X64-10767

(NASA-CR-138388) THE RANGER PROJECT Annual Report, 1961 (Jet Propulsion Lab.) 407 p

N74-74000

Unclas
00/99 37328

Technical Report No. 32-241

The Ranger Project:

Annual Report For 1961 (U)

JET PROPULSION LABORATORY
CALIFORNIA INSTITUTE OF TECHNOLOGY
PASADENA, CALIFORNIA

JUNE 15, 1962

This document contains information affecting the national defense of the United States, within the meaning of the Espionage Laws, Title 18, U.S.C., Sections 793 and 794, the transmission or revelation of which in any manner to an unauthorized person is prohibited by law.

CONFIDENTIAL

CONFIDENTIAL

NATIONAL AERONAUTICS AND SPACE ADMINISTRATION
CONTRACT NO. NAS 7-100

Technical Report No. 32-241

The Ranger Project:

Annual Report For 1961 (U)

CLASSIFICATION CHANGED
TO UNCLASSIFIED
By authority of E.O. 11652
Changed by L. Shirley Date 8-20-73

Copy No. 00362

JET PROPULSION LABORATORY
CALIFORNIA INSTITUTE OF TECHNOLOGY
PASADENA, CALIFORNIA

JUNE 15, 1962

EXCLUDED FROM THE GDS

CONFIDENTIAL

Copyright © 1962
Jet Propulsion Laboratory
California Institute of Technology

This document contains information affecting the national defense of the United States, within the meaning of the Espionage Laws, Title 18, U.S.C., Sections 793 and 794, the transmission or revelation of which in any manner to an unauthorized person is prohibited by law.

Contents

Preface v

I. Introduction 1

A. Background 1

B. Historical Summary 1

II. Preliminary Design and Project Planning 5

A. Preliminary Design 5

B. Project Planning 8

III. Project Management 11

A. Organization 11

B. JPL Activities 15

IV. Design and Development 17

A. Systems 17

B. Space Sciences 97

C. Telecommunications 154

D. Guidance and Control 225

E. Engineering Mechanics 263

F. Propulsion 299

G. Engineering Support Facilities 309

H. Ground Support Equipment 316

V. Assembly and Test Operations 331

A. Test Facilities 331

B. Assembly and Test Operations 334

VI. Launch Operations 351

A. Facilities 351

B. Pre-Flight Tests and Launch Operations 360

VII. Space Flight Operations 371

A. Facilities 371

B. Organization 375

C. Data Handling and Flow 376

D. Flight Operations Plans 376

E. Operations Procedures 377

F. Flight Operations 378

VIII. Deep Space Instrumentation Facility Operations 383

A. *Ranger I* Pre-Launch Operations 383

B. *Ranger I* Tracking Operations and Evaluation 384

C. *Ranger II* Pre-Launch Operations 394

D. *Ranger II* Tracking Operations 396

E. DSIF Preparations for RA-3 398

IX. Project Continuation Plan 403

References 404

Page Intentionally Left Blank

Preface

This report records the activities of the *Ranger* Project as a phase of the unmanned lunar exploration program of the Jet Propulsion Laboratory. The reporting period is retroactive to the inception of the project early in 1960, and extends through calendar year 1961. The following issues of this report will cover the subsequent calendar years.

Major sections of the report are: historical background, preliminary design and planning, project management, design and development, assembly and test operations, launch operations, space flight operations, deep space tracking operations, and project continuation planning.

The report covers the *Ranger I* and *II* missions, assembly and test of RA-3 and others of the lunar capsule series, and early effort on the follow-on TV subsystem group of spacecraft.

W. H. Pickering

W. H. Pickering, Director
Jet Propulsion Laboratory

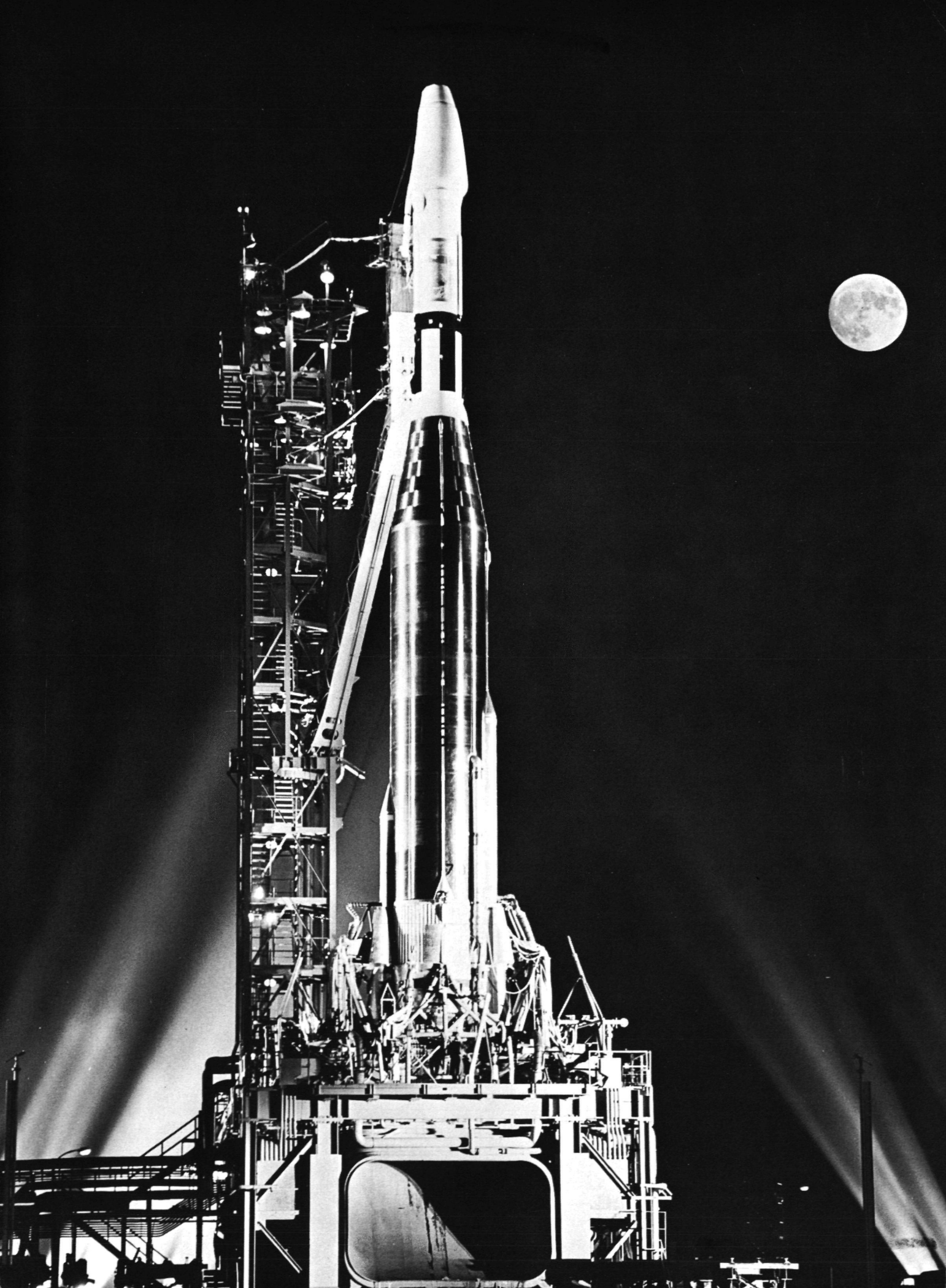

I. Introduction

A. Background

The *Ranger* Project began early in 1960. The first two engineering-test flights occurred in 1961, and the lunar mission series is planned to extend through 1962 and 1963. The objectives of the project are to demonstrate the technology of delivering scientific equipment from Earth to Moon, and to produce scientific and environmental data in support of the U. S. manned lunar flight program.

Major systems involved in the project are the *Atlas–Agena B* launch vehicle and associated launch and range facilities, the *Ranger* spacecraft, the NASA–JPL Deep Space Instrumentation Facility (DSIF), and a Space Flight Operations (SFO) system for in-flight control of the spacecraft.

This report records the efforts of the Jet Propulsion Laboratory from inception of the *Ranger* Project through calendar year 1961. The third flight test occurred early in 1962 and will be reported in the next annual report.

In the next section, the history of related work prior to 1960 is reviewed to record the circumstances under which the project began.

B. Historical Summary

1. Launch Vehicle System

During the *Juno I* (*Explorer*) and *Juno II* (*Pioneer*) experiments of 1958 and 1959, personnel of the Jet Propulsion Laboratory and the Army Ballistic Missile Agency made design studies looking toward improvement of the payload capacity of the *Jupiter* booster through the use of larger and more efficient upper stages. The first vehicle family considered was called *Juno III*, and was based on the use of a spinning cluster of solid rockets similar to, but larger than, the JPL-built clusters used on *Juno I* and *II*. The *Juno III* concept was rejected on the grounds that flight missions would soon require spacecraft guidance and stabilization, so that unguided, spinning upper stages would be undesirable.

The ensuing studies of a *Juno IV* vehicle family proposed the use of guided, liquid-propelled upper stages on the *Jupiter* booster. Power plants considered for these stages were:

(1) A proposed JPL 6K engine (6000-lb-thrust, pressure-fed, N_2O_4–N_2H_4, storable).

(2) The Aerojet *Able* or *Able–Star* propulsion system (7500-lb-thrust, pressure-fed, IRFNA–UDMH, storable).

(3) The Bell *Hustler* power plant (15,000-lb-thrust, pump-fed, IRFNA–UDMH, storable, later used in the Lockheed *Agena* stage).

(4) The General Electric 405 engine (33,000-lb-thrust, pump-fed, liquid-oxygen–kerosene, modified from the *Vanguard* first-stage power plant).

(5) A proposed JPL 45K engine (45,000-lb-thrust, pressure-fed, N_2O_4–N_2H_4, storable).

ABMA favored the pump-fed engines, while JPL preferred the pressure-fed power plants.

Concurrently with the *Juno IV* effort, ABMA was making studies, under the title *Juno V*, of million-lb-thrust class vehicles, which led eventually to the *Saturn* project. In mid-1958, ARPA ordered the development of both *Juno IV* and *Juno V*. In August 1958, ABMA was authorized to proceed with the 1½-million-lb-thrust, clustered-engine *Saturn*. Also in the fall of 1958, JPL was transferred to NASA while the von Braun team remained under ABMA, and the *Juno IV* project was cancelled. JPL's *Juno IV* effort is recorded in Reference 1.

The mission and payload design studies made during 1958 gave evidence that useful lunar and planetary experiments were barely feasible using payload weights available with IRBM-based (50-ton class) vehicles such as *Thor–Able* and *Juno IV*. It was, therefore, decided that future JPL deep-space missions should be based on ICBM (100-ton) boosters, although this was then regarded as a very risky and expensive step. The choice between *Atlas* and *Titan* was made in favor of *Atlas* because its flight tests had started earlier.

The selection of upper stages for the *Atlas*, coming as it did simultaneously with the organizational changes mentioned above, occasioned many problems. In addition to the list of rockets previously considered for *Juno IV*, there was also the *Centaur* (30,000-lb-thrust, pump-fed, liquid oxygen–hydrogen), which was then being proposed to USAF by Convair-Astronautics. In view of expected *Centaur* development difficulties due to use of hydrogen, NASA decided that Convair should also develop an interim stage to be known as *Vega*, using the GE 405 liquid-oxygen–kerosene engine. JPL studies, however, showed that another stage would have to be added for the deep-space missions, and early in 1959 NASA authorized development of the *Vega* vehicle, including the JPL 6K third stage for escape shots and using only the first two stages for launching Earth satellites. NASA let contracts to General Electric for the GE 405 engine and to Convair-Astronautics for the second stage development. JPL was requested to build the third stage and the deep-space payloads, and to assume technical direction of the vehicle development.

During the summer of 1959, personnel of the Ames Research Center of NASA were exploring various prospects for design of an attitude-stabilized meterological satellite to be launched by the two-stage *Vega*. One proposal was to use the *Agena B* satellite being developed by the Lockheed Missile Systems Division for USAF, with the propulsion system removed. An earlier version, *Agena A*, was already flying in the ARPA–USAF *Discoverer* program.

In the course of examining this proposal, JPL personnel became convinced that it would be better not to eviscerate the *Agena* stage, but simply to use it in place of the *Vega* stage on the *Atlas*. Further studies showed that, for most missions, the *Agena B* could perform better than the *Vega*. The turbo-pump-fed engine of the *Agena B*, powered by UDMH–IRFNA, developed 15,000-lb thrust. The system had a restart capability that could be used for transferring a spacecraft from a parking orbit into a lunar trajectory.

On December 11, 1959, NASA cancelled the *Vega* vehicle development and redirected the JPL 6K engine to propulsion-research status. The recommendations of a NASA group that included JPL personnel led to the February 1960 establishment of the NASA *Atlas–Agena B* program under direction of the von Braun team, which by then had joined NASA as the nucleus of the Marshall Space Flight Center. JPL's *Vega* effort is recorded in Reference 2.

2. Spacecraft System

During all of the launch-vehicle reprogramming events in 1958 and 1959, the spacecraft design and mission analysis effort at JPL continued fairly steadily. In addition to the interest in lunar missions, there was a strong desire by JPL to try for the next available planetary launch opportunities, viz., Mars in October 1960 and Venus in January 1961. Many of the principal design decisions on what later became the *Ranger* spacecraft were made with this goal in mind. For example, it was recognized that, for communicating at useful data rates from planetary distances, the spacecraft must have a high-gain, directional antenna pointed toward Earth. Thus, attitude stabilization became a requirement. This decision to control spacecraft attitude continuously made oriented solar power panels and direction-sensitive scientific instruments more feasible.

When it became evident that time was running out, and that both technical and fiscal constraints would prevent a U.S. planetary attempt in 1960–61, the *Vega* spacecraft design was reoriented to lunar missions only.

When the *Vega* vehicle development was cancelled, the lunar spacecraft development continued, and the hardware was modified to be compatible with *Agena B*. The resulting design became the present *Ranger* spacecraft.

3. Deep Space Instrumentation Facility

The historical development and background of the JPL Deep Space Instrumentation Facility are covered in two publications:

(1) Report No. 30-21, *A Description of Deep Space Net Facilities and Capabilities,* December 4, 1959.

(2) Technical Memorandum No. 33-83, *System Capabilities and Development Schedule of the Deep Space Instrumentation Facility—1963–1967,* March 2, 1962.

4. Space Flight Operations System

The problem of how to use the *Ranger* spacecraft after it had been launched was first given serious consideration during the spring of 1960. Deep space missions prior to *Ranger* were highly experimental and passive in nature; i.e., after launch, little if any control could be exercised from Earth-based tracking stations.

The *Ranger* spacecraft were to be considerably more sophisticated than their predecessors and were designed to be actively controlled from Earth. The particular measurements to be made by the spacecraft were grouped, and each group could be telemetered in turn on Earth-based or spacecraft-generated command.

The spacecraft were being designed so that their course could be altered in transit. The problem of attempting to hard-land an object on the Moon, coupled with the uncertainty in the time and distance between the Earth and Moon, necessitated active control from the Earth of the start of the landing sequence.

As the import of the need to control the spacecraft after launch became more apparent, more effort was devoted to attempting to devise a method and environment, both human and physical, within which the operation required to obtain and process data and control the spacecraft could be executed. This effort continued at JPL during the summer and fall of 1960. During November 1960, the policy and procedure by which JPL would plan and execute a newly defined category of functions called space flight operations was established. Space flight operations were defined as those functions necessary for the obtaining and processing of spacecraft information and commands required by JPL during the portion of flight from launch to the accomplishment of the mission.

The position of Space Flight Test Director was established. His assigned responsibilities were:

(1) To support the Project Manager in the preparation and execution of the Standard Operating Procedure (SOP) for space flight operations.

(2) To coordinate and integrate the requirements established by the cognizant divisions for the SOP.

(3) To interpret the SOP and place requirements consistent with the SOP on the various operating groups.

The standard operating procedure, by which the space flight operations would be executed during standard operation and anticipated departures from standard operation, was incorporated into the Space Flight Operations Plan (SFOP). The first SFOP was issued during January 1961 to describe the then-current best estimate of the space flight operations for RA-1.

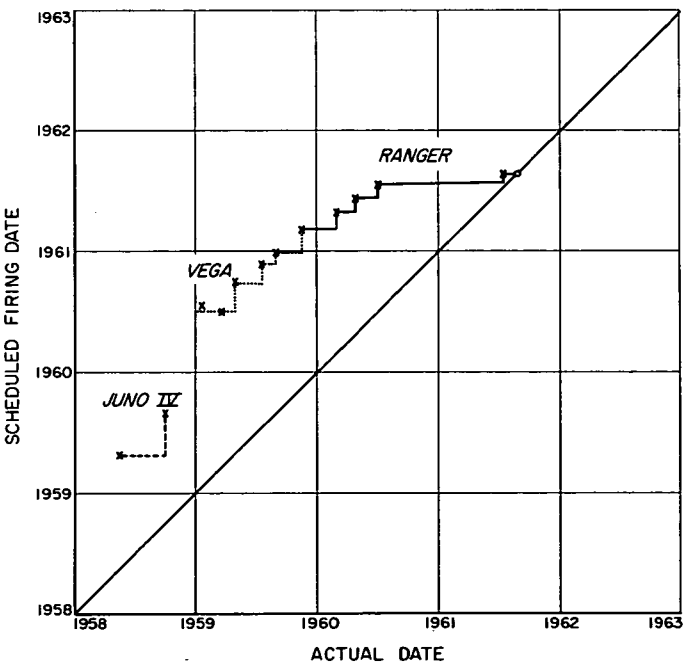

Figure 1. Schedule history of *Juno IV*, *Vega*, and *Ranger*

5. Schedule History

Figure 1 shows the history of schedule planning for the *Juno IV*, *Vega*, and *Ranger* efforts to date. The line plotted corresponds to the first planned flight-test date for each project. Periods during which the plan remained firm are shown as horizontal segments, and slippages are shown as upward jumps.

II. Preliminary Design and Project Planning

A. Preliminary Design

1. Mission Requirements

When the system analysis began, the critical mission requirement was the 1960–61 planetary opportunity. Lunar missions were also a requirement on the system design, but the planetary mission governed in areas such as (a) launch-on-time ability; (b) launch-to-injection tracking and instrumentation coverage; (c) spacecraft lifetime, communications range, solar power, and temperature control; (d) Deep Space Instrumentation Facility performance; and (e) total system reliability.

Certain lunar missions, such as the lunar orbiter for precision optical mapping, were more critical than the planetary mission in the requirement for spacecraft commands, control, and data handling. When the 1960–61 planetary mission had to be abandoned, design studies were made to determine what kinds of lunar experiments could best be performed within the system design capacities. It soon became evident that lunar orbiter precision mapping missions would require more payload weight, more time, and greater resources of personnel and funding than were available. The same conclusion applied to the lunar soft-landing mission, so both of these objectives were relegated to the next, larger generation of launch vehicles and spacecraft.[a]

[a]The soft-landing and orbiting missions are current objectives of the *Surveyor* Project at JPL.

This left, as possible lunar missions for spacecraft in the *Ranger* class, flights to unbraked impact, flights of the near-miss or circumlunar *(Lunik III)* type, and flights with retro-deceleration of part of the payload mass to an uncontrolled rough landing. It was decided to direct the system design toward the last class of missions.

2. Launch Vehicle System

When the *Atlas–Agena B* replaced the *Vega* as the launch vehicle for the lunar spacecraft, considerable work had already been done on the launch-to-injection system problem. Much of this work was directly applicable to the desired *Agena B* launch vehicle system design (Ref 4). Important conclusions of this preliminary design study were as follows:

(a) Celestial mechanics of the Earth-to-Moon transfer trajectory are such that launching must be over the Atlantic Missile Range, not the Pacific Missile Range, because range-safety azimuth limits at PMR would prevent eastward launching and, thereby, cause an intolerable reduction of payload weight.

(b) To maximize payload weight and relieve liftoff time constraints, it is necessary to include a variable coast phase, or "parking orbit" in the launch-to-injection sequence. The restart capability of the *Agena B* makes this phase possible without additional staging.

(c) No increase in guidance precision is required over that potentially available with the *Agena B* satellite guidance system, if the lunar spacecraft can make a midcourse maneuver for trajectory correction after injection.

(d) A standard USAF *Atlas–Agena B* vehicle with minor modifications can carry lunar spacecraft weighing 700 to 800 lb.

The *Ranger* launch vehicle is shown in Figure 2.

3. Spacecraft System

Early in the spacecraft design phase, it became evident that the opportunities for engineering-development flight test would be very limited because of the high cost and unreliability of the 100-ton class launch vehicles. Since the mission criteria unavoidably resulted in highly complex spacecraft designs, there would be little hope of ever reaching a useful single-shot probability of success unless major aspects of the spacecraft design remained the same from round to round to permit the growth of development experience. This view, together with the determination that only a fraction of the initial weight could be decelerated by retro-rocket at the Moon, led to the concept of a "bus and passenger" design. The bus would incorporate the basic functions of attitude control, power supply, support structure, telecommunications, and propulsion for flight-path correction, and would remain more or less the same from series to series; the passenger equipment could contain the items peculiar to a particular mission.

The shape and functions of the spacecraft were largely dictated by geometrical configuration constraints. Some of these for planetary and lunar missions are as follows:

(a) The spacecraft primary axis of symmetry should be pointed toward the Sun to simplify the problems of attitude acquisition, solar power, and temperature control.

(b) The high-gain antenna must continually track the Earth over a wide range of Earth–spacecraft–Sun angles, and must therefore be articulated relative to the spacecraft.

(c) Moon or planet scanners would have to be articulated independently of the antenna to provide enough degrees of freedom for satisfying all angular relationships during a flyby mission.

(d) The thrust of the midcourse propulsion system must act through the center of gravity of the spacecraft in the maneuver configuration.

(e) Since many kinds of scientific experiments are degraded by nearby equipment (limits on field of view, radio or magnetic interference, radiation from nuclear events in the spacecraft mass, etc.), tall structures, extensible booms, and such devices would be required.

(f) The spacecraft, which is required by the above constraints to assume a "spread-out" shape during cruise, must fold up into a relatively compact and rugged package to fit inside a reasonably-shaped aerodynamic nose fairing on the launch vehicle.

The JPL 6K stage for *Vega* had six longerons. Therefore, the spacecraft which later became the *Ranger* bus was designed with hexagonal symmetry. It now appears that JPL-built spacecraft will retain this hereditary characteristic for a long time, simply because there is no particular reason to change it.

Electronics packaging experience in the *Corporal* and *Sergeant* missile programs resulted in choice of plain rectangular boxes, with removable structural modules, as the basic technique for *Ranger*. A very stiff structure is required to avoid resonance amplification of vibration. Aluminum or magnesium alloy castings were used in the design of most of the boxes and the standard module frames, producing a rugged structure with good packing density and adequate heat rejection.

The present *Ranger* spacecraft configurations are illustrated in Figure 2, which shows the bus, the scientific-instrument superstructure for the first two flights, the lunar rough-landing retro-capsule for the current series, and the high-resolution TV passenger assembly for the later flights.

4. Space Flight Operations System

The entire complex of Earth-based facilities required to conduct space flight operations is called the Space Flight Operations Complex. The preliminary design and development of certain elements of this complex were well underway during the summer of 1960, i.e., the DSIF. Others, particularly the point of central control of the space flight operations, had not been designed or developed at that time.

A study was undertaken to determine and evaluate the advantages and disadvantages of exercising control of the various components of the Space Flight Operations Complex from JPL in Pasadena, or the DISF station at Goldstone, California. After it had been decided that control of the operations would be exercised from Pasadena, the problem of developing the control area and

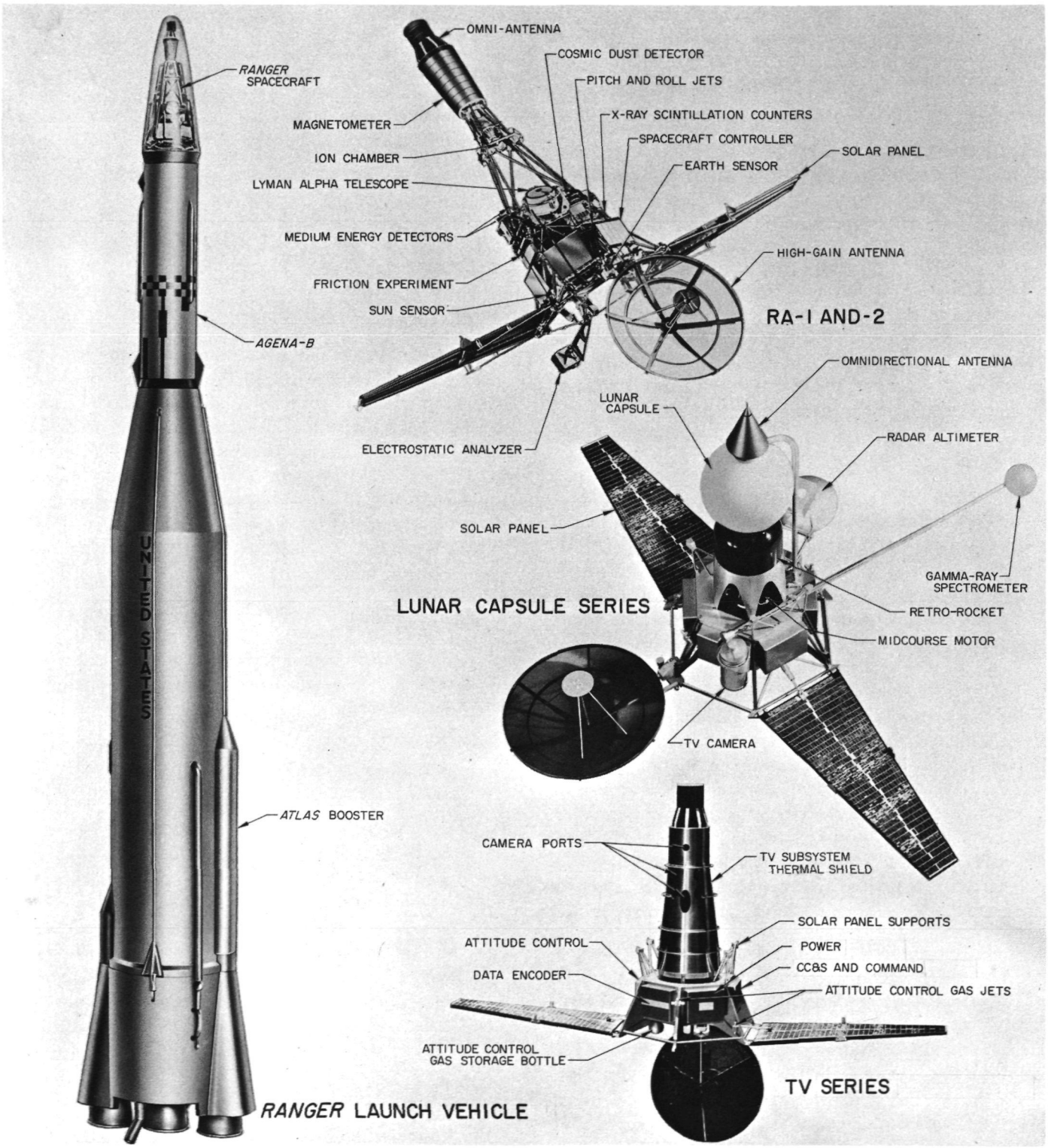

Figure 2. *Ranger* launch vehicle and spacecraft

other components of the complex was undertaken in earnest. The three areas requiring most effort were the instrumentation and computation capability at AMR, the integration of required facilities at JPL in Pasadena, and an adequate communication system by which data could be transmitted between various elements of the complex.

Late in 1960, the immediate and projected tracking, telemetry instrumentation, and computation capability required at AMR was established and placed on AMR in the initial issue of the *Ranger* Program Requirements Document No. 1800.

Recognizing that sufficient time did not exist prior to the launch of RA-1 to realize the desired capability, the injection of RA-1 and -2 was constrained to occur over Ascension Island, the only instrumentation facility existing far down range at AMR at that time. During 1961, additional capability was planned and implemented such that it would be available for later phases of the *Ranger* Project.

The nature of the activities conducted at JPL before the inception of the *Ranger* Project was such that no need existed for an operational "command post." The JPL facilities required for space flight operations were dispersed and a serious problem existed in attempting to physically and operationally interconnect them. The necessary communication lines were installed to transfer data and operational information between the various installations at JPL. The procedures established in the RA-1 SFOP were exercised to bring the human element of the Space Flight Operations Complex to an operational state. Experience during the RA-1 and -2 space flight operations and the projected requirements of the *Ranger* and subsequent projects, established the need for a centralized facility in which the operations would be exercised and controlled at JPL. The new Space Flight Operations Facility will be located at JPL in Pasadena, and may be operational in time for later launches in the *Ranger* Project.

Effective communication between elements of the complex and the spacecraft is accomplished through the DSIF and is particularly important to the execution of space flight operations. Data originated by the sensors in the spacecraft must be transmitted to the Earth-based DSIF stations for re-transmission in real time to Pasadena. Upon reception at Pasadena, the data is processed in the Central Computing Facility (CCF), using a data processing system built around an IBM 7090. Expeditious handling of the output of the data processing system is required to interpret, evaluate, and analyze the data and make decisions and generate commands to return to the spacecraft. Data recorded at the DSIF stations is forwarded to JPL, Pasadena, for non-real-time processing in the Data Reduction Laboratory, and subsequent reduction in the CCF.

Dissemination of information about the space flight operations is accomplished through the Office of Information and Education at JPL.

B. Project Planning

1. Mission and Design Philosophy

The definition of the best series of steps toward a given goal was difficult because of the inherent complexity of the deep-space missions. Should small satellites or vertical probes be launched first to test components in space? Should the final design be optimized in all respects for its first expected mission, or should it be compromised somewhat to gain long-term flexibility? These and many other questions were examined and, by the time the NASA *Agena B* program started, the following conclusions were in hand:

(a) The first flight should test the complete launch vehicle and most aspects of the spacecraft design. Flights with smaller, cheaper, more reliable launch vehicles or payloads would divert more effort than was justified.

(b) Every flight, including the early engineering tests, should carry scientific instruments, because there was no way of predicting which flights might succeed.

(c) Since the demonstrated reliability of the individual launch vehicle stages was of the order of 0.7, each flight would have less than half a chance of success, even neglecting the failures expected in the complex spacecraft. Therefore, it would be necessary to schedule a series of attempts at each objective in order to have a reasonable probability of at least one success. Numerical estimates related to this question are given below.

(d) In order to obtain maximum value from the experience accumulating in the USAF flight programs, changes on the *Atlas* and *Agena* relative to the standard production vehicles must be held to a minimum.

The basic objectives of the lunar investigation were initially agreed to be: (1) to create the spacecraft tech-

nology necessary for scientific experiments that could determine the origin, constitution, and history of the Moon; and (2) to exploit this technology, first in support of the purely scientific goal and second, in support of plans for eventual manned exploration. When the U.S. manned lunar landing effort changed from "eventual" to high-priority status, the *Ranger* objectives were adjusted accordingly and the order now is: (1) to support the manned program, and (2) to conduct lunar investigations of basic cosmological interest.

2. Scientific Experiments

a. RA-1 and -2. Scientific experiments were scheduled as passengers on board *Rangers* RA-1 and -2 to take advantage of the engineering feasibility flights, without reference to the lunar body.

The principal scientific objective of the RA-1 and -2 spacecraft was the further determination of the nature of the particles and fields in interplanetary space, with special emphasis on discovering the mechanisms responsible for the many terrestrial phenomena which appear to be related to solar disturbances. In particular, most of the instruments on *Rangers* RA-1 and -2 were directed toward the following aspects of solar-terrestrial relationships:

(1) Geomagnetic storms and the solar wind. The existence of a steady solar wind has not yet been either proved or disproved conclusively. It was hoped to directly determine the number, energy, and temporal fluctuations of those particles believed to be responsible for geomagnetic storms, the curvature of comet tails, and other observed phenomena.

(2) Replenishing of the Van Allen radiation by particles of extraterrestrial origin. There exists, at present, some controversy as to the origin of a large fraction of the trapped particles—whether they are of solar origin or come from the decay of low-energy neutrons created in the Earth's atmosphere of cosmic radiation.

(3) Production of high-energy particles by the Sun. The energy spectrum, time variations, and directions of travel of these particles must be determined in order to establish their times, places, and mechanisms of production and storage.

(4) Modulation of galactic cosmic rays as observed near the Earth—both the 11-year variation and the shorter-period Forbush decreases. The similarities and differences between these two types of variations are of great importance in determining their mechanisms.

In addition, it was hoped that the data from *Rangers* RA-1 and -2 would aid in understanding of those processes at the Sun which give rise to the various particles and modulations seen near the Earth.

b. RA-3, -4, -5. The first *Ranger* spacecraft designed to land instrument packages on the Moon will carry experiments designed to obtain scientific information which will increase our knowledge of the history and formation of the Moon and technical information which will help increase the chances of successful future Moon landings by unmanned or manned spacecraft. RA-3, -4, and -5 will carry the same four experiments: a vidicon camera, a gamma-ray detector, a radar altimeter to obtain reflectivity data, and a seismometer. The main body of the spacecraft, carrying the vidicon, gamma-ray, and radar instrumentation, will crash-land and be destroyed. The capsule, with the seismometer and its radio transmitter, will hard-land and is designed to withstand about 3000-*g* deceleration. The seismometer will then measure lunar seismic activity.

c. RA-6, -7, -8, -9. The primary scientific objective of RA-6 through -9 is acquisition of knowledge of lunar topography sufficient for determination of its gross effects on lunar landing vehicles. This objective will be achieved by means of relatively high-resolution photography of a portion of the lunar surface from the impacting spacecraft, and subsequent quantitative analyses of these photographs. This mission will be performed within the constraints of a *Ranger* standard impact trajectory which specifies a near-vertical impact with a velocity at impact of approximately 2700 m/sec.

A secondary scientific objective of the follow-on series is acquisition of knowledge of the radiation environment of cislunar and lunar space which may be of importance to manned lunar flights, or which may yield data pertinent to the origin of these environments. Specifically, the several radiation experiments to be carried on the spacecraft will provide data on radiation levels and the biological hazards resulting from high-energy particle radiation during flights to the Moon.

3. Engineering Development Planning

The major objectives of early development planning for *Ranger* were: (a) to fly the basic bus as soon as possible on an *Atlas–Agena B* vehicle, (b) to match the technical criteria to the resources available so as to have reasonable probability of a successful lunar mission in 1962, and (c)

to exploit the *Ranger* flights for the benefit of the planetary program.

Initially, the project was funded for five shots. Rough estimates of reliability showed that the complicated lunar rough-landing mission would be unlikely to succeed with fewer than three attempts, leaving two vehicles available for engineering flight tests. Accordingly, RA-1 and -2[a] were designed for a simplified test mission, namely, a near-escape elliptical trajectory without the midcourse and terminal maneuver functions. The lunar reconnaissance and rough-landing mission became the goal of RA-3, -4, and -5. The scientific passenger experiments for RA-1 and -2 were selected to take advantage of the engineering-test trajectory and had nothing to do with the Moon.

A very important decision concerned how much of the launch-phase complexity required for the lunar missions should be incorporated in the engineering test shots. After study, the conclusions were that the first two flights should include the parking orbit and *Agena* re-start functions, but not the variable launch time, variable azimuth, and variable parking-orbit coast times required for lunar injection. The latter functions were omitted (a) to simplify prelaunch operations; and (b) to assure telemetry coverage of the critical second-burn phase by using an Earth-fixed trajectory within view of Ascension Island. The tracking and telemetry ships, transoceanic communications, and other features required for the more complicated missions were included on an experimental basis.

In view of the RA-1 and -2 flight results, the decision to test the parking orbit and second burn was a fateful one, since second burn failed both times. It is questionable whether the early discovery of the two *Agena* faults compensated for the loss of spacecraft engineering and scientific data. Fortunately, both spacecraft remained in orbit long enough for engineering evaluation of most subsystems, but the scientific results were slight.

In addition to the technical development goals of the *Ranger* Project, a major objective was the early introduction of major subsystem contractors in order to: (a) encourage the spread of lunar flight technology, (b) gather experience quickly in the requisite management and procurement techniques, and (c) limit the JPL work load. After a design study competition and source-selection board procedure, NASA designated the Aeronutronic Division of Ford Motor Company to design and build the lunar rough-landing retro-capsule subsystem for RA-3, -4, and -5, under subcontract to JPL. When the manned lunar landing program assumed high-priority status, four additional *Ranger* spacecraft were ordered and a single-source procurement was negotiated with the Astro-Electronics Division of RCA for a high-resolution TV subsystem to be carried by *Rangers* RA-6 through -9. The change from a five-shot to a nine-shot program greatly improved the chance of obtaining at least one completely successful mission.

[a]*Ranger* flight spacecraft are numbered consecutively as follows: RA-1, RA-2, etc. NASA numbers flight missions in S (satellite) and P (probe) sequence; e.g., P-32, P-33, etc. After successful launch, the flight experiments are designated *Ranger I, Ranger II,* etc.

III. Project Management

A. Organization

The *Ranger* Project operates under the rules of NASA General Management Instruction 4-1-1, issued January 19, 1961. The cognizant office in NASA Headquarters is the Office of Space Sciences. JPL is the Project Management Center (Fig 3), and is also responsible for three of the project's four systems: the spacecraft; Deep Space Instrumentation Facility; and Space Flight Operations System. The fourth system (the *Atlas–Agena B* launch vehicle and associated facilities, including launch-to-injection range support) is under the cognizance of the Marshall Space Flight Center (MSFC) of NASA.

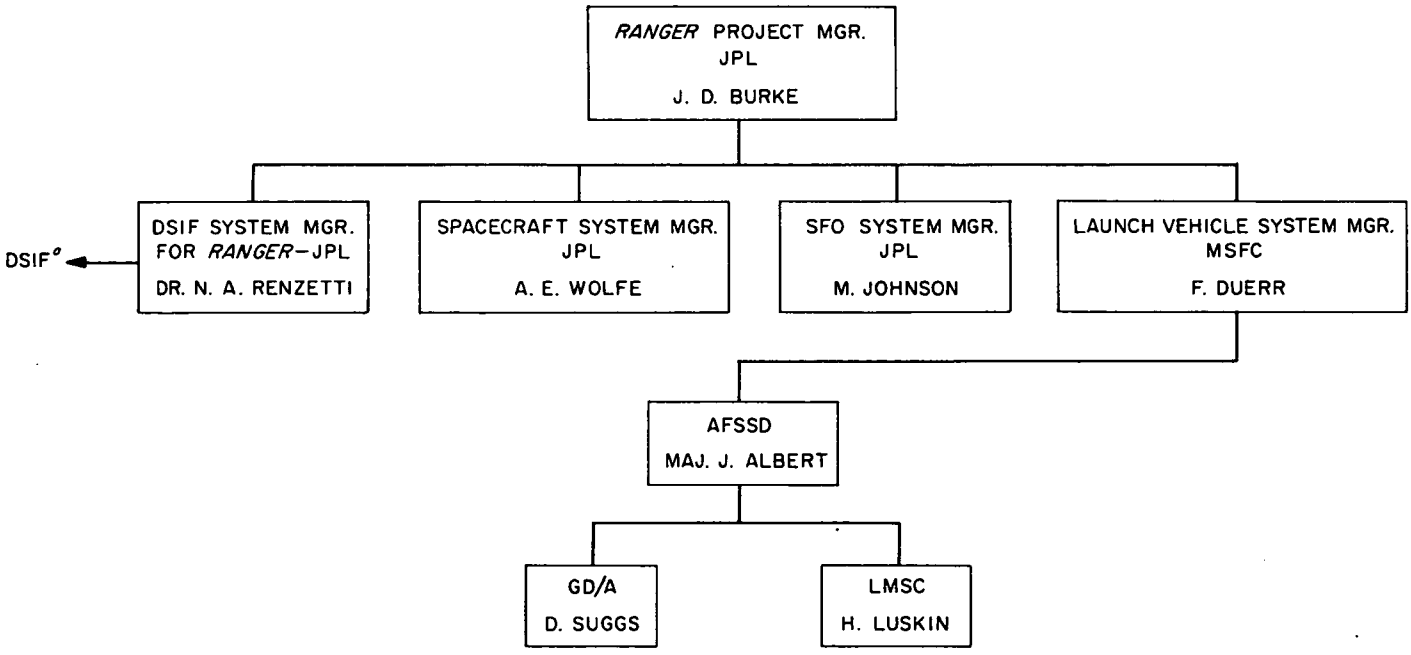

[a] GOLDSTONE, CALIFORNIA; STATION OPERATED FOR NASA BY JPL
JOHANNESBURG, SOUTH AFRICA; STATION OPERATED BY NATIONAL INSTITUTE FOR TELECOMMUNICATIONS RESEARCH OF COUNCIL FOR SCIENTIFIC AND INDUSTRIAL RESEARCH OF UNION OF SOUTH AFRICA
WOOMERA, AUSTRALIA; STATION OPERATED BY AUSTRALIAN WEAPONS RESEARCH ESTABLISHMENT

Figure 3. *Ranger* Project organization

MSFC procures the vehicles through the Air Force Space Systems Division (AFSSD). AFSSD administers the contracts and directs the contractors so that MSFC obtains maximum benefit from established USAF procedures, and so that interference between the NASA program and high-priority military programs is minimized. The Lockheed Missiles and Space Company (LMSC) supplies the *Agena* stage and is the vehicle system contractor in charge of such efforts as structural integration, trajectory and performance analysis, test and operations planning, and documentation. General Dynamics-Astronautics (GD/A) is the contractor for the *Atlas*.

At the launch base, the Launch Operations Directorate (LOD) of MSFC is in charge of pre-launch activities. Range support is obtained through the NASA Test Support Office of LOD, and the 6555th Test Wing of AFSSD directs the vehicle contractors. Figure 4 shows the organization for pre-launch and in-flight operations. JPL's internal organization for the *Ranger* Project is shown in Figure 5.

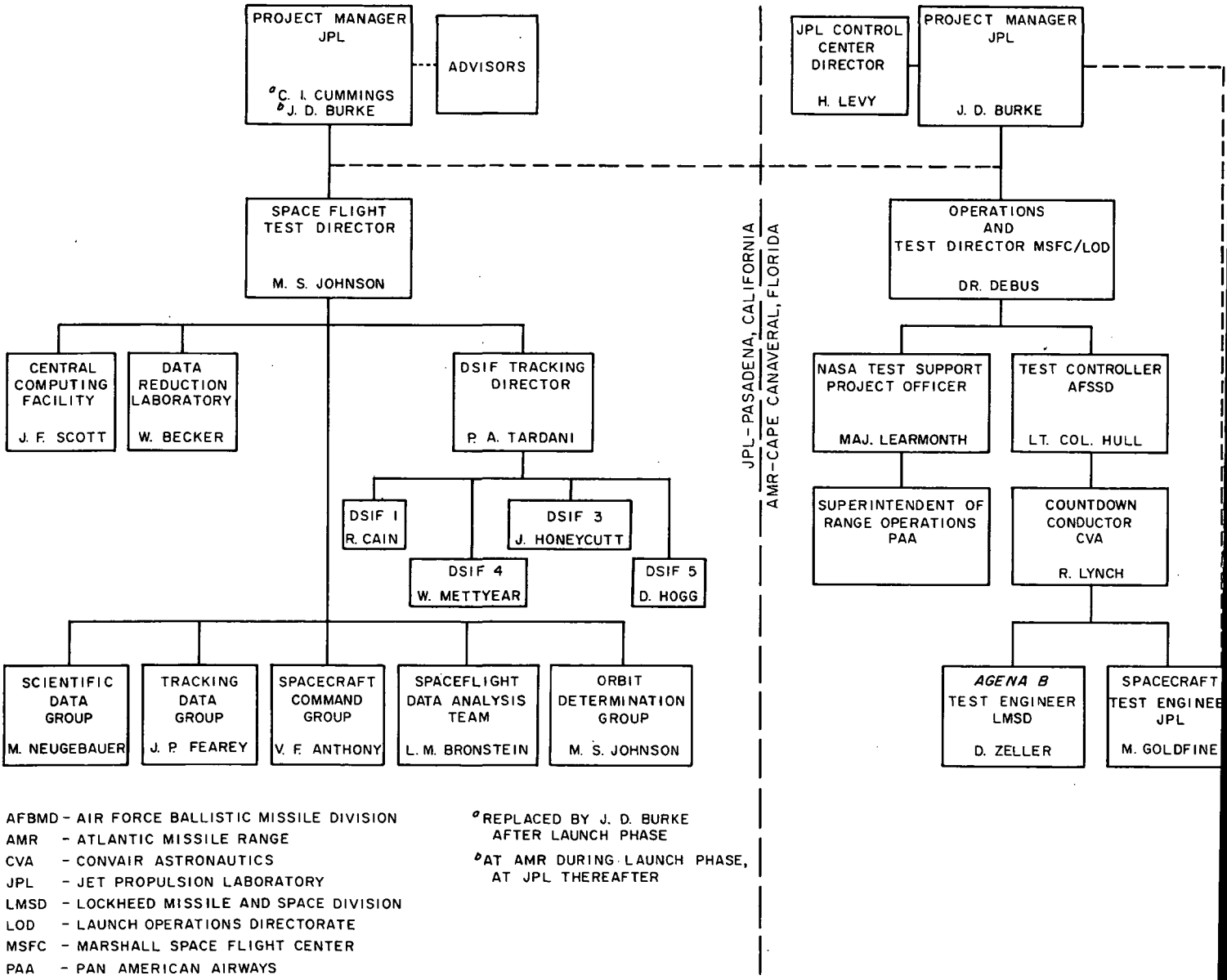

Figure 4. *Ranger* operations organization

ORGANIZATION
JET PROPULSION LABORATORY

Approved W. H. Pickering
Director
February 1, 1962

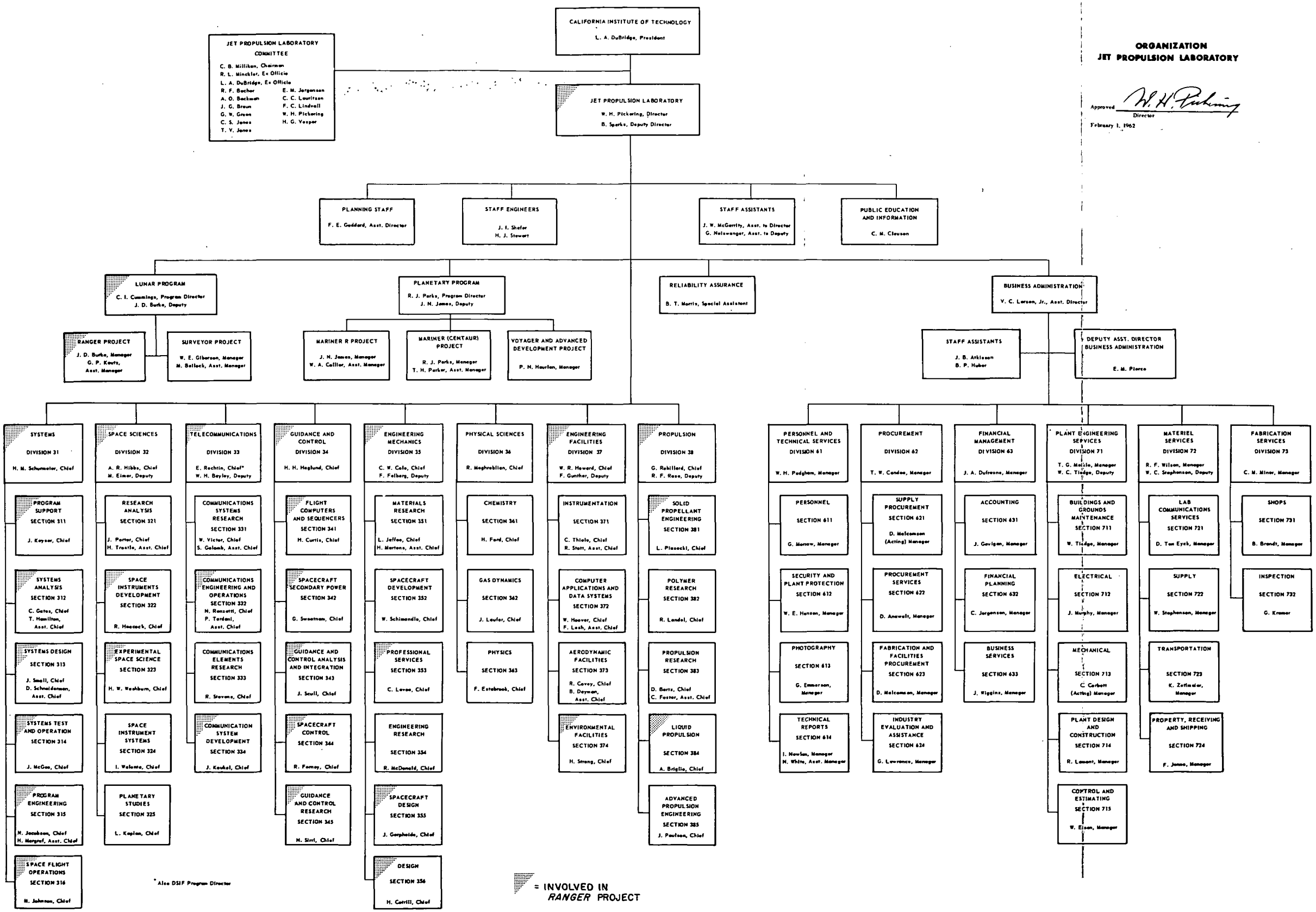

Figure 5. JPL organization for *Ranger*

Page Intentionally Left Blank

B. JPL Activities

1. General

During the first year of the project, prior to the issuance of Management Instruction 4-1-1, some difficulties resulted from poor definitions of authority and responsibility external to JPL. The troubles were most evident in interface and system-integration areas, where some of the engineering work was inadequate or late. The most serious incident was a performance analysis error that set off a major spacecraft weight-reduction effort later found to be unnecessary. Despite the difficulties, the project came up to its first flight date on time and within the budget, and the performance of the spacecraft in flight was completely successful, considering the orbit attained.

2. Launch Vehicle Liaison

Much of the early management effort was expended in liaison with MSFC, LMSC, and AFSSD on the problems of integrating the vehicle and spacecraft. LMSC is responsible for integrity of the vehicle with the spacecraft, and participates in the appropriate reviews by AFSSD and MSFC. Later in the project, when tests had demonstrated successful mating, this effort required less sustained emphasis, but it still remains an area of major management interest.

Launch-to-injection instrumentation presented difficult problems because of the number of interests involved. Solutions of conflicts and releases of required documents were often very late, with the result that, on one occasion, a flight attempt was cancelled because of delayed documentation for range-safety analysis. Eventually, satisfactory commitments were obtained, and the launch-to-injection coverage is now limited more by technical than by management considerations.

3. Spacecraft Development

Management of the spacecraft system development was relatively straightforward, being entirely internal to JPL. The JPL groups that later became the Systems Division executed the preliminary design in accordance with the criteria established by the Project Manager, with the aid of personnel assigned from the other technical divisions. Detail design, prototype fabrication, and procurement were handled by each division for its own equipment, with the aid of the administrative divisions. Assembly, test, and field operations were under direction of the Systems Division; the test crew included specialists assigned from each participating division.

Some difficulty arose as a result of conflicts between scientific and engineering objectives, particularly in the early flights where the science experiments were aboard as noninterfering passengers. Prior arrangements between NASA and participating scientists were sometimes inconsistent with JPL's project management approach, and placed the JPL Division of the Space Sciences in a difficult spot. Most of these problems were resolved without serious incident, but one of them did cause a last-minute cancellation of a launch attempt.

Since the selection, assignment, and execution of the scientific experiments is fundamentally a hard technical and managerial job, additional problems in this area are expected and substantial further management effort is indicated.

Page Intentionally Left Blank

IV. Design and Development

A. Systems

1. System Design

a. Rangers I *and* II. *Rangers I* and *II* were designed as engineering-development rounds having the primary objectives of demonstrating the desired performance and lifetime capability of the major engineering functions required to meet the ultimate objectives of RA-3, -4, and -5. The specific objectives were the development of the elements of spacecraft environment control, power conversion, attitude control, and communications. A secondary objective of *Rangers I* and *II* was to carry an integrated group of scientific experiments for investigating certain aspects of deep-space environment.

With the available techniques, experiments on these elements of spacecraft technology demanded a weight of several hundred pounds injected on a precisely controlled near-escape trajectory.

Figure 6 is a simplified block diagram showing the relationship of the major subsystems on *Rangers I* and *II*.

Attitude control. The attitude control of the spacecraft combines a primary and a secondary control system. The primary system controlling the pitch and yaw attitude

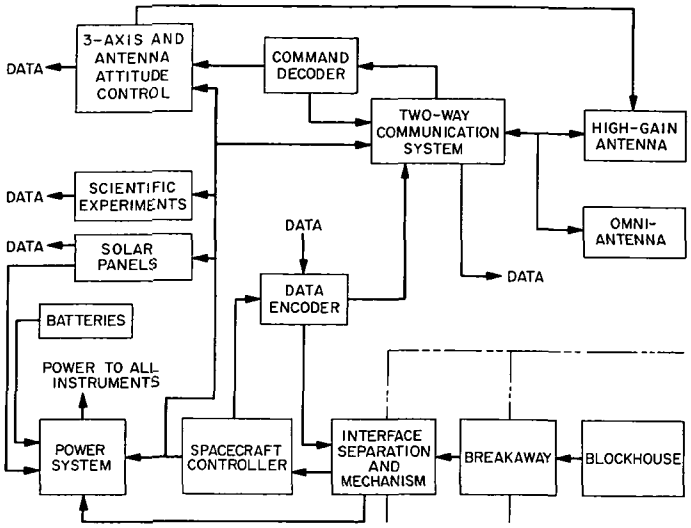

Figure 6. RA-1 and -2 spacecraft system block diagram

of the spacecraft is Sun-oriented. The secondary system uses Earth light to control the roll axis of the vehicle, and thus establish the plane containing the spacecraft roll and yaw axes. This system also rotates the dish antenna about a hinge axis to point it toward the Earth. Operation of the Sun-pointing system is entirely independent of the Earth acquisition experiment. The probe–Sun and probe–Earth lines establish the vehicle attitude references.

Attitude-control torques are produced by a cold-gas expulsion system. Pairs of on–off gas nozzles and valve assemblies, mounted on the spacecraft, are switched by a linear combination of position and rate signals. The pitch axis has one pair of nozzles, whereas the roll and yaw axes have two pairs of jets each. Figure 7 is a block diagram of the RA-1 and -2 pitch or yaw attitude control systems. (Figure 256 illustrates the over-all attitude-control system.)

The system is capable of pointing the roll axis of the spacecraft along the probe–Sun line with an accuracy of ± 1.5 deg.

The pitch axis of the spacecraft is maintained perpendicular to the Earth–probe–Sun (EPS) plane with an

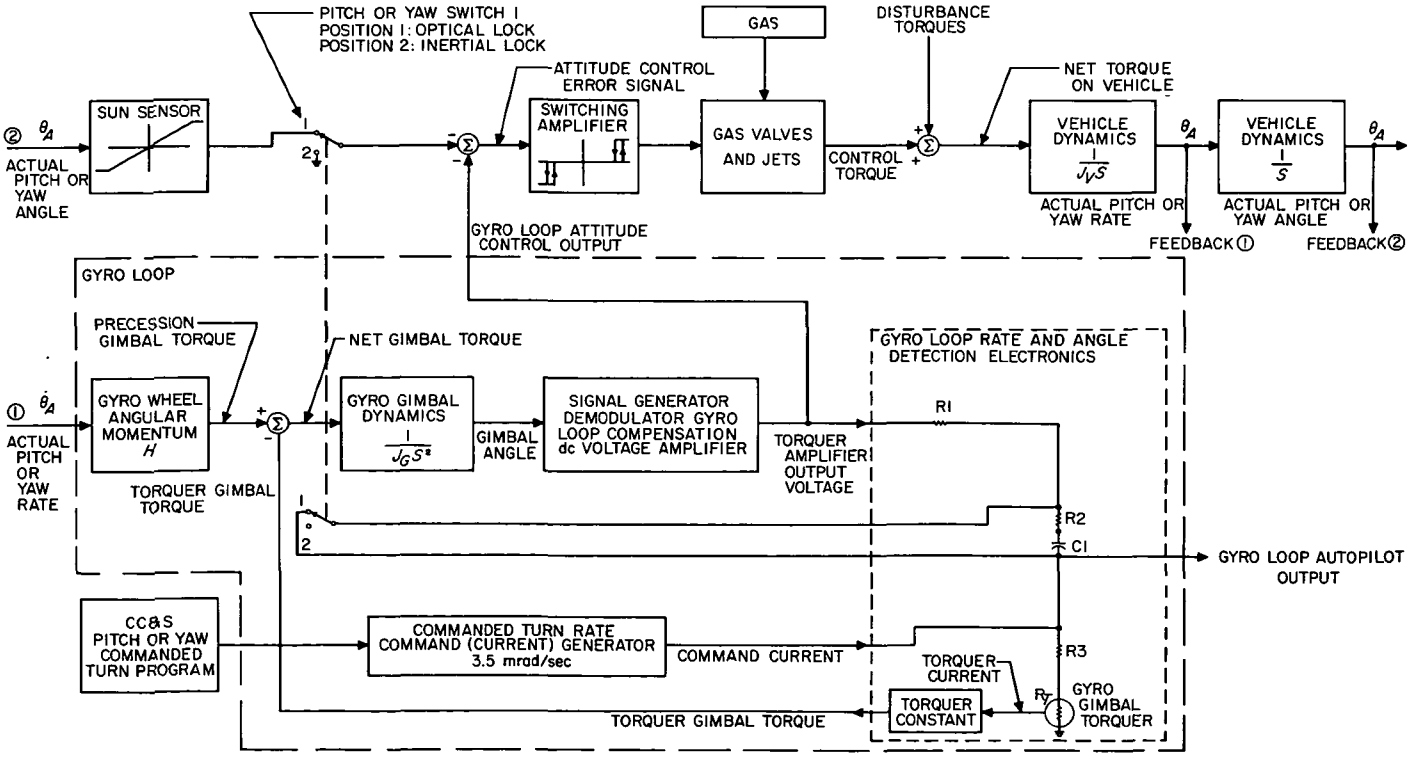

Figure 7. Pitch or yaw attitude control

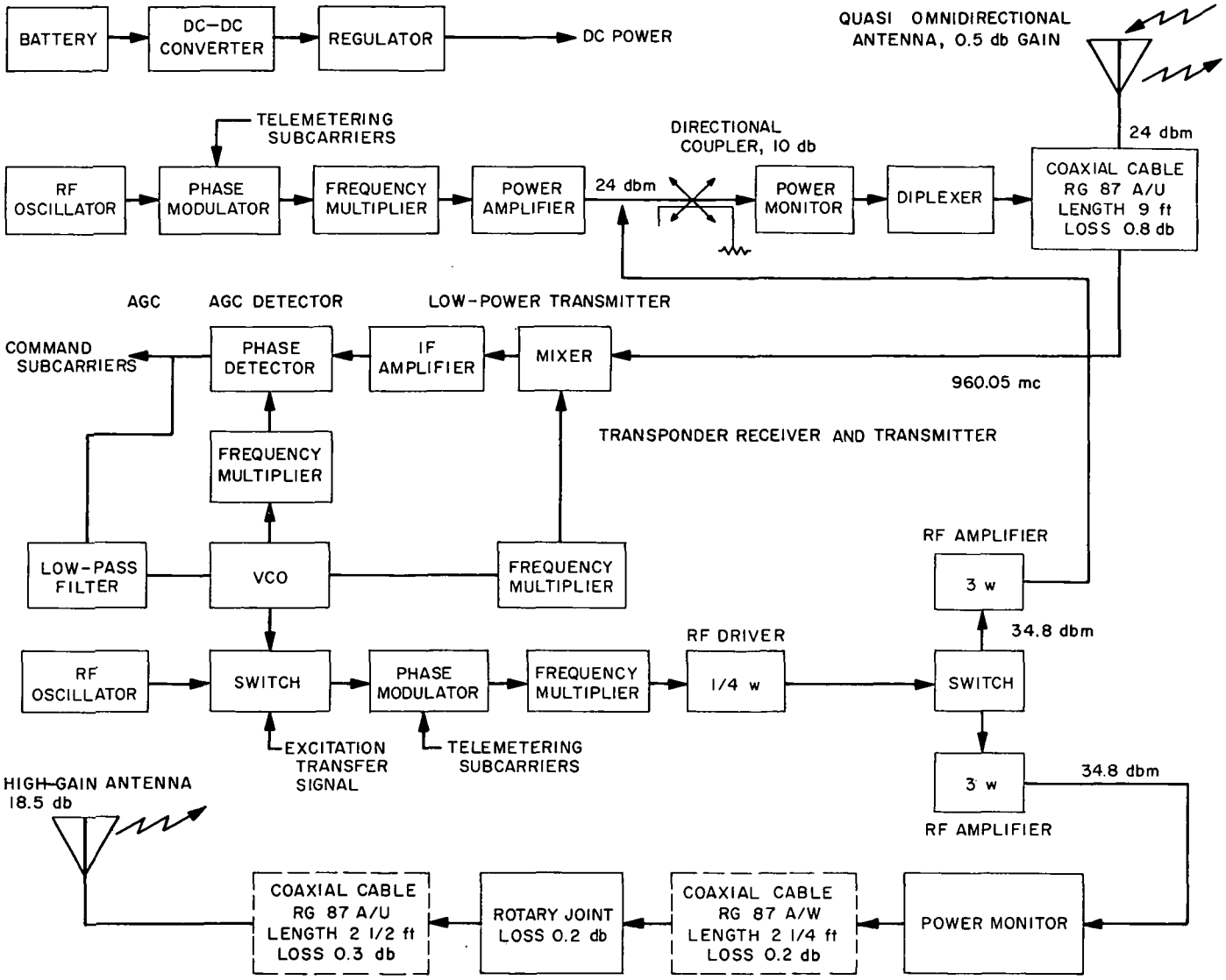

Figure 8. RA-1 and -2 communication system, functional block diagram

accuracy which varies with the vehicle's distance from the Earth, and with the EPS angle for any given trajectory. Maximum pointing accuracy is obtained when the EPS angle is 90 deg.

Communication system. The spacecraft communication system consists principally of a transponder containing a 3-w transmitter. Earth commands are received by the transponder through the omni-directional antenna. The transponder 3-w output can be switched on command from the Earth so that it is transmitted through either the spacecraft 18.5-db high-gain antenna or through the omni-directional antenna. A functional block diagram of communication system elements is shown in Figure 8.

In addition to the transponder, a 250-mw, self-contained transmitter was included to provide backup capability for the 3-w transmitter and/or the solar-oriented power supply. In order to be completely independent of the rest of the spacecraft systems, the transmitter was equipped with its own power supply and isolated battery capable of providing 7 to 10 days of continuous operation. Transmission beyond that time would be extremely marginal because of the Earth-to-spacecraft range, assuming a near-nominal trajectory.

Antenna system. The omni-antenna was mounted at the top of the spacecraft structure and provided a toroidal pattern symmetrical about the roll axis of the spacecraft.

Thus, transmission to the spacecraft would not be impaired by the loss of the secondary or Earth-pointing portion of the attitude system. In the event of such a mishap, it therefore would have been possible to transmit ground commands to the spacecraft, transferring the transponder output from the high-gain antenna to the omni-antenna.

The high-gain antenna consisted of a pointable 4-ft parabolic dish antenna having a gain of 18.5 db at the transmitter frequency of 960 mc. The antenna was hinged at one foot of the spacecraft and was provided with 180 deg of rotation in a plane containing the yaw and roll axes of the spacecraft. Pointing signals for the antenna actuator were provided by the attitude-control system.

Antenna drive mechanization. After considering the environmental requirements for the antenna gear drive in space, it was decided that a hermetically sealed enclosure for the drive would be required. The enclosure or gear box later became a part of the prime airframe structure.

The lifetime of the antenna drive in space required the box to be sealed so that the life expectancy of lubricants, motors, and potentiometers could be extended. Also, the possibility of vacuum welding or galling of metals is eliminated and temperature control is simplified. A positive pressure in excess of present day laboratory vacuum was maintained in the box for the duration of the mission.

The components which mechanized the drive were a servomotor, gear train, slip clutch, and position potentiometer. The servomotor was size 11 and is a special design requiring 3 to 4 w at stall and is lubricated with silicone fluid. The gear train provided a reduction of 234,000 to 1 from the motor to the antenna yoke, which was driven nominally at 1 rph. A rotary seal was used between the gear box and yoke. Worm gears in the train prevent back driving by the antenna. A slip clutch was employed as a safety feature so that ground checkout overloads would not damage the gear train. During flight, the clutch remained locked.

Command system. The purpose of the command system was to complement the r-f system and accomplish the transfer of command data from the Earth to the spacecraft. The system included the ground equipment, which accepted the command information in a form convenient to the flight unit, with discrete outputs for each command. It will encode commands into a form recognizable by the spacecraft command decoder and also employ a modulation technique which is compatible with the phase-coherent VHF transmission link.

To meet the requirements of *Rangers I* and *II*, a system capable of only three on–off functions was developed. Two of these were used to provide the hinge override and roll override capability to the attitude-control system required in the event that the Moon was acquired instead of the Earth. The third command was used for switching the transponder output between the two antennas.

For RA-3 and later spacecraft, a more complex and flexible system is required to accommodate a large number of on–off and proportional control commands.

Two types of systems were considered for RA-1 and -2 on–off functions: tone burst and discrete pulse modulation. Advantages of a tone approach are: relative simplicity for a small number of commands, adaptability to parallel redundancy, possibility of simultaneous initiation of more than one command, and experience with existing tone systems (AN/DRW-4 and AN/DRW-11). In addition, the tone system of control is the method most widely used at missile test ranges. Disadvantages include weight penalties associated with filter components and bandwidth limitations imposed by temperature, aging drifts in filter, and/or local oscillator frequencies.

Any pulse modulation system is necessarily time multiplexed so that simultaneous transmission of more than one command is not possible unless coding logic is employed. Advantages of this type of system include the use of simple digital building blocks (practically all switching mode operation), and a capability for extension to complex control functions (e.g., proportional control with the addition of a digital-to-analog converter). Disadvantages are: the system is new and will require an extensive development effort and most important, there is no worthwhile performance improvement over a tone system for the simple functions required of an RA-1 or -2 mission.

Based on these considerations, the conclusion was that a multiple tone-command system was the most logical way to implement RA-1 and -2 command functions. A tone burst system would logically take the form indicated in Figure 9. The ground system consists of an ensemble of tone generators (in this case, three) which are keyed independently to achieve a command.

In practice, a command would be initially generated with a push-button having a holding time of 3 sec. An electronic timer provided a standard command duration of 3 sec which could be lengthened by continued closure of the push-button switch. In case the electronic timer failed, the same function could be achieved by pushing the button for at least 3 sec. These tone signals

were used to phase modulate an 890-mc transmitter at a nominal total rms phase deviation of 0.8 rad.

Salient vehicle system components consisted of the transponder, capable of furnishing a phase-error reproduction of the transmitted tones, together with an audio decoding channel corresponding to each of the tones used. Each decoder channel consisted of suitable amplification, a narrow-band tone matched filter, and a threshold detector. Actual initiation of commands was furnished by momentary relay closures lasting for the duration of command generation, approximately 3 sec. Since the maximum tolerable delay between reception of a command tone and conversion of this information into a relay closure was 2 sec, the minimum permissible decoding channel bandwidth was approximately 1 cps, which was compatible with required system reliability (in a noisy environment) and available pre-decoder signal-to-noise ratios.

To guard against false operation, inhibiting functions, derived from a receiver coherent AGC loop, interrupt signal paths on both ends of all channels in the event that carrier-lock is lost or insufficient signal strength is obtained.

Data encoder. The data encoder accepts and encodes signals corresponding to voltage, temperature, pressure, and other telemetered variables for radio transmission. The data transmitted from the spacecraft fall into two categories. One is the engineering data which covers spacecraft structural, guidance, communications, power, and environmental data for use in evaluating the development of the elements of spacecraft technology. The second type of data is that taken primarily for scientific reasons.

In the design of a data communication link, either one of two general approaches may be taken. In the first, the number of data channels available, as well as power

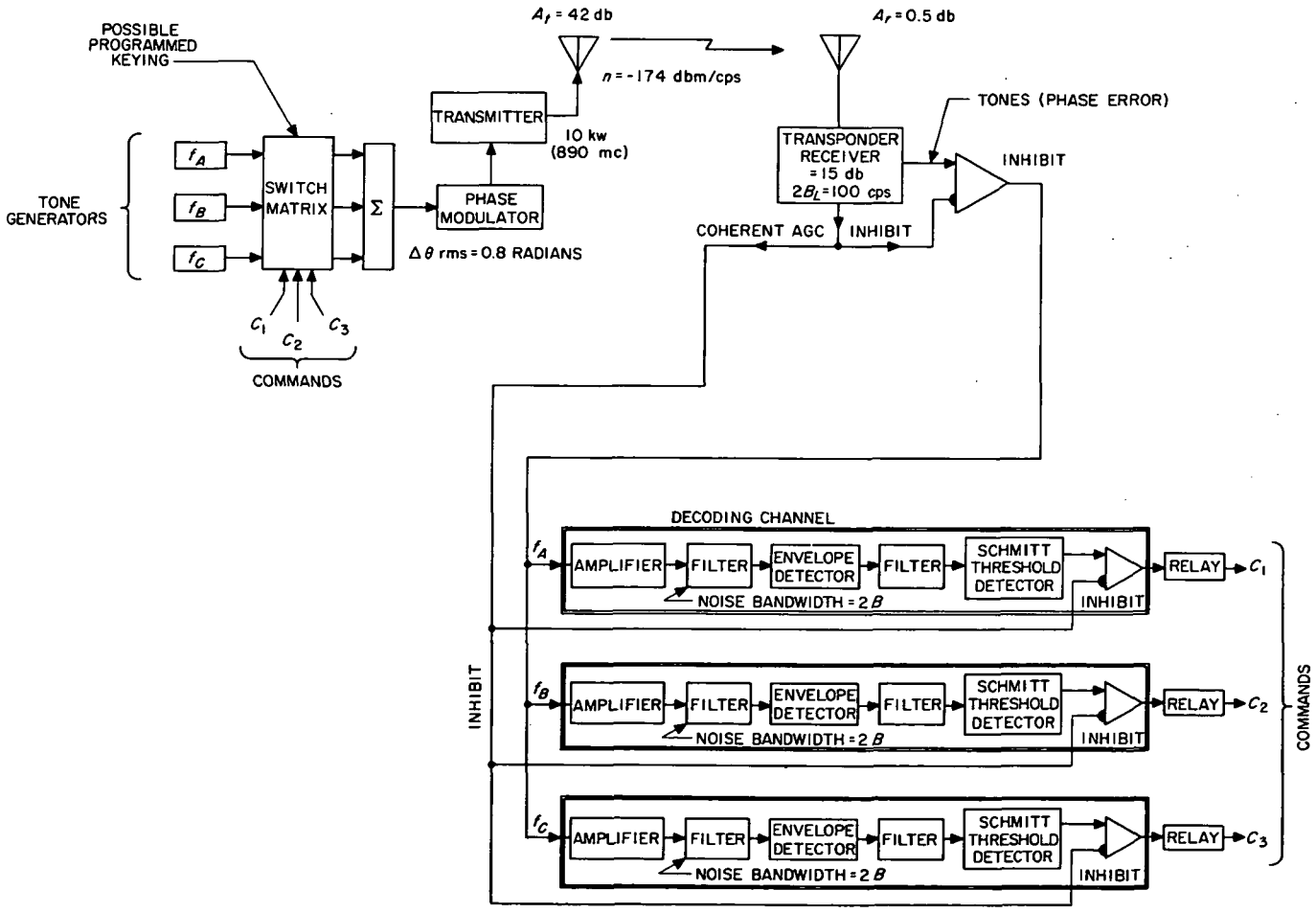

Figure 9. Command system

available per channel, may be arbitrarily fixed and the data then conditioned so as to pass through these channels. In the second method, the data rates and waveforms are fixed, and then the channel power is allocated for most efficient use of the available power. The *Explorer* satellites were an example of the former approach; an arbitrary division of power was made among the subcarrier channels with the thresholds allowed to fall where they might, as a function of the data rates and waveforms. In the *Pioneer* lunar probes, the first approach was again used but much more sensibly. In this case, the available channel bandwidths were chosen to achieve a specified threshold and the data conditions so as not to exceed the allowable rate.

In designing the spacecraft communication system, the second approach has been taken. The data waveforms, sampling rates, accuracies, and threshold distances were chosen and then the power required to achieve this data rate and fidelity was allocated to each channel.

An early module of the data encoding system used for RA-1 and -2 is shown in Figure 10. (A schematic of the system is shown in Figure 143.) Two types of frequency-multiplexed channels are used to provide the maximum data communication efficiency. One type of subcarrier (Channels 2, 3, 4, and 7.7) carries analog-type data, whereas the remaining channels (B-10 through B-13) carry binary or two-state information. Spectrum relationship for these channels is shown in Figure 11.

The binary data is prepared in serial form by the scientific instrument electronics which modulates the binary channel with a very low-frequency deviation. This binary data is reconstructed by the ground discriminators into binary pulse data of the form presented to the flight encoder.

Spacecraft controller. Primary function of the RA-1 and -2 spacecraft controller was to provide commands to the various spacecraft subsystems. These commands initiated, and sequenced spacecraft events. In addition to timed commands, the controller also provided 1-cps pulses to the data encoder and the science systems, plus an additional timing pulse once per thousand seconds to science. These pulses occurred in synchronization with the spacecraft power frequency (400 cps) to aid in identifying telemetered data.

A list of commands used on the RA-1 and -2 spacecraft and their functional description follows:

Command 1, issued approximately 30 min after launch, increases the radiated power from the spacecraft from approximately 1.5 to 3 w. It was necessary to radiate

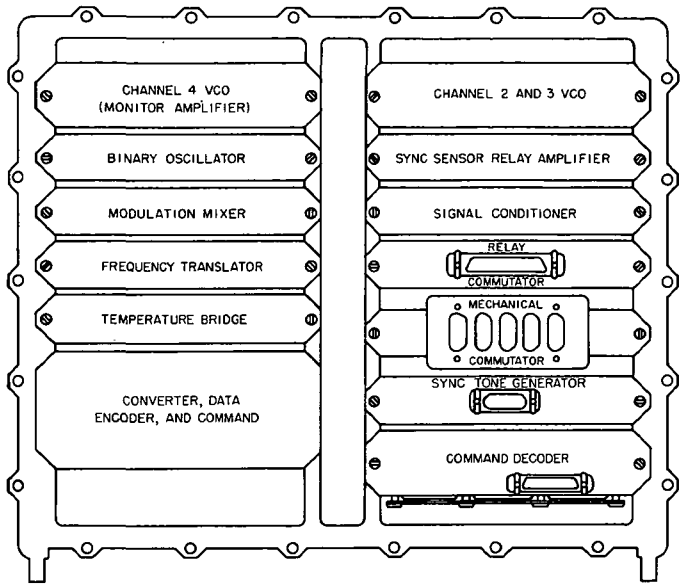

Figure 10. Telemetry-encoder command modules

at the lower power level during the launch phase in order to avoid corona discharge within the transponder power amplifiers.

Command 2, issued approximately 34 min after launch, permits the solar panels and a boom carrying scientific instruments to extend from their folded positions.

Command 3, issued approximately 59 min after launch, permits the attitude-control system to initiate the Sun-acquisition process and causes the high-gain antenna to move from the nested position to the pre-set acquisition angle.

Command 4, issued approximately 74 min after launch, turns on certain scientific instruments which had not been turned on because of corona discharge.

Command 5, issued approximately 87 min after launch, permits the attitude-control system to initiate the Earth-acquisition process.

Command 6, issued approximately 115 min after launch, changes the scale factor on the telemetry measurements of the spacecraft inertial rates, and turns off the instrumentation gyro which is useful only during the immediate post-injection and attitude acquisition phase.

Command 7, issued approximately 204 min after launch, changes the scale factor of one of the scientific instruments.

Command 8, issued approximately 247 min after launch, transfers the transponder output from the omni-

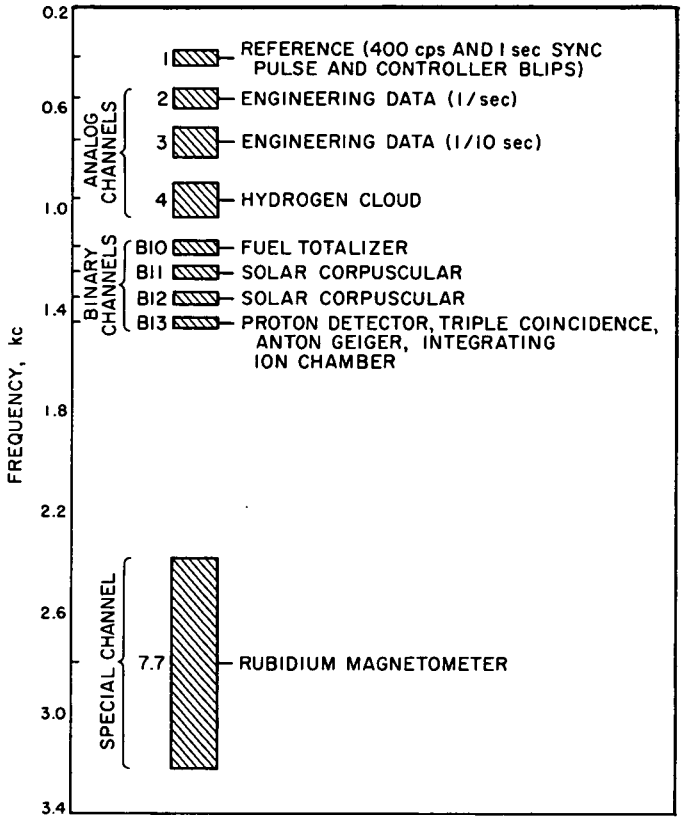

Figure 11. *Ranger* RA-1 channel layout

directional antenna to the high-gain antenna. This function can also be performed by ground command. It is performed by the controller, however, as a backup in the event of a command failure.

Command 9, issued approximately 364 min after launch, reduces the information rate on the 250-mw transmitter in order to extend the communication threshold range.

Command 10, issued approximately 367 min after launch, turns on an engineering experiment designed to investigate the effects of the space environment on the coefficient of friction between various bearing materials.

Power system. The spacecraft electrical power system consists of two oriented solar panels, a battery, a power-switching system, and several static converters, as shown in Figure 12.

The solar panels provide the primary power to the spacecraft. The battery provides power from launch to acquisition and backup capability should the attitude control or solar power systems fail. Since RA-1 and -2 were developmental rounds, it was decided to put all available weight margin, consistent with the vehicle capability and the growth requirements for RA-3, into excess battery capability.

A battery was selected which was a modification of one which had performed satisfactorily during satellite flights in another program. The battery was manually activated, weighed 120 lb, and could power the spacecraft for a period of 50 to 60 hr.

Each solar panel was capable of delivering 78 $+30$ w, -0 for a total raw power capability between 156 and 216 w. The larger tolerance on the power output for the panels is due to the uncertainty in our knowledge of the parameters which affect the power output. Some of these were the exact value of the solar constant, the transmissibility of the Earth's atmosphere, the temperature at which the panels will stabilize, the variations in distance from the Sun, and the effects of exposure to the space environment on the panels.

A list of regulated power required by each of the subsystems during various phases of the flight is shown in Figure 13. Also shown is a power profile expressing the regulated power requirements in terms of the raw power required at the input to the power conversion system.

After the first few hours of flight, the raw power requirements are well below the minimum power output from the solar panels.

Packaging and configuration. The configuration developed for the spacecraft was a direct consequence of the desire to maximize the solar panel area which could be carried within the *Vega* shroud design, and to develop a basic spacecraft capability which could be adapted to a variety of missions and scientific experiments.

The hexagonal shape was selected as a reasonable packaging and configuration compromise which permitted an efficient structural transition from the spacecraft to the 6K stage. The maximum diameter at the base of the hex and the taper of the solar panels were established by the maximum allowable envelope within the *Vega* shroud. Packaging for the spacecraft equipment was influenced to a great extent by the need for a versatile design, which was required in order to make the spacecraft capable of accepting equipment for various missions. From the standpoint of ease of fabrication and standardization, it was decided to package only in rectangular-shaped volumes, using modular packaging techniques. The form factor for the design was then established on the basis of optimizing the rectangular packaging volume and providing adequate clearance for the parabolic antenna and other equipment within the shroud constraints.

The basic shape of the instrument compartment was as shown in Figure 14. The six assemblies or boxes in the

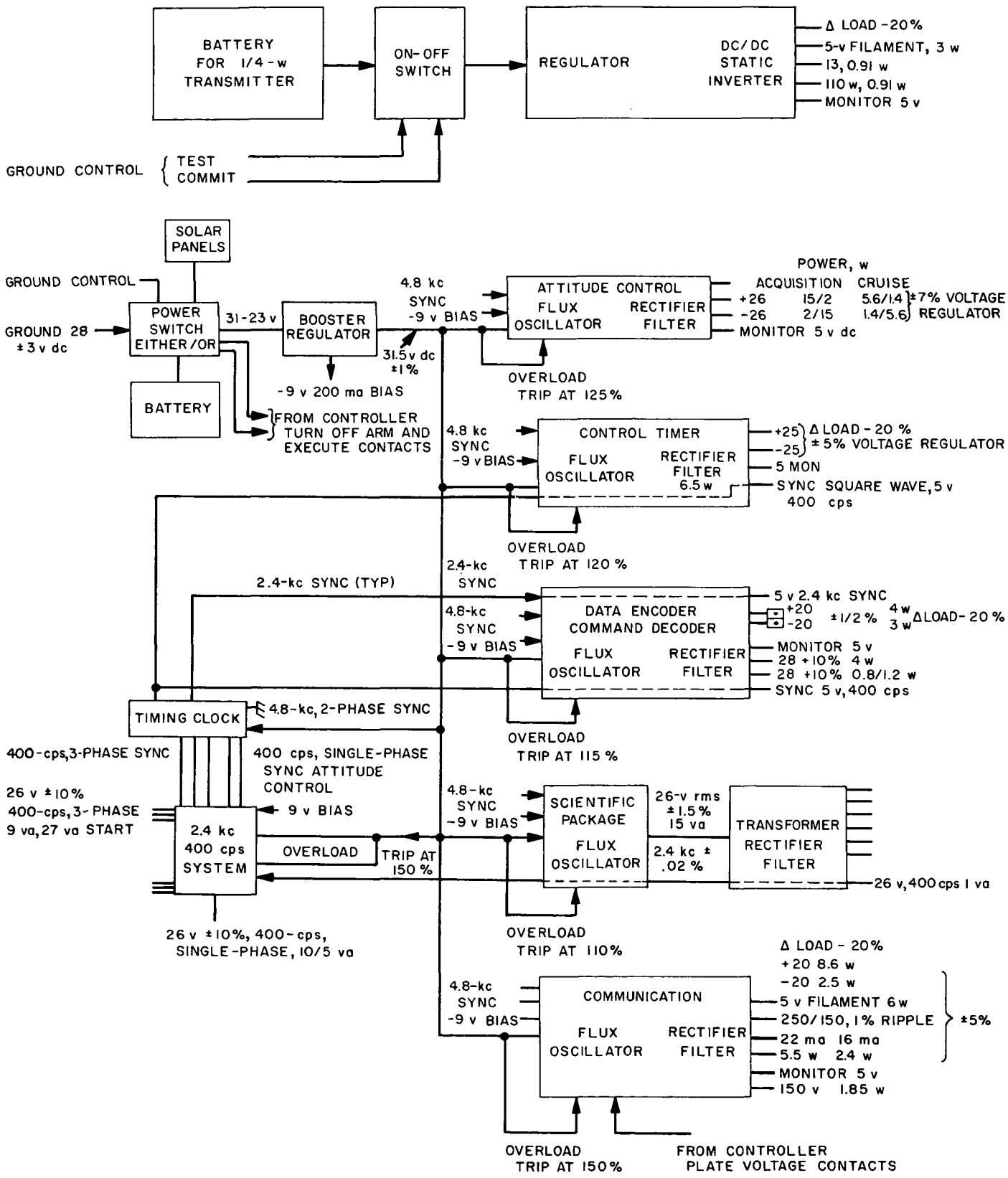

Figure 12. Spacecraft electrical power system

REGULATED POWER	LAUNCH	INITIATE SUN ACQUISITION	INITIATE EARTH	STEADY STATE
COMMUNICATIONS	19.0	20.4	20.4	20.4
ATTITUDE CONTROL 3ϕ	9.1	9.1	9.1	9.1
ATTITUDE CONTROL 1ϕ	2.8	6.8	0.8	0.8
ATTITUDE CONTROL dc	4.9	21.6	12.7	6.7
DATA ENCODER	10.8	10.8	10.8	10.8
CONTROLLER	6.8	6.8	6.8	6.8
SCIENTIFIC	10.4	10.4	10.4	10.4
RATE GYRO	9.8	9.8	9.8	0.0
TOTAL	73.6	95.7	80.8	65.0

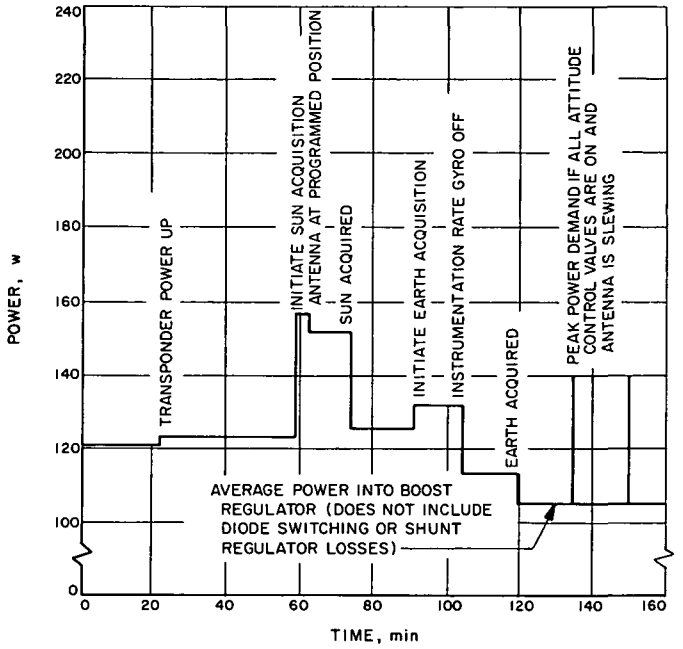

Figure 13. Subsystem regulated-power requirements

closed position served as structural members, while the modules provided gussetting for the assemblies. This integrated approach resulted in an efficient structural design having a low structure-to-total-weight ratio.

Upon cancellation of the *Vega* program and initiation of the *Ranger–Agena* project, it was decided to retain as much of the existing design as possible. The mission objectives were modified as described in Chapter II and the configuration developed as shown in Figure 15.

The principal elements of the configuration include the basic bus or hexagonal instrument compartment, the high-gain antenna, a scientific boom, two solar panels, and the forward structure.

The geometry of the forward structure was determined by considering the accommodations desired for the various components and experiments to be mounted, and by developing a structure that would most nearly attain these goals. Although not structurally optimized, it did in fact represent a satisfactory compromise between structural efficiency and experiment–component accommodation. For structural efficiency, the packaging of the scientific experiments would have taken the familiar form of the basketball or bullet configuration, typical of early spacecraft.

From the experiment accommodation standpoint, the magnetometer must be supported a minimum of 10 ft from the major source of spacecraft-generated magnetic field; the cosmic-ray experiment must be provided as nearly a 360-deg, solid-angle view as possible; the omni-antenna must be supported 125 in. above the plane of the solar cell panels; two solar corpuscular radiation (SCRE) experiments must be mounted to look in particular directions with unobstructed views outboard; one SCRE mounted on a boom must be latched at a point 16 in. above the bus during the boost phase; the Lyman-alpha experiment must be mounted outboard to provide as unobstructed a sweep as possible in the direction dictated by the 18-db antenna; and the solar panels must be latched during the boost phase at points approximately 13 and 50 in. above the bus. The forward structure of the spaceframe illustrated in Figure 16 is the result of considerations and parameters referenced above.

In addition, the design had to provide a protection system for the spacecraft during shroud separation. The protection was provided by six tubular guards attached to the spacecraft and tangent to the 9-deg spacecraft envelope. These guards provided initial guidance for the shroud, so that contact would not be made with the upper portions of the spacecraft.

b. RA-3, -4, -5 spacecraft. The RA-3, -4, -5 spacecraft design (Fig 2) is basically similar to the RA-1 and -2 configuration, with the modifications necessary to incorporate midcourse and terminal maneuvers, to transport a lunar capsule subsystem, and to mount equipment for a gamma-ray radiation experiment and vidicon photography of the Moon's surface. In addition, the spacecraft must fly within more restrictive trajectory constraints, meet sterilization requirements, and provide increased volume for electronics and power system packaging.

Capsule subsystem. The capsule subsystem weighs 328 lb and consists of an impact limiter, survival instrument sphere, retrorocket, and radar altimeter.

(1) *Impact limiter.* The crushable impact limiter weighs approximately 39 lb; it is constructed of balsa wood and protects the survival sphere during impact, at the residual speed remaining due to errors in the retromaneuver.

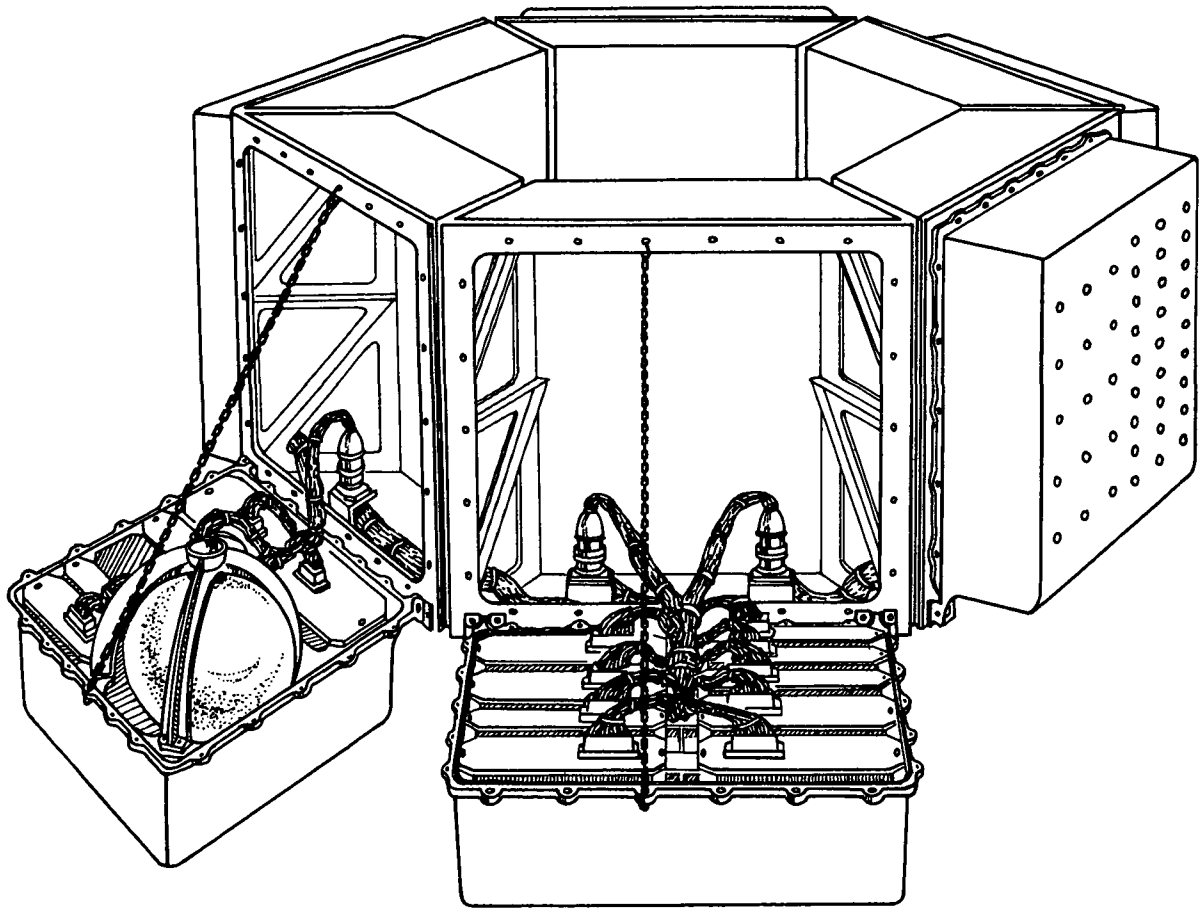

Figure 14. Spacecraft packaging

(2) *Survival sphere.* The 56-lb instrument sphere is designed to survive a rough landing on the Moon, to measure seismic activity on the lunar surface for up to 30 days, and to transmit the data back to Earth. The sphere is floated within the impact limiter and is insulated against the lunar environment. It is capable of righting itself after impact and orienting its antenna on Earth. Following impact, the seismometer is placed in the operational mode by venting its caging fluid to the lunar atmosphere. Internal power is provided for 30 to 60 days of operation.

(3) *Instruments.* The single-axis lunar seismometer can detect seismic disturbances in the surface material that will yield significant information about the composition and formation of the Moon. The data are transmitted back to Earth through an L-band transmitter operating at 960 mc, with an information bandwidth not less than 5 cps and a power output of not less than 50 mw.

(4) *Radar altimeter.* The radar altimeter serves a dual function. It acts as a range meter to generate a fuzing signal for capsule/spacecraft separation during the terminal maneuver, and it collects lunar surface radar reflectivity data.

(5) *Retrorocket.* The retrorocket motor slows the capsule after separation from the bus, nominally braking it from 6000 mph at 52,000 ft to zero velocity at an altitude no greater than 1100 ft above the lunar surface. The retromotor weighs 213 lb and develops 5080-lb thrust for 10 sec.

A small spin motor is attached to the retro system and can spin stabilize the capsule assembly at 300 rpm with its 20-lb thrust, lifting it free of the spacecraft bus.

Bus. Modifications to the RA-1, -2 spacecraft bus were held to a minimum.

(1) *Structure.* The RA-1, -2 superstructure was replaced with the lunar capsule subsystem. The omnidirec-

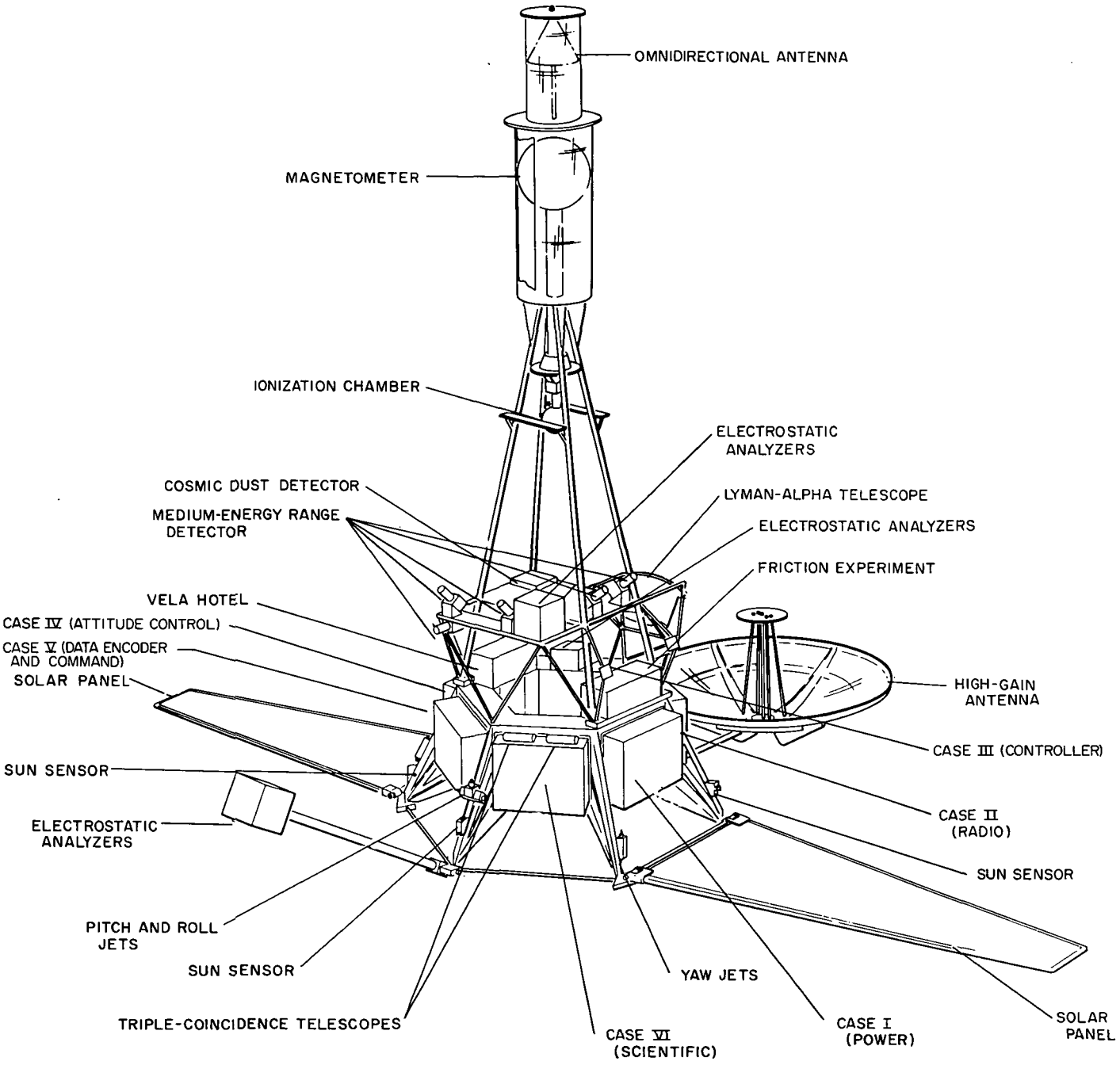

Figure 15. Early *Ranger* spacecraft configuration

tional antenna was modified to fit above the capsule sphere and was mounted on a movable arm. The basic hexagonal structure was retained. It measures 5 ft in diameter at the base. In the cruise mode, with panels out, the spacecraft extends 17 ft and is 10.25 ft in height. Total weight of the RA-3, -4, -5 spacecraft is approximately 727 lb.

(2) *Antennas.* The RA-3, -4, -5 spacecraft has three antennas. The high-gain directional antenna has a redesigned feed and supports, since it must deploy 45 deg to the roll axis at the midcourse maneuver. The omnidirectional antenna also must be moved before separation of the capsule subsystem and the bus. The radar altimeter antenna on the capsule subsystem is nested until the terminal maneuver, when it is extended to the operating mode.

(3) *Solar panels.* The solar panels are similar to those used for RA-1, -2 except for a modified latching

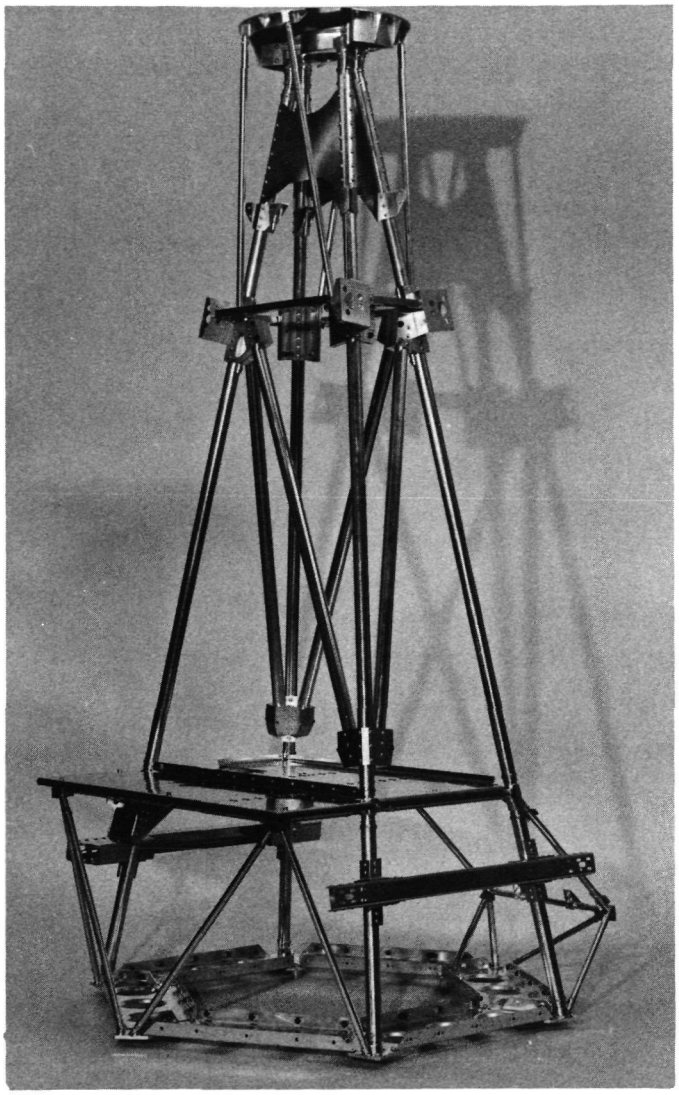

Figure 16. *Ranger* RA-1 forward structure

system. Each of the two panels has 4340 solar cells in a 10 ft² area. The power system is capable of producing a maximum of 210 w, and a minimum of 155 w, unregulated.

(4) *Packaging.* All packaging cases for RA-3, -4, -5 were fabricated from magnesium to save weight. The battery, vidicon camera, and attitude-control gas storage bottle were relocated on the bus.

Midcourse maneuver. The RA-3, -4, -5 spacecraft must perform a midcourse maneuver to reduce injection dispersion errors so as to place the spacecraft on a collision course with the Moon. The correction commands are computed and transmitted through the DSIF to the spacecraft, where they are stored in the CC&S, which assumes control upon transmission of the start command. After the high-gain antenna has been moved out of the way, the midcourse motor ignites and makes the proper incremental velocity corrections.

The midcourse motor is a liquid, monopropellant, helium pressure system weighing 36 lb and using hydrazine fuel. It develops 50-lb thrust over a maximum of 68 sec. The midcourse motor can increase the velocity of the spacecraft over a range of 1/10 to 144 ft/sec. Four jet vanes below the nozzle are used for attitude control during the maneuver, since the attitude control gas jet system is ineffective at that time.

Gamma-ray spectrometer experiment. A gamma-ray spectrometer is mounted on the bus in a 12-in. ball on a telescoping boom. The spectrometer measures gamma-ray radiation in cislunar and near-lunar space to determine the approximate concentration of radioactive materials on the lunar surface. The spectrometer remains in the retracted position until after completion of the midcourse maneuver, when it is extended on a 72-in. pneumatic boom so as to reduce the background count due to the proximity of the spacecraft mass.

Terminal maneuver. About 65 min before impact, a terminal maneuver places the spacecraft in position for the hard landing sequence. At 95 min before impact, pitch and yaw commands are transmitted. At 65 min, the radar altimeter antenna is deployed and the vidicon camera is energized for warmup. On signal from the radar altimeter at approximately 70,200 ft, the capsule and retro-motor separate from the spacecraft bus. The retrorocket is then ignited and the spacecraft is braked to zero velocity at not less than 1100 ft. The retrorocket and capsule are separated for the final impact. The spacecraft bus crashes into the lunar surface at 6000 mph and is destroyed.

Vidicon camera. The vidicon camera takes TV photographs of the Moon's surface at a rate of one picture each 13 sec, starting with capsule-spacecraft separation and continuing until spacecraft tumbling prevents the transmission of clear pictures.

c. Lunar capsule. *Ranger* flights RA-3, -4, and -5 are designed to carry a lunar seismographic capsule and ancillary equipments. As the spacecraft approaches the Moon, the capsule will be separated from the spacecraft and braked to allow a survivable landing which emplaces a sensitive seismometer on the lunar surface. Data from the seismometer are then relayed back to Earth receiving stations for an extended period of time.

Subsystem (Fig 17) includes following components: an altimeter for sensing the proper instant of separation;

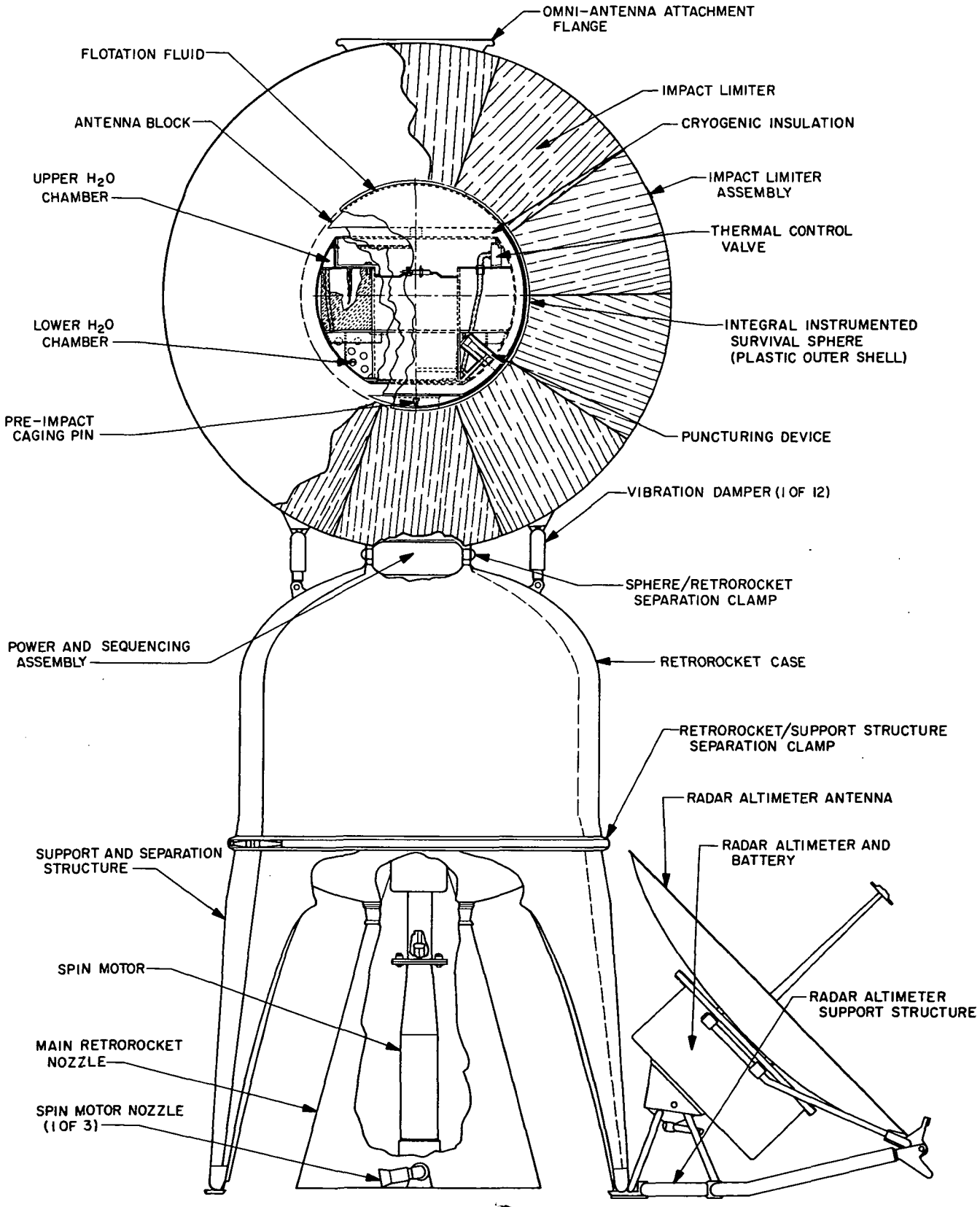

Figure 17. Lunar capsule system

a spin-rocket motor to provide stabilization during the retro-rocket braking; a retro-rocket; a crushable impact limiter to absorb residual energies; and the survival package. The survival package is a sphere which is fluid-floated inside the hollow, spherical impact limiter and will allow erection by Moon gravity to the local vertical after the assembly comes to rest.

Conventional chemical batteries are used to supply the required power. Near-constant temperature for the survival sphere equipments is provided by the use of a cryogenic insulation and a small quantity of water which cools by evaporation to the vacuum surroundings during the lunar days. The water also offers a safety feature for night operation by virtue of its latent heat of freezing.

The separation, braking, and landing are an open loop process; passive devices are used wherever feasible; and the number of independent and necessary events in the functional sequence is held to a minimum.

Contractual arrangement. Because of JPL's work load on the *Ranger* Project and the anticipated work load on future programs, it was decided to develop the lunar capsule with the aid of a subcontractor.

Fourteen prospective subcontractors were briefed on the technical requirements and were asked to submit a proposal for a 6-weeks' study of the capsule problems. The subcontractors were asked to outline the various technical problems and to state their approach to the solutions by February 15, 1960.

An 11-man JPL evaluation committee, consisting of representatives of the technical divisions and a procurement contract administrator, reviewed the proposals and on February 26, 1960, selected North American Aviation, Hughes Aircraft, and Aeronutronic Division of Ford Motor Company to carry on with the design-study program.

The study-contract final reports and program technical and cost proposals were received April 15, 1960. The evaluation committee, through a proposal scoring process, recommended Aeronutronic for the design and development of the equipment. NASA accepted this recommendation and JPL Contract N-21453, dated April 27, 1960, was issued to Aeronutronic.

System description. The following are the functional events performed by the capsule elements from pre-launch through post-landing operations:

Prior to launch and after acceptance testing, the system is assembled in a sterile manner, balanced, given a final check, and then installed on the spacecraft bus. Since bus guidance and control is the source of direction for the retro-velocity decrement, particular care is taken to ensure the following:

(1) Alignment of the separable capsule assembly itself to minimize capsule contributions to any separation errors.

(2) Weight (Table 1), center of gravity, and moment of inertia control the tolerances demanded by the bus control system.

(3) Dynamic balance of the capsule assembly to tolerances which minimize the velocity errors that could arise when the capsule subsequently is spin-stabilized and decelerated for landing.

A 1-*g* mercury position switch permits the turning on and off of the survival sphere battery during the long interval between landing-sphere closure and final assembly to the bus (approximately 4 to 5 weeks). An analysis of the thermal behavior from final assembly to landing shows that, since the insulation is ineffective prior to its evacuation on the Moon, the steady-state temperature increase will not exceed about 10°F due to the 1 w of internal power dissipation.

To accomplish both a safety-arming function and to ensure that the capsule transmitter is operating for tracking purposes during terminal maneuver, two acceleration switches are employed which close during boost at 5 ± 0.5-*g* acceleration. One is utilized in the power and sequencing assembly (P&SA) to keep the external power supply isolated from the squib circuitry. The other is located within the survival sphere to bypass the mercury switch, thus providing positive assurance that thereafter the transmitter will always be supplied power regardless of the acceleration field experienced by the sphere. These two acceleration switches are associated with integrating circuits that require a velocity increment of about 140 ft/sec before activating closure in a 5-*g* field.

During transit, the retro-motor (Fig 18) is protected by a thermal radiation shield which keeps temperature of the motor, and thus the burning distance, within limits. The design objective for the shield is an effective drop of the propellant temperature of not more than 11.5°F dur-

Table 1. Lunar capsule weights

Configuration	Weight, lb
Launch	325.7
After separation	308.8
At burnout	111.9
At impact	89.3

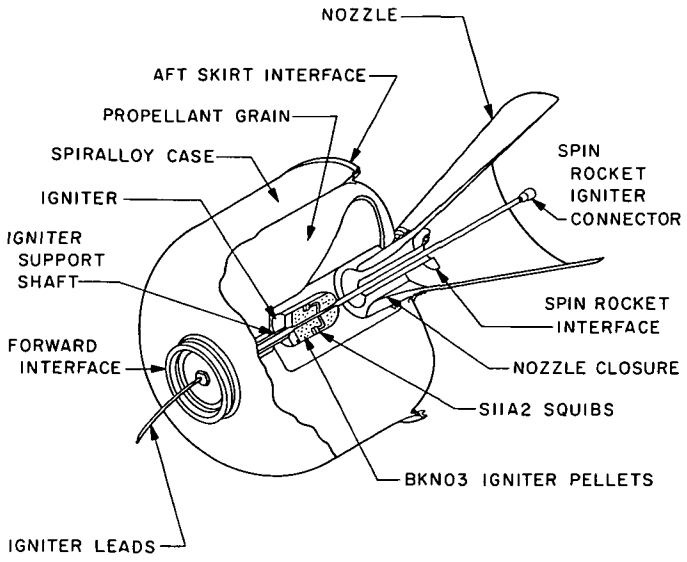

Figure 18. Retrorocket motor for RA-3, -4, -5

ing the 66-hr transit. To adjust the retro-motor initiation time to permit nominal burnout at a specific altitude (approximately 1000 ft), the temperature of the motor under this shield is measured with a thermistor. With an effective temperature drop anywhere between 4 and 19°F during the transit cooling period, and with an initial temperature (under the shield) anywhere from 57.3 to 87.3°F, the ignition timer circuitry controls the motor ignition time so that burnout occurs at the required altitude with no pre-launch adjustment.

The completion of the spacecraft terminal maneuver (Figs 19, 20, and 21) aligns the capsule-assembly roll-axis parallel to the trajectory. Upon command from the spacecraft, both bus omnidirectional antenna (on top of the landing sphere) and the capsule altimeter are deployed. The altimeter is released by either of a redundant pair of explosively actuated bolt cutters and erects to a position so that the r-f beam axis is parallel to the roll axis. This erection is such that it imposes a small net pitch impulse in order not to upset the spacecraft attitude. Once in position, the altimeter is held in place by redundant latches.

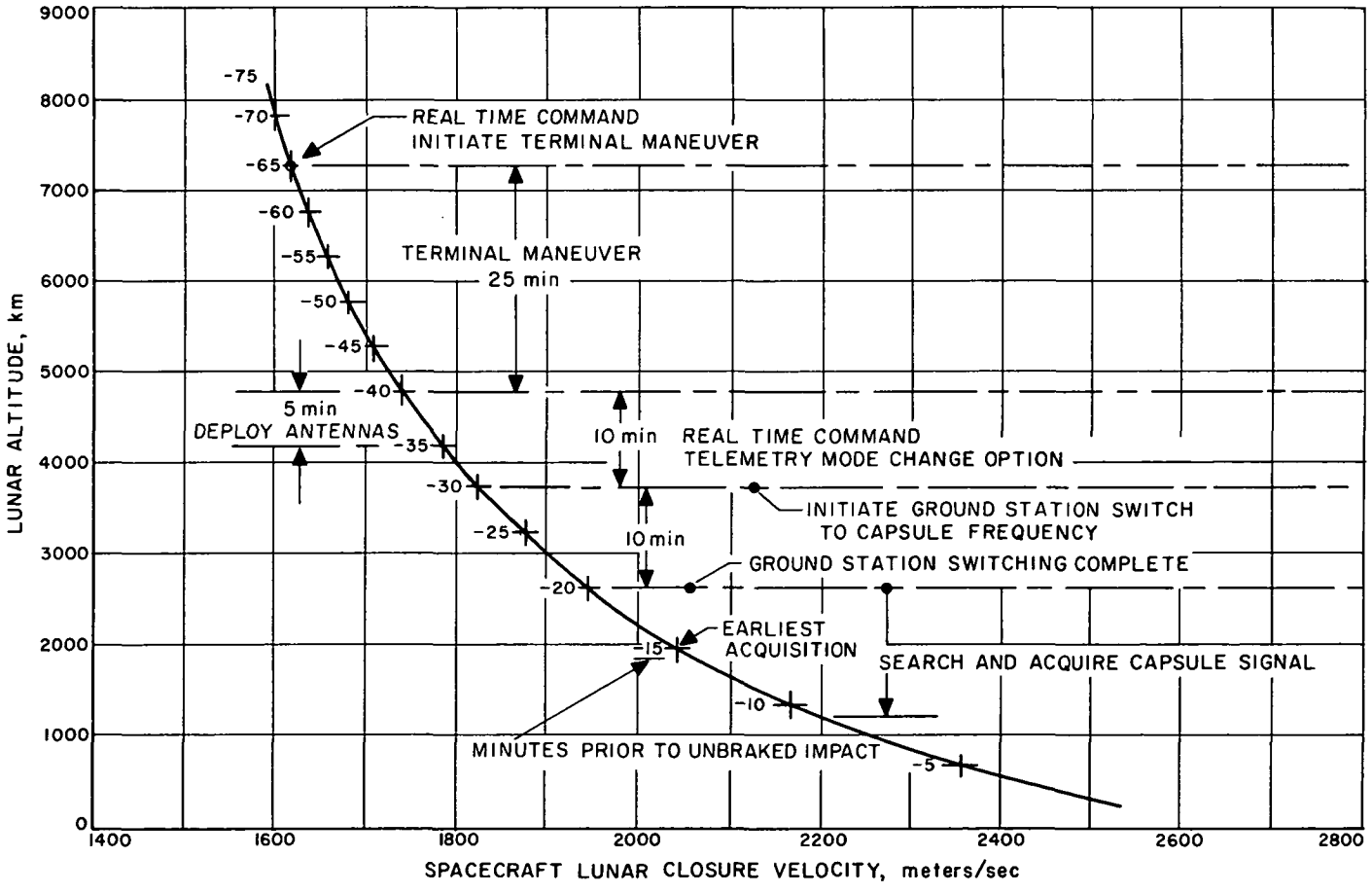

Figure 19. Impact trajectory

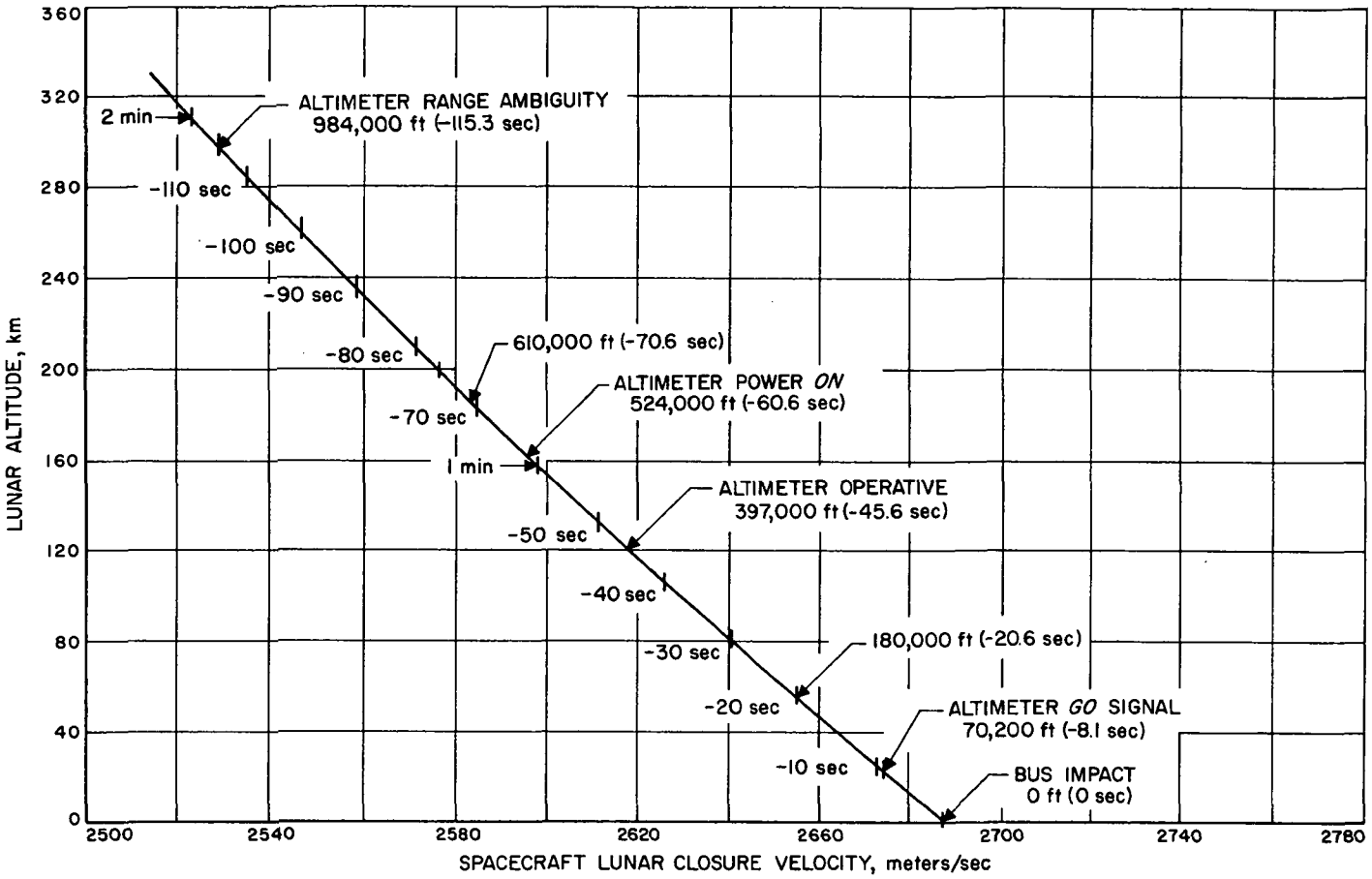

Figure 20. Terminal trajectory

At 60 sec prior to bus impact on the Moon, the spacecraft turns on the altimeter (Figs 22 and 23), using spacecraft power to actuate a thermal switch in the altimeter (Fig. 24). The altimeter has a warm-up time of 15 sec. It fuzes when the spacecraft reaches an altitude of approximately 70,000 ft. At this altitude, the altimeter closes a relay which connects bus power to accomplish (1) lower-clamp (primary) separation of the capsule from the support structure by firing four redundant bolt cutters, and (2) initiation of the power and sequencing assembly in the capsule itself by firing two parallel squib switches.

The power and sequencing assembly (Fig 25), in addition to providing power for all subsequent functional events prior to landing, contains three electrical timers, all three of which are initiated at the fuzing event. The first of these (spin-motor timer) provides a delay of 130 ± 20 msec to ensure release of the separation clamp prior to spin-motor initiation. The spin-motor initiation delay is always greater than 15 msec and the maximum clamp opening time does not exceed 125 msec. Hence, at the extreme, spin-motor ignition always occurs after clamp opening. Physical separation of the capsule from the support structure is accomplished by the axial component of impulse delivered from canted spin-motor nozzles (approximately 20 lb-sec). This impulse produces a velocity increment of approximately 2 ft/sec. The torque component of the impulse produces a minimum spin of 300 rpm. The spin-motor burning time does not exceed 1.3 sec.

The second P&SA timer accomplishes the firing of the retro-motor. The nominal delay of this circuit is 2 sec, but in flight the delay is automatically varied over the increment 1.7 to 2.3 sec, depending on the measured temperature of the retro-motor. The retro-motor burns for approximately 10 sec with the nominal burnout altitude occurring at 1000 ft.

The third P&SA timer fires two bolt cutters on the separation clamp between the landing sphere and the

retro-motor. This event occurs 13.0 ±0.5 sec after P&SA initiation.

The survival sphere is completely enclosed by the impact limiter (Fig 17) and no circuits pass through the fluid space. Hence, to activate the sphere functions, an integrating inertia switch (20 g for 1 sec) is closed by acceleration from the retro-motor thrust. This switch immediately closes the power circuit once more, causes pre-impact uncaging to occur, and initiates an internal sequence timer for the following post-impact events:

(1) A 15-min delay after initiation accomplishes post-impact caging.

(2) A 16-min delay after initiation accomplishes sphere venting by firing the two penetrator squibs. The penetrators pierce the shells and the impact limiter which releases the survival sphere flotation fluid to Moon vacuum. This release also vents the seismometer caging fluid, opens the vent line for the boil-off valve, and exposes the insulation to lunar vacuum.

(3) A 30-min delay after initiation turns on the seismometer centering motor and turns off power to the sequence timer itself.

After the seismometer is uncaged and centered, any motion of its pendulum provides the signal that modulates the transmitter (Fig 26). The carrier center frequency and the subcarrier center frequency are slightly temperature sensitive. Therefore, in addition to the primary seismic data, the thermal performance of the survival sphere in the lunar environment is also read out at the receiving sites of the Deep Space Instrumentation Facility (DSIF).

Dispersion analyses. Dispersion analyses completed to early 1961 were based entirely on the normal (along lunar vertical) approach trajectory and rigid body motion of the capsule. The effect of these differences did not seem significant, but it was included in the analyses.

Component and subsystem contributions to burnout altitude and velocity dispersions are summarized in Table

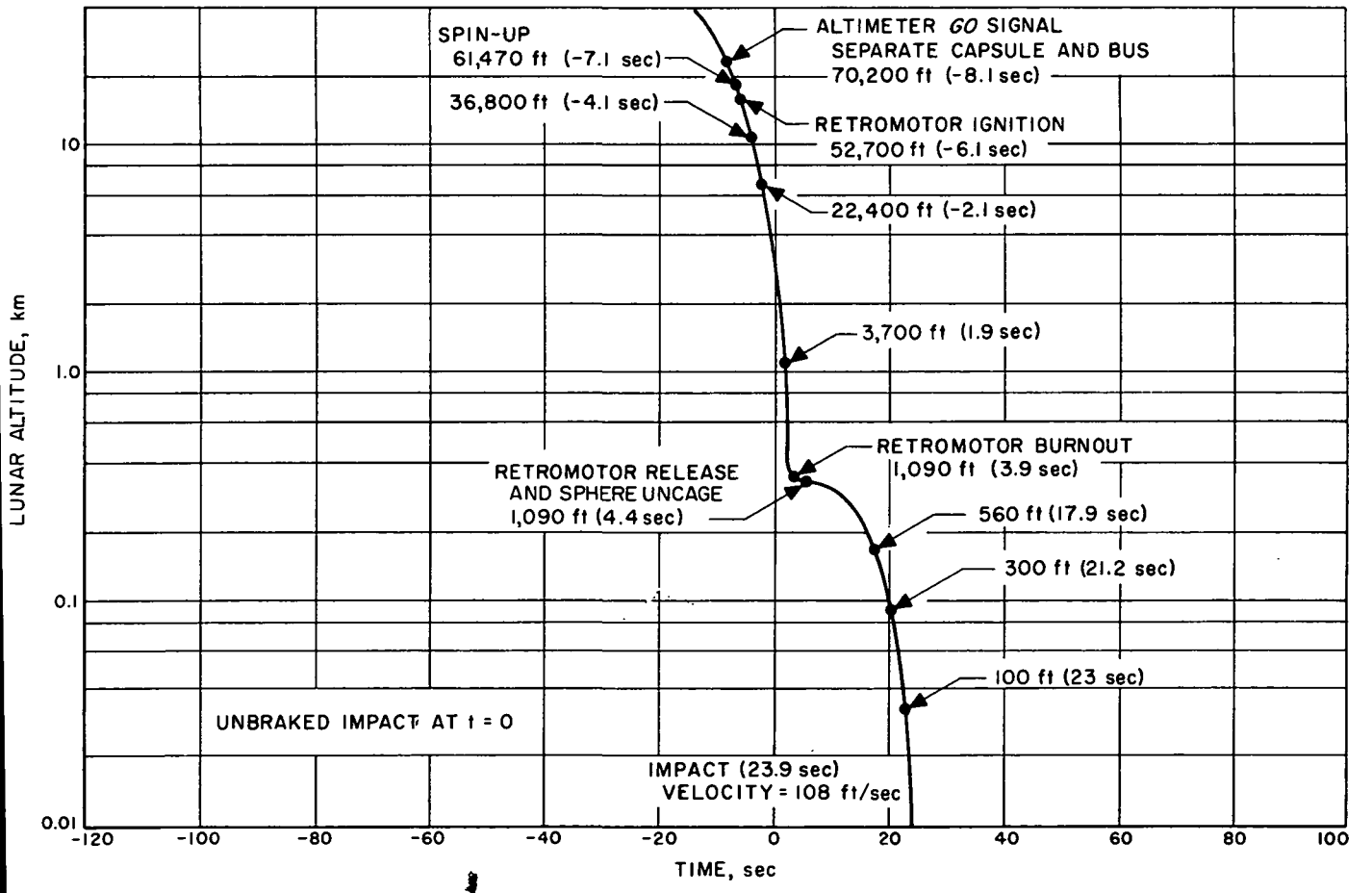

Figure 21. Final trajectory

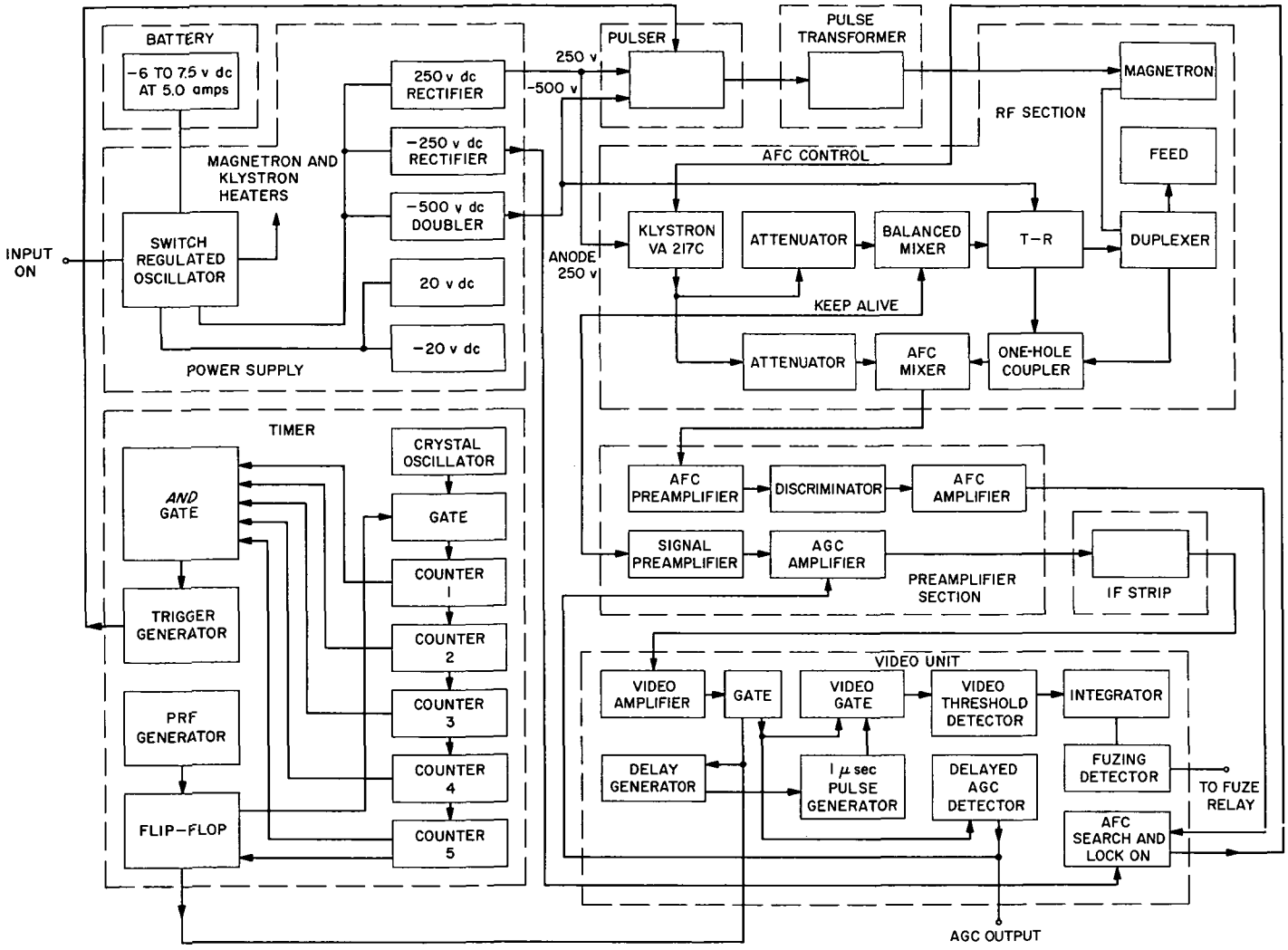

Figure 22. Altimeter block diagram

2. Two values of uncertainty in motor burning time were used in estimating the dispersion in burnout altitude. The lower value corresponds to a rms deviation of motor burning time of 0.22%. This is believed to be the probable lower limit for this error and gives an error of 125 ft (1 sigma) in burnout altitude. The higher value corresponds to an rms deviation of motor burning time of 0.66% and gives an error of 375 ft (1 sigma) in burnout altitude.

Dispersion analysis to evaluate the parametric influence of motor burn time errors on the impact velocity and, more generally, to determine the relative significance of other possible contributions to burnout altitude errors were completed for both cases (Fig 27).

A study was also completed to determine the effects of elastic bending of the capsule on the burnout dispersion. Results show that the bending and spin frequencies are well separated (by about a factor of 4) and that the effect of bending of the present configuration in burnout dispersion is not significant. This conclusion is subject to review when the final experimental data are available. However, component data obtained on both rigidity and damping have provided experimental values to the analysis which are probably representative.

The distance traveled during the retromotor burning must be accurately predicted to obtain a tolerable vertical component of the lunar impact velocity. One of the limiting factors of this prediction is the temperature of the motor grain at the time of motor ignition. An analog determination for the appropriate placement of the temperature sensor was completed. To check these results and to obtain quantitative information for flight adjustments, a

Table 2. Lunar capsule rigid body dispersions vertical approach

Source	Sigma values at burnout		
	Transverse velocity,[a] ft/sec	Axial velocity, ft/sec	Altitude, ft
Spacecraft trajectory and attitude	51	20	-220
Altimeter variances	—	—	130
Stage separation tip-off	32	—	—
Spin motor variances	26	—	—
Static imbalance	26	—	—
Retro-motor variations	25	13	125 (375)[b]
Motor temperature uncertainty	—	—	179
rms	74.5	23.8	336 (488)[b]

[a]Velocity dispersion occurs in each of two orthogonal directions.
[b]Numbers in parentheses represent conservative estimate of variance of retro-motor burning time.

thermal-vacuum simulation of the transit phase with an inert motor and thermal shield was planned.

During summer 1961, several changes occurred in the input conditions and statistical parameters describing position and velocity at retromotor burnout. Of greatest potential significance was the change to non-normal approach trajectory. Several 1000-sample Monte Carlo analyses (Fig 28) were performed to assess the effect of the non-normal approach and, additionally, to include the effects of the corresponding increase in altimeter fuzing altitude variance. The off-normal approach simulation required a minor computer program change, and an additional change in the program was made to obtain specific printout of information on those impacts which occurred before retromoter burnout.

Based upon current trajectory planning, a median off-normal approach of 10.1 deg was used. In addition to propagating a component of the roll-axis position and velocity errors into the horizontal velocity component, geometrical effects add an independent statistical altimeter measurement error variance of 50 ft. All other error sources remain the same relative to the nominal roll axis except that the altimeter instrument error used in the

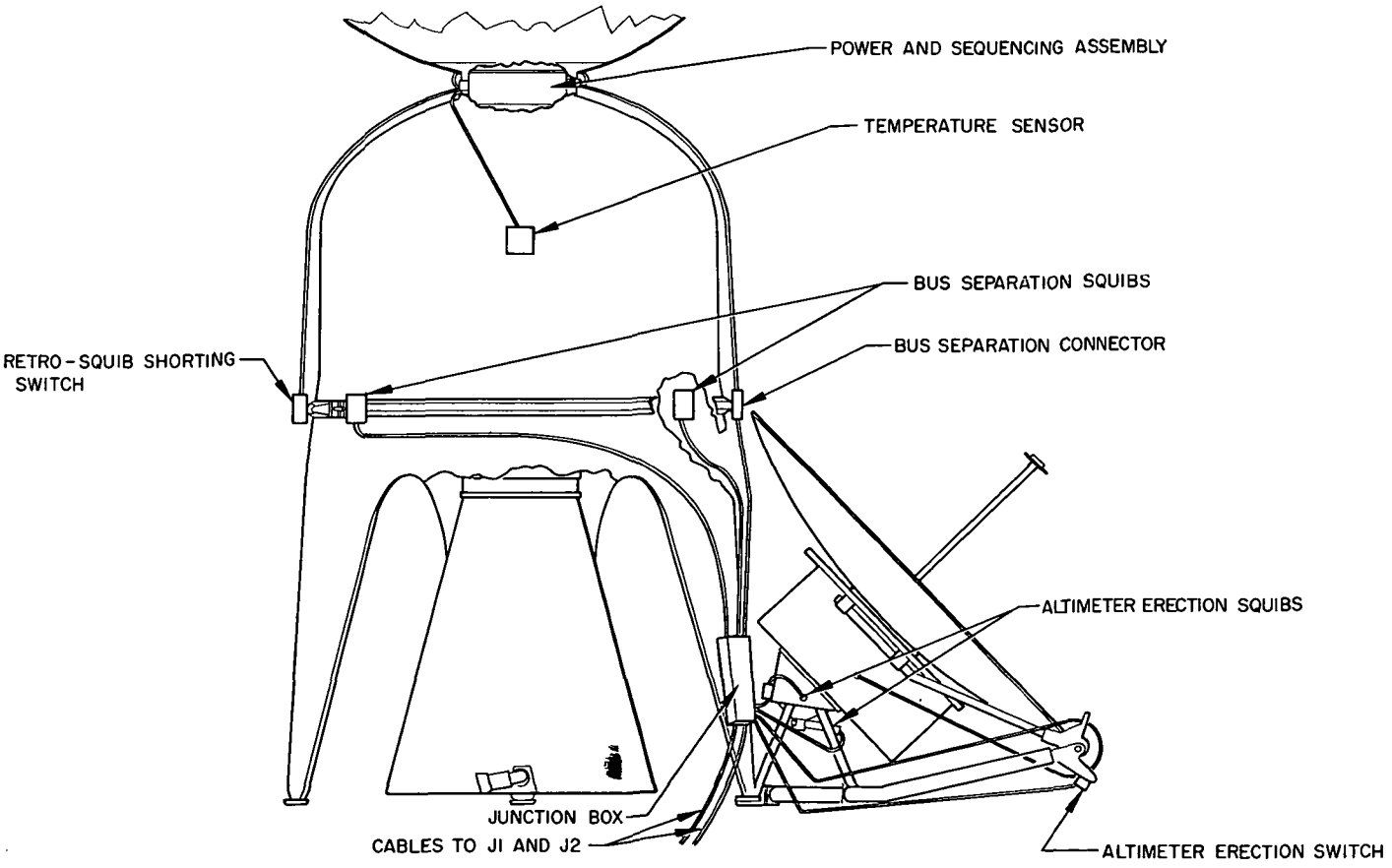

Figure 23. Timing, control, and ignition component location

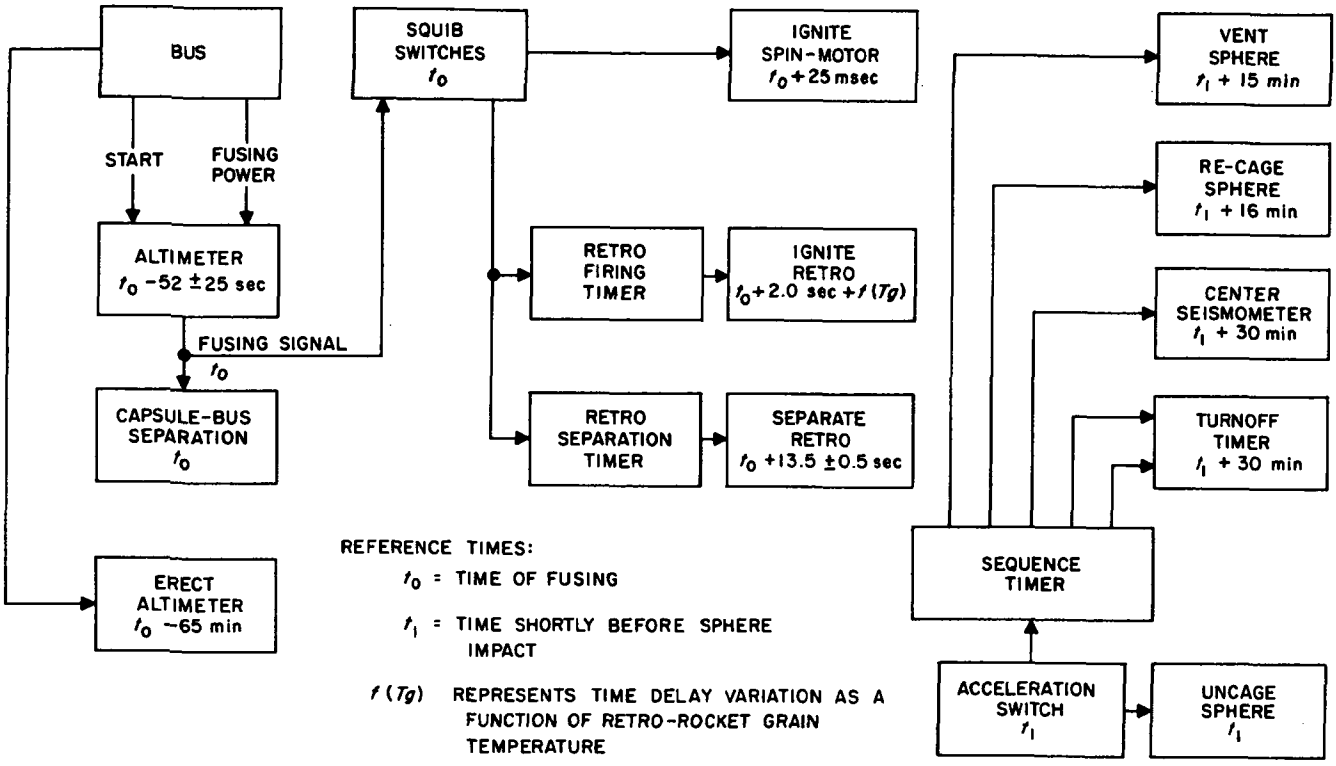

Figure 24. Lunar capsule timing, control, and ignition system

study was 165 ft vs 130 ft used in earlier studies to account for improved knowledge of the altimeter performance.

The results of these analyses showed that there was a negligible change in the statistical parameters at impact. The off-normal approach, considered independently, changed the mean impact angle by less than 1 deg. The increased altimeter variance (considered independently) increased the mean value of the vertical component of impact velocity by about 2% and the mean total impact velocity by about 1%. The mean impact angle steepened by 1 deg.

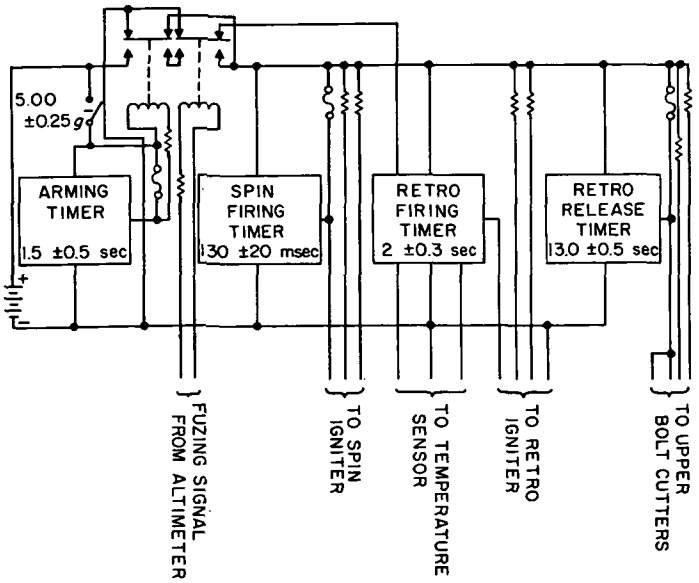

Figure 25. P&SA block diagram

Additional Monte Carlo simulations were performed using lower nominal burnout altitudes, thus examining the tradeoff between increased impact-before-burnout probability, and the corresponding lowering of the mean vertical impact velocity. Up to these studies, a value of 0.5% probability of impact before burnout had been chosen arbitrarily. Computer runs covering 5 and 10% premature impact probability were made using a modified Monte Carlo program which printed out the individual impact characteristics (negative burnout altitude, burnout velocity). These cases were modified by the actual motor thrust time curve near burnout to determine actual impact velocity and the sliver content that would remain.

The choice of a 5% likelihood of premature impact lowered the mean total impact velocity by 15%, and the mean impact energy by 20%, which appeared to be worthwhile reductions. But even correcting for the thrust decay in the last 0.4 sec of powered flight, the velocity-position profile has such a severe slope that 80% of the impacts

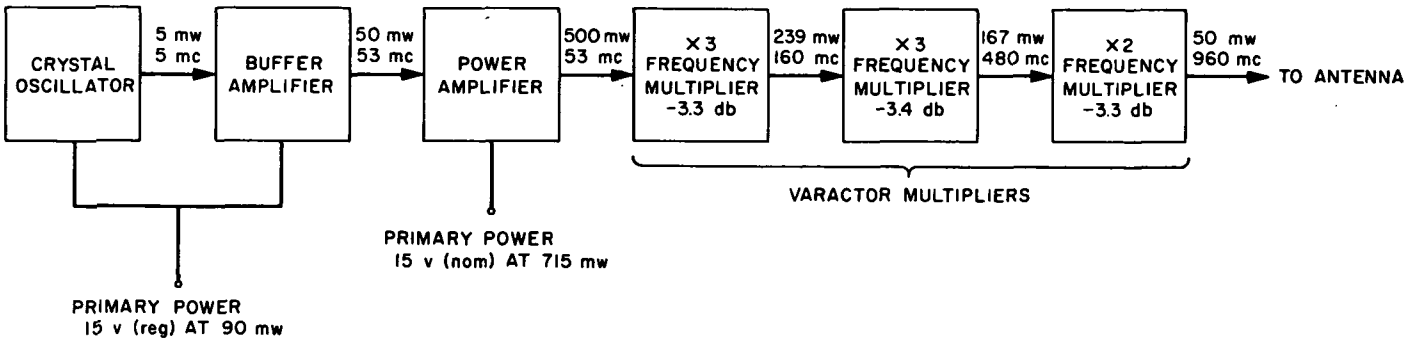

Figure 26. Transmitter block diagram

SOURCE	RMS VALUES AT BURNOUT		
	TRANSVERSE VELOCITY, ft/sec	AXIAL VELOCITY, ft/sec	ALTITUDE, ft
ALIGNMENT ERRORS	11	–	–
ALTIMETER	–	–	78
SEPARATION TIP-OFF	11	–	–
SPIN MOTOR	30(54)	0.2	2
SEQUENCE TIMER	–	–	73
RETROMOTOR	33(40)	16.2	253

Figure 27. Lunar capsule subsystem dispersions

before burnout would be fatal due to high-velocity impact. Thus, only a small downward revision of nominal burnout altitude will be possible or desirable.

Development chronology. The February 1960 study proposal by Aeronutronic Division of Ford Motor Company (AD/F) contained a concept of how a capsule could be designed to meet the lunar landing objectives of the *Ranger* Project. The ensuing study sought other ways to accomplish these objectives, analyzed in considerable detail the selected system arrangement, and produced plans and cost estimates for developing and providing flight capsules. It was found that in fact, the original concept was the best of many investigated, and remains basically unchanged. The study report and the development plan demonstrated to JPL the feasibility of accomplishing the objectives desired. At that time, the aspects that seemed to be the most difficult to achieve were: (1) meeting the delivery schedule, which called for two flight capsules in early May 1961; (2) staying within the 300-lb weight allocation, and (3) providing 90 days of lunar operation.

In June 1960, JPL notified Aeronutronic that delays in the booster vehicle program required slipping the September 1961 flight date to late January 1962. At about the same time, the Laboratory concluded that Aeronutronic should develop the amplifiers and related ground equipments needed to integrate the seismometer into the capsule. Originally, it had been planned that JPL would supply both the amplifier final design and the flight seismometers.

Aeronutronic prepared cost estimates for not only the amplifier and ground adapters, but also a product improvement effort to make modest use of the additional time made available by the flight date change. Included with the product-improvement proposal was a recommendation for parallel and competitive subcontracts for altimeter and retro-rocket development. The plan was to carry these developments up to a point where a choice could be made between the two competing designs. Then only one subcontract for each flight item would be let. This approach was apparently a good way to intensify the subcontractor's efforts, and to provide extra assurance of high-quality products.

The Laboratory accepted Ford's basic proposals and increased the estimated contract amount. However, the parallel subcontract options were not accepted on the assumption that subcontractor hardware would be available for early design proof demonstration tests. It was reasoned that sufficient time was available to institute if necessary, at a later date, new subcontracts for alternate designs which could also be proof-tested and still not endanger the flight date.

During these early phases of the program, JPL indicated to Aeronutronic that funding was tight and that prime emphasis should be placed upon producing a flyable capsule within the allocated funds. Each major subcontractor was instructed to organize his efforts to reduce costs.

In summer 1960, subcontracts were let to Hercules Powder Company for the retro-motor, and to Ryan Aero-

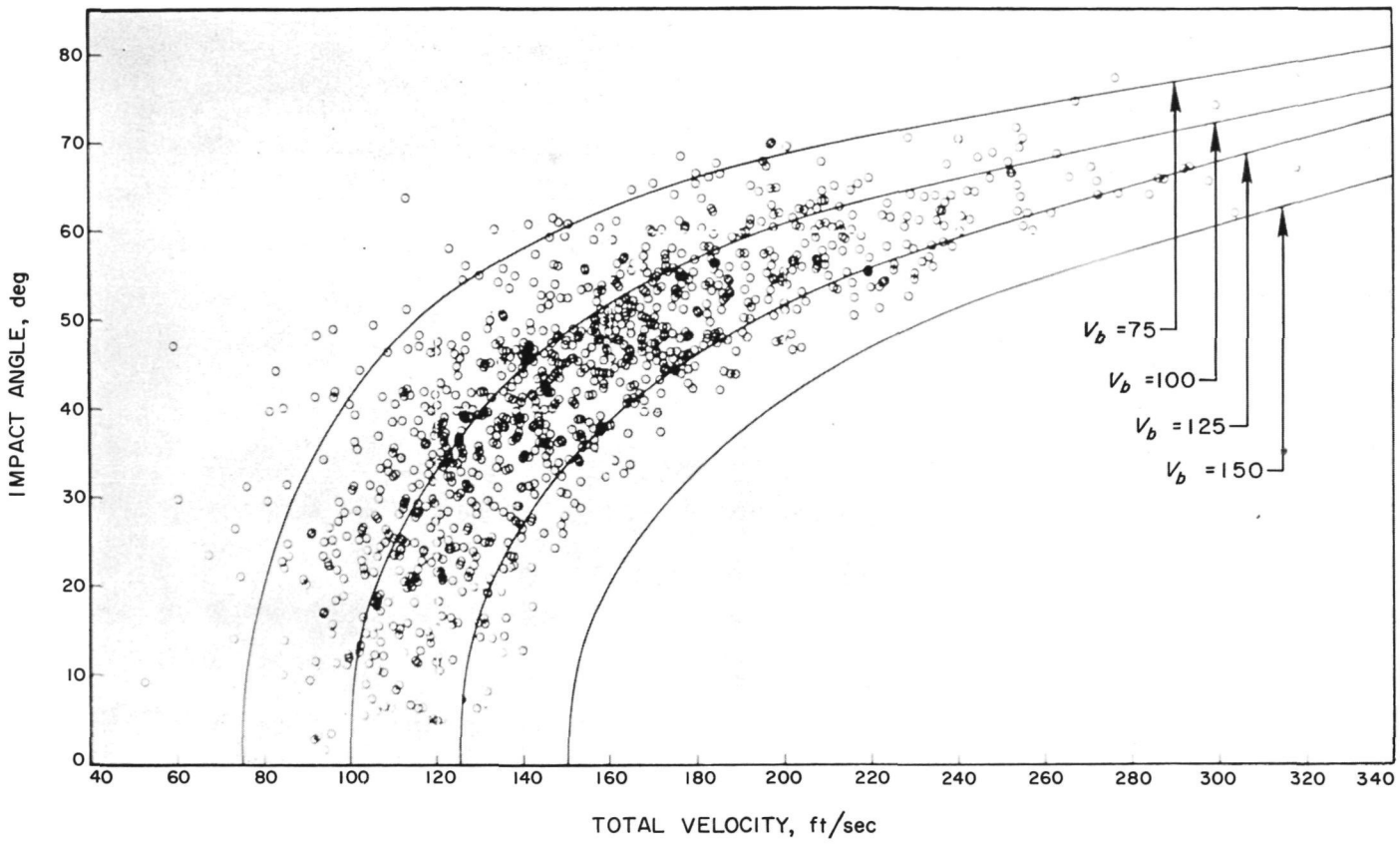

Figure 28. Scatter diagram—1000-point Monte-Carlo impact angle vs total velocity

nautics Company, Electronics Division, for the altimeter. Hercules began work on August 1, 1960, at its Bacchus, Utah, facility.

In March 1961, it was clear that the Ryan subcontract would not result in an adequate altimeter at an early enough time, and a parallel altimeter program was recommended. The Laboratory approved this addition, and work was undertaken by Wiley Electronics Company, of Phoenix, Arizona. During this period, a substantial amount of design effort was accomplished. However, early test program efforts were minimized and great reliance was placed on accomplishing systems tests to be finished just prior to and as a part of the simulated lunar landing tests programmed for April 1961.

In retrospect, the austerity phase seriously affected the eventual results of the program. The development testing should have been more comprehensive than that accomplished by April. The *Ranger* subcontract coincided with the award to Hercules of new major contracts at Bacchus, and the capsule effort was not staffed as well or regarded as urgentlv as it should have been.

The spheres for the simulated lunar landing tests in May 1961 were actually completed, but in April the inadequacy of the development test background raised a number of questions. Hercules was also scheduled for qualification tests of the retro-rocket in May, but by early April the development firings were still incomplete. At this point, the Laboratory asked AD/F to submit a proposal to cover the increased costs associated with the Ryan, Wiley, and Hercules subcontracts and any anticipated Ford overrun. AD/F suggested that late May would be a better time for such a proposal because Hercules had many development firings scheduled in that period, and by then the results of the AD/F simulated landing tests would be known. However, JPL required the figure immediately, so the April 17, 1961, request for additional funding was submitted, using optimistic assumptions about the outcome of both the Hercules tests and the simulated lunar landings. In May 1961, a moderately successful simulation of a lunar landing was conducted.

The expenditures through May were close to the original proposal figure although the rocket motor design at

that time was not yet flyable. The Wiley altimeter subcontract produced a crude, but flyable altimeter at the end of May.

In May and June 1961, the high technical risk inherent in the austere method by which the program had been conducted produced clearly unfavorable results. The Hercules motor developed intermittent failures that forced a long postponement of the qualification tests. The simulated lunar landing, while moderately successful, demonstrated that the survival sphere design was potentially unreliable in certain areas and that the assembly procedures required by that design presented much opportunity for problems in construction.

During July 1961, a careful analysis of the entire capsule system was made by AD/F. While the simulated lunar landing payload could probably have been sent to the Moon with a moderate chance of success, there were enough aspects unproven so that nearly every subsystem element needed further testing to give JPL and ADF the confidence necessary to commit the capsule to flight. The batteries, the cryogenic insulation, the ordnance devices, the electronics and sub-elements thereof, the impact limiter, the spin motor, and the altimeter support structure all required additional design effort and additional development test. If this testing were to be complete in time to provide useful data for the flight units, this work had to be accomplished before the end of October 1961.

Accordingly, a series of test programs using a larger number of test vehicles seemed the appropriate way to achieve the desired standard of mission success. The Hercules subcontract effort was drastically expanded, with additional AD/F assistance provided at Bacchus and increased emphasis at Ford. An intensive development effort was directed at repeating the simulated landing tests in September, with a markedly improved over-all design for the survival sphere. Ford obtained more and better engineering support from Hercules. Because additional motor troubles developed, it was necessary to place several additional AD/F engineers in residence at Bacchus. Simultaneously, AD/F began to meet the many development test deadlines necessary to precede the September demonstrations. No excuse was acceptable for failure to meet these deadlines. If there was any doubt about the chances for intermediate success, parallel efforts were begun at once. Every effort was expended to produce the best attainable assurance of success.

Fabrication of flight articles was scheduled to begin during late October with completion scheduled for early January 1962. To accomplish this schedule, an accelerated and increased test program was necessitated, resulting in a high rate of expenditure, trebling the rate at Hercules and doubling the rate at Aeronutronic. The financial reports clearly indicated from July forward this rapid increase in the rate of expenditures.

One other confidence-disturbing matter also occurred in July and August. Two capsule components (the main battery and the voltage-controlled oscillator) long-since qualified for flight and impact, suddenly developed failures. These failures occurred during development tests for which these components were merely necessary ancillaries. A significant additional effort was required to obtain and qualify proper components in time. As a result, the September tests were not accomplished until mid-October.

In November 1961, funding adjustments were made, resulting from a Hercules subcontract overrun and increased costs at AD/F in such activities as product qualification, electronics, fabrication and inspection, environmental testing, and research. The Hercules effort suffered from being a small element in a large facility at a time when that facility was expanding rapidly. "Garden variety" technical problems which should have been recognized and solved early in the program were allowed to drift despite AD/F surveillance until quite late. The solving of such problems, while not technically difficult, needed quick attention and considerable AD/F and JPL prompting was required to assure attention to the *Ranger* engine program.

With reference to the technical status of the capsule system development, every grave doubt that existed early in August had been resolved by November 30, 1961. The program had a rocket motor design, tested almost as successfully as any motor is tested before qualification firing in the Arnold Engineering and Development Center facility. The altimeter was fully qualified and needed only to be reproduced for flight. A new lot of VCO's was qualified, and several successful impact and capacity tests with the improved capsule battery had been conducted. Three of four demonstration impacts of landing spheres had been conducted. In every case, from the reference of the flight articles under construction, there was no evidence from these major tests that the flight capsule would not make a successful landing and communicate useful data back to Earth. The capsule development tests are reviewed in Table 3.

During the period November to January, the capsule program culminated in fabrication, testing, and delivery

Table 3. Lunar landing sphere test performance chart

Test vehicles	Functional equipment										
	Uncage and cage	Erection	Venting	Seismometer and amplifier	Control electronics	Transmitter and VCO	Antenna and feed	Battery	Thermal control and insulation	Impact limiter	Structure elements
DPT-1	Test wiring did not permit caging system to operate. OK in subsystem test	5 deg	No test. Penetrators fired in lab prior to test	OK (preliminary design)	OK	Preliminary design partial success	Coax broken	OK	Preliminary design no thermal data	Airplane drop 20-deg angle, 200 ft/sec. Good limiter	Good test of preliminary design
DPT-2	Preliminary design used	11 deg	System worked. Design changed to give bigger holes	—	OK	—	Antenna structure OK	One-half OK, other half poor before assembly	Preliminary design no thermal data	Airplane drop 45-deg angle, 200 ft/sec. Good limiter	Good test of preliminary design
ITV-1	—	—	—	—	—	—	—	—	Development models of insulation, fair thermally, poor structurally	No limiter, sled test, 154 ft/sec	—
ITV-2	—	—	—	—	—	—	—	—	Development models of insulation, fair thermally, poor structurally	No limiter, sled test, 138 ft/sec	—
ITV-3	—	—	—	—	—	—	—	—	Failed, insulation shifted in shell	No limiter, sled test, 136 ft/sec	Insulation shell cracked
ITV-4	—	—	—	—	—	—	—	—	Heat loss of 2.3 w	No limiter, sled test, 120 ft/sec	Insulation shell cracked
BOV-1	—	—	—	Seismometer operated with thermal valve. OK	—	—	—	—	Water boiloff system good	No test	—
ETV-1	—	—	—	Two diodes failed probably due to procedural failures	OK	VCO failed. Two capacitors failed mechanically	Coax broken but antenna OK	Electrolyte leak	—	No limiter, sled test, 179 ft/sec	Severe test in sled. Insulation shell cracked
OTV-1	OK	Failed due to antenna structure failure allowed fluid in top	Venting occurred but one blast shield malfunctioned	—	Battery lead unsoldered. Broken resistor	—	Shells failed	Only ½ battery tested. OK	Minor structural problems	Normal impact 168 ft/sec. Good limiter	Impacted on top, both shells broke, cover bent, structural sound valve seal leaked

CONFIDENTIAL

Table 3. Lunar landing sphere test performance chart (cont'd)

Test vehicles	Functional equipment										
	Uncage and cage	Erection	Venting	Seismometer and amplifier	Control electronics	Transmitter and VCO	Antenna and feed	Battery	Thermal control and insulation	Impact limiter	Structure elements
OTV-2	OK	7 deg after drying from leak due to antenna structure failure	—	—	Resistor immersed in fluid	—	Coax failed, antenna redesigned to include rubber cover	Only ½ battery tested. OK	Minor structural problems	45-deg impact, 187 ft/sec. Good limiter	Insulation shell broke at ground plane. New outer shell OK
BTV-2	—	—	—	—	—	VCO test only, OK	—	½ battery failed after discharge (7 days)	—	Normal impact, 174 ft/sec. Good limiter	New shell design good. Valve seal OK
DPT-3	OK	9 deg	System OK. One penetrator failed (not from qualified lot)	OK	OK	Capacitor broke loose	OK	Diodes separated. Parallel halves were bad	Insulation good structure but no thermal data	Airplane drop 32-deg angle, 220 ft/sec. Good limiter	All structural elements sound
DPT-4	—	—	OK	Mating technique test only, OK	Capacitor leakage	—	OK (no RF test)	Failed	Heat rate slightly high after impact and immersion	Normal impact, 166 ft/sec. Good limiter	Leaking brazed joint after impact and venting
DPT-5[a]	OK	OK	OK	OK	OK	—	—	Failed. Six v section had a short but sufficient power after impact to conduct test	Good insulation prior to impact. Little loss in perforation after impact	—	—

[a]Flight configuration.

of flight hardware to AMR. This hardware was used in support of the January 1962 launch of *Ranger III*.

d. RA-6 through -9 spacecraft design. For the RA-6 through -9 missions, the basic RA-3, -4, -5 type bus will be used to carry an RCA high-resolution TV package instead of the ADF capsule subsystem. The RA-3, -4, -5 type high-gain antenna will be replaced by a *Mariner R* type, which incorporates circular polarization.

Auxiliary science experiments have been tentatively chosen and the instruments will be mounted on the bus. At present, the experiments are: (1) ion chamber, (2) vertical flux detector, (3) cosmic dust experiment, (4) search coil magnetometer, (5) low-energy ions experiment, (6) electron flux experiment, (7) electron–proton spectrometer, and (8) low-energy solar proton experiment. Only the ion chamber and TV package will be flown on RA-6. All of the experiments will be on RA-7, -8, and -9. A data automation system will be used on RA-7, -8, and -9; RA-6 will have a wave shaper for this function.

The following bus subsystems require minor changes to accommodate the new mission: attitude control, CC&S, power, command, and midcourse propulsion. The data encoder will require slight modification, as will the squib firing assembly. Re-design will be required on the ring harness, the squib harness, and some of the case harnesses.

An S-band communications ranging experiment is planned for the RA-8 and -9 missions. This experiment will require a high-gain antenna capable of L-band, with circular polarization and S-band capability. The antenna can apparently be provided without introducing any untenable transients into the spacecraft design. In order to maintain a constant cg and moment-of-inertia design, it may be necessary to carry ballast on RA-6 and -7 to compensate for the ranging experiment to be added on later flights.

The RCA vidicon tower–spacecraft interface is being kept as clean as possible. The RCA "passenger" is relatively self-contained. Operating at full power only during the last 10 min of the mission, it contains its own transmitters, power sources, sequencer, and telemetry, as well as six high-resolution vidicon cameras. A directional coupler must be installed on the bus to allow the RCA transmitters to feed the high-gain antenna on the bus. During cislunar cruise, RCA telemetry will be fed through the bus communication system. A real-time ground-originated command will be used to turn on the experiment during terminal maneuver. The missions will be operated similarly to those on the RA-3, -4, -5 program, with midcourse trajectory correction and terminal positioning. The RA-6 through -9 missions will not orient the spacecraft's roll axis with the velocity vector in terminal maneuver, but instead will orient the camera cluster axis with the velocity vector. The camera axis is 38 deg out from the $+z$ axis of the spacecraft in the roll–yaw plane and in the $+y$ direction, i.e., directly opposite the high-gain antenna.

The science experiments output telemetry will be handled through a data automation system that will have a common output to the spacecraft data encoder. Power will be furnished by the RA-3, -4, -5 design science inverter and by a new science T/R unit. All major design problems have been recognized and solutions are underway. The data automation system will be housed with the ranging experiment in Case III. Although the ranging experiment will not be added until RA-8 and -9, ballast modules will be used on preceding flights.

e. RCA TV subsystem. In support of the manned lunar program, one of the required missions is a high-resolution TV experiment to be incorporated early in the *Ranger* Project. Accordingly, a contract was initiated with RCA to provide a primary experiment TV subsystem to mate with the JPL-produced bus—this bus to be essentially unchanged from the seismometer capsule series. RA-6 through -9 were selected for the high-resolution TV mission.

The primary objective of an advanced *Ranger* mission will be to obtain high-quality pictures of the lunar surface at a resolution that is sufficiently high to enable an evaluation of the nature of the detailed surface features. Data obtained from these pictures can then be used to improve understanding of origin and composition of the lunar surface, and to determine the effects of the surface on lunar landing vehicle requirements.

System description. In order to accomplish this primary mission within the constraints of the existing *Ranger* spacecraft system and supporting facilities, a TV payload is to be developed that will be fully compatible with the present spacecraft mechanical, thermal, and electrical interface requirements. The major elements of *Ranger* TV payload will consist of optics, television cameras, control sequencers, telemetry, and transmitters needed to acquire and transform the energy reflected from the lunar scene into a video signal for transmission to Earth. This equipment will be combined with a spaceframe and a passive thermal control design to form a fully integrated payload that is dependent upon the spacecraft only for the receipt of instructions through the command receiver,

transmission of the video signal over the high-gain antenna, and stabilization. The TV subsystem will remain structurally attached to the spacecraft throughout the entire mission and will impact on the lunar surface with the spacecraft at conclusion of the mission.

The TV payload will be supported on the ground by special equipment at the Goldstone (Calif.) DSIF Station, which will be used to receive, store, and reconstitute the TV data transmitted from the TV payload. Additional ground support equipment will be required at JPL, Cape Canaveral, and RCA.

Design. For reasons of mechanical simplicity, it is desirable to use a fixed focal length optical system with the television cameras. With such a system, it is possible to trade area coverage for resolution as the payload approaches the Moon. In light of environmental requirements for the payload, weight constraints, and problems of packaging and mechanical integration, it is desirable to employ the shortest focal length, dioptric lens system consistent with mission resolution goal. Moreover, high-speed optics are used to minimize the effects of uncompensated image motion by shortening the television camera exposure time.

The spacecraft TV subsystem functional block diagram is shown in Figure 29. The subsystem consists of six slow-scan vidicon cameras, a control programmer and camera sequencer, a telemetry system, a two-channel transmitting system, and a battery power supply with associated voltage regulators. The camera parameters and the system interconnections reflect the system design goals of (1) obtaining a high-quality television picture of the lunar surface at a resolution of about 0.2 m per optical line pair; (2) obtaining reasonable nesting of a sequence of television pictures, starting from a resolution of approximately 350 m per line pair; and (3) obtaining wide area coverage of the lunar surface. Another desirable goal achieved by the system design is to obtain a color image of the lunar surface.

The communication system is designed to make optimum use of a 2-mc bandwidth allocation centered at 960.05 mc, within which a channel allocation of 80 kc centered at 960.05 mc is required for the JPL beacon transmitter.

The first design goal, that of obtaining high-resolution pictures, is achieved by a system of four television cameras operating at a frame rate of 5 cps, and having a usable resolution of 35 optical line pairs per mm. The cameras are exposed sequentially and while one camera is being read out, the remaining three are being erased and prepared for the next sequence of exposures. At the impacting velocity of 2700 m/sec, and with a proposed 76-mm camera lens, the system has good probability of obtaining a full television picture at a resolution of 0.2 m per line pair. The last sequence of four pictures will have resolutions varying from 0.8 to 0.2 m per line pair and will include a 16-to-1 variation in area coverage. Cameras 1 through 4, the partially scanned cameras (Type P), provide these last four television pictures, which are scanned out and transmitted in real time, within an r-f bandwidth of about 1 mc. Cameras 1 through 4 are permanently connected to Transmitter 2.

The design goal for the nesting feature is to obtain a final set of pictures which can be located on present lunar maps. The initial pictures will be taken at 10 min from impact at an altitude of about 1300 km. Their resolution will be of the order of 350 m per line pair and will enable the photo interpreters to locate these images on the available lunar maps. Each subsequent set will increase the resolution and will permit location by reference to the previous set. This technique of picture location will proceed to the final set, where the highest resolution television pictures will then be located, permitting a more meaningful interpretation to be made of these images. Two fully scanned cameras on the mission have a frame time of 2.56 sec, and the same line density as the partially scanned cameras. Using the proposed 76-mm lens, they can account for a larger area coverage of 16-to-1 over that of the partially scanned cameras. Thus, both nesting and wide area coverage are achieved with this arrangement.

The arrangement of the fields of view of Cameras 1 through 4 and of Cameras A and B is shown in Figure 30. These overlapping fields ensure that the four partially scanned cameras are centered on the velocity vector. Cameras A and B (type F) are alternately scanned and erased, and their real-time readout is contained in the 1-mc r-f bandwidth of Transmitter 1.

The telemetry subsystem consists of cruise-mode telemetry elements as well as more detailed diagnostic telemetry elements for the terminal phase of the mission. A 15-point sampling switch, operating at a rate of 1 point per sec, samples critical temperatures and voltages. The output of this switch is used to drive a Channel 8, IRIG, subcarrier oscillator. An a-c amplifier and a transformer connect the output across the spacecraft interface, where it is mixed with other telemetry for transmission over the bus beacon transmitter.

During the terminal mode, a 90-point sampling switch, operating at a rate of three points per sec, samples the TV subsystem parameters. The switch output is used to drive voltage-controlled oscillators (225 kc) connected in

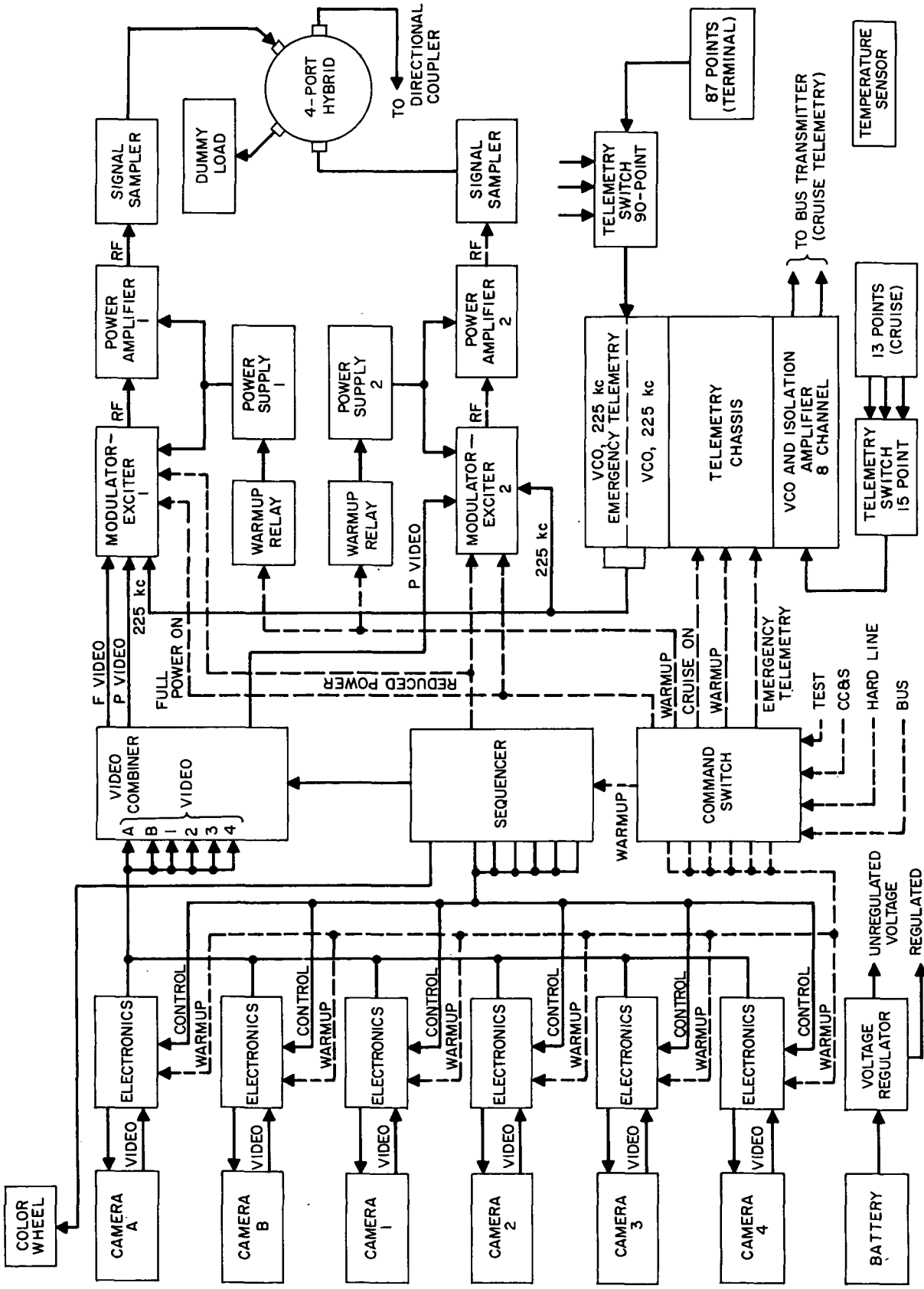

Figure 29. TV subsystem functional block diagram

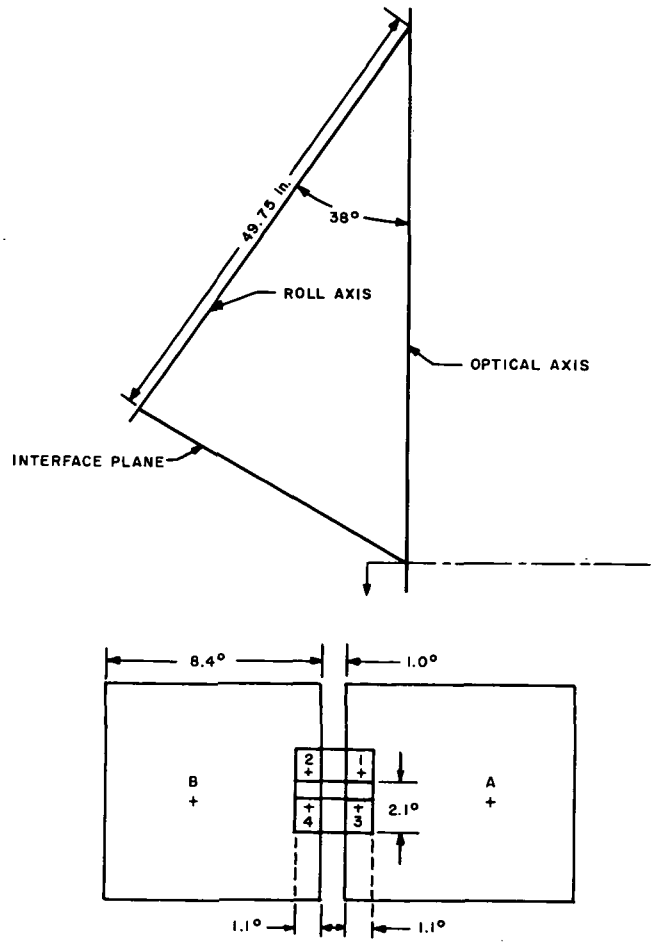

Figure 30. Terminal phase optical geometry

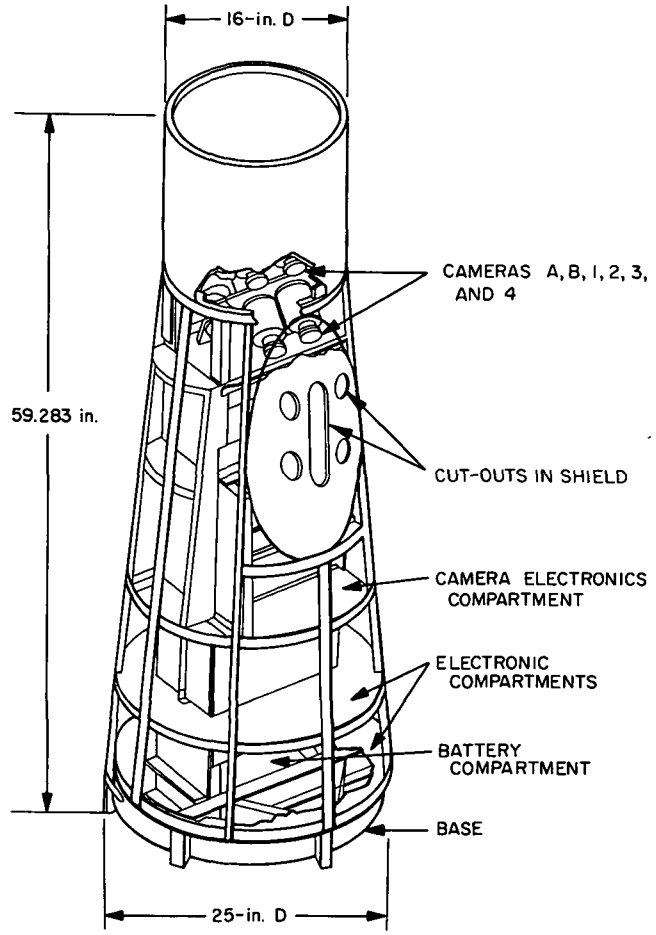

Figure 31. Basic structure of TV subsystem

parellel. These two outputs are connected so that one VCO is mixed with video at Modulator 1 and the other at Modulator 2. The VCO frequency was chosen so that it is located above the highest video frequency in the base band of the system.

In emergency mode, the video signals are switched out and the nine-point telemetry is used to modulate each of the transmitters directly. A possible condition requiring emergency telemetry would occur if video transmission were interrupted, and it became necessary to determine whether the TV subsystem was non-operational or the high-gain antenna was not locked to the Earth.

Flight sequence. The nominal trajectories for the TV payload flights will employ a nearly vertical descent to the lunar surface. In transit from the Earth to the vicinity of the Moon, the spacecraft will fly in a Sun-oriented attitude, with the solar cell panels perpendicular to the rays of the Sun. Thus, the optical axis of the television cameras will be fixed in vehicle body coordinate system. When the spacecraft reaches the vicinity of the Moon, it will undergo a commanded terminal maneuver to align optical axis of the television cameras with the spacecraft velocity vector for descent to the lunar surface.

Test set-up. The system test complex will be set up in a manner similar to that used on RA-3 and -4. The addition of 13 racks of RCA equipment will consist of: 7 racks for final picture recovery and recording; 2 racks for TV subsystem stimulation, monitoring, and control (hard line); and 4 racks for receiving equipment.

Basic structure. The mechanical design of the TV subsystem basic structure has been established to the extent that assembly and detail drawings have been prepared. Final drawings for the complete structure were released to Lavelle Aircraft Corporation, the structure subcontractor, in November 1961.

A full-scale plastic model of the structure has been fabricated and will be used to verify location of equipment and the assembly of the actual structures. A drawing of the structure is shown in Figure 31.

A detailed weight analysis of the structure was completed, using the final assembly drawings. Results indicated a weight of approximately 75 lb for the structure and thermal shield. The initial structure and thermal shield will be used in the mechanical test model without any special surface treatment.

TV cameras. Personnel have been assigned to the camera electronics in the RCA Camden (N. J.) facility. This group will complete the design of the circuits and their packaging, and fabricate the units.

The television equipment located in the payload consists of six 1-in. vidicon cameras. Of these cameras, two are fully scanned, producing a resolution of 800 TV lines over a tube format of 0.44 by 0.44 in., with a side field coverage of 8.4 deg. A reduced raster is utilized by four of the six cameras scanning a 0.11- by 0.11-in. central portion of the tube at approximately the same line density to produce a resolution of 200 TV lines. The side field of view is 2.1 deg and is achieved with the same focal length lens as specified for the fully scanned cameras. This leads to a natural categorization of Type-F cameras for fully scanned and Type-P for partially scanned. The Type-F cameras are used as Cameras A and B in the system configuration, and Type-P cameras are used as Cameras 1, 2, 3, and 4. The Type-F and Type-P cameras use the same imaging transducers and optical equipments and differ only in the detail of their electronic circuitry. The image transducer is an electromagnetically focused, 1-in. deflection vidicon photoconductor with a resolving capability in excess of 800 lines per picture height.

The Type-F or fully scanned camera utilizes 1152 active horizontal scan lines over the 0.44- by 0.44-in. faceplate area. The horizontal scan rate is 450 cps with 0.2 ms appropriated to horizontal blanking. The active scan lines plus 46.6 ms for vertical blanking add up to the 2.56-sec frame period. At the end of its active scan, the Type-F camera enters an erase phase which occupies an equal amount of time. Two Type-F cameras are alternately scanned and erased in such manner that one is being scanned while the other is being erased. This timing sequencer is illustrated in Figure 32.

The Type-P or partially scanned camera utilizes 300 horizontal scan lines over a 0.11- by 0.11-in. faceplate area. The horizontal line rate is 1500 cps with 111.1 μsec allocated for horizontal blanking. The vertical scan plus a 6.6-ms blanking period occupies 0.2 sec. At the end of the vertical scan, an erase procedure is initiated which occupies 0.64 sec. In the system, four Type-P cameras are sequentially scanned; while one is being scanned, the remaining three are in various portions of their erase cycles. A 40-ms pulse is used to separate each sequence

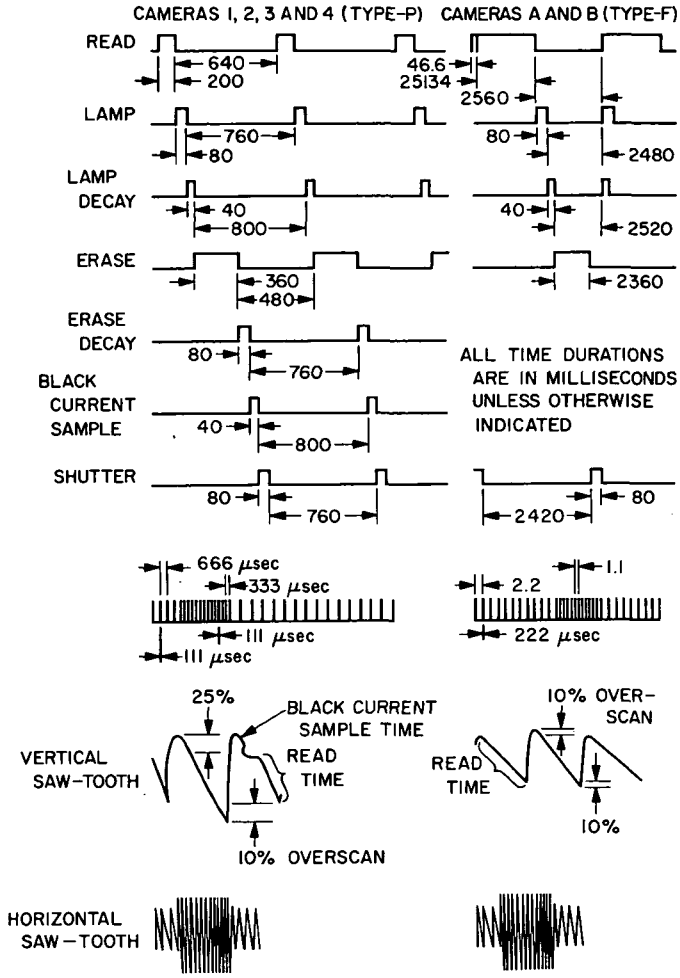

Figure 32. Camera timing and waveforms

of four Type-P camera exposures. The total period per sequence is then 0.84 sec. Figure 32 shows the basic camera timing, as well as the relationship of the four cameras in the system.

Each of the Type-F and -P cameras will derive its scan synchronization from the control sequencer. The cameras will each contain a preamplifier and video amplifier. The camera circuitry will also include a control grid current regulator, a focus current regulator, shutter drive circuits, dark current compensation, fast erasure circuits, and dc-to-dc converters for both high and low voltages.

The optics for Type-F and -P cameras will be identical lenses with a 76-mm focal length and an $f/2$ aperture ratio.

A color wheel containing three color filters and a single neutral density will be supplied with Camera A. The wheel will be caused to sequentially position a different filter in the optical path for each exposure of Camera A.

It will feed a coded signal to the control sequencer, which will be used to gate on the appropriate tone signals during the vertical blanking, signifying the color filter being used.

The mechanical portion of the filter wheel has been designed, and engineering releases have been issued for four assemblies. Spectral response tests have been conducted on vidicons for the color system.

Six Bausch and Lomb lenses and six Elgeet back-up lenses have been received and testing of the lenses has begun. If the Bausch and Lomb lenses meet all requirements, the back-up lenses will be used in breadboards and test set-ups.

Five Type-P camera housings have been released to the model shop. The housings will incorporate the mechanical focusing and centering of the vidicon yoke assembly with respect to the optics.

Camera sequencer. Work on the camera sequencer has been subcontracted and has been directed toward finalizing the logic design and testing the basic logic circuits. The addition of new inputs, and difficulties encountered in adhering to the −10 to +65°C temperature range, make it necessary to increase the number of circuits over that originally planned. A complete block diagram of the control programmer and camera sequencer is shown in Figure 33.

Communications and telemetry. Communication subsystem components for the transmission and reception of the multiplexed TV data and telemetry data consist of the following:

(1) Spacecraft telemetry components, including a 3-kc subcarrier oscillator (SCO), two commutators, two 235-kc SCO's, an a-c amplifier, and a dc-to-dc converter.

(2) Spacecraft transmitter.

(3) Spacecraft power supply.

(4) Spacecraft communication system integration components such as junction boxes, control panels, etc.

(5) Ground telemetry components.

(6) Ground receiver components, including a 30-mc mixer, two 5.0-mc IF amplifiers, and two 0.5-mc IF amplifiers with automatic frequency control.

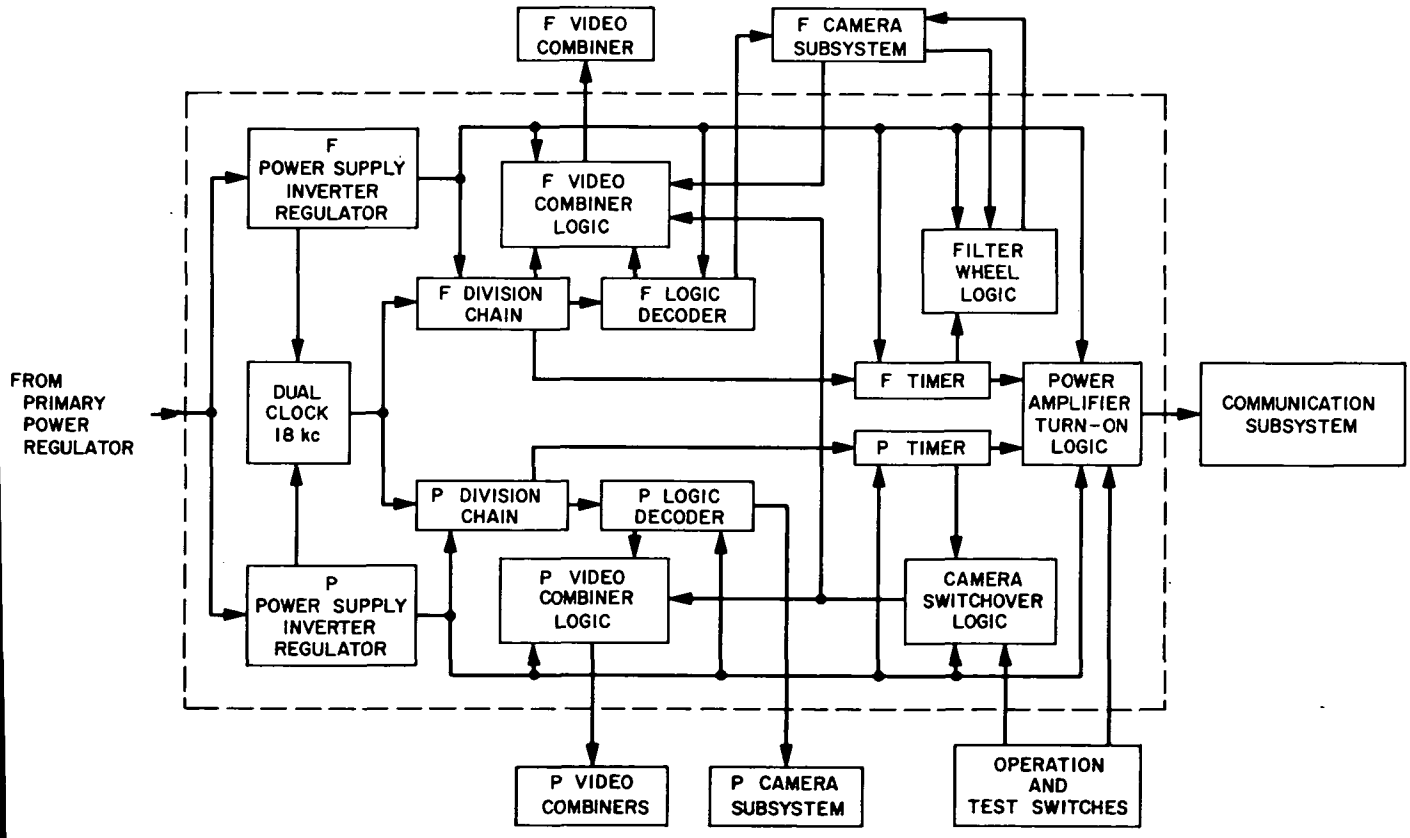

Figure 33. Control programmer and camera sequencer

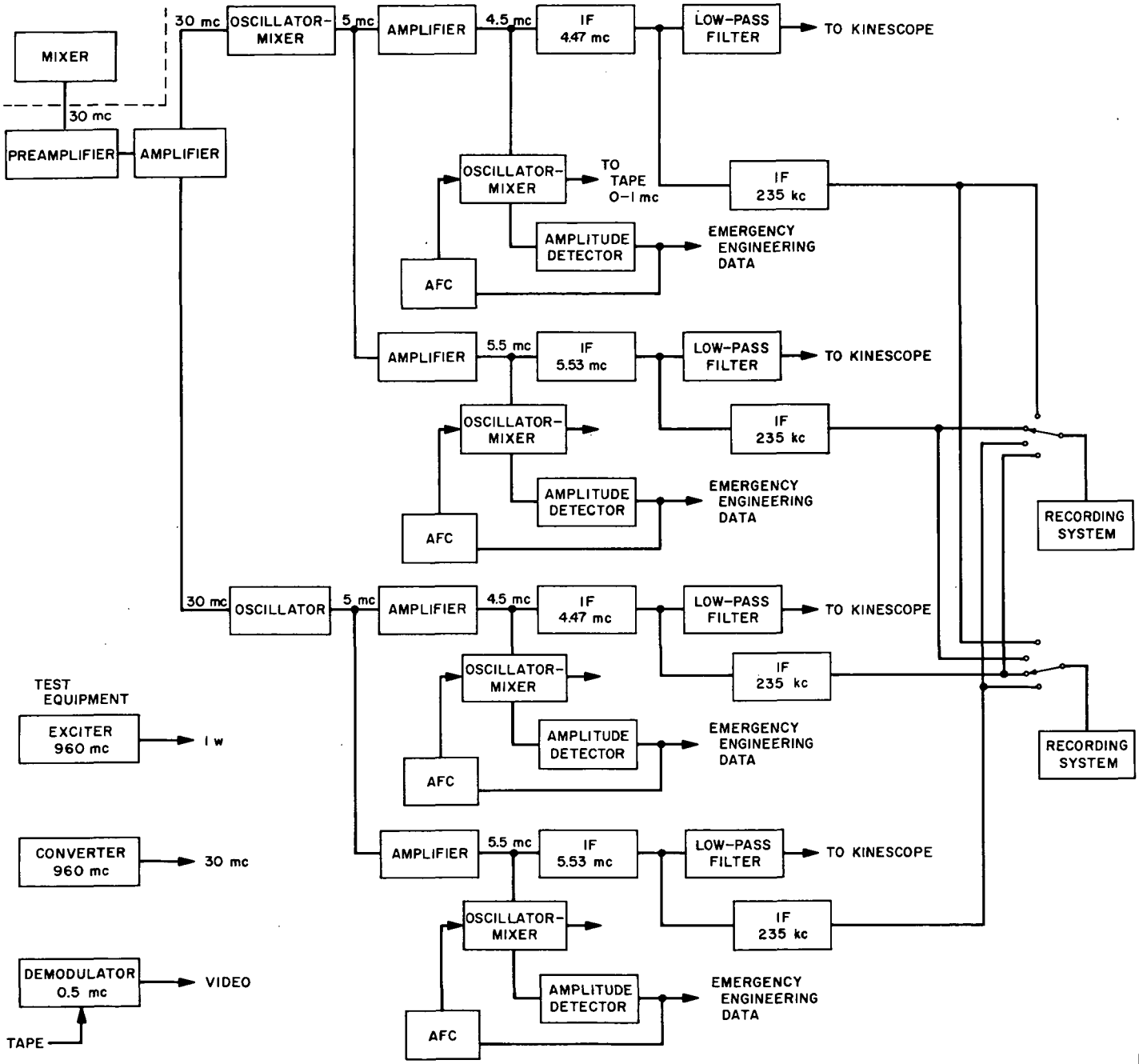

Figure 34. Goldstone receiving system

The current spacecraft and ground configurations are shown in Figures 29 and 34.

The modulator-exciter design reflects the reliability requirements of design simplicity and the utilization of the minimum number of circuit components. Temperature compensation is being performed on the oscillator circuits and it appears that the 0.001% requirement may be met without the use of a crystal oven. Frequency deviation requirements for the modulator have been met with less than 2% distortion of the modulating signal.

Power supplies. The preliminary design on two power supplies, a 150-w unit and a 15-w unit, has been completed. The changes to both voltage and current requirements necessitate replacement of the 150-w unit by two units of 190- and 390-w, each with an operating frequency of approximately 2 kc. The 190-w unit will supply 500

at 100 ma, 300 v at 50 ma, 100 v at 300 ma, 6.3 v ac at 1 amp, and 6.3 v ac at 8 amp. The 390-w unit will supply 1250/1000 v at 250 ma.

The 15-w unit will be housed in a separate shielded case. This unit is to supply 27 v regulated at 500 ma. Preliminary design of the larger two-unit power supply has been started. Mechanical design of the 15-w unit is underway.

Telemetry. The communications system analysis has been made for the carrier-to-noise ratio, picture signal-to-noise ratio, and tone code signal-to-noise ratio. An analysis of the effects of using pre-emphasis to gain an improvement in signal-to-noise ratio for video transmission has been made.

Primary power: batteries. The TV payload power supply subsystem will consist of two silver-zinc storage battery units which will feed a common series-type voltage regulator and furnish a regulated output of 27.5 ±0.5 v. Each of the battery packages will be capable of furnishing the total payload energy requirements as determined by the mission power profile, improving the over-all reliability of the system. In addition to the batteries and voltage regulators required for the payload power supply subsystem, battery chargers and external power supply units will be required for the development, testing, and checkout of the payloads.

A systems test set of batteries and a flight set will be used to furnish internal power during the integration and testing of the payload, and will be recharged as required during testing. The flight set will be inserted after the completion of the final systems tests, and before the payload is mated with the spacecraft, in order to minimize the accumulated test time on the flight units.

The problem of assuring the internal and external sterility of the battery units will be considered in design of the batteries and selection of the battery mounting locations in the payload structure. The Electric Storage Battery Company, Missile Battery Division, Raleigh, N. C., was selected to supply the batteries.

The external power supply and battery charger units will be adaptations of existing commercially available equipments.

Voltage regulator. A series-type voltage regulator will be used to provide −27.5 ±0.5 v. Two batteries will supply the unregulated power and the power to the regulators. The maximum battery terminal-voltage variation that can be expected is from −41.5 to −30.5 v dc. The TV transmitters and camera shutters will operate from unregulated battery voltage to reduce the current drain on the regulator. A reduced current drain will result in reduced size and weight of the regulator.

Power profile. The total power-drain profile for the TV subsystem has been modified in accordance with the new payload operational sequence and subsystem requirements. Figure 35 shows the major power-draining periods for the new sequence.

The new total energy required is approximately 896 w-hr. This estimate is based on the requirements of the clock and sequencer, voltage regulator, cameras, communications, and telemetry units for the entire mission.

Ground battery charger and monitor (launch pad area). The purpose of the ground battery charger and monitor of the launch-pad area (Fig 36) will be to maintain the full-charge capacity of the flight batteries when power drain during pre-launch test is continued for an appreciable time. Since battery charging should not take place while the payload equipment is operating from the battery, the test procedure will make provisions to prevent charging during the pre-launch tests.

Ground power supply charger and monitor (service area). The ground power supply charger and monitor of the service area (Fig 37) will have these purposes:

(1) To monitor the terminal voltage of each battery and to regulate battery charging by means of voltage sensing.

(2) To monitor individual cell voltages by selection and to also indicate continuously the temperature of each battery.

(3) To supply external power for payload equipment when desired.

All connections for battery charging and sensing will be made through the payload umbilical cord.

Battery and voltage-regulator bench test load. In order to test the battery and voltage-regulator power capabilities, a test load was designed. The bench test load

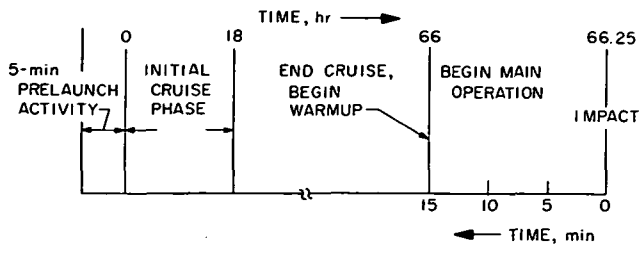

Figure 35. Major power consumption periods

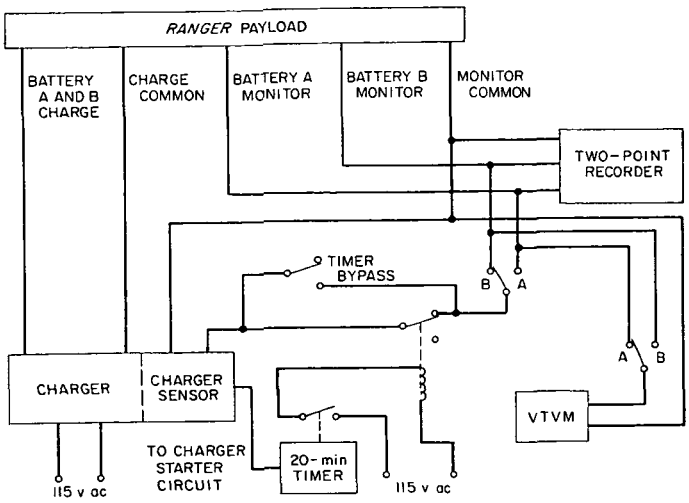

Figure 36. Ground battery charger and monitor, launch pad

(Fig 38) will enable simulation of any flight power profile. simulated.

Thermal control. A detailed thermal analysis to determine a continuous temperature–time history of the electronic modules throughout the mission was initiated and is continuing. Three separate computer programs are being used to analyze configuration, radiation-coupling factors, and mission temperature–time histories.

Thermal analysis directed toward a passive thermal control technique is being made. The primary design parameters of such a system are:

(1) Location of the electronic modules within the spacecraft.

(2) Emissivity and solar absorptivity of all exposed surfaces.

(3) Mass available for thermal heat sinks.

The TV subsystem consists of electronic modules that are in operation during limited time periods. Detailed examination of the modules indicates that there will be high thermal dissipation in some modules and little thermal dissipation in others. For this reason, the modules cannot be treated as gross isothermal bodies, but must be treated as individual units, and a temperature–time history predicted for each unit. Temperature–time histories will be predicted for the following modes of flight:

(1) 100-nm parking orbit.

(2) Passage through the Earth's shadow.

(3) Solar-oriented cruise (first phase).

(4) Midcourse maneuver.

(5) Solar-oriented cruise (second phase).

(6) Terminal camera orientation mode (11-hr duration).

(7) Terminal equipment warmup mode (5-min duration).

(8) Terminal operational mode (10-min duration).

The over-all result of thermal analysis will be a continuous temperature–time history of appropriate electronic modules from launch to impact on the Moon.

Three machine programs are being used to analyze the system. A program has been developed for the IBM 709 computer to evaluate configuration factors, using the principle of contour integration. The second program, for analog computing equipment, evaluates radiation-coupling factors, which are a function of surface emissivities, module areas, and configuration factors. An RCA-501 computer will be used to compute temperature–time histories of the modules. The program for this computer is designed for solution of the temperature–time dependence of a 30-day body system, with each body exchanging energy with all other bodies by radiation and conduction.

A detailed thermal model is being constructed for testing. The model will be placed in a vacuum chamber capable of simulating external energy flux by infrared radiation at pressures of 10^{-4} mm Hg or lower. After necessary design information has been obtained, a solar-simulation test should reveal any thermal design problems that might exist, in time to permit solutions for the Proof Test Model.

Design of the thermal model and Proof Test Model test facility was initiated. It is planned to use lamps to simulate incident solar energy on the TV subsystem. A test fixture is under development to provide a variable, uniform intensity on appropriate surfaces.

The results of the preliminary calculations to determine magnitudes of thermal mass needed to minimize terminal temperature rise indicate that many modules are sufficiently massive to require no additional heat sink. However, a few units are low in weight and have high dissipation densities; additional heat-sink material is required for these units. Change-of-state materials with favorable thermal properties (wax in particular) are being investigated for use as additional lightweight heat sinks.

Subsystems integration. The design has been established for command switching of the TV subsystem by real-time command (RTC) signals from the spacecraft bus. The purpose of this switching is to set the TV subsystem into the different modes of operation required by the mission sequence of events. The three RTC signals

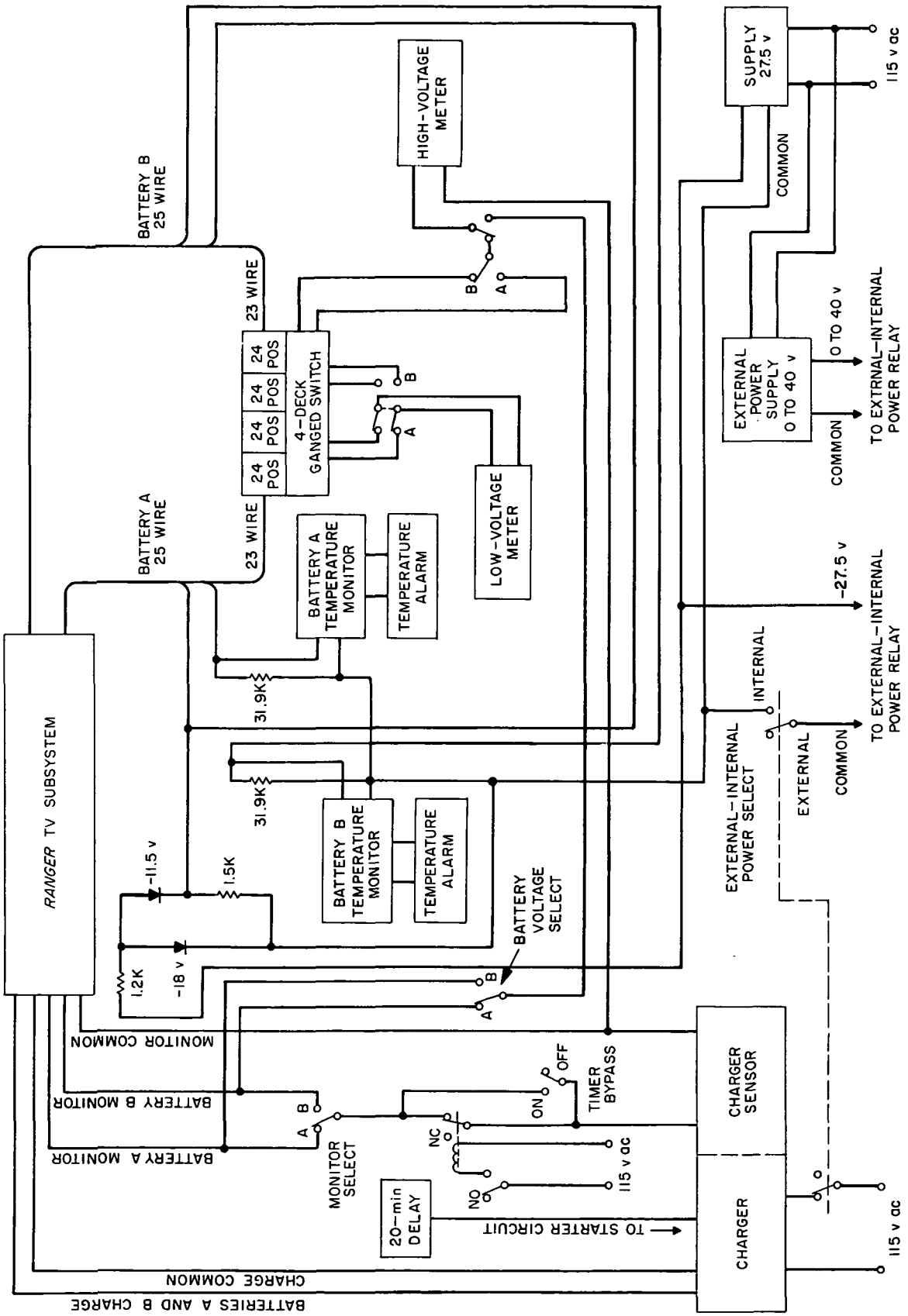

Figure 37. Service area ground power supply and monitor

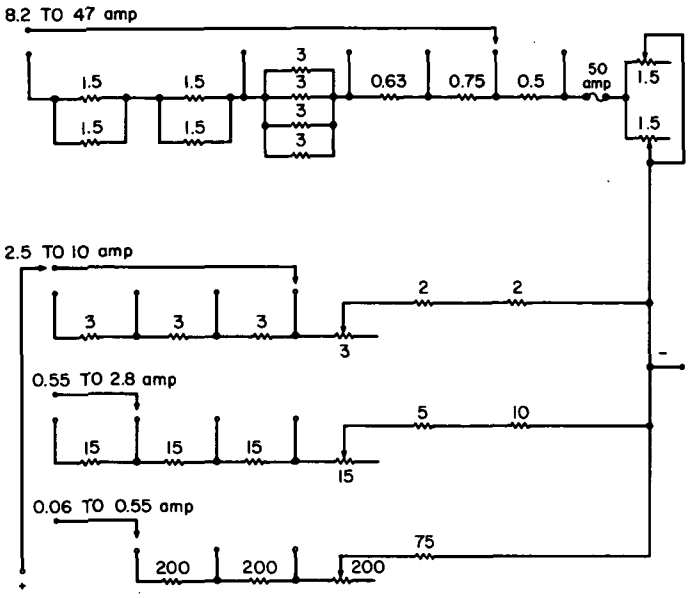

Figure 38. Battery bench test load

which operate the command switch are: (1) warmup signal, (2) emergency mode signal, and (3) emergency mode-off signal. When the warmup signal is received, the command switch advances from Position 0 to Position 1, energizing relays in the command switch, the transmitters, and the telemetry section.

The emergency mode signal causes the command switch to advance from Position 1 to Position 2 and the cameras become disconnected from the transmitters. The terminal telemetry signals are connected directly to the transmitters. In this position of the command switch, the warmup signal is still applied to the warmup relays to keep the TV subsystem in operation.

The final signal received from the bus is the emergency mode-off signal. This signal advances the command switch to Position 3; the cameras are again connected to the transmitters, and the TV subsystem performs in the normal operating mode. The warmup signal is applied to the appropriate relays as in the other modes. Position 3 is the final position to which the command switch will be advanced during the mission. It is not planned to use the switch during the subsystems tests, except to test operation of the switch itself.

Total payload weight for the missions is 350 lb, and the center-of-gravity location for the spacecraft–payload combination satisfies the JPL requirements.

Ground support equipment. The designs for the TV subsystem ground receiving equipment and ground checkout equipment have been finalized. Plans for the Goldstone equipment call for a 30-mc, caged preamplifier to be located on the antenna. The design provides for redundant receivers and tape recorders. Included also are two Kine-recorders which can be used for direct on-line or off-line photographic recording. The Channel 8 telemetry is selected by means of an appropriate filter, from the wide band telemetry. After demodulation, the telemetry data can be presented as a printout.

Signal processing and interconnection switching has also been finalized. A two-channel test transmitter is planned.

Designs for a TV subsystem panel and a single-channel test transmitter for the ground checkout equipment have been completed. The TV subsystem panel will permit exercising the spacecraft equipment by simulating command signals as well as making the correct connection to the checkout equipment.

The checkout panel to be included in the blockhouse equipment has been designed. This panel will permit a brief exercise of the spacecraft through hard-line connections while it is emplaced on the launch pad.

All primary power requirements for GSE have been established and equipment layouts for the various installations were reviewed. In addition, the interface between the RCA equipment and the ground support equipment at Goldstone was established.

The operational ground station comprises two major ground equipments: the TV data recording and display equipment, and the ground communications equipment.

Data recording and display. The TV ground support equipment provides three primary functions: (1) data recording (telemetry and TV information), (2) data reduction (TV information), and (3) control of checkout and exercising of the subsystem.

Data recording will provide interim as well as archival storage of events on a multi-channel, continuous-tape, magnetic recorder. Data reduction of information in the form of television signals will be recorded by a 35-mm film camera. GSE subsystems, intended for checking and exercising the system, will be provided by one kinescope and film–camera combination capable of recording either slow-scan or fast-scan video channels individually.

Figures 39 and 40 are block diagrams and equipment layout, respectively, of the TV data recording and display ground checkout equipment.

Tape recorder. The tape recorder is a four-channel, wide band, continuous linear magnetic-tape system which will record and play back the composite video and

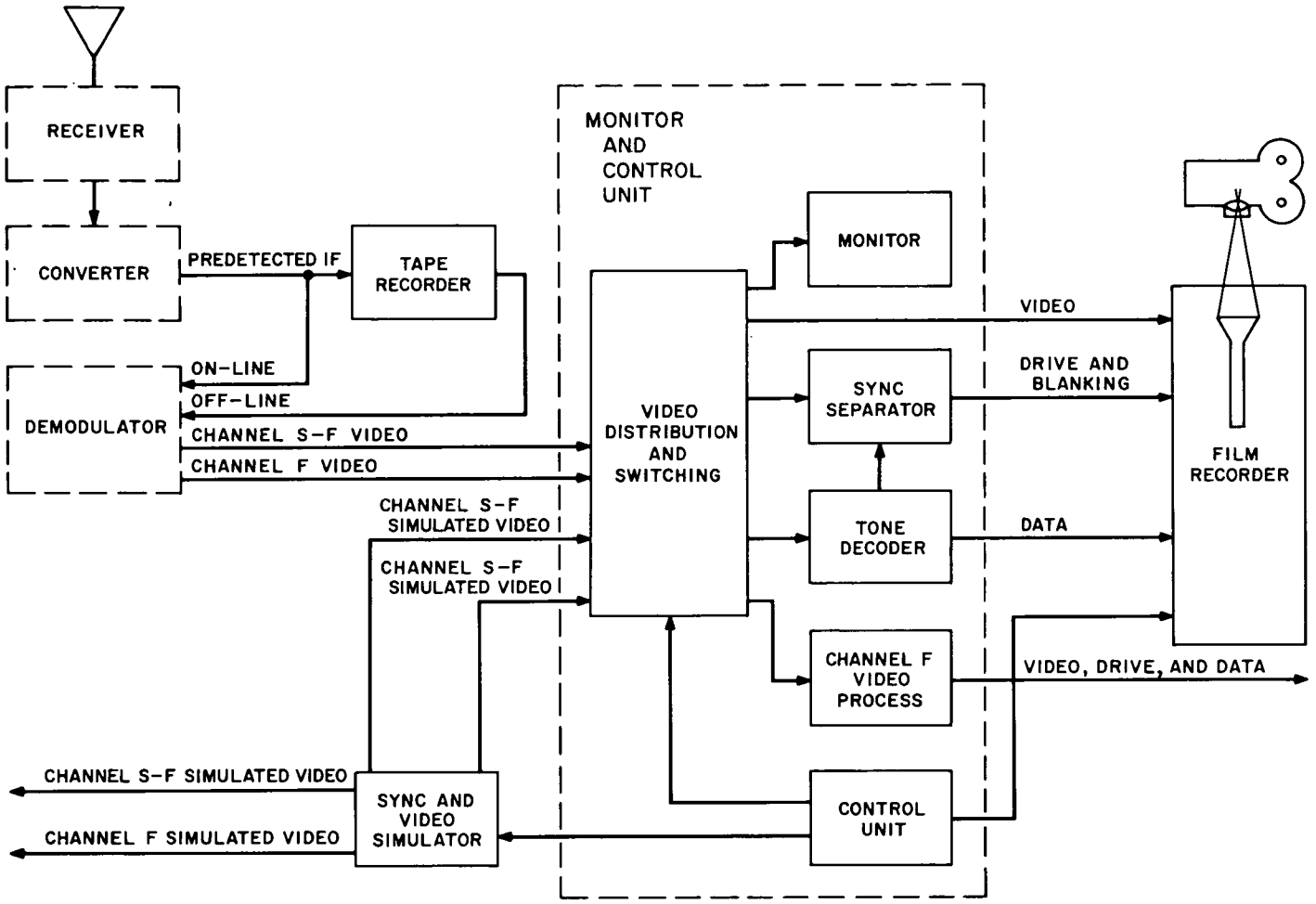

Figure 39. TV data recording and display, ground checkout equipment

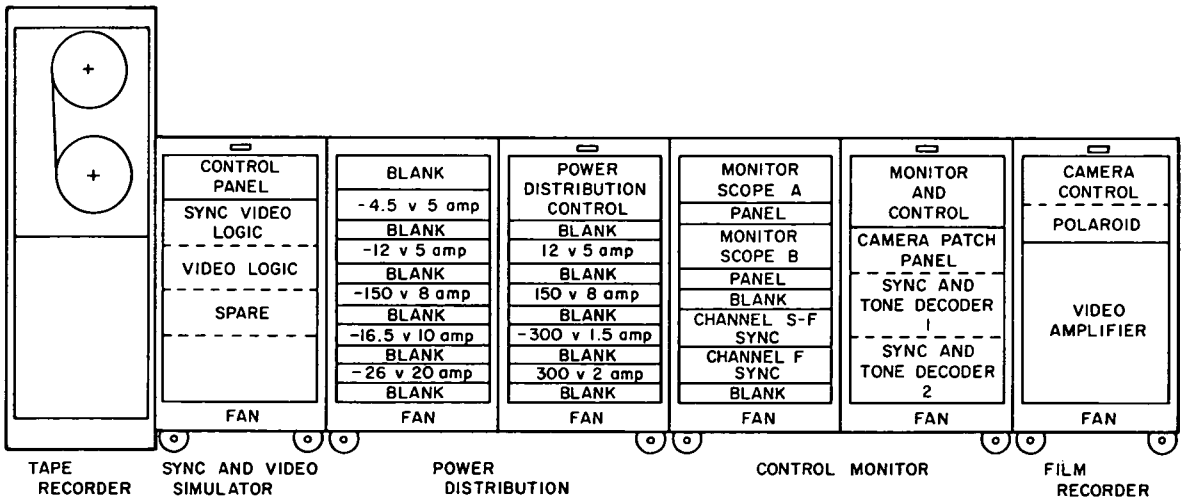

Figure 40. TV data recording and display checkout circuit, panel layout

telemetry signals received from the subsystem interface equipment.

Sync and video simulator. The sync and video simulator contains the test-pattern control, sync generator, and video-simulator circuits. These circuits produce the function necessary to perform a comprehensive subsystem test to determine equipment operability.

The generated video test signals are selectable by a rotary switch on the simulator unit. These signals comprise:

(1) Vertical bars (two raster lines wide).

(2) Horizontal bars (two raster lines wide).

(3) Grating pattern (horizontal and vertical bars).

(4) Gray scale.

(5) Resolution bars (five bursts of sine waves).

(6) Composite test pattern (grating, resolution bars, and gray scale).

The power distribution unit consists of a control panel, blower, and nine individual d-c voltage power supplies. This unit provides control of the a-c and d-c voltage requirements of the TV data recording and display subsystem.

Monitor and control unit. The monitor and control unit contains a monitor and control panel, camera patch panel, monitor scope (one in the checkout configuration, two in the operational configuration), Channel S-F sync chassis, Channel F sync and tone-decoder chassis, two sync and tone decoder-module nests, and a communication panel. This unit provides a central point from which the subsystem can be operated.

Film recorder unit. The film recorder consists of a 35-mm camera, Polaroid-Land camera, high-voltage power supply, camera control, kinescope, kinescope-control circuits, and deflection amplifier. The primary purpose of this unit is to provide a film record of the kinescope display. The kinescope display is transmitted from TV cameras on the payload, and a 35-mm camera photographs the picture produced on the face of the kinescope.

Ground communications. The purpose of the communications portion of GSE being supplied to the DSIF Goldstone facility is to reduce the composite 960-mc signal into two separate video signals and a print-out of the telemetry information. In order to accomplish this with maximum reliability, a completely redundant system is used (Fig 41).

960-mc information is received and translated into a 30-mc IF signal. To assure that a flat 2-mc bandwidth is provided, a separate 30-mc IF preamplifier is mounted on the antenna. This composite signal is coupled to the RCA equipment located in the operations building. At this point, the two channels are separated; one is processed by a 4.47-mc IF, the other by a 5.53-mc IF. After limiting, the signal is detected and the telemetry information is separated for further processing. The video signal then goes through a low-pass filter to suppress the telemetry channel, followed by a de-emphasis network to restore the flat video spectrum. This signal is then fed to the kinescope recorders for real-time display.

Tape recorders are used for predetection storage of received signals. For this purpose, the 5-mc IF is translated to a 500-kc carrier, recorded on two channels of a tape recorder. For playback, the outputs of the two channels are combined and fed to a 500-kc demodulator. This composite signal is then coupled (in place of the 5-mc demodulator output) through filter networks to the kinescope and telemetry reduction system.

The telemetry-reduction system has an analog-to-digital converter with printout. Analog information may be received in three ways:

(1) Cruise telemetry: Channel 8 over the bus transmitter. An IRIG demodulator is used to reduce the Channel 8 FM signal to an analog voltage.

(2) Terminal telemetry. A 225-kc subcarrier on the TV transmitter is demodulated to obtain the analog telemetry signal.

(3) Emergency telemetry. The 5-mc signal is fed to a narrow-band phase-locked loop. The output of the phase-locked loop is coupled to the Adcon unit.

To test the ground system, a TV simulator will be incorporated. To check the communication portion of the ground station, the signals from the simulator are preemphasized and fed to the test transmitter. The test transmitter signal is coupled with the bus signal and fed to the preamplifier for systems test. Power levels of the test transmitters are calibrated so that the DSIF equipment may be checked at a threshold signal level.

3. Systems Analysis

a. Trajectories.

RA-1 standard trajectory. Desired post-injection trajectory for RA-1 was highly elliptical, having a nominal first-apogee distance varying from 1,104,600 km for the 8:30

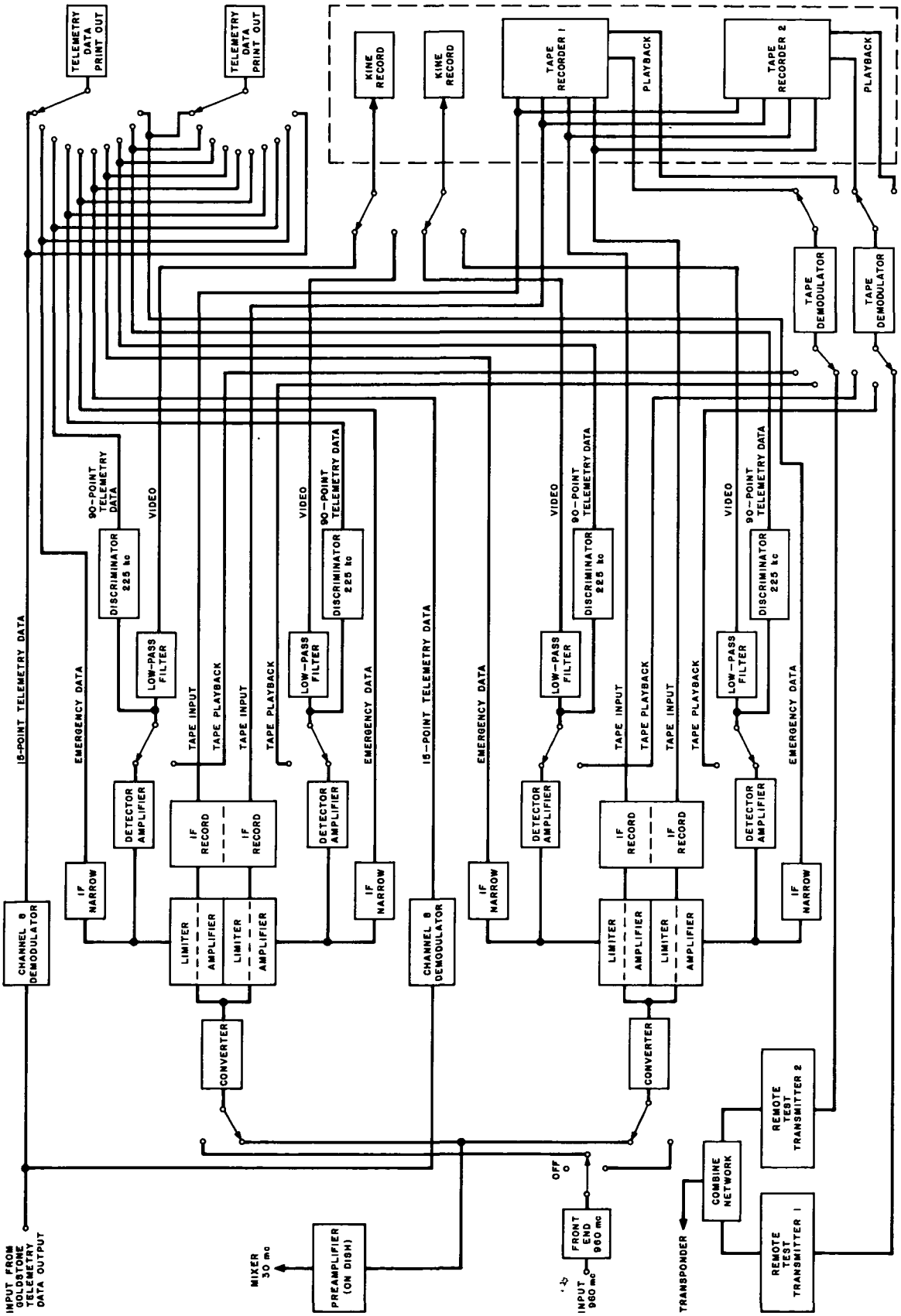

Figure 41. Goldstone ground receiving equipment

(GMTI)[a] trajectory to 1,178,300 km for the 11:00 (GMTI) trajectory (686,400 to 732,200 mi), a nominal first-perigee distance varying from Earth impact to 94,300 km, and nominal lifetimes varying from 45 days to over 120 days.

Further information concerning the RA-1 standard trajectory may be obtained from Reference 7.

Ranger I actual trajectory (Refs 8 and 9). The *Ranger I* spacecraft was placed in a low-altitude Earth–satellite orbit on August 23, 1961. Launch occurred at 0504:10 EST from Complex 12 at the Atlantic Missile Range. The standard trajectory was essentially achieved up to ejection from the parking orbit. At this point, a component failure in the propulsion system of the second-stage *Agena B* prevented *Ranger I* from achieving the required velocity increment for standard flight.

Liftoff was normal, with all systems operating properly. *Atlas* performance during ascent was satisfactory. The guidance system indicated the cutoff of the engines at near-nominal times, and the coast ellipse prior to *Atlas–Agena B* separation was within specification. The separation sequence was performed satisfactorily, followed by expected stabilization and pitch-down controls. The *Agena-B* timers were started, as planned by *Atlas* guidance commands, and the second-stage sequence of events was normal. *Agena* first-burn data indicated that the proper parking orbit was achieved.

A malfunction in the *Agena-B* engine second-burn ignition sequence allowed the gas generator to start but kept the main fuel valve closed, with the resulting lack of engine thrust. A small velocity gain of 70 m/sec was obtained during the programmed second burn due to the expulsion of oxidizer. The net loss of approximately 3100 m/sec of velocity to be gained during second burn resulted in an Earth orbit having an apogee altitude of only 313 mi.

Since second burn was not attained, the velocity meter did not initiate the engine shutdown function. This event was performed by the timer backup signal. Separation of the spacecraft from the *Agena* followed at 1530 sec. Telemetry indicated that a separation velocity of approxi-

[a]GMTI = Greenwich Mean Time at Injection.

Table 4. Orbital parameters of *Ranger I*

August 1961	Time of injection						Epoch of pericenter passage			Period, min Apogee, mi Perigee, mi
	X R	Y ϕ	Z θ	$\dot{X}$ v	$\dot{Y}$ γ	$\dot{Z}$ σ	a e	i Ω	ω ν	
23	8-23-61, 10:26:36						8-23-61, 10:27:23.106			91.1483
	−0.24370486E4[a] 0.65421648E4	0.60054081E4 −0.78371254E1	−0.89207321E3 0.34396299E3	−0.59845351E1 0.75058997E1	−0.30579307E1 −0.83381240E1	−0.41566759E1 0.12400118E3	6709.03 0.024911	32.9283 279.8169	197.788 −3.2601	313.337 105.597
24	8-24-61, 5:20:00						8-24-61, 4:38:42.202			90.8346
	0.15937675E4 0.68277538E4	−0.66002189E4 0.60346574E1	0.71780167E3 0.23132487E3	0.61159252E1 0.71507338E1	0.18709918E1 0.34833794E0	0.40379101E1 0.55444856E2	6693.63 0.020846	32.9237 274.1791	206.828 164.324	286.614 113.172
25	8-25-61, 1:50:00						8-25-61, 1:47:48.742			90.4836
	−0.36687562E4 0.65356489E4	0.48113055E4 −0.22215657E2	−0.24710883E4 0.12673406E3	−0.49436399E1 0.74935728E1	−0.53200141E1 0.19903683E0	−0.30874395E1 0.11633590E3	6676.37 −0.021334	32.9008 268.1813	215.029 9.084	277.692 100.645
26	8-26-61, 0:20:00						8-26-61, 0:23:29.176			90.1401
	−0.20031848E4 0.65393933E4	0.59413022E4 −0.16505720E2	−0.18579142E4 0.12961566E3	−0.61797660E1 0.74802883E1	−0.32606133E1 −0.27501244E0	−0.36375649E1 0.12057164E3	6659.47 0.018598	32.9074 261.3796	225.978 −14.448	255.625 101.686
27	8-27-61, 0:15:00						8-27-61, 0:22:46.763			89.7370
	−0.32633687E3 0.65485475E4	0.64037421E4 −0.11718777E2	−0.13300636E4 0.11416857E3	−0.66805933E1 0.74581758E1	−0.12279096E1 −0.51101682E0	−0.39452968E1 0.12282820E3	6639.59 0.016117	32.9141 254.2260	234.132 −32.182	232.818 99.806
28	8-28-61, 0:10:00						8-28-61, 0:16:1.986			89.1915
	−0.13595608E4 0.65346669E4	0.59559554E4 −0.20790533E2	−0.23194963E4 0.12437762E3	−0.65960181E1 0.74585742E1	−0.28048166E1 −0.32683821E0	−0.32160637E1 0.11760648E3	6612.66 0.012979	32.9076 246.9342	245.768 −24.974	202.914 96.231

X, Y, Z, $\dot{X}$, $\dot{Y}$, $\dot{Z}$ = a right-handed, Earth centered, equatorial, space fixed rectangular cartesian coordinate system. Z is assumed to lie along the Earth spin axis, positive north, X is normal to Z and positive in the direction of the vernal equinox, km, km/sec.

R, ϕ, θ, v, γ, σ = a right-handed, Earth centered, equatorial, Earth fixed spherical coordinate system. R is from Earth center in km, ϕ is geocentric latitude measured from equatorial plane positive north in deg, θ is longitude measured eastward from the Greenwich meridian positive eastward in deg, v is Earth fixed velocity in km/sec, γ is path angle of spacecraft with respect to local horizontal in deg, σ is azimuth angle of v measured east of true north in deg.

a = semi-major axis, km.
e = eccentricity.
i = inclination of orbit plane to equatorial plane, deg.
Ω = longitude of ascending node, deg.
ω = argument of perigee, deg.
ν = true anomaly, deg.
All times are in GMT.

[a]−0.24370486E4 = −2437.0486.

Table 5. Sequence of flight events

Event	Predicted time, sec	Actual time, sec
Liftoff (GMT)	0	10:04:10.32
Atlas booster cutoff	137.7	136.23
Atlas booster engine separation	—	138.90
Start *Agena* re-start timer	247.3	246.27 ±0.11
Atlas sustainer cutoff	276.4	273.50
Start *Agena* primary D-timer	285.8	288.06 ±0.11
Atlas vernier cutoff	295.3	289.91
Nose shroud pin puller squibs *Fire*	296.8	291.80
Midbody pin pullers and retrorockets *Fire*	299.8	294.97
Jettison horizon scanner fairing	307.56[a]	307.60
Initiate −180-deg/min pitch rate	314.06[a]	314.01 ±0.11
Transfer to −3.54-deg/min pitch rate	317.06[a]	317.07 ±0.11
Ullage rockets *Fire* (first burn)	337.06[a]	337.12
Telemeter signal acquire (Antigua, Station 9.1)	—	346.68
Gas Generator 1 *Fire* (first burn)	349.06[a]	349.05 ±0.11
Thrust attainment, 90% P_c (first burn)	350.31[a]	350.58
Telemeter signal loss (Cape Canaveral, Station 1)	—	458
Engine cutoff, 70% P_c (first burn)	499.41[a]	499.48
Burning duration (first burn)	149.10	148.90
Horizon scanner position squib *Fire*	516.06[a]	516.10
Helium valve Off Squib 2 *Fire*	516.06[a]	516.10
Stop *Agena* primary D-timer	520.06[a]	520.10
Telemeter signal loss (Antigua, Station 9.1)	—	766.00
Telemeter signal acquire (Ascension, Station 12)	—	1152.39
Re-start *Agena* primary D-timer	1266.27[b]	1267.25 ±0.11
Ullage rockets *Fire* (second burn)	1271.25[c]	1271.37 ±0.11
Transfer to −4.74-deg/min pitch rate	1271.25[c]	1271.37 ±0.11
Gas Generator 2 *Fire* (second burn)	1283.25[c]	1283.35 ±0.03
Thrust attainment, 90% P_c (second burn)	1284.50[c]	—
Engine cutoff, 70% P_c (second burn)	1373.50[c]	1380.32 ±0.03[d]
Burning duration (second burn)	89.50[c]	96.97[e]
Start telemetry calibrate	1380.25[c]	1381.35
Payload interface connector *Fire*	1525.25[c]	1525.35
Payload pin pullers *Fire*	1530.25[c]	1530.35
Agena-hanger separation complete	—	1530.51
Initiate +180-deg/min yaw rate	1533.25[c]	1533.31 ±0.11
Telemetry signal loss (Ascension, Station 12)	—	1583.08
Remove yaw program	1593.25[c]	—[f]
Transfer to 5.55-deg/min pitch rate	1593.25[c]	—[f]
Retro-rocket *Fire*	1920.25[c]	—[g]

[a]Adjusted for primary D-timer start of 288.06 sec.
[b]Adjusted for re-start D-timer start of 246.27 sec.
[c]Adjusted for primary D-timer re-start of 1267.25 sec.
[d]Shutdown of relay signal.
[e]Duration of gas generator operation.
[f]Not available.
[g]Verification of event only.

mately 0.6 m/sec with approximately 0.15-sec separation time resulted. Following separation of the spacecraft, the *Agena* performed the required yaw–pitch maneuver in preparation for firing of retro-rockets. The rockets fired and the subsequent altering of the *Agena's* trajectory to prevent it from following the spacecraft trajectory was successful.

The characteristics of the post-injection trajectory are presented in Table 4. These are the best obtainable parameters using the Orbit Determination Program (ODP) available at JPL. The JPL ODP is designed for use with deep-space probes similar to the RA-1 standard trajectory and, therefore, lacks certain features which are mandatory for the determination of orbits of low-altitude satellites. The most important of these features is the exclusion of any type of drag effect experienced by the spacecraft during the decay of its orbit. As a result, it was necessary to re-determine the orbit for each excursion about the Earth. The final orbit of *Ranger I* will be determined by Goddard Space Flight Center, using techniques developed especially for low-altitude satellites.

Six orbits are available in Table 4, one for each day. The epoch on each day was chosen to be just prior to the start of the set of new periods at Woomera. The orbit defined is representative of the actual orbit up to the last new period at South Africa, a duration of approximately 14 hr.

Comparisons of standard and actual trajectory parameters are presented in Tables 5 through 9. Table 5 compares the sequence of flight events; Table 6 compares the *Atlas* coast apogee conditions; Table 7 compares the parking orbit parameters; Table 8 compares the injection conditions; and Table 9 compares the orbit parameters at injection. In general, satisfactory agreement exists with the exception of Tables 8 and 9, which show large differences since nominal injection was not obtained. Figure 42 shows the result of the non-nominal injection.

Table 6. *Atlas* coast apogee conditions

Parameter	Predicted	GE-Burroughs Vector 1	Real time Vector 2	FPS-16 radar simulation
Inertial velocity, m/sec	5646.72	5654.65	5645.52	5650.08
Altitude, km	184.3369	181.9107	184.6296	184.4558
Orbital inclination angle, deg	32.62	32.63	32.62	32.61

RA-2 standard trajectory. The post-injection trajectory for the RA-2 mission is highly elliptical, having a nominal first-apogee distance varying from 1,106,535 km for the 8:00 (GMTI) trajectory, to 1,240,473 km for the 11:00

Table 7. Parking orbit parameters

Item	$N + N^a$	$A + N^b$	$A + N + S^c$	JPL data
Perigee, km	6553.477	6548.028	6554.054	6545.784
ΔPerigee		5.449	−0.577	7.693
Apogee, km	6567.648	6583.615	6596.530	6614.216
ΔApogee		−15.967	−28.882	−46.568
Period, min	88.139	88.245	88.436	88.531
ΔPeriod		−0.106	−0.297	−0.392
Eccentricity	0.00108	0.00271	0.00323	0.0052
ΔEccentricity		−0.00163	−0.00215	−0.00412
Apogee–perigee, km	14.171	35.587	42.476	68.422
Inclination angle, deg	32.699	32.770	32.778	32.85
Node, Ω, deg	—	—	—	279.80
Argument of perigee ω, deg	—	—	—	194.60
Position of epoch ω + ν_0, deg	—	—	—	136.50
Epoch	—	—	—	August 23, 1961 $15^h\ 12^m\ 28^s$

[a] $N + N$ = nominal *Atlas* + nominal *Agena*.
[b] $A + N$ = actual *Atlas* + nominal *Agena*.
[c] $A + N + S$ = [b] + actual ignition and burnout.

Table 8. Injection conditions

Parameter	Predicted	Actual (first orbit)
Time from launch, sec	1373.4233	1346.32
Radius vector, km	6569.4743	6542.1648
Earth-fixed velocity, m/sec	10,588.0223	7505.8997
Earth-fixed flight path angle, deg	1.6251180	−0.0833812
Geocentric latitude, deg	−9.1929791	−7.8371254
Longitude, deg	346.178965	343.962990
Earth-fixed azimuth, deg	122.970366	124.001180

Table 9. Orbit parameters

Conic parameters at injection	Predicted	Actual
Twice total energy/unit mass, C_3, km^2/sec^2	−0.622,272	−59.4131
Angular momentum, C_1, km^2/sec	72,155.9	51,696.9
Semi-major axis, *a*, km	640,561	6709.03
Semi-minor axis, *b*, km	91,470	6688.18
Eccentricity, *e*	0.989752	0.024911
Period of revolution, min	85,035.2	91.1483
Inclination of the plane of the orbit against the equatorial plane, *i*, deg	32.8032	32.9283
Longitude of the ascending node, Ω, deg	279.761	279.8169
Argument of perigee, ω, deg	194.003	197.788
Closest approach distance, km	6564.54	6564.19
Apogee distance, km	1,274,557	6876.11
Time from perigee passage, sec	32.83	−47.11
True anomaly, ν, deg	3.14822	−3.2601

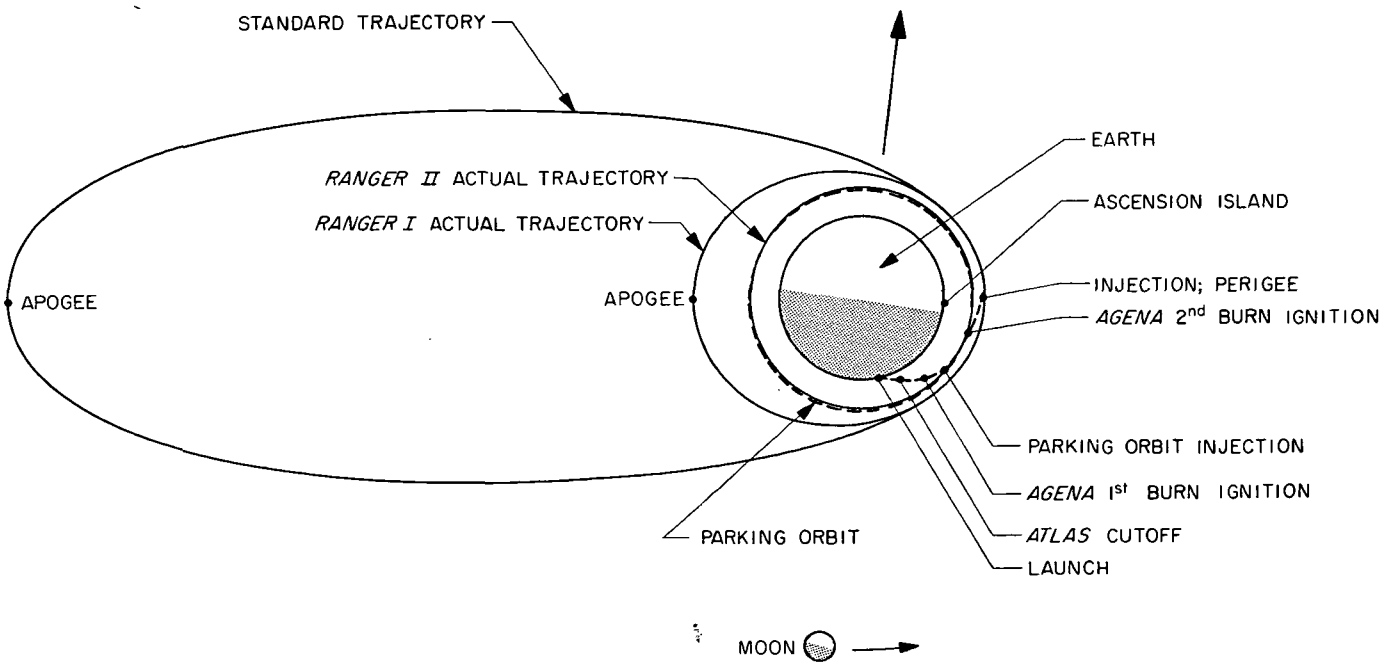

NOT TO SCALE

Figure 42. RA-1 and -2 orbits

(GMTI) trajectory (687,600 to 770,830 mi), a nominal first-perigee distance varying from Earth impact to 299,482 km, and nominal lifetimes varying from 45 days to over 120 days.

Further information concerning the RA-2 standard trajectory may be obtained in Reference 10.

Ranger II *actual trajectory* (Refs 11, 12). The *Ranger II* spacecraft was placed in a low-altitude Earth–satellite orbit on November 18, 1961. Launch occurred at 0312:21 EST from Complex 12 at the Atlantic Missile Range. The standard trajectory was essentially achieved up to ejection from the parking orbit. At this point, a component failure in the attitude-control system of the second-stage *Agena B* prevented *Ranger II* from achieving the required velocity increment for standard flight.

Liftoff was apparently normal. The guidance system initiated the cutoffs of the engines at near-nominal times, and the coast ellipse prior to *Atlas–Agena B* separation was within specification. The separation sequence was performed satisfactorily. After separation, the *Agena B* spacecraft vehicle exhibited instability in roll due to a failure in the *Agena B* roll gyro. Analysis of the *Agena B* flight data shows that the *Agena B* roll gyro stopped spinning between the gyro checks made at $T - 260$ min during the countdown, and the *Atlas* roll program executed shortly after liftoff.

The *Agena-B* pitch-down program, occurring shortly after *Atlas–Agena B* separation, was satisfactory, so that the *Agena-B* first burn carried the vehicle safely under the jettisoned shroud and into a nominal parking orbit. However, a high roll rate occurred during the first-burn period due to the roll gyro failure. As a result, *Agena-B* guidance gas depletion occurred shortly after the burn period. The exhaustion of guidance gas caused vehicle tumbling in all three axes.

Vehicle tumbling apparently prevented proper propellant ullage control. Engine shutdown occurred immediately after second-burn ignition, probably due to ingestion of pressurization gas. Second-burn ignition imparted approximately 6.2 m/sec impulse to the vehicle. The net loss of approximately 3176 m/sec of velocity to be gained during second burn resulted in an Earth orbit having an apogee altitude of only 146 mi.

Spacecraft separation and *Agena-B* retro-rocket firing occurred at the proper times. No 180-deg yaw maneuver was performed by the *Agena B* due to guidance gas depletion.

The characteristics of the post-injection trajectory are presented in Table 10. These are the best obtainable parameters using the Orbit Determination Program available at JPL. The final orbit of *Ranger II* will be determined by Goddard Space Flight Center, using techniques developed especially for low-altitude satellites.

Table 10 presents only one orbit since the lifetime of RA-2 was approximately 1 day. The orbit defined is representative of the first several actual passes. The decay due to drag was significant after this time.

Comparisons of standard and actual trajectory parameters are presented in Tables 11 through 15. Table 11 compares the sequence of flight events; Table 12 compares the *Atlas* coast apogee conditions; Table 13 compares the parking orbit parameters; Table 14 compares the injection conditions; and Table 15 compares the orbit parameters at injection. In general, satisfactory agreement exists, with the exception of Tables 14 and 15, which show large differences since nominal injection was not obtained. Figure 42 shows the result of the non-nominal injection.

RA-3 and -4 trajectories. The RA-3 and -4 launch dates are presented in Table 16. Changes in schedule affect the lunar missions because of the continuously changing position of the celestial bodies. The result of the schedule change of the RA-5 mission was to shift the injection locations over the Earth and to alter the flight time (and, therefore, the impact speed). RA-5 is tentatively scheduled for launch in the latter part of 1962. Specific launch dates for the RA-5 mission (and, therefore, trajectory characteristics) have not yet been determined.

RA-3 and -4 standard trajectories have been up-dated to reflect the changes in mission philosophy since the generation of the standard trajectories. The most significant changes have been the consideration of additional launch dates and the extension of launch azimuth range. In addition, the impact locations have been changed to increase the performance of the seismometer experiment.

From the experience gained during the launching of *Ranger I*, it is now evident that increased launch periods and launch windows would be of interest. This requires that all affected mission constraints be re-evaluated.

All months from January to May 1962 were considered to cover the possibility of slippage in the RA-3 and -4 launch dates. June and subsequent months are precluded because of conflict with the scheduled *Mariner-R* mission launch preparations. A launch period of 6 days encompasses all possible launch days in each lunar month under consideration. Further increase of the launch period in

CONFIDENTIAL

Table 10. Orbital parameters of *Ranger II*

August 1961	Time of injection						Epoch of pericenter passage			Period, min Apogee, mi Perigee, mi
	X R	Y ϕ	Z θ	$\dot{X}$ v	$\dot{Y}$ γ	$\dot{Z}$ σ	a e	i Ω	ω ν	
18	11-18-61, 8:33:44.302						11-18-61, 8:01:32.460			88.5274
	−0.63459188E4[a]	0.16854436E4	−0.65343558E3	−0.12939232E1	−0.64001960E1	−0.41955106E1	6579.81	33.3153	59.085	146.029
	0.65983621E4	−0.56833149E1	0.33954339E3	0.73638873E1	0.19510606E0	0.12490519E3	0.004292	336.4170	131.3020	111.231

$X, Y, Z, \dot{X}, \dot{Y}, \dot{Z}$ = a right-handed, Earth centered, equatorial, space fixed rectangular cartesian coordinate system. Z is assumed to lie along the Earth spin axis, positive north, X is normal to Z and positive in the direction of the vernal equinox, km, km/sec.

$R, \phi, \theta, v, \gamma, \sigma$ = a right-handed, Earth centered, equatorial, Earth fixed spherical coordinate system. R is from Earth center in km, ϕ is geocentric latitude measured from equatorial plane positive north in deg, θ is longitude measured eastward from the Greenwich meridian positive eastward in deg, v is Earth fixed velocity in km/sec, γ is path angle of spacecraft with respect to local horizontal in deg, σ is azimuth angle of v measured east of true north in deg.

a = semi-major axis, km.

e = eccentricity.

i = inclination of orbit plane to equatorial plane, deg.

Ω = longitude of ascending node, deg.

ω = argument of perigee, deg.

ν = true anomaly, deg.

All times are in GMT.

[a] −0.29985340E4 = −2998.5340.

CONFIDENTIAL

Table 11. Sequence of flight events

Event	Predicted time, sec	Actual time, sec
Liftoff (GMT)	0	08:12:21.502
Atlas booster cutoff	138.3	136.4
Atlas booster engine separation	—	—[b]
Start *Agena* re-start timer	249.0	253.9
Atlas sustainer cutoff	278.1	280.2
Start *Agena* primary D-timer	286.5	292.0
Atlas vernier cutoff	295.2	295.7
Nose shroud pin puller squibs *Fire*	297.5	297.7
Midbody pin pullers and retro-rockets *Fire*	300.5	300.7
Jettison horizon scanner fairing	313.0[a]	313.2
Initiate −173 deg/min pitch rate	318.0[a]	318.2
Transfer to −3.36 deg/min pitch rate	321.0[a]	321.3
Ullage rockets *Fire* (first burn)	341.0[a]	341.2
Telemeter signal acquire (Antigua, Station 9.1)	—	352.0
Gas Generator 1 *Fire* (first burn)	353.0[a]	353.0
Thrust attainment, 90% P_c (first burn)	354.5[a]	354.4
Telemeter signal loss (Cape Canaveral, Station 1)	—	473.0
Engine cutoff, 70% P_c (first burn)	506.6[a]	508.4
Burning duration (first burn)	151.7	154.0
Horizon scanner position squib *Fire*	523.0[a]	—[b]
Helium valve *Off* Squib 2 *Fire*	523.0[a]	—[b]
Stop *Agena* primary D-timer	527.0[a]	527.1
Telemeter signal loss (Antigua, Station 9.1)	—	783.0
Telemeter signal acquire (Ascension, Station 12)	—	1125.0
Re-start primary D-timer	1265.9[c]	1265.9
Ullage rockets *Fire* (second burn)	1269.9[d]	1269.9 (No. 3) 1282.7 (No. 1)
Transfer to −4.68-deg/min pitch rate	1269.9[d]	—[b]
Gas Generator 2 *Fire* (second burn)	1281.9[d]	1281.9
Thrust attainment, 90% P_c (second burn)	1283.9[d]	1282.8
Engine cutoff, 70% P_c (second burn)	1374.2[d]	1282.8
Burning duration (second burn)	90.3	0
Start telemetry calibrate	1381.9[d]	1382.4
Payload interface connector *Fire*	1526.9[d]	—[e]
Payload pin pullers *Fire*	1531.9[d]	1531.8
Agena–Ranger separation complete	—	—[e]
Initiate 180-deg/min yaw rate	1534.9[d]	1534.7
Remove yaw program	1534.9[d]	1595.0
Transfer to 5.55 deg/min pitch rate	1534.9[d]	1595.0
Telemetry signal loss (Ascension, Station 12)	—	1640.0
Retro-rocket *Fire*	1921.9[d]	—[e]

[a]Adjusted for primary D-timer start of 292.0 sec.
[b]Not available.
[c]Adjusted for re-start D-timer start of 253.9 sec.
[d]Adjusted for primary D-timer re-start of 1265.9 sec.
[e]Verification of event only.

Table 12. *Atlas* coast apogee conditions

Parameter	Predicted	G.E.-Burroughs	
		Veco + 0.5 sec	Veco + 0.1 sec
Inertial velocity, m/sec	5646.4	5650.7	5652.5
Altitude, km	185.5	185.9	184.3
Orbital inclination angle, deg	32.614	32.605	32.603

Table 13. Parking orbit parameters

Parameter	Nominal	JPL data
Perigee, km	6561.4	6502.331
ΔPerigee		59.1
Apogee, km	6575.1	6640.055
ΔApogee		−65.0
Period, min	88.3	88.354
ΔPeriod		−0.1
Eccentricity	0.00105	0.0105
ΔEccentricity		−0.00945
Apogee–perigee, km	13.7	137.724
Inclination angle, deg	32.584	33.173
Node, Ω, deg	—	336.62
Argument of perigee, ω, deg	—	54.04
Position of epoch, $\omega + \gamma_0$, deg	—	137.76
Epoch	—	November 18, 1961 $8^h\ 20^m\ 49^s$

Table 14. Injection conditions

Parameter	Predicted	Actual (first orbit)
Time from launch, sec	1373.4055	1282.8
Radius vector, km	6568.9782	6598.3621
Earth-fixed velocity, m/sec	10,587.8210	7363.8873
Earth-fixed flight path angle, deg	1.7238	0.1951
Geocentric latitude, deg	−9.0679	−5.6833
Longitude, deg	346.1921	339.543
Earth-fixed azimuth, deg	122.8447	124.9052

any lunar month would result in serious degradation of the mission objectives. A launch azimuth range of 90 to 114 deg is being considered to extend the launch window during each launch day. Firing windows based on permissible launch azimuths from 90 to 114 deg are given in Table 16.

The RA-3, -4, -5 standard trajectories might be classed as slow trajectories, in that their flight times are of the order of 66 hr. Choice of flight time is made on the basis of visibility of impact to the Goldstone Tracking Station

Table 15. Orbit parameters

Conic parameters at injection	Predicted	Actual
Twice total energy/unit mass, C_3, km^2/sec^2	−0.621,909	−60.5798
Angular momentum, C_1, km^2/sec	72,150.0	51,212.1
Semi-major axis, a, km	640,934.0	6579.81
Semi-minor axis, b, km	91,488.0	6579.75
Eccentricity, e	0.989760	0.004292
Period of revolution, min	85,104.0	88.5274
Inclination of the plane of the orbit against the equatorial plane, i, deg	32.6557	33.3153
Longitude of the ascending node, deg	325.832	336.4170
Argument of perigee, ω, deg	193.644	59.0854
Closest approach distance, km	6563.43	6551.57
Apogee distance, km	1,275,304.5	6608.04
Time from perigee passage, sec	34.82	1931.8
True anomaly, γ, deg	3.33910	131.3020

Table 16. *Ranger* launch dates and firing windows

Date	Firing window	
Ranger RA-3	90- to 114-deg launch azimuths[a]	
	h	m
January 22, 1962	2	58
January 23, 1962	2	50
January 24, 1962	2	42
January 25, 1962	2	34
January 26, 1962	2	26
January 27, 1962	2	18
Ranger RA-4	90- to 114-deg launch azimuths[a]	
	h	m
April 21, 1962	2	0
April 22, 1962	1	58
April 23, 1962	2	0
April 24, 1962	2	6
April 25, 1962	2	14
April 26, 1962	2	23

[a]The actual firing windows will be determined by the range of permissible launch azimuths determined by range safety and tracking considerations.

and guidance accuracy considerations. Injections occur about 3.3 deg past perigee of the near-Earth conic.

Previously, the RA-3 and -4 standard trajectories were designed so that the probe would descend vertically onto the lunar surface. This would give the most desirable pictures from the television experiment. These trajectories impacted approximately 42 deg from the Earth's projection on the Moon's surface, giving an acceptable Earth–Moon–probe angle for the seismometer experiment at impact. For Earth–Moon–probe angles greater than 45 deg, the seismometer antenna patterns indicate that the transmission of useful seismometer data is doubtful because librations of the Moon will cause the Earth–Moon–probe angle to vary after lunar impact. A typical result is shown in Figure 43. Clearly the Earth–Moon–probe angle is undesirable for large portions of the lunar month after impact.

The impact locations can be biased from the vertical impact locations to minimize the Earth–Moon–probe

Table 17. *Ranger* RA-3 and -4 trajectories

Mission	Launch conditions			Injection conditions			Impact conditions		
	Date, 1962	Azimuth, deg	GMT, hr	Geocentric latitude, deg	Geocentric longitude, deg	GMT, hr	Selenocentric latitude, deg	Selenocentric longitude, deg	Unretarded velocity, m/sec
RA-3	1-22	90	14.59	−10.5	21.6	15.11	−2.3	329.3	2684.9
		114	17.56	−11.5	339.5	17.93	−3.0	328.6	2692.2
	1-23	90	15.83	−6.4	14.0	16.32	−3.4	327.5	2684.9
		114	18.67	−7.4	333.8	19.01	−4.0	326.9	2692.2
	1-24	90	17.07	−2.1	355.4	17.52	−4.7	326.1	2684.8
		114	19.77	−3.1	328.3	20.08	−5.3	325.5	2692.2
	1-25	90	18.32	2.1	359.3	18.73	−5.8	325.0	2684.8
		114	20.88	1.0	323.0	21.16	−6.5	324.4	2692.2
	1-26	90	19.58	6.1	352.3	19.96	−6.7	324.2	2684.7
		114	22.00	4.9	317.9	22.25	−7.4	323.6	2692.2
	1-27	90	20.84	9.6	345.8	21.19	−7.2	323.9	2684.7
		114	23.12	8.3	313.4	23.35	−8.0	323.3	2692.1
RA-3 alt	2-21	90	16.10	0.6	1.8	16.52	−5.6	326.0	2684.9
		114	18.71	−0.4	324.8	19.00	−6.2	325.3	2692.1

Table 17. *Ranger* RA-3 and -4 trajectories (cont'd)

Mission	Launch conditions			Injection conditions			Impact conditions		
	Date, 1962	Azimuth, deg	GMT, hr	Geocentric latitude, deg	Geocentric longitude, deg	GMT, hr	Selenocentric latitude, deg	Selenocentric longitude, deg	Unretarded velocity, m/sec
	2-22	90	17.34	4.6	354.8	17.73	−6.5	325.1	2684.9
		114	19.81	3.5	319.7	20.07	−7.2	324.5	2692.0
	2-23	90	18.58	8.3	348.2	18.94	−7.1	324.6	2684.9
		114	20.91	7.1	315.1	21.15	−7.8	324.1	2692.0
	2-24	90	19.81	11.4	342.4	20.14	−7.2	324.4	2684.9
		114	22.00	10.0	311.2	22.22	−8.1	323.8	2691.9
	2-25	90	20.99	13.7	337.8	21.30	−7.0	324.4	2685.0
		114	23.06	12.1	308.3	23.26	−8.1	323.9	2691.6
	2-26	90	22.05	14.9	335.3	22.35	−6.5	324.6	2685.3
		114	24.05	13.2	306.8	24.24	−7.6	324.2	2691.2
RA-3 alt	3-23	90	17.74	11.0	343.2	18.07	−7.4	324.3	2670.2
		114	19.96	9.6	311.7	20.18	−8.2	323.7	2676.9
	3-24	90	18.92	13.5	338.3	19.23	−7.2	324.3	2670.2
		114	21.01	11.9	308.5	21.22	−8.2	323.8	2676.6
	3-25	90	20.00	15.0	335.2	20.30	−6.7	324.3	2670.4
		114	22.01	13.3	306.6	22.20	−7.9	323.9	2676.2
	3-26	90	20.92	15.3	334.6	21.21	−6.0	324.5	2670.6
		114	22.90	13.4	306.3	23.09	−7.2	324.2	2675.6
	3-27	90	21.64	14.2	336.8	21.95	−5.1	324.8	2670.9
		114	23.67	12.4	307.9	23.87	−6.3	324.6	2675.1
	3-28	90	22.18	11.9	341.5	22.51	−4.0	325.3	2671.0
		114	24.33	10.0	311.1	24.54	−5.2	325.2	2674.5
RA-4	4-21	90	18.05	15.3	334.5	18.35	−7.1	323.3	2648.4
		114	20.06	13.7	306.0	20.25	−8.2	322.8	2654.1
	4-22	90	19.01	15.8	333.4	19.30	−6.7	323.7	2648.6
		114	20.97	14.1	305.4	21.16	−8.0	323.3	2653.6
	4-23	90	19.76	15.0	335.0	20.06	−5.7	323.9	2648.9
		114	21.76	13.2	306.6	21.96	−7.0	323.7	2653.0
	4-24	90	20.33	13.0	339.3	20.64	−4.7	324.2	2649.1
		114	22.42	11.2	309.5	22.63	−5.9	324.1	2652.5
	4-25	90	20.74	9.9	345.3	21.09	−3.4	324.7	2649.2
		114	22.98	8.1	313.7	23.21	−4.6	324.6	2652.2
	4-26	90	21.06	5.8	352.7	21.44	−2.0	325.3	2649.4
		114	23.45	4.1	319.0	23.71	−3.0	325.3	2651.9
RA-4 alt	5-21	90	18.50	14.0	337.2	18.81	−4.9	322.7	2625.3
		114	20.56	12.3	307.9	20.76	−6.2	322.6	2628.6
	5-22	90	18.94	11.1	343.1	19.27	−3.8	323.3	2625.4
		114	21.13	9.4	312.0	21.36	−5.0	323.3	2628.2
	5-23	90	19.26	7.2	350.3	19.63	−2.4	324.0	2625.5
		114	21.61	5.5	317.2	21.86	−3.5	324.0	2627.9
	5-24	90	19.52	2.7	358.2	19.93	−1.5	324.8	2625.6
		114	22.02	1.0	323.0	22.30	−2.6	324.9	2627.8
	5-25	90	19.75	−2.2	6.6	20.20	0.2	325.6	2625.6
		114	22.40	−3.9	329.3	22.72	−0.8	325.7	2627.7
	5-26	90	19.96	−7.1	15.3	20.45	1.5	326.6	2625.6
		114	22.77	−8.8	335.8	23.12	0.5	326.8	2627.8

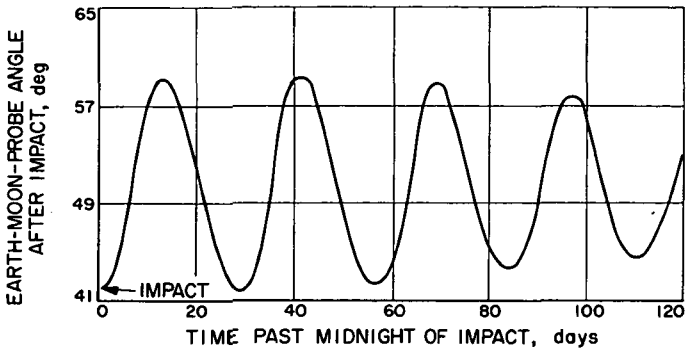

Figure 43. Effects of lunar libration on Earth–Moon–probe angle after impact

angle after lunar impact. These biased trajectories result in an unretarded velocity vector at lunar impact which is canted to the local vertical. This degrades the pictures from the television experiment.

Tradeoffs between the seismometer and television experiments were considered and a bias angle of 14 deg (Fig 44) was selected as a compromise. This bias angle gives an unretarded velocity vector at impact which is canted 10 deg from the local vertical. A bias angle of 14 deg is used in the up-dated RA-3 and -4 trajectories.

Some of the characteristics of the RA-3 and -4 up-dated standard trajectories are presented in Table 17 for all of the launch dates under consideration. Additional trajectory characteristics are presented in Tables 18 and 19 for the first and sixth launch days of the RA-3 and -4 missions, for January and April launch periods, respectively. The injection locations for launch periods in January and April are shown in Figures 45 and 46 for RA-3 and -4 trajectories of 90- to 114-deg launch azimuths, for the 6 successive days on which firings are considered. Each line represents the burning of the last stage.

The coordinates of injection are all relative to a rotating Earth, except the inertial speed. Latitudes are

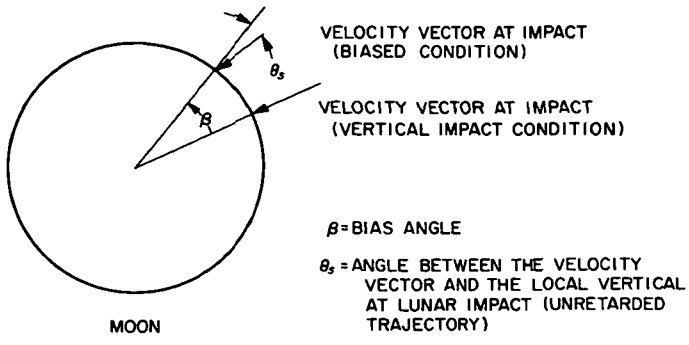

Figure 44. Lunar impact parameters

Table 18. *Ranger* trajectory conditions

Conditions	Launch azimuth, 90 deg			
	First launch day		Sixth launch day	
	RA-3	RA-4	RA-3	RA-4
Injection				
GMT, hr	15.1114	18.3461	21.1878	21.4442
Time after launch, sec	1882.54	1056.29	1247.98	1369.34
Radius, m	6569620	6568870	6569107	6569178
Speed, m/sec	10549.7	10534.4	10540.6	10530.5
Path angle, deg	1.754	1.748	1.752	1.744
Azimuth angle, deg	117.632	115.207	117.960	119.015
Latitude (geocentric), deg	−10.518	15.279	9.637	5.841
Longitude, deg	21.588	334.525	345.79	352.695
Speed (inertial), m/sec	10969.0	10954.1	10959.8	10949.5
Impact				
GMT, hr	9.2400	12.9153	13.6280	11.9815
Geocentric				
Latitude, deg	4.784	−19.686	−14.826	−11.504
Longitude, deg	274.234	220.631	264.061	300.344
Selenographic				
Latitude, deg	−2.308	−7.082	−7.186	−1.983
Longitude, deg	329.342	323.267	323.893	325.286
Earth–Moon–probe angle, deg	28.012	30.648	28.505	31.376
Flight time (from injection), hr	66.1285	66.5692	64.4404	62.5373
Speed (impact), m/sec	2684.1	2648.4	2684.0	2649.4
Lighting angle, deg	22.279	22.486	79.796	71.723

geocentric, path angle is measured from the geocentric local horizontal plane, and azimuth angle is measured in the geocentric local horizontal plane eastward from true north. Longitude is measured positive east of Greenwich. The Earth–Moon–probe angle indicates the impact location on the lunar surface since it is, in a sense, a measure of the impact lunar longitude referenced to the Earth–Moon line. Impact occurs approximately on the Moon's equator. Selenographic coordinates of the probe at impact are defined in Figure 47. (The selenographics of the true Moon–Earth line are time variant and are tabulated in "The American Ephemeris and Nautical Almanac.") The selenographic longitude λ and latitude μ, respectively, for the point P on the Moon's surface, are shown in the positive directions. The lighting angle is the angle between the Moon–Sun line and the impact vertical and indicates the time of impact during the lunar afternoon.

Table 19. *Ranger* trajectory conditions

Conditions	Launch azimuth, 114 deg			
	First launch day		Sixth launch day	
	RA-3	RA-4	RA-3	RA-4
Injection GMT, hr	17.9167	20.2474	23.35	23.7089
Time after launch, sec	1332.35	688.39	827.59	935.77
Radius, m	6567970	6568314	6568320	6568226
Speed, m/sec	10585.1	10569.1	10575.4	10565.4
Path angle, deg	1.721	1.718	1.720	1.712
Azimuth angle, deg	125.499	124.739	126.357	127.054
Latitude (geocentric), deg	−11.531	13.678	8.348	4.096
Longitude, deg	339.541	306.011	313.427	319.027
Speed (inertial), m/sec	10970.4	10954.6	10960.4	10950.3
Impact GMT, hr	12.0678	14.8368	15.7064	14.1985
Geocentric Latitude, deg	4.321	−19.776	−15.086	−11.122
Longitude, deg	233.021	192.838	233.938	268.300
Selenographic Latitude, deg	−2.948	−8.180	−7.979	−3.035
Longitude, deg	328.636	322.799	323.340	325.320
Earth–Moon–probe angle, deg	28.514	31.176	29.043	31.629
Flight time (from injection), hr	66.1358	66.5894	64.3563	62.4896
Speed (impact), m/sec	2691.4	2654.1	2691.4	2651.9
Lighting angle, deg	23.078	23.246	80.314	85.496

b. Injection guidance analysis. A statistical description of the coordinate deviations at injection is necessary to determine the midcourse correction capability needed to assure the desired lunar landing. An analysis of the *Atlas–Agena* injection guidance system was made to determine this information for the *Ranger* trajectories.

The analysis was carried on as follows:

(1) The 1-σ value of each independent error source and the sensitivity of injection coordinates to these errors were obtained from Lockheed Missile and Space Division.

(2) The 1-σ injection coordinate deviations were then obtained.

(3) This information was used to form a noise moment matrix (covariance matrix I) of injection coordinate deviations.

(4) This matrix, Λ^I, was used to calculate the target miss components in the absence of midcourse guidance.

(5) The Λ^I matrix was also used to compute the rms midcourse velocity capability needed for each flight.

(6) A units-of-variance analysis was performed to obtain the relative effect of each error on the midcourse maneuver.

Determination of injection errors. The following sequence of events occurs prior to the spacecraft injection (Fig 70):

(1) The *Atlas* burning interval gives the spacecraft less energy than the circular parking orbit requires.

(2) After a short coast, the *Agena* ignites and injects the spacecraft into a parking orbit.

(3) The *Agena* is re-ignited at the proper time to obtain the desired injection position, attitude, and velocity.

In the cases considered here, nonstandard trajectories have two important characteristics: (1) The source of error is a random quantity with zero mean. (2) The trajectories which are in error differ only slightly from the standard, so that linear perturbation theory may be used to calculate deviations.

Let the column matrix δE be the values of the independent random errors δe_j.

$$\delta E = \begin{bmatrix} \delta e_1 \\ \delta e_2 \\ \cdot \\ \cdot \\ \cdot \\ \delta e_n \end{bmatrix}$$

The first-order sensitivity of the six coordinates X, R, V, Γ, W, and $\dot{W}$ with respect to the errors δe_j may be written in matrix form as

$$A = \begin{bmatrix} \frac{\partial X}{\partial e_1} & \frac{\partial X}{\partial e_2} & \cdots & \frac{\partial X}{\partial e_n} \\ \frac{\partial R}{\partial e_1} & \frac{\partial R}{\partial e_2} & \cdots & \frac{\partial R}{\partial e_n} \\ \cdots & \cdots & \cdots & \cdots \\ \frac{\partial \dot{W}}{\partial e_1} & \frac{\partial \dot{W}}{\partial e_2} & \cdots & \frac{\partial \dot{W}}{\partial e_n} \end{bmatrix}$$

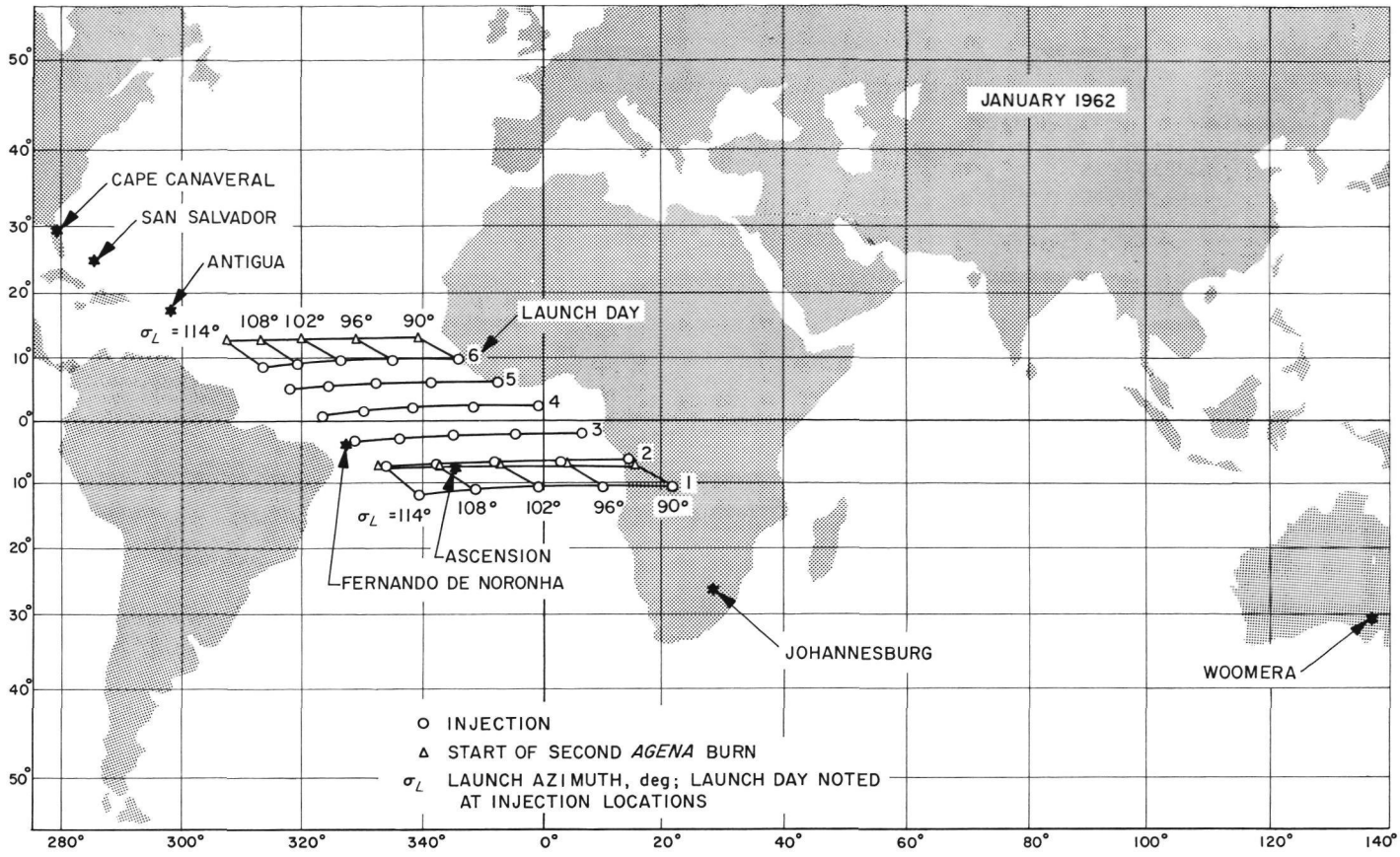

Figure 45. RA-3 injection locations

The δE-matric and the A-matric were obtained from Lockheed Missiles and Space Division. The first-order coordinate deviation at injection into the parking orbit (noted by subscript 1) is

$$\delta Z_1 \equiv \begin{bmatrix} \delta X \\ \delta R \\ \delta V \\ \delta \Gamma \\ \delta W \\ \delta \dot{W} \end{bmatrix}_1 = A_1 \, \delta E$$

The injection coordinate errors due to the *Agena* second burn (noted by subscript 2) are assumed to be independent of the preceding errors and of the parking-orbit duration; thus

$$\delta Z_2 = A_2 \, \delta E$$

By mapping the errors at injection into the parking orbit to the start of the last burn (Fig 48) by B,

$$B = \begin{bmatrix} 1 & \frac{R_0}{R_1}(2\sin\rho - 3\rho) & \frac{R_0}{V_1}(4\sin\rho - 3\rho) & -2R_0(1-\cos\rho) & 0 & 0 \\ 0 & (2-\cos\rho) & \frac{2R_1}{V_1}(1-\cos\rho) & R_1\sin\rho & 0 & 0 \\ 0 & -\frac{V_1}{R_1}(1-\cos\rho) & (2\cos\rho - 1) & -V_1\sin\rho & 0 & 0 \\ 0 & \frac{\sin\rho}{R_1} & \frac{2\sin\rho}{V_1} & \cos\rho & 0 & 0 \\ 0 & 0 & 0 & 0 & \cos\rho & \frac{R_1}{V_1}\sin\rho \\ 0 & 0 & 0 & 0 & -\frac{V_1}{R_1}\sin\rho & \cos\rho \end{bmatrix}$$

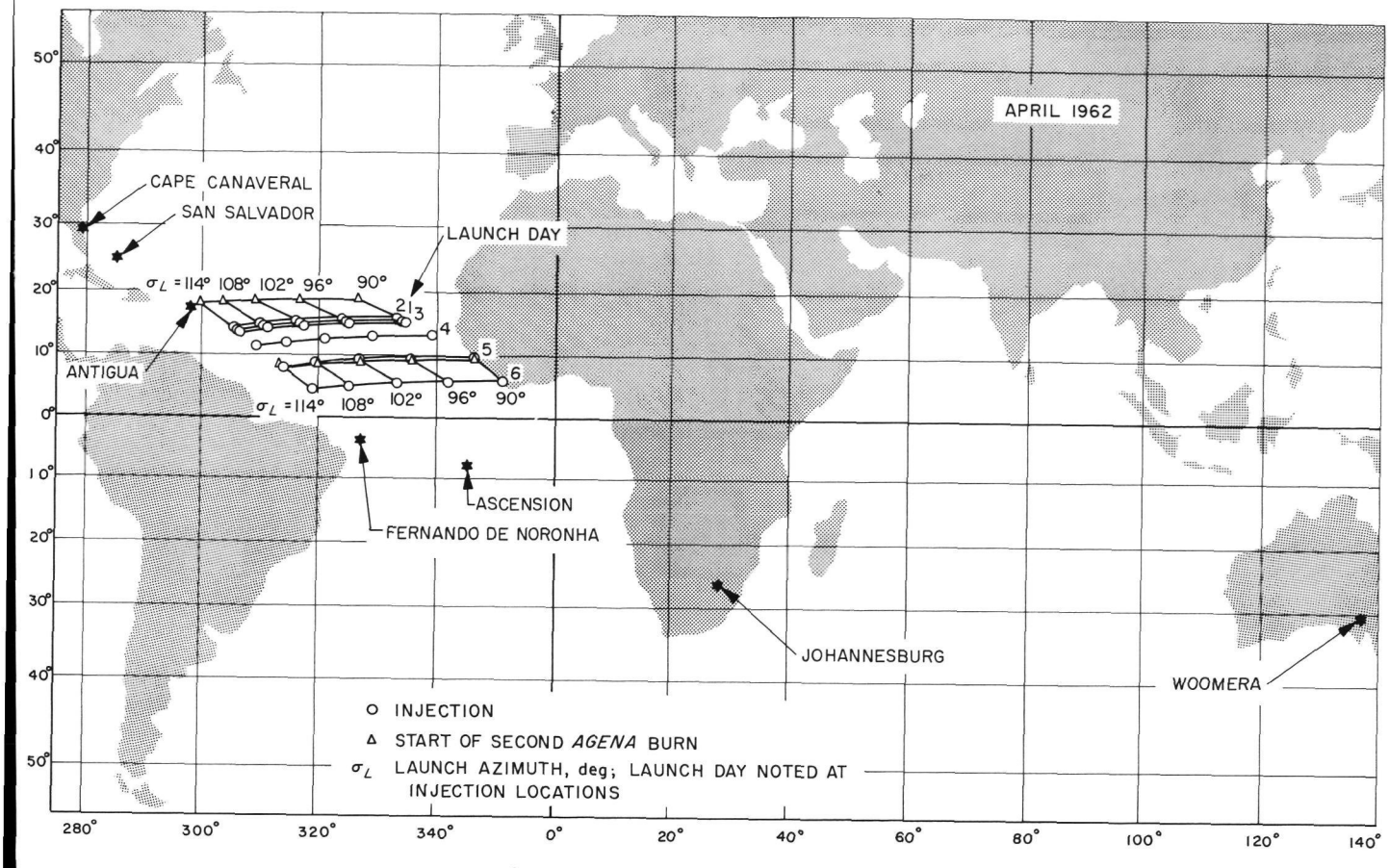

Figure 46. RA-4 injection locations

and then through the last burn by C,

$$C = \begin{bmatrix} \frac{\delta X_2}{\delta X} & \frac{\delta X_2}{\delta R} & \frac{\delta X_2}{\delta V} & \frac{\delta X_2}{\delta \Gamma} & 0 & 0 \\ 0 & \frac{\delta R_2}{\delta R} & \frac{\delta R_2}{\delta V} & \frac{\delta R_2}{\delta \Gamma} & 0 & 0 \\ 0 & \frac{\delta V_2}{\delta R} & \frac{\delta V_2}{\delta V} & \frac{\delta V_2}{\delta \Gamma} & 0 & 0 \\ 0 & \frac{\delta \Gamma_2}{\delta R} & \frac{\delta \Gamma_2}{\delta V} & \frac{\delta \Gamma_2}{\delta \Gamma} & 0 & 0 \\ 0 & 0 & 0 & 0 & \frac{\delta W_2}{\delta W} & \frac{\delta W_2}{\delta \dot{W}} \\ 0 & 0 & 0 & 0 & \frac{\delta \dot{W}_2}{\delta W} & \frac{\delta \dot{W}_2}{\delta \dot{W}} \end{bmatrix}$$

the injection coordinate deviations are obtained.

$$\delta Z = CB\delta Z_1 + \delta Z_2$$

Statistical description of injection errors. Having obtained a set of injection deviations corresponding to N different random component errors, one can form a noise moment matrix of injection errors which statistically describes the injection errors. To do this, form the product

$$\delta Z \delta Z^T = (CBA_1 + A_2)\, \delta E \delta E^T\, (CBA_1 + A_2)^T$$

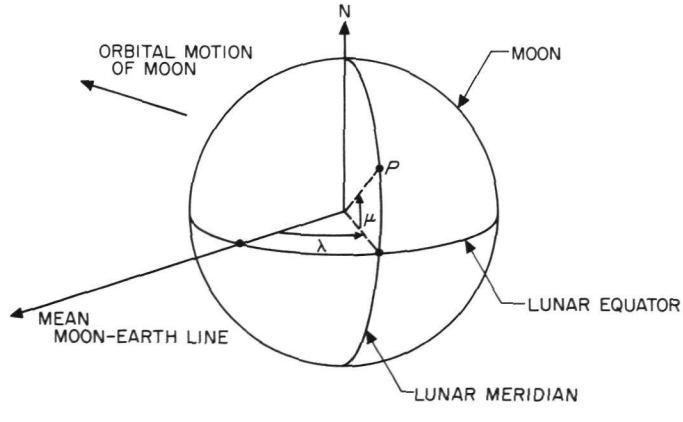

Figure 47. Selenographic coordinates

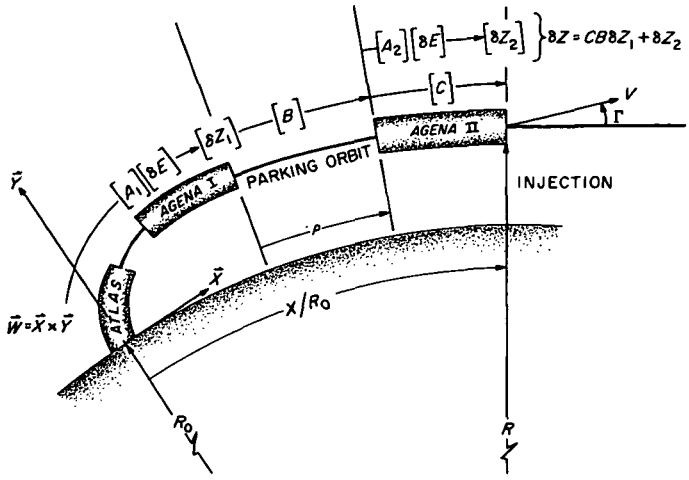

Figure 48. Launch to injection

where δZ^T is the transpose of δZ. The ensemble average is now taken of all terms in the matrices.

$$\overline{\delta Z \delta Z^T} = (CBA_1 + A_2)\,\overline{\delta E \delta E^T}\,(CBA_1 + A_2)^T$$

or

$$\Lambda^I = (CBA_1 + A_2)\,\Lambda^E\,(CBA_1 + A_2)^T$$

where the $(n \times n)$ symmetric matrix $\overline{\delta E\, \delta E^T}\,(= \Lambda^E)$ is the moment matrix of the independent error sources

$$\Lambda^E = \begin{bmatrix} \sigma_{e_1}^2 & 0 & 0 & 0 & \cdots \\ 0 & \sigma_{e_2}^2 & 0 & 0 & \cdots \\ 0 & 0 & \sigma_{e_3}^2 & 0 & \cdots \\ & & \cdot & & \\ & & \cdot & & \\ & & \cdots\ \sigma_{n-1}^2 & 0 & \\ & & & 0 & \sigma_n^2 \end{bmatrix}$$

and the noise moment matrix of injection coordinate errors, Λ^I, is of the form

$$\Lambda^I = \begin{bmatrix} \sigma_X^2 & \rho_{XR}\sigma_X\sigma_R & \rho_{XV}\sigma_X\sigma_V & \rho_{X\Gamma}\sigma_X\sigma_\Gamma & 0 & 0 \\ & \sigma_R^2 & \rho_{RV}\sigma_R\sigma_V & \rho_{R\Gamma}\sigma_R\sigma_\Gamma & 0 & 0 \\ & & \sigma_V^2 & \rho_{V\Gamma}\sigma_V\sigma_\Gamma & 0 & 0 \\ & & & \sigma_\Gamma^2 & 0 & 0 \\ & (Symmetric) & & & \sigma_{\hat{W}}^2 & \rho_{\hat{W}\dot{\hat{W}}}\sigma_{\hat{W}}\sigma_{\dot{\hat{W}}} \\ & & & & & \sigma_{\dot{\hat{W}}}^2 \end{bmatrix}$$

where σ_X is the rms injection error in X and ρ_{XR} is the coefficient of cross-correlation between X and R, etc. The coefficient $\rho = \pm 1$ for perfectly correlated variables and $\rho = 0$ for uncorrelated variables. The standard coordinate deviations and their correlations are given in Table 20 for a representative trajectory.

Uncorrected miss components at the target. A convenient system for expressing miss distances at the Moon resulting from injection coordinate deviations is one which defines two components of a miss vector to be normal to the asymptote of the standard approach hyperbola. Such a miss vector is independent of the transit time, which, in turn, is chosen as the third miss coordinate.

A U-matrix is now defined, having elements which are the first-order differential coefficients of each of the miss components with respect to each of the coordinate deviations at injection. Denoting the two components of the miss vector by M_1 and M_2 and the flight time by t_f, the U-matrix is given by

$$U = \begin{bmatrix} \frac{\delta M_1}{\delta X} & \frac{\delta M_1}{\delta R} & \cdots & \frac{\delta M_1}{\delta \dot{\hat{W}}} \\ \frac{\delta M_2}{\delta X} & \frac{\delta M_2}{\delta R} & \cdots & \frac{\delta M_2}{\delta \dot{\hat{W}}} \\ \frac{\delta t_f}{\delta X} & \frac{\delta t_f}{\delta R} & \cdots & \frac{\delta t_f}{\delta \dot{\hat{W}}} \end{bmatrix}$$

When the noise moment matrix Λ^I is multiplied by U and the transpose of U, a 3×3 B-matrix results as follows:

$$B = U\Lambda^I U^T = \begin{bmatrix} \sigma_{M_1}^2 & \rho_{1,2}\sigma_{M_1}\sigma_{M_2} & \rho_{1t_f}\sigma_{M_1}\sigma_{t_f} \\ (Symmetric) & \sigma_{M_2}^2 & \rho_{2t_f}\sigma_{M_2}\sigma_{t_f} \\ & & \sigma_{t_f}^2 \end{bmatrix}$$

Table 20. Standard coordinate deviations and correlations for representative RA-3 trajectory

Parameter	Representative value
σ_X, km	9.69
σ_R, km	7.57
σ_V, m/sec	8.70
σ_Γ, mrad	1.39
σ_W, km	24.79
$\sigma_{\hat{W}}$, m/sec	56.67
ρ_{XR}	−0.975
ρ_{XV}	0.972
$\rho_{X\Gamma}$	−0.869
ρ_{RV}	−0.991
$\rho_{R\Gamma}$	0.918
$\rho_{V\Gamma}$	−0.905
$\rho_{W\dot{W}}$	0.585

The 1-σ flight-time error is the square root of $\sigma_{t_f}^2$. A rotation of the $M_1 - M_2$ axes which makes $\rho_{M_1M_2}$ equal to zero, yields a new matrix, B', as follows:

$$B' = \begin{bmatrix} \sigma_{M'_1}^2 & 0 \\ 0 & \sigma_{M'_2}^2 \end{bmatrix}$$

where the semi-major and semi-minor axes of the 1-σ error ellipse are the square roots of the diagonal terms. These values are given for a representative trajectory in Table 21.

The miss components M_1 and M_2 used in the U-matrices for these calculations nearly represent miss distances at a massless target. The actual miss distances would be about 30% smaller than indicated.

Units of variance analysis for the midcourse maneuver. The statistically averaged magnitude of midcourse maneuver can be found once the noise moment matrix of injection coordinate deviations, the time of the maneuver, and the sensitivity of the target miss components with the maneuver are known. A units-of-variance analysis is performed to determine the relationship between the variance of the magnitude of the maneuver and the variances of the individual injection error sources.

A K-matrix is defined, having elements which are first-order differential coefficients of each of the miss components with respect to mutually orthogonal midcourse maneuver velocity components V_1, V_2, and V_3.

$$K = \begin{bmatrix} \frac{\delta M_1}{\delta V_1} & \frac{\delta M_1}{\delta V_2} & \frac{\delta M_1}{\delta V_3} \\ \frac{\delta M_2}{\delta V_1} & \frac{\delta M_2}{\delta V_2} & \frac{\delta M_2}{\delta V_3} \\ \frac{\delta t_f}{\delta V_1} & \frac{\delta t_f}{\delta V_2} & \frac{\delta_{t_f}}{\delta V_3} \end{bmatrix}$$

The sensitivity coefficient of the velocity components with the individual injection errors follows as

$$K^{-1}U(CBA_1 + A_2) = \begin{bmatrix} \frac{\delta V_1}{\delta e_1} & \frac{\delta V_1}{\delta e_2} & \cdots & \frac{\delta V_1}{\delta e_n} \\ \frac{\delta V_2}{\delta e_1} & \frac{\delta V_2}{\delta e_2} & \cdots & \frac{\delta V_2}{\delta e_n} \\ \frac{\delta V_3}{\delta e_1} & \frac{\delta V_3}{\delta e_2} & & \frac{\delta V_3}{\delta e_n} \end{bmatrix}$$

from which the first-order sensitivity coefficients of the total velocity increment, p_j, can be found.

$$p_j = \left[\left(\frac{\delta V_1}{\delta e_1}\right)^2 + \left(\frac{\delta V_2}{\delta e_1}\right)^2 + \left(\frac{\delta V_3}{\delta e_1}\right)^2\right]^{1/2}$$

Table 21. Uncorrected 1-σ target miss for representative RA-3 trajectory

Parameter	Representative value
Semi-major axis, km[a]	2332
Semi-minor axis, km[a]	1205
Time-of-flight error, hr	0.32

[a]These dimensions represent the ellipse in a plane perpendicular to the incoming asymptote, such that there is a 40% probability that the spacecraft will pass through the ellipse.

Since the individual error sources are uncorrelated, it follows that the variance of the midcourse maneuver is

$$\sigma_V^2 = \sum_{j=1}^{N} p_j^2 \sigma_{e_j}^2 \qquad j = 1, 2, 3, \cdots, N$$

The number of units of variance of the maneuver will be defined as 100 times the ratio of the actual variance to a figure of merit, FOM, where the FOM can be thought of as a "design standard deviation." The units of variance, UOV, given in percent is

$$UOV = \frac{\sigma_V^2}{(FOM)^2} 100$$

The units of variance for each error source is

$$UOV_j = \frac{100}{(FOM)^2} p_j^2 \sigma_{e_j}^2$$

Representative values for the sensitivity coefficients, p_j, and the corresponding units of variance (assuming $FOM = \sigma_V$) are given in Table 22.

c. Midcourse guidance. In developing the theory of midcourse maneuvers, we assume that the injection guidance system is accurate enough so that we may use linear perturbation theory with the preflight standard trajectory as the reference trajectory. This approximation is sufficiently accurate for engineering design of the system. In computing the exact maneuver during an actual flight, iterative schemes are used to refine the linear approximation.

In developing the basic theory of midcourse maneuvers, let the position and velocity coordinates of the spacecraft on a ballistic trajectory at some initial time, t_b, be denoted by $q_i, i = 1, \cdots, 6$. Let the difference in the coordinates on the actual and standard trajectory be denoted by Δq_i. Let $m_j, j = 1, 2$ be the miss components at some terminal time, t_f. Taking only first order terms of a generalized Taylor expansion

$$m_j = \frac{\partial m_j}{\partial q_i} \Delta q_i \qquad (1.1)$$

Table 22. Representative units-of-variance for RA-3 midcourse maneuver

Description of error source and dimension of p_j	Sensitivity coefficients (p_j)		Units of variance for miss and flight time correction, %
	Nature of midcourse correction		
	Miss components only	Miss and flight time	
(1) *Agena* angular offset in pitch plane, first burn, m/sec/rad	2,134	3,737	(See error No. 3)
(2) *Agena* angular offset in pitch plane, second burn, m/sec/rad	1,312	1,479	(See error No. 3)
(3) *Agena* angular offset in pitch plane, both burns, m/sec/rad	2,588	3,473	31.9
(4) *Agena* angular offset in yaw plane, both burns, m/sec/rad	438	559	3.8
(5) Vibration insensitive yaw drift, m/sec/rad/sec	7,817	31,079	0.02
(6) Vibration sensitive yaw drift, m/sec/rad/sec	2,898	3,534	0.0001
(7) *Agena* accelerometer bias, m/sec/m/sec^2	890	1,445	0.26
(8) *Agena* accelerometer scale factor, m/sec/%	214	348	1.02
(9) *Agena* first burn start time, m/sec/sec	4.50	7.92	0.98
(10) *Agena* second burn start time, m/sec/sec	2.89	3.94	0.78
(11) *Agena* first burn tail-off impulse, m/sec/lb sec	0.00489	0.00785	2.34
(12) *Agena* second burn tail-off impulse, m/sec/lb sec	0.0190	0.0311	36.8
(13) *Agena* specific impulse, m/sec/sec	1.13	2.00	1.47
(14) *Agena* propellant flow rate, m/sec/lb sec	6.91	10.27	15.4
(15) *Agena* empty weight, m/sec/lb	0.0202	0.0277	0.008
(16) All *Atlas* errors, m/sec/m/sec	3.36	5.34	5.22

where the repeated subscript implies summation. In addition to the six coordinate perturbations at t_b, let a further perturbation be added at t_g in the form of an impulse of velocity with orthogonal components $v_k, k = 1, 2, 3$. The miss components due to the maneuver alone are

$$m'_j = \frac{\partial m_j}{\partial v_k} v_k \tag{1.2}$$

Requiring that the velocity impulse correct for the original perturbations,

$$m'_j + m_j = 0 \tag{1.3}$$

or

$$m'_j = -\frac{\partial m_j}{\partial v_k} v_k \tag{1.4}$$

The partial derivatives can be computed on the standard trajectory for any given t_f and t_g. The miss, m_j, can be predicted from radio tracking observations of the orbit. Thus, the correcting velocity impulse can be computed from Equation (1.4).

We now refine some of the ideas in the last paragraph. Denoting the correcting velocity vector by $\bar{v}$, Equation (1.2) is rewritten as

$$\begin{aligned} m_1 &= \bar{v} \cdot \bar{\lambda}_1 \\ m_2 &= \bar{v} \cdot \bar{\lambda}_2 \end{aligned} \tag{1.5}$$

Vectors $\bar{\lambda}_1$ and $\bar{\lambda}_2$ are the gradient vectors of m_1 and m_2, respectively. The components of these gradient vectors are the partial derivatives in Equation (1.2). To find m_1 and m_2, project $\bar{v}$ onto the $\bar{\lambda}_1$ and $\bar{\lambda}_2$ vectors shown in Figure 49. Conversely, to find the v which will produce a certain m_1, construct a plane normal to $\bar{\lambda}_1$ and intersecting it at a distance $m_1/|\bar{\lambda}_1|$ from the origin. Repeating this procedure for the desired value of m_2, the two planes intersect in a line, L, which is normal to the plane containing $\bar{\lambda}_1$ and $\bar{\lambda}_2$. Any $\bar{v}$ terminating on L will produce the desired m_1 and m_2.

Since Equation (1.5) determines only a line in v_k space, there is 1 degree of freedom which may be used for one of the following:

(1) To minimize the magnitude of the correction, v.

(2) To control an additional terminal variable such as time, t_f, or speed of arrival, v_f.

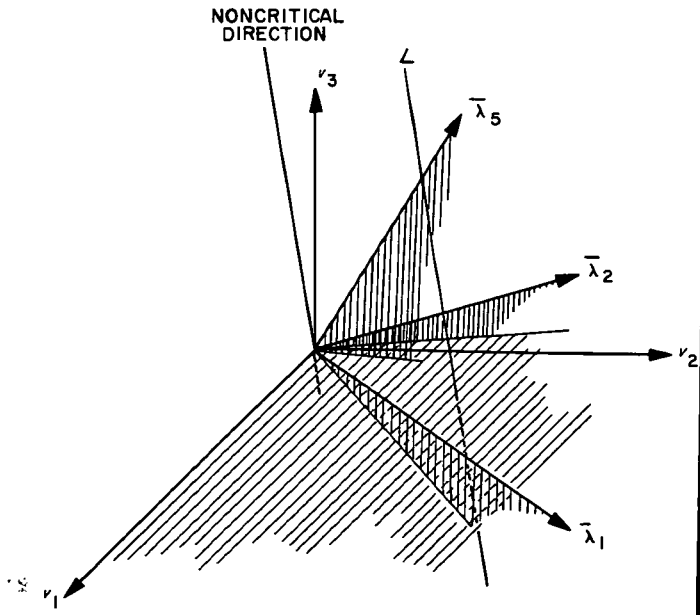

Figure 49. Gradient vectors of miss components

Consider Option (1), in which it is desired to minimize v subject to the constraints of Equation (1.5). The magnitude of $\overline{v}$ will be a minimum when $\overline{v}$ is normal to L or in the plane of $\overline{\lambda}_1$ and $\overline{\lambda}_2$. For this reason, the plane of $\overline{\lambda}_1$ and $\overline{\lambda}_2$ is called the critical plane and the normal to this plane is called the non-critical direction. Thus, for Option (1),

$$\overline{v} \cdot (\overline{\lambda}_1 \times \overline{\lambda}_2) = 0 \tag{1.6}$$

Combining Equations (1.5) and (1.6),

$$m = K_1 v \tag{1.7}$$

where $(m)^T = (m_1, m_2, 0)$, $v^T = (v_1, v_2, v_3)$ and the superscript T denotes transpose. Matrix K_1 is given by

$$K_1 = \begin{bmatrix} \frac{\partial m_1}{\partial v_1} & \frac{\partial m_1}{\partial v_2} & \frac{\partial m_1}{\partial v_3} \\ \frac{\partial m_2}{\partial v_1} & \frac{\partial m_2}{\partial v_2} & \frac{\partial m_2}{\partial v_3} \\ k_1 & k_2 & k_3 \end{bmatrix} \tag{1.8}$$

where k_1, k_2, k_3 are the direction cosines of $(\overline{\lambda}_1 \times \overline{\lambda}_2)$. Using Equation (1.3) and inverting

$$v = -K^{-1} m' \tag{1.9}$$

where $(m')^T = (m_1', m_2', 0)$. Equation (1.9) gives the three components of the correcting impulse in terms of the radio tracking estimates of the miss components.

For Option (2) we wish to null the variation in some other terminal variable, e.g., time of flight, t_f, or impact speed, v_f. We obtain the following equation analogous to Equation (1.5).

$$t_f = \overline{v} \cdot \overline{\lambda}_f \tag{1.10}$$

where $\overline{\lambda}_f$ is the gradient vector of t_f. Proceeding as before

$$v = -K_2^{-1} m' \tag{1.11}$$

where $(m')^T = (m_1', m_2', t_f')$. Note that vector m' is defined differently for the two options. Matrix K_2 is given by

$$K_2 = \begin{bmatrix} \frac{\partial m_1}{\partial v_1} & \frac{\partial m_1}{\partial v_2} & \frac{\partial m_1}{\partial v_3} \\ \frac{\partial m_2}{\partial v_1} & \frac{\partial m_2}{\partial v_2} & \frac{\partial m_2}{\partial v_3} \\ \frac{\partial t_f}{\partial v_1} & \frac{\partial t_f}{\partial v_2} & \frac{\partial t_f}{\partial v_3} \end{bmatrix} \tag{1.12}$$

When the correcting velocity is confined to a plane, e.g., the critical plane, it is convenient to transform v_k to rectangular components in the plane and normal to it. Let the new velocity axes be $u_k, k = 1, 2, 3$, with u_3 in the $(\lambda_1 \times \lambda_2)$ direction and u_2 in the v_1, v_2 plane. Then

$$v = G u \tag{1.13}$$

where $u^T = (u_1, u_2, u_3)$ and the rotation matrix G is given by

$$G = \begin{bmatrix} \frac{k_1 k_3}{k} & -\frac{k_2}{k} & k_1 \\ \frac{k_2 k_3}{k} & \frac{k_1}{k} & k_2 \\ -k & 0 & k_3 \end{bmatrix} \tag{1.14}$$

where $k = (k_1^2 + k_2^2)^{1/2}$.

We now compute the velocity components for Option (1) in the rotated system. Equation (1.7) becomes

$$m = K_1 G u \tag{1.15}$$

where $u^T = (u_1, u_2, 0)$ since the correction is restricted to the critical plane. Equation (1.15) is re-written as

$$m = Q_1 u \tag{1.16}$$

where $m^T = (m_1, m_2)$, $u^T = (u_1, u_2)$ and Q_1 is obtained from $K_1 G$ by omitting the third row and column. Applying Equation (1.3), the required velocity components are

$$u = -Q_1^{-1} m' \tag{1.17}$$

For Option (2), the velocity components in the rotated system are

$$u = -(K_2 G)^{-1} m' \tag{1.18}$$

where $u^T = (u_1, u_2, u_3)$ and $(m')^T = (m_1', m_2', t_f')$.

Statistical calculation of the required maneuver. We now regard the injection guidance errors as random variables and compute the probability density distribution of the correcting velocity components. Knowing this distribution, one may estimate the amount of midcourse rocket propellant that should be carried in the spacecraft.

Equation (1.1) is re-written in matrix notation as

$$(m_1', m_2')^T = W_1 \Delta q \tag{1.19}$$

where Δq is a 6×1 column vector of injection errors and W_1 is a 2×6 matrix of differential coefficients. If u_1 and u_2 are to correct for the miss components due to Δq, then using Equation (1.17), we have for Option (1),

$$u = -Q^{-1} W \Delta q \tag{1.20}$$

Let the six injection errors now be regarded as random variables. Multiplying each side of Equation (1.20) by its transpose and taking the ensemble average (denoted by a bar) over all possible injection errors,

$$\overline{uu^T} = Q^{-1} W_1 L W^T (Q^{-1})^T \tag{1.21}$$

Matrix $\overline{uu^T}$ is the covariance matrix of midcourse velocity components and $L = \overline{\Delta q \, \Delta q^T}$ is the covariance matrix of

injection errors. Matrix L is obtained from an analysis of the injection guidance system.

For Option (2), define

$$t_f' = W_2 \Delta q \tag{1.22}$$

where W_2 is a 1×6 matrix of differential coefficients. Combining Equations (1.19) and (1.22)

$$m' = W \Delta q \tag{1.23}$$

where $(m')^T = (m_1', m_2', t_f')$ and W is a 3×6 matrix formed from W_1 and W_2. Using Equation (1.18)

$$\overline{uu^T} = (K_2 G)^{-1} WLW^T (K_2 G)^{-1T} \tag{1.24}$$

Assume that Δq is normal with zero mean, so that u is also normal with zero mean. In order to estimate how much fuel should be carried in the spacecraft, we need to know the cumulative distribution of the maneuver magnitude v. Since the general form of this distribution is quite complicated, we write here only the limits on v for a given percentile. Thus, to obtain the 0.99 probability level for Option (1)

$$2.14\,(\overline{v^2})^{1/2} \leq v \leq 2.58\,(\overline{v^2})^{1/2}$$

where $\overline{v^2}$ is the trace of $\overline{uu^T}$. For the lower limit, the equiprobability contours for u_1, u_2 are circles and for the upper limit the contours are very narrow ellipses. To obtain the 0.99 probability level for Option (2)

$$1.94\,(\overline{v^2})^{1/2} \leq v \leq 2.58\,(\overline{v^2})^{1/2}$$

In this case the equiprobability contours are spherical and needle shaped. To be conservative, we use the upper limit in both cases.

Computation of the exact maneuver. In computing the maneuver during an actual flight, we would not assume linear perturbation theory. The exact maneuver would be determined by iteration, using a digital computer to integrate the equations of motion. Equation (1.18) could be used to obtain the first approximation to the maneuver. The method of computing the exact maneuver is described in detail in Reference 13.

Application of theory. In this section, the theoretical results of the previous section are applied to a lunar impact mission. The coasting trajectory for this mission is defined by the set of Earth-fixed injection conditions in Table 23. On the standard trajectory, the spacecraft impacts near the middle of the visible side of the Moon, 65 hr, 51 min, 32 sec after injection.

There are three possible methods of computing the differential coefficients:

(1) Direct computation of perturbed trajectories.

Table 23. Injection conditions

r	= radius from center of Earth: 6,611,167.7 m
ϕ	= latitude: 13.312895 deg
θ	= longitude: 351.85651 deg
v	= velocity with respect to a coordinate system (r, ϕ, θ) which rotates with the Earth: 10,531.770 m/sec
γ	= angle of velocity vector above local horizontal plane: 5.3912348 deg
σ	= angle measured in local horizontal plane from North to projection of velocity vector: 121.83937 deg
t_s	= injection time: November 1, 1961 at 23h 2m 31.4s GMT

(2) Solution of the differential equations satisfied by the differential coefficients.

(3) Analytical calculation from conic formulas.

In Method (1), differential coefficients such as $\partial m_1/\partial v_1$ are approximated by $\Delta m_1/\Delta v_1$ where Δm_1 is the change observed in m_1 when v_1 on the standard trajectory is perturbed by Δv_1. The choice of the size of the increments is important since, if the increments are too large, nonlinear effects appear, and if the increments are too small, the errors in the trajectory computation become important. Method (1) is used to obtain the results in this section.

For terminal coordinates, we choose $m_1 = \overline{b} \cdot \overline{r}$ and $m_2 = \overline{b} \cdot \overline{t}$, where $\overline{b}$, $\overline{r}$, and $\overline{t}$ are defined in the section on trajectories. For near-vertical descents, the time of closest approach to the center of the target, t_c, changes nonlinearly on perturbed trajectories. A linearized time of flight, t_f, is obtained as follows:

$$t_f = t_c - \left(\frac{a^3}{\mu}\right)^{1/2} \log e \tag{2.1}$$

where a is the semi-major axis of the approach hyperbola, μ is the gravitational constant of the target, and e is the eccentricity of the hyperbola.

The column vector of injection perturbations is defined as follows: $\Delta q^T = (\Delta r, \Delta\phi, \Delta\theta, \Delta v, \Delta\gamma, \Delta\sigma)$. The W matrix is shown in Table 24, where m_1 and m_2 are in meters and t_f is in seconds. A typical K_2 matrix, evaluated at 16 hr after injection, is shown in Table 25. Velocity component v_1 is in the direction of the vernal equinox of date; v_2 points north and v_3 completes the right-handed orthogonal system. The velocity components have units of meters per second.

Equation (1.20) gives the components of the midcourse maneuver (in the critical plane) which are required to correct for a specified set of injection errors. It is interesting to compute the maneuver magnitude, v, to correct for a typical error in a single injection coordinate only

Table 24. *W*-matrix[a]

0.6814 (3)	0.7647 (7)	−0.1595 (7)	0.7571 (6)	0.9230 (7)	−0.1562 (7)
−0.4874 (3)	−0.1202 (7)	−0.5443 (7)	−0.5548 (6)	0.8896 (7)	0.1307 (7)
−0.7720 (0)	0.1565 (3)	0.2979 (4)	−0.8580 (3)	−0.2650 (4)	0.4605 (4)

[a]Numbers in parentheses are decimal exponents.

Table 25. K_2-matrix[a] (at $t = 16$ hr)

−0.6609 (5)	0.3963 (5)	−0.1588 (6)
0.1434 (6)	0.1311 (6)	−0.1218 (3)
0.1166 (3)	−0.7100 (2)	−0.4312 (2)

[a]Numbers in parentheses are decimal exponents.

The results are shown in Figure 50 as a function of time of application of the maneuver. It can be seen that the application time which minimizes the maneuver magnitude will depend on the particular combination of injection errors. Thus, the application time which minimizes the rms maneuver depends on the covariance matrix, L.

Figure 51 shows the rms maneuver magnitude for a typical injection guidance system. The injection guidance system is characterized by the covariance matrix, L, in Table 26. The lower curve is for Option (1) and is computed by means of Equation (1.21). Note that the correlation of Δv and Δr is such that they compensate for each other when we compute the average maneuver.

Error analysis of midcourse guidance systems. There are four types of errors in a midcourse guidance system:

(1) In execution of the commanded maneuver.

(2) In the radio observations.

(3) Imperfections in the mathematical model used for trajectory computation.

(4) Unpredictable disturbances occurring after the maneuver.

In this section, equations are derived for the terminal dispersions due to Type (1) errors. Type (2) errors are treated in the section on orbit determination. Only a

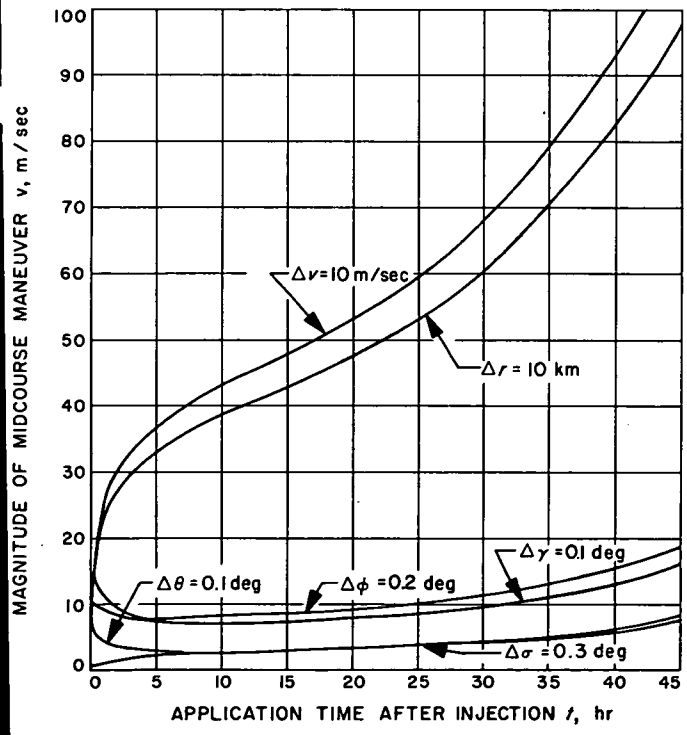

Figure 50. Midcourse maneuver to correct injection errors

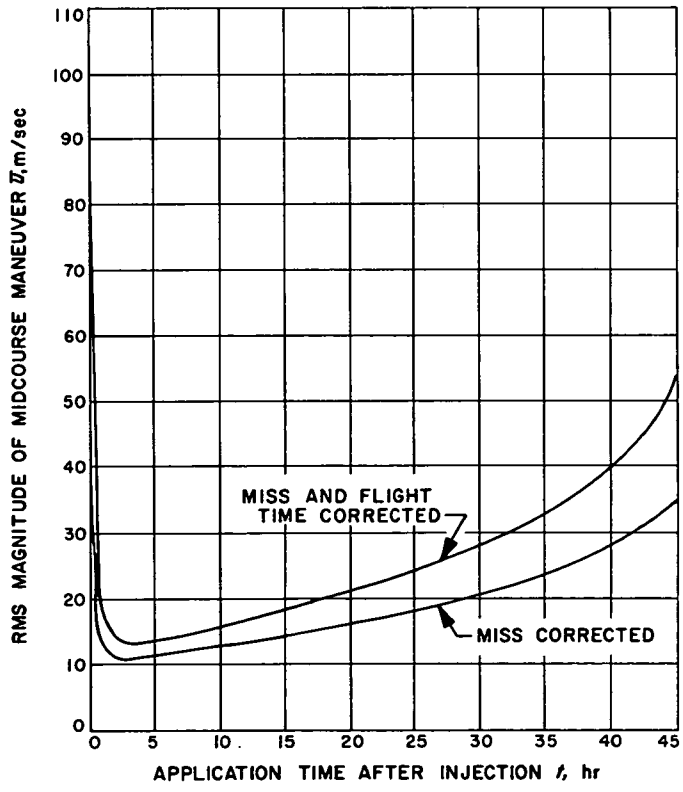

Figure 51. Midcourse maneuver for typical injection guidance system

Table 26. L-matrix[a]

0.5739 (8)	0.3249 (3)	−0.5659 (3)	−0.6841 (5)	0.5798 (3)	0.1581 (3)
	−0.3617 (−1)	0.1731 (−1)	−0.5897 (0)	0.3301 (−2)	−0.3341 (−1)
		0.1854 (−1)	0.5596 (0)	−0.5509 (−2)	−0.2248 (−1)
			0.8516 (2)	−0.6888 (0)	0.2722 (0)
				0.6858 (−2)	0.1326 (−2)
symmetrical					0.9824 (−1)

[a]Numbers in parentheses are decimal exponents.

brief discussion of Type (3) errors is presented, since they have not yet been thoroughly analyzed. An example of Type (4) error is the miss caused by corpuscular pressure if a solar storm should occur after the maneuver. Such errors are believed to be negligible for the lunar impact mission and are not considered further.

Execution errors. Figure 52 shows the desired midcourse velocity increment, $\overline{u}$. Vector $\overline{w}$, extending from the tip of $\overline{u}$, is the velocity error in executing $\overline{u}$. The components of $\overline{w}$ are w_k, $k = 1, 2, 3$, where w_3 is measured along $\overline{u}$; w_2 is normal to $\overline{u}$ and parallel to the u_1, u_2 plane and w_1 completes the orthogonal system. The w-vector depends on component errors in the midcourse system.

$$w = \begin{bmatrix} w_1 \\ w_2 \\ w_3 \end{bmatrix} = \begin{bmatrix} \alpha v + \zeta \\ \beta v + \eta \\ \gamma v + \theta \end{bmatrix} \tag{3.1}$$

where

α, β = pointing errors

γ = proportional error

ζ, η = lateral velocity errors

θ = axial velocity error

Pointing errors result from gyro and attitude sensor errors. Proportional errors are caused by accelerometer scale factor and null offset errors. Lateral velocity errors occur as a result of the midcourse autopilot correcting for thrust misalignments. Axial velocity errors are caused by accelerometer resolution and thrust tail-off errors.

We now transform the execution errors into the u_k system

$$\delta u = Hw \tag{3.2}$$

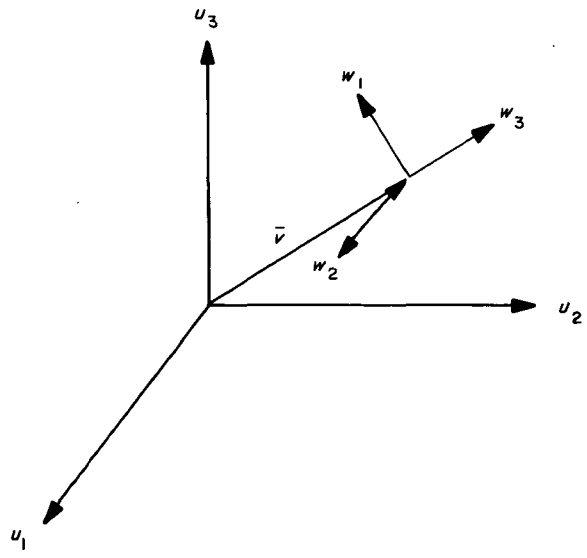

Figure 52. Execution error components

where $\delta u^T = (\delta u_1, \delta u_2, \delta u_3)$. The rotation matrix, H, is given by

$$H = \frac{1}{v} \begin{bmatrix} \frac{u_1 u_3}{y} & -\frac{v u_2}{y} & u_1 \\ \frac{u_2 u_3}{y} & \frac{v u_1}{y} & u_2 \\ -y & 0 & u_3 \end{bmatrix} \tag{3.3}$$

where $y = (u_1^2 + u_2^2)^{1/2}$.

The covariance matrix of execution errors is

$$\overline{\delta u \delta u^T} = \overline{H w w^T H^T} \tag{3.4}$$

If we know the commanded maneuver, the elements of H are not random. In that case, the ensemble average goes over the component errors only. In order to simplify the computation assume that the component errors are all

independent with zero mean and that $\overline{\alpha^2} = \overline{\beta^2}$ and $\overline{\zeta^2} = \overline{\eta^2}$. We obtain

$$\overline{\delta u \delta u^T} = (\overline{\gamma^2} - \overline{\alpha^2})\,\overline{uu^T} + (\overline{\theta^2} - \overline{\zeta^2})\,(\overline{v^{-2}uu^T}) + (\overline{\alpha^2 v^2} + \overline{\zeta^2})\,I \tag{3.5}$$

where I is a (3×3) unit matrix.

If we regard u_1, u_2, u_3, and v as random variables, the computation of $\overline{\delta u\, \delta u^T}$ is more complicated. In order to simplify the computation, assume that the component errors are independent of u_1, u_2, u_3, and v. We now obtain

$$\overline{\delta u \delta u^T} = (\overline{\gamma^2} - \overline{\alpha^2})\,\overline{uu^T} + (\overline{\theta^2} - \overline{\zeta^2})\,(\overline{v^{-2}uu^T}) + (\overline{\alpha^2 v^2} + \overline{\zeta^2})\,I \tag{3.6}$$

For Option (1) we are interested in the 2×2 partition of Equation (3.6) which involves δu_1 and δu_2 only. In order to simplify the computations, consider the particular case where u_1 and u_2 are normal with circular equiprobability contours. In this case, $\overline{u\,u^T} = \tfrac{1}{2}\overline{v^2}\,I$ and $(\overline{v^{-2}\,u\,u^T}) = \tfrac{1}{2}I$, where I is a 2×2 unit matrix. Thus, for Option (1)

$$\overline{\delta u \delta u^T} = (\tfrac{1}{2}\overline{\alpha^2 v^2} + \tfrac{1}{2}\overline{\gamma^2 v^2} + \tfrac{1}{2}\overline{\zeta^2} + \tfrac{1}{2}\overline{\theta^2})\,I \tag{3.7}$$

For Option (2), consider the particular case where u_1, u_2, and u_3 are normal with spherical equiprobability contours. In this case, $\overline{u\,u^T} = \tfrac{1}{3}\overline{v^2}\,I$ and $(\overline{v^{-2}\,u\,u^T}) = \tfrac{1}{3}I$, where I is a 3×3 unit matrix. Thus for Option (2)

$$\overline{\delta u \delta u^T} = (\tfrac{2}{3}\overline{\alpha^2 v^2} + \tfrac{1}{3}\overline{\gamma^2 v^2} + \tfrac{2}{3}\overline{\zeta^2} + \tfrac{1}{3}\overline{\theta^2})\,I \tag{3.8}$$

We now compute the miss due to execution errors. From Equation (1.16), we obtain for Option (1)

$$\delta m = Q_1 \delta u \tag{3.9}$$

where $\delta m^T = (\delta m_1, \delta m_2)$ is the miss due to δu. The covariance matrix of δm is

$$M = Q_1\,\overline{\delta u \delta u^T}\,Q_1^T \tag{3.10}$$

We now define the elements of K_2G (and thus, Q_1).

$$K_2G = \begin{bmatrix} a_{11} & a_{12} & 0 \\ a_{21} & a_{22} & 0 \\ a_{31} & a_{32} & a_{33} \end{bmatrix} \tag{3.11}$$

From Equations (3.7) and (3.10), the trace of M is

$$\overline{\delta m^2} = \overline{\delta m_1^2} + \overline{\delta m_2^2} = \phi^2\,(\tfrac{1}{2}\overline{\alpha^2 v^2} + \tfrac{1}{2}\overline{\gamma^2 v^2} + \tfrac{1}{2}\overline{\zeta^2} + \tfrac{1}{2}\overline{\theta^2}) \tag{3.12}$$

where

$$\phi^2 = (a_{11}^2 + a_{12}^2 + a_{21}^2 + a_{22}^2) \tag{3.13}$$

For Option (2) we obtain

$$M = K_2G\,\overline{\delta u \delta u^T}\,G^T K_2^T \tag{3.14}$$

From Equations (3.8) and (3.14)

$$\overline{\delta m^2} = \overline{\delta m_1^2} + \overline{\delta m_2^2} = \phi^2\,(\tfrac{2}{3}\overline{\alpha^2 v^2} + \tfrac{1}{3}\overline{\gamma^2 v^2} + \tfrac{2}{3}\overline{\zeta^2} + \tfrac{1}{3}\overline{\theta^2}) \tag{3.15}$$

The mean squared error in correcting t_f is

$$\overline{\delta t_f^2} = \psi^2\,(\tfrac{2}{3}\overline{\alpha^2 v^2} + \tfrac{1}{3}\overline{\gamma^2 v^2} + \tfrac{2}{3}\overline{\zeta^2} + \tfrac{1}{3}\overline{\theta^2}) \tag{3.16}$$

where

$$\psi^2 = (a_{31}^2 + a_{32}^2 + a_{33}^2) \tag{3.17}$$

If Option (1) is used, flight time variations occur not only due to injection errors but as a result of the midcourse maneuver itself. From Equations (1.15 and (3.11)

$$t_f = Ru \tag{3.18}$$

where $R = (a_{31}, a_{32})$. The total change in flight time is Δt_f where

$$\Delta t_f = t_f' + t_f = W_2 \Delta q + Ru = (W_2 - RQ_1^{-1}\,W_1)\,\Delta q \tag{3.19}$$

Thus, the mean square error in flight time for Option (1) is

$$\overline{\Delta t_f^2} = (W_2 - RQ_1^{-1}\,W_1)\,L\,(W_2 - RQ_1^{-1}\,W_1)^T \tag{3.20}$$

Mathematical model errors. In this category we include:

(1) Uncertainties in physical constants which affect the trajectory computation (e.g., gravitational constant of the Earth).

(2) Uncertainties in physical constants which affect the computation of observables (e.g., station location, speed of light).

(3) Computer errors (i.e., roundoff and truncation).

Type (1) errors affect the target error in two ways. First, errors in the computed trajectory cause errors in the computed observables which, in turn, cause errors in the estimated orbit. Second, the magnitude of the correction cannot be computed perfectly unless the motion after the correction can be exactly predicted. C. Tross (Ref 14) has estimated that the uncertainty in the Earth's gravitational constant and equatorial radius would cause an uncertainty of 78 mi in the impact point of a ballistic rocket at the Moon. This error will be reduced as improved values of the constants are obtained by tracking satellites and space probes.

Type (2) errors affect only the computation of observables. It is estimated that errors in station location cause an error of less than 20 km in predicting the lunar impact point. The uncertainty in station location can also be reduced by tracking Earth satellites. It is estimated that the uncertainty in the speed of light causes an error of about 10 km in predicting the lunar impact point.

In some cases, it may be desirable to treat the uncertainty in a parameter (e.g., the uncertainty in GM of the Earth) as an additional parameter to be estimated in the orbit determination process. This procedure is only effective if the observations are accurate and strongly dependent on the parameter. The effects of Type (1) and (2) errors are presently under study. It is assumed that Type (3) errors can be reduced until they are negligible.

Results of error analysis. In this section, the error analysis developed in the preceding section is applied to the lunar impact mission. Figure 53 shows the error coefficient ϕ, defined by Equation (3.13), as a function of execution time. Typical values of the component errors are: $(\overline{\alpha^2})^{1/2} = 0.01$ rad, $(\overline{\gamma^2})^{1/2} = 0.004$, $(\overline{\rho^2})^{1/2} = 0.06$ m/sec, and $(\overline{\theta^2}) = 0.03$ m/sec. Assuming that the correcting velocity components are spherically distributed and using Equation (3.15), we find that the rms miss is about 48 km if the maneuver is executed at 16 hr. Most of this miss is due to $\overline{\alpha^2}$, so that if one desired the miss for other than spherical distribution, he could probably neglect $\overline{\rho^2}$ and $\overline{\theta^2}$ in Equation (3.6). Note also that the miss due to $\overline{\alpha^2}$ and $\overline{\gamma^2}$ is relatively independent of time, whereas the miss due to $\overline{\rho^2}$ and $\overline{\theta^2}$ decreases with time in the same way as ψ.

The error coefficient ψ, defined in Equation (3.17), is shown in Figure 54. Using Equation (3.16) and the above component errors, the rms time of flight error is 23 sec if the maneuver is executed at 16 hr. Figure 55 shows the rms flight-time error, $(\overline{\Delta t_f^2})^{1/2}$, if Option (1) is used instead of Option (2).

The results are summarized in Table 27. In this table, Option (1) is used and the maneuver is executed at 16 hr. The percentage of spacecraft weight required for fuel is $2.58(\overline{v^2})/gI_{sp}$ and a specific impulse $I_{sp} = 230$ sec is assumed. Mathematical model errors are not included in the table.

In retrospect, it would seem more sensible for the *Ranger* mission to correct v_f instead of t_f in Option (2). This possibility was originally rejected because of the erroneous impression that v_f could not be predicted accurately from radio tracking. However, this point is not too important, since correcting t_f also tends to correct v_f.

d. Orbit determination. Orbit determination is treated in two sections. The first section reviews the three basic areas of activity in orbit determination in the JPL Systems Division: (1) mathematical theory, (2) accuracy studies, and (3) operational orbit determination. The second section gives some examples of the merging of these three activities in order to plan and execute the RA-3 operational orbit determination. The role of *Ranger I* and *II* flight experience in shaping plans for RA-3 is reviewed general block diagrams of data and information flow

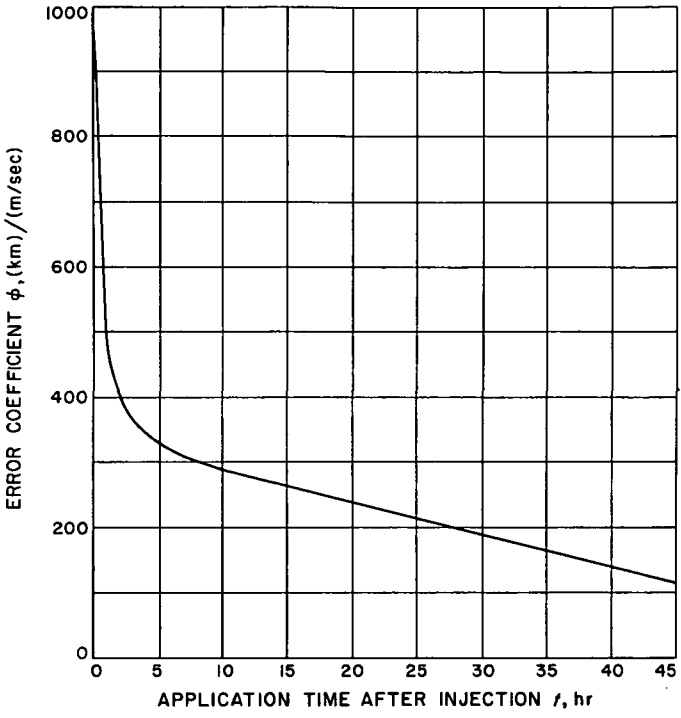

Figure 53. Error coefficient relating miss to pointing and shutoff errors

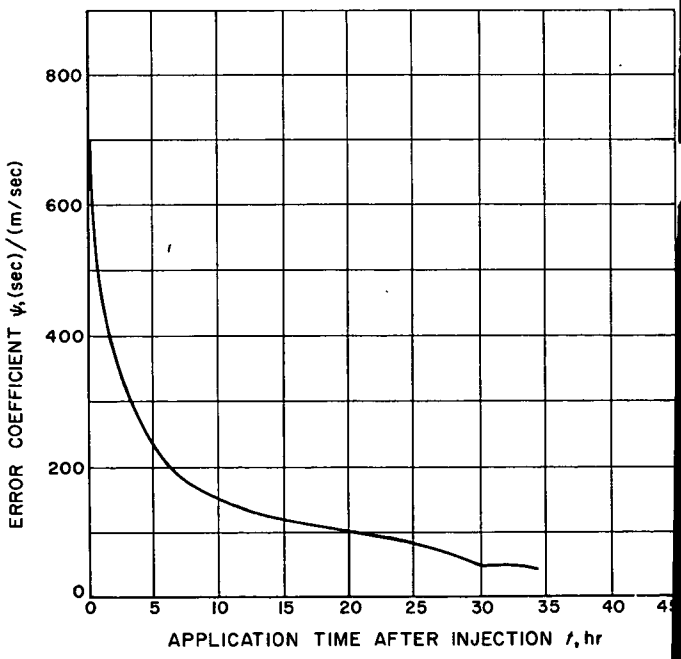

Figure 54. Error coefficient relating flight time error to point and shutoff errors

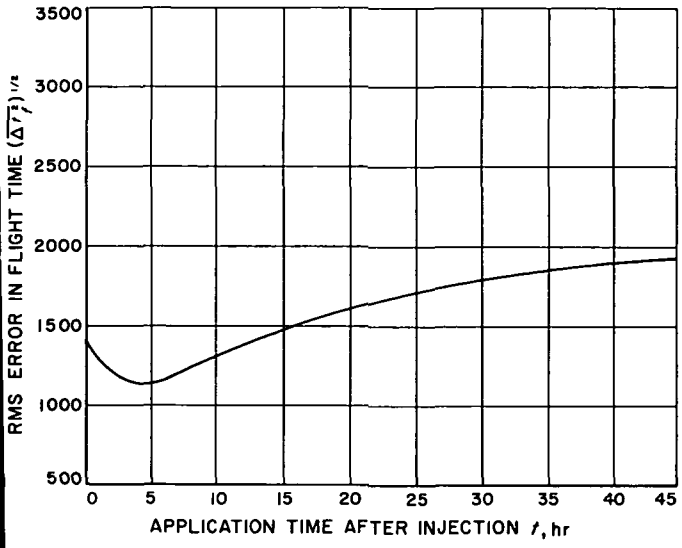

Figure 55. RMS error in flight time when only miss is corrected

are given. Two examples are given of pre-launch studies which helped to shape the DSIF tracking configuration and accuracy, as well as allowable launching azimuths.

Mathematical theory. The set of observations taken by the various Earth-based tracking stations and/or spacecraft-borne instruments supply redundant information from which a statistical estimate of the orbit parameters may be made. The well-known basic theory will be described briefly.

Let $\overline{y}$ be a column n-vector composed of all the observations. From the laws of physics and the geometry of the measuring instruments, the true value of the observables, $\overline{y}_T$, can be expressed as a known function of a set of p parameters represented by the vector $\overline{p}$. Thus we have

$$\overline{y}_T = \overline{y}_T(\overline{p})$$

In general, $\overline{p}$ represents the six injection position and velocity components at the chosen epoch, plus physical constants, station coordinates, systematic error coefficients in the observing instruments, etc. The regression equation is $\overline{y} = \overline{y}_T(\overline{p}) + \overline{N}$, where $\overline{N}$ is an n-vector of the noise on the observations. The weighted least-squares estimate, $\overline{p}_{WLS}$, minimizes the weighted sum of squares of the residuals, i.e.,

$$[\overline{y} - \overline{y}_T(\overline{p}_{WLS})]^T W [\overline{y} - \overline{y}_T(\overline{p}_{WLS})]$$

Here W is an $n \times n$ diagonal matrix with non-negative elements; the T denotes the transpose. When the non-linear system of equations is solved by linearization, the solution is expanded about $\overline{p}_0$

$$\overline{p}_{WLS} - \overline{p}_0 = (A^T W A)^{-1} A^T W [\overline{y} - \overline{y}_T(\overline{p}_0)]$$

The next $n \times p$ matrix A represents the partials of $\overline{y}_T$ with respect to the parameters $\overline{p}$

$$A = \left.\frac{\partial \overline{y}_T}{\partial \overline{p}}\right|_{p_0}$$

The covariance matrix of $\overline{p}_{WLS}$ depends on the covariance of $\overline{N}$, namely R. R = Expected Value $[\overline{N}\overline{N}^T]$ is an $n \times n$ matrix.

$$\text{Covar}(\overline{p}_{WLS}) = (A^T W A)^{-1} A^T W R W A (A^T W A)^{-1}$$

The problems of outstanding theoretical interest are:

(1) Estimation of the data noise properties.

(2) Finding optimal ways to select W to minimize some statistical measure of error.

(3) Evaluation of the performance of other estimators of $\overline{p}$ relative to $\overline{p}_{WLS}$.

During the past year, JPL has carried on studies in these areas in addition to sponsoring such work under a contract let to Space Technology Laboratories. The work was summarized in an annual report available in March 1962.

Orbit determination accuracy studies. If the errors at the target, $\overline{M}$, are related to the parameter vector by $\Delta\overline{M} = U\Delta\overline{p}$ the covariance of $\overline{M}$ is given by Covar $(\overline{M}) = U$ Covar $(\overline{p})\, U^T$. Thus, the covariance of target error can be expressed in terms of W, the weighting matrix, and R, the noise correlation matrix.

For each mission, the spacecraft trajectory with respect to the observing stations is different on each launch day, and for different launch azimuths on the same day. This feature is exhibited by changes in the A-matrix defined above. Accuracy is further dependent on:

(1) The particular stations available for tracking.

(2) The data types taken.

(3) The time of the first data point.

(4) The sampling rates.

Table 27. Summary of midcourse guidance characteristics

RMS maneuver, m/sec	Spacecraft weight for fuel, %	RMS execution errors, km	RMS observation errors, km	Total rms miss, km
15	1.7	48	20	52

(5) The amount of data available before the estimate of orbital parameters is made.

(6) The equivalent accuracy of the various data, characterized by the noise correlation matrix R.

Operational considerations require that assignment of tracking stations, sampling rates, data types, and accuracy be made in such a way that the mission objectives be met in the most reliable fashion possible.

Detailed analyses required to support the RA-3 mission are partially reported elsewhere in this publication. Such studies lead to the determination of the proper combination of Items (1) to (6) above. Various analytical tools have been developed during the year in order to more efficiently carry out these studies. One such tool is the Tracking Accuracy Prediction Program (TAPP), which is being developed under the space systems analysis study contract by Space Technology Laboratories.

Operational orbit determination. Once the mathematical theory has been embodied in a digital computer program (called the orbit determination program, ODP) and the tracking station configuration and accuracy requirements are established, there remains the problem of carrying out the procedures in the real flight conditions. Here, the major problems are data handling, data accuracy analysis, supplying acquisition information to the tracking stations and other trajectory estimates to all users, and adaption to unexpected circumstances. The operational ODP must be able to clearly present the relevant information in a manner such that control of the ODP may be adjusted to adapt to the new circumstances. The value of the operational ODP is measured by its flexibility in presenting diagnostic information and its susceptibility to easy change of control while maintaining high reliability and short delay times between the receipt of the last data point and the convergence to the estimate of the orbit parameters. The development of satisfactory presentation of information regarding the in-flight OD process and the methods of implementing control represent a significant step in achieving good operational capability. In addition, procedures must be determined in advance for the conduct of the operation assuming normal operation and all anticipatable nonstandard circumstances.

The final activity in this area is the post-flight analysis of the tracking data and the flight operation which results in the final orbit of the spacecraft, and in changes in operational procedures on future launchings.

Review of work supporting RA-3 orbit determination. The stated purpose of the orbit determination program for *Rangers I* and *II* was to assist in the development of the operational tracking configuration and operational ODP. While neither launch provided a near-parobolic trajectory, the objectives appear to have been well met. As a result of the experience gained, a clear picture of the operational problems and a satisfactory solution have evolved. The resultant picture of the operational ODP and examples of application of the results of accuracy studies are given in succeeding sections. No attempt will be made to detail the RA-1 and -2 programs; the contrasts to the RA-3 ODP will be described, however.

Development of the operational orbit determination configuration. On *Rangers I* and *II*, the block diagram of Figure 56 describes the processing of the incoming data. After conversion to IBM cards, the data cards were scanned manually for bad data condition words, transmission or conversion errors, missing characters, out-of-range data. Bad cards are rejected or re-punched with appropriate corrections. Doppler data which has been counted by alternate counters without re-set prior to next counting interval, so-called non-destructive counted doppler, was then processed to form equivalent destructively counted doppler. After the ODP has iteratively converged to the estimate of orbital parameters, predictions for the tracking stations and/or plots of the data residual vector are done on option. The orbital parameters are then read into the trajectory program to supply target conditions and/or other trajectory information for other users of trajectory-dependent information.

Changes in orbit determination configuration. On the basis of experience obtained during *Ranger I*, a Tracking Data Editing Program (TDEP) was written in time for RA-3, in order to automate the detection of errors on the data cards and to allow more flexible operation of the

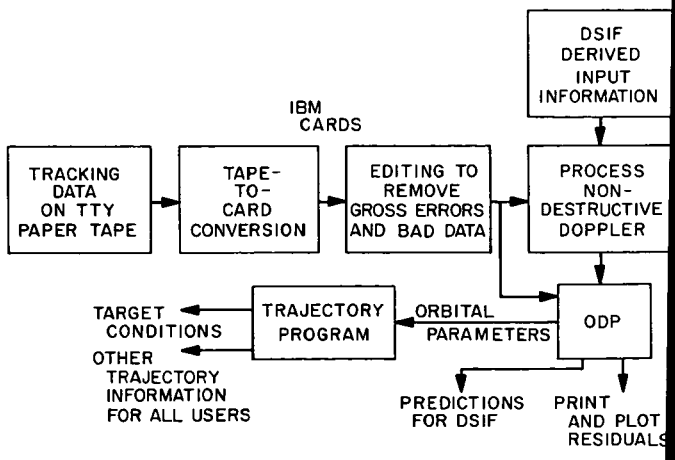

Figure 56. RA-1 and -2 orbit determination block diagram

ODP. The difficulties in handling non-destructive counted doppler were so great that it was decided to abandon that data type until all DSIF stations are equipped with revised counting systems. Some other changes were:

(1) The new TDEP and the ODP were linked together to increase flexibility. Many functions were transferred from ODP to TDEP.

(2) Greater flexibility in in-putting DSIF-derived constants into the ODP was established.

(3) The ODP was modified to supply target conditions and target error ellipse on option.

(4) Emphasis was shifted from *a posteriori* data weighting to *a priori* weighting because of the strong dependence of the optimal weights upon data rate, counting time, and range. (Allowance was made for frequent stepwise variation in weights for each data type at each station.)

(5) An option was added to allow the processing of additional blocks of data without iterating through all previous data. This procedure allows the efficient rejection of bad data points and speeds last-minute up-dating of the estimated orbit parameters.

(6) Provision for epoch forwarding of previous estimates and associated covariance matrices has been made to allow correct handling of the post-midcourse maneuver orbit determination. This capability also increases operational reliability and can be used to reduce computer running time where essential.

(7) Refinements in station coordinate descriptions and a refraction correction to doppler data were implemented.

(8) Many refinements in the calculation of observables were made in the ODP.

(9) The TDEP corrected DSIF angle data using error curves obtained from pre-flight star-track tests.

The revised block diagram is shown in Figure 57.

Orbit determination accuracy studies. The RA-3 objectives relevant to orbit determination accuracy are:

(1) Determine the orbit prior to the midcourse correction point to sufficient accuracy to land in the desired general area of the Moon.

(2) After implementing the midcourse correction, it is necessary to track further in order to estimate certain conditions at impact necessary to calculate the retro-rocket firing direction and to turn on the capsule altimeter. The conditions are: (a) orientation of the impact velocity vector in inertial space; and (b) impact time.

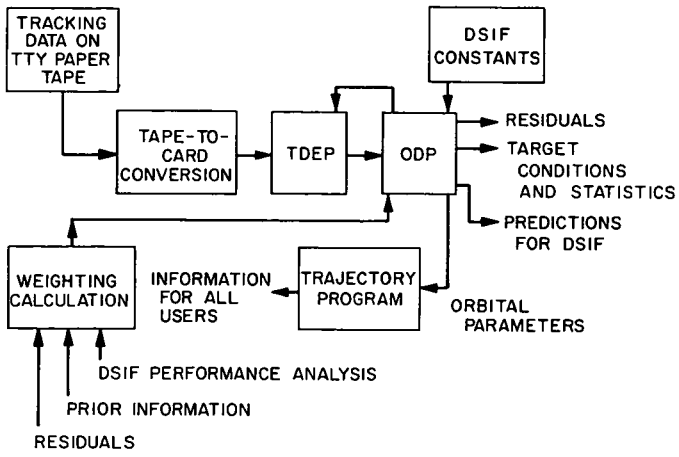

Figure 57. RA-3 orbit determination block diagram

The only DSIF stations equipped with two-way doppler capability for RA-3 were Goldstone and the Mobile Tracking Station, situated in South Africa. Since command capability existed only at Goldstone, the midcourse maneuver had to be made over Goldstone. For the case where the maneuver is executed at the earliest practical time in the Goldstone pass, a study was made of the influence of the ground transmitter oscillator drift on the ability to re-establish the orbit to meet the second objective above. Previous studies (Ref 15) had assumed that the effective noise was 1 cps everywhere (uncorrelated over 10 sec), whereas at lunar distance the drift of the Goldstone VCO reference oscillator during the transit time was a factor of 10 to 30 outside the required values because of the highly correlated drift rates introduced by moderate temperature variations over a couple of hours. Temperature control of the VCO crystal was quickly installed at Goldstone and a further analysis was performed to determine whether a similar change was required at the MTS. The results, described below, indicated that significantly greater accuracy could be obtained or significantly less early data would be required to obtain equivalent accuracy if the change were made. On the basis of these results, this change was also made.

The following section describes part of the results of the studies made to determine the lowest allowable launch azimuth on each day of the firing period. It was found that, for certain days, the spacecraft appeared only briefly over South Africa and then dipped down below 5-deg elevation angle for up to 2 hr. Since accurate data cannot be reliably expected this low on the horizon, the

resulting degradation of accuracy necessitated rejection of certain launch azimuths near 90 deg. Other studies were performed to select the best compromise sampling patterns, influence of loss of data near injection, and accuracy as a function of launch day and total time from injection. Various situations simulating varying degrees of failure in obtaining MTS data were simulated to determine the amount of Goldstone data which must be added to compensate the loss of some MTS data. This information will serve as a basis for back-up planning for the actual operation.

Dependence of orbit determination accuracy on launch azimuth and launch date. On each launch day, the required launch azimuth, ε_L, varies with the launch time during the window of permissible launching times. The spacecraft trajectory as seen from South Africa is a strong function of both the launch azimuth and launch date. The most critical dependence, for southeast launchings, occurs for the most southerly (downrange) injection points. Another significant parameter is t_D, the time delay between the spacecraft's rise to 5-deg elevation angle and the first valid two-way doppler point. Inaccurate predictions, communication difficulties, non-standard trajectory, or minor equipment or operational troubles can cause increases in t_D.

Figure 58 shows the variation of the semi-major axis of the error ellipse at the Moon, λ_1, as a function of t_D for a tracking configuration and accuracy corresponding to the MTS without temperature control of the VCO crystal. Angular data from the Johannesburg and Woomera antennas supplement two-way doppler from the MTS. Tracking data is assumed available from rise time plus t_D to 740 min after injection. The launch date was January 22, 1962, and the launch azimuth 102 deg. The flat portion of the curve between 50 and 80 min indicates that there is no degradation of accuracy caused by additional delays after 50 min, as long as those delays are less than 30 min. The reason for this situation is that during this time interval, the spacecraft is below 5-deg elevation angle and the data is assumed to be inaccurate or unavailable.

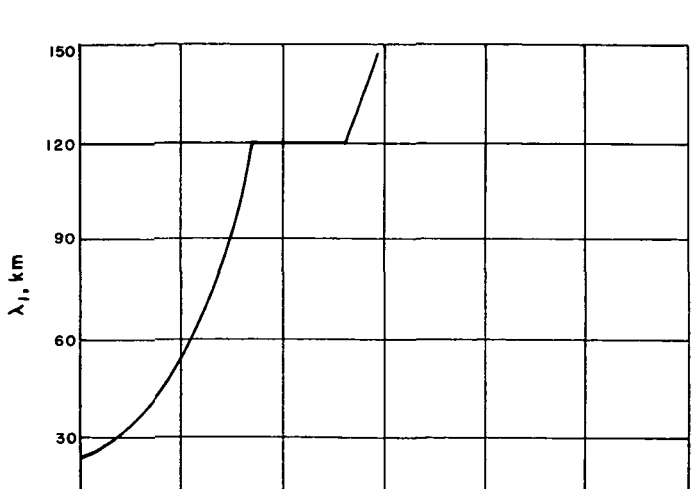

Figure 58. Effect of time delay to first valid data

In general, those trajectories with intervals of 30 min or more below 5 deg after initial rise are very sensitive to t_D. For RA-3, a nominal 40-km semi-major axis of the lunar error ellipse is desired, which would require, for the case in Figure 58, that t_D be less than or equal to 20 min. The launchings during the first half of the firing period will be restricted to the more southerly of the launch azimuths to avoid this significant degradation of accuracy. In the latter half of the period, injection occurs further north (uprange) and thus no low-elevation angle problems occur, even for the 90-deg launch azimuth.

Dependence of orbit determination accuracy on MTS oscillator drift. As mentioned, specifications were established for the Goldstone VCO frequency stability in order to allow adequate estimation of impact conditions. A study was made to determine the value of installing crystal temperature control at the MTS also. The two cases examined were (1) no temperature control, drift similar to Goldstone, and (2) temperature control equivalent to Goldstone specifications. Figure 59 shows the semi-major axis, λ_1, of the dispersion ellipse at the Moon as a function of t_D, the delay between rise at the station and the first valid doppler data point, for both cases. All other conditions are the same as Figure 58 with the exception that the launch date is January 24, 1962. To achieve a $\lambda_2 = 40$ km requires $t_D \leq 4$ min if the old system is used whereas $t_D \leq 50$ min will accomplish the job using the new system.

The more rapid degradation in accuracy with t_D in Case (1) is due to the fact that the contribution of the oscillator drift rate to the error is proportional to range hence, the most accurate data is taken near injection.

e. Performance evaluation.

Ranger I *flight summary. Ranger I* was launched from AMR, Cape Canaveral, August 23, 1961, at 10.26 sec after 5:04 a.m., EST. The GMT of liftoff was 235:10:04:10.26 Z (All subsequent references to time will be in GMT.) The ascent phase and injection into parking orbit were normal. The spacecraft shroud was ejected as programmed. The spacecraft transponder was kept in two-way lock

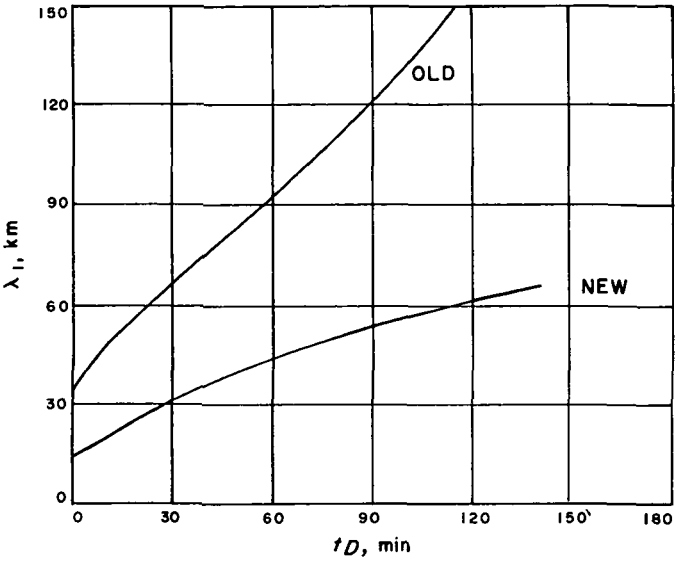

Figure 59. Influence of precision-frequency oscillator at MTS on orbit determination accuracy for a particular launching

with the launch checkout telemetry trailer (LCTT) for 7½ min after liftoff, except for an unexplained momentary dropout.

The *Agena* re-start sequence began at the proper time but the fuel valve failed to operate and ignition did not occur. Sufficient oxidizer gas was expelled to add a velocity increment of approximately 70 m/sec. The subsequent electrical and mechanical separation of the spacecraft from the *Agena* appears to have been normal. The spacecraft was injected at 10:27.23 Z into a satellite orbit with a period of 91.15 min and apogee and perigee of 313.3 and 105.6 statute mi, respectively. By August 28 (4.6 days later), the last day on which the spacecraft signal was tracked, the orbit had decayed to a period of 89.19 min with apogee and perigee of 202.9 and 96.2 statute mi, respectively.

The spacecraft controller is programmed to issue a sequence of discrete commands to different units in the spacecraft within 6 hr after injection. A list of these commands and the programmed times is given in Table 28.

The spacecraft can also accept commands (roll override, hinge override, and antenna transfer) from the ground as a back-up for controller commands 5 and 8, or to correct certain non-standard conditions.

Controller command 2 was programmed at the time indicated as the result of an incident which occurred during the countdown on August 3. When this command was sent from the blockhouse, it apparently caused the

Table 28. *Ranger* command sequence

Number	Command	Time from liftoff, min
1	Increase transmitter power	30.3
2	Turn-on scientific instruments high-voltage	78.7
3	Extend particle analyzer boom and solar panels	33.6
4	Start Sun acquisition	58.7
5	Start Earth acquisition	90.3
6	Change data encoder rate gyro scale	115.3
7	Open semiconductor detector aperture	203.7
8	Switch transponder transmitter to high-gain antenna	247.0
9	Reduce modulation on beacon transmitter	363.7
10	Turn-on friction-lubrication experiment	367.0

controller to issue all the other programmed commands. Subsequently, this step was eliminated from the countdown procedure and the time of the programmed command delayed in order to minimize the effect in case of a similar occurrence during flight.

Telemetry records indicate that all programmed events took place. The nature of the orbit was such that it is impossible to determine the exact time of any of the programmed commands. Command 1 occurred before the Mobile Tracking Station (DSIF 1) in South Africa acquired the spacecraft signal. At the time of Command 3, the signal was too noisy. All the other commands occurred during periods when the spacecraft was not in view of any tracking station. In each case, however, subsequent telemetry indicated that each commanded function did occur within the proper time interval.

Probably the most serious effect of the satellite trajectory was the fact that the spacecraft was in the Earth's shadow about 45% of the time during each orbital revolution. Each time the spacecraft returned to the sunlight, the attitude-control system, if operating normally, would commence its acquisition procedure with a consequent heavy drain on the supply of nitrogen gas used for activation. This gas supply was exhausted within 19 hr after injection, sometime after the fifth orbit (the last orbit tracked on August 23), and before the thirteenth orbit (the first orbit tracked on August 24).

A number of apparently related conditions appeared with the first data obtained on August 24, lasted throughout all passes tracked on that day (up to the twenty-first orbit) and did not show up again after that. (1) The attitude-control (A/C) power converter was overloaded, indicated by the converter monitor voltage reading of zero. (2) Spikes appeared on the analog trace of all the attitude-control measurements. (3) Except for the spikes,

all the attitude-control measurements (rates, positions, and light detector) had null values (due to the absence of d-c power). (4) The 400-cps tone on Channel 1 exhibited a considerable degree of what can best be described as amplitude modulation. The modulation was variable, especially in amplitude, with at least two identifiable frequency components present at times. (5) The data encoder commutator was stepped faster than normal by the controller generally increasing its speed to a maximum error of about 4% on the fifteenth and sixteenth orbits, then decreasing back to normal by the twentieth orbit. This apparently was done without skipping any segments. The Lyman-alpha telescope scanning times were also affected and it is quite likely the scientific data automation system (DAS) was similarly affected, but this has not yet been established.

The frequency of the spikes, occurring every 0.41 to 0.42 sec, corresponds to drops in amplitude of the 400-cps signal. It is believed that both phenomena resulted from the A/C converter overload interrogation process. The cause of some of the other events which were happening is still not known. It would seem logical to assume that the excessive current requirements in the A/C system which caused the converter to go into overload are the result of loss of nitrogen gas, but this cannot be proved. Nor does it explain why the overload condition subsequently disappeared.

The ground-to-spacecraft command link was successfully tested on August 25. The ground transmitter at Goldstone Az-El site (DSIF 3) switched the transponder transmitter from the high- to the low-gain omnidirectional antenna during the thirtieth orbit. During the following orbit, the same station switched the 3-w transmitter to the high-gain antenna and back again. Then the LCTT transmitter switched it back to the high-gain antenna, where it remained for the rest of the flight. The reason for leaving it on the high-gain antenna was that the received signal level at the DSIF stations was usually higher in this mode, even when locked on a side lobe, than it was when the transponder was transmitting over the low-gain antenna with its −10-db coupler.

On August 26, the hinge and roll override commands were transmitted by DSIF 2 at Goldstone, but there was no way to determine their effect on the spacecraft since the spacecraft was not stabilized due to the loss of A/C gas; and, hence, the rate gyros were usually saturated.

The first indication of the main battery failing was on the sixty-first orbit on August 27, approximately 91 hr after liftoff. The last good telemetry was recorded 40 min later at 05:49 Z. After that, the ¼-w transmitter, which has its own battery power supply, continued to operate, usually with no modulation, until after the eighty-third orbit, the last pass tracked on August 28. During this period, sporadic modulation appeared on the beacon signal when the solar panels were supplying enough current to activate the data encoding system. The transponder signal was occasionally heard at these times. The last signal received from the spacecraft was a momentary one from the transponder at 23:53.36 Z on August 28 during the eighty-ninth orbit. Apparently the beacon battery was dead by then.

The orbit of *Ranger I* created serious problems in recovering and reducing telemetry data. Of a total of 36 spacecraft engineering measurements, all of which are sampled by commutation, 23 are sampled by the data encoder only once every 1000 sec. All of the power system and temperature measurements are included in this group. Proper reduction of these telemetered measurements for evaluation requires that the ground decommutator be synchronized with the spacecraft commutators. This is done by using the 400-cps tone on IRIG Channel 1 and synchronization tones for each of the three commutator speeds. Since the sync tone for the slowest rate measurements (Rate 3) is sampled only once every 1000 sec, and because the station passes were always less than 10 min or 600 sec, the ground decommutators were seldom synchronized with the spacecraft Rate 3 commutator decks. As a result, these samples usually had to be decommutated by hand.

During the 92-hr lifetime of the main battery (through 61 orbital revolutions) portions of 39 orbits were tracked by the DSIF stations and the LCTT. The total tracking coverage was approximately 500 min, including all the periods when the spacecraft signal was lost or below receiver threshold in the middle of a pass. A reasonable estimate of the total amount of useful telemetry obtained would be 300 to 400 min. Table 29 shows a breakdown of this coverage by days.

Table 29. *Ranger* tracking coverage

Date	Tracking time, min	Stations
8/23	41	DSIF 1, 2, 3
8/24	109	DSIF 1, 2, 3, 5, LCTT
8/25	145	DSIF 1, 2, 3, 4, 5, LCTT
8/26	151	DSIF 1, 2, 3, 4, 5, LCTT
8/27	53[a]	DSIF 2, 3, 4, LCTT
	Total 499	

[a] Before battery failure.

General subsystem performance. The over-all performance of the *Ranger I* spacecraft was successful, considering the nature of the orbit flown. In most cases where an element did not perform as it was designed to do, it was because it was not designed to operate in a near-Earth environment. No malfunctions were detected that would warrant making any design or hardware changes in RA-2.

Space Sciences subsystems. The value of most of the scientific experiments was seriously reduced because of proximity to the Earth and lack of attitude stabilization. The data automation system exhibited occasional minor malfunctions, such as premature program re-set, data register re-set, and extra counts in the frame-count register. The scientific instruments, in general, performed as expected, considering their operating environment. The magnetometer was saturated by the Earth's field throughout the mission.

Telecommunications subsystems. All available information indicates that all elements of the communications system performed within their design tolerances. This includes the transponder, data encoder, command system, and ¼-w transmitter. The high-gain antenna drive indicated a higher power output than specified when the transponder was switched onto the high-gain antenna.

Guidance and control subsystems. The spacecraft controller apparently issued all programmed commands in the proper sequence but the exact times cannot be verified. It also provided a 1-pps signal to the data encoder for commutator stepping with a high degree of accuracy except on the second day of flight, when the stepping rate increased. The same is true of the 1 pulse per 1000 sec provided to the Lyman-alpha telescope. The accuracy of the 1-pps signal to other scientific instruments has not been thoroughly checked.

The performance of the attitude-control system was difficult to evaluate because of the limited amount of telemetry obtained before gas depletion. Sun acquisition, as indicated by solar panel current measurements, was only observed on one pass. On other occasions, it appeared that the Earth sensor had locked on the Sun. No valid conclusions can be drawn concerning limit cycle performance, antenna pointing accuracy, or gas consumption rate. Measurements of the rate gyros showed that they were usually saturated due to spacecraft tumbling after the nitrogen gas was gone.

Because the spacecraft was seldom oriented toward the Sun, the solar panels provided only intermittent power, resulting in an almost continuous drain on the launch back-up battery. This main battery's lifetime of about 92 hr is considered normal in view of the system power demands. The few correlated measurements of panel current and temperature available indicate normal performance under the circumstances prevailing.

The power conversion and distribution system apparently functioned normally. The overload in the attitude-control dc-to-dc converter on August 24 was probably caused by excessive power demand in that system resulting from gas depletion and marginal overload design conditions. Some of the other symptoms previously described, which occurred simultaneously, may have been caused by noise generated by the A/C converter's interrogation of its load.

The operating lifetime of the ¼-w transmitter battery was less than 5.6 days, compared to a design value of 10 days. Whether this was due to a discrete failure, or the battery life was reduced by its unexpected environment, is not known.

Not enough data was obtained to make any definite evaluation of the advanced development solar cell experiment.

Engineering mechanics subsystems. Shock, vibration, and acceleration levels during boost phase of the mission were generally as expected. Spacecraft separation, both electrical and mechanical, was apparently normal. The erection of the solar corpuscular analyzer boom and solar panels was apparently normal.

Temperature measurements of elements within the main hexagonal frame of the spacecraft showed good agreement with values calculated for the actual orbit. The temperature of such external elements as the solar panels, Earth sensor, and magnetometer showed more variation than the hex temperatures but this is to be expected, considering the orbit.

The friction-lubrication experiment was designed to measure coefficients of friction in the near-total vacuum of space. Although the value of the data obtained was greatly reduced due to the low-altitude orbit, the experiment apparently performed normally under the circumstances. Its self-contained battery power supply operated longer than its design expectancy.

Ranger II flight performance. The post-injection flight performance analysis of *Ranger II* was limited by the scarcity of telemetry data obtained from the low satellite orbit, which could not be tracked by the DSIF except for a few brief passes. A total of only 37 min of spacecraft telemetry was recovered by all stations after the spacecraft was separated from the *Agena.* This was sufficient, however, to indicate generally successful performance of

most of the spacecraft systems, considering the nature of the orbit. In most respects, the flight was almost a duplicate of *Ranger I* except for its shorter duration.

The *Atlas* performance was apparently normal. The times of ignition and cutoff for the *Agena* first burn were normal, but an excessive roll rate occurred during this period. A near-nominal parking orbit was achieved but no *Agena* second burn occurred, so the spacecraft remained in a satellite orbit somewhat lower than that for *Ranger I*. Separation occurred at the normal time but the calculated relative separation velocity and angular rates indicate that the nested spacecraft high-gain antenna dragged against the sterilization diaphragm on separating.

The initial orbit had a period of 88.31 min, apogee of 147.2 mi, and perigee of 97.5 mi. The spacecraft was in the Earth's shadow for approximately 37 min of each orbit. The Mobile Tracking Station in South Africa provided most of the tracking and telemetry data. After the fifth pass over that station, the orbit was below the horizon and no further passes were tracked.

Following separation, the spacecraft was designed to execute a programmed series of maneuvers and switching functions upon command from the controller:

(1) Increase transponder transmitter power.

(2) Extend particle analyzer boom and solar panels.

(3) Turn on attitude-control d-c power for Sun acquisition.

(4) Turn on high-voltage to scientific instruments.

(5) Turn on attitude-control a-c power for Earth acquisition.

(6) Change data encoder scale for rate gyros.

(7) Switch transponder transmitter from low-gain (omni) antenna to high-gain antenna.

(8) Remove scientific and fast-commutated engineering telemetry modulation from the ¼-w transmitter (beacon).

(9) Turn on friction-lubrication experiment.

All of these commanded functions apparently occurred in the proper sequence and approximately at the programmed time. All but the panel opening command were scheduled at times between tracked passes and the exact times are indeterminate. Event blips indicating boom and panel extensions were recovered. The beacon modulation change was not verified since the beacon signal was never tracked. All of the other functions (including beacon power output) were verified by telemetry from the affected subsystems.

The command for Sun acquisition was given shortly before the spacecraft left the sunlight and no acquisition data was obtained. The Earth acquisition command was given while still in darkness. Spacecraft attitude stabilization was not observed during any of the subsequent passes tracked.

The communications transponder and data encoder, as on *Ranger I*, showed no performance irregularities. The command system (for ground commands) was not tested.

The power supply system apparently obtained little solar power because of the lack of attitude stabilization, and, therefore, operated off battery power most of the time. Power regulation and distribution were apparently normal.

All scientific instruments on board *Ranger II* were operating. Most of them performed normally for the type of orbit flown although a few displayed some minor irregularities similar to *Ranger I*.

4. Vehicle Integration

JPL Specification 30331, issued on May 3, 1960, defined the spacecraft and system requirements necessary to effect interface design between the spacecraft and the *Atlas–Agena* launch vehicles. At this time, definition of interface demarcation was agreed upon by JPL, MSFC, and LMSC. Certain basic decisions relating to the interface equipment were also agreed upon. Efforts were made to utilize existing LMSC designs and design experience, as far as practical. Some of the agreements were:

(1) It was decided that a monocoque shroud would be utilized. The shroud was to be ejected axially, in a forward direction. This shroud was selected after consideration of design, fabrication, contractual, and weight problems associated with an r-f transparent clam-shell shroud.

(2) A spacecraft–*Agena* adapter section was necessary to provide support for the spacecraft, since the shroud was necessarily of a larger diameter than the *Agena*, and the spacecraft directional antenna required an extension in length.

(3) The spacecraft r-f signals would be monitored with the shroud in place through the use of

antenna coupler systems instead of hard-line, quick-disconnect systems.

(4) The spacecraft-shroud eject would be effected by using existing LMSC explosive-actuated pinpuller and spring devices.

(5) To accomplish spacecraft sterilization, it was decided to incorporate a sealing diaphragm and associated valving in the LMSC-designed spacecraft–*Agena* adapter.

(6) An *Agena* retro-system design was agreed upon. This was necessary to prevent the unsterilized *Agena* from impacting the Moon.

(7) The spacecraft would have a separate umbilical connector.

(8) Agreements were made relating to launch complex equipment.

a. Systems interface. The *Agena B–Ranger* spacecraft interface requirements are schematically presented in Figures 60 and 61. Note that r-f commands to the spacecraft when enclosed by the shroud utilize the external r-f system and the omni-coupler system. The high-gain coupler system is used for pre-launch checkout purposes only. Failure coverage is provided from launch to shroud ejection through the omni-coupler system, and from launch to separation from the *Agena* through the modulation of a composite *Agena* telemetry signal.

Hardware developed for the mounting of the spacecraft on the *Agena* vehicle consisted primarily of two items: (1) an adapter, pictorially represented in Figure 62, on which the spacecraft and shroud are mounted; and (2) the shroud, shown in Figure 63, which installs in an axial direction over the spacecraft and protects it during the boost phase of the flight. Just before the *Atlas–Agena* separation, the shroud is ejected axially so that it will not be necessary to further accelerate its weight. Following the end of the *Agena* second burn, the spacecraft is injected into its trajectory, leaving the adapter with the *Agena*.

After spacecraft injection, the *Agena* vehicle performs a 180-deg yaw maneuver and a retro-rocket is fired to

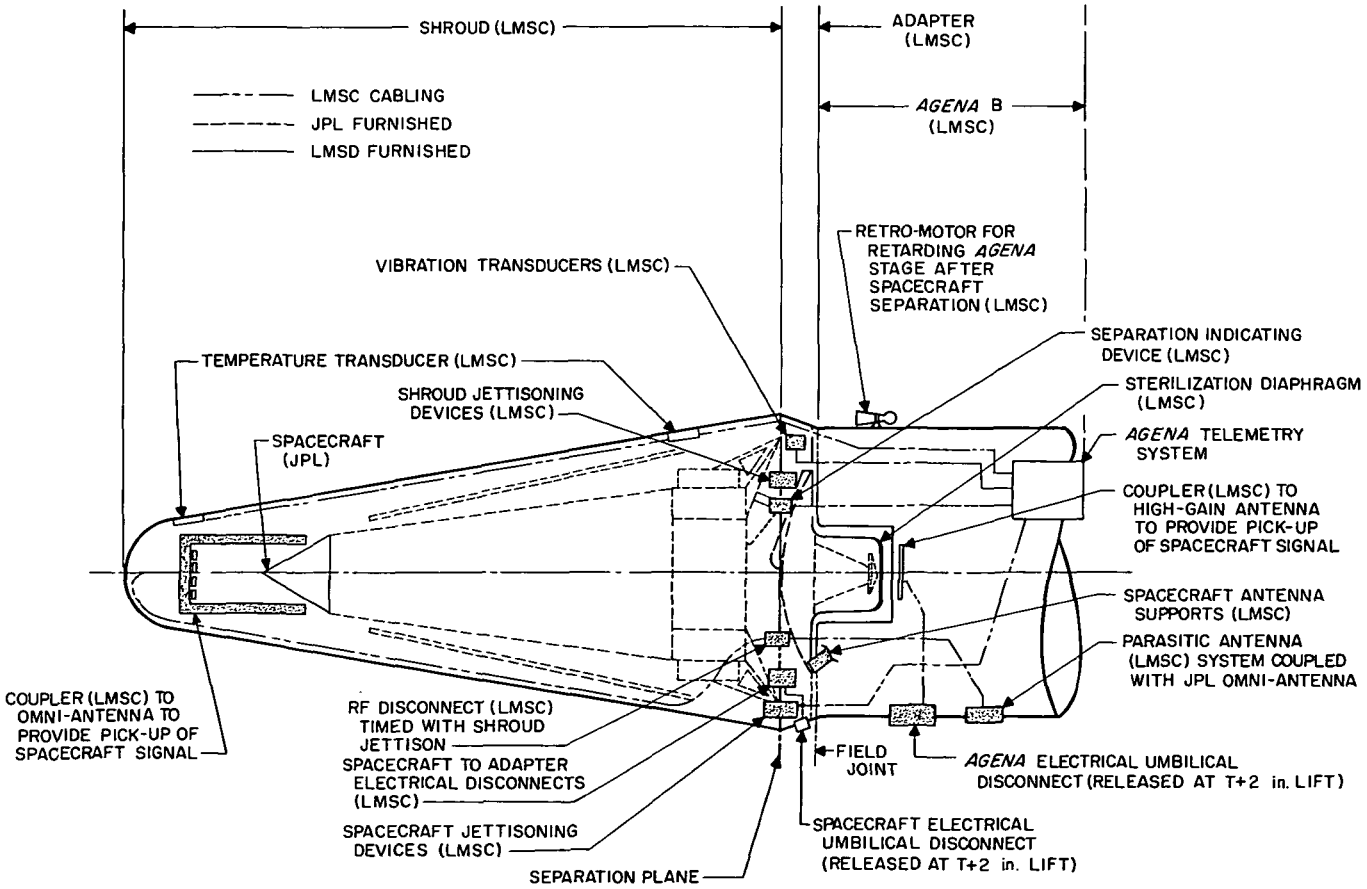

Figure 60. *Ranger–Agena B* interface

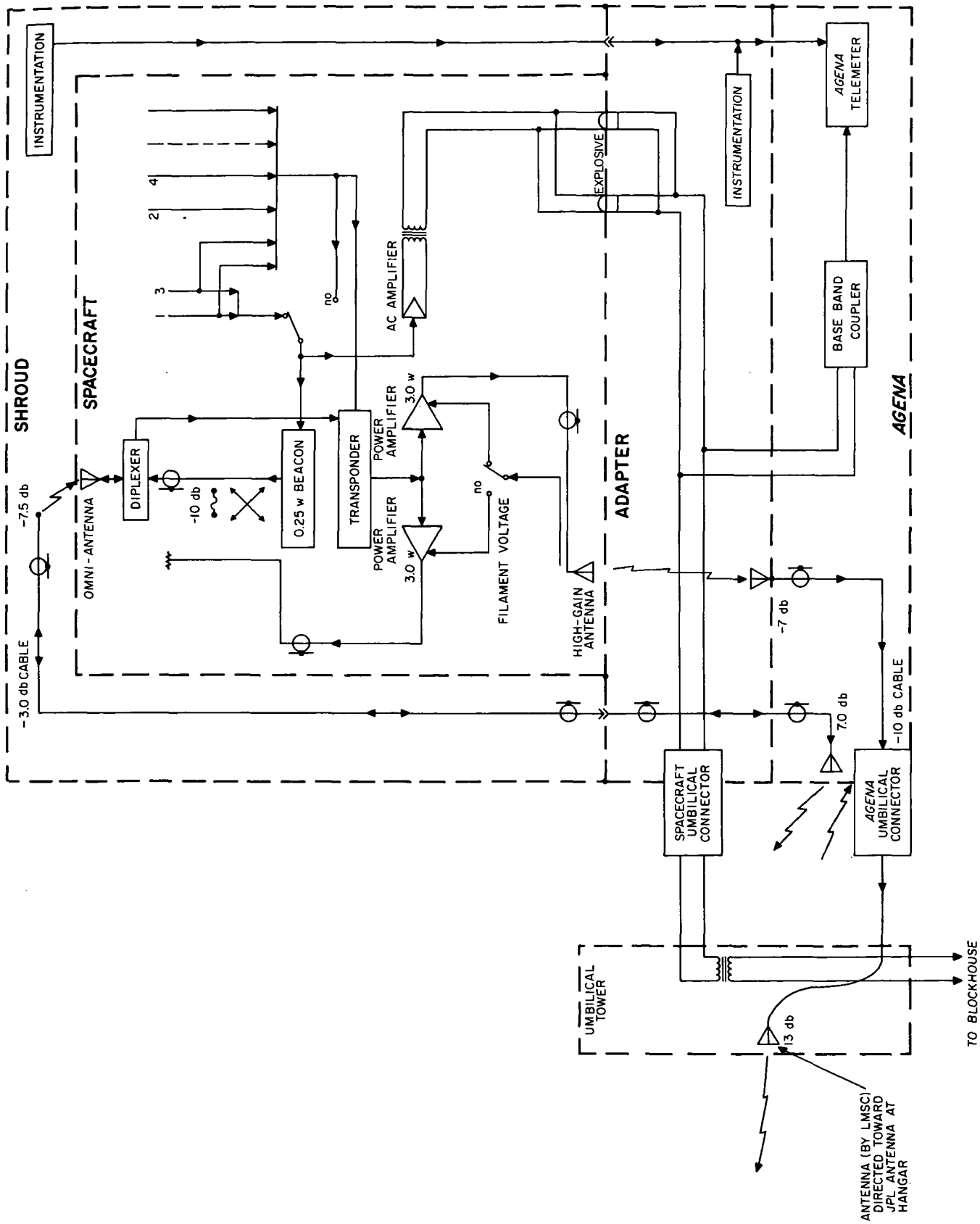

Figure 61. R-F and telemetry interface

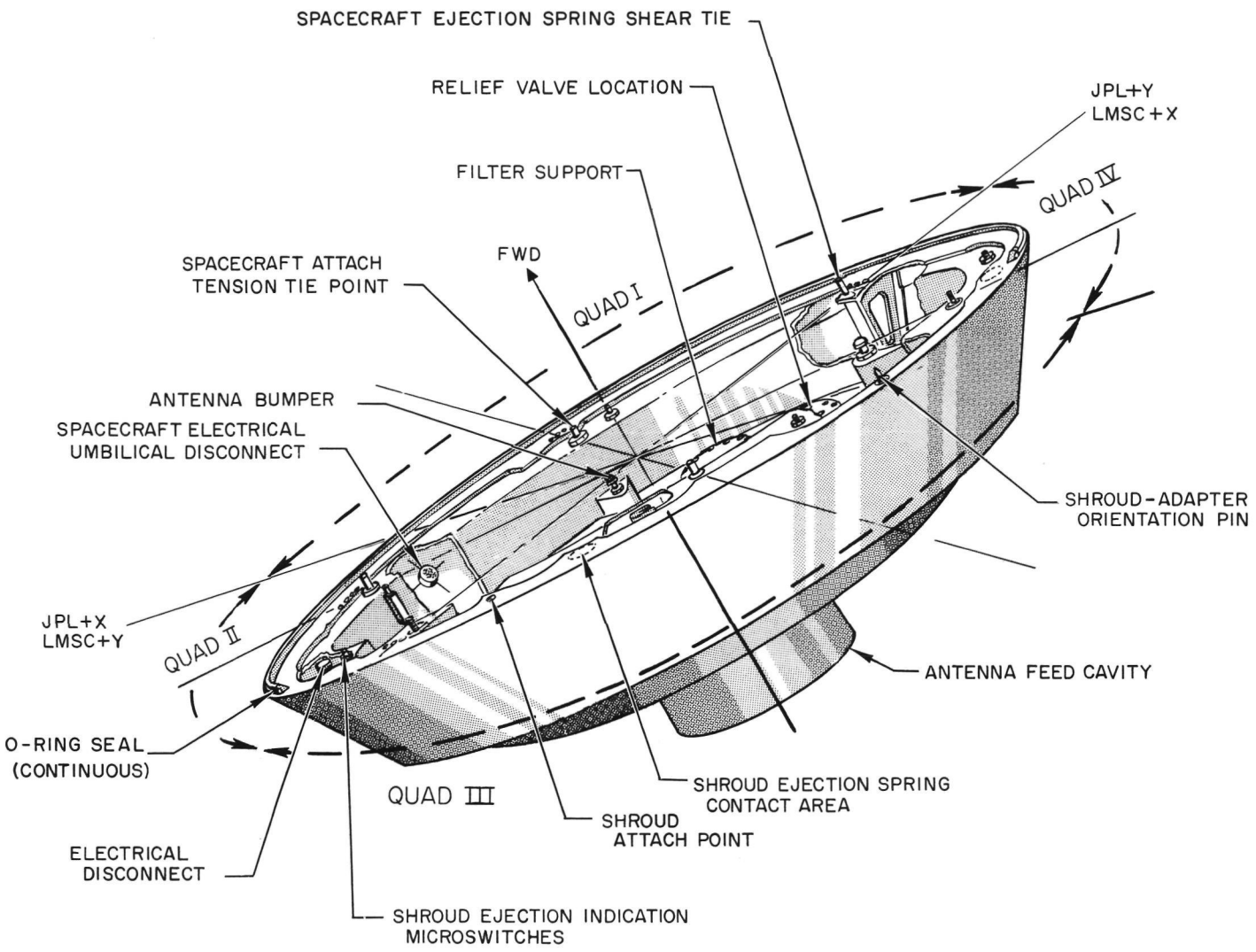

Figure 62. Spacecraft adapter

reduce the *Agena* velocity to prevent its impacting the Moon.

LMSC made several presentations of the shroud and spacecraft separation mechanisms and dynamics. At these meetings, the final sequence of events from launch to *Agena* retro-maneuver was developed, and a better understanding of the shroud and spacecraft separation dynamics was obtained.

A mockup of the adapter, shroud, and forward portion of the *Agena* vehicle structure was received at JPL in September 1960, but was immediately returned to LMSC because of inconsistencies in design and construction. The mockup was re-worked by LMSC and returned to JPL in January 1961. Match-mate tests of the spacecraft and this equipment proceeded.

b. Systems interface tests. Specifications were written and procedures for tests of the combined spacecraft–*Agena* systems were prepared. Movement of each major assembly for both tests and flight items is indicated in Figure 64.

Tests relating to the *Ranger–Agena* systems interface which have been conducted are as follows:

(1) Serrated plate shear connection tests.

(2) Smoke tests.

(3) Shroud ground cooling tests.

(4) Payload section assembly vibration tests.

(5) *Agena* hot-firing tests.

(6) Shroud and spacecraft separation tests.

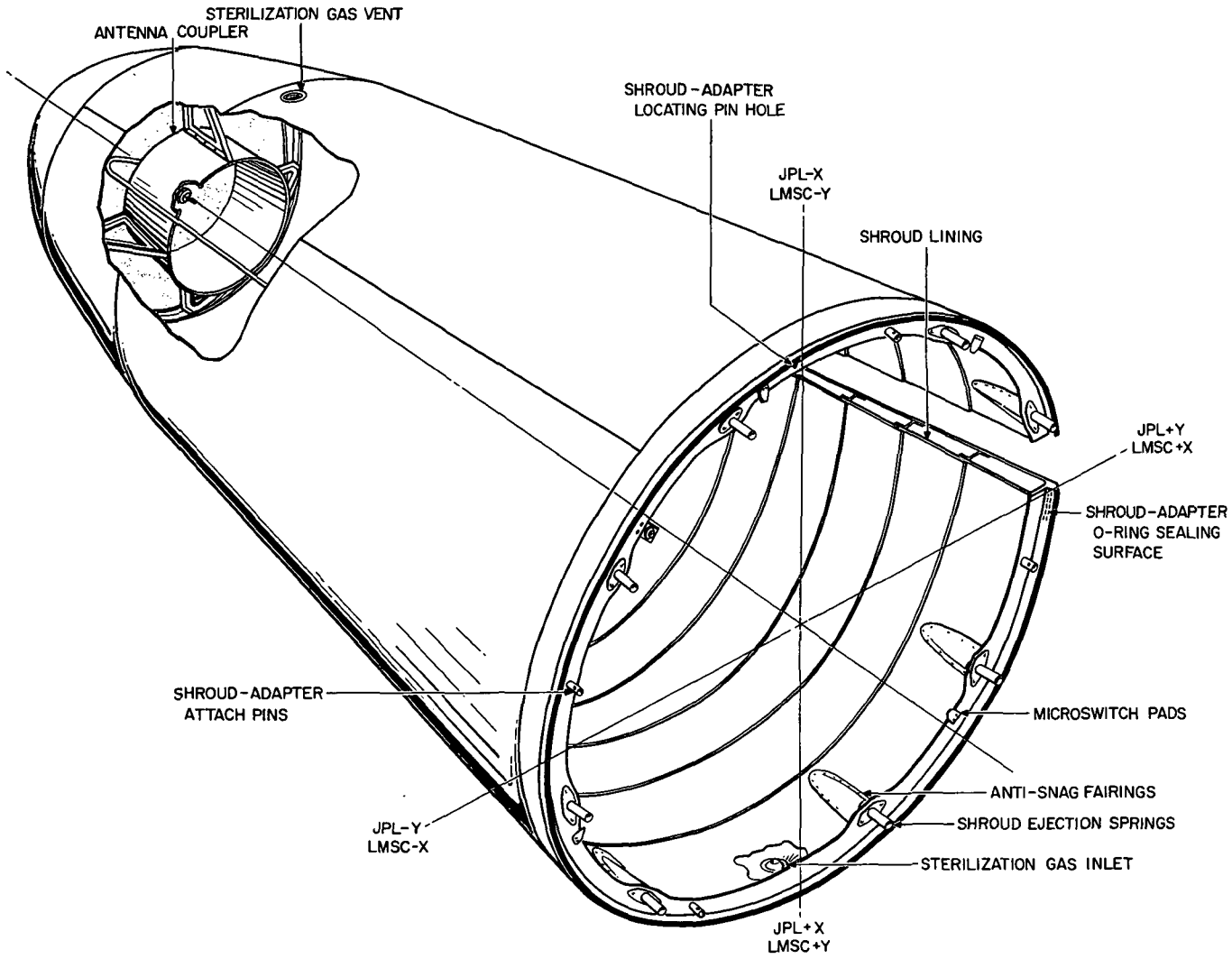

Figure 63. Spacecraft shroud

(7) Match-mate tests.

(8) Combined systems compatibility test.

The results of these tests indicated that the integration design was satisfactory for flight.

Serrated plate shear connections. The design of the shear attachment between the spacecraft and the adapter was investigated. The problem was whether to use a shear connection involving close tolerance, tight-fitting bolts and holes (JPL's suggested design), or a serrated plate type (LMSC's suggested design) which would permit some adjustment. The design was made so that either method could be selected. Hardware was fabricated of both types. On the match-mate tests of RA-1 and -2, both types of hardware were used. Both were satisfactory.

Structural tests indicated that the serrated washer type shear joint was satisfactory. It was, therefore, selected for use on all spacecraft because of its adjustability for varying tolerances.

Shroud material qualification smoke tests. During March and April 1961, LMSC conducted qualitative tests to prove the acceptability of the materials used inside the shroud. It was determined that a number of the materials initially considered for use on the shroud were unacceptable from the standpoint of contaminating spacecraft surfaces by smoke and/or gases generated from aerodynamic heating. These materials were eliminated and replaced by non-smoking materials.

Results of the tests indicated that degradation of the reflective surfaces on the Lyman-alpha mirror would be in the order of 10%. This was considered satisfactory for RA-1 and -2, as it was comparable to variations accompanying the handling, storing, and testing of the samples.

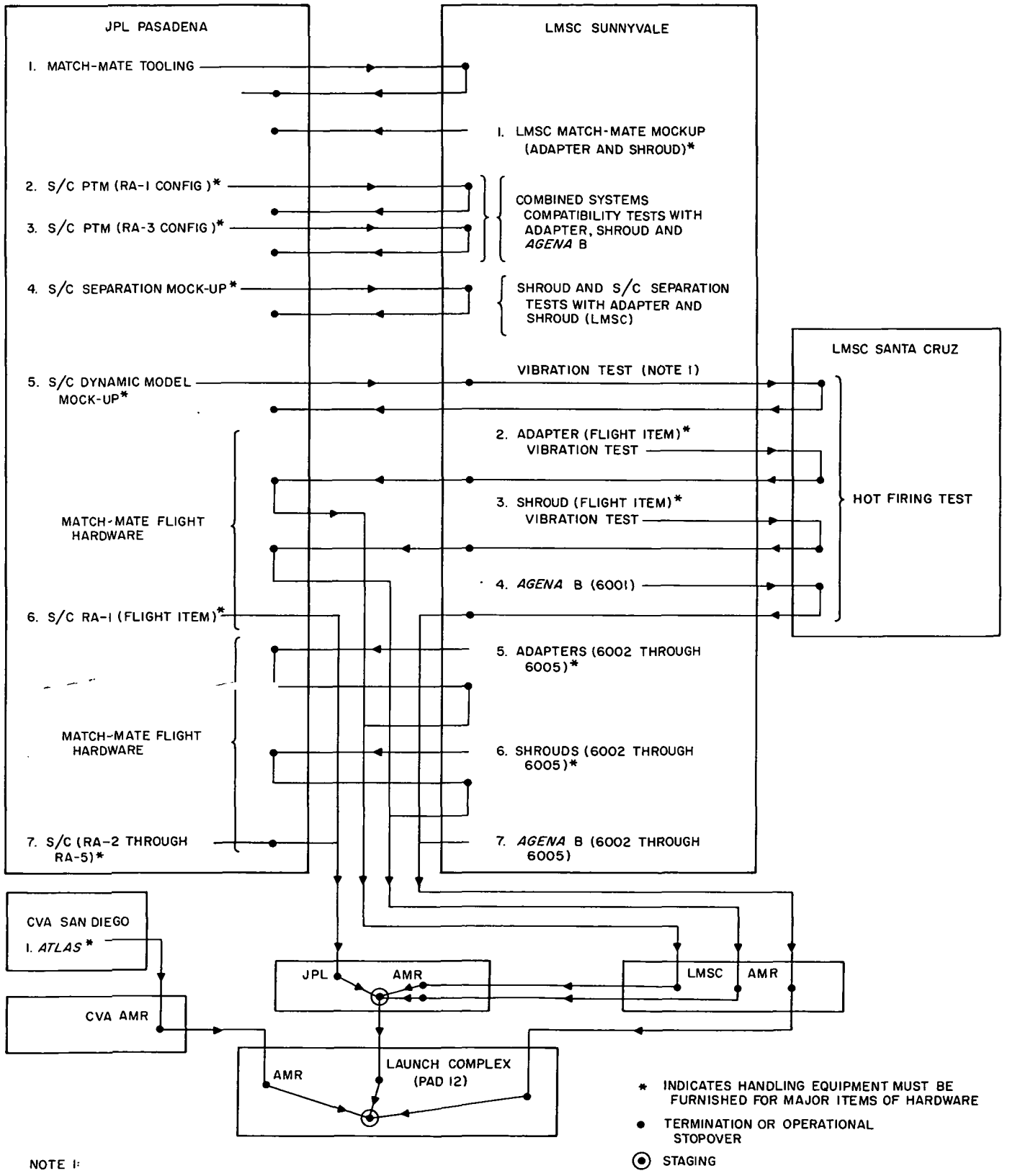

Figure 64. System assemblies flow diagram

All other tests of the JPL samples indicated satisfactory transmissibility in the visible light range.

Shroud ground-cooling tests. A demonstration of ground cooling of the shroud with spacecraft power dissipation simulated therein was made at Lockheed Van Nuys in April 1961. The method for cooling was a cooling blanket which fitted closely the exterior contour of the shroud. Varying quantities of controlled-temperature air were pumped through ducts to the blanket and distributed to annular ducts running around the shroud. Air flowing through the annular ducts picked up both solar heat from the outside and spacecraft dissipated heat from inside the shroud and exhausted it to the atmosphere. The blanket was to be left on the shroud until the missile actually lifts off the pad. A cable attached to the umbilical tower releases the blanket along its entire fore and aft length. As the umbilical tower moves away from the missile, it pulls the cooling blanket with it. The blanket is expected to be damaged and burned sufficiently by the missile exhaust to require a new one for each flight.

The weather was sufficiently cool to allow *Ranger I* to be fired without using a cooling blanket. On *Ranger II*, a cooling blanket was used with satisfactory results.

Vibration tests. JPL furnished a dynamic model of the spacecraft to LMSC in April 1961 for running a composite vibration test of *Agena*–spacecraft adapter, the spacecraft, and shroud. The purpose of these tests was to check the structural compatibility of the assembly under simulated vehicle vibration.

The package was shaken in all three axes over a range of 6 cps to 2 kc. Loads varied from 1 *g* at the low ranges to 7.5 *g* at the high range, with intermittent 0.5-*g* levels at particular table resonance conditions. Data from the test consisted of accelerometer data from the shake table, the adapter, the spacecraft, and the shroud, and data taken from distance probes on both spacecraft antennas to determine any possible bumping or interference. Results indicated the package was structurally sound and no interferences were detected. Upon completion of the vibration tests, the dynamic model of the spacecraft was sent to Lockheed's Santa Cruz test base for use in the *Agena* hot-firing tests.

Agena *hot-firing test.* A hot-firing test of the *Agena* system was conducted at the LMSC Santa Cruz Test Base. A dynamic model of the spacecraft instrumented with 12 accelerometers was furnished. Acoustical measurements were taken both inside and outside the shroud. The test was conducted with all functions of the *Agena* being monitored and a normal countdown followed. Data was taken by use of both land-line and telemetered signals. Both first and second burns of the *Agena* were of full duration. Results indicated that a working spacecraft would have survived the firing tests satisfactorily.

Shroud and spacecraft separation tests. Shroud and spacecraft separation tests were conducted by LMSC at its Burbank, California, Facility. The test was set up with the adapter mounted on a rigid steel framework with the centerline of the missile in a horizontal position. The spacecraft was attached to the adapter with the flight-type pins, ejection springs, and pinpullers. The weight of the spacecraft was supported precisely at its CG by means of a cable running to the building roof trusses approximately 65 ft above the floor. When the squibs in the pinpullers released the spacecraft, the springs ejected it away from the adapter. The precise movement was recorded by three high-speed motion picture cameras aimed at targets on the spacecraft. Shroud separation tests were run in a similar manner. Results indicated that no major difficulties would be encountered.

Match-mate tests. Match-mate tests were conducted at JPL, using mock-up equipment of the adapter, shroud, and PTM spacecraft. Further, match-mate tests of the actual flight hardware were accomplished on RA-1, -2, and -3. Although no major difficulties were encountered, enough minor discrepancies were discovered (different on each set) to warrant continuance of match-mate tests of flight hardware prior to shipment to AMR.

Combined systems compatibility test. The combined systems compatibility test was conducted at LMSC, Sunnyvale, California, during March 1961. For the performance of this test, MSFC provided over-all management direction. LMSC and JPL supplied personnel to perform the necessary tasks in their respective areas. These personnel were under the control of LMSC and JPL test directors, who reported to an LMSC test conductor. The test conductor reported to MSFC personnel.

The purpose of this test was to demonstrate the mutual compatibility of the RA-1 PTM and the *Agena B* 6001 vehicle. The test was conducted in accordance with LMSC specifications and was divided into three major areas.

Mechanical compatibility. This test was to go through, as completely as possible, the operations necessary to mate the spacecraft with the *Agena* shroud and adapter (Fig 65), and to determine if the ground handling equipment was compatible with the flight hardware.

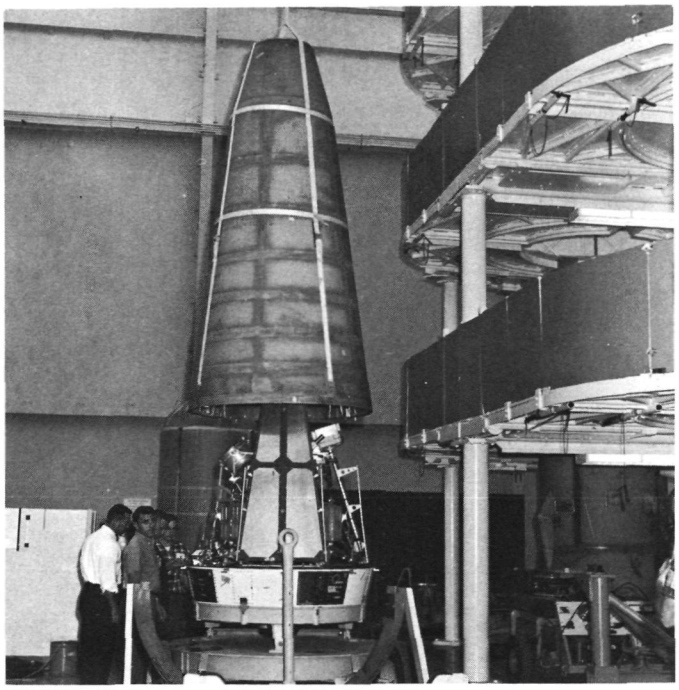

Figure 65. Installation of spacecraft shroud

Electrical compatibility. This test was to determine if the spacecraft–*Agena* adapter wiring was mutually compatible.

Radio-frequency compatibility. This test was to determine: (1) r-f compatibility between on-board electrical and electronic systems, and (2) r-f compatibility between on-board electronic systems and certain simulated AMR sources.

During this test, the *Agena* and spacecraft were simultaneously put through complete system checkout runs while being exposed to a simulated AMR r-f environment. Three different system runs were made: the first run was accomplished without the shroud installed (Fig 66). In the second run, the shroud was installed and was removed manually (Fig 67) at the time it is normally ejected during flight. During the third run, efforts were made to simulate flight conditions as nearly as possible. External monitoring cables were removed and the preflight countdown was simulated. At $T - 0$, the spacecraft and *Agena* umbilicals were removed and a simulated flight sequence was conducted.

The r-f environment equipment was designed to simulate AMR conditions as nearly as practical. The equipment consisted of signal generators feeding directional antennas aimed at the spacecraft (Fig 68). JPL acted as over-all coordinator for the environmental simulation.

The objectives of the mechanical, electrical, and r-f interference tests were met. A number of problems were encountered; however, these were minor and were resolved during the course of the test. Evaluation of the spacecraft telemetry and central recorder records has revealed no abnormalities in spacecraft operation due to the r-f environment. However, two incompatibilities were uncovered during the course of this test.

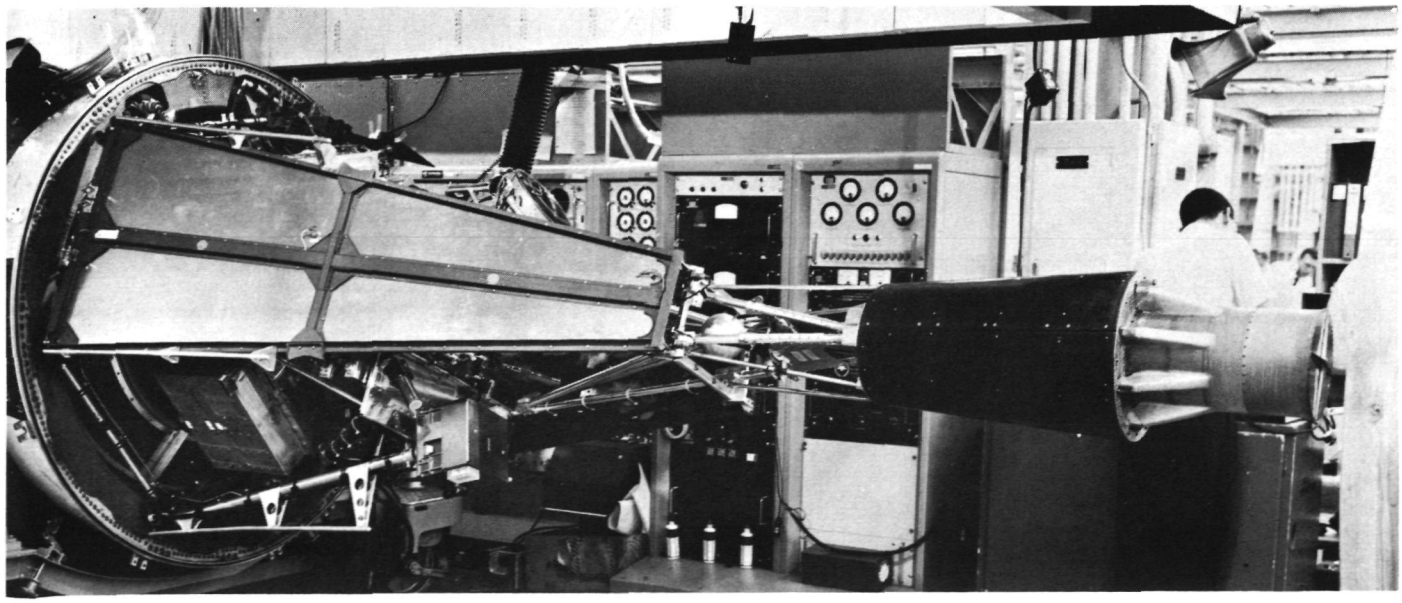

Figure 66. Spacecraft mated to *Agena*

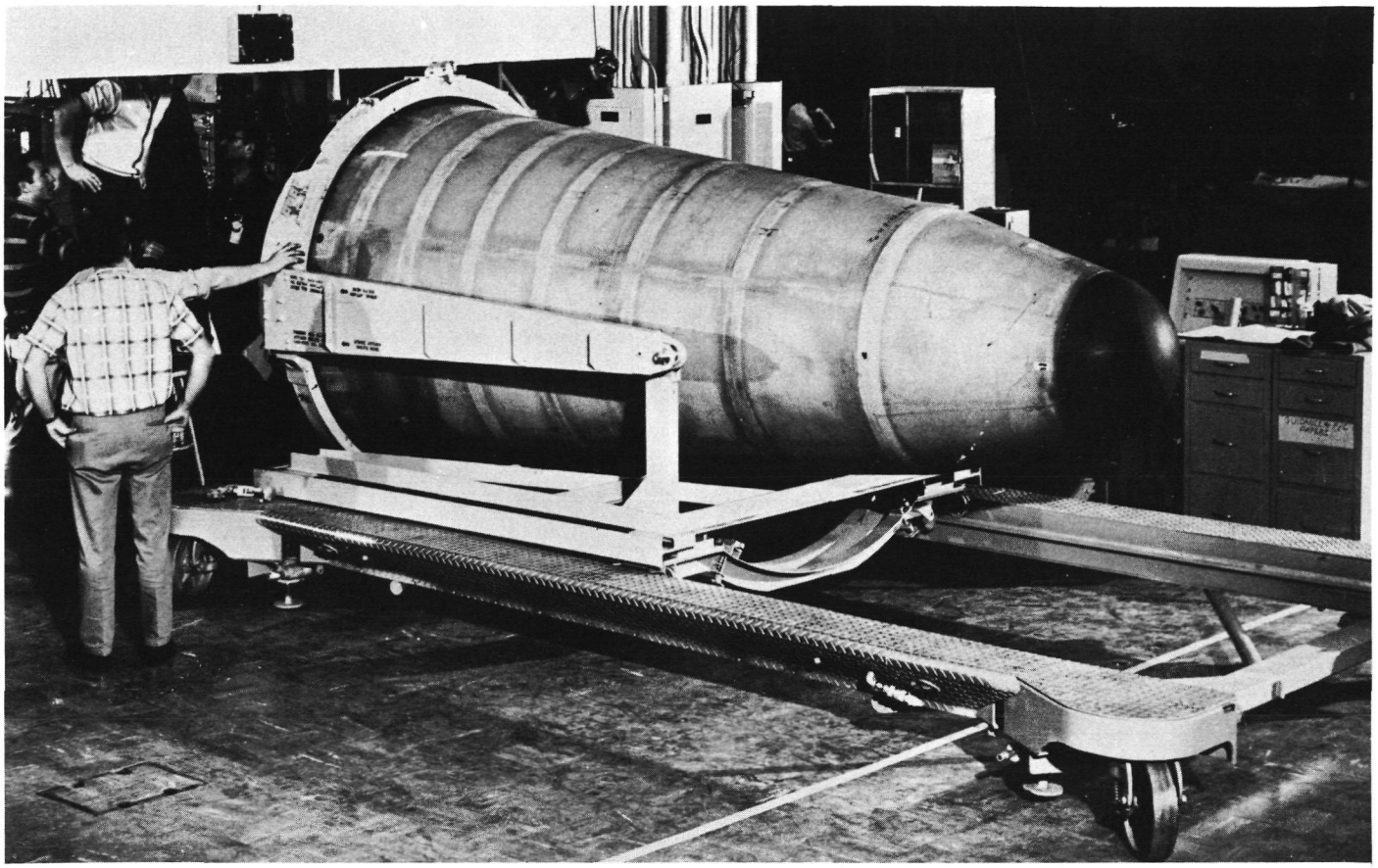

Figure 67. Spacecraft–adapter–shroud assembly

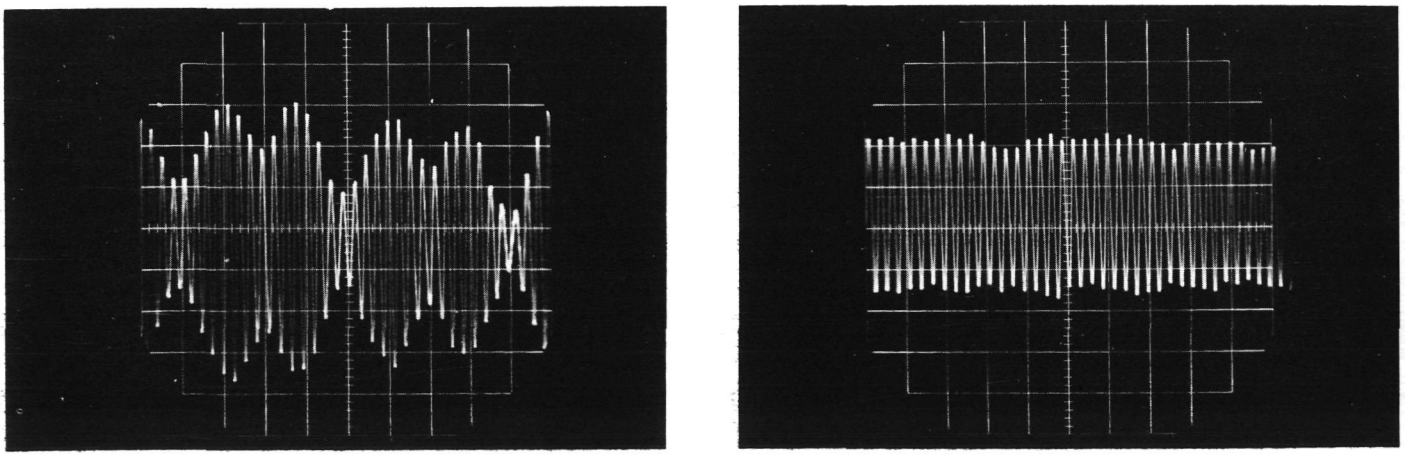

Figure 68. Channel 3 output

Electrical incompatibility. Observations of the spacecraft signals after coming through the *Agena* telemetry system showed a noticeable 800-cps component which interfered with the spacecraft Channel 3. This interference is shown in Figures 68, 69, and 70. Figure 68 was taken from the tape made during the tests. This shows Channel 3 on the spacecraft modulation line and after passing through the *Agena*. The two pictures were taken

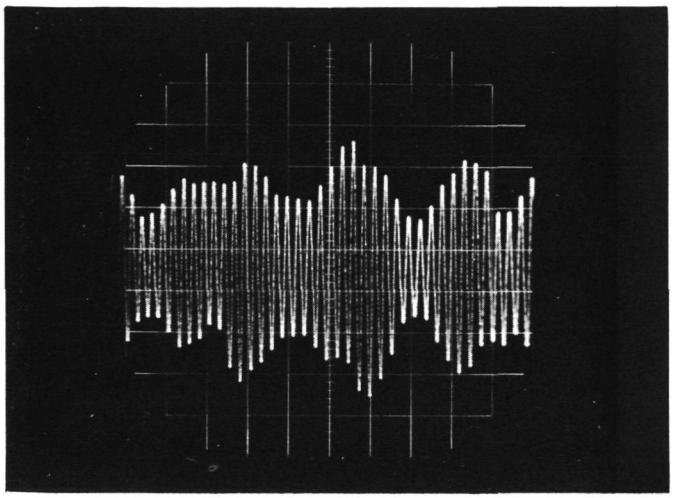

Figure 69. Channel 3 output taken from LMSC telemetry tape

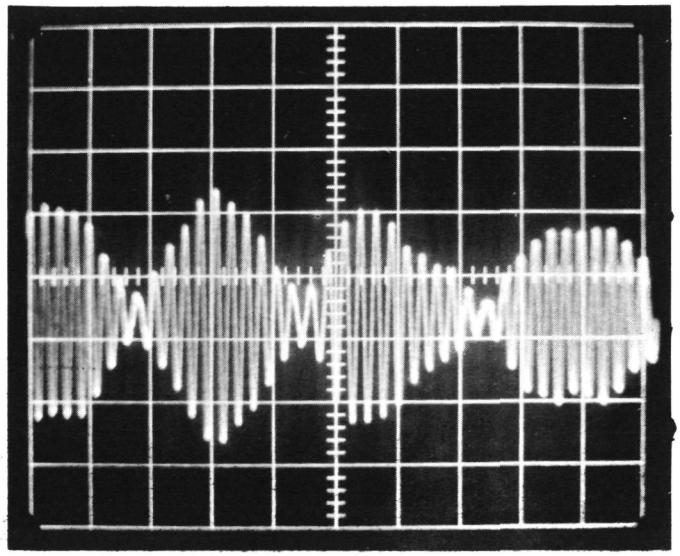

Figure 70. Channel 3 output on *Agena* telemetry signal

when Channel 3 was at the same frequency. Figure 69 was made from a dub of the recording made of the *Agena* telemetry signal by Lockheed during the test; it shows the same effect. Figure 70 was taken at Lockheed during the test.

It was determined that the 800-cps tone was not caused by the instrumentation gyro in the spacecraft. Analysis of the spacecraft and *Agena* signals with an HP Model 302A wave analyzer is shown in Table 30. Thus, the *Agena* telemetry signal contains an 800-cps component which is 20 db greater than that in the spacecraft and only 6.5 db below Channel 3.

Table 30. Analysis of spacecraft and *Agena* signals

Signal	Spacecraft signal, db	*Agena* signal, db
Channel 1	−12	−12
Channel 2	0	0
Channel 3	−7	−6.5
Channel 4	0	0
800 cps	−33	−13

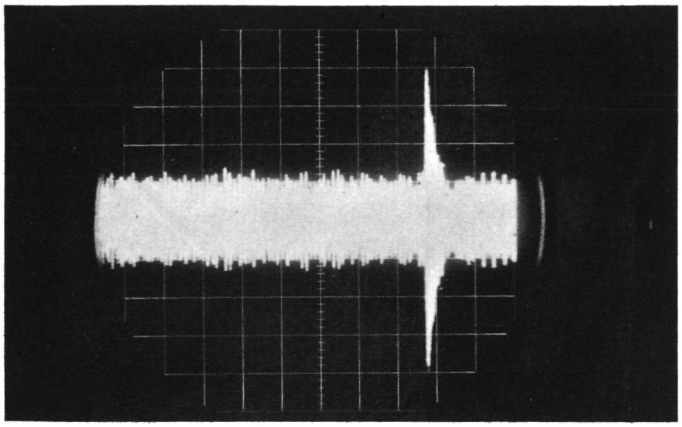

Figure 71. Channel 1 amplitude change

Another incompatibility is shown in Figure 71. This increase in amplitude occurred regularly every 40 to 45 sec, and only on Channel 1 of the *Agena* telemetry signal and nowhere else. This transient, under no-noise conditions, causes the Channel 1 discriminator to momentarily lose lock. This can cause an error in the 400-cps timing reference used in the decommutator and in decommutating the scientific data.

LMSC resolved the 400- and 800-cps problems by performing an additional test utilizing a JPL-furnished magnetic tape to simulate the JPL audio telemetry signal during an *Agena* 6001 systems test. When the reduced data failed to duplicate the prior problems, attention was redirected toward associated support equipment. The offending item was determined to be a recorder.

R-F incompatibility. From approximately 24 hr prior to launch until the shroud is ejected during the boost phase of flight, the spacecraft is completely enclosed within a metal box, i.e., the shroud, the adapter, and the *Agena* forward equipment rack. Thus, a fundamental incompatibility arises in that the antennas are not radiating into free space with the result that a large voltage

standing wave ratio (VSWR) exists within the r-f system (Fig 61).

As shown in Figure 61, the spacecraft has three r-f cavities which provide the r-f power output: two at 3.0 w and one at 0.25 w, through coaxial cables, etc., to the spacecraft antennas. Task Assignment Directive No. 007 from MSFC to LMSD established the feasibility of coupling a portion of this r-f energy from the antennas to the exterior of the vehicle, and the system design parameters are noted in JPL Specification No. 30331. Thus, two-way communication links are provided through an integrated r-f system.

The large VSWR was found to degrade the performance of the r-f cavities. The performance of the Lockheed-designed and -installed r-f couplers was not degraded.

The combined systems compatibility test showed degraded performance through the integrated r-f system, with especially poor performance (compared to the original LMSC laboratory tests) through the high-gain antenna coupler system. The power output through the omni-antenna to parasitic-antenna system was 5 db less than anticipated; and through the high-gain antenna *Agena* umbilical connector system it was 13 db less than anticipated. (Values shown in Figure 61 are the anticipated values.)

It was established that the large VSWR in the spacecraft coaxial cables, which is the load seen by the r-f cavities, was degrading the performance of the r-f cavities. The mismatch detuned the cavity with resultant reduction in power output; and detuning the cavity caused a large and supposedly detrimental increase in the plate current. The mismatch was alleviated by changing the length of the spacecraft coaxial cables so that each r-f cavity would see as little mismatch as possible.

Later, it was determined from laboratory tests that, although the plate current was large, it was not detrimental because only the low-power mode of the cavities is used until $T + 22$ min, when the transponder power is turned up. (The shroud is ejected at $T + 297$ sec.)

c. Conclusions. The flights of *Rangers I* and *II* have demonstrated that the design of interface equipment was satisfactory. Specifically:

(1) Design requirements for spacecraft communications through the coupler systems were achieved.

(2) Design requirements for shroud and spacecraft ejection were met.

(3) The shroud and adapter furnished the expected spacecraft environmental protection.

The results of these flights, as well as the results of interface tests, have provided a high level of confidence in the interface equipment design.

5. Cabling

a. RA-1 and -2. The *Ranger* spacecraft series has in the order of 20 distinct functional subsystems, depending upon the mission. The attitude-control subsystem, for example, which provides a basic function, appears in unvarying form on all the spacecraft, whereas the scientific experiments vary greatly in number and character. The basic design permits such variation without major change in the spacecraft cabling plan, and variations in cabling within the series will consequently not be discussed.

Each of the subsystems referred to contains a number of subassemblies performing mechanical and electronic functions. A typical subsystem is housed in an electronic assembly containing six to ten subassemblies, with additional components situated peripherally from the central electronics area. An electronics assembly occupies each of the six bays of the spacecraft hexagonal main structure. The numerous peripheral components also require electrical connection to the subassemblies within the electronic assemblies. Part of the power subsystem, for example, occupies electronic assembly No. 6; it also includes two solar panels which deploy outward in flight, and are connected with the power subsystem by means of flexible cabling.

The *Ranger* packaging design leads naturally to the interconnection of subassemblies by means of one harness per electronic assembly and the interconnection of electronic assemblies and peripheral components by means of a main "ring" wiring harness. Complexity of individual harnesses, from the standpoints of electrical design and physical realization, proved readily manageable. Design and fabrication of harnesses proceeded concurrently and with a large degree of independence. The ring harness, which couples to each of the electronic assembly harnesses by means of detachable connectors, completes the wiring. Ring harness electrical design was intentionally kept flexible, to accommodate the evolution into final form of the various subsystems.

A particular series of electrical connectors was designated as standard for subassemblies. All subassemblies requiring electrical connections were provided with one or more connectors of the proper size, taken from this

light-duty series. A second series of connectors was designated for interconnecting electronic assemblies to the ring harness. From one to six connectors from this heavy-duty series are required for each electronic assembly. The data encoding assembly requires a particularly large number of interconnections in gathering data for telemetering from many points in the spacecraft.

The electrical design of the wiring calls for splicing of wires within the harnesses; as a result, the assembly harnesses, and particularly the ring harness, perform functions of junctioning and distribution as well as interconnection. In addition to saving the weight of a more conventional junction box, the number of interconnections through connectors is substantially lowered, reducing potential failure correspondingly. The splices in the harnesses have proved reliable. The locations of splices are restricted to relatively rigid portions of the harnesses; flexible portions are spirally laid in conventional manner.

Two initial requirements were imposed on the choice of wire used in harnesses:

(1) Only wire with a particular formulation of poly-olefin insulation was used.

(2) Only AWG 22 and AWG 20 wire was used.

These two requirements are considered to have contributed greatly to the flexibility and durability of the harness wiring. The poly-olefin insulation diminishes problems of shorting as a consequence of cold flow, and the limited range of wire size (gage) reduces stresses on wires within the harness as it is flexed during installation and operations. Heavy currents in certain circuits are accommodated by paralleling two or three wires on both sides of the circuit. It was not considered practical to employ smaller than gage 22 wire during fabrication and subsequent manipulation of the harnesses.

The electrical design of the system interconnections was influenced by the presence on board the spacecraft of a sensitive magnetometer. For this reason, unusual care was given to the control of magnetic fields, including fields contributed by the wiring. Each circuit interconnecting two or more systems was wired such that the circuit current in the active wire was cancelled by the current in the return wire. To realize cancellation, a strict regimen of circuit return paths was instituted, placing each circuit return parallel to the active wire, and eliminating alternate return paths. A few low-current circuits were exempt from such treatment. The standard service for circuits was the twisted pair, which affords excellent current cancellation. A related advantage of this return-path control is the reduction in cross-talk between circuits.

A further step in cross-talk reduction was the physical separation, by an inch or two, of the wiring carrying "noisy" circuits from that carrying noise-sensitive circuits. Such separation was accomplished without significant increase in weight, since the size of the wire bundling was to be kept small for other reasons as well. Separation is in some instances more effective than shielding, since magnetic coupling is reduced, as well as electrostatic effects. The number of shielded circuits was limited because of the higher likelihood of shorts to shield, and other types of failure experienced in shielded circuits.

b. RA-3, -4, -5 cabling. The design of flight cabling for RA-3, -4, -5 is similar to the concept for RA-1 and -2. The main interconnection was by a cable harness (ring harness) contained within the hex structure, fabricated onto a separable fixture which became a part of the basic hex upon installation. All other connections to squibs, antennas, and scientific experiments are by a separate cable to each item external to the hex structure, but connected into the ring harness or directly to an assembly. Also, the cabling to the midcourse motor, inside the hex structure, required separate cables.

The design evaluation leading into testing for more reliability and selection of improved materials, etc., was increased for RA-3, -4, -5. Improved methods of potting to reduce the leakage of the potting material through the connector insert material, adjacent to the pins, resulted in the use of a two-layer potting technique, one layer of Silastic RTV to act as a barrier around the connector pins, and a second layer of Epocast H-1368 to act as a more secure support to the wires from the potting cup. Series D connectors to the ring (system) harness were used instead of Pigmy connectors. This change was predicated on structure requirement of the spacecraft. However, Pigmy connectors were used for separation, test access, midcourse motor, and AD/F interfaces.

The critical requirements for the gamma-ray boom dictated a complete departure from normally accepted cabling techniques. The extension of the boom required 130 in. of cabling be also extended without degradation of critical electrical parameters of the cable. The solution was the use of teflon-insulated wire laid flat with a coaxial cable at each side forming a ribbon. The cable was then interlaced with glass-teflon lace to maintain the ribbon shape. The cable was contained in a dispenser prior to extension of the boom.

The cable for the midcourse motor required extensive design testing to determine the temperature effects from the motor propulsion. Contractor facilities were utilized for this evaluation. The use of a thicker neoprene insulation, normal fabrication techniques, plus very specific routing of the cable, resolved the problem.

GSE required a complete redesign and fabrication of cabling for RA-3, -4, -5. This cabling is to accommodate the SAF, JPL environmental, and AMR facilities. No departure from normal techniques was required. All cabling was fabricated by subcontract.

Cable harness design and fabrication were in full progress by June 1961, when ECR action was required. ECR requirements were completed by December 1961. Repeated fabrication and testing were required because of ECR's, either by direct change of a cable, or unforeseen mutual effects upon another cable, causing a cable to be fabricated and tested up to ten times to gain flight acceptance. This situation was present 4 weeks before actual launch of the spacecraft.

Because of extensive testing, evaluation of the midcourse motor and gamma-ray cables, fabrication, and flight testing were very close to schedule requirements.

6. Quality Assurance

a. Subsystems. Virtually all of the electronics and electrical wiring on the RA-1 spacecraft were inspected to a nominal quality level. All flight harnesses and GSE cables received continuity and short check per print, and a thorough visual inspection. Only the ring harness received additional high-pot and leakage resistance tests.

From RA-2 spacecraft on, all of the electronic modules were inspected microscopically at least twice, and one or more times at AMR. All subsequent flight harnesses were checked for continuity, shorts, and leakage resistance.

The Quality Assurance Group electrically tested and visually inspected all electrical items on the *Agena* adapter prior to each match-mate test. These inspections revealed serious discrepancies, which were corrected by LMSD.

b. AMR cables. Quality assurance personnel witnessed the installation of all Complex 12 long-line cables during the early part of 1961. All soldering and molding of connectors were also witnessed at AMR. This effort proved worthwhile because it prevented lowering of quality standards because of a pressing schedule.

c. Liaison with vendors. Comparatively few of the vendors who manufactured RA-1 and -2 electronics were surveyed. Moreover, source inspection was spotty. More modules were inspected after modules entered the assembly building at JPL than before. For the RA-3, -4, -5 program, most of the spacecraft modules were inspected both at the source and at JPL. Less than 70% of the RA-3, -4, -5 vendors were surveyed at all.

d. Inspection at SAF and AMR. From the beginning cognizant RA-1 engineers were required to certify that their assemblies met the basic requirements for flight equipment. RA-1 and -2 requirements provided that:

(1) A like unit pass type-approval test.

(2) The assembly itself successfully pass the flight-acceptance test.

(3) The weight requirements be met.

(4) The magnet field requirement be passed.

The requirements were changed for the RA-3, -4, -5 program by not including the magnet field requirement, but requiring sterilization. On all launches to date, few of the assemblies were fully certified when first accepted into the SAF. In fact, as many as 10% of the flight modules at AMR were not fully certified until a few weeks before launch.

The role of the spacecraft inspector evolved slowly, beginning with RA-1. Initial responsibilities included monitoring the engineering change system (ECR and EDFU), and witnessing all "button-down" operations prior to systems tests.

RA-3 spacecraft was more closely controlled. The quality assurance personnel performed more microscopic inspections per module, were at all times aware of the flight-worthy status, and aware of what changes were pending. The spacecraft inspector participated in the packing and shipment of spacecraft equipment and cables to and from AMR. An informal procedure of the spacecraft inspector's job and responsibilities was evolved into a written procedure.

e. Conclusion. The trend has definitely been established for stricter control of equipment and higher quality levels for spacecraft systems. The cognizant subsystem engineers have responded well to the quality assurance requirements. The over-all result has been production of spacecraft of significantly good quality and comparatively trouble-free in operation.

B. Space Sciences

1. Scientific Experiments

a. Scientific objectives. The principal scientific objectives of the *Ranger I* and *II* missions were discussed in Chapter II-B-2 of this report. For the investigation of these phenomena, the *Ranger I* and *II* spacecraft carried a family of radiation detectors designed to monitor the intensity of charged-particle radiation from energies of about 10 ev to about 100 mev. A summary of the portions of the particle spectrum covered by each of the several detectors is given in Figure 72. The dynamic ranges of these instruments were so chosen that studies could be made of quiet conditions in interplanetary space, as well as of the phenomena associated with solar disturbances. A magnetometer for determining the interplanetary magnetic field and its relation to the particle flux was also carried.

Other scientific experiments on the first two *Ranger* spacecraft were a telescope sensitive to Lyman-alpha radiation for obtaining information on the distribution of neutral hydrogen atoms in the vicinity of Earth, an instrument for the analysis of the mass and velocity distributions of cosmic dust particles, and an experiment using a pair of scintillation counters to investigate the statistics of solar X-rays.

Since the orbital altitudes actually reached by *Rangers I* and *II* were so low, most of the scientific objectives of these missions were not achieved. Table 31 summarizes the performance and probable scientific value of each of the instruments flown on *Rangers I* and *II*. The RA-1 and -2 scientific experiments, agencies, and cognizant JPL personnel are listed in Table 32.

b. Solar corpuscular radiation electrostatic analyzers. General description. The solar corpuscular radiation electrostatic analyzers, developed for RA-1 and -2 spacecraft were to measure the low-energy solar particle flux as a function of charge sign, energy per unit charge, and direction of travel. By changing the polarity of the deflection plate voltage, electrons or positive ions could be measured. For the measurement of particle energy, four electron-energy intervals between 13.7 and 110 ev, and eight positive-ion-energy intervals between 13.7 and 5490 ev (for singly charged particles) were selected.

Direction of travel was determined by means of six detectors, each with an acceptance angle of approximately 15 deg about the normal direction. These detectors were assembled in pairs and so situated on the spacecraft that they pointed in six orthogonal directions: toward and away from the Sun, approximately forward and backward in the ecliptic, and approximately north and south

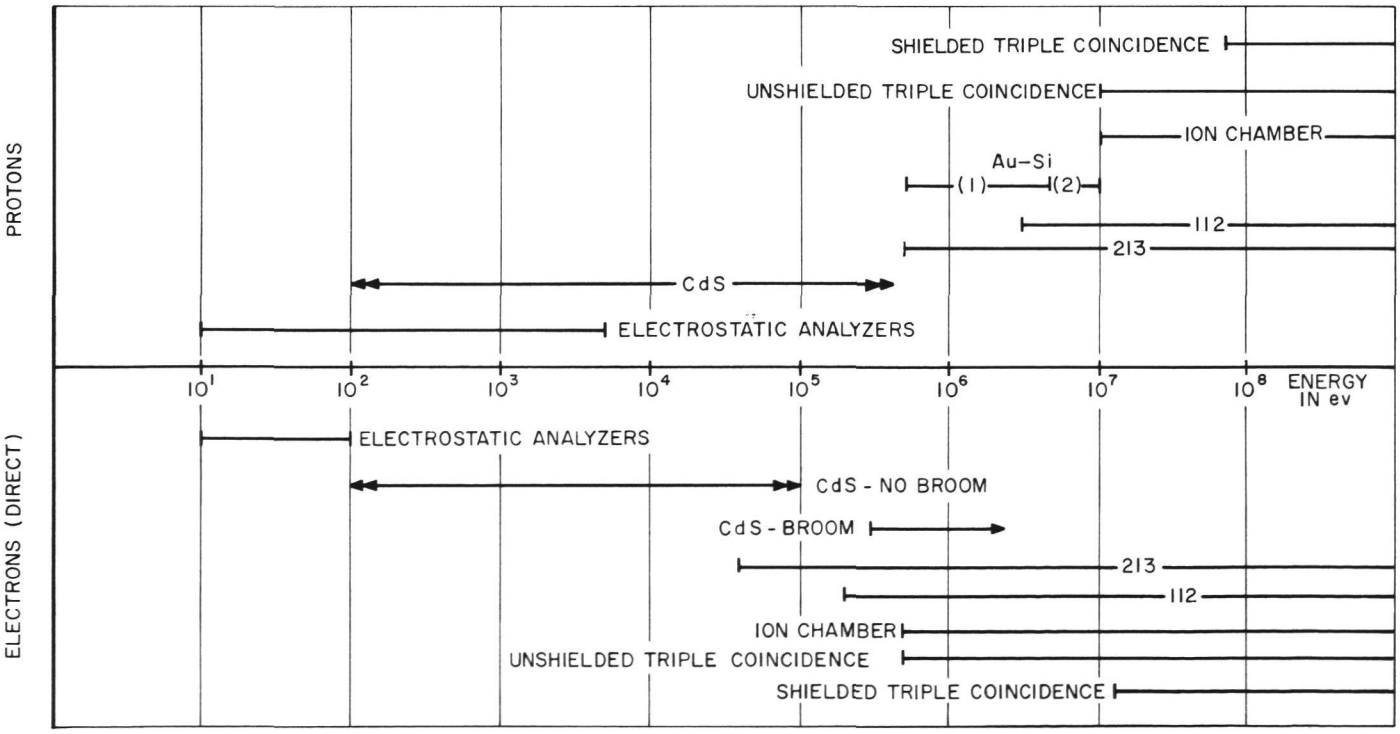

Figure 72. Energy ranges of radiation detectors for RA-1 and -2

of the ecliptic. (The analyzer assembly pointing toward and away from the Sun was located on a boom which was intended to place the analyzers beyond the plasma sheath of the vehicle itself.)

This determination of the direction of travel of the particles, although not extremely detailed, should have made it possible to choose among three principal theoretical models for the interplanetary plasma. These theoretical models are as follows:

(1) The particles spiral around the field lines of a solar dipole magnetic field. This theory is consistent with the *Pioneer V* magnetometer data (Ref 16).

(2) The flow away from the Sun is relatively more important than the magnetic effects, and the particles travel, for the most part, radially out from the Sun (Ref 17). This view is consistent with the observation of the excess curvature of comet tails away from the Sun (Ref 18). Preliminary information from *Explorer X* supports this theory, but due to the short duration of flight, it is not known whether this is a steady-state condition.

(3) Neither the flow nor the magnetic field is of special importance, and the expansion velocity of the plasma is less than its proton thermal velocity (Ref 19).

Table 31. Summary of performance and scientific values of *Ranger I* and *II* scientific experiments

Instrument	*Ranger I*	*Ranger II*
Magnetometer (Goddard Space Flight Center)	c	c
Triple-coincidence cosmic-ray telescopes (University of Chicago)	a*	a*
Cosmic-ray integrating ionization chamber (California Institute of Technology & JPL)	a*	a*
Geiger tube(s) (State University of Iowa)	a	a*
Au-Si medium-energy-range particle detector (University of Chicago)	a	a
CdS medium-energy-range particle detectors (State University of Iowa)	b	b
Solar corpuscular radiation electrostatic analyzers (JPL)	b	b
Composite cosmic dust detector (Goddard Space Flight Center)	a* (Dark) b* (Sun)	b
Lyman-alpha telescope (Naval Research Laboratory & JPL)	a (*?)	b (*?)
Vela Hotel x-ray detectors (Los Alamos Scientific Laboratory)	a*	c

Key: a Operation normal.
b Experiment a qualified success. Any malfunctions are explainable in terms of the unexpected environment.
c No data at all and none expected for such low altitudes and/or short flights.
* Data probably has at least minor scientific value.

The basic operation of the electrostatic analyzers can be shown in Figure 73. Charged particles entering the instrument are deflected by an electric field which is

Table 32. *Ranger I* and *II* scientific experiments, sponsoring agencies, and cognizant JPL personnel

Division of the Space Sciences
Program Representative: M. Eimer.
Project Scientist: M. M. Neugebauer.
Project Engineer: R. L. Heacock.

Experiment	Sponsoring agency/experimenter(s)	JPL cognizant scientist	JPL cognizant engineer
Triple-coincidence cosmic-ray telescopes	University of Chicago/C. Y. Fan, P. Meyer, and J. A. Simpson	M. M. Neugebauer	J. D. Allen
Integrating cosmic-ray ionization chamber	California Institute of Technology and JPL/H. V. Neher and H. R. Anderson	H. R. Anderson W. S. McDonald	H. R. Anderson W. S. McDonald
Medium-energy particle detectors:		C. W. Snyder	J. D. Allen
(a) Geiger tubes and and CdS detectors	(a) State University of Iowa/J. A. Van Allen		
(b) Au-Si detectors	(b) University of Chicago/C.Y. Fan, P. Meyer, and J. A. Simpson		
Solar corpuscular radiation electrostatic analyzers	JPL/M. M. Neugebauer and C. W. Snyder	M. M. Neugebauer C. W. Snyder	C. S. Josias J. L. Lawrence, Jr.
Rubidium vapor magnetometer	NASA Goddard Space Flight Center/J. P. Heppner	D. E. Jones	M. B. Gumpel
Lyman-alpha telescope	Naval Research Laboratory and JPL/T. A. Chubb, and R. W. Kreplin	H. T. Bull	D. D. LaPorte
Cosmic-dust detectors	NASA Goddard Space Flight Center/W. M. Alexander	M. M. Neugebauer	E. S. McMillan
Data Automation system	Jet Propulsion Laboratory	R. Nathan	W. E. Brown, Jr.
Ground support equipment	Jet Propulsion Laboratory		G. F. Baker

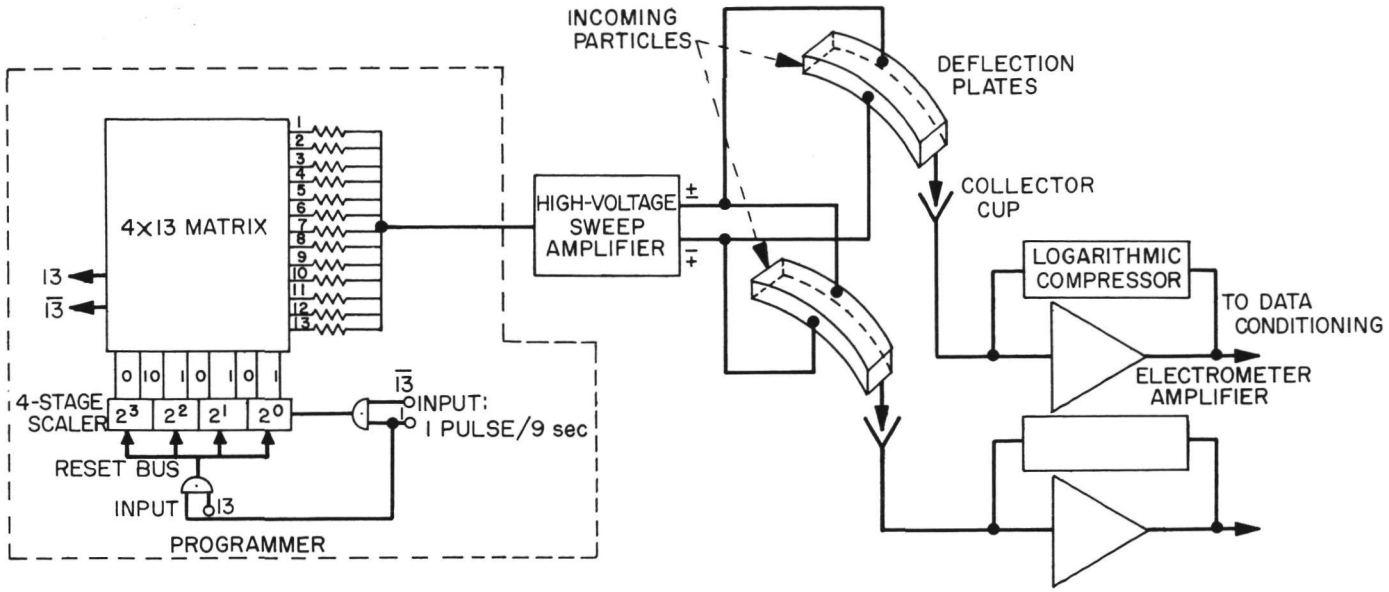

Figure 73. Solar corpuscular radiation experiment

approximately transverse to the particle velocity. Those particles with a particular charge sign, a certain range of energy per unit charge, and a certain angle of incidence are deflected onto the charge collector cup. Particles which enter the deflection plates with the wrong charge sign, energy per unit charge, or angle of incidence strike the deflection plates and are not recorded. The energy distributions of both positively and negatively charged particles entering the instrument can be determined by varying the sign and magnitude of the deflection voltage. The spread in particle energy for each deflection voltage setting is demonstrated in Figure 74 where the fraction of a beam of singly-charged particles with energy E/E_c, normally incident on an analyzer, which reaches the collector cup is plotted vs E/E_c. (E_c = 2.743 times the deflection voltage = energy required for a constant radius of curvature for normally incident singly-charged particles).

Deflection voltage system. The deflection voltages for the analyzer plates are generated by two fully transistorized subassemblies: the programmer and high-voltage sweep amplifier (Fig 75). The programmer consists of 4×13 diode matrix which consecutively gates a reference input voltage to one of the 12 input resistors of the high-voltage amplifier. The matrix is driven by a four-stage binary counter which accepts one pulse per 9 sec from the data automation system (DAS). A reset pulse from the DAS every 120 sec recycles the counter for another measurement sequence. The measurement cycle is shown in Table 33.

The high-voltage amplifier subassembly consists of an operational amplifier with a differential output and large dynamic range (± 100 to ∓ 1000 v dc), in conjunction with two subsidiary amplifiers for generation of the low-voltage steps. This logic was adopted, since the main amplifier is not carrier stabilized in the present design and since the subsidiary operational amplifiers with their limited output range (± 20 v dc) could maintain the smaller voltage increments at sufficient accuracy over the expected ambient temperature range (0 to 80°C). A diode disconnect circuit is utilized in which the deflection plates are clamped to the subsidiary amplifier outputs for the first seven steps and to the main amplifier for steps 8

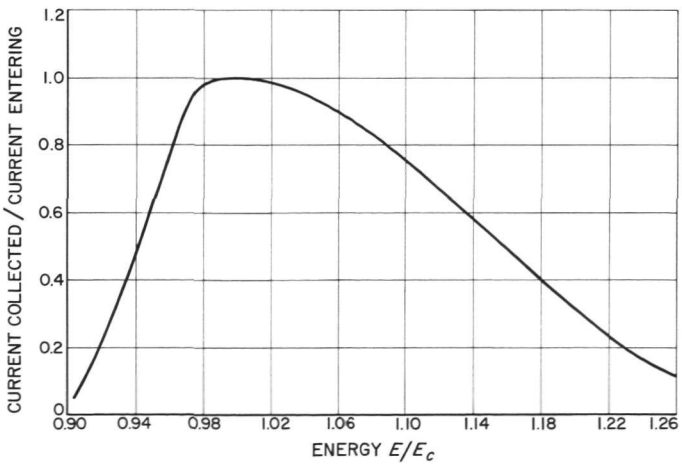

Figure 74. Experimental energy resolution curve for electrostatic analyzers

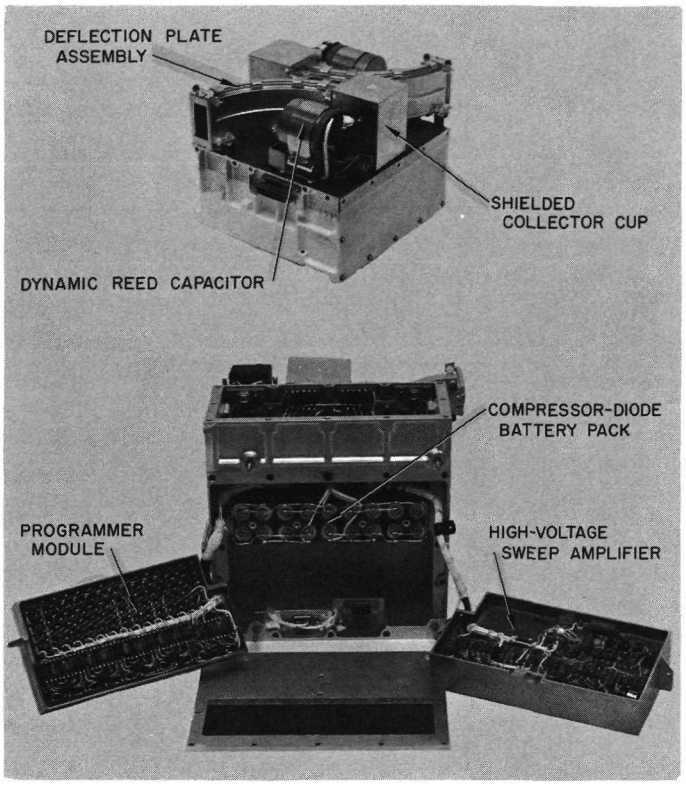

Figure 75. Solar corpuscular radiation electrostatic analyzer

through 12. The differential voltage across the deflection plates and the corresponding particle energy level is shown in Table 34.

Electrometer amplifier. The electrometer amplifier (Fig 76) designed for *Ranger* differs from the usual dynamic reed electrometers in the mechanization and return mode of its primary feedback loop. Transistors are used exclusively in the amplifier design; the necessary high input resistance is obtained by use of the dynamic reed modulator. It resembles a conventional carrier-stabilized operational amplifier, except that the chopper modulator is replaced by the dynamic reed capacitor which has an

Table 33. Measurement cycle for solar corpuscular radiation electrostatic analyzers

Time, sec	Operation
0 to 9	Deflection voltages are held at Step 1
8 to 9	Outputs of all six electrometers are converted and stored by the DAS
9 to 18	Deflection voltages are held at Step 2
• •	•
• •	•
• •	•
108 to 120	Deflection voltages are held at Step 1 but the electrometers are not sampled in this period

Table 34. Particle energies corresponding to voltage across deflection plates

Step number	Deflection plate voltage (outer and inner)	Particle energy, ev
1	−40	109.7[a]
2	−20	54.9[a]
3	−10	27.4[a]
4	− 5	13.7[a]
5	5	13.7[b]
6	10	27.4[b]
7	20	54.9[b]
8	65	178[b]
9	151	414[b]
10	365	1000[b]
11	840	2300[b]
12	2000	5490[b]

[a]Electron.
[b]Proton.

extremely high input resistance. The reed capacitor has a nominal resonant frequency near 2.4 kc, a mechanical Q of about 150, and a conversion efficiency of about 10% at resonance. No effort is made to buck out the amplifier offset due to reed contact potential, since the contact potential and its temperature coefficient are small. Any initial offset due to these effects is compensated in the instrument calibration.

The feedback element of the electrometer, which determines the amplifier transfer function, is the bipolar logarithmic current to the voltage transducer. This device

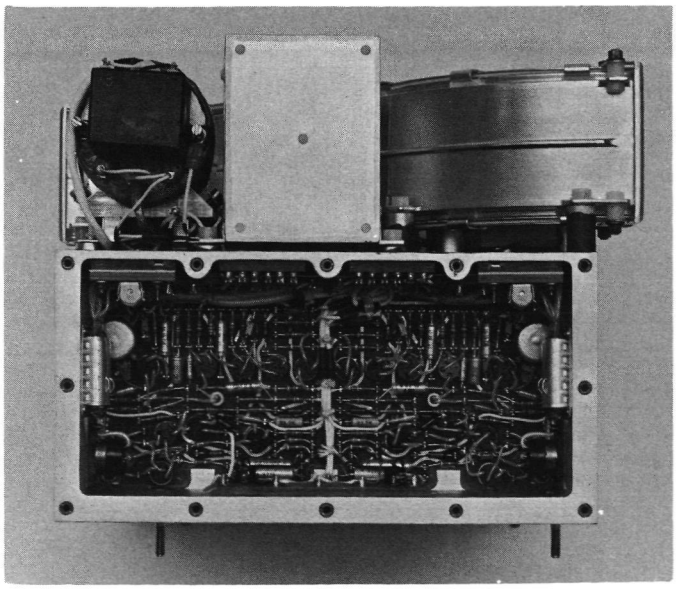

Figure 76. Electrometer compartment

consists of a pair of 5886 pentodes, used as diodes, operating in the retarded field region. The voltage across the diode is then proportional to the logarithm of the current through the tube. The electrometer input current will flow through one diode or the other depending on its polarity and will thus determine the amplifier output voltage. Since the filament of the diode which compresses the electron current is at the electrometer input, it was necessary to provide a battery for this filament in order to maintain a high input resistance. A bias network is incorporated into the feedback loop so that when the input currents are below the electrometer sensitivity ($\pm 10^{-13}$ amp) the nominal null output is about 3.5 v. Figure 77 illustrates a typical amplifier transfer characteristic. The electrometer measures current between $\pm 10^{-6}$ and $\pm 10^{-13}$ amp, which for the deflection plate geometry used, corresponds to particle fluxes between 8.6×10^{4} and 8.6×10^{11} cm^{-2}/sec^{-1} for each energy level.

The compressed analog output is converted to digital form by the data automation system (DAS) for transmission accuracy and convenience. Each electrometer is sampled during the last sec of the 9-sec energy interval

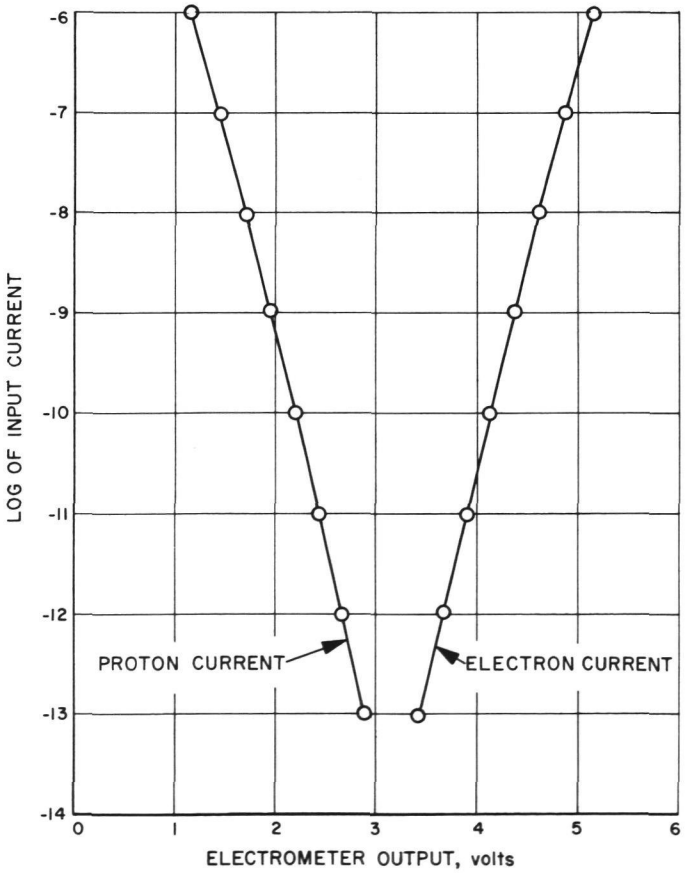

Figure 77. Typical amplifier transfer characteristics

to ensure that the electrometer has reached a steady-state condition. The data are presented in the form of eight-bit numbers and, as the data are the logarithms of the currents measured, the relative accuracy is constant over seven decades. The rms current-measuring accuracy of the experiment, based upon the anticipated environment and duration, is expected to be about ¼ of a decade.

Instrument history. The development contract for the dynamic reed capacitor was let to Applied Physics Corp. in January 1960. Evaluation of prototype reeds in June 1960 indicated that the reed should have a natural resonant frequency near 2.4 kc. Factors considered were conversion efficiency, mechanical Q, drive power, source impedance, and temperature stability of the reed resonance characteristic. At this time, the need for a reed tracking oscillator was considered; that is, a device which would sense the drift in reed resonant frequency due to temperature change, and which would synchronously drive the demodulator in the electrometer amplifier.

The first six prototypes were evaluated in the electrometer with both the reed and the demodulator driven from a fixed 2.4-kc signal. The data indicated that the change in amplifier loop gain suffered at the demodulator (due to phase shift between the reed output signal and the demodulator drive signal) would not seriously degrade the electrometer performance. Realizing this, and considering the limited period for development of the experiment, it was decided in September 1960 to drop the tracking oscillator concept and start production on reeds to be driven at 2.4 kc, a point near their natural resonant frequency. The decision proved to be a costly one, however, since simultaneous control of both the resonant frequency and reed Q in actual production led to a poor yield of reeds with desirable characteristics. A subsequent contract let to Applied Physics in April 1961 has resulted in a dynamic capacitor with a piezoelectric crystal mounted on the reed which can sense reed resonance and thus control a driving oscillator.

The plasma probe project was adequately staffed in June 1960 and circuit development began in earnest. The first prototype instrument was completed and tested in October 1960. Evaluation of one of the proof test model instruments in January 1961 in a particle accelerator showed that ultraviolet photons could reflect down the gold walls of the deflection plates and indirectly illuminate the suppressor grid in the collector cup. This caused the release of photoelectrons, which were recorded as a background current by the electrometer. It was realized that this current would be large enough to cancel the expected positive ion current seen by the analyzer, which looks directly at the Sun. This problem was solved by

evaporating gold onto the deflection plates and collector cup surfaces in a partial atmosphere of hydrogen. The resultant coating was extremely black to visible light as well as Lyman-alpha radiation, and appears to have reduced the photoelectron effect below the sensitivity of the instrument. In RA-2, a stairstep "mirror" was also used to deflect photons back out the entrance.

The first of the three flight packages for RA-1 was delivered to the spacecraft in January 1961. Subsequent effort in construction, evaluation, and flight acceptance testing led to a full complement of spares for RA-1 and flight units for RA-2. The final flight spare was completed in August 1961.

Flight performance summary. The currents measured by these detectors on *Rangers I* and *II* appeared to be independent of the nominal programmed voltage across the deflection plates. A possible explanation is that the positively charged deflection plate collected enough electrons from the ionosphere and the plasma sheath around the spacecraft to cause an overload of the deflection-plate power supply. This should not have been a problem if a nominal orbit had been achieved. A rough idea of the spacecraft orientation and tumble rate can be obtained from these data.

c. Rubidium vapor magnetometer.

General description. In order to determine the magnitude and direction of interplanetary magnetic fields as well as their temporal and spatial fluctuations, a rubidium vapor magnetometer was flown on *Rangers I* and *II*.

There is a strong tendency for any plasma flow from the Sun to drag the local solar magnetic field with it; the field, in turn, impedes the flow of the plasma. Furthermore, the interplanetary magnetic field probably plays a major role in the modulation of cosmic rays reaching the solar system from interstellar space. Thus, the correlation of the magnetometer data with the data from plasma and cosmic ray experiments, as well as with terrestrial observations, should be especially enlightening. Measurements of the geomagnetic field, from ~6 Earth radii out, were to be made in order to obtain information concerning the interaction mechanism of the solar plasma with the Earth's field, and the distribution of electric currents in the outer radiation belts. The quiescent interplanetary magnetic field is perhaps of the order of 1 or 2 ($\gamma = 10^{-5}$ gauss). The magnetometer which was used for this experiment was an alkali-vapor type, using rubidium gas as the sensing element. The magnitude of the Zeeman splitting in the energy levels of the rubidium 87 isotope appears as a Larmor precession, the frequency of which is given by

$$f = kB \tag{1}$$

where k is 6.996 cycles per γ and B is the magnitude of the magnetic field.

In the present configuration, the magnetometer (Figs 78 and 79) is a self-oscillating unit, generating a sine-wave signal whose frequency as a function of the field is given by Equation (1).

A beam of light (Fig 80) at the appropriate frequency and intensity, is used to achieve the optical pumping

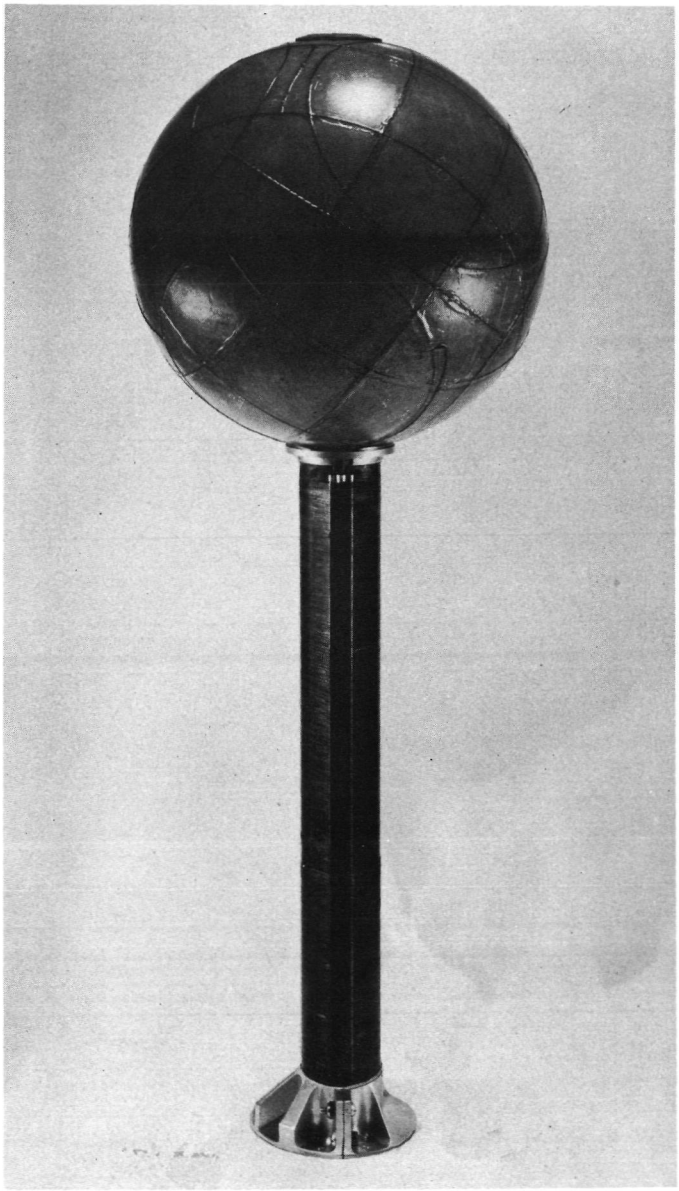

Figure 78. Magnetometer assembly

necessary to increase the population of a certain energy level of the rubidium 87 isotope in the gas cell. Zeeman splitting of this energy level results in an amplitude modulation at the Larmor frequency of the light passing through the gas cell. This variation in light intensity is detected by a silicon mosaic cell. An amplifier is then used to raise the level and shift the phase (90 deg) of this signal. The resulting positive feedback signal is then inductively applied to the gas cell, thereby supplying sufficient energy to the system to increase the duration of this phenomenon, which is normally of the order of milliseconds.

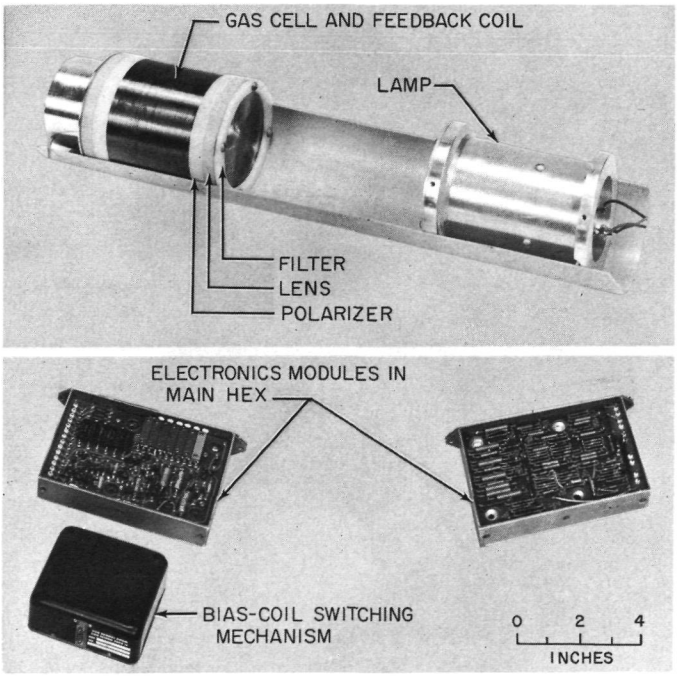

Figure 79. Components of rubidium vapor magnetometer

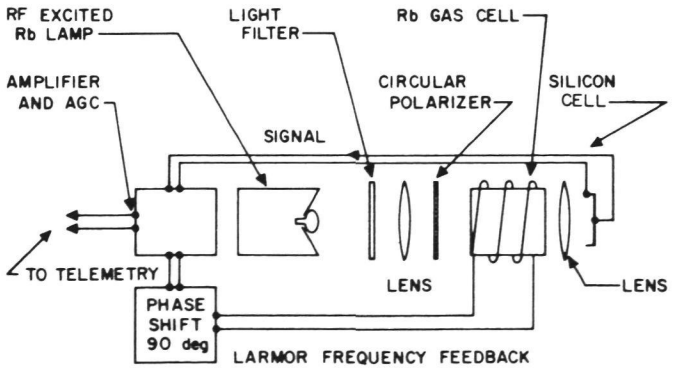

Figure 80. Magnetometer experiment

Bias coils. In this instrument, which differs from earlier models in that one light beam is used for both the pumping and the monitoring operation, a maximum amplitude signal is achieved when the magnetic field is at 45 deg to the light beam; there are nodal cones of no response near 0 and 90 deg. In order that field measurements can be obtained for any field direction, bias fields of 10-gamma strength are applied in each of six orthogonal directions consecutively for 10 sec per direction. The bias fields are also required because the limiting value of magnetic field which can be detected by the present model is about 2 gammas. The bias field gives a reference of 10 gammas (chosen for telemetry reasons) upon which the ambient interplanetary field is superimposed. Since the bias field is known to within 0.01 gamma, the instrument still is capable of accurately measuring very weak magnetic fields. The bias coils are also required to obtain the average (over 1 min) direction of the field.

Sensor. The rubidium cell mechanism consists of the following parts:

(1) Rubidium lamp.

(2) Interference filter.

(3) Convex lens.

(4) Polarization filter.

(5) Rubidium gas cell.

(6) Feedback coil wound over the rubidium cell.

(7) Lens.

(8) Photo cell.

(9) 100-mc oscillator.

The signal from the 100-mc oscillator is used to generate the necessary light beam in the rubidium lamp. The output light from the rubidium lamp is passed through an interference filter, a convex lens, and a polarization filter in order to obtain the 7947 Å right-circularly-polarized parallel beam necessary to optically pump the rubidium gas in the gas cell. The light leaving the gas cell is focused onto the photo cell by another lens.

The variation in intensity of the light beam caused by the precession of the excited, or pumped, atoms in the gas cell at the Larmor frequency, is detected with a silicon cell and this signal is amplified, phase-shifted through 90 deg and inductively applied as a positive feedback to sustain the modulation of the light beam.

Environment and spacecraft integration. In order to keep the magnetic background due to the spacecraft and its components to a minimum, the magnetometer was

placed at the front end of the spacecraft, with only the omni-directional antenna ahead of it. In this operation, the magnetic sensing element was 8½ ft from the main spacecraft. (It was hoped that this placement would help keep the background field to less than ½γ.)

Both the gas cell and the r-f lamp are temperature sensitive. The center operating temperature for the gas cell is about 43°C with a working tolerance of ±18°C. The r-f lamp temperature during operation is required to be about 50°C. The temperature sensitivity of this lamp results from the fact that the pressure inside the bulb has to be kept above a certain minimum in order to ignite the lamp. To maintain this required pressure, the r-f lamp temperature should be held at a minimum of 18°C. This temperature sensitivity makes it rather impractical to light the lamp after the payload has been injected into orbit; therefore, it was energized prior to liftoff. To maintain temperature required for the gas cell it was necessary to thermally integrate the design of the omnidirectional antenna, located immediately above the magnetometer, so that the solar radiation falling on it could be transmitted by conduction to the gas cell. Since the temperatures of the gas cell and the light source are critical, they were telemetered.

Electronics. The magnetometer electronics schematic diagram is shown in Figure 81. The power required to operate the magnetometer is 4.1 w, of which 3.66 w will be used to generate the 100-mc r-f signal that excites the rubidium lamp. The amplifier bias switching and bias coil system used 443 mw. A breakdown of the currents and voltages required is given in Table 35.

Data handling. The output signal of the magnetometer is a sine-wave which will vary in frequency as the magnetic field surrounding the magnetometer changes. The frequency range of present models is 70 to 800 cps, corresponding to a maximum field strength of 105 γ. The signal was sine-wave with an amplitude of 3 v peak-to-peak. In order to obtain the 2400-to 3150-cps signal bandpass required, the 400-cps reference signal of the spacecraft was multiplied 8 times and then added to the magnetometer signal. A block diagram of this signal chain is shown in Figure 82.

Since the solar corpuscular radiation experiment completed its energy range coverage for both electrons and protons in 2 min, it was desirable to obtain a complete magnetic field measurement within this time. To accomplish this, the commutator which switches the bias coils was triggered (by a pulse) every 10 sec. By using this mode of operation, at least two average field measurements could be obtained for each complete scan of the solar corpuscular radiation experiment. Actually, it may often be possible to obtain a field reading every 30 sec if each of 3 successive resultant (ambient plus bias coil) magnetic fields is greater than ~72 because of the low probability of any resultant vectors falling in the narrow nodal cones of the magnetometer. To obtain rapid variations of the magnetic field, the frequency variations within each 10 sec will be studied. The telemetering system will follow field change rates of up to 30 γ per sec.

Spacecraft magnetic field and calibration. Considerable effort went into the task of assuring that the magnetic field generated by the spacecraft would be minimal. A system was set up to check individual components, subassemblies, structures, etc., against magnetic specifications generated for the mission. When the spacecraft was completed, it was magnetically calibrated in a field-free facility and, after transportation, these results were verified at Cape Canaveral by rotational calibration in the Earth's magnetic field.

Flight performance summary. Since neither *Ranger I* nor *II* got far enough from the Earth for the field strength to be less than 105 γ, the signal was always out of band and no flight data were obtained. Furthermore, due to the lack of attitude stabilization, the instant temperatures were outside the range necessary for proper operation.

d. Triple-coincidence cosmic-ray telescopes. The purpose of the triple-coincidence telescopes was to monitor and to determine some of the properties of the high-energy radiation in interplanetary space. The design and analysis of this experiment, which had the highest threshold energies of the entire complex of radiation detectors on RA-1, was the responsibility of the University of Chicago.

Each of the two triple-coincidence telescopes carried on RA-1 and -2 consisted of an assembly of seven proportional-counter tubes arranged in the same manner as in the units successfully flown on *Explorer VI* (Ref 20) and *Pioneer V* (Ref 21). Six of the seven counters were grouped in a concentric ring around the seventh counter,

Table 35. Magnetometer power requirements

Voltage	Deviation, %	Stability, %	Ripple, %	Spikes, mv	Current, amp
6.3 ac	±2.5	±2.5	—	—	0.150
150 to 170	Current regulated ±3% total			—	0.016
6	±1	±1	1	20	0.005
12	±1	±1	1	20	0.010
−12	±1	±1	1	20	0.024

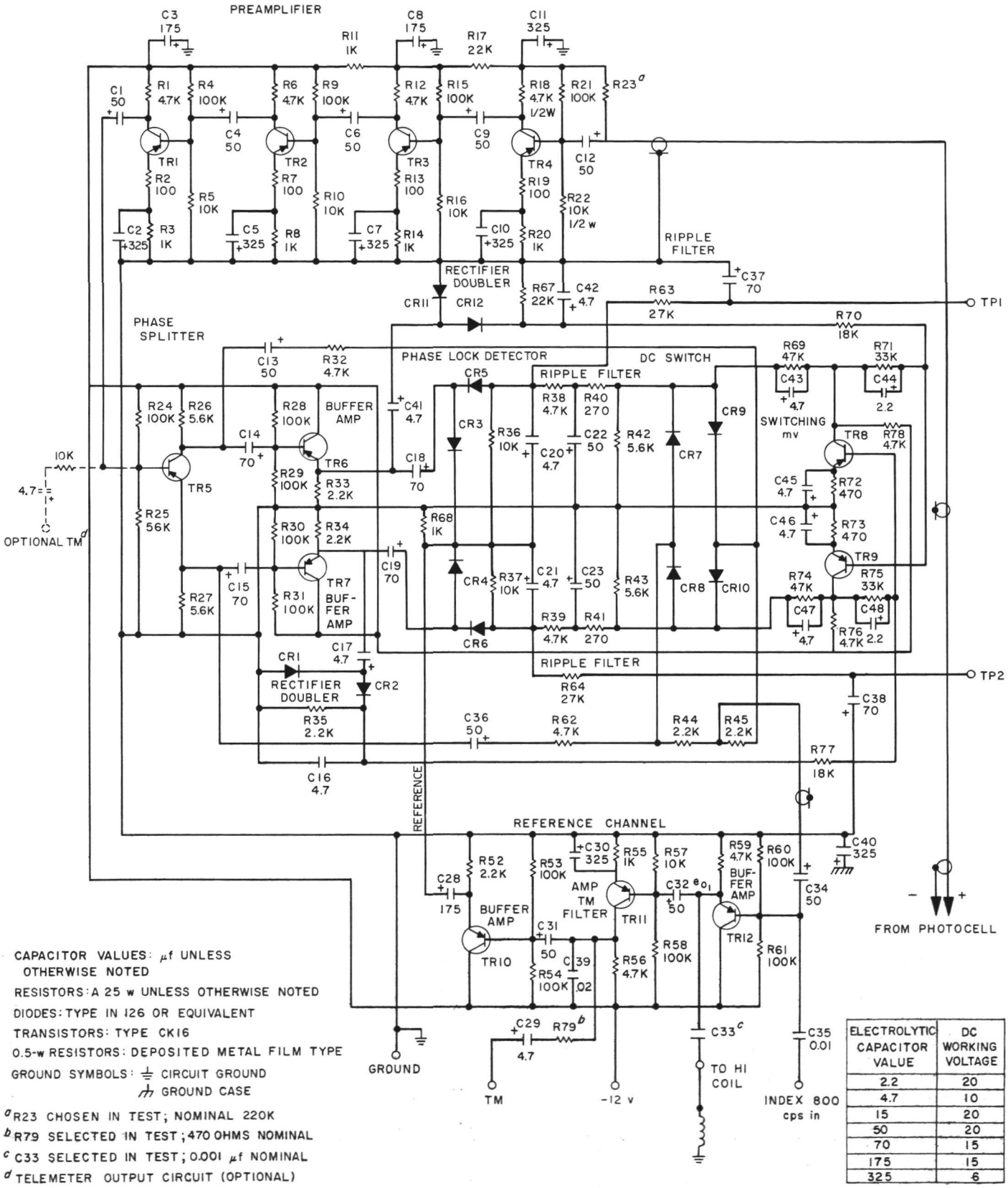

CAPACITOR VALUES: μf UNLESS OTHERWISE NOTED
RESISTORS: A 25 w UNLESS OTHERWISE NOTED
DIODES: TYPE IN 126 OR EQUIVALENT
TRANSISTORS: TYPE CK16
0.5-w RESISTORS: DEPOSITED METAL FILM TYPE
GROUND SYMBOLS: ⏚ CIRCUIT GROUND, ⏚ GROUND CASE

[a] R23 CHOSEN IN TEST; NOMINAL 220K
[b] R79 SELECTED IN TEST; 470 OHMS NOMINAL
[c] C33 SELECTED IN TEST; 0.001 μf NOMINAL
[d] TELEMETER OUTPUT CIRCUIT (OPTIONAL)

ELECTROLYTIC CAPACITOR VALUE	DC WORKING VOLTAGE
2.2	20
4.7	10
15	20
50	20
70	15
175	15
325	6

Figure 81. Magnetometer electronics, schematic diagram

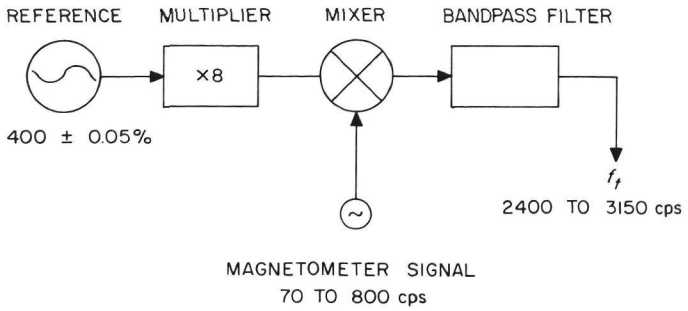

Figure 82. Magnetometer signal chain

with the outer counters connected in two adjacent groups of three (Fig 83). The pulses from each of the three groups of counters were first amplified and then entered a pulse shaper, which accepted pulses of only a given amplitude or greater, and thus acted as a pulse-height discriminator. A standardized pulse was generated and coupled into a triple-coincidence circuit. The outputs of the coincidence circuits and of the center counters alone were then coupled first to scaling stages and then, after scaling by a factor of 2^5, to the 14-bit counters which were read out by the data-automation system at a rate of once per min. The maximum counting rate of these counters is such that counting rates up to about 2000 times the normal cosmic-ray background rate can be accommodated.

High-energy telescope. One of the two telescopes, the high-energy unit, consisted of counters whose walls were 0.5-in.-diameter brass tubing, 3 in. in length with a 0.028-in. wall thickness. Lead shielding of 5 gm per cm^2 thickness surrounded this assembly of seven counters. The telescope had a threshold of 75 Mev for a triple-coincidence count due to protons; the corresponding threshold for electrons was 13 Mev. The threshold for detection of electrons through their bremsstrahlung radiation was approximately 200 Kev. This bremstrahlung radiation was monitored through the central-tube counting rate rather than by the triple-coincidence counting rate because of the exceedingly low probability that a gamma ray would cause a pulse in each of three counters. In this manner it is possible to obtain a separation of the high-energy-particle radiation from other radiation (gamma rays, electrons between 200 Kev and 13 Mev, and other charged particles with a sufficient energy to

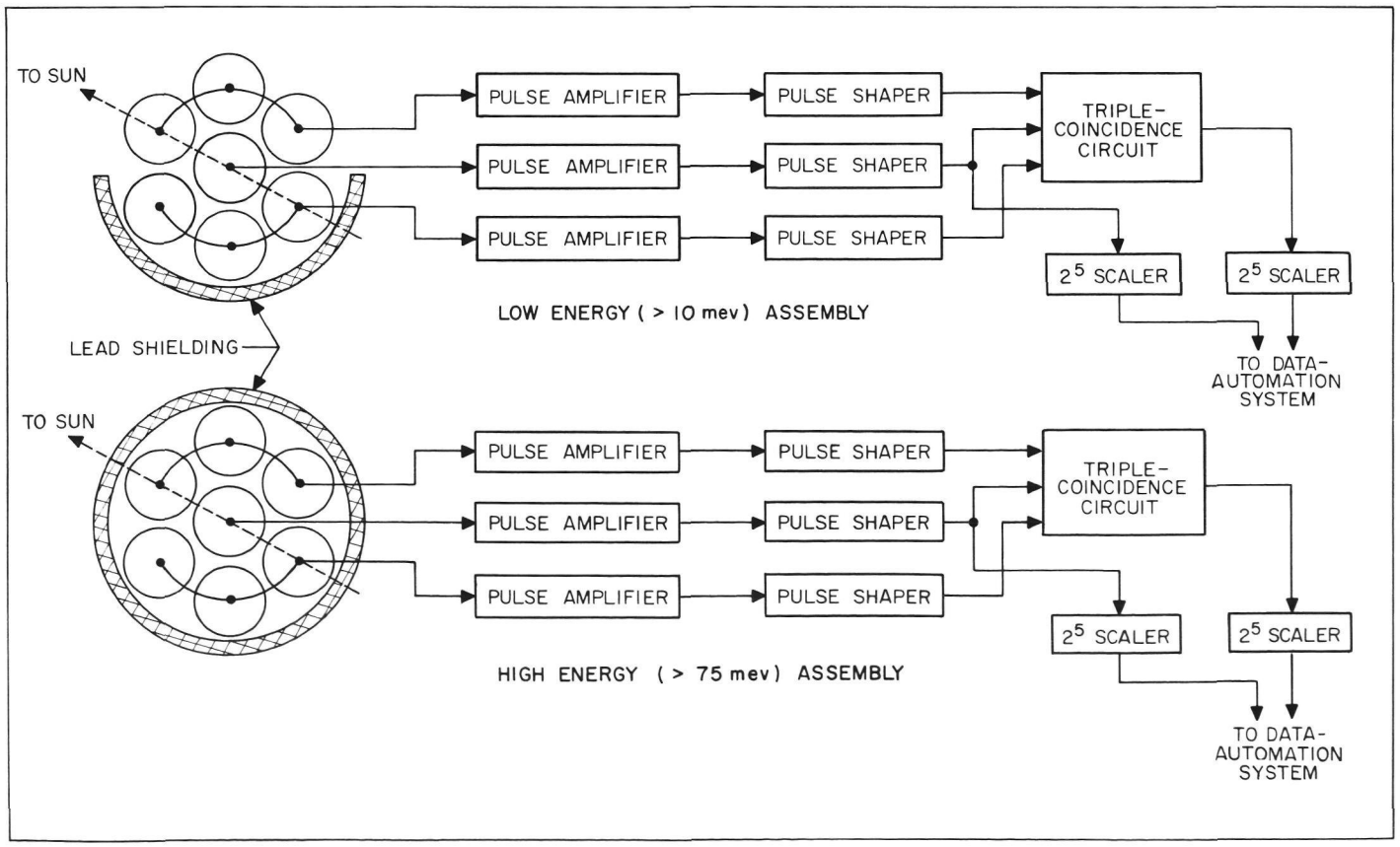

Figure 83. Triple-coincidence cosmic-ray detector

penetrate the lead shield plus greater than three but less than five counter-wall thickness).

Low-energy telescope. The low-energy telescope had counters with 2.0 ±0.1-mil steel walls. One half of this assembly had lead shielding (5 gm/cm²) along the length of the tubes, whereas, the other half of the assembly (the half for which particles could reach the detector without encountering spacecraft structural material) had no shielding. Since particles which encounter any spacecraft structure must also penetrate the lead shielding before detection, the effects of spacecraft material could be neglected here. A knowledge of the counting rates of the high-energy telescope permits the correction of the low-energy telescope data in order that the particle flux incident on the unshielded portion of the low-energy-unit can be calculated. Calculations indicate that a dead angle ϕ, as shown in Figure 84, will exist for low-energy-particle detection; thus, the actual look angle Ψ for low-energy particles will not be quite 180 deg. The thresholds for triple-coincidence counts by particles incident in this angle Ψ are approximately 10 Mev for protons and 0.5 for electrons.

Testing, calibration, and spacecraft integration. Electrical and environmental tests were performed on each unit after an initial incoming inspection had been completed. Count rate data were recorded as a function of environment.

Both units received final calibration while mounted on the spacecraft at Cape Canaveral, using both background cosmic radiation as well as radioactive sources mounted on the spacecraft. A period of 36 hr was utilized to obtain the calibration data. Twelve hr were utilized for radioactive source data and two 12-hr periods for background cosmic rays. These tests were performed overnight on a non-interference basis, both from the standpoint of overall spacecraft testing, as well as interference with the calibrations from spacecraft operations. The spacecraft was placed in a flight configuration with the triple coincidence instruments being activated and monitored externally.

The two telescopes were placed with their axes of symmetry on a line which is approximately 1.5 in. above one of the electronics boxes on the main spacecraft. The probe–Sun line is shown in Figures 83 and 84; the geometry is such that particles incident from the direction of the Sun can be seen by the low-energy part of the low-energy telescope, as well as by the high-energy telescope.

The total weight of this experiment was 9 lb, and the total power requirement was 500 mw.

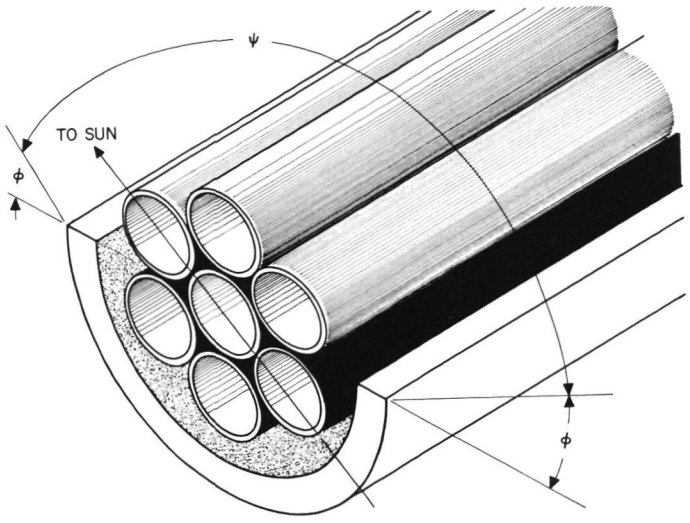

Figure 84. Low-energy triple-coincidence telescope assembly

Flight performance summary. The triple-coincidence telescopes on *Rangers I* and *II* appeared to function normally, with the exception that the cumulative count of high-energy triple-coincidence would occasionally increase by an extra 64 between successive readouts.

e. Medium-energy particle detectors. The characteristics of the radiation in the energy region from a few Kev to a few Mev was measured by a group of relatively small and simple charged-particle detecting modules. It was planned that the modules be as nearly identical as possible with regard to voltage requirements, power requirements, output-signal characteristics, telemetry requirements, shape, and method of attachment to the spacecraft. This would permit interchanging of the modules for the yield of the most information for a given flight. Although this plan proved not to be entirely feasible, the modules are sufficiently similar that different combinations of these detectors were flown on RA-1 and -2.

Geiger counters. The State University of Iowa developed two modules containing Geiger counters. One of these modules used an Anton 213 end-window counter, flown in several successful space probes, which has an effective counting area of approximately 0.12 cm² and a 1.2 mg per cm² mica window through which can pass electrons above 35 Kev or protons above 500 Kev. The maximum apparent counting rate of this tube is approximately 20,000 per sec; however, by laboratory calibration, the dynamic range can be extended to over 500,000 counts per sec. The second Geiger-tube module uses an Anton 112 cylindrical thin-wall counter which has a 30 mg per cm² steel wall (corresponding to cut-off energies

of 3 Mev for protons or 200 Kev for electrons). The maximum effective counting area (perpendicular to its axis) of this counter is about 13 cm^2, and its minimum area (parallel to the axis) is about 3 cm^2. Its maximum counting-rate characteristics are similar to those of the 213. Prescaling factors of 2^7 were utilized for both tubes. Figure 85 is a photograph of the two Geiger tubes.

Cadmium-sulfide detectors. A group of charged-particle-detecting modules developed and constructed by the Department of Physics and Astronomy, State University of Iowa, has a sensitive element which is a small crystal of photoconductive cadmium sulfide (CdS) approximately 2-mm square and between 0.1- and 0.3-mm thick. The electrical conductivity of such a crystal is proportional to the rate of deposit of energy of ionization in the crystal; hence, if a constant voltage is impressed, the circuit flow through the crystal can be calibrated in terms of energy flux.

The typical radiation sensitivity of a CdS crystal is 4×10^{-7} amp per unit energy flux (erg/sec-cm^2) for protons, electrons, and X-rays over a wide energy range. The upper limit of this proportional region is the energy required to pass through the CdS crystal (a few hundred Kev for electrons and a few Mev for protons). The lower limit of the region has not been determined accurately, but it may be below 100 ev for both protons and electrons. Actually, the sensitivity of most crystals is slightly energy-dependent and may vary by a factor of 2 to 4 for electron energies between 5 Kev and 80 Kev. The variation, when present, is approximately the same for protons, electrons, and X-rays.

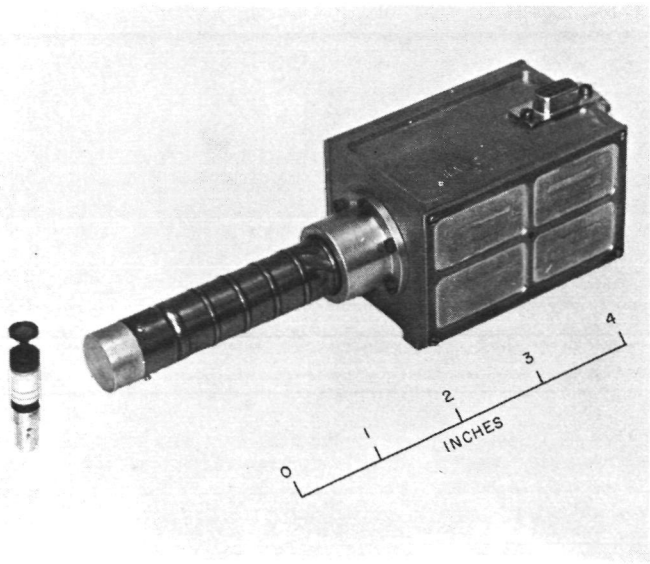

Figure 85. Anton type 213 (left) and 11w Geiger tubes

Because of their photoconductivity, these CdS detectors cannot measure low intensities of corpuscular radiation when their axes are closer than 20 deg to the solar vector (35 to 40 deg for the large solid-angle unit). The dynamic range of the detectors is limited at the lower end by a dark current of about 10^{-10} amp; the upper limit is about 5×10^{-5} amp with present circuitry. If the particle flux and the entrance aperture are large enough to give a flux of greater than 10 erg per sec-cm^2 on the crystal, a permanent increase in dark current occurs. It was hoped that the modules would have apertures small enough that this limit would not be reached in passing through the radiation belts of Earth. Modules with larger aperture had shutters which were to be opened after passing beyond the belts. The modules were designed in such a manner that their apertures could easily be modified.

A "magnetic broom," which deflected low-energy electrons (below about 500 Kev) away from the crystal, was incorporated in some of the modules. The magnetic broom is a small permanent magnet; tests have shown that its stray field at the magnetometer in the spacecraft could be kept within acceptable limits (less than 0.5 gamma).

The parts of a CdS detector are shown in Figure 86. In the lower right-hand corner, the crystal itself, a modified Clairex Type CL-2 photocell, is shown with two leads coming out of it. A series of light baffles are laid out in the adjoining row; the third baffle from the right incorporates the magnetic broom. The modules for the spacecraft incorporated these parts together with the circuitry shown in Figure 87. The current from a 160-v supply charges a capacitor through the resistance of the crystal until it reaches the firing potential of a neon bulb across it. The resultant pulses are shaped and fed out to a 14-bit shift register which was read out by the DAS once per min. The circuit parameters are adjusted in such a manner that the saturation current through the crystal corresponds to about 100 pulses per sec.

Gold-silicon detector. The Cosmic-Ray Group at the University of Chicago developed a module for measuring protons in the energy region from 0.5 to 10 Mev; this module incorporates gold-silicon (Au-Si) surface-barrier detectors. The sensitive elements are thin wafers of high-resistivity silicon with a very thin film of gold evaporated on the front surface. A space-charge region (also called the depletion region) extends from the Au-Si interface into the bulk of the silicon. The thickness of this region is adjusted (by adjusting the potential difference across the wafer) to approximate equality with the range of a 2-Mev proton. A charged particle incident on the detector will penetrate the thin gold film and produce electron-

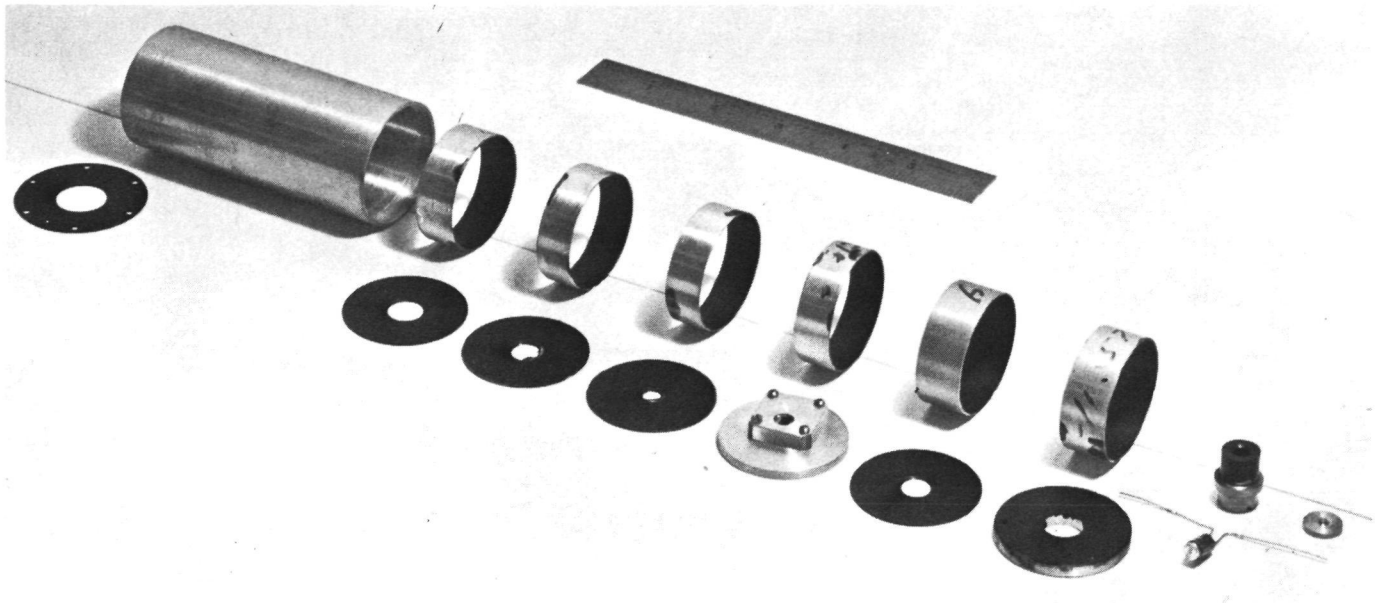

Figure 86. Cadmium sulfide detector

hole pairs as it passes through the space-charge region. The liberated ion pairs are swiftly swept apart by the high electric field in the space-charge region; this results in a measurable voltage pulse proportional to the amount of energy lost by the particle in passing through the region. An amplifier discrimination level is set in such a way that pulses are produced by protons only if their energy lies between 0.5 and 10 Mev; an electron or gamma ray of any energy cannot lose this much energy in so short a distance. It has been found experimentally that the pulse height and shape from the detector for 5.3 Mev alpha particles in the presence of an X-ray background flux of about 100 R per hour were essentially unaffected. However, at fluxes near 1000 R per hour, the alpha pulses could not be distinguished from the radiation-induced noise.

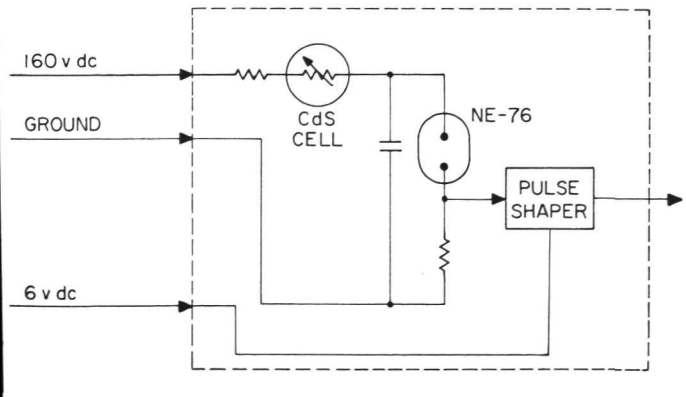

Figure 87. Circuitry for cadmium sulfide detector

The module, a block diagram of which is shown in Figure 88, contained two Au-Si wafers (approximately 5 mm diameter and 0.2-mm thick) in a coincidence-anticoincidence scheme. Since a proton must have about 5 Mev energy to penetrate completely the first wafer, a coincidence output pulse, which results from a particle triggering both detectors, represents the passage of a proton with energy between 5 and 10 Mev. An anticoincidence pulse represents a proton which triggers only the first detector and, hence, has an energy between 0.5 and 5 Mev.

Since the detectors are photosensitive, a thin foil ($\sim$¼ mil) of aluminized mylar was placed above the first detector as a shield against sunlight.

Testing, calibration, and spacecraft integration. Electrical and environmental tests were performed at JPL after an initial incoming inspection had been completed. Count-rate data was recorded as a function of the environmental conditions. Detailed calibrations were performed at the two sponsoring universities for the appropriate instruments.

Preflight calibrations were performed at Cape Canaveral a few weeks prior to the flight to look for any shifts in characteristics due to storage. These calibrations were performed with radioactive sources while the instruments were removed from the spacecraft.

It was possible to carry a total of 6 modules on each flight. The data-automation system (DAS) read out a

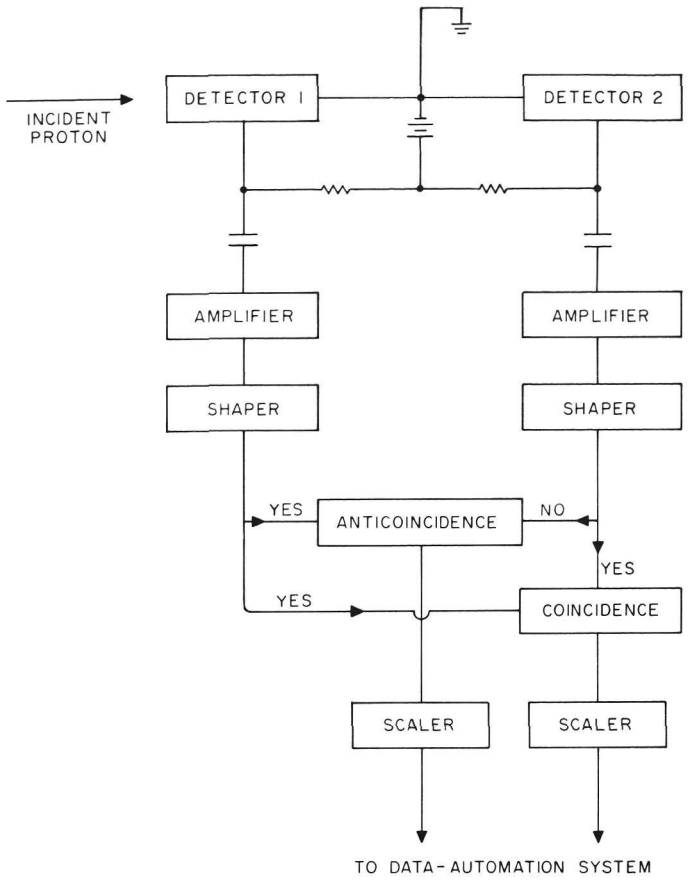

Figure 88. Block diagram of gold-silicon detector

14-bit word once per min from each of the six modules. One of these six shift registers was divided into two 7-bit words to accommodate the Au-Si module (7 bits each for the coincidence and anticoincidence counts) and another was divided into 13-bit and 1-bit words for the CdS module with a removable shutter; the one bit signified the aperture of the detector.

The six detectors flown on RA-1 and -2 are listed and their properties are summarized in Table 36. The six RA-1 modules weighed a total of 3.8 lb and consumed approximately 160 mw of power. The RA-2 modules had essentially the same weight and power requirements as those on RA-1.

Flight performance summary. The Geiger tubes and the Au-Si detectors on *Rangers I* and *II* apparently worked perfectly. The data from the CdS detectors will probably have little, if any, scientific value because the detectors were almost always either saturated by sunlight (or Earthlight) or in the recovery phase after having looked at the Sun.

f. Integrating cosmic-ray ionization chamber.

General description. The RA-1 and -2 ionization chamber was intended to measure both the primary cosmic radiation in space beyond the Earth's atmosphere and magnetic field in such a way that:

(1) Intensities measured at different times during a flight of many months may be compared with one another and with other quantities measured during the flight. This requires that the calibration of the instrument remain constant.

(2) The intensities measured during the flight of one spacecraft may be compared with those measured by another at a different time. This comparison may be accomplished by using the same kind of instrument on every vehicle or by using instruments which will give an absolute value of the intensity.

(3) One may relate the cosmic-ray intensity measured in space with intensities measured in the Earth's atmosphere or at its surface. The best way to do this appears to be to obtain absolute values of the

Table 36. Medium-energy-particle detectors for *Rangers* RA-1 and -2

Ranger flight	Detector	Angle of axis with expected probe–Sun line, deg	Angle of axis with expected ecliptic, deg	Proton energy	Electron energy
RA-1 and -2	CdS with magnet 10^{-2} sterad	45	45	≧ 400 ev	≧ 500 Kev
RA-1 and -2	CdS 10^{-2} sterad	45	45	≧ 100 ev	≧ 100 ev
RA-1 and -2	CdS with shutter 10^{-3} to 5×10^{-2} sterad	45	0	≧ 100 ev	≧ 100 ev
RA-1	CdS 10^{-3} sterad	45	0	≧ 100 ev	≧ 100 ev
RA-1 and -2	Au–Si	90	90	0.5 to 5 Mev 5 to 10 Mev	—
RA-1	213 Geiger tube	90	0	≧ 0.5 Mev	≧ 35 Kev
RA-2	112 Geiger tube	0	—	≧ 3 Mev	≧ 200 Kev
RA-2	112 Geiger tube	90	0	≧ 3 Mev	≧ 200 Kev

intensity in space at the same time that measurements are made at the Earth.

The ionization chamber consists of a spherical volume of argon gas contained by a thin steel wall and placed near a bulky spacecraft. What is actually measured is the ionization produced in the argon by naturally occurring (i.e., primary) particles able to penetrate the wall, that produced by those secondaries generated in the spacecraft which can penetrate the wall, plus the ionization caused by secondary particles generated in the ion chamber walls and gas.

The ionization in the argon can be reduced to the ionization in a unit volume of standard air by suitable calibration of the ion chamber. The effect of the wall can also be accounted for since it is thin and has spherical symmetry. The effect of secondaries produced in the bulk of the spacecraft is difficult to calculate, and so the chamber is located as far as possible from the main bulk of the spacecraft.

Figure 89 shows the ion chamber and its internal mechanism. The entire working mechanism is made of fused quartz, an excellent electrical insulator. The areas which are shown black in Figure 89 are covered with a conducting coat of aquadag. When no voltage is applied, the fiber, which has a conducting coat, lies about 0.020 in. from the collector. When the power is connected, the fiber is bent by electrostatic attraction and touches the collector, charging it to the battery potential. The fiber then moves back to its rest position away from the collector since the fiber, collector, and shield can are all at the same potential.

The electric field between the collector and the outer shell is more than sufficient to collect all ions formed in the argon. The ionization current discharges the collector until the fiber again touches and recharges it, simultaneously producing a voltage pulse across a load resistor. Hence, the time between pulses varies inversely with the rate of ionization in the argon; a pulse occurs after about 10^{-10} coulombs have been collected from the argon.

Accuracy and sensitivity to radiation. The wall thickness determines the minimum-energy particle which can reach the filling gas from the outside. In this case, the thickness was chosen to match the thickness of the unshielded, triple-coincidence, proportional-counter telescope made by the University of Chicago. This thickness is 0.2 g/cm^2 of stainless steel for the proportional counters and, in the case of the ion chamber, the same total thickness of stainless steel plus copper and silver plating. The minimum-energy particle which can be detected by either of the two instruments is 10 Mev for a proton, 40 Mev for an alpha particle, and 0.5 Mev for an electron, approximately.

Hence, by combining the flux measured by the proportional-counter telescope and the rate of ionization measured by the chamber, the average total specific ionization of the particles may be obtained. Since the average total specific ionization is a function of energy, some information could be obtained about the energy of the particles present.

Experience with similar ion chambers made at CIT over a period of years suggests that the ion chambers may be calibrated to within $\pm 1\%$ absolutely, and $\pm 0.5\%$ relative to each other, and that they may be expected to hold their calibration within $\pm 0.5\%$ for many months. The approximate relationship between pulse rate and the rate of ionization is shown in Table 44. The filling pressure may be varied from one instrument to another, with proportional variation in calibration.

As indicated in Table 37, the pulse rate varies linearly with ionization over a wide range. However, the maximum rate at which the chamber can operate is about 100 pulses per sec, and somewhere between 20 and 100 sec^{-1} the response deviates significantly from linearity.

The steady galactic cosmic ray ionization is expected to lie between 100 and 1000 ion pairs per cm^3 sec atm of air, depending upon the phase of the 11-year sunspot cycle. However, bursts of solar particles can produce ionizations of the order of at least 400,000 ion pairs per cm^3 sec atm, and because there are very few experimental results, this number must be regarded as a lower limit of what may occur. Thus, the pulse rate was expected to be a few pulses per hr most of the time, with occasional increases to 1 pulse per sec or more.

Development effort at JPL. Ionization chambers have been used to measure ionizing radiation for many years, and various sorts of current measuring devices have been applied to the basic gas-filled chamber. The mechanism which uses a quartz fiber to integrate the charge collected and automatically recharges the collecting electrode was developed by Prof. H. V. Neher and his associates at CIT beginning about 1950 (Ref 22 and 23). It has been used extensively for cosmic-ray measurements in the atmosphere by the CIT cosmic-ray laboratory.

The development of a rugged version of the integrating ion chamber to carry out the measurements listed at the beginning of this discussion was begun in June 1959, and was carried out jointly at JPL and at CIT.

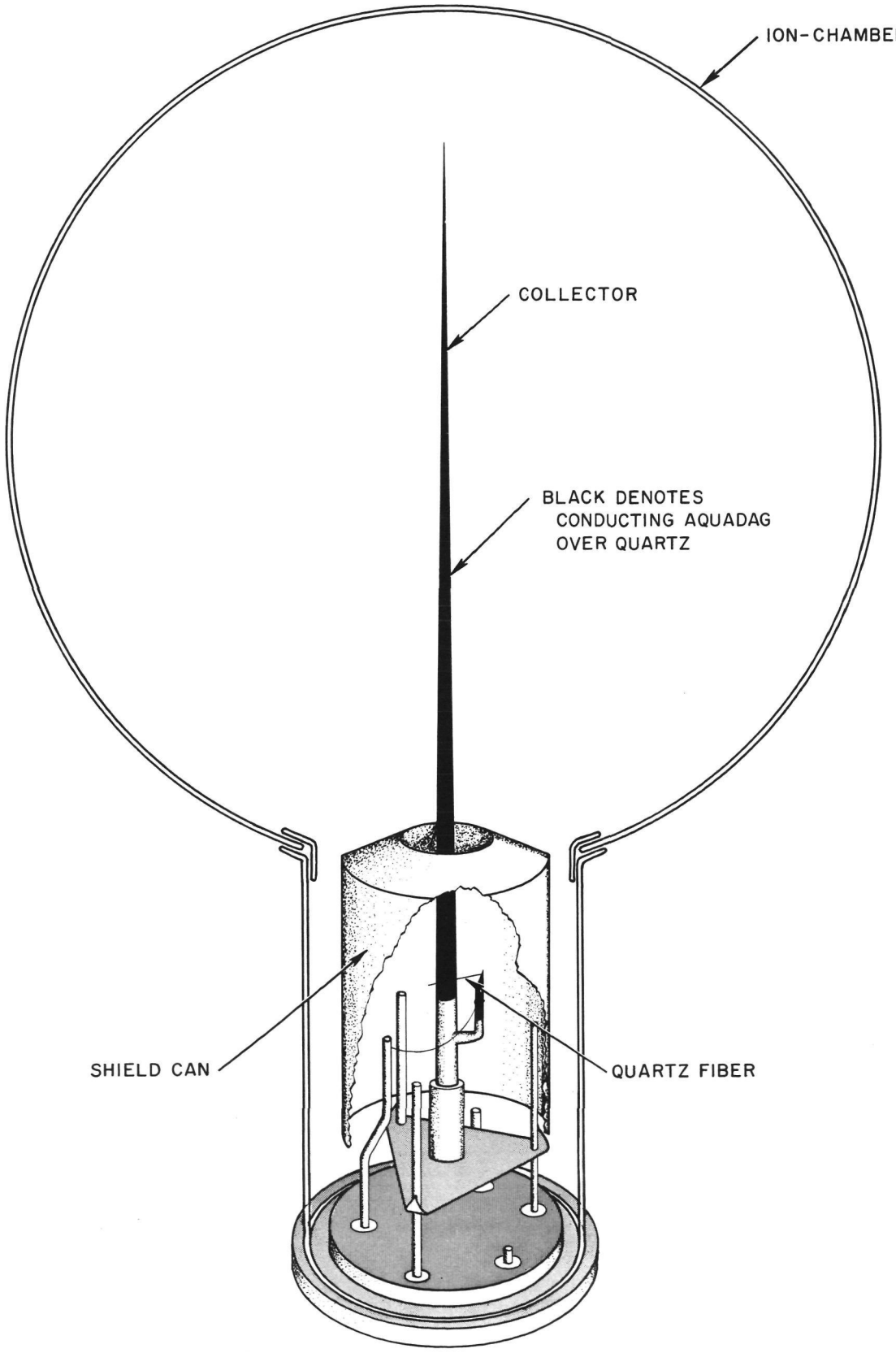

Figure 89. Cross section of ion chamber and quartz integrating system

Table 37. Pulse rate as a function of ionization

Pulse rate	Ionization	
	Ion pairs/cm³ sec atm of std air	Roentgen/hr
1/hr	106	1.8×10^{-4}
1/min	6400	0.011
1/sec	384,000	0.66
100/sec	2.8×10^{7}	66.4

A new mechanical design was drawn up at JPL and parts were fabricated there. JPL designed an emitter follower output amplifier, and the circuit was tested and assembled at JPL. After the ionization chambers were complete, they were tested in the JPL environmental facilities. A new quartz integrating mechanism was built at CIT. The complete chambers were assembled, filled, and calibrated at the CIT laboratory. The first flight units were made in November 1960.

Environment and spacecraft integration. Ideally, the ion chamber should be located at least 10 or 15 ft from the main mass of the spacecraft in order to reduce the effect of secondary radiation produced in this mass. Because of structural limitations, however, the chamber was mounted midway between the main spacecraft hexagon and the omni-directional antenna on the forward structure. The hexagon subtended about 5% to 4π sterad at this position. Total mass in the hexagon was about 500 lb. In addition, some 15 to 20% of 4π sterad was subtended by superstructure members, the magnetometer, and the omni-directional antenna, which in general presented less absorbing material than did the hexagon.

The complete ion-chamber experiment weighed about 500 gm and required about 0.01 watt for operation.

Data handling. Pulses from the chamber were fed to the central data-automation system. A 14-bit word was assigned to this experiment. This word was sampled and transmitted every 28 and 32 sec, alternately. Eleven bits constituted the ion-chamber pulse register; the other 3 bits constituted the time-count register. Both registers reverted to zero after accumulating $(2^{11}\text{-}1)$ and $(2^{3}\text{-}1)$ counts, respectively, and neither was ever reset; i.e., reading out or sampling did not change the number in the register. The pulse register counted every ion chamber pulse except during an insignificant 100 microsec dead time while it was being sampled.

The time-count register connected through a switch to a clock which generated a pulse every 4 sec. The count in this register increased by 1 every 4 sec until an ion-chamber pulse occurred, at which time the switch was opened and no more counts could be accumulated until the next readout, when the switch was closed again and count accumulation restarted. Thus, the DAS could determine the time when each pulse occurred to within 4 sec.

Flight performance summary. The operation of the ion chamber during the *Ranger I* and *II* flights was completely normal. However, the contents of the time-count register were occasionally incorrect (see discussion of Data Automation System).

g. Lyman-alpha telescope.

General description. The principal purpose of the Lyman-alpha scanning telescope is to obtain a series of low-resolution pictures of the Earth and its exosphere in ultraviolet light near the Lyman-alpha wavelength, 1216Å. The source of most of the Lyman-alpha radiation from the vicinity of the Earth is the result of the excitation of neutral hydrogen atoms by either direct or scattered solar Lyman-alpha radiation, or by charged particle bombardment. Hydrogen is formed by photo-dissociation of water vapor by sunlight at about 90 km altitude; the hydrogen gas then diffuses outward and is believed to form the main constituent of the exosphere (Ref 24). Thus, this hydrogen cloud is the last remnant of the Earth's atmosphere and may extend several Earth radii before merging with the gas of interplanetary space or being swept away by a solar wind or radiation pressure.

There is disagreement among interested scientists as to whether or not sufficient hydrogen is concentrated near the Earth to account for the Lyman-alpha radiation in the night sky as observed on high-altitude rocket flights (Ref 25). One school of thought is that the night-time Lyman-alpha radiation originates through scattering of solar Lyman-alpha radiation by hydrogen atoms in interplanetary space (Refs 25 through 27). However, Johnson and Fish (Ref 28) have argued that, if the atoms which scatter the solar Lyman-alpha radiation were in interplanetary space, the orbital velocity of the Earth would produce a doppler shift which would reduce the reflectivity of the Earth's atmosphere below the value observed on the night-time rocket flight. They also believe that there is very little neutral hydrogen in interplanetary space because either charge exchange with solar-wind protons or the outward radiation pressure on neutral hydrogen atoms by solar Lyman-alpha would sweep the inner solar system clean of neutral hydrogen. By combining the results of the night-time Lyman-alpha observations with the atmospheric temperature and density derived from the *Vanguard I* orbital decay data, Johnson and Fish have constructed a model neutral

hydrogen atmosphere. There is some disagreement as to whether or not the Johnson-Fish atmosphere fits the observation of solar Lyman-alpha radiation made on a day-time rocket flight (Ref 29). The data from the Lyman-alpha telescope and the simultaneous measurement of any solar wind by the electrostatic analyzers and CdS detectors will be of considerable value for the resolution of these problems.

Because of its relatively broad frequency response (1050 to 1350Å), the Lyman-alpha telescope can also obtain very valuable information on the geographic extent of any auroral activity which may be occurring during the time of the Earth scan. The Lyman-alpha scanning telescope was developed for these investigations jointly by the Naval Research Laboratory and JPL.

The telescope consists of a parabolic mirror with an ionization chamber located at its focus. A cylindrical radiation shield provides protection against undesirable scattered light and also allows some temperature control. This assembly is mounted in a gimbal system which permits motion of the telescope axis in two perpendicular planes (Figs 90 and 91).

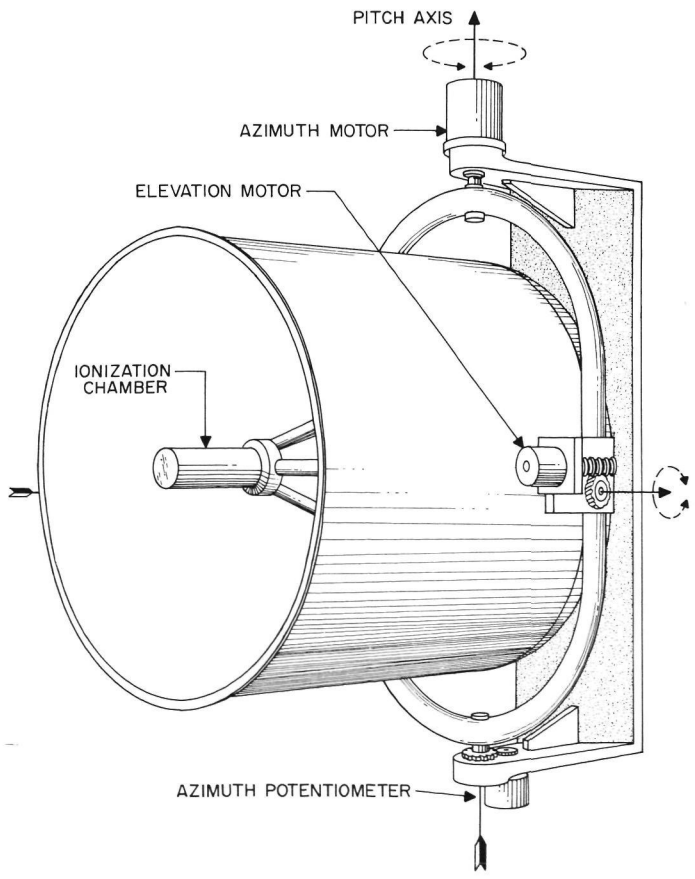

Figure 90. Lyman-alpha telescope

In order to furnish the required optical gain and provide a narrow field of view, a prime-focus telescope was used. The received power P from any sample area is given by

$$P = BA\Omega = \frac{\pi BS}{4F^2} \tag{2}$$

where

B = effective brightness of source

A = effective collecting area (after correction for obstructions and reflectivity)

Ω = solid angular field of view

S = field stop area

F = effective focal ratio

The mirror was a parabola of 10-in. diameter and $F/0.6$; whereas, the field stop was 0.116 in. diameter. The optical gain was approximately 100 and the field of view was 1.1-deg full-cone angle.

The mirror was made by casting epoxy between a preformed Mg shell and a convex glass master which had the proper figure. After the glass master was stripped from the Mg shell-epoxy mirror, the resulting optical surface was coated with aluminum and then coated over with MgF_2 to provide reflectivity enhancement at 1216Å. This technique yields a light-weight mirror with a reflectivity of 0.6 to 0.8 at Lyman-alpha, with a low scattering coefficient.

The ionization chamber was filled with 15-mm pressure NO gas, which is the active constituent, and 35 mm of a filler gas, CO_2. It was 1 in. in diameter and 1.5 in. long,

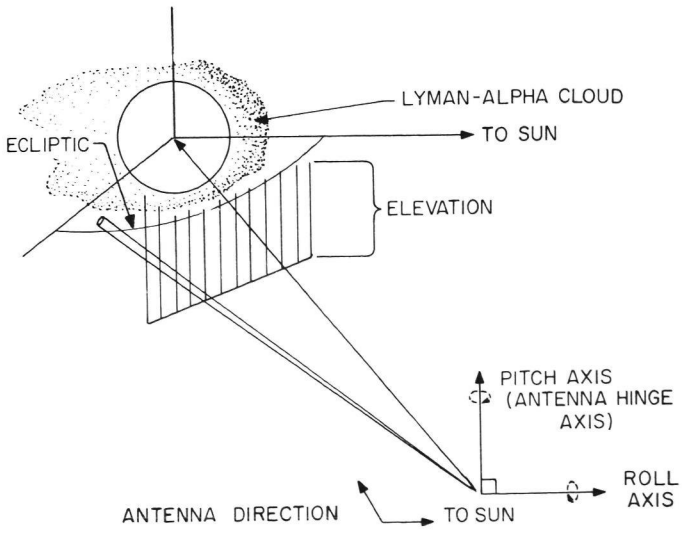

Figure 91. Scanning raster of Lyman-alpha telescope

with a 0.4-in. diameter LiF window cemented with AgCl on one end. The spectral sensitivity of a similar ionization chamber is shown in Figure 92. The long-wavelength sensitivity cutoff is due to the ionization threshold of NO at about 1350Å; whereas, the short-wavelength cutoff is due to the increasing absorption by the LiF window. The ionization-chamber voltage can be adjusted to give the desired gas gain. A typical set of voltages would give gas gains of 650 and 13, alternately, for which brightness levels between 8×10^{-6} and 1.6×10^{-3} ergs per sec cm^2 sterad, and between 4.2×10^{-4} and 8×10^{-2} ergs per sec cm^2 sterad, respectively, can be detected without either overloading the ionization chamber or having a signal which cannot be distinguished from the noise.

Scanning mechanism. The sequence of events for each picture can be described as follows:

(1) The telescope moves to a position such that its axis of symmetry points 20 deg away from the center of the Earth in the roll-yaw plane and the pitch-yaw plane of the vehicle. This is done by use of the high-gain-antenna position and by a simple position-control servomechanism. The telescope is then switched into its programmed scanning operation.

(2) The axis of the telescope sweeps out a raster, as indicated in Figure 91. Elevation drive is effected by a synchronous motor with the direction of drive determined by two-element commutators. The upper contact reverses the direction of motion while the lower one initiates the azimuth motor to step out 2 deg in the azimuthal plane. On the completion of this azimuthal motion, the elevation motor is permitted to drive again, the azimuth remaining unchanged, while another line is scanned. During the upward motion of the elevation scan, the gas gain is 13; during the downward motion, it is 650. The final data are then two series (1 for each gas gain) of 20-strip pictures of brightness versus elevation; each strip is 1.1 deg wide, 40 deg long, and separated from the adjacent strips by 2 deg.

(3) After completion of the scanning operation, the telescope remains in its final position and takes background data at gas gain 650 until the next picture is to be taken. Table 38 presents the program of the series of pictures.

The total weight of this experiment is 14 lb and the total power requirement is 1.15 w.

Environment and spacecraft integration. The problem of temperature control and the hard-vacuum environment were the two most critical environmental problems.

Since the telescope is a moving object, the temperature control surfaces must see both the sunlight from various angles and the cold of space.

The major portion of the electronics was placed in the hex due to the temperature control available there.

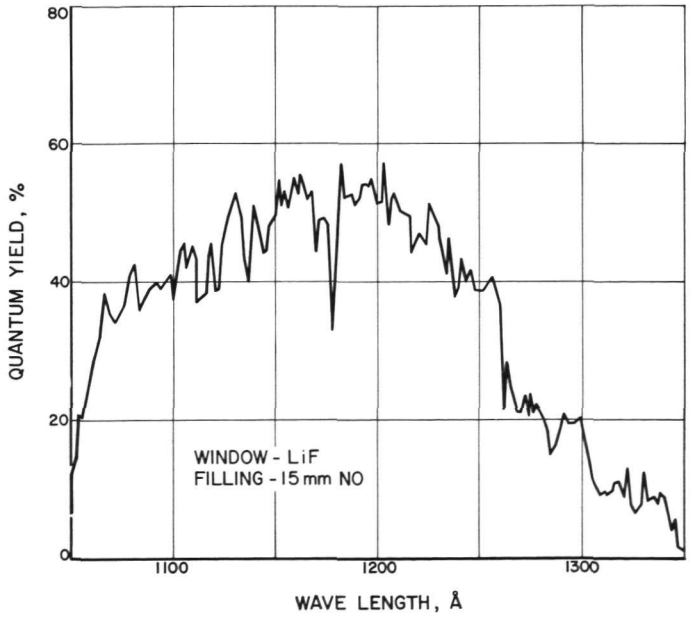

Figure 92. Spectral sensitivity of Lyman-alpha ion chamber

Table 38. Program of Lyman-alpha scanning operations

Picture No.	Distance from Earth at time of picture, Earth radii	Linear size of picture, Earth radii
1	8.9	±3.3
2	11.0	4.0
3	12.9	4.7
4	14.6	5.3
5	16.2	5.9
6	17.7	6.4
7	21.3	7.8
8	27.9	10.2
9	37.6	13.7
10	67.4	24.5
11	99.2	36.1
12	130	47.4
13	153	55.6
14	174	63.3
15	183	66.5

The ionization chamber required a temperature between 0 and +40°C. The problem was solved by extensive use of Sun shields and thermal conductivity control.

The position of the telescope on the spacecraft was a compromise between the 40-deg scan pattern of the telescope and the Earth-probe-Sun angle range of 104 to 50 deg (which meant a total range of telescope look angle of 94 deg), and the structure of the spacecraft.

The hard vacuum presented a serious problem with lubrication of bearings and outgassing of material on the mirror. Dissimilar metals were used on all sliding or rolling surfaces that were exposed and low leak rate seals were used on all high-speed parts.

No material with a high outgas rate was allowed to have a line-of-sight to the mirror surface, as it is known that the reflectance at 1216 Å is reduced sharply as contaminations form on the surface.

Data handling. Data was transmitted back to Earth by an analog channel. A strip chart of each line is read for intensity as a function of telescope position and then plotted as equal intensity lines on a map with the Earth at its center.

Flight performance summary. Part of five picture scans (*Ranger I*) and several inflight calibrations (*Rangers I* and *II*) were observed, as well as background measurements of Lyman-alpha intensity. However, nothing is known about the direction in which the telescope was pointing and the pictures are completely smeared due to the spacecraft tumble. Some of the observed signals from *Ranger II* are not yet understood.

h. Cosmic dust detector.

General description. The cosmic-dust experiment on RA-1 and -2 was designed to measure the flux of dust particles in interplanetary space, as well as to obtain rough values of the particles' energy and momentum distributions. From these data, something can be determined about the dust density and the effects of the Earth's gravitational field on this density, the mass and velocity distributions of the dust particles, and any time variations of these properties which may exist.

Dust particle bombardment may adversely affect the spacecraft surface, the erosion of solar cells, the change in reflectivity or transparency of optical equipment. (Refs 30 and 31.)

The micrometeorite bombardment on the Earth may also be of importance to the understanding of many geophysical phenomena; for example, the formation of the sporadic E layer, noctilucent clouds, airglow, etc.

The composite detector used two sensors physically attached together, one for the measurement of energy and one for the measurement of momentum.

Energy impact detector. This light flash detector measured the light emission during crater formation; the assumption is then made that the intensity of the light emitted is roughly proportional to the kinetic energy of the impacting particle. The detector was a photomultiplier 1⅜ in. in diameter with an 800 Å thick aluminum layer deposited onto the outer front surface of the tube to shield the photocathode against extraneous light from the Sun, Earth, and Moon, during spacecraft altitude-control maneuvers. The minimum energy with which a particle must impact in order to be detected by this device is roughly 0.005 erg.

Outputs were taken from the anode, the tenth dynode, and the ninth dynode of the photomultiplier. Each signal was separately amplified. The ratio of pulse sizes from the anode, the tenth dynode, and the ninth dynode circuitry were approximately 1000:31.6:1, respectively. The greatest sensitivity output (anode circuitry) was fed into a 5-bit counter. The tenth and ninth dynode outputs fed three- and two-bit counters, respectively.

The RA-2 five-bit counter was modified to include an inhibit circuit that prevented recycling in the event of an overflow condition.

Momentum impact detector. This sensor is a piezoelectric crystal microphone mechanically coupled to the sensitive surface of the photomultiplier tube. If it is assumed that the response of this detector is proportional to the momentum of the impacting particle, then the threshold is approximately 10^{-4} dyne sec.

Output of the microphone drove a parallel resonant amplifier, having a mid-frequency of 100 kc and a voltage gain of 80 db. The output drove both a 2-bit counter circuit and another amplifier, having a voltage gain of 20 db. The latter fed into another 2-bit counter. The binary trigger circuits were arranged so that the binary counters would not see microphone "ring" from a particle impact; instead, only the first pulse from the shock wave.

In-flight calibrations. It can be seen from the system diagram shown in Figure 93 that a 14-bit data word was parallel-fed into the Data Automation System. The period of data accumulation was 60 sec, less readout and calibrate time (about 10 msec). While the shift register of the Data Automation System scanned the experiment's binary states, a +5 v 100 μsec wide pulse was received, delayed 5 μsec, used to reset all binaries to zero, delayed another 5 ms, and used to initiate the calibration circuitry.

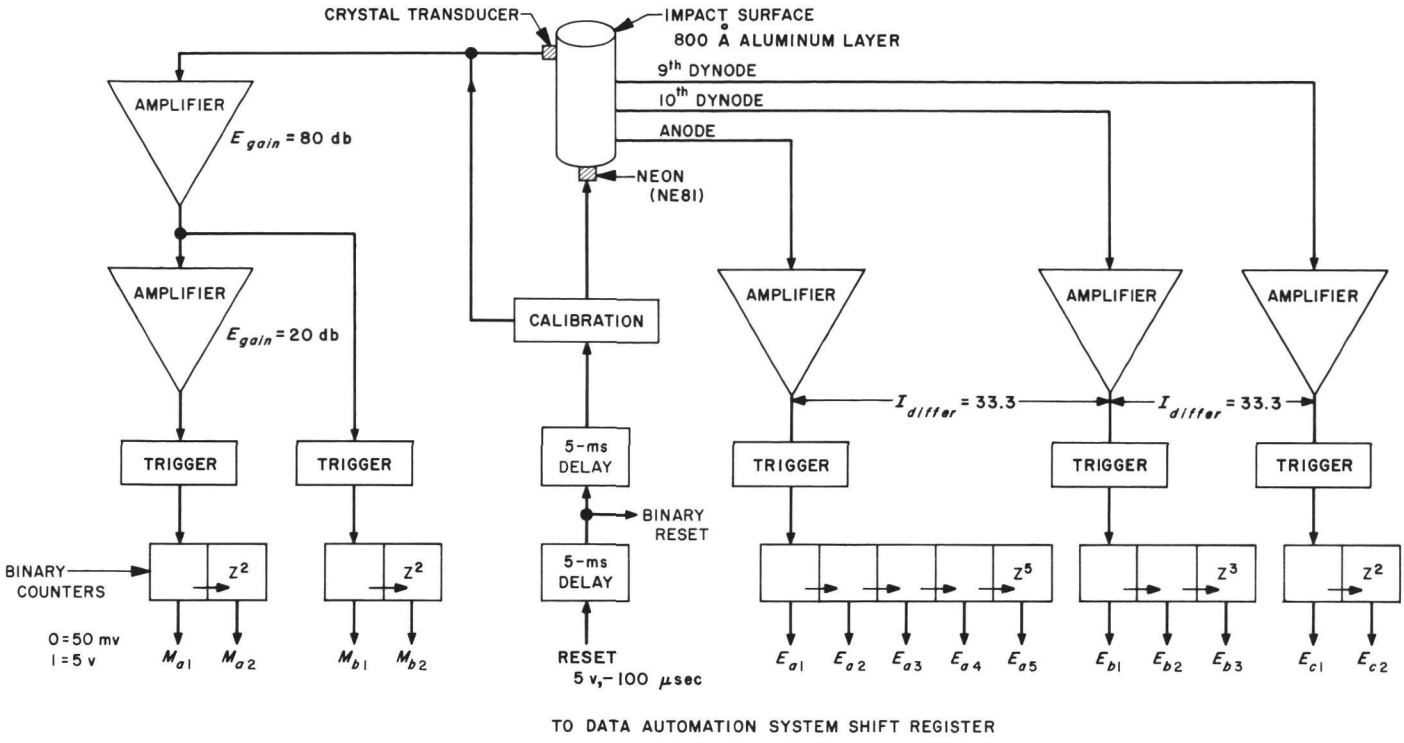

Figure 93. Composite dust detector

In-flight calibration was thought to be worthwhile, in that the sensitivity may reduce in the environment of space.

Calibration of the light-flash detector was provided by a neon flash within the base of the photomultiplier tube of approximately 200-μsec duration, and of such an intensity that a count of 1 appeared in each binary counter, and simultaneously, a pulse was electrically injected across the microphone of sufficient amplitude to insert a 1 in each of its binary counters.

The composite package (Fig 94), housing sensors and all the associated electronics (Fig 95), was extruded magnesium, 0.002-in. 24k gold plated (for a stabilized operating temperature of 60°F), 3⅜ in. × 6 in. × 6 /in. in

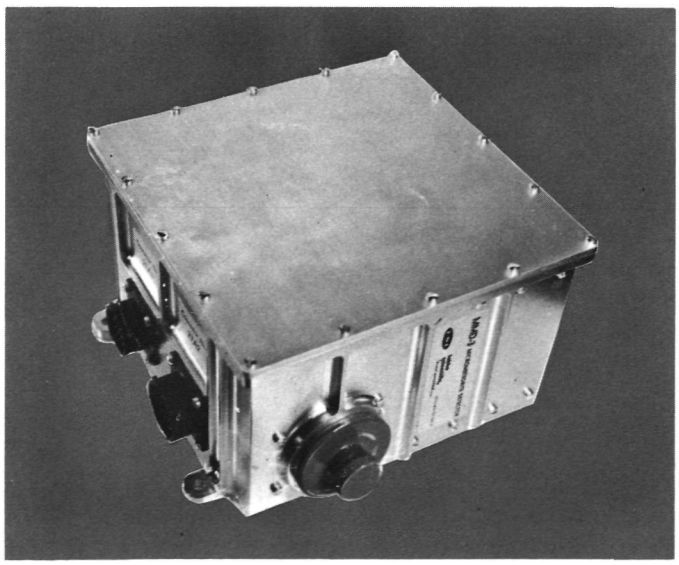

Figure 94. Cosmic dust detector, with protective cover

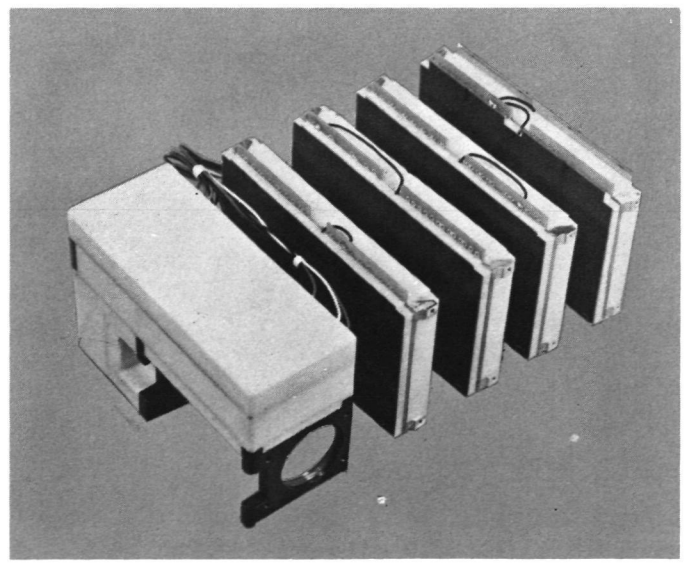

Figure 95. Cosmic dust detector, exploded view

over-all dimensions. Weight was 3.55 lb and required +7 v, 120 mw and −7 v, 80 mw of power. The package was located on the top of the main spacecraft structure and the detectors were pointed at 90 deg to the expected probe–Sun line and in the Earth–probe–Sun plane.

To avoid high-voltage corona problems encountered at critical altitudes, power was supplied to the experiment 78.5 min after lift-off.

Flight performance summary. Anomalously high counting rates were often recorded by the light-flash detector; this was presumably due to direct or reflected sunlight, reaching the photocathode through pin holes in the aluminum protective surface from previous particle impacts. For the first several hours after launch, the microphone output was erratic, probably because the instrument was picking up acoustic noise from the outgassing process.

i. Data automation system.

General description. The purpose of the RA-1 and -2 Data Automation System (DAS) was to process, store, control, and translate the data from six scientific experiments on the spacecraft. These experiments had 25 sensor outputs, sampled on a 120-sec time base, and utilized three digital telemetry channels.

The complete data system consisted of an on-board Data Automation System digital converter for telemetry station equipment (TSE). A general functional diagram of the data flow is shown in Figure 96.

The general performance of the data system was satisfactory. During prelaunch spacecraft systems testing and post-launch operations, spacecraft noise affected less than 1% of the data. The TSE-TTY link shown in Figure 96 was originally relegated the role of a back-up link. However, the TSE-TTY link proved to be more successful than expected and served as the primary source of scientific data, except for the case of the Mobile Tracking Station (MTS), which was not equipped with the TSE-TTY units. The processing of the data by the computer, virtually in real time, has been proven a valuable and desirable mode of operation for the data user.

Flight equipment. The flight unit served several functions which varied with the experiment. In some instances, the DAS furnished control pulses to the experiments, in others it only processed the incoming data. A functional diagram of the flight unit is shown in Figure 97. The final configuration of the DAS was a function of the design boundary conditions which were:

(1) Handle the data with wide dynamic ranges from an array of 25 sensors.

(2) Meet the weight and power requirements of 13 lb and 1 w.

(3) Design and construct a prototype in 60 days and a flight unit in 120 days.

(4) Limit the output data rate to 4 bits per sec per channel on three channels.

The principal considerations used to meet these conditions were:

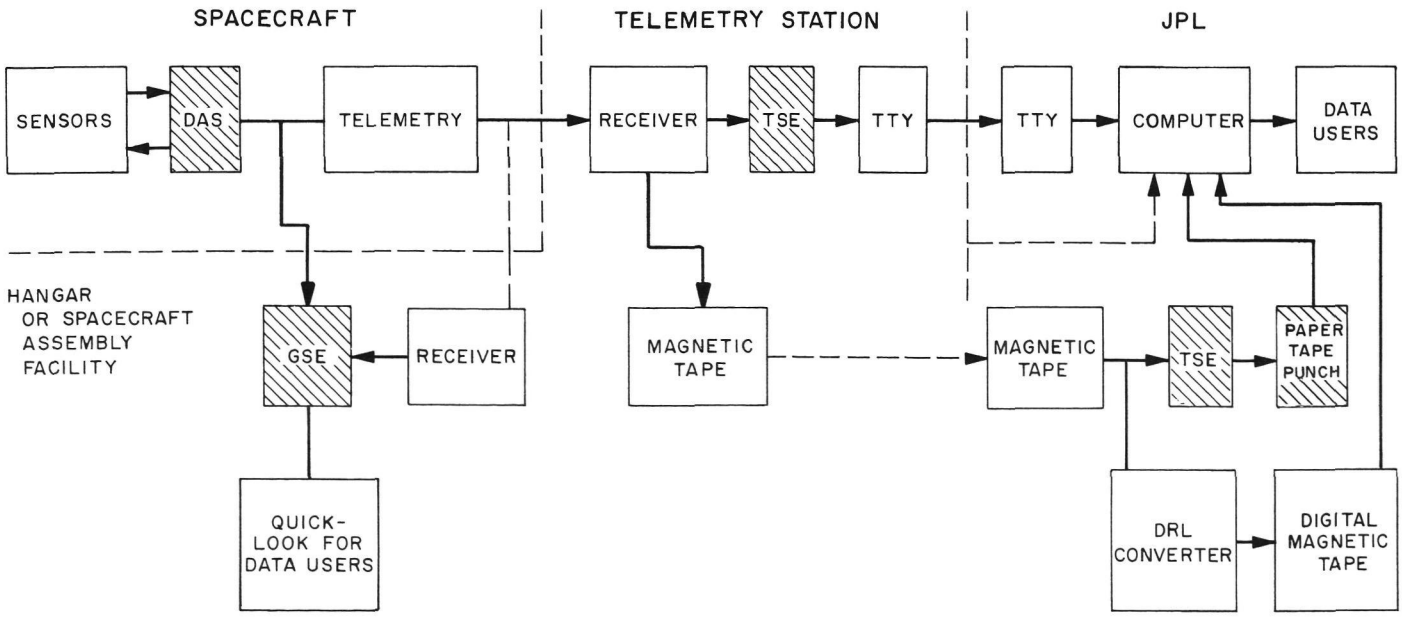

Figure 96. Data handling system for science data on RA-1 and -2

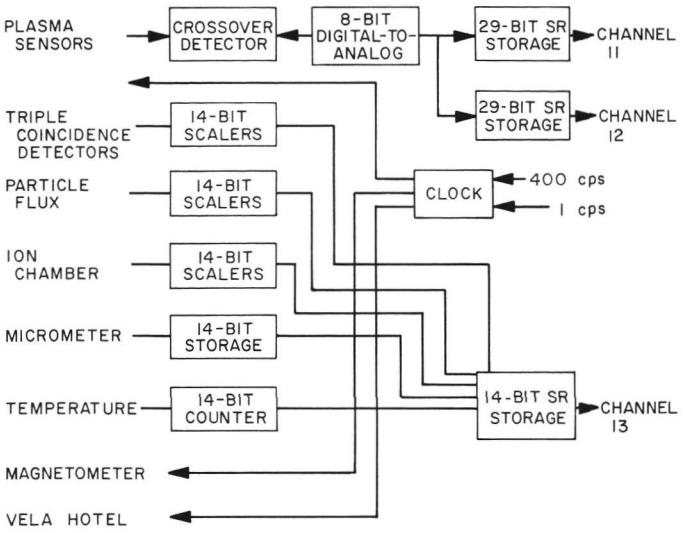

Figure 97. Functional diagram of data automation system flight unit

(1) The use of 14-bit non-resetting scalers and 8-bit A−D converter sampling six sensors simultaneously

(2) Package the components in as small a space as possible and use low power logic.

(3) Use off-the-shelf circuit designs such as flip-flop storage.

(4) Divide the telemetry into two channels for the six plasma sensors and a third channel for all the particle experiments.

The resulting device contained 932 transistors, 1478 diodes, and 6633 total components.

The scaling binaries used 700 μw each and the clock binaries used 1.2 mw each. The components were packaged in modules, cordwood style, and the entire system was mounted on 8 six-in. squares. The average component density was approximately 24 components per square in.

Functional description. The flight unit can be divided into three major areas:

(1) Digital processing

(2) Analog processing

(3) Sub-programming

The digital processing consisted of fourteen 14-bit data binary stages. Each could be connected as single 14-bit scalars or as two 7-bit scalars, or as any combination totalling 14 bits. These scalars were not reset and were sampled once per 60 sec. The expected dynamic range of incoming pulse rates from the particle experiments was 1 per 1000 sec to 2000 per sec. These scalars were read out by sequentially transferring the 14 bits to an output shift register and unloading the shift register at a 4-bit sec rate. A parity and a "1" completed the 16-bit word. This data was transmitted on telemetry channel B13. A bit or frame sync word and a clock monitor count or temperature word completed the 60-sec subframe.

The analog processing consisted of six cross-over detectors and a staircase generator or D-to-A converter. All six conversions were made simultaneously, and stored in six 8-bit shift registers every 9 sec for 12 consecutive samples. The six 8-bit shift registers were divided equally into two telemetry channels, B11 and B12. A parity bit and 4-bit identifier completed the 29-bit word transmitted each 9 sec via B11 and B12. Master frame sync was transmitted from B11 and B12 simultaneously with sub-frame sync on B13. The word format for all three channels is shown in the timing diagram (Fig 98).

The sub-programmer consisted of a clock actuated by the 400-cps signal from CC&S. If the 400-cps signal was interrupted for any reason, the clock would run at 385 cps. The various outputs from the clock included:

Bit rate	4 cps
Vela Hotel (sync)	1 cps
Ion chamber (word sync)	1/4 cps
Solar plasma (read and switch)	1/9 cps
Magnetometer (switch)	1/10 cps
Sub-frame	1/60 cps
Master frame	1/120 cps
Temperature (read)	1/240 cps
Temperature (read)	1/300 cps
Temperature (read)	1/480 cps
Clock monitor	1/1,966,080 cps

The purpose of the clock monitor was to check the timing operation of the DAS. As the power per clock binary was relatively low (1.2 mw), the noise margins were also low. It was presumed that the presence of abnormal noise levels would, therefore, be detected by irregular changes in the clock monitor or frame count. These data were not designed to have any scientific significance, but if the noise were normal, the frame count could be used to identify the approximate time of transmission and might assist the data user.

Circuit design. A typical binary circuit is shown in Figure 99. Circuit d-c stability analysis was made on all

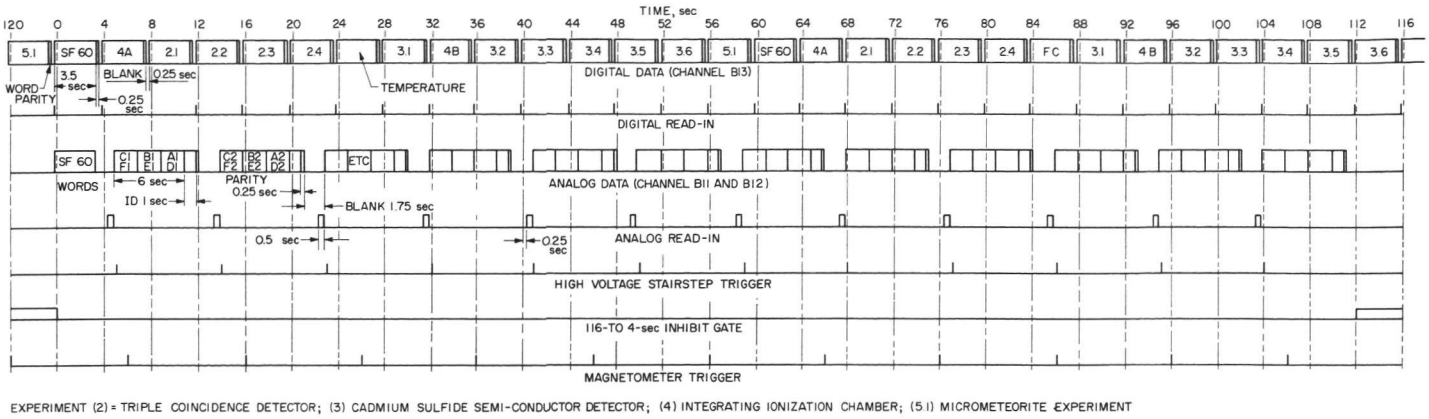

EXPERIMENT (2) = TRIPLE COINCIDENCE DETECTOR; (3) CADMIUM SULFIDE SEMI-CONDUCTOR DETECTOR; (4) INTEGRATING IONIZATION CHAMBER; (5.1) MICROMETEORITE EXPERIMENT

Figure 98. Timing diagram of data system

the circuits used in the DAS. All the transistors selected had $B \geqq 60$ and the analysis was performed assuming a degradation of a factor of 3 or more ($B = 20$). The analysis is presented in Reference 32.

Packaging. The type of construction used is illustrated in Figure 100. The components were stacked cordwood-style between two printed circuit boards. Each circuit was separately potted and called a module. A set of 14 modules placed side by side constituted a stick. Four sticks were placed on each side of four castings. The leads from each module projected through eyelets on printed interconnection boards that were printed on both sides. The module leads were bent over and soldered to the outside of each eyelet. Intercasting wiring was soldered to the eyelets both above and below the interconnection boards and went to 37 pin connectors at the top of the castings.

As a consequence of the hidden soldered connections below the printed boards, module exchange was very difficult. Replacing modules also required the complete disassembly of the unit from the casting. However, the packaging technique did provide a means of meeting the weight requirement.

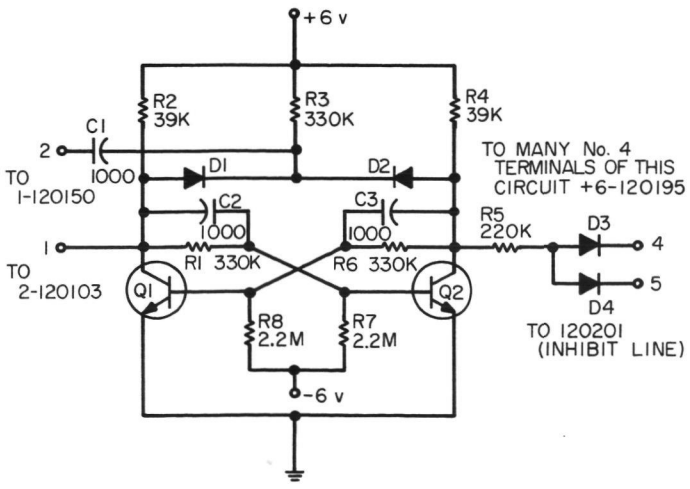

Figure 99. Data binary circuit

Pre-launch checkout ground support equipment. The pre-launch checkout equipment was designed to convert the data format, as generated by the flight unit, into a decimal print-out for quick-look analysis and a paper-punched tape for computer use or a detailed analysis of the data. A functional diagram of the GSE is shown in Figure 101. The GSE logic was constructed with standard commercial logic modules.

The principal boundary conditions affecting the design and construction of the GSE were cost, reusability, and schedule. Except for a few interface circuits, the entire GSE was constructed within 30 days from commercial units. After the launching of *Rangers I* and *II*, two of the three GSE units were dismantled and the logic was modified to serve as MA-R DAS check-out equipment. The third unit, shown in Figure 102, remains intact for testing the RA-2A system.

GSE implementation. The DAS-GSE consists of:

(1) Clocking and bit frame sync logic drawer.

(2) Down counter logic drawer.

(3) Visicorder.

(4) Patch panel.

(5) Oscilloscope.

(6) Tape punch.

(7) Tape reader.

(8) HP counter.

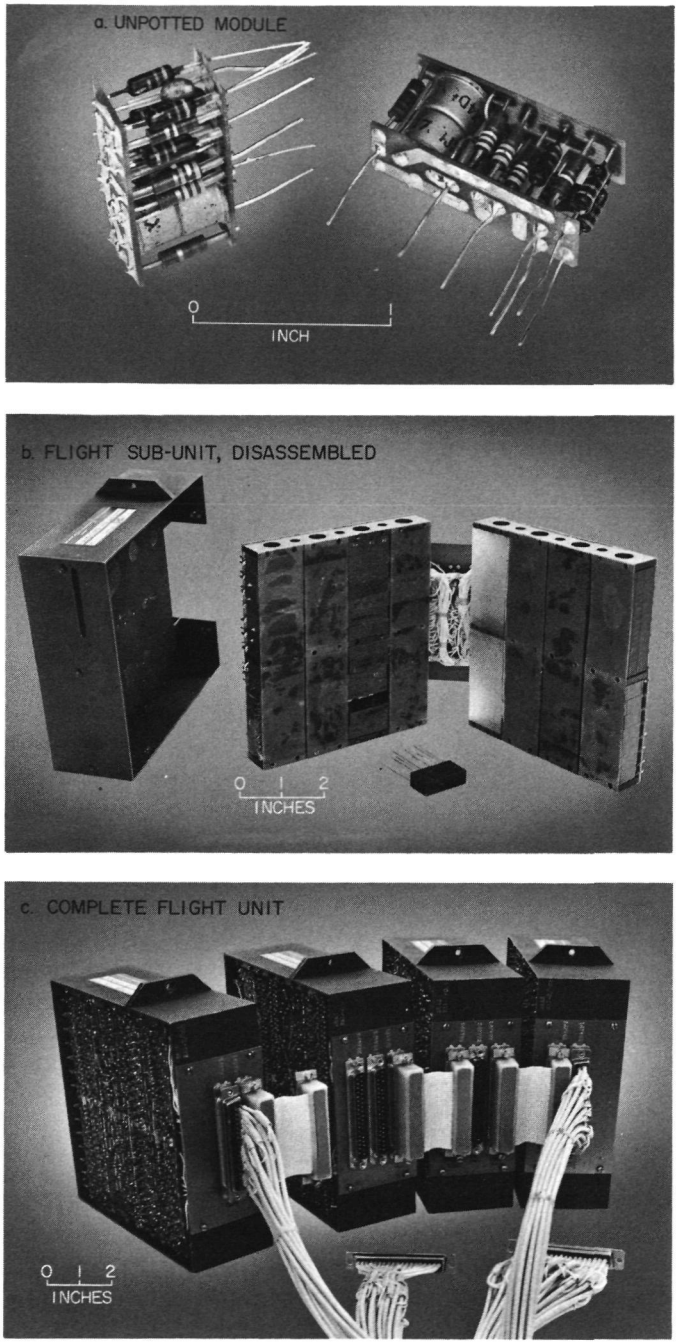

Figure 100. Data automation system flight unit

(9) HP printer.

(10) Dymec clock.

The DAS–GSE can accept digital data directly from the spacecraft, telemetry or tape reader or analog data from the telemetry discriminator outputs. Bit and frame sync are checked and corrected every 480 bits by use of a special sync word. Each bit is sampled midway in the 250 ms bit for a duration of 20 ms. The sampling interval is controlled by the 400 cps generated on the spacecraft and telemetered on a separate channel. An example of the data is shown in Figure 103.

The operation of the GSE was completely satisfactory. For most of the system testing, the mode of operation which utilized the telemetry analog output was found to be best. The bit sampling system would allow discriminator analog drifts of ±30% of peak-to-peak values. The stability of the telemetry system was excellent and seldom exceeded ±5%.

Telemetry support equipment (TSE). The TSE units were duplicates of a fraction of the GSE. Their primary purpose was to convert the discriminator outputs at the DSIF stations into a paper-punched tape which could then be handled by standard teletype equipment to relay the data back to JPL. Two of each of the units were installed at the DSIF stations at Johannesburg, Woomera, and Goldstone, one unit for operation and one for stand-by. A detailed description of the TSE is given in Reference 33.

The data recovered by the TSE's was nearly errorless and their operation is considered completed satisfactory. One of the TSE units was also used with complete success in the JPL Data Reduction Laboratory to translate the MTS data from magnetic tape to the paper-punched tape. An example of the data as read from the magnetic tape through the discriminators is shown in Figure 103. It can be seen that even though wow and flutter added appreciable noise to the signal, the data recovery was satisfactory.

Flight-unit reliability. The two types of degradation of major concern were the abrupt failures and fadeout. All abrupt failures, such as broken wires or diodes, occurred in environmental testing. No fadeout failures were experienced. Parts of the flight units were operated at elevated temperatures (80°C) for several months with no apparent degradation. All of the weak points in the flight units were eliminated by repeated environmental tests and at no time during any of the pre-launch system testing or post-launch operations did any component of the RA-1 and -2 flight units fail to operate properly.

Reliability of DAS-GSE/TSE units. The major problems with the ground equipment were associated with interface problems, ground loops, and spurious noise. Once these sources of trouble had been traced and corrected, no additional failures occurred. The equipment appeared to be rugged and insensitive to transport. It was often moved about at AMR, and when returned to

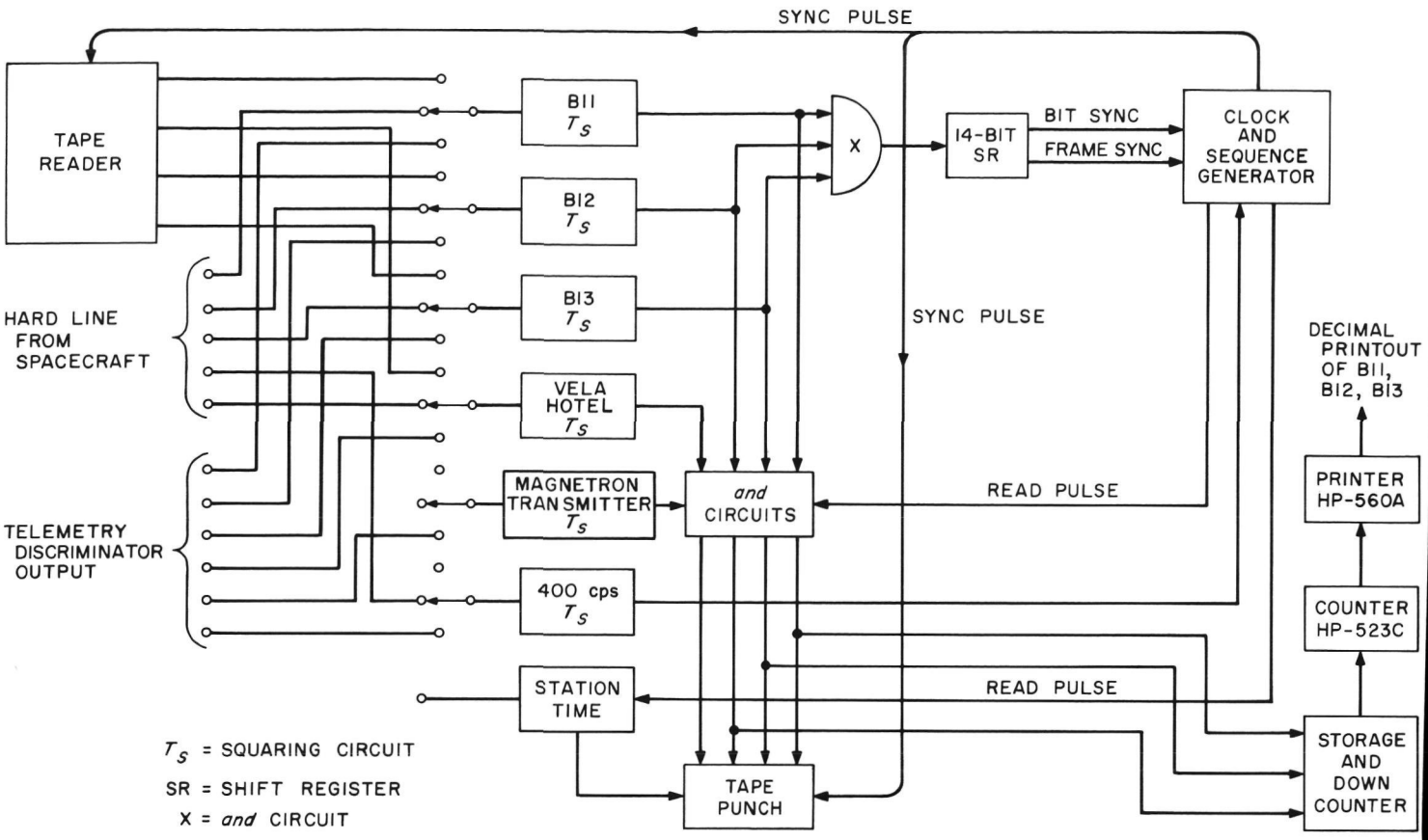

Figure 101. DAS ground support equipment, functional diagram

JPL after *Ranger II*, the ground equipment operated correctly with no adjustments within a few sec after being turned on.

Testing and calibration. Environmental and systems tests were performed on the flight unit. The environmental testing consisted of:

(1) Vibration and shock (flight acceptance).

(2) Temperature (flight acceptance).

(3) Voltage margin ($\pm 5\%$).

The procedure of testing followed in the above order. After vibration test, the unit was subjected to the temperature test and if any modules failed to operate properly they were replaced. The unit was reassembled and sent back for another vibration test. This procedure was repeated until the unit passed all tests, consequently all units were subjected to the FA tests several times. A tabulation of the number of tests and number of modules replaced is given in Table 39.

During systems tests, a number of problems occurred with the interfaces between the flight unit and the science sensor check-out equipment. These problems, the DAS indication, and the corrective action taken are listed in Table 40.

The only calibrations required were associated with temperature and solar plasma A-D conversions. A typical temperature calibration curve is shown in Figure 104. The analog-to-digital converter was calibrated by comparing

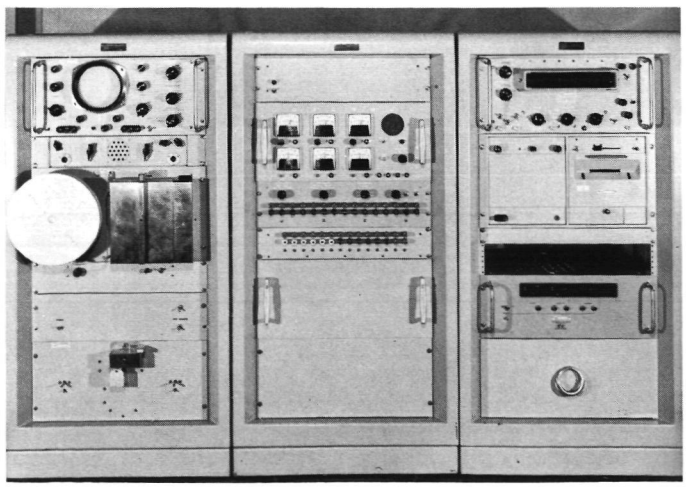

Figure 102. DAS ground support equipment

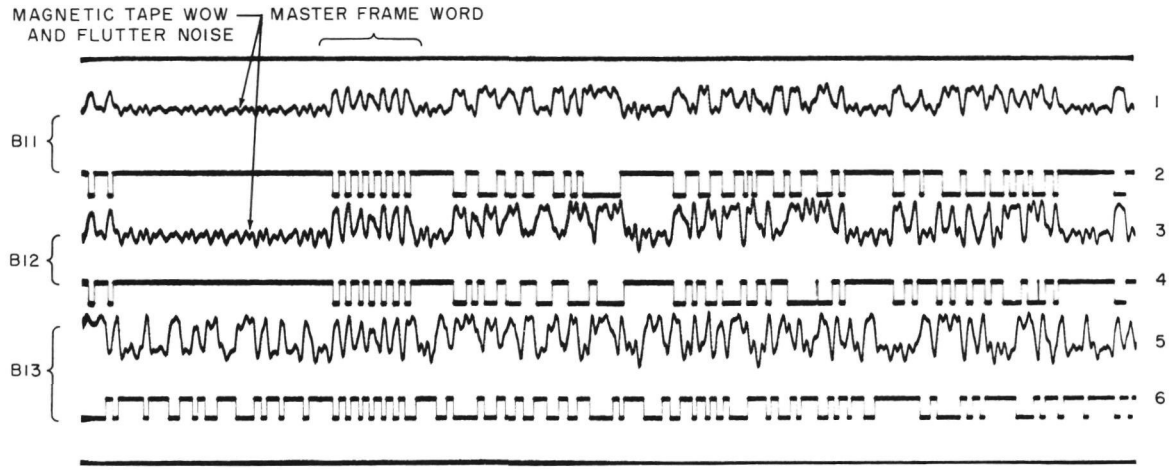

TRACES 1,3 AND 5 ARE DISCRIMINATOR OUTPUT VOLTAGES. THE SIGNAL IS BEING REDUCED FROM MIXED-TONE ON MAGNETIC TAPE

TRACES 2,4 AND 6 ARE INTERMEDIATE RECONSTRUCTION SIGNALS IN THE DAS-GSE. THE FINAL RECONSTRUCTION SIGNAL IS OBTAINED BY SAMPLING THE CENTER OF EACH BIT AND CONVERTING THE SAMPLES TO PUNCHED PAPER TAPE

Figure 103. Example of *Ranger I* data, from MTS intercept

Table 39. Flight unit flight-acceptance tests and modules replaced

Unit	Modules replaced[a]	Reason[b]	Shake tests
5	9	Failure	
	7	Design change	4
6	13	Failure	
	7	Design change	3
7	1	Failure	
	7	Design change	2
8	16	Failure	
	7	Design change	5
9	5	Failure	
	7	Design change	3

[a]The total number of modules in a DAS Flight Unit is *448*.
[b]Nearly all failures were due to the inability of the module to operate with satisfactory voltage margins over the entire temperature range.

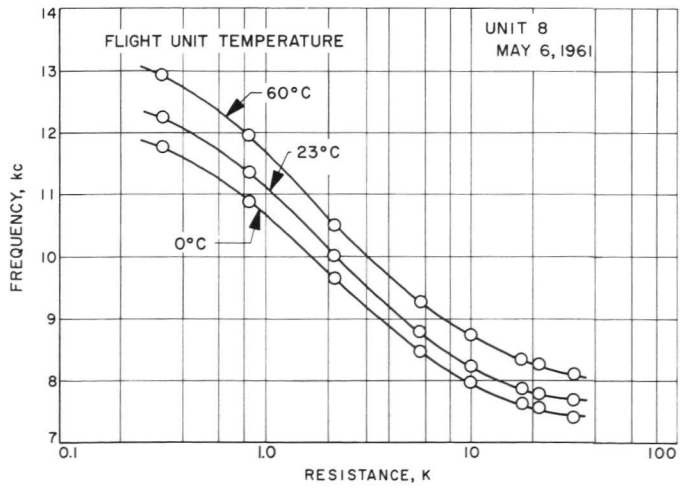

Figure 104. Typical temperature calibration curve

a known voltage with the DAS readout. Little variation was found over the required temperature range. An example of the staircase waveform is shown in Figure 105. The leading edges of the steps were purposely rounded off to prevent overshoot from furnishing erroneous readings.

Performance summary. The total operating time of each of the flight units was 1000 to 1200 hr. At all times during pre-launch or post-launch operations, the behavior of the flight units was satisfactory. During launch and after Command 2 was actuated, anomalies were noted in the clock monitor and in the ion chamber time-count register. Some of the anomalies appeared to be caused by errors

Table 40. Systems tests problems

Indication	Problem	Correction
No signal out of DAS to telemetry	4-cps driver overloaded by GSE cable capacity	Isolated GSE cable with 10 KΩ resistors in DAS
No ¼-pps/pulse present	CC&S 1-pps oscillated at 100 cps	Isolated CC&S from DAS with 5.6 KΩ resistor in DAS
No sub-frame indication	A −5-v signal was erroneously fed to DAS by Scientific GSE (SGSE)	Capacity coupled the signal to SGSE in SGSE
Asynchronous data print-out	Noise on ¼-pps DAS–GSE line	Installed pulse-width detector on ¼-cps DAS–GSE line in GSE
No data out of DAS	A 3-v signal existed between System common and DAS common	Replaced pin connectors in Case 6 harness
Improper operation of solar plasma	⅛ pps running at ⅓ pps	Replaced cabling to boom unit
No data out of DAS	*Short-circuit in Case 6 harness*	*Removed short-circuit*

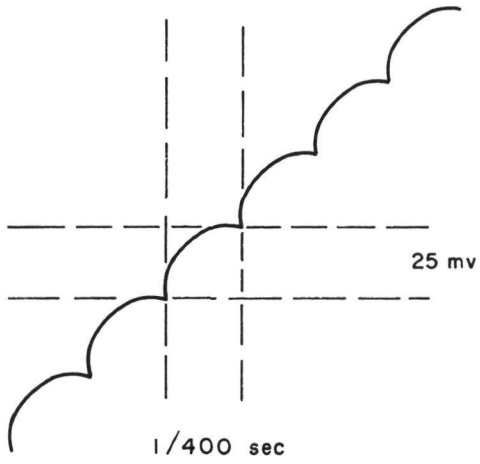

Figure 105. Example of staircase waveform

in the reduction or transmission link. A preliminary analysis of the digital scientific data resulted in the approximate figures given in Table 41.

Spacecraft noise

(1) One noise pulse was detected on both RA-1 and RA-2 between 3 and 4 min after lift-off. It was of sufficient strength to reset all registers.

(2) No noise was detected prior to Command 2 other than the one noted above.

(3) After Command 2 was actuated, noise pulses were occasionally detected and one type was found to be in synchronism with the solar plasma sequence. These noise pulses were relatively low in energy and were only apparent in the clock monitor.

(4) The rate of synchronous noise pulse occurrences decreased with time and occurred most often near perigee.

(5) Large noise pulses, of the type the caused all registers to reset or a major shift in the clock monitor, occurred occasionally and for the most part, at times when the spacecraft was either entering or leaving sunlight.

(6) A total of 20 noise pulses was recorded by the clock monitor on RA-1. Only three of these were actually observed; the presence of the other 17 were made known as a result of the storage properties of the clock monitor. The average time between noise pulses was:

Type of pulse	Avg time, hr	No. occurred
Synchronous noise	7.5	7
Asynchronous noise	8.8	8
Complete re-sets	6.2	5

There are 30 frames of data transmitted per hr and only 20 of the 4170 frames transmitted were affected by the various kinds of noises in the clock monitor.

(7) There were 24 and 2 observed data frames (out of total of 256 and 32) from RA-1 and -2, respectively, in which the contents of the ion chamber "time" register were obviously in error on board the spacecraft.

Conclusion. The performance of the DAS flight units was satisfactory and indicated that the pre-launch testing, calibration procedures and design margin checks are adequate. The DAS properly performed all designed operations. The performance clearly indicated that low-power, high-density packing digital date devices are useful in a spacecraft system. Furthermore, the relatively low percentage of errors suggests that short period framing can circumvent the noise and short duration of intercept problems.

Table 41. Scientific data system performance

	RA-1	RA-2
Transmission time, min	5460	408
Received data, min	417	55
Bits transmitted	4×10^6	2.9×10^5
Bits received	3×10^5	4.0×10^4
Data points readable	20,300	2700
Data points lost (sync noise)	54	18
$\frac{\text{Data received}}{\text{Data transmitted}} \times 100$, %	7.6	13.5
$\frac{\text{Data points readable}}{\text{Data points received}} \times 100$, %	99.3	99.1
Data errors (all causes), %	0.67	0.92
Data errors (spacecraft noise), %	0.27	0.66

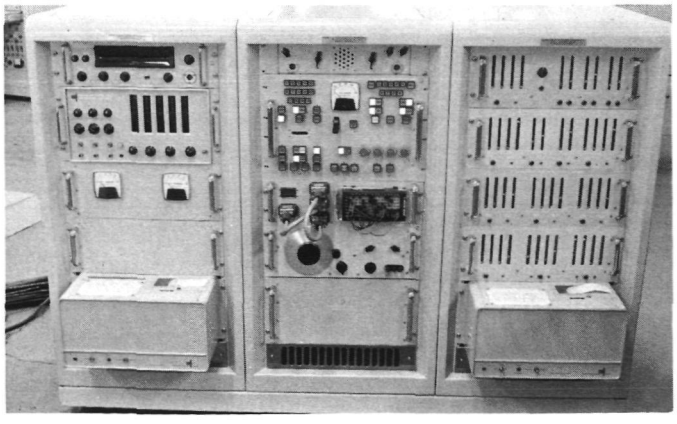

Figure 106. Master GSE consoles

The performance of the ground data handling devices was satisfactory. All units operated without failure or special adjustment. The successful operation of these digital devices indicates the usefulness of sampled data and bit-framing synchronization techniques in reconstructing the data. Near-real-time data reduction proved to be feasible and desirable for both pre-launch and post-launch operations.

j. Ground support equipment.

General description. The RA-1 and -2 ground support equipment (GSE) was designed to individually test the seven scientific experiments aboard the spacecraft and to obtain data from these experiments during the spacecraft systems test for evaluation of the operation of these experiments. Figure 106 displays the three master GSE consoles, while Figure 107 shows the remote cart which is operated in conjunction with the master station. Two new ideas were incorporated into this equipment. The first was the use of a patchboard system which could pre-setup the testing operation of the GSE system. A separate patchboard was arranged for both the individual experiment tests and for the systems test. The other innovation was the remote cart which can be moved to the vicinity of the spacecraft for directly monitoring certain scientific instruments.

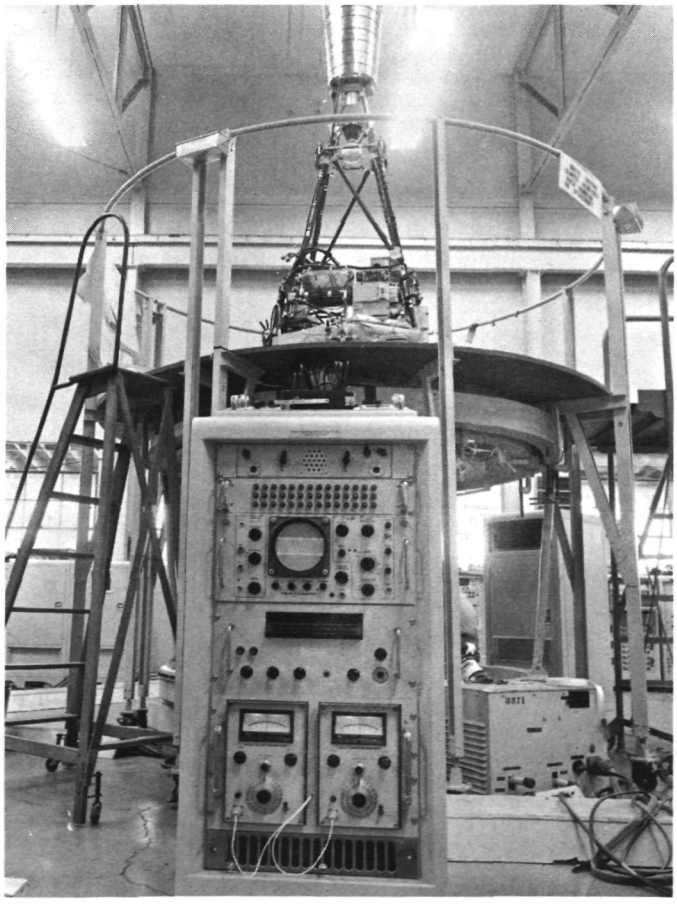

Figure 107. Remote GSE installation

By means of the data automation system GSE and the central recorder, all scientific instruments could be monitored during the countdown. The GSE illustrated in Figures 106 and 107 was only used when there was direct access to the spacecraft.

Stimulus and response. Integrating cosmic-ray ionization chamber, Geiger counter, gold-silicon detector and triple-coincidence cosmic-ray telescope experiments were excited by radioactive sources which were placed in the vicinity of the spacecraft. The output rates of these instruments were monitored by display-type counters in the GSE and permanently recorded by a printer. Other display counters were used to monitor the medium-energy cadmium-sulfide detectors which were activated by lights placed at the sensor of the instrument. All of these GSE counters were read-out in the same sequence as the data automation system GSE. The rates of the two GSE systems were then compared.

The solar corpuscular radiation electrostatic analysis experiment received a known amount of current injected into its sensor from a test fixture placed on top of this instrument. Nine decades of current injection were used and the analog output of the unit was printed-out on a recorder after each new step of current injection. These results were then compared with previous calibrations.

The cosmic-dust detector was stimulated by a trigger signal from the GSE which had the same effect as a micrometeorite striking the sensor of this instrument. The condition of the binary counters in the micrometeorite experiment was automatically read-out after each triggering input.

Since the rubidium vapor magnetometer created a special problem because of its saturated condition near the Earth the GSE was used to modulate the B+ to the rubidium vapor lamp. This procedure produced the same effect as a changing magnetic field and caused the frequency output of the magnetometer to be identical to the input test frequency.

Integration. The design and construction of the scientific case harness proved to be a very complex problem because of the numerous monitoring functions required for testing the scientific instruments. After several attempts, a reliable harness was produced.

Although the scientific power supply passed all environmental tests, the high output impedance of the

magnetometer d-c supply caused an oscillation in the magnetometer system when the two items were mated in the spacecraft. As a result, the power supply system was modified to lower the output impedance. Figure 108 displays the scientific power supply (T/R). Figure 109 shows the scientific case which contain the scientific electronics and data automation system used in RA-1 and -2.

Throughout the testing of the scientific instruments, numerous detrimental noise and ground problems were discovered. After considerable effort, most of these problems were resolved.

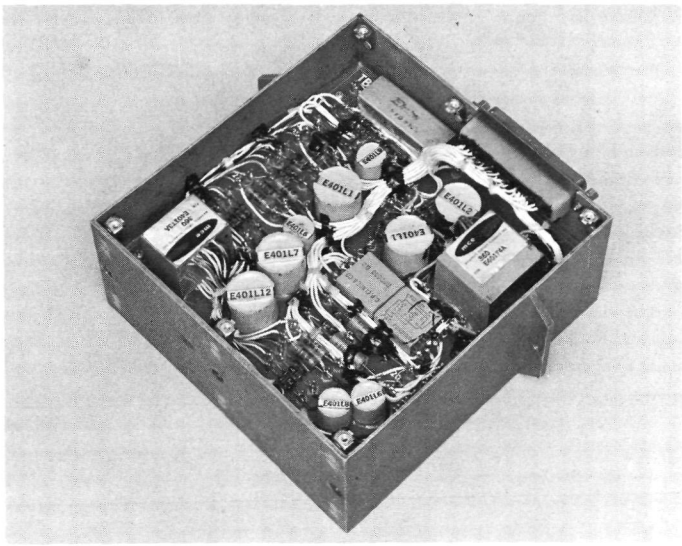

Figure 108. Scientific power supply T/R unit

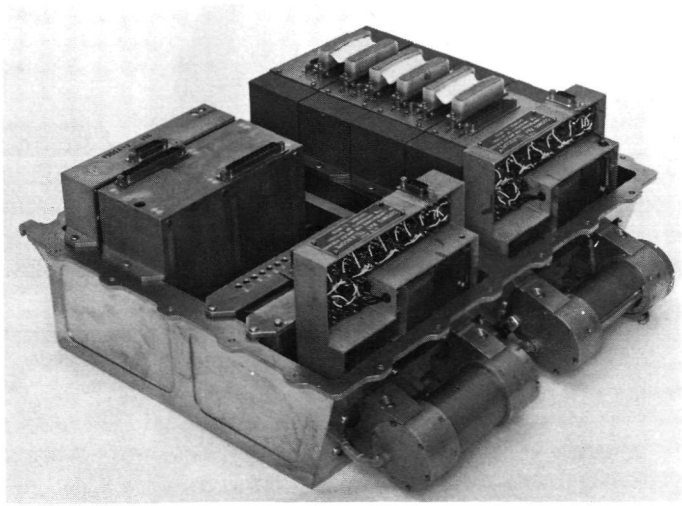

Figure 109. Case containing scientific electronics and DAS for RA-1 and -2

Subsystem and system testing. Aside from the testing described above, oscilloscope monitoring of certain functions, such as the solar corpuscular demodulator wave forms, was incorporated as an important part of the analysis of the instruments. The power supply system, which required 26 measurements, was automatically programmed to a voltmeter and recorded on a printer.

The Lyman-alpha system was tested by inserting a discrete number of input pulses to start the scan of this instrument at a specific time. This scan was visually observed and the output of the device was monitored on the central recorder. The observation of the scanning of the instrument was considered as part of the test.

A systems test involving the testing of all seven scientific instruments required four hr of test time. Two of these hr were for testing just the solar corpuscular unit.

A problem existed concerning the contamination of the Lyman-alpha telescope mirror when it was exposed to the atmosphere for any length of time. The mirror surface was preserved by feeding nitrogen to the telescope through a plastic plate covering the telescope opening.

Data analysis. During some portions of the subsystem testing, during all portions of the systems tests, and during the countdown, the scientific data was sampled and manually reduced. By this method, the scientific GSE and data automation system GSE readouts could be compared immediately. In addition, punch-tape data was obtained from the DAS GSE and sent to the computer at JPL by teletype for verification of the manual scientific data reduction.

Calibrations. Several times during the testing of the spacecraft, medium-energy detectors were removed from the spacecraft and accurately calibrated with radioactive sources. The calibrations were compared periodically to ascertain the stability of the instruments.

The triple-coincidence detectors were calibrated by obtaining a total of 36 hr of background radiation data of the instrument on the spacecraft. An instrument was considered flight-worthy if the rates of this test were within the accuracy of the predicted data.

The solar corpuscular test fixture was calibrated prior to installation on the spacecraft and produced known outputs from the solar corpuscular instrument. These outputs were then compared with the predicted data from the DAS system.

Voltage and current measurements were taken at AMR in detail to determine the characteristics of the power supply system while operating in the spacecraft. These

measurements were taken in a condition with the high voltage turned off and then again with the high voltage activated. The switching of the high voltage was required to eliminate arcing problems during the initial portions of the flight.

Maintenance. After the initial problems when the ground support equipment was first tested with the flight instruments, the GSE has required a minimum of maintenance. Approximately 700 hr of operating time was accumulated on one of the systems.

Documentation. Two complete files have been established—one at JPL, the other at AMR. These files contain all drawings and literature that has been released on every flight instrument and GSE system.

Log books are maintained on all operations and a complete record of each test and modification has been recorded in these log books.

Analysis of GSE and subsystems tests. The use of a patchboard system for setting up tests provides flexibility and saves considerable testing time. Throughout the testing of the RA-1 and -2 scientific instruments, it was established that there was no interaction between the various instruments or between the scientific instruments and other spacecraft subsystems. The testing of the scientific instruments during the countdown permitted the detection of instrument malfunctions when the spacecraft was being prepared for launch.

Some areas which require considerable thought in future designs are:

(1) Elimination of ground loops.

(2) Reduction of system noise.

(3) Conditioning of signals for operation over long cables between the GSE and the spacecraft.

(4) Elimination of leakage problems in low-current devices.

In general, the RA-1 and -2 scientific ground support equipment provided complete evaluation of the spacecraft scientific instruments and met all design requirements.

Reduction and presentation of received data. The data-handling system that was to have been used with the *Ranger* program was designed to utilize the IBM 7090 high-speed, automatic digital computer as the major information-transforming device. This computer is capable of performing 250,000 arithmetical or logical operations each sec.

The RA-1 and -2 spacecraft transmitted their data in both analog and digital form. Each mode required special ground equipment to effect the transformation of data to a form suitable for the computer. Specifically, the Lyman-alpha data was in analog form and the magnetometer data was in the form of frequency-versus-time; all other data was received in digital form as encoded by the data-automation system on board the spacecraft.

The data was recorded on magnetic tapes at each antenna site, and these tapes were then transported to the JPL telemetry Data Reduction Laboratory (faster teletype transmission was also used), where the signals were demodulated from the carrier frequency and the noise was removed. All digitized data was transformed by a specially built data translator and recorded on a magnetic tape that could have been fed directly into the computer.

The computer accepts this information serially into its memory. The first operation is to check the data to determine whether or not they pass certain parity tests and frame-synchronization markers inherent as check points in the transmitted data. Such tests will not be passed if noise has so distorted the data that a "one" appears as a "zero," or vice versa, since all of the digital data are in binary form. Once it is established that the data is correct, calibration factors are applied to each experiment in order that the numbers will be of significance to the reader. Since many of the experiments use counters which accumulate information rather than reset each time, the computer calculates successive differences between readings and also calculates averages, ratios, and other desired parameters. The computer also makes comparisons with the results of other experiments.

An output format is created which labels each experiment and gives the time the measurement was made in the spacecraft. It is in this capacity that presentation for useful interpretation by the scientific community becomes important. All of the transformed data will be printed numerically on the IBM tabulator, which prints 120 digits per line and 8 lines per in. (1 line generally represents 1 min worth of data). Approximately 6 pages laid side by side will be necessary to represent 1 line for 1 min. It would still be very difficult to examine visually these large amounts of numbers with the immediate hope of establishing any trends within any single experiment or to compare one experiment with any of the other experiments. Therefore, it is valuable to convert a pertinent number of the columns of printed data into a graphical form using an x, y plotter with time along the base at a

rate of 1 hr per in. Several experiments can then be plotted above each other such that it is much easier to see any correlation and trend with time among the various experiments, relevant geophysical data, and terrestrial observations of solar events which will be noted on the same plots. From these observations, it should be possible to deduce a mathematical model which can be placed into the computer for testing.

Since neither *Ranger I* nor *II* followed its predicted path, this system, which was designed for massive data flow, has not had a chance to be tested.

2. RA-3, -4, -5 (Impact Capsule System)

a. Scientific objectives. Rangers RA-3, -4, -5, the first spacecraft designed to land instrument packages on the Moon's surface, will carry experiments designed to obtain scientific information which will increase our knowledge of the history and formation of the Moon, and technical information which will help increase the chances of successful future Moon landings by unmanned or manned spacecraft.

The three spacecraft will carry the same four experiments:

(1) Television subsystem.

(2) Gamma-ray spectrometer.

(3) Radar altimeter to obtain reflectivity data.

(4) Seismometer.

The superstructure of the spacecraft, carrying the television, gamma-ray, and radar instrumentation, will crash-land and be destroyed. The capsule, with the seismometer and its radio transmitter, will hard-land at about 3000-g deceleration. The seismometer will then measure lunar seismic activity.

One objective of the present missions is to obtain pictures that contain more detail than do the photographs of the Moon now available. These pictures will indicate the type of surface on which the seismometer capsule will land and assist in the proper evaluation of the seismometer data. The pictures will also give some geological information relative to a coarse surface structure, small-scale geological land forms and features, and attitudes and slopes of surface features. The same information will help in the selection of landing sites for future instrumented and manned lunar probes. It is expected that the resolution of the final picture obtained will correspond

Table 42. RA-3, -4, -5 scientific experiments, sponsoring agencies, and cognizant JPL personnel

Division of the Space Sciences
Program Representative: M. Eimer.
Project Scientist: H. W. Washburn.
Project Engineer: R. L. Heacock.

Experiment	Sponsoring agency/experimenter(s)	JPL cognizant scientist	JPL cognizant engineer
Television subsystem	Jet Propulsion Laboratory G. P. Kuiper E. M. Shoemaker H. C. Urey A. R. Hibbs R. L. Heacock E. F. Dobies	E. F. Dobies	R. C. Heyser
Gamma-ray spectrometer	University of California at La Jolla, Los Alamos Scientific Laboratory, Jet Propulsion Laboratory J. R. Arnold E. C. Anderson M. A. Van Dilla A. E. Metzger	A. E. Metzger	A. E. Metzger
Radar altimeter	Jet Propulsion Laboratory W. E. Brown, Jr.	W. E. Brown, Jr.	H. E. Wagner
Seismometer	California Institute of Technology, Columbia University F. Press M. Ewing	R. L. Kovach	D. F. Adamski
Scientific data system	Jet Propulsion Laboratory	L. G. Goforth	H. E. Wagner
Ground support equipment	Jet Propulsion Laboratory		

to a 3-meter line spacing, which is substantially better than the resolution secured from Earth-based telescopes operating under the best conditions.

The objective of the gamma-ray experiment is to determine the approximate concentration of several of the radioactive materials expected to be present on the surface of the Moon. The radioactivity compared to that of meteorites will indicate the degree of differentiation of rocks on the Moon. Furthermore, a comparison of the radioactivity of the potassium with that of the heavy element decay series will indicate if such differentiation is similar to that occurring in the Earth.

The radar altimeter aboard RA-3, -4, and -5 serves a dual purpose. Its function as range meter is to initiate the separation of the capsule from the spacecraft bus at a predetermined height (52,700 ft) above the Moon. Its purpose as a scientific experiment is to produce information regarding the character of the Moon's surface structure. This information is not only of fundamental value, but can be an important factor in selecting lunar landing sites. For example, comparison of the simultaneously obtained radar reflection data and vidicon pictures may serve to establish a standard for the interpretation of more sophisticated Earth-based radar systems. The Earth-based radar reflection data could then be more effectively used in selecting future landing sites, as well as getting better information regarding the surface structure of the Moon.

The investigation of lunar seismic activity is a very effective means of determining important factors in the history of the formation of the Moon. Information on the seismicity of the Moon will give an insight into the thermal history and tectonic processes which might be operating. Seismic body wave data will give information on the presence or absence of a solid or liquid lunar core; it will also give information on the depth of focus of moonquakes and seismic energy release. This information is related directly to the depth and magnitude of thermal activity on the Moon.

Information on the mechanical properties of the materials making up the Moon will be obtained from seismic wave absorption data. Finally, the presence or absence of a lunar crust and information on the lunar dust layer can be determined from the presence (or absence) and character of the surface waves recorded from moonquakes, from meteoric impact disturbances, or from small bombs exploded at some distance from the seismometer.

The scientific experiments, sponsoring agencies, and cognizant JPL personnel, are shown in Table 42.

b. Television subsystems.

General description. A telescopic television subsystem (Fig 110) has been developed by JPL to go aboard RA-3 and -4 and -5 to accomplish the high resolution photography mission in the 30 min before impact of the spacecraft. It can be demonstrated that, with 40-in. equivalent focal length telescope for the *Ranger* payload, photographs secured with a 200 TV line scan vidicon camera at 4000-km distance will just about equal the best resolution secured from Earth-based telescopes. Therefore, there is little purpose in attempting recordings at a greater distance from the Moon. The present vidicon camera-optical telescope system will transmit from 4000-km down to 24-km altitude, where the capsule is ejected and Earth contact with the high-gain antenna will probably be lost due to subsequent tumbling of the spacecraft. The spacecraft and camera-telescope assembly longitudinal axes will be aligned nearly normal to the lunar surface during the recording period. The lunar phase-angle, as viewed from the spacecraft may vary from approximately 20 to 70 deg, depending upon the date and azimuth of launch within the proposed launch windows. This will result in a sufficiently oblique Sun angle to yield shadows on the lunar surface, thus providing greater surface detail rendition. It is anticipated

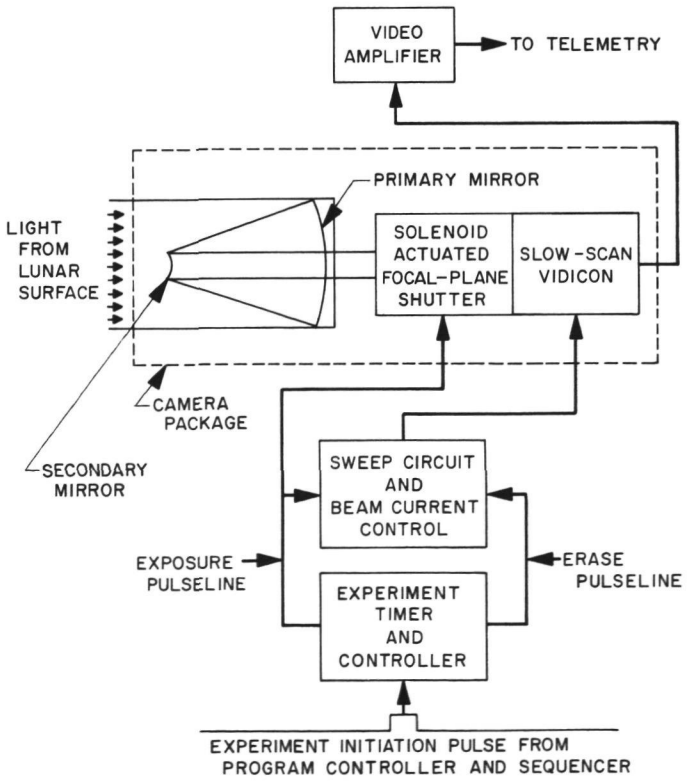

Figure 110. Television subsystem

that the improvement in lunar surface resolution will be from 100 × to 1000 × that secured from Earth-based telescopes under the best conditions, depending upon a number of instrumental and environmental factors which will be encountered by the television subsystem.

The television recordings of the lunar surface from RA-3, -4, and -5 will be put to a number of uses. Primarily, the images will indicate the type of lunar terrain in which the seismometer capsule will land, and should assist in the proper evaluation of the data. The vidicon images will also permit determination of the coarse surface structure, small scale geological land forms and features, altitudes and slopes of lunar surface features, and the general environmental condition close to the Moon. At the same time, the vidicon photographs will be a first approach to the selection of possible landing sites for future instrumented and manned lunar probes.

The complete RA-3, -4, and -5 proof test model (PTM) television subsystem (Fig 111) was mounted on the PTM spacecraft at the spacecraft assembly facility (SAF); the PTM system tests were completed without serious problems and the spacecraft, complete with TV subsystem, delivered to the Environmental Test Laboratory for vacuum-chamber testing prior to type-approval shake testing of the entire structure.

The first two flight models of the television subsystems assembly were received, assembled, and operationally checked in the laboratory. One flight model was assembled on the RA-3 flight model spacecraft at the SAF. Subsystems testing was nearly completed, prior to starting of the flight model systems test.

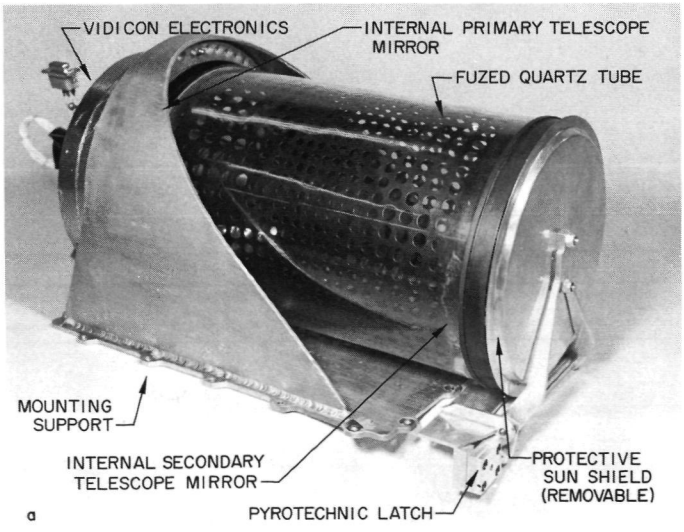

Figure 111. PTM of RA-3, -4, -5 television subsystem

The PTM systems tests of the vidicon camera electronics and optical telescope were completed through Type-Approval shake and vacuum testing.

The RA-3 flight model camera-telescope assembly was received and assembled on the RA-3 spacecraft; Flight-Approval systems tests were completed. The RA-3 flight unit and flight spare were shipped to AMR and received there intact. Subsystems testing at AMR indicated that the optical telescope and vidicon camera electronics were in satisfactory operating condition and flightworthy.

Another minor design change resulted in considerable additional vidicon-pointing capability in case of an inadvertent lunar flyby, without affecting the spacecraft's normal mission. In the former design, the terminal yaw maneuver (which is the second of three motions required to position the spacecraft for lunar encounter without losing Earth lock), has only a 0- to 6-deg capability. This was considered more than sufficient for any normal mission resulting in spacecraft–lunar contact. However, it was felt that additional angular correction capability would enhance the vidicon experiment in case the spacecraft could not complete a normal mission and "flew by" the Moon. This may happen if the *Agena* injection errors are too great to be corrected by the spacecraft's midcourse maneuver, or if the spacecraft cannot complete a midcourse maneuver. The terminal yaw maneuver has been opened up to a maximum of 120 deg. This is the maximum practical, in that higher angles would result in vidicon visual field obstruction by the high-gain antenna. However, the additional angle capability allows more flexibility in pointing the vidicon for an emergency flyby mission. The actual hardware change only involved relocation of some diodes in the CC&S subsystem timing matrix.

Doubling the angular capability did increase the time required for the entire terminal maneuver from 25 to 30 min. To prevent adding this time to the total required from the beginning of the maneuver to lunar impact (65 min), 5 min formerly allowed for settling time (later found to be unnecessary) were eliminated. Functionally, the terminal maneuver will be performed as follows:

Impact −65 min: Initiate terminal maneuver by ground command.

−65 to −55 min: First pitch maneuver + settling time.

−55 to −45 min: Yaw maneuver (formerly required only 5 min).

−45 to −35 min: Second pitch maneuver + settling time.

−35 to −32 min: Altimeter and omni-antenna deployment + settling time.

−32 min to −8.1 sec: Vidicon experiment, starting with stable spacecraft at 4000 km.

−8.1 sec: Retro maneuver of lunar survival capsule; no further telemetry expected from spacecraft.

The RA-4 flight model camera-telescope assembly has been received and assembled on the RA-4 spacecraft, which is undergoing systems tests.

The RA-5 flight model telescope and flight spare telescope have been received at JPL.

Vidicon camera. The television subsystem for RA-3, -4, and -5 has been tailored specifically for the experiment and thus departs in several areas from typical designs. A vidicon sensor was chosen for imaging because of its simplicity and ease of operation. Quite unlike other vidicon camera systems, an all-electrostatic deflection and focus vidicon is employed which combines a special *sticky* target with rapid erase capability. In operation an image is shuttered onto the faceplate for 20 millisec and the slowly decaying image is subsequently scanned at a rate which yields one complete frame in 10 sec. Two hundred scanning lines are employed per frame in order to achieve the desired resolution. The video bandwidth out of such a system for equal vertical and horizontal resolution is of the order of 2000 cycles.

Since each frame is different from the rest, no averaging technique for a large number of frames may be employed for background shading or d-c restoration; thus, the lowest frequency in the video signal must be considered to approach d-c. In order to accommodate this, the vidicon beam current is modulated by a high frequency which chops the target current and creates an amplitude-modulated signal. After sufficient amplification, the demodulated video is mixed with blanking pulses to form a composite video signal for presentation to telemetry. The line-deflection circuit is triggered from a 20-cps generator clocked, in turn, from the spacecraft 400 cps. Since this 400-cps clock is available in the ground receiver, line synchronization is guaranteed even in the presence of rather severe noise; or, in turn, the 400-cps clock may be retrieved from the line sync pulses should the 400-cps signal be lost. The commands for shutter and erase are obtained from the CC&S in the form of 1-msec switch closures. The shutter command terminates erase, triggers the shutter solenoid drives and, following a fractional second delay, causes initiation of the frame sweep. The erase command terminates the frame sweep and initiates the erase mode, which consists of illumination of six filamentary lamps mounted on the periphery of the vidicon target, acceleration of line and frame scan rates over the surface of the target, and increased beam current. Although this process normally requires less than 1 sec, circuit simplicity is maintained by continuing erasure for the full 3 sec allotted for readout of the gamma-ray data.

Vidicon sensor. The proper vidicon sensor was chosen as the result of an extensive evaluation program. All available sensors were investigated by RCA as a preliminary phase of the impact television contract. The specific requirements on the vidicon are:

(1) Adequate sensitivity for low light levels anticipated.

(2) Sufficient dynamic range to allow perception of detail for lower than normal illumination as well as possible strong highlight detail.

(3) Capability of survival of the thermal requirements of bulk sterilization.

(4) Minimum weight and power requirements.

(5) Adequate storage time of a shuttered image combined with ease of erasure prior to shuttering of a new optical image.

These requirements of the sensor were not mutually compatible in light of present commercial practice. Thus, it was evident that a completely new sensor would have to be developed which combines the best features of existing sensors and yet meets the rigors of spacecraft environment. Since this is an evolutionary development which normally requires extensive time, it is a credit to the participating organizations that a task of this nature was actually accomplished within the demands of the *Ranger* schedule. The resultant sensor combines all the required features.

The target material chosen for this vidicon is an antimony sulfide oxysulfide surface, which is a proprietary development of RCA and combines the necessary retention of the image for slow-scan readout, together with rapid erase capability. The latent image may be scanned slowly off the target with less than 10% reduction in highlight detail for periods in excess of 10 sec. Sensitivity of the surface is maintained at light levels as low as 0.01 ft-candle-sec following the 24-hr soak at 125°C for sterilization; the useful dynamic range of some units extends

from 0.001 to 0.1 ft-candle-sec with an opening of *f*/6 and 20-msec exposure. The image may be erased in 700 msec.

The electron gun structure and deflection system is a ruggedized version of the 1-in. diameter electrostatic unit manufactured by General Electrodynamics Corporation (GEC). Electrostatic focus is accomplished by a saddle field lens arrangement and electrostatic deflection is accomplished through the use of special deflection plate configuration designed by Schlesinger called a Deflectron. The conventional crossed-pair deflection plates cause the electron beam to be deflected sequentially; that is, in passing between the first set of plates, it is deflected in one plane and, then, when reaching the second set of plates, it is deflected in the other plane. The Deflectron causes the beam to be deflected both horizontally and vertically simultaneously, as in magnetic deflection. This common center of deflection reduces the undesirable effects of fringe fields, defocusing, and other distortion found in conventional plate scanning.

Physically, the Deflectron is a tube of insulating material, the inside of which contains the printed deflection plate pattern. This yields an exceptionally rugged structure capable of surviving present spacecraft environment. In addition, the use of an all-electrostatic structure removes the considerable weight and power penalty of electromagnetic deflection yokes, while resolution comparable to electromagnetic systems is maintained through the use of post-deflection focusing.

The faceplate, complete with target material, is supplied by RCA and is bonded by GEC to their gun structure by an indium-glass seal process tailored specifically for this particular vidicon. The electron gun structure has been modified to permit a larger beam diameter. This was done in order to facilitate rapid erasure of the sticky target, since erasure is accomplished by simultaneous application of external light stimulus and rapid-scan of the target in *fire-hose* fashion by the electron beam. Dark-current clipping over wide temperature ranges is facilitated by including a deposited mask on the faceplate to obscure a portion of the image. This mask covers a narrow strip along the faceplate which obscures less than 5% of each scan line. Present vidicons have this mask vapor deposited externally; however, experimentation with internal deposition is in process and, if successful, will eliminate the slight amount of optical defocusing presently observed with this mask.

Vidicon. By far the greatest difficulty that has been experienced has been in the procurement of vidicons. The camera tube used in this impact experiment has been designed specifically for the *Ranger* mission and was developed to (1) be lightweight, (2) consume minimum power, (3) be sticky enough to hold an image for 10 sec with virtually no degradation and yet be erased completely in 3 sec, (4) be sterilizable, and (5) be extremely sensitive in order to provide minimum weight optics. The tube design is a composite of a faceplate and target fabricated by Radio Corporation of America (RCA) and an electron gun structure fabricated by General Electro-Dynamics Corporation. Joint agreement between RCA and GEC evolved the following assembly procedure:

(1) Deposit of the faceplate at the RCA Tube Division, Lancaster, Pa.

(2) Shipment of the completed faceplate to GEC, Garland, Texas.

(3) Assembly of the RCA faceplate with a GEC ruggedized electrostatic deflection and focus gun structure.

(4) Shipment of the completed vidicon to RCA, Astro Electronics Division, Princeton, N. J., for test and integration with the spacecraft electronics.

(5) Shipment of the complete flight assembly to JPL for flight acceptance testing and delivery to the SAF.

Considerable difficulty was experienced at first with shipment of faceplates across country without damage or contamination. Each of these problems has finally been solved.

Optical telescope. Basically, the telescopic optical system (Fig 112) developed by JPL is a conventional Cassegrain-configuration astronomical telescope employing a primary concave parabolic mirror and a centrally located, secondary, convex hyperbolic mirror to reflect the lunar image picked up by the primary back to the vidicon photoconductive image surface 0.5 in. in front of the primary mirror. An aperture of 7 in. and equivalent focal length of 40 in. is provided, yielding an equivalent light grasp of *f*/6.3. An initial optical resolving power of 5 sec of arc, or 40 optical line pairs/mm on the optical axis with some degradation over the 1 deg telescope field of view will be secured. This will, of course, be deteriorated by the vidicon scan to approximately 34 sec of arc or 6 optical line pairs/mm resolution.

The significant deviations from usual astronomical telescope design consists of the use of fused quartz for the telescope mirrors, Invar for all temperature sensitive metallic parts and, primarily, the use of an 8 in. diameter

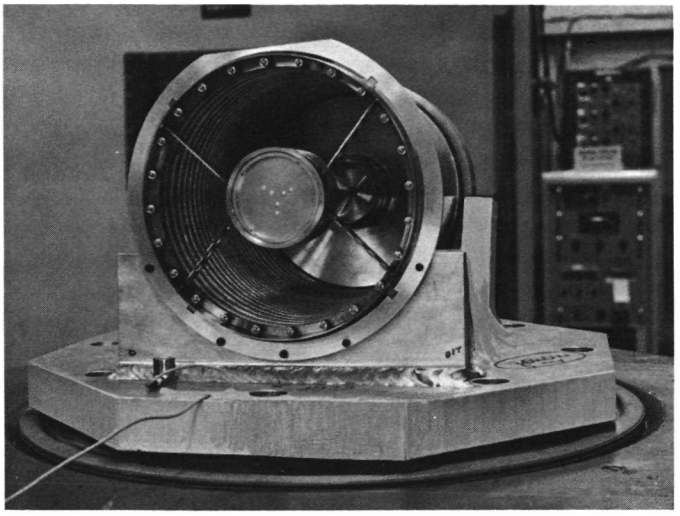

Figure 112. Vidicon telescope

fused quartz tube under spring loading as the basic rigid tubular structure separating the primary and secondary mirrors. These features have been emphasized in the design because of the large range of vehicle temperatures anticipated in the cislunar environment. Engineering models of the telescope employing this JPL design have successfully survived the simulated *Atlas–Agena* takeoff vibration tests without mechanical or optical deterioration.

A mechanical rotating sector shutter operating on inertial principles with solenoid actuation has been included in front of the vidicon face. This provides an exposure time of 20 msec on the photoconductor surface with a uniformly illuminated field. The shutter will prevent blurring of the optical image of the lunar surface, due to motion of the spacecraft during the exposure time, and will also provide a closing of the optical system during the 13-sec scan and erase operation of the vidicon electronic system.

The unit for holding the telescope optical elements and the vidicon tube and associated electronics within the telescope structure has been carefully designed to survive the shake, shock, and temperature environments anticipated. An auxiliary capping mechanism is provided to shield the telescope optics and the vidicon surface from the light of the Sun during midcourse maneuver, and to provide protection from micrometeorites and a proper temperature balance within the telescope in cislunar space. The telescope structure will be mounted to the spacecraft in such a way as to minimize misalignment of the longitudinal optical-mechanical axes during takeoff and under the temperature environment anticipated.

In the generation of the present optical telescope design, three different optical firms were contacted for detailed design studies. In addition, a fourth, backup design was undertaken by JPL. Three engineering models resulted from these design studies. These were all subjected to optical tests for image quality, resolving power, and position of the image plane with reference to the vidicon face before and after *Ranger* system vibration testing. The only design which satisfied the strict optical-mechanical requirements both before and after shake was the JPL backup telescope. This design has been constructed by a vendor for RA-3, -4, and -5 to meet the mission schedule requirements. Two separate identical orders for flight models were placed, one to Tinsley Laboratories, Inc., and one to Penn Optical and Instrument Co., to assure a backup for the required flight model spacecraft assembly date of RA-3.

Following assembly and checkout experience with these flight model telescopes and with the PTM telescope, several minor changes in mechanical design have been accomplished. These include the following modifications to the rotating sector shutter and the vidicon holding unit:

(1) A new micarta insert for proper electrical insulation of the vidicon replaces the original teflon spray coating which was difficult to apply and gave unsatisfactory insulation.

(2) Additional ball bearings and minor tolerance changes have been made in the mechanical shutter to reduce friction and give more reliable operation.

(3) The structural shape of the shutter mounting and housing was changed to permit easier assembly within the telescope, without removing the optical elements.

(4) The holders and reflectors of the lamps, used to give edge-lighting for erasure of the image on the vidicon photocathode, were modified for more reliable electrical operation and illumination.

(5) All nylon washers and O-rings were removed and replaced by teflon units because of difficulties heating to 125°C for sterilization.

Two new Zoomar optical collimators have been procured so simultaneous alignment and checkout of the camera-telescope system, mounted on the spacecraft, and the new TV electronics and optics, located in the laboratory, can be accomplished. New reduced-scale, TV-type, resolving-power, chart transparencies were made at JPL to replace the original Zoomar Air Force-type resolving-power targets in these collimators. One of these collimators later

accompanied the camera-telescope and spacecraft to the launch site for final checkout.

More sophisticated and reliable fixtures for holding the viewing microscope in the telescope for focusing the vidicon and optics were designed and constructed at JPL. The original units employed for the PTM and first RA-3 flight model were assembled strictly as an emergency measure to meet the tight time schedules for spacecraft assembly.

The only serious problem that has been encountered with the RA-3, -4, and -5 optical telescopes and spares, has been poor operation of several of the camera shutters. Inasmuch as the first several shutters operated satisfactorily and consistently over long periods of time, it is certain that the difficulty is not in the shutter design. It has been determined that the faulty shutters all showed poor machining, poor bearing fits, and lack of adherence to JPL tolerances. Though these shutters were manufactured by an outside firm, it was possible to correct their operation by rework and adjustment at JPL.

Some difficulty was experienced with the nylon insulation which covered the shutter electrical wiring, which tended to crack during the heat sterilization. Corrective measures have been taken.

A photoelectric shutter tester employing an oscilloscope tube presentation has been designed and constructed at JPL for determining the shape and duration of the telescope shutter exposure on the vidicon camera, and for determining the exposure level in conjunction with the collimator used for electronic gain adjustment of the vidicon as discussed previously.

A third Zoomar Service collimator was ordered. Three collimators are needed to perform simultaneous calibrations of RA-3, -4, and -5 flight model camera-telescope assemblies in the following locations: final checkout of the RA-3 flight model at AMR; checkout of the RA-4 flight model at the JPL Spacecraft Assembly Facility; and alignment and calibration of the RA-5 flight model in the JPL test laboratory.

The complete electronic package (Fig 113) for the first flight model vidicon camera comprising video processing, timing, and sweep electronics, and the transformer-rectifier power supply was successfully bulk sterilized at 125°C for 24 hr. This marked the first time that the integrated assembly has been so tested, although complete subassemblies were previously sterilized independently. Following sterilization, a mechanical and electrical inspection disclosed:

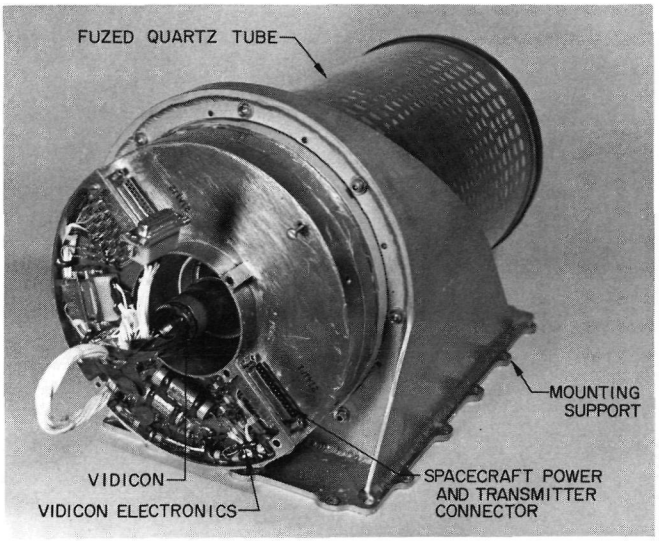

Figure 113. Complete electronics package, first flight model of vidicon camera

(1) Severe bubbling of the gold plating on the support used to mount the camera-telescope structure to the spacecraft. Bubbling was not in evidence on any other plating, and it is believed that improper cleaning prior to plating was the cause. No change of thermal characteristics of the plating could be caused by this bubbling; however, steps were taken to reduce this effect in future mounts.

(2) A thermofit insulator used on a coaxial cable termination was found to have split. It was replaced by a larger insulator and the cable successfully sterilized.

(3) Spring tension within the shutter assembly was lost. This condition was corrected.

(4) A nylon ring used to position the vidicon faceplate experienced severe deformation. Because of this difficulty, a teflon ring is proposed for use on all flight models.

(5) No change of performance of the electrical circuitry was found.

All remaining units were successfully passed through sterilization and no subsequent difficulty was observed. The optical telescope was subjected to both 125°C for 24 hr and to ethylene oxide gas sterilization for 24 hr, with no observable deteriorating effects or deposits on the optical surfaces.

Lunar photometric calibration of vidicon. Because of the rather poor lunar resolution obtained from Earth-based observation, detail knowledge of high-resolution

imaging and anticipated reflection for high-resolution, lunar photography is totally lacking. RA-3, -4, and -5 photographs will provide an analysis of lunar detail in the tens-of-meters range; therefore, electronic gain adjustment of the vidicon camera is of paramount importance for maximum utilization of telemetry capability. Detail analysis of all known data on lunar luminance (brightness) has yielded data against which all flight model television subsystems are adjusted for gain, employing the TE collimator.

The luminance of the lunar surface at the expected impact point has been calculated for the successive days of the firing window, using Van Diggelen's lunation curve adjusted to a 10-deg observation angle (from the normal). Results of these calculations are shown in Table 43.

It should be observed that highlight luminance drops off rapidly with each succeeding firing day. If the electronic gain were to be adjusted to take maximum advantage of first day illumination, then the fifth and sixth days would be seriously degraded due to inefficient utilization of telemetry. Conversely, a gain adjustment for optimization of later firing days would tend to saturate telemetry for an early firing day. To circumvent this problem, the flight model cameras are delivered with the gain adjusted to take maximum advantage of telemetry for a first day firing. Each camera, however, has also been calibrated to take maximum advantage of the illumination to be expected for a third day firing. Each flight model camera can be adjusted, at AMR, from first day illumination to third day illumination by rotation of an accessible gain adjustment by the proper number of turns appropriate to that particular camera. Full reproducibility of laboratory calibration may thus be expected at AMR without recourse to an optical laboratory environment.

The process used in adjusting the electronic gain of the vidicon camera consists of establishing the appropriate light level from the TE Co. optical collimator and projecting this light directly into the optical telescope of the vidicon camera. The electrical output of the camera is then adjusted so that this maximum image brightness will provide a 2-v signal to telemetry referred to electrical neutral. The luminance of the collimator, as measured with the spectra brightness spot meter (photometer with ½-deg field), is 1800 ft-lamberts. Based on this, the 2-v ft-candle of the RA-3 vidicon tube corresponds to 0.229 ft-candle-sec for a first-day firing.

This gain adjustment procedure automatically compensates for the shutter exposure time. However, since maximum vidicon signal-to-noise ratio and optical image smear due to relative image motion is affected by the shutter time, each flight telescope-shutter combination receives a calibration prior to gain adjustment. Calibration of the shutter consists of adjustment of shutter blade spring tension so that the total illumination of an image point on the vidicon target lasts for 20 ms. To determine this exposure time, a finely focused spot of light is projected through the shutter blade and into a 0.013-in. pinhole in a mask placed in the optical focal plane. A photomultiplier is then used to pick off this focal plane illumination and display the time relationship on an oscilloscope. Figure 114 shows an oscillogram of a typical flight shutter. The vertical scale is in arbitrary light units and the horizontal scale is 5 ms per large division.

Data presentation. Examination of the Russian photographs of the back of the Moon indicates clearly that noise has been a severe handicap to their analysis. Techniques exist which are more credible than applying corrections on the pictures with a paint brush. These corrective techniques involve the use of analog equipment and include superposition of several photographs, which tends to cancel out random noise. It is also possible through techniques of dodging and through the use of different chemical developers to enhance the grey level of certain portions of the photograph.

Table 43. Luminance of the lunar impact point for *Ranger* RA-3

Day	Highlight luminance ($p = 0.2$), ft-lamberts	Maria luminance ($p = 0.07$), ft-lamberts
1	1800	655
2	1350	473
3	1030	360
4	700	245
5	450	158
6	275	97

p = geometric, or *normal*, albedo.

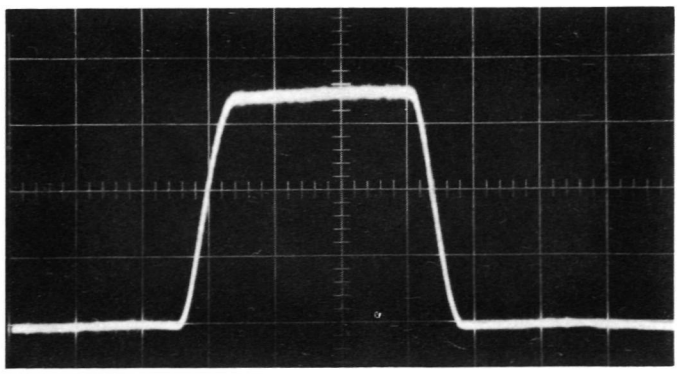

Figure 114. Typical flight shutter exposure time

Clean-up techniques which use dodging or the paint brush are rather haphazard. Analog techniques for cleaning up also suffer from the need to work with a large portion of the picture at one time. If each resolvable point of the picture were converted to a numerical intensity, then digital computers could be introduced. Each point could be tested with respect to the presence of noise, the grey level could be enhanced, and averaging over several photographs could be performed using weighted values dependent upon the acceptability of each photographic point.

Several lunar missions will be conducted by NASA which involve a great deal of lunar photography. *Ranger* and *Surveyor* will each produce large numbers of photographs which will require careful analysis. The techniques discussed below are new insofar as the digital computer has not previously been used to substitute for analog corrections of photographic materials. Simply because it is new does not mean that it is not practicable for these particular missions. For RA-3, -4, and -5, there will be a straightforward application of the computer to remove noise by comparing each line to its neighbors and watching for unusual events.

In addition to the added power for cleaning up, which is made possible by introducing digital computers, it now becomes possible to do research in pattern recognition and, thereby, automate a large portion of a lunar photographic mission which would otherwise saturate any group of observers. The computer will be asked to recognize the various lunar features and to categorize them according to the relation of certain features to their neighbors, the numbers of such features, and their description. The basic concept will require that the length of lines, the orientation of lines, and the length and orientation of curved and complete circular lines be listed.

The programming flow diagram shown in Figure 115 outlines the computer program for handling the televised data. The program assumes that video data has been converted into digital form and stored on magnetic tape nominally with 6 bits/point, which represents 64 grey levels and is more accurate than is required by the signal-to-noise ratio of the vidicon camera. It is then possible to expand those particular regions of the photographing process which were non-linear and allows the user to see more detail by intensifying the grey levels at each end of the photometric spectrum. Each photograph for RA-3 consists essentially of 200 lines, with 250 resolvable elements along each line. This creates 50,000 elements for each picture, and since there are 6 bits for each element, we obtain 300,000 bits per picture. Since each computer

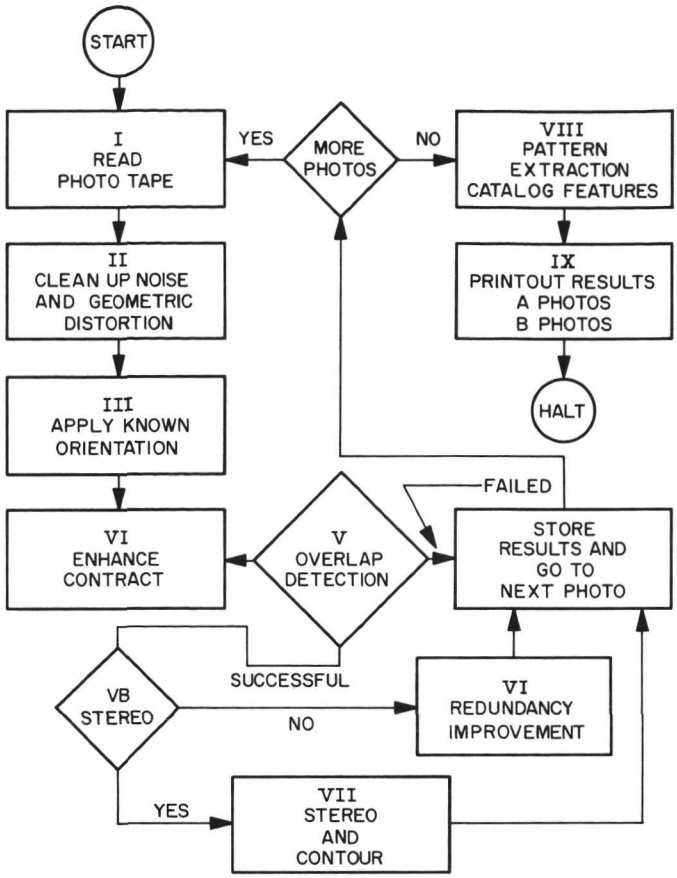

Figure 115. Video data IBM 7090 flow chart

word contains 36 bits, it is possible to store one complete photograph in approximately 8400 computer words. In the IBM 7090 at JPL, it is possible to store in memory 32,768 computer words. Assuming that it may take up to 5000 words of memory for the program, it should be possible to store three complete pictures of the RA-3 type in the computer at one time.

Information from the vidicon camera on board the vehicle is transmitted to Earth antennas, where it is monitored and recorded on magnetic tapes. The signal recorded on these tapes is converted into digital form and recorded on magnetic tapes for computer use without loss of resolution.

Some burst noise can be removed by performing a comparison to each of the line-sweep neighbors. If it is seen that there is noise, then a weight of zero will be recorded for this particular set of points so that when the pictures are averaged later, these points will not contribute to the averaging. The magnitude of these noisy points can be modified also so as to match that of the average of its two neighbors, thereby cleaning up the noise from the photograph if there were no others to average it against.

Noise also comes from an incomplete erasure of the previous photograph from the vidicon tube. Anywhere from 10 to 30% (depending on the particular tube) of the previous picture may not be erased, thereby leaving a ghost. This phenomenon is easily subtracted out by the computer.

Ground calibrations will remove geometric distortions which can be expected to be constant throughout the mission. This distortion, whether linear or nonlinear, can be corrected by the computer.

On the surface of the vidicon there is a known grid which will have to be found by the computer program automatically. A calculation will be performed to decide on the amount of geometric displacement which has occurred to the image, and a program will perform these corrections automatically. The grid will be subtracted from the final image.

Trajectory information is used as a first approximation to perform magnification of the image and rotation and translation to the degree known.

By comparing the recorded grey level against a calibration table, it can be replaced by the correct photometric value. If more than just a return to real values is desired, an artificially distorted scale can emphasize one end of the intensity spectrum while squeezing the other.

To find where one picture is relative to another requires a correlation of some area in one photograph to a similar area in the other. Cross-correlation is a point-by-point multiplication from the corresponding part of each of the two pictures, the results of which are summed together. We then shift one of the pictures by one coordinate unit and perform the same operation. In another part of the memory, the various sums created by this operation are mapped. When the two photographs have been shifted completely relative to each other and this summed multiplication has been performed, the resulting map is examined for a strong peak.

Once the coordinates of the picture have been established relative to the prior pictures, a test on the coordinates of the camera can be made to determine whether there is a sufficient parallax for stereo. This particular direction of research has been successfully investigated by IBM for the Army; it could be pursued at this time but was not the prime purpose of the RA-3 experiment.

The initial correction for noise was not dependent on any other photographs; that is, tests were performed with each line scan compared to its neighbors. There now exists a more powerful test of information by checking one photograph against another. The intensities of the successive photographs for the same portion of the lunar surface can be averaged in accordance with the weights that were determined from the noise calculations and the resolution.

Pattern extraction is a research area and although it holds great promise it was not in final form for the RA-3 mission. Automation techniques should speed up the data handling that would otherwise be bottlenecked by human handling. It is expected that computer techniques will be usable to locate lines by means of enhancing edges, and will be performed in the computer by a delta x and a delta y subtraction technique. Once these edges have been enhanced, the computer can be programmed to trace along them and catalog the coordinates according to lengths or orientations of the lines and circular features which have been brought out.

Printout. Once the computer has created a master photograph or has cleaned up the sets of photographs, it is ready to print them out. This printout can be done by converting the signal from the digitized magnetic tape output onto another magnetic tape in analog form. This magnetic tape can be fed into a film recorder, which will then produce the cleaned-up photographic images.

A large programming effort is required to accomplish the processing described above. It is not expected that all portions of this program will be written in time for the lunar capsule missions. Since this is a developmental research effort, more confidence will have to be attained with this kind of processing for each succeeding mission before this approach can become integrated into the overall flight operations.

c. Gamma-ray spectrometer.

General description. A measurement of the gamma-ray spectrum generated by lunar surface rocks or dust will provide direct information about the composition of this material. Since the heat production of a body is largely determined by its radioactive content, and since those elements which possess natural radioactivity are indicative of differentiation (at least in the Earth), gamma-ray spectroscopy on the Moon appears capable of contributing evidence to both problems (Ref 34).

Lunar gamma-ray activity will consist of the decay of those isotopes which are naturally radioactive and of isotopes whose activity is induced by solar and cosmic radiation. The most abundant naturally occurring radioactive isotopes are K^{40}, Th^{232}, U^{235}, and U^{238}, plus the radioactive daughters of the last three. In the Earth's crust, the mean concentration of potassium is 25 to 30

times greater than that found in chondritic meteorites; for uranium and thorium, ratios are about 150 to 200. The response (or lack of response) of the gamma-ray spectrometer to natural radioactivity will indicate the extent to which the surface of the Moon, to a depth of 10 cm or so, represents differentiated material. Of particular interest in this regard is the subject of the tektites, whose composition, appearance, and distribution over the Earth seem to indicate a direct or indirect extraterrestrial origin. Should they be representative of the lunar surface, their high potassium content will be detectable by the spectrometer.

The gamma-ray spectrometer consists of three units; a detector, a high-voltage supply, and a pulse-height analyzer.

Detector. The detector system (Fig 116) was designed at the Los Alamos Scientific Laboratory and is being assembled by the Packard Instrument Company. In addition to the inorganic scintillator and phototube, which constitute a standard scintillation counter, a ⅛-in.-thick plastic scintillator completely surrounds the inorganic crystal. The plastic scintillator discriminates between gamma rays and charged particles by not responding significantly to the former. Both scintillators transmit light to the one phototube. A charged particle, interacting with both the plastic and the inorganic crystal produces a signal from the phototube, which generates an anti-

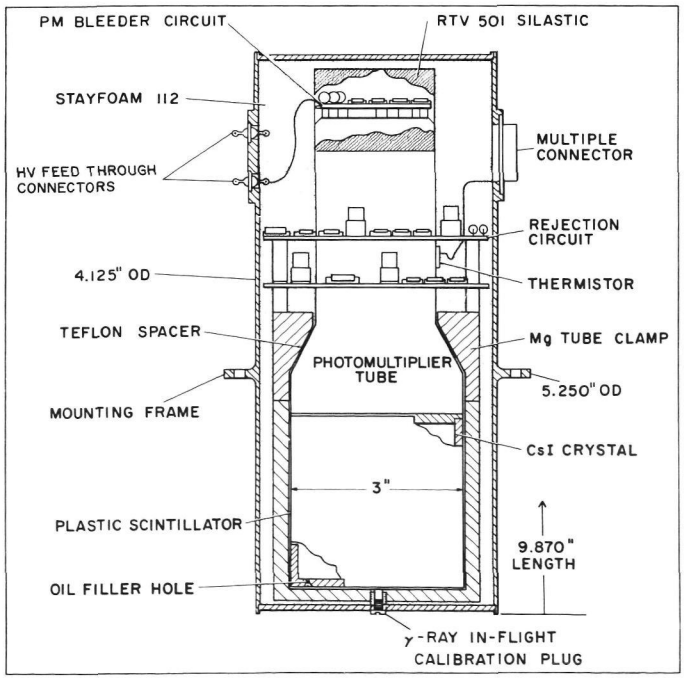

Figure 116. Gamma-ray detector assembly

coincidence pulse. Gamma rays of interest do not have sufficient energy to interact appreciably with the plastic.

The inorganic scintillator is a cylindrical crystal of thallium-activated cesium iodide measuring 2¾ x 2¾ in. The plastic scintillator is composed of polyvinyl toluene with an added quantity of diphenystibene. The phototube is a ruggedized unit with a window 3 in. in diameter. A teflon jacket surrounds the crystal–plastic assembly and serves as a light reflector to increase the efficiency of the two scintillators. The teflon jacket is attached to a magnesium clamp which is anchored around the yoke of the phototube. This clamp provides the principal structural support to hold the teflon jacket and the scintillators to the phototube. The dynode bleeder circuit is mounted on a circular board near the base of the tube. Silicone oil is inserted between the two scintillators and between the plastic and photomultiplier tube face to give optical coupling between these surfaces. Two larger circuit boards, also placed around the neck of the phototube but closer to the center, contain the anticoincidence circuitry as well as an emitter follower for the signal pulse. The entire assembly is contained in an aluminum cylinder. A threaded hole is provided at the crystal end, as shown in Figure 116, to allow installation of a plug containing a weak source of low-energy gamma rays which is used for calibration both before and during the flight.

High-voltage supply. A compact high-voltage supply has been developed for this experiment (Fig 117). It is a dc-to-dc converter, utilizing a zener bridge, operating off the transformer secondary to achieve excellent regulation, both for long periods of time and over a wide temperature range. A potentiometer permits the output voltage to be matched to the signal level of the phototube in the detector.

Pulse-height analyzer. The pulse-height analyzer has been designed by the Radiation Instrument Development Laboratory and performs the following functions: It determines the energy of the voltage pulse from the photomultiplier through analog-to-digital conversion, it stores this information in a ferrite core memory, and it is capable of reading out this stored information on command. Thirty-two channels are provided, of which one is devoted to all pulses greater than a certain value.

A functional diagram of the entire system is shown in Figure 118. Gamma rays and charged particles which pass through the plastic scintillator and enter the inorganic scintillator will be transformed into light. This light reaches the cathode of the photomultiplier tube either directly or by reflection from the teflon jacket. The resultant electrical signal is taken from the eighth dynode of

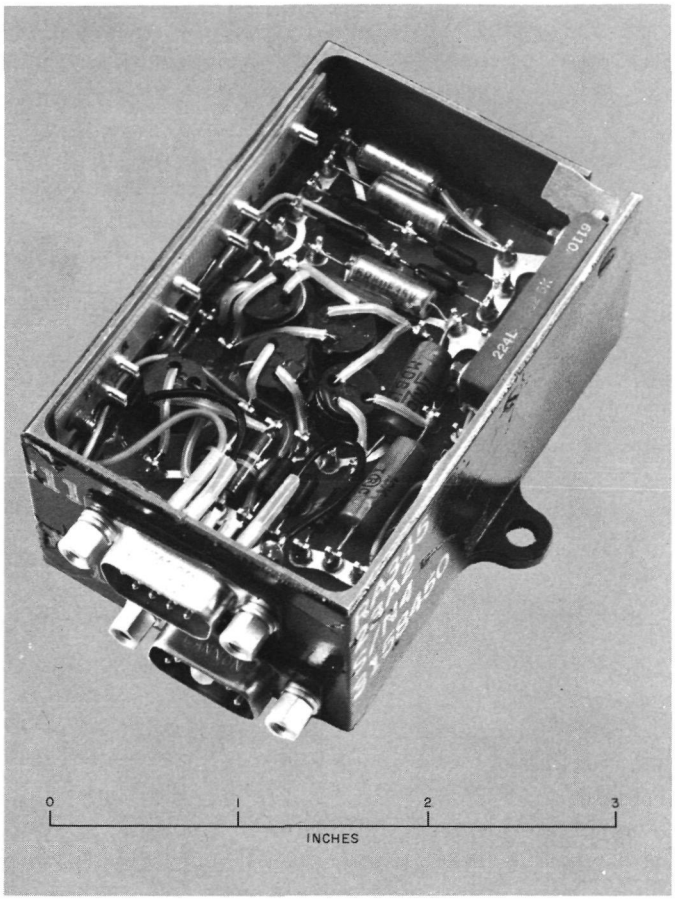

Figure 117. Gamma-ray spectrometer high-voltage supply

the photomultiplier tube to an emitter follower. The emitter follower signal has a variable output of 0.01 v to more than 1 v depending on the type and energy of the incident radiation. These signal pulses will have a rise and fall time of approximately 1 to 10 μsec, respectively. When a charged particle interacts with the plastic scintillator and deposits at least 0.1 Mev of energy, the resulting light flash produces a comparatively fast pulse at the anode of the phototube. A fast clipping circuit drives a univibrator, which in turn generates a 5-v blocking pulse with a rise time of 0.1 μsec. The blocking pulse closes the gate of the analyzer for a sufficient length of time to prevent the slower cesium iodide pulse from passing into the analyzer.

Analog-to-digital conversion is accomplished by charging a capacitor with the cesium iodide signal, sensing the charging peak, and allowing pulses from a 500-kc oscillator clock to enter a channel address scaler as the capacitor discharges. The state of the cores belonging to the channel which has been addressed is then examined, starting with the least significant. If a "one" is found, the core is set to "zero" and the next most significant core interrogated. The first core found at "zero" is set to "one," completing the process.

Programming of the analyzer is controlled by the central computer and sequencer. The latter periodically supplies a pulse which causes the analyzer to go from the store to the read mode. This pulse is followed by a series of pulses on a separate line which read out information in the memory to telemetry.

Sterilization. The high-voltage supply and pulse-height analyzer are sterilized thermally. The detector cannot be sterilized so simply, since neither the scintillators nor the phototube can be subjected to 125° for 24 hr.

These components are, however, internally sterilized in the course of their manufacture. The procedure followed is to sterilize all the other parts by preheating and

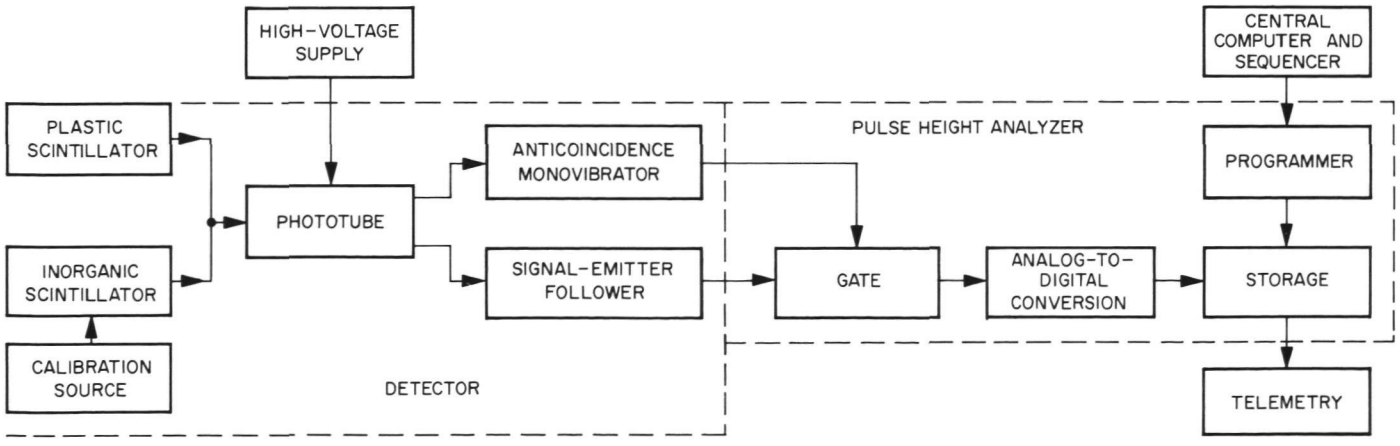

Figure 118. Gamma-ray spectrometer system, functional diagram

then to assemble the entire system in an atmosphere of ethylene oxide.

Environment and spacecraft integration. The high-voltage supply and the detector are located at the end of a telescoping boom. The extension of this boom to a length of 6 ft is designed to reduce the contribution of secondary gamma rays which are produced by the interaction of cosmic rays with the bulk of the spacecraft. These two units are enclosed in a thin aluminum sphere in order to equalize the temperature distribution as much as possible.

The pulse-height analyzer is mounted on five standard modules in one of the cases of the bus. A picture of the module containing the memory matrix is shown in Figure 119.

The weight of the entire experiment is a little over 12 lb. It occupies a volume of 850 cu in. The power required is less than 2 w.

The mission sequence calls for the gamma-ray spectrometer to be turned on 4 hr after lift-off. Data storage and transmission begin at once. At 16 hr after lift-off, the gamma-ray boom will be extended to reduce the background counting rate. By acquiring data with the boom, both stowed and extended, it will be possible to estimate the fraction of the counting rate due to background when the detector is in the extended position.

A measurement of gamma-ray spectrum over most of the RA-3, -4, and -5 trajectory is designed to serve two purposes: to distinguish between the lunar and the nonlunar gamma-ray spectrum, and to search for solar photons. In addition to solar photons, the nonlunar background will consist of secondary gamma rays produced by the interaction of primary cosmic rays with the spacecraft, and a certain amount of radioactive material, mostly potassium, in the detector.

Data handling. The memory of the pulse height analyzer, into which signals from the detector are processed, has a capacity of 16 bits in each of its 32 channels. The total storage in bits is then $32 \times 16 = 512$, which represents the number of readout pulses which the central computer and sequencer must supply to empty the memory and transmit its information to telemetry. After the memory has been read out, the analyzer automatically returns to store mode. The digital transmission represents data "one" and data "zero" by different voltage levels.

To distinguish readout periods on the telemetry line, the output is clamped to the data "one" level during the store period and released only at the initiation of readout. In the cruise mode, the start-read pulse causes a change

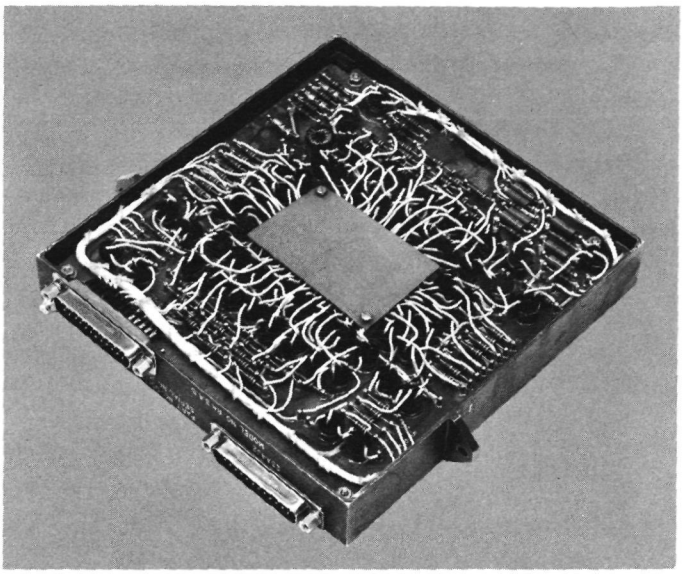

Figure 119. Memory module, gamma-ray spectrometer system

of state in the telemetry level with a duration one and one-half times greater than each memory bit. This invariable change of state marks the initiation of a line of data. Commutation with the vidicon in the terminal mode raises the possibility that the start-read pulse will not always be seen, so an additional identification pulse is provided following the start pulse. This identification pulse is also one-half times as long as a memory pulse.

Each store/readout duty cycle in the cruise mode is 8 min in length. The readout portion of the cycle requires 512 memory pulses, each 40 msec apart (25 pps), plus a start-read pulse which occurs 60 msec after the first memory pulse. This rate of readout allows transmission with the omnidirectional antenna as well as the high-gain antenna.

In the terminal mode, a readout will occupy slightly more than 2.5 sec of each 52-sec duty cycle, since it will be at the rate of 200 pulses per sec. The gamma-ray telemetry line is time-shared with the vidicon experiment, and the radar altimeter and gamma-ray data will be read out during every fourth vidicon erase period. Choice of this interval reflects a desire to have as much time as possible to store lunar radiation, while reading out frequently enough to establish a lunar effect.

The pulse-height analyzer contains provisions for two levels of gain: high and low. The latter, which can be considered the lunar, or standard, setting, will cover an energy range of 0 to 3 Mev. The high gain will scan between 0 and 0.6 Mev for the purpose of improving the

resolution in this range, in which are to be found the peaks from the calibration sources. The choice of gain level is controlled through a relay which is actuated by a signal from the command controller sequencer. During the cruise mode, the high and low gains alternate with each 8-min cycle. At the beginning of the terminal mode, calibration is established with six consecutive periods of high gain followed by a change to low gain for the remainder of the mission.

The quantity of data involved in this experiment is comparatively moderate. Decoding of information received in the cruise mode will be accomplished automatically. The terminal mode data—about 10% of the total—may have to be decoded manually because of the difficulty of distinguishing the start of gamma-ray readout from vidicon data by machine.

The computer program is under development. It will average the data on a channel-by-channel basis for equivalent periods of operation, thus providing a background rate to subtract from rates recorded as the Moon is approached. Successive readouts in the terminal mode will be differenced to provide a sensitive indication of lunar activity as the distance to the Moon is decreasing. Finally, the gamma-ray peaks seen will be analyzed by fitting standard spectra to the composite curve and stripping. This analysis will be performed at the University of California (La Jolla) as well as at JPL.

d. Radar altimeter.

General description. During the past 15 yr, numerous lunar radio reflection measurements have been made with various frequencies with wavelengths ranging from 3 meters to 10 cm (Refs 35 and 36). Nearly all of these measurements were of the backscatter type; that is, the transmitter and receiver antennas were located either within a few miles of each other or were the same antenna. All measurements exhibited a highlight, or specular effect, in the central region of the disk. This brightening of the central region is not observed at optical wavelengths; instead, the reflectivity, on the average, appears uniform from limb to limb. It is not certain that the specular component will be predominant at 3 cm, which is the wavelength used by the lunar altimeter. Consequently, the signal strength of the scatter component, which appears to be independent of wavelength, was used for the altimeter design. One of the scientific objectives of this experiment is to ascertain the relative strength of the specular component for the case where the radar is located near the Moon.

Another area of uncertainty associated with the lunar reflection properties is the variation of reflectivity. Earth-based radar measurements allow estimates to be made of the average reflection coefficients of very large areas (10^6 sq km) of the lunar surface. The altimeter will view areas of 100 sq km or less and may serve to establish a "standard" area for the calibration of more sophisticated Earth-based radar systems. The range of reflectivity is particularly important in the design of future radar systems for soft landers. Thus, the measurement of the effective reflection coefficient for small areas of the lunar surface is of engineering and scientific interest.

Values of the average reflection coefficient depend on the various interpretations of the radar data by the researchers and generally fall in the region of 0.01 to 0.1. The value chosen as the design parameter for the altimeter is 0.01. It is not known why the lunar surface exhibits such low values; the equivalent value for the Earth's land masses is 0.33. It could be a property of the material, the porosity of the material, the result of a multiple bounce of the incident energy, or any combination of these effects.

As mentioned above, most of the Earth-based radar measurements have yielded backscatter data. At the present stage of theoretical development, electromagnetic theory is not capable of providing surface profile information from backscatter data alone. Therefore, backscatter radar data cannot determine which of the proposed models (Refs 37, 38, 39) concerning the lunar surface is closest to being the actual case, even though these models are widely divergent, varying from vast areas of dust layers to jagged surfaces. Some information about the surface profile can, however, be determined from forward scatter experiments in which the transmitter and receiver antennas are located at separate points in space. Two such experiments have been conducted by Earth-based systems, one between Washington, D. C., and Palo Alto, California, and the other between England and Texas (Ref 40), where the forward scatter angles were about 1 to 2 deg, respectively. In both cases the data were noisy, and the specular or highlight effect appeared reduced or nonexistent. These measurements imply that the low reflectivity results from the mutiple bounce or jagged surface model. However, as the data are noisy, there continues to be some doubt about this model. Therefore, a third scientific objective of the radar experiment is to obtain surface properties by correlating trajectory, optical, radar, and, perhaps, seismic data. Should the surface be jagged, the radar data may aid the optical data in determining the depths of the jags.

The lunar radar altimeter was designed to initiate the capsule separation and retrorocket ignition at a preset

altitude of 19 to 25 km from the lunar surface. The altimeter design is predicated on an estimate of the average lunar reflectivity obtained from Earth-based radar measurements. In addition to its primary engineering function, the altimeter will provide a coarse measure of the lunar radar reflectivity in the impact region and serve to establish closer brackets on the lunar radar reflection properties.

The lunar altimeter is a standard pulse-type radar. A functional diagram of the altimeter is shown in Figure 120. The transmitter is a magnetron with a peak power output of 150 to 400 w. The radar parameters are:

Pulse width, 2 μsec

Pulse repetition rate, 500 to 600 pps

Frequency, 9400 mc

Receiver bandwidth, 12 to 16 mc

Receiver noise figure, 11 to 12 db

Antenna beamwidth, 4.5 deg

The altimeter will be turned on by ground command at a distance from the Moon between 198 and 55 km, with 137 km nominal. The function height[a] of the altimeter is designed for an altitude of 19 to 25 km. The relative velocity of the bus and Moon will be 2.5 to 2.9 km/sec during the time of altimeter operation, and the function height resolution is about 150 m for a near-normal velocity vector.

[a]Function height is the distance above the Moon at which the altimeter initiates the separation of the capsule from the bus.

Automatic gain control. The radar receiver is a superheterodyne with a klystron local oscillator. The transmitter pulse and receiver recovery are gated out in the video amplifier so that they will not affect the AGC (automatic gain control). The AGC signal is generated by passing the video signal through a pulse stretcher amplifier and integrator. The AGC voltage controls the static operating point of two IF stages in a manner that forces the dynamic operation into saturation and thereby reduces the amplitude of the IF signal. The AGC action begins when the signal-to-noise ratio exceeds 10 db; that is, the AGC voltage begins to build up after the peak signal-to-rms noise ratio reaches 10 db and continues to be a measure of the peak signal strength thereafter. This AGC voltage is relayed to telemetry and represents the source of radar data. A pulse-by-pulse account would be preferred but the necessary telemetry bandwidth is not available. The AGC dynamic range is 40 db and has a time constant of 0.01 to 0.05 sec.

The AGC voltage varies from 0 to -8v; the required input to the telemetry system is ± 2.5. The AGC voltage is passed through a chopper insolation amplifier with output characteristics which match the input characteristics of the telemetry system. The transfer characteristic of this type of AGC is a very strong function of temperature. Comprehensive pre-launch calibration procedures will be conducted to establish a family of AGC transfer function curves, at various temperatures, in order that the data may be accurately evaluated.

Data handling. After the altimeter is turned on, the AGC voltage is sampled for 3-sec intervals every 10 sec during the TV erase period. Every fourth 3-sec interval,

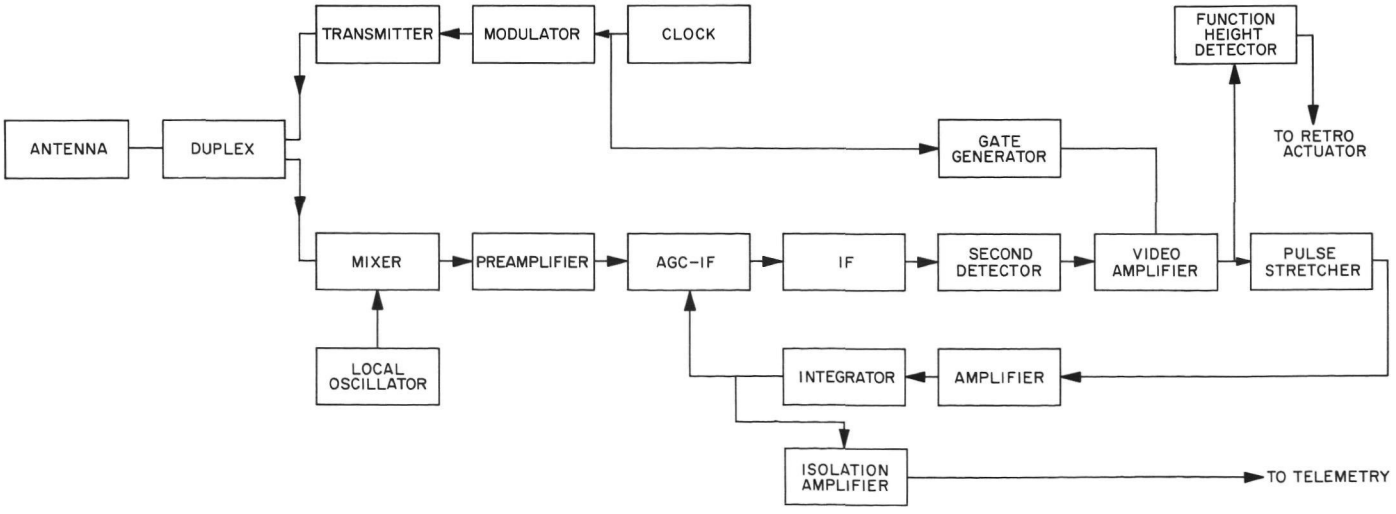

Figure 120. Radar altimeter functional diagram

the telemetry is switched to the gamma-ray experiment. The total operation time of the altimeter is nominally 42 sec, and can vary between 66 and 9 sec. For the nominal case there will be 9 to 12 sec of AGC data. After function height is reached and the capsule is ejected, the altimeter will continue to operate for about 20 sec until impact of the bus. However, the bus may be tumbling and little or no telemetry data will be available.

The analog AGC signal will be recorded in real time on an oscillograph recorder and magnetic tape for subsequent non-real time analysis. The purpose of the real-time recording is to separate data variations from the magnetic tape machine wow and flutter variations.

The data will first be converted to power returned vs range and compared with the expected variation. The mean reflection coefficient will be calculated and certain theoretical assumptions will be tested. Second, the major deviations from the smooth-power-vs-range curve will be examined and correlated with bus stabilization and TV pictures of the target region. Third, a study of the smaller and more rapid variations will be made. The AGC time constant is approximately 50 millisec; consequently variations with frequency components up to 10 cps are significant. One of the possible methods for determining the strength of the specular component of the echo is to examine the amplitude of the fluctuating component.

e. Seismograph.

General description. The lunar seismograph (system) consists of a seismometer (seismic transducer), a lunar-based data processing system (lunar capsule electronics), and an Earth-based data processing system, as shown in Figure 121. The bandpass of the system is 0.05 to 0.5 cps. Response characteristics depend on the filter characteristics used in the two terminal data processing systems located at the Caltech Seismological Laboratory (CIT) and the Lamont Geophysical Observatory (LGO). The CIT filters were chosen to simulate a standard short-period and a standard long-period Benioff seismograph. Magnification of the CIT system based on the filter which simulates the short-period Benioff seismograph is 3.3×10^5 at 1 cps. Magnification is defined as recorder trace per ground amplitude seen by the seismometer and it is directly proportional to the seismometer output, which in turn is a function of ground period. The minimum detectable ground motion at the lunar seismometer corresponding to this magnification is 3×10^{-6} mm at 1 cps, based on a signal-to-noise ratio of 2.5 in the capsule amplifier and a minimum resolution of 1 mm (minimum resolution of the human eye) on the seismogram (seismograph record). As a comparison, the Earth-bound short-period seismograph located at CIT consists of a standard Benioff seismometer, a short-period galvanometer, and a photographic drum recorder. Magnification of this system is approximately 2.5×10^4 at 1 cps. Thus, the lunar seismograph is approximately 13 times as sensitive as its Earth-bound equivalent at CIT. The greater sensitivity of the lunar system allows detection of the lunar microseismic level (seismic background signals), which is estimated to be approximately 1/10 that on Earth.

Due to miniaturization, the seismometer used in the lunar seismograph is about 1/10 as sensitive as a standard

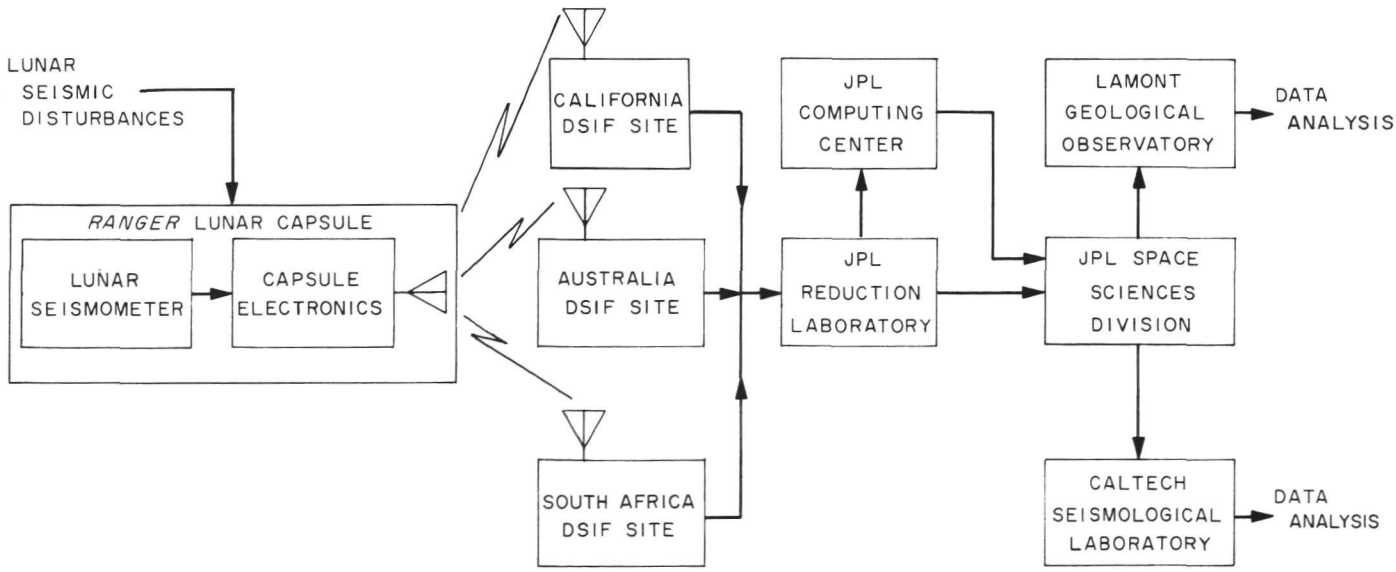

Figure 121. Lunar seismograph data flow

short-period Benioff instrument after which its characteristics were patterned. Sensitivity is defined as voltage output per ground amplitude seen by the seismometer. It is a function of coil impedance, the size of the inertial mass, and the type of damping employed. The capsule amplifier, which has a gain of 5.0×10^5 in its linear region, compensates for the low sensitivity of the lunar seismometer and provides the increase in magnification of the lunar seismograph.

The seismometer was designed and fabricated by the CIT Seismological Laboratory. The capsule, including its amplifier, was designed, developed and fabricated by Aeronutronic, a Division of Ford Motor Company. JPL conducted environmental tests on the seismometer, sterilized it, and monitored the operations of both CIT and Aeronutronic to ensure proper integration of the seismometer in the lunar capsule and integration of the capsule into the *Ranger* spacecraft.

The seismograph data processing system was developed and assembled jointly by the co-experimenters (CIT and the Lamont Geological Observatory) and JPL. Evaluation of the seismic data will be carried out separately by each co-experimenter.

Seismometer. The lunar seismometer is a single-axis, suspended-magnet type instrument consisting basically of a coil, a spring-suspended magnet, a centering system, and an internal calibration device. The relationship of these components is illustrated in Figure 122. Figure 123 is a schematic of the transducer. The inertial mass consists of a permanent magnet suspended from the body of the instrument by a helical spring and two cantilever spring rings. The spring rings act to maintain concentricity of the mass within the body. This allows the seismometer to operate at any inclination of its longitudinal axis from 0 to 90 deg at lunar gravity. Movement of the coil, which is rigidly attached to the body, relative to the inertial mass generates the voltage output of the transducer. Several additional permanent magnets are embedded in the body so as to repel the mass, thus extending the natural period of the instrument from approximately 0.4 sec to a range of 0.9 to 1.2 sec.

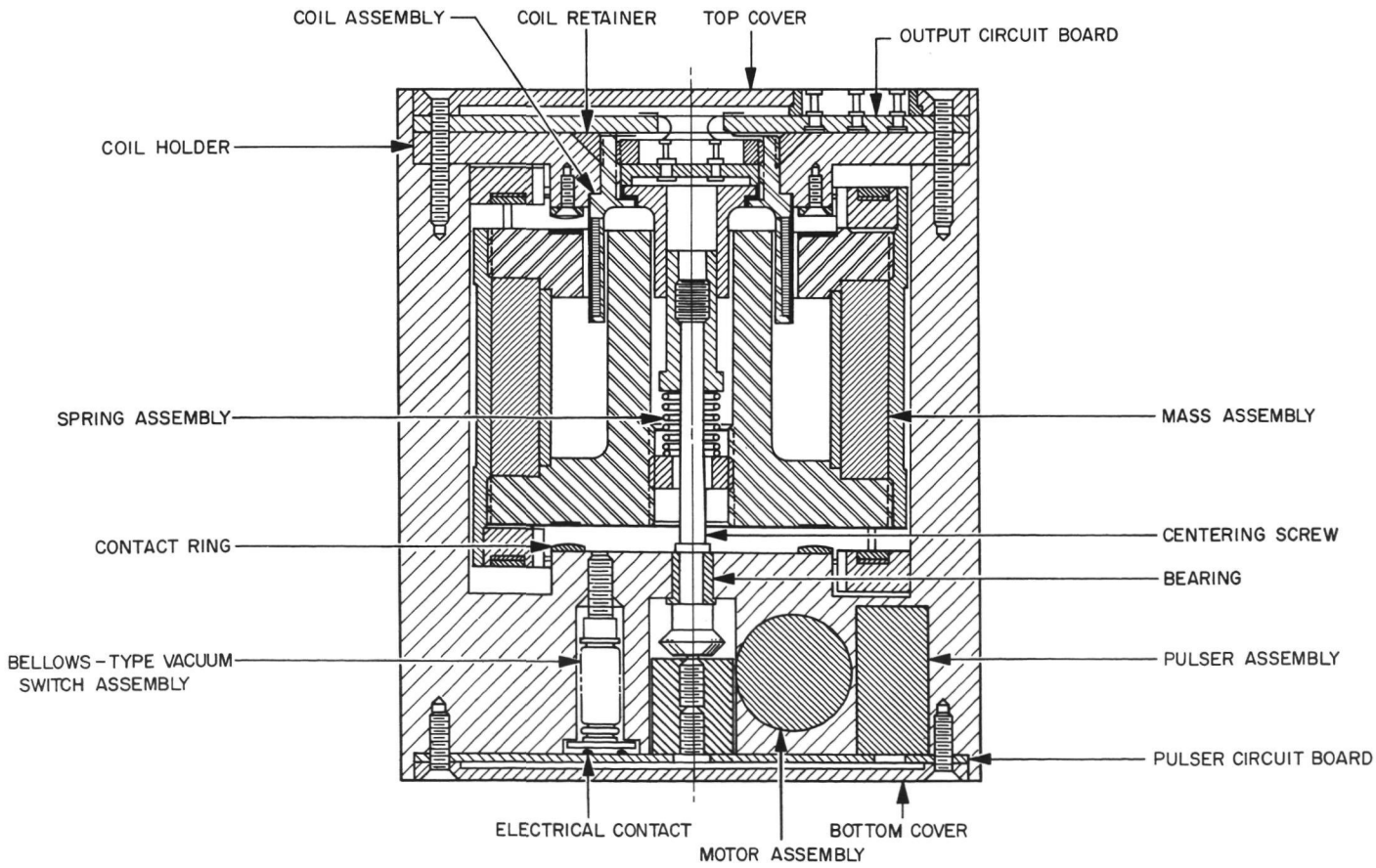

Figure 122. Suspended magnet seismometer, internal view

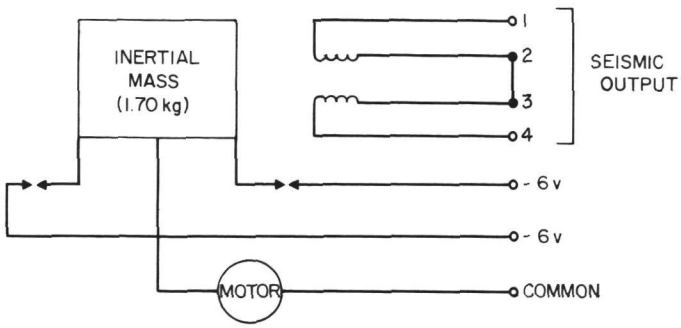

Figure 123. Suspended magnet seismometer schematic diagram

The seismic transducer is self generating and requires no external or internal power. At 1 cps its output is 0.80 microvolt per millimicron of ground motion. The transducer characteristics provide a 6 db/octave rise for periods short compared to the natural period of the instrument, and 18/db octave fall-off for periods long compared to the natural period. The mass is critically damped at all frequencies. Power loss in the combined resistance of the transducer coil and the external mating circuit (amplifier) generates the electro-magnetic viscus damping.

Movement of the inertial mass is limited to 0.25 in. by stops. The instrument contains a closed-loop servo system designed to keep the mass from resting on these stops regardless of the orientation of its longitudinal axis. A motor is activated whenever the mass makes electrical contact with the stops. The motor drives the center shaft through a gear system, thus, shifting the frame end helical spring attachment point. This shift causes an increase or decrease of the force exerted by the spring on the mass, thereby lifting it off the contact ring and breaking the circuit. Over-run of the motor is sufficient to balance the mass at a free position.

Calibration of the seismometer output and monitoring of its operation will be provided by the pulser throughout the lifetime of the experiment. The pulser circuit consists of two asymmetrical free-running multivibrators plus an "and gate" which periodically energizes a coil magnet. The generated magnetic field displaces the inertial mass, thereby generating a standard output signal. A schematic of the circuit is shown in Figure 124. Figure 125 illustrates the cordwood-type technique used in packaging the circuit for high-g survival. The pulser will be activated by an internal bellows-type pressure switch which closes at 0.50 to 0.05 atmosphere of pressure.

Power for the pulser circuit is provided by six nickel-cadmium batteries embedded in the body of the seismometer. These batteries are arranged in a series-parallel network to supply +2.4 v and −1.2 v with a nominal capacity of 575 maH. This capacity operates the pulser

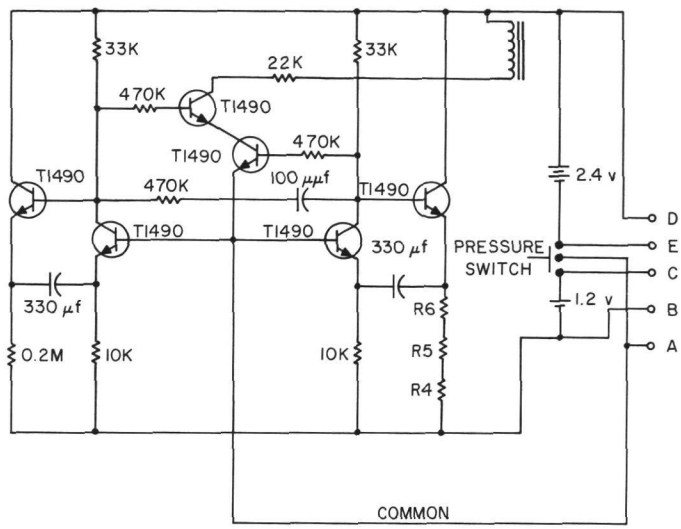

Figure 124. Seismometer pulser circuit

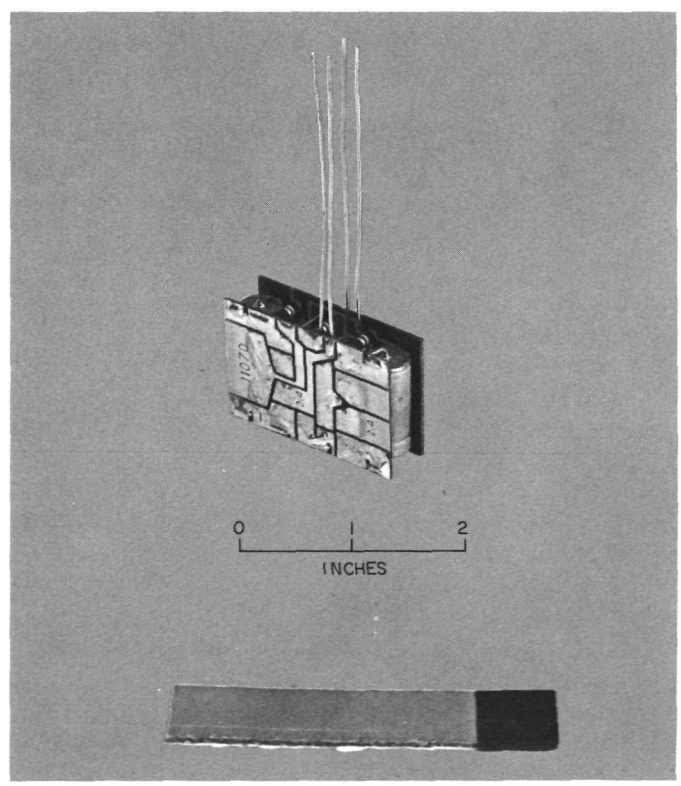

Figure 125. Cordwood technique used in packaging seismometer for survival

for approximately 90 days. The centering motor for the inertial mass requires 48 mw of power at 6 v, externally supplied by the lunar-capsule power supply batteries.

The seismometer package is a cylinder 5.50 in. long and 4.375 in. in diameter. It weighs 7.98 lb when filled with caging fluid and 7.55 lb when empty. The inertial mass weighs 3.75 lb (1.70 kg). Figure 126 shows the physical appearance of the instrument.

The body of the seismometer is composed of high-temperature, epoxy-glass laminate. The ring magnet used in the inertial mass and the bar magnets used to lengthen the period are made of Alnico V. The spring rings are composed of hardened beryllium copper. All bearings within the instrument are run dry.

Seismometer environmental tests. The seismometer was designed and tested to withstand all environmental limits prescribed for equipment inside the survival capsule. Unusual requirements include a 300-*g*, 4-msec, sawtooth shock along the longitudinal axis and at 45 deg to it in two perpendicular planes, and a 24-hr heat soak at 125°C. Pretesting of the pulser circuit package was carried out by the CIT Seismological Laboratory. No failures were experienced for shocks up to 12,500 *g* peak and 7000 *g* average for 5 msec.

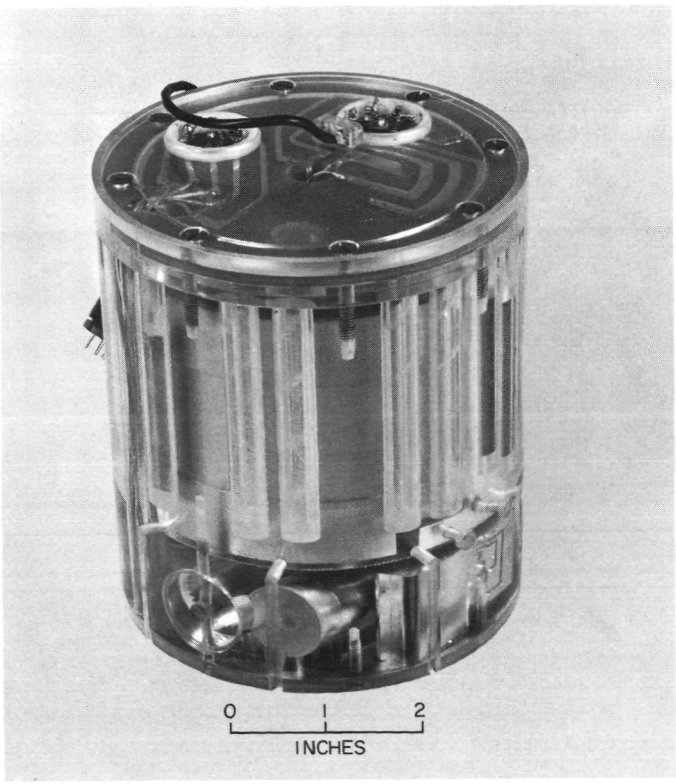

Figure 126. Lunar seismometer unit

During all environmental tests, the seismometer was housed in a fixture which simulated its packaging in the survival sphere. The mass was caged with N-Heptane. Provisions were made to bring out signal leads. Following each test, the seismometer was returned to the CIT Seismological Laboratory for a standard performance test on a seismometer pier. Records from these tests were compared to a master record obtained from the seismometer prior to the testing program. A block diagram of the setup for obtaining these records is illustrated in Figure 127.

During the design proof tests, only one deficiency was exposed in the seismometer's design despite the fact that a single instrument had undergone the abuse of many fillings and dryings and each of the impact, vibration, heat, cold, gas and vacuum exposures. It was found that the original epoxy-glass laminate body material was changed to a more suitable high-temperature epoxy-glass and the body design was modified to a two-piece instead of a one-piece assembly.

All flight units and spares were subjected to Flight-Acceptance tests, which consisted of a heat soak, static acceleration, vibration and two 100-*g*, 2-msec, terminal, peak saw-tooth shocks in three mutually perpendicular planes.

Seismometer sterilization. Construction of the instrument and the packaging techniques in the lunar capsule necessitated the use of both thermal and ethylene-oxide gas sterilization in order to comply with the NASA lunar impact sterilization policy. The seismometer and pulser circuit package, less the pulser batteries, were heat-soaked at 125°C for 24 hr after temperature stabilization. The batteries and pulser were potted within the instrument, using a sporicidal potting compound. The

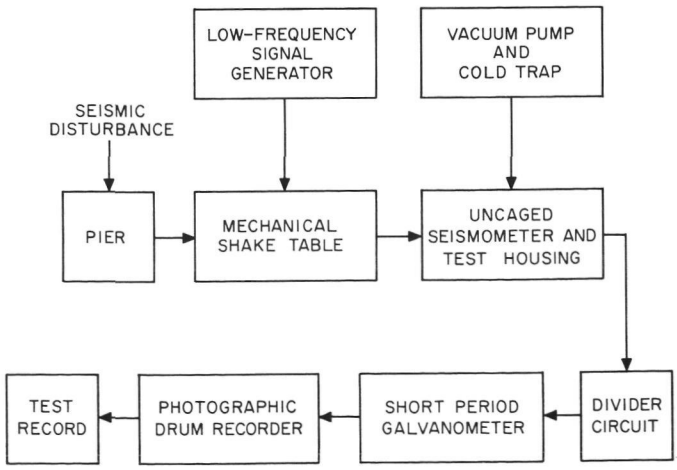

Figure 127. Seismometer performance test setup

seismometer was inspected for mechanical and electronic defects at JPL. A 24-hr pier check was conducted at CIT.

The completed flight seismometer, the environmental test fixture, the caging fluid, and all equipment used to vacuum-fill the test fixture were surface-sterilized by exposure to an ethylene-oxide-freon mixture for 8 hr inside a glove box. Two ultra-violet lamps inside the box were turned on during the gas soak and subsequent assembly operations. Commercial spore strips and ethylene-oxide exposure indicators were used to verify the sterilization process. The caging fluid was bulk-sterilized in the glove box by filtering with a sterile 0.22 micron filter and then sealed in a polyethylene bottle. All vacuum and fluid lines were connected to the fixture before removal from the glove box. The fixture was evacuated and filled with fluid. Flight-Approval tests were then conducted. Figure 128 shows the glove box loaded prior to gas sterilization. Following the flight-approval tests, a second 24-hr pier check was conducted at CIT. The seismometer was then packaged in an air-tight container, following a second gas sterilization, and delivered to Aeronutronic.

Spacecraft integration. Inside the lunar capsule, the seismometer is packaged in a rigid breech so that it is supported everywhere except at the terminals and drain vents. To damp the rapid movement of the inertial mass during lunar impact, the instrument is filled with a fluid. The fluid (N-Heptane) was chosen because of its relatively high vapor pressure, viscosity, density, and its compatibility with the materials of the instrument. Internal details of the survival capsule payload are shown in Figure 129.

Data processing. Upon impact on the lunar surface, the survival package will be permitted to float into an upright

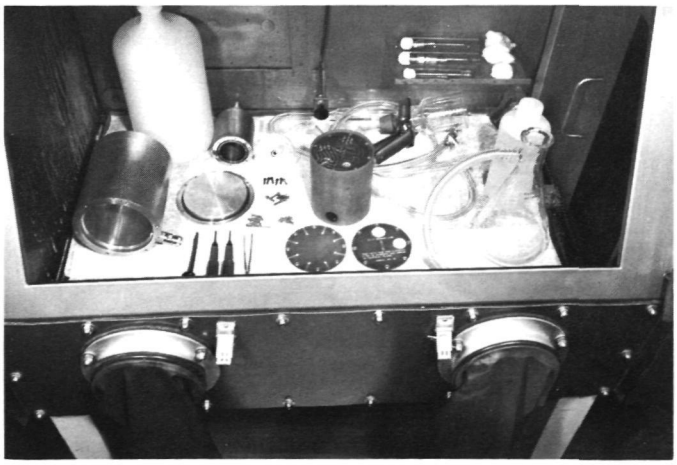

Figure 128. Glove box loaded prior to gas sterilization

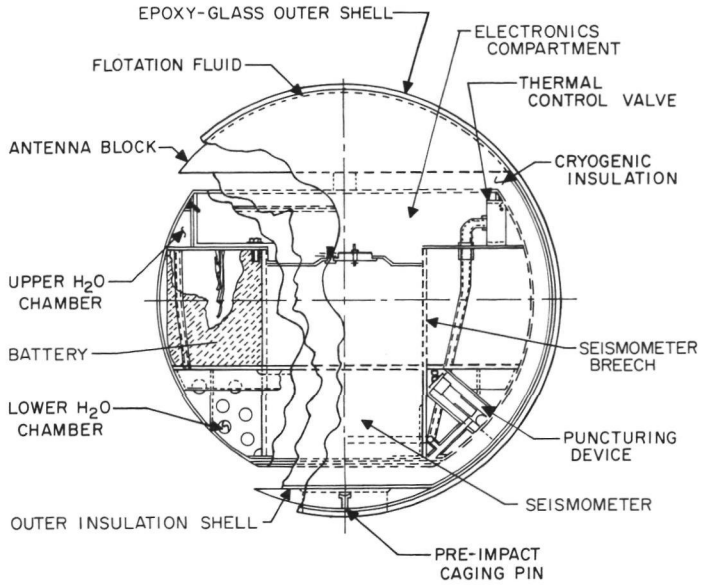

Figure 129. Lunar capsule payload, cross section view

position within the impact limiter. Fifteen min after impact, the survival package will be rigidly caged within the impact limiter by three post-impact caging squibs. One min later, the impact limiter will be punctured by two venting squibs permitting the seismometer caging fluid to drain. The subsequent reduction of pressure within the seismometer will actuate the pressure switch and activate the pulser. Thirty min after impact, the centering motor feedback system will be energized by the sequence timer within the capsule, initiating the seismic experiment. Data from the experiment will be processed as illustrated in Figure 130.

Lunar seismic disturbances will be detected and converted into electrical analog signals by the seismometer. These signals are then processed in the capsule data system, which consists basically of an amplifier and a FM-PM transmitting system, as shown in Figure 131. The amplifier compresses, clips, shapes and amplifies the signals received from the seismometer. The conditioned signal then frequency-modulates the standard Channel 2 subcarrier frequency (560 cps) of the voltage-controlled oscillator (VCO). The FM subcarrier then phase modulates the voltage-controlled oscillator (VCO). The FM subcarrier then phase modulates (PM's) the 960-mc r-f carrier of the capsule transmitter.

JPL's three DSIF sites will alternately receive the telemetered data. The FM subcarrier will be recovered from the main carrier in the phase-locked-loop receiver, recorded on magnetic tape along with standard timing signals and other receiver performance characteristics,

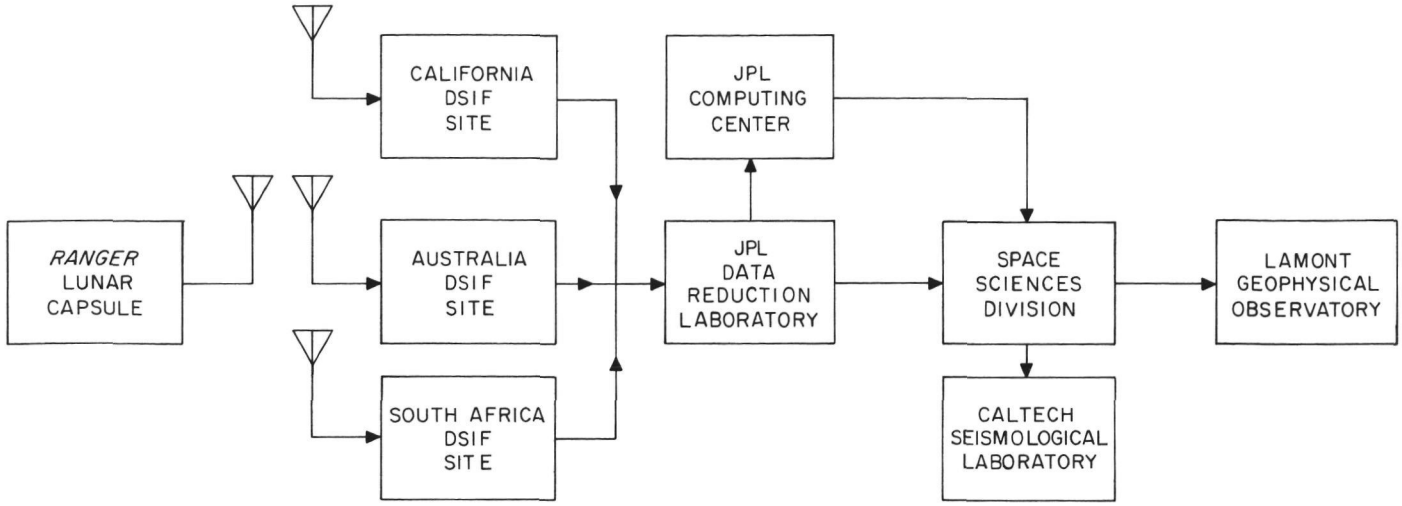

Figure 130. Seismic data flow

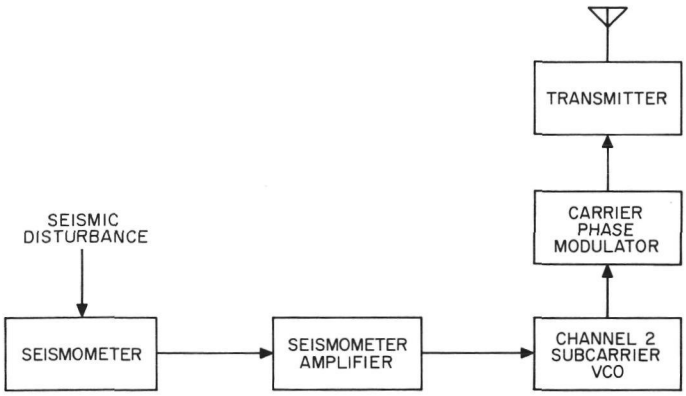

Figure 131. Capsule data system

and forwarded to the JPL Data Reduction Laboratory (DRL).

The system used by the DRL for processing the tapes received from DSIF is shown in Figure 132. The data subcarrier will be dubbed onto one track of a ¼-in., 1-mil mylar magnetic tape multiplexed with a 1-kc reference frequency used for flutter compensation. A direct-record voice label will precede the data on this track. Timing signals, to an accuracy of 0.1 sec, will be recorded on the other track. In addition to the analog processing, the data will be digitized for input to the JPL IBM 7090 computer. Each co-experimenter, the CIT Seismological Laboratory and the Lamont Geological Observatory, will receive one set of analog data tapes. The digitized data will be made available upon request.

The analog tapes produced at the DRL will be processed for final analysis in the terminal data-systems at CIT and LGO. The CIT system is illustrated in Figure 133. Two identical systems of this configuration will be available for the *Ranger* experiments. The two systems located at LGO are identical to those at CIT, except for the choice of filters.

The data subcarrier discriminator in the terminal data processing system separates the analog data signal (the same analog signal used to FM the subcarrier in the lunar capsule) from the 1-kc reference frequency on the DRL tapes. The ground adapter inverts the processing performed by the capsule amplifier and expands the signal so that it is the same as that received from the seismometer.

To facilitate analysis of the seismic information obtained from the ground adapter, CIT will filter the signal before it is recorded so that it corresponds to that obtained from familiar seismograph systems. Those which will be simulated are a Benioff short-period seismometer with a short-period galvanometer, and a Benioff short-period galvanometer. Specifically, the seismometer period (T_0) and the galvanometer period (T_g) will be as follows: ($T_0 = 1.0$, $T_g = 0.2$; $T = 1.0$, $T_g = 90$ sec). After filtering, the seismic signal is amplified and recorded on a direct-writing drum recorder along with timing signals. Figure 134 shows a typical Earthquake trace from the lunar seismometer. The signal was filtered through the CIT system, which simulates the Benioff short-period seismograph.

Data processing system test. An over-all system test was conducted by JPL. To facilitate the test, a magnetic "instant quake" tape was prepared, using the system of Figure 135. A portable FM recorder/reproducer was used to record live seismic signals from a lunar seismometer located at the CIT Mt. Wilson Seismological Station. A

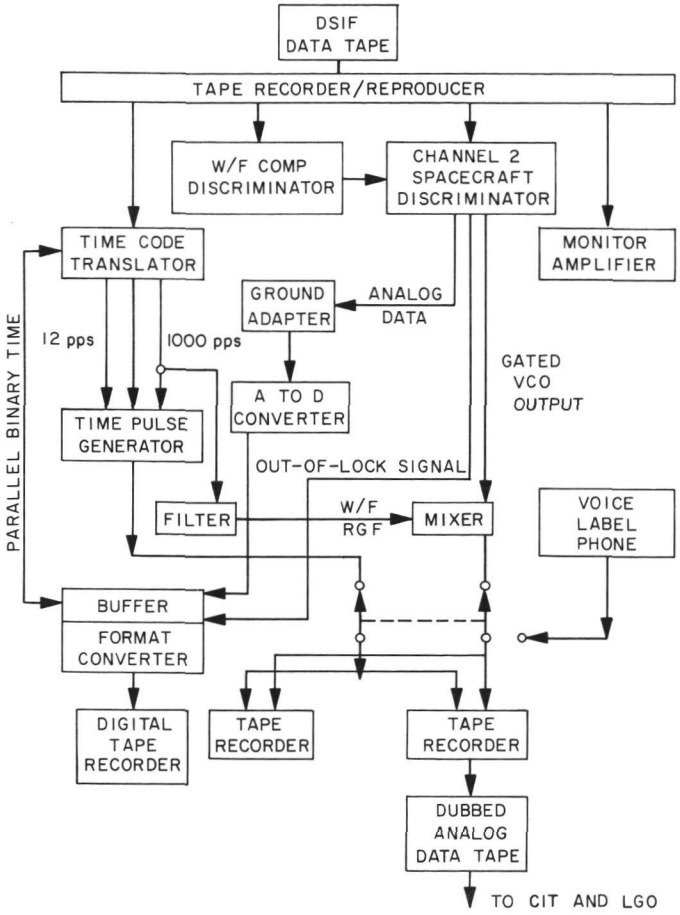

Figure 132. Data Reduction Laboratory seismic data

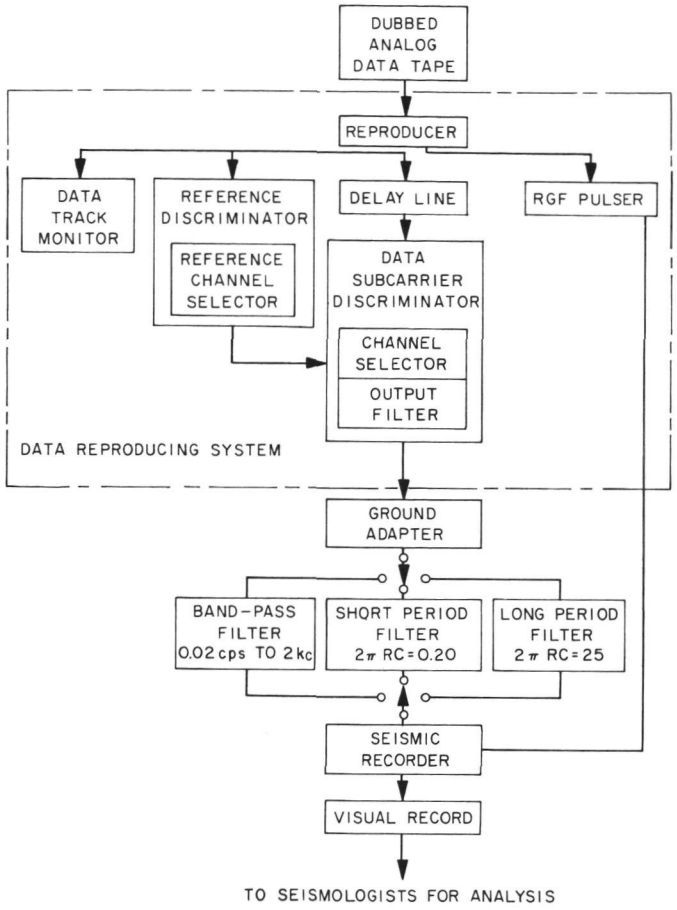

Figure 133. CIT terminal data processing system

visual record was recorded simultaneously with the magnetic tape for the purpose of preparing a time log of the signals recorded. This log was used to edit the Mt. Wilson tape. The final "instant quake" tape contained a series of seismic signals of various types, ranging from microseismic levels to severe quaking levels. Time length of the tape was approximately 1 hr. The "instant quake" tape, the FM reproducer, and a low-pass filter then constituted the electronic equivalent of the lunar seismometer capable of producing seismic signals on command.

During the test, the electronic-equivalent seismometer was used to replace the seismometer itself. The capsule amplifier was maintained at the upper limit of the capsule temperature-control system (77°F). This temperature produced the greatest noise from the amplifier. The capsule VCO and transmitter were contained in a "quiet box" which allowed attenuation of the transmitted r-f signal below the DSIF receiver threshold. The "quiet box" was connected to the receiver by a hard line. The remaining portion of the system was the same as that which is used during the *Ranger* flights.

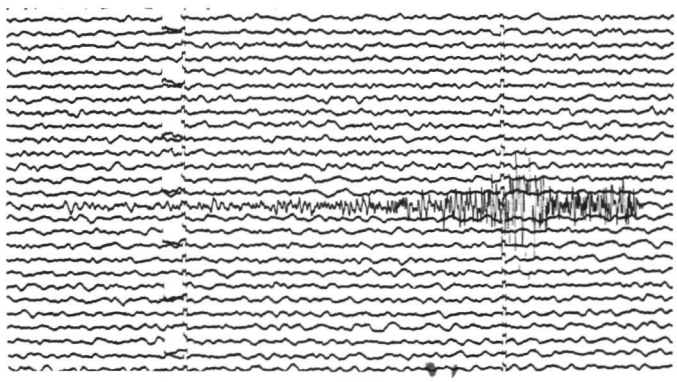

Figure 134. Typical earthquake trace

Analysis of the test records by seismologists at CIT, LGO, and JPL indicate that the quality of the data recovered from the over-all system is satisfactory for scientific purposes.

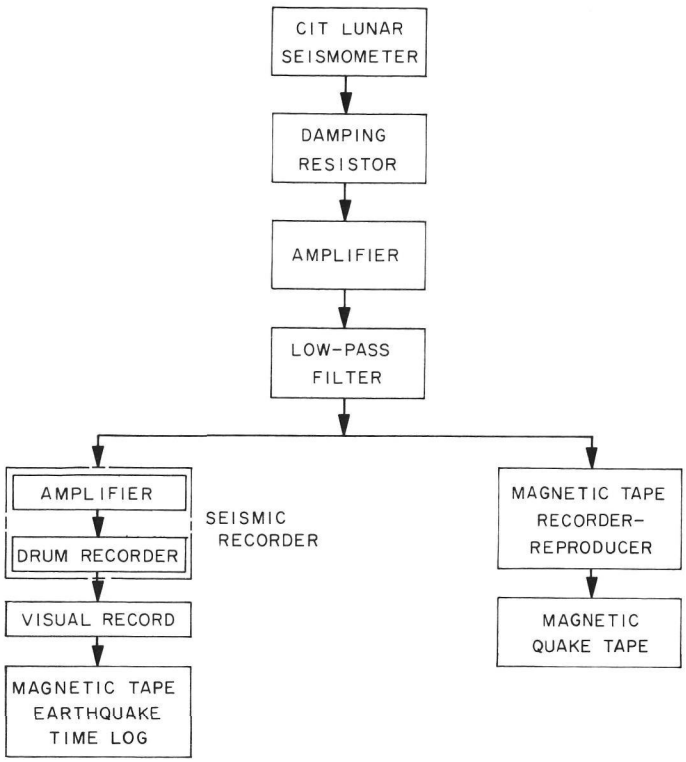

Figure 135. Mt. Wilson seismic recording system diagram

f. RA-3, -4, -5 ground support equipment.

General description. The ground support equipment for the RA-3, -4, -5 scientific instrumentation, when operated in conjunction with the appropriate stimuli applied to the instruments, provides an over-all check on instrument performance. Both visual monitoring of outputs and a printed record of test results are provided. Additionally, a punch-tape record suitable for teletype transmission and a film strip recording are available.

In general, the purpose of the GSE checkout procedure is to establish a *"go-no-go"* condition of the equipment, rather than to check the absolute calibration of each experiment, in terms of the physical units being measured —i.e., light intensity or gamma-ray energies. Such absolute calibration will have been performed by the individual scientific experiment groups prior to installation on the vehicle.

Physically, the ground support equipment consists of five equipment racks. Three of the racks are associated with the telescopic television system and the other two are associated with the gamma-ray spectrometer. Aeronutronic, Division of Ford Motor Co., has cognizance over the lunar capsule and its associated GSE. The ground support equipment largely utilizes commercial-type units. Figures 136 and 137 are photographs of the equipment.

Stimulus and response. The stimulus utilized with the telescopic television subsystem is an infinitely focused or collimated light source. This light is modulated by a standard RETMA television test pattern. The television system scans this test pattern and creates an analog video signal whose bandwidth is 2000 cycles. The GSE displays this signal both in electrical and visual form. The stimuli used in conjunction with the gamma-ray spectrometer include background, cesium 137, sodium 22, and strontium 90. The spectrometer converts the gamma radiation into binary coded numbers of counts. The GSE decodes these binary numbers and records the decimal equivalents.

Integration. Inasmuch as the scientific ground support equipment must be capable of simulating other spacecraft subsystems which supply signals to the scientific subsystem, the GSE outputs are designed to match those

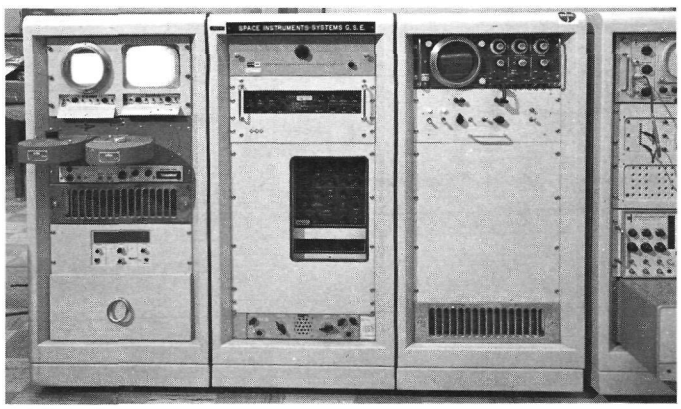

Figure 136. TV test rack

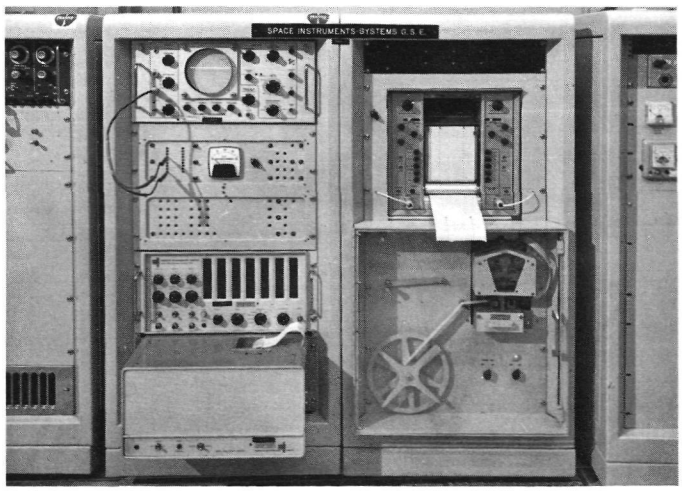

Figure 137. Gamma-ray test rack

spacecraft subsystem signals that they simulate. The capacitance introduced by the long cable lengths between the spacecraft and GSE is offset, as much as possible, by line amplifiers and isolation amplifiers. Since the central controller and sequencer (CC&S) provides all the control for the scientific subsystem on RA-3, -4, -5, the timing, amplitude, wave shape, and rise time of the CC&S commands are all that need simulating. This reduces the magnitude of integration to one major item. Such things as spacecraft power and data output loads are also supplied.

Subsystem and system testing. The subsystem test phase provides an opportunity to completely evaluate a flight-configured subsystem in simulated spacecraft operation. This is generally the first time the individual components that make up the subsystem are mated wth each other to verify interfaces within the subsystem. Subsystem testing reveals the minor integration oversights present on the initial spacecraft assembly. A major area to be tested at this time is the intercabling of the subsystem. The RA-3, -4, -5 scientific subsystem testing was handled as a parallel operation. Since only two of the experiments were to receive subsystem testing and the support equipment for each was a separate entity, parallel testing could be accomplished during all subsystem operations. This allowed a more thorough evaluation per given increment of test time than a single integrated test console could have provided. Since it was possible to simulate both experiments completely external to their equipment, the experiments received a complete evaluation.

Once the individual subsystems had been verified, the entire spacecraft system was intercabled and the various system interfaces were verified. In a pre-system test environment, each of the subsystem interfaces is investigated and verified separately until the complete system configuration is operating properly. From this point, system testing consists of confidence checks of the entire spacecraft operation. Careful records were taken of the operation of the scientific package during the system tests to build a history of operation. This was necessary to establish a trend of scientific performance against elapsed time. As no scientific checks can be accomplished on the launch pad, an accurate estimate of scientific operation over extended periods of equipment off-time is a necessary condition for the actual countdown predicted performance.

Data analysis. The television subsystem data was of two types—measured voltages and visual signals. A record of voltages from test to test displayed proper operation and revealed any trends. The visual (video) indications were displayed in real time by means of television monitors so that an on-the-spot evaluation could be accomplished. In addition, two other recordings were made for later, more complete analysis. These recordings included a pictorial record (kinescope picture) and an oscilloscope record.

The gamma-ray spectrometer data was primarily limited to the output signal. This binary output was decoded in a binary-to-decimal converter and printed out by a decimal printer for on-the-spot evaluation. To preclude decoding errors from biasing the evaluation, the binary data was recorded undecoded on a punch tape. This tape was decoded either manually or by computer at some later date to verify the real-time evaluation.

Calibrations. The one component calibration required for every test was the scan-conversion system in the television support equipment. A special calibration unit was added to the support equipment to accomplish the calibration requirement. The calibration unit provided a standard Indian Head television test pattern for use in calibrating the scan conversion system. Figures 138 and 139 are photographs of these two units.

Documentation. Individual document files were set up and assigned to each spacecraft undergoing test. This documentation included all the necessary drawings and procedures to intelligently conduct the testing, troubleshooting, and repair of the ground support equipment and flight experiments. A subsystem log was kept for each spacecraft to record all operation. To document the scientific support to the operation of the RA-3, -4, -5 program, Technical Memorandum 33-80 was published. In addition, a motion picture was prepared to provide a comprehensive history of all scientific flight instruments, scientific ground support equipment, and tests involving the scientific equipment.

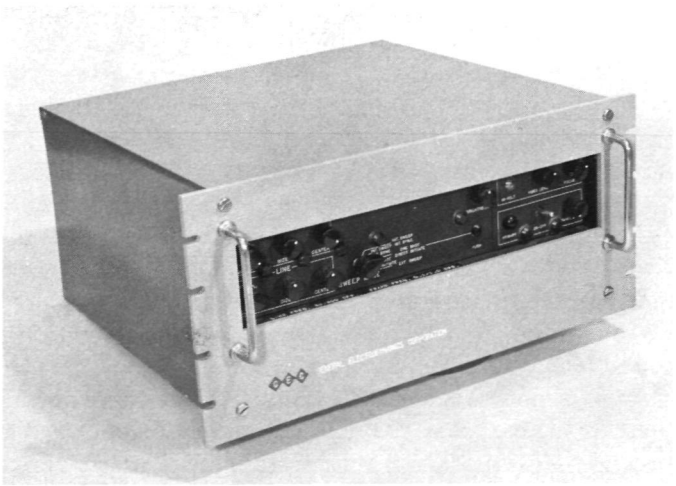

Figure 138. Monoscope

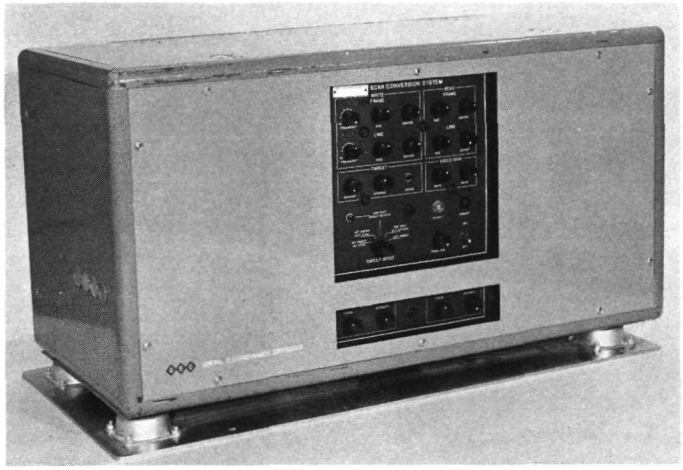

Figure 139. Scan converter

3. RA-6, -7, -8, -9

a. Scientific objectives. The primary scientific objective of the *Ranger* 1963 missions (RA-6 through RA-9) is acquisition of knowledge of lunar topography sufficient for determination of its gross effects on lunar landing vehicles. This objective will be achieved by means of relatively high-resolution photography of a portion of the lunar surface from the impacting spacecraft, and subsequent quantitative analyses of these photographs. This mission will be performed within the constraints of a *Ranger* standard impact trajectory which specifies a near-vertical impact with a velocity at time of impact of approximately 2700 m/sec.

Achievement of this objective requires that the system provide a resolution in the photographs as received on Earth at least 10 and preferably 50 times better than the RA-3 camera system was expected to obtain. Photography must be started at a time before impact, or a distance from the Moon such that the initial photographs are comparable in resolution with the best now available from Earth-based astronomical observatories, and this photography must be continued at a regular rate until impact.

The desired quality of the photographs is directly linked to their usefulness in planning the design of unmanned vehicles and the initial manned lunar exploration program. To be of value, the pictures should indicate the suitability of the lunar terrain for landing and launch and the problems of surface mobility. On consideration of these objectives and the ultimate scientific use of the *Ranger* follow-on photographs, resolution of the final image as received on Earth must be at least 0.5, and preferably 0.1 m.

A secondary scientific objective of the follow-on mission is acquisition of knowledge of the radiation environment of cislunar and lunar space which may be of importance to manned lunar flights, or which may yield data pertinent to the origin of these environments. Specifically, the several radiation experiments to be carried on the spacecraft will provide data on radiation levels and the biological hazards due to high-energy particle radiation during flights to the Moon.

In consideration of these scientific objectives, the following scientific experiments are planned for the *Ranger* follow-on missions.

Primary objective—high-resolution photography. The television experiment for the follow-on consists of six 1-in. vidicon cameras. These are arranged as two wide-angle cameras, designated Camera A and Camera B, and four narrow angle—high resolution—cameras designated as cameras 1, 2, 3, and 4. The A camera is aligned to the expected spacecraft velocity vector at impact and has a color wheel attached. The color wheel has three color filters and a neutral filter which are exposed in sequence. Camera B is set to view the lunar surface obliquely some 30 deg away from the velocity vector and the look-angle of Camera A; thus, its field of view is designed to scan the lunar surface. The four narrow-angle, high-resolution cameras, each with a 2.1 deg field of view, have 1-deg overlapping fields-of-view, directed as Camera A is, along the expected spacecraft velocity vector at impact.

Cameras A and B are fully scanned, producing 800 TV line resolution over the tube format of 0.44 in. by 0.44 in. with a side field coverage of 8.4 deg. The four clustered cameras utilize a reduced raster, scanning a 0.11-in. by 0.11-in. central portion of the tube at the same line density, thus giving 200 TV line resolution. The angular resolution of each camera is then the same; however, the reduced format of the partially scanned system enables a much faster picture cycle and, thus, pictures may be taken at lower altitudes than with the fully scanned system.

This leads to a natural categorization of Type-F cameras for fully scanned and Type-P for partially scanned. The Type-F and Type-P cameras use the same imaging transducers and optical equipments and differ only in the detail of their electronic circuitry. The image transducer is an electromagnetically focused and deflected 1-in. vidicon with an ASOS photoconductor with a resolving capability in excess of 800 lines per picture height.

The Type-F or fully-scanned camera utilizes 1,152 active horizontal scan lines over the 0.44-in. by 0.44-in.

faceplate area. The horizontal scan rate is 450 cps with 0.22 msec appropriated to horizontal blanking. The time required to cover the active scan lines plus 46.6 msec for vertical blanking adds up to the 2.56-sec frame period. At the end of its active scan, the Type-F camera enters an erase phase which occupies an equal amount of time. In the *Ranger* television system, two Type-F cameras are alternately scanned and erased in such a manner that one is being scanned while the other is being erased.

The Type-P or partially-scanned camera utilizes 300 active horizontal scan lines over a 0.11-in. by 0.11-in. faceplate area. The horizontal line rate is 1500 cps with 111.1 μ sec allocated for horizontal blanking. The vertical scan plus a 6.6-msec blanking period occupies 0.2 sec. At the end of the vertical scan an erase procedure is initiated which occupies 0.64 sec. In the system four Type-P cameras are sequentially scanned and while one is being scanned the remaining three are in various portions of their erase cycles. A 40-msec pulse is used to separate each sequence of four Type-P camera exposures. The total period per sequence is then 0.84 sec.

Secondary objective—radiation environment. Three separate radiation experiments will be performed on RA-6 through -9 missions. These are:

(1) A Dosimeter, composed of three tissue-equivalent ionization chambers, each with a different wall thickness, to measure the radiation dose rate under various amounts of tissue-equivalent material. Each tissue-equivalent detector consists of a spherical ionization chamber constructed from a plastic which is similar in chemical composition to human muscle tissue. The sensitive volume of this detector is filled with a gas at 1 atmosphere pressure that is as nearly tissue-equivalent as feasible. A voltage is maintained between a cylindrical collecting electrode inside the chamber and the external spherical wall. This voltage must be high enough to collect all of the charges formed in the gas by the incident ionizing radiations. The current to the collecting electrode is a measure of the radiation dose. This current is monitored by means of an electrometer circuit and amplifier.The data from the instrument appears in the form of an analog voltage.

The basic spherical chamber has an inside diameter of 3½-in. and a ¼-in. TE (tissue-equivalent) plastic wall. Several basic chambers will be flown on each flight (within weight limitations), each surrounded with different thicknesses of TE plastic shielding in order to determine the radiation dose under varying depths of simulated tissue.

(2) An ionization chamber to measure total integrated radiation. The detector for the integrating ionization chamber experiment is a quartz fiber instrument of the Neher type. It consists of a thin spherical metal shell filled with gas at a pressure of several atmospheres. The wall thickness is such that protons above 10 Mev in energy and electrons above 0.5 Mev can pass through into the gas. A voltage is maintained between a cylindrical collecting electrode inside the chamber and the external spherical wall. This voltage is high enough to collect all of the charges created in the gas by the incident ionizing radiations. When a known amount of charge is collected, the quartz fiber system activates a recharging pulse from the chamber power supply. The time interval between recharging pulses is inversely proportional to the radiation dose rate. The recharging pulse is amplified and shaped by the chamber amplifier into a form suitable for processing by the data conditioning system.

(3) Three Geiger-Müeller counter tubes to measure charged particle flux in various energy ranges. Two of these counters are type RCL 10311 and each is shielded such that protons above 10 Mev in energy can penetrate into the sensitive gas volume and be detected. One of these counters is shielded with material that is essentially identical in composition and thickness to that of the wall of the integrating ionization chamber which is also being flown. Since they will each be detecting the same type of particles, and since the ion chamber measures the total ionization, the combined data from this counter and the ion chamber will enable the average ionization per particle to be computed. The other 10311 tube is shielded with beryllium. This provides some discrimination between protons and electrons. The two RCL 10311 tubes will also be operated in coincidence to give directional information. The other Geiger counter is an Anton 213 with a thin end window which allows lower energy particles (protons above 0.5 Mev and electrons above 35 Kev) to be counted.

A Data Conditioning System (DCS) will be an integral part of the radiation experiments for spacecraft RA-7 through RA-9. This system will monitor the frequencies of four separate pulse inputs, and generate digital numbers proportional to five separate temperature analog voltage inputs and three digital inputs.

The data from the follow-on DCS will be transferred to telemetry in a format similar to the format used by the port unit for both systems.

Mariner R DCS. This enables the use of one ground support unit for both systems.

The data from the DCS will enable the determination of the frequencies of the pulse inputs with 1% accuracy, and time intervals of frequencies below 1 per sec within 1.28 sec. The data from the DCS will also include PN sequences and frame count for synchronizing and identifying the data.

The follow-on DCS consists of a timing counter, two 3-bit data counters, two 13-bit data counters, an 8-bit shift register with an output storage flip-flop and a parity generator, an analog-to-digital converter, a 5-bit shift register for coincidence count, and other logical circuits for data selection and controls.

C. Telecommunications

1. Spacecraft Instrumentation

a. Introduction. Telecommunication support of the *Ranger* Project, like that for other operations, has extended over the past 3 years. Figure 140 illustrates the relative times allocated to conceptual design, detailed design, production, and operations for the program. As the project progressed, the time allocations were adjusted until a general plan was evolved. This plan, shown in abbreviated form in Figure 141, permitted the design engineers sufficient time to produce flight hardware, ground support equipment, drawings, specifications, procedures, and to deliver them to the Spacecraft Assembly Facility on the dates required by the Program Director. Whenever this schedule has been followed, there has been sufficient time to put together an integrated telecommunications system. Lesser time scales have resulted in an unintegrated operation.

Scope. This section will review the conceptual design philosophy of the various telecommunications subsystems, followed by a brief explanation of special design problems encountered during the program, and a summary of their solutions. Finally, where appropriate, there is a discussion of telecommunications operations at JPL and in the field. Discussion in this area will be limited to special tests which were performed with telecommunications hardware.

Telecommunications subsystems. The *Ranger* telecommunication system was designed to perform these specific functions:

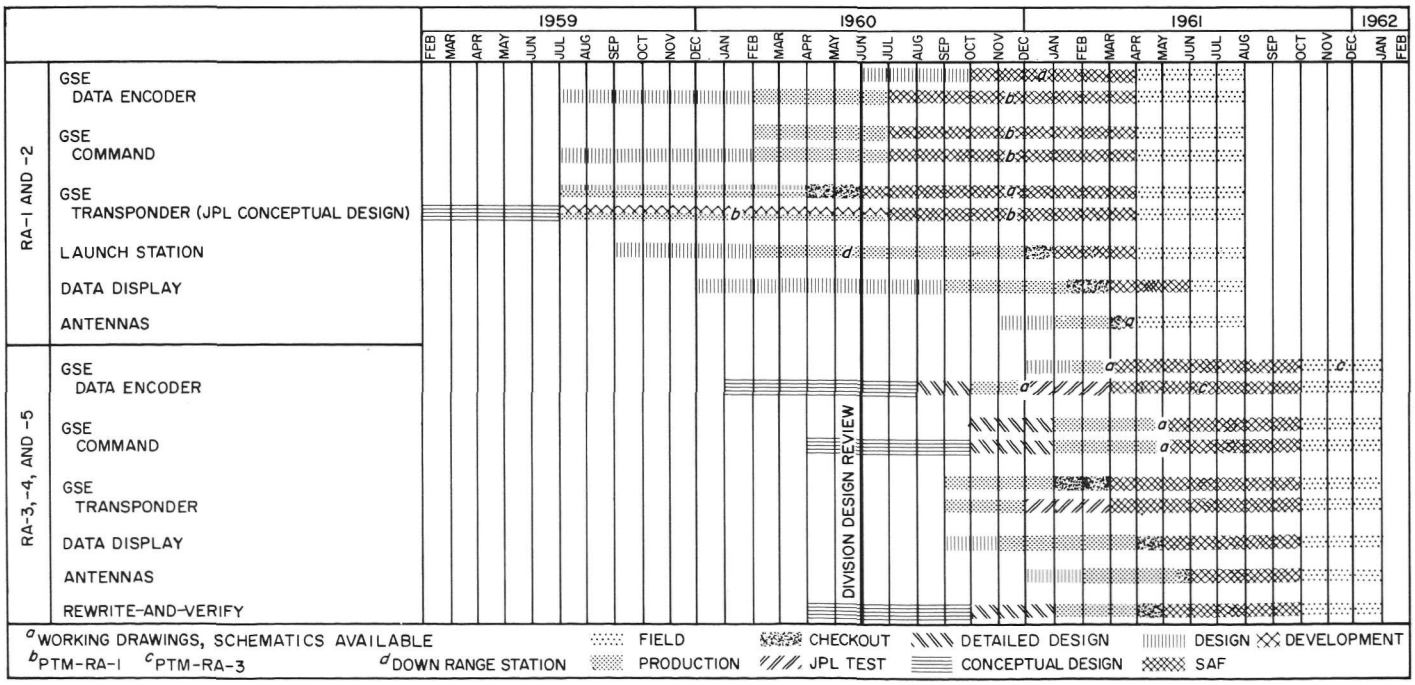

Figure 140. Telecommunications support of *Ranger* Project

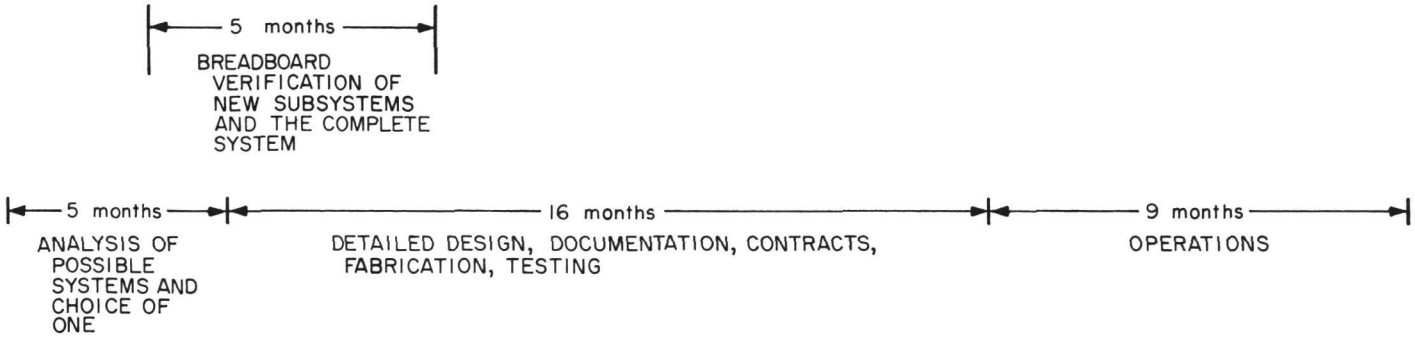

Figure 141. Condensed schedule of instrumentation operations

(1) Communicate commands from the designated command decision location to the recipient spacecraft subsystems.

(2) Telemeter certain engineering parameters and scientific phenomena from the spacecraft to designated ground locations.

(3) Track the relative motion of the spacecraft with respect to designated coordinate systems to enable the Central Computing Facility to compute the parameters of the spacecraft trajectory as a function of time.

The telecommunication equipment required to perform these functions is comprised of the following subsystems:

(1) Spacecraft command subsystem, ground support equipment, and the ground command subsystem.

(2) Spacecraft radio and associated ground support equipment.

(3) Spacecraft telemetry and associated ground support equipment.

(4) Ground telemetry as required for data acquisition and reduction.

(5) Launch stations—R-F Trailer and Telemetry Trailer.

The relationship of subsystem components to the over-all communications system is shown in Figure 142. The launch station may be considered as an appendage to the Ground Telemetry System required for data acquisition.

b. Data encoder. The data encoders for RA-1 and -2 and for RA-3, -4, -5 were quite similar in over-all concept. They differed in the design detail required to implement the respective channel assignments.

RA-1 and -2 design concepts. The telemetry data requirements for the RA-1 and -2 spacecraft are indicated in Table 44. In Part A, there were approximately 36 engineering measurements divided between attitude control, the power system, telecommunications, and the spacecraft environment. In Part B, there were 9 scientific measurements.

The telemetry data encoding plan used to implement these requirements is shown in Figure 143. Channel 1 carried 400-cps for timing and synchronization purposes. It was also the event channel and recorded event pulses as they were generated in the spacecraft. Channels 2 and 3 carried engineering information which required some type of signal conditioning and commutation because all of the measurements were time multiplexed. The rest of the channels were specially designed to handle the scientific measurements shown.

Two types of frequency-multiplexed channels were used to provide maximum communication efficiency for each of two types of data characteristics. Channel 2 carried only three measurements at 1 sps in order to provide adequate frequency response for data analysis. Channel 3 carried measurements where frequency response was unimportant.

The system also required the use of two types of subcarrier oscillators. Analog types were used on Channels 2, 3, 4, and 7.7; whereas, the remaining units (Channels B-10, B-11, B-12, and B-13) were binary oscillators. That is, they were designed to operate at either one of two frequencies in order to accept the two-state information from the scientific packages. The binary data was prepared in parallel-serial form by the scientific instrument electronics, and modulated the binary channels, which had a low frequency deviation. Subsequently, this binary data was reconstructed by the ground discriminators into binary pulse data in the form originally presented to the flight encoder.

The spectral relation for these channels is shown in Figure 144. The power allocated to each was a departure from the concepts used on previous space programs. On

Table 44. RA-1 and -2 telemetry data requirements

System	Measurement	Time between commutated samples, sec	Required coverage distance, km	
			Transponder	Beacon
Part A, Engineering measurements				
Telecommunication	Transponder static phase error, coarse	10	1.6×10^6	5.3×10^4
	Transponder static phase error, fine	100		
	Transponder AGC, coarse	10		
	Transponder AGC, fine	100		
	Transponder local oscillator drive	1000		
	Transponder plate voltage	1000		
	Transponder power out	1000		
	High-gain antenna drive	100		
	Low-gain antenna drive	1000		
	Transponder temperature	1000		
Power	Primary system voltage	1000	1.6×10^6	5.3×10^4
	Primary system current	1000		
	Converter voltage, attitude control	1000		
	Converter voltage, controller	1000		
	Converter voltage, data encoder	1000		
	Solar panel 4A9 current	1000		
	Solar panel 4A10 current	1000		
	Solar panel 4A9 temperature	1000		
	Solar panel 4A10 temperature	1000		
	Launch back-up battery temperature	1000		
	Case I temperature	1000		
	Solar cell open circuit voltage	1000		
	Solar cell short circuit current	1000		
Attitude control	Pitch rate gyro	10	1.6×10^6	5.3×10^4
	Yaw rate gyro	10		
	Roll rate gyro	10		
	Roll position	10		
	Pitch position	10		
	Yaw position	100		

System	Measurement	Time between commutated samples, sec	Required coverage distance, km	
			Transponder	Beacon
Part A, Engineering measurements				
Altitude control	Gas bottle pressure	1000	1.6×10^6	5.3×10^6
	Gas bottle temperature	1000		
	Light detector	100		
	Earth sensor temperature	1000		
	Case IV temperature	1000		
Controller	Events	Blips		
General	Friction experiment	10		
Data encoder	Synchronization, Rate 1	100		
	Synchronization, Rate 2	1000		
	Synchronization, Rate 3	1000		
	Temperature bridge calibration	1000		
	Channel 2 mid-band reference	10		
	Channel 3 mid-band calibration	100		
	Channel 3 high-band calibration	1000		
	Channel 3 low-band calibration	1000		

Measurement	Type of data	Channel No.	Required coverage distance, km	
			Transponder	Beacon
Part B, Scientific measurements				
Magnetic field intensity	Analog (continuous)	7.7	1.6×10^6	5.3×10^4
Magnetometer temperature	Analog (sampled every 1000 sec)			
Lyman-alpha telescope	Analog (continuous)	4	9.7×10^5	—
Solar corpuscular detectors	Binary (4 bits/sec maximum)	B-11, B-12, B-13	1.6×10^6	5.0×10^4
Semi-conductor detectors				
Ionization chamber				
Triple coincidence telescopes				
Micrometeorite detector				
Vela Hotel experiment	Binary (1 bit/sec maximum)	B-10		

Explorer I and *Pioneer IV*, the power was divided among the channels to reach threshold at approximately the same time, regardless of its importance to the system. On the *Ranger* spacecraft, power was allocated according to the importance of the various channels as a function of time. The extreme case of power allocation per channel is shown on the quarter-watt beacon. At a given point in time, when the engineering measurements were near

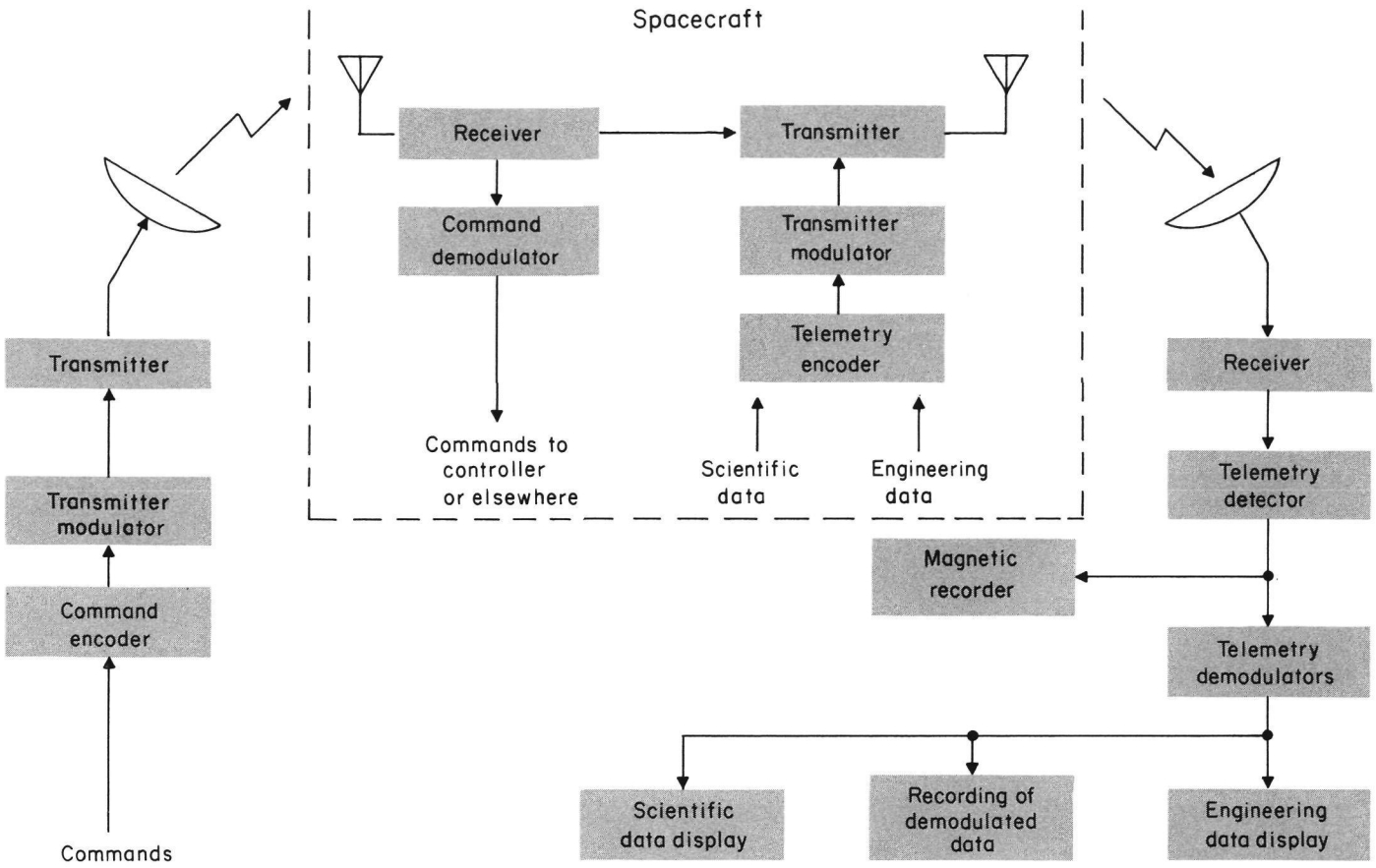

Figure 142. Command and telemetering system

threshold in signal-to-noise ratio, the scientific measurements were switched off and all available power, and associated bandwidth, was allocated to Channels 1 and 3. This can be seen by referring again to Figure 143.

Special design problems. The RA-1 and -2 spacecraft telemetry subsystem was designed to perform the functions of transducing, signal conditioning, commutation, encoding, and modulation.

The first two functions were quite straightforward and were accomplished through well-known telemetry techniques. Some problems were encountered in temperature transducers, but these were principally because of manufacturing errors rather than problems in theory.

Commutation was quite a different problem. In assembling the RA-1 data encoder, it was necessary to use hardware and techniques which were available commercially or at JPL. Because of this requirement, a mechanical commutator was selected as the heart of the commutation scheme, as shown in Figure 145.

The commutator selected (Fig 146) was a commercially available unit. However, it was not properly designed for use in spacecraft work and each unit flown had to be modified significantly before satisfactory operation was attained. Some of these modifications follow:

(1) Hermetically sealing the unit.

(2) Use of gold-plated contacts.

(3) Development of lubrication-free bearings.

(4) Use of nylon gears rotating on stainless steel shafts to replace brass gears, which froze together under vacuum.

(5) Modification of the electrical drive system to operate within the spacecraft power limits.

(6) Modification of the drive circuitry to avoid stepping with noise pulses.

Most of these modifications were incorporated to resolve particular problems which were encountered during or subsequent to RA-1 PTM testing.

The commutator operation, shown in block diagram form in Figure 145, is similar to that of an odometer in an automobile. That is, Deck A is advanced at a rate of

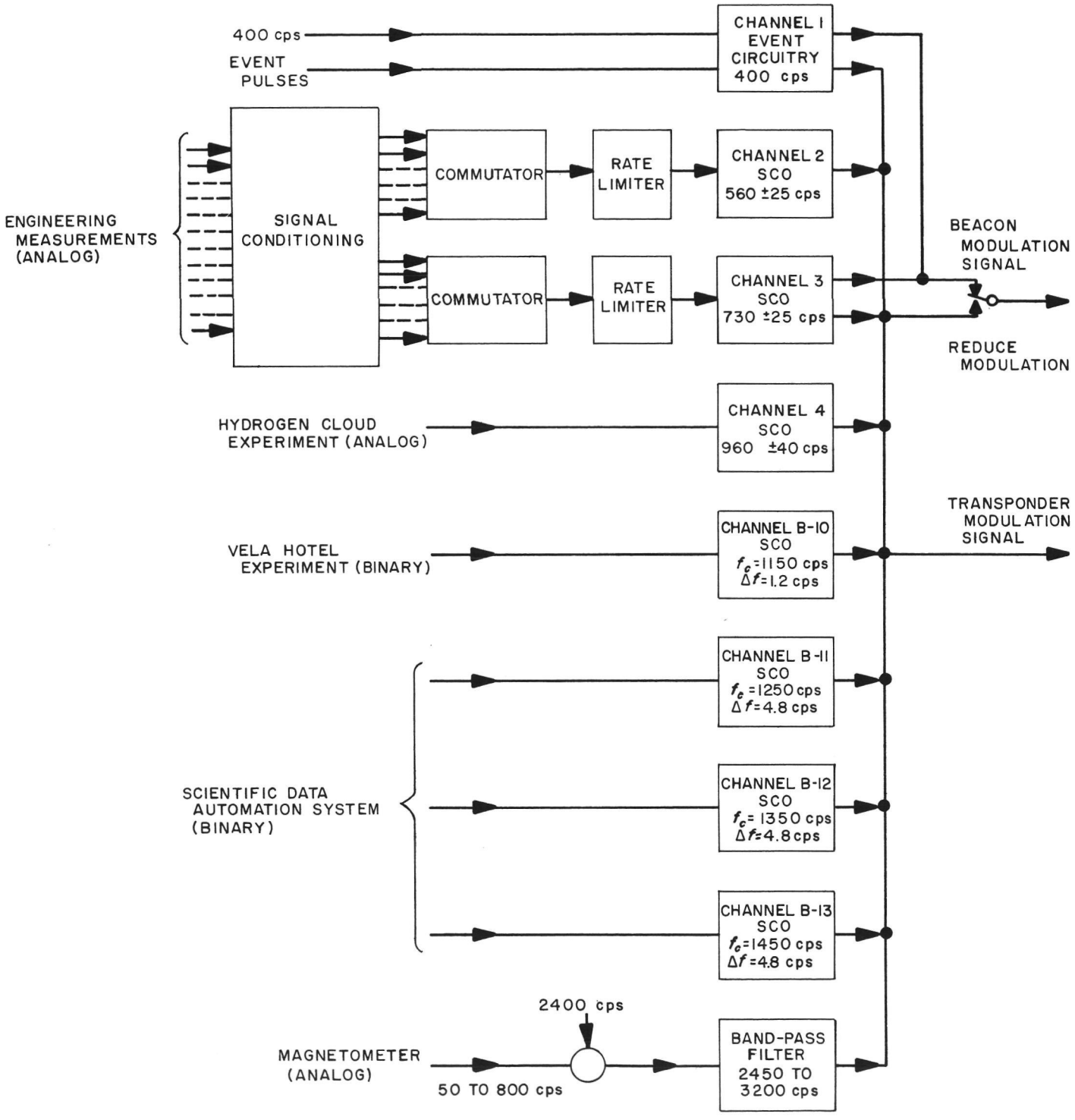

Figure 143. RA-1 and -2 data encoder, block diagram

one position per sec and it completes one revolution every 10 sec. Deck B is advanced one position for every complete rotation of Deck A and completes one revolution every 100 sec. Decks C, D, and E are pinned together and simultaneously advance one position for every rotation of Deck B.

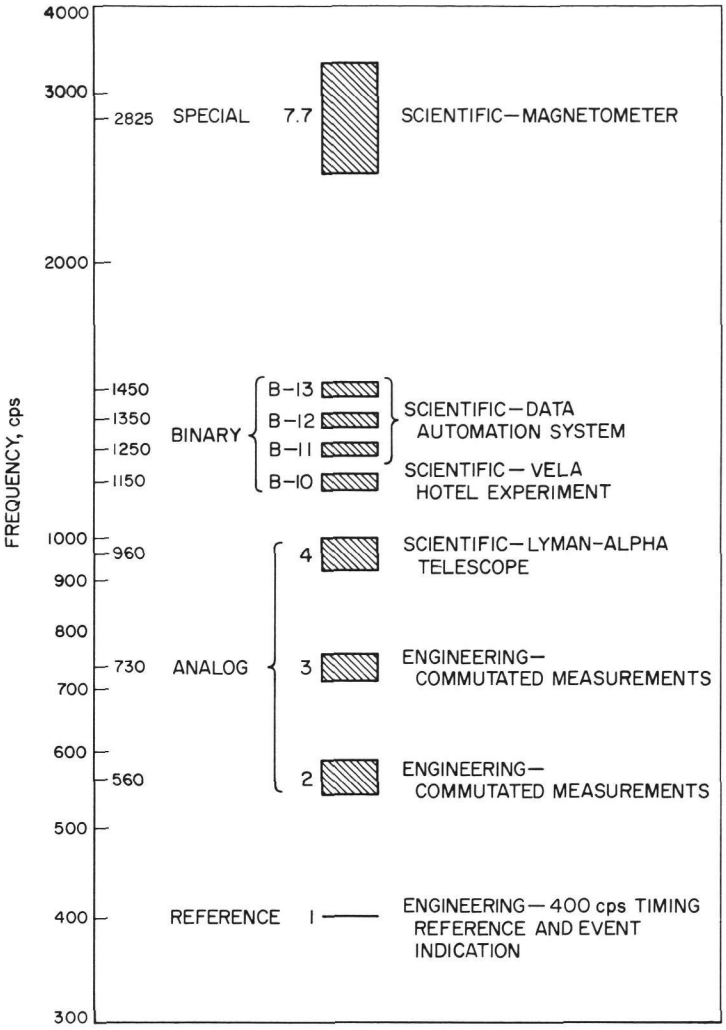

Figure 144. Spectral relationships for RA-1 and -2 telemetering subcarriers

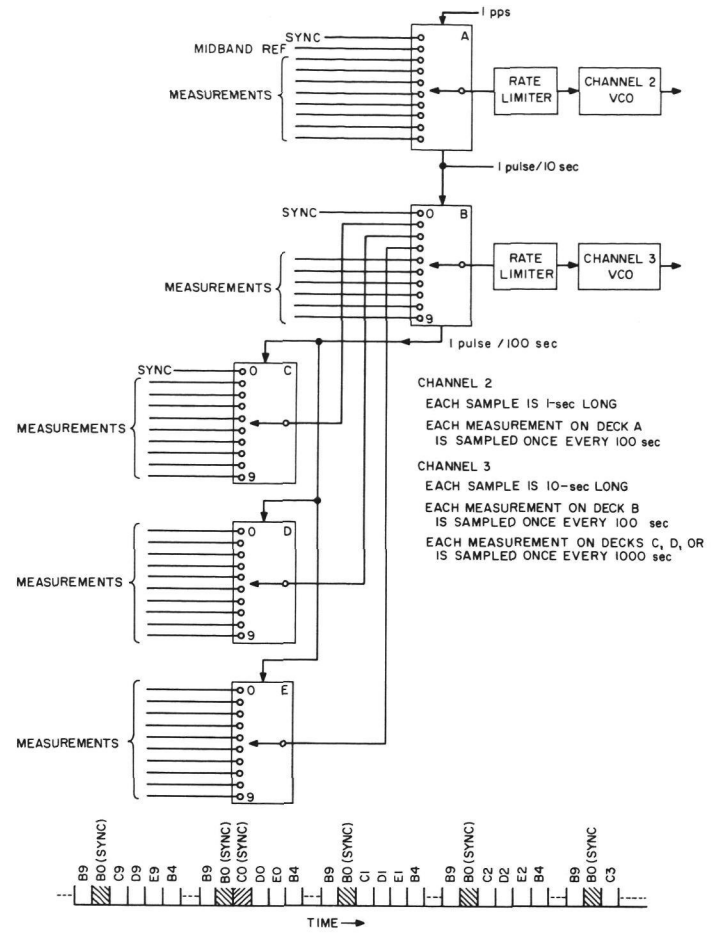

Figure 145. Commutation on Channels 2 and 3

With this type of operation, the principal problem was in the generation of a synchronization scheme which could be used on the ground for automatic data reduction. This was accomplished through use of sync tones supplied to the system as shown in Figure 145. Channel 2 is a simple example of the system since sync appears once every 10 sec and quickly identifies the segments in Deck A.

Segment location on Channel 3 is somewhat more complex in that the sync tone on Deck C appears only once every 1000 sec. However, once it appears the position of the commutator is uniquely determined and the automatic data reduction equipment can be locked up.

Operation of the aforementioned system requires the use of a sync-tone generator and a sync-sense relay amplifier. The sync-tone generator consisted of three

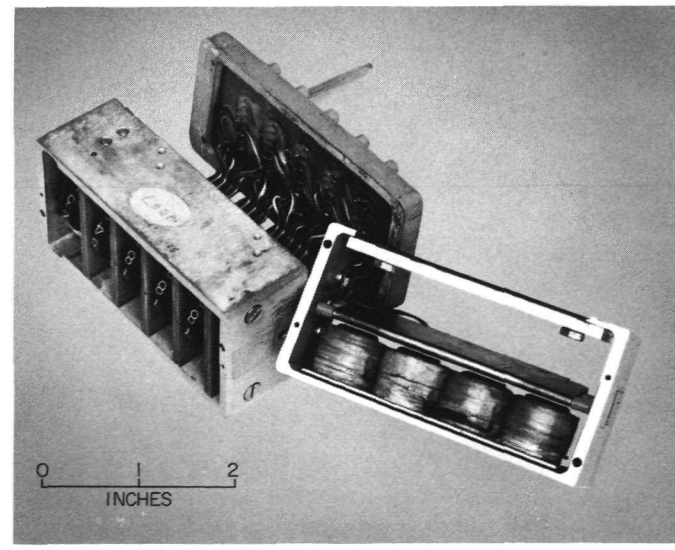

Figure 146. Mechanical commutator

stable, low-frequency oscillators and provided tones at 18, 24, and 30 cps, respectively.

The sync-sensor relay amplifier had the task of sensing when the mechanical commutator is switched to the sync contact. Since there were three different commutator deck rates, three separate sync sensors were required. These were all packaged in a single module, as shown in Figure 147.

The principle of operation of the sync sensor is as follows: A high-frequency transistor oscillator is held in a non-oscillating state except when a small capacitor is switched from emitter to ground (of the grounded base transistor). This increases the gain of the transistor stage, which starts its ocillation. The output from the oscillator is then rectified, amplified, and used to close the sync tone relays (Fig 148). The relay then ties the output of the sync-tone oscillator to the appropriate VCO.

Rate limiter development. In order to obtain satisfactory threshold performance phase-locked-loop (PLL) subcarrier discriminators were used in RA-1 and RA-2 telemetry. The nature of the PLL discriminator is such that when the loop bandwidth is designed for good threshold performance, the discriminator cannot maintain lock if there is a large step change in the input frequency. This restriction regarding step changes in data complicates the problem of mechanizing commutated measurements. Calculations show that the shortest discriminator settling time compatible with satisfactory threshold performance is achieved if the commutated data is modified before transmission such that successive sample levels are approached at a selected constant rate rather than in discrete steps.

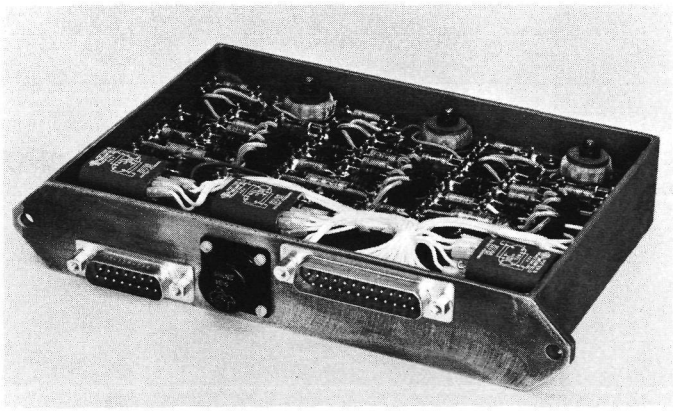

Figure 147. Sync sensor relay amplifier

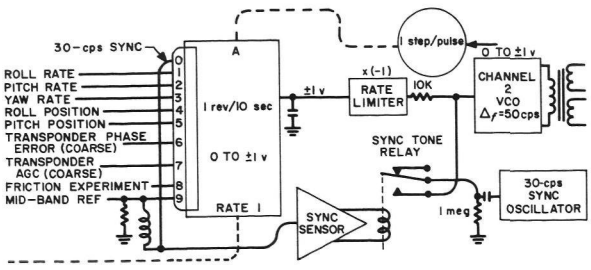

Figure 148. Sync sensor schematic

The device used to accomplish this task is called a rate limiter. A block diagram of a rate limiter is shown in Figure 149. Since no commercially available rate limiter was known to exist a JPL design became mandatory. To design a satisfactory rate limiter, three basic approaches were pursued. The first approach utilized only passive elements; the second approach utilized controlled constant-current generators; and the third approach utilized operational amplifiers.

Passive rate limiter designs are suited to accomplishing the transitions in a fixed time at a rate not to exceed the selected rate rather than at the fixed selected rate. Three of the passive circuits which were evaluated are shown in Figure 150. Each of these circuits performs satisfactorily if the load impedance is much larger than the network characteristic impedance. The use of these circuits without the addition of other components, such as diodes, requires that critical damping be used to achieve optimum results. However, if diodes are used, then a circuit which possesses some overshot can be employed, resulting in a good approximation to the ideal rate limiter. The diode is used as a feedback element around the filter network to clip the output waveform when its amplitude reaches that of the input (Fig 151). Two such networks must be connected in cascade to properly shape both positive and negative step inputs. Unfortunately the size of this type of unit was prohibitive at the slow rates required.

The second basic design approach utilized controlled-current generators. A schematic of this circuit, in its current state of development, is presented in Figure 152. Q1 and Q2 are current generators which, depending on the voltages across CR1 and CR2, coordinate to increase, hold, or decrease the charge on capacitor C1. When the current generated by Q2 is adjusted to be twice the current generated by Q1, the output of this circuit approaches the input at a constant rate. This circuit has operated satisfactorily, but it has the disadvantage that the signal input source impedance must be less than 100 ohms.

The third approach to designing a rate limiter utilized operational amplifiers. A block diagram of the operational

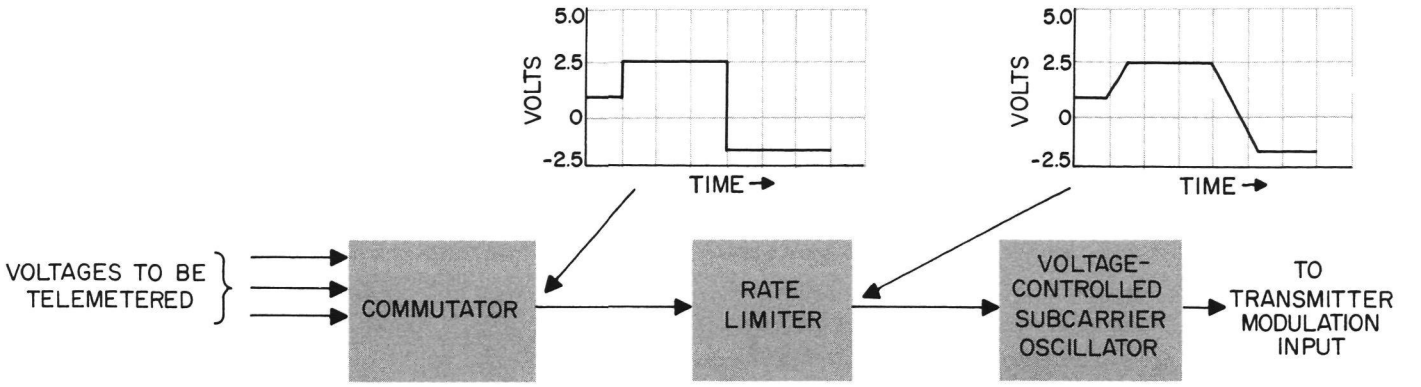

Figure 149. Block diagram of commutated measurements

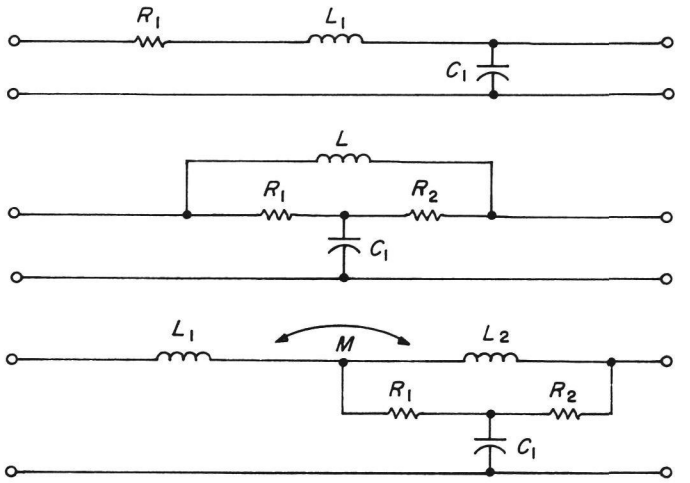

Figure 150. Passive rate limiters

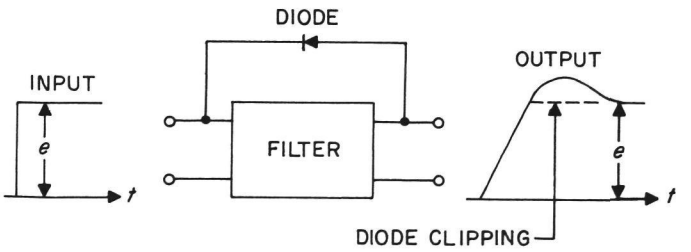

Figure 151. Passive rate limiter with diode clipping

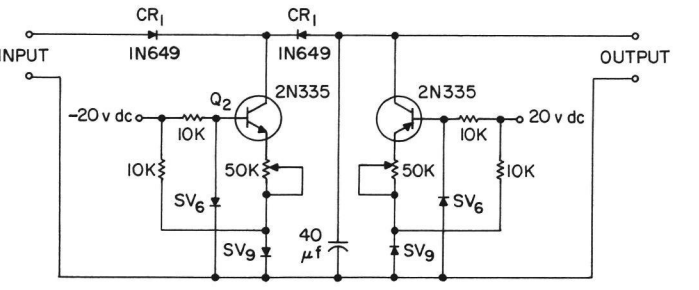

Figure 152. Current generator rate limiter

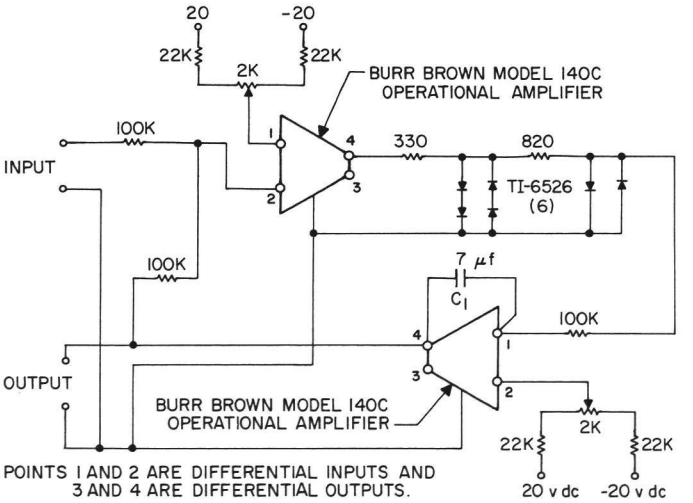

Figure 153. Operational rate limiter

rate limiter is presented in Figure 153. This circuit is composed of three basic elements: an operational summing amplifier, a bi-polar amplitude limiter, and an operational integrator. The operational summing amplifier gain is selected so that an output error greater than 0.1% of the input range will cause the amplitude limiter to saturate. The integration of the constant voltage output of the amplitude limiter causes the output voltage to approach the input voltage at a constant rate. This circuit has demonstrated good performance. The input impedance is 100K ohms and the output impedance is less than 100 ohms. This circuit was eventually used on RA-1 and -2.

Voltage-controlled oscillator. The problems attendant on building a quality, transistorized, voltage-controlled

oscillator (VCO) led to a 3-year JPL study of such devices, from 1956 to 1959. Unfortunately, most of the units tested proved to be undesirable. In late 1959, however, several excellent VCO's became available, and of these, a unit was selected for *Ranger* spacecraft use.

The VCO selected (Fig 154) was a proprietary design of Teledynamics, Incorporated, and exhibited very stable operating characteristics under a wide latitude of supply voltage, set range, set output voltage, set zero point, and temperature.

In spite of its advantages, the VCO developed severe drift problems during life tests at JPL. Some units exhibited as much as 15% drift in 1 week and indicated a stabilizing tendency only after that period time.

This peculiar drift characteristic was discovered too late for modification on RA-1 and -2 and was overcome only through use of in-flight calibration of the VCO's.

In 1960, Bendix Pacific produced a VCO which seemed to have all of the desirable characteristics of the Teledynamics unit plus stability over a long life test. It was, therefore, decided that Bendix oscillators would be used on all *Ranger* flights after RA-2.

Data encoder, RA-3, -4, and -5. The data encoder for RA-3, -4, and -5 used extensions of techniques developed for RA-1 and -2. It is essentially an analog system using frequency multiplexed subcarrier oscillators. When data was to be telemetered in binary form a narrow deviation, two-state subcarrier oscillator was used.

A simplified block diagram of the data encoder is shown in Figure 155. This system is packaged on printed wiring boards and installed in magnesium modules very similar to those used in RA-1 and -2. A list of the major components comprising the data encoder and an estimate of their weights are given in Table 45.

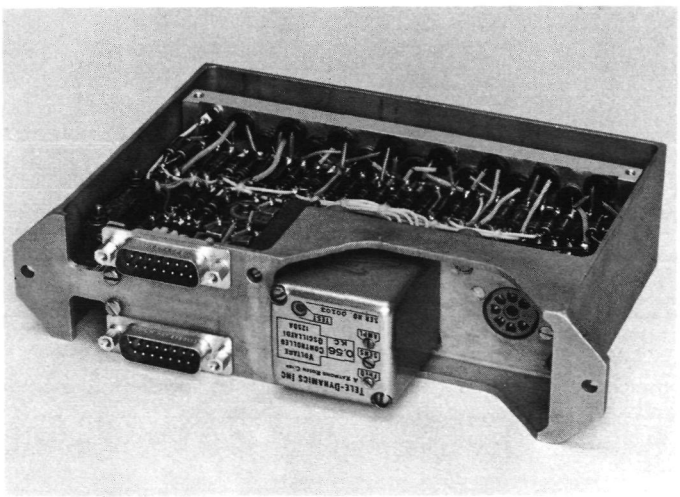

Figure 154. Voltage-controlled oscillator

Table 45. Component list, data encoder RA-3, -4, and -5

Component	Estimated weight, lb
VCO module I	1.6
VCO module II	1.3
VCO module III	1.6
Commutator I	1.1
Commutator II	1.2
Commutator III	1.2
Commutator IV	1.2
Temperature bridge I	1.2
Temperature bridge II	1.3
Signal conditioner I	1.3
Signal conditioner II	1.2
Binary oscillator	1.2
Modulation mixer	1.2
Data selector	1.2
Transducers	4.0
Cables	4.5

A total of 87 engineering and scientific measurements was planned to be telemetered by the data encoder. A list of these measurements and their ranges is given in Table 46. Not all these measurements are telemetered at all times during the mission. Some measurements are switched out and replaced by others during particular portions of the flight. There are five such conditions or modes for these rounds. They are as follows:

Mode I. Launch to start of midcourse maneuver; duration of this mode is about 16.5 or 40.5 hr. (This variation is due to possible midcourse maneuver during the second Goldstone tracking period.)

Mode II. Midcourse maneuver phase; high-gain antenna not used; duration of this mode is about 40 min.

Mode III. Includes post midcourse maneuver acquisition to terminal maneuver; duration of this mode is about 47 hr.

Mode IV. Scientific instrumentation from end of terminal maneuver to capsule ejection; duration of this mode is about 30 min.

Commutator design problems. Two basic types of switches that were considered for RA-3, -4, -5: (1) a solid-

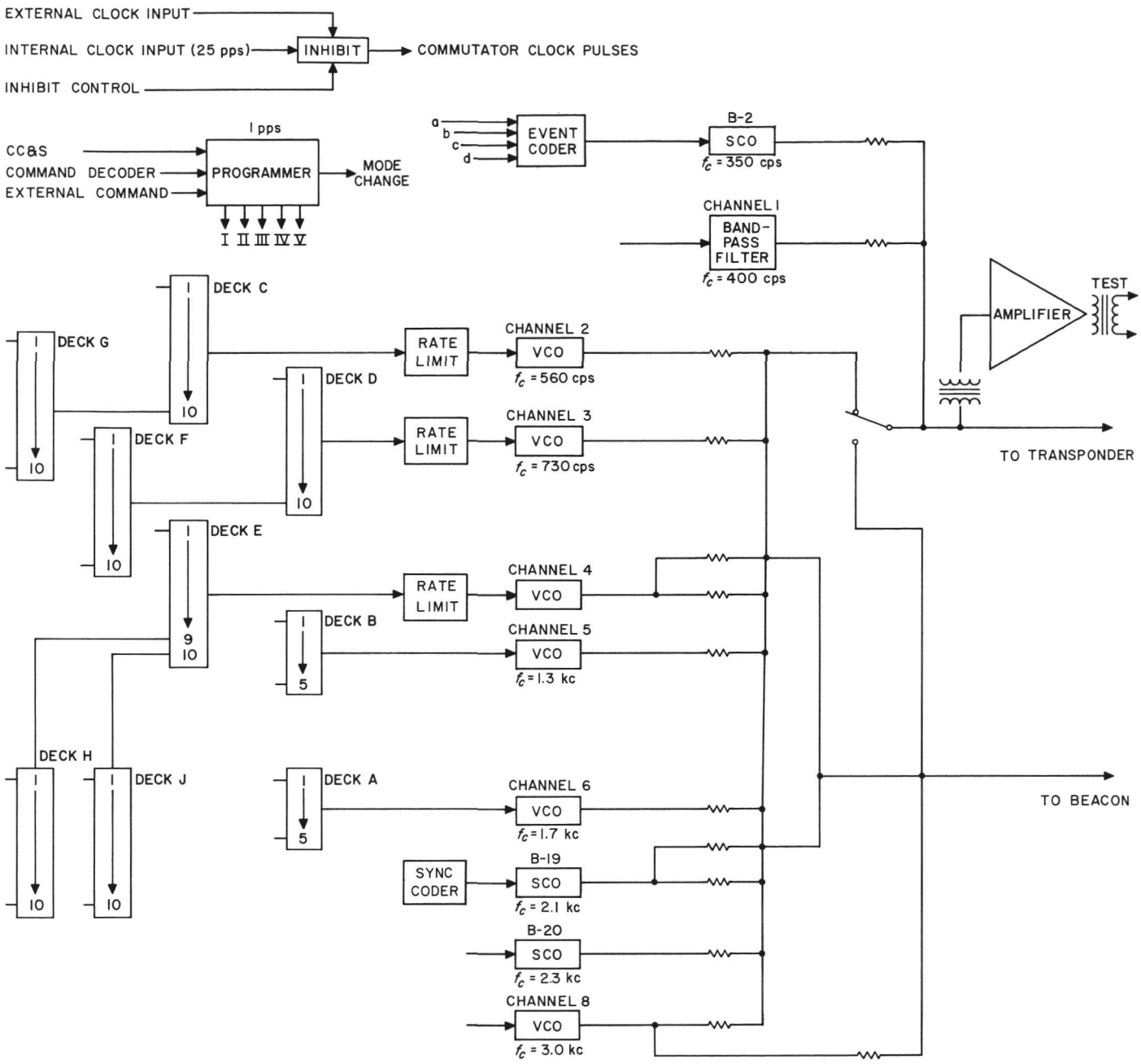

Figure 155. Data encoder

state type either using diode or transistor gates, or (2) a mechanical switch. The solid-state type of switch is preferred for high-rate sampling or applications where extremely long life is required. However, this type of switch is rather expensive, requires a large number of components and, because of the complexity, may be less reliable for short flights, at least initially.

Considering the metal-to-metal contact switch, there are three general types of commutator construction. These are:

(1) Motor-driven rotating-brush mechanism.

(2) Pulsed stepping switch.

(3) Sequenced drive of crystal can relays.

The first two are undesirable from a size, weight, and power consumption basis and are difficult to operate reliably for long times in a space environment. The third is the mechanization that was used to multiplex the inputs to the *Sergeant* flight-monitor supplement, analog-to-digital encoder. This type requires a rather large number

Table 46. Telemetering measurements, RA-3, -4, and -5

System	Measurement	Range	System	Measurement	Range
Attitude control	Pitch rate gyro, coarse	±1500 deg/hr	Attitude control	Nitrogen tank temperature	−25 to 165°F
	Yaw rate gyro, coarse	±1500 deg/hr		Pitch Sun sensor output	±0.9 deg
	Roll rate gyro, coarse	±1500 deg/hr		Yaw Sun sensor output	±0.9 deg
	Yaw gyro torquer	±0.4 deg/sec		Antenna hinge angle	0 to 180 deg
	Pitch gyro torquer	±0.4 deg/sec		Earth sensor temperature	±100°F
	+*y* yaw jet vane angle	±25 deg		Differential Sun sensor temperature	±36°C
	−*y* yaw jet vane angle	±25 deg		+*y* Pitch Sun sensor temperature	+14 to +140°F
	+*x* pitch jet vane angle	±25 deg		−*y* Pitch Sun sensor temperature	+14 to +140°F
	−*x* pitch jet vane angle	±25 deg			
	Roll gyro torquer	±0.4 deg/sec			
	Roll earth sensor output	±2.5 deg	Central computer and sequencer	400 cps	±1 cps
	+*y* yaw jet vane actuator temperature	0 to 500°F		CC&S program	Event
	Hinge earth sensor output	±2.5 deg		Midcourse velocity increment	0 to 204.7 ft/sec
	−*y* yaw jet vane actuator temperature	0 to 500°F		Midcourse acceleration	0 to 25 pps
	Pitch switching amplifier output	±12.5 v dc	Central power	Power system voltage	18 to 31 v dc
	+*x* pitch jet vane actuator temperature	0 to 500°F		+*x* solar panel current	0 to 5 amp
	Yaw switching amplifier output	±12.5 v dc		−*x* solar panel current	0 to 5 amp
	−*x* pitch jet vane actuator temperature	0 to 500°F		Solar cell short circuit	0 to 0.2 amps
		±12.5 v dc		Solar cell open circuit	0 to 0.25 v dc
	Pitch rate gyro, fine	±62 deg/hr		Power system current	0 to 10 amp
	Yaw rate gyro, fine	±62 deg/hr		+*x* solar panel voltage	20 to 35 v dc
	Roll rate gyro, fine	±62 deg/hr		−*x* solar panel voltage	20 to 35 v dc
	Earth sensor light intensity	0.01 to 17 ft/candles		+*x* solar panel temperature, front	+45 to +145°F
	Nitrogen tank pressure	0 to 3500 psia		+*x* solar panel temperature, back	+45 to +145°F
Central power	−*x* solar panel temperature, front	±200°F		−*x* solar panel temperature—front	+45 to +145°F
	−*x* solar panel temperature, back	±200°F		−*x* solar panel temperature—back	+45 to +145°F
	Power converter, a/c	0 to 4.5 v dc			
	Power inverter data encoder	0 to 4.5 v dc			
	Power converter command	0 to 4.5 v dc			
	Power inverter scientific	0 to 4.5 v dc	Communications	Receiver AGC, fine	2.0 to 4.5 v
	Power boost regulator temperature	0 to 200°F		Transponder high-voltage supply	0 to 250 v
	Power converter temperature	0 to 200°F		Receiver mixer current	0 to −0.10 v dc
	Power inverter, 400 cps, 1 phase	0 to 4.5 v dc		Commutator sync	
	Power converter, 3-phase inverter	0 to 4.5 v dc		Command system output	17 bits
	Battery temperature, main	32°F to 158°F	Scientific	Gamma-ray experiment temperature	+32 to-109°F
	Switching and logic temperature	0 to 200°F		Gamma-ray boom extension	Event
Midcourse propulsion	Midcourse motor chamber temperature	0 to 2000°F		Gamma-ray intensity	±2.5 v
	Fuel tank temperature	−25 to 165°F		Vidicon output	0 to −2 v
	Helium tank pressure	0 to 3600 psia	Miscellaneous	Capsule ignition	Event
	Fuel tank pressure	0 to 460 psia		Solar panel extension	Event
Communi-cations	Receiver AGC, coarse	−2.0 to 5.5 v		Gyro temperature	0 to 70°C
	Receiver phase error, fine	0 to 0.5 v		Temperature control temperature	−25 to +165°F
	Receiver phase error, coarse	±1.5 v		Altimeter echo strength	±2.5 v
	Transponder temperature	+14 to 158°F		Squib fire	Event
	Low-gain antenna drive	0 to +0.5 v dc		8-mm antenna extension	Event
	High-gain antenna drive	0 to +0.5 v dc		Tele mode indication	±0.5 v
	Transponder r-f drive level	0 to 0.5 v			

CONFIDENTIAL

of components as compared to the first and second method.

One JPL approach to the multiplexer problem was to use magnetic latching relays which operate from pulses that transfer the armature from one contact to another. In a multiplexer there is an obvious advantage in using the latching type relay at low sampling rates. With the conventional pull-in type of relay, the average power consumption is independent of the sampling rate. With the latching relay, power is required only at the transfer times, and the average power will reduce with the clock rate. Also, since the relay is a bistable device, it has the inherent binary memory properties of a flip-flop circuit. Since much of the circuitry required to sequence the relays consists of logical memory, the possibility of implementing both the sequencing logic and the switch with the relay results in a considerable reduction in the total number of components required for a relay multiplexer, when contrasted with electronic sequencing using semiconductor circuits.

Operation of the magnetic latching relay is shown in Figure 156. Application of a positive voltage on Pin 1 (with respect to Pin 5) will close the relay as shown. When the voltage is removed, the relay will remain in this position. However, if a positive voltage is now applied to Pin 10 (with respect to Pin 9), the armature will transfer to the opposite position and remain there even if the voltage is removed.

Design of this relay multiplexer avoids the condition known as *relay hazard* in which the armature may vibrate as in the doorbell circuit. This is caused by attempting to transfer the armature of a relay by a current through its own contacts. Since the excitation current is lost as soon as the contacts open, the armature may never transfer but rather just vibrate. This condition is avoided by use of a two-phase clock to separate in time the gating function of the relay and the alteration of its state.

The multiplexing scheme for RA-3, -4, and -5, using magnetic latching relay commutators is shown in Figure 157. Each deck is comprised of 10 inputs; since more than one deck at each sampling rate is required, relays are operated in parallel, thus gaining two additional signal decks with one additional set of relays. This is called double-deck operation.

Figure 158 gives the data interconnections of one deck of the multiplexer. Only nine relays are required for a deck with 10 inputs and, thus, 18 relays are required for a double deck comprised of 30 inputs. This comes about because each relay has two poles; since only one set of

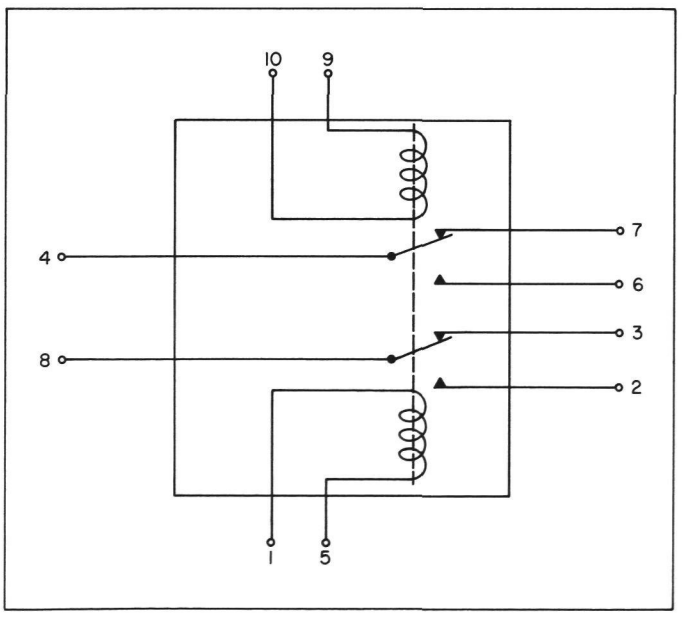

Figure 156. Magnetic latching relay detail

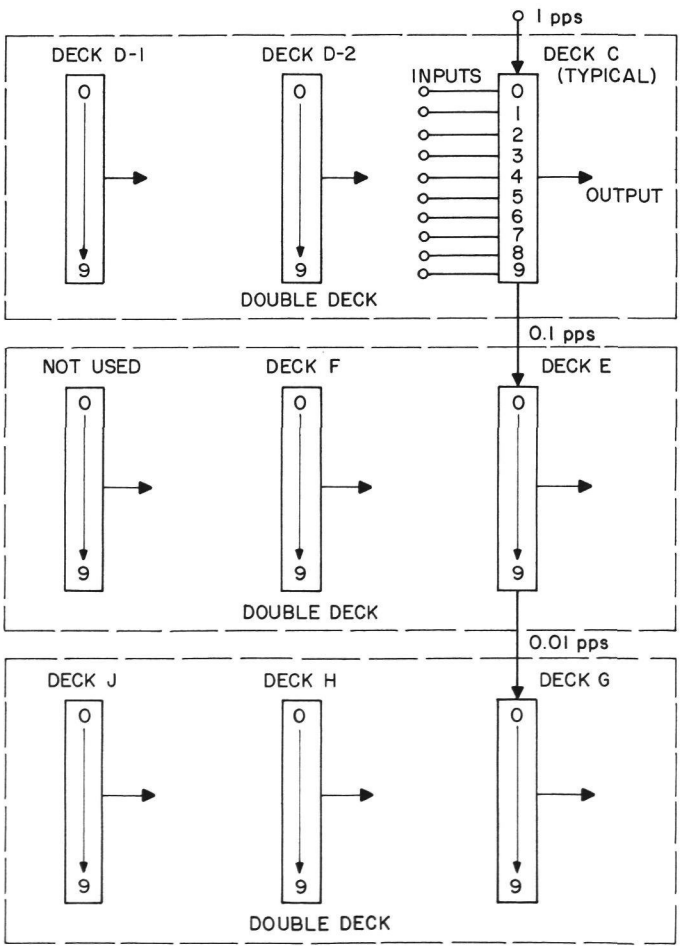

Figure 157. Multiplexing scheme

CONFIDENTIAL

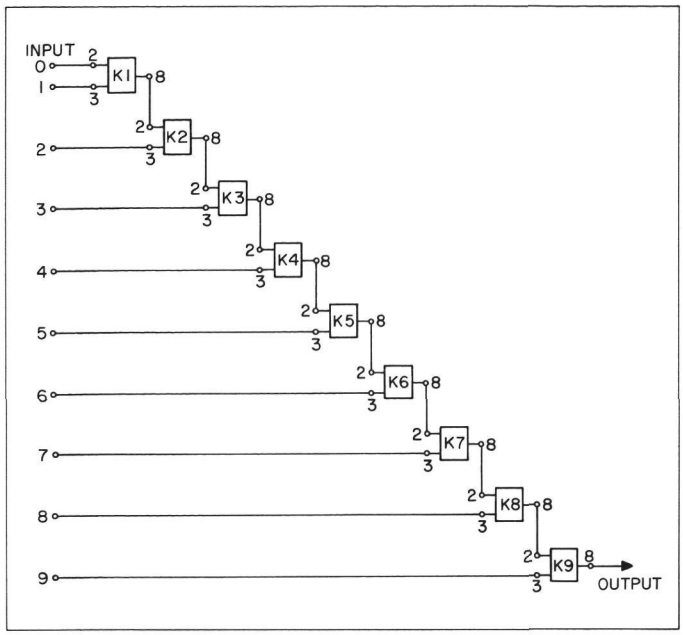

Figure 158. Relay commutator data interconnection

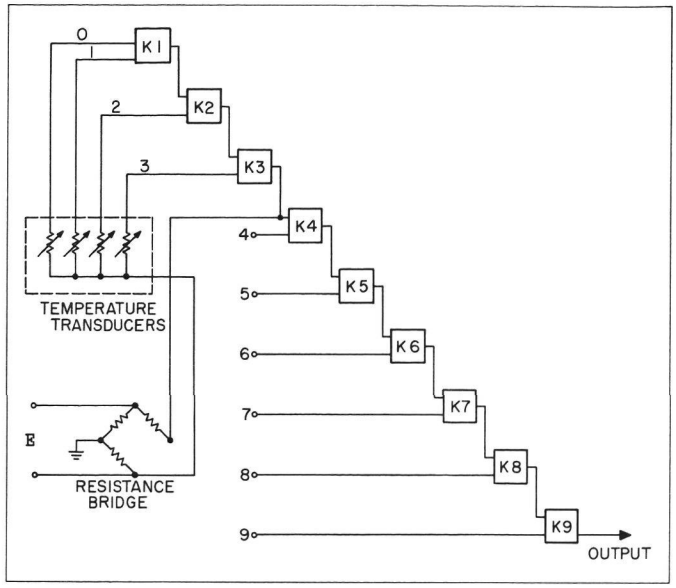

Figure 159. Data interconnection for reducing signal conditioning

poles is required for logic, three data inputs are available from double-deck operation.

If a specific signal conditioning requirement is not common to all measurements on a particular deck, the tree-type interconnection offers a possible reduction in the amount of signal conditioning circuits. The method shown in Figure 159 is used in four decks of the RA-3, -4, and -5 multiplexer to enable both temperature and voltage measurements to be sampled with one deck.

The double-deck relay commutator (Fig 160) is packaged into a standard spacecraft module, with a double deck occupying both sides of the module. This design has successfully passed the *Ranger* TA tests.

Since the latching relays as procured are sealed and inspection of their quality is not possible, JPL has initiated a 100% visual inspection at the relay manufacturer prior to canning the units. This inspection is performed by JPL or JPL contractor personnel using 20-power microscopes.

Electrical and mechanical characteristics of a double-deck unit are given in Table 47. The quiescent power consumption for the double deck is approximately 50 mw and is supplied by the −20-v source. During the transient periods at the reception of the clock pulse, the maximum required peak power from the 20-v supply is approximately 5 w. However, this power is required for only a short duration of time (10 msec) as compared to the clock period (1-sec minimum). Therefore, through simple RC integration of the supply current, the peak loads may be reduced considerably. A peak power of 67 mw from the +20-v supply is required by a double-deck commutator using a simple RC network.

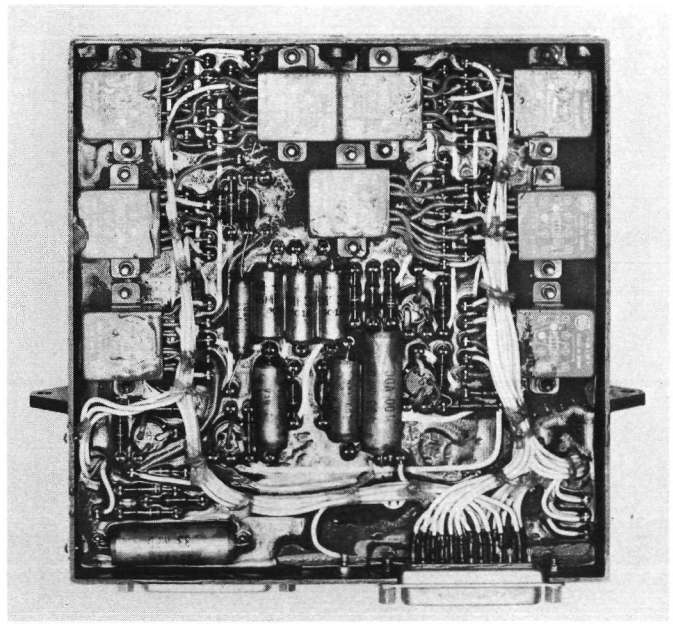

Figure 160. Data encoder

Sampling switch. An important part of the data encoding system is the device that samples the data, which is commonly called the commutator or sampling switch. One

Table 47. Relay commutator characteristics

Parameter	Dimension
Input trigger pulse	
Input resistance, ohms	15K (min)
Voltage, v	5
Rise time, μsec	<50
Width, μsec	>800
Source resistance, ohms	<100
Output trigger pulse	
Voltage, v	>5
Rise time, μsec	<50
Width, μsec	<800
Synchronizing pulse output	
Voltage, v	−6
Rise time, μsec	<1
Duration	1 segment
Peak power requirements	
+20-v dc supply, mw	67
−20-v dc supply, mw	50
Weight of double deck (including module), lb	1.7
Size of module, in.	6.2 × 6.0 × 1.2

type of commutator used in the RA-3 is a commutator using magnetic latching relays and is used for the majority of measurements on RA-3, -4, and -5. Another type that is used for higher sampling rates where relay life is a limiting factor, is called a solid-state commutator. This type uses transistors as switches which are turned on in sequence by an electronic ring counter.

The solid-state commutator used in RA-3, -4, and -5 has two decks, each with five gates. A block diagram of this unit is shown in Figure 161. The five-stage ring counter is stepped by the input clock pulses. As the counter sequences, each stage, in turn, causes a gate to be closed. An a-c voltage of about 30 kc is thus gated to the data switches, where it is then rectified and used to close this switch. The use of an a-c voltage allows transformer coupling to the data switch and permits high d-c isolation between the gating signal and the data signal. The output trigger occurs once per frame or once every five input pulses. This trigger is used to pulse other commutator decks operating at slower rates. A photograph of this device is shown in Figure 162.

Rate limiter. Data encoders for *Rangers* RA-1 through -5 incorporate a rate limiting signal conditioner for PAM relay–commutated data. This was required to perform three important functions:

(1) To limit the rate of change of voltage step inputs.

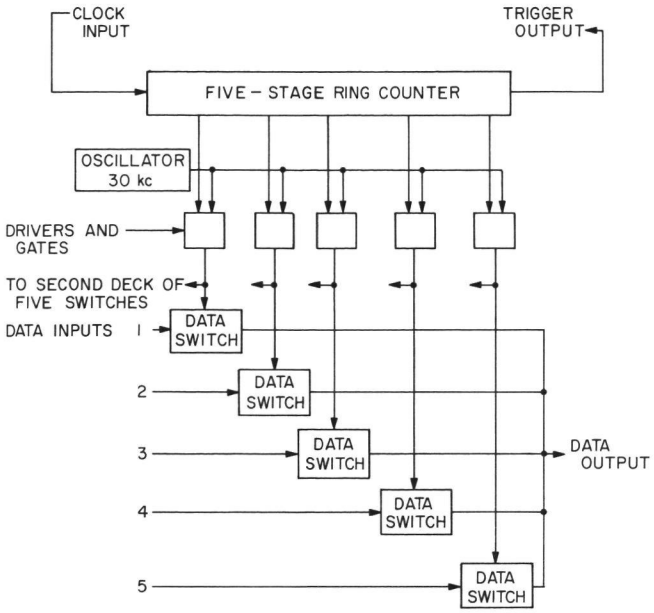

Figure 161. Solid-state commutator block diagram

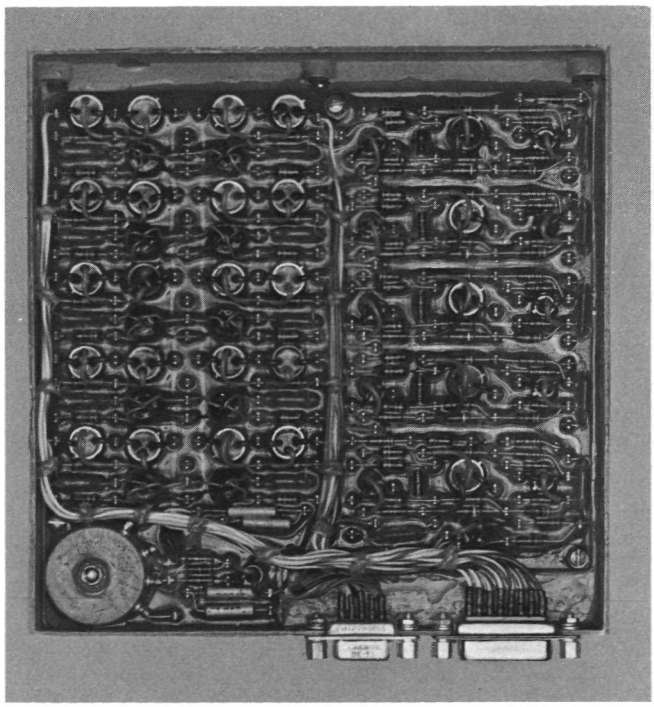

Figure 162. Solid-state commutator

(2) To provide voltage amplification for low-voltage signals.

(3) To provide amplitude limiting for signals of greater amplitude than the measurement ranges. Failure to confine these voltages results in interference between measurement channels.

The first model rate-limiting data amplifier was developed using two operational transistorized d-c amplifiers. It is shown in the simplified schematic (Fig 163). Diodes D5 and D6 and resistors R42, R43, R44, and R45 were added to provide output-voltage limiting for off-scale voltages which exceed the desired measurement ranges.

As RA-1 and -2 progressed into the hardware stages, it became evident that cumulative drifts with temperature, time, and vacuum were greater than anticipated, and a redesign for RA-3, -4, and -5 was undertaken. Table 48 lists the basic characteristics of the RA-1 and -2 rate limiter vs those called out for RA-3, -4, and -5.

The rate limiter selected for use on RA-3, -4, and -5 is shown in Figure 164. This model employs a modulated-carrier technique using voltage-variable silicon capacitors for modulation, a silicon transistor carrier amplifier, a silicon transistor demodulator and a 1-mc silicon transistor carrier generator. After demodulation, the signal is further amplified by a direct-coupled silicon transistor amplifier. the output stage of this direct-coupled amplifier is supplied from positive and negative current limiters so that it cannot supply more than a certain fixed current to a large value capacitor placed across the output. The value of this capacitance, together with the settings of the current limiters, determines the maximum output rate of the system. In order to produce the desired voltage-limiting characteristics, two silicon diodes are used to clamp positive and negative voltage excursions.

Voltage-controlled oscillator. An important part of this system is the analog subcarrier oscillator, commonly called voltage-controlled oscillator (VCO). The VCO is a device that has an output frequency directly proportional to its input voltage. Five VCO's in the audio frequency range are used for analog measurement encoding. The VCO characteristics are given in Table 49.

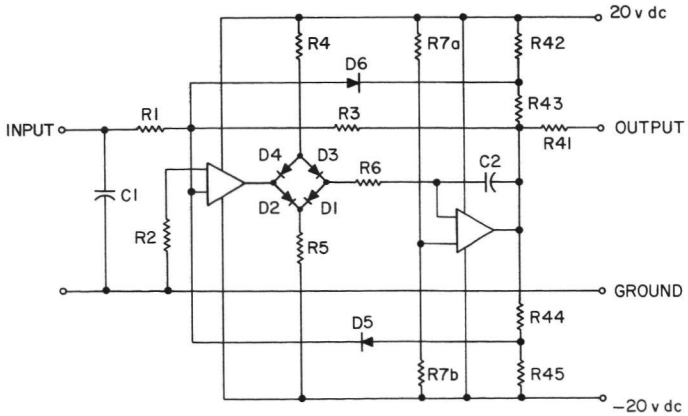

Figure 163. Rate limiting data amplifier

For RA-3, -4, and -5, Model TOE 305 VCO made by the Bendix-Pacific Division of Bendix Aviation was selected. Detailed specifications on this unit are given in Table 50. Two encapsulated VCO's are mounted in a magnesium module with two voltage rate limiters, which are constructed on printed wiring boards and are mounted on the flat surfaces. Figure 165 shows a VCO-rate limiter module as used in the RA-3, -4, and -5 data encoder.

Ground support equipment. The data encoder systems test console (Fig 166) is used for controlling and analyzing the data encoder operation during the spacecraft test and calibration phase. To accomplish this, the console comprises several major equipment groups:

Table 48. Rate limiter characteristics

Specifications	RA-1 and -2	RA-3, -4, and -5
External source resistance, ohms	10K ±20%	—
Input impedance, ohms	100K	100K ±1%
Gain stability, %	±2	±0.20
Output ramp stability, %	+10, −0	±5
Output impedance, ohms	1K	1K
Gain range	−1.0 to −4.0	−1 to −10
Linearity, %	—	±0.15
Zero stability, mv	±50	±10[a]
Ramp linearity, %	—	1
Power, mw	400	250
Weight, oz	4.5	3.6

[a] Referred to the input.

Table 49. *Ranger* RA-3, -4, and -5 VCO characteristics

IRIG channel	Center frequency, cps	Bandwidth, cps	Voltage input, v dc
2	560	±25	±1.0
3	730	±25	±1.0
4	960	±37	0 to −2.0
5	1300	±60	±1.0
6	1700	±60	±1.0

Table 50. Bendix TOE VCO specifications

Item	Value
Input impedance	300K ohms, minimum
Output amplitude	5 v (rms), minimum
Output distortion	1% total, maximum
Linearity	Less than ±0.25% from best straight line
Power requirement	28 v dc ±3 at 15 ma
Temperature range	0 to 85°C
Stability (zero shift)	Less than 2% of bandwidth during environmental extremes
Stability (sensitivity shift)	Less than 1% of bandwidth during environmental extremes
Output voltage variation	Less than 1 db during environmental extremes
Size	1.31 by 0.78 by 1.60 in.
Weight	2.5 oz

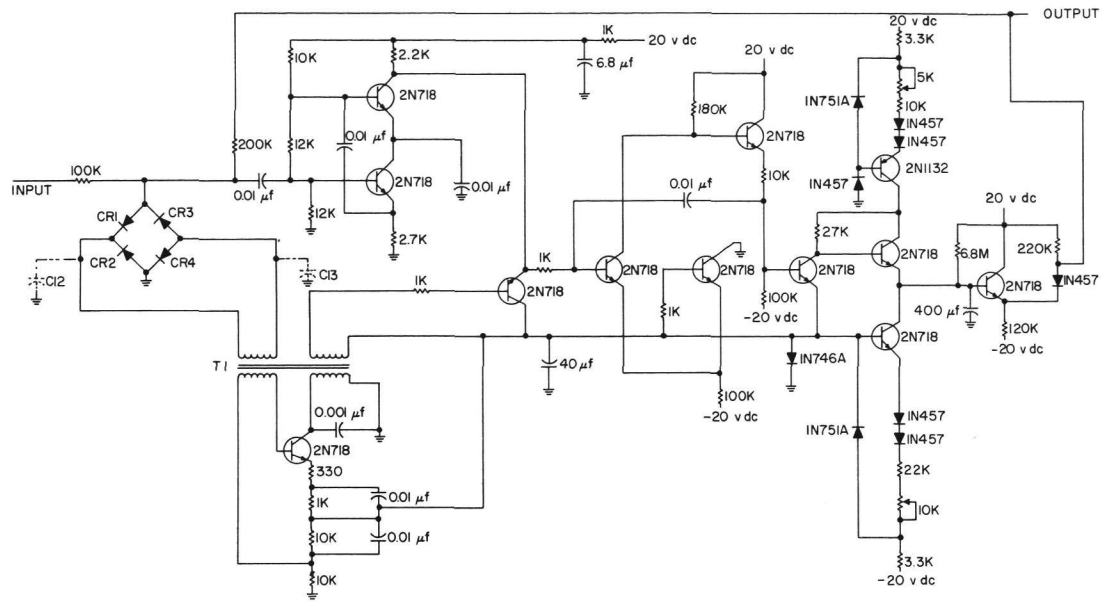

Figure 164. Voltage rate limiter

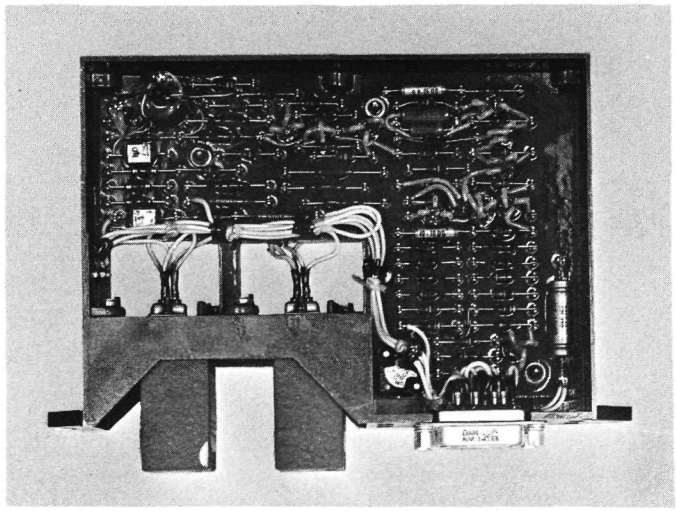

Figure 165. VCO rate limiter module

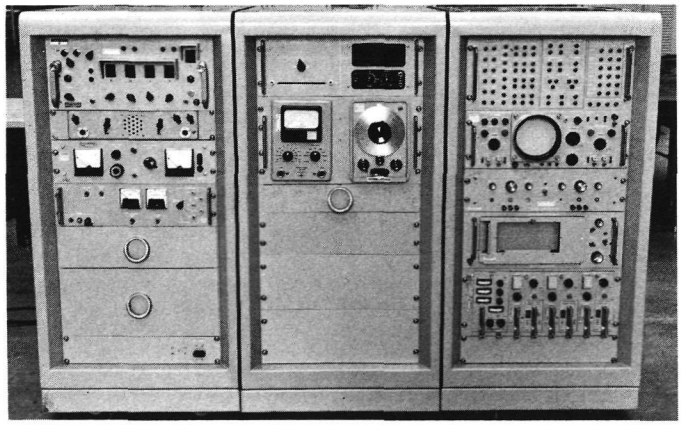

Figure 166. Data encoder systems test console

(1) Power supplies to enable the data encoder to function if spacecraft power is not available.

(2) A commutator-programmer control unit (CPCU), which can control the data encoder commutator and programmer. With this unit, the commutator can be set to any desired position and the programmer can be set to any desired data mode.

(3) Test equipment to examine and record the frequency, amplitude, and waveshapes of the data encoder output.

For checkout and control of the data encoder when the spacecraft is on the launch pad, a data encoder blockhouse console is used. Figure 167 shows this console. It uses the same type of equipment as the systems test console and functions in a similar manner.

Since a relatively long cable connects the blockhouse to the spacecraft, several isolation units are used by the data encoder. These isolation units are mounted in a J-box which is installed on the umbilical tower adjacent to the spacecraft. The data encoder units contained in this J-box are:

(1) Mixed signal line amplifier.

(2) Mode indicator line amplifier.

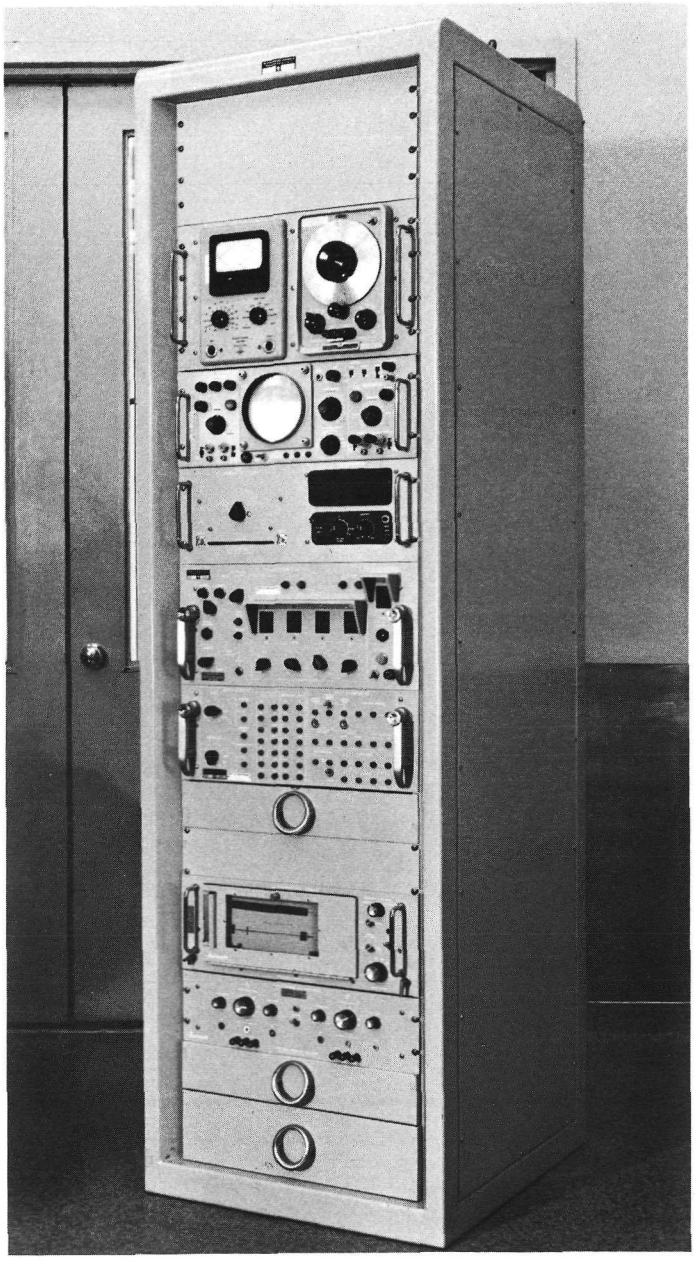

Figure 167. Data encoder blockhouse console

(3) Mode change pulse amplifier.

(4) C sync line amplifier.

c. Data Reduction Laboratory.

Design philosophy—RA-1 and -2. Spacecraft RA-1 and RA-2 contained a telemetering encoding system with approximately 36 engineering measurements and various scientific measurements. The primary responsibility of the Data Reduction Laboratory is to decommutate the engineering measurements, perform data cleanup on the scientific measurements, and prepare quick-look records.

Figure 168 is a block diagram of the *Ranger* telemetering Data Reduction Laboratory. The laboratory is functionally divided into two sections: data processing station and data record production station. Tasks performed in the data processing station are (1) preparation of a computer entry magnetic tape, (2) preparation of a digital magnetic tape containing engineering measurements for the digital record production station, and (3) producing calibrated analog records. The digital record production is concerned only with engineering measurements with an end product of a combined record consisting of an analog and digital printout of each measurement separately.

A brief description of the equipment used in the data processing station (as depicted in Fig 168) follows. The magnetic tapes received from the field stations are reproduced at 373 times the recorded speed. The composite spacecraft signal is fed into the phase-lock-loop discriminator bank where the signal-to-noise ratio of each channel is enhanced by reducing the noise bandwidth. The loop bandwidth of each discriminator is selected for a desired signal-to-noise ratio at the output of the discriminator at the required mission distance.

Each discriminator has three output signals. There are (1) VCO output, which is an oscillator that is phase-locked to the input frequency, (2) analog output which is a voltage proportional to the input frequency, and (3) an out-of-lock monitor. One or more of these output signals are used, depending on the type of data contained on the channel. The VCO and out-of-lock monitor for Channels 1, 2, and 3 (engineering channels and clock channel) are fed to the digital decommutator. The decommutator is basically an EPUT meter that is synchronized to the spacecraft signal and generates a unique address for each engineering measurement. The output of the decommutator is a binary-coded decimal frequency count plus a binary bit indicating whether the data is considered valid. This output is delivered to (1) the digital format converter used to produce a magnetic tape for the digital record production station, (2) the format converter for computer entry, and (3) to a tabular printer. Each measurement is time-tagged with the actual time of day (GMT) that the data was received from the spacecraft. This time is obtained from the time code translator which decodes the recorded time from the magnetic tape and connects it to a parallel output for time tagging engineering data, and to a serial output for recording analog signals on an oscillograph.

CONFIDENTIAL

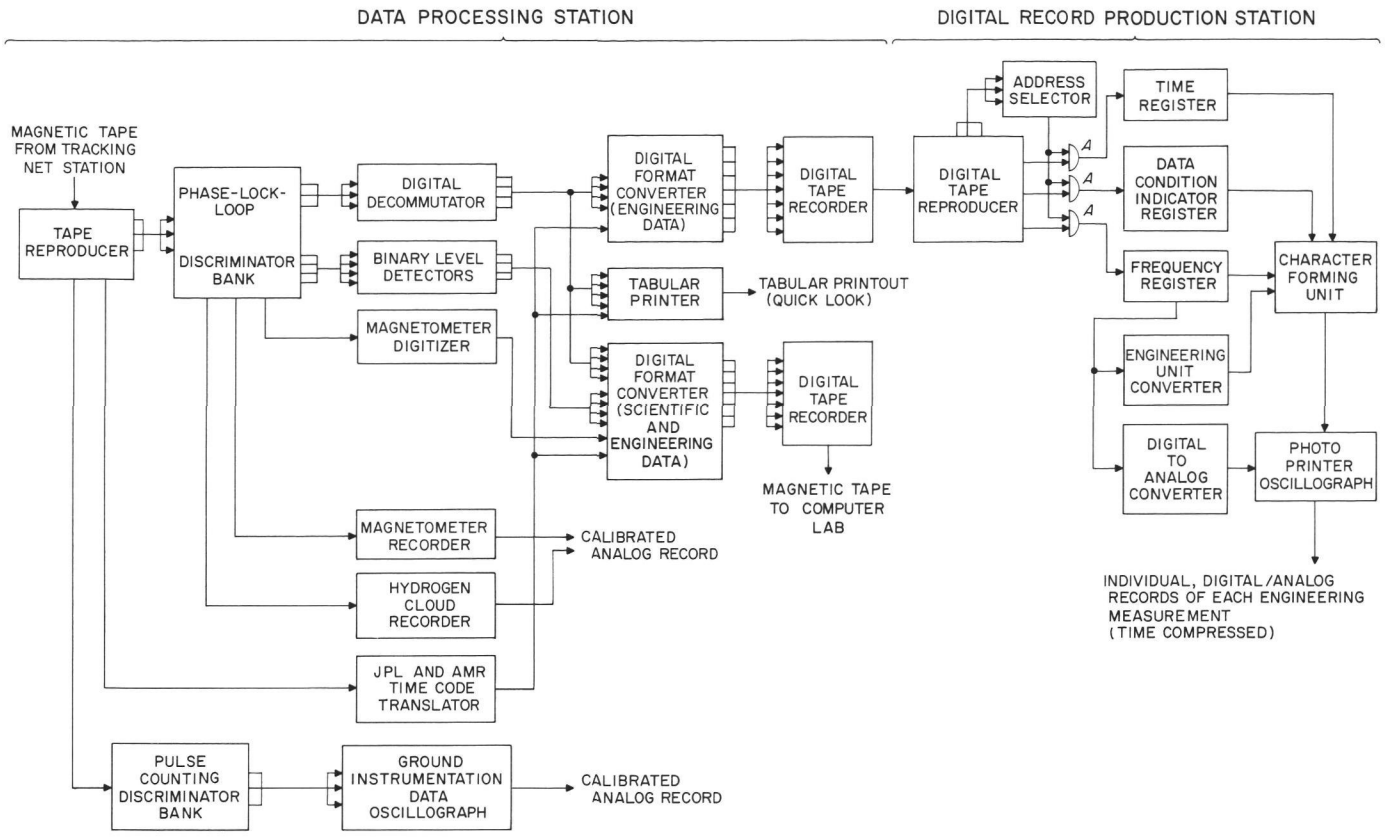

Figure 168. *Ranger* telemetering data reduction station

The scientific data consisting of hydrogen cloud (Channel 4), magnetometer (Channel 7.7), Data Automation System (Channels B-11, B-12 and B-13) and Vela Hotel (Channel B-10) is, in general, handled on a signal conditioner basis.

Magnetometer data was digitalized at a 10-sample-per-sec rate and recorded on a digital magnetic tape recorder for computer reduction. A calibrated analog oscillograph record of this measurement was also made to establish that the digitalizing rate was adequate and to provide a quick-look record of this measurement.

Hydrogen cloud data was recorded on a calibrated oscillograph in analog form. These records were then to be analyzed by the scientific groups.

Binary telemetering Channels B-10, B-11, B-12, and B-13 were separated and demodulated by the phase-lock-loop discriminators. The rate-limited output of the discriminators (analog) was reshaped into "square waves" by the level detectors. This "square-wave" binary data was then recorded on the digital tape recorder for computer reduction.

Ground instrumentation data was converted from an FM signal to an analog voltage by the pulse-counting discriminators and recorded on a calibrated analog oscillograph. Upon request, these measurements were reduced and recorded in this form during the reduction period.

Figure 168 shows the equipment required for the data processing and digital production station. The criteria used in this design of the engineering record-production portion of the station are as follows, in their order of importance:

(1) Produce reduced data that can be analyzed in the shortest possible time.

(2) Produce reduced data at a rate equal to, or greater than, the rate it is being generated.

(3) The reduced records should contain data in its most elementary form to preserve system accuracy and to give assurance to the operations analysis groups of proper systems operations.

The data reduction system shown in Figure 168 met the system design objectives. Points (1) and (3) of the design objectives were met by the records made by the

CONFIDENTIAL

photo-printing oscillograph shown at the output of the digital record production station. These records gave a combined analog and digital printout of selected data points with respect to time. The calibrated analog data covered 6 in. of the 12-in. record; the other 6 in. of record width was used for the digital printout. The digital printout consisted of a complete time report (GMT) of when the data point was taken, a printout of data point in engineering units with sign and decimal point and a printout of the telemetering subcarrier frequency for selected data [Point (3) in the design objectives].

Point (2) of the design objective is met by a magnetic tape speed-up (time compression) process of 117 to 1. This was done by reproducing the field recorded tape at four times recorded speed (3¾ to ≃15 in./sec) in the data processing station. The digital data at the output of this station was recorded at a low tape speed (1⅞ in./sec). At the input of the digital record production station the digital tape was reproduced at 32 times the recorded speed (60 in./sec), giving an over-all speed-up of 117.

Considering this speed-up process in each individual station, this means the data processing station produced all of the engineering and scientific data output indicated in Figure 168 for a 10-hr field recording in 2½ hr. The digital record production station can produce an individual analog-digital record for each engineering measurement for a 10-hr field recording in approximately 2½ hr (30 measurements × 10 hr divided by 117).

RA-1 and -2 operations. The Data Reduction Laboratory was designed for long periods of received data so that, by using time-compression techniques, a large volume of data could be produced in a short time. Because RA-1 and -2 trajectories were both orbital, the basic design concept of volume data was invalidated. Instead of having hours of received data from the tracking stations, each pass lasted from 4 to 10 min. Consequently, the data processing station had to be converted to operate with no speed-up factor.

In general, the signal-to-noise ratio of the signals was lower than expected for the normal trajectory and this further aggravated the problem. Due to the short periods of data, it was difficult to obtain correct address synchronization in the decommutator, especially for the slowest data rate (sync correction for the slowest rate occurs approximately every 16 min).

It is believed, however, that the Data Reduction Laboratory performed as well as could be expected under the adverse signal conditions.

RA-1 and -2 data-display consoles. The data-display consoles were designed for real-time data monitoring of the spacecraft telemetry signals while the spacecraft was undergoing tests (for example, in the environmental laboratory).

A signal flow diagram of the data-display console is shown in Figure 169. Basically, the data display console consists of a phase-lock-loop discriminator bank, an engineering measurement decommutator, tabular printer, remote engineering measurement display, time-of-day clock, and level detectors. A front view picture of the console is shown in Figure 170, and the remote display is shown in Figure 171.

The operation of the data-display console is not unlike the data processing station in the Data Reduction Laboratory. The composite telemetry signal is fed to the phase-lock-loop discriminators, where each subcarrier is filtered by the predetection filter and the phase-lock-loop discriminator. All analog signals are recorded on an oscillograph record located in another console.

The engineering measurements on Channels 2 and 3 are decommutated, sampled, and tagged with a unique address by the decommutator. This information (plus time) is then printed on a tabular printer. Selected measurements may be displayed on the remote display for viewing by cognizant personnel located in the checkout area.

In general, the data-display console performed its functions satisfactorily. Some operational inconveniences were observed, such as the narrow viewing angle for the remote display.

RA-3, -4, -5 design philosophy. The requirements of the RA-3, -4, -5 ground telemetry subsystem are to provide equipment that will perform the functions of filtering, demodulating, decommutating, decoding, signal reconstruction, and data-processing signals from the data encoder in the spacecraft. This equipment will be used for ground checkout of the telemetry subsystem as well as be an integral part of data processing and data reduction of flight data.

The data encoder subsystem employed in the RA-3, -4, and -5 spacecraft is basically the same in operations as the one used on *Ranger I* and *II* missions but more complex in configuration. The present configuration allows for one additional high speed rate and five additional decks, plus approximately a 100% increase in the measurement capabilities of the encoder. Twelve telemetry channels are used to accommodate the measurement program. Channel 1 is used for the spacecraft clock only and Chan-

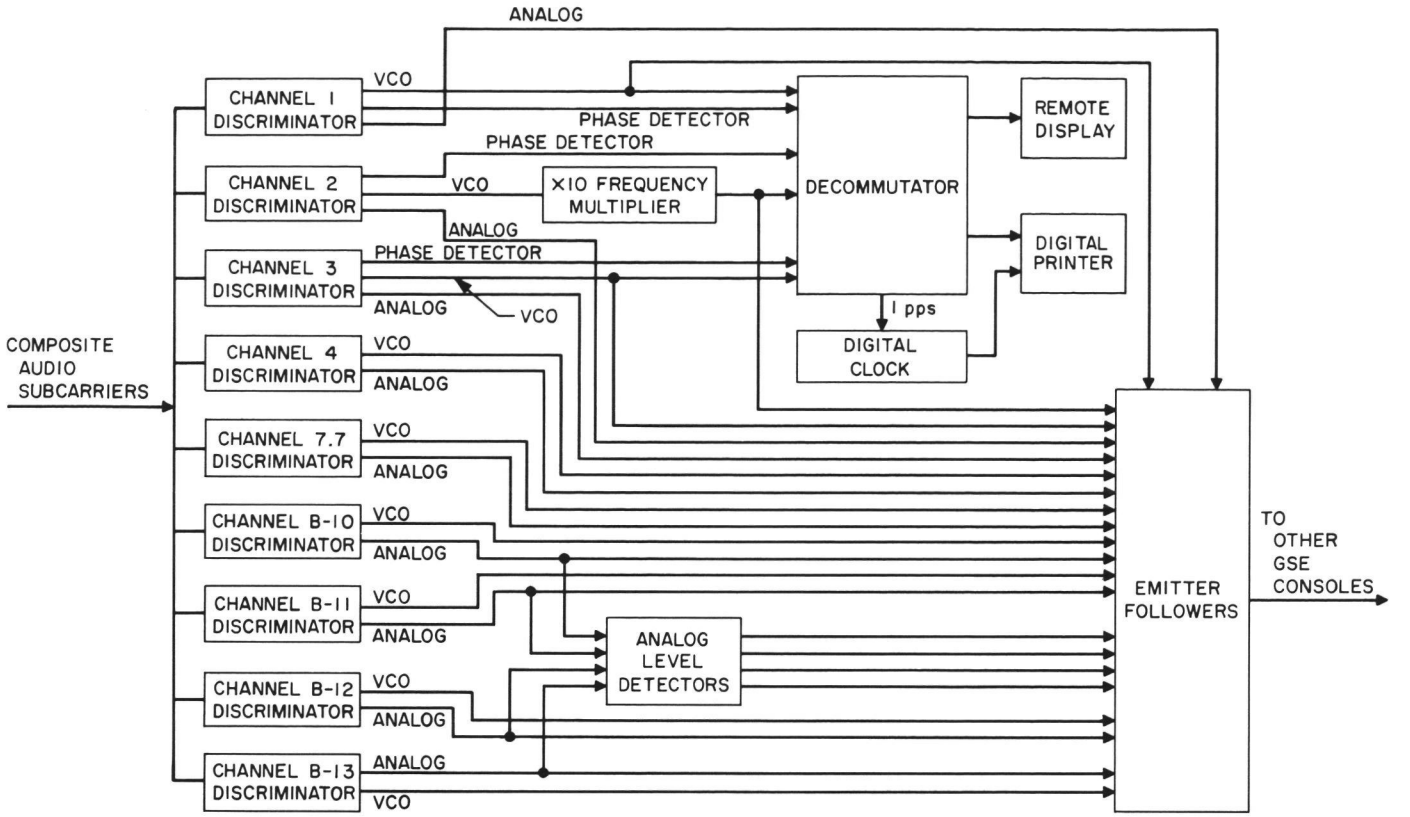

Figure 169. Flow diagram, data display console

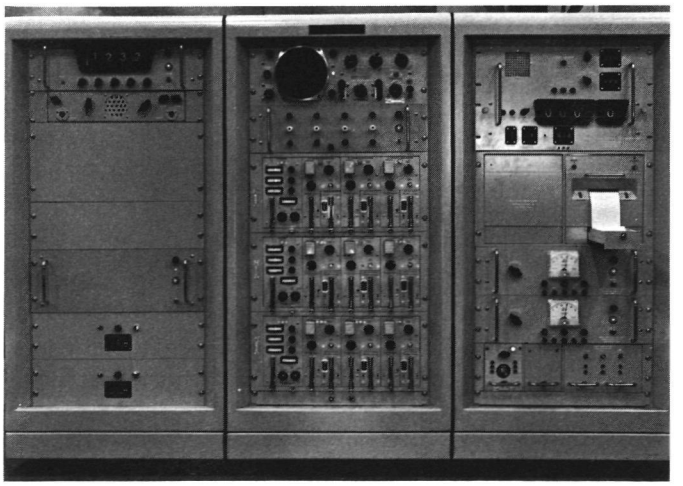

Figure 170. RA-1 and -2 data display console

nel B-19 is used for the commutator sync reference only. The remaining channels are time-shared by various measurements.

A ground telemetry subsystem was designed to meet the above requirements and perform the functions described. Actually, it was a redesign of the system employed in the *Ranger I* and *II* missions. This subsystem, like the data encoder, is basically the same in operation but more complex in configuration than the previous subsystem. Figure 172 is a block diagram of the digital decommutator. Figure 173 shows the complete subsystem, and Figure 174 shows the subsystem as it is used in data reduction. Probably the most redesign was in the digital decommutator.

These areas of redesign and/or upgrading are as follows:

(1) Synchronization scheme: the original decommutator depended upon a tone reference modulating the commutated channels. Due to the low frequencies of these tones (18, 24, and 30 cps for rates 1, 2, and 3, respectively) there was considerable time error in the detection process. The data encoder for RA-3 used the two distinct commutator-stepping pulses (Rate 2, and Rate 4) to modulate Channel B-19. The pulse output of this channel was fed into a level detector and provided a reasonably accurate reference for sync comparison.

(2) Decommutator countdown logic to generate gating pulses for the higher rate (25 pps).

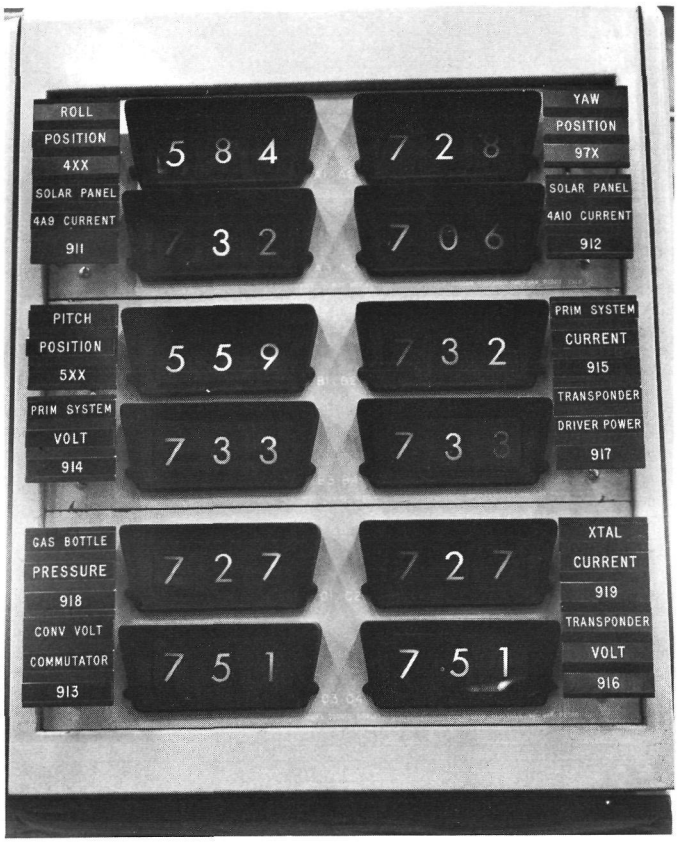

Figure 171. Remote display, RA-1 and -2

(3) Data condition indication logic to provide a "go" or "no-go" bit for each data sample.

(4) Address logic to provide a 2-digit identification to each data sample.

(5) Solid-state, phase-coherent frequency multipliers to restore the original frequency count accuracy lost in the short sampling time.

(6) A high-speed, digital photo printer designed to print out all the data samples from the data encoder commutator.

Locations of these subsystems are as follows:

(1) JPL Spacecraft Assembly Facility.

(2) JPL Environmental Testing Laboratory.

(3) JPL Dummy-Run Facility.

(4) JPL Data Reduction Laboratory Checkout Station.

(5) JPL Data Processing Laboratory.

(6) AMR—Hangar A.E. Checkout Facility.

(7) AMR—Launch Checkout Telemetry Trailer.

(8) AMR—Blockhouse Facility.

(9) DSIF—Goldstone Facility.

(10) DSIF—Mobile Tracking Station, South Africa.

(11) DSIF—Johannesburg, South Africa.

The degree of completeness at each location depends upon the requirements at that site which are, in general, the same. The only exception is in the data processing station of the Data Reduction Laboratory. At this site, all data is handled in non-real time from magnetic tapes received from the DSIF locations.

Equipment operation. The operation of the Data Reduction Laboratory during the data processing and data reduction of the RA-3 flight test was planned with no time compression, since the duration of the flight was programmed for 66 hr. However, due to the volume of data, it was decided to speed up the process by a factor of 3.667 in order to speed up the handling of the data tapes. The equipment performed as expected and all requirements were met with the exception of generating a good computer entry tape for the gamma-ray measurements. The problem was that, in order to make an acceptable computer entry tape, the gamma-ray bits must be clocked onto the tape. There is sufficient noise on the data tapes to cause considerable jitter in these bits with respect to the clock pulse. An improved level detector is being designed which is expected to solve this type of problem. This is the only serious problem encountered during data-reduction processing of the flight data.

d. R-F development.

R-F communications. The communications system flown on RA-1 and -2 spacecraft consisted of a low-power transmitter and a 3-w transponder (Fig 175). The low-power transmitter operated on 960.10 mc and radiated 0.25 w essentially omnidirectionally. It was designed to telemeter information about the gross operation of the payload and its scientific instrumentation for ½ million mi and to be powered by its own separate battery. The low-power transmitter, therefore, functioned independently of the attitude of the spacecraft.

The purpose of the 3-w transponder was to provide two-way doppler velocity information, to receive commands sent from Earth, and to provide telemetering to a maximum range. It was powered by solar power (after the solar panels had been erected). Prior to erection, the transponder was energized from batteries. The transponder received a signal at 890.046 mc, using the same antenna as the low-power transmitter. It also transmitted the 960.05-mc signal over this antenna prior to the time

CONFIDENTIAL

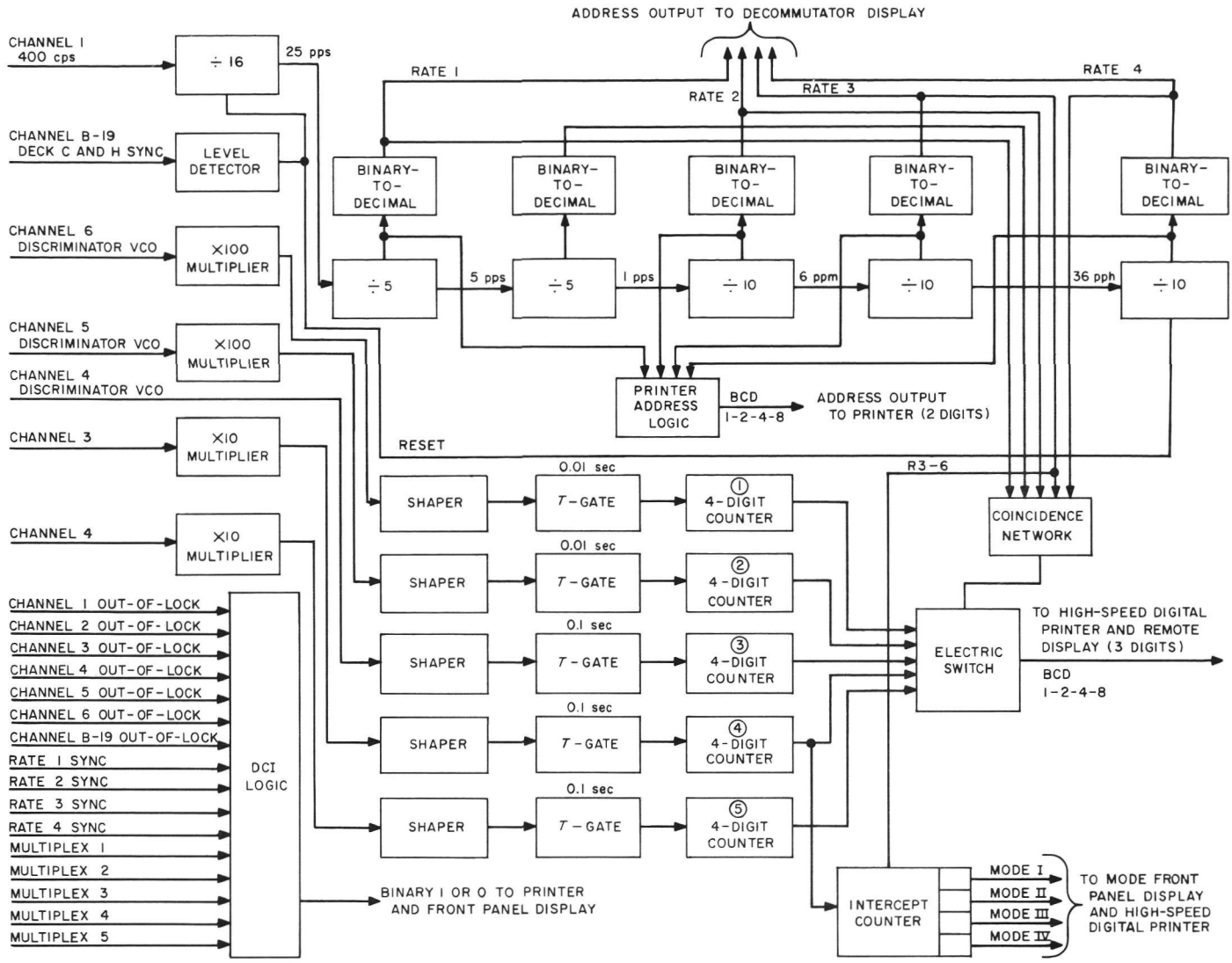

Figure 172. Digital decommutator, flow diagram

of attitude acquisition. After acquisition, the transmitted signal was switched to the high-gain directional antenna.

The low-power transmitter and ¼- and 3-w cavity amplifiers were designed by JPL and produced by Resdel Engineering Corp. in Pasadena. The transponder design was accomplished through a joint effort between JPL and Motorola, Inc., and was produced by Motorola.

Transponder. The design objective was to develop a transponder with maximum long-term reliability, minimum power consumption, and minimum weight consistent with the desired electrical performance.

Figure 176 shows a functional block diagram of the transponder. Note that the unit consists basically of a double superheterodyne, crystal-controlled, phase-coherent receiver and a 960-mc transmitter. The entire circuitry, with the exception of the two UHF vacuum tube cavity amplifiers, is contained within this structure (Fig 177). Transistor and solid-state devices are used throughout. Note also that the mechanical design consists of a casting containing 12 separate shielded compartments. Each compartment contains a module such as a 50-mc IF amplifier, 10-mc IF amplifier, phase detector, VCO, etc. This technique was used primarily to ensure adequate r-f isolation between the highly sensitive circuits. All circuits within the compartments are mounted on removable plates. Therefore, if a component failure occurs, the faulty module can be replaced. Another important feature of this technique of packaging is its improved vibrational characteristics. Experimental vibrational data indicates that the structure is free of resonances from 20 to 700 cps. At 740 cps, where the first resonance occurred, the displace-

CONFIDENTIAL

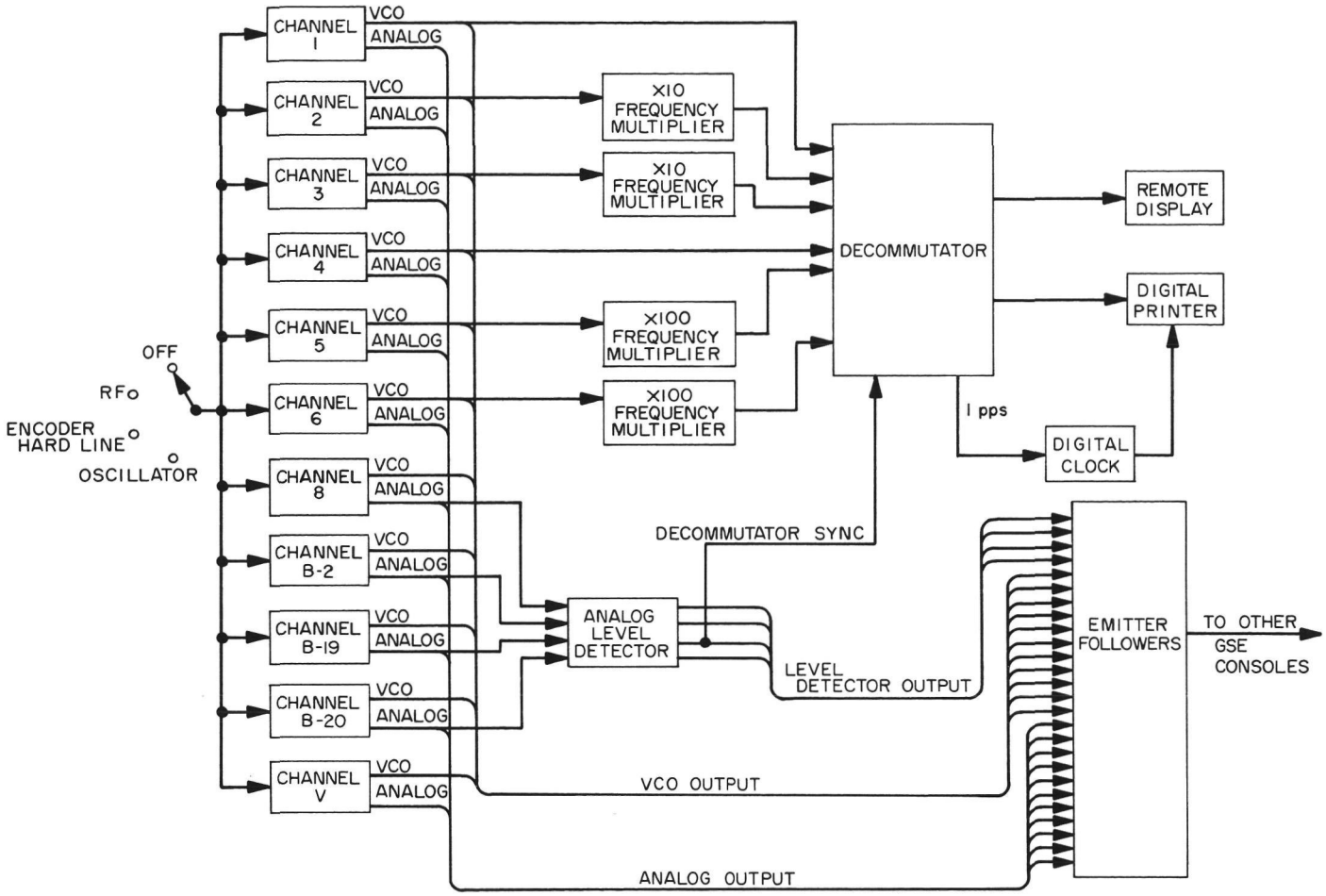

Figure 173. Data display console, flow diagram

ment had a negligible effect on the transponder's performance.

UHF cavity amplifiers. The spacecraft transponder system for RA-1 included two cascaded 960-mc cavity amplifiers. This series of UHF amplifiers is used to boost the transponder's 5-mw output to 3 w. This 3-w signal is then fed to the spacecraft transmitting antenna.

The first amplifier boosts the transponder 5-mw signal to a level of 250 mw, which is then amplified again to a level of 3 w by the second amplifier.

The principal criteria affecting the design of the cavity amplifier were reliability, high efficiency, high gain, wide bandwidth, and low incidental phase modulation as a function of vibration. Design, fabrication, and testing have been completed on the first amplifier. Figure 178 shows an assembly view of the amplifier. The electrical characteristics of the 250-mw unit have been measured and are compared with the specifications in Table 51.

The amplifier is designed to operate in a partially saturated condition to provide some stabilization of the output signal for variations of the input signal. The r-f power output vs r-f power input curve of Figure 179 shows the saturation characteristic. The data in Figure

Table 51. UHF cavity amplifier characteristics

Characteristic	Design	Measured
Power input, mw	5	5
Power output, mw	250	300
Gain, db	17	17.8
Bandwidth, mc	5	5
Plate efficiency, %	31	41.6
Over-all efficiency, %	8	8.4
Input impedance (nominal), ohms	50	50
Input VSWR	1.5	1.25
Output impedance (nominal), ohms	50	50
Output VSWR	1.5	1.06
Plate voltage, v	100	100
Plate current, ma	8	7.2
Filament voltage, v	4.75	4.75
Filament current, ma	600	600

CONFIDENTIAL

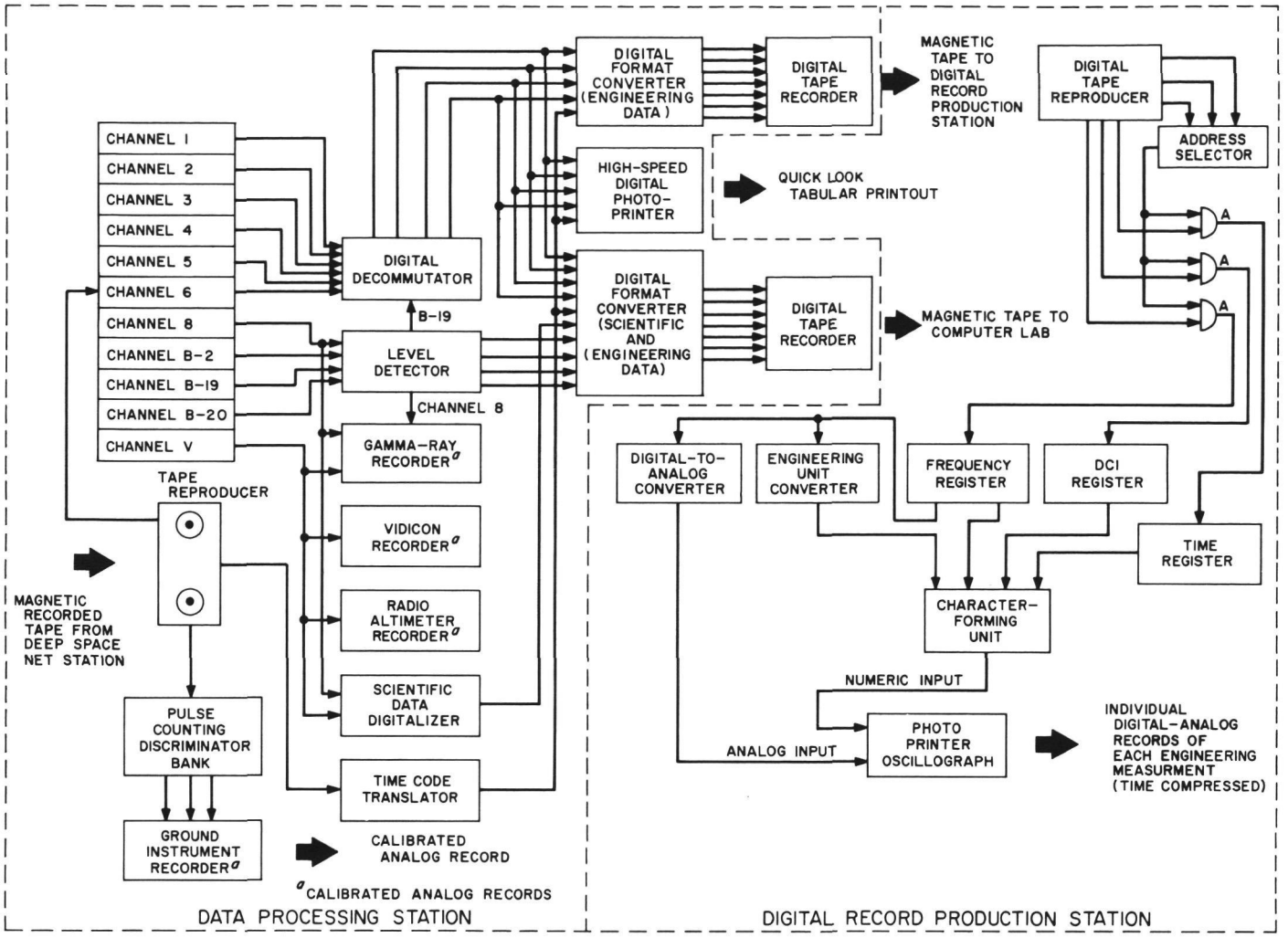

Figure 174. *Ranger* telemetering data reduction station

179 indicates that a 3-db decrease in drive level will result in a 1.4-db decrease in output power. Figures 180 and 181 show the effects of B+ and filament power supply variations on amplifier performance. Within the spacecraft B+ and filament power supply regulation tolerance of ±5%, the curves show that the output of the amplifier will vary ±0.25 db. The actual supply voltages were chosen for highest efficiency and greater life expectancy.

The thermal characteristics of the unit are shown in Figure 182. It can be seen that the output power will decrease 2 db at the temperature extremes of −10 and 80°C. The mechanical parts of the cavity are fabricated from 2024 aluminum alloy. This material was chosen for light weight and ease of machining and surface plating. The thermal expansion and contraction of this material de-tunes the cavity and causes the power to drop as indicated in Figure 182. It is desired that the effect of temperature on the power output be limited to 1 db. This figure has been accomplished by the addition of a thermally sensitive tuning adjustment.

The unit was tested environmentally to the flight equipment specifications listed in Table 52. As a function of mechanical shock and vibration, the amplifier was required to meet that portion of JPL design specifications No. 30317 covering performance. The results of the tests are compared with the specifications in Table 52.

The electrical characteristics of the 3-w amplifier are shown in Table 53. As expected, the operating efficiency of this unit (38%) is considerably greater than that of the 250-mw driver stage (6%). This is due in part to operating the tube closer to its optimum design power level but mainly to the larger ratio of r-f to filament power at this level of output. Greater bandwidth was obtained in the higher powered unit due to the lower plate impedance

CONFIDENTIAL

Table 52. UHF cavity amplifier environmental test specifications and performance

Test	Definition of limits	Maximum phase jitter, deg	
		Design	Measured
Vibration	3 planes, complex wave		
	12.5 g rms noise, 4 sec	2.5	0.7
	5 g rms noise / 5 g rms sinusoid } 10 min	1.0	0.5
	5 g rms noise / 8 g rms sinusoid } 10 min	1.6	0.6
	4 g rms sinusoid, 20 to 2000 cps, 10 min	0.8	0.5
Shock	3 planes		
	50 g 6.0 msec	10.0	1.0
Thermal	−10 to 82°C at 1 micron pressure	—	—

Table 53. Cavity amplifier performance data

Power input, w	0.25
Power output, w	3.0
Gain, db	10.8
Bandwidth (3 db), mc	13.0
Plate efficiency, %	60.0
Overall efficiency, %	38.0
Input impedance (nominal), ohms	50
Input VSWR	1.5/1
Output impedance (nominal), ohms	50
Output match	1.05/1
Plate voltage, v	250
Plate current, ma	20
Filament voltage, v	4.75
Filament current, amp	0.6
Weight, lb	1.44
Size, in.^{3}	36

loading of the output cavity. The r-f power output vs r-f power input of the 3-w amplifier is shown in Figure 183. It will be noted that the unit is operated near saturation for optimum power stability, where a ±1.0-db variation in r-f input power results in less than ±0.25-db change in the output power. Thermal data on the unit is shown in Figure 184 which indicates a 2-db variation in output power over the temperature range of −10 to 82°C. Due to the mechanical identity of the two units, the output power vs temperature characteristics of the 3-w amplifier are essentially the same as that of the 250-mw unit. Variations of 2 db are permitted in the electrical specifications of these units, assuming no temperature compensation.

The electrical performance of the two units operating in cascade is shown in Table 54. The resultant over-all efficiency of 25% represents an acceptable performance for a transmitter subsystem using planar tubes at this frequency and power level. Figure 185 shows the over-all bandwidth of the two units, measured by phase-modulating the r-f signal. A 3-db bandwidth of 6 mc was

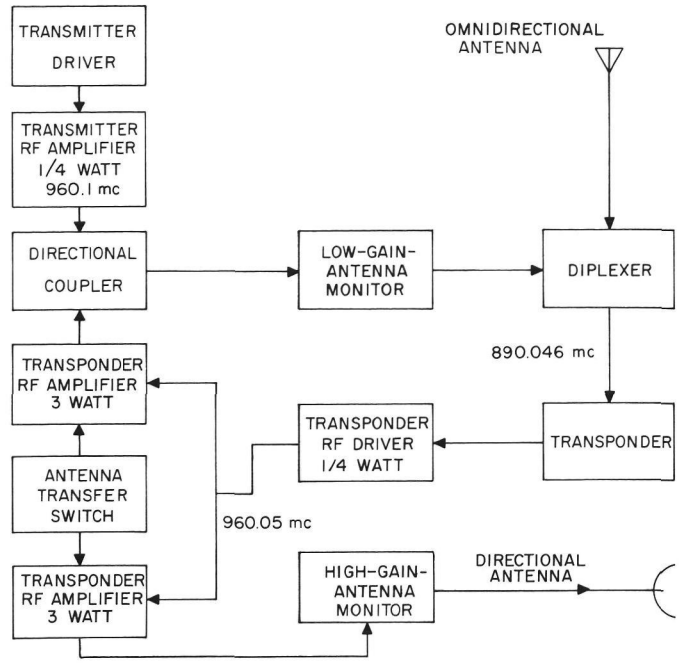

Figure 175. *Ranger* communications system

obtained and is considered adequate in view of the 5-mc system-design goal. The input–output characteristics, which show that drive level fluctuations as large as ±3 db (from the 5-mw design point) will result in an over-all output power variation of 0.9 db, are illustrated in Figure 186. The thermal properties of the cascaded units (Fig 187) show that variations in output power due to temperature change are similar to that of the individual units. Thermal compensation devices and materials are currently under test and will be incorporated in the cavity design when such techniques prove beneficial.

R-F switching. At launch and until the directional antenna is properly positioned, the high-power transponder will transmit from the omni-directional antenna.

Table 54. Cavity amplifier cascaded performance

Function	Driver amplifier	Final amplifier	Total
Plate power (dc), w	1.2	5.0	6.2
Filament power (dc), w	2.85	2.85	5.7
RF drive power (960 mc), w	0.005	—	0.005
RF output power (960 mc), w	—	3.0	3.0
Plate efficiency, %	20.8	60.0	48.5
Over-all efficiency, %	6.0	38.0	25.2
Input impedance, ohms	50.0	—	50.0
Input VSWR	1.5/1	—	1.5/1
Output impedance, ohms	—	50.0	50.0
Output match	—	1.05/1	1.05/1
Bandwidth (3 db), mc	8.0	13.2	6.0
Weight, lb	1.44	1.44	2.88
Size, in.^{3}	36.0	36.0	72.0

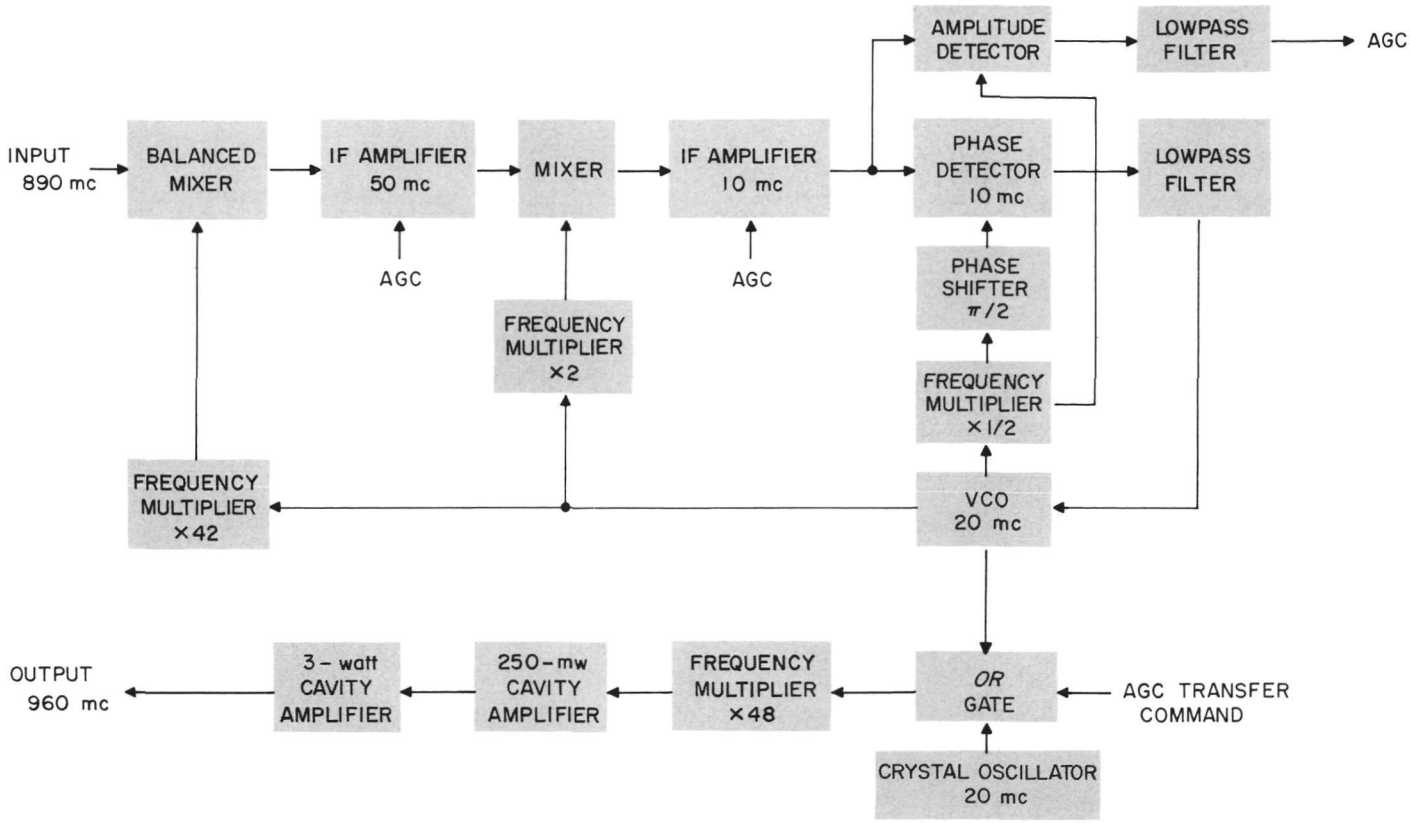

Figure 176. Transponder functional block diagram

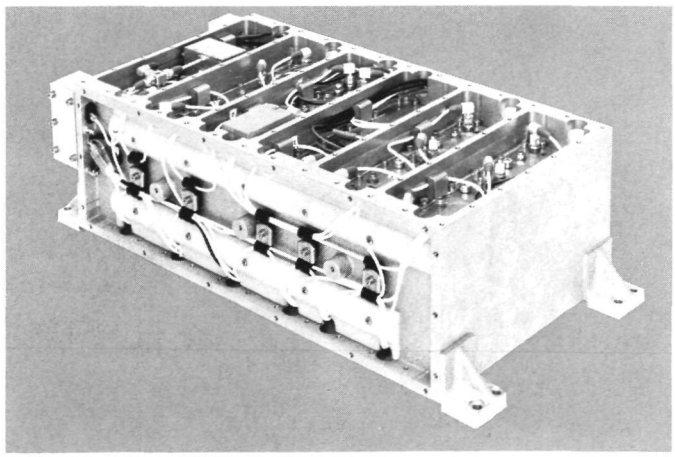

Figure 177. Transponder assembly

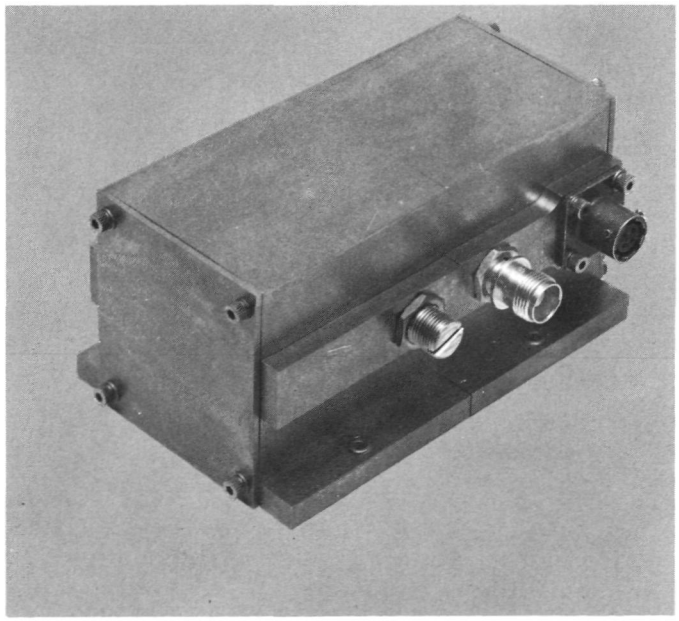

Figure 178. UHF cavity amplifier

After the directional antenna has been properly positioned, the transponder output signal will be switched to the high-gain directional antenna. D-C power switching instead of r-f power switching has been selected for the *Ranger* flights to obtain greater reliability. The switching is accomplished by feeding the transponder r-f driver output to two 3-w r-f amplifiers in parallel, each amplifier feeding one of the two antennas. Plate voltage to these amplifiers is applied at all times while

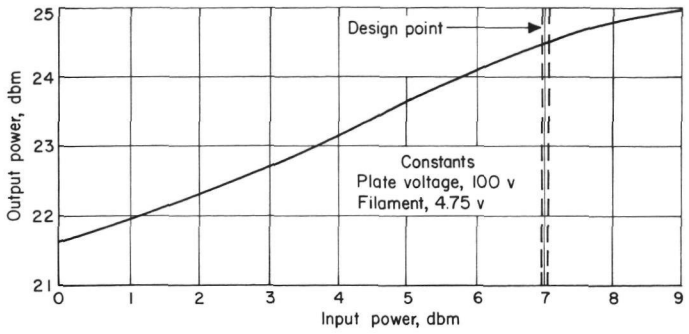

Figure 179. Input vs output power

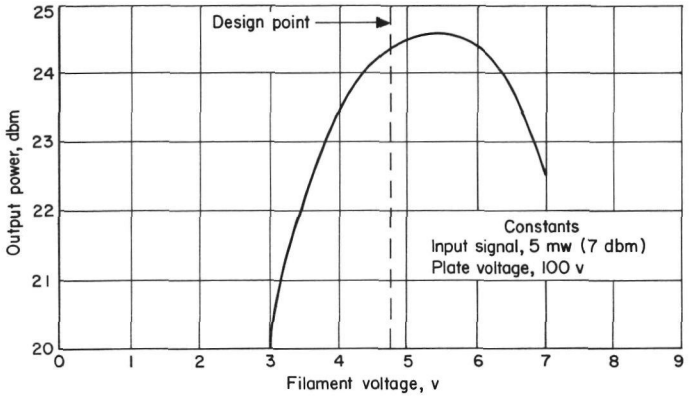

Figure 180. Output power vs filament voltage

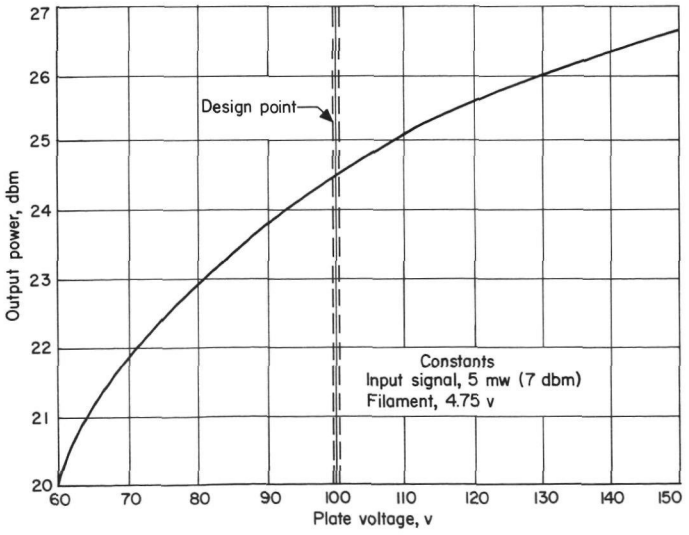

Figure 181. Output power vs plate voltage

the filament voltage is applied only to the amplifier feeding the antenna to be used. Filament voltage is transferred from one 3-w cavity to the other through a relay switch controlled by command from the ground.

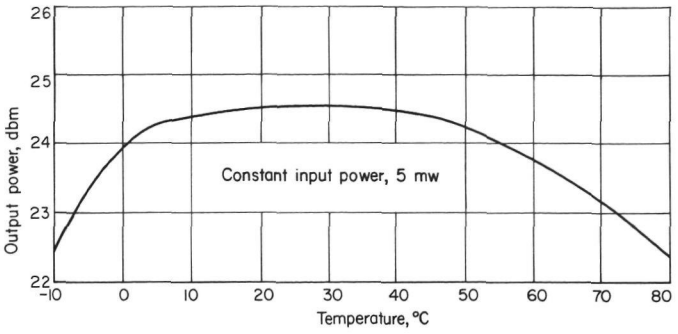

Figure 182. Output power vs temperature

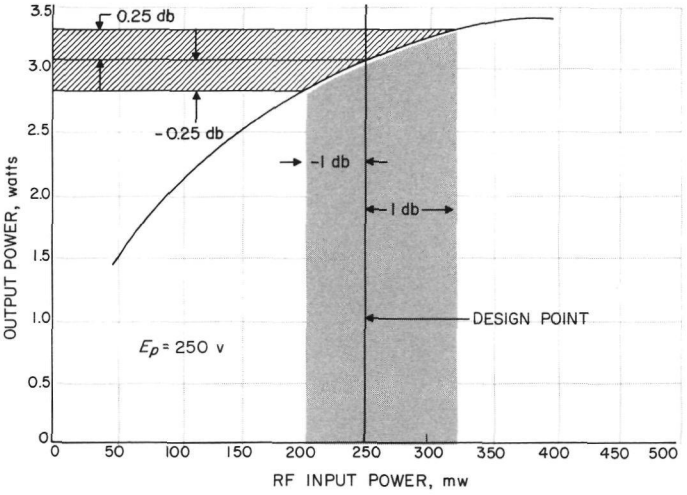

Figure 183. Cavity amplifier input–output characteristics

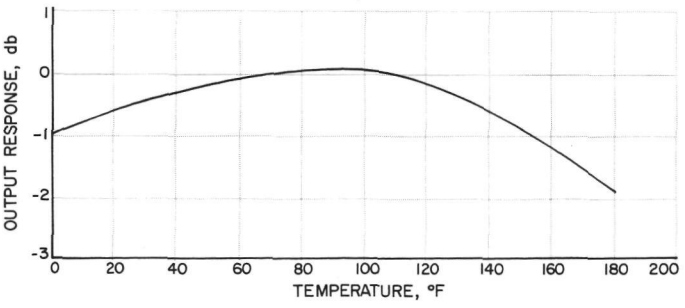

Figure 184. Cavity amplifier thermal characteristics

GSE transponder test set. In order to provide a convenient and efficient means of testing and calibrating the spacecraft radio communication equipment, a test set was designed by the Motorola Western Military Electronics Center to specifications prepared by JPL. The test set consists of an 890-mc transmitter, a 960-mc receiver, a transponder mount and power supply, and a number of general purpose test instruments. It was designed to measure the following characteristics of the spacecraft

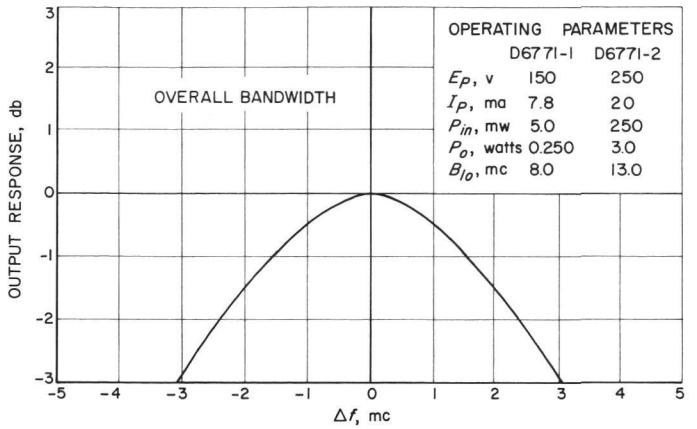

Figure 185. Cavity amplifier bandwidth characteristics

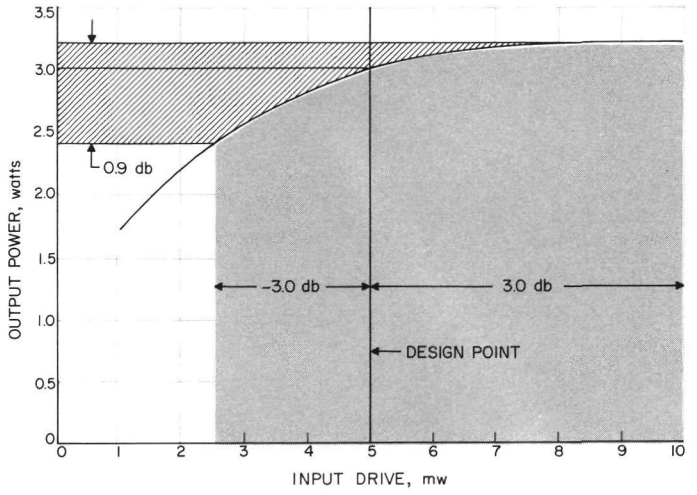

Figure 186. Input–output response for cascaded amplifiers

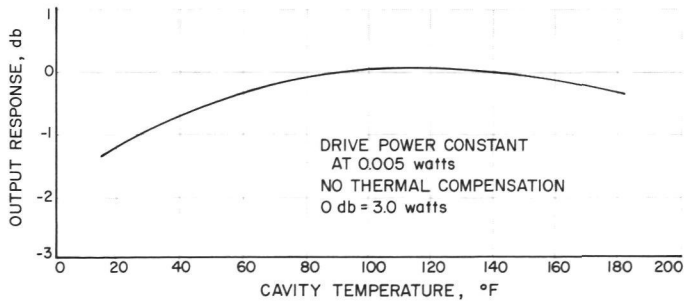

Figure 187. Thermal characteristics for cascaded amplifiers

communication equipment under static and environmental test conditions: transmitter frequencies, power output, phase stability; modulated output spectral distribution; receiver threshold sensitivity, automatic gain control response, phase stability; and transponder phase transfer function. The functional relationship of the test set components is shown in Figure 188.

The *test transmitter* (890 mc) provides a test signal for the receiver portion of the Mark I transponder. Means are provided for modulating the amplitude, frequency, or phase of the test signal and for accurately controlling its average power level. The principal design characteristics of the transmitter are:

(1) *Frequency:* 890.046 mc.

(2) *Tuning range:* ± 5 parts in 10^5.

(3) *Frequency control:* voltage-controlled crystal oscillator.

(4) *Power output:* -39 dbm down to -170 dbm.

(5) *Modulation:* Frequency, phase, and amplitude.

(6) *Frequency-modulation response:* 0 to 2 kc.

(7) *Phase-modulation response:* 0 to 5 mc.

(8) *Amplitude-modulation response:* 0 to 2 kc.

(9) *Output impedance:* 50 ohms resistive with a VSWR of no greater than 1.2 to 1.

(10) *Auxiliary outputs:* 29.6682-mc VCO signal.

As shown in Figure 189, the test transmitter is assembled in a single instrumentation rack with its power supply and power output monitor.

The *test receiver* (960 mc) is the single-conversion, superheterodyne type designed for three different modes of operation. In the first mode, it is an automatic phase control receiver which may be operated completely independently of the other test set components. In this mode, the amplitude and phase-detector reference signals are internally generated.

In the second mode, the system also acts as an automatic phase-control receiver; however, the phase detector reference signal is derived from the precision frequency standard of an electronic frequency counter. With this arrangement, the output frequencies of 960-mc transmitters may be conveniently determined by measuring the receiver VCO frequency with the electronic counter when the receiver is synchronized to the transmitter signal.

In the third mode, the receiver is operated as a phase detector in conjunction with the test transmitter. Both the phase detector reference and the local oscillator signals are derived from the transmitter VCO signal by means of coherent frequency shifters. By use of this tech-

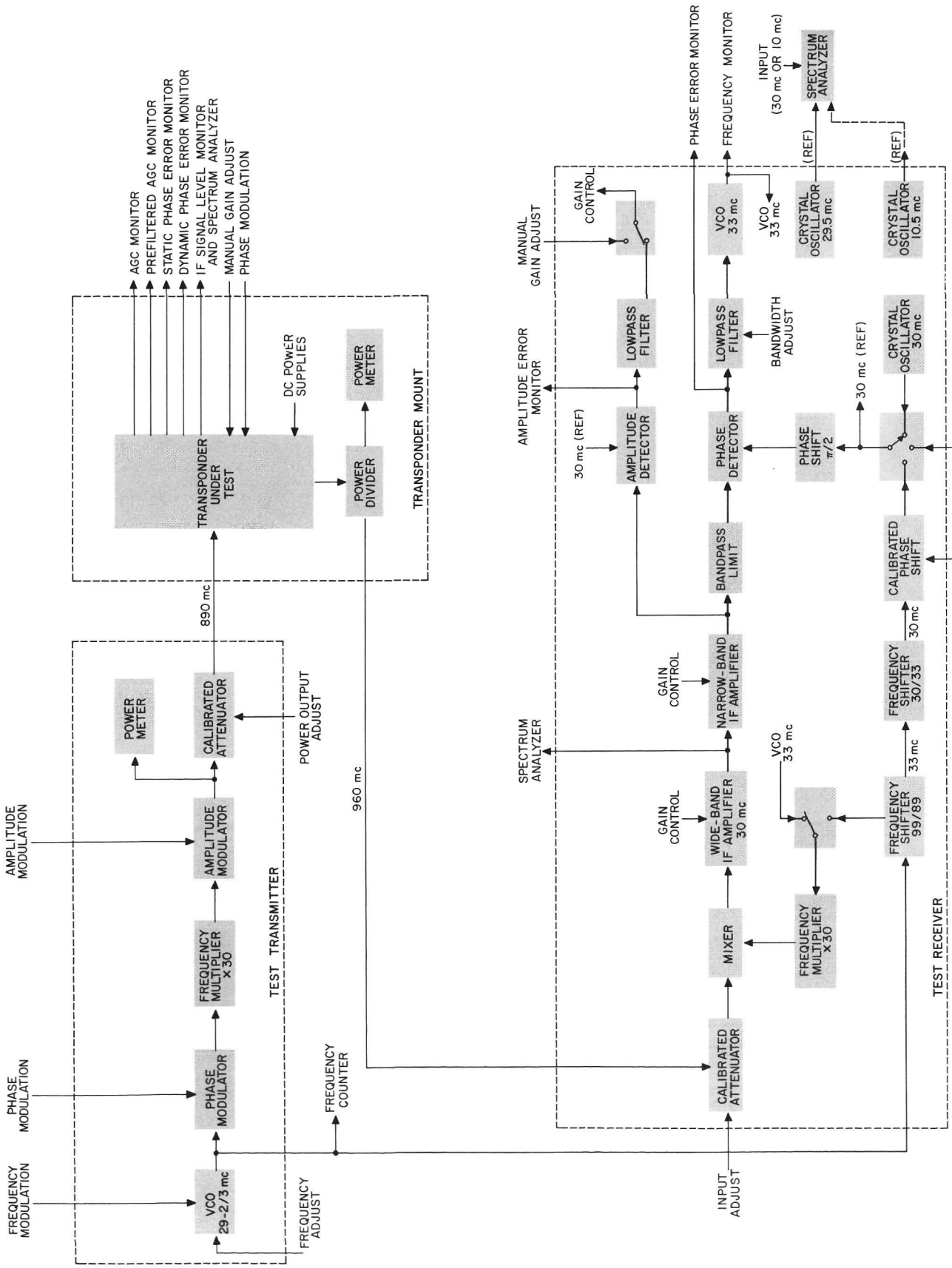

Figure 188. Transponder test set

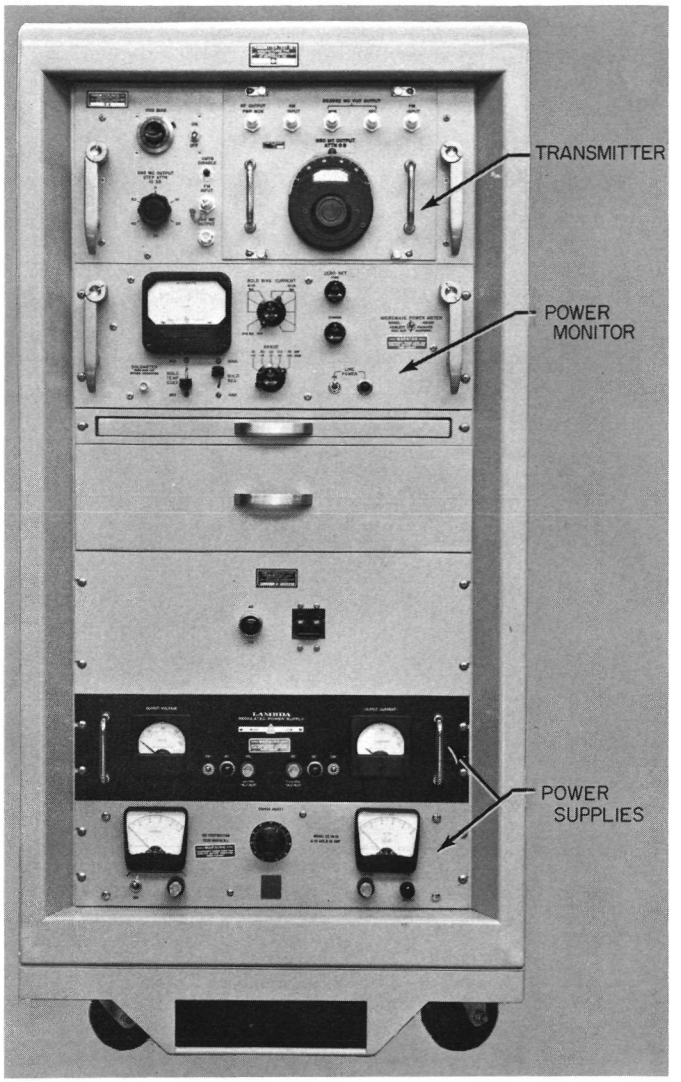

Figure 189. Test transmitter

nique, the transponder phase transfer function and modulation characteristics may be observed without the distortion introduced when an automatic phase control receiver is used.

The principal characteristics of the test receiver, which include means for both manual and coherent automatic gain control, and both amplitude and phase modulation monitoring are:

(1) *Center frequency:* 960.050 mc.

(2) *Tuning range:* (a) ± 1 part in 10^5 by automatic phase control, (b) ± 5.5 parts in 10^5 by manual steps of 1.5 parts in 10^5.

(3) *APC loop noise bandwidth:* selectable 5, 10, 20 or 100 cps.

(4) *Design point:* signal level -50 dbm.

(5) *Dynamic range:* 0 dbm down to -100 dbm.

(6) *Gain control:* manual or coherent automatic.

(7) *AGC loop noise bandwidth:* 10 cps at design point.

(8) *Amplitude-modulation response:* 0 to 5 kc (manual gain control mode).

(9) *Phase-modulation response:* 0 to 5 kc when used as a phase detector.

(10) *Input impedance:* 50 ohms resistive with a VSWR of no greater than 1.25 to 1.

In addition, the receiver provides either a 29.5-mc or a 10.0-mc reference signal for the panoramic spectrum analyzer, which is a part of the test set.

As shown in Figure 190, the receiver is assembled in a double instrumentation rack with its power supplies, an oscilloscope, a d-c-vacuum tube voltmeter, and an a-c-vacuum tube voltmeter. A modular design, illustrated in Figure 191, has been employed in the construction of the r-f components. These components, with the interconnecting circuits designed to accommodate manipula-

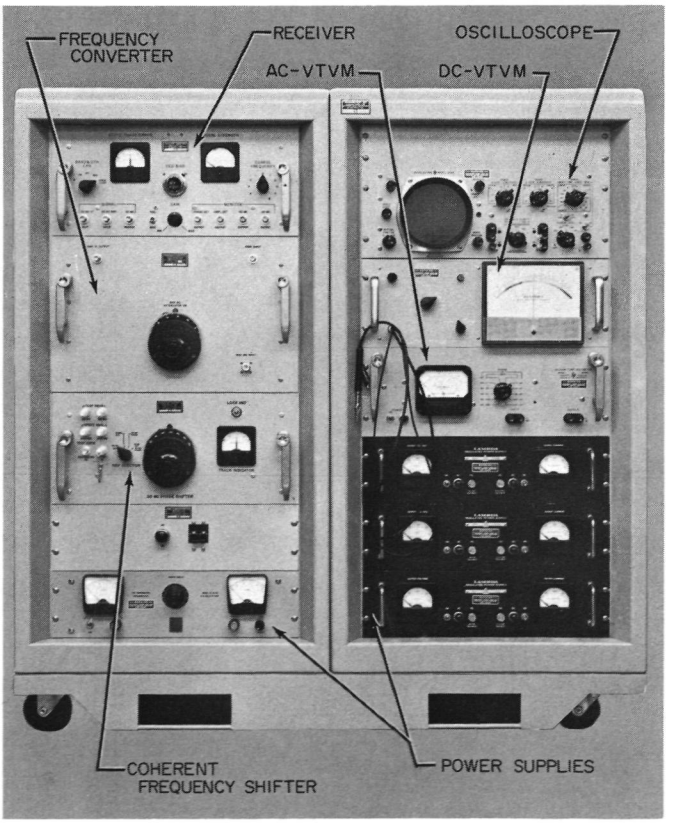

Figure 190. Test receiver

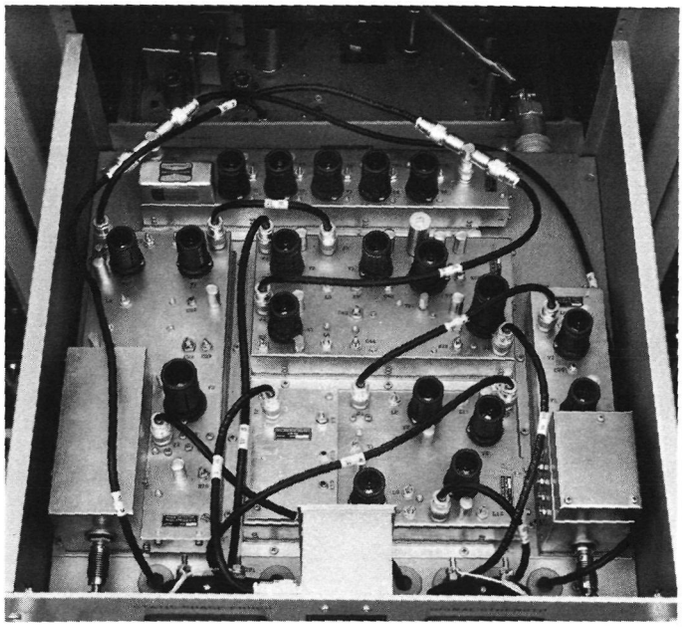

Figure 191. Internal view of receiver

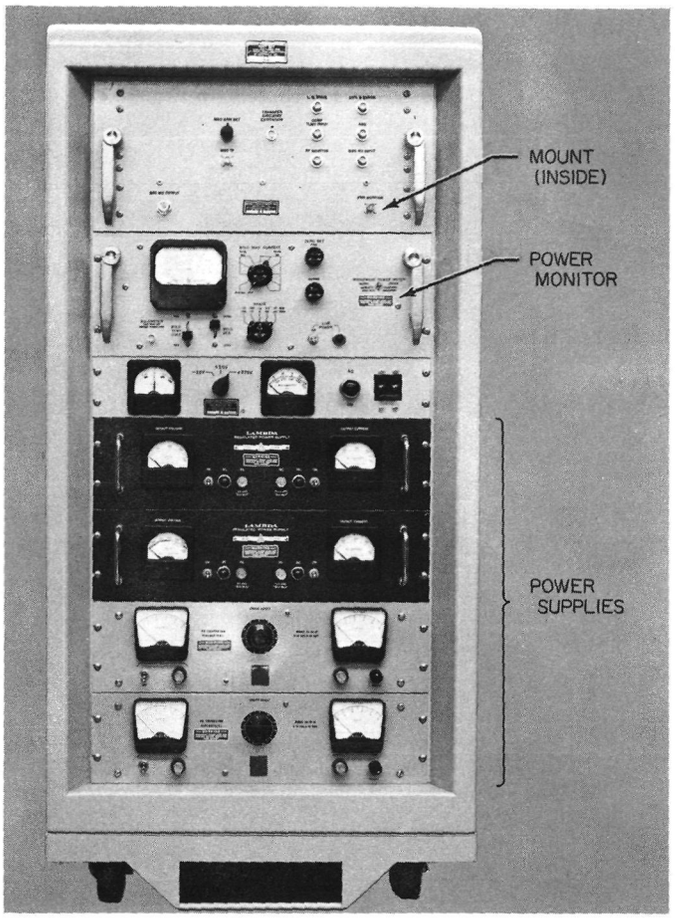

Figure 192. Transponder mount

tion of the interconnections, are often required by special tests.

The *transponder mount* provides a convenient means for operating the transponder for test purposes. It includes provisions for powering the transponder and its associated r-f cavity amplifiers (up to 25 w output). r-f power dividers, dummy r-f loads, and an r-f power meter are also provided in the assembly, which is shown in Figure 192.

The *test instruments* which complete the test set are an electronic frequency counter, an a-c vacuum-tube voltmeter, a d-c vacuum-tube voltmeter, a cathode-ray oscilloscope, a panoramic spectrum analyzer, a telemetering test oscillator, and a low-frequency function generator. These instruments are assembled in a double rack, as shown in Figure 193. As with the other assemblies of the test set, the racks are approximately 51 in. high, 28 in. deep, and of standard 19-in. panel width. They are equipped with large rubber castors for ease of handling and have recessed panels in order to protect the knobs, meters, and terminals.

e.* Ranger *antenna systems. The problem of providing antennas for the *Ranger* spacecraft involves two general requirements. The first requirement is to provide a high-efficiency communication link for telemetry, to be utilized for the later portions of the *Ranger* flight. The function demands a high-gain, vehicle-mounted antenna which can be directed toward the Earth. However, there are times when the high-gain antenna is incapable of being oriented toward the Earth: (1) before the spacecraft is stabilized in space; (2) during the period when the spacecraft is undergoing its midcourse maneuver; and (3) any time when the spacecraft is in a failure mode such that the high-gain antenna cannot be pointed toward Earth.

A second type of antenna is required to accommodate such situations, incorporating "quasi" omni-directional pattern characteristics. With such a radiation pattern, communications can be provided almost independently of the spacecraft orientation. However, this increased pattern coverage is obtained at the penalty of reduced antenna performance. This antenna can be used for telemetry purposes during the early portion of the spacecraft flight, when the spacecraft is undergoing attitude stabilization, and during the period of midcourse maneuvers. When this antenna is used for long-distance communication, it provides low information bandwidth.

Therefore, there are basically two antennas systems required. An omni-directional system providing telemetry coverage during the early portions of the flight, and a high-

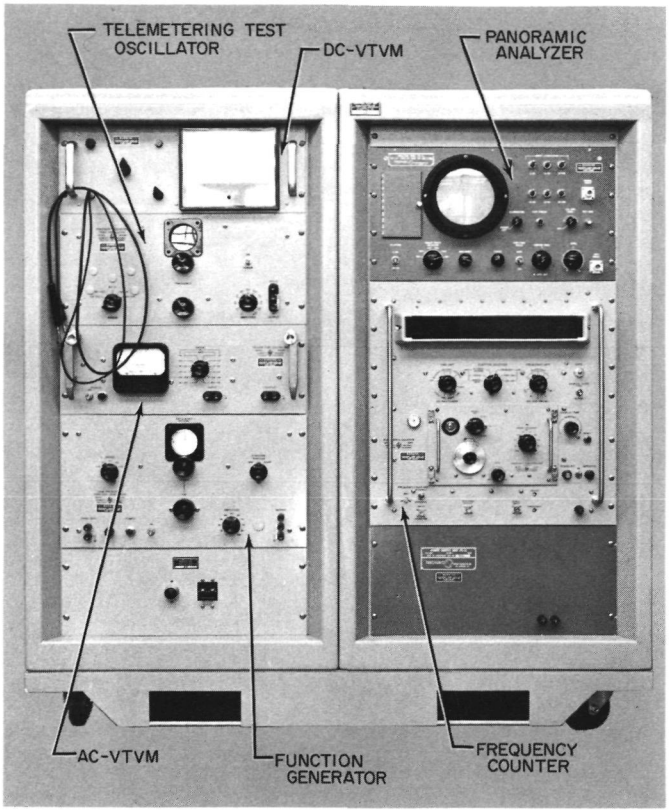

Figure 193. Test instruments

gain antenna system, giving required communication-system performance during the long-distance phases of the flight.

A third requirement is the capability of receiving commands sent to the spacecraft. Since one of the purposes of the ground command system is to override various spacecraft-generated commands or maneuvers when the spacecraft malfunctions, it is necessary to get commands through to the spacecraft no matter what the spacecraft orientation happens to be. This means that an omni-directional antenna is required for command purposes. Since there is already an omni-antenna aboard for telemetry, it is logical to use it to satisfy the omni-directional command requirement. A diplexer is needed to allow both the transmitter and receiver of the spacecraft transponder to operate on the same omni-antenna.

The antenna system must have a rotary joint to point the high-gain antenna back at the Earth through 2 deg of rotational freedom. One deg of freedom is obtained by rolling the spacecraft on its axis. The second deg of freedom results from moving the antenna relative to the spacecraft. This means the transmission line, which connects between the antenna and the spacecraft communication pan, must have bending capability. The best way to meet this requirement is to use a rotary joint.

High-gain antenna system. The original constraints imposed on the high gain antenna system were that its maximum size would be 4 ft in diameter and the weight of the reflector and feed structure should be less than 10 lb. The high-gain antenna is a 4-ft paraboloidal reflector, with a focal length-to-diameter ratio of 0.35. The reflective surface of the dish consists of ¼-in. square mesh, giving a surface coverage of approximately 19%. This mesh is supported by a structural system consisting of six radial arms and three concentric hoops. The feed for this antenna consists of a dipole mounted ¼ wavelength in front of a 9-in. diameter ground plane. A linear polarized radiator was chosen for simplicity; it matched the polarization of the omni-antenna.

Since this feed is driven from an unbalanced coaxial transmission line, and the feed is a balanced type of antenna, some type of balun was required. The balun type selected consisted of a one-half wavelength axial slot cut into either side of the outer conductor of the coaxial transmission line, thus splitting the outer conductor into two halves. Half of the way along the slot, one side of the outer conductor is shorted to the center conductor of the coaxial transmission line; the dipole feed is driven at this point. The 9-in. ground plane is mounted onto the outer end of the balun slot. The other end of the balun slot becomes the coaxial transmission line which runs from the feed area down to the base of the reflector. The feed structure position is stabilized by a fiberglass quadripod.

RA-1 to -5 configuration. As mentioned above, the feed type used for the RA-1 to -5 high-gain antenna (Fig 194) consisted of a half-wave dipole, mounted ¼ wavelength in front of a 9-in. diameter ground plane. For this particular configuration, the antenna was slightly defocused. Displacing the feed from the nominal focus has certain advantages. With the feed at the focus of the reflector, very sharp nulls were produced at either side of the maximum lobe whenever there was no phase variation in the illumination of the antenna aperture. By slightly moving the antenna and causing a variation in the phase of illumination, these nulls fill in, and therefore provide additional reliable angular coverage when the antenna is not closely directed toward the Earth. This advantage, however, can be utilized only during the early portions of the spacecraft flight when there is a sufficient signal margin. The performance parameters for the antenna are as follows, all measurements being made at 960 mc: The voltage standing wave ratio is 1.1 to 1 (Fig 195). The half-power beamwidth in the E plane is 17½ deg

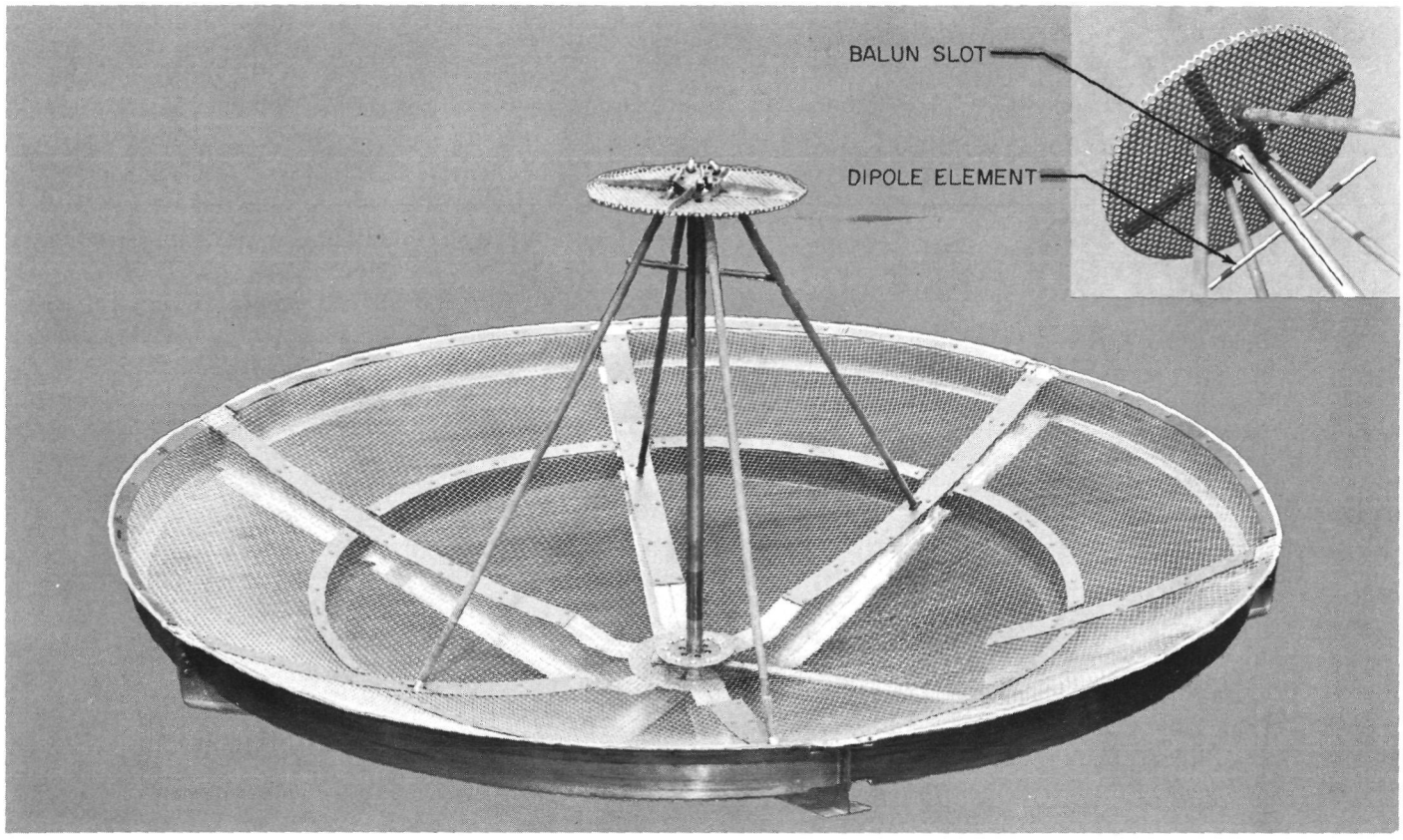

Figure 194. RA-1 to -5 high-gain antenna

and in the H plane it is 15½ deg. The 1-db beamwidth in the E plane is 10.5 deg and in the H plane is 9.5 deg. The highest side lobe level in the E plane is down by 22.5 db, whereas in the H plane it is down by 16 db. The gain of the antenna is 19.5 db. The E and H plane antenna patterns are shown in Figure 196.

The matching section of the antenna system consisted of a quarter-wave coaxial transformer located approximately 1 in. below the balun slot (toward the base of the reflector). The balun slot itself was resonant at 0.454 wavelength or 5.587 in. The final length of the dipole element was 6.25 in. over-all and, it was spaced 3.13 in. from the 9-in. diameter ground plane.

Only minor difficulties occurred with this antenna during the initial development stage. One particular problem was a variation in the impedance of the antenna during type-approval tests. In an effort to isolate this trouble, higher-level tests were run, and it was noted that the disturbance occurred during a resonance in the feed structure. During the high-level test, the quadripod longerons failed. When the deficiencies in the longerons were correct, the impedance variations noted before were no longer found.

RA-6 and -7 high-gain antenna development. When the requirements for the RA-6 and -7 program were established, it was considered desirable to use a circularly-polarized high-gain antenna. A circularly-polarized high-gain antenna had already been developed for the *Mariner* program, and it was decided to use that antenna for the RA-6 and -7 vehicles (Fig 197). The antenna is similar to the RA-1 to -5 type high-gain antenna, with the following differences: in order to circularly polarize the antenna, the ½-wave dipole on the feed of the RA-1 to -5 antenna was replaced by a turnstile (two crossed dipoles). Since the turnstile changes the impedance of the high-gain antenna, the ¼-wave matching transformer required redesign. This involved changing the diameter and location of a ¼-wavelength enlarged section of the center conductor of the coaxial transmission line. Some mirror modifications were made to the reflector structure to enhance the reliability of the reflector surface and the focus was adjusted. With the high-gain antenna right-hand circularly polarized, its performance is essentially the same as the RA-1 to -5 antenna.

RA-8 and -9 high-gain antenna development. The performance required of the high-gain antenna for RA-8

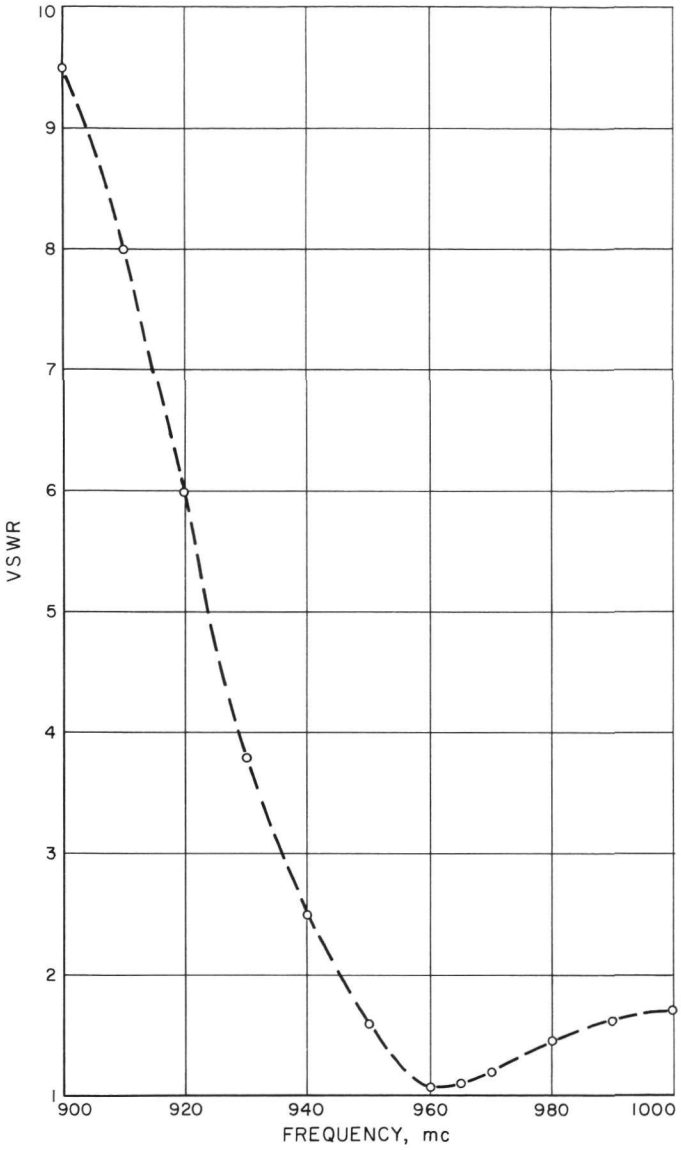

Figure 195. VSWR of RA-1 to -5 high-gain antenna

and -9 is the same as that for RA-6 and -7 at 960 mc. However, RA-8 and -9 will carry an S-band communication and tracking experiment. It is required that a high-gain antenna be used with the S-band experiment. Because it was not feasible to put a second high-gain antenna on the spacecraft, the decision was made to broadband the existing antenna to cover the S-band frequencies, as well as the 960-mc frequency. Again, a design was borrowed from the *Mariner* program (Fig 198). The reflector is the same as that used for RA-6 and -7. The major difference is in the feed structure and the feed structure support. To meet the bandwidth requirement for the feed, a conical spiral periodic antenna structure was used (Fig 199). Since this type of antenna has to be fed at the small end of the cone, by a balanced line with an impedance of over 100 ohms, a broadband balun transformer is required to connect the antenna to the 50-ohm unbalanced coaxial line. The design used consists of a coaxial line which has been peeled open (Fig 199). Since the impedance of the slotted coaxial line is higher than that of a closed line, and also is a function of the width of the slot, this type of balun can be used to give the required impedance transformation.

During the development of this broadband feed, it became apparent that conducting material in close proximity to the feed was highly undersirable. Therefore, the final configuration incorporates a dielectric feed-support structure. Gain measurements versus focal distance (Fig 200) of the original *Mariner A* high-gain broadband antenna indicated that the minimum distance for good operation at all three frequencies required (960, 2113 and 2295 mc) is about 22 in. This focal distance is also the maximum allowable feed protrusion into the RA-1 to -7 sterilization diaphragm without requiring a change to that structure.

Impedance measurements of the antenna with the feed at 22 in. indicated that an impedance transformation of 50 ohms unbalanced to 200 ohms balanced is required. A photo of a disassembled feed and 200-ohm balun is shown in Figure 199. Figure 198 shows the all-dielectric support structure and the antenna feed in a prototype spun-aluminum parabola.

R-F rotary joint. Two different types of rotary joints are required for the *Ranger* program. The rotary joint for RA-1 to -7 is required to operate at 960 mc only and, therefore, is a single-frequency design. The rotary joint to be used for RA-8 to -9 has to pass 960 mc and S-band, since the high-gain antenna will be operating both at 960 mc and at S-band.

RA-1 to -7-type rotary joint. A survey was made to see if there were any commercially available rotary joints that would be adequate for a space environment. Several requirements would have to be met by the rotary joint: (1) It would have to operate reliably over a long period of time and at extremely low pressures. This puts a severe limitation on the rotary joint bearing since normal bearings will probably seize under sustained vacuum environment. (2) The rotary joint had to have very low insertion loss and negligible wow.

Since there were no commercial joints considered acceptable in these areas, a program was started at JPL to develop a suitable rotary joint. The basic configuration chosen was a rotary joint with r-f chokes. This technique eliminates any metal-to-metal relative motion joints at

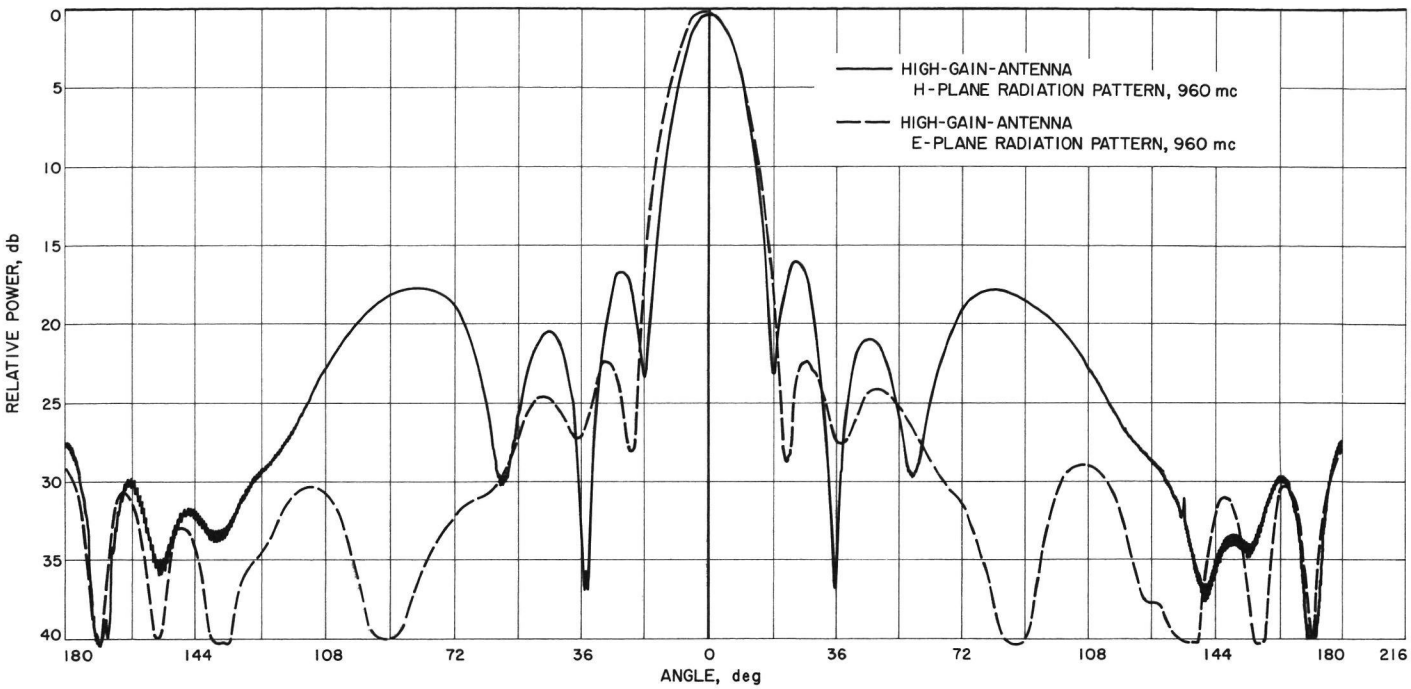

Figure 196. RA-1 to -5 high-gain antenna radiation pattern

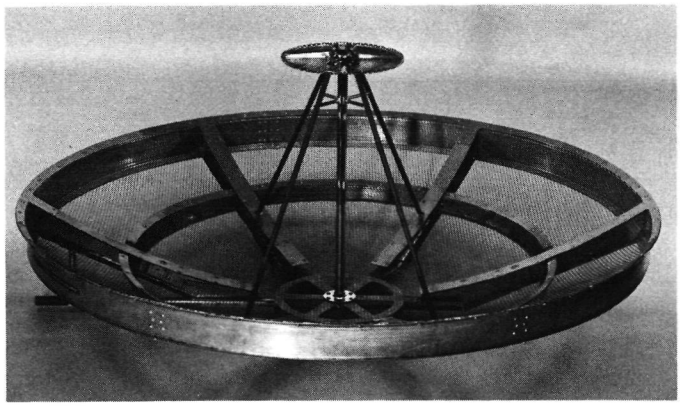

Figure 197. RA-6 and -7 high-gain antenna

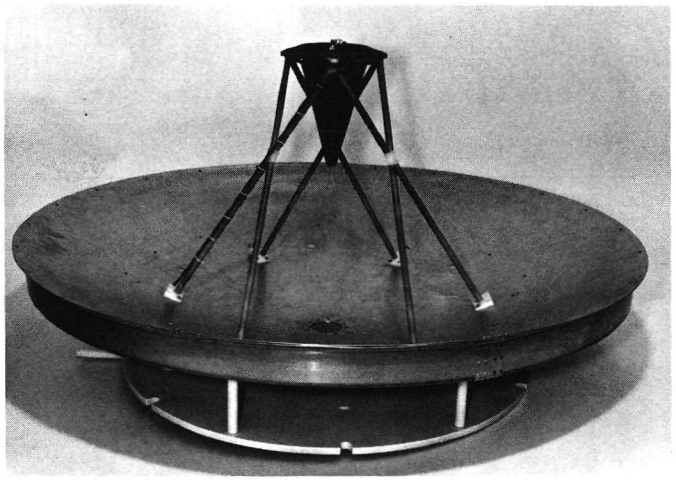

Figure 198. RA-8 and -9 high-gain antenna prototype

low impedance levels which could cause seizing of the rotary joint or could cause noise because of corrosion or dirt in the joint. The conventional joint where the relative motion is taken through fingerstock was eliminated at the start, since it was believed that the fingers could conceivably weld to the mating portion of the joint. The choke for the center conductor of the rotary joint consists of an open circuit ¼-wavelength choke. It reflects the high impedance at the open end of the choke into a very low impedance at the point where the ¼-wavelength choke enters the transmission line. The choke in the outer conductor is a shorted ½-wavelength choke; the short is reflected through ½ wavelength into a short at the point where the choke enters the transmission line at the outer conductor. The only metal-to-metal contact in the rotary joint occurs in the center of this ½-wavelength choke. However, this is not critical since at this point the choke is at a very high impedance level and noisy or erratic performance would be greatly attenuated by transformation through the ¼ wavelength down to the point where the choke intercepts the outer conductor.

It was desired to optimize the performance of the rotary joint at the spacecraft transmitting frequency.

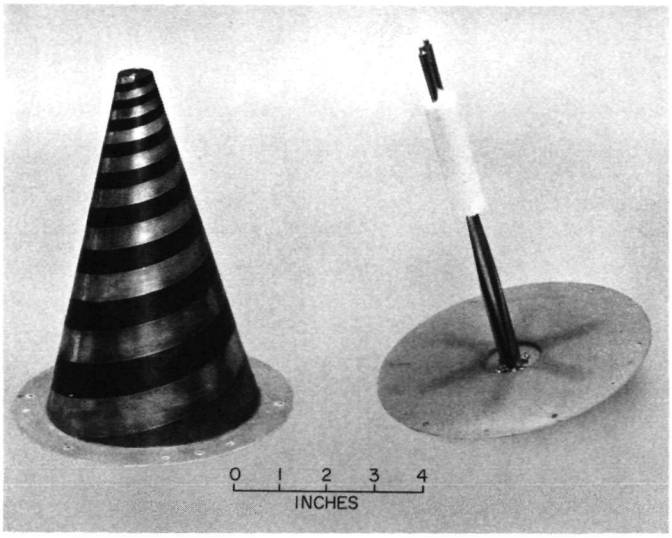

Figure 199. RA-8 and -9 broadband feed, disassembled

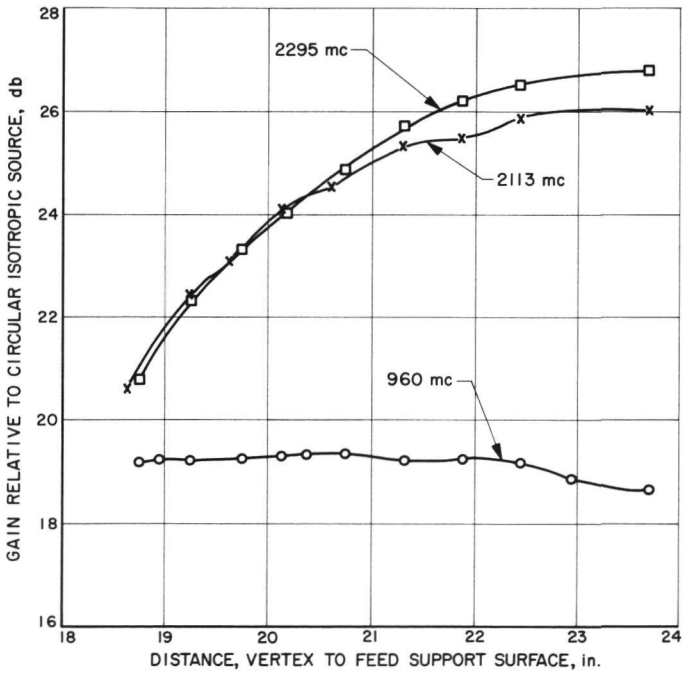

Figure 200. RA-8 and -9 high-gain antenna gain vs feed position, fiberglass struts

However, sufficient broadbanding was included so the rotary joint could be used at the receiving frequency in case a two-way system ultimately is needed. Considerable effort was expended designing the bearing system of the rotary joint. Due to the low expected angular rates of the antenna, the rotary joint was designed with dry bearings. This eliminates the problem of lubricants and the probability that the lubricants would evaporate in a vacuum environment. The selection of the bearings for the rotary joint was complicated for several reasons:

(1) Due to the size of the rotary joint, conventional ball bearings would not fit.

(2) Lubrication of conventional bearings would be difficult because of the basic requirement that the rotary joint could not be pressurized.

(3) The bearings within the coaxial section of the rotary joint itself must not degrade the electrical performance of the joint.

In the final design, one main bearing is used at the rotating end of the joint and is located in the center of the ½-wavelength outer choke (Fig 201). This arrangement consists of a sleeve bearing with silicon copper running on 303 stainless steel, with a molybdenum disulfide dry lubricant. A tungsten carbide needle bearing, running dry in an aluminum oxide ceramic jewel, carries the axial loads of the rotary joint in a compressive direction. This bearing is located within the ¼-wavelength open-circuit choke, which is within the center conductor of the rotary joint. A 303 stainless steel collar on the sleeve bearing keeps the rotary joint from separating in the axial direction. To maintain the concentric tubes of the joint in line, aluminum oxide spacers are used. Alumi-

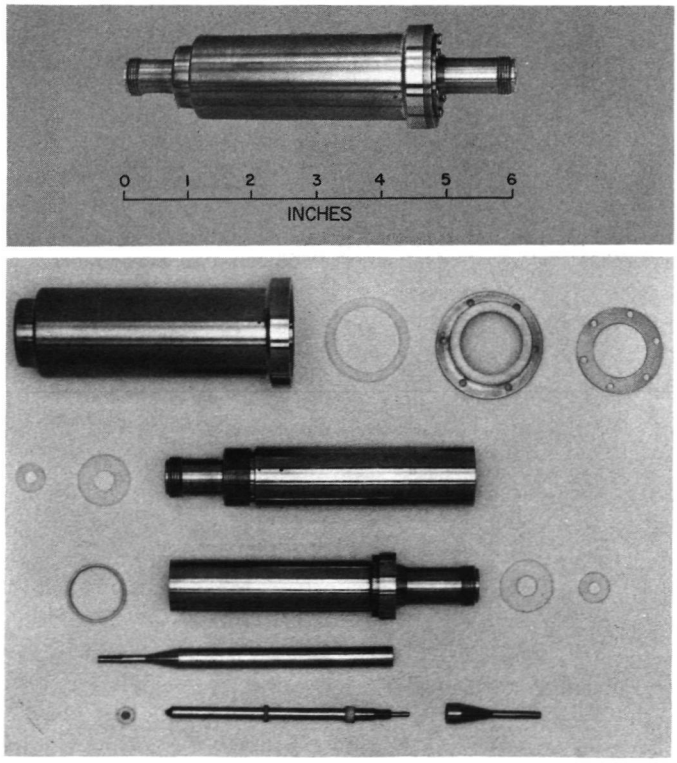

Figure 201. Prototype rotary joint, disassembled

num oxide is ideal in this application because it has low r-f losses and is a very hard material. The design approach on the bearings was conservative due to the lack of information on bearing performance at extremely low pressures.

The final version of the rotary joint is 5½ in. long and 1⅜ in. in diameter and weighs 0.99 lb (Fig 202). The chokes in the rotary joint were determined to be quite broad, providing a VSWR of less than 1.1 over a frequency range of 770 to 1000 mc. The insertion loss turned out to be 0.05 db at 960 mc and the wow is within 0.01 db, the measuring accuracy of the insertion loss measurement.

The rotary joint was run through an environmental testing program to test the life expectance of the unit. The unit has successfully completed 970 hr of continuous running (58,565 revolutions) at 1 rpm in a specially designed cycling test fixture under a normal room environment. At the beginning of the tests, the torque necessary to drive the rotary joint was 1.0-in. oz maximum with an average of 0.5-in. oz. At the end of the test, it required a 1.5-in. oz maximum driving torque with an average of 0.7-in. oz. This running rate is approximately 60 times faster than the choke could run if the antenna on the spacecraft was moving continuously at its maximum rate. Therefore, it is believed that this is a very conservative life test. At the completion of this test, the dry bearing showed no indication of wear and there were no changes in the electrical performance of the rotary joint.

In order to determine if operation in a vacuum would affect the operational life of the rotary joint, the unit underwent a test in the cycling fixture in a vacuum chamber at pressure of 10^{-6} mm of mercury. The rotary joint remained in the vacuum chamber for approximately 1 week. Upon termination of the test in the vacuum chamber, the rotary joint was subjected to electrical measurements. There was no sign of degradation or changes of the electrical performances of the rotary joint as a result of the vacuum test. In order to determine the effect of high temperature on the driving torque requirements of the rotary joint, tests were made at 200°F. During these tests, the drive torque exceeded 15-in. oz, well above the room temperature requirements of about 2-in. oz.

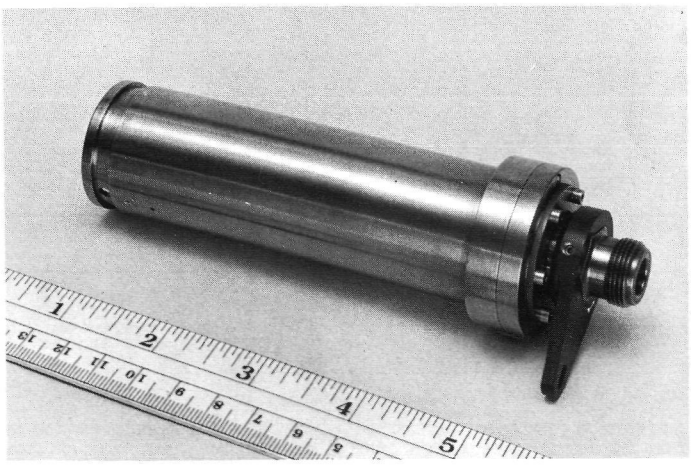

Figure 202. Flight r-f coaxial rotary joint

Internal examination showed one of the ceramic spacers to be broken with one piece of the ceramic completely out of place. Examination of the breakage planes of the ceramic led to the conclusion that the failure was caused by localized stress concentration as the beryllium copper conductor expanded within the ceramic. The stress concentration was probably brought about by improper distribution of the adhesive between the ceramic and the conductor. Further evaluation of the expansion breakage of these spacers was conducted. Five dummy conductors with a total of nine ceramic spacers cemented in place were baked at temperatures ranging from 125°F to 400°F in 25°F increments. Pieces were baked for 30 min at each temperature. No total failure occurred during any of the tests. Each failure that did occur consisted of only single hairline cracks occurring at 400°F. Because the bearing loads carried by the spacers are low, it was believed that a hairline crack failure would not impair the reliability of the rotary joint. Dynamic environmental tests using some of these hairline-cracked ceramic spacers indicated this to be true; therefore, no modifications were made to the rotary joint for the RA-1 to -5 series. However, for RA-6 and -7 the rotary joints were modified slightly to eliminate the problem. Instead of cementing the ceramics in place, they were machined with a clearance from the supporting conductor. To hold these ceramics in place, shoulder sleeves were soldered onto the supporting conductor to keep the ceramics from moving back and forth. Tests on units using this fabrication technique indicated that it was a feasible solution.

Rotary joint for RA-8 and -9. Since on RA-8 and -9 an S-band experiment was to be flown which would use the high-gain antenna, the rotary joint had to be re-designed to handle not only the 960 mc, but also 2295 mc, which is the S-band transmitter frequency, and 2113-5/16 mc, which is the S-band transponder receiver frequency. The requirements were met by the use of resonant chokes in the following manner: The inner choke was designed to be a ¼-wavelength, open-circuited choke at 700 mc, and a ¾-wavelength, open-circuited choke at 2200 mc. The

outer choke was designed to be a ½-wavelength shorted choke at 1100 mc, and 1-wavelength shorted choke at 2200 mc. Since, at the lower frequency, the two chokes were not resonant at 960 mc, the length and impedance of the chokes were so set that they exhibited equal and opposite reactance at 960 mc, giving a series resonance effect which allowed the passage of L-band energy. In essence, the rotary joint was designed with two resonant passbands: one at 960 mc and one at 2200 mc. The 2200-mc passband was sufficiently broadband so that it covered both 2113-5/16 mc and 2295 mc. In order to match out the effects of the coaxial supporting beads, two impedance-matching transformers were included in the rotary joint. One transformer matches the effect of the beads at S-band, the other transformer, designed to be ½-wavelength long at 2200 mc so that it would have minimum effect at S-band, matches the effect of the beads and of the S-band transformer at 960 mc. Tests on two prototype rotary joints show that the S-band losses are less than 0.2 db and the VSWRs at 2113-5/16 mc and 2295 are 1.17 and 1.21, respectively. The loss at 960 mc was less than 0.05 db and the VSWR was less than 1.05 to 1.

Omni-antennas. The basic requirement for the omni-antenna is to provide as uniform a pattern coverage over a sphere as possible. Giving coverage over a complete sphere increases the communication flexibility if the spacecraft is not properly oriented, or allows the spacecraft to assume different attitudes during its flight. The requirement for uniform coverage makes it possible to evaluate the performance of the communication system, since a knowledge of the radiation properties of the antenna on the spacecraft would be available. Also, this eliminates the possibility of looking at a null on the antenna on the spacecraft for some particular attitude of the spacecraft, thus jeopardizing the communication link to the spacecraft.

RA-1 and -2 omni-antenna. Rangers RA-1 and -2 required omni-communications with the spacecraft for Sun–probe–Earth angles of 40 deg to 140 deg, and for any angle about the roll axis.

Constraints were imposed on the spacecraft, to help meet this communication requirement. One such constraint was that no spacecraft hardware could lie within the specified communication angle. A second was that the bulk of the spacecraft below the antenna should appear symmetrical. A number of antenna configurations were considered and evaluated (Fig 203):

(1) Sleeve dipole.

(2) ¼-wavelength stubbed cone.

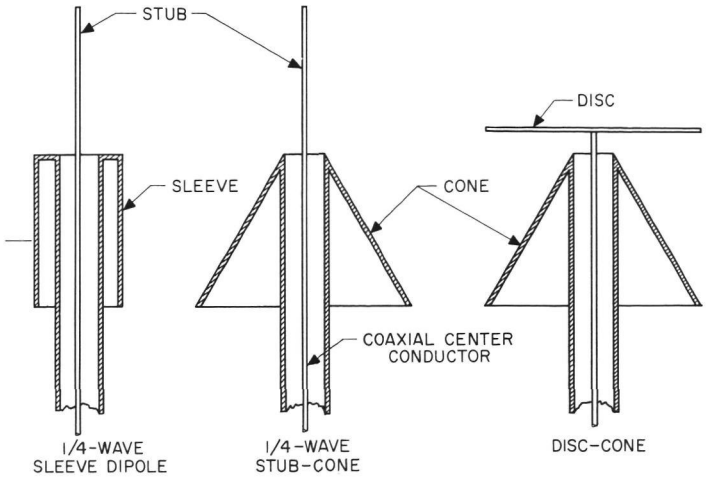

Figure 203. Omni-directional antenna types

(3) Disc-cone antenna.

To meet the requirement that the spacecraft should not interfere with the antenna field of view, the only location acceptable for the antenna was above the spacecraft, on its roll axis. It was in this location that the above configurations were tested. To maintain the requirement that the spacecraft appear symmetrical and to control the points where reflections could originate, a diffraction structure was used to isolate the antenna from the spacecraft.

The first two types of antennas were initially evaluated with an 80-deg diffraction cone. Apparently, traveling waves were excited on the cone and a considerable amount of energy was radiated toward the spacecraft and then reflected, causing a number of deep serrations in the basic pattern of the antenna (Fig 204). It was found that placing chokes between the antenna and the diffraction cone had little effect in controlling the serrations. A diffraction disc was tested and found to be effective in reducing the amount of energy directed toward the spacecraft. However, it was determined that, if a sufficiently large disc was used to minimize the amount of energy directed toward the spacecraft, it subtended a large enough angle to adversely effect the pattern coverage aft of the spacecraft. A typical pattern obtained with the sleeve dipole above a diffraction disc is shown in Figure 205. This disc subtended an angle of approximately 80 deg, as viewed from the antenna center. It can be seen that the major direction of the radiation is toward the forward end of the spacecraft, with very little toward the aft end.

The sleeve dipole was eliminated because of the relatively narrow-band characteristics of this type of antenna. (A wide bandwidth is required because the

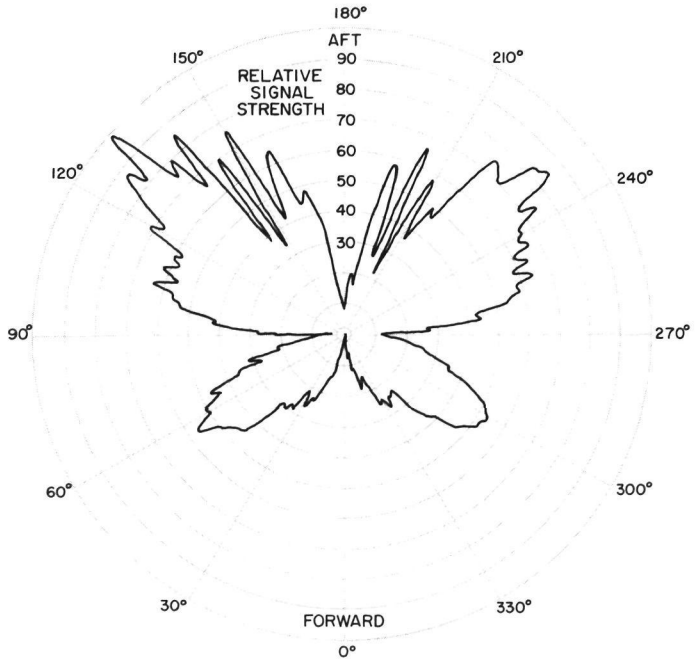

Figure 204. Sleeve dipole with diffraction cone

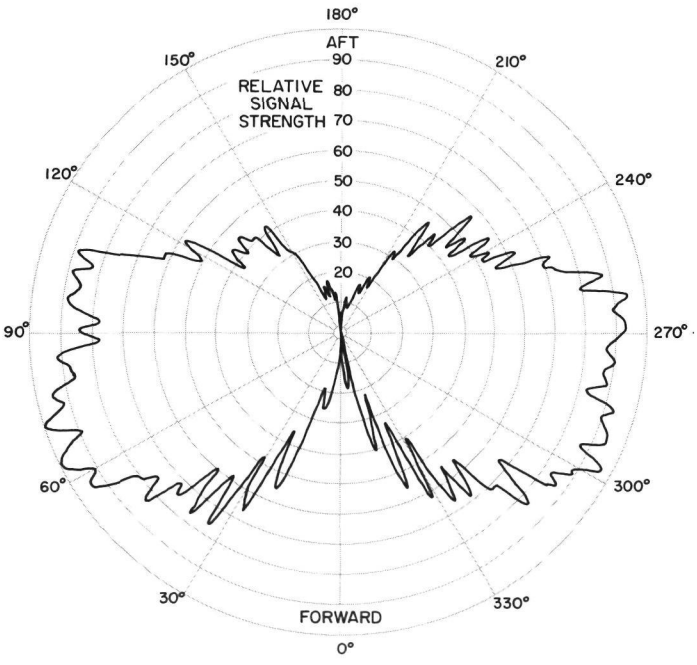

Figure 205. Sleeve dipole with diffraction disc

antenna must operate at both 890 mc and 960 mc.) The bandwidth is narrow because the design requires a resonant choke in the sleeve portion of the dipole. The ¼-wave, stubbed-cone antenna was considered next, since it was believed that the problem of choking a cone-type antenna was less severe than for the original sleeve dipole. The next step was to replace the stub with a disc. This type of antenna is sufficiently broadband to handle both the 890 mc and 960 mc. The antenna also has a lower silhouette, providing a shorter all-around spacecraft system. This antenna was found to be versatile, since there are many parameters (the length and the angle of the cone and the diameter of the disc) that can be used to vary the pattern shape. The pattern shape of a disc-cone antenna with a ¼-wavelength diameter disc and a ¼-wavelength cone is similar to that of a dipole. Tests made with the disc-cone antenna indicated that the radiation can be directed toward the aft end of the antenna when either the cone angle is made smaller (i.e., going from 80- to 60-deg cone), or if the length of the cone is increased. Increasing the diameter of the disc to more than ¼ wavelength shifts the pattern toward the forward end of the antenna. It was found that a combination of increasing the length of the cone and increasing the diameter of the disc provided the required pattern coverage. The final configuration used a disc approximately ¾ wavelength in diameter and a cone approximately ½ wavelength long with an angle of 80 deg. The pattern of a full-scale disc-cone without the spacecraft is shown in Figure 206.

Next, measurements were made to determine the effect of a diffraction disc on the disc-cone antenna pattern. It was found that the diffraction disc had an appreciable effect on the resultant pattern of the disc-cone antenna. Depending upon the position of this disc, a pattern could be produced which was predominately forward directe

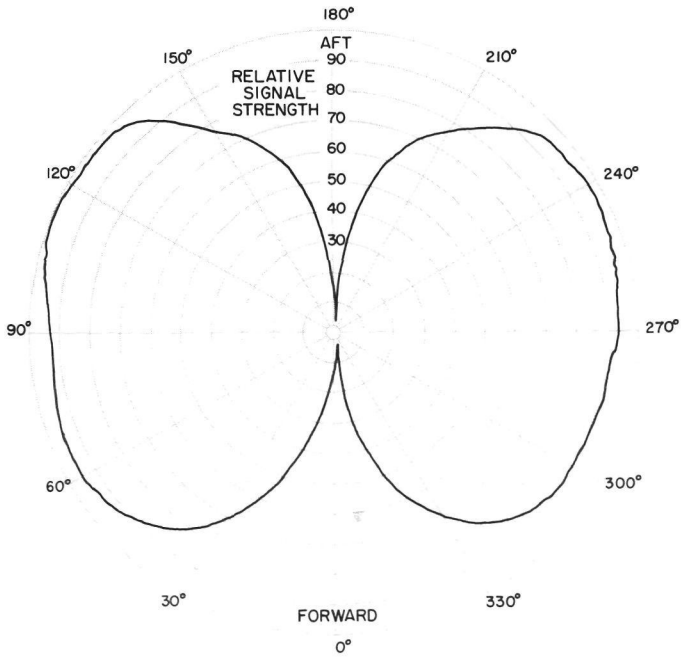

Figure 206. Full-scale disc-cone antenna

aft directed, or apparently independent of the disc. It was found that a 16-in. diameter diffraction disc placed 16 in. from the forward end (i.e., the disc) of the antenna gave the best results (Fig 207). By comparing with previous pattern (Fig 206), it can be seen that the disc causes approximately a 1-db dip at the equatorial plane of the pattern, and somewhat reduces the energy radiated toward the aft end of the antenna. In order to determine whether the effect of the diffraction disc could be minimized, absorbers were mounted on the side of the diffraction disc facing the antenna. It was found that the absorber only had a small effect on the diffraction disc. Since the absorber would add considerable weight to the antenna and would provide mechanical problems, the small increase in antenna performance was not sufficient to warrant its use. The prototype antenna is shown in Figure 208.

A ¼-scale disc-cone antenna was built and mounted on a ¼-scale disc-cone antenna was built and mounted on (Fig 209). There is a considerable amount of amplitude ripple along the maximum of these patterns. This results from a small amount of energy still getting onto the spacecraft and being re-radiated. Since the spacecraft is located a number of wavelengths from the antenna, a large number of low-amplitude lobes are formed. Most of the ripple is within about 1-db magnitude, with the exception of one large peak in a forward direction. From the pattern with the solar panels in an extended position,

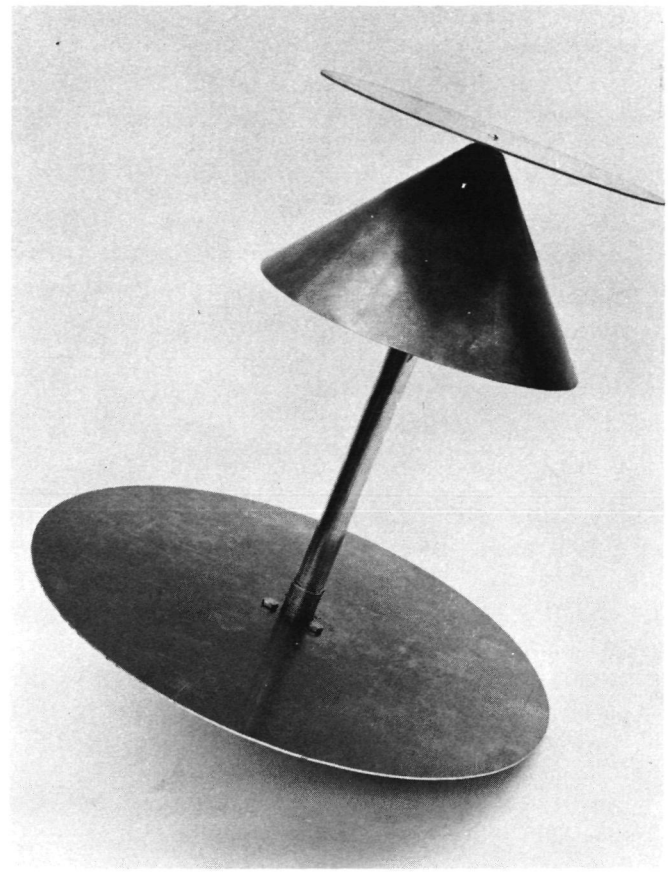

Figure 208. Disc-cone antenna with diffraction disc

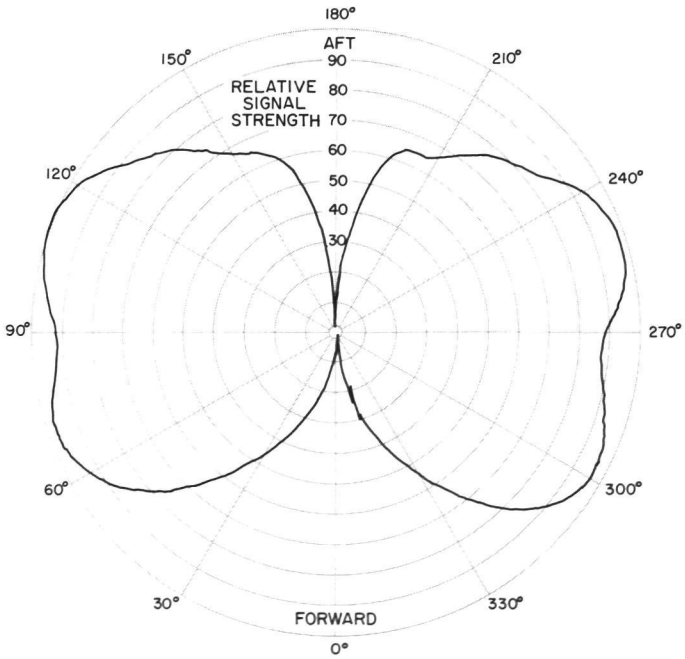

Figure 207. Full-scale disc-cone antenna plus diffraction disc

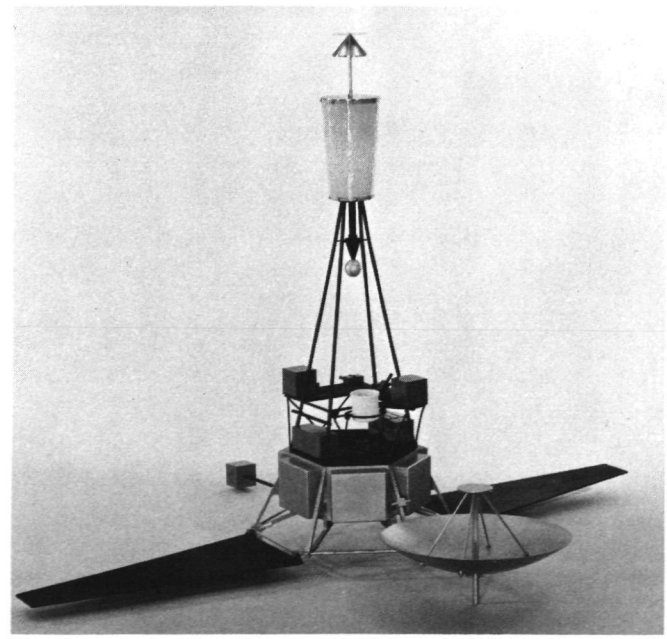

Figure 209. One-quarter scale spacecraft and antenna system

it was found that the solar panels affect the pattern only in a forward direction, primarily in the area between 20 and 50 deg from the forward end of the spacecraft. The effect of the solar panels and spacecraft could be reduced by using a considerably larger diffraction disc and locating it at a greater distance from the antenna. However, this was not practical for two reasons:

(1) The antenna with the large diffraction disc would require considerably more room under the shroud of the launching vehicle than was available.

(2) A sacrifice in radiation toward the aft of the spacecraft would result, limiting the coverage in that direction to within approximately 30 deg of the spacecraft equatorial plane.

Figure 210 shows the final flight configuration of the omni-antenna. A fiberglass cylinder is used to support both the disc at the top of the antenna and the rim of the cone (Fig 210). The fiberglass cylinder mates with the ground plane. Because the antenna is supported by the outer rim of the ground plane, buttresses were used to carry the loads up from the edge of the ground plane to the fiberglass cylinder. The disc-cone antenna is fed by a coaxial transmission line which travels up the center of the fiberglass cylinder. Within this transmission line is a ¼-wavelength matching transformer; it is located where the phase of both the 890- and the 960-mc impedance is the same. The original design of the antenna had a lip at the top of the antenna where the disc and the fiberglass cylinder were laced together. It was feared that this lip might hang up on the shroud, as it was ejected. To eliminate this possibility, a modification was made to the antenna by adding a small fairing. The fairing began approximately 2 in. below the top of the antenna and ran up to the edge of the disc. This modification did not appreciably affect the electrical characteristics of the antenna.

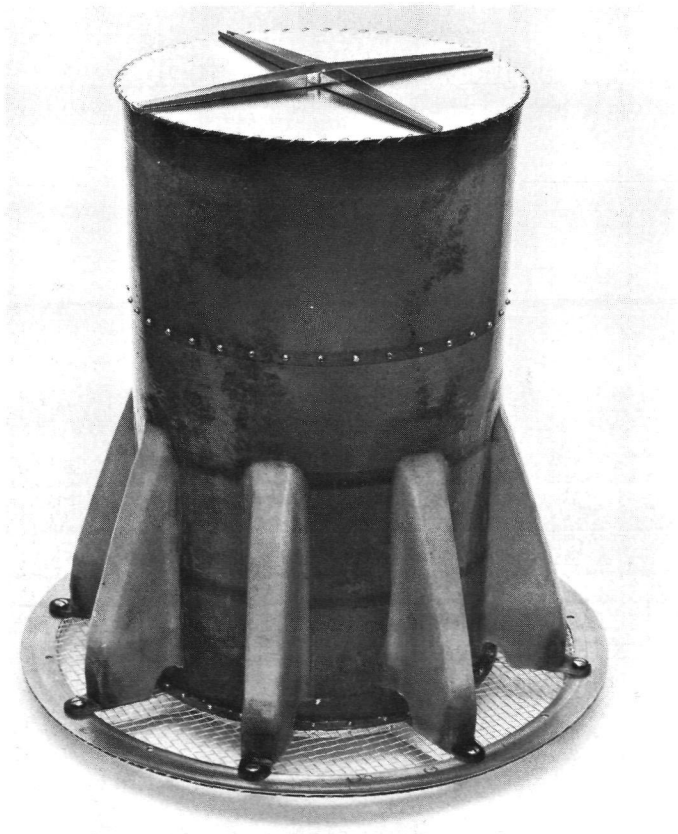

Figure 210. RA-1 and -2 omni-directional antenna

The VSWR of the antenna at both 890 mc and 960 mc was below 1.2. The gain was approximately 1.6 db above isotropic at 960 mc, and 1.7 db at 890 mc. Its weight is approximately 3.3 lb.

RA-3 to -5 omni-antenna. The RA-3 to -5 spacecraft was designed to carry a lunar landing capsule. This capsule is located on top of the spacecraft, and at the separation time, the capsule is separated from the spacecraft by traveling forward along the spacecraft axis. Since the omni-antenna that was used on RA-1 and -2 was located on the top of the *Ranger* spacecraft, there was a mechanical conflict between the antenna and the capsule. In order for the capsule to separate, the omni-antenna had to be moved out of the way of the capsule. Several techniques were proposed. One was to support the omni-antenna on a boom which could be deployed before capsule separation. A second was to mount the omni-antenna directly to the capsule and jettison it before the capsule was separated. Since the capsule was being designed by a subcontractor to JPL, it was believed that mounting the antenna on the capsule would create serious coordination and integration problems. Therefore, it was decided to mount the omni-antenna on a boom. However, deploying the RA-1 and -2 antenna on a boom presented a serious problem due to the weight (3.3 lb) of the omni-antenna. It was determined, in order to keep the boom weight to a reasonable value and to make the operation reliable, that the omni-antenna should not weigh more than 1 lb.

It was recognized that with the additional constraints of a lighter, more simplified antenna, it would no longer be possible to provide the coverage from the equatorial plane of the spacecraft, as specified for RA-1 and -2. Analysis of the trajectories indicated that a coverage of ± 30 deg from the spacecraft equatorial plane would be acceptable, in view of the essential requirement of a reliable antenna deployment system.

Because of the limited time available for the redesign of the omni-antenna, the antenna was restricted to configurations which were well understood. One configuration that seemed to lend itself to the application was the antenna designed and used with the *Pioneer III* and *IV* spacecraft. The design was a stub cone, where the cone portion of the antenna consisted of fiberglass plated with a conducting surface. The principal modifications required to the *Pioneer III, IV* antenna were a reduction in the length of the plated portion on the cone, and the addition of a modified matching section for the antenna (Fig 211). Considerable trouble was encountered in fabricating the cone for the antenna—the gold plating failed to adhere properly to the fiberglass. Various techniques were attempted to correct this, including metal-spraying the fiberglass and bonding foil onto the fiberglass. However, none of these techniques properly solved the problem. It was determined that the cones could be plated as on the original *Pioneer III, IV* antennas but the process required severe quality control. It appeared that the original vendor, who had done the earlier *Pioneer* work, could no longer maintain the quality of his process to get a reliable plating job. A comprehensive survey of other platers finally located one vendor who could control the process sufficiently well to get a reliable bond between the plating and the fiberglass. The VSWR of this antenna was below 1.2 to 1 and the gain was 2.7 db at 890 mc, and 2.4 db at 960 mc. The final antenna weight was 0.7 lb.

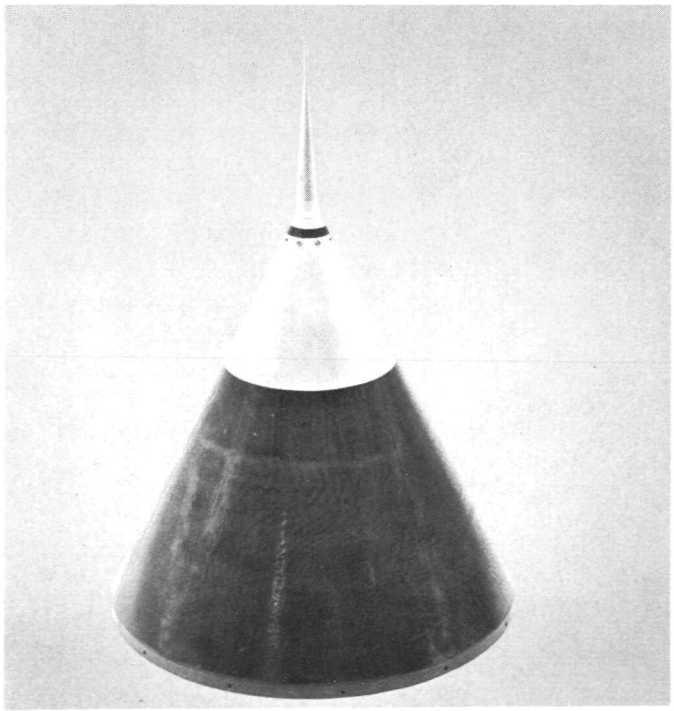

Figure 211. RA-3 omni-directional antenna

RA-6 to -9. Since RA-6 to -9 spacecraft do not carry a landing capsule, deploying the omni-antenna is not necessary. Therefore, the RA-1 and -2-type antenna was used, because of the improved pattern coverage obtained with that antenna. A short study was made to see if the antenna on RA-6 to -9 had to be put in the same location as on RA-1 and -2, or whether it could be located at the lower position used on RA-3 to -5. It was determined that the RA-6 to -9 antenna could be located at the same location as the RA-3 to -5 antenna and still provide adequate pattern coverage for the mission.

Omni-directional antenna patterns. Before an accurate analysis of the performance of the RA-1 and RA-3 types of omni-directional antennas could be made, the radiation patterns of these antennas, mounted on the appropriate spacecraft, had to be known to a reasonable degree of accuracy. To accomplish this, full-scale mock-ups were made of a typical spacecraft for each major *Ranger* configuration (i.e., RA-1, -3, and -6). As each type of mock-up was completed, an omni-antenna was mounted on it and radiation pattern measurements were made on the Mesa Antenna Range.

The Antenna Range initially used to make these measurements is shown in Figure 212. A spacecraft was mounted with the roll axis horizontal (Fig 213), on the small tower to the left in Figure 212. This tower is rotatable about a vertical axis. In addition, the spacecraft was mounted in such a manner that it may be rotated about its roll axis. An illuminating antenna was mounted on the illuminating tower, the large tower to the right in Figure 212. Thus, the omni-antenna radiation pattern could be measured for any combination of vehicle roll, pitch, and yaw angles.

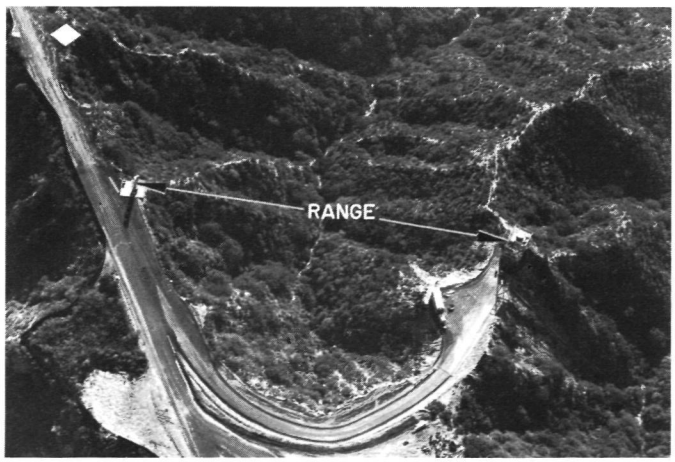

Figure 212. Initial pattern range for full-scale omni patterns

Figure 213. RA-1 mock-up on pattern rotator

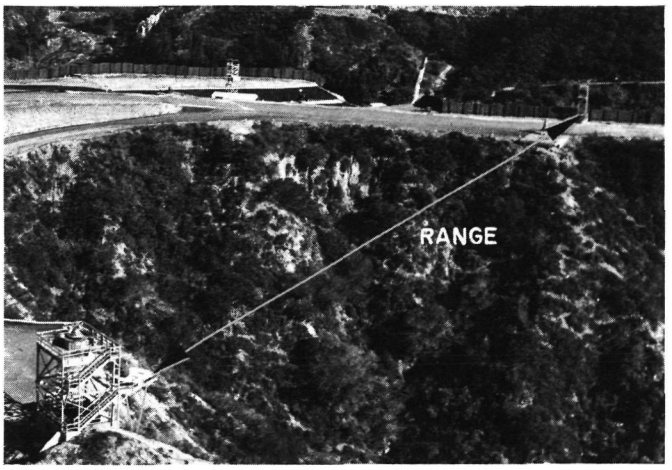

Figure 214. Final pattern range for full-scale omni patterns

The first measurement attempts on an RA-1 configuration showed that spurious range reflections made the patterns unreliable. An analysis of the reflection problems indicated that a change in the location of the rotator on which the spacecraft was mounted, and the use of a sector-type of illuminating antenna would increase the accuracy of the measurements. These changes were made (the new rotator location is shown in Figure 214), resulting in an estimated antenna pattern accuracy of ± 0.75 db over the look angles most likely to be encountered, and ± 1.5 db over most of the remainder of possible look angles. (No pattern accuracy guarantees could be made for aspects within 24 deg of the nose and tail.)

After reworking the pattern range, measurements were completed on the RA-1 type vehicle. These measurements indicated that the omni-antenna, mounted on the vehicle, met the program requirements for pattern coverage.

Next, measurements were made on an RA-3 type vehicle, with an RA-3 omni-antenna mounted on it. This configuration is shown in Figure 215. Again, the measurements confirmed the required pattern coverage of the configuration.

However, a clamshell-like thermal shield was proposed for thermal control of the capsule retro-rocket propellant.

Figure 215. RA-3 cruise mode mock-up without thermal shield

This shield was to be closed during cruise, as shown in Figure 216, then opened during the terminal maneuver, as shown in Figure 217, to allow escape of the caspule and retro-rocket. Thus, it became necessary to repeat the omni-antenna measurements to determine the effects of the thermal shield. These measurements demonstrated that this shield had little effect on omni-antenna pattern coverage. The clamshell arrangement was later discarded in favor of an aluminized mylar shield similar to a shower curtain, as shown in Figure 218. Pattern measurements were again taken and showed that program requirements for antenna pattern coverage were still being met.

The advent of the *Ranger* 6–9 program provided still another vehicle configuration to be evaluated. A mock-up was built, based on the information then available about the TV subsystem configuration. This mock-up is shown in Figure 219. Measurements taken on this vehicle indicated that antenna pattern coverage was still adequate, even though there was a large conducting mass near the omni-antenna.

In the evolution of the *Ranger* TV subsystem, sufficient changes were made in the payload structure to require modification of the mock-up, as shown in Figure 220, and measurements were again made on the mock-up.

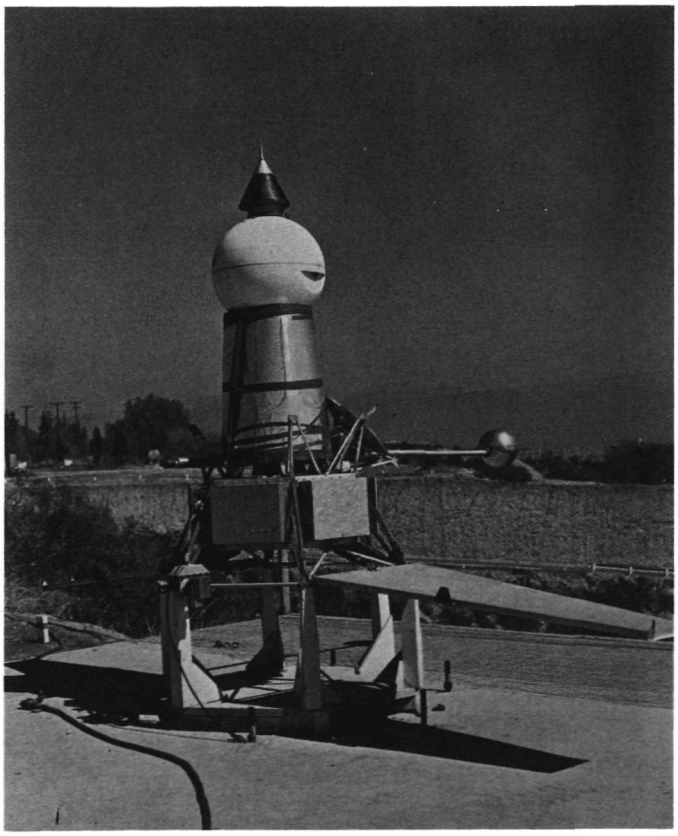

Figure 216. RA-3 cruise mode mock-up with thermal shield

Figures 221 to 225 are typical measurements made on the omni-antennas of the *Ranger* vehicles. These patterns were taken at a frequency of 960 mc, for 360 deg about the vehicle in a plane determined by the roll axis and the high-gain antenna hinge point, this being the expected spacecraft attitude in relation to the ground antennas. The omni-antenna pattern is plotted in db relative to an isotropic source versus the look angle, where the 0 deg is a nose-on view of the spacecraft. The isotropic reference is a fictitious antenna that radiates equally in all directions.

Diplexer. A diplexer (Fig 226) was required on the *Ranger* series, so that the command receiver and the telemetry system could operate over the same omni-antenna. The diplexer serves two basic functions. It isolates the power of the transmitter from the receiver, since the high power level could disturb the operation of the receiver. The diplexer also matches the transmitter to the antenna so that no power is lost into the receiver, which would cut down the efficiency of the transmitter communications link. The receiver arm consists of four coaxial cavities tuned to 890 mc and, therefore, pass the receiver frequency. The location of the first 890-mc cavity relative to the input antenna terminal of the diplexer is adjusted such that at 960 mc the receiver arm looks like a high impedance; thus, essentially no transmitter power can be dissipated in the receiver arm. The transmitter arm has a coaxial cavity which is designed to be a band-reject filter at 890 mc. In this way, essentially none of the receiver 890-mc signal is lost in the transmitter arm, which would reduce the sensitivity of the receiver.

The transmitter arm was not designed to have a band-pass filter at 960 mc in order to eliminate any resonant elements in the diplexer at the transmitter frequency. If there were any resonant elements at 960 mc, considerable precautions would have to be taken to ensure that these resonant elements did not break down under the power supplied by the transmitter. These diplexers were designed and built by Rantec Corporation.

The performance of the original diplexers is as follows: The insertion loss in the transmitter arm at 960 mc is 0.15 db and in the receiver arm at 890 mc is 0.8 db. The VSWR is below 1.1 to 1 for both frequencies when looking into the antenna terminal of the diplexer. Subsequent to the delivery of the original diplexer units, the diplexer was re-designed to improve its mechanical integrity. At the completion of the re-design, the diplexer was re-

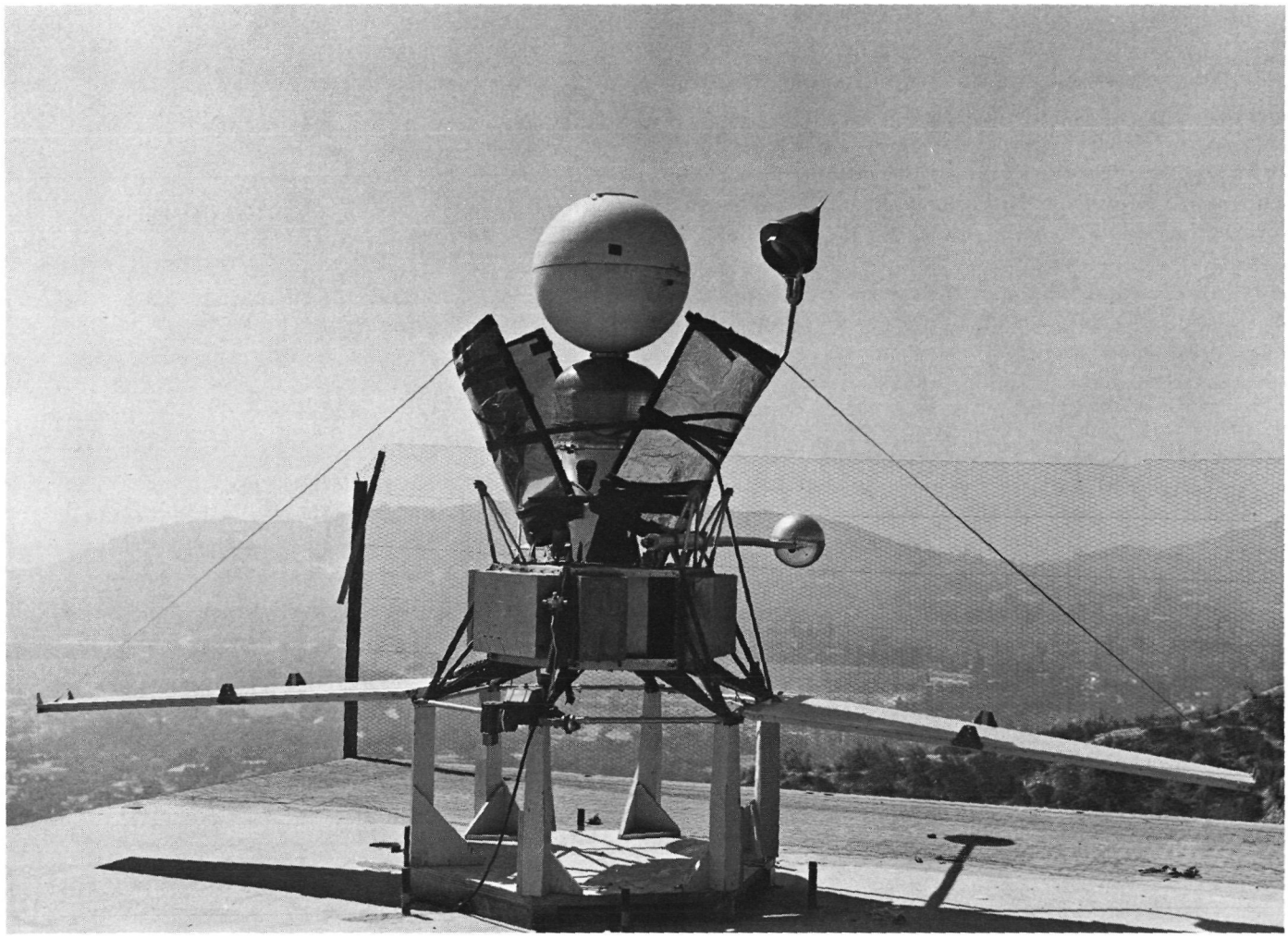

Figure 217. RA-3 terminal mode mock-up with terminal shield open

evaluated and it was found that the insertion loss at the transmitter frequency was only 0.1 db. This improvement was achieved with an increase in the insertion loss at the rejection frequency from approximately 30 db to 40 db in the transmitter arm. In the receiver arm, the passband insertion loss was reduced to 0.7 db with an increase in the 3-db bandwidth of approximately 50%. The transmitter frequency rejection remained at the same level (100 db).

Shroud coupler and parasitic-antenna system. During the boost-phase of power flight, the spacecraft will be enclosed in a metallic shroud. Since communication with the spacecraft is required during this portion of flight, it is necessary to provide a parasitic-antenna system within the shroud which will couple energy from the omni-directional antenna and carry the energy through a transmission line to an externally mounted antenna on the *Agena* stage. Although the high-gain antenna will not be used until after powered flight, it is necessary to provide a similar high-gain antenna coupler for pre-launch checkout purposes. The design and fabrication of the shroud parasitic antenna system was performed by Lockheed Missile System Company, and is illustrated in Figure 227. The omni-directional antenna coupler consists of a cylindrical metallic cavity placed over the omni-antenna and supported by the spacecraft shroud. A radial line probe at the top of the cavity provides the coupling to the omni-antenna. Since the coupler is a part of the shroud, the coupler is removed when the shroud is separated. An r-f quick-disconnect is located between the shroud and the *Agena* stage, to accommodate the separation between the shroud which contains the coupler, and the *Agena* stage which contains the externally mounted antenna (Fig 227).

In order to monitor the high-gain antenna while the spacecraft is on the launching pad, a monitoring probe

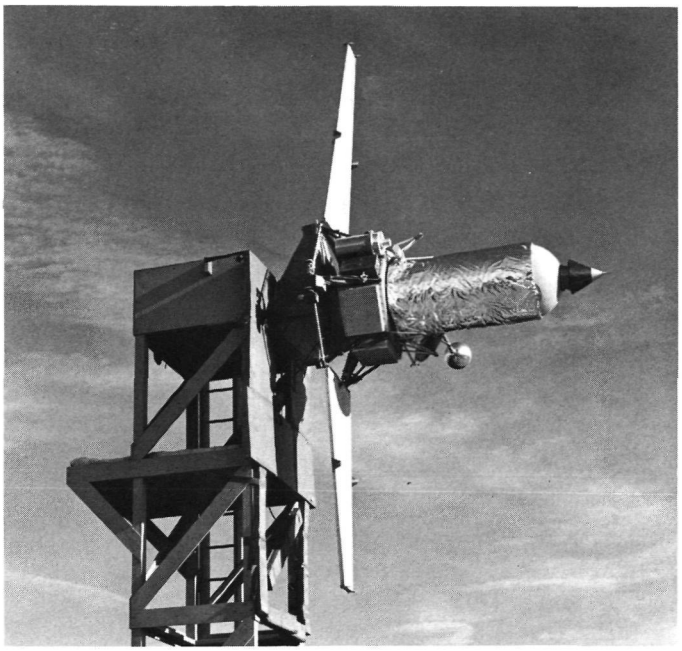

Figure 218. RA-3 with shower curtain thermal shield

was mounted in the *Agena* forward equipment rack opposite the location which the high-gain antenna protrudes into this forward equipment rack (Fig 228).

From the probe, a cable runs to the *Agena* umbilical connector, from where it goes up the umbilical boom to an antenna mounted on the top of the umbilical tower. From there, the high-gain antenna signal is radiated to the launch r-f checkout van. In order that the omni-antenna might also be monitored on the pad, a removable coupler was designed to be bolted over the *Agena*-mounted external antenna. From the output of this coupler, a cable ran to a high-gain antenna mounted on top of the gantry. This antenna then radiated the omni-antenna signal also to the launch r-f checkout trailer. To determine the effectiveness of the coupler systems, several tests were made on the vehicle while it was located at Cape Canaveral.

The coupling loss between the high-gain antenna output connector on the communications pan on the spacecraft and the input to the umbilical plug on the *Agena* was 6.0 db at 960 mc. The coupling loss between the omni-antenna output connector on the communications pan on the spacecraft and the quick-disconnect connector on the shroud was 11.3 db at 960 mc and 4.1 db at 890 mc. The losses for the external pad communications link are as follows:

(1) *Omni-antenna coupler system:* The loss between the cable connecting to the external *Agena*-

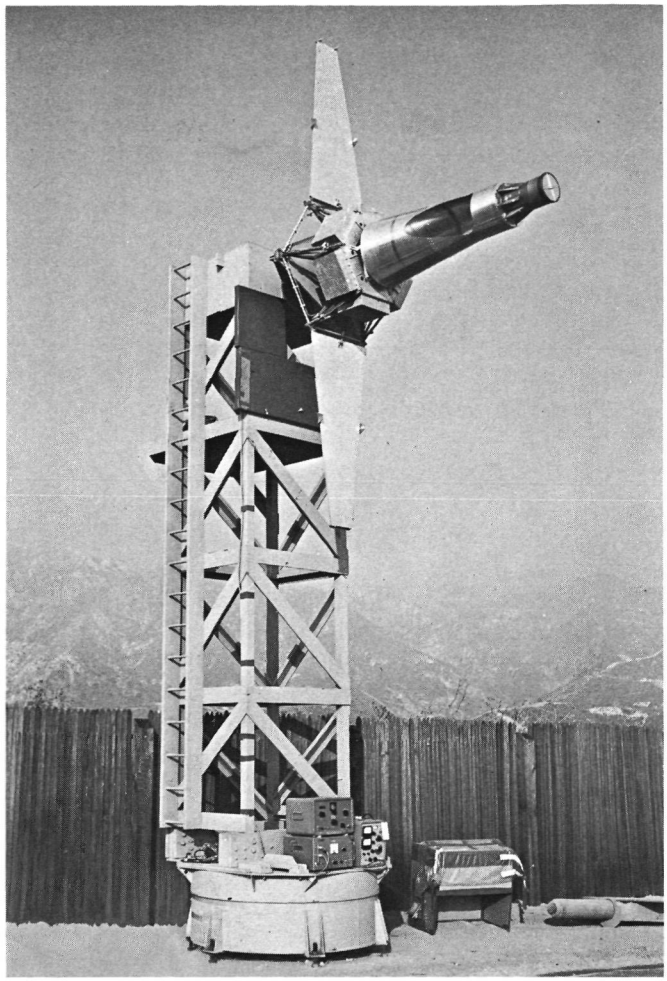

Figure 219. *Ranger* 6–9 with RCA superstructure mock-up

Figure 220. *Ranger* 6–9, final configuration

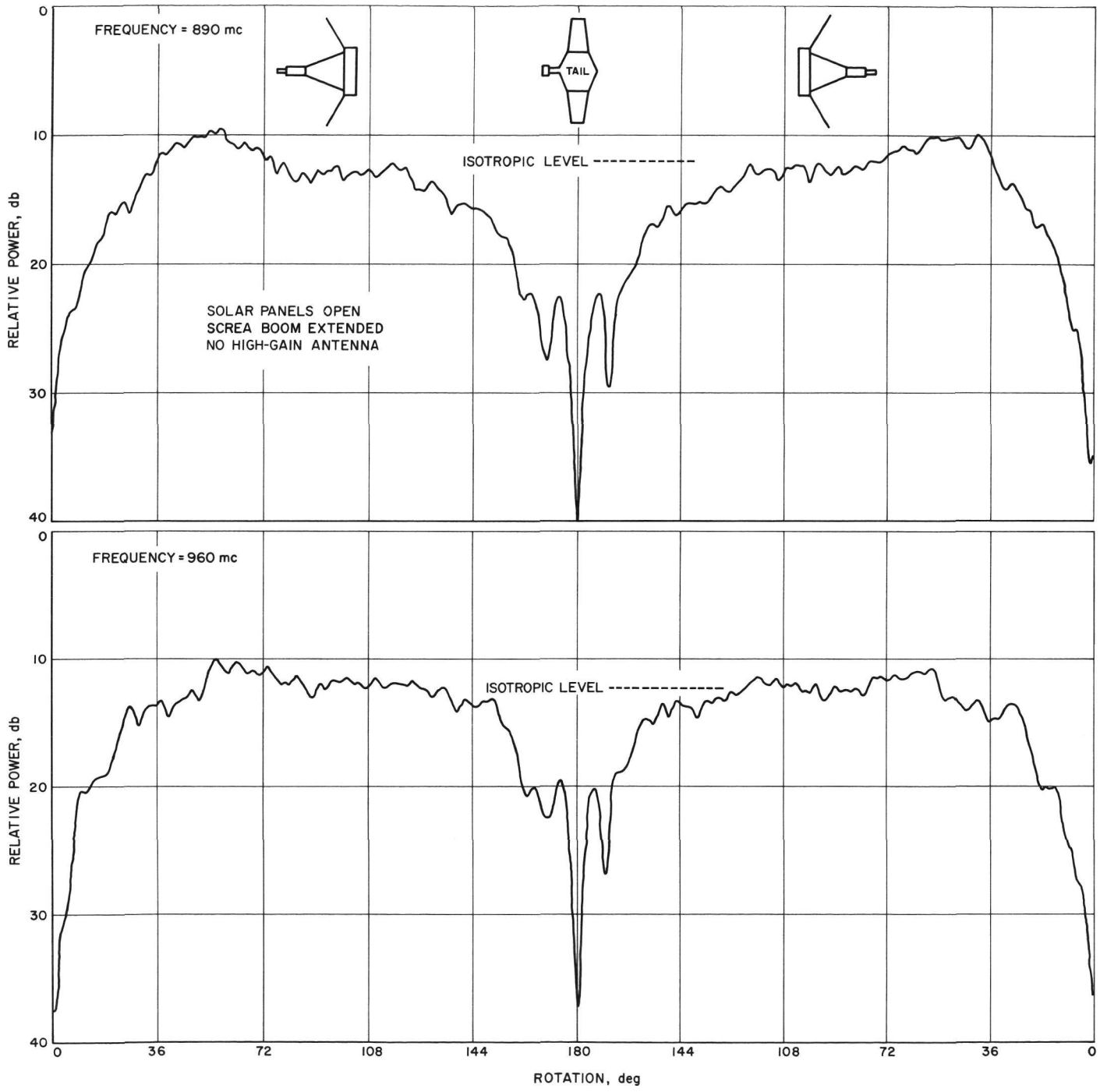

Figure 221. Full-scale RA-1 omni-antenna patterns

mounted coupler and the diplexer located in the r-f checkout trailer was 82.5 db at 960 mc and 83.8 db at 890 mc.

(2) *High-gain coupler system:* The loss for the high-gain coupler system between the *Agena* umbilical plug and the diplexer located in the launch r-f checkout trailer was 87.9 db at 960 mc.

(3) *RA-3 omni-antenna coupling configuration:* Due to the different type of the omni-antenna used on the RA-3 vehicle, the coupler parameters measured between the omni-antenna and the omni-antenna coupler are different from those measured on the RA-1 and -2 vehicles. Measurements show a loss of 14.3 db at 960 mc and 12.5 db at 890 mc between

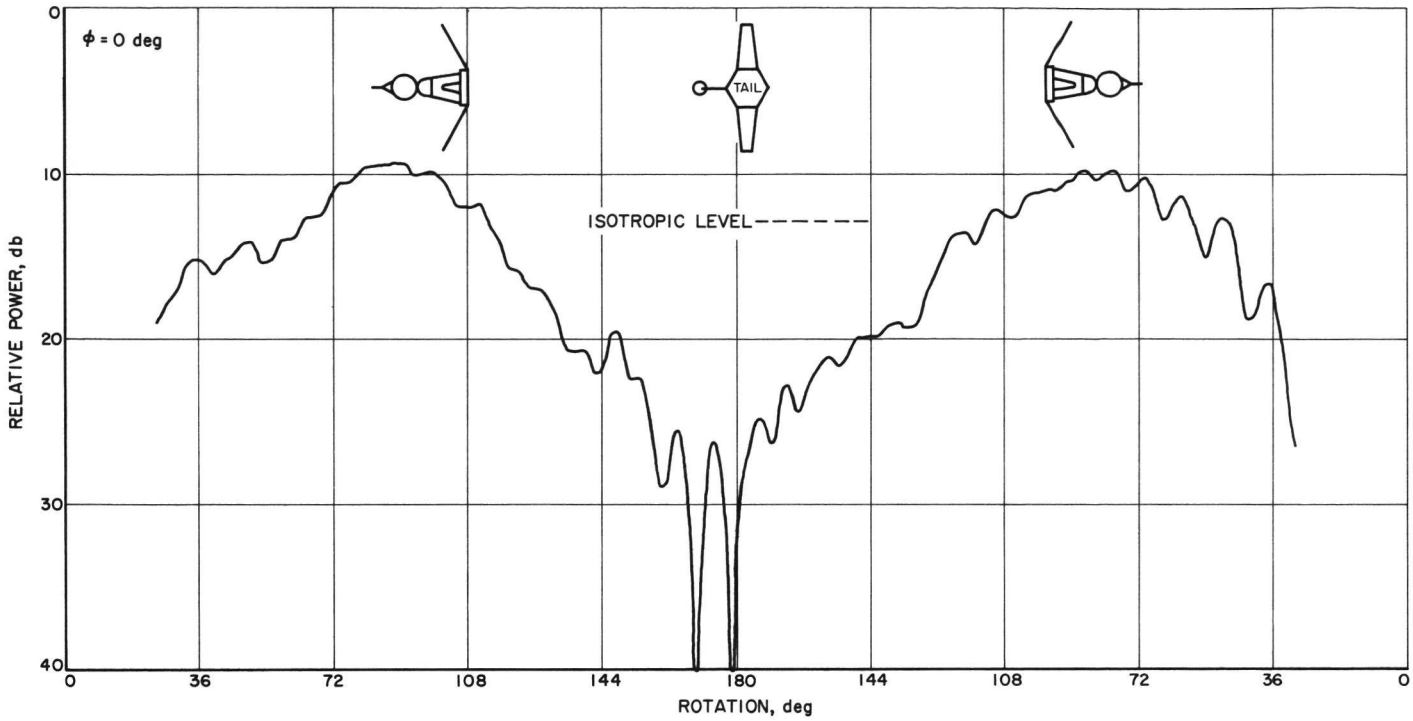

Figure 222. RA-3 omni-antenna pattern without thermal shield

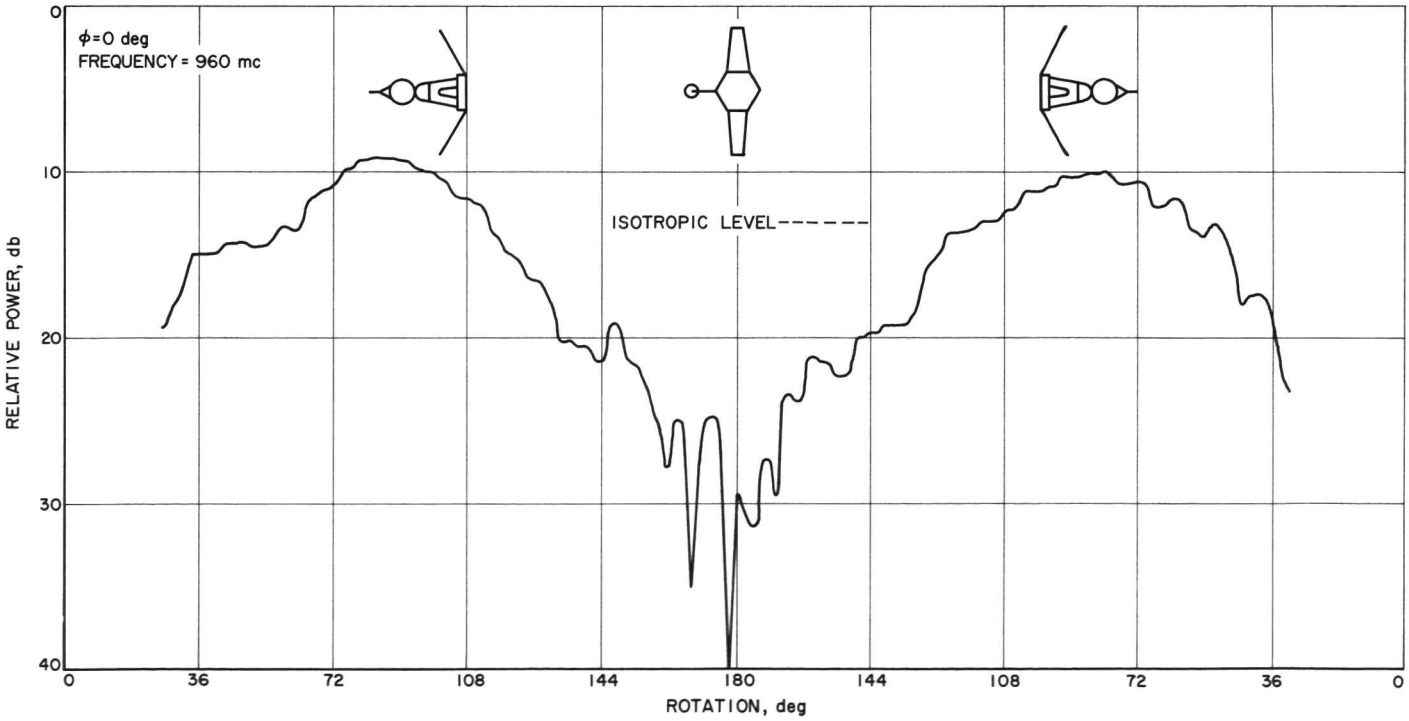

Figure 223. RA-3 omni-antenna pattern, clamshell thermal shield configuration

the output connector of the spacecraft communications pan and the quick-disconnect connector on the spacecraft shroud. It is interesting to note that the survival sphere transmitter, located just below the omni-antenna, was picked up by the coupler system at a level approximately 30 db below the

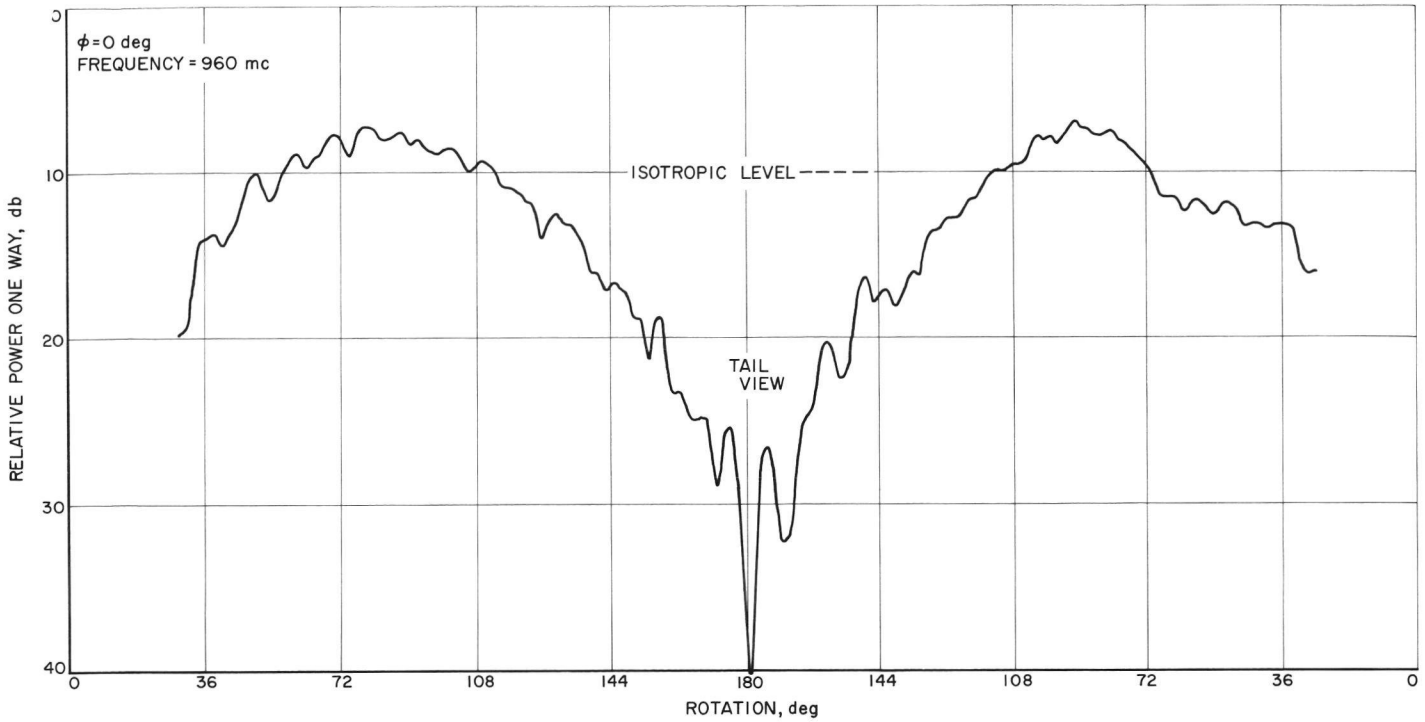

Figure 224. RA-3 omni-antenna pattern, shower curtain thermal shield

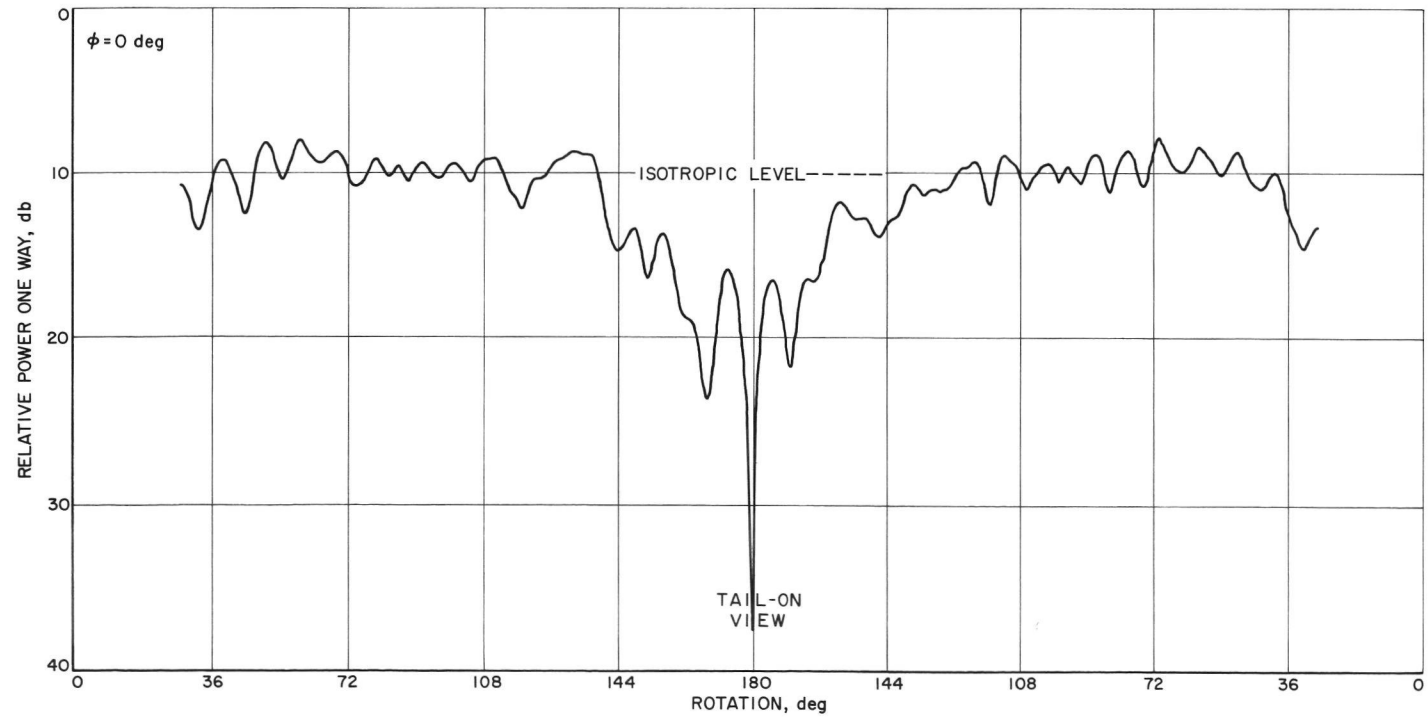

Figure 225. *Ranger* follow-on omni-antenna pattern, with prototype TV package

capsule transmitter level. These particular tests were run on an RA-3 PTM spacecraft, utilizing a flight-type shroud and a mock-up of the *Agena* forward equipment rack.

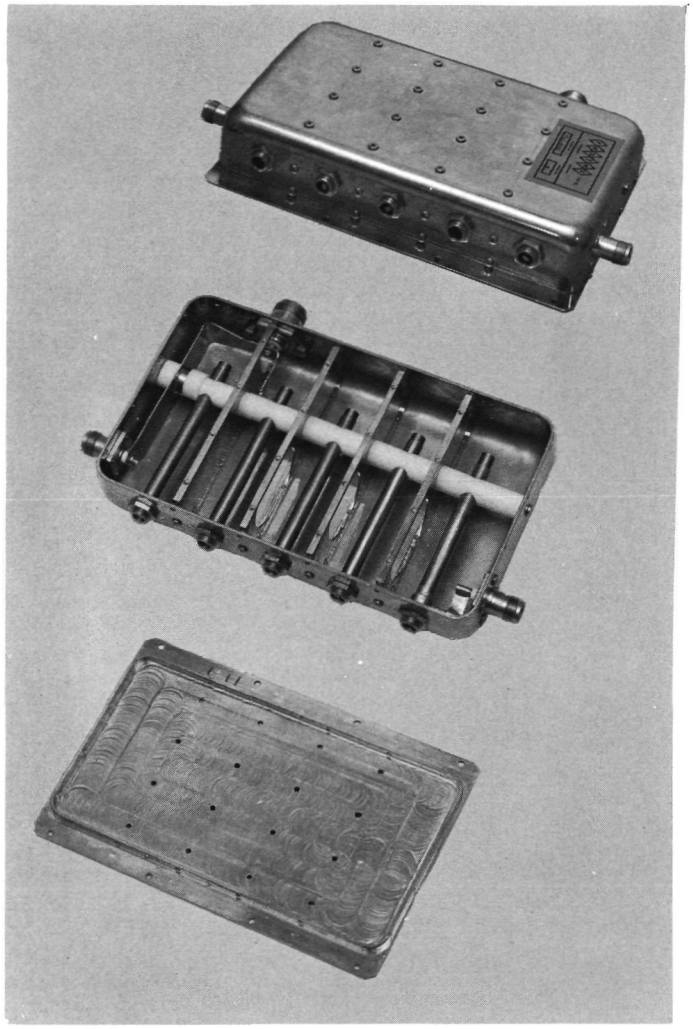

Figure 226. Diplexer

Mobile Tracking Station (MTS) antenna system. A contract to modify the MTS antenna feed system from its *Pioneer III, IV* configuration was let to Rantec Corporation on May 18, 1960. The purpose of this contract was to broadband the feed so that an 890-mc transmitting command channel could be efficiently diplexed with the 960-mc amplitude comparison monopulse tracking and listening channels. A secondary objective of the contract was to ruggedize the feed elements so that they are less susceptible to mechanical damage to which the electrical performance characteristics of the antenna are highly sensitive. The amplitude comparison monopulse used for the Mobile Station has four turnstile antennas in a square array supported by a center column to feed a ten foot parabolic reflector. Four hybrid rat-races located at the end of the center column behind the dish are used to provide the sum and azimuth and elevation difference signals.

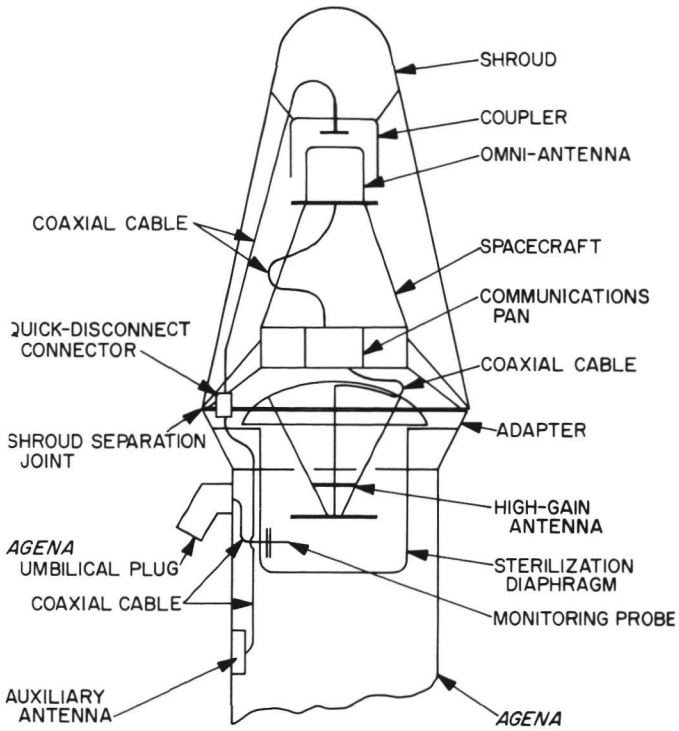

Figure 227. *Ranger–Agena* r-f coupler system

In conjunction with the feed redesign a contract was also let with Rantec to design and fabricate the diplexer and error channel filters necessary to operate the downrange antenna at 890 mc and 960 mc simultaneously. The error channel filters and receiver arm of the diplexer are of the bandpass type and are composed of seven resonant cavities. The error channel filters pass 960 mc with an insertion loss of less than 0.3 db, with the response down 70 db at 930 mc and 990 mc, and down 120 db at 890 mc and 1030 mc. The half power bandwidth of the error channel filters as well as the reference channel filter of the diplexer are 24 mc.

The transmitter arm filter of the diplexer, using bandpass techniques, consists of two resonators. The insertion loss at 890 mc is less than 0.1 db, and the unit provides a 3-db bandwidth of 47 mc. The response is down 20 db at 820 mc and 960 mc. These units were delivered in October 1960 and met specification as described above.

Due to the rather tight delivery schedule set up at the outset of the feed redesign, it was decided to accomplish the redesign with as few changes as possible to the original system built by Collins Radio Corp. for the *Pioneer* mission in 1958. Under these restrictive requirements, Rantec ran into design problems on the first prototype. These problems involved failure to meet the axial ratio (gain variation vs polarization angle) specification

of less than 1 db at 960 mc and less than 5 db at 890 mc. It was found that appreciable secondary reflected energy from the dish surface was intercepted by the feed and reradiated toward the dish surface adding with the primary feed energy in the opposite sense of polarization. The resulting magnitude of the secondary axial ratio with an essentially perfected circularly polarized feed was found to be 6 db.

Primary patterns of the feed confirmed the need to make a design change in that the first null of the array pattern occurred at 41 deg. Since the edge of the dish subtends a ± 50-deg angle from the focal point, this placed a null on the dish. Beside reducing the over-all antenna gain, this high illumination taper concentrated more energy in the center of the dish, and hence aggravated the feed reflection-axial ratio problem. Both of these problems were traced to the array spacing factor which was left unchanged from the original design at $\frac{3}{4}\lambda$.

A second prototype was made using a 0.6λ array spacing factor and incorporating a ridge loaded cupped ground plane design around each of the array elements. This design was proposed in order to reduce mutual coupling between array elements and to give more nearly equal E and H plane patterns. Figure 228 shows the feed array with one of the fiberglass radome covers removed. By decreasing the array spacing factor two benefits were realized. First, better primary sum channel illumination of the dish, and hence higher secondary gain were obtained. Second, the physical size of the feed could be made smaller, thus decreasing the aperture blocking effect and increasing the gain by a smaller amount. The combination of the more uniform illumination and the smaller feed resulted in a smaller secondary axial ratio. However, in order to produce axial ratios within specification at both frequencies, it was necessary to make the primary energy elliptical and critically focus the feed.

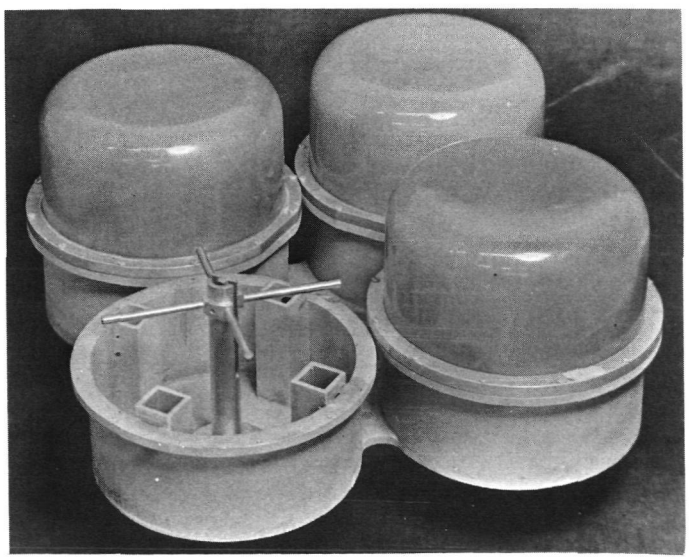

Figure 228. MTS monopulse tracking feed

Prior to shipment from the Rantec Corporation, the feeds were extensively tested at the subcontractor's facility. The final results of these tests are presented herein. Secondary pattern r-f performance characteristics of the new 890–960-mc feed (VSWR, ellipticity, gain and pattern data) will be compared with the original 960-mc monopulse tracking and listening feed wherever possible.

Table 55 shows the VSWR of the various antenna outputs (sum, azimuth error and elevation error) for feeds 1 and 2 for 960 mc ± 1 mc and 890 mc ± 1mc. No comparative data is available for the original feed. Table 56 shows the axial ratio of the peak of the sum channel beam versus frequency between 970 mc and 880 mc. A

Table 55. VSWR of feed system installed in dish as measured at output of sum and difference hybrids

Frequency	Sum channel			Azimuth difference channel			Elevation difference channel		
	Feed 1	Feed 2	Specification	Feed 1	Feed 2	Specification	Feed 1	Feed 2	Specification
961	1.12	1.09	<1.2	1.58	1.48	<1.5	1.21	1.52	<1.5
960	1.13	1.09	<1.2	1.56	1.51	<1.5	1.22	1.34	<1.5
959	1.13	1.09	<1.2	1.61	1.61	<1.5	1.18	1.30	<1.5
891	1.31	1.18	<1.5						
890	1.32	1.21	<1.5						
889	1.33	1.19	<1.5						

Table 56. Axial ratio (ellipticity) vs frequency

Frequency	Feed 1		Feed 2		Axial ratio specification (voltage)
	Axial ratio (voltage)	Angle of major axis, deg	Axial ratio (voltage)	Angle of major axis, deg	
970	1.6	+90	1.8	+90	
960	1.04	+30	1.10	−15	<1.12
950	1.55	+20	1.6	+20	
940	2.0	+20	1.95	+20	
930	2.4	+30	2.25	+35	
920	2.2	+50	2.2	+50	
910	1.8	+60	1.75	+55	
900	1.3	+80	1.16	+80	
890	1.36	−10	1.40	−15	<1.78
880	2.2	0	2.2	−5	

considerable improvement has been achieved in this parameter over the original feed, particularly in feed number one. At 960 mc, the improvement was from 2.1 db with the original feed to 0.3 db with feed number one, and from 13 db to 2.6 db at 890 mc.

Antenna system gain as measured at the output of the sum channel hybrid is shown in Table 57. The antenna system with the original feed exhibited a nominal gain (mean gain relative to linear polarization) of 22.2 db compared with 22.8-db nominal gain for the new feeds. It is interesting to note that the combined improvement in ellipticity and gain of the new feed will result in a 1.7-db increase in minimum gain due to polarization angle.

The higher gain values at 890 mc (Table 57) obtained for the new feeds are due to a much higher (approximately 14 db) dish edge illumination. This compares favorably with an optimum low noise listening feed. The edge illumination at 960 mc is −24 db. Tables 58 and 59 summarize the secondary pattern measurements on the new feeds.

f. Launch checkout r-f trailer. The primary purpose of the launch checkout station is to verify, by means of r-f communications, that the spacecraft is functioning properly when on the launching pad. In addition to providing this function, the station is mechanized to enable evaluation of the spacecraft during the booster phase of the flight. Basically, the r-f launch trailer consists of a radio system, a command checkout system, and various types of commercial test equipment. The radio system consists of the following:

(1) Transmitter, 890 mc.

(2) Receiver capable of receiving the 960.05-mc transponder or the 960.1-mc beacon.

Table 57. Antenna system gain as measured at output of sum channel hybrid

Frequency, mc	Polarization angle, deg	Gain (above linear isotropic source), db	
		Feed 1	Feed 2
960	0 (vertical)	22.85	23.3
	45	22.8	23.2
	90	22.8	22.4
	135	22.75	22.65
890	0	24.4	24.9
	45	—	23.3
	90	22.3	22.1
	135		23.1

(3) Phase-coherent frequency shifters.

(4) General purpose test instruments.

This equipment will be capable of measuring the following characteristics of the spacecraft communication system:

(1) Transmitter frequencies.

(2) Phase stability.

(3) Modulated output spectral distribution.

(4) Automatic gain control response.

(5) Command reception.

A block diagram of the r-f system is shown in Figure 229. Note that the mechanization philosophy is basically the same as in the DSIF system.

Transmitter. The transmitter has the capability of being phase-modulated and having the average power output level accurately controlled. The principal design characteristics of the transmitter are as follows:

(1) Frequency, 890.046 mc.

(2) Tuning range, ± 4 parts in 10^5.

(3) Frequency control, voltage-controlled crystal oscillator.

(4) Short-term frequency stability, 1 part in 10^7 after initial warmup.

(5) Power output, fixed +44 dbm, nominal variable +41 dbm down to −79 dbm.

(6) Phase modulation response, 0 to 25 kc.

(7) Output impedance, 50 ohms resistive, with VSWR no greater than 1.2 to 1.

The transmitter frequency is obtained by multiplying a voltage-controlled oscillator frequency 30 times. This frequency multiplication is obtained with the use of a $\times 5$ VHF frequency multiplier and a $\times 6$ VHF varactor frequency multiplier. The 25-w power output level is obtained by cascading three vacuum tube cavity amplifiers. A requirement of the launch station is to accurately control the average power output level and thus obtain the transponder signal strength vs AGC characteristic. A variable attenuator is incorporated which allows the power output to be varied from +41 dbm down to −79 dbm.

The transmitted output spectrum can be observed by means of an up-frequency converter. This conversion may be obtained by taking a small portion of the transmitted

Table 58. Sum channel pattern data

Feed	Pattern	Frequency, mc	Polarization angle, deg	Beamwidth at 3 db points, deg	First side lobe level, db	Maximum side lobe level for angles > 20 deg	
						db	Angle, deg
1	Azimuth sum	960	0	10.5	−17.8 −16.5	—	—
			45	9.0	— —	—	—
			90	7.8	−17.8 −17.5	—	—
			135	8.8	−19.2 −18.7	—	—
		890	0	8.7	−19.8 −20.1	—	—
			45	7.6	−17.5 −17.8	—	—
			90	7.0	−19.0 −19.5	—	—
			135	8.3		—	—
2	Azimuth sum	960	0	12.3	14.0 13.0	−19.7	100
			45	10.4	11.3 11.3	−21.2	100
			90	9.0	17.5 16.6	−26.5	100
			135	11.0	16.5 15.8	−21.9	90
		890	0	9.9	16.9 16.3	−29.5	115
			45	8.8	16.0 15.8	−29.0	100
			90	8.1	19.3 19.4	−25.3	123
			135	9.9	20.1 19.7	−25.8	123

signal and mixing with a 70-mc crystal-controlled oscillator resulting in an output frequency of 960.05 mc. The transmitted output spectrum and phase stability can now be observed with the receiver instrumentation.

Receiver. The receiver is of the double-conversion superheterodyne type, designed to receive signals from the transponder, 0.25-w beacon, and the ground transmitter through an up-frequency converter. When receiving signals from the transponder, the receiver reference is derived from the ground transmitter VCO by means of phase-coherent frequency shifters. The arrangement allows the precise measurement of the absolute doppler rate along with the transponder output frequency. When receiving signals from the 0.25-w beacon, fixed oscillators are used for the receiver reference. The output frequency of the beacon can be determined by measuring the receiver voltage-controlled oscillator (VCO) and the

Table 59. Error channel pattern data

Feed	Pattern	Frequency, mc	Polarization, deg	Null depth below error peak, db	Error peak below sum peak, db	First side lobe level, db	Maximum side lobe level for angles > 20 deg	
							db	Angle, deg
1	Azimuth difference	960	0	37	1.8	−13.5 −14.8	—	—
			45	33	5.3	— —	—	—
			90	33	2.0	−8.9 −8.8	—	—
			135	33	0.7	−12.5 −13.3	—	—
2	Azimuth difference	960	0	34	1.3	−12.0 −13.1	−13.0	110
			45	39	3.3	−6.4 −6.3	−9.0	110
			90	32.5	1.5	−7.1 −7.5	−12.7	115
			135	25	0.3	−9.7 −10.5	−16.0	105

receiver reference oscillators. A list of the receiver design parameters are given in Table 60. Figure 230 shows the receiver construction and mounting technique used to obtain temperature stability and ease of maintenance.

Control console. The console, which is the control center of the communication system, gives the operator remote control of the receiver and transmitter and the means of monitoring the internal frequencies, phase errors, received signal spectrum, and the ground-transmitted signal spectrum. The test instruments include an electronic frequency counter, d-c vacuum tube voltmeters, a cathode ray oscilloscope, and panoramic spectrum analyzers. Figure 231 is a photograph of the console, and Figure 232 shows the trailer interior.

Testing of the communication system indicates that all of the design objectives as outlined in Table 60 have been met. A plot of receiver sensitivity vs AGC voltage for the two bandwidths is shown in Figure 233. Note that the receiver met the threshold level on the 150-cps bandwidth position and is within 0.5 db on the 20-cps position.

Field operation. The launch stations were installed at a prepared site at AMR. The site was 2.2 mi from the launching pad and was selected for the clear, unobstructed view of the missile from launch to horizon.

The communication system makes use of two semi-fixed antennas mounted on an 18-ft tower. A low-gain, broadband antenna is positioned toward the spacecraft and is used for on-pad checkout. A 6-ft parabolic, high-gain antenna is positioned at a point in space to intercept the missile trajectory and is used to obtain information during the booster phase of the flight.

An 18-ft collimation tower and antenna were erected for the purpose of evaluating the ground communication system. An antenna system was installed on the missile gantry and umbilical tower to direct the spacecraft signals to the r-f station.

All of the above antenna systems were measured and compared with the theoretical values within 1 db. These measurements are obtained prior to each launching to enable accurate spacecraft evaluation.

Figure 234 is a photograph of the launch checkout site with the r-f trailer on the left and the telemetry trailer on the right. The antenna tower is shown on the left.

The launch checkout r-f station has been thoroughly evaluated and has met all of the design objectives. The station was used successfully for three *Ranger* pre-flight tests and has tracked these spacecraft to the horizon, providing data for evaluation during the booster phase of the flight. The station was important in *Ranger I* and *II*

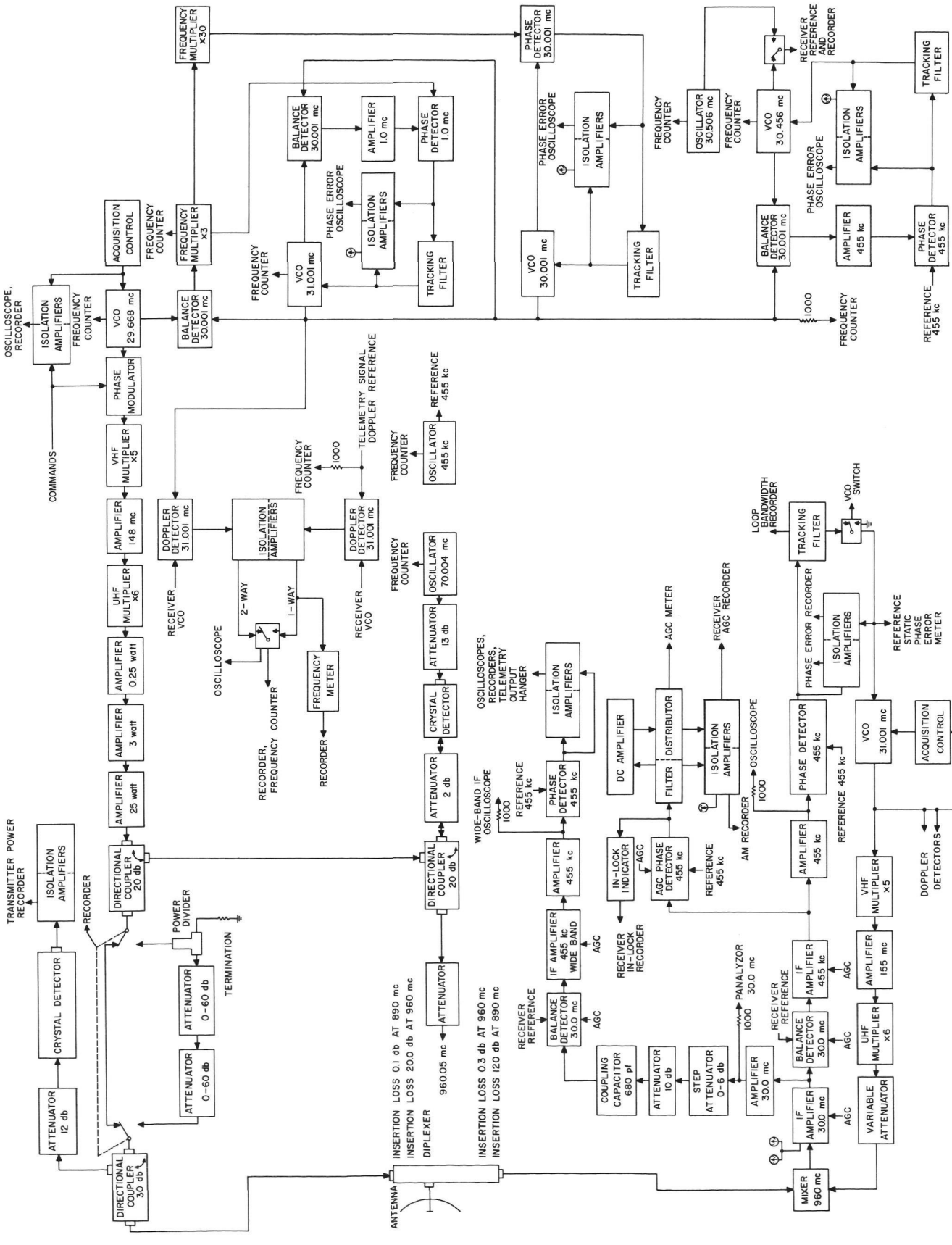

Figure 229. Launch checkout station radio system

Table 60. Receiver design parameters at 960.05 or 960.10 mc

Parameter	Units	$2B_{L0} = 20$	$2B_{L0} = 150$
Input impedance	ohms	50	50
Input VSWR		< 1.2 to 1	< 1.2 to 1
Receiver noise, including preselection	db	6.5	6.5
Predetection bandwidth	kc	2.0	2.0
Receiver threshold signal level, unity P_n/P_s in $2B_{L0}$	dbm	154.5	145.7
Predetection P_n/P_s at RF threshold	db	20	11.25
Maximum receiver RF gain	db	169	—
Dynamic range to threshold	dbm	−50	−50
Modulation response	kc	0 to 5	0 to 5
Suppression factor	—	0.0884	0.236
Detector gain K_m	v/deg	0.698	0.698
VCO gain at 30 mc K_v	cps/v	800	800
Frequency multiplication factor	—	30	30
Open-loop gain $G_0 \times 10^5$	1/sec	5.33	14.25
Nominal loop filter component values			
C	pf	93	93
$R_0 + R_1$	megohms	16.1	0.712
R_2	ohms	807	107.5
AGC loop threshold			
Receiver gain K_a	db/v	2	
AGC detector gain K_d	v/db	0.44	
Amplifier gain K_1	v/v	10	
Open-loop gain G	—	8.8	
Filter time constant τ	sec	33	
Frequency response f_3, db	cps	0.042	
Loop noise bandwidth $2B_1$	cps	0.133	

tracking because of the unfortunate orbital paths these spacecraft achieved.

The launch station will achieve more versatility in the antenna system by mounting the now existing 6-ft parabolic antenna on a manual-positioned 360-deg rotating pedestal.

g. Launch checkout telemetry trailer (LCTT). Aluminum Body Corp. was asked to build the launch checkout telemetry trailer to JPL drawings. Eight racks were to be supplied by Stone and Smith. JPL did the mounting, wiring, diagrams, and checkout of all equipment.

The trailer equipment consisted of the following (Fig 235):

(1) Phase-lock-loop discriminators.

(2) Direct-write oscillograph.

(3) Magnetic recorder.

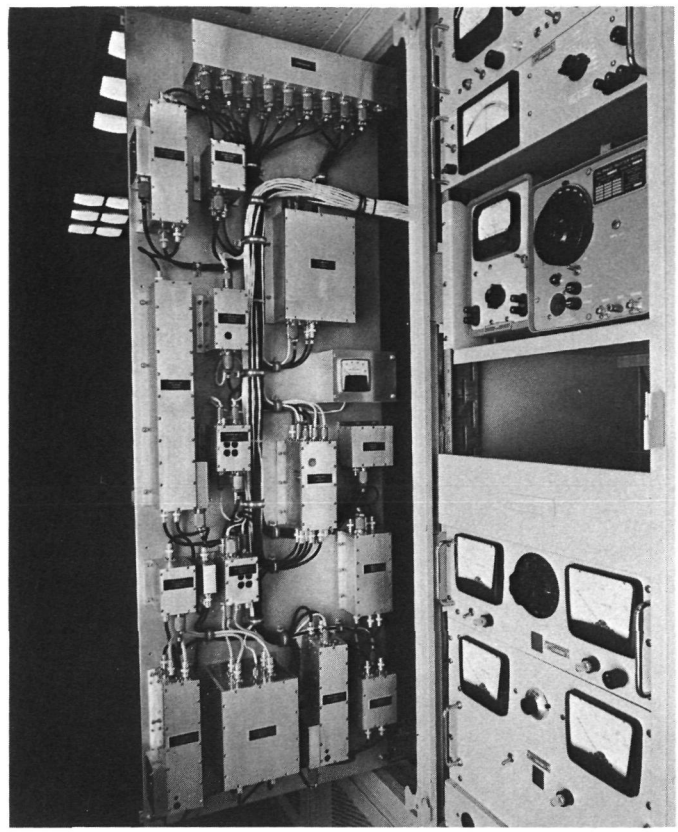

Figure 230. Checkout station 960-mc receiver

(4) Other equipment included: time generator, decommutator, galvo control panels, calibration oscillator, dual-trace oscilloscope, d-c VTVM, function generator, a-c millivoltmeter, audio oscillator, subcarrier oscillator (VCO), active mixer, electronic counter, adjustable BPF, speaker assembly, line-voltage regulator, power supply for battery, control panel, patch panel, stable oscillator, WWV receiver, batteries, power supplies, digital printer, and receivers.

It was decided that the LCTT at AMR would act as a data reduction laboratory in checking out the spacecraft in the SAF (AE Hangar). When the spacecraft was on the pad, the station would check out and record the r-f receiver and its functions. A secondary objective was to track the missile from lift-off to the horizon. The functions to be recorded on magnetic tapes are shown in Table 61. The functions to be recorded on direct-write oscillograph are in Table 62.

The LCTT supplied 100 kc and 30.99 mc to the r-f trailer. Also, the LCTT supplied display output to the r-f trailer, for AGC fine and coarse, and static phase error fine and coarse measurements as received by telemetry. Figure 236 is the signal flow diagram.

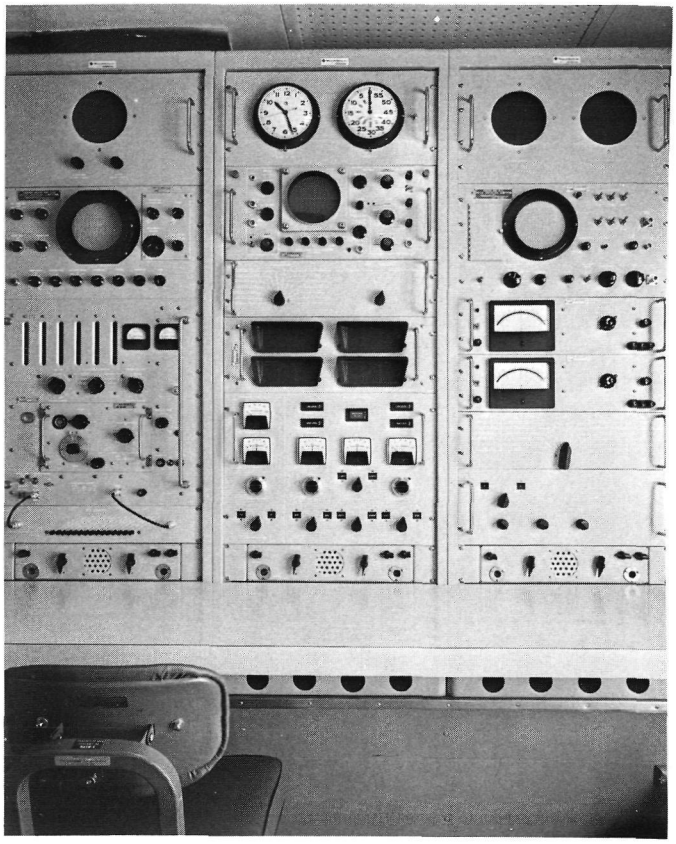

Figure 231. Checkout station control console

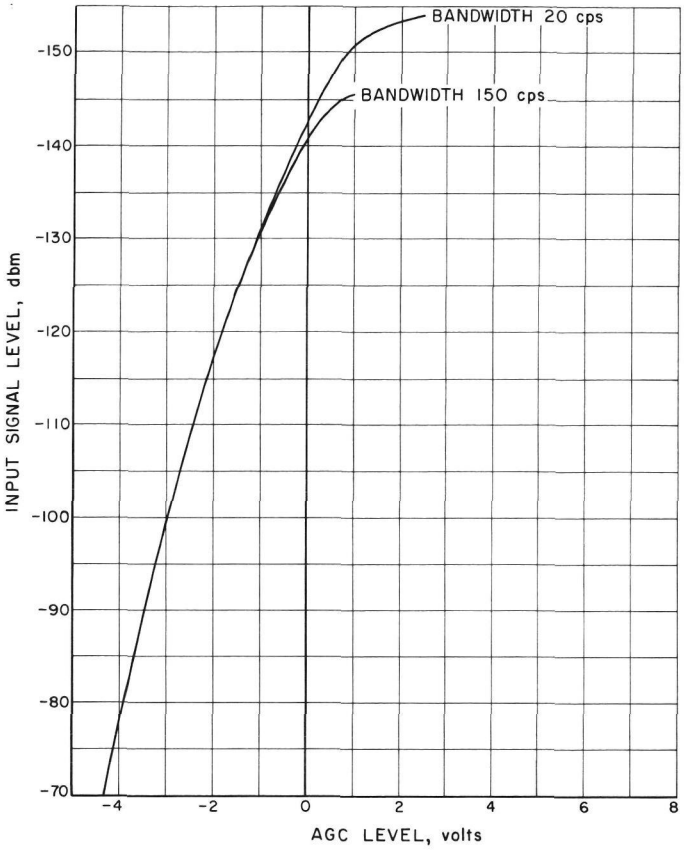

Figure 233. Receiver sensitivity vs AGC gain

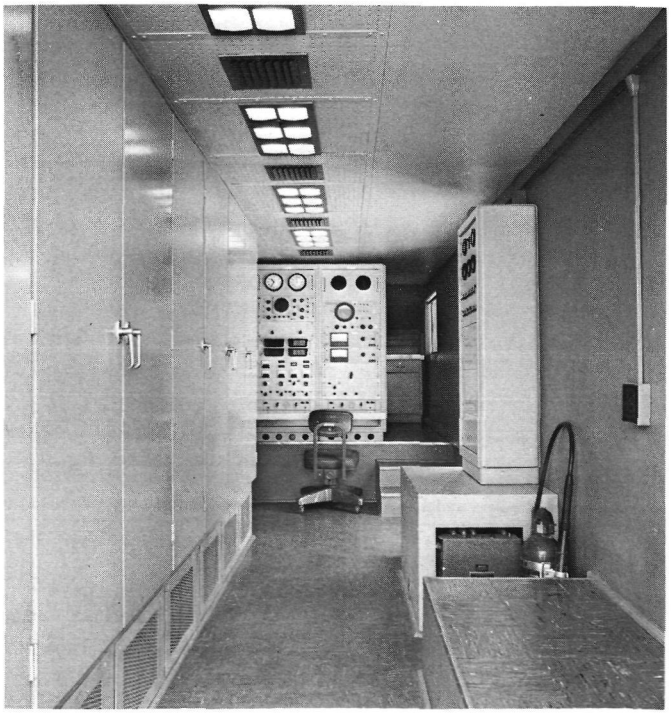

Figure 232. Trailer interior

Figure 234. Launch checkout site; r-f trailer at left, telemetry trailer at right

LCTT field operations. The function of the LCTT when the spacecraft is in the AMR SAF (Hangar AE) is to make a magnetic tape of all the tests conducted by the spacecraft test director. Also, the LCTT makes a real-time recording on direct-write oscillograph of the spacecraft when the commutator is running. This tape is back-up for the test director and central recorder tapes. If spacecraft trouble develops and the test director needs magnetic tapes played back, the LCTT has provided the

Table 61. Ampex in LCTT

Track 1 In	Mixer No. 2	3E18	Mixtone	ALL output, v	1.0
1	VCO 6	3E16	1,572–1,700–1,828	Receiver AGC, v	0.5
3	VCO 5	3E12	1,202–1,300–1,398	Reference rec. static Ø error, v	0.5
2	VCO 8	3E8	2,775–3,000–3,225	Reference rec. dynamic Ø error, v	0.5
5	VCO 7	3E37	2,127–2,300–2,473	Pre. Fil AGC 150 amp, v	0.5
4	VCO 3	3E33	675–730–785	Transmitter power, v	0.5
6	VCO 4	3E30	888–960–1,032	Antenna switch position, v	0.5
7	—	3E36	10 kc–5 kc–10 kc	One way doppler, v	0.5
8	VCO 1	3E41	370–400–430	Cape timing, v	0.5
9	—	—	100 cps	Readout/hour, v	0.5
Track 2		3E31		Agena	1.0
Track 3	9J2-12, R6	3D51	Mixtone	Telemetering output rf	±3.0 P/P
Track 4 In	Mixer No. 3	3E40			1.0
1	5AJ16	5E3	6.25 kc	Reference tone	1.0
2	5AJ14	5E2	100 cps	Readout/min	1.0
3	5AJ13	5E1	1000 cps	Readout/sec	1.0
Track 5	9J2-2, 20	3E35	0 to 10 kc	Doppler frequency	±3.0
Track 6		3E44		MOPS voice labeling	
Track 7		9J13	Mixtone	Encoder tones	±35 P/P

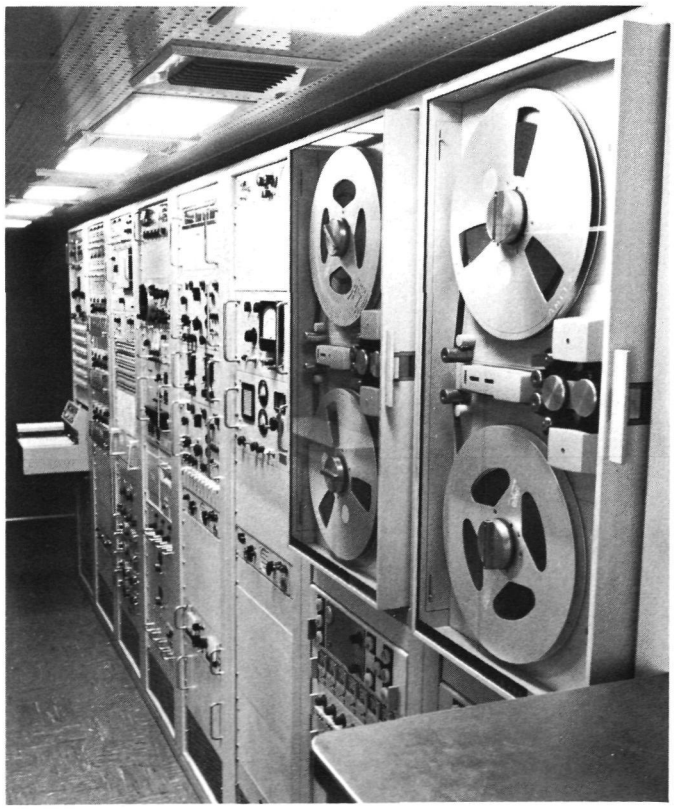

Figure 235. Launch checkout trailer, interior view

capability of running any needed special test. These playback tapes are on a 7-in., direct-write oscillograph.

When the spacecraft is moved to the pad, the r-f trailer is turned on and the LCTT checks and records the r-f functions on magnetic and direct-write oscillograph tapes. On launch day, the r-f and LCTT track the missile from lift-off to the horizon (about 7 min).

On RA-1 and -2, a tripod-mounted antenna was installed on the r-f tower to track the spacecraft from horizon to horizon during orbital passes. Data obtained during these passes was good.

h. Command system development.

RA-1, -2. The command functions required for the RA-1 and -2, consisted of three on-off commands to initiate a roll override, an antenna hinge-angle override, and switching between omni- and directional antennas. Since the only requirements placed on the command link were that the probability of recognizing and acting upon a command should be 0.9, and the probability of initiating a false command due to receiver noise be 0.01, a simple tone-burst system was evolved for RA-1 and -2. To fulfill the above requirements, each command was recognized in the spacecraft command detector as a discrete tone or frequency by means of a tuning-fork filter and level detector, which in turn activated a relay to perform the

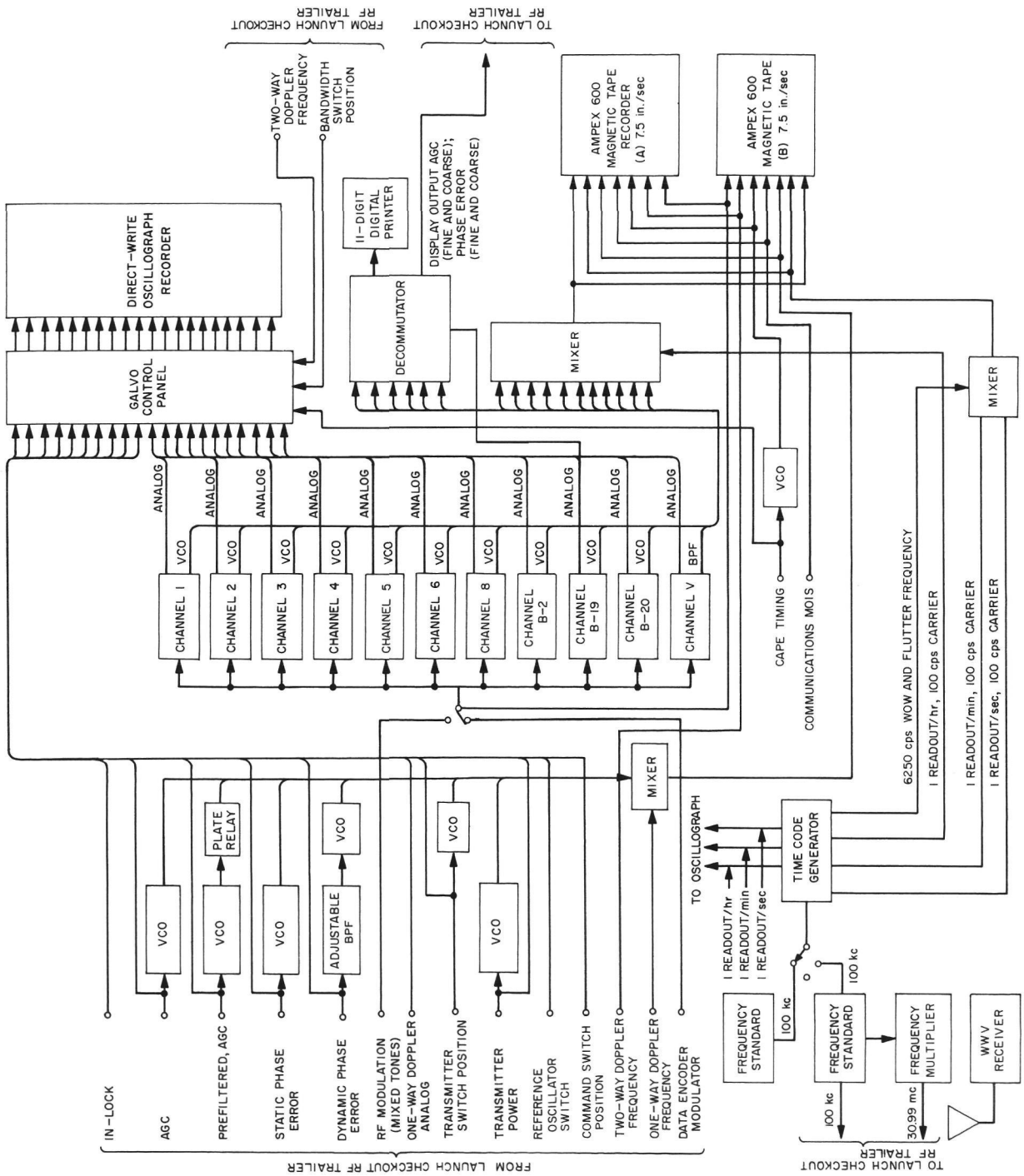

Figure 236. Launch checkout telemetry trailer, signal flow diagram

Table 62. Functions recorded on direct-write oscilloscope

Galvo	Position	Volts	Deflection	Test point	Plug and pins	Attenuation	Name
1	−6	0	0	0	0	Off	Reference trace 1 (dummy)
2	−5.7		−0.2	5EJ2	5AJ11	0.1M	Readout/min (2 pps)
3	−5.4	−0.2			5AJ12	0.1M	Readout/hr (1 min)
4	−5.3	2 or 3 v dc	+0.1	3E26	9J1-4 and 22		Reference OSC switch position
5							
6	−5.1	2 or 3 v dc	+0.1	3E27	9J1-14 and 28		Doppler switch position
7							
8							
9	−4.4	±3 v dc	±0.5	3E10	9J1-6 and 23		Reference receiver static phase error
10							
11				3D42			Discriminator
12				3E1			Discriminator
13				3E11			Discriminator
14				3E21			Discriminator
15	0		0				Reference trace 2 (dummy)
16	−4.5		±0.25	3D12		1.0M	Discriminator Channel 4 (analog)
17	−1.0	±3 v dc	±3.0	3 EH	9J1-12 and 26		Receiver AGC
18	−4.0		±0.25	3D21		5.0M	Discriminator Channel 7.7 (analog)
19	−3.7		±0.1	3D22		0.1M	Discriminator Channel B-10 (analog)
20	−1.2	±3 v dc	±0.5	3E24	9J1-16 and 29		Prefiltered AGC 150 amp
21	−3.4		±0.1	3D31		0.1M	Discriminator Channel B-11 (analog)
22	−3.1		±0.1	3D32		1.0M	Discriminator Channel B-12 (analog)
23	−2.8		±0.1	3D41		0.1M	Discriminator Channel B-13 (analog)
24	+2.5	±3 v dc	±0.25	3E4	0J1-2, 20		Reference receiver dynamic phase error
25	−2.5	dc	+1.0	3E32	9J2-6, 23		Doppler analog
26	+0.7	0 to +3 v dc	+0.1	3E25	9J1-10, 25		Receiver in-lock (relay)
27	+1.2	2 or 3 v dc	+0.1	3E29	9J1-32, 33		Transmitter switch position
28	0		+0.1	3D1		10K	Discriminator Channel 1 (analog)
29	+2.0		±1.0	3D2		0.1M	Discriminator Channel 2 (analog)
30	+35		±1.5	3D11		1.0M	Discriminator Channel 3 (analog)
31	+4.6	2 or 3 v dc	+0.1	3E28	9J1-18, 31		Antenna switch position
32	+4.8	0 to 1 v dc	+1.0	3E31	9J1-35, 36		Transmitter power
33	+5.0		+0.1		9J		Cape timing
34	+5.2	4, 2 or 100 C	+0.4	3E38	9J2-4, 22		Command, switch position
35	+5.7		+0.2		SAJ	0.1M	Readout/min, 1 pps
36	+6.0		0		—		Reference trace 3 (dummy)

desired function. Inception of the command at the ground transmitter was produced by depressing the proper command switch, resulting in automatic transmission of the command for a period of 3 sec. Figure 237 shows a general block diagram of the RA-1 and -2 command link.

When the command requirements for RA-3, -4, -5 began to evolve, it became apparent that the simple tone-burst type command system would not be practical because of:

(1) The greater volume of commands to be handled; (Table 63).

(2) The need for quantitative command data in the form of command words for midcourse and terminal maneuvers;

(3) The higher received bit accuracy required to achieve mission success; $P_e \leq 10^{-5}$.

Concurrently, the problems of transmitting commands over interplanetary distances were being investigated and it was concluded that a great degree of sophistication would be required to maintain an acceptable bit error probability level because of limited transmitter power, antenna gains, etc. As a result, the development of the

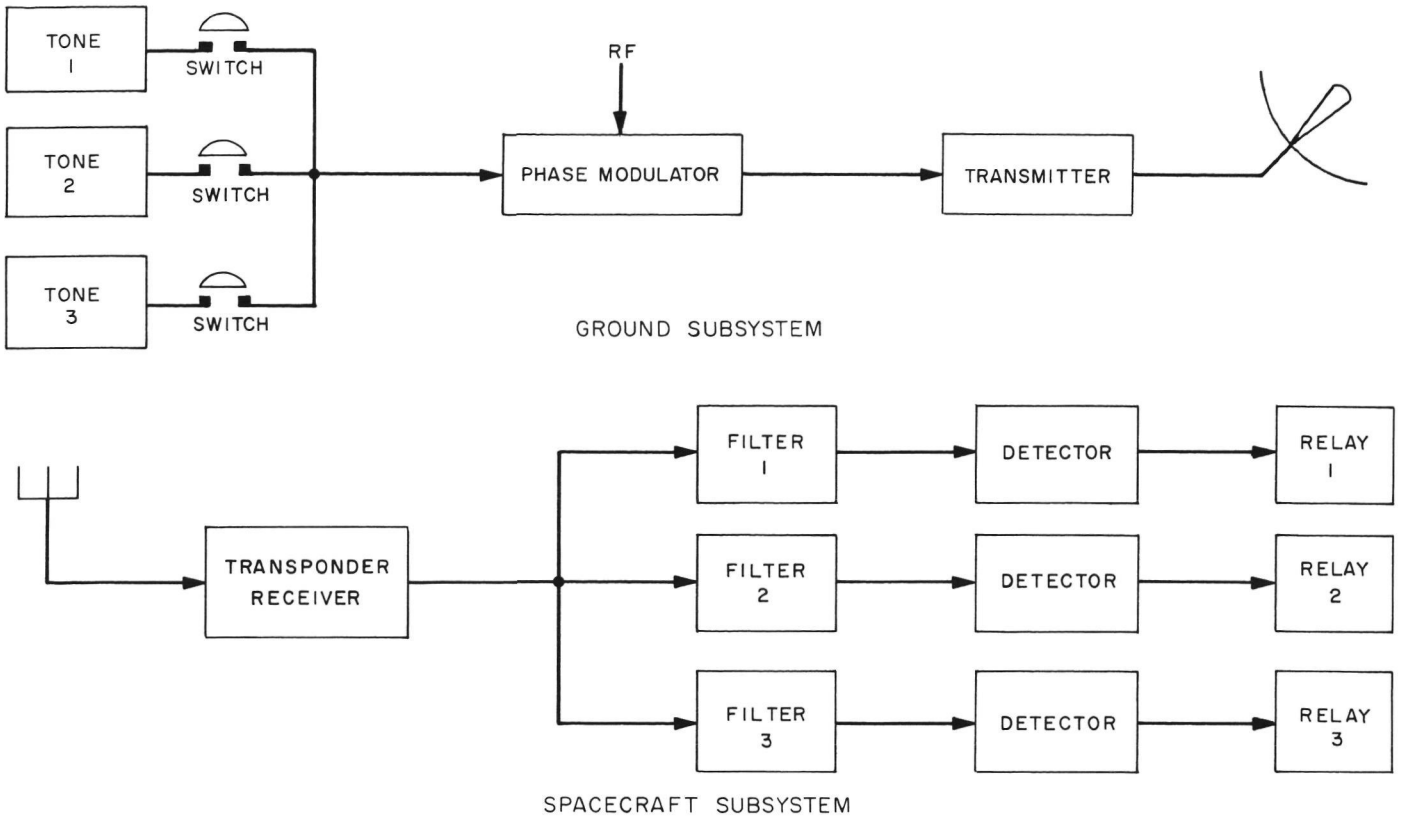

Figure 237. RA-1 and -2 command system

Table 63. *Ranger* RA-3 commands

Command	Address	Data block	Function
Clear	1-00000	All zeros	Clear detector and decoder
RTC 1	1-01010	All zeros	Roll vo override
RTC 2	1-10100	All zeros	Hinge angle override
RTC 3	1-11010	All zeros	Switch 3-w transmitter to high gain antenna
RTC 4	1-10110	All zeros	Begin midcourse maneuver
RTC 5	1-10010	All zeros	Telemetry mode change
RTC 6	1-00101	All zeros	(a) Begin terminal maneuver (b) Vidicon power on
RTC 7	1-0110	All zeros	Altimeter power on (back-up)
SC 1	1-10101	00110011001X[a]	Midcourse roll maneuver duration and direction (10 sec)
SC 2	1-11101	01101001100X	Midcourse pitch maneuver duration and direction (15 sec)
SC 3	1-00011	010000100100	Shut off midcourse motor (velocity increment)
SC 4	1-10011	00110011001X	Terminal first pitch maneuver direction and duration (10 sec)
SC 5	1-01011	01101001100X	Terminal yaw maneuver direction and duration (15 sec)
SC 6	1-11011	01001011010X	Terminal second pitch maneuver direction and duration (20 sec)

[a]X may be either a "1" or a "0" to indicate direction of maneuver.

RA-3, -4, -5 command detection system was directed toward designing a command link which could also be used for interplanetary missions. Command bits were to be transmitted and received in a near-optimum manner by employing phase-coherent and matched filter detection techniques (1). A special synchronizing code would also be transmitted in conjunction with command bits to provide coherent detection references and bit sync to the spacecraft system. Because of system complexity, it was also decided to develop a back-up detector, not unlike the tone-burst detector used for RA-1 and -2, (for use with RA-3, -4, -5) in the event that the phase-coherent system development fell behind schedule because of technical problems.

As mentioned earlier, quantitative data as well as on-off commands would be required by RA-3, -4, -5, and as a result, command words consisting of a fixed number of serial data bits were formulated. Each word would consist of an alert or start bit, five address bits to identify which command was being sent, and 12 bits to indicate the quantitative magnitude. In the event that the command would be of the on-off variety, the 12 magnitude bits would be deleted by sending zeros. Typical command word structures are shown in Figure 238.

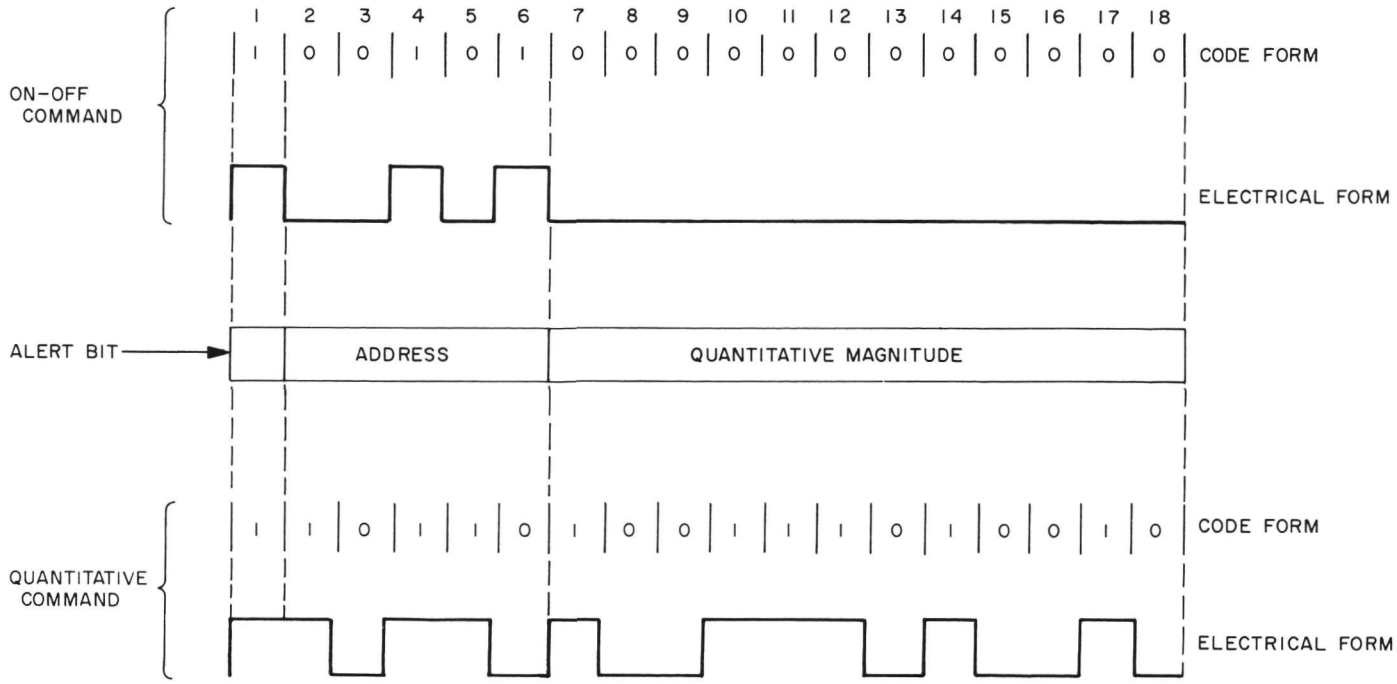

Figure 238. Command word structures

In order to facilitate handling of the commands at the ground transmitter and to prevent errors in the command to be transmitted a command Read- Write–Verify (RWV) system was devised. Figure 239 shows a functional block diagram of the RWV system. A command to be transmitted would be received from the originating source in the form of a punched teletype tape and read into the RWV storage memory; the contents of the memory were displayed in the form of an octal code. Prior to transmission, a simulated command transmission would be performed to check all ground equipment exclusive of the transmitter, and would result in the command being stored in a second memory and displayed. If the two displays were identical, a "go" condition would exist and the command could be transmitted. During actual command transmission, the transmitted command would be received by identical equipment to that used in the spacecraft and stored and displayed as a final verification of correct system operation. In addition, the RWV also generates the command timing and synchronizing signals to modulate the transmitter.

Upon receipt of the command by the spacecraft command detector, the serial command bits are transferred to the command decoder. It is the function of the decoder to recognize the start of the command word and store the address bits for further decoding. When the address bits are properly positioned in the storage register, interrogation of the address decoding gates occurs and a relay corresponding to the transmitted command is activated. In the event that the command is quantitative in nature, the address serves to alert the spacecraft Central Computer and Sequencer (CC&S), following which the 12 magnitude bits are transferred to the CC&S memory for further processing.

The final RA-3, -4, -5 command system block diagram is shown in Figure 240. During final system component selection, the back-up detector was chosen because of technical delays and manufacturing difficulties encountered with the phase-coherent detection system.

i. Read–Write–Verify (RWV) system. The Read–Write–Verify (RWV) system provides positive verification of actual transmissions and checkout of the communication link between computer and transmitter.

The teletype (TTY unit) bridges the gap between the Central Computing Facility (CCF) at Pasadena, Calif., and the transmitter site at Goldstone, Calif. Command decisions originating at CCF are transmitted redundantly three times over the TTY. The Kleinschmidt tape output is read by RWV and electronically compared. Complete agreement establishes valid TTY transmission (Fig 241).

Proper operation of the command modulator is ascertained by electronic comparison of the output of a ground detector with modulator input. Subsequent modulation of the transmitter occurs. R-F energy sensed by an

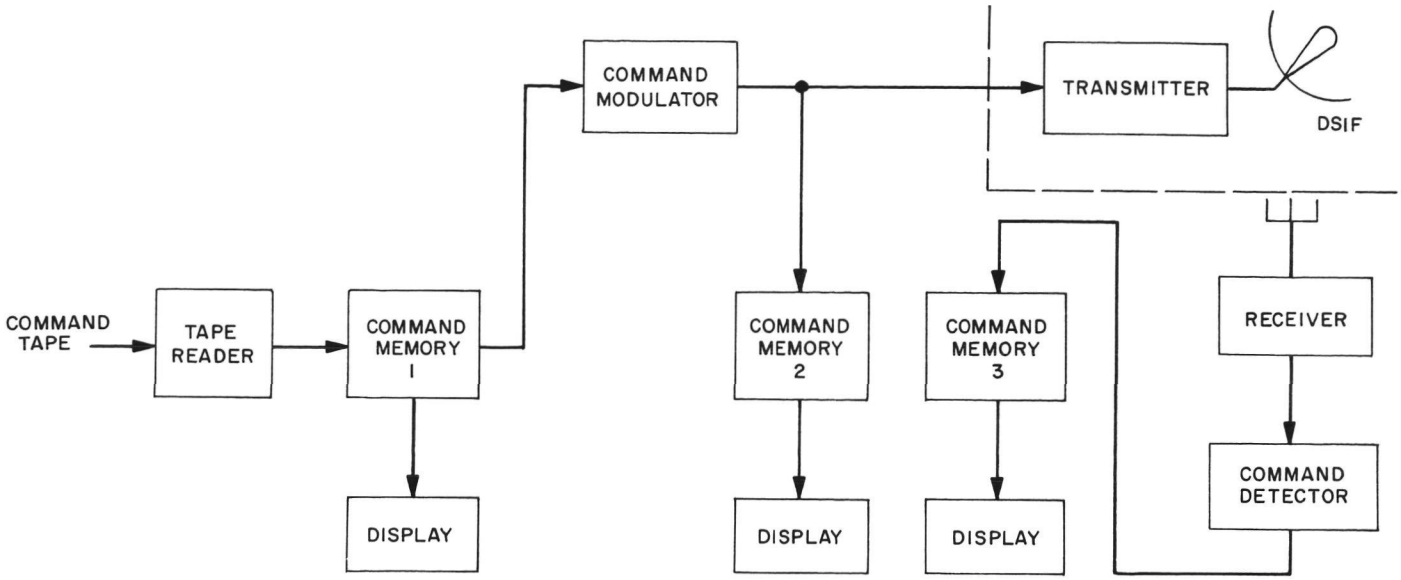

Figure 239. RWV functional diagram

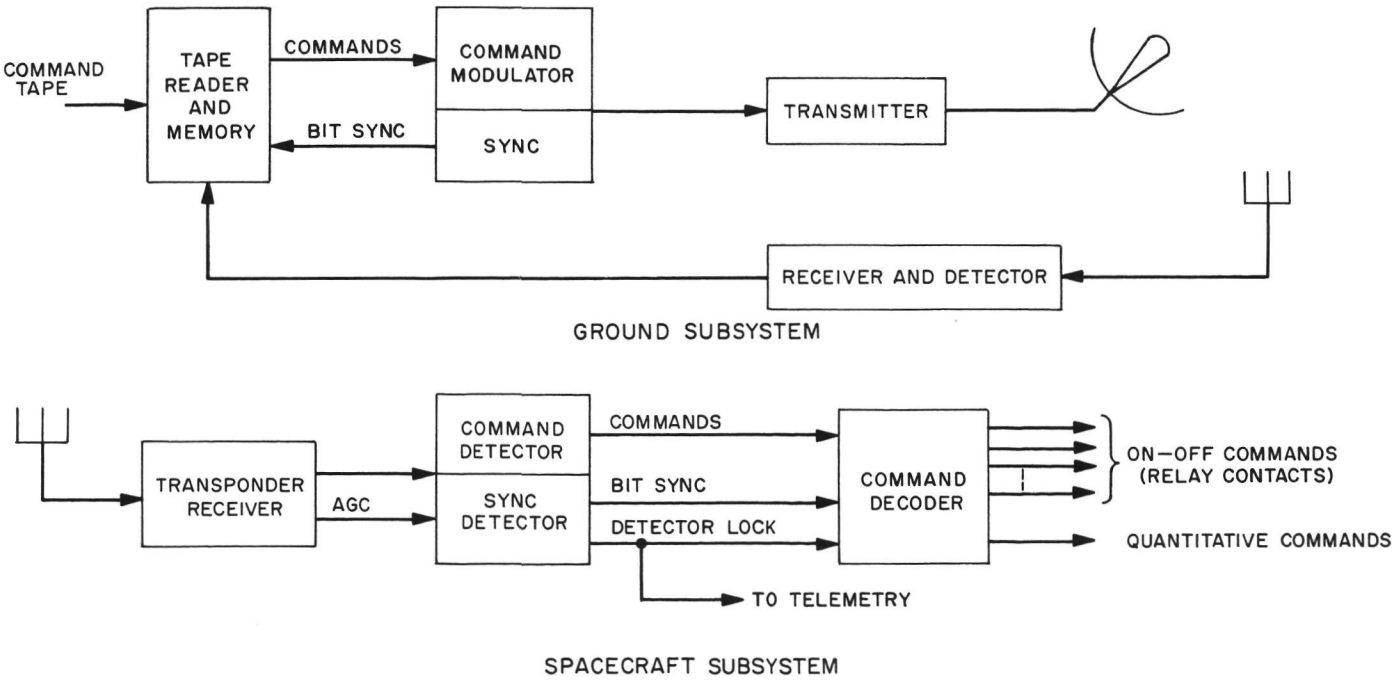

Figure 240. RA-3, -4, -5 command system

antenna probe is detected, demodulated, and is recompared with modulator input. Any discrepancy causes inhibition of the transmission (Fig 242).

It was decided to use an asynchronous detector rather than a synchronous system. This decision necessitated several revisions in the RWV system. Both modulator and detector were replaced with an FSK (frequency shift keying) system. Timing and display logic were revised to accommodate the FSK hardware. All revisions were made to permit convertibility for subsequent use of the design with the pseudo-noise system in later programs.

j. Command detector. The command detector was designed to accept the command subcarrier and AGC voltage from the spacecraft transponder. The command

subcarrier information was then converted into binary form and sync information was obtained from an internal clock started by the first binary "one." AGC was used as an indication of the received signal-to-noise ratio. If the received signal-to-noise ratio was below a preselected value, the output of both the detector and decoder was to be blocked. When a command with sufficient S/N ratio was received, the command word and sync pulses were to be sent to the command decoder.

The logical design of the command detector is presented in Figure 243. The first "one" tone from the transponder is filtered, detected, shaped, and then used to initiate the start of the detector operations. The shaped "one" from ST1 is one of three inputs to the command word and gate A5, which controls the command word output of the detector. A second input to A5 is from ST2 which is in the "one" state when the AGC voltage is above a preselected level. The first "one" sets F/1 which in turn Resets F/F2, which is the third input necessary to A5 to allow the command to leave the detector. Another function of F/F1 is to gate "and" gate 3 which controls the 25-pps clock signal, received from CC&S. This signal is divided by 25 to produce the 1-pps sync pulse. The command word from A5 is only usable by the decoder when accompanied by the 1-pps sync pulse for sampling. A low AGC voltage switches ST2, which sends outputs to "and" gate 5, "and" gate 1, and "or" gate 1. The output of "or" gate 1 is the dump signal which prevents an incomplete or false command by the decoder. "And" gate 1 sets F/F 2 to keep the dump signal on for the remainder of a command cycle when it has been initiated. F/F 2 is then reset by F/F 1 at time t-56 sec, at which time the detector is ready for the next command.

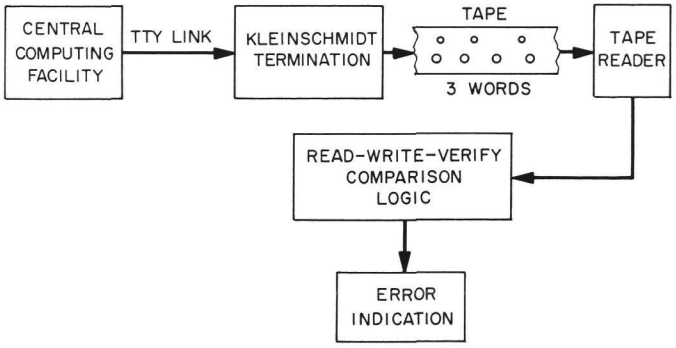

Figure 241. RWV teletype verification flow diagram

The major field operations problem was bit error tests to verify a design requirement for a bit error rate of 10^{-5}. The only test run was quite crude in nature. It consisted of testing the detector under various S/N ratios from a band-pass limited noise, simular to the pass band of a typical transponder. A series of "ones" were transmitted to the input of the detector and any "zero" out of the detector was considered an error. The S/N ratio at which 1×10^{-5} bit error rate was achieved was about 0.35 or -127 to -132 dbm. This was satisfactory because at lunar distance the received signal strength was expected to be better than -120 dbm.

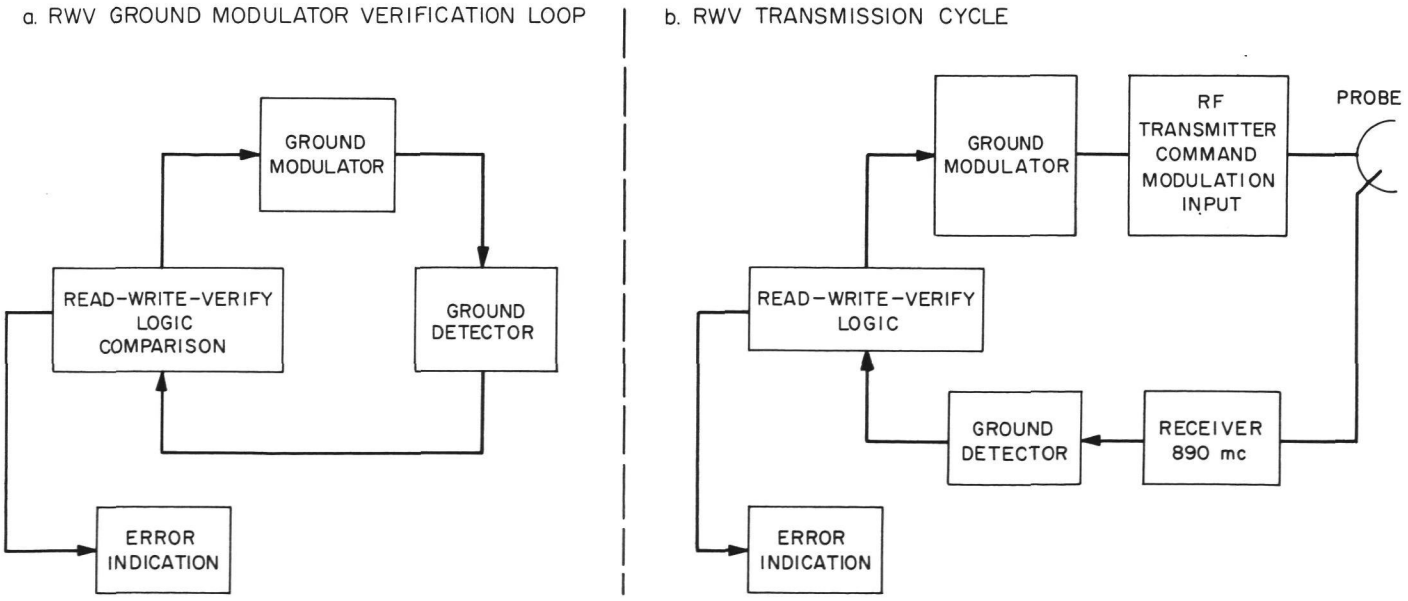

Figure 242. RWV ground modulator verification loop (a) and RWV transmission cycle (b)

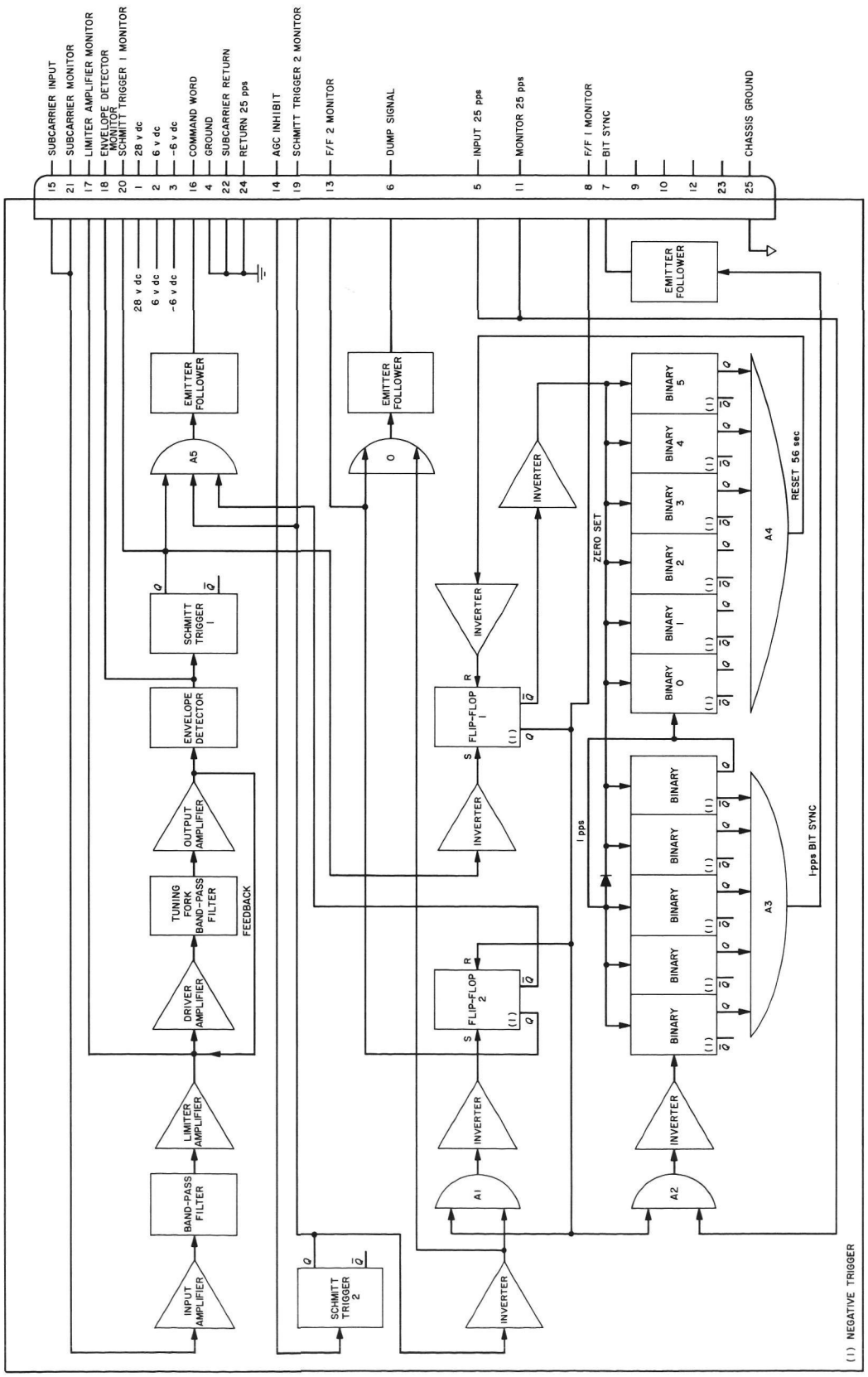

Figure 243. Command detector logical design

CONFIDENTIAL

Command decoder. The basic function of the command decoder was to examine each incoming command, decide whether it was real time or a stored command, and process the command appropriately. A real-time command is executed by the momentary actuation of the designated relay, while a stored command is routed to the CC&S in an appropriate form.

The highest resolution required for a stored command magnitude is 1 part in 1200 (the velocity increment command). Since the CC&S was designed so that the least significant digit was weighted at two tenths of a unit, 13 digits are required to obtain the needed resolution. It was observed, however, that the required resolution could be obtained by expressing the command to the nearest 0.8 sec, so that the first two digits were always zero. It is then possible to eliminate these two digits from the command transmission, thus increasing the probability of obtaining an accurate command.

The logical design of the decoder is presented in Figure 244. The first digit of each command word, always a binary 1, causes $F/F1$ to be set. This opens the appropriate gates to cause the program control scaler to begin counting sync pulses and to cause the address, magnitude, and polarity digits to be read into the shift register. The nineteenth sync pulse causes the address decode matrix to be interrogated. If the address is that of a real-time command, the appropriate transistor switch is energized to cause a 150 $\pm$50-msec relay closure for the command user. If the command address is that of a stored command, $F/F2$ is set, thereby allowing the address block and the data block to be read out of the shift register. The readout of the command is completed at the occurrence of the thirty-fifth sample pulse. The thirty-sixth sync pulse causes $F/F1$ to be reset. This in turn causes $F/F2$ and the binary scaler to be reset, thus rendering the command decoder ready to accept another command. The command decoder is so mechanized that the occurrence of an unused address results in no command output.

The decoder required modifications on two different occasions for the following reasons: (1) an additional hold-off function was required to eliminate a possibility of error upon power turn on and (2) the use of the RTC 8 channel to produce a clear bit for CC&S.

The interface problems which arose during system testing were associated with the CC&S clear pulse and degradation of CC&S 25-pps signal. The first problem resulted because the decoder output impedance and CC&S input impedance were not matched, making it difficult to clear the CC&S circuit. The 25-pps degradation was solved by using additional drive current on the 25-pps input to the detector.

System tests. The RA-3 system functioned without error during system tests. The system test on the PTM indicated some source of interference with the command system. Two major sources were found to be the voltage scanner and CC&S clear-reset. The voltage scanner created 4-6-v · transients on the plus and minus 6-v power supplies. This condition confused the logic in both the detector and decoder by causing random settings of the binary counter, shift registers and the program control flip-flops. Scanning the voltage before start and after finish of the system test or cross bar switching eliminated this problem in system tests. The CC&S clear–reset transient did not initiate a false command but it did insert a count in the decoder program control binaries and a "one" in the decoder shift register. This caused the decoder to sample before the correct command was complete and could have resulted in a false command. Transmission of a clearing command will always prevent this type of action.

Clearing commands became an essential part of the command operating procedures when the PN sync system was abandoned for RA-3. (See Command Development.) In the PN system, the PN generator was continuously running and supplying sync pulses to the decoder. This kept the programmer and shift register continuously clear of information which might have been introduced by spacecraft power transients. In using the asynchronous backup detector, this feature was lost and it became necessary to send clearing commands to avoid false command problems.

The worst case of possible error occurs with random setting of program control binaries. In this case, two clear commands (1000—0) are necessary. The first command starts the detector cycle which clears the "dump" signal at count 56. The second clear command allows sync-pulses to enter the decoder, which will then reset itself at count 36. The system is now clear for desired commands.

Since the two clear commands are insurance against an unknown interference causing an error, they are included as part of the command procedure and precede each group of commands.

RA-3 operation provided an excellent test of the command system. The continued correct operation of the command system beyond lunar distances indicates the safety factors considered in basic design were sufficiently conservative.

CONFIDENTIAL

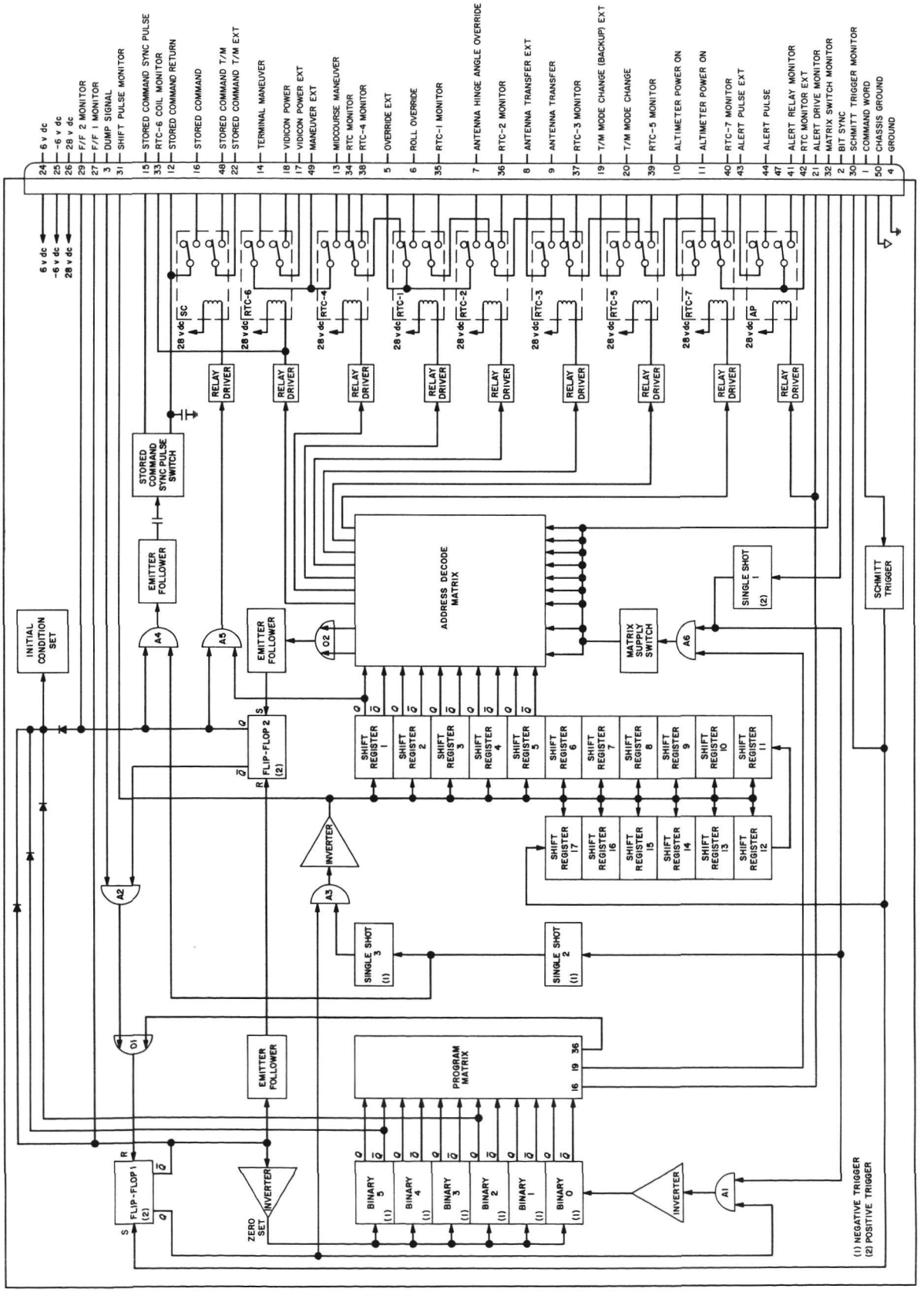

Figure 244. Command decoder

2. Deep Space Instrumentation Facility

a. General. The Deep Space Instrumentation Facility (DSIF) comprises a network of three tracking stations spaced approximately 120 deg apart in longitude around the world, and within ±36 deg latitude of the Earth's equator. Being so located, they have essentially uninterrupted tracking capability for spacecraft that are injected into orbits that carry them away from the Earth, on orbits intended to reach the Moon, one of the planets, or much of interplanetary space.

Figure 245 illustrates why the DSIF is not capable of continuous tracking of Earth satellites at relatively low altitudes. On the other hand, three DSIF stations spaced approximately 120 deg about the Earth provide continuous and overlapping coverage, except for the unshaded regions, for deep space probes.

The DSIF stations are located at Goldstone, California; Johannesburg, South Africa; and Woomera, Australia. The exact coordinates of each station are listed in Table 64. These stations are equipped with 85-ft parabolic antennas and phase-locked-loop receivers for automatic tracking of spacecraft. Figures 246 through 250 show the DSIF network stations during the operational periods for RA-1 and -2.

To coordinate the activities of the three DSIF tracking stations, and to provide a means for rapidly transmitting the data received by each station back to the Jet Propulsion Laboratory for analysis, a world-wide NASA-operated teletype and telephone network was used to support the stations. Through this network (Fig 251), the tracking data obtained at each station is sent in near-real time to the computing facilities at JPL for an orbit determination and a preliminary telemetry data analysis.

As a network, the DSIF is capable of tracking spacecraft whose orbit or ephemeris lies within the bounds shown in Figure 252. The heavy black line that originates at Cape Canaveral, Florida, shows the anticipated nominal trajectories for RA-1 and -2 spacecraft. Had these been attained, the spacecraft would have been injected from a near-Earth orbit into a deep-space orbit somewhere between Ascension Island, in the South Atlantic Ocean, and the southern tip of Africa. The timing of this final injection was such that accurate tracking data from the Atlantic Missile Range (AMR) would be marginally available to direct the Johannesburg antenna immediately onto the spacecraft.

Table 64. Deep space station locations

DSS location	Code	Geodetic latitude	Geodetic longitude
Goldstone, Calif., U.S.A.	GS	35.389° N	116.848° W
Johannesburg, South Africa	J	25.891° S	27.675° E
Woomera, Australia	W	31.382° S	136.886° E

For this reason, the Mobile Tracking Station (Fig 250) was deployed to that site so that its wide beam width and high tracking rate capability could be used for early acquisition of the spacecraft. Data obtained from the MTS was to assist the JPL facility in computing an initial trajectory, for directing the other DSIF stations onto the spacecraft signal. MTS tracking was to take place along the path indicated in Figure 252.

Booster vehicle difficulties prevented achievement of the desired deep-space orbits for both the *Ranger I* and *II* missions. Each of these craft achieved only an Earth–satellite status, which meant that the spacecraft's passes over the DSIF stations would be infrequent and that much of its lifetime would be spent in the non-visible regions, as shown in Figure 245. Because of this circumstance, the DSIF was able to recover but a small percentage of the total data transmitted by the RA-1 and -2 spacecraft.

b. DSIF station configuration for **Rangers I** *and* **II.** All DSIF stations were operational for *Ranger I* and *II* missions, using 960-mc phase-locked-loop receivers. Each receiver consisted of two angle-tracking channels and a sum signal channel from which doppler data and telemetry information were derived.

The outputs of the receiver's angle channels were d-c error voltage signals that drove the antenna servo systems to maintain the antenna pointed at the spacecraft within 0.03 to 0.05-deg rms error. Digital sensors on the antenna structure converted the physical shaft positions of the antenna into signals which were teletyped back to the JPL computer to serve as angle-tracking data. The forces of gravity slightly distort the antenna and its structure with respect to the readings of the digital sensors. These are bias errors and amount to as much as ±0.1 deg. However, optical calibration techniques permit accurate pre-determination of most of the biases as a function of angle. For *Ranger*, the known bias errors of each station were removed from the observed data by the JPL computer.

The sum channel of the DSIF receiver had two outputs: (1) a wide-band output which fed the telemetry discriminators; and (2) a narrow-band output which contained the doppler (velocity) data pertaining to the space-

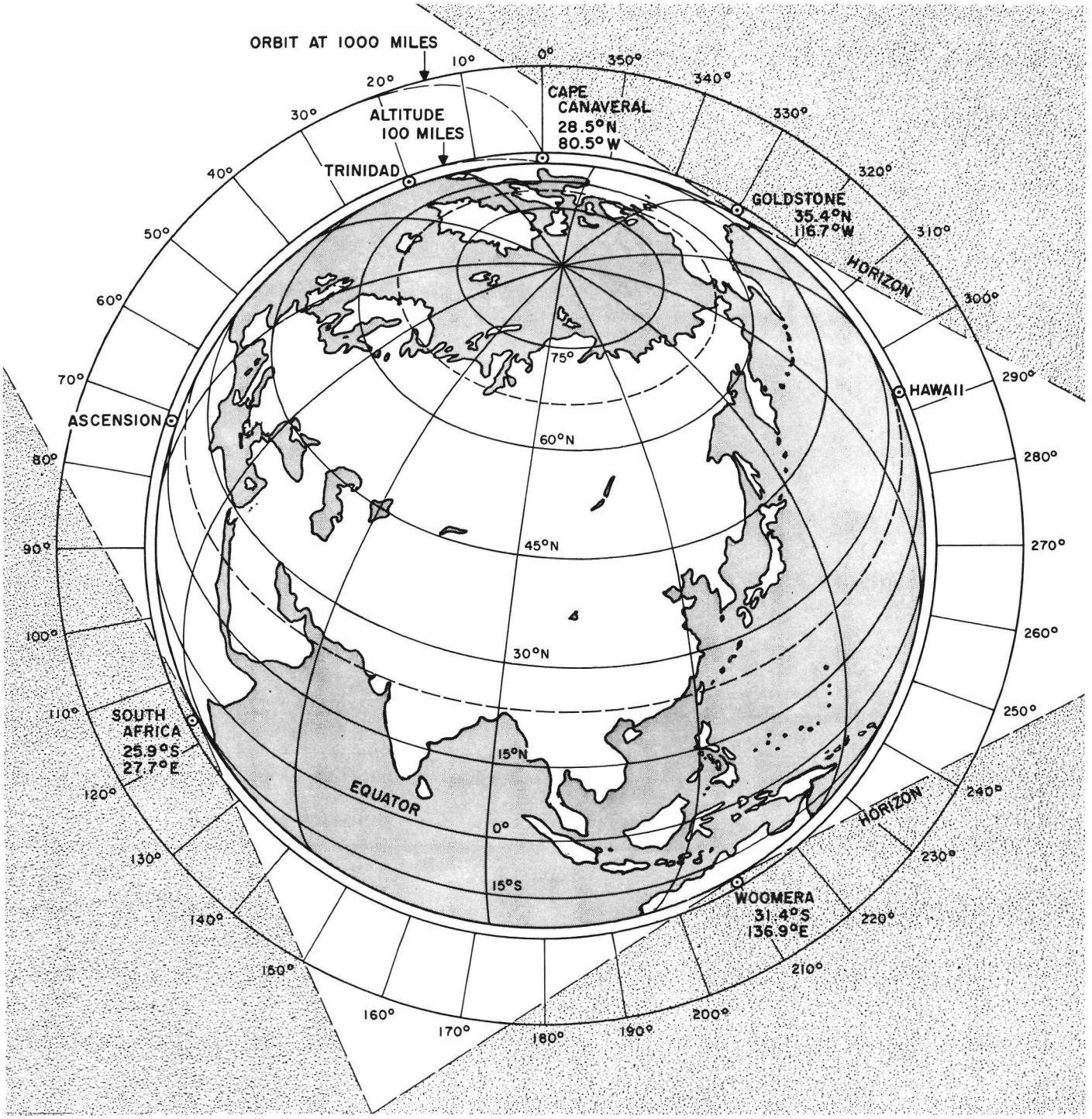

Figure 245. Line-of-sight tracking capability of DSIF

craft trajectory. Angle, doppler, and telemetry data were converted into teletype format and sent through the intersite communications network (Fig 251) to the JPL computer facility. The doppler data was sent in near-real-time with the angle data. The telemetry data was sampled at the DSIF stations and selected portions were teletyped to JPL at scheduled intervals during the tracking mission. All telemetry was tape-recorded at each station, and these tapes were mailed to the JPL Data Reduction Laboratory at the conclusion of each mission.

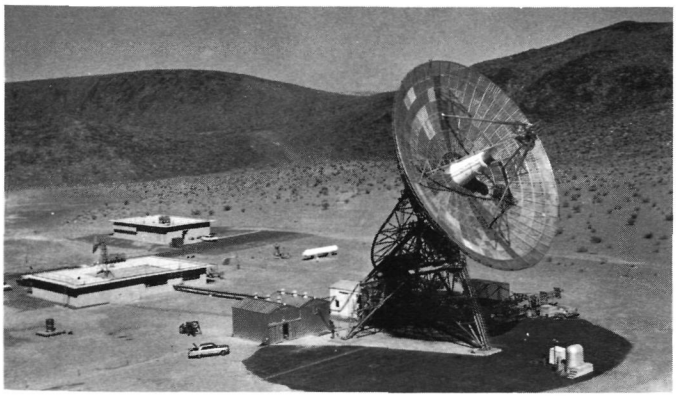

Figure 246. Goldstone Station Pioneer site

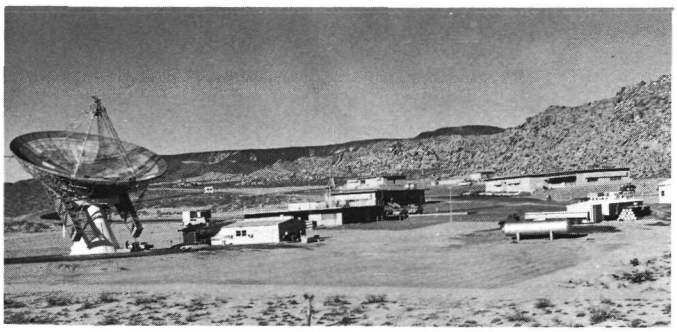

Figure 247. Goldstone Station Echo site

Goldstone configuration. The altazimuth antenna at the Goldstone *Echo* Site had prime tracking responsibility for both *Rangers I* and *II*. A block diagram of this station's configuration is shown in Figure 253. The Echo Site station (DSIF 3) also had the responsibility for transmitting commands to the spacecraft, and, along with the Mobile Tracking Station, the unique capability to make two-way doppler measurements. (In two-way doppler, the ground station transmits a signal to the spacecraft, where it is transponded—i.e., multiplied—by an exact ratio and retransmitted back to the ground station receiver.)

The polar-mount antenna at the Goldstone *Pioneer* Site also had tracking responsibility during *Ranger I* and *II* missions—the exception being that the 6-ft calibration shown in Figure 253. *Pioneer* Site had a 25-w transmitter but no on-site command capability, and employed a HA/Dec antenna instead of an altazimuth antenna.

With one exception, the Goldstone configuration remained as indicated throughout the *Ranger I* and *II* missions—the exception being that the 6-ft calibration antenna mounted on the 85-ft dish was connected into the receiver's sum channel. This modification increased the usable beamwidth to 15 deg, but left the angle tracking beamwidth for telemetry and doppler at approximately 1 deg. The 34-db reduction in gain could be toler-

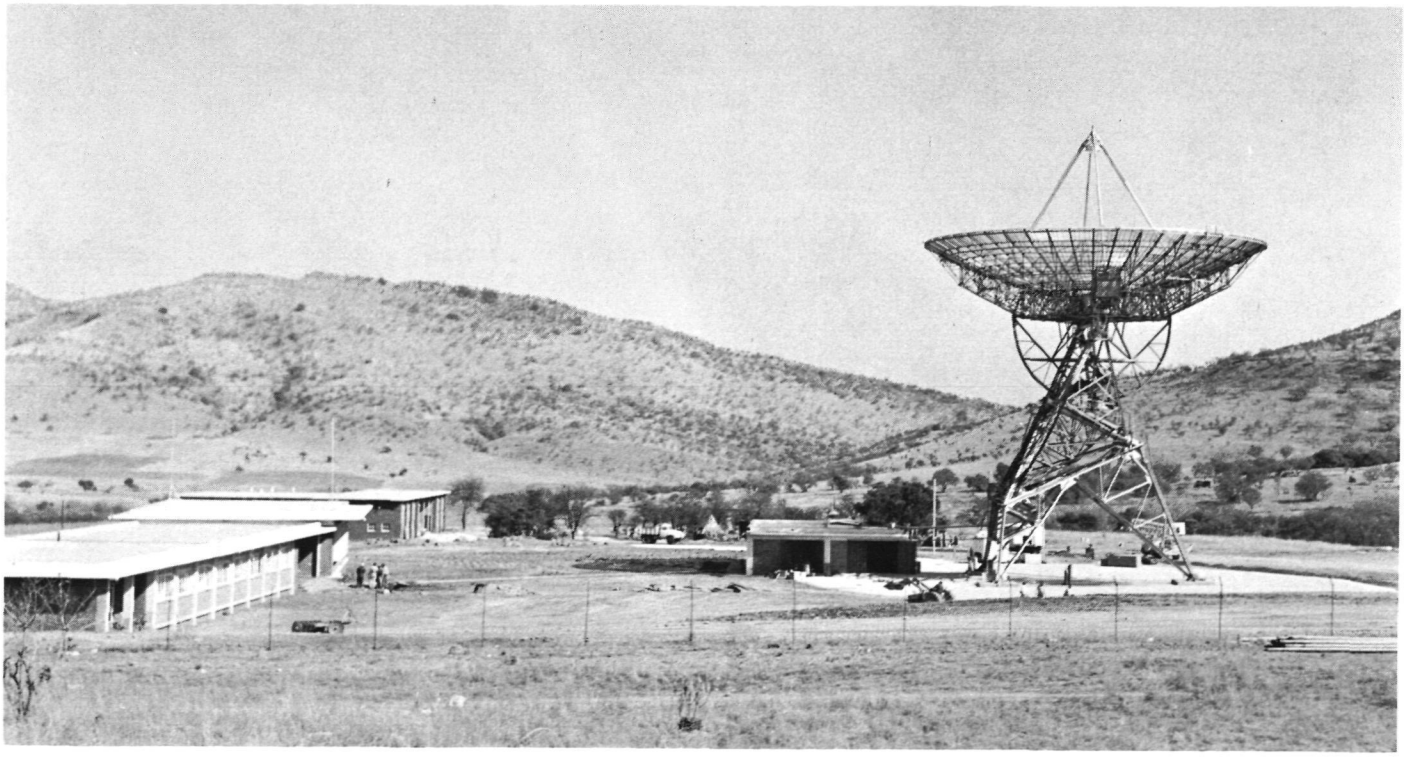

Figure 248. Johannesburg tracking station

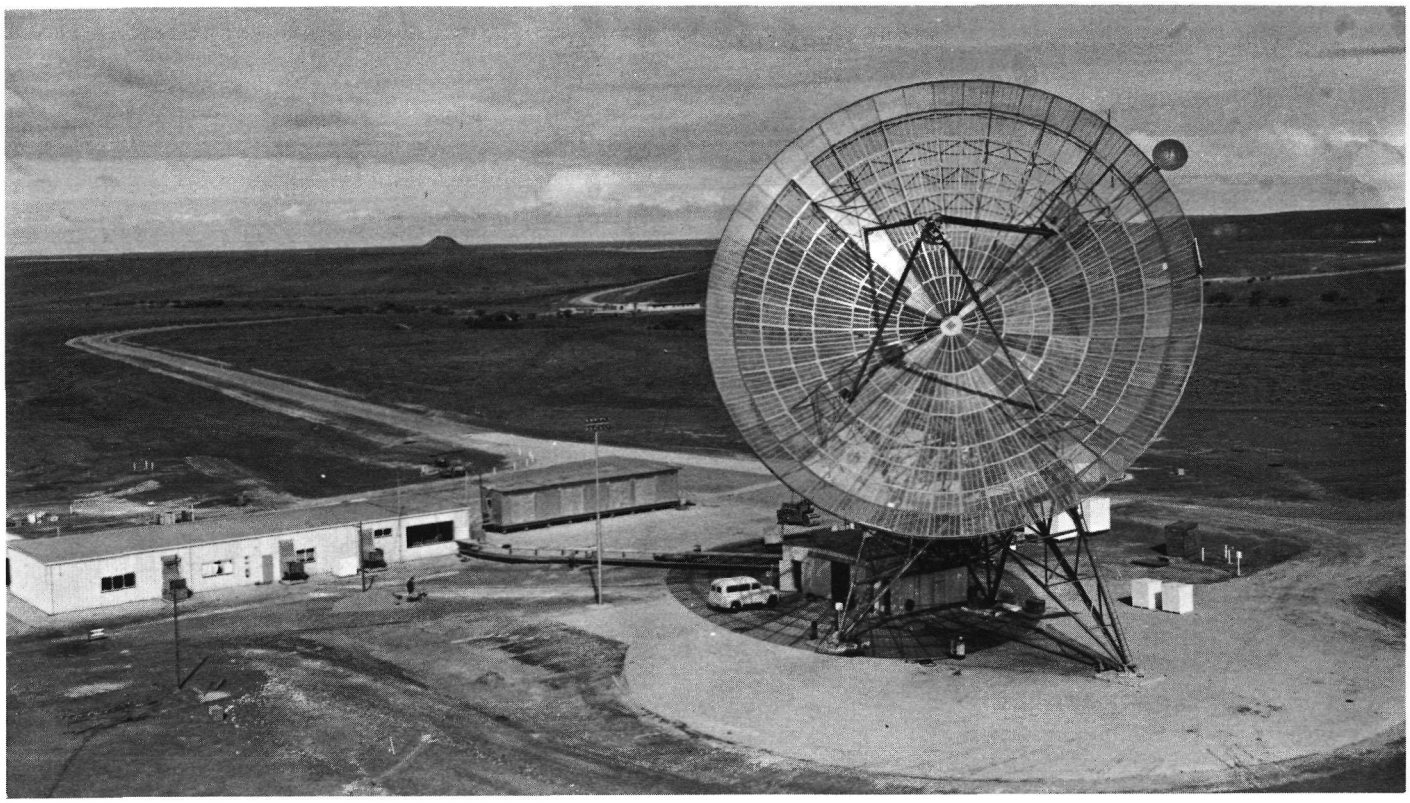

Figure 249. Woomera tracking station

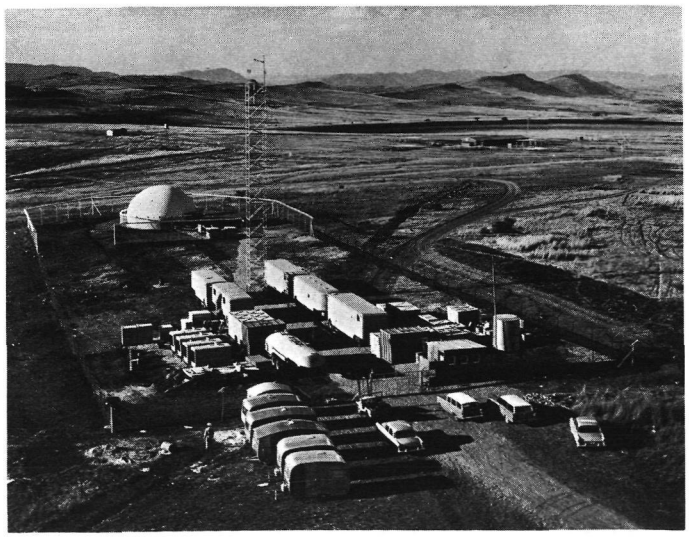

Figure 250. MTS deployed at South Africa site

ated because of relatively strong signal strength received from *Rangers I* and *II*, and the increased beamwidth was a definite advantage in making a quick acquisition of the telemetry data as the spacecraft appeared above the station horizon.

The command capability of the DSIF was successfully demonstrated during Orbits 30 and 31 of *Ranger I*. *Echo* Site transmitted several antenna switchover commands and the spacecraft responded by switching the transponder output back and forth between the omni-antenna and the high-gain antenna.

Command capability from *Pioneer* Site was also demonstrated when signals were sent from the command unit at *Echo* Site over the Goldstone microwave link to *Pioneer's* 25-w transmitter. During Orbits 46 and 47, *Pioneer* Site sent hinge over-ride commands.

Johannesburg and Woomera station configurations. The polar-mount antennas at Johannesburg and Woomera tracked the *Ranger I* and *II* spacecraft whenever these vehicles were visible and within the station tracking-rate capability. Their station configurations are shown in Figure 254. These stations differed from the Goldstone *Echo* configuration principally in the lack of a transmitter and in the type of antenna, tracking rate, etc. Thus, neither station could have command capability or use two-way doppler. However, the stations did have full capability for one-way doppler, angle tracking, and telemetry recovery. Both stations performed above specification on these first lunar missions.

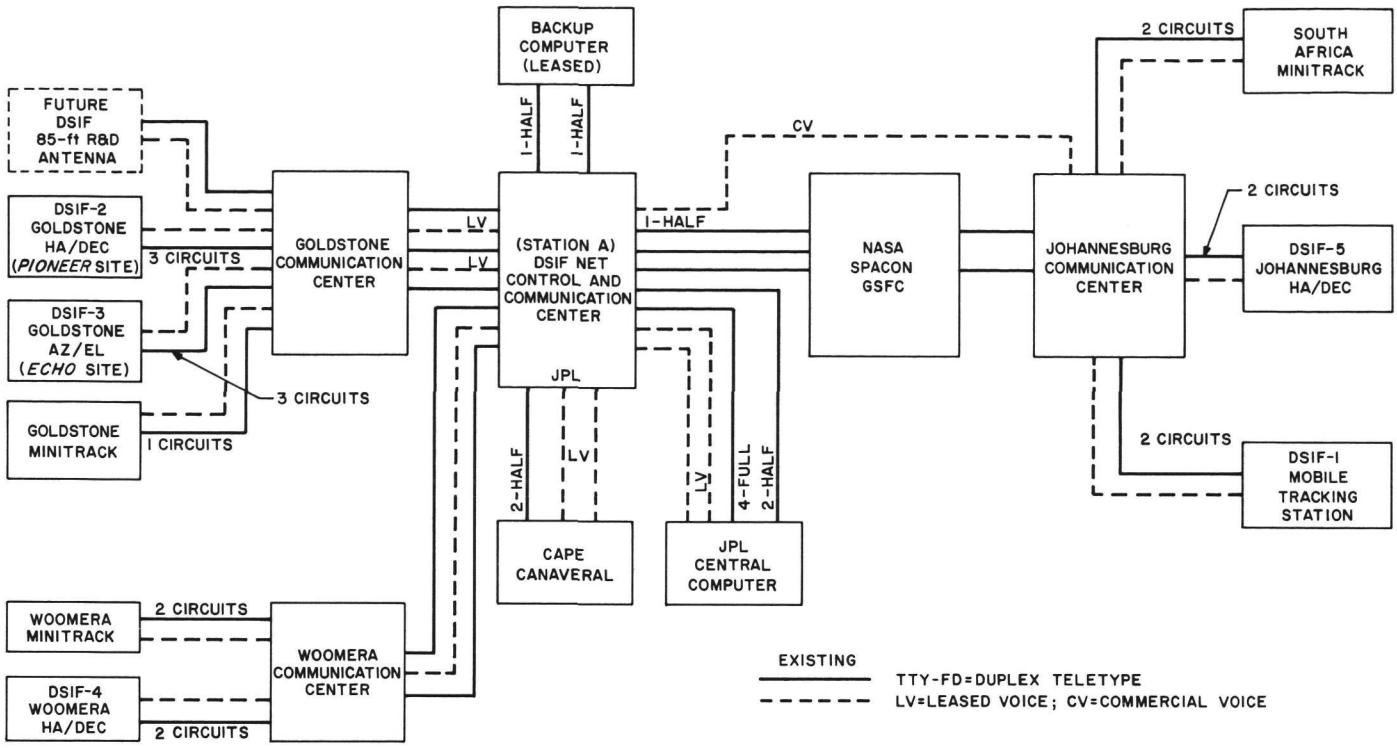

Figure 251. DSIF intersite communications network for *Ranger*

Due to the Earth-orbit status of *Rangers I* and *II*, these stations employed two last-minute modifications to the standard station configuration. The first was the use of the 6-ft calibration antenna for feeding the receiver sum channel, as was done at Goldstone *Pioneer* Site. The second was to replumb the servo hydraulic system to remove the anti-backlash feature and set-up the servo motors to aid rather than buck each other. This change increased the angular tracking rate capability of these stations from 1 deg per sec to 1.5 deg per sec, at a slight sacrifice in tracking accuracy. While the latter modification proved very helpful, the increased tracking rate was still below that of the Goldstone *Echo* Site and the Mobile Tracking Station. For this reason, the Johannesburg and Woomera DSIF stations were not able to track all the *Ranger I* and *II* passes that were visible to them. Despite this handicap, these stations did obtain valuable data on many passes.

Mobile Tracking Station configuration. For *Rangers I* and *II*, the Mobile Tracking Station was deployed to South Africa and located in an area approximately 1 mi from the permanent DSIF station. As shown in Figure 255 the MTS had a 25-w transmitter which permitted two-way doppler capability. It did not, however, have command capability. Since the MTS already was equipped with a widebeam antenna (approximately 10 deg), and a servo drive system capable of a slewing speed in the range of 10 to 20 deg/sec, it was not necessary to make emergency changes to the station, as was done at the other DSIF sites. As a result of this intrinsic capability, the MTS performed exceptionally well and, along with the Goldstone *Echo* station, produced much of the data obtained from the *Ranger I* and *II* missions.

D. Guidance and Control

1. RA-1 and -2 Subsystems Description

a. Attitude-control subsystem (block diagram, Fig 256).

Design considerations. The primary function of the attitude-control subsystem is to provide three-axis orientation and stabilization of the spacecraft in flight according to pre-established spatial relationships.

Ranger I and *II* missions required that two major assemblies be oriented, so that: (1) the solar panels faced the Sun, and (2) the high-gain, narrow beamwidth antenna pointed toward the Earth.

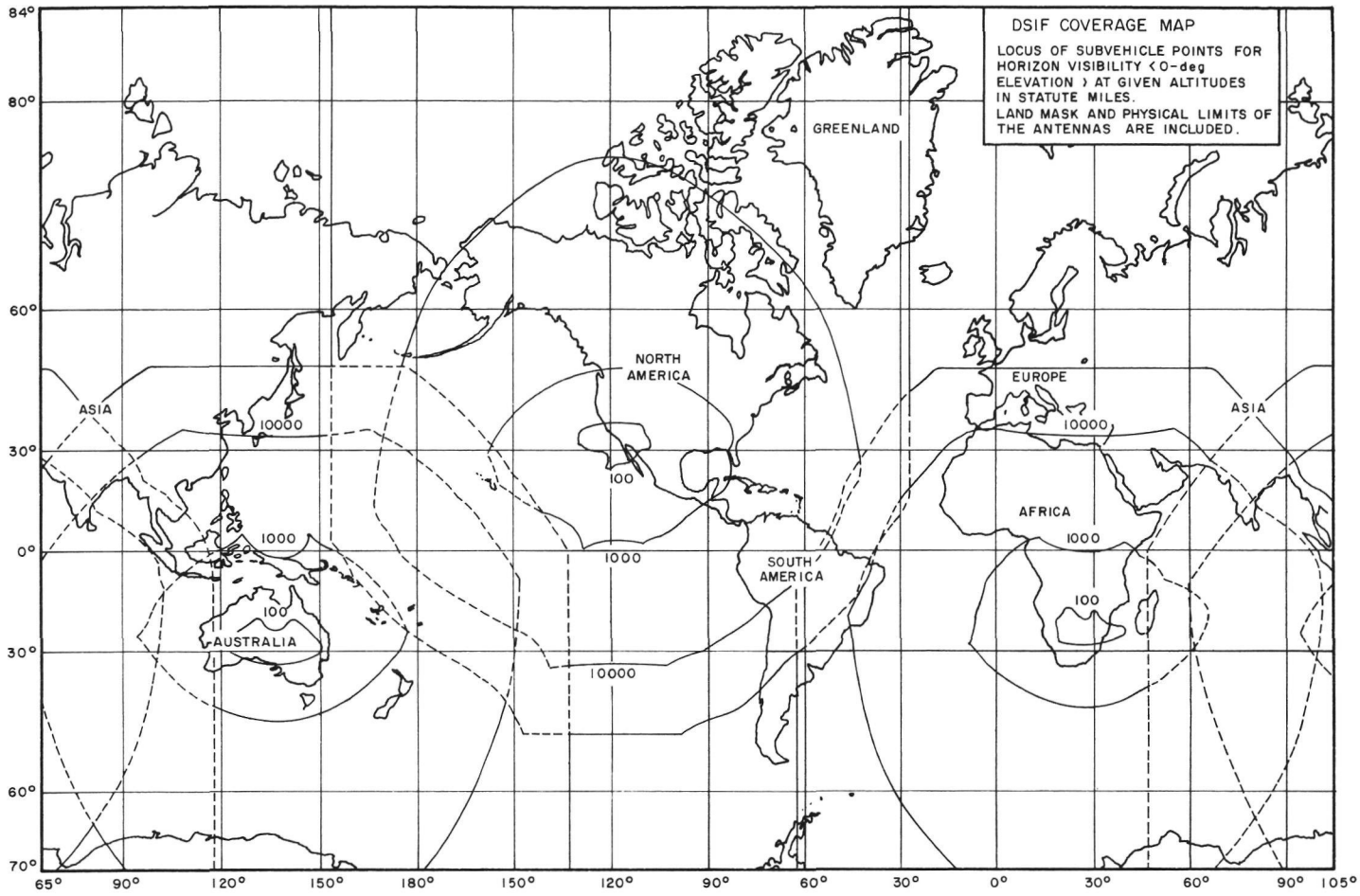

Figure 252. DSIF station coverage

Secondary, but important, design requirements imposed by the missions were:

(1) To operate for a lifetime of approximately 50 days (see trajectory requirements).

(2) To be adaptable to future, more sophisticated missions.

(3) Simplicity.

(4) Reliability.

(5) To operate in the expected environments.

(6) To conform to the structure-packaging concept.

(7) To satisfy weight limitations.

Mechanization. Several methods and systems were considered, including combinations of momentum devices, hot-gas systems, star trackers, etc. A cold-gas, on–off, expulsion torquing system, and a system of photosensitive reference-sensing devices were selected for simplicity, adaptability, and reliability. Development and performance of the attitude-control subsystem is discussed in more detail under subsystem development and flight performance.

b. Controller subsystem (block diagram, Fig 257).

Design considerations. The RA-1 and -2 controller coordinates the activities of the various spacecraft subsystems and causes the correct operations to be initiated at the proper time during the flight of the vehicle. In general, the controller is not involved in the internal operation of the various subsystems, but it is required to initiate functions by timed switching.

The controller also generates one-pulse-per-sec pulses for use as a time base for the controller and other spacecraft subsystems.

Figure 258 diagrams the relationships of the controller with the spacecraft subsystems, and the flight sequence

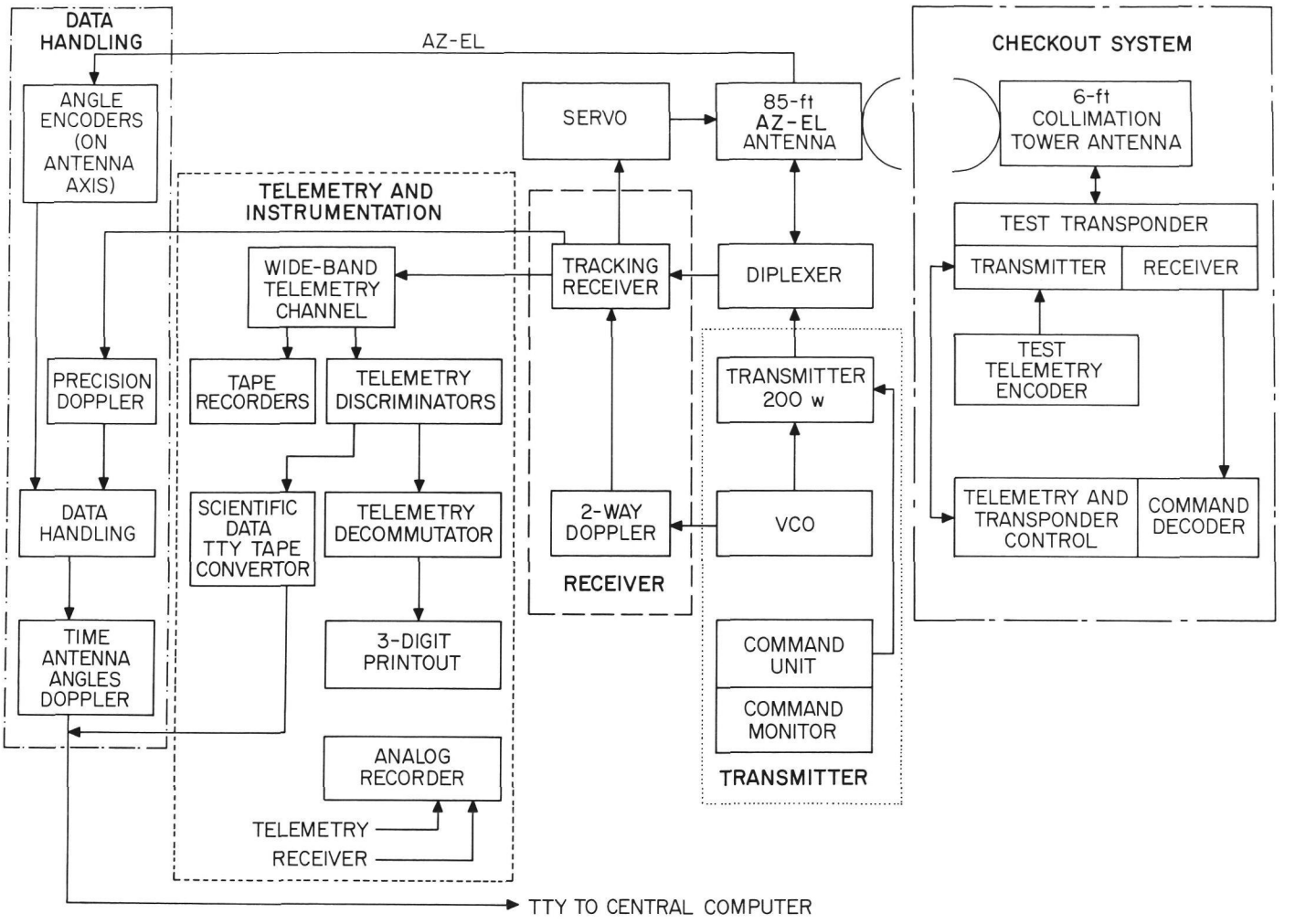

Figure 253. Goldstone Echo station block diagram

in Table 65 describes the events begun by instruction from the controller.

Mechanization. The RA-1, -2 controller consists of a clock pulser and dividing network, a counter, a command gate, relay drivers, and relays.

The subsystem is mechanized to be easily expanded for the future, more sophisticated systems, and is designed to operate reliably within the environmental, packaging, and weight restrictions imposed.

A photograph of a typical module, the main counter, is shown, prior to potting, in Figure 259.

Development and performance of the controller described above is discussed in more detail under subsystem development and flight performance.

c. Power subsystem (block diagrams, Fig 260).

Design considerations. The RA-1 and -2 spacecraft system required a power source which was capable of:

(1) Supplying power in the amount required for the expected lifetime of the mission (approximately 50 days).

(2) Supplying power tailored to the needs of the various users.

(3) Providing an accurate (0.01%) timing and synchronization reference to the spacecraft.

(4) Accomplishing the above requirements with a maximum of efficiency and reliability within the restrictions of size and weight.

Mechanization. Primary power for the spacecraft was provided by a battery and solar panels. The battery sup-

Table 65. RA-1 and -2 flight sequence

No.	Time[a] (ref only)	Type[b]	Origin[c]	Destination[d]	Designated command Nos.	Occurrence
1	X−3 min	C	EA	CL		Start timer
2	X−3 min	I	CL	EA		Timer has started
3	X−3 min	I	CL	TM		Timer has started
4	X+22 min	T	CL	RF	1	Transfer transmitter to high powered transmission
5	X+22 min	I	CL	TM		A command was issued
6	X+34 min	T	CL	ST	3	Unfold solar panels and release solar corpuscular analyzer arm (1)
7	X+34 min	T	CL	SC		Turn on solar corpuscular radiation and semiconductor plasma detector experiments
8	X+34 min	I	CL	TM		A command was issued
9	X+59 min	T	CL	AC	4	Attitude control command one (2)
10	X+59 min	I	CL	TM		A command was issued
11	X+32 min	T	CL	SC	2	Power on (scientific instruments)
12	X+32 min	I	CL	TM		A command was issued
13	X+90 min	T	CL	AC	5	Attitude control command two (3)
14	X+90 min	I	CL	TM		A command was issued
15	X+115 min	T	CL	TM	6	Rate gyro scale change
16	X+115 min	I	CL	TM		A command was issued
17	X+204 min	T	CL	SC	7	Open apertures of the remainder of the semiconductor plasma detectors
18	X+204 min	I	CL	TM		A command was issued
19	X+247 min	T	CL	RF	8	Antenna switchover
20	X+247 min	I	CL	TM		A command was issued
21	X+364 min	T	CL	TM	9	Reduce data rate to primary transmitter
22	X+364 min	I	CL	TM		A command was issued
23	X+367 min	T	CL	FE	10	Turn on friction experiment

[a]Time at which an event is expected to occur in the RA-1 and flight sequence.
[b]Nature of an occurrence. C = a command resulting from an event, I = an information signal announcing the occurrence of an event, and T = a command generated as a result of controller-produced timing information.
[c]System in which the occurrence originates.
[d]System receiving the information or command and acting on it. The systems are identified as follows:

A/C = attitude control
CL = controller
EA = Earth checkout and launch systems except via RF link
FE = friction experiment
PR = power system
RF = communication system
SC = scientific instruments
ST = structures
TM = telemetry

(1) It will take approximately 45 sec for the solar panels to open and approximately 60 sec for the solar corpuscular arm to erect.
(2) This command enables the attitude control system to acquire the Sun and to position the high gain antenna and the Earth sensor.
(3) This command enables the attitude control system to acquire the Earth.

plied power from shortly before take-off to Sun acquisition, at which time the solar panels assumed the electrical power load. From this point on, the battery became a back-up source, sharing the load if greater than the panel capacity, or assuming the load if the panels were not illuminated.

A power switch and logic circuit performed the functions of switching from external to internal power and governing the load sharing between battery and panels.

The booster–regulator acted on the output of the power switch and logic and supplied 31.5-vdc ±1% for the operation of the various users.

Converters and inverters suited to the needs of each particular subsystem were the local power supplies for the subsystems.

In addition to the above items, a separate battery, switch, regulator, and inverter were provided for the exclusive use of the ¼-w transmitter. It was reasoned that in case the solar panels are not illuminated, the ¼-w transmitter would be operative as a back-up for the 3-w transmitter, relaying engineering and scientific telemetry data, and as a tracking beacon for an extended period after the main battery was exhausted.

All secondary power equipment was of the static transistor-magnetic type and the general characteristics are shown in the block diagram (Fig 260).

2. RA-3, -4, -5 Subsystems Description

The addition of midcourse and terminal maneuver requirements in the RA-3, -4, -5 spacecraft further complicates the guidance and control subsystems as described for RA-1 and -2. The subsystems, while similar to RA-1 and -2, have been expanded in some instances and redesigned in others. The capabilities of the RA-3, -4, -5 subsystems can perhaps best be described by considering the functional requirements for the subsystem on a block diagram basis.

a. Attitude-control subsystem. The RA-3 attitude-control subsystem consists of error detectors (optical sensors), electronic signal circuits, and gas jet control components. The autopilot and midcourse guidance subsystems are interconnected to share attitude control circuits. Figure 261 shows this relationship in block diagram form; Table 66 explains the operation. Sun and Earth sensors determine the spacecraft attitude and generate the error signals to align the spacecraft properly with the Sun and Earth. A switching amplifier circuit is used to establish a limit cycle mode of attitude control. The switching amplifiers control ten valves and reaction jets about the spacecraft pitch, yaw, and roll axes in a cold-gas (nitrogen) expulsion subsystem.

Table 66. Flight operations

0. Conditions at launch:
   A. Gyro power for motors and torquer amplifiers on
   B. All other attitude control power off
1. Sun acquisition:
   A. Turn on remaining A/C power except to
      1) Earth sensor
      2) Acquisition rate command generator
      3) All autopilot components, and
      4) Midcourse motor shutoff system
2. Earth acquisition:
   A. Turn on Earth sensor and acquisition rate command generator
3. Antenna exit:
   A. Step S3 to Position 2 regardless of its prior position
4. Inertia lock any axis:
   A. Command S1 to Position 2
   Note: With the present sum sensor S1P and S1Y will always operate together
5. Prepare for Earth loss:
   A. Reverse Step 2
6. Command turn any axis:
   A. Turn on calibrated rate command generator in proper direction
   B. Reverse Step 6A after allotted time
7. Prepare for midcourse motor:
   A. Turn on autopilot and motor shutoff systems
8. Midcourse motor ignite:
   A. Give ignite command simultaneously with 8B and 8C
   B. Command S5P and S5Y to Position 2 simultaneously with Steps 8A and 8C
   C. Open shutoff gates simultaneously with 8A and 8B
9. Midcourse motor shutoff:
   A. Give shutoff command
   B. Reverse Step 7A after allowing time for shutoff transient
10. Sun re-acquisition:
    A. Command S1P, S1Y, and S1R to Position 1
    B. Step S3 one position
11. Earth re-acquisition:
    A. Same as Step 2A
12. Hinge override:
    A. Step S3 one position
13. Roll over-ride:
    A. Command S2 and S4 to Position 1
14. Threshold gain (logic operation, internal):
    A. Pulse S2 and S4 to Position 2
15. Threshold loss (logic operation, internal):
    A. Pulse S2 and S4 to Position 1

Switch operations

S1: Operated solely by the central computer and sequencer (CC&S).

S2: This switch latches in both directions. It is pulled to Position 1 by the threshold crossing detector whenever signal threshold is lost (or when the Earth sensor is turned off) and to Position 2 whenever threshold is gained providing the Earth sensor is turned on). S2 may also be returned to Position 1 by the roll override command from the CC&S.

S3: This switch must be in Position 1 when Sun acquisition power is turned on. The antenna exit command from the CC&S causes S3 to step to Position 2 regardless of its prior position. The Sun reacquisition command from the CC&S causes S3 to step one position. The hinge override command causes S3 to step one position.

S4: Same as S2.

S5: The ignite command from the CC&S causes S5 to go to Position 2.

NOTES:

1. Switches must be in position shown and midcourse shutoff gates must be closed when power is initially turned on.
2. Solid boxes and circles represent control system or other components. Dotted boxes and circles represent vehicle dynamic characteristics.
3. Any mechanization shown is for illustration only and is subject to change by the cognizant engineers without notice.

Attitude-control operation and flight description. The attitude-control subsystem is designed to be adaptable to any programmed lunar trajectory by proper selection of the antenna hinge angles (hinge axis control portion of block diagram, Figure 261) and operation of the roll and hinge overrides. The roll and hinge override command feature also provides the capability of partially salvaging the mission in the event of gross trajectory errors. Simplicity has been given a very high priority in the design of the attitude-control subsystem to maximize the likelihood of mission success.

To describe the attitude-control subsystem and its functions, the spacecraft guidance sequence is discussed in chronological order.

The flight begins for the attitude-control subsystem at spacecraft and *Agena* separation. The subsystem has completed pre-launch checks before lift-off and at injection only the gyros are activated. The spacecraft is tumbling and will continue to do so until the attitude-control subsystem is activated.

Next, the solar panels are opened at A + 30 min and the tumbling rate slows (A + 0 is time of launch).

The "acquire-Sun" command is given by the Central Computer and Sequencer (CC&S) at A + 33 min. The directional high-gain antenna is extended, the gas jets and Sun sensors are activated, and the solar acquisition sequence commences. The spacecraft first eliminates the initial tumbling rates and then, as part of the same process, when the rate feedback voltage drops below that of the saturated position sensors, the vehicle automatically turns to face the Sun. Eliminating the tumbling rates requires a period of 15 min maximum and uses less than ½ lb of the 2.5-lb nitrogen capacity. Turning to face the Sun takes 22 min, maximum.

At A + 3 hr, the CC&S gives the attitude-control subsystem the "acquire-Earth" command. The command activates the Earth sensor and introduces a 3.5-mrad/sec roll rate. The directional high-gain antenna is in the acquisition hinge position following the A + 33 min command. Within 30 min, the Earth enters the field of view of the Earth sensor and the Earth is acquired. If the Moon should be acquired first, the roll and/or hinge override commands must be given. The spacecraft then rolls, gives up the Moon and acquires the Earth. The Earth will be acquired within four hr after injection for RA-3, -4, and -5.

The cruise mode is established when the Earth is acquired. In the cruise mode, the spacecraft performs a limit cycle about each axis. The dimensions of the pitch

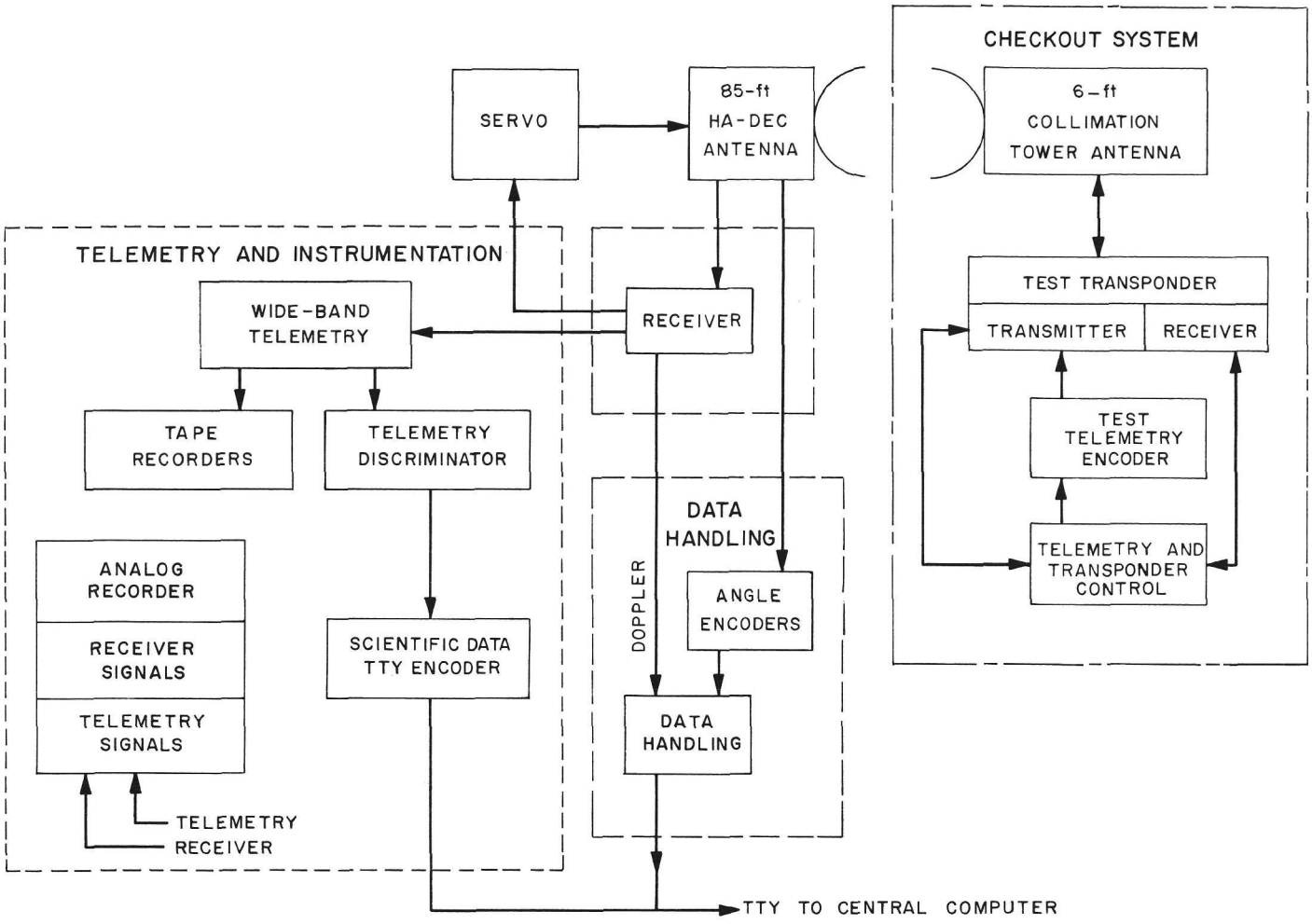

Figure 254. Johannesburg and Woomera station block diagram

and yaw limit cycles are ± 10 μrad/sec and ±2.9 mrad in the cruise mode. The limit cycle dimensions increase to ± 5 mrad in the commanded turn mode. The dimensions of the roll limit cycle are ± 14.7 μrad/sec and a gradually decreasing angular limit set for ±5 mrad at nominal midcourse and thereafter. This gradually decreasing angular limit in the roll limit cycle is due to the gradually decreasing angle which the Earth subtends. This roll limit cycle is flown in the cruise and maneuver modes all the way to the Moon. The gas consumption required by the limit cycle is approximately 0.03 lb per axis. Solar pressure may increase the gas consumption about 50%.

At approximately 16 or 40 hr after launch, the spacecraft performs the midcourse maneuver on receipt of a radio command. The radio command consists of the velocity increment, the roll and pitch turn durations with polarity, and the execute command. The CC&S, on receipt of the execute command, first commands the attitude-control subsystem to switch the roll axis from optical to inertial lock, to connect the roll capacitor, to turn on the autopilot, and to withdraw the directional high-gain antenna to the exit angle, which is 180 deg from the nested position. This command switches S2 to Position 2 and S3 to Position 2 as shown in the block diagram, Figure 261.

The calibrated roll turn is switched in at this time for the calculated roll duration. This duration, as well as the other commanded turn durations, is determined on the ground in advance from the tracking data and transmitted prior to the maneuver via the ground command and r-f link to the CC&S, where it is stored. The polarity of the turn is included in the command. At the conclusion of the roll turn duration, the calibrated command rate generator is switched off and the spacecraft remains stationary until the next CC&S command is given.

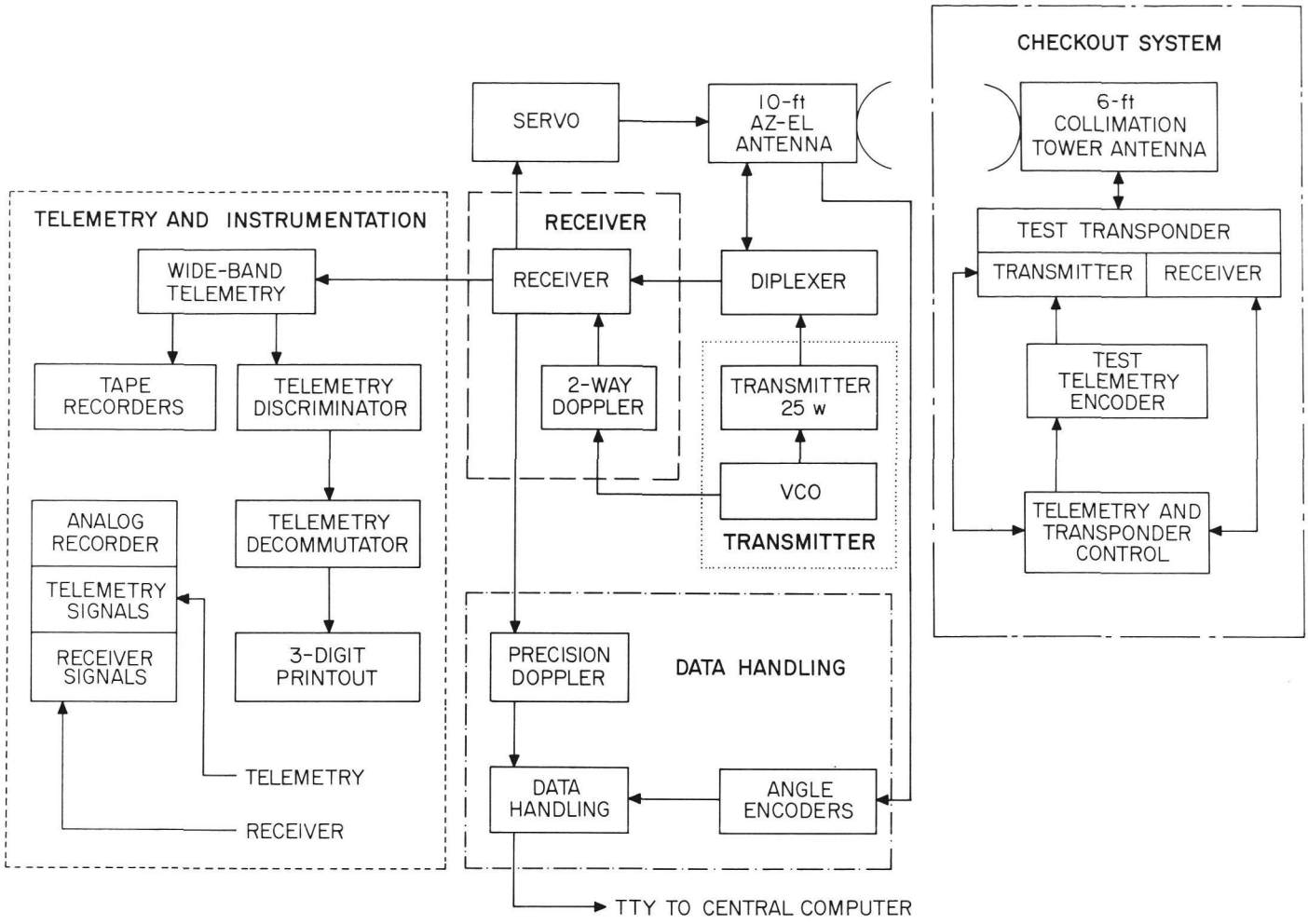

Figure 255. MTS block diagram

The next CC&S command in the sequence switches the pitch and yaw axes from optical lock to inertial lock. The pitch and yaw capacitors are connected and a pitch turn is performed in a similar manner to the roll turn. The CC&S commands the start of each turn at a fixed time after the receipt of the execute command. The interval between the start time of the turn allows sufficient time for the maximum turn plus 2 min settling time for the turn transients to dampen out.

The CC&S next ignites the midcourse motor and, for simplicity, the coasting attitude-control subsystem is left on. While the gas jets on all three axes are probably on continuously during motor burning, there is no harmful effect. The gas consumed is insignificant, and the perturbations to the thrust vector direction and magnitude are small. The midcourse motor is turned off by CC&S command. The required velocity increment is determined from tracking information on the ground and sent to the spacecraft by ground command through r-f link, where it is stored in the CC&S in the form of a required accelerometer count. The pulses of the digital accelerometer are counted and the midcourse motor is shut off when the required count is reached. The autopilot remains on for the shut-off transients to dampen.

The CC&S next turns off the midcourse autopilot, jet vane actuators, accelerometer, and shut-off computer. The roll, pitch, and yaw capacitors are switched out, the antenna is repositioned, and solar acquisition is started. Thirty min are allowed for solar reacquisition. The CC&S next gives the roll search command for Earth reacquisition. If Earth–Moon ambiguity exists, the roll override command procedure will again be used. The cruise mode is again established when the Earth is acquired and the attitude-control subsystem continues in this mode until the terminal maneuver.

The terminal maneuver is a sequence of single axis turns performed in the order: pitch, yaw, pitch. Again

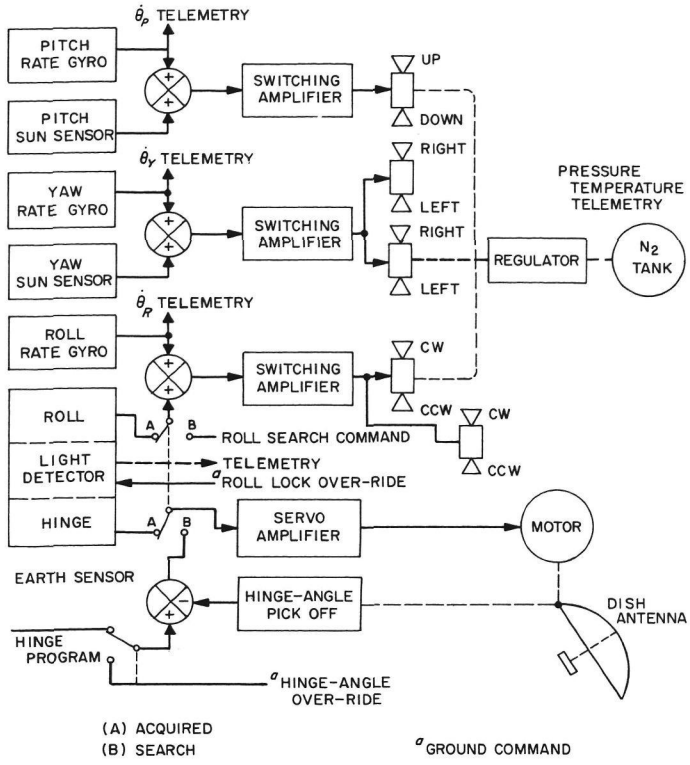

Fig. 256. RA-1 and -2 attitude control system, block diagram

the turn durations are sent to the CC&S in the spacecraft through the r-f command loop. On the execute command from the ground, the Sun sensors' signals are switched out, the pitch and yaw channel capacitors are connected, and the first pitch turn is started. The roll axis remains in optical lock (Earth sensor) with the antenna slaved to the Earth until lunar impact. After the turns, the attitude-control subsystem maintains the final spacecraft orientation for photographing the lunar surface and for launching the lunar capsule.

Attitude-control requirements. The spacecraft guidance control equipment must orient the spacecraft with the following pointing accuracies:

(1) Pointing error of roll reference line in cruise: 8.7 mrad -3σ

(2) Pointing error of antenna axis in cruise: 5 deg -3σ

(3) Pointing error of thrust vector in midcourse maneuver: 25 mrad -3σ

(4) Pointing error of roll reference line in terminal maneuver: 28 mrad -3σ

The widths of the limit cycle for each axis and the turning rates were mentioned above. These factors and trajectory limitations dictate dynamic requirements and alignment tolerances. With the establishment of the location of center-of-gravity accuracies, moments-of-inertia limits, products of inertia, etc., the component alignment and operational accuracies are specified. The development of the subsystem components within these specifications is then accomplished.

Attitude-control components. The description of the various components will be given in terms of the requirements placed upon each.

The Sun sensor error detectors must have a pointing accuracy of 3.5 mrad and have a field-of-view over the complete sphere about the spacecraft. The Sun sensors, consisting of primary and secondary pairs, are interconnected to produce these proper error characteristics. When the Earth sensor acquisition signal is given, the circuit to the secondary sensors is open and only the primary sensors are used in cruise. The primary Sun sensor pairs have a field of view of ± 45 deg in the plane of control and ± 30 deg in the plane perpendicular to the control plane.

The Earth sensor must have a pointing accuracy of ± 10 mrad 3σ in roll and ± 17.5 mrad 3σ in hinge. The Earth sensor is similar to that used for RA-1 and -2, except where the RA-3, -4, -5 application has required sensitivity changes and the addition of a Sun shield over the shadow box.

The pitch and yaw gyro loops are shown in Figure 262. The steady-state response of spacecraft to the turn command is 3.5 mr/sec, with a saturation turning rate of 10 mrad/sec minimum. The loop has a rise time response (application until 95% of steady state) of 100 msec maximum.

The switching amplifier performs a limit cycle mode of operations with the following requirements:

Roll dead zone in acquisition, cruise, and commanded turn .... 5.0 ± 0.5 mrad 3σ

Pitch and yaw dead zone in acquisition and cruise..... 2.9 ± 0.29 mrad σ

Pitch and yaw dead zone in commanded turn ..... 5.0 ± 0.5 mrad 3σ

The rise and fall time response requirements are 200 and 50 msec, respectively.

The gas subsystem acceleration level for each axis for steady flow is 0.28 mrad/sec^2. Valve opening and closing times are 50 and 20 msec, respectively. The gas capacity is 2.5 lb with a leakage rate for the three axes of less than 0.05 lb/day.

The antenna drive or hinge angle servo tracks the Sun–probe–Earth angle to better than 22 mrad maximum and positions the antenna to the preset angles with an accuracy of ± 3 deg maximum. The switch-on angle is ± 20 mrad and the switch-off angle is ± 10 mrad. The antenna drive turning rate is about 5 mrad/sec.

b. Midcourse guidance subsystem. The midcourse guidance subsystem controls the magnitude and direction of the midcourse correction velocity increment. The RA-3 autopilot subsystem consists of the autopilot jet vane actuator loop, the gyro rate and position loop, and the various signal mixing, integrating, etc., circuits. The autopilot controls the spacecraft motion about the pitch, yaw, and roll axis during the midcourse maneuver. The autopilot intrafunctional relationship with the attitude-control subsystem is shown in Figure 261, which indicates how the various components as gyros are used at different flight times. The components in the pitch or yaw autopilot loop are shown in block diagram form in Figure 263. The components in the roll loop are shown in Figure 264. A velocity shut-off control circuit shuts off the midcourse motor when the desired velocity increment has been obtained.

Midcourse guidance operation and flight description. At approximately 15.5 hr after launch, the spacecraft starts receiving the radio command information for the midcourse maneuver. The received signals consist of the roll and pitch turn durations (with polarity), the velocity increment, and the execute command. On receipt of the execute command, the CC&S commands the attitude-control subsystem to switch the roll axis control from optical to inertial lock, to connect the roll capacitor, to turn on the autopilot, and to extend the directional high-gain antenna to the exit angle, which is 180 deg from the nested position. (This sequence is further described in attitude control and CC&S flight operations descriptions.)

The midcourse motor is ignited after the sequence of commanded turns has been completed and the autopilot controls the jet vanes to perform the midcourse maneuver correction. The accelerometer senses the velocity increment and the CC&S shuts off the midcourse motor when the desired value has been reached.

Autopilot control requirements. The autopilot functions in a limit cycle mode during the midcourse maneuver after each commanded turn. The pitch and yaw limit cycle increases to ± 5 mrad during midcourse, while the autopilot must maintain a thrust vector pointing error in the midcourse maneuver of 25 mrad -3σ.

Using midcourse motor parameters, spacecraft moments of inertia, etc., midcourse motor calibration and mounting requirements are specified. Jet vane alignment, asymmetrical impingement of the exhaust gases, midcourse motor alignment, jet vane control calibration of the resultant thrust vector about the pitch and yaw axis, as well as cg and measurement of the cg position, etc., are all specified by the autopilot design.

Autopilot components. The autopilot is comprised mainly of control loops. The pitch and yaw channels of the autopilot have two control loops. The inner loop (the autopilot loop) controls and stabilizes the vehicle attitude in inertial space in response to the autopilot command angle. The inner loop is slower acting than the outer or path guidance loop. The further description of these loops becomes involved with time constants, damping ratios, loop gains, null offsets, etc. Therefore, let it suffice to note that the selection of loop parameters must satisfy multiple modes of operation where components are used in several circuit connections.

The jet vane actuator loop must function with the required stability. The pitch and yaw restoring moment capability about the spacecraft center of gravity must be 3.2 ft-lb, minimum. Any combination of pitch and yaw moments within the above capability must not reduce the net available roll moment capability below 0.1 ft-lb.

The gyro loop requirements in addition to those listed for the attitude-control operation, specify time constants and a torquing amplifier voltage saturation of 53 mrad, minimum.

c. Central computer and sequencer subsystem. The RA-3, -4, -5 central computer and sequencer (CC&S) is the subsystem which supplies internal timing in the spacecraft for synchronization, timer control, and operational sequence programming. The CC&S functions with fixed inputs to perform predetermined events. It receives quantitative radio inputs (to store and use later) and radio-execute commands for the midcourse and terminal maneuvers, as well as accelerometer signals during the midcourse maneuver. These input signals and commands are in a serial digital form. The CC&S outputs actuate spacecraft functions which occur at predetermined, commanded, or computed times. Various pulse train and waveform outputs also are supplied to the spacecraft.

CC&S functions. An over-all listing of input and output functions required of the CC&S is shown in the Figure 265. Functional operations are separated into the subsystems with which the CC&S is associated prior to launch and during flight. Input functions are indicated by arrows and appropriate relay and electronic switches are indicated by the initials *R* and *ES*.

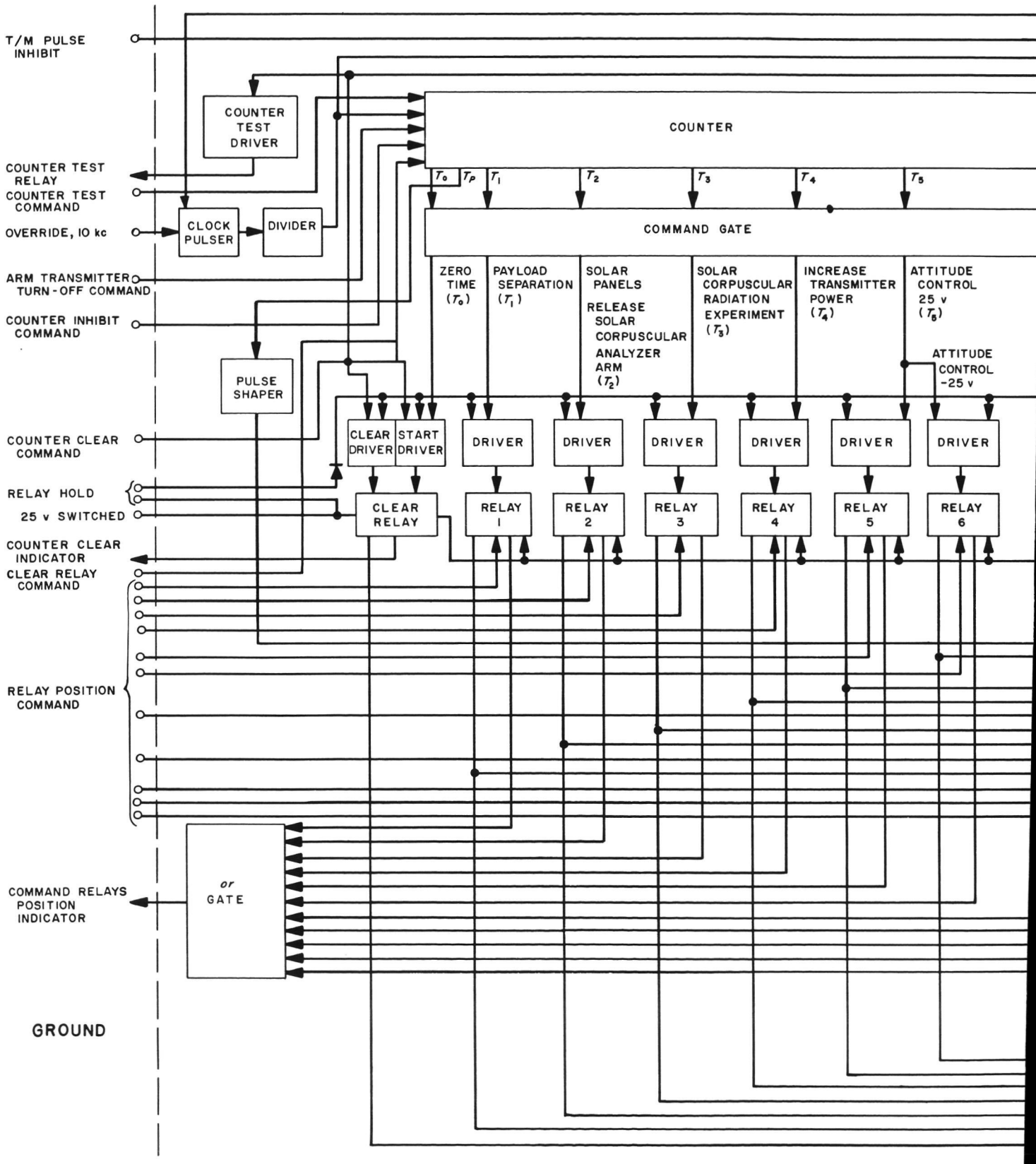
T/M PULSE INHIBIT
COUNTER TEST DRIVER
COUNTER
COUNTER TEST RELAY
COUNTER TEST COMMAND
OVERRIDE, 10 kc
CLOCK PULSER
DIVIDER
T_0 T_P T_1 T_2 T_3 T_4 T_5
COMMAND GATE
ARM TRANSMITTER TURN-OFF COMMAND
COUNTER INHIBIT COMMAND
ZERO TIME (T_0)
PAYLOAD SEPARATION (T_1)
SOLAR PANELS RELEASE SOLAR CORPUSCULAR ANALYZER ARM (T_2)
SOLAR CORPUSCULAR RADIATION EXPERIMENT (T_3)
INCREASE TRANSMITTER POWER (T_4)
ATTITUDE CONTROL 25 v (T_5)
ATTITUDE CONTROL -25 v
PULSE SHAPER
COUNTER CLEAR COMMAND
CLEAR DRIVER
START DRIVER
DRIVER
RELAY HOLD
25 v SWITCHED
CLEAR RELAY
RELAY 1
RELAY 2
RELAY 3
RELAY 4
RELAY 5
RELAY 6
COUNTER CLEAR INDICATOR
CLEAR RELAY COMMAND
RELAY POSITION COMMAND
COMMAND RELAYS POSITION INDICATOR
or GATE
GROUND

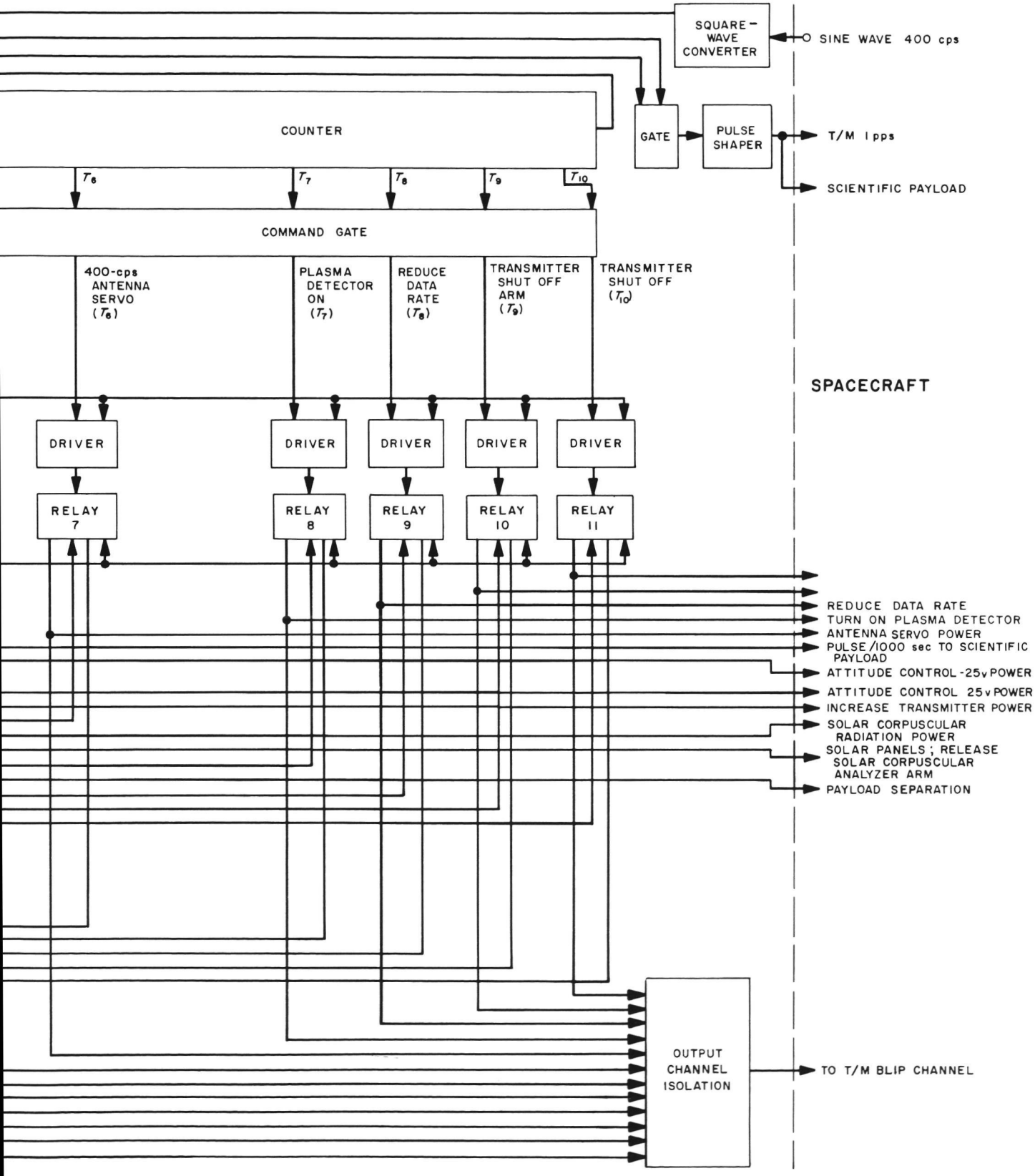

Figure 257. RA-1 and -2 controller, functional block diagram

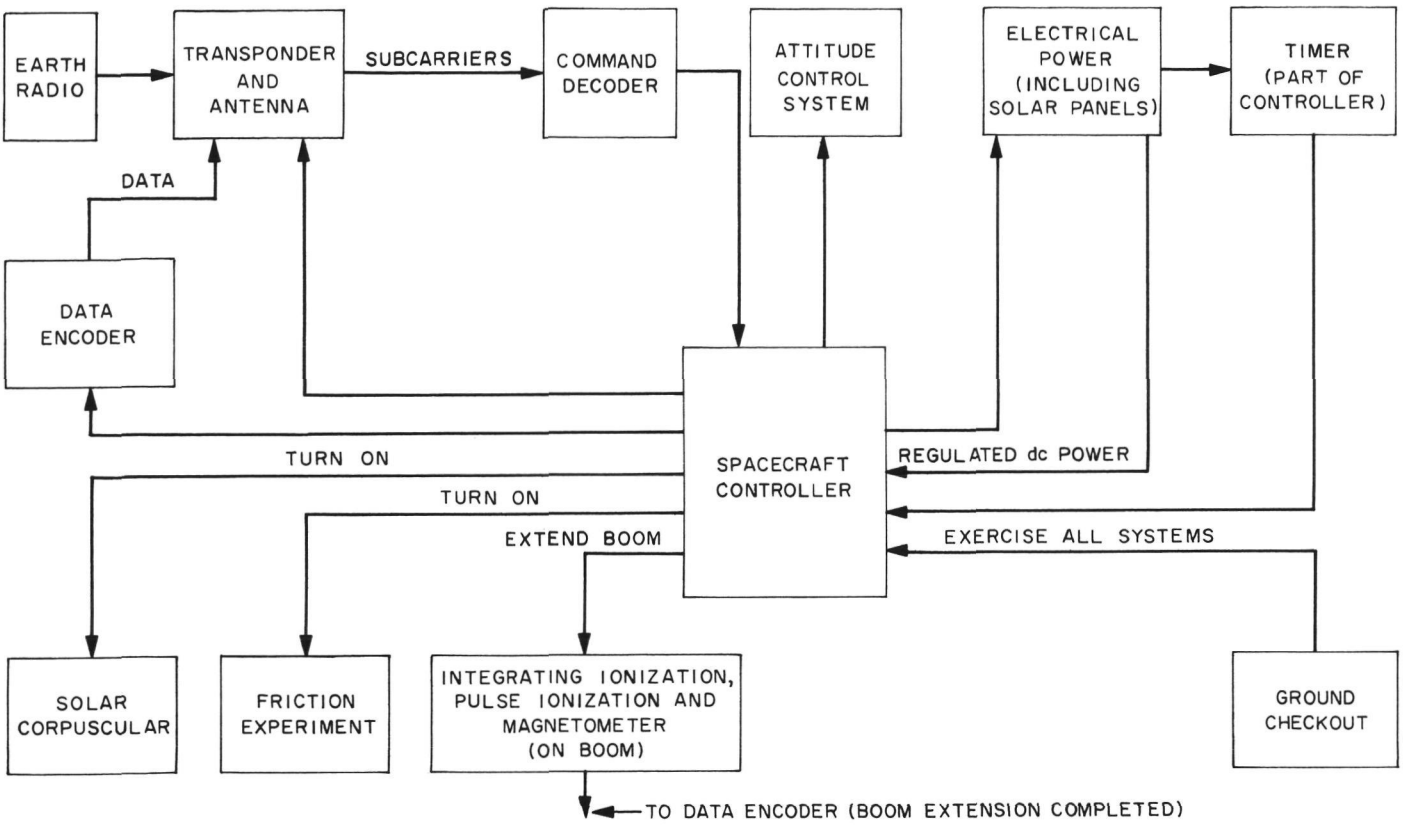

Figure 258. Controller relationship

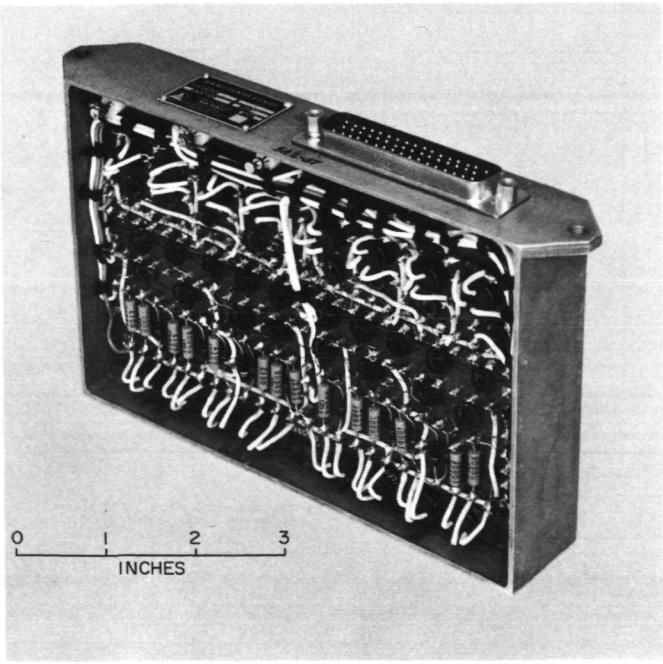

Figure 259. Controller counter

Since timing, gating, and switching are the main functions of the CC&S, for a complete description, the functional requirements of each subsystem would need to be considered in specific detail as to input and output wave shapes. This description can only show the sequence by which the CC&S supplies the desired control. Table 67 shows the order in which the CC&S receives inputs, performs switching operations, and provides the required waveforms. The tabulation is divided into the prelaunch–launch, midcourse maneuver, and terminal maneuver phases of the flight.

CC&S timing accuracies and parameters. The CC&S contains the master time standard or clock by which the spacecraft operations are synchronized and timed. A 38.4 kpps (kilopulses/sec) signal is supplied to central power to sync the 400-cps power inverter. The data encoder and scientific experiments are also supplied a 400-cps frequency reference signal. The accuracies required are:

(1) Timing

Clock frequency accuracy	$0.01\% - 3\sigma$
Lift-off time accuracy (launch time)	± 30 sec

Table 67. CC&S functional operations requirements

Launch, injection, and cruise		
1. A > − 180 min	CC&S—GSE Control Power On (precedes spacecraft power turn on), Counter inhibited, Clear logic and/or relays (observe re-set condition)	Command—Blockhouse
2. A − 3 min	Start CC&S counter	Command—Blockhouse
3. A − 0	Lift off	Event
4. A + 22 min	Increase transmitter power	CC&S—stored time command
5. A + 30 min	Unfold solar panels	CC&S—stored time command
6. A + 33 min	Turn on A/C d-c power Extend antenna Activate gas jet system Activate Sun sensor system Commence solar acquisition	CC&S—stored time command
7. A + 63 min	Sun acquisition complete	Event—A/C
8. A + 3.5 hr	Turn on A/C 1Ø, 400 cps Activate Earth sensor system Start roll search command	CC&S—stored time command
9. >A + 3.5 hr	Earth sensor attains light signal Stop roll search Start hinge servo	Event—A/C
10. A + 4 hr	Acquisition complete	Event—A/C
11. A + 4 hr	Turn on gamma ray system	CC&S—stored time command
12. A + 4 hr and 1 min	Initiate timing pulses	CC&S—stored time command
Midcourse maneuver		
13. A + 15.5/39.5 hr	From midcourse tracking and correction computation, transmit midcourse maneuver roll and pitch duration and impulse magnitude information	Ground command to the CC&S
14. A + 15.5/39.5 hr +	A/C capacitor cycling pulse receipt of roll address	Ground address command to CC&S
15. B	Initiate midcourse maneuver sequence, TM Mode II	Ground command to the CC&S for start midcourse maneuver subsequence
16. B + 5.0 sec	Turn on midcourse autopilot, jet vane actuators, accelerometer. Turn off Earth sensor system (1Ø, 400 cps). Connect roll channel capacitor, initiate command polarity, command roll angle turn, provide antenna 180 deg command	
17. B + 5 sec to B + 455 sec	Stop roll angle turn, switch to pitch channel	CC&S sequence command
18. B + 9.5 min	Switch out Sun sensor signals, connect pitch and yaw channel capacitors, initiate command polarity, command pitch angle turn	CC&S sequence command
19. B + 9.5 to B + 24.5 min	Stop pitch angle turn, switch to roll channel	CC&S sequence command
20. B + 26.5 min	Gate accelerometer into the shut-off computer, command midcourse motor ignition, disconnect autopilot integrator reset	CC&S sequence command
21. B + 26.5 to B + 27.6 min	Midcourse motor shut off (computation)	CC&S sequence command
22. B + 28 min	Turn off midcourse autopilot, jet vane actuators, and accelerometer; stop shut-off computer; switch out yaw, roll, and pitch channel capacitors, provide antenna reposition, commence solar acquisition. Initiate T/M Mode III	CC&S sequence command
23. B + 58 min	Turn on A/C 1Ø 400 cps; activate Earth sensor system, start roll search command	CC&S sequence command
24. ≥ B + 58 min	Earth sensor attains light signal; stop roll search, start hinge servo	Event—A/C
25. B + 88 min	Re-acquisition complete	Event—A/C
26. B + 2.5 hr	Extend gamma ray boom, 3-w transmitter switched to directional antenna (back-up)	CC&S sequence command
Terminal maneuver		
27. A + 64.5 hr	Transmit spacecraft turn duration (pitch-yaw-pitch) information	Ground command to the CC&S
28. A + 64.5 hr +	A/C capacitor cycling pulse (receipt of first pitch address)	Ground address command to CC&S
29. C + 5.0 sec	Initiate terminal maneuver sequence. Select terminal mode, switch out Sun sensor signals, connect pitch and yaw channel capacitors, initiate command polarity, command pitch angle turn	Ground command to the CC&S for start of terminal maneuver subsequence
30. C + 5.0 to C + 455 sec	Stop pitch angle turn, switch to yaw channel	CC&S sequence command
31. C + 9.5 min	Initiate command polarity, command yaw angle turn	CC&S sequence command
32. C + 9.5 to C + 19.5 min	Stop yaw angle turn, switch to pitch channel	CC&S sequence command
33. C + 21.5	Initiate command polarity, command pitch angle turn	CC&S sequence command
34. C + 21.5 to C + 29 min	Stop pitch angle turn, initiate vidicon pulse train, initiate T/M Mode IV Deploy omni and altimeter antennas	CC&S sequence command
35. C + 64 min	Turn on radio altimeter	CC&S sequence command

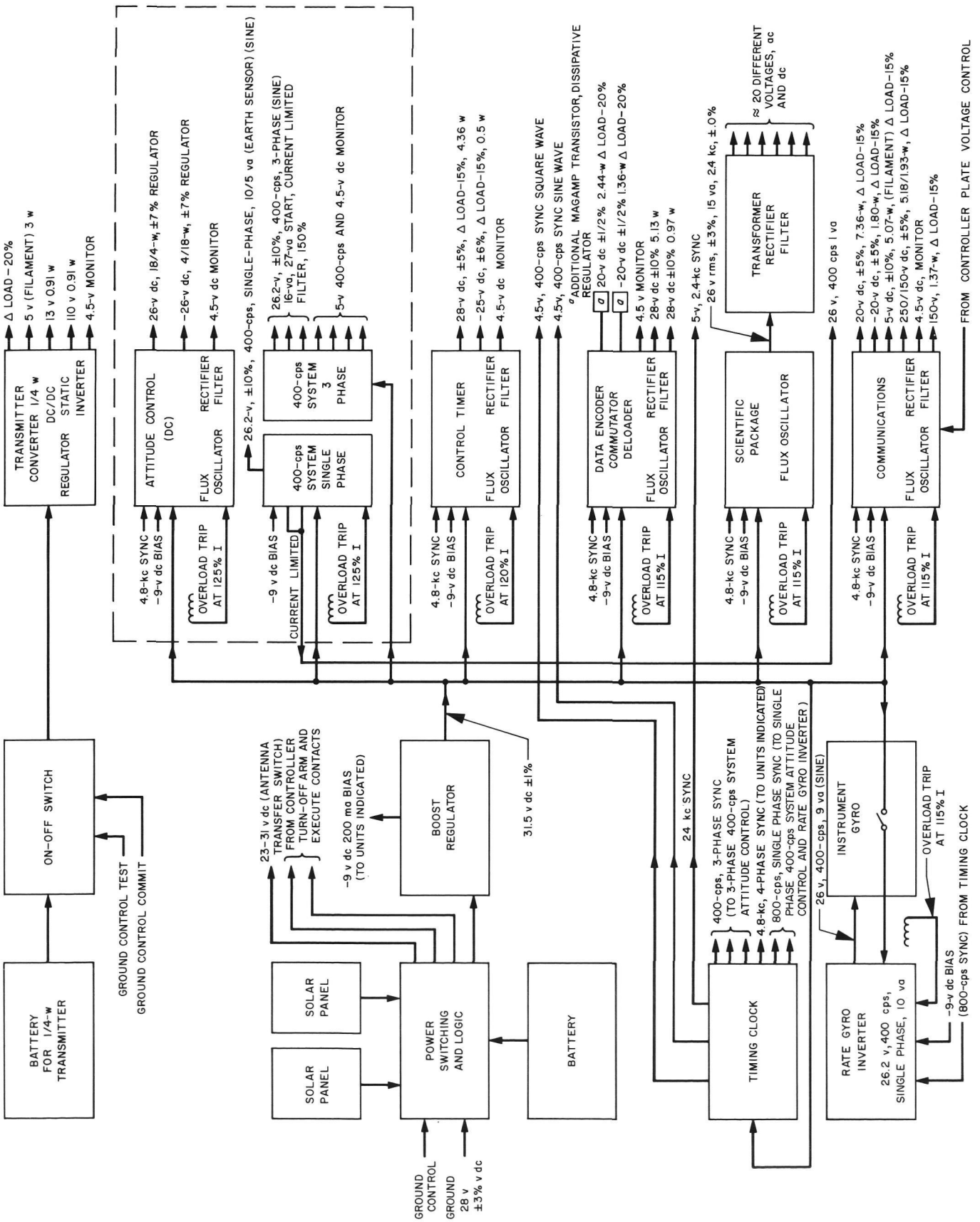

Figure 260. Power subsystem block diagram

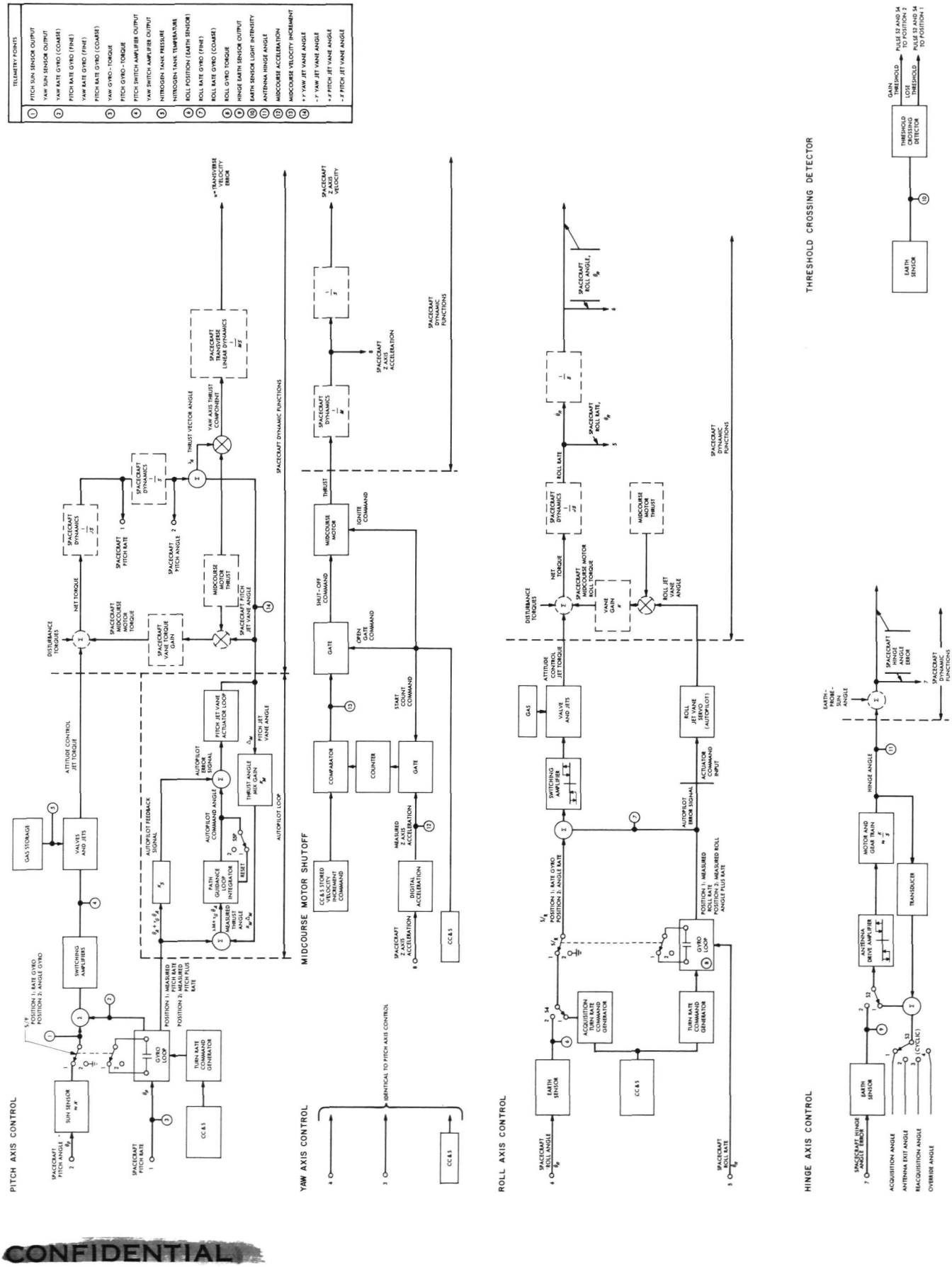

Figure 261. RA-3 attitude-control subsystem, block diagram

CONFIDENTIAL

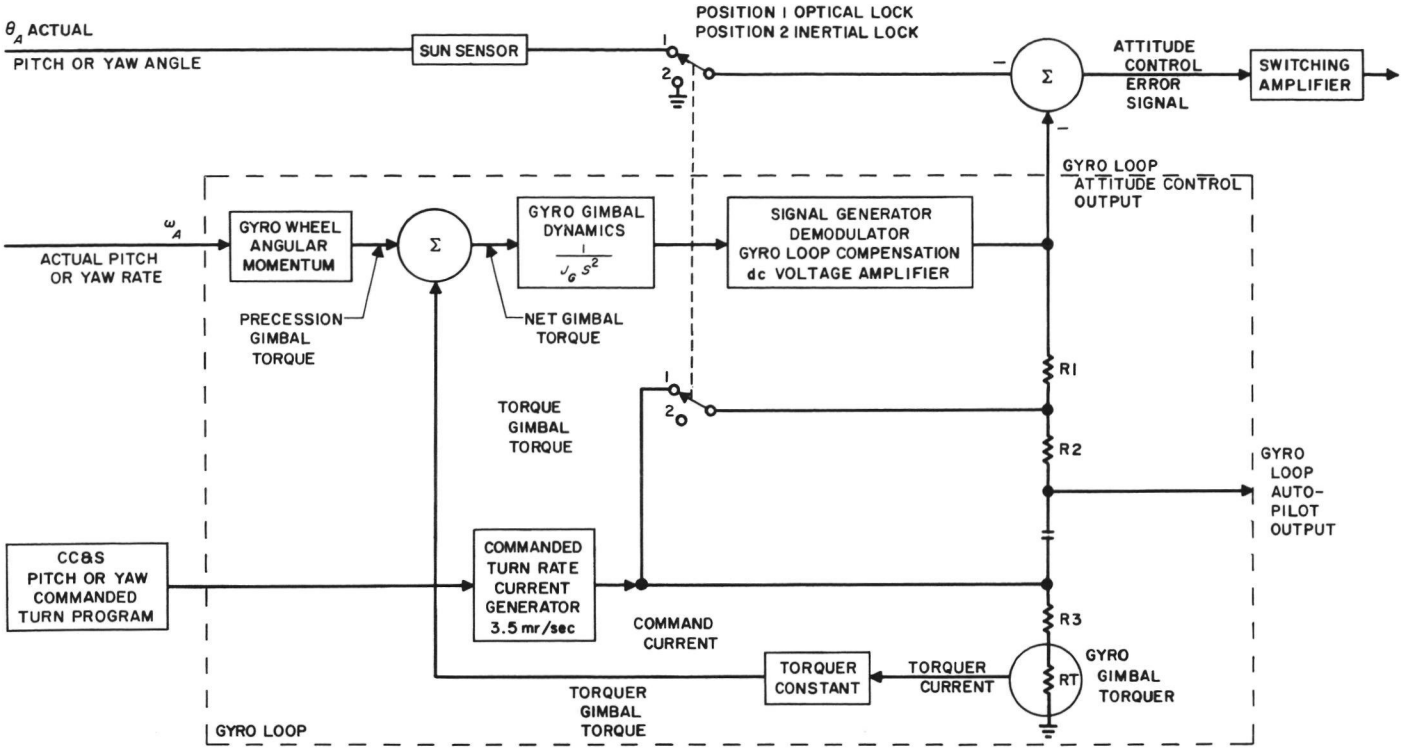

Figure 262. Gyro loop block diagram

Required time resolution

(a) Start commands ±7.0 sec
(1) Launch phase ±1 min
(2) Midcourse and terminal ±10 sec
(b) Maneuver turn duration 1.0 sec

Maximum time capacity required

(a) Launch sequence 1,000 min
(b) Manuever sequence 10,000 sec

(2) Radio command information

Resolution required for commanded turn duration 1.0 sec
Maximum required turn duration 900 sec
Polarity ±
Input data rate 1 bit/sec

Start maneuver accuracy

(a) Midcourse ±5 min
(b) Terminal ±7 sec

(3) Parameters

Memory

(a) Word length
(1) Information 11 bits
(2) Polarity 1 bit
(3) Address 5 bits
Total 17 bits
(b) Velocity resolution required 0.1 ft/sec
(c) Maximum velocity capacity 204.7 ft/sec
(d) Memory capacity:
Preset event times required 15 events
Radio command storage required 4 words
(e) Time resolution required 1.0 sec

Radio command information

(a) Velocity increment, resolution required 0.1 ft/sec
(b) Maximum velocity increment required 200 ft/sec
(c) Polarity None

Accelerometer information

Average accelerometer rate 25 pps

Although the above figures are in some detail, they describe the performance and the capacity required of the CC&S.

CONFIDENTIAL

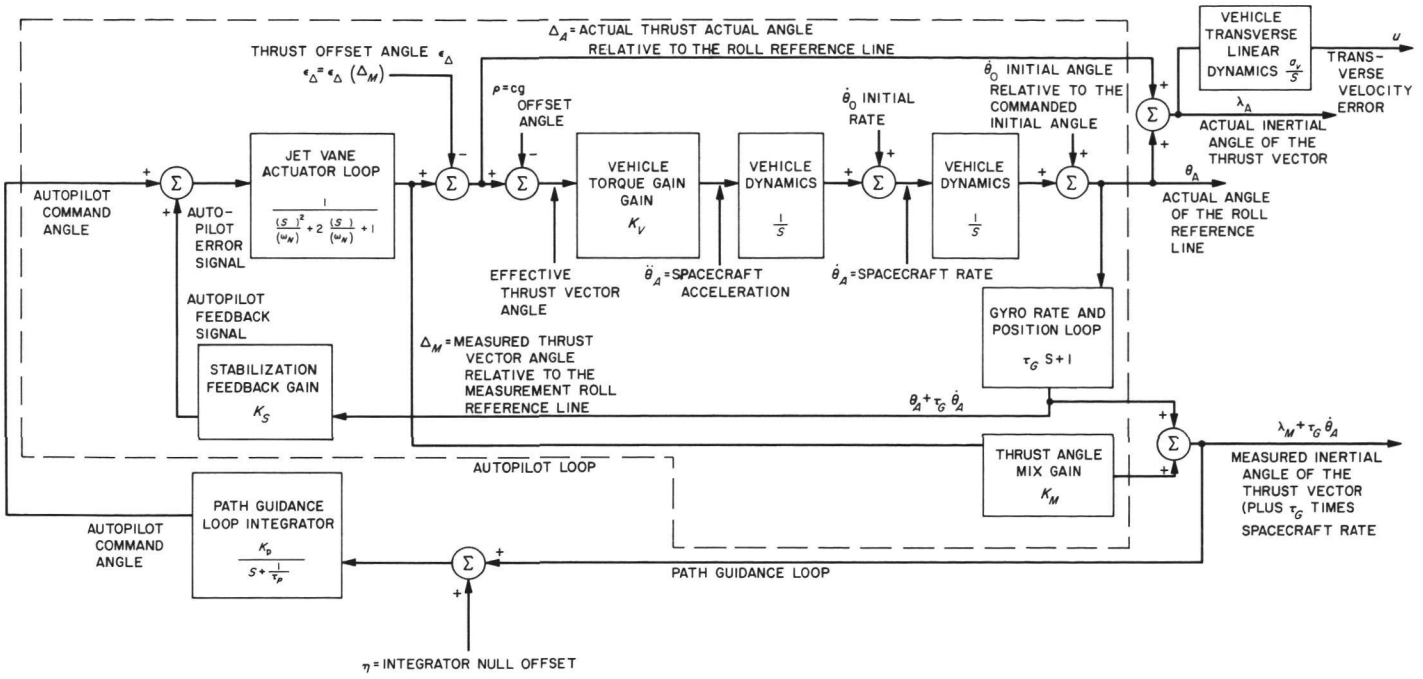

Figure 263. Autopilot (pitch and yaw) block diagram

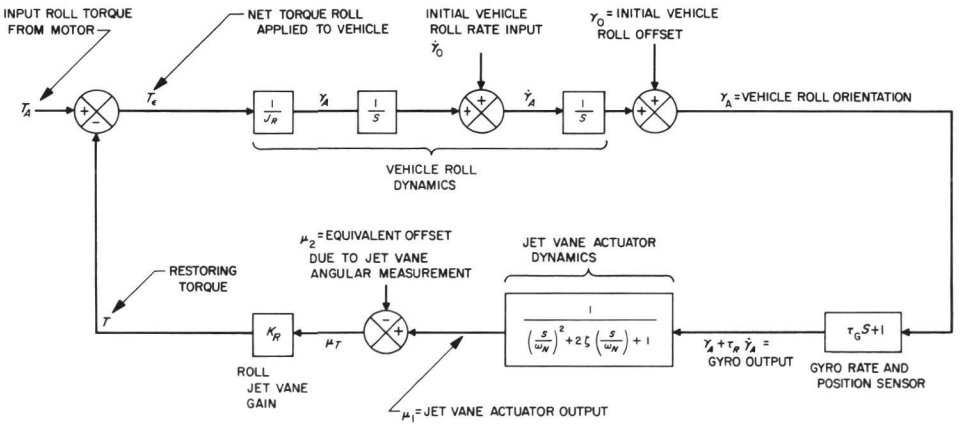

Figure 264. Autopilot roll channel block diagram

d. Power subsystem. The RA-3 power subsystem consists of a solar panel source, a battery source, and the converter and distribution equipment to power the spacecraft during pre-launch, launch, and flight phases. The various components of the power subsystem are shown in Figure 266. The voltage outputs, required regulation, and noise constraints are listed. The raw power requirements during launch, cruise, midcourse maneuver, and terminal maneuver are shown in Figure 267.

The RA-3 power subsystem is similar to that of RA-1 and -2. The 400-cps 3-phase, 400-cps 1-phase, communications, and power switch and logic units are nearly identical to their RA-1 and -2 counterparts. The data encoder converter, scientific inverter, attitude control converter, and power synchronizing supply, are expansions of RA-1 and -2 packages. The command converter and CC&S inverter are new additions, with the CC&S inverter quite similar to the scientific inverter. The RA-1 and -2 booster–regulator has also been redesigned for increased reliability and power. The RA-3 power subsystem contains two solar panels, identical to the two panels for RA-1 and -2.

The primary battery for the RA-3 mission supplies power for the postlaunch or Sun acquisition period, the midcourse maneuver period, and the terminal maneuver period. It has a reserve capability to supply power

CONFIDENTIAL

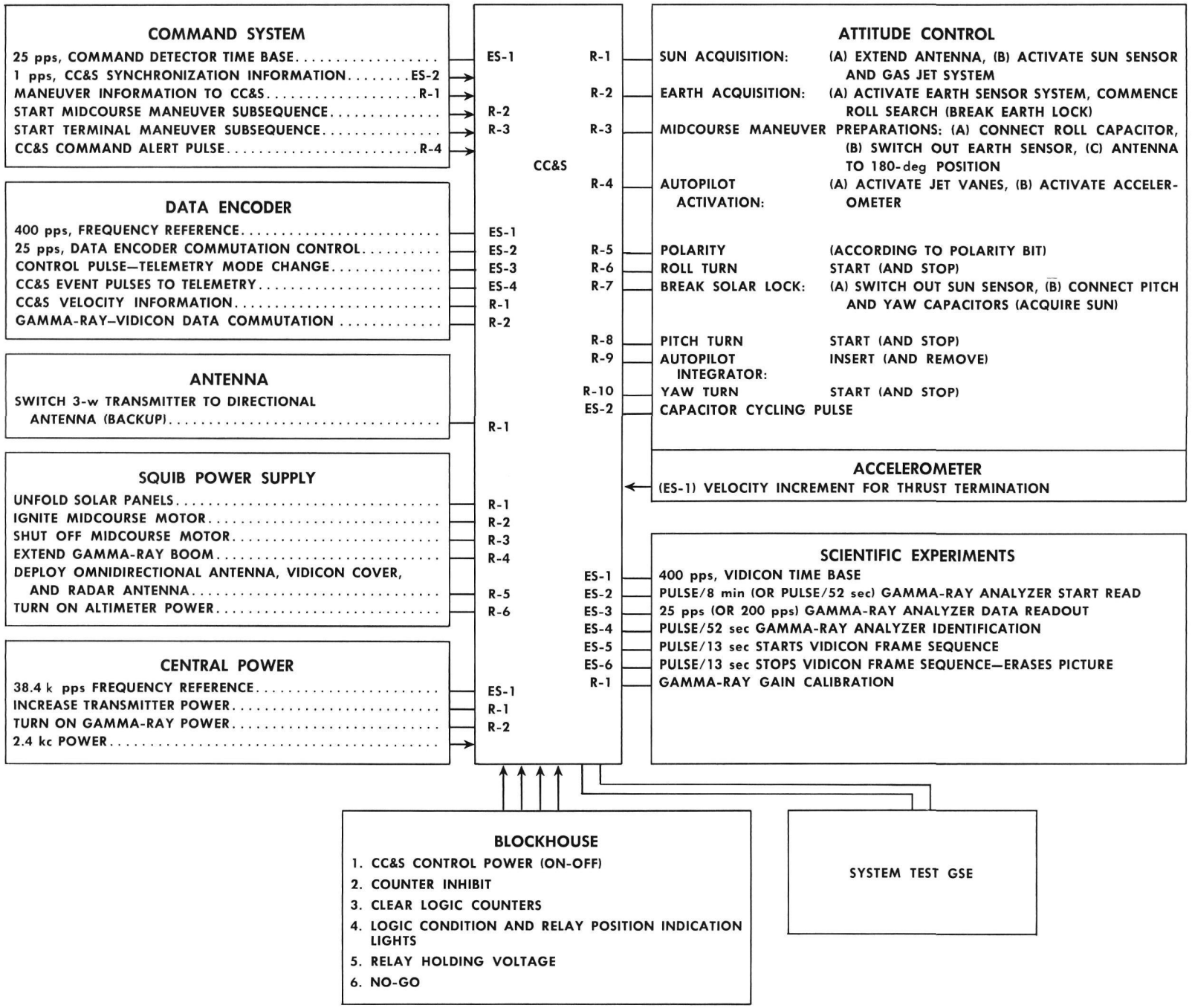

Figure 265. Functions of CC&S

CONFIDENTIAL

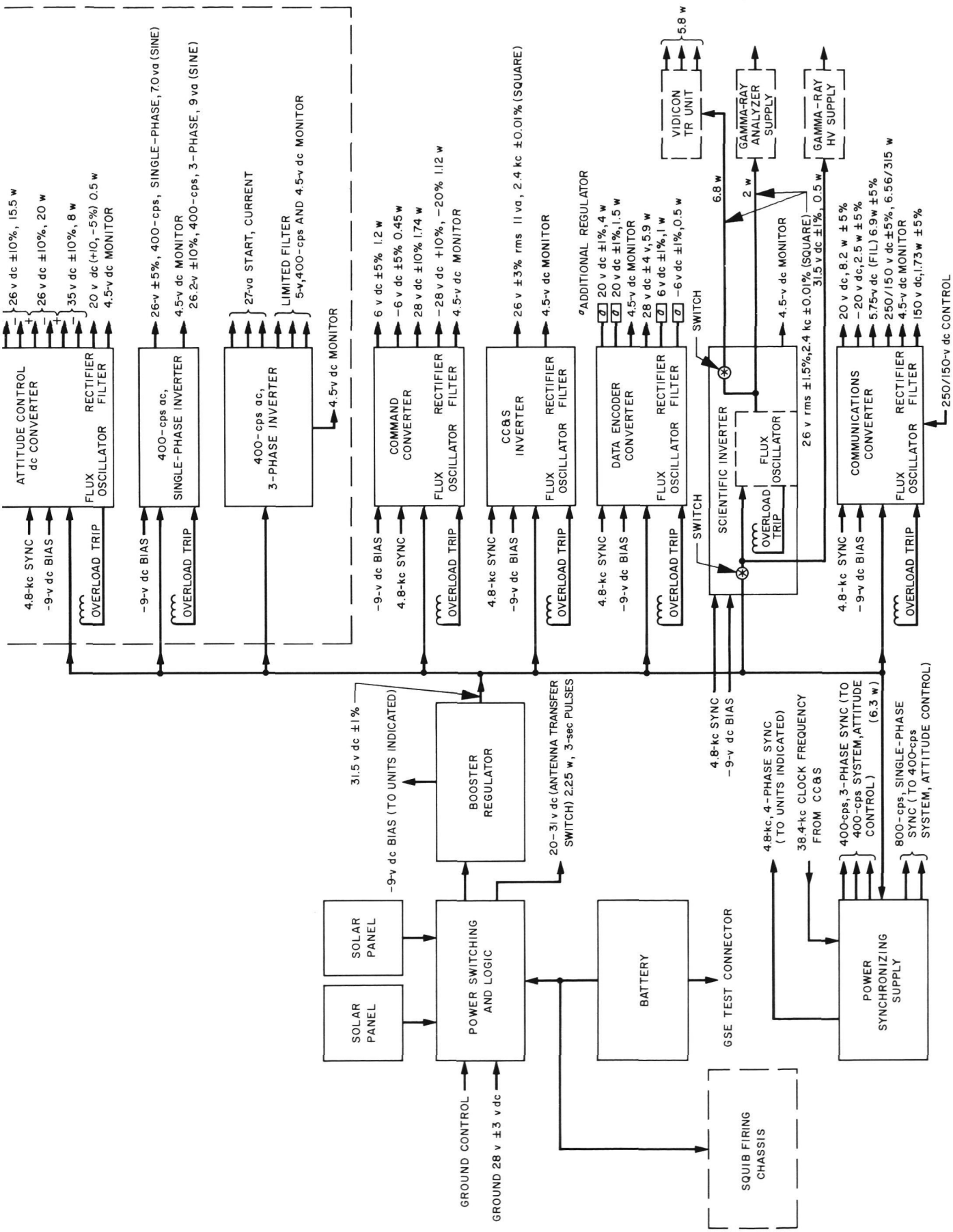

Figure 266. RA-3, -4, -5 power subassembly

for two meteoric perturbation (contingency) maneuver periods.

3. Subsystem Development and Performance

a. Attitude control. Attitude control of the RA-1 and -2 spacecraft combined two control systems. The primary system controlling the pitch *(X)* and yaw *(Y)* attitude was Sun-oriented. The secondary system used Earth light to control the roll (Z) orientation of the vehicle. The Earth light sensing system also controls the rotation of the high-gain antenna about its hinge axis to point the antenna toward the Earth. Probe–Sun and probe–Earth lines establish the vehicle attitude references.

Three body-fixed, single-degree-of-freedom, floated gyroscopes, their sensitive axes aligned orthogonally with the pitch, roll, and yaw axes of the vehicle, are inserted in the control loop (Fig 256). Their purpose is to rate-limit the torquing functions, with a resultant conservation of gas. Also, rate data telemetered from the three gyros provides valuable information for the analysis of spacecraft behavior in flight.

The controlling functions are performed in the following sequence:

(1) Point the roll (Z) axis of the spacecraft along the probe–Sun line and extend the antenna to a preset angle.

(2) Rotate the vehicle about the roll axis until the pitch (and antenna hinge axis) is perpendicular to the Earth–probe–Sun plane.

(3) Turn the antenna about its hinge axis until the antenna points toward the Earth.

(4) Maintain the vehicle and antenna attitude in these configurations.

Two radio commands, hinge over ride and roll override, can be initiated from the ground. The hinge override is used in case the trajectory is highly nonstandard, the Earth being at an angle out of the field of view of the sensor. The hinge rotates upon command to a second preset angle and the search in roll continues until a body comes into view. Roll override is initiated in the event the Earth sensor locks onto a body other than the Earth. In this event, the spacecraft is commanded to resume roll search until the Earth is finally acquired.

The gyros, electronic control subassemblies, the gas pressure vessel, and power supply subassemblies are mounted in an RA-1 spacecraft case as shown in Figure 268. The other sensors, actuators, etc., are mounted to the spacecraft.

The RA-3, -4, -5 attitude-control subsystem includes the following features not present on RA-1 and -2:

(1) Midcourse orientation maneuver, consisting of two commanded turns that orient the body-fixed midcourse motor in the required direction.

(2) Midcourse autopilot which controls spacecraft orientation during motor burning.

(3) Reacquisition phase similar to the initial acquisition phase.

(4) A second cruising phase.

(5) Terminal maneuver consisting of three commanded turns that orient the capsule and vidicon axes in the required direction.

(6) A final phase for maintaining the spacecraft in a fixed orientation for Moon surface photography until the capsule retromotor is fired.

The RA-3 attitude-control subsystem has a smaller limit cycle (2.9 mrad) than RA-1 (8.5 mrad) since a more accurate attitude reference is required for the midcourse and terminal maneuvers. For a more complete description of the attitude-control development and mechanization, the various components are discussed by functional groups.

Sensors. RA-1, -2 requirements do not demand high spacecraft pointing, orientation, or stabilization accuracies. The most rigid requirement is the control of roll (about the Z axis). Motions about this axis affect the pointing alignment of the high-gain, narrow beam width antenna. The antenna hinge has a single degree of freedom, in the pitch plane, so that motions in roll are not compensated for by the hinge servo system; therefore, pointing in the yaw direction (about Z) is directly affected. The antenna beam is approximately 10 deg (cone angle) wide, which is much greater than the pointing capability of the system.

RA-3, -4, -5 missions demand greater orientation and stabilization accuracies, particularly prior to the midcourse maneuver, at which time spacecraft orientation must be known precisely as a starting reference for the commanded turns. The RA-1, -2 system was developed with this in mind so that items would be reusable with a minimum of change on the following programs.

Sun sensors. The Sun sensor is a simple device requiring no optics, an advantage gained from the high-energy output of the Sun source, and the transfer efficiency of the detector.

Electrically, the detectors are connected in a bridge circuit (Fig 269a). The output of each photosensitive

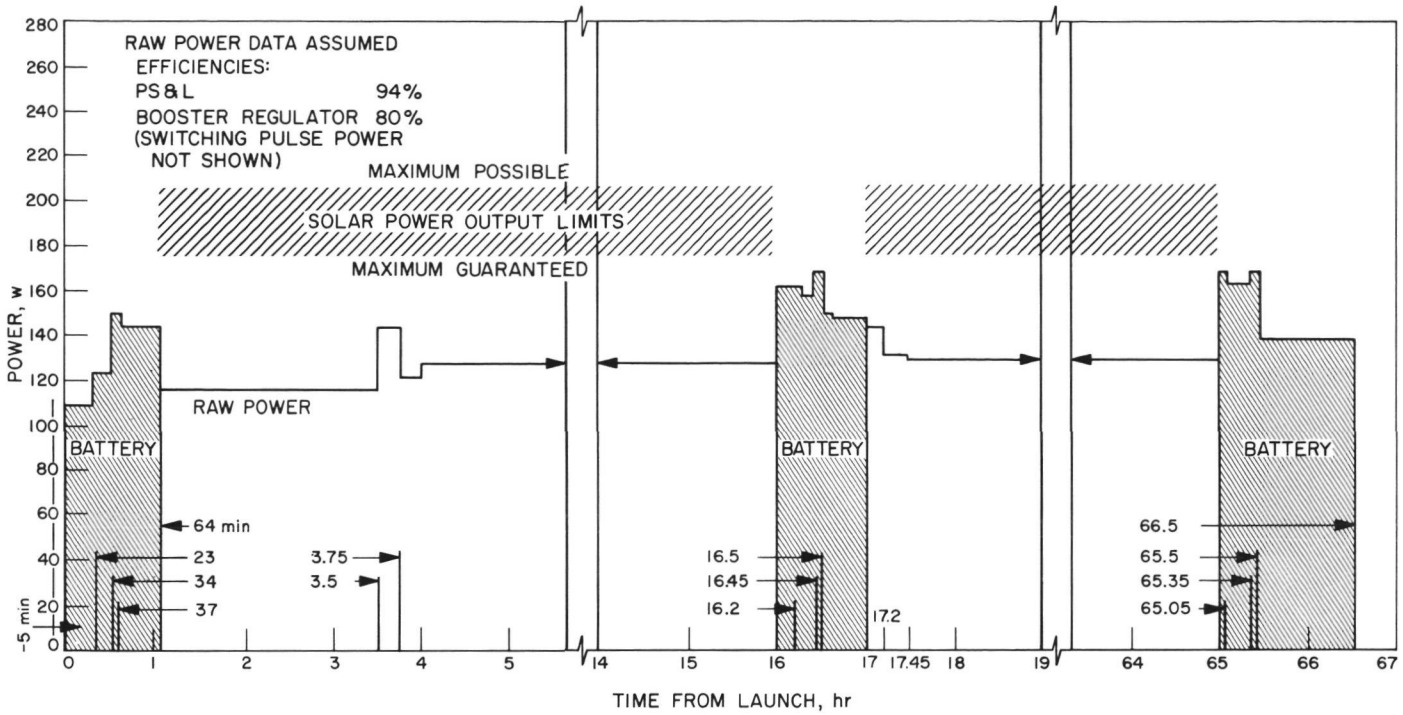

Figure 267. RA-3, -4, -5 raw power consumption

detector is 9 v/deg of angular change across a 50,000-ohm resistive load. Because of the high output, no preamplifier is necessary, the output feeding directly into the switching amplifier. Repeatable angular resolution of the sensor is 5-10 sec of arc and system resolution is 0.053 deg, 1σ.

The Sun sensing subsystem is composed of two sets of Sun sensors, primary and secondary (Fig 270).

A primary sensor consists of two small (¼-in. diameter) matched cadmium selenide detectors mounted parallel to each other with a shadow vane between. The amount of light received by each of the pair of detectors is determined by the sunlight incidence angle, and the shadow vane (Fig 269b, c). One primary sensor senses angular deviations from the probe–Sun line in the pitch *(X)* direction, and another mounted at 90 deg to the first, senses deviations in the yaw *(Y)* plane, controlling Sun orientation to an accuracy of ± 1.5 deg in the linear range.

For practical reasons (unobstructed field of view), each of the sensors is "split" and mounted on opposite sides of the spacecraft.

The secondary Sun sensors, similar to the primary, are mounted on the tips of the solar panels, arranged in a manner such that the combination of primary and secondary sensors covers a full spherical field of view around the spacecraft. The secondary sensors are operative only during the initial acquisition period, or until the Sun is within the field of view of the primary sensors.

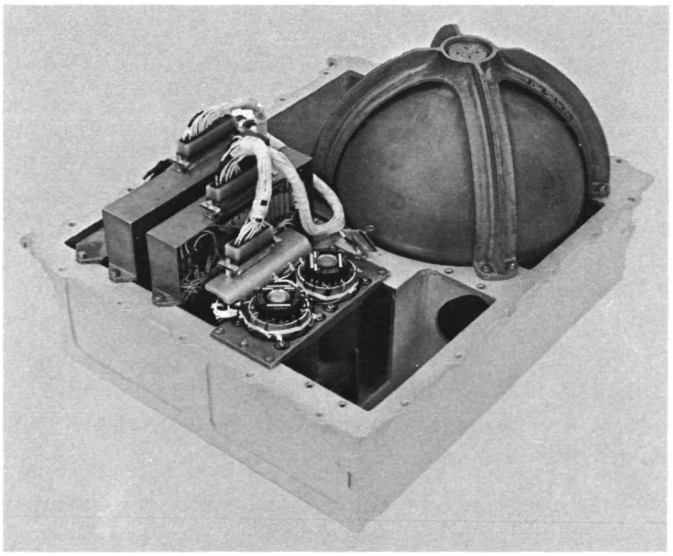

Figure 268. Attitude-control subassembly

Cadmium sulfide detectors replace the cadmium selenide detectors on the RA-3, -4, -5 systems with an improvement in day-to-day null stability in the operating temperature range.

Earth sensor. The Earth sensor controls the vehicle–Earth relationship of the spacecraft, and with the Sun

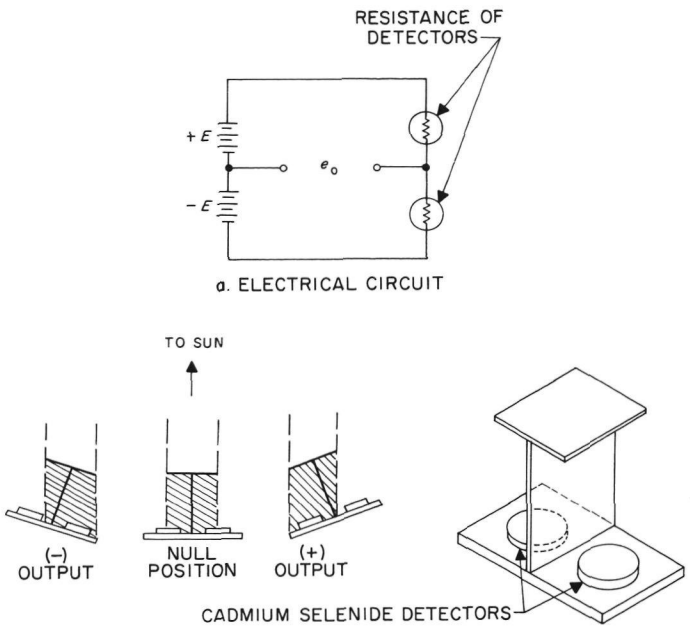

Figure 269. Sun sensors

sensors, completes the sensing subsystems required to orient and maintain the attitude of the vehicle in an Earth–vehicle–Sun plane.

The Earth sensor consists of three ¾-in.-diameter photomultiplier tubes, with their field of view constrained by a cover mask in which slits are cut, as shown in Figure 271. The Earth sensor is a two-axis device which yields information about angular deviations around two axes. It seeks the center of reflected sunlight in the case of a partially illuminated Earth.

The physical arrangement of the Earth sensor photomultiplier tubes and cover masks, and the wiring schematic, are shown in Figure 270. The output signals of the three photomultiplier tubes are designated as A, B, and C. A − B is the error signal for one axis (hinge), and A + B − C is the error signal for the other axis (roll). The

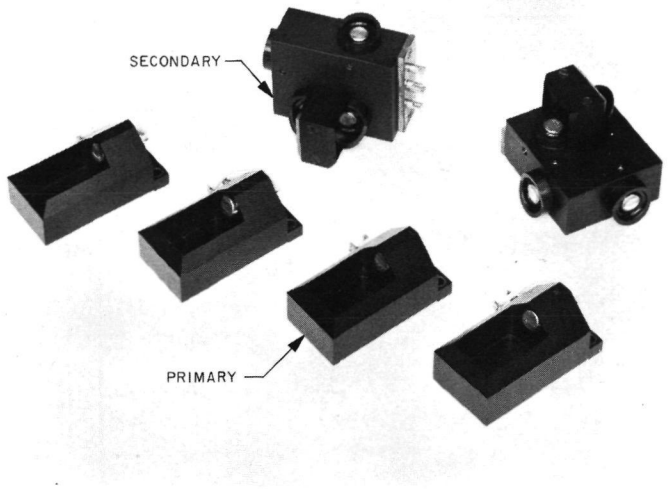

Figure 270. Primary and secondary Sun sensors

Earth sensor has a 20 by 30-deg field of view. As the Earth sensor moves away from the null position, there is a 2.5-deg linear range in each direction. After these points, the system saturates and holds its output for the remainder of the field of view. The sum signal A + B + C is used in a closed loop to adjust the excitation voltage for the photomultiplier tubes. This loop controls the output of the tubes to a constant voltage independent of range (decreasing Earth light).

The output of the Earth sensor is 2 v/deg in pitch (hinge) and 8 v/deg in roll. Taking into account the 5-mv noise level, the system has a maximum tracking error of 0.45 deg in each axis.

As the vehicle rolls in the Earth acquisition search mode at a rate of 0.2 deg/sec in a minus direction, the antenna and Earth sensor are held at a pre-selected angle based on the expected Sun–vehicle–Earth angle at the time of acquisition. When the Earth comes into the sensor field of view, the roll search is terminated by sensor command, and Earth lock is accomplished. At the same time, the antenna and Earth sensor are servo-driven about the hinge axis, correcting differences between the preset hinge angle and the actual Earth–vehicle–Sun angle. Earth acquisition is now complete, and the vehicle is in the cruise mode of operation. (See *switching amplifier.)*

The early a-c version of the Earth sensor was replaced by a d-c model which includes electrostatic shielding for the photomultiplier tubes. The main improvements are

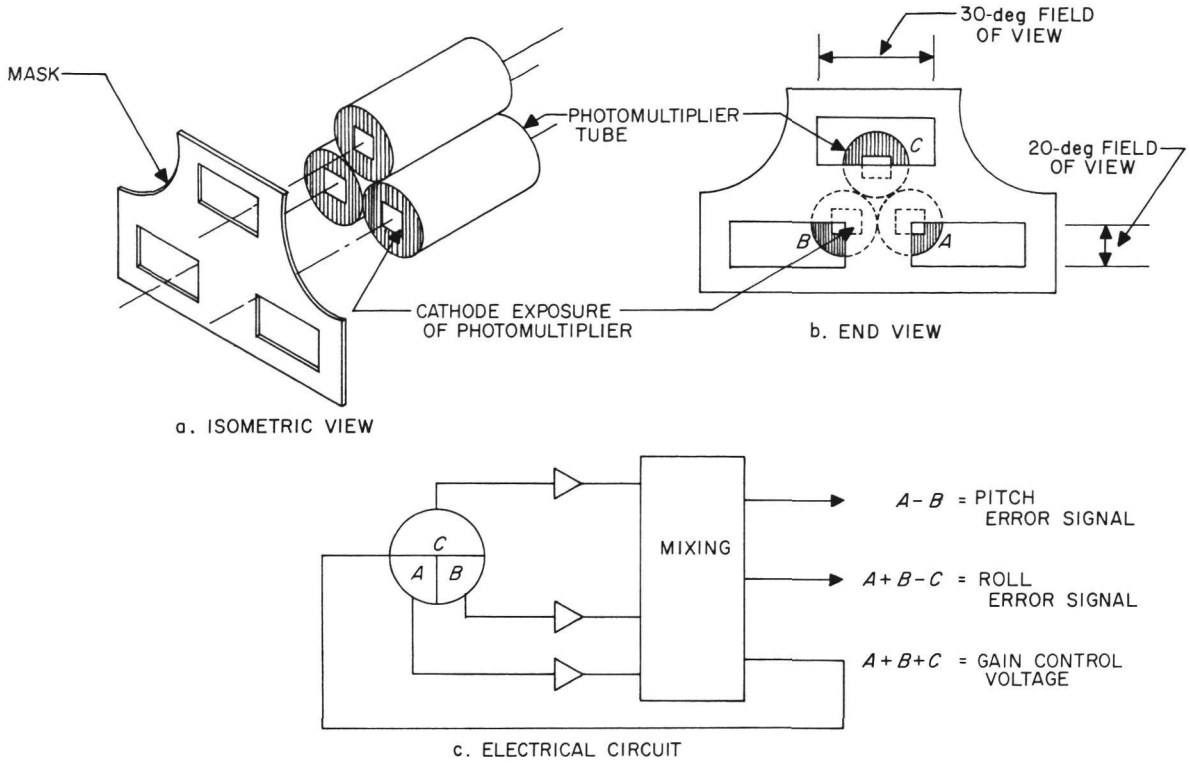

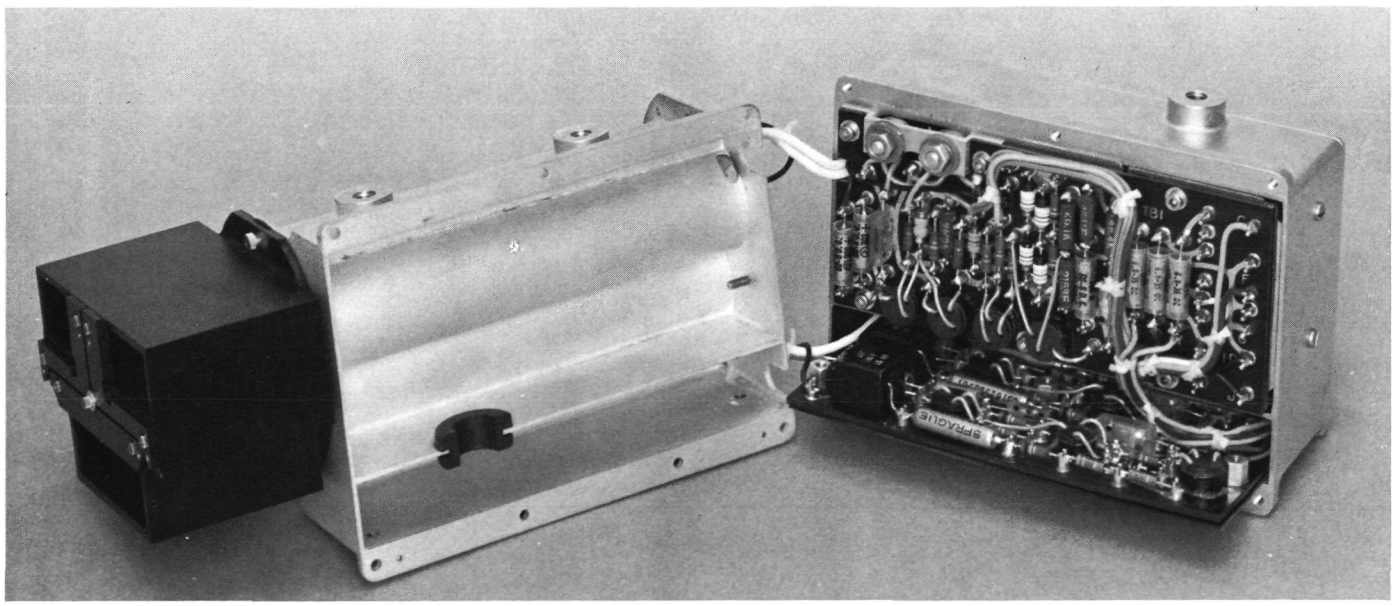

Figure 271. Earth sensor

better reliability, acquisition at lower light intensities, and lower dark-currents. The RA-3, -4, -5 Earth sensors are built into an aluminum housing with a combination netic and conetic magnetic shield around the tubes, a further improvement in shielding over the mumetal housings used in the earlier models.

The sensor has the estimated capability of locking on the half-illuminated Earth at a distance of 10 million mi. At this distance, the light flux is 1.76×10^{-9} w/cm^2 and the input to each detector is approximately 8×10^{-11} w. Tube output is about 0.4 amp/w, dark current about 0.02 μamp, and a signal-to-noise ratio of 20.

Gyros and gyro electronics. The gyros and associated electronics provide angular rate and angular position information about the spacecraft's three axes. The gyro selected to sense this information was the Minneapolis-Honeywell miniature integrating model GG49E5. This model differs from the typical GG49 in that it is filled with a damping fluid having a minimum viscosity. This fluid eliminates the need for gyro heaters yet provides the desired density for full flotation. The required loop damping is designed into the electronics.

The gyro is a single-axis floated unit, with electronic circuits, which amplifies and demodulates the gyro signal generator output and applies the resulting current back to the gyro torquer. The feedback or torque rebalance current holds the gimbal at null, with the magnitude and polarity of current determined by the turning rate about the gyro input axis.

In RA-1 and -2, the three GG49E5 gyros were filled with MO-10 fluorolube and were operated in a rate feedback mode. This fluid provided a coefficient of viscous restraint of 258 dyne-cm sec/rad and lowered the gyro operating temperature to 115°F. The three-gyro subassembly is shown in Figure 272. This subassembly was the result of extensive static and dynamic gyro tests, and of loop, life, environmental, and subsystem tests.

The RA-3, -4, -5 spacecraft uses the MIG model GG49E12 gyro for rate stabilization and to provide a reference for angular position maneuver during midcourse and terminal maneuvering. The E12 design is essentially the same E5 design used in RA-1. The model designation distinguishes a gyro which the manufacturer guarantees to meet all *Ranger* design approval requirements. Although the E5 gyro has met the same testing requirements, the E12 gyro has seal material improvements which further increase the design margin in thermal and gas sterilization.

During thermal sterilization testing, it was necessary to replace the signal generator windings because of insulation breakdown. Five gyro failures were caused by insulation breakdown in the signal generator, torquer, Dualsyn windings. The double Formvar insulated wire used in the Dualsyn winding proved a marginal choice for the high-temperature application and was replaced by Nyleze insulated wire.

The spacecraft maneuvering is accomplished at a constant rate of turn by applying a fixed current to the gyro torquer for a commanded period of time while closing the loop through the spacecraft reaction jets. During the commanded turn, the position error of the spacecraft is stored on a bank of capacitors connected between the

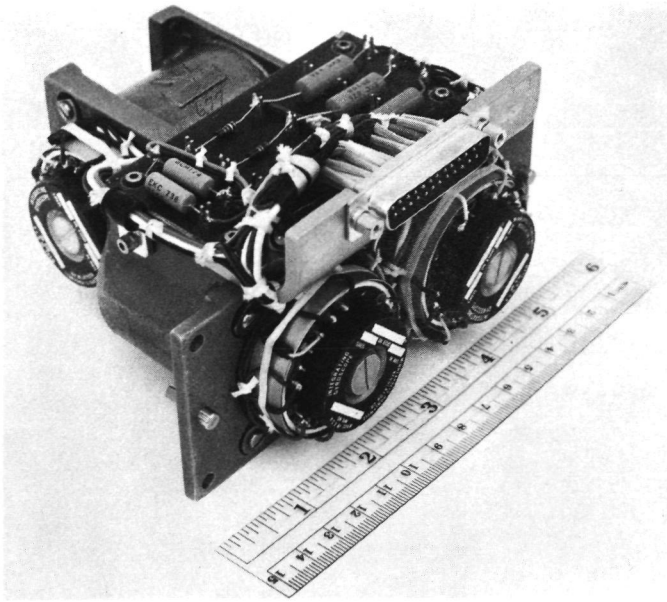

Figure 272. Three-gyro module

gyro rebalance amplifier and the gyro torquer. Four tantalytic capacitors, totaling 4080 μf per gyro, are packaged in the same chassis as are the gyros. The constant current required during the commanded turn will be dependent upon gyro temperature, since the gyro scale factor changes as a function of temperature. Therefore, to provide a compensated level of command current, a compensation circuit referenced to the total resistance value of the three gyro temperature sensors is employed.

The accuracy of the commanded turn is further dependent upon the stability of gyro drift rates from the time of calibration of the gyros until their actual usage. The most significant part of the gyro drift will be that resulting from restraint and reaction torques, referred to as acceleration insensitive drifts. The resultant drift rates of each gyro are determined after assembly of each gyro into the module, and then compensated by applying a bias current to the gyro torquer. This amount of bias current is adjusted with a trim potentiometer until the drift rates have been reduced to less than 0.1 deg/hr.

The RA-3, -4, -5 gyro subassembly thus includes the gyro module containing the gyros, a bank of capacitors (the passive integrators), and various trim capacitors for adjusting the power factor. The subassembly is shown in Figure 273.

The gyro control electronics subassembly contains the gyro loop circuits for the damping and the spring restraining force necessary to control the miniature integrating gyro. A block diagram of the electronics is shown in Figure 274.

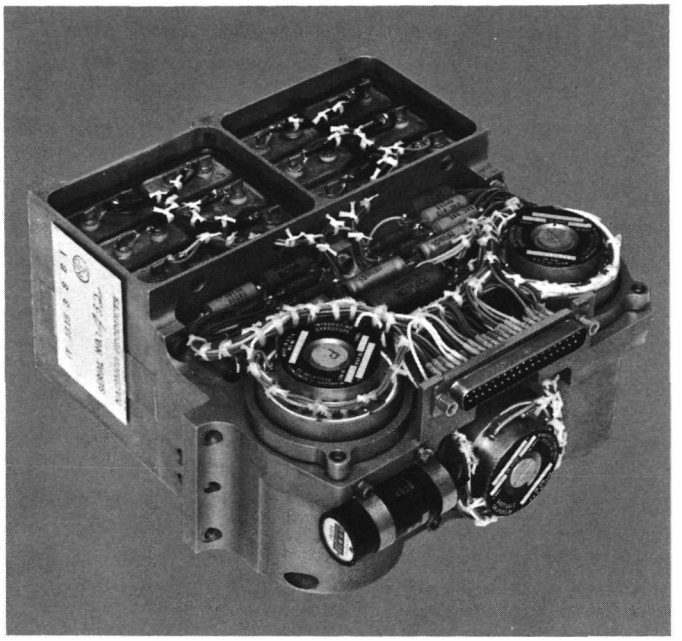

Figure 273. Control gyro module

The gyro control electronics may be roughly divided into three parts: (1) the loop electronics, which hold the gyro output axis in capture, (2) the pattern field current and command current regulators, and (3) the relay control section, which provides all the necessary switch closures for operation of the gyro loop.

Each set of capture electronics consists of a high-gain a-c preamplifier which boosts the 400-cps suppressed carrier output of the gyro dualsyn pickoff winding. The amplified signal is demodulated by a double ring demodulator, after which an 800-cps parallel-T network and a low-pass filter are provided to reduce the ripple. A Class B d-c amplifier is used to compensate and power amplify the signal. The output of the d-c amplifier feeds the gyro torquer control field. A resistor is placed in series with the gyro torquer to provide the proper rate scale factor. During the maneuver mode, a series capacitor is also inserted to provide position, as well as rate information, from the gyros.

Two current regulators are also provided in the gyro control module. The first is a pattern field regulator which supplies 50 ma of current to the three series connected pattern fields. The second current regulator is responsible for providing an accurate current for a timed period to the control fields of both the pitch and yaw (one at a time) gyros. This requirement is necessary during the maneuver mode, when the spacecraft is reoriented prior to firing the midcourse rocket. Due to the requirements of the angular pointing accuracy of the maneuver, both regulators were designed to be 0.1% devices.

The relay control section provides the following switching function: unshorting of the series capacitors during maneuver, shorting of the Sun and the Earth-seeker input lines to the switching amplifier, polarity switching for the command current regulator, pitch or yaw signal routing for the current field regulator, activation of the current field regulator, and disconnection of the gyro loop from the switching amplifier during the autopilot phase of the maneuver mode. (The seven relays are activated by the controller or CC&S.)

Attitude control actuators. The actuation system applies torques to the vehicle, correcting deviations between the actual attitude and the desired attitude. The main elements of the *Ranger* cold-gas actuation system are the storage vessel, the pressure regulator, the valve-nozzle assemblies, the interconnecting piping, and the dry nitrogen gas.

The storage bottle on RA-1 and -2 was a single 8-in. diameter, spherical, titanium pressure vessel, located in attitude-control Case IV. It was mounted in brackets which constrained the vessel but allowed for expansion during pressurization. On RA-3, -4, -5, three vessels are used, similar in construction to the one above except 5.5 in. in diameter and located on the spacecraft hex

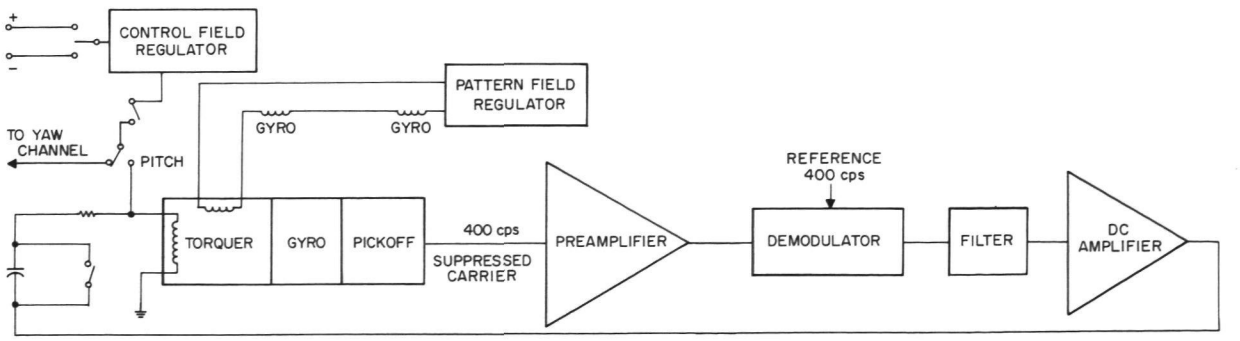

Figure 274. Gyro control loop

structure. The three bottles provide extra gas capacity required because of increased spacecraft moments of inertia, and for the midcourse and terminal maneuvers during the RA-3, -4, -5 missions.

The regulator is a poppet ball and seat type and drops the storage pressure to 15 psig for use by the nozzle (jet) valves.

Miniature, solenoid-operated, on-off, directional nozzle-valve assemblies are used on the *Ranger* spacecraft to apply attitude torques. Four valves each are used to control the yaw (Y) and roll (Z) axes, providing pure couples, and two valves control the pitch (X) axis. Significant shifts of the center of mass of the spacecraft are expected along the Z axis, and the couple arrangement minimizes cross-coupling effects, thereby conserving gas. The axis of each valve is oriented to prevent the impingement of exhaust gas on the spacecraft structure during valve actuations.

The nozzles are removable from the valve bodies, and are sized or tailored to meet the inertia-acceleration requirements for each axis of the spacecraft. The nozzles have a throat diameter range of 0.0135–0.028 in. and a thrust range of 3–6 gr operating in a vacuum.

The dry nitrogen gas has a specific impulse of 76 sec (lb of force/lb/sec of gas consumption) at 80°F operating temperature. It was chosen because of its high specific impulse, inertness, and lubricating properties. The dew point of the gas is kept below −60°F to prevent icing in the system.

The following is a comparison of expected gas consumption for RA-1, -2, and RA-3, -4, -5, based on expected maximum acquisition and maneuver times, leakage, and 15% surplus.

	RA-1, 2	RA-3, -4, -5
Number of bottles	1	3
Storage capacity, lb	2.31	2.64
Storage pressure, psi	3000	3640
Quantity used:		
Injection, lb	0.28	0.49
First acquisition, lb	0.10	0.15
Midcourse, lb	—	0.11
Second acquisition, lb	—	0.21
Terminal, lb	—	0.17
Cruise, lb	1.25	1.10[a]
Leakage at 100 cc/hr, lb	0.32	0.01
Length of mission	approx 50 days	66 hr

Limit cycle velocity assumed 2 × ideal, and dead band 0.75 × ideal.

Acceptable system leak rates are set at 100 cc/hr maximum. Rigorous cleanliness demands are met by clean-room assembly techniques. Charging nitrogen goes through a bacteriological filter on RA-3, -4, -5 because of the sterility requirement.

A portable charging cart has been developed for boosting supply bottle gas pressure up to system storage pressure.

Switching amplifier. The switching amplifiers are the electronic links between the Sun and Earth sensors, gyros, and actuation system. Summed position and rate information is received from the sensors and gyros, is acted upon by the amplifier, and sent to the proper actuator as a direction and duration signal.

A switching amplifier consists of an operational preamplifier with a nonlinear feedback network, followed by two Schmitt trigger circuits and output amplifiers. The preamplifier is a two-stage, direct-coupled circuit having a differential input stage to minimize input offset variations. The resistor-diode feedback network produces a non-linear transfer characteristic as shown in Figure 275. It establishes a prescribed dead-band region and a controlled slope beyond this region. The output switching commands are produced by the Schmitt triggers, which also introduce hysteresis into the amplifier. Two triggers are required to handle the three possible states necessary for the operation of the system.

For the *Ranger I* and *II* missions, the dead-band is set at ±1 deg for all axes, and on RA-3, -4, -5, the dead-band is ±2.9 mrad on the pitch and yaw axes and ±5 mrad on the roll axis.

During the cruise phase, the spacecraft oscillates slowly back and forth in the dead-bands, receiving a correcting impulse from the actuation system at each limit. The rate of turn in limit cycle operation is 2 deg/hr.

b. Midcourse guidance subsystem. The midcourse guidance subsystem, which controls the magnitude and direction of the midcourse correction velocity increment, consists of the autopilot for positioning the spacecraft and the velocity shutoff control for adjusting spacecraft velocity. The autopilot serves the functions of maintaining spacecraft stability in three axes and of stabilizing the direction of the motor-thrust vector in inertial space. The mechanization of the midcourse autopilot is shown in Figure 276.

The thrust-vector direction is controlled by means of jet vanes mounted in the motor nozzle. The displacement of each jet vane is produced by a direct-coupled d-c

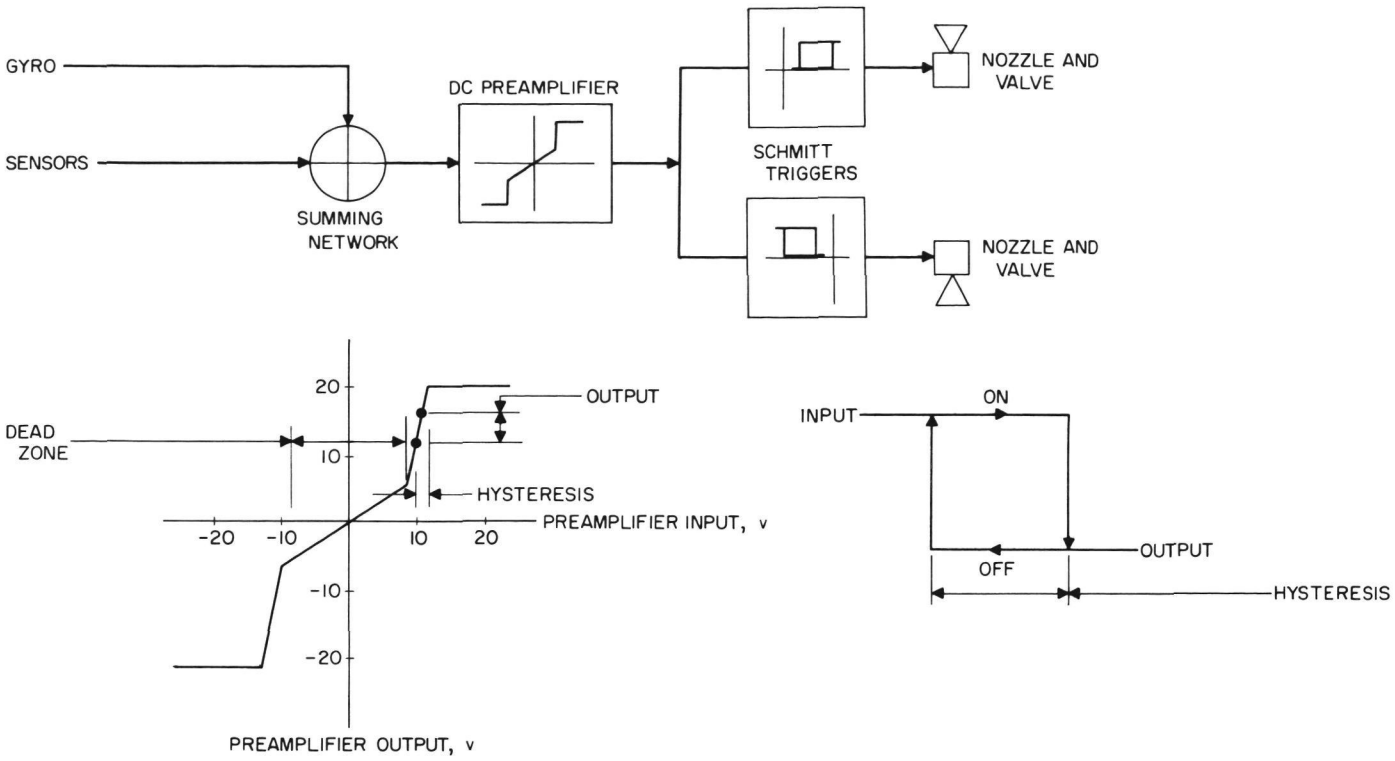

Figure 275. Switching amplifier, attitude-control preamplifier transfer characteristics

torque motor. The ratio of thrust-vector deflection to jet vane angle is precalibrated so the thrust direction can be determined from the jet vane angle. The jet vane angle is measured by means of a precision potentiometer mounted on the jet vane motor assembly.

The jet vane actuator has a d-c torquer, a ± 25-deg deflection, output torque capability of 2 oz-in., stiction not to exceed 1 oz-in. and an acceleration constant of 70 rad/sec^2. The jet vane actuator is shown in Figure 277.

As shown in the mechanization diagram, each of the four jet vane actuators is driven by a separate actuator amplifier. A pitch command is produced by a common-mode signal at the inputs to the No. 1 and 3 actuator amplifiers. A command-mode input to the No. 2 and 4 actuator amplifiers produces a yaw command. A roll command is introduced by differential inputs between Nos. 1 and 3 and between Nos. 2 and 4 amplifier inputs.

The thrust-vector deflection in pitch is measured by summing the No. 1 and 3 jet vane potentiometer outputs at the integrator input. These signals are combined with the rate plus position signal and integrated.

The autopilot integrator employs a high-gain, solid-state chopper amplifier. The d-c input to the amplifier is modulated by the 8-diode modulator circuit. The modulated signal is amplified and demodulated.

Velocity shutoff subsystem. The magnitude of the velocity increment added to the spacecraft during the corrective midcourse maneuver of RA-3, -4, -5 is measured by an accelerometer and integrator combination. Since the digital computer is carried in the CC&S unit, and the size of the corrective velocity increment is transmitted digitally from the Earth, a digital accelerometer is required. This subsystem was developed at JPL and is used in combination with the CC&S digital computer for midcourse motor shutoff.

This digital accelerometer system consists of a force balance accelerometer with a pulse torqued rebalance loop to provide capture current to the proof mass. In this mode of operation, the pulsing rate is directly proportional to the applied acceleration and each pulse produced represents a constant value of velocity increase (or decrease, depending on the direction of the applied acceleration). In the *Ranger* system application, this value or scale factor is 0.1 ft/sec of velocity increase per pulse.

The accuracy in this type of subsystem is determined to a large extent by how accurately the current pulses to the torquer can be measured. The subsystem uses an

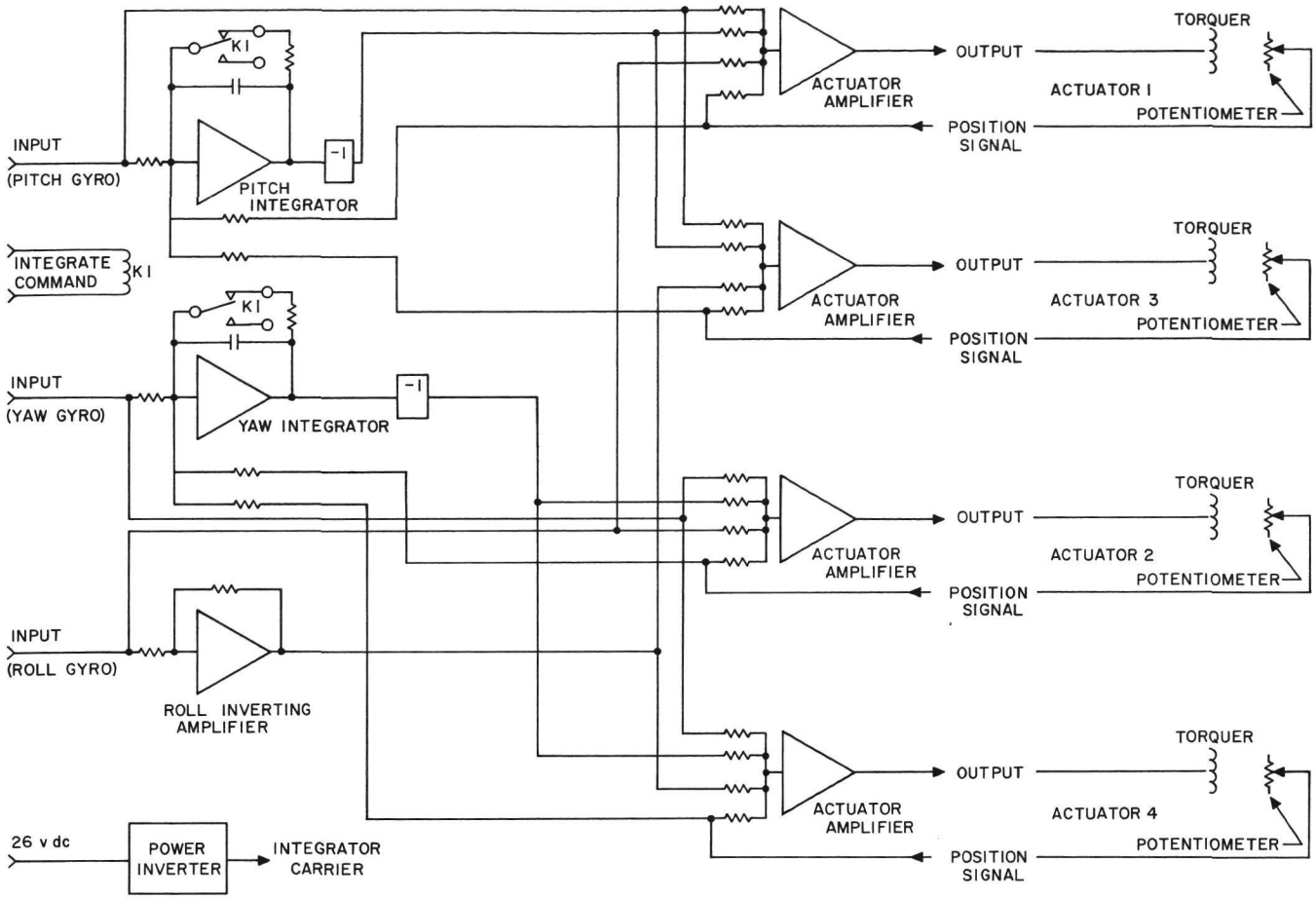

Figure 276. Autopilot block diagram

accurate frequency from the CC&S clock to control the pulse width and an accurate voltage, controlled from a precision zener diode, to determine pulse height. The subsystem is shown in Figure 278, while a block diagram of the electronics is shown in Figure 279.

The accelerometer pickoff is a capacitive type excited by a 200-kc oscillator, and the decision device is a Schmitt trigger circuit. The switch is supplied with 8.4 w from a precision zener diode. This diode voltage is stable to $\pm 0.1\%$ over a 100°F temperature range.

Laboratory testing under constant temperature and no vibration conditions has shown the accelerometer subsystem is stable to a 3σ accuracy of 0.03% of applied acceleration. The system can retain capture up to 1 g of acceleration while the expected *Ranger* midcourse maneuver acceleration is 0.07 g. The greatest change in the accelerometer during environmental testing occurs during the 125°C 24-hr soak for sterilization. This was a null torque shift and was adjusted for after heat sterilization.

c. Controller and Central Computer and Sequencer subsystems.

RA-1 and -2 controller. The RA-1 controller was designed to perform the following general functions: (1) generate timing information; (2) receive information and/or commands from Earth-based control during preflight system tests, and from the timer; and (3) when required, generate commands based on information from the timer on the Earth. The subsystem, as shown functionally in Figure 257, is composed of six main building blocks. These are the square-wave power converter, clock pulser, frequency divider, the counter, the command gate, and the output command driver-relay array. The controller mechanization consists of seven modules mounted in one side of a spacecraft case as shown in Figure 280.

In operation, the converter-pulser-divider block is fed by a 400-cps sinusoidal source and provides, as its output, three pulse trains to the counter with count pulses occurring at a one-per-second rate. The count pulse

Figure 277. Jet vane actuator

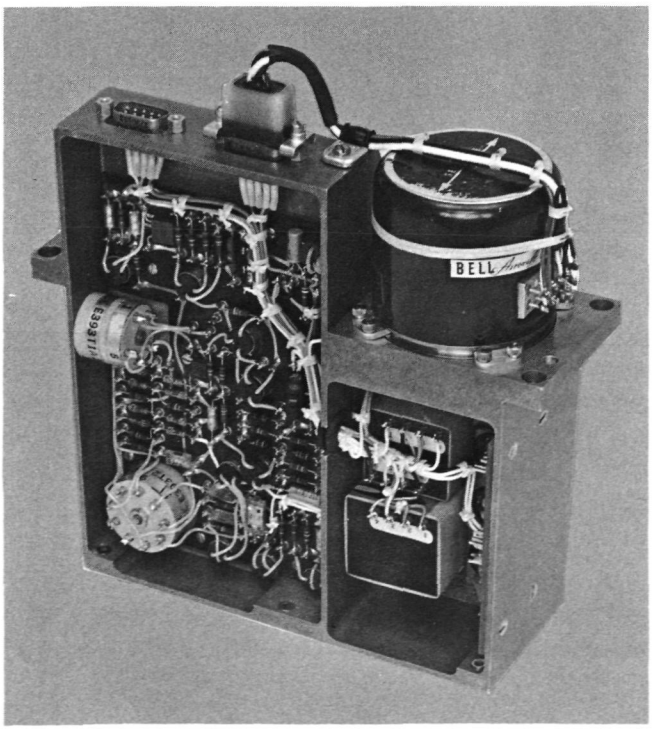

Figure 278. Velocity shutoff subsystem module

channel output, in addition to feeding the counter, also connects to a gate which controls a pulse shaper. The time counter has a basic resolution of 1 sec and a total time count capacity of more than 8 months. Its output is given in the form of pulses on eight binary-coded decade stages. The command gate is essentially a diode matrix which allows the passage of a pulse from the counter to the output relay drivers whenever the count time coincides with the preset command time. Commands to the various spacecraft subsystems are then given in the form of relay closures.

Magnetic latching relays have been chosen as controller output devices to satisfy the functional requirement that a momentary power failure must not cause the controller to issue (or to remove previously given) commands. As a consequence of this choice, the command relay position at any time depends on the previous history of the relay so that precautions must be taken to prevent any one relay from being in the command state when spacecraft power is first turned on. A 10-kc override into the clock-pulser is provided to permit the speeding up of the time count by a factor of 25 for systems test.

Clock pulse generator. The clock pulse generator (Fig 281) is used to provide the pulse power required to operate the digital counter and logic circuits. Its input is derived from the spacecraft 400-cps power supply, which is converted to a square-wave and then drives a blocking oscillator. This oscillator feeds the sequential clock pulse blocking oscillators which, in turn, provide the current to drive the count reset and read pulses for both the frequency divider and main counter. A fourth pulse is used for gating and extra logic drive. The output repetition frequency of the clock pulses is 100 cps.

Frequency divider. A frequency divider is used to reduce the 100-cps rate of the clock pulse to the 1-cps rate required for the operation of the main counter. Other clock pulses occur at the 100-cps rate, and are used to govern the operation of the divider and counter.

The divider consists of two decade units which obtain the decade count from a modified binary-coded decimal code. Its circuitry is composed mainly of ferrite cores, which perform the feedback, counting, and storage functions. There is one transistor per stage of the counter. This transistor is used to compensate for core and pulse transfer losses.

Main counter. The main counter provides a means of counting time from launch, or some time before launch, to a maximum of 13 months in 1-sec increments. The latest time required was 8 months. In order to accom-

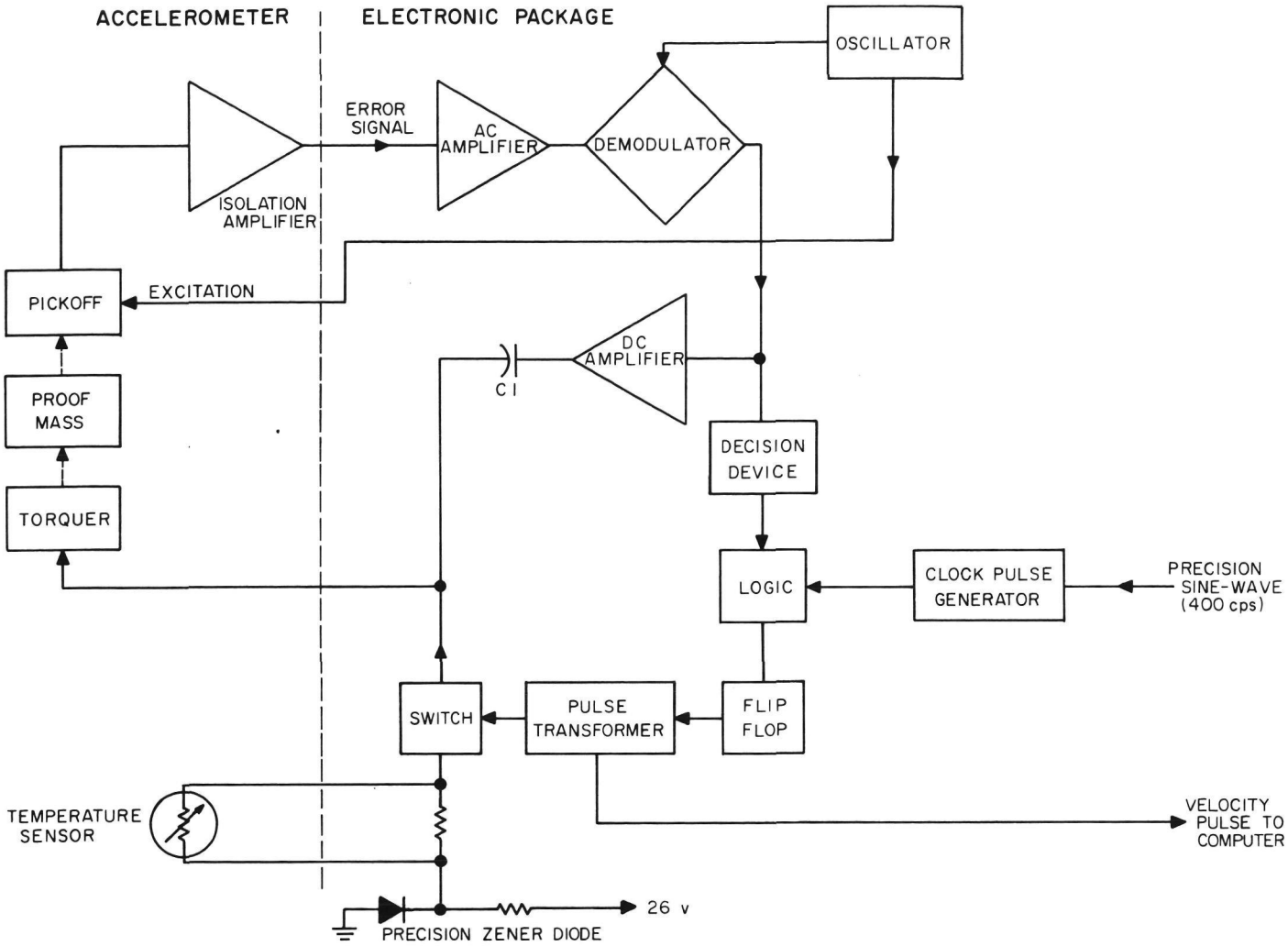

Figure 279. Velocity shutoff system

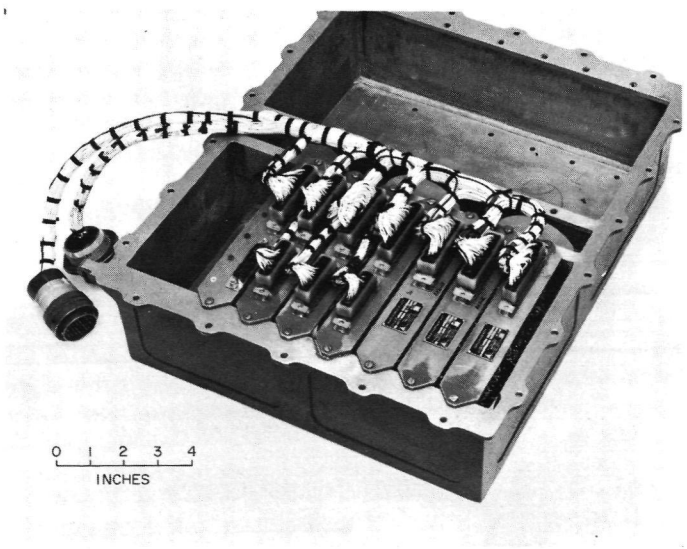

Figure 280. RA-1 and -2 controller

plish a count of this magnitude, 32 stages of binary-coded decimal circuits are required. These stages are used in decades, and time information is given in seconds.

The counter is of the multiaperture magnetic core type, selected primarily because of its non-destructive read-out capability. Information is retained in event of unexpected power interruption so the counter resumes the count from the point of interruption when power is restored.

Tests of the two subassemblies which comprise the main counter pointed up the necessity to encapsulate the subassemblies with a nonrestraining, Eccofoam to protect the fine wires and cores. Figure 282 shows a main counter subassembly prior to potting.

Command output subassembly. To facilitate the design and construction of the RA-1 and RA-2 controllers, it was established that the commands delivered by the

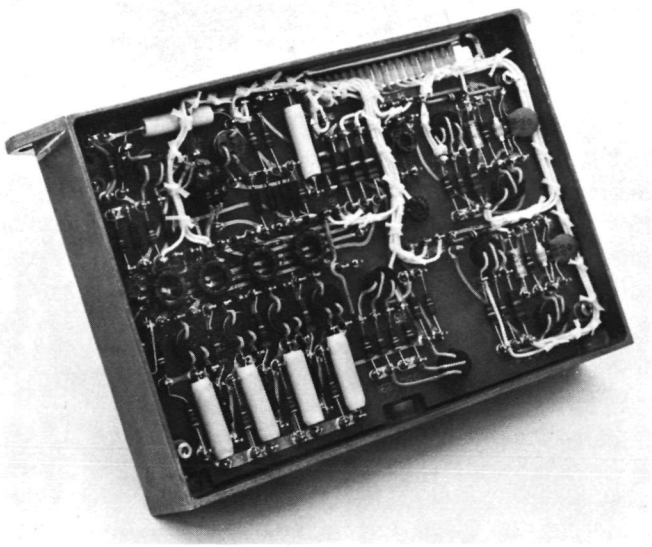

Figure 281. Clock pulse generator

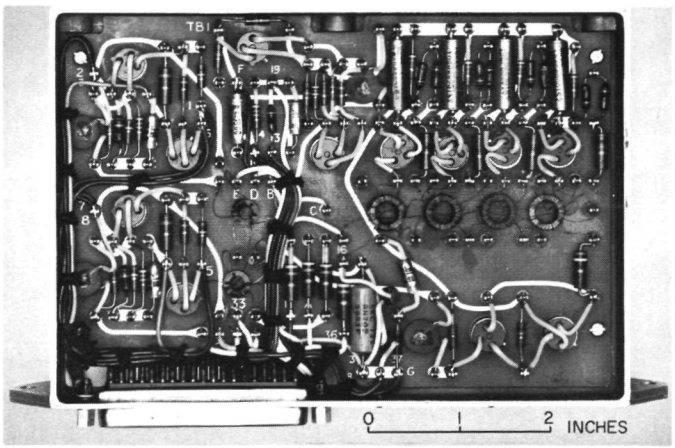

Figure 282. Main counter subassembly before potting

controller be in the form of relay-contact closures or openings. The circuitry required to actuate these relays, the relays themselves, and the circuitry necessary for monitor and checkout purposes, were contained in the command output module. The number of commands the controller was required to execute necessitated that the command output circuits be mechanized into at least two subassemblies.

The inputs to the command output subassemblies were obtained from the command gate in the form of positive pulses of 2-v amplitude and 5-μsec duration. When spacecraft power was turned on, capacitors in the output gate circuits were charged. Then, when an input pulse from the command gate was applied to the gate electrode of the SCR, it turned on, discharging the capacitor through the coil of a magnetic latching relay.

This method of actuating the relay was chosen for two reasons: (1) The SCR provides the necessary gain and pulse stretching required to actuate the relay. The relay requires approximately 10 msec to operate. (2) Capacitive coupling to the relay removes the necessity of supplying turn-off signals to the SCR, as it will automatically turn off when the combined currents through the anode resistor and capacitors have dropped to a value below the minimum holding current of the SCR (approximately 1 ma). Thus, the only current required from the spacecraft supply is that necessary to charge the capacitors.

Auxiliary circuitry is provided to supply monitoring functions and to permit the performance of the necessary test sequence prior to application of general spacecraft power. There are three controller monitoring functions: two are used during test, and the other is used during flight. The test monitoring functions are the command relay position and clear indicators. The command relay position indicator is mechanized as a diode or gate, the inputs of which are connected to a contact on each of the command relays. If any one of the command relays is in the command position, the *or* gate provides an output to light an indicating bulb in the controller test equipment. The clear indicator monitors the position of the clear relay and turns on a light when a clear command is given. The telemetry function occurs during flight and is mechanized similar to the command relay position indicator, except that each input of the *or* gate has a capacitor in series with it. When a command relay is energized, a pulse is sent through the *or* gate and delivered to telemetry. One of the command output subassemblies is shown in Figure 283.

RA-3, -4, -5 Central Computer and Sequencer subsystem. The equipment mechanized to fulfill the timing, switching, and computing requirements outlined above has a much greater functional capability than the RA-1 controller and consists of only nine subassemblies mounted in one side of the standard case (Fig 284). The CC&S is capable of performing two additional operations over that of the controller. The new CC&S operations (1) provide for storage of commands transmitted to the spacecraft through the r-f radio link, and (2) perform computations associated with the midcourse maneuver motor shutoff. The complexity of the timing, switching, and gating functions performed by the CC&S for the RA-3 spacecraft is also much greater due to the midcourse and terminal maneuvers requirements.

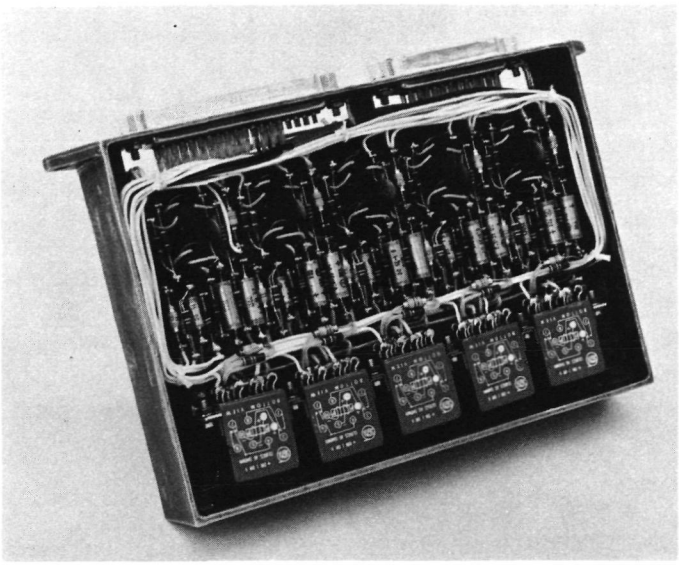

Figure 283. Command output subassembly

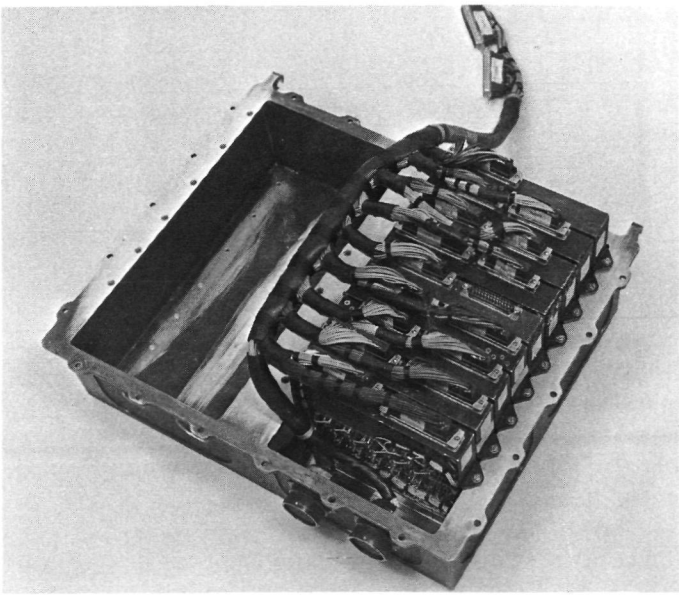

Figure 284. CC&S

The CC&S subsystem was developed at JPL and will be discussed by subassemblies since this divides the subsystem on a functional basis.

Reliability, launch area safety, and automatic testing were considerations in the design of the total CC&S systems. Efforts to increase reliability of operation were made wherever possible within the schedule constraints. For example, magnetic counters and shift registers were used to benefit from the greater reliability of magnetic devices. These circuits require no standby power to hold information and, consequently, their contents are unaffected by loss of power. In addition, these are low impedance circuits and, therefore, less sensitive to noise.

Component selection for increased reliability was limited to relays. Relays used in the CC&S system are procured under a specification requiring a JPL inspector on the manufacturing line to monitor pre-canning inspection and acceptance testing to JPL standards for each relay before purchase.

For greater reliability, relay logic was used instead of transistorized bistable circuitry in one critical application; i.e., for the initiation of the midcourse and terminal sequences upon receipt of the appropriate real-time command.

Another approach toward greater reliability was the use of clamps on the inputs of logical bistable circuits and relay drivers to prevent erroneous commands due to noise. These clamps are maintained either by (1) the solar acquisition command relay, up to launch +33 min, or (2) the midcourse and terminal sequence start relays up to the start of each sequence.

Central clock. The basic function of the central clock (Fig 285) is to provide the time reference for all spacecraft and CC&S functions. Output frequencies include 38.4 kc for the spacecraft power system; 400.0 pps for the vidicon electronics; 400.0 pps for telemetry synchronization; 25.0 pps for telemetry data communication; and 25.0 pps for the command system, to allow examination of the phase-lock loop. Each CC&S output is completely isolated from the receiving system by means of a transformer-coupled transistor switch. Except for the 38.4-kc frequency output, all pulse widths are nominally 1.0 msec.

The basic timing source is a 307.2-kc crystal oscillator circuit with a frequency accuracy of $\pm 0.01\%$. Frequency division down to 25.0 pps is accomplished by 14 transistorized bistable stages with appropriate feedback. Division from 25.0 to 1.0 pps is done magnetically with a transfluxor-transistor divider. In addition to the divider electronics, the subsystem contains three pulse circuits which provide the necessary count, re-set, and sense pulses to the magnetic frequency dividers as well as the launch and maneuver counters.

Provisions have been made to permit overriding of the central clock frequency with a manually controlled frequency of 10.0 kc at the 400.0-pps point. Thus, the CC&S has the capability to speed all timing by a factor of 25, a feature which is used during laboratory and

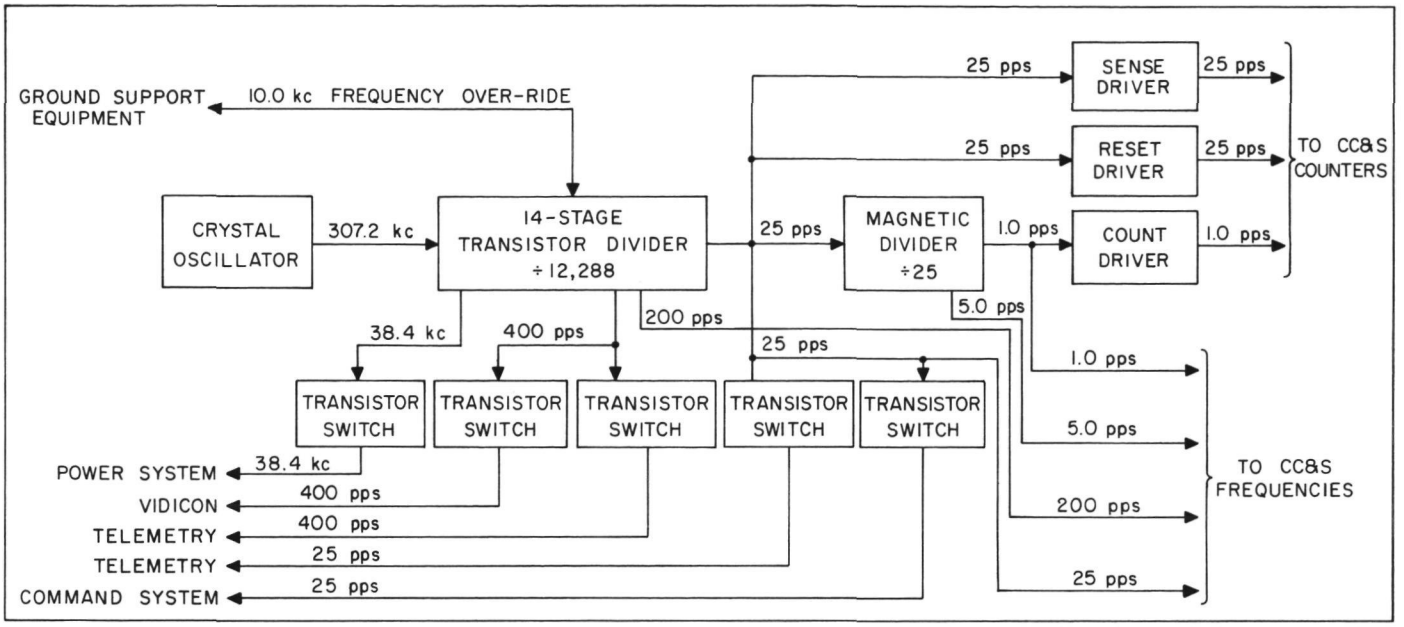

Figure 285. Central clock block diagram

systems testing. The central clock subassembly is shown in Figure 286.

Launch phase subsystem. The basic function of the launch phase subsystem (Fig 287) is to give a sequence of commands to various spacecraft systems at predetermined times referenced to launch. The commands are in the form of relay closures. Spacecraft functions controlled by this subsystem include solar acquisition, Earth acquisition, transmitter power control, activation of the gamma-ray system, and antenna and solar panel erection.

Count pulses (1.0 pps) from the central clock are divided by 60 in a magnetic divider. The launch counter then counts these 1-min pulses up to a capacity of 1000 min. The counter uses transfluxors for nondestructive readout of time. The output of each counter stage connects a matrix of diode and gates to yield a command pulse at particular times. The desired times are stored prior to flight in the matrix configuration. A command pulse from the matrix energizes an appropriate relay driver circuit which closes, or opens, a corresponding relay. The command relays are the magnetic latching type and are driven by the discharge current of a capacitor upon receipt of a command pulse.

Maneuver clock. The basic function of the maneuver clock (Fig 288) is to generate two independent sequences of command times which control various spacecraft functions. Each sequence is referenced to a separate real-time command received through the command system. The first sequence contains the midcourse maneuver, while

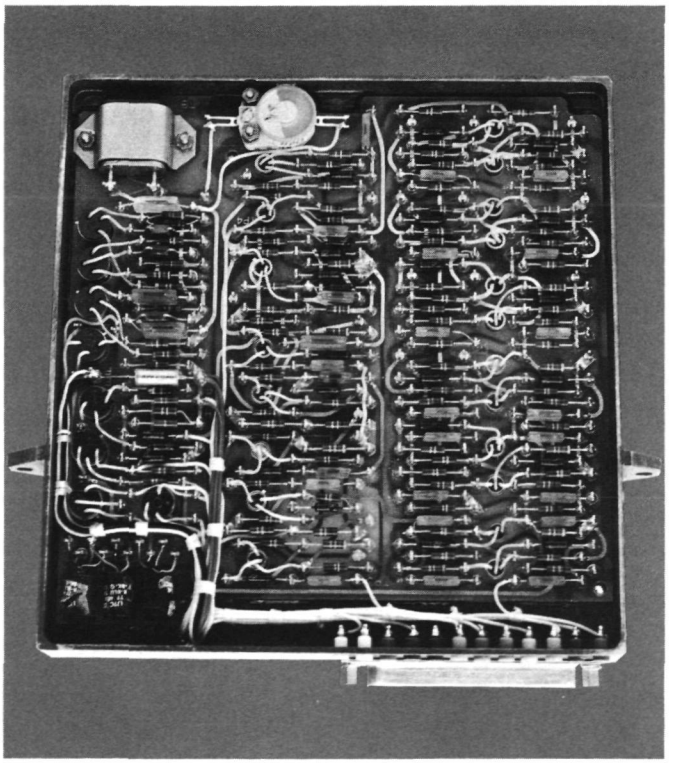

Figure 286. Central clock subassembly

the second contains the terminal maneuver. Spacecraft functions controlled by the midcourse sequence include the breaking and reacquisition of solar and Earth locks; power turn-on to accelerometer, autopilot, etc.; maneuver

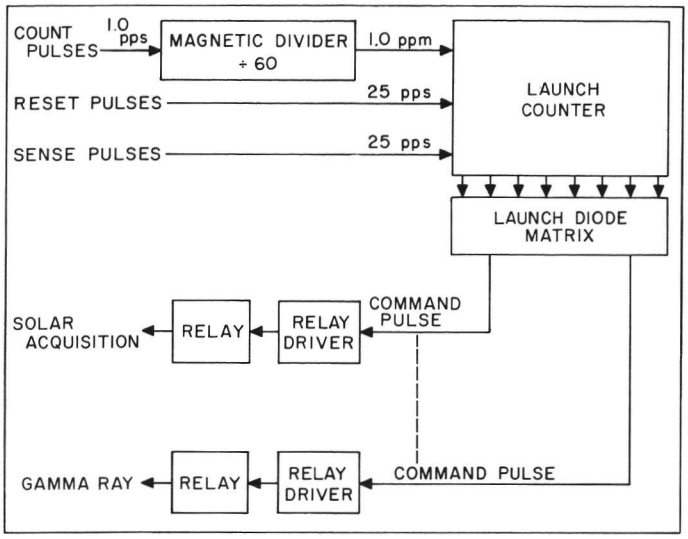

Figure 287. Launch phase subsystem

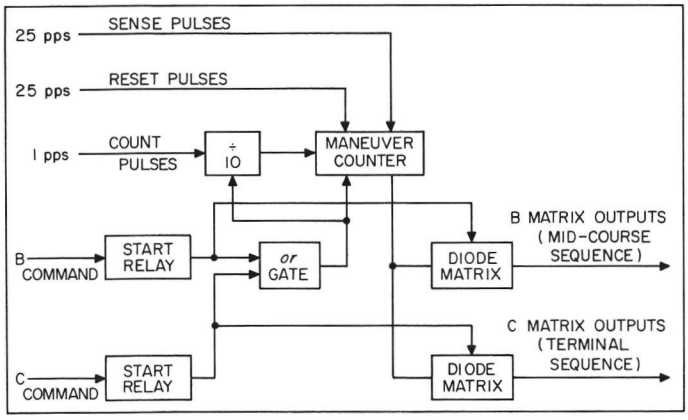

Figure 288. Maneuver clock

turn starts; motor ignition; and extension of the gamma-ray boom. Those functions controlled by the terminal sequence include the breaking of solar lock; maneuver turn starts; start of gamma-ray and vidicon data handling and sequencing; antenna deployment; and power turn-on of the capsule's radar altimeter. Both sequences also contain telemetry mode changes.

The maneuver clock counts with a resolution of 10.0 sec following one decade of frequency division of the central clock count pulse rate (1 pps). Following the magnetic divider is another counter of 10,000-sec capacity identical in mechanization to the launch counter. Two diode matrices are required in order to store the command times for the two sequences. The counter can be used for both sequences, since it resets itself to zero after reaching its capacity following the completion of the midcourse sequence. Starting of the counter and selection of the proper matrix is controlled by two magnetic latching relays, each of which is closed by the appropriate real-time command.

Maneuver output subsystem. The maneuver output subsystem contains the command relays, relay drivers, and one output transistor switch, all controlled by the maneuver clock except for the maneuver turn relays which are contained in the maneuver duration subsystem. The output transistor switch provides a pulse for each telemetry mode change. As in the central clock, the switch is transformer-coupled for ground and power isolation. In addition, this subsystem contains a second output transistor switch which delivers event pulses to telemetry for ground recording of all CC&S command relay position changes during flight.

Maneuver duration subsystem. The basic function of the maneuver duration subsystem (Fig 289) is to command the stop of each maneuver turn when the commanded duration has elapsed. The digital words representing the command durations are received from the command system through the CC&S input decoder.

The subsystem uses three 11-bit magnetic core serial shift registers, one register for each of the spacecraft axes about which the maneuver turns are executed. The shift register consists of two cores per bit and requires a two-phase mode of operation. Current steering logic is used to transfer the binary information through the register. When information is being stored, each bit of the digital word received serially from the input decoder is accompanied by synchronization pulses used to generate the two-phase shift pulses required. When counting down a duration, the shift register receives 1.0 pps from the central clock to generate the required shift pulses. In addition, a feedback loop between the ninth and eleventh register stages and the input is closed through an exclusive circuit. This feedback shift register configuration generates 2047 unique 11-bit patterns of binary zeros and ones (excluding the all-zero pattern) at the rate of 1/sec. The condition of all ones, detected by an 11-bit input and gate, generates the stop turn command pulse. Thus, the turn duration, in seconds, is the number of pattern changes (a maximum of 2046) between the stored and the all-ones patterns in the shift register.

The same registers are used for both maneuvers but not necessarily for the same axis in each maneuver. The subsystem also contains the three maneuver turn relays as well as a turn polarity relay controlled by the input decoder. Each maneuver turn relay is closed by a start command from the maneuver clock and opened by the

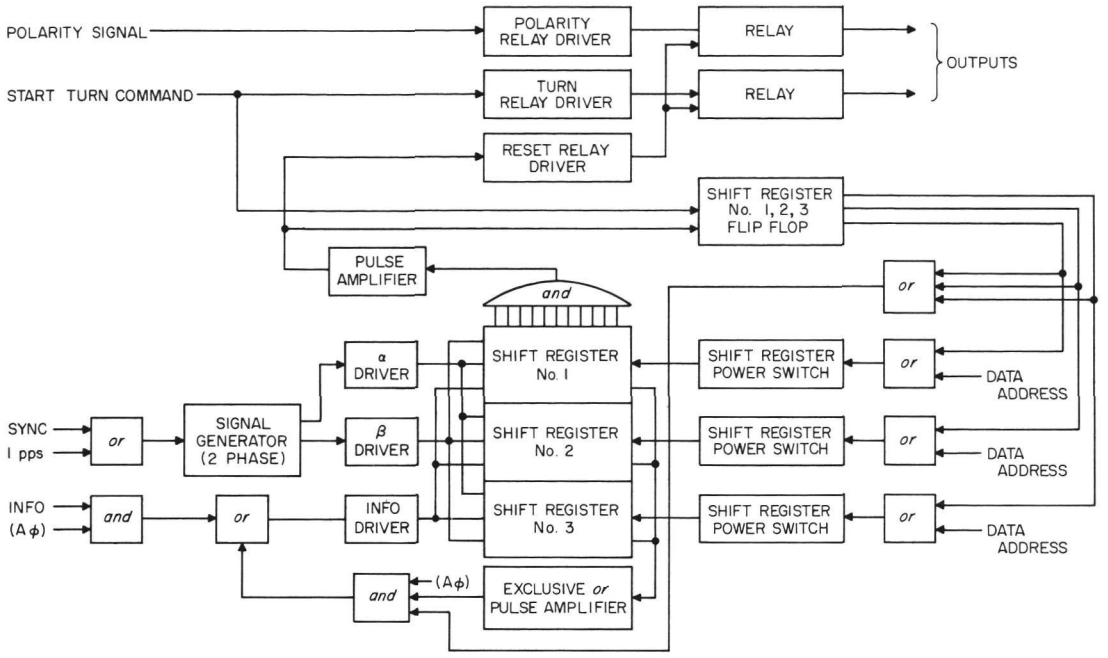

Figure 289. Maneuver duration subsystem

stop turn command pulse from the corresponding shift register.

Accelerometer integration subsystem. The basic function of the accelerometer integration subsystem (Fig 290) is to command the motor shutoff when the required midcourse velocity increment is achieved. The digital word representing the velocity increment is received from the command system through the CC&S input decoder. In addition, the subsystem sends to telemetry, for postflight analysis, samples of the velocity word during computation.

A transfluxor shift register, functionally the same as those employed in the maneuver duration subsystem, is used for the velocity storage and computation functions. Mechanization with transfluxors is necessary since the register must be read out nondestructively to telemetry. Another difference is that the pattern of binary zeros and ones does not change at a constant 1/sec rate during computation. Instead, the change occurs at a rate controlled by a digital accelerometer whose individual pulses are weighted 0.1 ft/sec.

The appropriate pattern of the digital word to be stored is selected from the table used for the turn durations. Since separate relays control motor ignition and shutoff, a zero velocity increment can be obtained by transmission of the all-ones pattern. Once the shutoff relay is closed, ignition relay closure by the maneuver clock can no longer start the midcourse motor.

Input decoder. The basic function of the input decoder subsystem (Fig 291) is to accept information from the command system and transfer this information to the appropriate storage register. Polarity information is included with the maneuver duration information but is stored in the input decoder. Coincident with the start of the duration count, the polarity information positions the polarity relay in the maneuver duration subsystem. Synchronization pulses accompany the information to distinguish the non-return to zero bits.

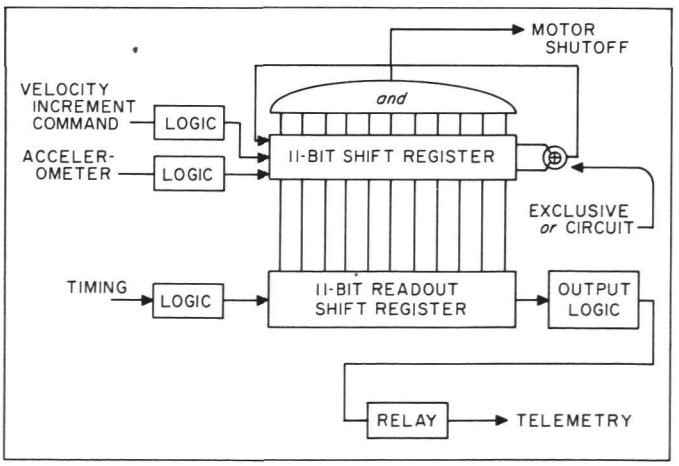

Figure 290. Accelerometer integration subsystem

CONFIDENTIAL

Since the word sent to the CC&S from the command system contains no bits identifying its components, a transistorized counter is used to separate the address, information, and polarity portions of the word. The counter employs five bistable elements in a minimal-logic configuration to obtain the required 17 states.

The first two bits of the address data are sufficient to identify the correct storage register and, hence, only two bistable elements are used for address storage. Synchronization pulses (Aϕ) are delayed (Bϕ) by use of a monostable element for delayed logical operations in the input decoder and for shift pulse generation in the maneuver duration subassembly.

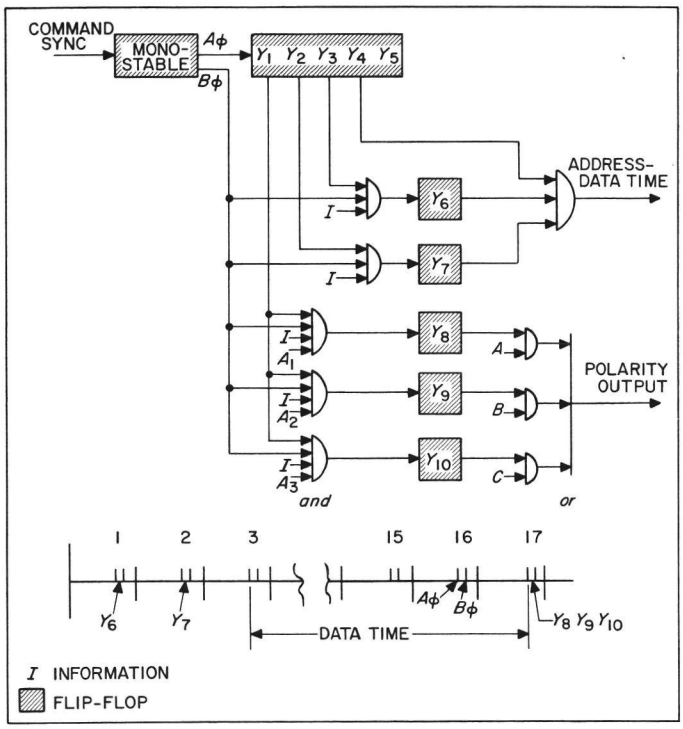

Figure 291. Input decoder

Pulse sequencer. The basic function of the pulse sequencer (Fig 292) subsystem is to provide time-sequenced pulse trains for execution of the gamma-ray and vidicon experiments. The pulse sequencer receives time information from the CC&S central clock and provides gating outputs. Solid-state devices are utilized for all binary logic and gating functions.

The operation of the pulse sequencer is divided into two discrete modes. The gamma-ray mode operates from launch +4 hr to the beginning of the second pitch maneuver in the terminal sequence. The gamma-ray and vidicon mode commences from the end of the second pitch maneuver in the terminal sequence and continues to impact.

Power converter. The basic function of the power converter subassembly is to accept 2.4-kc, 24-v rms square-wave power from the central power supply and convert it to the required d-c voltages for the CC&S system. A power transformer with four separate secondary windings followed by full-wave rectifier circuits furnishes unregulated 3-, 15-, 28-, and 60-v d-c power. The 28-v power is regulated to ±3% in a zener diode regulating circuit. Efficiency of power conversion has been measured at 82%.

d. Power subsystem (Fig 260).

The *Ranger* power equipment satisfies the design and mechanization requirements outlined above.

Batteries. The primary battery serves a launch and back-up function on the RA-1, -2 spacecraft. It provides spacecraft power for the launch period prior to illumination of the solar panels. It also provides power in case the spacecraft does not acquire the Sun. The expected life under these conditions is about 5 days.

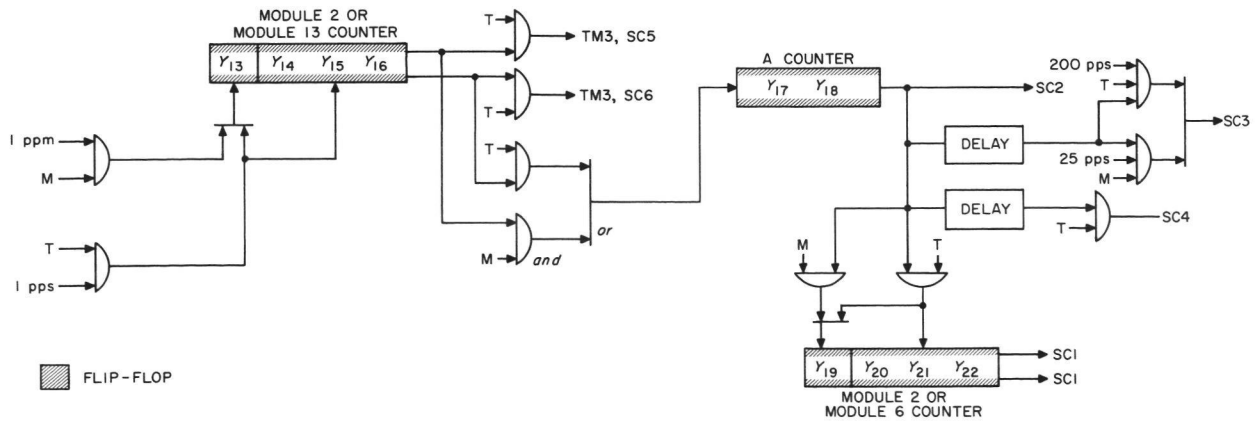

Figure 292. Pulse sequencer

CONFIDENTIAL

The RA-1, -2 battery (Fig 293) is a 16-cell, silver-zinc, non-rechargeable type. It is sealed in a JPL-designed magnesium case with provision for the expulsion of generated gas through a pressure-actuated relief valve. The case is of egg-crate construction designed to lend support to the cells and to dissipate heat generated within the cells. Battery operating voltage range is 25.5 to 29.5 v, and it has a capacity of 360 amp-hr.

The RA-3, -4, -5 battery performs a launch and flight function. It must supply power during the launch phase and, in addition, during the midcourse and terminal maneuver, at which times the solar panels lose illumination. The RA-3, -4, -5 battery is a 14-cell, silver zinc, rechargeable type. It is located in Case VI on the spacecraft (Fig 294), and is sealed with no provision for gas expulsion. Its operating voltage range is 20.0 to 23.5 v and its capacity is 45 amp-hr, sufficient for the 66-hr RA-3, -4, -5 flights.

Solar panels. The *Ranger* solar panels were developed within the limits of two conflicting criteria. It was necessary to present a large active area to the sunlight in order to be able to satisfy the spacecraft power demands. At the same time, the size is limited by space under the shroud. The *Ranger* panels are two in number, each 10 ft^2 in size and of a plane trapezoidal shape (Fig 295). They are hinged to the spacecraft frame at the bottom edge and in the nested position are folded up against the spacecraft. They are deployed to their active positions, normal to the Sun, after injection.

The panels are composed of an aluminum honeycomb backing or frame to which are attached the active silicon solar cells, shingle fashion (Fig 296). Each of the silicon cells is 2 cm^2 in size. 6-mil thick glass slides cover the cells. The glass slides are front surfaced with a non-reflective coating which increases the light absorption. The back sides of the slides are treated with a series of proprietary deposited coatings acting as an ultraviolet filter. The purpose is to increase radiation and reduce operating temperatures.

Minimum output power is 78.5 w/panel and the maximum is 97 w/panel based on a solar constant of 1323 w/m^2 minimum and 1477 w/m^2 maximum.

The cells are connected together in a series-parallel arrangement with redundancies in the parallel circuitry to assure a minimum power loss per cell damage.

Shunt regulator zener diodes are inserted between the solar panels and the battery and distribution system. The diodes clamp the output voltage to prevent supplying over-voltage to the booster–regulator.

A solar cell advanced-development experiment is flown on the *Ranger* spacecraft. The experiment is designed to measure short-circuit current and open-circuit voltage on a small sample "panel." Information will provide cell efficiency and atmosphere-space correlation data. The RA-1, -2 missions were so nonstandard that no useful information was retrieved.

Power conversion equipment. The power switch and logic circuitry switches the spacecraft system from external to internal (battery) power shortly before takeoff. It also controls the sharing of the load between the battery and solar panels during flight.

The booster–regulator accepts a varying, load-dependent voltage (18 to 31 v) from the power switch and

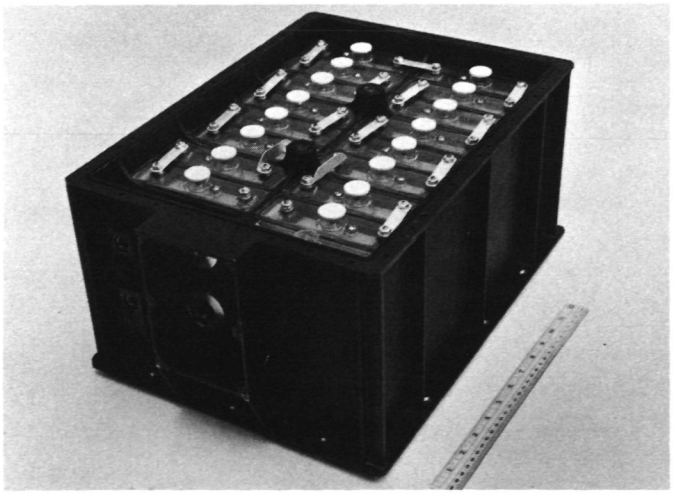

Figure 293. RA-1 and -2 battery

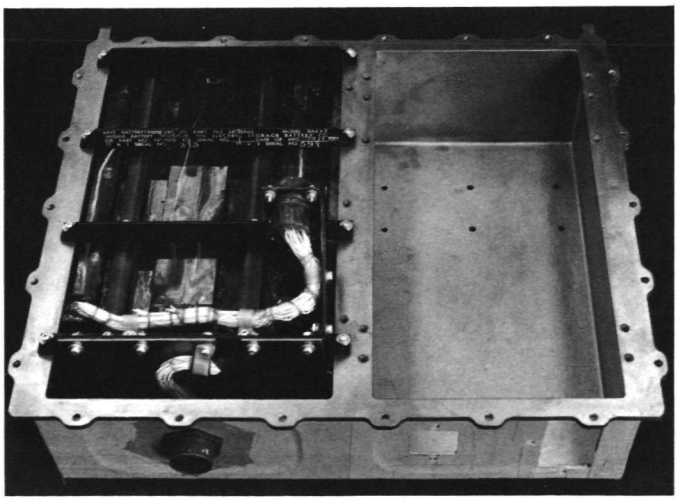

Figure 294. RA-3, -4, -5 battery

logic and provides a regulated output of 31.5 v dc ±1% to the various user's converters or inverters.

Each converter or inverter is tailored to the requirements of the individual subsystems they supply. Essentially, the converters consist of a flux oscillator, a transformer–rectifier unit, and an overload circuit. Characteristics of the converter and inverter outputs are listed in the power block diagram (Fig 260).

A feature of the conversion subsystem is the power synchronizing subsystem. A power synchronizer controls the turn-on time of each converter in a "phasing" manner. The converters are free running at a frequency lower than the synchronizer and the synchronizer adjusts the on-point so that each converter turn-on is sequenced and the system load fluctuations are reduced.

Another feature of the converters is the overload circuitry. In case of overload in any converter, the load is tripped out, but sampled once each sec. Damage is prevented, and if the overload should disappear the converter will return to normal output.

The system is designed so that failures within the system may cause degradation but not complete failure. For example, the boost regulator is fused, but if the fuse is blown, the booster will continue to supply power unregulated. Or if the synchronize circuit is disabled, the system will function, but with more line ripple.

4. Flight Performance

Both *Ranger I* and *II* flights were similar and nonstandard. Both spacecraft were put into circular orbits around the Earth instead of the anticipated highly elliptical orbits away from the Earth. Within the orbital conditions imposed, the Earth-probe-Sun relationships were unusual and continuously and rapidly changing. Earth light was presented to the spacecraft as a large flat illuminated surface, as opposed to a finite, well-defined "source," and cyclic periods of light and dark were encountered as the vehicles continued their orbital trips around the Earth. In addition, because of the short, fast passes over the various receiving stations, engineering telemetry was recovered in short, disconnected bursts, or in many cases lost completely. The circumstances made it impossible to piece together a continuous history of spacecraft guidance and control performance. However, the following comments on guidance and control performance can be made, based on telemetry information received:

(1) All controller events took place at the times designated.

(2) The controller one-pulse-per-sec pulses were generated.

(3) Attitude control on at least one occasion acquired the Sun and Earth.

(4) The attitude-control nitrogen gas supply was exhausted at approximately 19 hr after injection (fifth orbit) because of the unusual demands placed on the system by the orbit.

(5) The battery was exhausted approximately 91 hr after liftoff. This is considered normal, since the

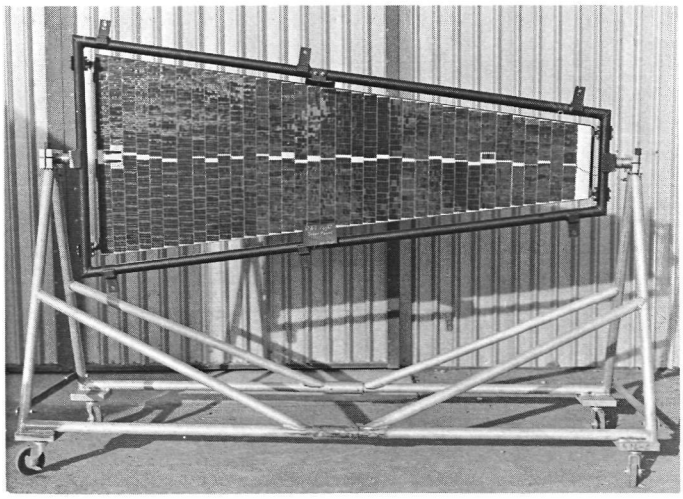

Figure 295. Solar panel in test rack

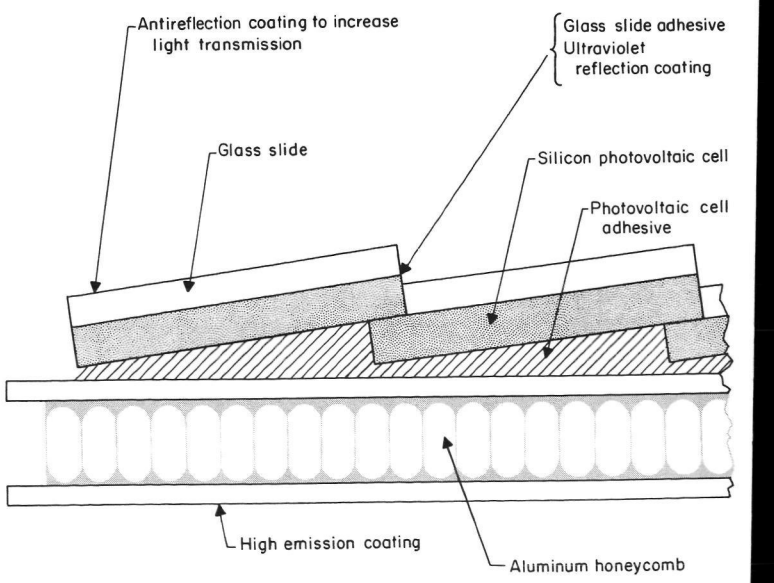

Figure 296. Solar panel cross section

solar panels shared the load intermittently for only short periods of time.

(6) The only recognizable malfunction was that the attitude power converter went into overload on the second day, probably due to heavy demands by the system. The converter recovered on the third day (after the twenty-first orbit) and functioned normally thereafter. RA-2 overload trip was set up from 1.2 to 1.5 amp.

The above comments apply to the *Ranger I* flight, but are in general typical of both the *Ranger I* and *II* flights.

E. Engineering Mechanics

1. Introduction

The responsibilities of the JPL Engineering Mechanics Division with respect to the *Ranger* Project are well summarized in these categories: structure, pyrotechnics, mechanical elements, electronics packaging, temperature control, friction experiments, and terminal sterilization. In addition, there has been a substantial engineering effort in support of the Systems Division with respect to the *Agena*/spacecraft interface (system integration), the lunar capsule system, the lunar capsule/spacecraft interface, and the follow-on TV package/spacecraft interface. These activities cover the fields of temperature control, structure, structural dynamics, flight dynamics, and pyronetworks.

With respect to the *Agena*/spacecraft interface, effort was expended in conjunction with Marshall Space Flight Center and Lockheed Missiles and Space Company to achieve satisfactory separation of the aerodynamic shroud and the spacecraft from the *Agena* through design refinements and an intensive test program. Great care was taken to reduce all known perturbations affecting proper separation to the practical minimum. As a further safeguard, all possible areas of contact between separating parts were designed to prevent snagging, or "hang up."

In the temperature control area, effort was expended to define the requirements for adequate temperature control during countdown and ascent periods. Joint MSFC-LMSC-JPL tests and analyses were conducted to determine the structural compatibility of the spacecraft and the *Agena* stage.

Engineering effort on the ADF lunar capsule system and the lunar capsule/spacecraft interface has consisted of analysis to determine the adequacy of the capsule spin-up and separation system, and temperature control system. In addition, a dynamics test program was conducted at JPL which led to the achievement of a capsule structural design compatible with bus and *Agena* requirements.

With regard to RA-6–9 TV package bus interface, a cooperative program has been established between JPL and RCA to evaluate the TV package temperature control system, to ascertain the compatibility of that temperature control system with the bus system, and to determine the structural compatibility of the TV package structure and the bus structure.

2. Structures

a. Spaceframe.

RA-1 and -2. The principal structure of RA-1 and -2 consists of a spaceframe and a forward structure. Other major structural components include an 18-db antenna and two solar panels. See Chapter IV A-1a for a discussion of the geometry of the RA-1 and -2 forward structure.

The basic geometry of the spaceframe was derived from such criteria as: placement of spacecraft weight near support points of previous stage to reduce bulging truss work; maximizing packaging volume; and separation of electronic packaging from prime structure. The spaceframe thus became a hexagonal framework to which six electronic cases of approximately 1 cu ft each may be bolted. The prime structure consists of six vertical support members of cast AZ63 magnesium connected together with aluminum angles and tubes. The entire structure is bolted together to ensure the tight tolerances required. Reference surfaces are aligned to within 0.25 mrad. A pair of K-braces is installed on the spaceframe to reduce the excessive gains of the first torsional mode of the spacecraft.

With the major portion of structural development for RA-1 and -2 completed, primary effort was directed toward integrating the structural framework into the over-all spacecraft system. Much coordination was required to provide compatibility with other elements of the JPL spacecraft, as well as the transition structure provided by Lockheed Missile and Space Division (LMSD). The combined spacecraft and LMSD transition structure were evaluated to ensure structural adequacy of the combination.

RA-3, -4, and -5. The RA-3 series of vehicles had four scientific experiments on board which were designed to investigate the lunar surface. This basic difference in mission from RA-1 and -2 (together with other resultant effects) was sufficient reason to cause modifications to the initial *Ranger* structural and mechanical equipment. The resultant effects arise from the fact that the RA-3 is a

lunar impact vehicle. Specifically, trajectory constraints were tightened, a midcourse maneuver capability was required, sterilization and weight control were mandatory, and increased electronic packaging volume resulted from the increased mission complexity. The following paragraphs describe those design changes which were made to accommodate the RA-3 mission.

Certain steps were taken to reduce structural weight, based on the results of RA-1 static and dynamic structural testing. Final confirmation of the changes occurred after completion of further static and dynamic testing. All interconnecting angles, tubes, and fittings between the vertical support castings are now made of ZK60A magnesium alloy. All sheet metal covers on the top and bottom of the spaceframe, with the exception of two bottom covers, are AZ31B magnesium alloy. The vertical sheet-metal covers on the inside of the spaceframe were replaced with 2024-T3 aluminum-alloy X-braces. All machining bosses, other than those used for direct support of the attitude-control jets and Sun sensors, were removed. The estimated weight saving brought about by these modifications was 6 lb. Long lead time delivery of ZK60A material from the mill caused a slippage of 1 month in the spaceframe delivery schedule. This slip delayed the structural test 1 month; however, there was no effect on delivery of flight spaceframes.

At one time, the total spacecraft weight problem was thought to be quite critical and drastic action was taken to reduce weight (Fig 297). The 250-mw transmitter was eliminated from the design, along with its power supply and directional coupler. The instrumentation gyros and their power supply were also eliminated. Further reduction was made by replacing some steel components with titanium or aluminum where possible, drilling lightening holes in non-stress-critical areas, removing shielding covers on power modules, and generally replacing components with lighter similar items if possible. The lighter counterparts were often more expensive and had longer procurement lead time, the reason for not having been used in the original design. Other areas of weight savings have been under continuing study, including lighter cable manufacturing techniques, smaller coaxial cable, machining-off tooling bosses on castings, eliminating nonflight hardware prior to flight (door hinges, etc.), and re-packaging the main battery.

"Weighed" weights were solicited as components were received for installation on the Proof Test Model (PTM). These weights were compared with the estimated weights, which are listed in the Design Parameter Functional Specification and used as weight allotments, to provide a practical look at the final weight of the spacecraft. In the main, "weighed" weights have been comparable with, or lower than, the weight estimates.

The weight savings effort on RA-3, -4, and -5 has been successful. The weight of the *Ranger III* spacecraft as flown was 736.60 lb.

Cursory studies have been initiated to determine how utilization of an increased weight allotment might aid in the reliability of the mission. Some thought has been given to increasing the amount of fuel in the midcourse motor to the maximum allowable within the temperature restraints consistent with range safety. At first look, it appears that sufficient additional fuel could be added to increase the velocity change capability of the midcourse motor from the present 120 ft/sec to approximately 135 to 150 ft/sec. This would increase the reliability of the mission of the spacecraft in the event that the *Agena B* injection errors were greater than nominal.

Various modifications have been incorporated on the spaceframe to accommodate various components. Briefly,

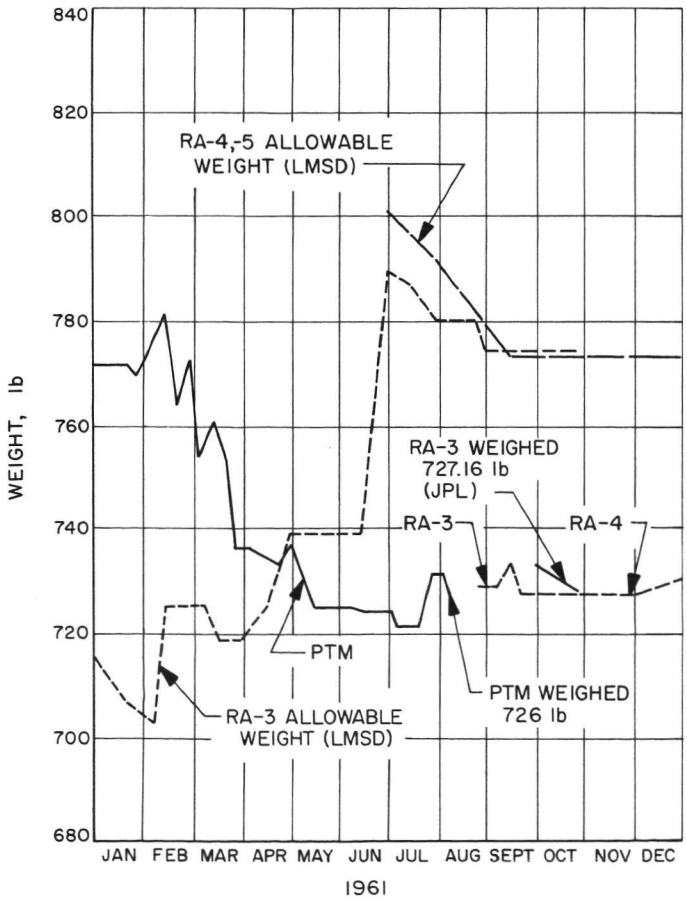

Figure 297. RA-3, -4, -5 weight history

these are: integral stiffening members on the support castings for rigidity of attitude-control jets and Sun sensors; bolt holes for attachment of the attitude-control nitrogen-gas supply bottles, which are now slung below the spacecraft; a vertical member in the center of Bay III to which a reduced Chassis III may be bolted, as well as the vidicon support mounting; small pads on the top of the spaceframe in Bay VI to which the altimeter for the lunar capsule may be bolted; the addition of Keenserts on the top of the spaceframe on a 25¼-in. diameter bolt circle for the attachment of the solar panel latching structure and the altimeter.

The changes which have been made along with the weight savings are shown in Table 68. The design changes which accrued due to the weight control program caused various delays in hardware fabrication. These delays, however, were absorbed into the schedule with no slippage in delivery of the flight hardware.

The RA-3 bus was subjected to thermal sterilization at 125°C. Inspection after the sterilization test confirmed that all dimensions were within tolerance.

RA-6 to -9 spaceframes. The RA-6 to -9 primary mission is to take high-resolution television pictures of the lunar surface throughout the approach to an unimpeded impact on the Moon. The spacecraft consists of essentially the same spaceframe as was used on RA-1 to -5, with a tower-like structure payload containing six cameras mounted on top of the spaceframe. This structure replaces the seismic capsule, retro-motor, spin motor, support structure, radio altimeter, and capsule thermal shield of RA-3.

A primary objective in the follow-on (RA-6 to -9) program is to minimize changes from the RA-3 to -5 configuration. Changes have been limited to only those necessary to accommodate, first, the television mission, and second, the scientific experiments. A few minor changes for improving assembly processing or reliability have also been incorporated.

Table 68. Spacecraft weight savings

Structure	Weight, lb
Spaceframe	
Additional machining of support castings	2.16
Replacement of steel bolts with titanium	1.00
Replacement of aluminum components with magnesium	0.65
High-gain antenna	
Conversion to aluminum feed	1.06
Redesign antenna supports	1.90
Additional machining of yoke	0.15
Solar panels	
Replacement of steel screws with aluminum	2.25
Midcourse propulsion support	
Remove redundant members	0.48
Total weight savings	10.23

b. Solar panels. Power requirements dictated that 20 ft² of area be available for solar cells. This area is divided equally between two trapezoidal panels placed diametrically opposite each other on the spacecraft. The design was based upon resonant frequency and weight criteria. An optimization study has shown that a combination of a honeycomb panel with a stiffening framework best meets the design requirements. Aluminum is used throughout because of its light weight and high thermal conductivity. The panels are hinged at the feet of the spaceframe to permit in-flight actuation to a horizontal position. During the boost phase, each panel is folded and latched to the forward structure at four points. A squib-actuated pinpuller is mounted at each of these locations with 3 deg of adjustment to remove tolerance mismatch.

The presence of the lunar capsule on RA-3 altered the method of support of the solar panels used on RA-1. There was no structure available for latching the upper part of the panel and, therefore, a testing program was initiated to determine the effects of leaving the panels cantilevered with supports only at the midpoint and the aft end. Under dynamic testing, deflections at the panel natural frequency far exceeded the allowable limits. A permissible deflection and a design goal were less than 4 in. peak-to-peak at Type-Approval loads.

The honeycomb panel with solar cells was left untouched, and efforts were placed on adding damping material to the solar panel frame. The firm of Barry Controls was selected for the task. The sheet metal stiffeners were changed from 0.060-in. aluminum to a laminate of three sheets of 0.020-in. aluminum, with approximately 0.005 to 0.010 in. of damping material between the three aluminum layers. Stiffening angles were added at the mid-panel point, and an extra layer of laminate and damping material added at mid-panel in the center hat section. The resultant effect under dynamic testing was 3½-in. peak-to-peak deflection, under Type-Approval loads. For additional protection of the solar cells in case of impact with the capsule, a snubber consisting of ½ in. of rubber was located at the center tip of the panel. Tests of the snubbers show impact acceleration of less than 100 *g*.

A truss-type magnesium alloy structure to support the solar panels at their mid-point (when in the folded posi-

tion) was designed, fabricated, and tested satisfactorily to Type-Approval requirements. The decision to mount the gamma-ray experiment on a telescoping boom, which must then be stowed on top of the spaceframe, led to a redesign of the panel support structure to include a mounting arrangement for the boom. The weight of the redesigned structure is approximately 2 lb and represents essentially no increase over the previous design.

c. High-gain antenna.

Antenna feed. Two significant modifications were attempted with respect to the high-gain antenna assembly on RA-3, both of which stem from the weight control program. The first was a redesign of the antenna supports from the spaceframe to the antenna and the second was the substitution of a brazed aluminum feed assembly for the steel one used on RA-1 and -2. Two prototype feeds were constructed, checked electrically, and showed a discrepancy with respect to matching impedances. Hardware was fabricated to permit relocation of the transformer on the inner conductor and subsequent impedance matching. This modification could not be made in time for the RA-3 flight unit delivery. Therefore, RA-3 flew with a stainless-steel feed. Although the electrical characteristics of the first aluminum feeds are not flight quality, they were still subjected to environmental testing to evaluate their application to flight units. One of these feeds underwent dynamic testing and the results indicated that structurally the aluminum outperforms the steel with an increase in natural frequency from 60 to 75 cps and a reduction of 50% in the gain at resonance.

The impedance-matching problem could not be resolved without an excessive amount of testing. The electrical characteristics changed through the brazing process which could only be performed twice on each test feed without damaging the parts. This program was subsequently dropped, and RA-4 and -5 will fly with stainless-steel feeds.

Pivot-arm insulator. An epoxy-fiberglass joint was used to provide thermal and electrical insulation between the high-gain antenna and the spacecraft frame. The tube was bonded into the main aluminum tube of the pivot arm with an epoxy adhesive. In addition, thin-wall aluminum sleeves were bonded into the epoxy-fiberglass tube to provide a ductile surface for riveting.

Antenna actuator gearbox. The antenna actuator shown in Figure 298 drives the antenna at a nominal speed of 1 rpm. The prime mover for the drive is a size 11 a-c servomotor. The gear reduction from the motor to the output gear shown in the upper right of the figure is 234,000:1. Included in the gearplate assembly (center) is the motor, a flywheel, slip clutch, output position potentiometer, and spur and worm gearing. The flywheel mounted on the high speed motor shaft provides momentum counterbalance for the antenna. The slip clutch serves two functions. It provides mechanical overload

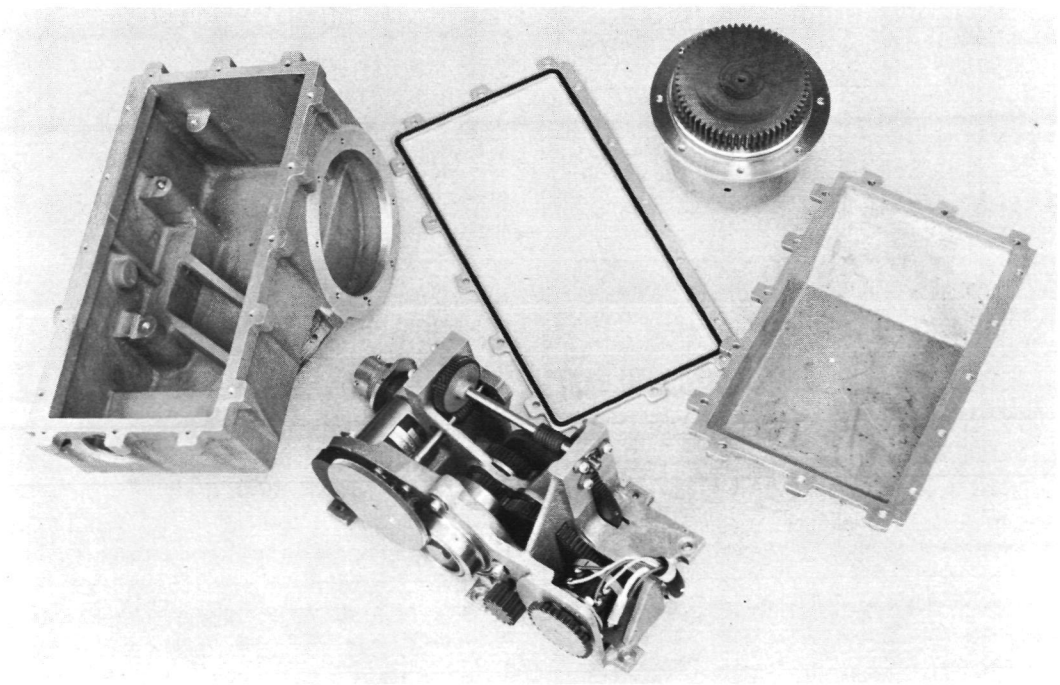

Figure 298. Antenna gearbox

protection for the output gearing during ground checkout and it also allows the antenna to be placed in any position (i.e., the nested position) without driving from the motor.

The gearbox actuator assembly is hermetically sealed, using elastomers. Ten seals are required, including an outboard bearing seal for the motor shaft (not shown) and the rotary seal on the output shaft. For the rotary seal, two O-rings are used on the output shaft separated by a reservoir of silicone fluid which constantly feeds both O-rings during actuation. Silicone fluid has also been used as the lubricant for the bearings. The gears are lubricated with silicone-bonded molydisulfide.

Type-approval and flight-approval antenna actuators were tested with favorable results. Early testing indicated a weakness in the heavily loaded motor shaft and, subsequently, an outboard bearing support was added. The seal integrity of the assembly has been typically below 1 cc/hr leakage of helium.

The antenna drive gear box required modification of the output rate capability to permit tracking the Earth in the terminal maneuver of the spacecraft. This change permits a maximum output speed of 3 rph and is accomplished by changing the gear ratio. In addition, dynamic performance of the hinge loop was improved by the removal of the angular momentum cooperation of the antenna. The total velocity added to the spacecraft equals 0.035 times the antenna velocity and is a negligible disturbance.

Electro-film plating on the gear teeth has not proven to be a complete solution to gear lubrication requirements. After short periods of running, the molydisulfide coating flaked off and appears to have caused excessive wear on some gear teeth. This problem was discussed with the developers of this technique and it was finally decided to add a small amount of General Electric G-300 silicone grease over the electro-film. This suppressed the severe scoring condition.

RA-6, -7, -8, and -9. The feed was changed from a dipole for RA-1 to -5 to a turnstile for RA-6 and -7 to provide circular polarization to the r-f radiation. The transformer was modified to match the impedance of the new feed. This change will be more compatible with the Goldstone equipment and double the effective power transmitted from the spacecraft. This new antenna is to be used on RA-6 and -7.

RA-8 and -9 are to carry the ranging experiment, which is to operate in both S and L frequency bands. A new multi-band antenna with a conical helix feed has been designed and is being tested for r-f characteristics. Since the feed and feed supports on this antenna extend further away from the antenna dish than previous designs, it has been necessary to put a joggle-like bend in the pivot arm to permit the antenna to nest higher up into the spacecraft. This provision affords approximately 1-in. clearance between the feed supports and the *Agena* sterilization diaphragm, and thus, interchangeability in this area with the earlier *Ranger* spacecraft remains unimpaired.

High-gain antennas of the RA-1 through -7 types have previously been test-shaken while assembled on the spacecraft in accordance with type-approval requirements of Specification 30232B. The shake tests to be run during the first quarter 1962 on the MTM (Mechanical Test Model) will be made with the RA-8 and -9 multi-band antenna on board.

d. Attitude-control tubing joints. Studies are being made to determine the adequacy of welded tubing joints for the attitude-control system. This design is being studied as a replacement for the mechanical flare-type fittings currently in use on *Ranger*. Although the all-welded system should be more reliable, it does pose some problems.

One of the problems being studied is the determination of internal tube cleanliness after welding. Any deposits formed inside the tube on welding, which could subsequently loosen and enter the gas stream, would be detrimental to control-jet operation. Studies so far on this problem have proved that it is possible to weld tubing, keeping the interior clean.

Additional tests are being run to determine the probability of making leak-free joints. This poses a problem, as it may not be possible to adequately inspect all joints after installation. During preliminary tests using a specially designed joint, it appears that 100% reliability can be obtained.

e. Testing.

RA-1 and -2. Although environmental survival has many different classifications such as temperature, humidity, vacuum, sterilization, blown particle, etc., the prime factors in the design of the structural components were static acceleration, shock, and vibration. The relative importance of these three tests varied with the component. For example, the bus design was primarily a static acceleration consideration; the forward structure was principally a problem in natural frequency and excursion control and, thus, vibration criteria predominated; the 18-db antenna was critical in vibration and shock; and the solar panels were primarily of concern in a vibration environment.

To verify the suitability of the structure to withstand the critical environment and also to verify the compatibility of the experiments or components to the resulting environment provided by the structure, an extensive test program was followed. The test program began in May 1960 with preliminary static testing of the bus. Testing of the other components developed rapidly from this time and continued until March 1961. A test outline is given in Table 69.

Generally, a preliminary test was run to determine the adequacy of the test equipment and to provide a first look at the performance of the structure. These tests were largely of an exploratory nature to assure that any load condition that might require design refinement had been thoroughly investigated. The second test was usually run strictly to type-approval loads to qualify the design for flight. The specimen for this test represented a final design ready for production upon satisfactory completion of the test.

Table 69. Testing history: RA-1 and -2

Program	Date of test			
	Bus	Forward structure	18-db antenna	Solar panel
	Static acceleration			
Component test				
Preliminary investigation	5/60	—[a]	—[a]	3/15/60
Design refinement	—[a]	—[a]	—[a]	—[a]
Type approval	7/6-7/15/60	10/13/60	10/12/60	8/60
	Vibration evaluation			
Component test				
Preliminary investigation	—[a]	8/60	4/27/60	2/60, 6/60
Design refinement	—[a]	8/60[b]	5/60, 10/60[c]	3/60[d]
Type approval	8/22/60	10/60	10/60-11/60	7/60
Composite structure test				
Preliminary investigation	9/14-10/1/60	9/14-10/1/60	—[a]	9/14-10/1/60
Design refinement	10/60[e]	—[a]	—[a]	—[a]
Type approval	10/22/60	10/22/60	10/22/60	10/22/60
Investigation of system compatibility problems	12/23/60	12/21-12/27/60	—	—
Type approval of guide rails	3/10/60	—[a]	—[a]	3/10/60
	Shock survival			
Component test	—[a]	—[a]	—	—[a]
Preliminary investigation	—	—	—[a]	—
Design refinement	—	—	—[a]	—
Type approval	—	—	10/14/60	—

[a]Not required.
[b]Incorporation of diagonal braces and relocation of SCRE.
[c]Revision of pivot/arm antenna interface; change in material of ground-plane attachment hardware.
[d]Joint redesign.
[e]Incorporation of torsional braces (k-truss) into bus.

After completion of the component tests, an assembly of the primary structure was tested. This testing also proceeded in two stages: (1) preliminary exploration of the interaction of major components, and (2) a type-approval test on a refined test specimen. Upon completion of these tests, the RA-1 structure was considered qualified for flight.

The proof of the qualification procedure of the structural design was the satisfactory completion of a vibration test of a vehicle with operating electrical components. Obviously, any malfunction of equipment previously operative and certified by component type-approval testing would have made the component environment provided by the primary structure extremely questionable. The functional test in this case was conducted on the PTM vehicle. As a result of this test, two separate areas were given careful investigation:

(1) The launch and backup battery had begun to malfunction a short time after activation. Vibration studies with thorough instrumentation of the battery support system, and later history of the battery itself, revealed that the detrimental effects were an internal component problem and not due to vibration.

(2) A mock-up of the solar corpuscular radiation experiment (SCRE) was present on the PTM and the large resonant gains encountered by the boom raised fears the SCRE might not survive the structural resonance condition. Vibration studies were run with an operative SCRE mounted on a structural vehicle and type-approval loads applied through the structural resonant range with no malfunction of equipment.

RA-3, -4, and -5. A majority of the type-approval tests performed on RA-1 hardware were also applicable with respect to RA-3; however, a significant number of tests still had to be performed. Hardware peculiar to the RA-3 series of spacecraft, as well as new groups of ordnance devices, must pass qualification tests, and there existed a continuing quantity of hardware to undergo flight acceptance (FA) tests. Table 70 gives a breakdown of the number of units tested, the time involved, and the test schedule.

Table 70. Test program details: RA-3, -4, and -5

Component	Type of test	No. of units	Total time days	Date of test initiation
High-gain antenna	FA	7	7	3/13, 4/17, 5/22, 6/26, 8/7, 9/18, 11/6/61
Solar panels (less cells)	FA	10	5	2 through 5/61
Solar-panel latching structure	TA	1	6	3/16/61
Omni-antenna support assembly	DEV	1	5	3/16/61
Omni-antenna support assembly	TA	1	20	4/10/61
N_2 bottle installation	TA	—	—[a]	—[a]
Gamma-ray boom	TA	2	20	3/20/61
Gamma-ray boom	FA	8	20	4/24, 5/22, 5/29, 6/12/61
Thermal-heat shields	TA	1	5	3/20/61
Midcourse propulsion system	TA	1	5	3/20/61
Pinpullers	TA, FA	30	25	4/3/61
Omni-antenna boom actuators	TA	2	20	3/20/61
Omni-antenna boom actuators	FA	6	10	4/17/61
Composite test vehicle	TA	1	20	4/17/61

[a]Included in TA Testing of omni-antenna support assembly.

NOTATION:

DEV = Experimental and developmental type testing.
TA = Type approval testing.
FA = Flight acceptance testing.
CTAT = Composite TA test. This is the dynamic testing of a complete structural model of the spacecraft to TA loads, which shall be performed on a full-scale vehicle with as many flight-type components as possible aboard. All items not available shall be mocked up as to their general structural properties. No structural component shall be considered qualified unless it has satisfactorily passed this test.

Composite vehicle dynamic test. A complete structural vehicle was assembled for the purpose of evaluating the dynamic characteristics of the spacecraft. This vehicle included all major structural assemblies mocked up to the proper weight. The first test consisted of a sine sweep from 1 to 40 cps at 0.5 *g* zero to peak along the *X*-axis. All components behaved normally including the lunar capsule, which again showed the first and second modes occurring at 12 and 24 cps, respectively. Under the type-approval lateral level of 1.25 *g*, one of the retro-rocket support structure legs failed. This appeared to result from improper bonding between the honeycomb core and the fitting at the foot, thereby reducing the load-carrying capability at that location (i.e., the load passed from the honeycomb structure to the fitting through the sheet metal facing alone). A new support structure was supplied with additional bonding at the feed and doublers bonded on both sides of the honeycomb and extending 1 in. above the lower extremity of the core. Type-approval testing of this vehicle indicated a shift in the first and second modes to 8 and 18 cps, respectively. A substantial increase of activity at 18 cps was noted and the test was halted. Investigation of the support showed that the honeycomb core had pulled away from the facing in several areas and the latter was buckling. Further investigation showed that the flange on the lunar capsule sphere had pulled away from the balsa wood in one area.

The oscillograph records of this test showed that during the second mode the table input was approximately 1.75 *g* zero to peak and a further gain through the bus placed the input to the capsule up to between 2.0 and 2.5 *g*. The lunar capsule support structure was designed for 1.25 *g*.

Three plans of action were followed: (1) an investigation to maintain tighter control on the table input; (2) a bus-capsule combination tested at low levels to investigate gains through the bus and secondary effects to lunar capsule components; (3) a model analysis conducted to determine the natural frequencies and mode shapes.

The test was rerun, with gains through the system as predicted. Having successfully completed this test, the vehicle was released for a model analysis.

f. Sterilization. Heat sterilization is apparently the most effective method of sterilizing spacecraft components. Eventually, entire spacecraft will be heat-sterilized in one operation. Twenty-four hours at 125°C will ensure that no viable organisms exist; but in a large, complex spacecraft, will 24 or even 48 hr ensure that all parts have been exposed to 125°C for 24 hr?

As a preliminary step in answering this question, a program was initiated. Two spheres of Stycast 2850 6T (a typical filled epoxy potting compound) were cast which had thermocouples located at the center at half the radius, and at the outer surface.

The spheres were placed in a forced convection oven, at ambient temperature with the oven set to control at 125°C. Figure 299 shows the resulting curve for the 1½-in. sphere while Figure 300 shows a similar curve for the 1¾-in. sphere. It is apparent that the thermal lag under the conditions of this test is not significant, essential equilibrium being obtained at all specimen locations in 15 to 25 min after the oven had stabilized. Further evaluation is required to determine thermal diffusivity of complex assemblies.

3. Pyrotechnic Subsystem

The squib firing assembly for the *Ranger* spacecraft has one basic requirement: upon external command, the unit must switch electrical power to reliably initiate a number of squibs. The squib firing assembly has under-

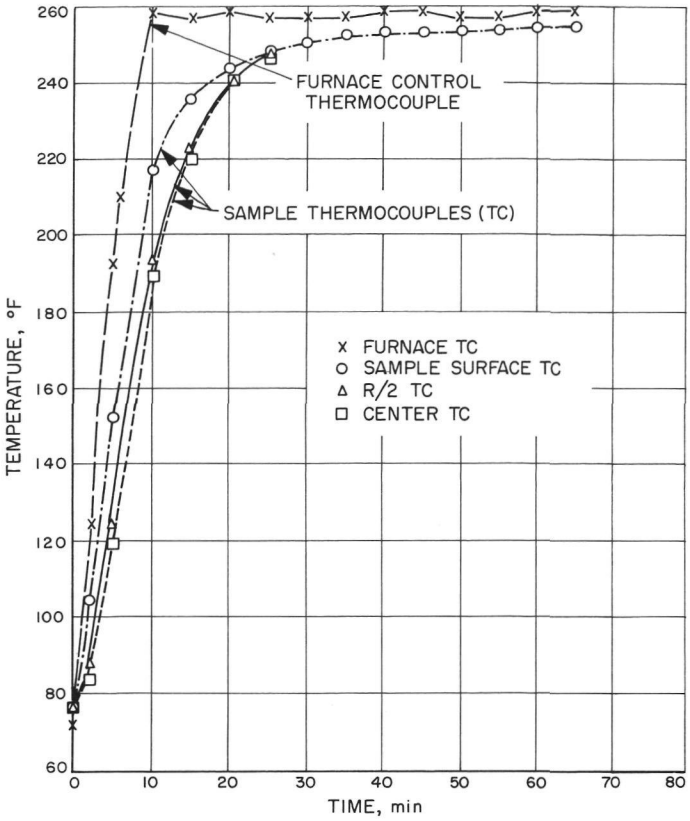

Figure 299. Thermal diffusion into 1 ½-in. sphere of Stycast

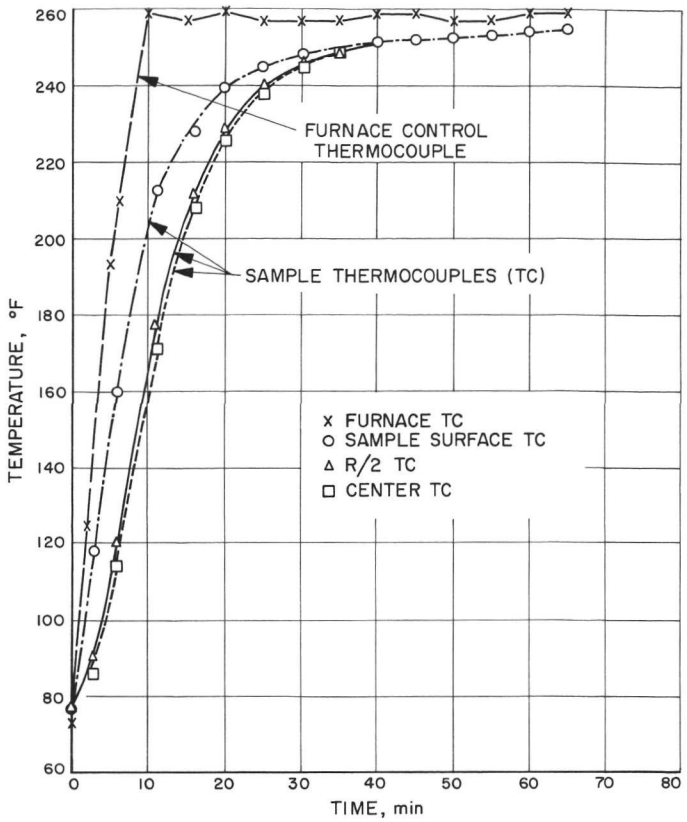

Figure 300. Thermal diffusion into 1 ¾-in. sphere of Stycast

gone many changes between RA-1 and -2 and RA-3, -4, and -5. The RA-1 and -2 squib power supply had an integral power pack (batteries). The RA-3, -4, and -5 squib firing assembly uses the main spacecraft battery power and has acquired many secondary functions.

a. RA-1, -2 squib power supply. Two electrically identical squib power supplies (Fig 301) are provided as part of the redundant erection system. Each squib power supply consists of a battery pack containing 12 nickel-cadmium cells, 11 current-limiting resistors, and a silicon-controlled rectifier power switch.

The nickel-cadmium cells used in the battery pack are rechargeable. A large portion of the GSE consists of an automatic high-rate charger and trickle chargers (Fig 302). The cells proved to be quite reliable. However, there were many attendant difficulties associated with the battery pack. The adjustment of operating procedures and charging methods and the venting of cells all were implemented to reduce the effects of cell gassing. Potting techniques were developed to restrain and seal the plastic cases of the cells.

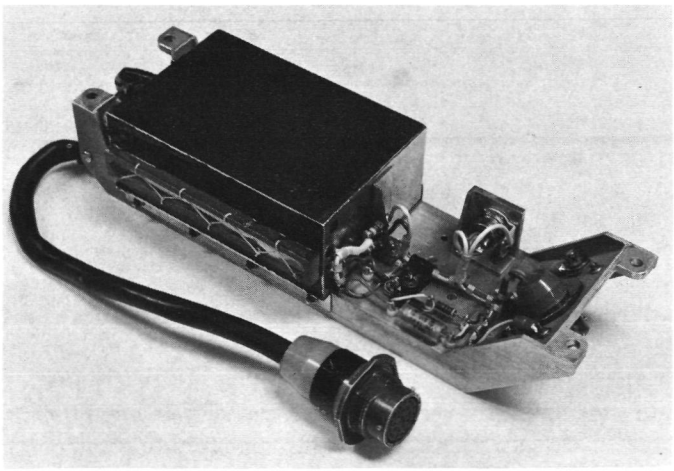

Figure 301. Squib power supply

Stycast 3050 was the most acceptable type of potting compound for use in sealing and encapsulating the cells. This compound has low viscosity when mixed, has high tensile strength when cured, is essentially unaffected by KOH, and can be cured at room temperature.

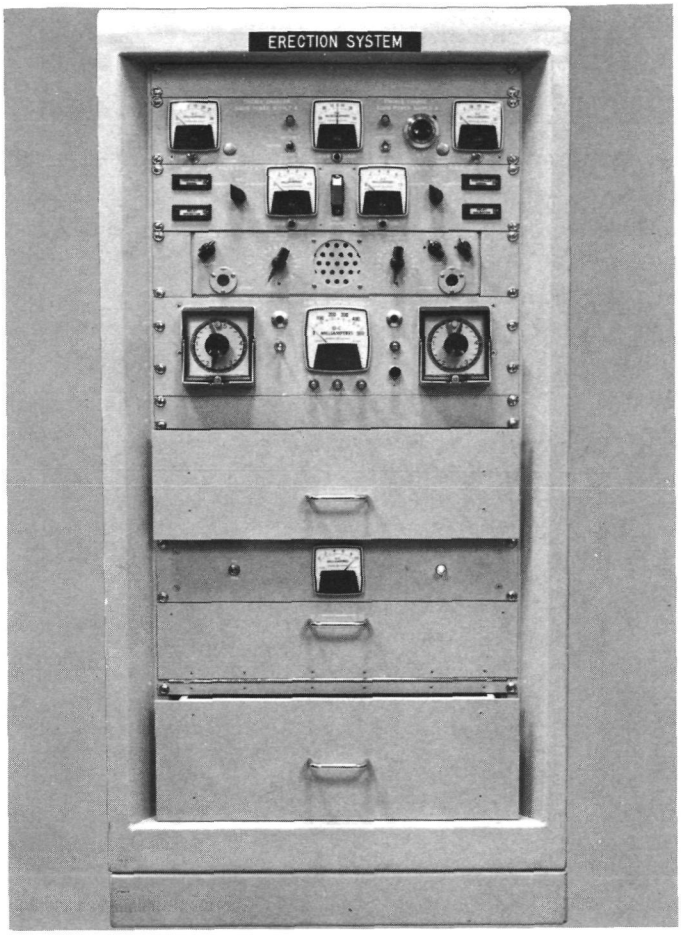

Figure 302. GSE erection system console

A change was made in the installation of the absorbent material used to contain the slight amount of electrolyte which escapes through the vent caps of the battery cells. The original design consisted of one continuous pad which was common to all 12 cells. An electrical leakage path was noted through the stainless-steel vent-caps when the pad was damp; this condition tended to discharge the cells slowly. A method of using individual pads for each cell was implemented to avoid the problem.

At one stage of development, a high failure rate of the silicon-controlled rectifier power switch became apparent. Excessive changes in the gate firing characteristics, as well as failure by shorting, were observed. Due to the limited time available to solve this problem, every known solution was applied. A functionally equivalent component of a different manufacturer was selected. This component carried a USN number, which implied that Navy qualification test conditions had to be met. Additionally, discussions with both the old and new manufacturer revealed that the latter employed much better quality control and component test programs. Burn-in tests were performed on all of the controlled rectifiers received. Gate circuit parameters were adjusted so that the current, voltage, and power remained well below the maximum allowable ratings. All components were subjected to a Radiflo leak test.

Although the exact cause of the failure was not determined, the referenced changes resolved the problem. No failures were observed in the new components, and a repeatable gate-firing characteristic was observed.

Figure 303 shows the RA-1, -2 pyrotechnic subsystem as it appears in the systems test configuration. Battery charging lines for the two supplies were carried through the separation connectors. In the prelaunch configuration, there was a trickle charger and voltage monitoring panel in the AMR blockhouse. The battery packs were maintained on trickle charge until approximately 20 min before launch.

Figure 303 shows that the system was completely redundant. Triggering of either squib power supply by the controller fired one of the squibs on all of the devices; firing of either squib on a device should have actuated that device. Both squib power supplies were triggered by a common command from the controller at approximately 30 min after launch. Each squib power supply delivered approximately 30 amp to a parallel combination of one squib on the solar corpuscular radiation experiment boom latch, eight squibs on the solar panel latches, and the two dimple motors on the Lyman-alpha telescope latches.

The command at this event was not turned off. Because the squib power supply had completed its job at this one firing, no special means were incorporated to remove battery power drain due to the trigger load, shunt resistor load (on the Lyman-alpha dimple motors), or post-fire shorted squib loads. The battery under those loads was depleted in approximately 30 min. During system testing, special procedures were implemented to prevent battery depletion. This action was required to prevent damage to some of the individual battery cells which would undergo excessive gassing during the final phases of battery depletion.

Although no direct telemetering indication was incorporated into the RA-1, -2 squib power supply, it is known by indirect indication that the unit functioned correctly on the *Ranger I* and *II* flights.

b. Squib firing assembly (RA-3, -4, -5). The RA-1 and -2 squib power supply was essentially a self-sufficient unit (requiring only an external command) and operated only

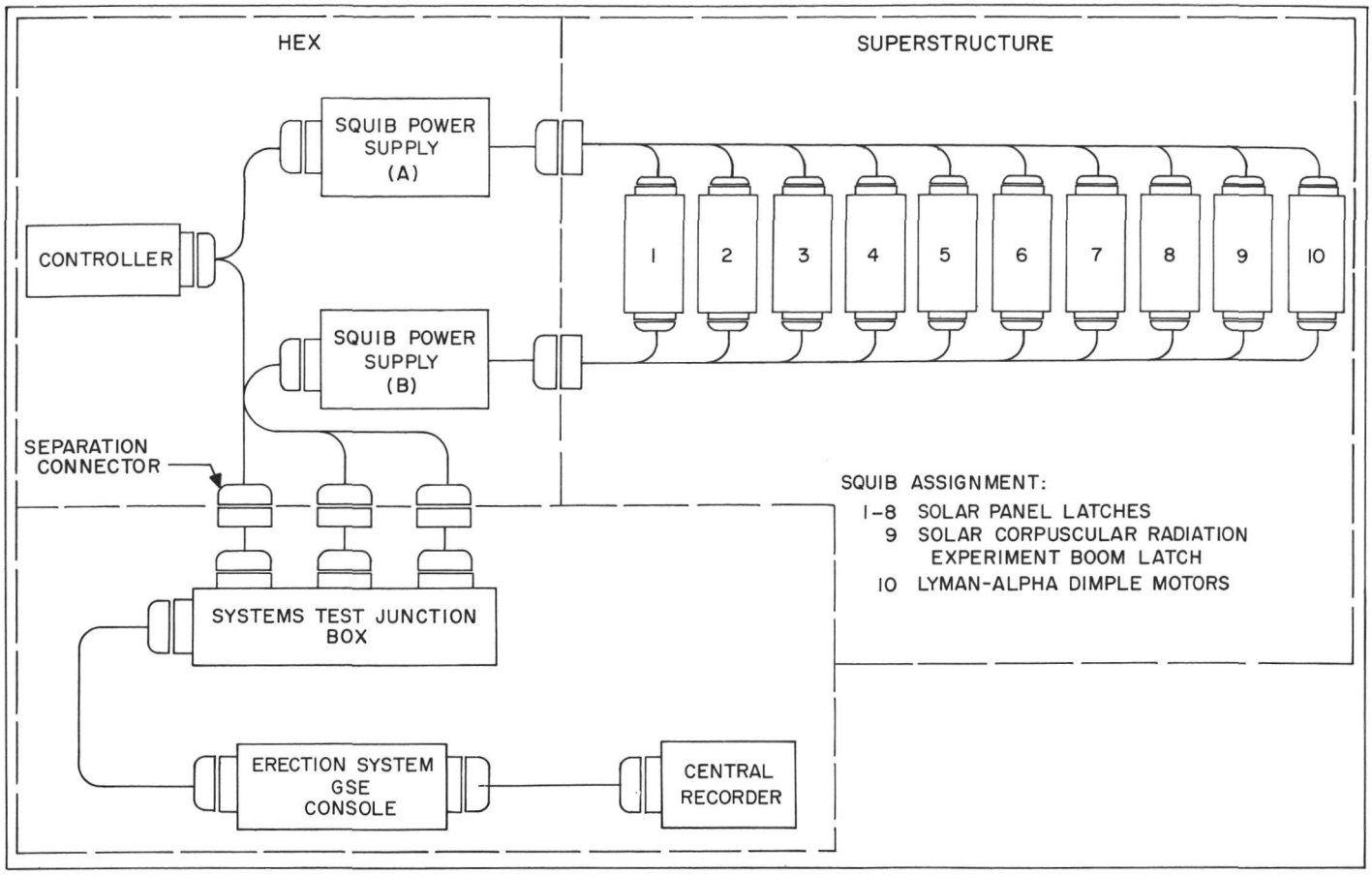

Figure 303. RA-1 and -2 erection system

once; it was somewhat isolated, both electrically and mechanically, from the rest of the spacecraft system. However, the RA-3, -4, and -5 squib firing assembly utilizes the main battery power, must be capable of repeated operation of six time-separated events, performs a power-pulse gating function at each of the six events, performs a time-delay function at one of the events, incorporates a safe-arm function, includes a toroidal transformer for telemetry information, and is electrically integrated into the over-all spacecraft system.

Originally, the squib firing assembly was only required to act as a power amplifier for the CC&S by switching battery power to the squibs upon command from the CC&S. There were five time-separated events: (1) solar-panel deployment, (2) gamma-ray boom deployment, (3) midcourse motor ignition, (4) midcourse motor shutoff, and (5) deployment of the low-gain and altimeter antennas.

A basic design problem developed because of the following circumstances: (1) the CC&S did not remove the event-initiating command; (2) an unpredictable number of squibs yielded a post-fire electrical short condition; and (3) current from the main battery had to be limited both in magnitude and time. It then became necessary to have the design of the squib firing assembly incorporate a built-in pulsing network, such that both squib firing current and command current would be turned off after the squibs had been fired.

A time period of 1 to 2 sec is sufficient to ensure squib firing, yet short enough to minimize power drain from the battery. The peak current demand from the battery, at a given event, is controlled by the choice of suitable current-limiting resistors in series with the output to each squib. Individual current limiting is also required to prevent a fired and shorted squib from bypassing available current from non-fired squibs during the 1-sec gate time of an event.

Due to the changed requirements elsewhere in the spacecraft system, the squib firing assembly picked up many new functions, not initially envisioned. It was determined that Event 5 (deployment of the low-gain and altimeter antennas) had to be delayed by 2 min. Rather

CONFIDENTIAL

than add an event to the CC&S, it was decided to incorporate a 2-min delay in the squib firing assembly. Also, upon determining that the CC&S could not switch the required current to the lunar capsule system for the altimeter turn-on event, it was decided to add this function as Event 6 in the squib firing assembly.

AMR range safety required that a safe-arm feature be incorporated into both the spacecraft and capsule systems to reduce the probability of premature firing of the midcourse motor, or premature actuation of the capsule system (which would eventually result in firing of the retro-motor by the capsule timing system). A safe-arm function was added to the squib firing assembly, so that all spacecraft pyrotechnic devices were "safed." The system is armed by actuation of an inertial switch during the *Atlas* boost phase of the flight. The "safed" voltage was routed to the lunar-capsule system to supply power for the pyrotechnic events associated with the altimeter fuzing (firing of the separation clamp bolt cutters and firing of the squib switches in the power and sequencing assembly).

Because of weight considerations, it was requested that a toroidal transformer (located in the lunar-capsule system) be moved into the squib firing assembly. The primary of this transformer was in series with the "safed" voltage line to give indication of current delivery at the altimeter fuzing event. The transformer secondary was routed to the data encoder to yield telemetry readout on event channel B2(2). The requested change was made; however, the transformer primary was relocated so that squib firing current was detected at all SFA events, rather than at only the altimeter fuzing event.

Sometime later, additional changes were incorporated into the squib firing assembly functional requirements, although the design was ostensibly frozen.

The first of these changes consisted of the addition of a squib-actuated device to unlatch the vidicon lens cover. It was originally planned to add this function to SFA Event 4. However, due to thermal considerations, it was found to be undesireable to open the lens cover this early in the flight sequence. It was then decided to add the function to SFA Event 5. However, this event had a total load that already approached the maximum current capabilities of the battery at this point in the flight sequence. During the investigation of this problem, it was learned that only one latch was required on the low-gain antenna deployment device; the vidicon latch was then substituted for the low-gain antenna latch.

Due to the possible battery load problem which still existed, it was decided to split SFA Event 5 into two subevents by delaying the firing of the redundant squibs on the devices associated with this event. This change was relatively easy to accomplish because the squib firing assembly already delayed this CC&S command for 2.0 min. The resulting configuration had SFA Event 5A delayed for 2.0 min and SFA Event 5B delayed for 2.5 min after receipt of the command.

After RA-3 had been shipped to AMR, one more change was made in the pyrotechnic subsystem. The reason for this change follows:

A retractable heat shield was used on the lunar-capsule system retro-motor. The lanyards which hold the shield in place are released when the omni-antenna is deployed. The system design was such that the omni-antenna was deployed at the same time as the altimeter antenna. It was believed certain that fouling of the radio altimeter by the heat shield would occur.

The deployment of these antennas occurs at SFA Event electrical channels. In the design that existed at this time, SFA Event 5A occurred 2.0 ± 0.2 min after command, at which time current was switched to one squib on the omni-antenna pinpuller, one bolt cutter on the altimeter antenna, and one squib on the vidicon lens cover pinpuller. SFA Event 5B occurred 2.5 ± 0.2 min after command, at which time current was switched to the second squib on each of the redundant devices mentioned.

Because of the *Ranger* schedule and the certainty and seriousness of the problem, the following fix was made:

The output from SFA channel 5A was routed to both bolt cutters on the altimeter antenna. The output from SFA channel 5B was routed to both squibs on the omni deployment pinpuller. The result was that the altimeter antenna would be deployed 0.5 min (nominally) before the omni was deployed and the thermal shield was retracted. The change was accomplished by replacing the existing squib harness with a redesigned harness.

A result of the fix was the fact that the redundancy was destroyed in the SFA electrical circuitry.

In summary, the RA-3, -4, -5 squib firing assembly (Fig 304) now incorporates the following functions:

(1) Arming of the system during the *Atlas* boost phase of the flight. Upon arming, the "safed" voltage is supplied to the lunar capsule system.

(2) SFA Event 1: Solar panel deployment (4 pinpullers, 8 squibs).

CONFIDENTIAL

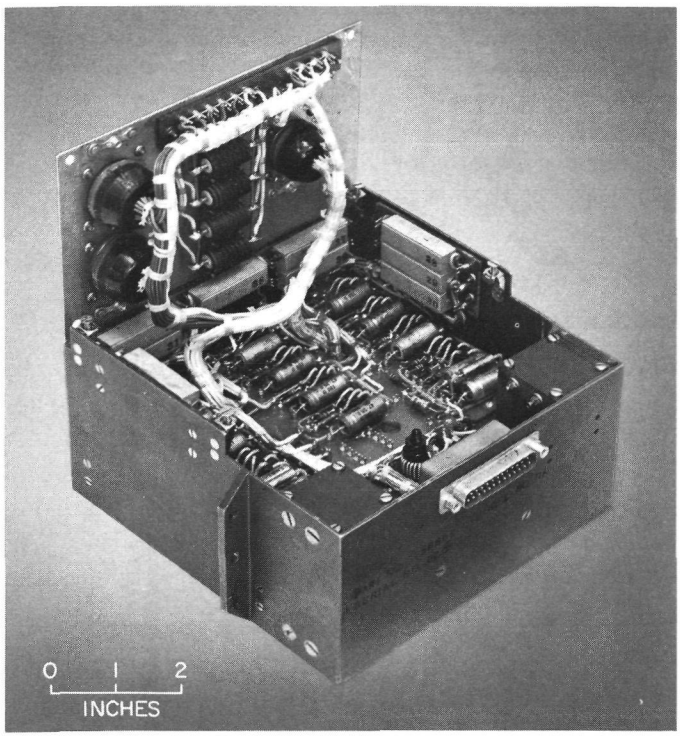

Figure 304. RA-1 squib firing assembly

(3) SFA Event 2: Midcourse motor ignition (3 valves, 3 squibs).

(4) SFA Event 3: Midcourse motor shutoff (2 valves, 2 squibs).

(5) SFA Event 4: Gamma-ray boom deployment (1 pinpuller, 2 squibs).

(6) (a) SFA Event 5A: Altimeter antenna deployment (2 bolts, 2 squibs). Uncover vidicon lens (½ pinpuller, 1 squib).

(b) SFA Event 5B: Omni-antenna deployment (1 pinpuller, 2 squibs). Uncover vidicon lens (redundant) (½ pinpuller, 1 squib)

(7) SFA Event 6: Turn on altimeter (1 thermal switch). Initiate scientific commutation (1 thermal switch).

Figure 305 is a schematic diagram of the RA-3, -4, squib firing assembly.

One major change was made in the RA-5 (and subsequent) system: this was the use of dual bridgewire squibs in the midcourse motor valves. The squib firing assembly for RA-5 was redesigned to implement this change. Figure 306 shows the RA-5 pyrotechnic subsystem block diagram.

c. Follow-on squib firing assembly. The *Ranger* follow-on missions require much simpler functional requirements for the squib firing asembly. The only pyrotechnic events for RA-6 through -9 are:

(1) Arming of the SFA during the *Atlas* boost phase.

(2) SFA Event 1: Solar panel deployment (4 pinpullers, 8 squibs).

(3) SFA Event 2: Midcourse motor ignition (3 valves, 3 squibs—dual bridgewire).

(4) SFA Event 3: Midcourse motor shutoff (2 valves, 2 squibs—dual bridgewire).

d. Design philosophy and problems. A conservative approach has been used in the design and development of the squib firing assembly. Maximum current demand on the spacecraft battery and minimum current delivery to the squibs are calculated on the basis that one-third of all squibs associated with a given event develop a zero-ohm short before the other two-thirds of the squibs have fired. Later experimental evidence indicates that this is a very conservative assumption.

The output load, as well as the comand current, is maintained for a period of 850±150 msec. The command signal is routed through the "normally closed" contacts of a magnetic-latching relay to the coil of a power-switching relay. Shutoff of the circuit is accomplished by feeding voltage from the output side of the power-switching relay to a R-C/UJT timing circuit; the UJT fires into the "turn-off" coil of the magnetic latching relay, thus removing the command.

The only problem encountered in the shutoff circuit was in the low-voltage, high-temperature operating mode. A change from 12-v to 6-v latching relays was incorporated into the design for the RA-5 and subsequent SFA units. It is expected that reliable shutoff operation down to 17 v at 65°C can be attained, without component selection. Operation down to 18 v at 65°C was reached on the RA-3, -4 SFA units, but component selection was required in some instances.

Selection and qualification of an inertial-arming switch type proved to be one of the most difficult problems encountered in the design and development of the SFA. Four types of non-latching inertial switches, obtained from three different manufacturers, were tested unsuccessfully. The failures ranged from slightly out-of-tolerance operation to intermittent non-operation before any environmental tests had been performed.

An MC-1107 inertial mechanical-latching, resettable switch was obtained from AEC/Sandia. Complete functional and environmental tests were performed with satisfactory results. Of approximately 20 switches tested,

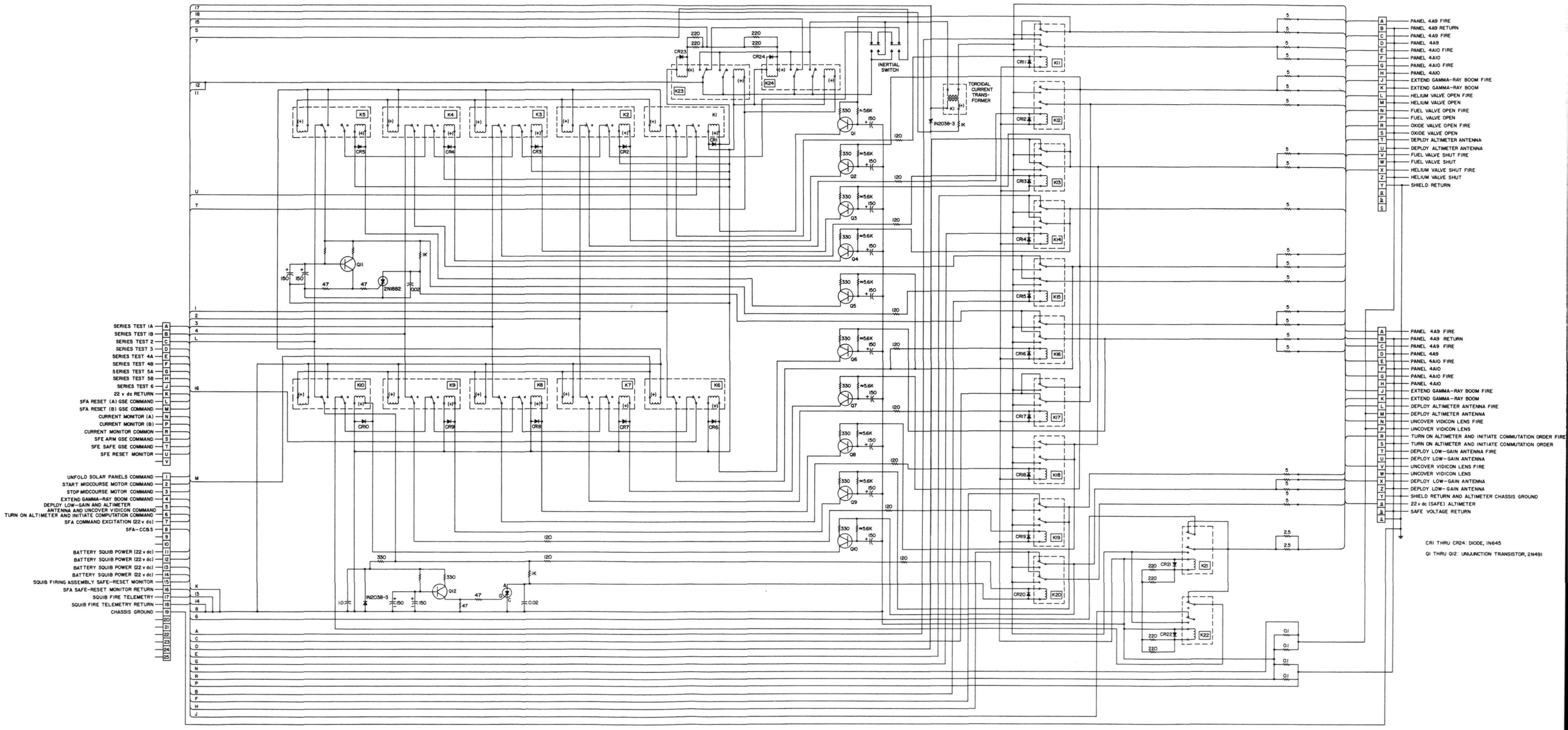

Figure 305. Squib firing assembly, schematic diagram

Page Intentionally Left Blank

only one indicated conditional out-of-tolerance operation, under a relatively severe environmental condition.

In the entire pyrotechnic subsystem, an attempt has been made to incorporate complete redundancy. In most cases, this goal has been achieved—with the exception of the fix required for the retromotor thermal shield problem on RA-3, -4, -5. Where redundant squibs cannot be used, as in the midcourse motor valves, a redesign has been instigated to incorporate dual bridgewire squibs; the effectivity of this change is RA-5.

A component screening program was started. Every component assembled into flight equipment has been subjected to a defined test. No failures or out-of-tolerance parameter changes of components have been detected on any flight unit, to date.

One undesirable design aspect exists in the pyrotechnic subsystem: squibs which short to case after firing will tie the spacecraft battery to frame ground. The positive side may be tied momentarily (until the shutoff circuit operates). The return side may have a permanent short to frame, which violates the spacecraft system grounding philosophy. There has been no confirmation that this shorted condition causes degradation in the spacecraft system. Repeated ground tests indicate that no undesirable effects should be expected in the flight configuration, except for transient effects which can be time-correlated with the event occurrence.

4. Mechanical Elements

a. Solar panel.

Actuation system. The solar panel actuation system on RA-1 and -2 was composed of one actuator, two hinges, and four latches on each panel. This system supports the panel during the boost phase of the trajectory and, on command, releases and extends it at a controlled rate. The system is operable in both 0- and 1-*g* gravitational fields.

Figure 307 shows the actuator and the two mid-point latches installed on the spacecraft. The actuator is mounted between the bus and the panel directly below Chassis IV, and the latches are mounted on the cross member above Chassis IV. The tubular panel alignment tool is shown in place between the latch bracket on the panel and the left-hand pinpuller on the cross member.

The system functions as follows: In the folded position, the panel is supported at six points (two hinges and four latches) to give it the proper dynamic characteristics to survive the boost phase. Panel opening is initiated by a controller command which triggers the squib power supplies. The power supplies fire the explosive cartridges at each latch, and the latch pins are retracted. With the latch restraints removed, the panel is free to move and the actuator pushes it into the open position, where it is locked.

In a 0-*g* field with the system at 80°F, the panel will open in about 45 sec. The opening time is affected by both temperature and load. Figure 308 is a plot of opening time as a function of temperature. Silicone oil is used for the damping fluid in the actuator in order to minimize the temperature sensitivity of the system. Panel position versus time is plotted in Figure 309 for 0- and 1-*g* loadings. Zero time is taken as the time of latch release.

The system performed properly on the flights of *Rangers I* and *II*. Operating times for the two panels were 188 and 150 sec indicating actuator temperatures to −5°F and +15°F, respectively. The difference in actuator temperatures was purposely produced by changing the heat radiating properties of one actuator. The panels on RA-2 opened considerably faster than on RA-1. Both panels opened in about 55 sec, suggesting actuator temperatures of 60°F. On this flight, the radiating properties of the two actuators were the same. The difference in actuator temperatures between the two flights is attributed to the fact that RA-2 was tumbling before and during panel opening, whereas RA-1 was not.

The RA-3 through RA-9 system configuration is the same as that described above, except for the latching. The major change was removal of the two latches at the tips of the solar panel and use of damping in the panel structure to control deflections. This in turn required minor changes at the remaining two latch points to handle the resulting larger loads.

This system performed properly on RA-3 flight. Panel opening time on this flight was between 41 and 141 sec. Since the "started opening" and "completed opening" signals were commutated, it is not possible to determine opening time to better than 100 sec.

Actuator. Figure 310 shows the actuator assembly. The principal parts of the actuator are the power spring, damping system, and three-part latch. The damping system is composed of a cylinder, piston (with orifice), rod, and volume compensator. Actuator characteristics are as follows: weight, 16½ oz; output (retracted), 150 lb, (extended), 30 lb; over-all length (retracted), 10 in.; stroke, 3⅜ in.; diameter (maximum), 2⅛ in.; operating time (unloaded at 80°F), 45 sec.

Two malfunctions were observed during the test program, neither of which, in itself, was severe enough to

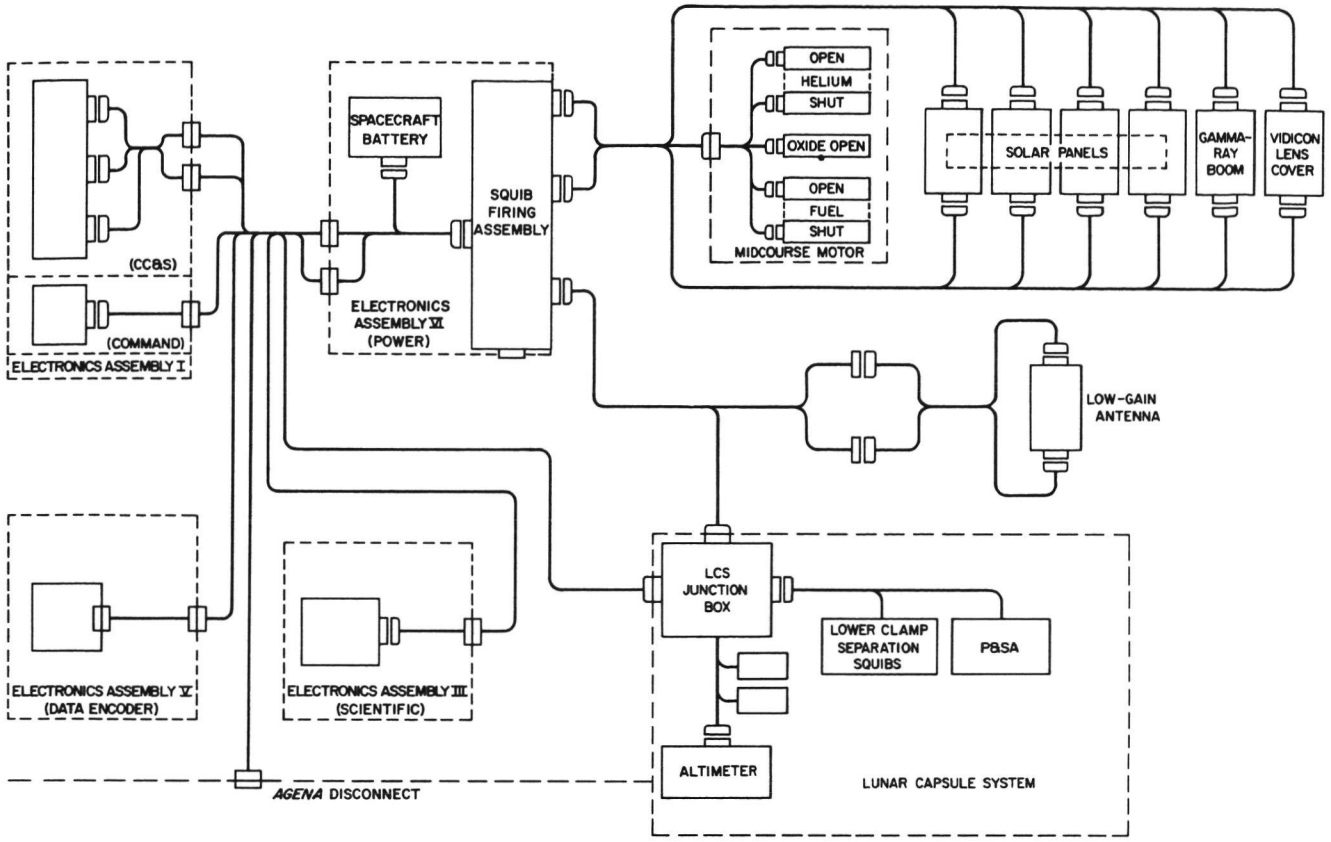

Figure 306. RA-5 pyrotechnic subsystem, block diagram

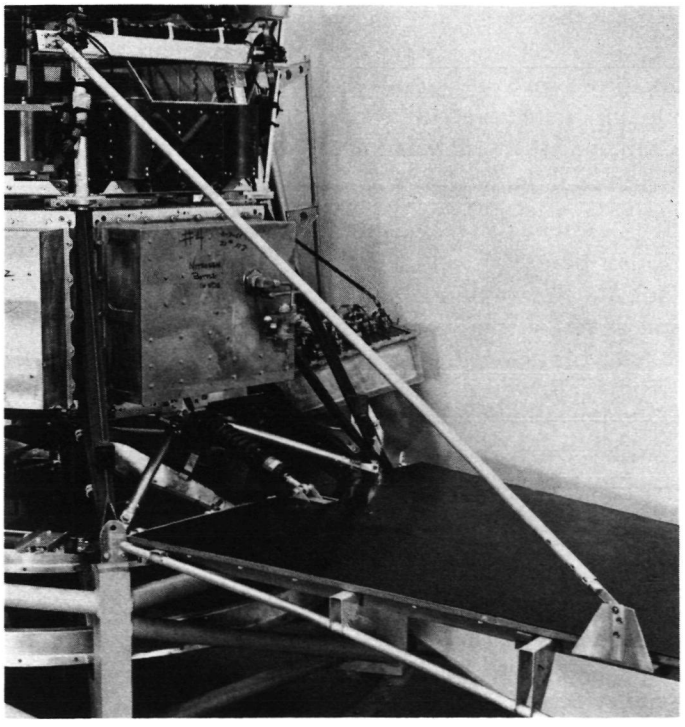

Figure 307. Solar panel actuator system

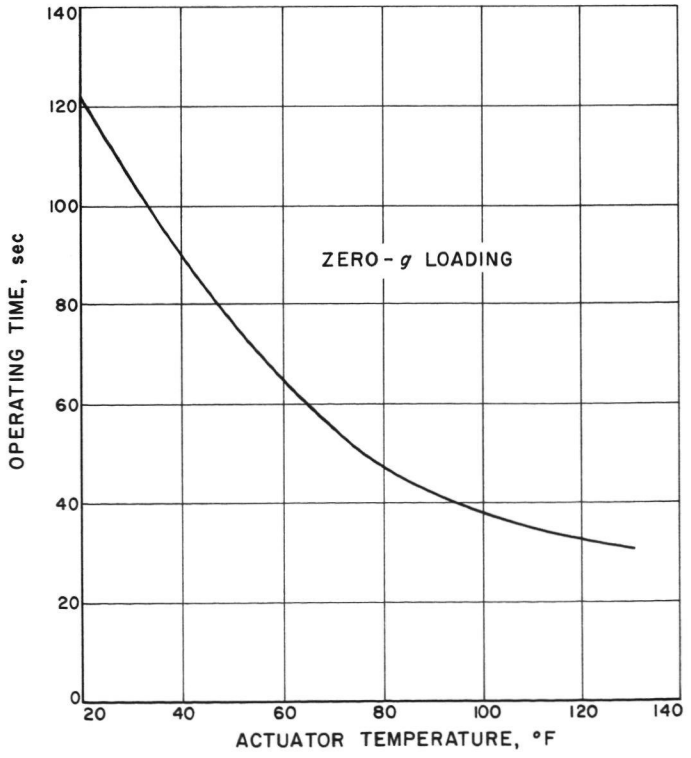

Figure 308. Actuator opening vs temperature

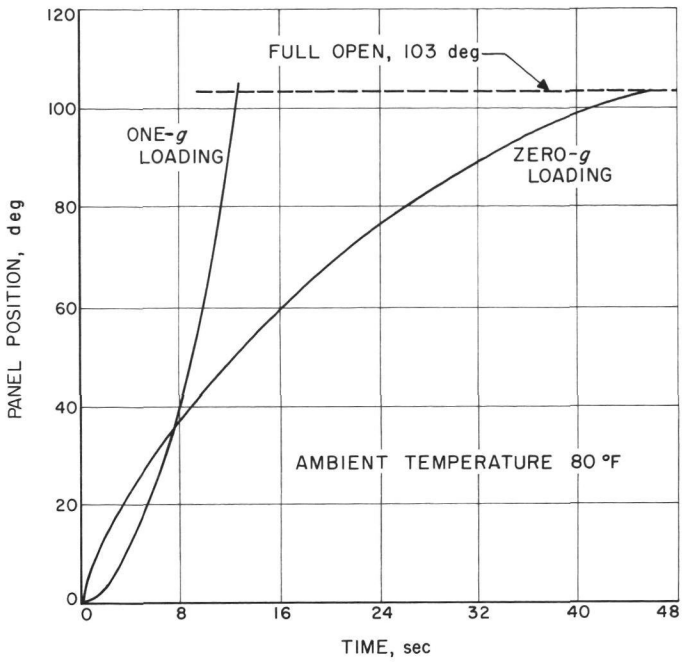

Figure 309. Actuator position vs time

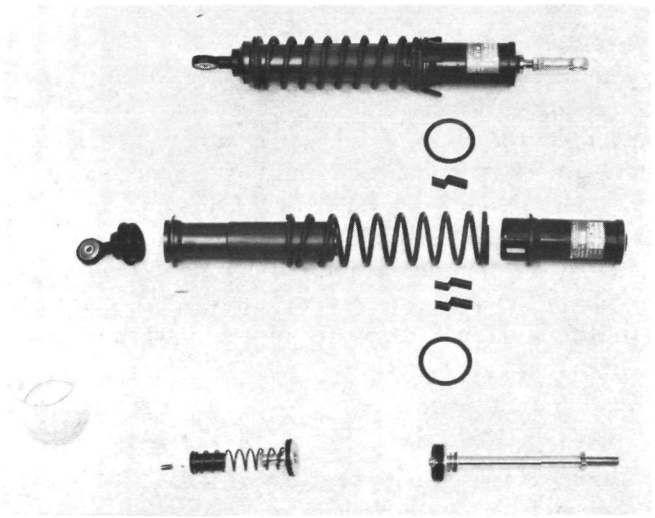

Figure 310. Solar panel actuator

cause a gross failure of the system. The first was excessively long and erratic operating time, caused by high friction loads between the barrel and the guide and was solved by coating the barrel with molybdenum disulfide. The second malfunction was a decrease in operating time of one actuator from the nominal 45 sec to about 20 sec. The cause here was found to be a dirt particle caught in the orifice; steps were taken to assure cleanliness in the subsequent units.

Latches. The solar panel latch assembly is shown in Figure 311 and consists of a pinpuller, tongue, ramp, and bumper-plunger. The tongue is permanently fastened to the solar panel and the other components are mounted on the forward structure. The pin of the pinpuller passes through a hole in the tongue and holds the tongue to the forward structure. The bumper-plunger takes up the clearance in the joint and, when the latch is released, supplements the actuator output force over the first ⅛ in. of panel motion. The ramp keeps the tongue on the bumper during boost and guides the tongue after pin retraction. The upper latch (shown) is connected to the panel through a slider shaft to permit compensation for thermal distortion. This feature is not required at the mid-point latch since thermal distortions here are less severe.

The RA-3 type latch is pictured in Figure 312. The ramp has been removed and both the tongue and bumper strengthened.

Components of the pinpuller are the body, integral piston and pin, and two explosive cartridges (Fig 313). Expansion of the gaseous products from combustion of the explosive on the pin side of the piston retracts the pin. O-ring seals are used in this unit to protect the cartridges from the vacuum of space and also to minimize the possibility of depositing combustion debris on the solar cells. One cartridge is sufficient to operate the pinpuller, but two are used to increase reliability through redundancy. The redundancy technique is also used in the cabling and squib power supplies, one cartridge and cable set per power supply.

Type-approval test results show that the operating characteristics of the pinpuller are not affected by *Ranger*

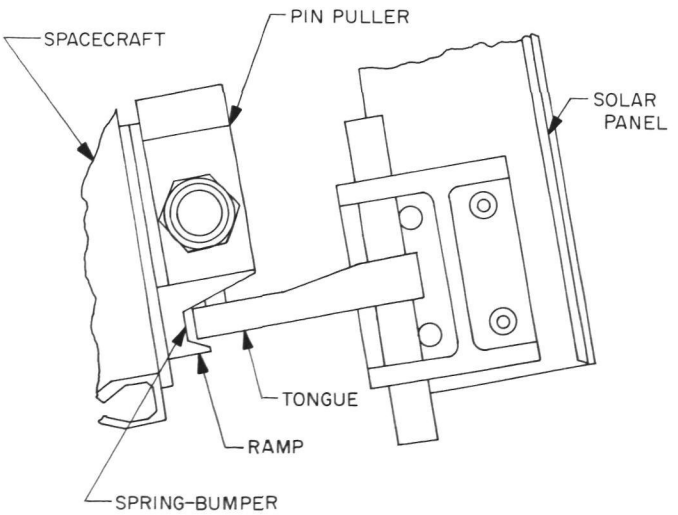

Figure 311. RA-1 upper solar panel latch

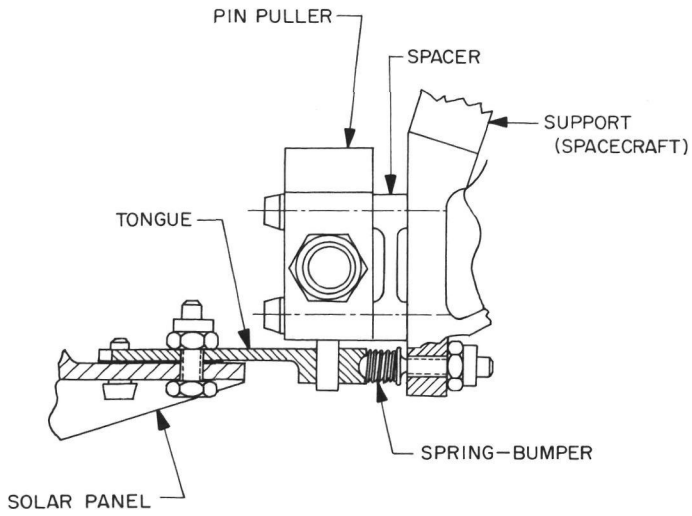

Figure 312. RA-3 solar panel latch

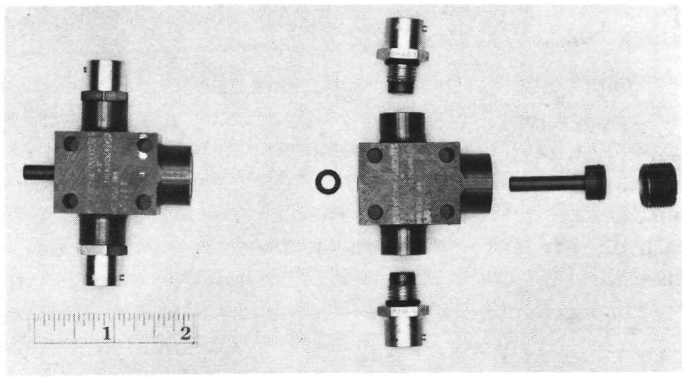

Figure 313. Pinpuller assembly

environments. Supplementary tests, however, indicated two weaknesses in this pinpuller. First, the O-ring seal at the pin was not adequate to prevent all hot gas leakage. Leakage past this seal has been observed in about half the firings. While the operation of the pinpuller is not jeopardized by this leakage, it does present a hazard if operated in the presence of an explosive atmosphere which may exist when the shroud is in place around the spacecraft. However, the pinpullers are not required to operate while the explosive atmosphere is present and with the proper safety features in design and procedure, this leakage should not be a problem.

Second, the original glass-to-metal seal in the cartridge was excessively porous, and in about one-fifth of the firings, leakage past this seal was observed. This problem could jeopardize the proper operation of the pinpuller, since a leak here before firing would expose the explosive to the vacuum of space and possibly cause a misfire. The cartridge vendor, in cooperation with JPL, has corrected this problem. For assurance, JPL has required helium leak detector inspection of the seals prior to loading the explosive.

b. SCRE boom actuation system. To satisfy the look angle requirements of the RA-1 and -2 solar corpuscular radiation experiment (SCRE) without violating the constraints imposed by shroud envelope and boost vibration, one of the three SCRE packages has been mounted at the end of an extendible boom. The opposite end of the boom is attached to a foot of the basic structure through the spring-powered boom actuator.

During the initial portion of the trajectory (through *Atlas* and *Agena* burn) the boom is held close to the spacecraft by the latching system as shown in Figure 314. After spacecraft separation, an electrical signal releases the latch. The actuator is then able to rotate the boom until its axis is perpendicular to the roll axis of the spacecraft. When this position is reached, a locking pin in the actuator drops into place and prevents further rotation. A hydraulic damping system has been built into the actuator to control the rate of rotation.

The system performed properly on *Rangers I* and *II*. Operating times were 88 and 43 sec, respectively.

Actuator. Figures 315 and 316 show the actuator and its components. The principal parts are the drive shaft, power spring, linear damper, volume compensator, locking pin, and housing. The boom is attached to one end of the drive shaft and the damper is connected to the other end through an eccentric. The torsional power spring fits around the shaft. One end of the spring is referenced to the housing and the other to the shaft. The damper is similar to the system used in the solar panel actuator and, in fact, many of the parts are interchangeable.

Several sources of high friction were encountered in the development program. All but one of these were the result of the small clearances between drive shaft, power spring, and housing and were eliminated by positively locating the radial position of the power spring. In addition to these problems, it was found that thrust loads caused an undesirable reduction of output force. This problem was solved by adding a teflon lubricating washer between the thrust collars on the shaft and housing. Characteristics of the boom actuator are given in Table 71.

Boom. The boom is fabricated from a 1.5-in. OD aluminum tube with a fitting at one end to adapt to the actuator and a bracket at the other to mount the experiment. Over-all length is 42 in. No problems have been found with the boom.

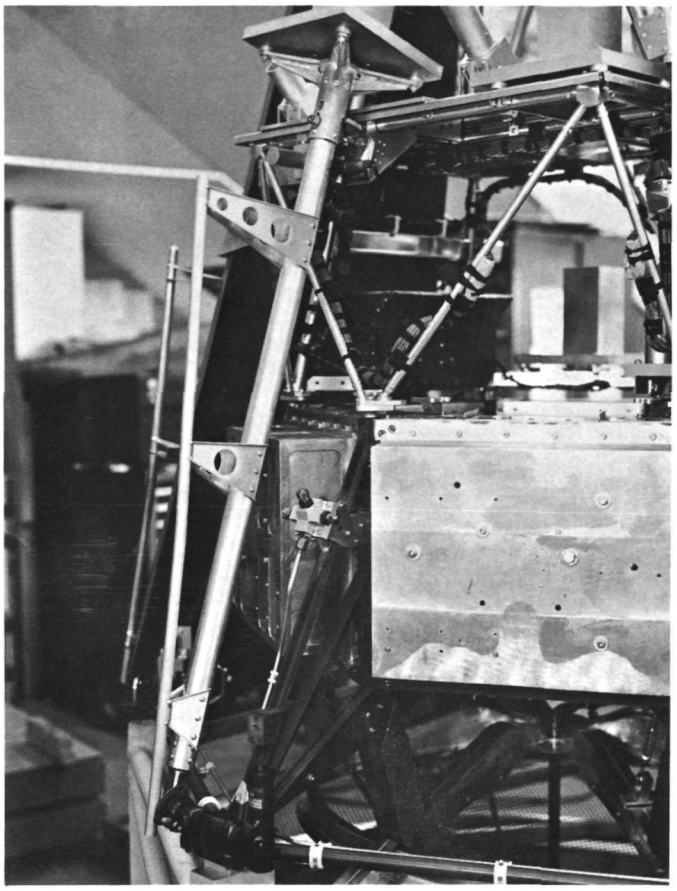

Figure 314. Boom assembly

Table 71. Boom actuator characteristics

Weight, lb	1-6
Output torque, in.-lb	
retracted	67
extended	36
Operating arc, deg	108
Operating time, sec[a]	
80°F	30
0°F	97
140°F	18

[a]Zero-g loading.

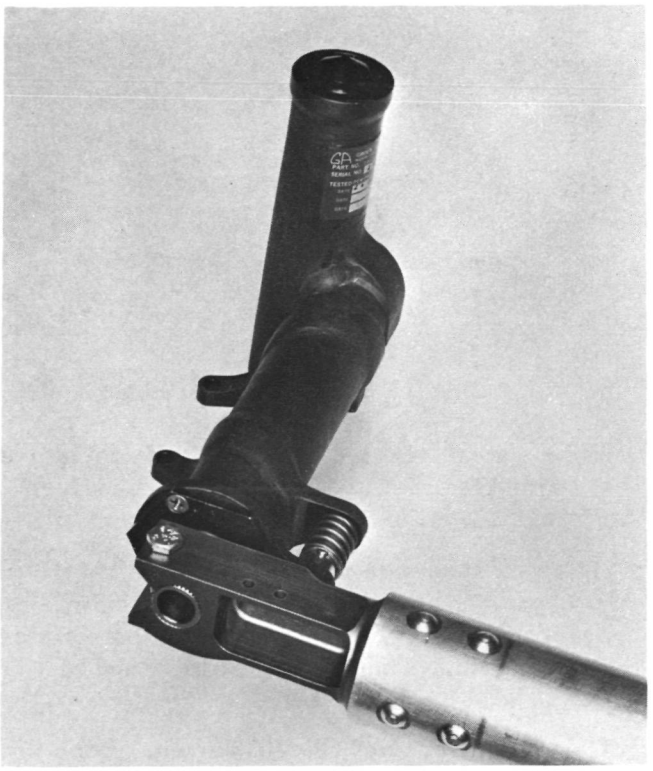

Figure 315. Actuator assembly

Latch. In the folded position, the boom is latched (Fig 317) at the forward structure by an eye-bolt-retractable pin arrangement. The retractable pin is part of the explosively actuated pinpuller described in detail as a component of the solar panel actuation system. The effective length of the eye-bolt is adjustable so that the boom can be pulled in tightly against the rubber-covered semicircular yoke. This latching technique has proved satisfactory.

c. Omni-antenna support and development system.

Design and test. Initially, a series of design studies was undertaken to determine the most reliable and lightweight omni-antenna support system for RA-3. An alternate antenna location from that used on RA-1 was first investigated. A technique which showed promise involved placement of a redesigned antenna on the tips of the solar panels; however, this would have involved significant system modifications and was subsequently dropped. The remainder of the studies considered only those techniques involved in placing the antenna forward of the lunar capsule and resulted in the following conclusions:

(1) The omni-antenna would be the type flown on the *Pioneer III* and *IV* payloads. This configuration is compatible with the *Ranger* communication system, has a similar r-f pattern to the RA-1 antenna, is flight proven, and is approximately 3 lb lighter.

(2) The omni-antenna was moved aft (along the roll axis) of the RA-1 position to the proximity of the lunar capsule. Specifically, this results in a considerable weight saving with a small decrease in performance.

(3) The lunar capsule served as the primary structural support of the omni-antenna. An auxiliary boom connected to the antenna served to deploy it after

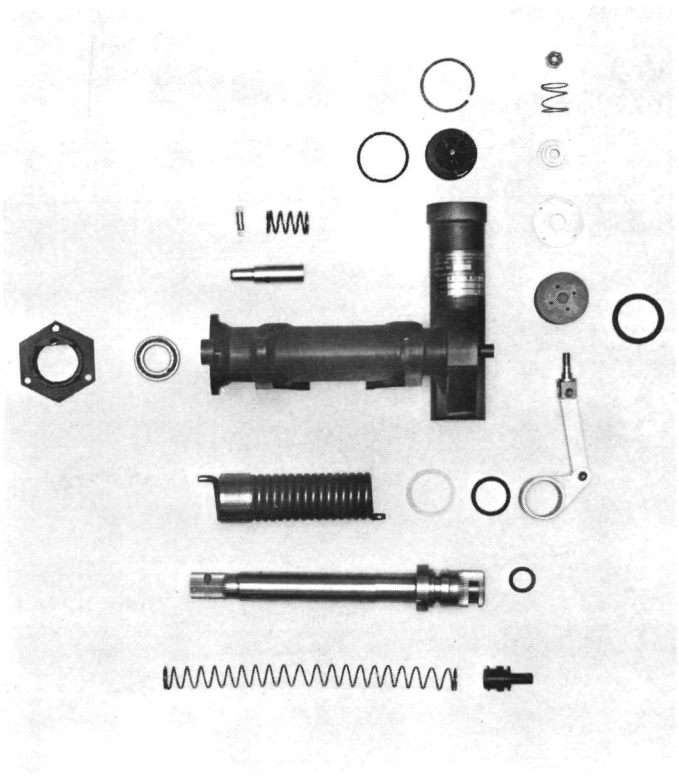

Figure 316. Actuator disassembled

separation from the capsule. This boom also supported the r-f cable and the squib circuitry for the ordnance devices in the separation joint.

(4) This system reduces to a sequence of two events: separation and deployment. The reliability of these events has been maximized in that ordnance devices and actuators can be used which have been qualified for use on RA-1 and -2.

The design involves the attachment of the omni-antenna through an adapter to a Marman-clamp-type separation joint. The lower half of the joint is firmly fixed to the impact limiter of the lunar capsule. The clamp is held in position with a single pinpuller attached to the adapter. The pinpuller is activated by either of two squibs. Also attached to this adapter is a curved boom of circular cross section. The lower end of the boom is fixed to a damped torsional spring actuator which, upon separation of the antenna from the impact limiter, deploys the antenna to a new location which has an axis at 45 deg to the vehicle roll axis. The boom is designed so that its natural frequency in the closed position is higher than that of the first bending mode of the lunar capsule. Its stiffness, however, when compared with the capsule is much lower and, thus, presents no significant structural inputs to it.

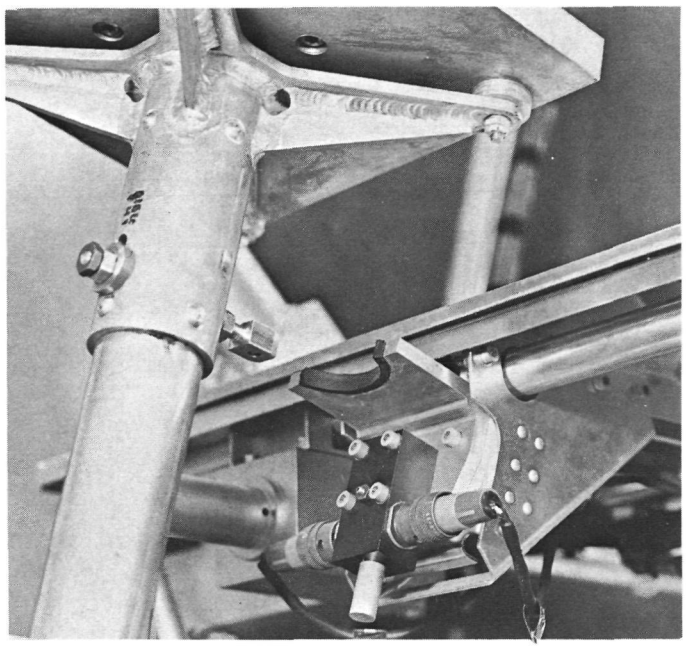

Figure 317. Boom latch

A dynamic test involving the lunar capsule and an early model of an omni-boom was conducted at Aeronutronic in May 1961. The purpose of this test was to establish whether or not any serious dynamic cross coupling existed between the two units. It was demonstrated that neither system significantly affects the other, with natural frequencies and gains at resonance remaining the same. Several prototype units have been fabricated of which one was delivered for assembly to the proof-test model. Another unit was assembled to a flight type omni-antenna and underwent complete type approval testing in July. All rotary actuators for RA-3, -4, and -5 successfully passed type-approval and flight-acceptance testing.

Omni-antenna cable. Two problem areas were noted in the fabrication and assembly of the coaxial cable into the omni-antenna boom. These were identified as follows:

(1) Because of vibrational loads, the cable must be supported at least intermittently inside the boom.

(2) The cable must be supported axially to minimize the load on the connector pin attachment points.

To damp the vibrational loads, it was decided to use semi-resilient spacers attached to the cable. These spacers were dimensioned to have a nominal interference fit with the boom of 0.010 in. They must also be stable at 125°C, resilient enough to pass through a necked-down portion of the boom (ID 0.93 to 0.80 in.), and as lightweight as possible. The material selected was Emerson and Cum-

ming's Eccosil 4640, a silicone rubber syntactic foam (i.e., the silicone rubber is filled with 150-micron hollow glass spheres). The density is, therefore, reduced to 40 lb/ft^3. Samples of the Eccosil 4640 were cast and evaluated. Except for a rather low tear resistance, the material was acceptable.

Before a mold could be designed and fabricated, a cable assembly had to be made for the PTM. Two alternate materials for the spacers were proposed:

(1) A medium sponge neoprene (AMS-3198).

(2) A medium sponge silicone rubber (AMS-3195).

Because of availability, the former was selected and bonded to the cable with a neoprene adhesive. A prototype assembly was made and exposed to 125°C for 24 hr with no deleterious effects noted. The cable, together with the two squib leads, was assembled into the boom without undue difficulty.

To provide axial support, a collar attached to the connector was bonded to the cable. Because the cable shielding had to be grounded carefully into the connector prior to application of the adhesive, a special bonding technique had to be used. An annular clearance of only 0.010 to 0.015 in. between the cable and the connector sleeve required that a 0.063-in. hole be drilled into the sleeve to permit introduction of the adhesive.

Electrical coating of the antenna cone. A high rejection rate was encountered in the bonded gold and silver electrical coating for the fiberglass RA-3 omni-antenna cone. The difficulty was in obtaining a sufficiently sensitized surface by chemical means so that adherent copper, silver, and gold electroplates result.

A recently initiated backup technique consists of adhesive bonding 0.001-in. silver foil to the fiberglass surface, high temperature soldering (antimonial tin) a doubler to the longitudinal seam to maintain electrical continuity during the RA-3 aerodynamic heating phase, followed by gold electroplating.

Other processes being evaluated for possible immediate or future use are:

(1) Gold plating of electrically conductive (70% Ag) epoxy soldered (Ecobond 56) fiberglass.

(2) Electroless precious metal deposition onto fiberglass.

(3) Flame spraying precious metals onto fiberglass treated with special adhesives.

(4) Elevated temperature firing of precious metal organic compounds.

RA-6, -7, -8, and -9. The follow-on spacecraft are not required to survive a landing on the Moon. Therefore, it is not necessary to deploy the omni-antenna during the mission and, consequently, these spacecraft will have no omni-antenna boom or boom actuator.

d. Gamma-ray boom.

RA-3, -4, -5. A pneumatically driven telescoping boom for the RA-3, -4, and -5 gamma-ray experiment has been developed by Groen Associates, Inc., Sun Valley, California, and JPL. The boom mounts on top of the spacecraft hex, and extends following the midcourse maneuver. The 6-ft extension reduces background gamma-ray count in the instrument caused by proximity to the spacecraft mass.

The boom consists of three 2-ft sliding tubes and one stationary tube housing mounted concentrically and sealed to retain internal pressure. A latch mechanism retains the boom in the retracted configuration, and for release utilizes an explosive pinpuller identical to those used for release of the spacecraft solar panels. The central tube serves as the pressure chamber and is charged to 100 psi with dry nitrogen. An annular flow restrictor is employed to control flow of the pressure charge from the central tube during actuation, thereby controlling actuation speed.

Double O-ring packings are used on all sliding seals; the rings are Viton A material, which has good vacuum and high-temperature characteristics, acceptable permanent set, and good resistance to abrasion. The lubricant used is F-50 silicone oil. The unit includes a small helical bourdon tube pressure gage for pre-launch monitoring. Comparison of successive enlarged photographs of the gage yields quite accurate pressure monitoring—to approximately ± 1 psi.

The boom extends 6 ft from the fully retracted to the extended position; its collapsed length is approximately 30 in. Diameter of the boom is 2½ in. and its weight is 5 lb.

A cable dispensing device was also developed to allow the instrument cabling to extend as the boom extends. A flat strap cable is used for flexible, controlled deployment. A microswitch is incorporated in the dispenser to provide telemetry confirmation of boom extension.

A plexiglass vacuum chamber 9 ft long and 8 in. in diameter was constructed in which to test the boom. The

complete flight boom can be actuated in this apparatus. Vacuum condition of 0.1 mm Hg or less can be produced, which is adequate for functional testing, and zero-*g* condition is accomplished by supporting the simulated detector mass on a monoball caster free to roll on a leveled surface. The entire functional cycle may be witnessed through the walls of the chamber and instrumented through fittings and connectors provided for this purpose.

The gamma-ray boom extension event was changed from before midcourse maneuver (8 hr after launch) to 2.5 hr after midcourse maneuver initiation (timed from the beginning of the maneuver), to prevent an incompatible center of gravity for the maneuver in the event that the boom failed to extend. The extension system has also changed in design. The boom is now a telescopic tube, gas-activated. This change allows the gamma-ray spectrometer to be extended out the distance required for the experiment without the problem of a double-articulated arm.

RA-6, -7, -8, and -9. These spacecraft will carry no gamma-ray spectrometer experiment. This change causes a slight modification in the solar panel latch support structure which supported the gamma ray boom on RA-3 and -4. The latch structures on both sides of the spacecraft will be the same.

e. Capsule separation sensor. In order to provide a secondary capsule separation input for RA-3, a separation sensor was mounted on the midcourse propulsion propellant tank. An analysis of the attachment problem indicated that adhesive bonding would be preferable and that the adhesive system should have the following attributes:

(1) High shear and peel strength.

(2) Good vibration resistance.

(3) Heat resistance (125°C for 24 hr).

(4) Hard vacuum stability.

(5) If possible, nonnutrient and sporicidal.

The propellant tank was annealed 6Al-4V titanium, while the separation sensor body was 6061-T6 aluminum. Three adhesive systems were considered: (1) a filled epoxy (Armstrong A-g), (2) a silicone rubber (Products Research Corp. PR-1930), and (3) a polyurethane (Products Research Corp. PR-1927).

Because of its high peel strength, high temperature stability (300°F continuous service), shock resistance, and sporicidal characteristics, the polyurethane was selected.

The need for a heat resistant (<300°F), high peel strength adhesive which can be applied with contact pressure and cured at ambient temperature was apparent in this application. The materials selected met all the requirements but were formulated as a potting compound. Silicone adhesives are heat stable but have poor shear and peel strength. Epoxy adhesives, modified for flexibility, lose much of their heat stability. A polyurethane or possibly a polyurethane modified epoxy could be developed for high temperature (>300°F) adhesive joints, requiring flexibility.

5. Electronic Equipment Packaging

a. RA-1 and RA-2.

General. Packaging for the *Ranger* spacecraft electronic equipment has been influenced to a great extent by the need for a design which is versatile. This versatility is required in order to make the spacecraft capable of accepting equipment of various power dissipations, shapes, sizes, and operating environments. Nevertheless, it was considered advantageous to achieve an integrated design by using modular packaging for the electronic equipment.

The basic shape of the electronic equipment compartment used for RA-1 is shown in Figure 318. The compartment with the assemblies in the closed condition was originally designed to be capable of retaining 1 atmosphere of pressure. For the initial missions, the compartment was not sealed; however, it was felt that for subsequent missions it may be desirable to seal the compartment for the following reasons:

(1) *Temperature control.* Temperature limiting of the critical components could be accomplished by forced convection of air or other suitable gas contained within the spacecraft.

(2) *Electrical problems.* Electrical problems associated with high-vacuum conditions can be avoided by a pressurized compartment.

(3) *Materials problems.* Sublimation of some of the materials is known to occur under high-vacuum conditions; therefore, pressurization may be necessary.

Due to flight experience gained with *Rangers I, II,* and *III,* it now appears obvious that sealing will not be required.

In order to reduce the design and fabrication time, the *Ranger* subassembly chassis are uniform in profile and vary in width as necessary. Cables run down the center of the assembly and connect to the spacecraft harness

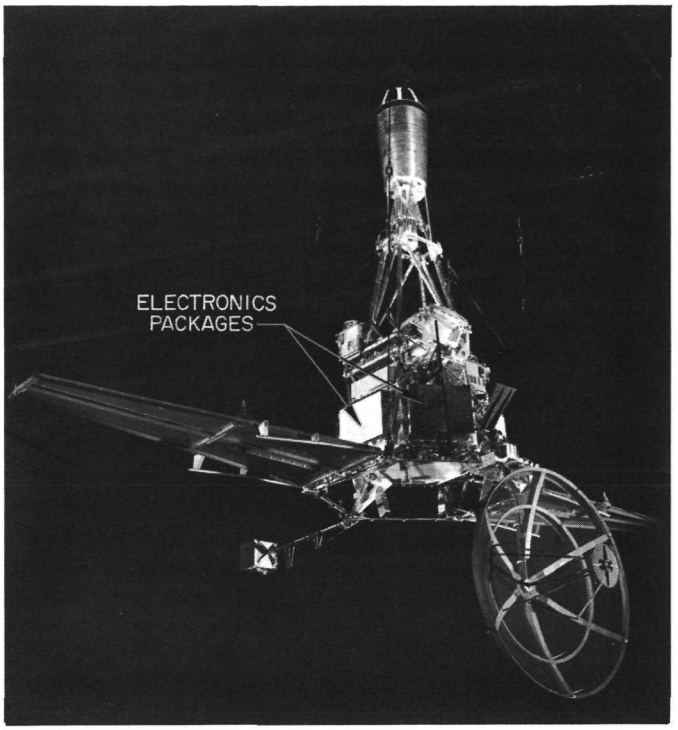

Figure 318. Spacecraft packaging

critical cabling, however, can be isolated from the main trunk. Use of subassembly chassis of uniform profile enables subassemblies to be interchanged from one assembly to another in order to accomplish mass and heat balance as required from flight to flight.

b. Equipment temperature control.

General concept. Temperature control of the electronic equipment was accomplished in the following manner for the *Ranger* flights: All heat dissipating parts conduct heat to the subassembly chassis which, in turn, is in good thermal contact with the assembly chassis. The heat is then rejected at a rate dependent on the absorptivity and emissivity of the outer surface of the assembly chassis. This rate is established to allow the equipment to operate under favorable temperature conditions.

Preliminary thermal testing. It was believed that sufficient surface area was available on the instrument compartment of the *Ranger* spacecraft to ultimately dissipate the heat generated within the compartment. There were many problems, however, associated with transferring the heat from the source to the external radiating surface while maintaining a satisfactory temperature distribution within the compartment.

As all of the heat transfer and distribution problems were made more severe by the necessity of operating in a vacuum, preliminary tests were conducted to determine the temperature differences that exist between a typical chassis operating at room ambient pressure and the same chassis operating under a vacuum of approximately 10 mm Hg. Thermal testing was conducted on typical chassis assembly equipment contained within the instrument compartment. The configuration consisted of eighteen subchassis in a typical chassis assembly fitted with a cover. Four of the subchassis had heat-dissipating resistors mounted on them. The power was adjusted so that 10 w was being dissipated on each of the four subchassis (40 w total). The assembly was then placed in a vacuum chamber at a pressure of 7×10^{-5} mm Hg and an ambient temperature of 78°F. Under these conditions the stabilized temperature directly under the heat dissipating resistors was 180°F and the outer surface temperature was 158°F.

The test was repeated using a vacuum grease (Dow-Corning-11) applied to the faying surfaces of the subchassis to determine if the thermal conductivity of the joint would be increased. Only a slight improvement was noted; however, the test was not considered conclusive.

The thermal tests were not comprehensive nor were they intended to replace any of the thermal tests to be conducted on the complete spacecraft. They were conducted to gain information on the basic method of cooling. This series of tests indicated that passive techniques for temperature control of the instrument compartment assemblies would be adequate, provided that a reasonable distribution of power dissipation between the various assemblies could be achieved.

c. Assembly chassis.

Vibration testing. The assembly housings used for RA-1 and -2 were vibration tested. These tests were conducted with both the aluminum and magnesium cast housings, of varying wall thickness, both loaded and unloaded. In general, the unloaded housings had their first primary resonance near 500 cps; again in general, the loaded housings had their first primary resonance at approximately 1000 cps. On the basis of these vibration tests, the nominal wall thickness of the assembly housings was reduced from 0.150 to 0.120 in.

A prototype chassis for the data encoder and controller electronics was used for further vibration testing in order to find the primary resonances of a typical chassis. Figures 319, 320, and 321 show the test setups, location of accelerometers, and type of loading. The weight of each subassembly (chassis and added weights) was adjusted to be 1 lb for the test. Tests were also conducted to determine the vibration characteristics of reduced weight

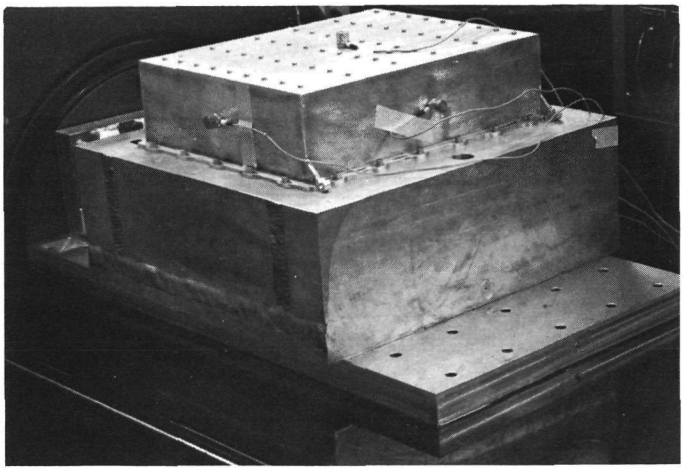

Figure 319. Basic chassis

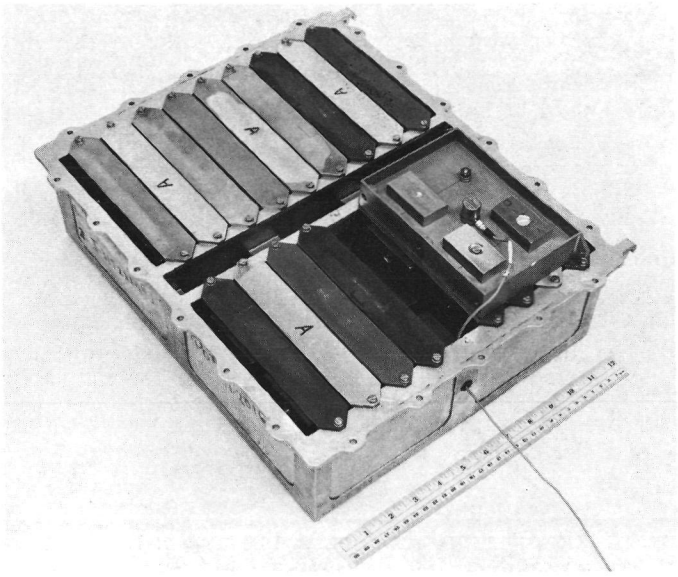

Figure 320. Thin-wall chassis

versions of the basic chassis where the weight was to be removed by machining the wall of the basic chassis. The first series of tests was conducted on a basic chassis as shown in Figure 319. The weight of this empty chassis was 6.25 lb. A second series of tests was conducted on a chassis with locally thinned walls, as shown in Figure 320, which weighed 5.00 lb. The third series of tests was on a chassis weighing 3.75 lb, which had holes machined through the walls of the chassis (Fig 322). The resonant frequencies along the sensitive axis for the three chassis configurations are shown in Table 72.

One of the original design considerations for the electronic chassis was the desirability of having the primary

Table 72. Test chassis resonant frequencies

Sensitive axis	Resonant frequency, cps		
	Basic	Undercut walls	Through holes
Transverse	550	510	400
Longitudinal	680	650	570
Vertical	630	600	520

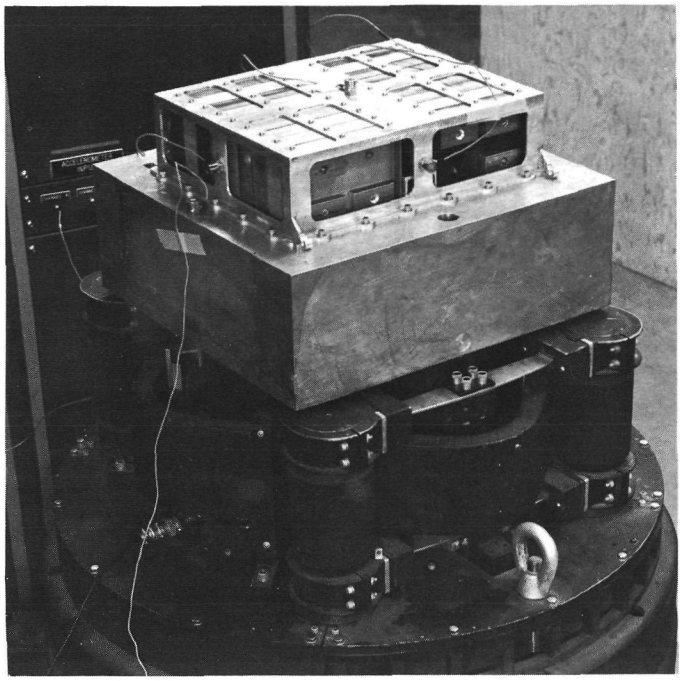

Figure 321. Ported chassis

resonant frequency as high as possible. Past experience with the design of this type of equipment has indicated that 500 cps is a reasonable goal for the primary resonance. Attempting to achieve a higher frequency generally results in severe weight penalty, and the acceptance of a lower first resonance frequency can jeopardize the reliable performance of the electronic equipment under a vibration environment.

On the basis of these design criteria, the partially thinned chassis (Fig 320) appeared to be satisfactory, whereas the completely cutout chassis (Fig 321) would have to be used with caution. Because of other field-handling difficulties with a perforated electronic assembly, only the basic (Fig 319) or the partially undercut chassis (Fig 320) was considered for the flight application

Chassis design. Figure 322 shows the six assembly chassis used for the RA-1 spacecraft. These chassis are

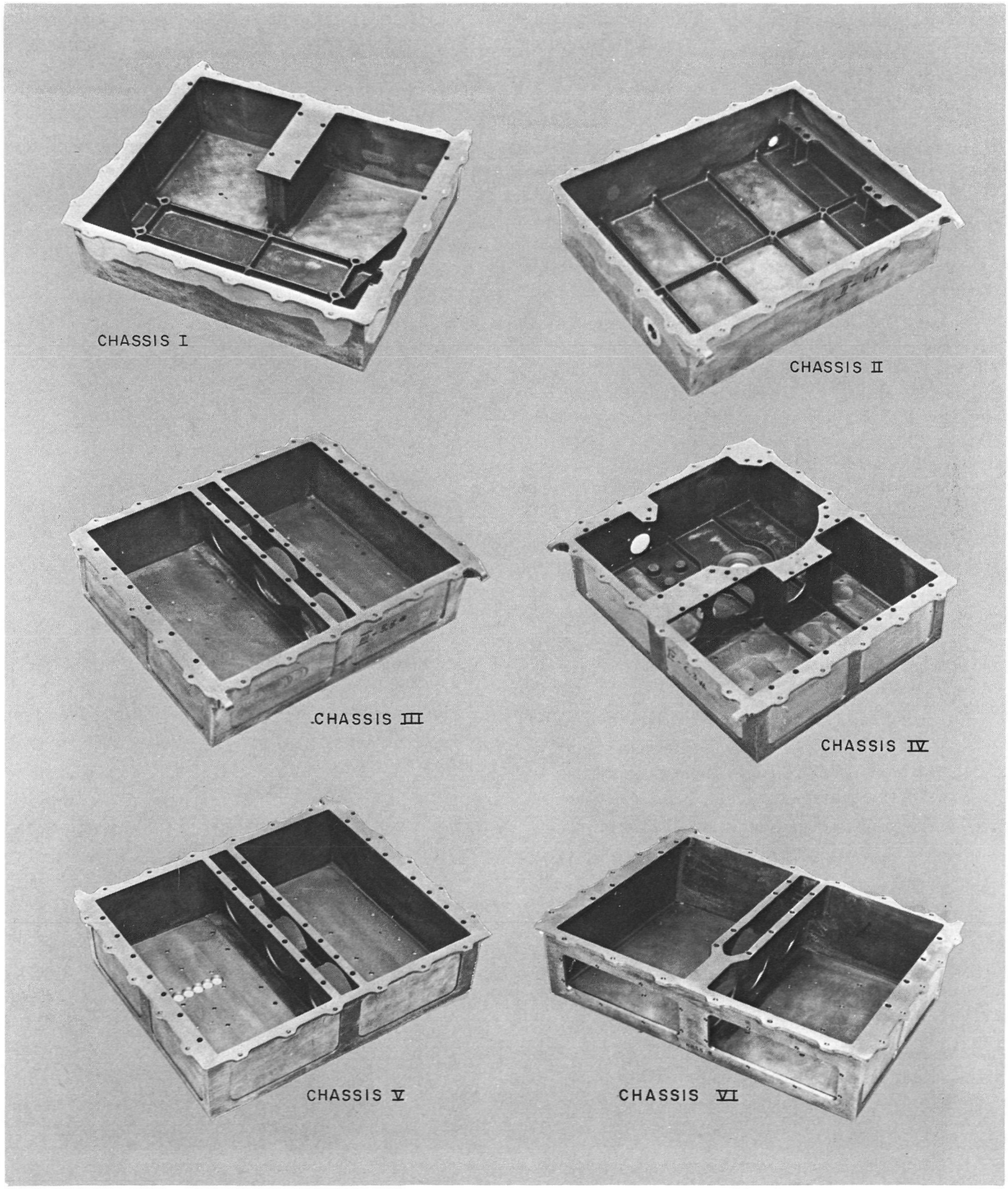

Figure 322. RA-1 and -2 assembly chassis

aluminum castings made from one basic external pattern. The internal configuration was modified to meet specific mounting requirements of the equipment to be contained.

Chassis I was modified for mounting the ¼-w transmitter battery. Chassis II was modified to accommodate the r-f cavities on the bottom surface and has mounting flanges for the transponder. A new design was completed which utilizes a standard assembly configuration for communications equipment. The transponder was divided into ten subassemblies of the standard profile, and the cavities were packaged into one subassembly of similar profile.

Chassis III was a standard assembly chassis; i.e., all subchassis in this assembly were of a standard profile. Chassis IV had the necessary modifications for mounting the attitude-control gas storage bottle and the gyro subassembly. Chassis V was also a standard assembly chassis. Chassis VI had two cutouts and the necessary angular modification so the triple coincidence detectors could look at the Sun during the flight. All six chassis were also machined in particular areas around the sides and the bottom to reduce weight.

d. Attitude-control assembly. Vibration tests of the RA-1 equipment indicated that the environment of the gyro subassembly in the attitude-control assembly was too severe. This environment was aggravated by the gas storage bottle; therefore, various means were explored to improve the bottle mounting:

(1) A stiffening channel was riveted on the outside of the chassis.

(2) The bottle was clamped with metal washers underneath the spider bracket hub.

(3) The bottom of the bottle was foamed in place.

(4) With the bottle foamed, washers were added as in (2).

(5) With the bottle foamed, sponge rubber dampers were added under the spider legs.

(6) To the condition described in (5), Aquaplas F-102-C coating was applied to the inside of the chassis walls.

At the end of these tests it was concluded that foaming alone as in (3) gave the best results.

The improvement to the gyro subassembly environment can be summarized as follows:

(1) The original design configuration gave a gain from 7.5 *g* noise input to 50 *g*. The foamed bottle reduced this gain to 35 *g*.

(2) The original design configuration showed the resonant frequency at 650 cps, and with the flight-acceptance vibration tape input, the peak output was 100 *g*. The foamed bottle raised the frequency to 750 cps and reduced the gain to 50*g*.

(3) The original design configuration showed some resonance in the 400-cps frequency range, which disappeared as a result of the corrective action.

These tests were performed with an empty subassembly chassis, with the bottle unpressurized, and without other pneumatic hardware, which ultimately is attached to this assembly. Further tests were conducted with complete flight hardware and with the bottle pressurized. The fix again proved satisfactory.

e. Primary battery. The primary battery was repackaged because of difficulties experienced with the original configuration during vibration and thermal testing. As a result of a study of these failures it was concluded that the new configuration should:

(1) Utilize internal stiffening to prevent excessive deformation of the chassis due to pressurization.

(2) Provide internal heat conduction paths from the cells to the exterior of the chassis.

(3) Allow potting of the cells in the chassis.

(4) Provide more attachment points to the battery support.

The new chassis (Fig 323) was machined from a forged billet of AZ80-F magnesium alloy and was subsequently surface treated per MIL-M-3171, Type III.

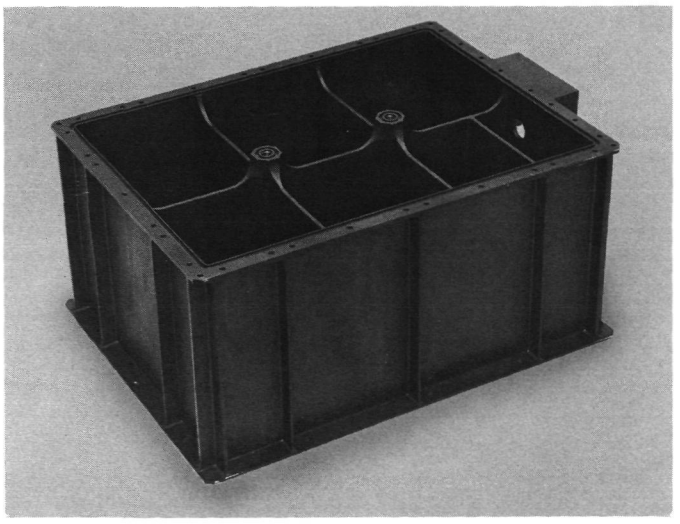

Figure 323. Primary battery chassis

A view of the inside of the chassis cover (Fig 324) shows the extruded rubber which was bonded to the ribs of the cover. When the cover was assembled to the battery this rubber was compressed against the top of the cells in order to retain the cells in the event the potting band should fail. Figure 325 shows the battery with cells potted in place and electrically connected.

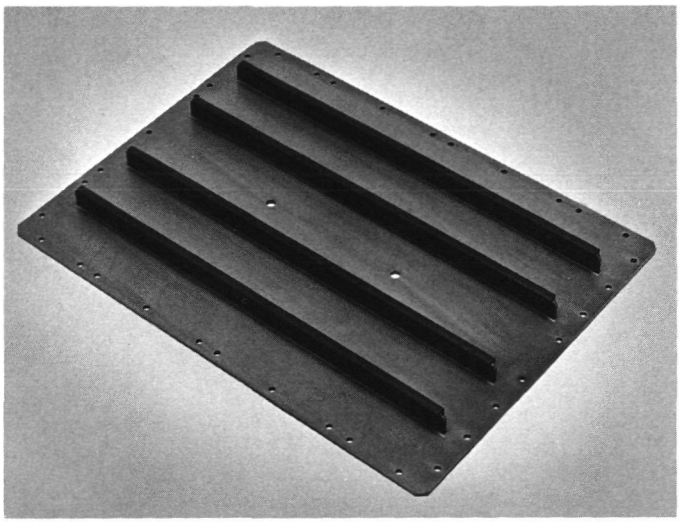

Figure 324. Battery chassis cover

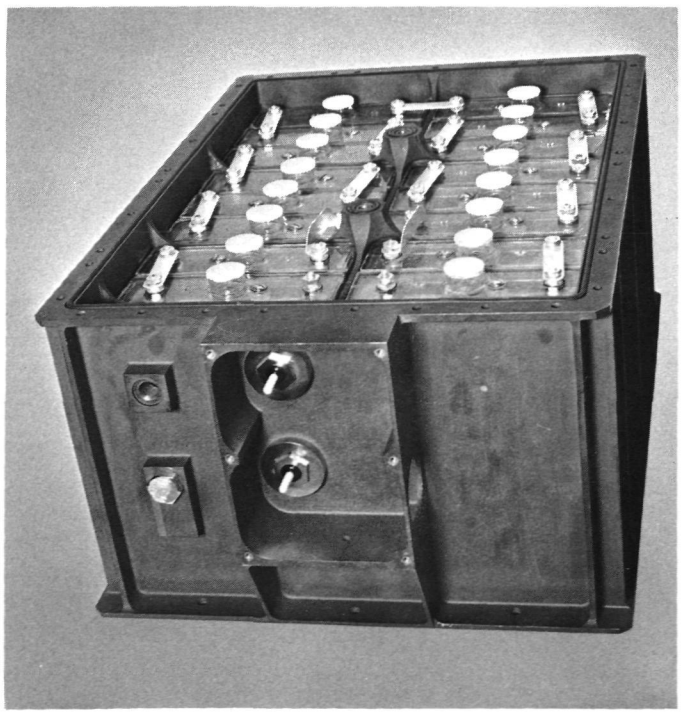

Figure 325. Battery internal configuration

f. Rangers RA-3, -4, and -5.

General. The packaging philosophy for RA-3, -4, and -5 was basically the same as that for RA-1 and -2. The major differences were (1) the use of magnesium for all chassis and subchassis to reduce weight, (2) the location of the primary battery within a chassis in the hexagonal compartment, (3) the removal of the attitude-control gas storage bottle from the chassis, and (4) mounting of the vidicon on the outside of the hexagonal structure which necessitates the use of a half box for the balance of the scientific equipment in the compartment.

The assembly chassis were required to have a high emittance surface on the exterior and a low emittance surface on the interior walls. In trying to conserve weight, several attempts were made to accomplish this requirement without plating and painting the interior surfaces. No other acceptable method was found; thus, interior side walls were painted after plating.

Weight reduction. Methods to reduce the weight in packaging of the electronic assemblies included changing to magnesium from aluminum for the assembly and subassembly chassis, and the removal of metal where not absolutely necessary; reducing the terminal board and insulating board thickness where feasible; changing to lighter weight encapsulation materials and more judicious application of the conformal coating which was applied to circuit boards. It was anticipated that these methods would afford a total weight reduction of approximately 30 lb. Figure 326 shows the standard RA-3, -4, and -5 chassis in magnesium. Figure 327 shows a lightened subassembly chassis with a 0.032 terminal board and 0.008 insulating board.

Chassis and subchassis parts machined from AZ31-B magnesium tooling plate were used for RA-3. The vibration environmental tests were made and, although some degradation was experienced in the magnesium parts as compared with RA-1 aluminum parts, the fundamental resonances (design goal of 500 cps) have been adequately high. The reason for the procurement of chassis (Figs 328 and 329) machined from tooling plate rather than the use of machined castings (as was done for RA-1 and -2) was to obtain a superior surface for finish and plating, thus alleviating some of the problems experienced on RA-1 and -2 equipment in attempting to achieve good temperature control surfaces.

Integration. The vidicon telescope assembly required considerable liaison between the vendor supplying the electronics and the two groups building the optics as a parallel effort. The original vendor proposal for the electronic packaging was not acceptable as it (1) lacked

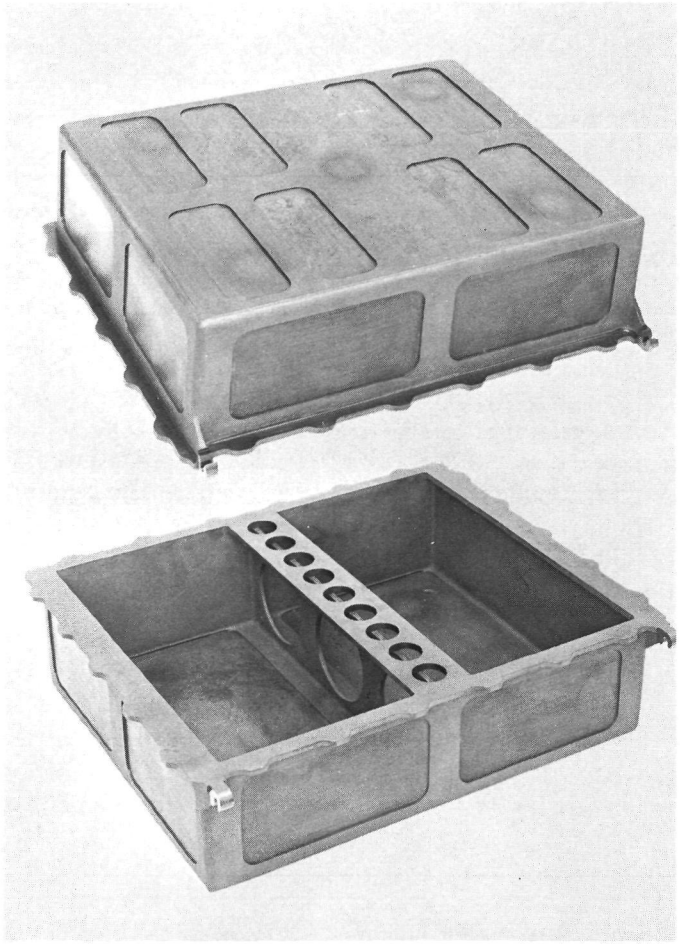

Figure 326. Standard RA-3 to -5 electronics magnesium chassis

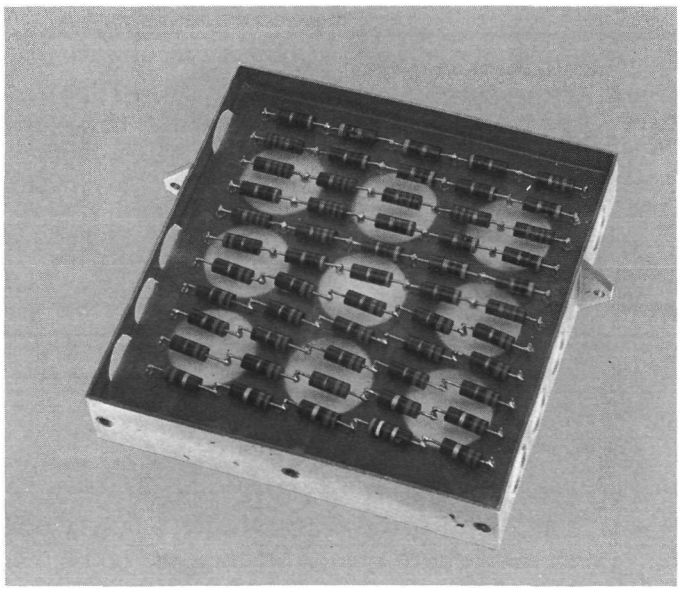

Figure 327. Lightened subchassis

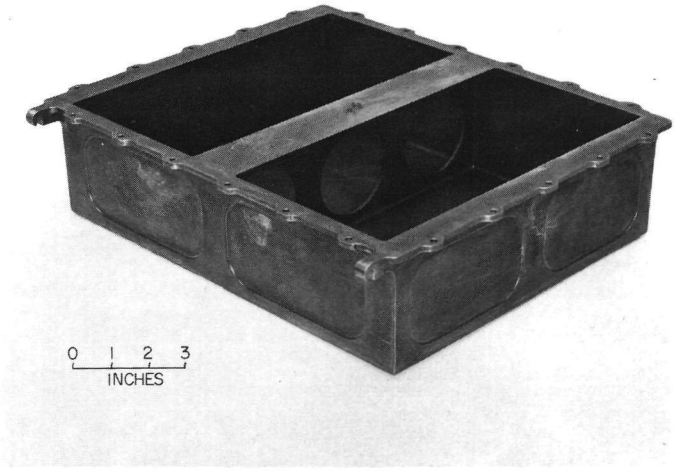

Figure 328. Chassis machined from tooling plate

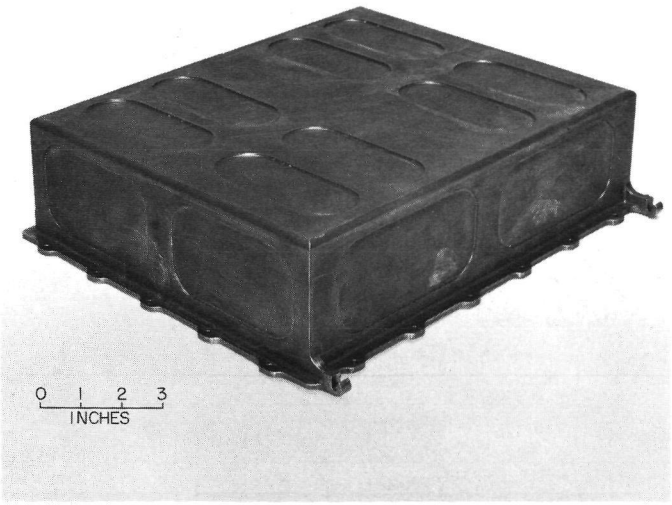

Figure 329. Chassis machined from plate

environmental reliability, (2) eliminated over 50% of the structural supports for one optic unit, and (3) required too great a volume because of poor packaging density. A proposal layout was then generated by JPL and presented to the vendor from which an acceptable package was agreed upon.

With the vidicon assembly outline defined, a physical interference was detected with the radar altimeter mounted above the hex structure proper. This necessitated relocating the vidicon assembly to Case III and the CC&S and command assembly from Case III to Case I. This relocation resulted in the vidicon and scientific assembly receiving the benefit of the solar load in Case III, which should improve the thermal performance of these units. The power assembly was moved to Case VI

to obtain the benefit of solar shading during the cruise portion of the flight.

Primary battery for RA-3, -4, 5. The battery for use in RA-3, -4, -5 was planned to be built directly in the chassis for Case VI. Although this required JPL to perform final machining and plating of this chassis prior to furnishing it to the vendor for fabrication of the battery, it resulted in approximately a 5-lb weight savings for the system as compared with a separate battery case which would be attached to the Case VI chassis with the consequent redundancy of structure. These chassis were machined and gold electroplated prior to being sent to the fabricator where the battery is potted directly into the assembly chassis (Fig 330). The booster–regulator subassembly was redesigned and required a slightly wider subchassis. This increase in size did not result in any other changes in this assembly.

g. RA-5, -6, -7, -8, and -9. In keeping with the requirement of limiting changes to those areas that contribute directly to the successful fulfillment of RCA TV mission and the S-Band ranging experiment, the major portion of the hardware associated with equipment packaging remains unchanged from the RA-3, -4, -5 configuration. However, there are some additions and changes which were necessitated due to the repackaging of the L-Band communications assembly, the replacement of the scientific instruments and telescope electronics assembly of electronics assembly III with the S-Band ranging experiment, and finally, the addition of scientific instruments for radiation measurements. The following brief summary outlines developments relative to electronic packaging of these assemblies.

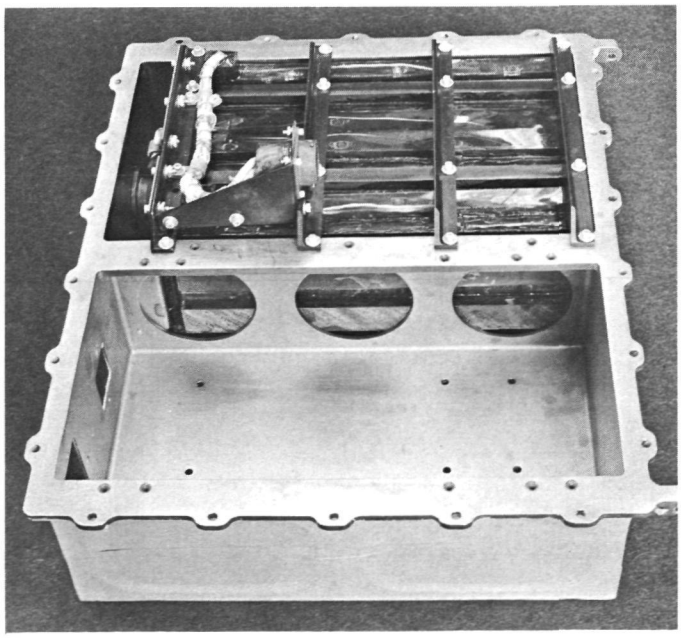

Figure 330. Battery in power chassis

Electronics assembly II—L-Band communications. This assembly has been completely repackaged to incorporate the electronics and other r-f equipment into standard JPL modular form. Due to the requirement of a band separator to be housed in the communications chassis when the S-Band ranging experiment is flown, this will necessitate a change to be recognized between RA-5, -6, -7, and RA-8 and -9. This additional subassembly is present on RA-8 and -9.

Electronics assembly III—S-band ranging experiment. This is a completely new electronic assembly that is to replace the equipment that occupied this bay on RA-3. Since this assembly will only be flown on RA-8 and -9, it requires that "dummy" modules be installed in this assembly case for RA-5, -6, -7. In addition to the modules required for operation of the S-Band, four modules will be housed in this assembly case that comprise the data conditioning system (DCS), required for operation of the scientific experiments aboard the spacecraft. This system will be aboard RA-5 through -9. The S-Band assembly consists of three transponders similar to those of the L-Band communications assembly, a diplexer, a power converter, and a shielded isolator.

Scientific instruments. These instruments consist of a series of three radiation experiments: a tissue equivalent ionization chamber, a particle flux detector, and a Neher-type ionization chamber. The particle flux detector and the Neher ionization chamber are similar to those to be flown on *Mariner*; however, the tissue equivalent ionization chamber is a completely new unit. Since the success of these experiments depends upon the "look" at the lunar surface, their mounting must be in such a manner so as to accomplish this. In order not to interfere with the functioning of any other instruments aboard the spacecraft, the radiation experiments are located beneath the hex electronic assemblies and between the hex and the high-gain antenna. Since the Neher chamber is identical to that of *Mariner*, it becomes a problem of location and mounting to the spacecraft structure. The particle flux detector will use the basic electronics of *Mariner;* however, a change is required in the chassis to facilitate the necessary orientation of the detector tubes when attached to the bus structure.

6. Temperature Control

a. Introduction. The temperature control system for *Ranger* is a passive system that maintains the temper-

ature of the spacecraft functional components within the required limits as specified for the respective components. Passive temperature control is defined as control without using moving parts or fluids. Control is achieved by the selection of surface finishes and by controlling spacecraft internal heat-transfer capabilities. Thus, spacecraft local temperatures are the composite result of solar energy absorption, energy absorption from the Earth, radiation of energy into space, heat from internal power dissipation, and heat transfer to or from other spacecraft components.

Primary emphasis was on the selection of local surface treatments and coatings that provide local equilibrium temperatures within the specified ranges during normal Sun-stabilized flight attitude. In addition, the local surface treatments and coatings maintain the component and instrument temperatures and temperature gradients within maximum limits for the duration of the various transient conditions.

The following transient conditions were considered in the design analyses and testing of the temperature control system:

(1) Heating during the countdown.

(2) Radiant heat from aerodynamic heating of the shroud.

(3) Shroud-off aerodynamic heating.

(4) Shroud-off Earth shadow cooling.

(5) Parking orbit attitude in the sunlight.

(6) Random tumbling in the sunlight.

(7) Variations of the internal power dissipation.

(8) Non-Sun oriented maneuvers.

b. Analysis. The basic means of controlling the spacecraft external surface temperatures is by radiation. The primary temperature control emphasis pertaining to the spacecraft equilibrium temperatures during the cruise or Sun-oriented attitude is as follows. For the over-all spacecraft the following equation must be satisfied:

$$q_{in} = \sum_i (\varepsilon_i A_i F_i \sigma T_i^4)$$

where

q_{in} = heat input; solar and internal power

a_i = area of surface i

F_i = view factor (geometrical term, giving % of surface area radiating to space)

σ = Stefan-Boltzmann constant

T_i = temperature of surface i

ε_i = emissivity of surface i

When considering the temperature distributions of separate components, Equation (1) will hold, provided two terms are added—the first to represent heat lost or gained by conduction at the component interfaces, and the second to include the inter-radiation effects of other components.

Conduction is governed by the temperature gradient at the boundary, while the inter-radiation depends on the difference between the fourth power of two temperatures, the surface properties, and the geometrical relationship.

Consequently, much effort has been expended to reduce the conduction term in Equation (1) by making an isothermal body or by insulating the component from the structure around it. The vehicle has been analyzed thermally by considering an isothermal hex assembly and numerous instruments, sensors, and other components isolated from the connecting structure.

The hex assembly in this analysis is considered to be the electronic chassis, the support structure not including the legs, and the center section covered by aluminized mylar radiation shields. Since each chassis, or case, has a different internal power and a different area exposed to the Sun, the requirement for keeping an isothermal structure would seem to demand conduction. However, each chassis was considered separately, assuming no heat transfer across the boundaries, and the corresponding effective or average emissivity determined for the desired temperature.

In general, the components of the hex assembly have a low power-to-surface-area ratio. Also, the area presented to the Sun is low. Consequently, the solution called for an average emissivity varying between 0.2 to 0.5 for the various chassis. At the present time, there is no known surface treatment which can give these values satisfactorily. The effective emissivities of 0.2 to 0.5 are obtained by combining various amounts of low- and high-emissivity areas. This required a low- and a high-emittance material that was highly reproducible, durable, and cleanable. For *Ranger*, gold and polished aluminum have been used for the low-emittance surfaces, white and grey paint for the high-emittance surfaces.

The legs were not considered in the above analysis because it has been determined that they do not exert a strong influence on the bus, due to the poor conductivity

of cast magnesium. However, since there are temperature-sensitive components attached to the legs, great effort was expended to ensure that they be as warm as possible by minimizing the emissivity of all leg and associated surfaces.

The basic method of applying this philosophy has been to incorporate the low-emittance surfaces and insulation during the design phases. The remainder of the surface treatment is performed at JPL by painting specified areas to provide the proper average emissivity. The JPL space simulator was then utilized to verify the thermal treatment or dictate minor changes in configuration.

c. Testing of RA-1 and -2. The RA-1 and -2 temperature control test program began late in October 1960 with the buildup of the temperature control model of the bus. (The space simulator was not large enough to test the *Ranger* spacecraft even when the foldout components were detached.) The temperature control model consisted of a spacecraft hexagonal structure, six electronics cases with dummy heat-dissipating modules inside, antenna gear box, triple coincidence telescopes, attitude-control jets, Sun sensors, and an attitude-control pressure regulator. These units were installed in their respective positions to properly represent the flight spacecraft. Electrical resistance heaters were attached to the surfaces which were to see the Sun and then covered with materials which duplicated the desired surface emissivities. Initially, the effects of the legs, cables, and solar panels were ignored as they were all determined to be negligible by the preliminary computations.

The temperature control model hex was then installed in the space simulator and tested. After many weeks of testing, including improved test techniques and improved simulator operation, the experimental temperatures obtained on the electronic chassis correlated with the calculations. The tests also indicated that the calculations were approximately correct for the legs. A truncated superstructure (the chamber was too small), with electrical heaters to simulate the Sun, was attached to the bus. As in previous tests, the test was valuable but limited. The space chamber solar simulation was improved to the point where it was usable. Another series of tests was performed.

The PTM never was tested in the space simulator because it did not have temperature control surface preparations (schedule limitations).

A series of tests was performed on the RA-1 and -2 flight units. These tests involved only the bus without superstructure or any foldouts. The tests resulted in bus temperatures of approximately 35°F. However, this resulted from a limited solar simulation intensity. When extrapolated to the one solar constant in space, near the Earth, the bus temperature should have been approximately 85°F during Sun-oriented flight. In addition, many separate tests, with and without solar simulation, were performed on the RA-1 and -2 science experiments which did not readily lend themselves to analytical solutions. All testing was completed approximately one week prior to RA-1 scheduled flight date and appropriate modifications incorporated on the flight vehicle.

d. Testing RA-3 to -5. The RA-3 test program drew from the experience gained during the RA-1 and -2 operations. Emphasis was upon determining the effect of the Earth shadow, the midcourse, and the terminal phases, as well as refining the Sun-oriented portions of the flight.

The largest unknown from the previous test program involved the simulation of solar energy absorption. Thus, the RA-3 to -5 temperature control hardware was designed to make use of the superior solar simulation (better collimation, greater intensity, and more uniformity) available at an off-laboratory facility. Unfortunately, this facility was too small to test an entire spacecraft hexagonal bus structure. As scaling laws do not exist for radiative thermal problems, the RA-3 temperature control model was a 120-deg "pie section" of the bus incorporating one full bay (⅙ of the hex) with half a bay on either side. Any unrealistic heat losses from the cut planes were eliminated by cryogenic type insulation. Electrical resistors simulated the power dissipation of the electronic subassemblies. This unit was tested in the configuration of three of the six bays, for Sun-oriented operation and for shaded operation. The results of these tests defined the paint patterns used on PTM and flight tests conducted in the JPL 6-ft diameter space simulator.

e.* Ranger I *and* II *flight results. The highly unstandard flight path of *Ranger I* necessitated the re-calculation of all temperature estimates based on the following assumptions:

(1) *Stability:*
   (a) Spacecraft had acquired the Sun, Earth sensor had locked on the Earth, placing Cases II and III facing the Earth at all times.
   (b) Spacecraft was in the shadow of the Earth 40% of each orbit.
   (c) One orbit lasted 90 min.

(2) *Tumbling:*
   (a) Spacecraft was in the shadow of the Earth 40% of the time.
   (b) One orbit lasted 90 min.

(c) Spacecraft was tumbling at a constant rate about all axes.

In order to account for the effect of the Earth and sunlight reflected from the Earth, appropriate geometrical view factors and average values for albedo and Earth radiation were estimated. The geometrical configurations in themselves limit the accuracy of the results to an indication of trends only. Aerodynamic heating was included in the calculations, but it too is only a very rough estimate. Values of the above items at apogee and perigee were averaged.

The hex, the magnetometer, the ion chamber, the solar panels, and the Earth sensor were analyzed for both the stabilized and tumbling conditions.

Average temperatures were calculated for the hex, the magnetometer, the ion chamber, and the Earth sensor, since these items have a high enough thermal inertia to remain fairly constant throughout an orbit. These are presented below in tabular form, along with measured flight temperatures:

	Stabilized temperature °F		Tumbling temperature °F	
	Calculated	Flight	Calculated	Flight
Hex	115	102 to 115	123	118 to 122
Magnetometer	142	140 to 149	144	140 to 158
Ion chamber	50	50	39	50
Earth sensor	150	130	130	110

The solar panels respond much too rapidly to calculate any average temperature. Calculations show that during a Sun-oriented orbit, the panels will vary from −50 to +140°F during the sunlit and shaded portions of the orbit, respectively. Unfortunately, flight data does not correlate well with upper temperature calculated. By determining the local time of each reading, it can be seen that very few of the readings are at a time in the orbit when the panels would be at either extreme of temperature. In this light, most of the points are at least reasonably close. Apparently, we do not have good enough information about the surface properties of the panels to accurately predict their operation.

The best inference that can be made for the rest of the superstructure and experiments is that everything was running too hot, probably in the range of 86 to 140°F. The two semi-conductor experiments and the friction package seem to bear this out.

In conclusion, it appears the temperature control system would have functioned properly in deep space and no changes were made on RA-2.

The flight of *Ranger II* was also highly nonstandard, and the vehicle was only tracked for five passes. Very little temperature data was obtained. However, that which was received showed the same trends as *Ranger I*, with indications of stabilized temperatures similar to *Ranger I* after it started to tumble.

7. Flight Friction Experiment on RA-1 and RA-2

For the engineering for future spacecraft, it is most important to be able to provide mechanical motions in space. Such devices as solar panels, antennas, and aimed vidicons require moving parts. The sampling of the Moon's surface or operating a surface vehicle on the Moon also implies many moving parts. All of these devices require that bearing surfaces and gear surfaces of some sort be used. It will not always be practical to have all bearings and gears completely sealed and pressurized. Accordingly, it will be necessary to be sure that bearings and gears will operate reliably in a deep-space environment.

Available data indicate that the ability of unlubricated bearings and gears to operate without seizure in many cases depends on the presence of adsorbed monomolecular films of air or water on the bearing surfaces. Under Earth conditions, such films will almost always be present. In a space vacuum, they will almost certainly not be present. To simulate a space vacuum of the order of 10^{-12} mm of mercury in a laboratory is beyond the present state of the art. The best that can now be done on Earth, in a chamber of practical experimental size, is probably about 10^{-9} to 10^{-10} mm of mercury; calculations indicate that this degree of vacuum is probably insufficient to completely remove adsorbed monolayers.

It is true that some data will be slowly obtained from the successful or unsuccessful operation of various spacecraft. Such an approach is slow in that data are obtained only on one pair of bearing materials and one lubricant per episode, not quantitative in that coefficients of friction are not measured, unreliable in that the cause of failure may not be adequately telemetered or identified, and extremely risky in that it means jeopardizing the scientific experiment or the whole mission. Therefore, an experiment specifically designed to provide information on frictional behavior in deep-space vacuum was flown on *Ranger I* and *II*.

The friction experiment assembly consisted primarily of disks, arranged along a shaft, rotated at 3 rpm. Four hemispherical riders with a 0.3-lb load applied by a coil spring rode against the two surfaces of each disk in concentric wear paths. The tangential frictional force was measured by the deflection of thin metal strips in the form of a cantilever spring at right angles to the disk. This deflection in turn was measured by strain gages cemented to opposite sides of the cantilever spring. Strain gage voltages were amplified and transmitted through the 10-sec deck of the telemetering commutator.

The friction assembly was a self-contained package with its own battery power and a sub-commutator for data sequencing. The package received a starting signal from the controller at 367 min after launch.

By choice of rider and disk materials, the frictional behavior of a number of pairs of materials was evaluated. These consisted primarily of bearing and gear materials of engineering interest, including metal alloys, plastics, and ceramics. Some pairs were commercially pure metals selected on the basis of mutual solubility to check existing theories on the seizing of clean surfaces. Several of the material pairs were run in replicate in order to insure the reliability of the friction measurement.

Friction data obtained by other investigators in vacuum or inert atmospheres indicated that steady-state coefficient of friction was reached in approximately 100 revolutions of the apparatus. Therefore, an operating lifetime of over 300 min was designed into the friction assembly.

To prevent stoppage of the assembly by seizure of a rider to its disk, each rider mounting included an overload mechanism set to operate when the friction coefficient approached seizure. Operation of the overload mechanism provided an overload signal to the appropriate sub-commutator bar of the friction assembly.

Note that the number of magnetic materials combinations in the flight friction assemblies was limited because of the spacecraft requirement of 0.5 γ magnetic field resulting from the presence of other experiments on board.

The RA-1 and -2 flight friction assembly is shown in Figure 331. Figure 332 shows the friction assembly in flight configuration. Temperature control surfaces and spacecraft mounting brackets can be seen. The polished aluminum surfaces of the lower thermal shields are protected with a strippable coating which is removed just prior to flight. The friction disk drive motor housing and the strain transducer cable harness are covered with plastic reinforced aluminized mylar for additional thermal control.

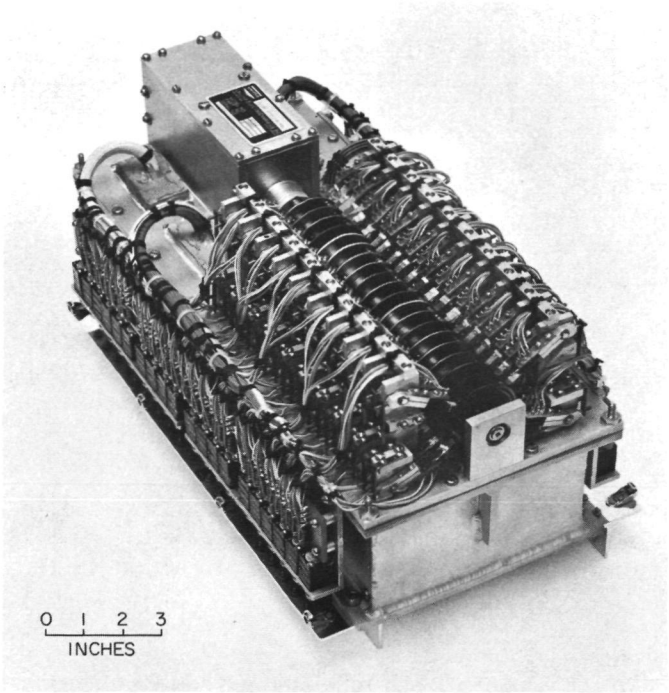

Figure 331. Flight friction assembly, RA-1 and -2

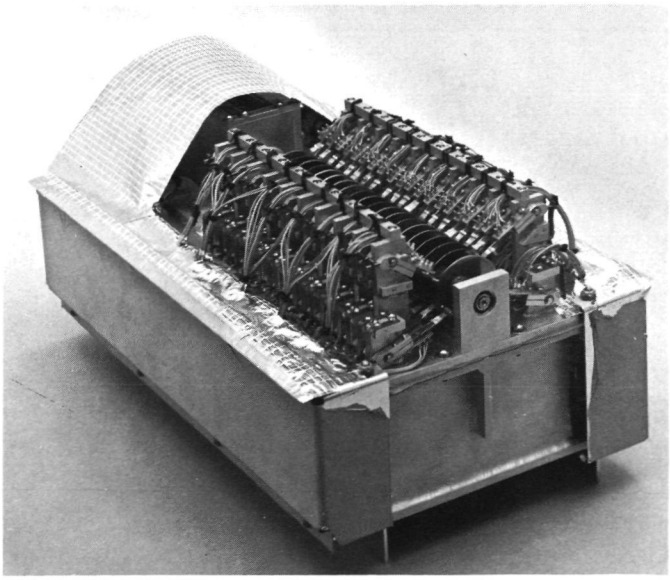

Figure 332. Flight friction assembly, flight configuration

Figure 333 illustrates a typical curve of coefficients of friction obtained from a prototype assembly in a vacuum of 10^{-6} mm Hg for several metal combinations. The vacuum coefficient of friction data, as well as the data

CONFIDENTIAL

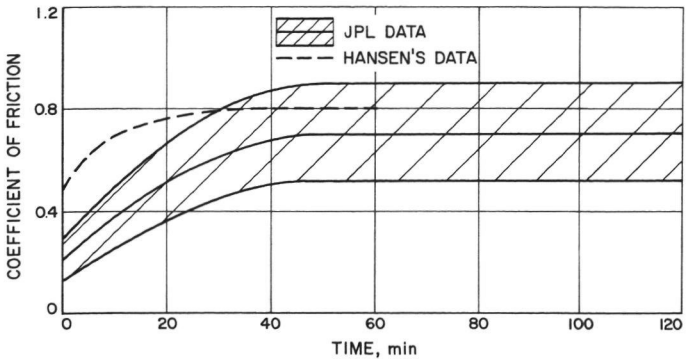

Figure 333. Average coefficients of friction in vacuum (10^{-6} mm Hg) for several metals

from preflight systems test in air and the RA-1 flight data for all of the combinations, are summarized in Table 73. For comparison, some data obtained in vacuum by Hansen (Ref 41) are also shown in Figure 333 and Table 74.

a. **Ranger I *flight results.*** *Ranger I* was launched August 23, 1961 at 1004 GMT from the Atlantic Missile Range, with flight friction assembly S/N 004 on board. Telemetry shows that the assembly was not operating at about 1522 GMT on August 23. The assembly was scheduled to start at 1611 GMT on that day; at this time the spacecraft, because of the nonstandard orbit, was between passes. Therefore, it is not known from telemetry whether the friction assembly was started on time. At the next period, during which spacecraft telemetry was received during a pass over the Atlantic Missile Range launch checkout trailer at about 0528 GMT on August 24, satisfactory coefficient-of-friction data from the flight friction assembly was received. Therefore, there is no reason to doubt that the start of the assembly took place as scheduled.

It is known that satisfactory coefficient-of-friction data was received from several passes over AMR and the Mobile Tracking Station and during the pass over the Mobile Tracking Station at 1401 GMT on August 24. The

Table 73. Coefficients of friction for several combinations of materials

Number of replicates	Number of RA-1 flight data points	Disk material	Rider material	Coefficients of friction		
				Vacuum 10^{-6} mm Hg[a]	Pre-flight system test data in air[b]	RA-1 flight data[b]
4	20	Copper	Tungsten	0.23 ± 0.09	0.22 to 0.41	0.23 to 0.54
4	19		Silver	0.28 ± 0.09	0.22 to 0.41	0.44 to 0.94
4	18		Nickel	1.09 ± 0.18	0.25 to 0.45	0.30 to 1.05
4	16		Aluminum	0.88 ± 0.32	0.22 to 0.41	0.30 to 1.60
4	17	A286	A286	0.43 ± 0.21	0.19 to 0.37	0.39 to 0.89
	18		Teflon	0.05 ± 0.01	0.03 to 0.07	0.02 to 0.09
	18		2024T4	0.31 ± 0.18	0.10 to 0.41	0.15 to 0.50
	19		4340	0.34 ± 0.15	0.13 to 0.52	0.49 to 0.89
3	16	Teflon; glass fiber reinforced; impregnated with molybdenum disulfide	440C	0.07 ± 0.06	0.07 to 0.13	0.02 to 0.12
	14		2024T4	0.08 ± 0.02	0.01 to 0.10	0.02 to 0.06
3	13	Aluminum–bronze	A286	0.50 ± 0.20	0.19 to 0.48	0.38 to 0.52
	15		Aluminum–bronze	0.69 ± 0.44	0.25 to 0.45	0.25 to 0.65
3	16	A286; coated with phenolic bonded molybdenum-disulfide	A286	0.08 ± 0.02	0.05 to 0.22	0.02 to 0.14
	16		Aluminum–bronze	0.11 ± 0.02	0.13 to 0.22	0.02 to 0.13
	16		4340	0.08 ± 0.01	0.07 to 0.31	0.02 to 0.24
	15		2024T4	0.09 ± 0.03	0.12 to 0.15	0.02 to 0.14
2	10	440C	440C	0.20 ± 0.05	0.07 to 0.19	0.09 to 0.15
	9		Sapphire	0.18 ± 0.04	0.07 to 0.22	0.07 to 0.18
2	10	A286; gold plated	A286	0.22 ± 0.11	0.15 to 0.25	0.08 to 0.20
2	9	A286; silver plated	A286	0.19 ± 0.04	0.13 to 0.41	0.33 to 0.59
2	11	A286; coated with flames sprayed tungsten carbide	440C	0.17 ± 0.08	0.15 to 0.24	0.11 to 0.25
	13		Teflon	0.05 ± 0.01	0.07	0.02 to 0.06
2	11	2024T4	2024T4	0.72 ± 0.15	0.37 to 0.83	0.18 to 0.54
	10		Teflon	0.08 ± 0.01	0.01 to 0.07	0.09 to 0.24
2	11	A286; lubricated with ETR-H grease	A286	0.17 ± 0.16	0.19 to 0.37	0.19 to 0.29
	13		2024T4	0.17 ± 0.13	0.13 to 0.28	0.10 to 0.18
	12		4340	0.19 ± 0.18	0.02 to 0.15	0.04 to 0.13
	12		Aluminum–bronze	0.18 ± 0.10	0.07 to 0.15	0.02 to 0.07

[a]Average value after 100 min of travel of the rider in the same disk wear path. Laboratory vacuum with flight prototype friction assembly.
[b]Flight friction assembly. Range is lowest and highest value of data recorded.

CONFIDENTIAL

Table 74. Coefficients of friction in vacuum 10^{-6} mm Hg data of Hansen (Ref 1)

Lower block material	Upper block material	Average[a] coefficient of friction
2024T4	2024T4	0.59
Brass	Brass	0.71
304 stainless steel	2024T4	0.34
304	304	0.93
52100 steel	52100 steel	0.45

[a]Average value after 60 min of travel over the same wear path.

assembly was not operating during a pass over the MTS at 1536 GMT on August 24. Therefore, it can be concluded that the assembly functioned for at least 22 hr and switched itself off at a predetermined low battery voltage. The designed operating life of the assembly was 10 hr. It can also be concluded that the assembly was operating about 13½ hr before the first telemetry data was received, a fact which, because of the high wear rates of some of the materials tested, can account for the wide ranges of coefficients of friction reported.

Table 75 is a summary of the stations, times and orbits for *Ranger I* during which friction assembly telemetry data was received. For the passes over the Mobile Tracking Station, the altitude and vacuum (Ref 42) are also given.

The coefficients of friction telemetered from *Ranger I* flight friction assembly for most of the material combinations were slightly higher than the telemetered data during final systems test from the same assembly on the ground at AMR, and also slightly higher than data obtained from a prototype assembly in laboratory vacuum. The space vacuums at the altitudes of the spacecraft during the periods that telemetry was received were (10^{-8} mm Hg) slightly better than can be readily obtained in laboratory vacuums (10^{-6} to 10^{-7} mm Hg). Therefore, it was expected that the coefficients of friction in flight would be higher than the ground data and also slightly higher than the coefficients of friction obtained from the prototype assembly in laboratory vacuum. The space vacuum at the RA-1 spacecraft altitudes was not as good as the vacuum expected in deep space (10^{-12} mm Hg). It is probable that coefficients of friction for these same materials would be higher at deep-space vacuum than those obtained in *Ranger I* flight.

b.* Ranger II *results. At 0812 GMT, on November 18, 1961, *Ranger II* was launched from Atlantic Missile Range with flight friction assembly S/N 005 on board.

The spacecraft controller command to start the flight friction assembly was to occur at 1419 GMT which, because of the nonstandard orbit of the spacecraft, was between the fourth and fifth pass of tracking by the Mobile Tracking Station.

During the fourth pass over the MTS at 1322 to 1328 GMT, telemetry indicated that the friction assembly was not running.

During the fifth MTS pass with acquisition at 1456 GMT, 26 pieces of telemetered information were received from the flight friction assembly.

The coefficients of friction from telemetered information from final systems test on the ground at AMR and from the *Ranger II* flight are shown in Table 75. As can be seen, the coefficients of friction of most of the non-lubricated combinations in flight are only slightly higher than those in air. This behavior is as expected, since the vacuum at *Ranger II* apogee is 5.6×10^{-7} mm Hg and at perigee is 3.5×10^{-6} mm Hg (Ref 41). Data of the coefficients of friction of the materials used on the *Ranger II* flight will be obtained at a later date in laboratory vacuum for comparison with flight data.

Contained in the group of coefficient-of-friction measurements were four duplicates of material combinations flown on *Ranger I*, the A286 uncoated disks with associated riders. Four more are readily comparable with similar combinations flown on *Ranger I*. In this latter case, the combinations flown on *Ranger I* (Table 73) were A286 disks with a phenolic bonded molybdenum disulfide coating.

Table 75. Summary of *Ranger I* orbits from which coefficient-of-friction data were obtained

Station	Time GMT	Orbit	Altitude km	Vacuum (Ref 2) mm Hg $\times 10^{-8}$
AMR[a]	0528	13	—	—
Goldstone 2	0658	14	—	—
AMR	0705	14	—	—
Goldstone 2	0334	15	—	—
AMR	0842	15	—	—
MTS[b]	0915	16	456	2.49
Goldstone 2	1007	16	—	—
Goldstone 3	1007	16	—	—
AMR	1017	16	—	—
MTS	1049	17	453	—
Goldstone 2	1145	17	—	—
Goldstone 3	1145	17	—	—
MTS	1226	18	426.5	3.24
MTS	1401	19	378.4	5.62
MTS	1536[c]	20	336.7	11.87

[a]Atlantic Missile Range, Launch checkout telemetry trailer.
[b]Mobile tracking station, South Africa.
[c]RA-1 Friction Assembly, automatically shut off after Orbit 19.

In the RA-2 flight, the material combinations (Table 83) were A286 disks with sodium silicate bonded molybdenum disulfide coating. The major variable between the RA-1 and RA-2 molybdenum disulfide coated combinations is the binding material. In most cases, the rider materials were the same; therefore, these combinations should be readily comparable.

c. Conclusions. The flight friction assembly on RA-1 performed as designed and coefficient of friction data from a low-altitude earth satellite were obtained. Apparently, the assembly was started on time by spacecraft controller command, and was turned off by the self-contained low battery voltage cutoff circuit. The assembly operated for about 22 hr.

Table 76. Coefficients of friction from *Ranger II* flight

Number of replicates	Number of flight data points	Disk material	Rider material	Coefficients of Friction	
				Pre-flight systems test data	RA-2 flight data
2	—	Aluminum	Lead	0.13 to 0.34	—
	—	Electrical grade	Tungsten	0.19 to 1.24	—
	—		Magnesium	0.31 to 0.50	—
	—		Iron	0.25 to 1.24	—
2	—	René	René 41	0.22 to 0.43	—
	1		Teflon	0.02 to 0.06	0.11
	1		2024T4	0.50 to 0.57	0.62
	1		4340	0.19 to 0.69	0.61
2	1	A286	A286	0.25 to 0.34	0.65
	1		Teflon	0.02 to 0.06	0.06
	1		2024T4	0.25 to 0.53	0.61
	1		4340	0.22 to 0.53	0.70
2	1	Beryllium-copper	Beryllium-copper	0.16 to 0.37	0.52
	1		René 41	0.16 to 0.31	0.51
	1		Tungsten carbides	0.08 to 0.22	0.15
	1		2024T4	0.25 to 0.53	0.45
2	1	A286 coated with Sodium Silicate bonded Molybdenum-disulfide	A286	0.11 to 0.13	0.08
	1		Beryllium copper	0.06 to 0.08	0.06
	1		2024T4	0.06 to 0.13	0.05
	1		4340	0.04 to 0.11	0.07
	1				
2	1	Silver (Fine)	Silver (Fine)	0.22 to 0.57	0.56
			Palladium	0.25 to 0.34	0.41
2	1	René 41	Pyroceram	0.16 to 0.50	0.42
	1		Nylasint	0.04 to 0.11	0.28
2	—	René 41 with Teflon wiper	Beryllium-copper	0.13 to 0.50	—
	—		René 41	0.16 to 0.43	—
2	—	2024T4 with Teflon wiper	2024T4	0.28 to 1.10	—
	—		A286	0.25 to 0.43	—
2	1	Silver (Fine)	Paleney 7	0.28 to 0.34	0.29
	1		Tungsten	0.13 to 0.28	0.65
	1		Platinum	0.19 to 0.47	0.20
	1		Silver-graphite	0.13 to 0.31	0.09
2	1	Copper-plated 0.003-in. hard nickel plus 0.0001-in. gold	Paleney 7	0.13 to 0.31	0.55
	—		Tungsten	0.11 to 0.25	—
	—		Platinum	0.22 to 0.81	—
	—		Silver-graphite	0.22 to 0.37	—
2	—	A286 lubricated with G300 grease	A286	0.08 to 0.22	—
	—		Aluminum-bronze	0.08 to 0.19	—
	—		2024T4	0.22 to 0.28	—
	—		4340	0.11 to 0.25	—

The flight friction assembly on RA-2 was started on time by the spacecraft controller. This fact was ascertained by comparing estimated friction assembly starting time from launch and controller starting time data with the 10-sec pulses of the coefficient of friction data and the acquisition time for the fifth pass over the Mobile Tracking Station. The assembly was destroyed when the spacecraft re-entered to lower altitudes and, therefore, the assembly apparently did not run long enough for the built-in low voltage battery cutoff to operate. A small amount of correlated coefficient of friction data was obtained.

It would be advantageous to have an assembly similar to the flight friction assemblies on RA-1 and -2 on some spacecraft in a higher altitude orbit—one at least at an altitude of 4000 mi or better where the vacuum of space would be low enough to ensure that new adsorbed gaseous or metal oxide layers would not form. In the absence of regenerated adsorbed surface layers, the freshly generated metal surfaces between disk and rider would be in intimate contact. Information of the possibility of unlubricated metal surfaces cold welding and the coefficients of friction of clean metal surfaces in the deep-space environment would thus be obtained. In addition, by incorporating certain selected dry film or grease-lubricated combinations, some data on the behavior of some lubricated material combinations could be telemetered to Earth from the deep-space environment.

8. Terminal Sterilization

The introduction of sterilization as a design requirement on the *Ranger* series of payloads necessitated the development of a method of sterilizing the spacecraft exterior surfaces just prior to flight and maintaining this condition until the spacecraft has moved safely out of the Earth's atmosphere. Terminal sterilization is one facet in the over-all sterilization program, supplementing component and assembly sterilization techniques.

In designing the required system, the first consideration was to develop a sealed cavity within the *Agena* shroud to house the spacecraft during flight and to contain the sterilization gas (12% ethylene oxide and 88% Freon 12) during sterilization. Scheduling demands necessitated completion of shroud design prior to designing the ground support equipment (GSE). The second step was to develop the necessary support equipment to service the sealed cavity with the sterilant and purging gases.

a. System concept. After the spacecraft is completely assembled and ready for flight, it is installed on the

Agena adapter (in the JPL assembly area). This adapter contains a diaphragm that seals the spacecraft from the *Agena* stage. The sealed cavity is completed by installing the shroud over the spacecraft. The shroud is equipped with valves that permit the introduction of sterilant and purging gases. The diaphragm contains a biological filter element that permits it to breathe without contaminating the spacecraft. It is also equipped with a pressure relief valve that protects the shroud against excess pressures during flight. The valve finally locks in the open position during the boost phase when it is subjected to maximum flow, maximum *g* conditions.

b. Ground support equipment. The terminal sterilization equipment developed to service the *Agena* spacecraft sealed cavity with sterilant and purging gases was designed with the following criteria in mind:

(1) To obtain spacecraft surface sterility with a minimum of interference with vehicle countdown operations.
(2) To obtain surface sterility without damaging spacecraft surfaces or decreasing the inherent reliability of the spacecraft and vehicle.
(3) To safeguard personnel from ethylene oxide vapor.

In line with the first criterion, the sterilization equipment was designed as a mobile unit capable of servicing the sealed cavity on the gantry or in the assembly building; however, it is generally agreed that performing the sterilization operation in the assembly building is highly preferable. Essentially, the terminal sterilization unit is composed of the following major assemblies:

(1) Sterilant and purge gas supply.
(2) Gas vaporizer and heater assembly.
(3) Humidification supply.
(4) Test plenum chamber.
(5) Purge-gas filtration assembly.
(6) Ethylene oxide disposal system.

All spacecraft material and component suppliers were concerned about the effects of the sterilant gas. In line with this, a series of tests was conducted and it was found that if the gas is kept well above its dew point (50°F), it has little effect on most engineering materials. However, all flight equipment must undergo environmental tests to determine material compatibility with the sterilant gas. The high dew point of ethylene oxide reinforces the desire to perform the sterilization work in the assembly area rather than on the gantry. The temperature control in the assembly building makes it possible to ensure that all surfaces are at a temperature greater than the dew point of ethylene oxide.

c. Determination of exposure time. Tests were run to determine exposure to ethylene oxide required for effective sterilization of spacecraft surfaces. Resistant strains of spores were conditioned and located in critical areas of the spacecraft cavity. Terminal sterilization runs were made with exposure times varying from 8 to 11 hr. After the various ethylene oxide exposures were completed, sterile media were aseptically introduced to the test spores, which were then incubated at 37°C for 14 days. Growth in any test tube constituted a positive, indicating an insufficient exposure. Test results are summarized in Table 77. Results of the tests established the 11-hr exposure time to be used on all *Ranger* terminal sterilization operations.

Table 77. Exposure times for ethylene oxide sterilization

Test date, 1961	Soak period, hr	Average relative humidity, %	Average ethylene oxide concentrate, %	Effectiveness, %
11/10	8	32	21.1	98
11/14	9	45	22.3	98
11/20	10	42	23.1	99
11/28	11	38	23.1	100
11/29	11	45	22.8	100
11/30	11	40	22.9	100

F. Propulsion

1. System Concept and Design Philosophy

The capability of a midcourse maneuver in order to assure a collision trajectory with the Moon is necessary for the lunar impact mission requirements of RA-3, -4, -5 spacecraft and the *Ranger* follow-on series. This maneuver will be accomplished through the use of a small monopropellant-hydrazine fueled, 50-lb vacuum thrust propulsion system capable of delivering, upon command, a variable total impulse. Use of this type of propulsion system is based upon system simplicity, the high degree of flexibility with regard to total impulse, adaptability to vehicle design, and general state of development.

The propulsion system (Fig 334) is functionally a pressure-fed, constant-thrust rocket. Injection pressure is derived from compressed helium or nitrogen gas, which passes through a pressure regulator and forces the fuel from a bladdered propellant tank into the rocket engine. The rocket engine contains a particulate catalyst to accel-

COMPONENTS

1 ROCKET ENGINE
2 IGNITION CARTRIDGE GN_2 FILL VALVE
3 IGNITION CARTRIDGE GN_2 RESERVOIR
4 IGNITION CARTRIDGE ACTUATION VALVE
5 IGNITION CARTRIDGE OXIDIZER RESERVOIR
6 IGNITION CARTRIDGE BURST DIAPHRAGM
7 SHUTOFF PROPELLANT VALVE
8 START PROPELLANT VALVE
9 PROPELLANT TANK FILL VALVE
10 PROPELLANT TANK
11 PROPELLANT TANK BLADDER
12 PROPELLANT TANK PRESSURIZATION VALVE
13 HELIUM PRESSURE REGULATOR
14 HELIUM FILTER
15 HELIUM START VALVE
16 HELIUM TANK FILL VALVE
17 HELIUM TANK
18 VISUAL PRESSURE GAGE, 0-4000 psi
19 VISUAL PRESSURE GAGE, 0-500 psi
20 PROPELLANT FILL BLEED
21 HELIUM SHUTOFF VALVE
22 IGNITION CARTRIDGE VISUAL PRESSURE GAGE, 0-500 psi

INSTRUMENTATION

PRESSURE

P_1 HELIUM TANK
P_2 PROPELLANT TANK

PRESSURE MONITORING GAGES

G_1 HELIUM TANK
G_2 PROPELLANT TANK
G_3 IGNITION CARTRIDGE RESERVOIR

TEMPERATURE

T_1 ROCKET MOTOR

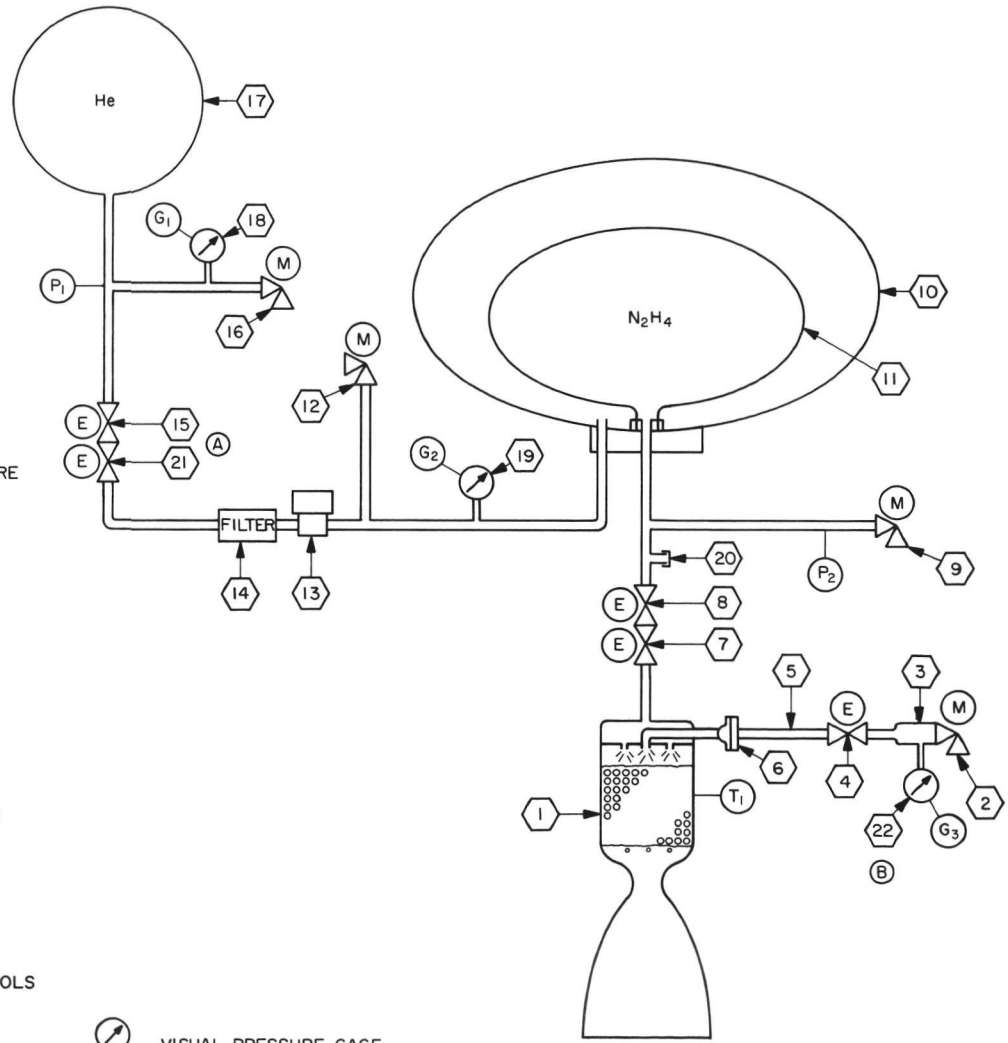

SYMBOLS

E TWO-WAY VALVE, EXPLOSIVELY OPERATED
M ANGLE VALVE, MANUALLY OPERATED
BURST DIAPHRAGM
FILTER FILTER
PRESET REGULATOR
VISUAL PRESSURE GAGE
17 COMPONENT NUMBERS
P_1 INSTRUMENTATION NUMBERS
CAPPED TUBE END

Figure 334. Monopropellant propulsion system

erate the decomposition of anhydrous hydrazine. Engine ignition is accomplished through the injection of a small quantity of a hypergolic oxidizer, nitrogen tetroxide. Five explosively actuated valves are used to operate the device.

a. Design concepts. The design and operational philosophy of the propulsion system have been predicated upon the following concepts:

(1) To utilize the highest performance monopropellant system consistent with present technology.

(2) To maximize system reliability and reproducibility.

(3) To minimize pre-flight handling and interaction with other subsystems on the spacecraft.

(4) To minimize in-flight electrical signals to the propulsion system.

(5) To avoid electrical or mechanical sequencing.

(6) To minimize the number of components.

(7) To utilize to as great an extent as possible the techniques, methods, and components previously developed by JPL for storable liquid propellant systems.

b. System criteria. In addition, the following basic system criteria have been utilized in the design of the propulsion system for the *Ranger* spacecraft:

(1) The unit must ignite and operate in a gravitationless environment.

(2) The unit must ignite and operate in a vacuum environment.

(3) The spacecraft will be essentially stationary in attitude (not spinning).

(4) The device will be capable of one ignition and one termination.

(5) The rocket engine thrust will be 50 lb (vacuum).

(6) The ambient temperature range of the propulsion system will be +40 to 160°F.

(7) The thrust axis of the rocket motor will lie along the spacecraft roll axis.

(8) The volume within the spacecraft generally occupied by the propulsion system will consist of that volume bounded on the sides by the internal hexagonal structure supporting the electronic chassis, on the top by the upper surface of the hexagonal compartment (capsule mounting plane), and on the bottom by an imaginary plane several inches below the lower surface of the hexagonal compartment, consistent with the closed position of the antenna.

(9) Thrust vector control will be accomplished by jet vanes inserted in the engine exhaust jet.

(10) The magnitude of total impulse delivered by the propulsion system will be determined by an on-board integrating accelerometer system.

One electrical signal is sufficient to initiate operation of the midcourse propulsion system and to terminate its operation. In order to accomplish this, the propellant tank is pre-pressurized, and hence rocket engine ignition can occur concomitantly with the release of high-pressure gas to the pressure regulator without allowing time for the propellant tank pressure to build up to its normal operating level.

The specific sequence of events during in-flight operation is as follows:

(1) At a command signal to ignite the rocket, normally closed, explosively actuated valves (4) (8) and (15) in Figure 334 are activated, allowing regulated gas pressurization of the propellant tank, propellant flow to rocket engine, and injection of a small quantity of nitrogen tetroxide to rocket engine.

(2) Hypergolic ignition ensues, followed by continuous monopropellant decomposition of the anhydrous hydrazine.

(3) At a command signal to shut off the rocket, normally open, explosively actuated valves (7) and (21) are activated, terminating propellant flow to the rocket engine and retaining the residual gas in the pressure reservoir. Typical operating parameters anticipated in flight are shown in Table 78.

Table 78. System parameters

Station	Item	At ignition	At termination
	Pressure, psia		
A	Pressure reservoir	3000	370
B	Regulated pressure	320	320
C	Propellant tank	275	320
D	Oxidizer ignition cartridge	350	208
E	Fuel injection pressure	320	320
F	Thrust chamber (avg)	200	200
	Temperature, °F		
G	Pressure reservoir	40 to 160	~ −100
H	Propellant tank	40 to 160	40 to 160
I	Thrust chamber (wall)	1800 to 1900	1800 to 1900

2. Development of the Rocket Engine Decomposition Chamber

The design of an efficient, minimum-size decomposition chamber for monopropellant-hydrazine requires determination of the optimum combination of injector design, catalyst bed sizing, and ignition system. During early 1960, approximately 125 engine firings were made in which the following parameters were varied: (1) injector configurations, including evaluation of single jet designs, multi-jet designs, spray coarseness, distance of injector from catalyst bed, and positions of jets in relation to reactor walls; (2) catalyst bed volumes; (3) catalyst particle size; (4) chamber pressure; (5) quantity of oxidizer used for ignition; and (6) ignition system pressure. The result of this investigation is the flight engine configuration shown in Figures 335 and 336.

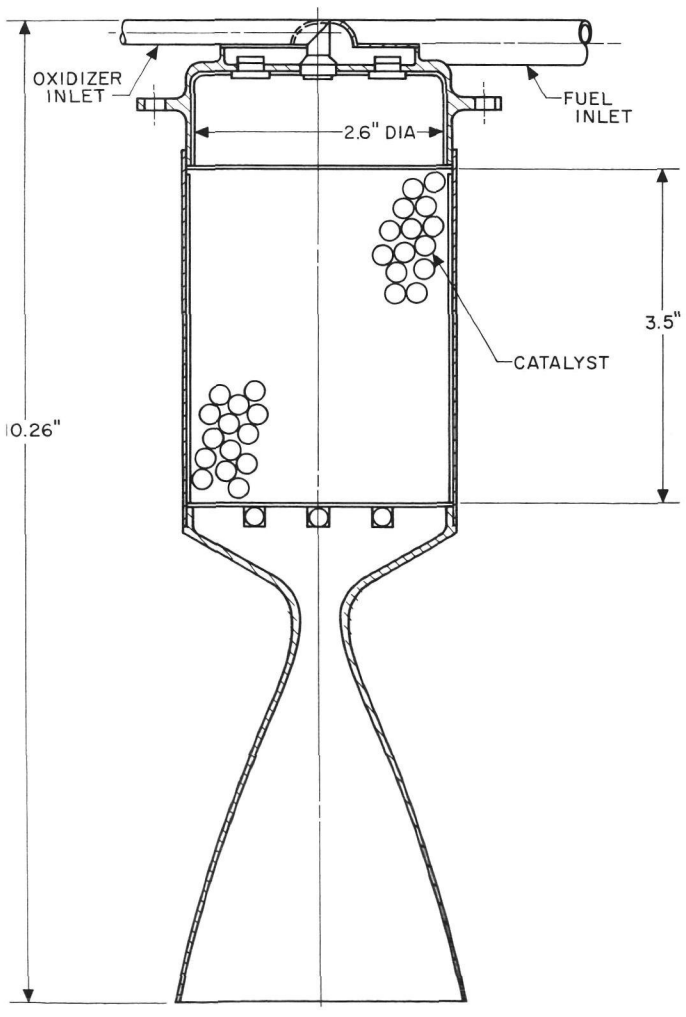

Figure 335. Monopropellant hydrazine engine

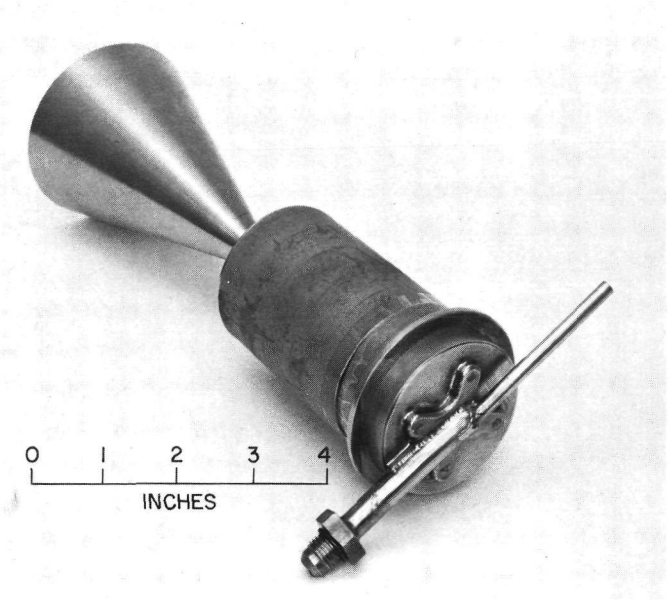

Figure 336. Prototype monopropellant hydrazine engine

Figure 335 is a sectioned sketch showing the internal configuration of the rocket engine. Fuel is supplied through a common manifold to four atomizing spray jets. The oxidizer required for ignition is injected through a centrally located atomizing spray jet. The catalyst bed is nominally 2.6 in. in diameter and 3.5 in. in length. The JPL Type H-7 catalyst is prepared from aluminum oxide catalyst support, impregnated with an equimolal solution of iron, nickel, and cobalt nitrates. The catalyst is then heated to reduce the nitrates, leaving only the base metals on the support. The $\frac{3}{16}$-in. catalyst particles are spherical.

Figure 336 is an external view of a partially assembled rocket engine and indicates principally the injector head, showing the integral design of the fuel manifold and oxidizer inlet tube.

3. Development of the Ignition System

The requirement of zero-gravity ignition for the propulsion system necessitated the development of a unique ignition system. During 1958 and 1959, considerable work was accomplished at this Laboratory toward obtaining a simple, reliable, rapidly operating, hypergolic ignition system for monopropellant-hydrazine gas generators. A summary of this work is contained in Reference 43. Most of this summary describes a simple system employable in positive gravity environments. The general principle of the device was to place in a small common reservoir a quantity of hypergolic oxidizer (nitrogen tetroxide, in

general) and gaseous nitrogen under pressure. The outlet from the "cartridge" was sealed with a normally closed, explosively actuated valve. Energizing the valve thus allowed the pressurized mixture to be blown into the decomposition chamber. Several hundred tests of this simple system were made with consistent success. In development of the zero-gravity cartridge, the experience gained in these earlier studies was used extensively. In this case, however, a means of separating the liquid oxidizer and the pressurizing gas was required. Several variations of the system were tried; the final version is shown in Figure 337.

This figure shows a prototype flight engine in a typical test setup. The zero-gravity ignition system is shown at the right of the picture. From right to left, the system consists of a pre-pressurized nitrogen gas reservoir, a normally closed explosively actuated valve, an oxidizer, reservoir, and a burst diaphragm holder. The optimum quantity of oxidizer was found by experience to be 12 cubic centimeters; the optimum length-to-diameter ratio for the oxidizer reservoir was found to be approximately 90. Upon actuation of the valve, the nitrogen gas forces the oxidizer into the chamber. In tests wherein the tube was placed at various attitudes, virtually all oxidizer was evacuated from the tube and successful and consistent ignitions were obtained.

4. Design of the Expansion Nozzle

The contour of the divergent portion of the rocket exhaust nozzle was optimized to deliver the maximum thrust coefficient consistent with the physical boundary conditions imposed by the spacecraft configuration and the design of the attitude-control jet vanes. An electronic computer program was undertaken to calculate the nozzle dimensions and Mach number distribution along the wall for nine divergent contour nozzles, utilizing the method described in Reference 44 for axisymmetric hypersonic wind tunnels. The thrust coefficients along the wall were computed from equations in Reference 45. The specific heat ratio γ was estimated to be 1.27 for the hydrazine decomposition products. The other computation parameters were the exit Mach number, M_E; and the expansion angle, θ_A. The magnitudes of these parameters for the nine cases were: $M_E = 5$, 6, and 7 for 100% of maximum θ_A; $M_E = 5$, 6, and 7 for 90% maximum θ_A, $M_E = 7$ for 90% of maximum θ_A and 5% partial cancellation (a device to reduce contour discontinuity, Ref 44); and $M_E = 8$ and 9 for 90% of maximum θ_A. The computations resulted in dimensionless wall-coordinate parameters with corresponding thrust coefficients, Mach numbers, and pressure ratios.

The space limitations imposed by the spacecraft interfaces and the midcourse propulsion system design configuration resulted in an allowable length for the divergent nozzle of 4.05 in. Figure 338 shows the variation in thrust coefficient, nozzle exit diameter, and dynamic pressure with exit Mach number for this nozzle length for the last six contours mentioned previously. They appear in Figure 338 from left to right, respectively, for each curve. (The three contours for 100% maximum θ_A were not considered for reasons of engineering practicality.) From

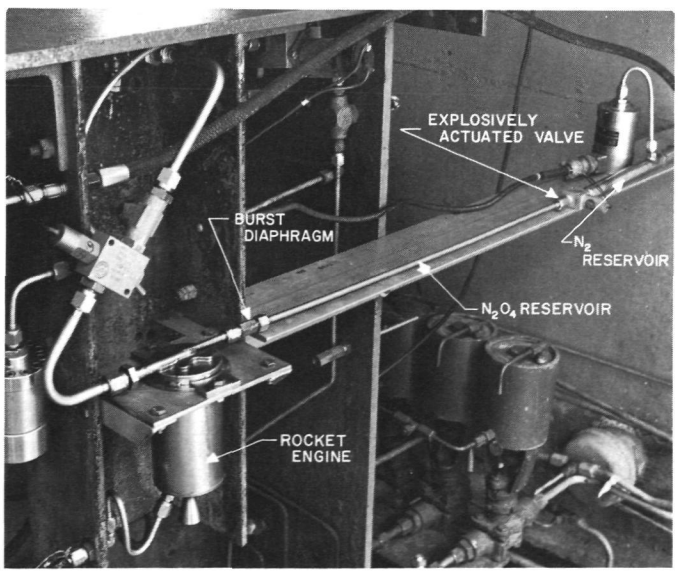

Figure 337. Rocket engine test firing set-up

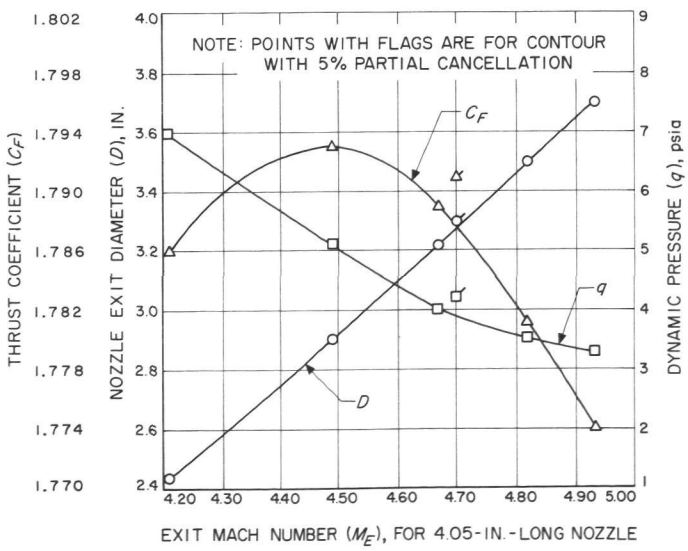

Figure 338. Thrust coefficient, nozzle exit diameter, and dynamic pressure vs exit Mach number

these comparisons, it was found that a nozzle diameter of 2.904 in., dynamic pressure of 5.11 psia, and Mach number of 4.49, associated with the maximum thrust coefficient 1.793 would most satisfy the jet vane requirements. Thus, the nozzle contour providing these values was considered optimum for both the propulsion system performance and the jet vane design.

5. Rocket Engine Testing

Subsequent to the engine firings conducted during the determination of the optimum configuration for the rocket engine catalyst bed, static test firings were conducted, consisting of the proof testing of the flight design rocket-engine injector and its associated feed plumbing (including the complete flight design ignition system). The tests were generally satisfactory, and the engines performed as anticipated. During the tests, a problem was encountered in the fuel feed line at engine shutoff. The explosively actuated valve functioned so rapidly that it caused an instantaneous over-pressure (hydraulic hammer). This over-pressure, on one occasion, ruptured the fuel inlet line. This problem was resolved through the substitution of a flexible, teflon-lined, wire-jacketed fuel line in place of the thin-walled aluminum tubing originally specified. This redesign allowed the line to absorb the energy of the over-pressure without rupture.

As a portion of the flight-acceptance test procedure, each flight injector was water-flow calibrated to ascertain its pressure-drop characteristics for later use in determining the proper setting for the gas-pressure regulators. After the water calibrations, each injector was test-fired in a "standard" thrust chamber. This series of tests provided a comparison of injector efficiency reproducibility for a production lot of seven injectors. The data was readily comparable since each injector was tested in the same thrust chamber. This chamber was constructed so that each flight injector could be slipped into the top of the chamber, held gas tight with an O-ring, and bolted down. The catalyst bed was changed for each test and the nozzle throat was water cooled. In this way, it was felt that variations of parameters other than those associated with the injector could be minimized. The water-cooled throat made it possible to ascertain throat area accurately for each of the static firings (not possible with flight nozzles since they are uncooled and, therefore, more subject to thermal effect variations). The average characteristic exhaust velocity obtained for the seven injectors was 4292 ft/sec $\pm$ 0.75%. This value compares favorably with the theoretical value, being on the order of 98 to 99% (depending upon the specific amount of ammonia decomposition assumed in the theoretical calculations).

After this series of tests the flight engines were welded and machined to their final flight configuration.

As indicated previously, the total impulse of the propulsion system is variable. During the spacecraft flight, the magnitude of impulse required for the midcourse maneuver will be determined from ground computation of the spacecraft trajectory. This information will then be sent to an integrating accelerometer system aboard the spacecraft, which will determine when the rocket has imparted the proper total impulse. The low thrust-to-weight ratio of the midcourse propulsion unit to the overall spacecraft necessitates that a sensitive accelerometer be used. Some concern existed early in the program as to whether the random vibration and noise produced by the operation of the rocket and induced into the spacecraft structure might produce spurious signals to the accelerometer and cause it to count improperly. Consequently, a series of tests was undertaken in which a test model of the *Ranger* spacecraft, weighted to simulate the flight unit, was elastically suspended in an acoustically lined chamber. A test rocket engine, mounted as it would be in the flight system, was placed aboard. Flexible propellant lines were used to introduce the fuel. A flight model of the accelerometer system was mounted in its proper location in the spacecraft. Figure 339 shows the experimental arrangements used in the tests. Two sets of 1-min duration each were made. The accelerometer system sensitivity is such that if 1 g of noise is present, erroneous counting will occur. The actual noise output of the propulsion unit was found to be 50×10^{-3} g in the first test and 55×10^{-3} g in the second test. Thus, it is evident that the vibration induced by the propulsion system will have no effect on the accuracy of integration of the accelerometer system.

6. Development of the Propulsion System Tankage

Early in the program, a decision was made to design the propulsion system tanks as large as was consistent with volume availability in the spacecraft. It was hoped that excess propellant, above that actually required to attain the desired statistical confidence level for accomplishment of the mission, could be added at the time of final spacecraft assembly as insurance to cover the cases of partial spacecraft failure. As the design of the spacecraft proceeded, in the summer of 1960 it appeared that this desirable feature could not be accommodated from a spacecraft weight standpoint and, therefore, carrying oversized tankage was not practical. The velocity incre-

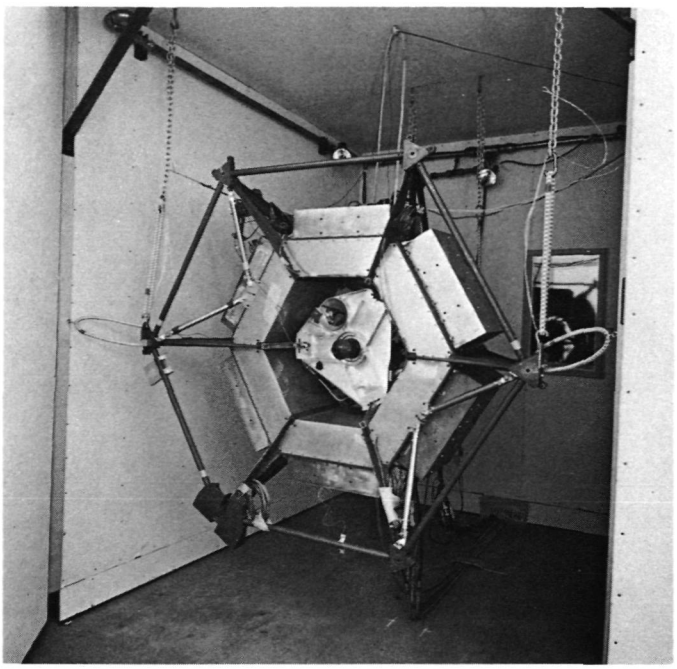

Figure 339. Midcourse rocket test set-up in acoustical chamber

ment for the RA-3 midcourse maneuver was originally specified as 120 ft/sec. Utilizing this data as well as considerations of propellant reserves and specific impulse loss due to the jet vanes in the exhaust nozzle, it was determined that, for an expected 750-lb spacecraft, the propellant weight should be 13.7 lb. The propellant tank design and pressure reservoir design based upon this capacity were undertaken and completed. It was determined that both tanks would be fabricated of titanium alloy (6% aluminum, 4% vanadium).

The basic design philosophy of the spacecraft requires that personnel be in close vicinity of the propulsion system tanks when they are pressurized to full operating pressure. The design of the vessels has been based upon Laboratory specifications regarding minimum safety factors to be used in vessels pressurized in the vicinity of personnel. In all cases, these specifications are more stringent than the USAF safety regulations in effect at AMR. The minimum safety factor used in the design of the tanks was that the burst pressure be 2.2 times the maximum operating pressure.

The pressure reservoir tank is spherical in shape, and the propellant tank is an oblate spheroid. This shape was necessitated by space limitations in the spacecraft. Initial models of the completed tanks were subjected to a proof-test program consisting of several combinations of vibration and pressure cycling. Several units of each different tank design were ultimately tested to the burst point. In every case, the burst pressure was above the minimum design safety factor. All remaining flight tanks were subjected to a flight-acceptance test consisting of three cycles of hydrostatic pressure to approximately 75% of burst pressure, and one cycle of high pressure at liquid nitrogen temperatures.

7. Development of the Propellant Expulsion Bladder

One of the most interesting design and development aspects encountered in the midcourse propulsion system was the fabrication of the bladder for the propellant tank. This device consists of a flexible, butyl rubber bag which contains the propellant and maintains a positive separation from the pressurizing gas. Space and weight limitations in the spacecraft caused the unique requirement that the pressurizing gas inlet and the liquid hydrazine outlet be at the same end of the tank. This requirement necessitated that the gas inlet be accomplished through an annular ring around the fuel outlet and that the bladder be constructed with ribs on its external surface so that a free passage was always available for the gas to pressurize the tank uniformly. For compatibility and reliability reasons, the bladder could not contain any seams, but was required to be of one-piece construction. The design restraints proved to be an extremely difficult problem for rubber fabrication, and necessitated the development of unique tooling and many sample fabrications before a satisfactory unit could be made by the subcontractor. The finished bladder is shown in Figure 340.

8. Development of the Pressure Regulator and Valves

Detailed design of the gas pressure regulator and the explosively actuated valves was subcontracted to appropriate commercial vendors. Concurrent with the type-approval testing of the propulsion system tanks, the pressure regulator and the explosive valves were subjected to an equally rigorous type-approval test program, consisting of vibration, shock, and temperature, in accordance with Laboratory environmental specifications for *Ranger*. All components passed the tests satisfactorily. Of special interest is the fact that the regulator was temperature-soaked at 257°F for 24 hr as would be accomplished in the sterilization procedures, with no indication of performance degradation in subsequent operations.

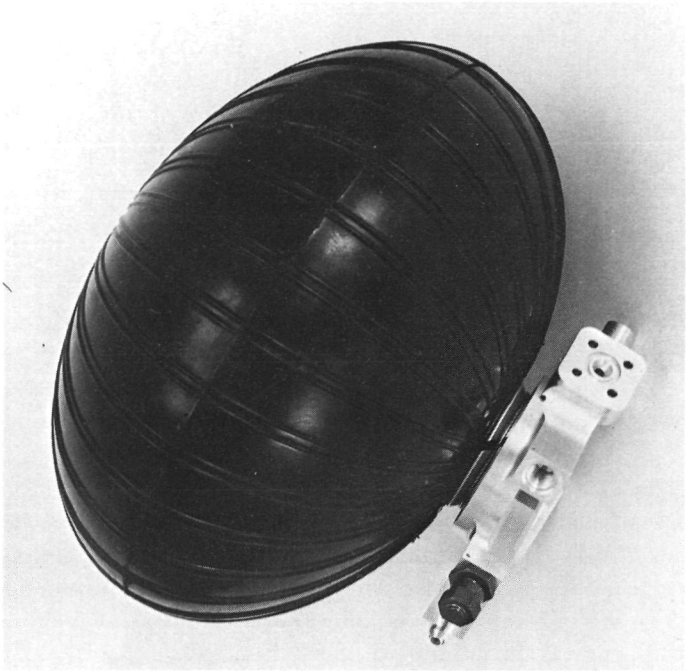

Figure 340. Propellant tank bladder

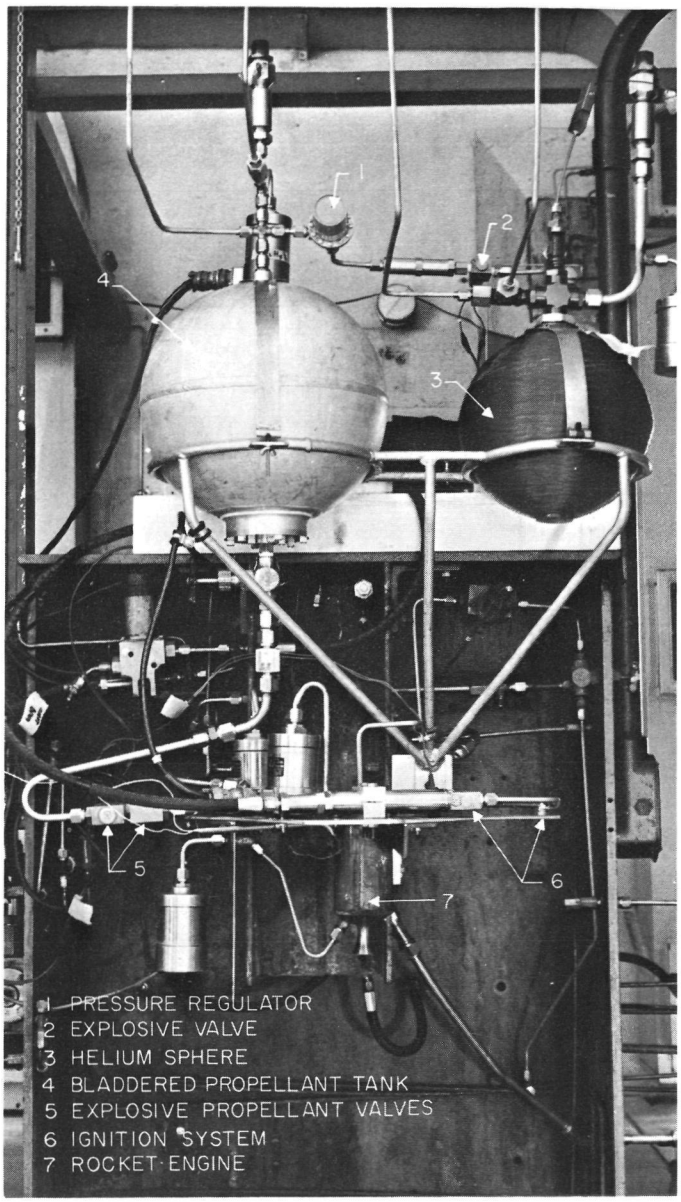

Figure 341. System functional test set-up

9. *Systems Testing*

A functional systems test model of the propulsion unit was constructed in the test cell and is shown in Figure 341. This unit was used to study system-starting transients and shutoff transients, effects of pre-pressurization level on such transients, verification of system pressure drops, the determination of minimum impulse capabilities of the system, and the effects on the system of complete propellant runout. The procedure in each of the tests simulated actual system operation as closely as possible. Explosively actuated valves were used throughout the test system. The system was fueled and pre-pressurized as in the actual system, and the firing procedure consisted only of one electrical signal to fire the necessary explosive valves at ignition and one signal to terminate the system at shutoff. The tests concerned with start-up transients at various pre-pressurization levels in the fuel tank and ignition cartridge produced results consistent with the design. Pressure levels chosen were equivalent to those which would exist in the pressure reservoir, fuel tank, and ignition system at three different temperatures: the design minimum operating temperature, 40°F; nominal operating temperature, 70°F; and maximum operating temperature, 165°F. In all cases, successful ignition and satisfactory operation were attained. In addition, one test was made to determine the effects of propellant runout. The system was started normally and the engine valving was left open until the propellant was completely exhausted, thus stopping the motor. No problems were encountered with this procedure, and it would appear that no explosions or damage will occur in flight if the shutoff signal is not given by the spacecraft. However, the wrong velocity increment would be delivered to the spacecraft.

With the receipt of complete sets of flight hardware, a series of system tests culminating in static firings was undertaken to evaluate the entire flight system in its final packaged condition: to determine system response rates, transients, and regulator characteristics when close-

coupled with the other system components. The test series initially consisted of expelling water from the bladdered propellant tank to observe whether the technique employed was suitable to hold the bladder onto the tank manifold and to determine propellant hold-up as the bladder collapsed.

In the course of these tests, it was found that the tank outlet baffle required redesign to assure that the bladder would not collapse incorrectly and trap a large quantity of fuel. Under various conditions of negative and positive gravity (accomplished by placing the tank at various attitudes) flow blockage occurred in some instances. The initial design consisted of a raised grating in the shape of a spherical segment. In the redesign, a cantilevered pylon was placed with a ball on top at the tank outlet, thus leaving an annular series of holes at the pylon base as a propellant drain. This design apparently forced the bladder to collapse more uniformly and assured an open channel to all parts of the bladder until it is virtually empty. The redesign was tested thoroughly and produced a propellant hold-up of less than 1%.

Next, the propellant tank circuit was mated to the helium pressurization circuit, and pressure regulator and water pumping tests were made using various pressurization levels in the propellant tank which would be present at the environmental temperature extremes. An explosively actuated valve was used to release the high-pressure gas, as in the flight unit. Good results were obtained with the exception of the performance of the gas filter, which is positioned between the gas blocking valve and the gas pressure regulator. The explosively actuated blocking valve opened so rapidly that a transient pressure differential occurred across the filter of such magnitude as to collapse the unit. The unit was redesigned after the initial test and now performs satisfactorily.

After establishing the characteristics and acceptability of the pressurization circuit, the system was mated to a rocket engine and ignition systems. The system was fueled and pressurized as it would be in the field. A series of three static firings was made, each of 55-sec duration. The over-all system functioned well, all system pressures and temperatures being within tolerance. Two photographs of the actual flight system (without cabling for clarity) are shown in Figure 342.

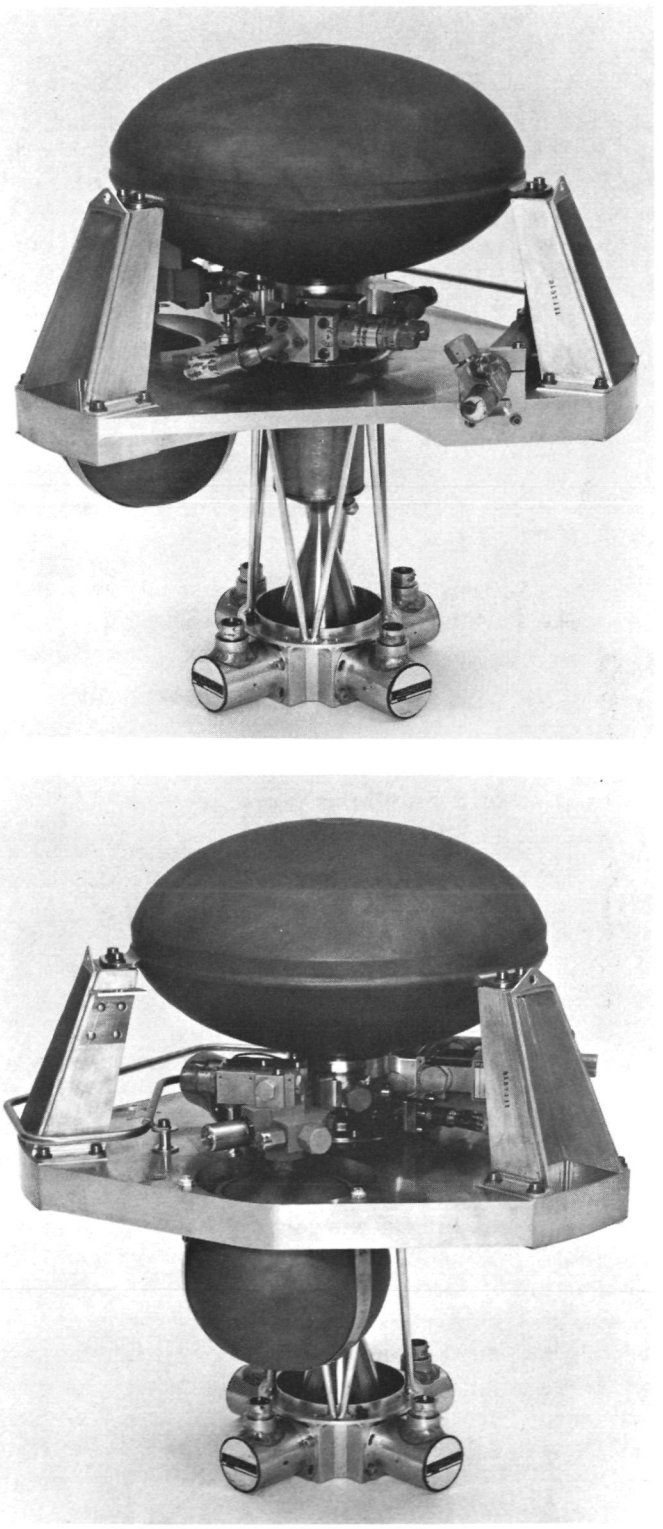

Figure 342. Midcourse propulsion system

One of the most critical items in establishing the over-all performance and operating characteristics of the flight propulsion system is its actual operation in a vacuum environment. This Laboratory does not possess suitable facilities, and, therefore, vacuum facilities were contracted for on a rental basis for this portion of the test program. The rented facilities allowed the rocket engine to be fired continuously into a steady ambient pressure

equivalent to approximately 100,000 to 130,000 ft. This pressure was sufficiently low to allow the rocket engine nozzle to flow full.

A total of 27 static firing tests were made at the leased facility. The tests were divided into three general categories: (1) defining rocket-engine performance (these tests employed a flight-design rocket engine, ignition system and fuel valving system, but utilized an externally located fuel supply system); (2) calibration of the jet vane (these tests utilized the same type equipment as the first tests with the addition of the jet vane system mounted below the engine); and (3) tests of the complete flight propulsion system.

Over-all, the following conclusions resulted from the tests:

(1) Ignition was achieved without difficulty in all cases. The starting transient appeared virtually identical to that obtained under normal atmospheric pressure.

(2) Engine operating characteristics (i.e., chamber pressure roughness, chamber wall temperature, and catalyst life) appeared to be identical to those found in tests at atmospheric pressure.

(3) The jet vanes and electromechanical jet vane actuators can withstand the high temperature environment at the rocket engine nozzle exit for the maximum run time (approximately 61 sec) without degradation.

(4) The entire system operated under vacuum. No malfunction. No excessive heat transfer was noted in any of the close-coupled components. Operating characteristics of the pressurization system were identical to those noted at atmospheric pressure.

Although all system components were found to be capable of surviving the various environmental rigors without loss in operational performance, it remained to determine how the over-all unit would perform when assembled into a complete system. Perhaps the most severe environmental condition encountered in the spacecraft flight from a structural standpoint is the vibration environment induced during firing of the booster stages. Accordingly, a series of tests was conducted to simulate such conditions. A complete propulsion unit was mounted in a prototype *Ranger* spacecraft which, in turn, was placed in a vibration tester. The test setup is shown in Figure 343. Physically, the propulsion unit was fueled with water to obtain the proper flight weight of the unit, and was pressurized to approximately 100 psig (low

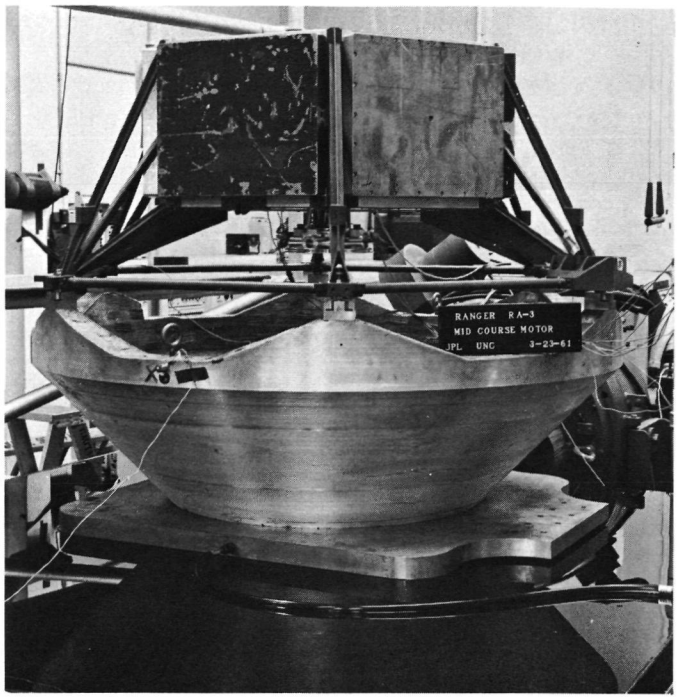

Figure 343. Propulsion vibration test set-up

enough to afford large safety factors for personnel in the vicinity during vibration tests). The test procedure consisted of exciting the unit and spacecraft with a sinusoidal vibration program from approximately 40 to 1500 cps at various *g* levels with the points of resonance being dwelled upon. In the course of these tests, two problems were encountered. A failure occurred in the structure that supports the jet vane actuator assembly below the rocket engine. This support, which is essentially a cantilevered structure, incurred weld cracks. Also, an abnormal excursion of a portion of the oxidizer ignition system was observed which, although it did not result in any failure, was felt to be a potential reliability problem. A modified design of the jet vane support structure consisting of the addition of three diagonal stabilizing struts was introduced, and the oxidizer ignition system was supported with an additional tie-down.

The tests were then repeated without incident. The propulsion unit was then subjected to the *Ranger* TA test vibration specification in three planes. After the tests the system was visually inspected and leak checked. No indications of system degradation were found. In view of the success of these tests and the desirability to reduce the weight of the spacecraft, modifications were made to the support structure that holds the propulsion unit in the spacecraft to minimize this weight. The TA test sequence was then run again. The unit once again suc-

cessfully withstood the vibration environment without leakage or damage. No further vibration tests of a proof-test nature are anticipated.

One of the fundamental design criteria of the RA-3, -4, and -5 spacecraft is the requirement of sterility. Currently, the most desirable method of assuring sterile equipment is high temperature. The approved Laboratory standard is 257°F for 24 hr. In addition, ethylene oxide gas diluted with freon will be pumped into the spacecraft shroud prior to launch. Thus, the flight equipment must withstand high temperature for long duration internally and externally, as well as the effects of the gas mixture externally.

A complete unit empty of liquids or gases was placed in an oven and soaked for 24 hr at 257°F. The unit was cooled down and then placed in a chamber filled with the ethylene oxide sterilizing gas mixture for another 24 hr. After these tests, the unit was visually inspected, leak tested, fueled, pressurized and statically fired. No abnormalities were noted in the physical appearance of the unit or in its operation.

G. Engineering Support Facilities

The accomplishment of a spacecraft development and flight program requires, in addition to the hardware design work, a number of supporting engineering activities and facilities. This section describes such activities as they have been employed at JPL in support of the *Ranger* Project. Included are the following:

(1) Environmental Test Laboratories.

(2) Instrumentation support.

(3) Computer applications and data systems.

1. Environmental Test Laboratories

The *Ranger* Project required the development of lightweight, vibration-resistant packaging techniques and equipment capable of extremely reliable operation in the space environment. Providing adequate testing facilities for the program necessitated constant improvement in environmental testing techniques and facilities.

The size and construction of the *Ranger* spacecraft itself created a need for increased vibration testing capabilities, and increased emphasis was placed on low-frequency vibration testing, due to the low resonant frequencies of the spacecraft structure in bending and torsion.

New techniques were developed, such as space simulation for the spacecraft and vacuum-temperature testing for components and assemblies. These were needed because the space environment drastically alters heat-transfer and material evaporation rates because of the reduced atmospheric pressure.

Because spacecraft equipment must also operate in the Earth environments, there has been a continuing need for conventional environments such as climatic testing. The need for sterilization of the spacecraft and its components has created a new requirement: sterilization testing.

a. Vibration testing. The testing of a complete spacecraft of the *Ranger* class requires vibration testing facilities capable of handling large-sized packages and fixture-plus-spacecraft weights of 2,000 to 2,400 lb. To accommodate such tests, a Ling L-249, 30,000-lb vector-force rating vibration exciter, and a Ling 175 KVA power supply and control console were installed in the new Environmental Laboratory during the summer of 1961. This system has the capability of testing *Ranger* spacecraft and fixture combinations at levels in excess of 5 *g* rms. Because of the size and unique construction of the *Ranger* spacecraft, it was necessary to design new and larger test fixtures, and to provide a means of testing these spacecraft in the pitch and yaw axes. This was done with a special granite oil table and horizontal test fixture with a hole in the center of both to allow clearance for the high-gain antenna feed. Figure 344 shows the vibration exciter, granite block, and horizontal test fixtures.

In vibration testing the spacecraft in the thrust axis, a 1,200-lb, cast conical fixture was used. Figure 345 shows the RA-3 structural model with this test fixture mounted on the L-249 vibration exciter.

To accommodate the increased *Ranger* component and assembly testing work load, a smaller granite block and oil slider plate test fixture was also installed in the Environmental Laboratory (Fig 346). Under normal operating conditions one of the vibration exciters shown in Figure 346 is kept in a vertical orientation, while the other remains horizontal. Consequently, changing of the axis of vibration can be accomplished by running vertical axis tests on one vibration exciter and the two transverse axes on the second vibration exciter. The use of these facilities has greatly improved the quality and control of the vibration tests, as well as aided in speeding up the *Ranger* environmental testing program.

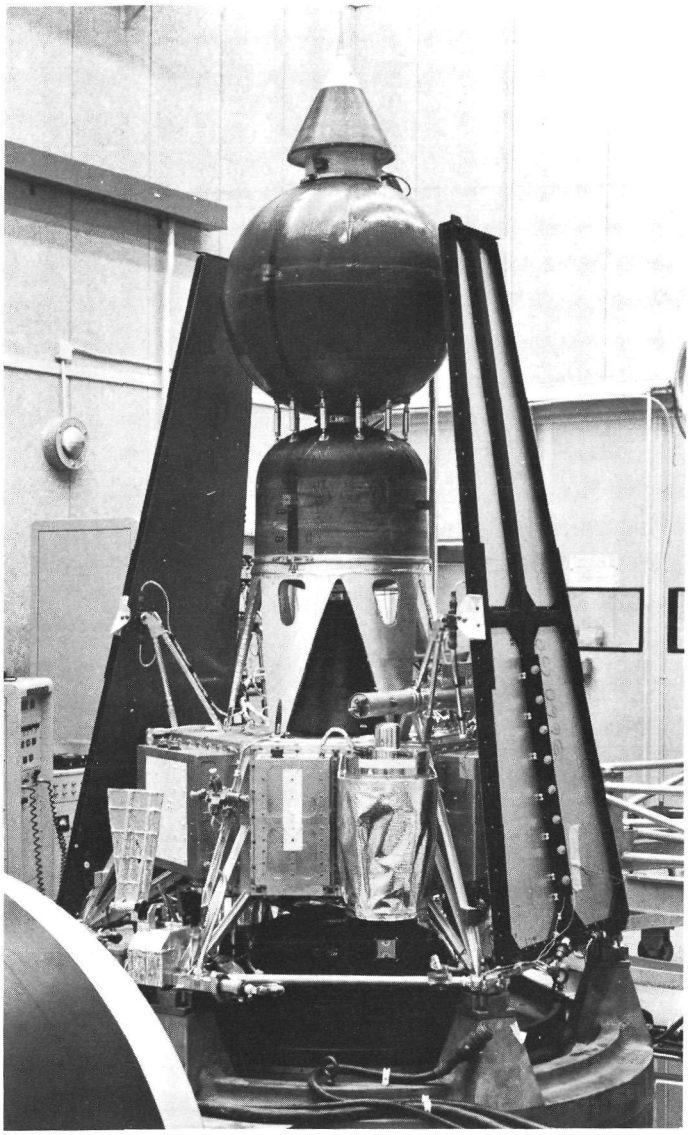

Figure 344. Test set-up, showing vibration exciter, horizontal test fixtures, and granite block

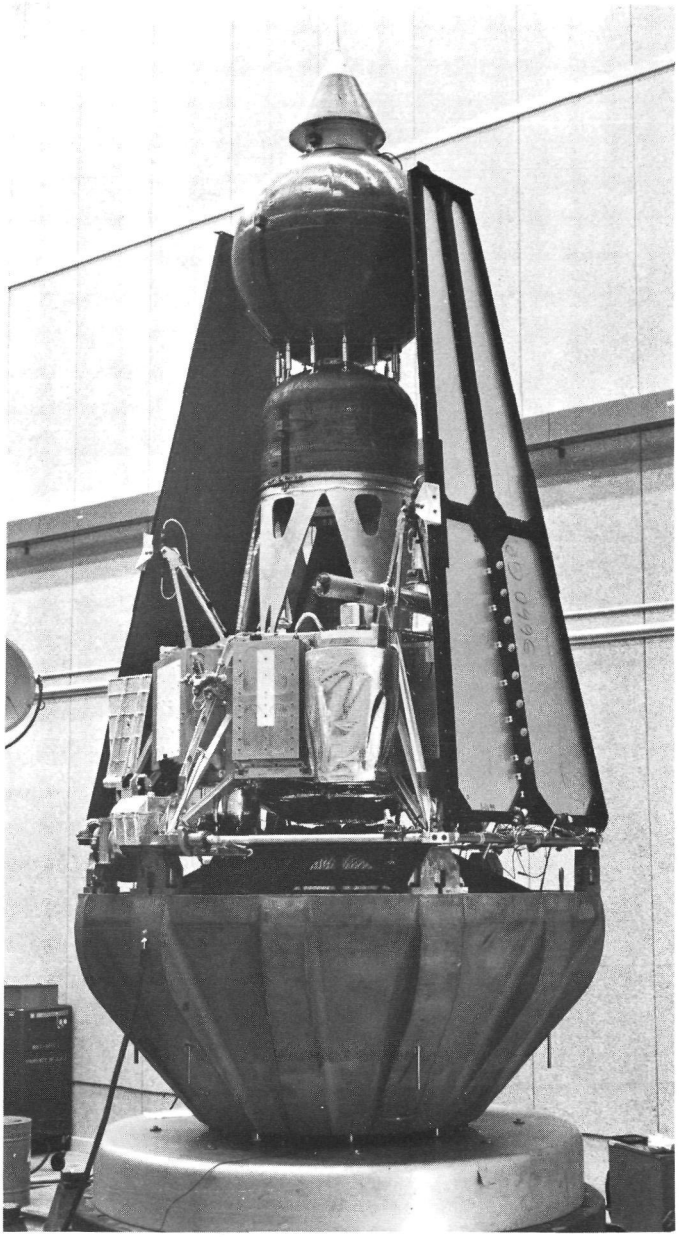

Figure 345. Vibration test set-up, showing thrust-axis test fixture

b. Vacuum–temperature testing. The vacuum–temperature testing capabilities of the Environmental Test Laboratory have been expanded and improved to handle the testing needs of the *Ranger* Project.

In the area of high-vacuum and temperature environmental-test equipment, six vacuum chambers were purchased, equipped with JPL-built, automatic temperature control systems, and installed in the new Environmental Test Laboratory. Two of these are 30-in. × 50-in. metal, horizontal-chamber, high-vacuum systems such as shown in Figure 347; and four are 18-in. × 30-in. glass, bell-jar, high-vacuum systems as shown in Figure 348. These systems are capable of an ultimate chamber pressure of 10^{-7} mm Hg when using their automatically filled, liquid-nitrogen, chevron baffle cold traps.

Automatic temperature control devices were installed on each of these vacuum systems, using liquid or gaseous nitrogen from a 1300-gal Dewar. These devices are used to control the temperature of components inside the vacuum chambers either by direct conduction from heat exchangers connected to the components, or by radiation to cold wall shrouds. The systems are capable of controlling the temperature in the range between −320°F

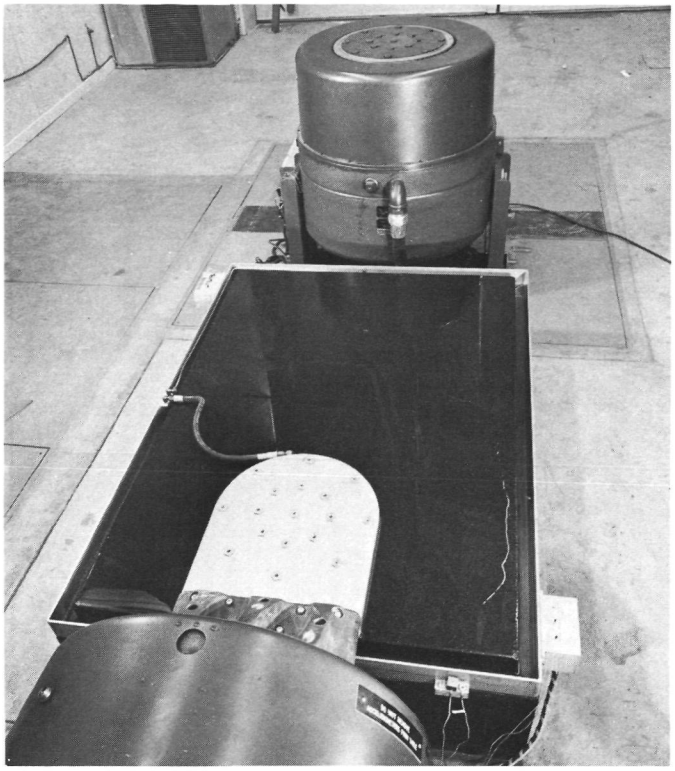

Figure 346. Vertical and horizontal vibration exciters, oil slider plate, and granite block

Figure 347. 30- by 50-in. metal chamber high-vacuum systems

(−195°C) and +300°F (149°C). The temperature is controlled and continuously recorded by Leeds and Northrup Model H recorders. These installations became operational during November 1961.

To provide for long-duration, high-vacuum exposures, four 18-in. × 30-in. glass, bell-jar systems were installed and placed in operation during May 1961. These systems are capable of an ultimate chamber pressure of 10^{-7} mm Hg when using their automatically filled, liquid-nitrogen, chevron baffle cold traps. Many tests to study the effects of long-term vacuum exposure on equipment have been run in these and other ETL facilities. One study of the drift in telemetry oscillators ran for a period of 6 months.

Space simulation. A 6-ft vacuum chamber was modified for use as a space simulator by the addition of liquid-nitrogen cooled walls and four Strong Electric Company carbon arc lamps. This system became operational in October 1960. Many *Ranger* environmental tests have been run in this facility, including the PTM, RA-1, RA-2, RA-3 PTM, RA-3, and RA-4.

Figure 349 shows the 6-ft space simulator and Figure 350 shows a test setup in the simulator of the RA-3 hex.

c. Environmental testing for the* Ranger *Project. Environmental test work on the *Ranger* Project started during late spring 1960. During the period covered by this report, 3696 tests associated with the RA-1, -2, RA-3, -4, -5, and RA-6, -7, -8, -9 programs have been handled by the JPL Environmental Test Laboratory. This number includes 69 systems vibration tests and 25 space simulator tests which, by virtue of their complexity and relative importance in the programs, have required more test personnel and time than the assembly level tests.

Total *Ranger* usage of ETL test facilities follows:

	Number of tests			Number of tests
6-ft space simulator	25	Temperature		452
Vacuum	162	Temperature/ humidity		56
Vacuum–temperature	343	Gas sterilization		50
Vibration	1470	Salt spray test		12
Low-frequency vibration	148	Off-Lab Facilities	Explosive atmosphere	6
Centrifuge	568		Altitude	1
Shock test	388		Temperature	15

The following is a breakdown of these tests by program and type:

Spacecraft	Experimental	Type approval	Flight acceptance	Total tests
RA-1, -2	397	794	1232	2423
RA-3, -4, -5	239	446	581	1266
RA-6, -7, -8, -9	1	4	2	7
			Total	3696

2. *Instrumentation Support*

The most important of the supporting activities in the instrumentation specialties are summarized here.

a. Vibration testing. In order to support the large number of type-approval and flight-acceptance vibration tests for the *Ranger* program, an enlarged instrumentation system was assembled. Included in this system were accelerometers of high- and low-frequency response, amplifiers, direct-write oscillograph recorders, and magnetic tape recorders. This equipment was mounted in racks that could be readily moved to various test locations and could be expanded to handle large assignments. The maximum signal-handling capacity was 30 oscillograph channels and 25 magnetic tape channels.

Most of the original instrumentation equipment will be installed in the recording room of the new Environmental Test Laboratory building. It will be centrally located to handle tests conducted in any part of the testing facilities.

Instrumentation support was provided for tests on a large variety of spacecraft components including the solar panel, high-gain antenna, battery boxes, component cases, magnetometer boom, and midcourse propulsion system. In addition, a large number of composite-structure tests were supported, using a maximum instrumentation capacity.

b. Structures testing. The structural proof tests of the *Ranger* bus and its various adapters were performed on the Structures Test Model, the Proof Test Model, and various other subassemblies that included antenna structure, traverse boom, and the *Ranger–Agena* adapter. The purpose of these tests was to check the design concept with experimental evidence in the form of measured strain and deflection with applied forces simulating the first and second boost phase of the spacecraft.

The data was recorded in digital form on punched paper tape, using a low-speed data logging device with a sampling rate of 2 sec per point and a total system capability of 192 channels plus calibration and computer programming information. The recorded tape was reduced to engineering units by the Datatron 205 computer.

Figure 348. 18- by 30-in. glass bell-jar high-vacuum systems

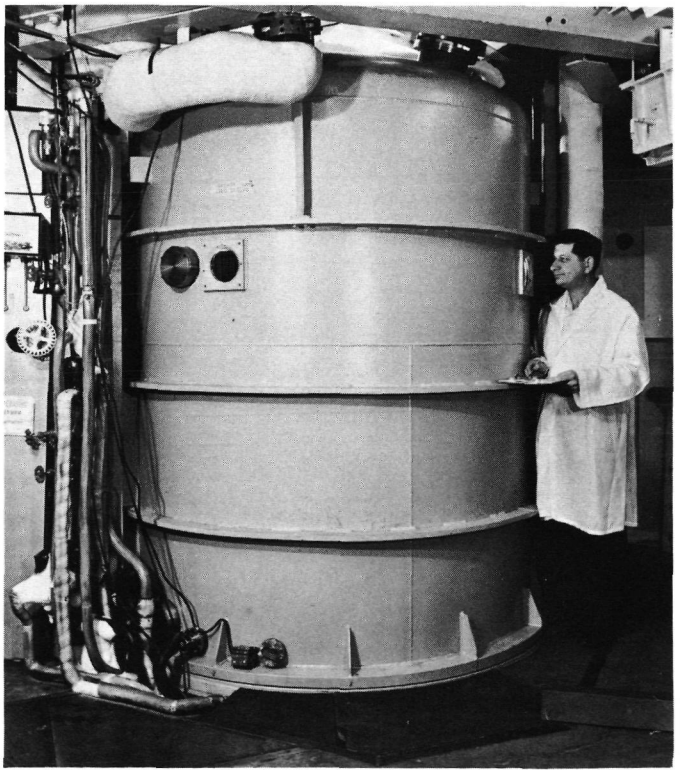

Figure 349. 6-ft space environment simulator

c. Thermal testing. Thermal environment tests were conducted on the *Ranger* Temperature Control Model and the Proof Test Model, and the critical areas of the spacecraft were monitored during the "dry runs" of RA-1,

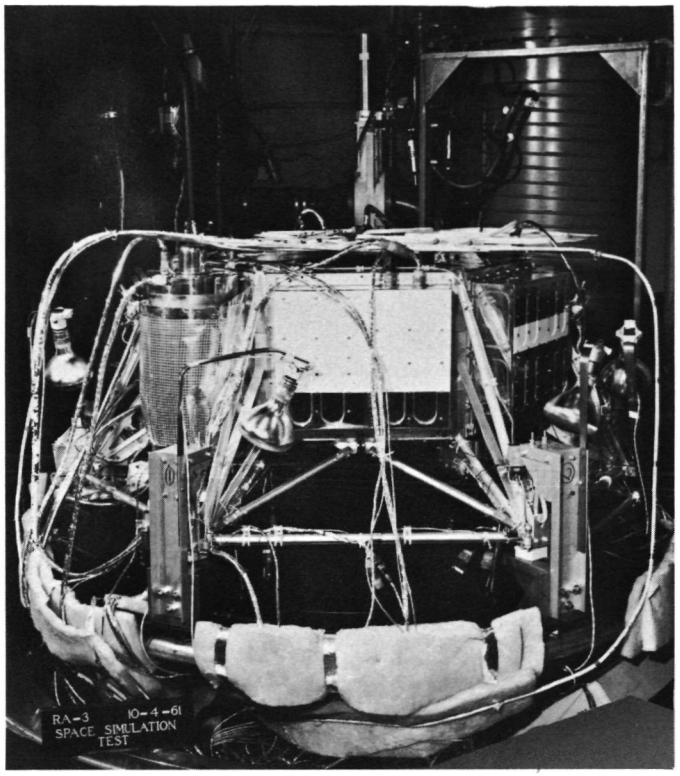

Figure 350. RA-3 hex prepared for test in 6-ft space environment simulator

RA-2, and RA-3. An installation technique for thermocouples was developed that allowed rapid installation and good thermal transfer, with no welding necessary. This method utilized thermo-setting conductive plastic.

The tests were performed with the spacecraft inside the 6-ft space simulator, with all thermocouples and control cables passed through the vacuum chamber wall with special feed-through plates. Many test hours included the establishment of heat balance conditions within the spacecraft, during which heat dissipated in various areas of the spacecraft was simulated and programmed according to the planned flight sequence.

Thermal monitoring operations were also conducted during separate tests of various instrument subsystems and components such as the magnetometer, Lyman-alpha telescope, and main battery and regulator.

d. Pyrotechnic tests. The design and evaluation of squib-actuated devices used in the *Ranger* spacecraft required a test program for which special transducers were designed and instrumentation equipment provided and operated. Several "bombs" were designed to measure pressure characteristics of the squibs fired, at high and low temperatures and in vacuum. The pin-puller tests that followed required the measurement of pin position and acceleration and squib current. Pin-position instrumentation required the design of a high-response, non-contacting linear transducer. About 300 tests were made in this squib firing program.

e. Systems tests. Performance evaluation of the ground support equipment for each *Ranger* spacecraft requires a central recorder which handles up to 44 signals during the systems test operations. This recorder is a direct-write oscillograph operating at various speeds and bandwidths to suit the test requirements. As a part of the system test complex, it is moved to various test locations at JPL and to Cape Canaveral. Three such recorders and operators constitute the instrumentation support for the *Ranger* operations.

f. Field tests. In addition to tests conducted in various JPL facilities, instrumentation, equipment, and operators have been provided for a variety of "field-test" operations. For this type of testing, transducers, portable oscillographs, tape recorders, and associated equipment were systematized to meet the requirements. The tests included the RA-1 Lockheed system-test at Sunnyvale where telemetered signals were recorded, the static firing test at Santa Cruz where vibration signals were recorded, the RA-3 capsule drop-test where accelerations were recorded, the midcourse propulsion system vibration tests at Wyle Laboratories, and RA-3 AD/F package vibration tests at the Aeronutronic facility.

g. Space Science instrument development. In addition to the test instrumentation support described above, important contributions were made to the design, development, fabrication, and testing of the electrostatic analyzers for the solar corpuscular radiation experiment.

3. Computer Applications and Data Systems

a. Computation facilities. The *Ranger* Project has been supported by the JPL Central Computing Facility. This facility consists of three types of equipment: conversion devices, general-purpose computing equipment, and display devices. These facilities were used to provide both pre-flight design support and flight operation data processing.

Conversion devices. These devices convert data into a form suitable for entry into the IBM 7090 system.

(1) *Telemetry-to-magnetic-tape translator.* This data translator accepts up to seven channels of digital data (asynchronously), converts this data into blocked IBM

format and records it on magnetic tape for entry into the IBM 7090 computer. All spacecraft telemetry data has been converted to IBM format magnetic tapes by this device, which is functionally part of the telemetry data reduction laboratory.

(2) *Digilog.* This device, developed at JPL, is a general-purpose data recorder. It is capable of bilaterally converting data in a number of analog or digital forms into blocked IBM format magnetic tape. Its principal uses in support of the *Ranger* Project have been converting teletype paper tape into IBM magnetic tape and serving as an interim vidicon translator.

(3) *Vidicon conversion system.* This system was developed to allow computer manipulation of spacecraft vidicon data. It converts the analog video signal contained on magnetic tape into blocked IBM format magnetic tape. It also converts blocked IBM format tape of computer manipulated video data into an analog tape of the data, or into an analog signal to drive a kinescope camera.

(4) *Paper-tape-to-card (IBM 047) and card-to-paper-tape (IBM 063).* These devices are used primarily in the flight operation. The data which arrives by teletype from the tracking sites is punched into IBM cards by the IBM 047 for entry into the IBM 7090 computer. Prediction data which is sent to the tracking sites is punched into IBM cards and converted to teletype tape by the IBM 063.

General-purpose computing equipment. The general-purpose computing equipment available at JPL consists of both analog and digital computers. These are general laboratory facilities and, as such, are used by all JPL programs. The *Ranger* Project used 26% of the analog facility in 1961 and used 52% of the digital capability in 1961. The digital computer facilities consist of an IBM 7090 computer and associated input–output equipment.

(1) *IBM 7090.* The IBM 7090 is a large, high-speed, geenral-purpose digital computer. The JPL installation includes a 32, 768-word, magnetic core memory, two input–output data channels, 12 magnetic-tape units, and on-line printer, card reader, and card punch.

(2) *IBM 1401.* Two IBM 1401 systems are available for input/output processing off-line from the 7090. These are general-purpose digital computers used for translating magnetic tape output from the 7090 printed copy or to punched cards, and for translating punched cards to magnetic tape for computer entry. Each of these computers includes 4000 characters of magnetic-core memory, two magnetic-tape units, a 600-line-per-min printer, and 800-card-per-min reader, and a 250-card-per-min punch.

(3) *Analog computer support.* The analog computing facility incorporates four consoles of Electronic Associates analog computers, including a total of 250 operational amplifiers with a complete complement of associated non-linear equipment, input and output devices. The four consoles may be operated independently to simultaneously solve four different problems, or two, three, or four consoles may be slaved together to handle problems of unusually high order or complexity. The facility has a balanced complement of both precision low-speed and high-speed non-linear components, such as function generators, multipliers, and trigonometric resolvers, which enable handling of a wide range of types of problems. For outputs, there are x-y 30-in. by 30-in. plotters, a total of 34 channels of strip chart recorder outputs, and 17-in. oscilloscopes.

Data display devices. In addition to tabular listings prepared by the IBM 1401, trajectory parameters, time histories of measurements, and the results of calculations are displayed on two other devices.

(1) *Moseley 575 magnetic tape plotter system.* This system uses IBM magnetic tape as an input and creates an inked graph for the output. Scaling and plot control are under 7090 program control. Multiple traces may be made by selecting several traces on the input tape and plotting one on top of the other.

(2) *4020 printer-plotter.* The SC 4020 is a high-speed microfilm recorder produced by Stromberg Carlson, a division of General Dynamics Corporation. It records on microfilm data supplied from the IBM 7090 on magnetic tape. The basic unit will accept characters at a rate of 17,400 per sec or plot coordinates at 12,500 per sec. Records are produced on standard 35-mm film; the raster is a 17.5 × 17.5 mm square. Film magazines contain 400 ft of film, which may be program-advanced at a rate of 10 frames per sec, maximum.

Quick-look is available in the form of a hardcopy camera option, which will generate one copy, 7.5 × 7.5 in., of each frame of information generated by the SC 4020. The copy is made on Du Mont Linowrit 4 photorecording paper and is processed on-site through the F-85 oscillogram processor making quick-look hardcopy available in 30 min.

b. Spacecraft design support.

Digital computer support. The digital computer facilities have been used to solve a large variety of problems in support of the *Ranger* spacecraft design and in analysis of the lunar missions. In many cases, general computer

programs were developed representing a capability used by several missions. In other cases, the computer program was developed for a particular design problem.

(1) *Trajectory programs.* The problem of trajectory computation represents the major area of computational support on the digital computer facility. An extensive set of IBM 7090 programs has been developed during the past 2 years and used for lunar trajectory studies. The trajectory programs fall into two areas: high-precision numerical integration of the total accelerations and conic section approximations to the trajectory. In the high-precision numerical integration programs there are two major capabilities: A three-dimensional, powered flight simulation program with guidance simulation capability and a general-purpose lunar and interplanetary space trajectories program in which gravitational accelerations and simple thrust acceleration are integrated. Both of these programs are coupled with a variety of subroutines to transform rectangular coordinates resulting from the numerical integration to required output coordinates and to transform from desired input systems to rectangular coordinates.

Conic section approximations have been developed allowing single conic approximation of a near Earth conic, followed by a transit conic, which is in turn followed by a lunar approach conic. These programs are used for general surveys of possible trajectories. Conic approximations offer the advantage of fast computation, but are, of course, not precise enough for the standard trajectory computation.

A trajectory program monitor has been developed and is used to run most of the trajectory computations. This monitor allows the automatic coupling of the powered flight program, the space trajectories program, conic approximation programs, and plotter output programs under input parameter control. A flexible system allows rapid response to a large variety of production computations. Standard computer input forms are available, providing easy communication of input information.

(2) *Structural analysis.* A structural analysis program has been developed to study truss structures with pinned or fixed jointed members. The calculation is in two parts. Part one requires a definition of the structure in terms of the lengths, areas, modulus of elasticity, and Poisson's ratios of the connecting members, as well as the corresponding coordinate end points. From this data, a stiffness matrix is generated, and with a matrix of loads at the joints, the static displacement is found. Optionally, part two uses a diagonal mass matrix with the stiffness matrix to find the lowest six mode shapes and frequencies. The program can include up to 60 joints and up to 130 deg of freedom.

(3) *Midcourse guidance analysis.* The midcourse-guidance error analysis program considers the distribution of position and velocity errors at injection of the spacecraft with distribution of errors in components in the spacecraft control system at midcourse maneuver time to characterize the miss error distribution at the target planet. The program uses a Monte Carlo technique, which selects an injection error, guarantees a velocity error at the time of midcourse maneuver, simulates the maneuver including the errors produced by the maneuver itself, and calculates the miss distance at the target. This repeated calculation defines the distribution of miss at the target.

(4) *Attitude-control simulator.* The attitude-control simulator accepts inertial data which defines a spacecraft, data which defines the spacecraft attitude-control system, and initial position and tumbling rates. The program then simulates the sequence of functions which tend to stabilize the vehicle within a preset sequence of attitude-control events. Although the program was initially written for *Ranger,* it may be used for any spacecraft that uses as a reference some rectangular coordinate system having the vehicle at the origin.

(5) *Miscellaneous.* A significant amount of effort has been devoted to space instrument analysis and communications systems analysis.

The analog computer facility has been used primarily for control system design and simulation. One-, two-, and three-axis simulations of the spacecraft with the effects of the appendages and control system were made in roll, pitch, and yaw. The dynamic effects during maneuvers of the solar panels, high-gain antenna, the omnidirectional antenna, and the flexible boom were simulated to determine their effects on the control systems and structures. Detailed studies were made through simulation of such components as the gyros, power-supply regulators, the integrating capacitors, and sensors. The results of these component studies were then incorporated into the over-all system simulations. One of the more important aspects of these studies depended on the ability to introduce noise into the systems artificially by using the analog computer noise generators.

c. Flight operations.

General participation. The Central Computing Facility supported the *Ranger* flight operations by preparing computer programs to carry out the required orbit-determination, midcourse-guidance and telemetry redue-

tion calculations; operating the computer application and data system facilities; developing special hardware for translation of data to computer format; and developing procedures to handle the data from receipt of raw data to delivery of reduced data to the user. In addition to supporting the actual flight, programs and equipment were developed to allow the facility to support spacecraft subsystem and systems tests and the countdown operation at Cape Canaveral.

Orbit determination. This program minimizes the weighted sum of the squares of the differences between actual observables and those observables calculated by the space trajectories program to determine the spacecraft injection initial conditions. For the RA-3 mission, the tracking data editing program was added to the orbit-determination process to automate the elimination of faulty data points.

Midcourse and terminal-maneuver program. This program computes the required spacecraft maneuvers to allow a successful lunar impact mission. The program computes the velocity impulse required to accomplish lunar impact at the desired location at a favorable time, while meeting constraints necessitated by the propulsion and other spacecraft systems and DSIF capability. The program allows for nonstandard operations and assists operations personnel in rapid selection of alternate landing areas and flyby trajectories. The terminal-maneuver portion of the program computes the turn necessary to orient the braking rocket correctly, or in the case of a flyby, to orient the vidicon camera.

Scientific telemetry data reduction. All scientific telemetry data from *Rangers I, II,* and *III* have undergone computer reduction. The RA-1 and -2 scientific reduction program gives a comprehensive reduction of all the scientific experiments aboard those spacecraft. RA-1 and -2 scientific data arrived at the Central Computing Facility in both real and non-real time, in a commutated from. A 7090 computer program was written which successfully decommutated the data and performed extensive error detection upon the data. Programs were also developed for the RA-3 gamma-ray and seismic experiments. All scientific measurements for RA-1 and -2 were computer-reduced for ground systems tests, and, during the countdown, to verify the science package readiness. Equipment was developed to gather data from gamma-ray ground test equipment for RA-3, and a 7090 computer program was developed to reduce it.

Vidicon telemetry data reduction. In addition to the development of the vidicon translator, a set of programs was developed for digital computer clean-up of the RA-3, -4, and -5 pictures. Attempts have been made to effect single picture clean-up, and planning has been done for multiple picture processing. The programs written so far have been designed to remove burst noise, correct geometric distortion, remove sweep non-linearity, and remove random noise by additive techniques.

Engineering telemetry data reduction. Programs have been developed to reduce to engineering units and time correlate these measurements for all *Ranger* missions. These programs are run both on selected measurements which are teletyped to JPL from the DSIF tracking sites, and on the complete data which arrives at JPL by mail. For RA-3, the capability was developed to provide plots of all engineering measurements using the SC 4020 printer-plotter as described above. Both time plots and cross plots are available using the SC 4020.

H. Ground Support Equipment

a. Introduction. Originally, on the RA-1 Proof Test Model (PTM), it was recognized that equipment and techniques would have to be evolved to allow comprehensive testing of the first *Ranger* spacecraft. The equipment originally planned and utilized on RA-1 PTM and RA-1 and -2 operations formed the nucleus of the equipment that has been utilized through the RA-4 test program.

Basically, the System Test Complex (STC) consists of various racks of equipment arranged in orderly fashion, comprised of test portions corresponding to each of the major subsystems within the spacecraft. As such, the test positions are basically oriented toward the testing of each subsystem, but sufficient direction and coordination of this equipment has been maintained so that the result is a true spacecraft System Test Complex. As the projects have changed in concept through RA-4 and into the follow-on phases, various deletions and additions of specific equipment have been necessary so that the STC keeps in step with the various changes in the spacecraft mechanization.

Throughout this evolution, improvements of basic techniques and test hardware have been incorporated to allow not only an up-dating of the complex, but also a steady improvement in its utility. Improved techniques in cabling and connectors, as well as expeditious routing of test cables constitute examples of this philosophy. The prime

example that has required complete obsolescence of old equipment and replacement by new is in the scientific area, where with each mission, the concept of this portion of the GSE changes significantly.

Certain other equipments augment the System Test Complex, while not directly associated with the testing of a specific subsystem on the spacecraft. Examples are the data display equipment, the central recorder, system test timer, and the system test J-box. These units constitute an essential portion of the STC, but provide an over-all service to the test area in general.

The GSE required to support the RA-1 and -2 programs consisted of three sets of System Test Complex equipment, two sets of blockhouse equipment, and one set of laboratory equipment. Two sets of STC equipment were used for spacecraft verification at JPL; the third set was used for final checkout in the spacecraft assembly area at AMR.

One set of blockhouse equipment was used to perform launch operations at AMR; the other was used for dummy-run operations at JPL. The set of laboratory equipment was used to test the spacecraft subsystems before delivery to the SAF at JPL.

b. System Test Complex. The System Test Complex is the basic test equipment used for performing the ground system test, which is intended to verify that the spacecraft will perform properly in a flight sequence.

Capabilities. The STC has the capability for stimulating and monitoring the spacecraft, and in addition:

(1) Operates the entire spacecraft in a manner simulating the countdown and flight sequence.

(2) Monitors system functions as well as subsystem inputs and outputs for quantitative evaluation of spacecraft performance.

(3) Exercises all elements of the spacecraft through their entire dynamic ranges for the purpose of evaluating their performance under influences produced by the presence of the complete spacecraft.

Break-in boxes. Break-in boxes or in-line cable adapters which allow access to all leads at a connector interface are permitted during spacecraft testing, except during system test. These adapters generally consist of a short length of cable with a male and female plug at either end and with a terminal or plug box in the middle. Each lead in the cable bundle is connected to a terminal or binding post so that each electrical circuit in the cable is made available. Normally, shorting plugs are connected across these connectors to complete the circuits, but may be removed to allow current measurements.

Dummy loads. As a precautionary measure, dummy loads are used in place of the actual subsystem cases during the initial turn-on operations following spacecraft assembly. A dummy-load box is required for each of the six cases around the hex. These boxes simulate the load each case would normally draw from the spacecraft main harness and power supply.

Self-power capability. The system test equipment has the capability of providing power to individual subsystems in the spacecraft at times when basic spacecraft power is not available due to the temporary absence of the spacecraft power supply or ring harness, and during certain types of trouble-shooting or noise isolation. Each subsystem test position is required to be equipped to provide this independent operation through a special cable to be plugged into the appropriate spacecraft subsystem directly.

R-F environment. The spacecraft performance is evaluated in an r-f environment which simulates the *Atlas–Agena* telemetry and beacons, ground r-f, radars, missile guidance r-f, all as part of the r-f compatibility test. The r-f simulators are not a permanent part of the System Test Complex.

Central recorder. A 50-channel recorder is provided as a part of the STC. It is used to provide a record of spacecraft performance during system test and records some telemetry as well as subsystem monitor data.

Spacecraft adaptations required for test. In general, the System Test Complex is made to conform to spacecraft requirements and not the spacecraft to GSE requirements. As such, the direct-access connectors are the only permanent adaptations made to the spacecraft for the convenience of test operations.

Test Complex checkout. All test equipment which forms a part of the System Test Complex is completely checked out with an actual spacecraft subsystem by the cognizant group prior to delivery of the equipment to the spacecraft assembly facility. Spacecraft power is normally supplied by the spacecraft batteries and solar panels; however, during systems test, alternate sources of power must be used because of the limited life of the spacecraft battery and other considerations.

In order to preserve the longevity of the spacecraft battery, it is used only when the test being performed requires actual spacecraft battery power to satisfactorily evaluate the test results. Sometime during test operations, the spacecraft battery is used for one simulated flight sequence to assure proper operation, preferably during space simulator tests.

Power ground support equipment. The system test power ground support equipment (GSE) for RA-3, -4, -5 (Fig 351) incorporates all of the required functions of spacecraft secondary power, monitoring, and control. It provides detailed subsystem analysis capability for test operations, beginning with initial power turn-on and extending to the final spacecraft integrated system test conducted just before transport to the launch pad.

The launch support test set contains some of the basic monitor and control features of the system test equipment, but reflects the constraints and design considerations imposed by the launch complex operations. It consists of a modified monitor-control panel and other assemblies similar to those in the systems test set.

Figure 351 shows the RA-3, -4, -5 power GSE (assemblies extended on quick-disconnect integral slides) prior to delivery to the JPL system test facility. Relatively high density packaging is used with the test set assemblies mounted at the front and the back of the consoles (Fig 352).

Self-test capability. A simulator-tester assembly (Figs 353 and 354) is provided to simulate all spacecraft power functions monitored and controlled by the GSE. A transfer assembly, on command from the control panel, switches between the spacecraft and the calibrator-tester assembly.

Tolerance detectors. In the transfer assembly (Fig 355) a system of go, no-go primary continuous monitors (Fig 356) is incorporated to detect malfunctions, rapid changes, and complementary troubles occurring in the spacecraft power subsystem. The output of each of these monitors is a descriptive fail indication on the operator control panel. During self-test, the detectors are required to respond to signals that are out-of-tolerance low, out-of-tolerance high, and normal. If, and only if, all self-test conditions are satisfied for all detectors, a single test complete indication is given. Diagnosis, if required, is possible

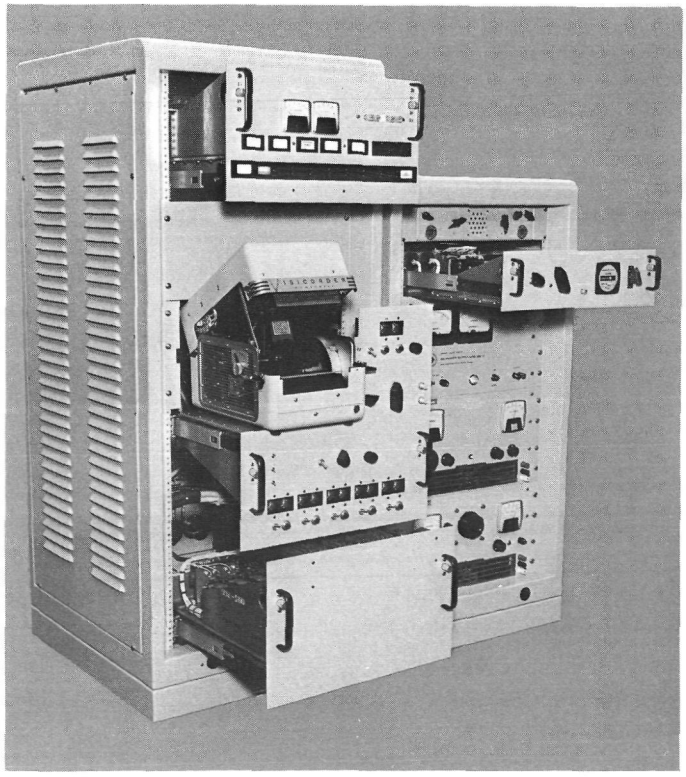

Figure 351. Power GSE for RA-3, -4, -5

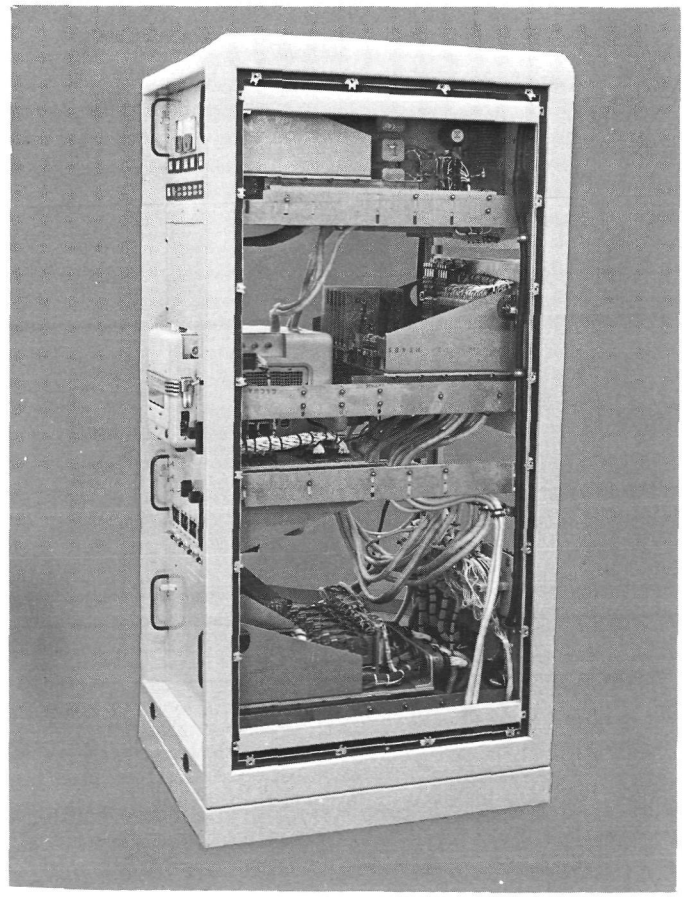

Figure 352. Power GSE with side panels removed

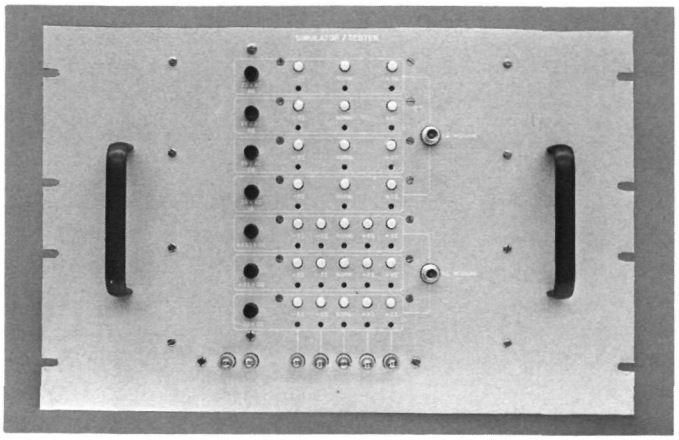

Figure 353. Simulator–tester

as the self-test is slow enough (3 to 4 sec) that the operator may view the front panel indications.

Secondary power. The primary functions of the secondary power GSE are to provide ground power, switching between internal and external power, ¼-w transmitter power control, and monitoring of voltages supplied to the spacecraft subsystems. Provisions for analysis and trouble-shooting of spacecraft power failures are also to be provided.

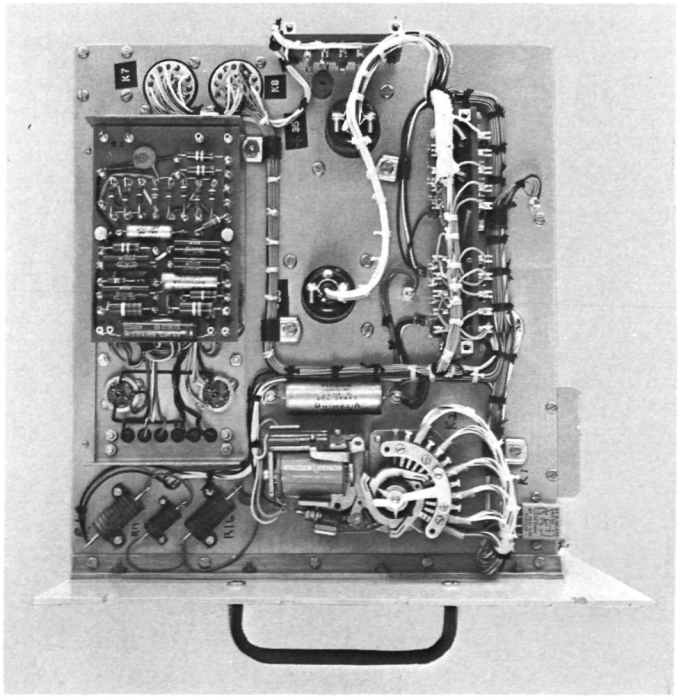

Figure 354. Power GSE packaging

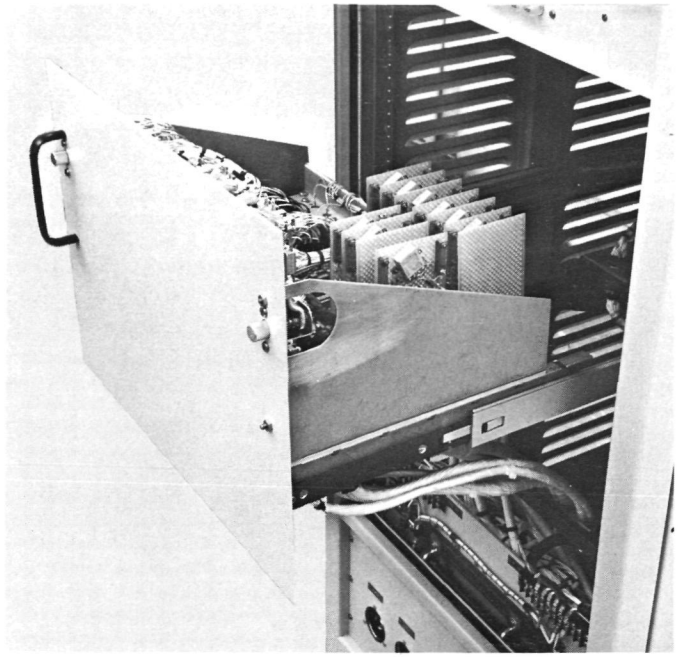

Figure 355. Transfer assembly power GSE

Control functions. A control panel (Fig 357) presents all primary controls and monitors normally encountered in system test and launch operations. The operator may elect to conduct a GSE self-test, a test on the spacecraft power system, or both. The controls include: external power, internal power, solar panel simulated power, GSE test, and GSE operate.

Monitors. Monitors available at the control panel include: external power supply current, booster regulator

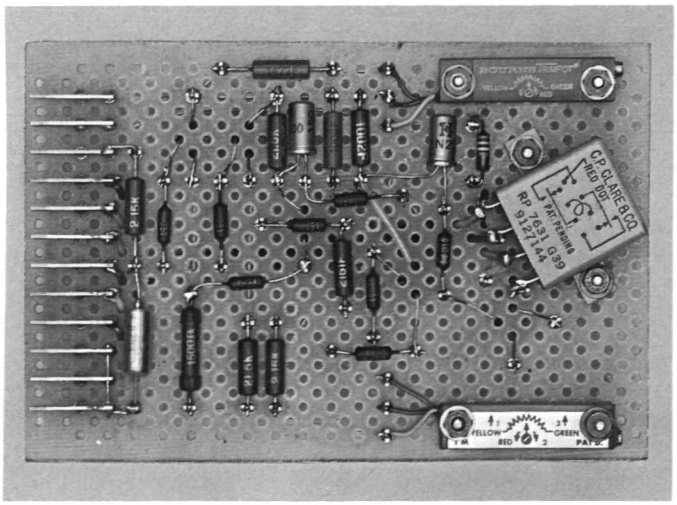

Figure 356. Tolerance detector

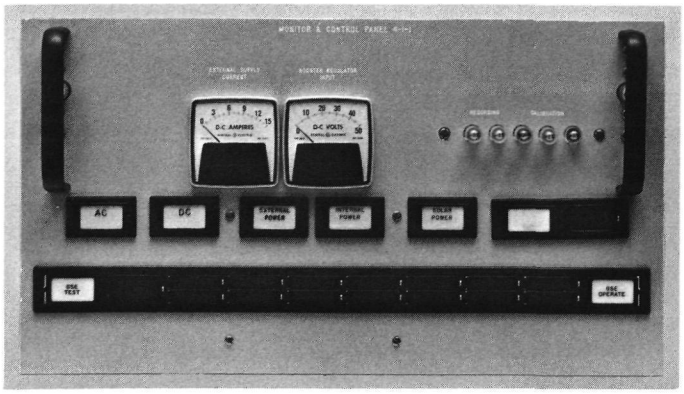

Figure 357. Power GSE control panel

input voltage, and an indication for each of the controls—a visible indication in the *fail* condition only, of the following primary monitors:

(1) Communications converter.

(2) Attitude-control three-phase inverter.

(3) Attitude-control single-phase inverter.

(4) Attitude-control d-c converter.

(5) CC&S converter.

(6) Data encoder converter.

(7) Scientific inverter.

(8) Command converter.

(9) Launch battery terminal voltage.

(10) Launch battery temperature.

(11) Launch battery current.

Positive indications are given for GSE self-test complete, battery charge required, and battery charging.

Recording. A multiple channel galvanometer type recorder (Fig 358) is used during PTM testing for transient behavior and special effects. This unit operates in conjunction with a circuit selector assembly to provide a record of 50 spacecraft power functions. Channel identification and selection controls are present at the recorder assembly. This equipment provides essentially two distinct records: one is a serial presentation of all power monitor functions, and the other is a block of five related functions recorded simultaneously. Each selector may be manually or automatically controlled.

All functions monitored are available at the front panel and, in addition, are distributed to connectors at the rear of the console to allow use of a supplementary digital display and recording system. The functions depend on the positioning of the transfer assembly. During the operate condition, actual spacecraft functions are available. In the self-test mode, these outputs are of internal GSE simulation.

Power supply equipment. The GSE power supply equipment furnishes external spacecraft power, solar panel power simulation, GSE auxiliary power, and precision monitoring excitation. All supplies are short-circuit protected so that a failure in the spacecraft or associated cabling does not destroy cabling. Although a battery charger is not a standard part of the system-test GSE, provisions for its use are made to include: (1) monitoring condition of and charging each battery cell, and (2) charging and monitoring automatically total battery condition.

The test equipment for missile launch operations will provide ground power and switching control for internal–external power. Apart from normal flight telemetry, only limited power monitoring will be undertaken during these operations.

Figure 359 shows a simplified layout of the three racks of test equipment to be used during spacecraft assembly facility and AMR hangar tests. Group 1 contains the control panel, a stepping switch, a pulse generator, an attenuator–rectifier system, a reference voltage power supply, a frequency meter, and a Leeds and Northrup

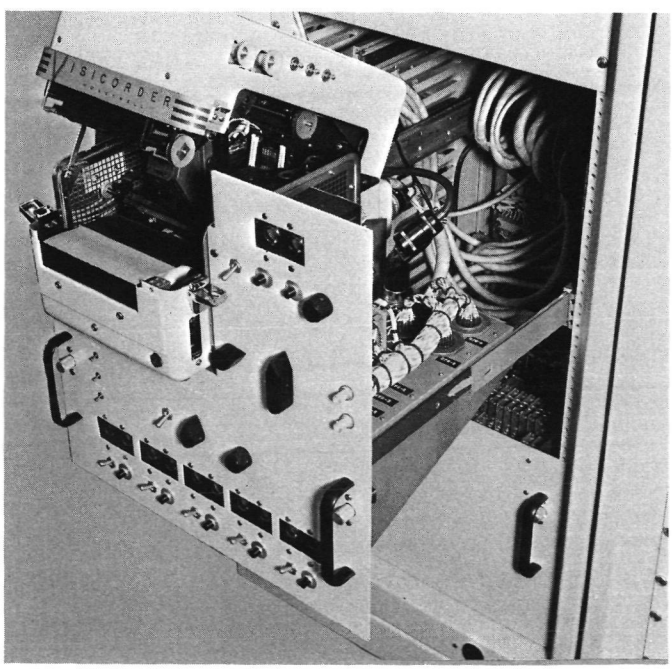

Figure 358. Recorder assembly

recording potentiometer with pre-set tolerance adjustments. An automatic out-of-tolerance alarm is provided. Primary monitor and control functions are provided in Group 1.

Group 2 provides redundancy of voltage monitoring through a digital voltmeter and printout. This group also includes a manual and/or automatic voltage scanner, and an oscilloscope for waveform analysis.

Group 3 contains the ground power supply, solar simulator, and communications facilities. Figure 360 depicts the support equipment to be used during blockhouse operations. Again, a control panel for internal–external power, ¼-w transmitter control, and the ground power source, are included. As previously stated, only limited monitoring will be provided. The monitoring portion of the power monitor and control equipment is designed to provide a sampled record of each power system voltage or to selectively monitor a particular one for any period of time. Each voltage will be attenuated to a level of 40 mv and serially presented to the self-balancing potentiometer recorder. If all sampled voltages are in tolerance, the record will consist of a series of 1/16-in. long dashes at the center of the chart. A precision power supply will provide calibration and channel identification. A tolerance detector as a part of the recorder is switched as required to designate any out-of-tolerance condition that may occur. Recorder speed is such that an 8-hr run will produce a record 80 ft in length.

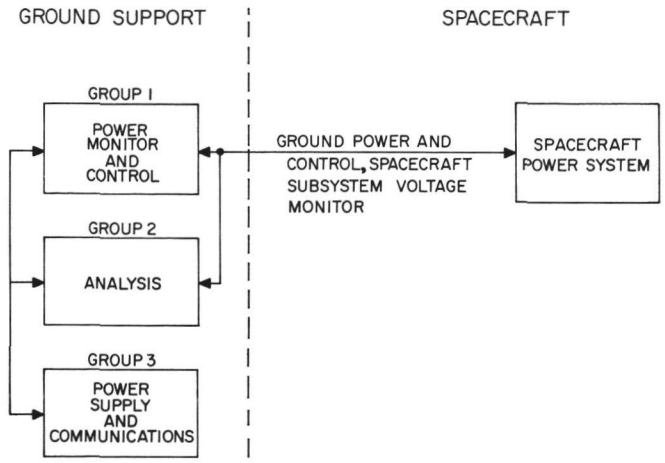

Figure 359. GSE layout

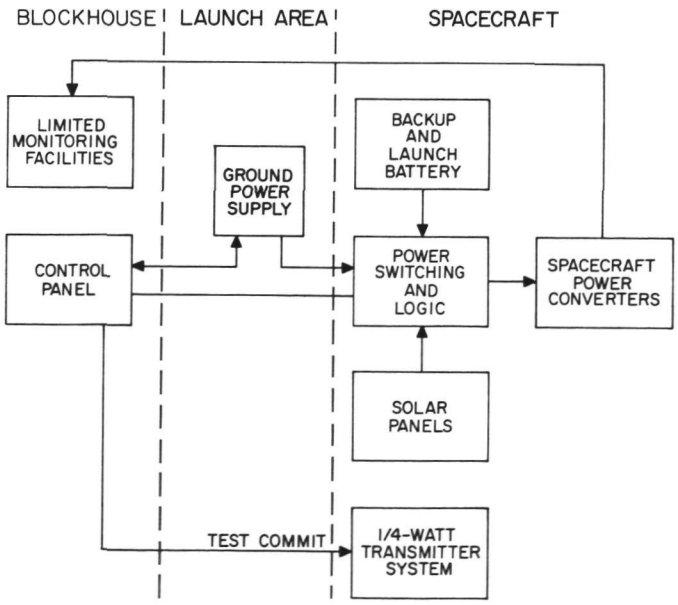

Figure 360. Blockhouse support equipment

The analysis system will be capable of observing the same voltages as the monitoring equipment. The circuit selector portion will handle 100 channels or any group within this value and feed a digital voltmeter. Final data will be printed by a digital recorder.

Controller–timer. The controller–timer ground support equipment for RA-1 and -2 was designed to provide the following capabilities:

(1) Supply power to operate the controller in the absence of spacecraft power.

(2) Inhibit the controller–timer count.

(3) Clear the controller counter.

(4) Provide a counter clear indication.

(5) Provide an indication of the closure of any of the command relays.

(6) Permit manual control of the command relays.

(7) Override the 400-cps input with 10 kc, giving an acceleration of controller time by a factor of 25.

(8) Provide preset counts at a 10-kc repetition rate.

(9) Determine accuracy of controller time pulses.

(10) Advance the count to 1 min before the transmitter arm command (9.9×10^6 sec).

(11) Advance the counter to 1 min before the counter overflows.

The equipment required to supply these functions is divided into two categories: that required for the missile launch operations, and that used for system testing prior to mating the spacecraft with the entire vehicle. The

equipment required for the missile launch operations consists of one panel and has the capability of inhibiting the controller count, clearing the controller counter, providing indications of the inhibit and controller clear conditions, and providing an indication of the closure of any of the command relays. The second category includes the above panel plus a commercial six-decade preset counter and a panel to provide the remaining capabilities.

Central computer and sequencer (CC&S) GSE. The GSE for RA-3, -4, -5 CC&S consists of three basic categories of equipment: (1) blockhouse, (2) system test, and (3) automatic checkout. The blockhouse equipment contains the functions necessary to operate and monitor the CC&S during a launch countdown. The identical functions are also part of the system test GSE, in addition to other functions required for more comprehensive CC&S testing and evaluation. The system test GSE is used for testing of the CC&S subsystem, both in the laboratory and in the spacecraft assembly (system test) area. By requiring that the blockhouse GSE be a part of the systems GSE, two important points are accomplished: (1) personnel familiar with systems GSE can readily operate blockhouse GSE, and (2) spare blockhouse equipment is provided.

Because it is difficult to test the CC&S manually, and because a permanent record of test results is required, an automatic checkout system has been developed. This equipment provides a printed paper record of the state of all event commands and the times of their occurrence. The contacts and electronic switches representing CC&S outputs to other systems in the spacecraft are energized and monitored by the checkout equipment. A printout cycle is initiated by any change of state of a relay or electronic switch, resulting in a readout whenever a command is set or re-set. The automatic checkout equipment is presently used primarily in the laboratory and for initial checkout of the CC&S in the spacecraft assembly area. In case of suspected trouble, the automatic checkout equipment is connected and a complete CC&S test cycle is made. The resulting printed tape is then compared to a standard tape to isolate problem areas.

Figure 361 is a photograph of a complete set of equipment as used in the laboratory or in the spacecraft assembly area for RA-3. This set contains all equipment described and, with proper cabling, will operate and check the CC&S in any of the test areas. Figure 362 is a block diagram of the GSE and its relations with the CC&S. The block diagram is broken into the same physical, functional blocks that are found in the actual GSE. A brief description follows for each block.

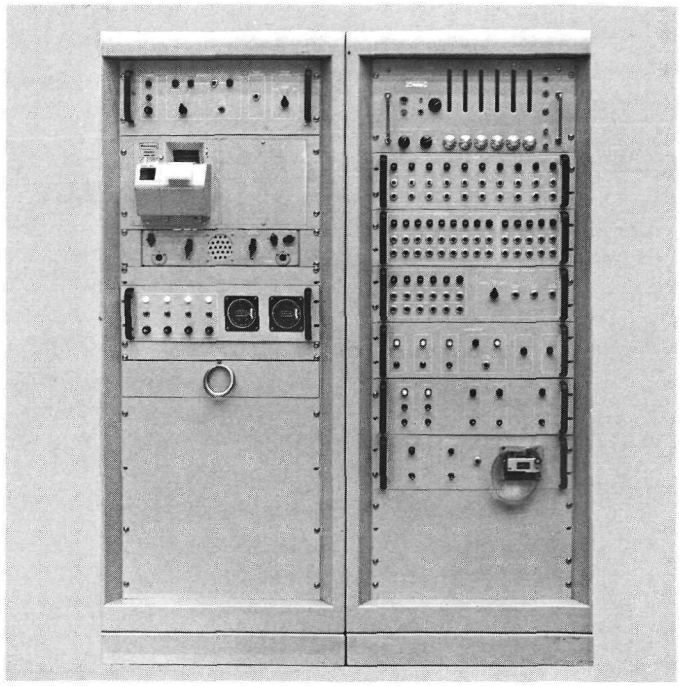

Figure 361. CC&S test set

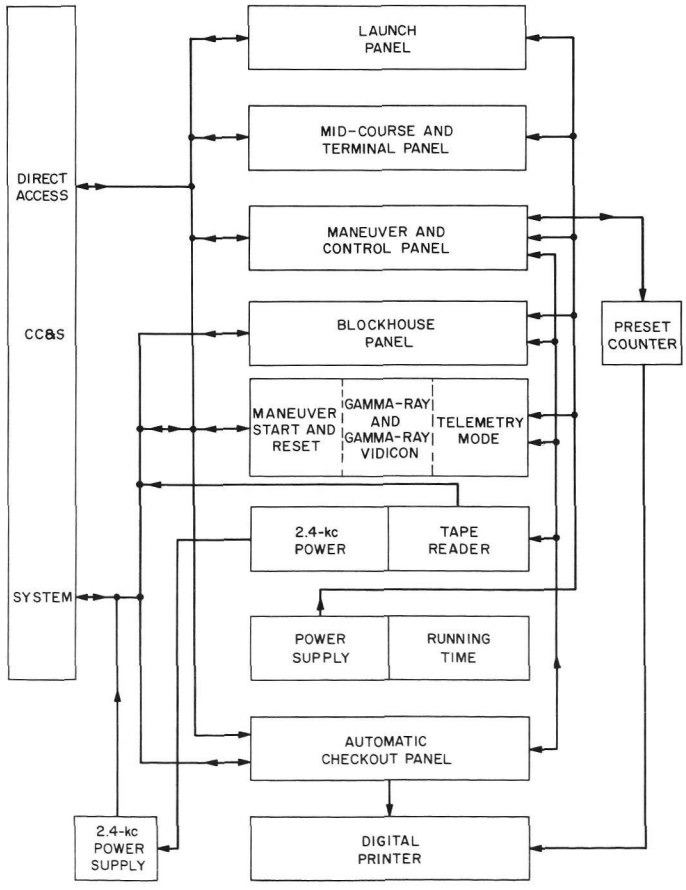

Figure 362. CC&S test set block diagram

Launch panel. This panel provides manual control of the relays in the CC&S associated with the flight launch sequence. Accordingly, a particular command may be manually initiated prior to its prescribed time in the CC&S launch sequence.

Midcourse and terminal panel. This panel provides manual control of the CC&S relays associated with the midcourse and terminal phases of the spacecraft mission. Operation is the same as for the launch panel.

Maneuver and control panel. The maneuver section of this panel manually controls the relays associated with the roll, pitch, and yaw attitude-control functions. Operation is the same as in the launch panel.

Blockhouse panel. Controls on the blockhouse panel inhibit the CC&S countdown, electrically hold all the relays in the re-set or safe state, and clear the CC&S counter back to its zero state. These functions and their indications are all accomplished from GSE power and are always done before turning on spacecraft power to ensure that no false commands result. An additional indication used primarily in the blockhouse area is the no-go light. Sixty sec from the release of the inhibit, a CC&S relay is set which indicates that the CC&S is counting down properly in the first stages of its counter. An electric timer within the blockhouse GSE is used to generate limits on the release of this relay. If the clear relay operates outside of these limits, a no-go indication will occur; this is a mandatory hold. Any red light on the blockhouse panel is a mandatory hold.

Maneuver start and re-set, gamma-ray, and telemetry mode panel. When the command system is not available, the initiation of the midcourse or terminal modes may be accomplished from this panel. Special cabling is needed, since parallel inputs to the CC&S are not provided.

Power and tape reader. In the absence of spacecraft power and with the proper cabling, 2.4-kc power may be supplied to the CC&S through this panel. The tape reader is used in the absence of the command system to load the maneuver shift registers in the CC&S for checkout of these systems.

Power supply and running time. The power supply furnishes power to operate all GSE functions and to perform necessary prepower-on checks: i.e., inhibit, relay hold, and clear. The running time meters provide total CC&S running time and running time for the CC&S counter.

Automatic checkout. This function consists of special logic circuits used in conjunction with the CC&S and the GSE to provide an automatic operational check and record of the CC&S operation.

Digital printer and preset counter. The digital printer is used in conjunction with the automatic checkout system for the printed record. The preset counter is used to check CC&S time. The contents of the preset counter as well as the coded states of all outputs from the CC&S are printed upon command.

Power supply. This unit supplies the 2.4-kc square-wave to operate the CC&S in the absence of spacecraft power.

Each subsystem is constructed with a quick-disconnect connector in series with a terminal strip to facilitate changes. The subsystems are also mounted on slide rails, and sufficient slack is allowed in the rack wiring harness to permit trouble-shooting of each subsystem while it is operating in the system. As a result of the ease of trouble-shooting, removal, and replacement, down-time is greatly reduced.

Attitude control. GSE requirements for the attitude-control (A/C) system center about Sun and Earth sensor system stimulation for the purpose of ensuring operation of pitch, roll, and yaw jet nozzles. Also, continuous monitoring of A/C gyros is supplied in order to provide go, no-go information as to gyro loop operation and calibration polarities for telemetering. High-gain antenna hinge angles are monitored to determine accuracies of the preset angles and motion polarities of the antenna.

Functions performed by A/C GSE in relation to the previously mentioned requirements include: (1) stimulation of Sun and Earth sensor systems, (2) monitoring of A/C system reactions to stimulation of sensor systems and rate gyros, (3) high-gain antenna hinge angle measurements throughout the A/C program, (4) monitoring of gyro stabilization amplifier outputs, (5) supplying A/C power when necessary, (6) A/C dummy load for spacecraft power, (7) valve and gyro simulation for laboratory subsystem tests, (8) gyro running-time monitoring.

For testing purposes, all RA-3, -4, -5 attitude-control cruise system functions are controlled and monitored by the same test equipment as was used on RA-1 and -2. GSE to test the RA-3, -4, and -5 midcourse guidance system consists of one additional panel and a five-digit electronic computer (top of Fig 363). The complete RA-3, -4, -5 attitude control test set is shown in Figure 363. All tests which determine the operational status of the attitude-control and midcourse guidance systems are simple open-loop checks.

The same basic test set (Fig 363) is used for laboratory testing and for field test operations. Laboratory testing requires additional equipment: power supplies, gas nozzles, Sun sensors, and a nitrogen supply to operate pressure-sensitive switches which monitor proper gas-jet operation and phasing. A laboratory central junction box integrates the various flight components to permit testing of attitude control and midcourse guidance as complete subsystems.

With the addition of the midcourse guidance test panel, all attitude-control and midcourse guidance flight maneuvers may be tested individually or sequentially. System phasing is determined by confirming that proper nitrogen jet valve operation results from stimulation of the Sun and Earth sensors and from induced gyro error signals. The jet vanes on the midcourse motor are monitored electrically by using algebraic sums and differences of the actuator position potentiometer signals. The vane (fin) positions or the composite positions of roll, pitch, and yaw (plus a drag component as a measure of error or malfunction) can be indicated by the four panel meters. Electrical monitoring of antenna hinge movement is obtained from a potentiometer attached to the antenna hinge yoke, using the spacecraft airframe as a reference. Monitoring of the gyro integrating capacitor charging has been incorporated to ensure proper capacitor forming for maneuvers. Gyro integration is checked as a function of time by using the gyro meters as polarity and voltage indicators.

The electronic counter is used to count and totalize the output of the digital flight accelerometer using internal counter gating after autopilot turn-on or, during motor firing, external gating by the integrate command from the CC&S or midcourse guidance test panel.

All tests performed are highly reliable because of the positive, fail-safe indications presented to the GSE and because of the simplicity of the GSE circuitry. Use of the GSE has helped to locate miswirings of cabling, gyro noise problems resulting from impedance mismatches, and numerous other malfunctions.

The GSE requirements of the attitude-control system are simple. Means are provided for stimulating the Sun and the Earth sensors. This stimulation produces operation of the pitch, roll, and yaw jet nozzles which are monitored by the GSE. Also, continuous monitoring of the A/C gyros is provided in order to supply go or no-go information on gyro operation. The antenna hinge angle will also be monitored to determine if specified hinge-angle changes are carried out.

Illumination sources are required to stimulate the Earth and the Sun sensors on command. Shielding is supplied to eliminate all extraneous illumination. These shields, or hoods, consist of opaque material formed to attach over each sensor unit (Fig 364). The sensor unit contains either a Sun or an Earth detector. Each sensor unit is equipped with at least one detector. Included in the body of each hood is an illumination source which consists of a 6-v lamp. Individual control of each lamp is accomplished from the A/C GSE test panel and incorporates intensity adjustments. Proper intensities are essential to the Earth sensor system to simulate Earth acquisition. Panel power is self-contained.

Operation of appropriate jet nozzles due to detector stimulation is monitored by means of pressure-sensitive switches attached externally to the jet nozzles. Upon activation of a switch, indication of jet nozzle operation is represented by a light on the A/C test panel (Fig 365). Each light is designated as a pitch, roll, or yaw—clockwise or counterclockwise.

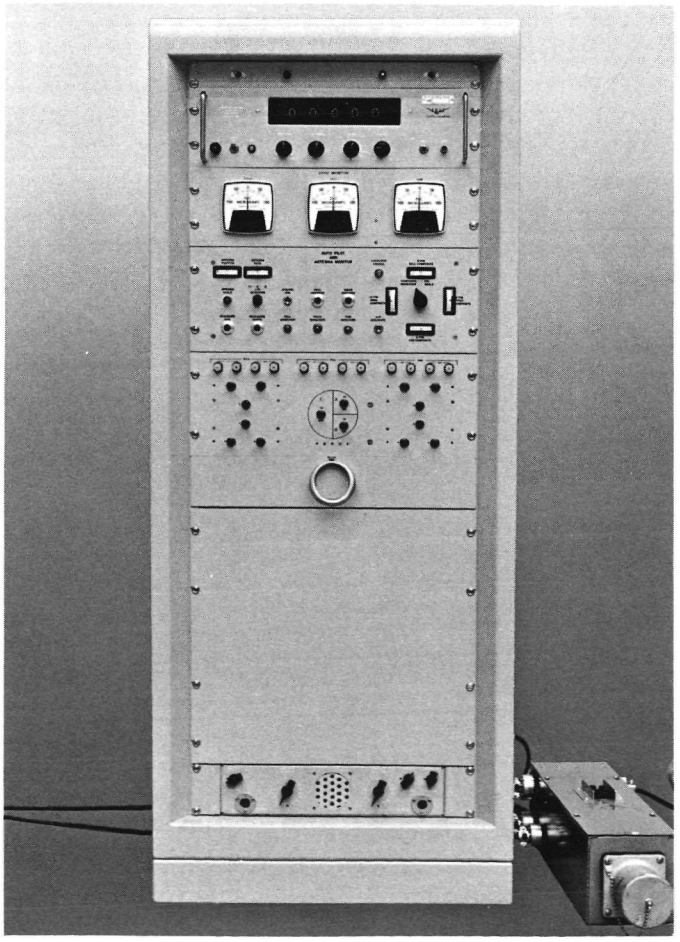

Figure 363. Attitude-control system test set

The jet nozzle monitoring pressure switches activate at approximately 3 psi, with a delay of 50 msec for on and off conditions. Figure 366 shows a complete pressure switch assembly.

Antenna hinge angle is checked mechanically by observing the actual angle of the antenna visually with the aid of a simple optical system. Angles to be observed consist of two preset angles. Changes in preset angles are accomplished by override commands to the antenna electronics. Tolerances will be ± 2 deg of all preset hinge-angle monitoring.

Operation of each of the three A/C gyros is monitored by picking off a voltage from the gyro torquer amplifier, and applying this voltage to a d-c amplifier. Each gyro amplifier has a separate d-c amplifier and meter circuit. The meter panel housing the pitch, roll, and yaw monitor meters is shown in Figure 365, directly below the functional test panel. Specifications met by the gyro monitor amplifiers are: (1) input impedance not less than 750,000 ohms; (2) amplification sufficient to allow full-scale meter indication for abnormal gyro functions, 75% of full scale for gyro tumbling due to a 0.5-deg/sec rate input, and 25% of full scale for normal gyro operation; (3) less than 10 μamp over-all drive from 40 to 120°F; (4) a floating signal return; and (5) a self-contained power source.

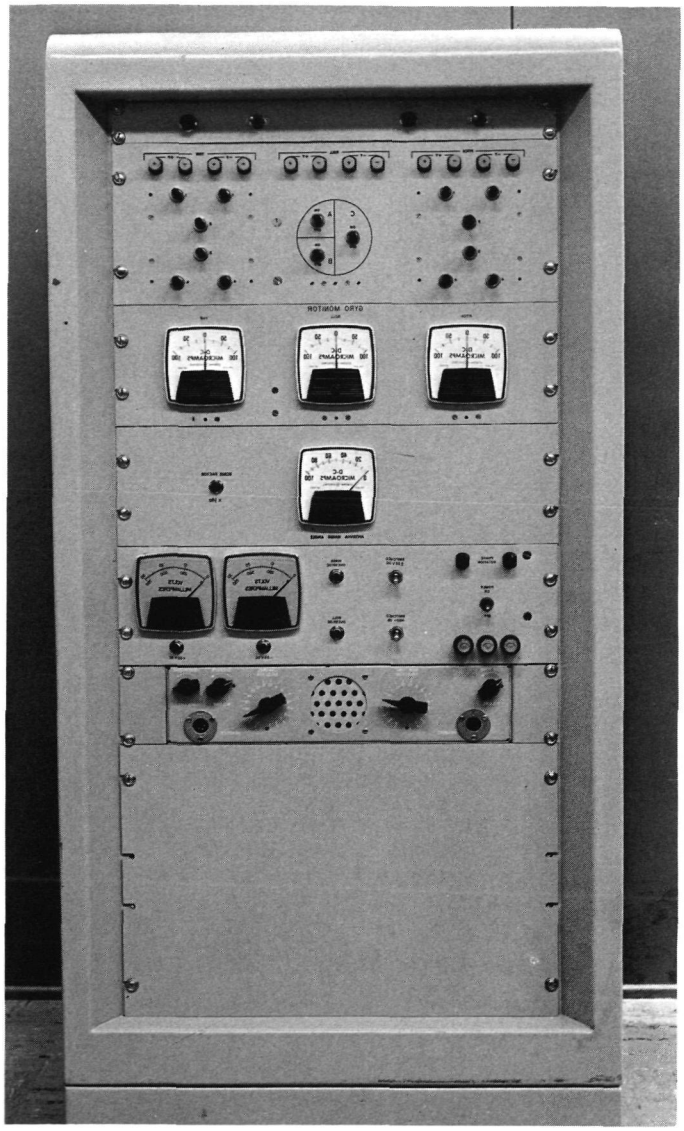

Figure 365. Attitude test console

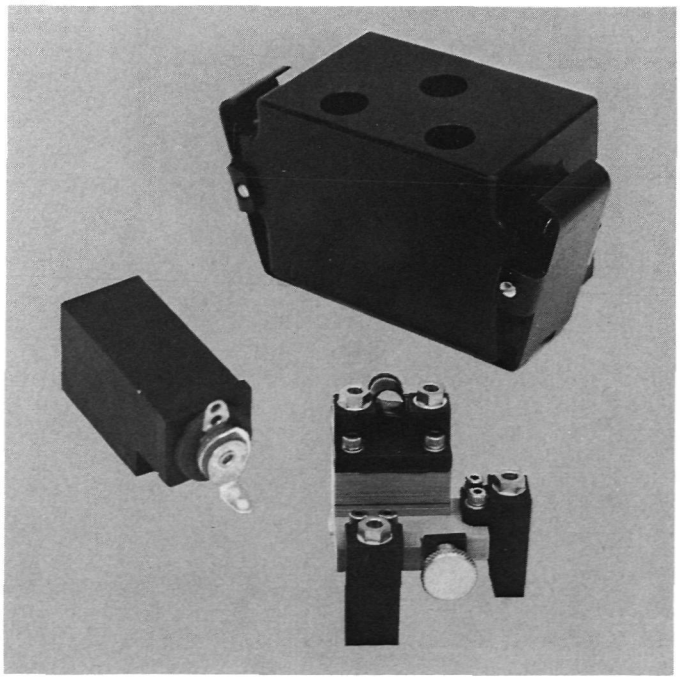

Figure 364. Sun and Earth sensor hoods

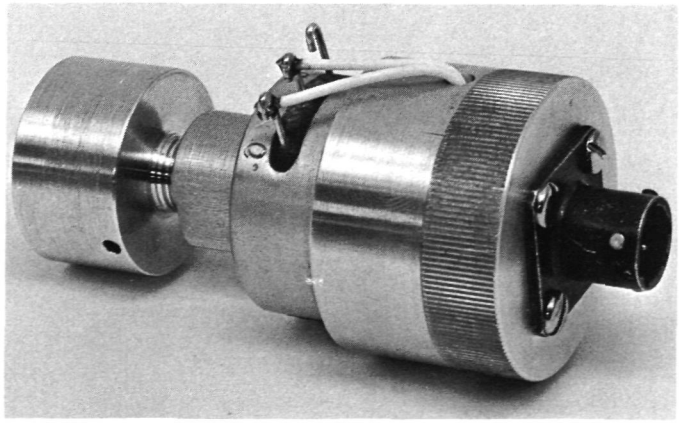

Figure 366. Pressure switch assembly

Power for the d-c amplifiers is supplied from a separate unit which is contained in the junction box with the amplifiers. The gyro monitoring system is the only phase of the A/C GSE that enters the spacecraft cabling. All other test functions are external to the spacecraft cabling.

The A/C GSE also is capable of supplying external power to the A/C flight equipment during special tests at times when spacecraft power is not available. The power supply is shown in Figure 365 and is located directly above the MOPS panel. A/C voltages are constantly monitored as to phase rotation to protect the gyros and assure proper Earth sensor and high-gain antenna operation. High-gain antenna hinge angles are monitored electromechanically.

Transponder test set. In order to provide a convenient and efficient means for testing and calibrating the spacecraft radio communication equipment, a test set was designed by the Motorola Western Military Electronics Center to specifications prepared by JPL. The test set consists of an 890-mc transmitter, a 960-mc receiver, a transponder mount and power supply, and a number of general-purpose test instruments.

The r-f phase detector is representative of the design and performance of the individual test set components. The appearance of the component is shown in Figure 367, wherein liberal use of r-f gaskets and shielding is evident. Table 79 summarizes the measured electrical performance which meets the specification requirements with sufficient margins. Tests have revealed that the system measurements made by Motorola and JPL are better than the tolerances of the measuring instruments.

c. Power launch support equipment. The launch support equipment (Fig 368) contains seven basic assemblies:

(1) Blockhouse control panel.

(2) External power supply.

(3) Power control assembly.

(4) Self-test assembly.

(5) Battery charger assembly.

(6) Auxiliary power supply assembly.

(7) Transfer and tolerance detector assembly.

Blockhouse control panel. This blockhouse unit is essentially identical to that used in system test. All of the controls previously described are available except those concerning solar simulated power and recording. Monitoring reflects flight readiness of two areas: power conversion system and launch battery. The blockhouse control panel remotely (1200 ft) controls the power control assembly in the launch control shelter, where the remaining power launch support equipment is located.

External power supply. This unit provides external spacecraft power and power for external commands to the spacecraft power subsystem.

Power control assembly. All commands from the control panel are received at the power control assembly

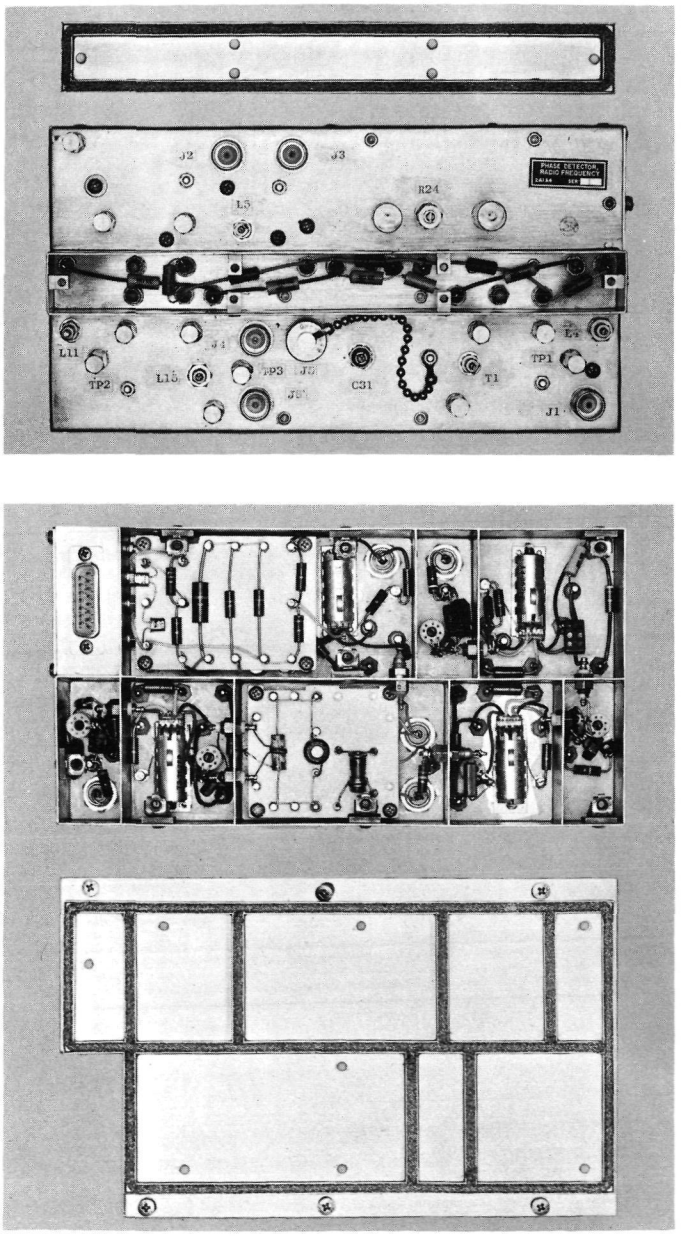

Figure 367. R-F phase detector

Table 79. R-F phase detector performance

Characteristic	Measured value	Required value
Peak S-curve, v	9.48	10 nominal 5 minimum
Reference channel unbalance, mv	20	100 maximum
Signal channel unbalance, mv	−20	100 maximum
Discriminator action, mv	24	100 maximum
Output frequency response	Constant within ±0.5 db from 0 to 8 kc	Constant within ±0.5 db from 0 to 5 kc
Reference channel input impedance, ohms	50	50 ±20%
Signal channel input impedance, ohms	46.2	50 ±20%
R-F signal level on power circuit, mv	8 maximum many < 1	10 maximum

and routed through the transfer assembly to the spacecraft in *operate*, and to the self-test assembly in the *test* mode.

Self-test assembly. The self-test assembly is a separate unit whose removal does not affect the normal operation (excluding self-test) of the launch control shelter equipment. It is a simplified version of the system test unit and does not include simulation for recording.

Battery charger. The battery charger assembly ensures that the flight battery is at full capacity prior to launch. This device automatically starts and terminates charging as required by the battery.

Auxiliary power supply. This unit contains the precision power supplies and auxiliary power units for monitor and control.

Transfer and tolerance detector assembly. This unit is essentially identical to that used for system test.

d.* Ranger *RA-6–9 GSE. Planning for the RA-6–9 GSE was started during the latter part of 1961. Since it was not known whether the first TV spacecraft would be RA-5 or -6, the planning provided the capability of testing the RA-5 spacecraft for either a TV or lunar-capsule mission.

Changes to the existing GSE are to be kept to a minimum in order to maintain reliability and to help meet schedule requirements. The GSE (supplied by RCA) required for the TV subsystem is to be integrated into the existing System Test Complex. All new equipment interfaces are to be kept as simple as possible. The interfaces for the TV GSE shall consist of eight leads through the separation connector and J-box for control of the TV

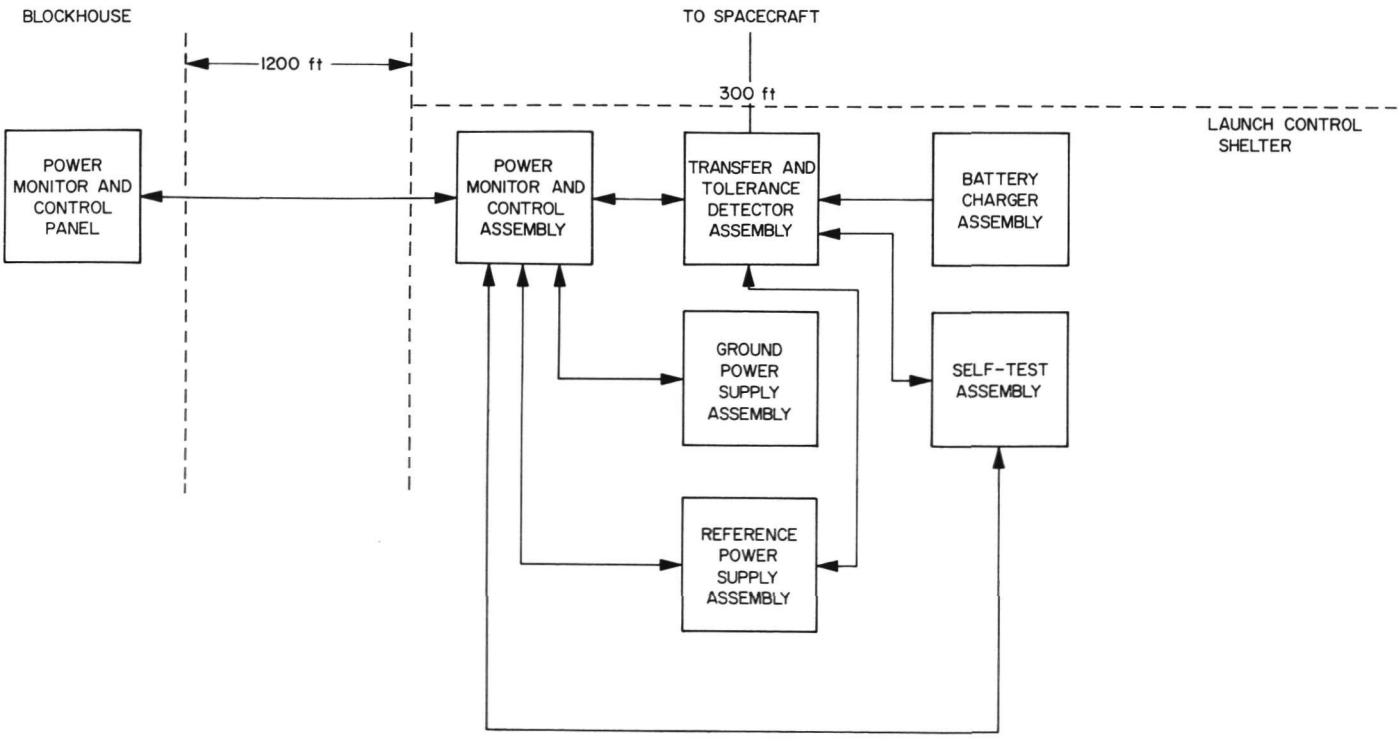

Figure 368. Launch support equipment

subsystem during system test and launch operations, a coaxial cable to the communication console to receive the r-f signal from the spacecraft for picture evaluation during system test, and two leads to the data display console to receive the composite telemetry signal from the spacecraft to evaluate the TV engineering data during test.

As presently planned, RCA will deliver the GSE to be used for AMR operations directly to the Cape. This is contrary to normal procedure calling for all portions of the STC to be checked out and used together at JPL before delivery to AMR. Since the electrical interface between the RCA GSE and the rest of the STC is minimum, and because of the need for two sets of GSE at RCA to check out the TV subsystem, it is more important to have the AMR-destined GSE at RCA to perform tests with the flight TV subsystem than it is to have the GSE compatibility verified with the rest of the STC at JPL.

The countdown testing philosophy calls for a minimum amount of testing to be performed during launch operations. However, since the TV subsystem is the prime experiment of the mission, and the only modification required to make a rather comprehensive check of the TV subsystem is to supply a light source for each camera, such a light for each camera will be located in the shroud, allowing a simple picture to be sent during the countdown.

The hard-line monitoring of the TV subsystem is to conform to the "direct-access cable" philosophy. This concept calls for those functions that are to be monitored during testing operations to be brought to the GSE through separate test connectors and cables. After testing is completed, the test cables are removed and the spacecraft remains in a flight-ready configuration. This technique allows all flight connections to remain intact before, during, and after spacecraft test operations.

A tape recorder is to be used to record the telemetry modulation signals during system test. If any discrepancy is noted during system test, the recording can be analyzed to determine the cause. Not only should the tape recorder prove to be a valuable trouble-shooting aid, but it should also help keep the operation time of the spacecraft to a minimum by reducing the number of times a system test has to be operated to isolate a malfunction.

Since the safety of the spacecraft partially lies with the test equipment and facilities, a temperature test model of the spacecraft will be tested in the space simulator before the flight spacecraft is subjected to this critical environment. To ensure that the spacecraft will not be damaged by the GSE, a spacecraft simulator will be used to verify the GSE and cabling before the flight spacecraft is connected to the GSE at the different test complexes, particularly the launch complex.

An equipment usage schedule has been prepared showing how all TV spacecraft can be supported with three sets of system test equipment.

A block diagram defining all the interconnecting cables for the System Test Complex is shown in Figure 369. The use of a standard cable system was considered, but since many of the cables that exist from earlier *Ranger* missions are usable for the RA-6–9 series, and the use of standardized cables would require some modification to existing GSE, a standard cable concept was not adopted.

Equipment layout diagrams have been generated for the areas where an STC is to be used. These areas are the Spacecraft Assembly Facility, the Environmental Test Facility, and the Space Simulator at JPL, as well as the Spacecraft Assembly Facility at AMR. Attention is given to the equipment layouts to ensure compatibility between the various test positions in reference to signal flow, cable routing and length, accessibility of equipment for trouble-shooting, and ease of operation.

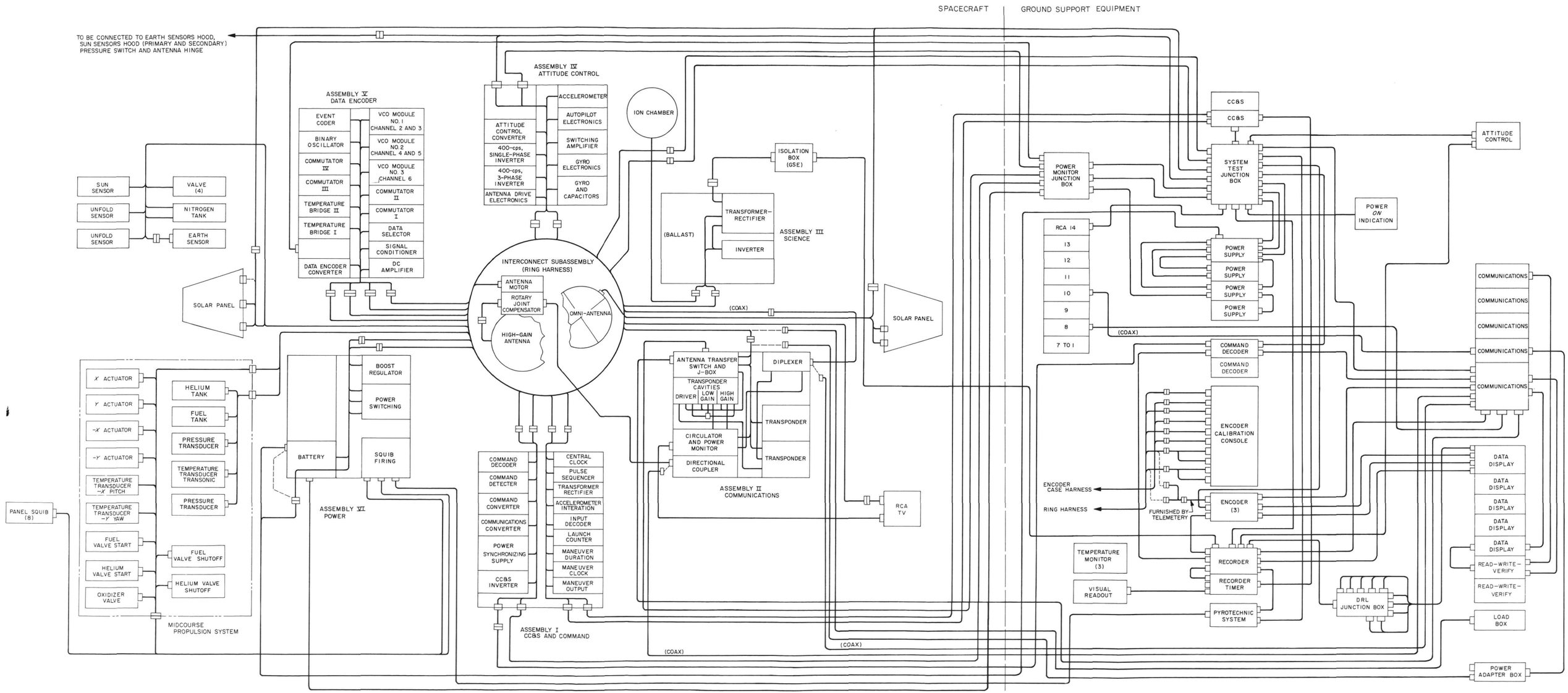

FOLD-OUT #1

FOLD-OUT #2

Figure 369. System Test Complex block diagram

V. Assembly and Test Operations

A. Test Facilities

1. General

Test facilities utilized for the *Ranger* operations are located at JPL, Pasadena; LMSC, Sunnyvale; and at AMR, Cape Canaveral. The JPL, Pasadena, test facilities and the AMR, Cape Canaveral, test facilities have been planned to take advantage of similar physical arrangement insofar as is practicable. (See Chapter VI for AMR facilities.)

2. JPL, Pasadena, Test Facilities

a. General. Test facilities at JPL, Pasadena, comprise the Spacecraft Assembly Facility (SAF), the Environmental Test Laboratory, and supporting facilities, e.g., Data Recording Laboratory (DRL), computing facilities, electronic laboratories, electrical shops, and machine shops.

b. Spacecraft Assembly Facility (SAF). RA-1 PTM (Proof Test Model) operations were conducted in temporary facilities while the Spacecraft Assembly Facility was being completed. *Ranger* operations were transferred to the new SAF with the installation of the Spacecraft Test Complex May 8, 1961. Thereafter, the activities required to prepare the *Ranger* spacecraft for flight readiness centered about that facility. This building (Figs 370 and 371) is utilized for assembly; subsystem and system testing; weight, center of gravity, and moment-of inertia measurements; and shipping preparations. The building contains a stock room, machine shop, cabling shop, potting shop, laboratories, offices, and inspection facilities in the two-story wing. The 80-ft × 120-ft main bay area contains the System Test Complexes and the necessary fixtures and jigs for assembly and mechanical operations.

c. Environmental Test Laboratory. RA-1 PTM, and the RA-1 and RA-2 spacecraft environmental tests were also conducted in temporary facilities at JPL while the present

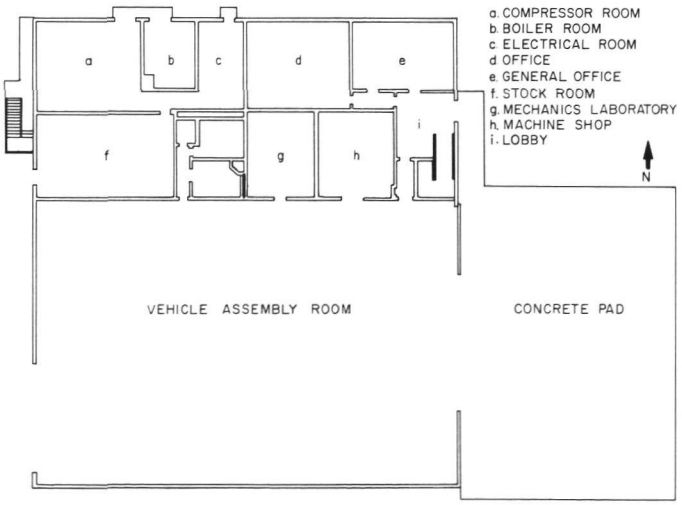

Figure 370. Spacecraft Assembly Facility (SAF), main floor plan

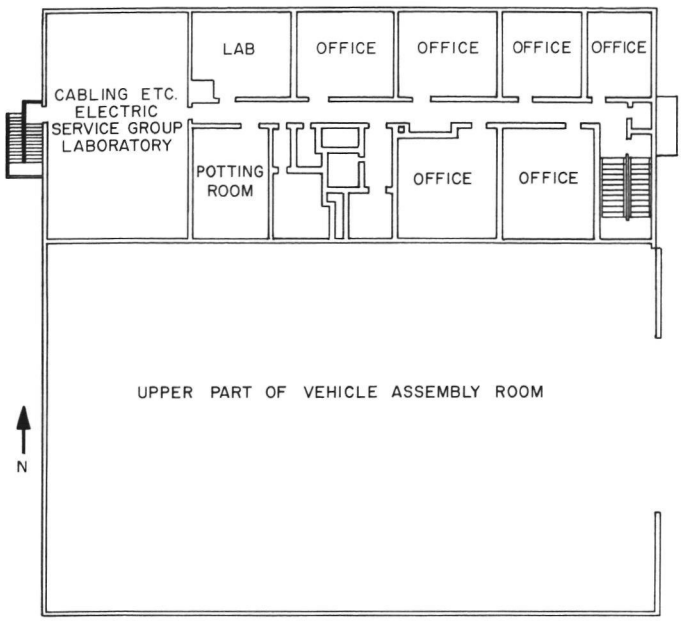

Figure 371. Spacecraft Assembly Facility, floor plan

Environmental Laboratory was being constructed. These facilities were utilized to test the spacecraft and all subsystems under a variety of environmental conditions. Layout of the present Environmental Laboratory is shown in Figure 372.

Equipment was available for simulation of the following conditions:

(1) In-flight dynamic environments.

(2) Spatial conditions by use of a space simulator.

(3) Storage and transportation environmental conditions.

(4) Sterilization techniques on the subsystem assemblies.

For the vibration testing of complete spacecraft, two vibration machines were used. A large, 28,000-lb force, output electrodynamic shaker is used for high-frequency vibration testing (15 to 1500 cps) and a hydraulically activated vibration machine (15,000-lb force output) is used for low-frequency (1 to 40 cps) vibration testing. Both

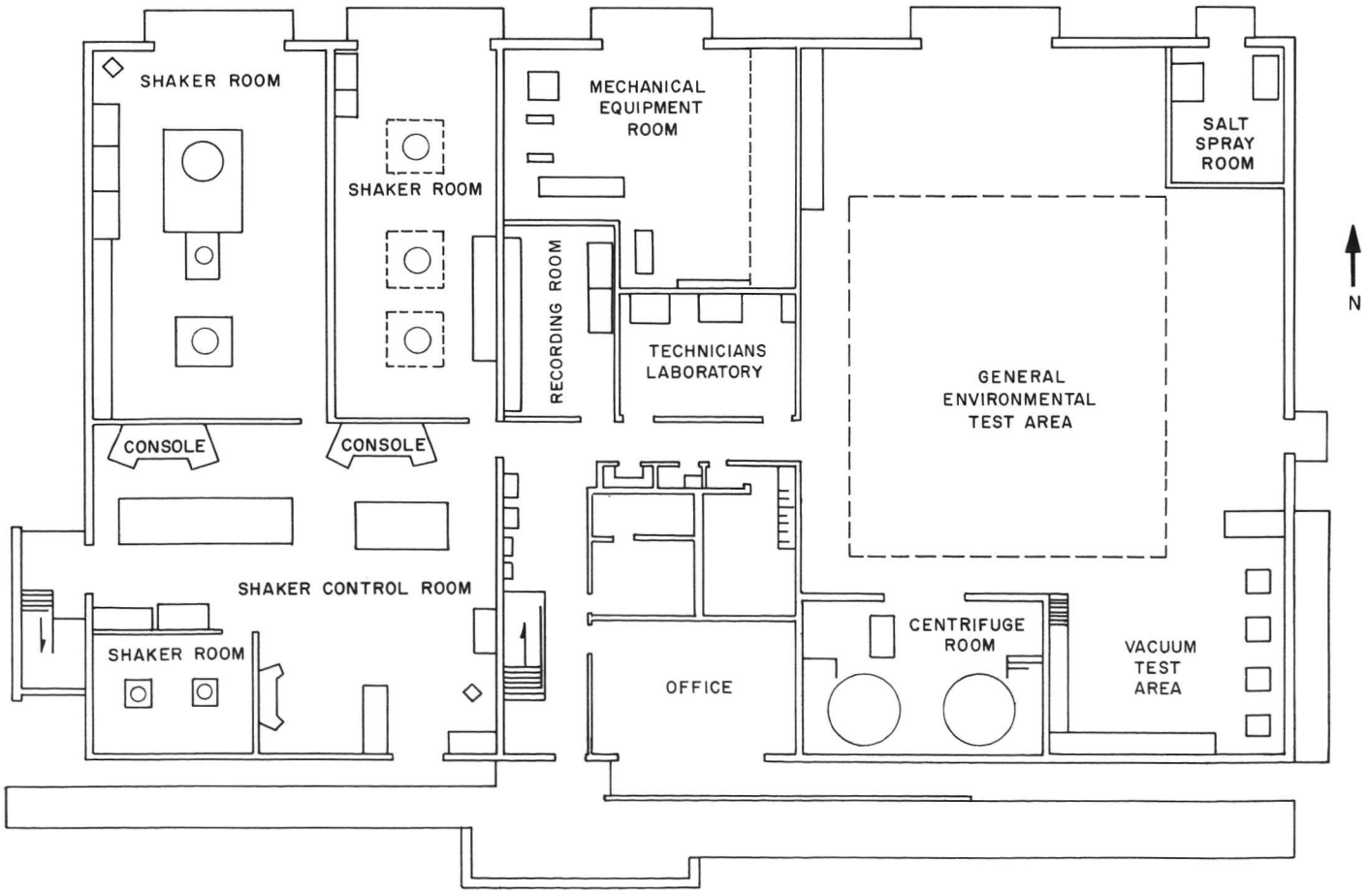

Figure 372. Environmental Laboratory, floor plan

exciters are located so that an oil table may be used for shaking in the directions in which difficulties arise from aligning shaker thrust with the spacecraft center of gravity. In addition, other vibration machines and test equipment were available for spacecraft environmental test operations as required.

Also used was a space simulator consisting of a large, stainless steel, vacuum chamber approximately 6 ft in diameter and 7 ft high. The space simulator provided, over an area for testing the spacecraft components, a pressure of less than 5×10^{-5} mm Hg, a 77°K radiation background, and simulated solar radiation.

3. Test Ground Support Equipment

a. General. Three classes of system-oriented Test Ground Support Equipment (TGSE), specifically designed for the test operations were supplied, as follows:

(1) System Test Complex (STC).

(2) Launch Complex Equipment (LCE).

(3) Special Test Equipment.

b. System Test Complex (STC).

General. Three complete sets of System Test Complex Equipment were used: two sets at JPL, Pasadena, and one set at AMR, Cape Canaveral. The STC is the basic unit for the testing of the assemblage of units that comprises the spacecraft. The STC was used in tests and operations (environmental tests, calibrations, etc.) designed to verify adequacy of design and fabrication, and flight readiness of the spacecraft.

Capabilities. The capabilities of the STC are to:

(1) Power the complete spacecraft and each of the units independently.

(2) Command the spacecraft and verify the receipt of commands.

(3) Monitor over-all spacecraft performance by the display of data transmitted through the telemetry system.

(4) Monitor pertinent unit inputs and outputs by direct access leads.

(5) Exercise all units (circuitry, mechanical devices, and sensors) through their entire operating ranges.

(6) Monitor transducer outputs for calibration in various environments.

Description. The STC, located in the JPL SAF and duplicated in the AMR SCF, consisted of test consoles designed to support the testing of the individual subsystems. These consoles were arranged as needed to support spacecraft assembly and operations such as system and environmental tests. The equipment layout used in a typical SAF STC is shown in Figure 373. The test consoles were distributed around the perimeter of the test area enclosure, facing the spacecraft test fixture. Cables enabling necessary test functions were routed from the test consoles to the spacecraft through a junction box. Direct access cables routed selected functions from their respective consoles to the spacecraft, bypassing the junction box. Direct access connections were made to the direct access connectors externally located on the spacecraft equipment cases. Communication between consoles, spacecraft, and the Test Director's console was provided by a Missile Operations Intercom System (MOIS). A system test recorder was installed to observe and time-correlate events, noise, transients, and other test characteristics.

Spacecraft System Test Stand. For system testing, the spacecraft was mounted on the System Test Stand. This test stand is designed to position the spacecraft in any required attitude for testing and is capable of providing rotational rates for roughly checking the gyros or for following the Sun during sensor alignment. The stand is approximately 5 ft high and has an inner ring diameter of 5 ft. The spacecraft is bolted to the inner ring by means of six mounting pads.

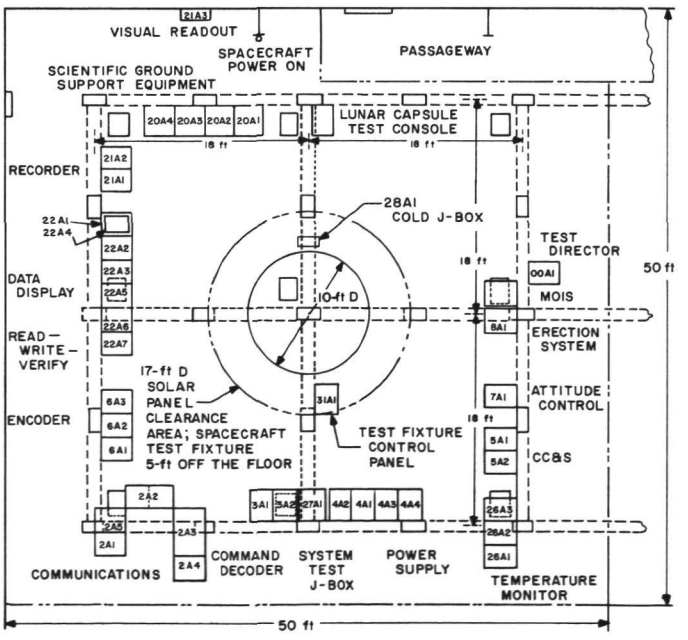

Figure 373. SAF System Test Complex

c. Launch Complex Equipment. The dummy-run equipment is required in the blockhouse to help evaluate the spacecraft and test techniques, to verify countdown procedures, and to train operating personnel. The dummy run is also used to verify the actual Launch Complex Equipment prior to initial installation and, therefore, initially contained additional JPL equipment such as the Launch Control Shelter electronics. The umbilical junction box was located so that its physical distance from the spacecraft during dummy run was approximately the same as their physical relationship during gantry operations. The same type of cable is used for the dummy run as used at AMR. For RA-1 and RA-2 spacecraft, the dummy-run equipment was installed in a dummy-run trailer to facilitate its use.

B. Assembly and Test Operations

1. Plans and Methods

a. Introduction. Assembly and Operations Plans were prepared by JPL for use in the RA-1 and -2 operations and reflected the policies of the *Ranger* Project Office.

b. Purpose. In addition to the spacecraft design specifications which define the mission objectives and spacecraft, further implementation of the *Ranger* Project required the creation of a plan of testing whereby the verification of the spacecraft's design integrity, its capacity to function as intended, and its readiness for flight would be accomplished. An Assembly and Operations Plan was created for planning purposes and presented such an overall operations plan for RA-1, -2, and -3 with the intent of achieving coordination and uniformity of all operations within the stated scope.

c. Scope. All tests performed on portions of a spacecraft were considered a part of the development and fabrication of that equipment. The JPL divisions supplying units were responsible for devising a test plan for their own subsystems (including environmental testing, both Type Approval and Acceptance) in keeping with the basic philosophy. The Assembly and Operations Plans are based on the assumption that these requirements have been met. Therefore, the Assembly and Test Operations commence with the assembling of the spacecraft from tested and accepted components and concludes with the launching and subsequent injection of the spacecraft.

2. Test Philosophy

Since JPL is involved in all phases of spacecraft development, it is imperative that consistent methods be developed to demonstrate accurately spacecraft performance and ensure mission success. Verification of the final design of the spacecraft by means of formal testing and evaluation is accomplished as a normal step of the developmental effort.

The controlling philosophy applicable to both the spacecraft and to the designing of test equipment is established as a part of the spacecraft design criteria of the Spacecraft Design Specification. In all areas where the design was influenced by the type of test program planned, the design criterion used was that first preference be given to designs that can be analyzed, and that testing is used primarily for the purpose of confirming analysis or resolving system interactions. When subsystem qualification tests were the only way of determining readiness for assembly and flight, the design must of course incorporate the necessary test provision. In general, however, the objective was to obtain reliability by design rather than by testing. In system test, the purpose was primarily to simulate flight operations. The burden of simulation, as far as possible, fell on equipment external to the spacecraft.

The schedule for the *Ranger* Project development dictates that reliability goals be achieved by extensive use of proven design techniques; i.e., limiting the use of the advanced state of the art to only those items upon which other subsystems are not dependent.

3. Constraints Imposed by Test Philosophy

a. Electrical and mechanical interfaces. Electrical interface operations between the spacecraft and the System Test Complex imposed constraints on the spacecraft design by requiring separate access test connectors on the subsystem cases and by requiring subsystem cases capable of being pivoted to effect access within.

The design of the spacecraft and the System Test Complex permitted power to be applied to each subsystem of the spacecraft from the System Test Complex equipment. An external power source was provided to allow trouble-shooting of the individual subsystems when the spacecraft-supplied power was unavailable. A special cable, separate from the direct access system test cable, provided this capability. Power supplied to each subsystem was that regulated voltage (not necessarily the usual 28 v supplied by spacecraft power) required to operate the individual system. In all instances, nonelectrical interface problems placed on the test equipment, test methods, and test philosophy the constraint of accommodating the spacecraft design. Examples of this were the test fixture design to accommodate the spacecraft, the sensor stimulus sources, and the attitude control gas jet monitor vanes.

b. System Test Complex interface. During all spacecraft operations, with the exceptions noted below, the System Test Complex connections were made directly to the spacecraft-adapter separation connectors through a J-Box electrically simulating the umbilical tower. Further, direct access connections by means of connectors located on subsystem cases were used during the LMSC Compatibility Test the direct-access connection was through the spacecraft adapter electrical access opening.

c. Dummy-run test interface. During dummy-run operations, the dummy-run adapter cable simulating the spacecraft-adapter cable-umbilical disconnect was used to connect the dummy-run trailer equipment.

d. Dummy loads and in-line cable adapters. Dummy loads were required during initial turn-on operations immediately following SAF spacecraft assembly. In-line cable adapters (break-in-boxes) were required to allow access to all leads at a connector interface for spacecraft test operations.

e. Calibrations design. All equipment must be designed to permit three-point verification calibrations after arrival at AMR.

f. Operations sequence design. The spacecraft was so designed that it can execute a reasonably complete flight operations sequence during the systems test. Additional design restraints imposed by the test philosophy are presented in Chapter VI.

4. Types of Test

a. General. The test scheme, projecting the above test philosophy comprised two basic kinds of tests: type-approval tests and acceptance tests. Acceptance tests are divided into flight-acceptance tests and use-acceptance (non-flight) tests. All flight article subsystem assemblies of the spacecraft, the completely assembled flight spacecraft, and GSE are subject to acceptance tests only. Prototype models of subsystem assemblies of the spacecraft as well as a Proof Test Model (PTM) spacecraft are subjected to type-approval tests.

b. Type-approval tests. Type-approval tests are performed on one or more samples of an item that are identical to the equivalent flight article. These tests are devised to verify that the design permits performance or endurance in environments in excess of those expected, thereby establishing the safety margins of the environment to which actual flight articles will be subjected during acceptance testing. Because of the rigorous nature of the type-approval tests, no item subjected to these tests is used as a flight article. Proof Test Model operations are a form of type-approval test of the prototype spacecraft.

c. Acceptance tests. Acceptance tests are devised to verify the workmanship and quality of components, the correctness of their assembly, and the adequacy of their performance. In purpose, acceptance tests are a quality assurance measure whereby verification of proper performance of flight articles in expected environments is obtained; for flight articles this environment is that established as normal by the type approval testing. Acceptance tests are devised and performed in a manner that avoids rework of the assembly after testing.

d. Operations. Each flight article is certified for use at the SAF before being assembled into the spacecraft. This certification is the verification by the cognizant division that its assembly has satisfactorily passed division tests including type-approval tests of a prototype of the flight article. A Proof Test Model of the RA-1 and -2 spacecraft is the only completely assembled spacecraft subjected to type-approval tests. The flight articles and the completely assembled RA-1 and -2 spacecraft, were subjected to flight acceptance tests only.

5. Test Organization

The operation of tests to prepare and launch each spacecraft for its mission is the responsibility of a test direction team. This direction team comprises a Test Director and subsystem representatives as shown in Figure 374. The subsystem representatives are operation personnel assigned to represent each JPL division contributing to the spacecraft. Each representative is responsible for understanding the essential and critical details of the subsystem contributed by the division he represents. The direction of test operations flows through the representative to and from the other JPL activities which complete the effort to build a spacecraft. As a team, the subsystem representatives are responsible for understanding each of the subsystems, the requirements for testing and operating the subsystems, and the facilities to be used during the testing and operations effort.

6. Sequence of Operations and Flight Preparation Schedule

a. Sequence of operations. Figures 375 and 376 show the assembly plan, sequence of operations, and the test equipment used in testing the PTM and the flight spacecraft. This flow diagram depicts only the events and movements as planned for tests and operations and does not establish the schedule of time required. For an overall analysis of the projected operation the flow diagram should be correlated with the JPL-Pasadena Preparation Schedule (Figs 377 and 378) which show the assembly and operations on the PTM, the flight spacecraft, and the

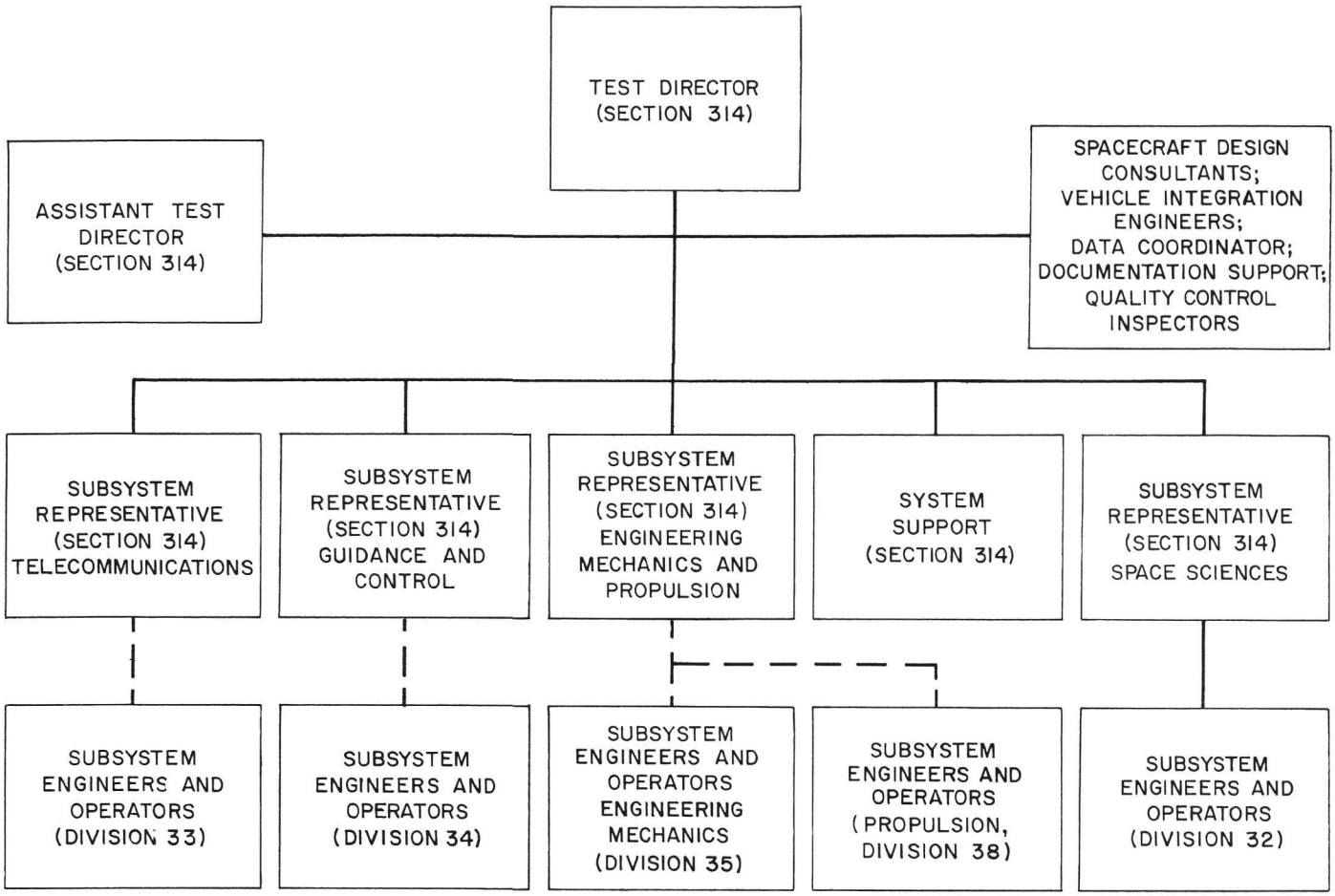

Figure 374. Test direction team

GSE requirements. (AMR Flight Preparation Schedule is presented in Chap. VI, JPL, AMR Operations.)

b. RA-1. The assembly and test schedule for RA-1 is shown in Figure 377. The entries prior to March 15 represent the time actually used in performing the related tests. All items after March 15 represent the necessary work to be completed before shipping to AMR.

Assembly. Approximately 70 to 80% of the spacecraft equipment and GSE was delivered to the spacecraft assembly facility on schedule. This allowed sufficient latitude for scheduling of tests and assembly work to prevent serious delays. A compatibility test, not indicated on the schedule, was performed between the RA-1 spacecraft and the Lockheed flight *Ranger–Agena* adapter. Several discrepancies in adapter wiring were found by JPL. These were reported to Lockheed and corrective action was taken.

The RA-1 final flight configuration was completed with the delivery and installation of the following items:

(1) Modified SCRE boom with guard rails.

(2) Modified solar panel with guard rails.

(3) New Earth sensor shade.

(4) Modified omni-antenna.

(5) Flight magnetometer.

(6) Newly designed launch and back-up battery.

(7) Modified solar panel zener diode brackets.

(8) New bracket and tripping switch for solar panel extended indication circuitry.

Items 1 through 4 were necessary from results obtained during the PTM's compatibility test with the LMSC adapter and shroud. They were intended to prevent shroud interference upon separation from the spacecraft.

All the items were installed prior to the weight, center of gravity, and moment-of-inertia tests scheduled for April 1, 1961.

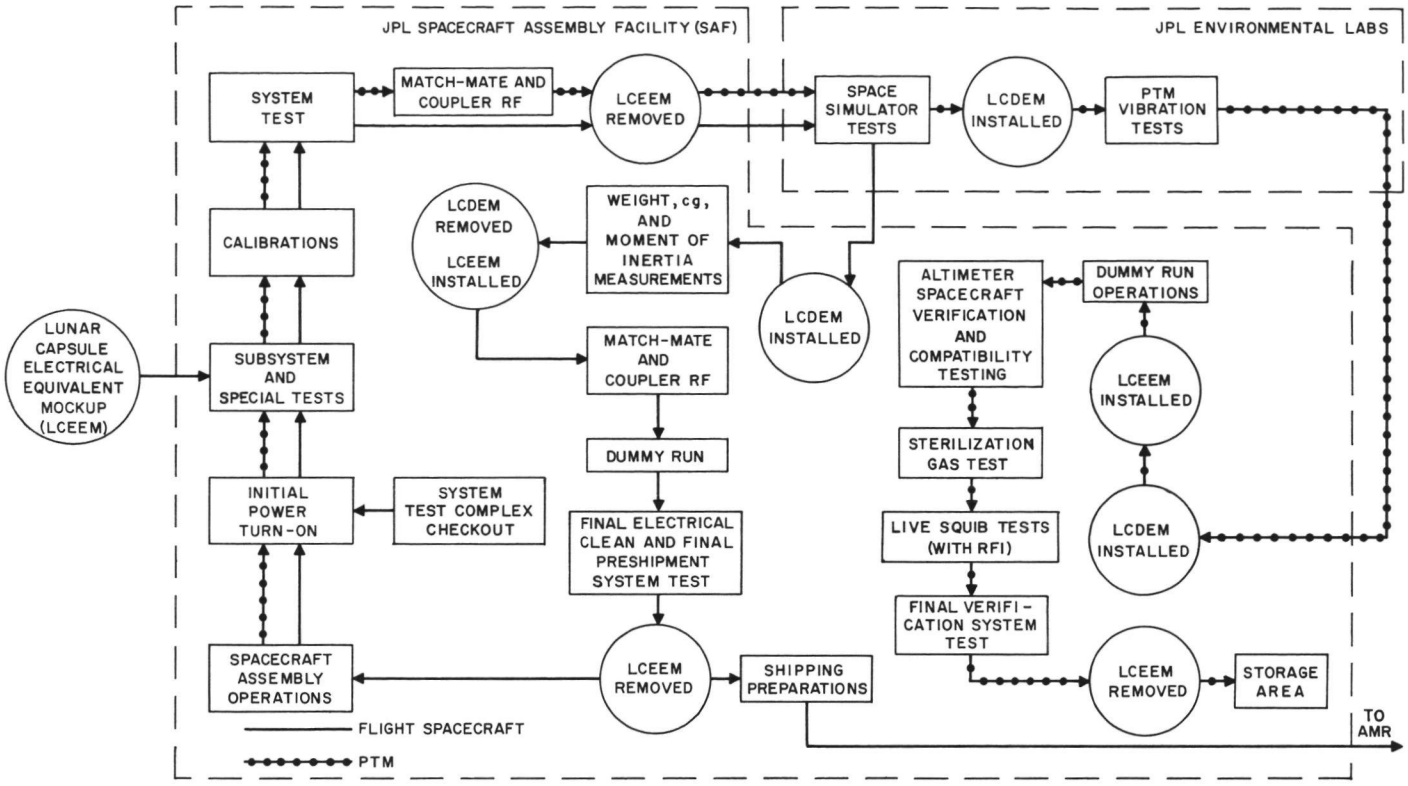

Figure 376. RA-3 and -4 sequence of operations

formally starts. The order in which subsystems were checked is:

(1) Power.

(2) Data encoder.

(3) Communications.

(4) Controller.

(5) Attitude control.

(6) Boom extension (erection).

(7) Scientific instruments.

Power. The power subsystem had a total of four failures discovered during the initial turn-on. Since then it accumulated approximately 480 hr of operating time without any additional malfunctions.

Attitude control. This subsystem experienced no difficulties with its electronics but was affected by a leaky gas system. The bottle and plumbing were carefully checked and defects corrected to achieve an acceptable leak rate of 65 cm^3/day.

Data encoder. The data encoder experienced more difficulty with GSE than its flight hardware. A complete "black-box" calibration was first performed, followed by calibration with the flight electronics. More explicitly, all subsystems other than the data encoder, after having performed their own checks satisfactorily, then underwent checkout with the telemetry and the system central recorder in operation. This procedure allowed a subsystem to have its maximum information read out as early as possible. Approximately 95% of the spacecraft was calibrated with telemetry by the end of the subsystem test period.

Communications. Communications performed methodic and extensive checkouts. Other than system noise having caused excessive phase jitter and removal of the cast for a change in the crystal-securing mechanism, no failures occurred.

Controller. No troubles were experienced with the controller once all the cables and circuit modifications were installed. These changes were made because of the analysis of the troubles experienced with the controller on the PTM.

Boom erection system. A design change on the packaging of the squib power supply battery was mandatory due to leakage of electrolyte.

CONFIDENTIAL

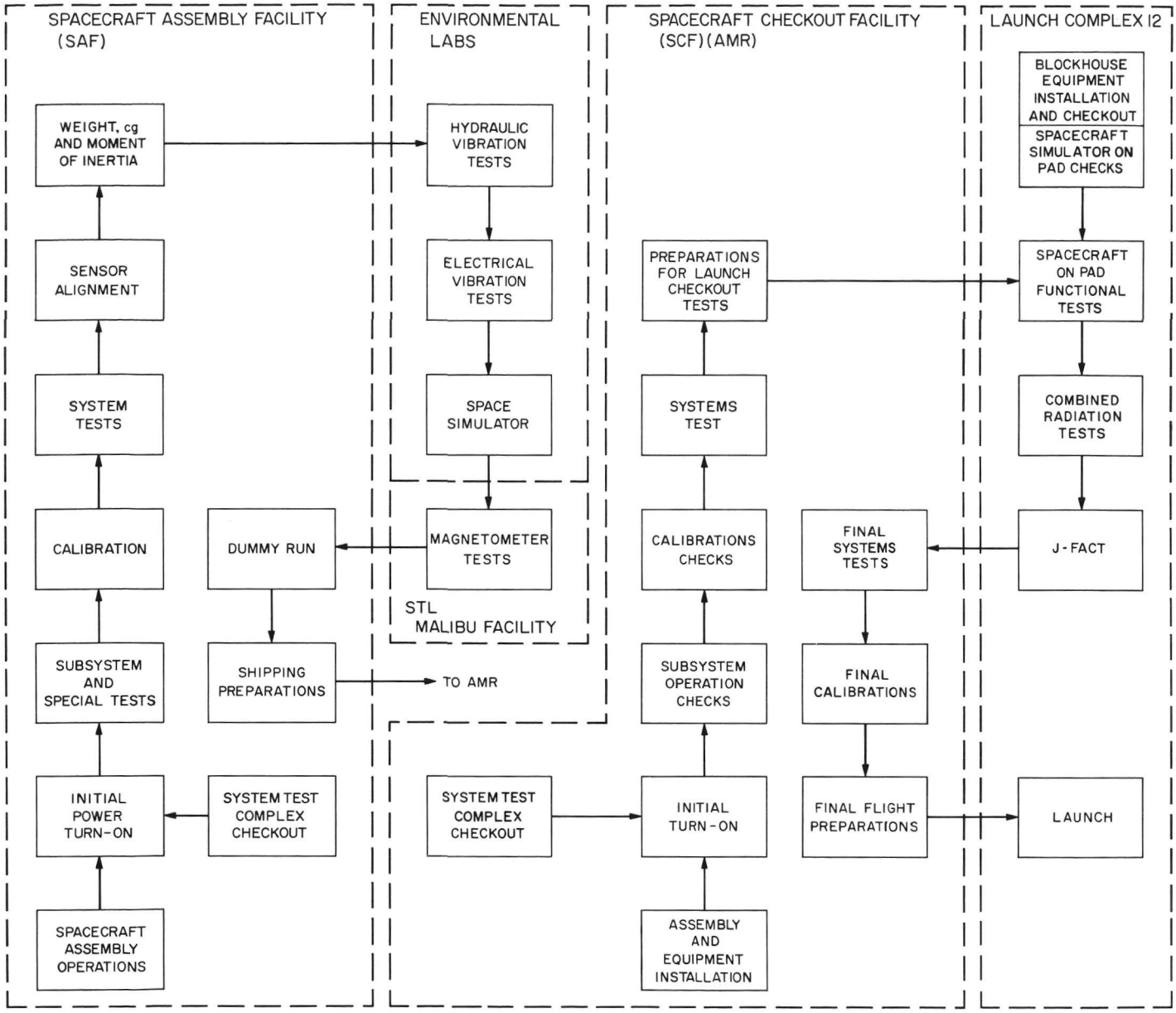

Figure 375. RA-1 and -2 assembly and operation plan

Subsystem test. The general plan of this test is to allow each subsystem representative an opportunity to verify that his equipment is functioning and has undergone no performance degradation in the spacecraft environment. To minimize interference and possible false indications, only one subsystem at a time is allowed to be checked. When all subsystems are reported working satisfactorily, the inter-subsystem checks (e.g., telemetry calibrations) are performed.

Prior to starting of the subsystem tests, comprehensive wiring integrity and ground checks were performed. Several errors in wiring, documentation, and ground ties were found during the RA-1 checks. These were corrected, permitting the start of the initial turn-on procedure. The initial turn-on objective is to allow safe application of power to the spacecraft electronics. Briefly, each converter, inverter, and transformer–rectifier is connected to a simulated normal load, and prime power applied. Each connector pin, by use of specially designed break-out boxes, is examined for a proper voltage or no-voltage indication. Once satisfied that all voltages are normal, the dummy loads are removed and the power module connected to its spacecraft load. The subsystem test then

CONFIDENTIAL

CONFIDENTIAL

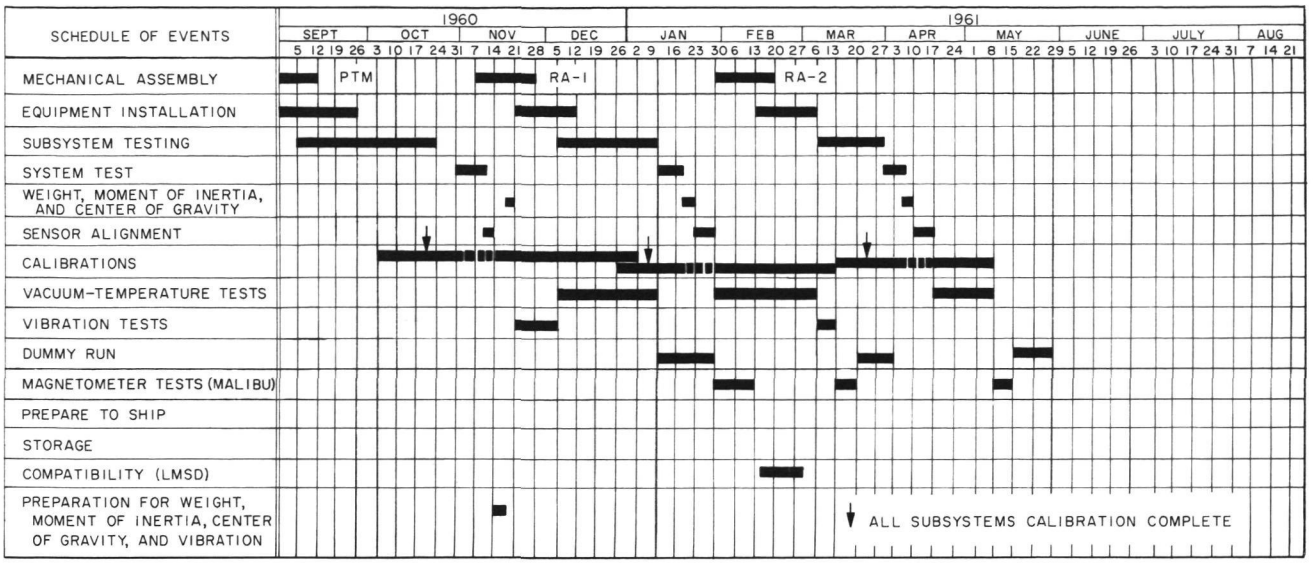

Figure 377. RA-1 and -2 PTM spacecraft preparation schedule (typical)

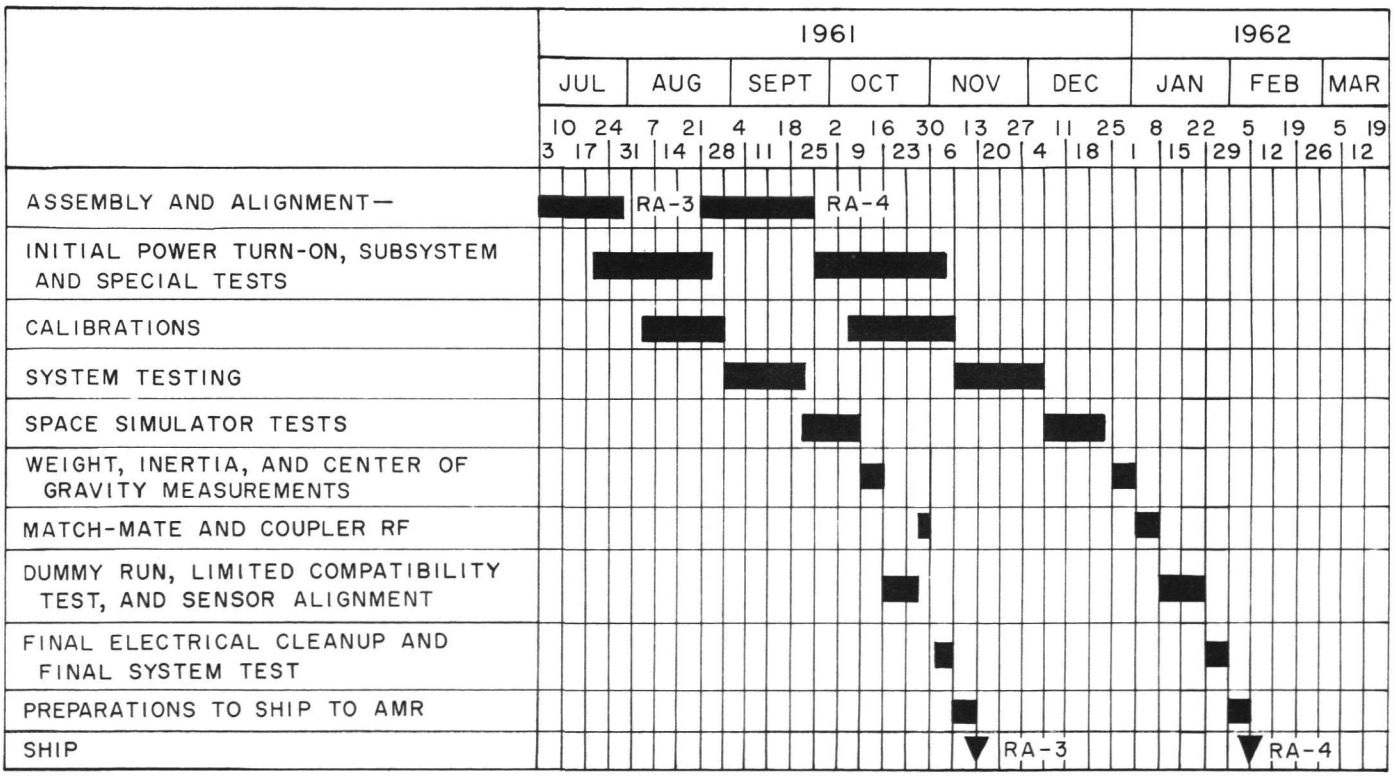

Figure 378. RA-3, -4 preparation schedule (typical)

Scientific. For various reasons, the scientific area required more subsystem test time, had more failures, and required more equipment modifications than any other area. However, the major part of the troubles was cleared.

The GSE, data automation system, and the evaluation and data equipment had many problems which delayed analysis of the scientific experiments aboard RA-1. The GSE instrument counters were extremely susceptible to

CONFIDENTIAL

noise, resulting in display of erroneous information. Usable data was obtained only after a complete and major repair of grounds and returns in the GSE.

The data automation system and scientific GSE simultaneously read out most of the experiments. It was not until near completion of systems test that good correlation data was obtained. The Lyman–alpha and magnetometer experiments corrected and modified many deficiencies in equipments. The JPL electrostatic analyzers were delivered late, but only minor design changes were necessary in order to obtain proper operation in the spacecraft. The Vela Hotel experiment required only one spacecraft wiring change. No other problems existed. The JPL friction experiment checked out normally, and the data obtained was satisfactory.

Systems test. The main objective of this series of tests is to ensure that the spacecraft's subsystems are operational and compatible. To this end, the maximum amount of instrumentation and monitoring is used. The GSE and associated direct-access and separation plugs are connected to the spacecraft. The central recorder, data display, and scientific GSE printers are all used.

The duration of the test was approximately 8 hr, of which 2 hr were used to verify the readiness of the GSE. All subsystems' representatives performed their own special tests according to procedure and under direction of a system test conductor. Upon completing these tests, time was started at X − 5 min. At X − 3 min the controller was activated and simulated real time run until controller command 7 was issued. Controller time was then accelerated by a multiple of 25 until the friction package experiment on-command was issued; the remaining controller commands were manually given and the test completed. The system test fixture was actuated in roll, pitch, and yaw during the T + times, and the overall data loops checked.

Vibration. The entire spacecraft was placed on the axial, the shake fixture transversed, and the spacecraft was subjected to the following flight-acceptance program:

High frequency, axial: (1) white Gaussian noise: 3.5 g rms, 15 to 1500 cps for 6 sec, and (2) 1.0 g rms, 15 to 1500 cps plus 1.0-g peak sinusoid superimposed on noise. The frequency of the sinusoid was swept from 15 to 1500 cps in 5 min.

Low frequency, pitch and yaw: sinusoidal frequencies between 1 to 40 cps for 20.5 min. The displacement of vibration was ±1 in. from 1 to 2.2 cps and 0.5-g peak from 2.2 to 40 cps.

The elements of the over-all test were as follows:

(1) System verification Test 1.

(2) Shake in axial plane.

(3) System verification Test 2.

(4) Shake in pitch plane.

(5) Verification Test 3.

(6) Shake in yaw plane.

(7) System test in spacecraft assembly facility.

The purpose of the system verification test was to establish a set of comparison data for both before and after shake. All connections to the GSE complex were used for this test. (Only the separation connectors were used during the actual vibration.)

Two days were used in completing the over-all vibration test, and no failures in electrical or mechanical components were observed. The accelerometer data showed no serious mechanical resonances.

Sun sensor alignment test. The primary Sun sensor mechanical–electrical alignment was verified by pointing the roll axis of the spacecraft at the Sun and monitoring the electrical output from the sensors (Fig 379). Sun tracking was accommodated by the azimuth elevation features of the system test fixture. The system test fixture drive was placed in low-speed range, and both azimuth

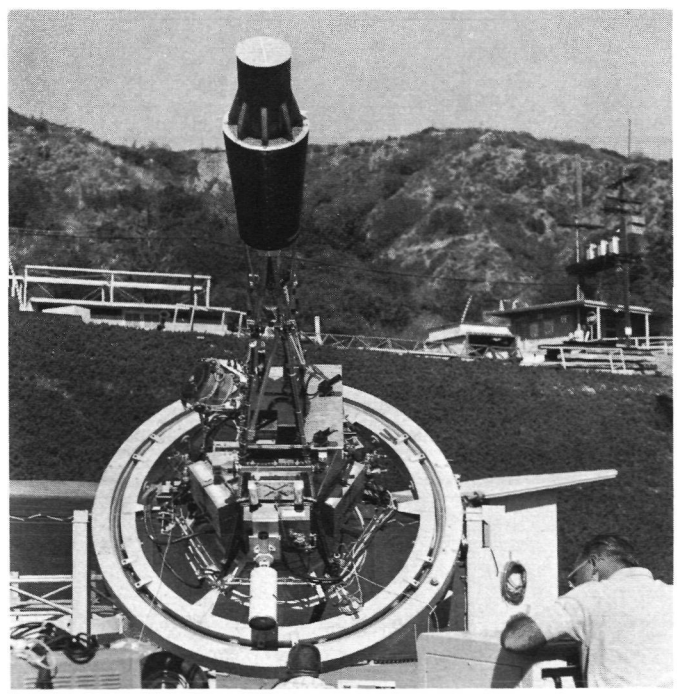

Figure 379. RA-1 test set-up

and elevation speeds controlled by manually adjusting the drive rheostats. The orientation of the roll axis of the spacecraft with respect to the Sun was monitored by an optical device illustrated in Figure 380. The device was aligned optically with respect to its mounting base and fitted to a bracket mounted on the attitude control surface of the support frame. The Sun's image was projected onto an opal glass screen on which a grid had been scribed to represent the Sun's position in various attitudes of the device.

The sensors' outputs were monitored by dynamic voltmeters for various attitudes of the roll axis with respect to the Sun. The results of the test were satisfactory even though the light intensity was less than desirable.

Vacuum–temperature. The purposes of this test were: (1) life-test the spacecraft in a simulated space environment, and (2) verify the design of thermal control surfaces. The requirements were to have a vacuum equal to or greater than 0.1 micron of Hg and a radiation intensity from arc-lamps of less than 1 solar constant (0.033 calorie/sec on a surface area of 1 cm^2).

The limitation in size of the chamber only allowed the installation of the engineering hex (Fig 381). The forward structure was placed outside of the chamber and connected to the spacecraft by extension cables. This configuration only allowed verification of effectiveness of the case thermal control design, since the hex legs could not be checked because of the inability to irradiate the legs with

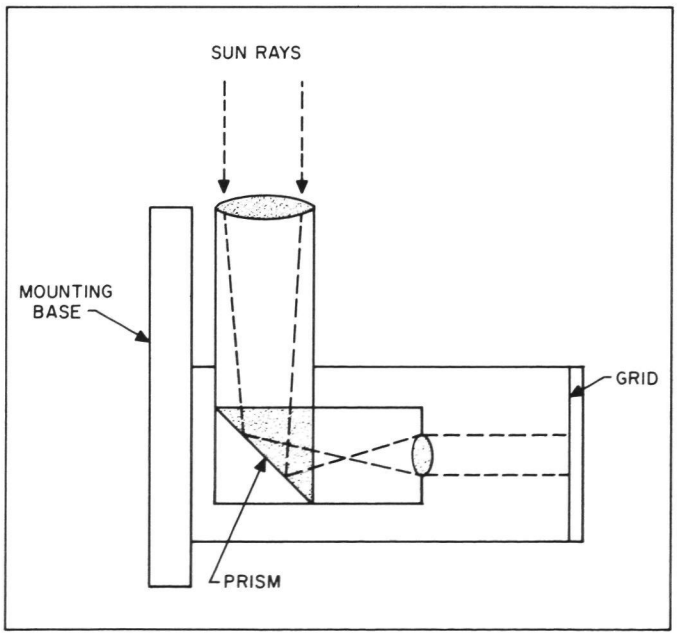

Figure 380. Sun sensor alignment fixture

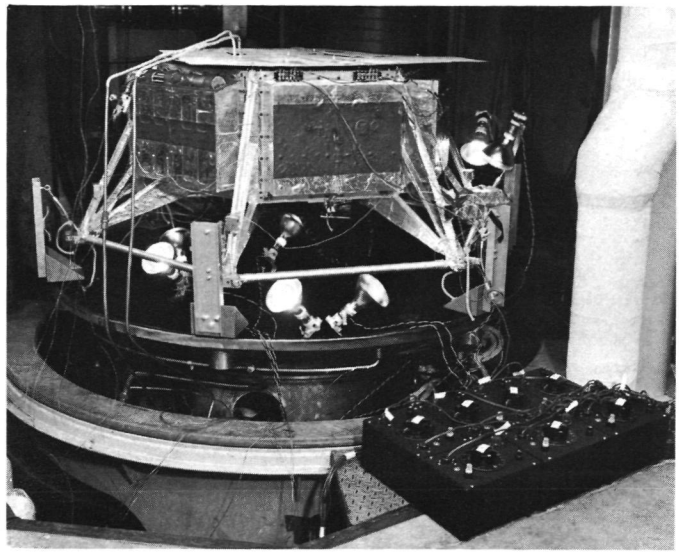

Figure 381. RA-1 temperature control model in space simulator

present lens and arc light system. Leg heaters were used instead. The purpose of having the forward structure connected was for assurance of the data links; telemetry and communications packages were on the hex and, therefore, located in the chamber. A shadow pattern plate was installed above the hex to simulate the forward structure.

Magnetometer tests at Malibu (Fig 382). The spacecraft flight articles were taken to the Malibu low-field magnetic site to measure the spacecraft residual specific conductivity for magnetic flux and to determine the flux components of the spacecraft in its operation modes. During the Malibu tests on RA-1, it was found that the spacecraft battery was not within its designed specification; however, there was no time to change this design for RA-1, but a redesign was accomplished for the RA-2 spacecraft. A modification to the scientific transformer rectifier, determined to be necessary during the Malibu test on the PTM, was evaluated and found to be adequate. The RA-1 flight spacecraft permanent magnetic flux density, as seen at the magnetometer, was determined to be approximately 4 gamma which was higher than desirable but adequate to achieve a meaningful measurement in the interplanetary field.

To assure that the permanent magnetic flux density of the spacecraft had not changed because of components being modified, magnetic calibrations of the spacecraft were performed at AMR utilizing a method developed by JPL. The spacecraft was mounted on a specially prepared turntable. A station magnetometer was mounted at a fixed

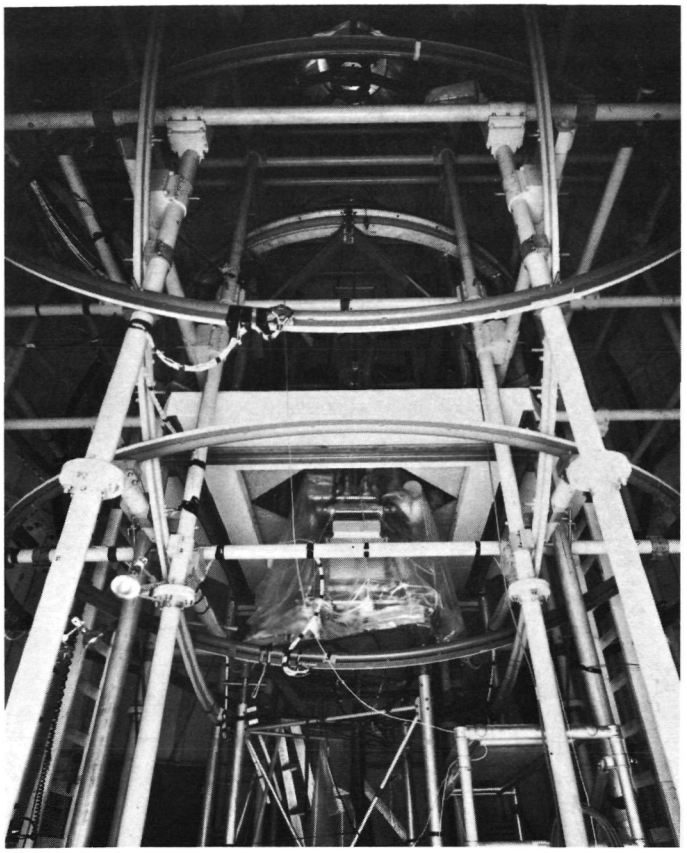

Figure 382. Magnetometer under test at Malibu

distance from the spacecraft. The spacecraft was then rotated about the roll axis and the short-term variations of the fixed station magnetometer were attributed to the permanent magnetic flux density component normal to the roll axis and the induced field, which had been low during the Malibu tests. The spacecraft was then quickly removed from the calibration fixture, the observed change in the reading of the station magnetometer being recorded as the permanent field of the spacecraft along the roll axis. It was a necessary condition that this method be accomplished in a short period of time to avoid local variations in the Earth's field insofar as possible. To validate subsequent data from the spacecraft, another station magnetometer monitored the Earth's field and its control information was used to correct the spacecraft data for local variations. These measurements were in very close agreement with the data obtained at the Malibu site.

Weight, center of gravity, and moment of inertia. The spacecraft was set up in a near-flight configuration for the weight, center-of-gravity, and moment-of-inertia tests. The major deviation from flight configuration was the lack of a backup battery. The center-of-gravity was determined in the *XZ* and *YZ* planes. The moments-of-inertia were determined about the *X-X*, *X-Y* and *Z-Z* axes with those of the *X-X* and *Y-Y* taken about arbitrary but known distances from spacecraft station 500. The spacecraft weight was determined with an electronic weighing kit using a load cell with a readout in micro-inches per in., the readout being converted to lb.

Dummy runs. The primary objectives of the dummy-run test were to check out the final countdown procedure, to acquaint the operators and evaluation personnel with the spacecraft in its launch configuration, and to verify the compatibility among the blockhouse, spacecraft, hangar, and launch checkout trailers.

The blockhouse equipment is designed to provide essential controls, e.g., applications of spacecraft power and a minimum of functional monitoring. The main spacecraft evaluation takes place in the AMR hangar or Spacecraft Checkout Facility (SCF) which receives information either over hard lines interconnecting with the spacecraft, or through an r-f telemetry link. The launch-checkout station comprises an r-f trailer containing both a transmitter and associated receiver for purposes of evaluating the launch communication system. The launch-checkout telemetry trailer supports the r-f trailer and spacecraft in providing real-time and tape memory storage of data. All of the equipment used to support RA-1 dummy runs was in its launch configuration.

Three dummy runs were performed, during which operating procedures were developed by extensive revision of existing rough drafts. The final procedure used in the actual AMR countdown was a result of the dummy-run procedure revisions.

Final JPL system test. Evaluation of the spacecraft prior to shipment to AMR required that a complete system test be performed. Only minor deficiencies were detected during this test, and the spacecraft was shipped to AMR on April 6, 1961.

The pre-launch operations and testing at AMR are detailed in Chapter VI.

c. RA-2. The basic testing philosophy for the RA-2 spacecraft followed closely that developed for the PTM and RA-1 spacecraft: (1) After the various equipment was assembled, a period of time was allotted to each subsystem for a thorough checkout to verify that each subsystem was capable of meeting the performance requirements on an individual basis. (2) Following this test was an integrated system test for all available subsystems on the spacecraft. (3) After satisfactory completion of a systems test, additional tests on the systems level were conducted

to establish a reasonable degree of confidence that the spacecraft would accomplish its mission.

Figure 377 presents the assembly and test schedule for the RA-2 spacecraft. The RA-2 spacecraft completed the first two test phases as shown on the schedule. The equipment assembly and preliminary checkout proceeded smoothly because of a thorough follow-up of the problems encountered on the PTM and RA-1 spacecraft. Very few documentation errors were noted on any of the basic engineering hex equipment. In addition, the acquisition of a spacecraft electrical simulator proved to be a valuable aid during the preliminary checkout test phase. The wiring integrity and ground checks discovered only minor problems that were easily resolved.

The following is a summary of the status of each spacecraft subsystem as of March 20, 1961:

(1) Power: subsystem ready for system testing.

(2) Controller: preliminary checkout completed and the subsystem ready for system testing.

(3) Erection system: preliminary checkout satisfactory and the subsystem ready for system testing.

(4) Attitude control: a preliminary leak check on the gas system completed and subsystem testing completed prior to March 31.

(5) Communications: subsystem completed its preliminary checkout and was in process of performing subsystem calibrations with the data encoder. Except for the omni-antenna, delivery of the communications equipment was complete.

(6) Data encoder: preliminary checkout of this subsystem resulted in a failure of a solid-state relay. A space was procured, and calibrations with other subsystems progressed.

(7) Data display: preliminary subsystem checkout satisfactory. Additional checkout continued as required by other subsystems.

(8) Central recorder: calibrations with other subsystems were being performed as required.

(9) Command decoder: a minor problem of ground support equipment indicator reversal was corrected and the subsystem was ready for system testing.

(10) Scientific data automation system: the ground support equipment received a preliminary checkout; however, the basic electronics for Chassis VI was not delivered, delaying complete subsystem testing.

(11) Scientific instruments: late delivery of much of the equipment for scientific instruments resulted in a postponement of subsystem testing. Ground verification checks and ground support equipment checkout were in progress. The equipment that remained to be delivered consisted of a magnetometer, two medium-energy detectors, and the third SCRE experiment.

After the vacuum–temperature test, a final system test was made to confirm flight readiness of the spacecraft. Minor problems were found in the GSE; flight equipment performance was completely satisfactory.

Assembly and testing of the RA-2 spacecraft proceeded smoothly and this activity was several weeks ahead of schedule. At the end of April, RA-2 was placed in the Space Technology Laboratories magnetic test facility at Malibu and the magnetic field calibration was accomplished. Following this test, vehicle match-mate and vacuum–temperature tests were planned. A portion of the time gained was used in an extended life test in the space simulator; however, this test was shorter than it could ideally be because of the limited number of available personnel. RA-1 experience indicated that round-the-clock operation of the space simulator and monitoring of the spacecraft is a demanding, exhausting task.

d. RA-3. During the assembly of the RA-3 PTM, the midcourse propulsion unit and the lunar capsule electrical mock-up were on hand, and other components were in qualification test. However, some late deliveries were expected and a part of the value of the RA-3 PTM was lost because there was not enough time to incorporate changes between tests of the PTM and of the actual RA-3 flight spacecraft.

Basic test plans for the RA-3, -4, and -5 program, and particularly RA-3 PTM, called for a test program similar to the one followed for RA-1 PTM. The main changes were replacement of the scientific superstructure by the lunar landing capsule and specific testing to accommodate this mission. Notably, the special requirements, time, and facilities necessary for magnetometer checkout and calibrations were deleted. The remaining subsystem testing of the assembled spacecraft, calibrations, system testing, weight and inertia measurements, sensor alignment, environmental tests, dummy run, and match-mate checking followed the same basic concepts used in RA-1 PTM testing.

The capsule assembly was checked out by Ford Aeronutronic. Electrical and dynamic equivalent mock-ups were furnished JPL for use in spacecraft testing. Operating and monitoring the capsule electrical equivalent mock-up was limited to specific test operations on the spacecraft. R-F or electrical interference between the spacecraft and capsule were the main items checked. The

limited hardwire interfaces, mainly for squibs, between the two units also had their functioning and compatibility verified during system test operations.

The System Test Complex was set up in the new spacecraft assembly facility. Originally a 50- by 50-ft test complex was planned to allow utilization of the cable trenches built into the floor, but previous commitments necessitated the reduction to a 40- by 40-ft test area. Test positions were turned around in the test area to best utilize the existing trenches rather than have the floor covered by protective troughs as was done for RA-1 and -2 testing.

The test complex was set up during the week of May 8, thus allowing 2 weeks to check out the test complex and incorporate any last minute changes or additions. May 29 was the scheduled date for the initial power turn-on of the spacecraft.

The test equipment utilized for nearly all the test positions was fabricated exclusively for and was initially used with the RA-3 PTM program. On April 27, the GSE used with RA-2, through its system test phase, was made available for direct use or modification for use with RA-3. Approximately 50% of the RA-2 GSE was usable directly with RA-3 or was economically modified. The GSE used with RA-1 and -2 was made available on August 10 for conversion into a system test complex for RA-4 and -5.

Test operations for RA-3, -4, and -5 followed much the same plan as PTM, but with a different sequence and without a vibration test of the assembled spacecraft.

Scheduled testing was completed on the PTM; however, the bus was used for some special unscheduled tests. These tests consisted of a dynamic modal analysis (determination of vibrational modes), command receipt tests, and DSIF receiver threshold checks. It was planned that the PTM would be kept as an RA-3 design entity, at least until after the first flight of the design. In the interim, it was made available for any pertinent special tests.

One such test was to check operational compatibility between the spacecraft and the altimeter. This test ideally should have been accomplished during the subsystem and system test operations, but due to unavailability of a test altimeter, this was impossible. It was, therefore, believed advisable to perform such a test at the earliest possible time, even at the expense of adding a couple of days to the over-all schedule. This appeared justified since Wiley Electronics would be at work on the flight altimeters shortly after delivery of the first test unit and, if system incompatibilities or shortcomings did exist, it was essential to know of these and take corrective measures quickly. Fortunately the tests worked out well, obviating the necessity for any significant circuit changes.

The PTM was subjected to low and high composite vibrational tests, dummy-run testing, a sterilization gas test, and a live squib test.

The configuration used for the vibrational testing consisted of the basic bus with all operating electronics fitted with dynamic mock-ups of the solar panels, lunar survival capsule, and radio altimeter. The spacecraft was shaken in each of three planes (normal to the x, y and z axes of the spacecraft) in accordance with JPL specifications. The attitude-control gas system was pressurized (1000 psi), the gamma-ray boom was pressurized (125 psi) and the midcourse motor fuel tank was filled with 14.6 lb of water. Post-shake verification tests were run after each plane of vibration exposure. No failures were noted during the low-frequency vibration tests that were directly attributable to vibrational environment. A shorted capacitor in the three-phase inverter was traced to a design fault.

The same configuration as that used for low-frequency checks was employed for the high-frequency testing and verification testing was also performed. Again, no failures were noted that were directly traceable to environmental testing. However, a somewhat spectacular event did occur due to high-frequency shaking normal to the z axis (centerline or roll axis of the spacecraft). As previously mentioned, the gamma-ray boom, a pneumatic telescoping extension device, was pressurized to 125 psi for these tests to ensure that no leaks would occur during vibration. The collet used to retain the boom in the retracted position was locked by a pyrotechnically operated pin puller (live pyrotechnics were not employed in this test). The collet used on the PTM was made of aluminum, whereas the flight design utilized stainless steel. The aluminum collet was used on the PTM because of early delivery requirements on the PTM. The three axes of low-frequency vibration and the x and y axes of high-frequency vibration had peened the soft aluminum collet with the pin of the retaining pinpuller sufficiently to allow the collet to disengage, thereby allowing the boom to extend. This was not felt to be a design problem since the flight collets were of stainless steel and therefore not subject to the peening effect. This incident represented the first time the boom was extended (other than on models or in artist's conceptions) on a spacecraft and in a 1-g field. A post-incident photograph is shown in Figure 383.

The PTM was next subjected to dummy run testing. The configuration used was similar to that used for RA-1

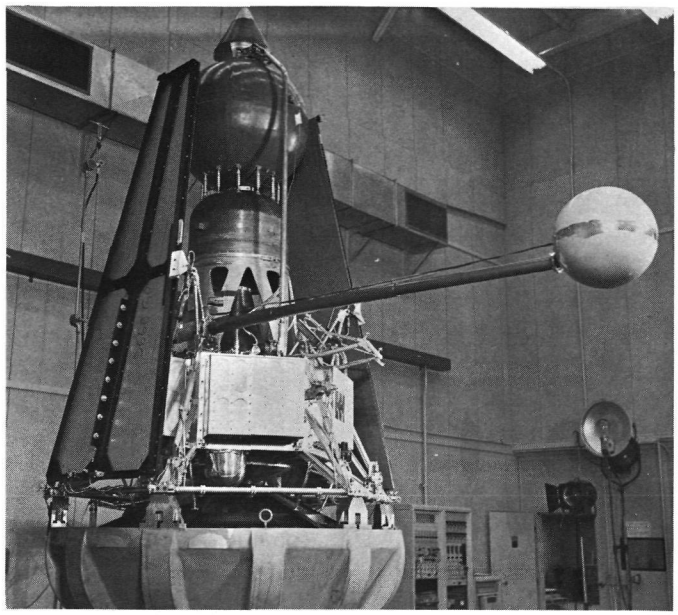

Figure 383. Gamma-ray boom extended

and -2. The spacecraft was mounted on the *Agena*-adapter-forward equipment section and was connected to the blockhouse–hangar complex through the umbilical cable. Precountdown and countdown procedures were executed three times each. Early operations were poor, since sufficient time was not available to check out the launch complex equipment before the beginning of dummy-run testing and many errors in cabling and console wiring were noted. These were reworked as discovered. The read-write-verify (RWV) equipment was used to issue commands to the spacecraft. This was the equipment used at the Goldstone DSIF site to modulate the transmitter for commands during the actual mission.

Early in the testing, it was noted that issued commands were not being received in the spacecraft with the desired repeatability; i.e., every fourth or fifth command would either be garbled or not received at all. The RWV GSE was checked for accuracy and some modifications were made. This did not, however, completely cure the problem. Eventually, the trouble was traced to the spacecraft command subsystem. Evidently, the command registers were being upset whenever power to the spacecraft was turned off, so that when power was turned on again, the issuance of a clear command (a normal procedure used prior to the issuance of any commands) could not efficiently clear all the registers. Therefore, when a command was issued, the registers were somewhat biased, depending on how badly they had been upset at last power turn-off. Two circuit modifications were made and subsequent testing showed that the problem was resolved.

The flight spacecraft were not bothered nearly as badly by this problem as was the PTM; however, the modifications were applicable to the flight spacecraft and assured an even higher reliability of correct commands being transmitted during flight. The Space Flight Operations Plan was revised to include the issuance of the clear command prior to the issuance of any group of commands in flight (e.g., midcourse maneuver and terminal maneuver stored commands, real-time commands, etc.) in case spacecraft noise, solar flares, etc., upset the registers. This would also lend more reliability to the issuance of commands. The balance of the dummy-run testing was conducted without incident.

Following dummy-run testing, a quick test was made with the spacecraft shroud coupler. A test at LMSC showed that ethylene oxide gas (used for terminal surface sterilization) affected the harp material used on the coupler by increasing its transmissibility by a factor of 50%. The retest of the output of the spacecraft's omni-antenna through the spacecraft shroud coupler showed no degradation in performance.

An opportunity was then afforded to test the PTM with the first operable prototype of the lunar capsule radio altimeter. The test was conducted in two parts: first, by allowing the radio altimeter to run free-radiating to determine if any r-f interference were noted on the spacecraft due to the altimeter or if spacecraft r-f could trigger the altimeter's fuzing signal (capsule sequence initiation) prematurely; and second, to inject simulated received signals into the altimeter to allow calibration of the altimeter lunar reflectivity telemetry. The first test revealed no r-f interference problems on either the spacecraft or the altimeter. The second test enabled the development of a technique for calibrating the telemetry, although the PTM system was not actually calibrated. This type of calibration must be tailored for each spacecraft and time did not allow a complete calibration of the PTM. However, information was received from the altimeter on the correct channel and the commutation system operated as designed.

The PTM was then set up for the live squib test (pyrotechnic and extension system). This test included the mounting of accelerometers to measure shock levels; AMR r-f interference simulation, with checks at each squib location as to received energy levels; and the actual operation of all squib-operated extensions and events.

For this test, the spacecraft was mounted on the *Agena* mock-up. Live squibs were installed, including simulation for *Agena*-spacecraft separation squibs (pinpullers and separation plug spin-offs). The lunar capsule and radio

altimeter extension pyrotechnics were also included (capsule-separation bolt-cutters, squib-switches, etc.). Before the actual squib test, the shroud was installed and the spacecraft was subjected to terminal surface sterilization gassing for 10 hours. Subsequent visual inspection (and later electronics tests) revealed no damage to the bus equipment, lunar capsule, or prototype altimeter due to the gassing. The spacecraft was then removed to the safe area, the umbilical was installed, and recorders were attached to the accelerometers. With the spacecraft shroud removed, the PTM was then radiated with simulated powers of *Atlas*, *Agena*, and AMR tracking r-f sources (nine in all). A thermistor was installed at each squib location and direct energy levels were measured with spacecraft power on. Subsequent analysis showed that no location received more energy than −40 db of that considered to be sufficient to ignite a squib. The r-f opaque spacecraft shroud was considered to be capable of at least an additional 10 db of isolation, giving a total of −50 db margin.

The next portion of the test involved firing the squibs. This was done by transferring to internal power and disconnecting the umbilical (thus, testing the live squibs against any incurred transients) and allowing the spacecraft to time its way to the first squib event, solar-panel extension. This event occurs 30 min after launch. The umbilical was then reconnected and the CC&S GSE was connected by direct access to allow stimulation of each squib event without having to go through a 66-hr mission. The next event was midcourse motor turn-on and turn-off (Conax valve operation), followed by gamma-ray boom extension, deployment of the omni and radio altimeter antennas, vidicon lens cover opening, capsule-spacecraft separation bolt-cutter actuation, and capsule squib switch initiation. The latter started the lunar capsule sequence by actuating the spin-motor initiator, the retro-motor initiator, and the payload-motor separation squibs (bolt-cutters). The test was considered successful with all squibs blown, excepting some of the bolt cutters on the capsule. This failure was subsequently traced to a discontinuity in the separation plane contacts (caused by the presence of foreign material) and, in one case, a broken wire. These devices were eventually fired successfully.

In order to extend the gamma-ray boom in a 1-*g* field, a trough was constructed that allowed the spectrometer sphere to ride out on nylon slides. The clamp that retains the omni-antenna, which normally separates violently from the spacecraft in a direction normal to the roll axis, was tethered by a cord and attached weight. The test showed that the clamp will separate cleanly from the spacecraft. The simulated *Agena* separation squibs were fired at the time of normal injection without effect on the spacecraft.

Flight spacecraft. Most of the design problems were detected in the PTM and subsequent modifications were enacted. However, some problems were noted that are unique to the flight spacecraft and bear mentioning. Component failure rates were much higher on the flight spacecraft than those recorded on the PTM. This was an exact reversal of the experience noted on the RA-1 and -2 program. The only difference between the RA-3 PTM and the flight spacecraft was heat sterilization. Although no failures were directly traceable to heat damage, it is believed that heat sterilization does shorten the expected life of electronic components and circumstantial evidence seems to bear this out. In any case, the failure rate on the flight spacecraft is not alarmingly high.

A design fault has been noted on the gamma-ray spectrometer. The unit was originally designed to be hermetically sealed. However, vacuum chamber tests have shown that the seal is not perfect and a slow leak results in arcing and permanent damage after about 15 to 18 hr in vacuum. The design is being changed to vent the unit to atmosphere, so that it will not be turned on, in the mission, until 4 hr after launch. This will allow internal surface sterilization, previously accomplished by using the sterilant gas as the pressurant.

RA-3 flight assembly. The assembly of the RA-3 flight model followed schedule, despite some early difficulty with internal sterilization of the basic bus assembly. It was planned that bus sterilization would be accomplished by building up the basic bus with all attitude-control gas jet hardware, primary harnesses, high-gain antenna gear box, and solar panel supports. The entire assembly would then be baked at 125°C for 24 hr to accomplish internal sterilization. However, the weight savings program dictated the extensive use on the bus of magnesium castings and titanium fasteners, as well as some aluminum parts that could not be made of magnesium. The first such "mixed metals" bus to be fabricated was the RA-3 flight bus. Considerable apprehension was expressed that the mixed metals bus might warp when heated. It was, therefore, considered advisable to heat the bus "bare," before build-up, in case it did warp and would have to be machined after heating. All parts to be assembled to the bus were heated separately and installed with the use of sterile fluid on all mating surfaces that would not later be exposed to terminal gas sterilization. The heating of the bare bus did result in a slight warpage, but fortunately, in a direction to be nearer in tolerance than that which existed before heating. No machining was required. Sufficient confidence was generated to heat

RA-4 and -5 in the built-up condition, thereby obviating the use of sterile fluid during buildup.

Initial power turn-on and subsystem testing. Initial power turn-on and subsystem testing took place during the period from July 24 through September 21, 1961. Most of the problems discovered during the period were those which remained unresolved from the PTM testing. The problems included a transient resulting from exciting the Earth sensor with a step function light input and the starting of the antenna hinge motor. The power converters showed a marked instability during switching transients.

Because of delivery problems, many of the equipment tested during this phase were nonflight items. As a result, some of the testing had to be repeated when flight items were delivered.

System testing. System testing was conducted during the period from August 22 through September 18. During this period, three systems tests were conducted. Many of the problems discovered in the first two systems tests were resolved by procedural change, recalibrations, and equipment adjustments. System Test Number 3 was postponed for approximately a week to allow additional time for the vidicon and gamma-ray subsystems to resolve existing problems. System Test Number 3 showed several additional procedure, operator, and GSE problems that were definitely resolved following the actual test. Prior to environmental testing, calibrations on several transducers were checked to insure a valid environmental test.

Environmental testing. The basic RA-3 spacecraft engineering equipment, without the lunar capsule, omni-antenna, and the radio altimeter, was subjected to a series of environmental temperature tests during the period from September 23 to October 9. This test series was conducted to calibrate spacecraft temperature transducers, temperature-sensitive communications measurements to verify theoretical temperature control calculations and to evaluate the flight-system interface problems in real time during a normal flight sequence.

Specifications indicated that the vacuum pressure should have been less than 10^{-5} mm Hg. The lowest pressure that could have been obtained with existing equipment was 2.5×10^{-4} mm Hg.

During the temperature calibration period, several discrete equipment failures were noted. None of the failures could be directly attributed to the near-space environment.

The mission verification portion of the test proved satisfactory, with the exception that operation and discrete equipment failures with the vidicon and gamma-ray equipment were noted. None of the failures detected was directly attributed to the near-space environment. The malfunction noted with the gamma-ray equipment was later resolved by repeating that portion of the test using the spacecraft PTM and the flight modules of gamma-ray equipment.

Weight, center of gravity, and mass moments of inertia. During the period from October 16 through 19, 1961, the basic bus weight as well as the center of gravity and moments of inertia for both launch and midcourse maneuver configurations of the spacecraft were determined. Due to the state of the lunar capsule assembly, it was decided to establish the basic bus parameters at that time and integrate the lunar capsule unit parameters as these became available.

Dummy-run testing. During the period from October 16 through 19, a precountdown test and two dummy-run tests were conducted. The results of the second dummy-run test showed that the procedure and equipment problems were well defined; therefore, further dummy runs at JPL were cancelled.

Pressure vessel calibration and leak checks. The weekend of October 21 and 22 was devoted to pressure vessel telemetry loop calibrations. A multiple-point calibration was performed on the midcourse motor fuel (300 psi) and helium (3000 psi) tanks and the attitude-control nitrogen (3000 psi) system. A quantitative leak-check of the attitude-control, cold-gas system indicated that the system was leaking at approximately 25 to 30 times the 100 cc/hr maximum allowable rate, according to the specification.

Live pyrotechnic firing test. A pyrotechnic firing test was conducted on October 23 to verify the ability of the spacecraft to fire live pyrotechnics. Review of test data showed that procedural errors invalidated portions of the telemetered event indications. Sensitivity of other telemetry channels to the event checking pulses was noted and investigated prior to shipment of the spacecraft to AMR.

Match-mate. A series of tests with the RA-3 flight adapter and shroud were conducted. These tests showed that several shields in the adapter wiring harnesses were loose and one plug on the spacecraft separation connector was incorrect. Prior to the mechanical match-mate, a leg spring constant determination was conducted. Mechanical match-mate of the spacecraft to the spacecraft adapter was conducted according to flight operational procedures. During the r-f coupler retro fitting to the omni-antenna, an interference was noted between the Earth sensor cable and spacecraft shroud. Techniques for the coupler retro

fitting were developed and will be incorporated in future testing. R-F loop checks were performed to establish radiating characteristics preparatory to the AMR on-pad checkout.

Following the match-mate testing, approximately 1 week was allowed for mechanical and electrical preparations for the final systems test at JPL. During this period, the spacecraft electronic support cases received final temperature control painting, cable securing, and system calibrations. A period was allowed for testing with the Deep Space Instrumentation Facility receiving equipment and alignment of the various optical sensors. The final system test in the SAF at JPL, Pasadena, was conducted on November 6, 1961, with all subsystems and GSE participating except the lunar capsule, which was to be delivered directly to AMR. No major discrepancies were noted at that time, and the RA-3 spacecraft was shipped to AMR on November 15, 1961.

Extensive investigation is underway to determine if reflections from the spacecraft can enter and affect proper operation of the Earth and Sun sensors. Light baffles are being added to the Earth sensor and reflection tests are being run on the Sun sensors. Some aging effects have been noted on the Sun sensors, particularly after heat sterilization. However, it has not yet been proven that this effect impairs their operation.

Testing of the RA-3 spacecraft at AMR did not reveal any serious problems. Pre-J-FACT tests were completed and the spacecraft had been removed to the Explosion Safe Area for final "button-up" prior to transportation to the pad for the J-FACT tests.

The final button-up did not utilize live pyrotechnics, fueled midcourse motor, or the flight lunar survival capsule. An electronic mock-up of the capsule and retro-motor were employed, as well as a prototype radio altimeter. The object of final assembly in the Explosion Safe Area was to establish safe operational procedures and to gain practice in operating around dangerous motors and pyrotechnics at the time of final assembly for flight. All sterilization precautions were adhered to; the spacecraft was mounted to the *Agena* adapter and the *Agena* shroud was installed in this area.

During final assembly, the new capsule retro-motor heat shield was installed for the first time on RA-3. No difficulty was noticed but the installation did reveal certain procedural requirements in maintaining safety protective devices during heat-shield installation. It was noted that clearance between the heat shield and the inboard edges of the radio altimeter was less than expected, but should not offer any difficulty.

Operation at the Explosion Safe Area also included a simulated midcourse motor fueling and installation and a simulated capsule assembly, dynamic spin balance and installation. The entire operation helped resolve many undecided areas and firmed a logical assembly sequence for actual flight preparation use.

During early testing in Hangar AE, it was noted that on occasion, the data encoder would inadvertently change modes during the switching operation from external to internal power. This is not a flight problem, but could cause some consternation on the launch pad. There is a blockhouse control to switch modes as required; however, use of this control causes loss of sync in the data display equipment, which requires 16 min to re-sync. The problem was resolved by swamping the power changeover relay coils with diodes in the ground support equipment. This swamping prevents the transient that was causing the trouble and subsequent tests showed that the modification was successful.

One failure was noted early in the testing. The 4A4 communications converter suffered a collector-to-emitter short in the input transistor. Subsequent investigation showed that a defect in the transistor's coating near the emitter had caused the short. The converter was replaced with a spare and the failed unit was repaired and returned to stores.

Considerable testing has been conducted at the Pasadena facility on the possibility of stray light reflections entering the Earth sensor and causing lock-on confusion or ambiguity. As a result, severe "shiny" areas in the vicinity were dulled by painting with a flat black paint and in some chronic areas, covering with a black cotton "coffin" cloth. This effort was coordinated with cognizant thermal control personnel and handled in a manner that did not jeopardize the thermal characteristics. RA-3 was so modified at AMR, with the exception of the shroud bumper (a guard rail that prevents the *Agena* shroud from drifting into the spacecraft) that is mounted adjacent to the Earth sensor.

***e.* Ranger *RA-4*.** Mechanical assembly and alignment of RA-4 was started on August 21, 1961, and completed to the extent that initial power turn-on testing was started on September 26. The problems associated with the mechanical assembly were as follows: (1) Sterilization of the bus assembly resulted in warping the structure so that Plane A (Station 500) was out of flat by 0.115 in. (allowable tolerance is 0.005 in.). This, however, was compensated for by suitable shimming. (2) A wire in the ring harness was found to be parted near a splice. This damage occurred sometime during the sterilization process.

By October 31, initial power turn-on, system grounding checks, and a large portion of calibrations were completed. During these calibrations and testing, the following difficulties were encountered:

(1) The transponder was returned to the cognizant engineer because of AGC difficulties.

(2) The antenna drive unit had a faulty potentiometer, and is believed to be a sterilization problem.

(3) The attitude-control pressure regulator had an O-ring failure.

(4) The autopilot electronics unit failed.

RA-4 problems were resolved by the end of December 1961. Recalibration of the transponder and data encoder was scheduled for January 8, 9, 1962, and final system test at JPL was scheduled for February 8, 1962. The RA-4 spacecraft was scheduled to be shipped to AMR on February 19, 1962.

f. RA-5. RA-5 is being prepared as though it were to be a follow-on mission. The decision as to which mission it would fly was to be reached before testing began. A thorough test program was worked out to assure an integrated design prior to flight. A spacecraft PTM was not to be used. Rather, the flight bus would utilize a PTM version of the passenger for a major portion of the testing, with the flight passenger being added at a later date.

Pursuant to the practice followed on *Mariner R*, it was suggested that dual bridge-wire squibs be used to fire the midcourse motor valves on RA-5. These were not available for use during the early stages of RA-3, -4, -5. However, their use was considered mandatory on *Mariner R* and a rather complete and elaborate testing program was devised. It was determined that the testing program would be complete early enough to be of value on RA-5 and should yield sufficient quantities to supply the flight needs. This change involved certain wiring alterations in the midcourse motor squib harness, the bus squib harness, and the squib firing assembly. Use of the dual bridge-wire valves for RA-6 through -9 (follow-on) was adopted for all flights. RA-5 will use the new arrangement, regardless of its mission.

A major design change was found necessary at a late date. The final decision on the use of a retractable heat shield for the capsule retro-motor brought to light the fact that the deployment of the omni-antenna (which releases the lanyards that hold the shield in place) occurs simultaneously with the deployment of the radio altimeter, resulting in an almost certain fouling of the radio altimeter by the heat shield as it drops. Since the altimeter is not forcibly deployed, but rather depends on "mouse-trap" springs operating in a zero-*g* field, this situation could be serious. Elastic bands maintain tension between the top of the shield, which is supported by lanyards that are contained by the base of the omni-antenna, and are released when the antenna is deployed, allowing the shield to retract to the base of the support structure.

The problem was solved in a unique manner. The deployment of the two antennas is controlled by initiation of redundant pyrotechnics. Each of the redundant squibs at each location is initiated by redundant firing circuitry, referred to as Channels A and B for clarity. The signal which actuates these squibs is derived from a CC&S signal, "stop pitch," which is the last signal given in the attitude-control terminal-maneuver sequence. Since it was required to allow sufficient damping time for the spacecraft to remove pitch motion prior to these deployments, it was an early design decision to initiate a 2-min time delay after the receipt of "stop pitch" and before the antenna deployments. It was further decided to allow a 2.5-min delay for the redundant channel to permit sufficient time spread between the redundant squib events to read out on telemetry. The result is that the Channel A squib at both locations is initiated after a 2-min time delay, and the Channel B squib is initiated at both locations after a 2.5-min time delay. The "fix," then, was to deploy the radio altimeter by the use of both A-channel squibs, at 2 min, and to deploy the omni-antenna (and heat shield) with both of the B-channel squibs at 2.5 min. Thus, the altimeter should be completely deployed and out of the way of the heat shield when it is dropped 30 sec later. The mechanization was simple, involving only the interchange of two wires in the bus squib firing harness. The disadvantage, of course, is that some of the redundancy has been sacrificed. Although there are still redundant squibs at each location, they will both be fired by the same signal. This is not believed to be a serious sacrifice, in that the squib firing circuitry is the only redundant circuitry on board the spacecraft.

g. RA-6, -7, -8, -9 (follow-on). Preliminary planning for test operations on the *Ranger* follow-on TV experiment incorporating the RCA supplied TV subsystem indicated that most of the three sets of system test equipment used on RA-3 and -4 will be suitable also for these operations. The anticipated schedule for the follow-on testing would require only three sets of system test equipment, as are now being used on the existing *Ranger* programs, with a fourth set as a spare in the event of failure. This appears justified by the fact that the GSE will have had a great deal of time on it by the time the last of the *Ranger* follow-on spacecraft has undergone test operations.

The existing basic system test equipment will be augmented by RCA-furnished equipment of two basic categories, each of these in different quantity.

(1) Flight-operation type information-recovery equipment.

(2) TV subsystem analysis-type equipment.

The first of the two types will be furnished to the Goldstone tracking station and, in addition, two sets will be utilized during system test operations at JPL and one (additional) at AMR.

VI. Launch Operations

A. Facilities

1. General

This section describes those basic facilities and test ground support equipment (GSE) that were utilized at AMR for direct operation support of the *Ranger* spacecraft pre-launch and launch activities. These facilities comprise the JPL Spacecraft Checkout Facility (SCF), Launch Complex 12, and the JPL Launch Checkout Trailer Site (LCTS) (Fig 384). Included in the description of each of the aforementioned facilities is a description of the test GSE that was utilized in that facility. Range facilities used for support and maintenance services are not discussed.

2. JPL Spacecraft Checkout Facility (SCF)

a. General. The SCF, located in Hangar AE, comprises the System Test Area, the JPL Operations Center, the JPL Communications Center, Administrative and Engineering Offices, supporting Laboratories, and GSE. The hangar located in the industrial area at Cape Canaveral is a metal-clad building measuring 120 by 265 ft. Large paved areas are provided at the front and rear with wide roadways on both sides of the building. A loading dock is adjacent and parallel to the northeast side of the hangar (Figs 385 and 386).

JPL is using the high-bay area with its adjoining wings, and the northeast wing of the building. The center low-bay area and the southwest wing of Hangar AE are utilized by the Goddard Space Flight Center. A portion of the central low-bay area has been made available to JPL.

b. System Test Area (STA). Spacecraft assembly and system test operations were conducted in the high-bay area, known as the STA, which measures approximately 50 by 64 ft. The STA is equipped with a 5-ton capacity, traveling bridge crane with a 35-ft hook height.

The spacecraft checkout equipment contained in the STA is a duplicate of the System Test Complex (STC) located in the SAF at Pasadena (Chapter V). Separate arrangements of the STC equipment shown in Figure 387 are necessary to meet the requirements of the pre-launch operations and the launch operations. The wings adjoining the STA contain the mechanical and electronic stock room and the following laboratories, all opening into the STA:

(1) *Electronic laboratory.* This laboratory was used for JPL (and associated contractor) activities involving electronic testing and checkout of subsystems and components. The laboratory contains an r-f screen room which was used for electronic equipment calibration and interference testing.

CONFIDENTIAL

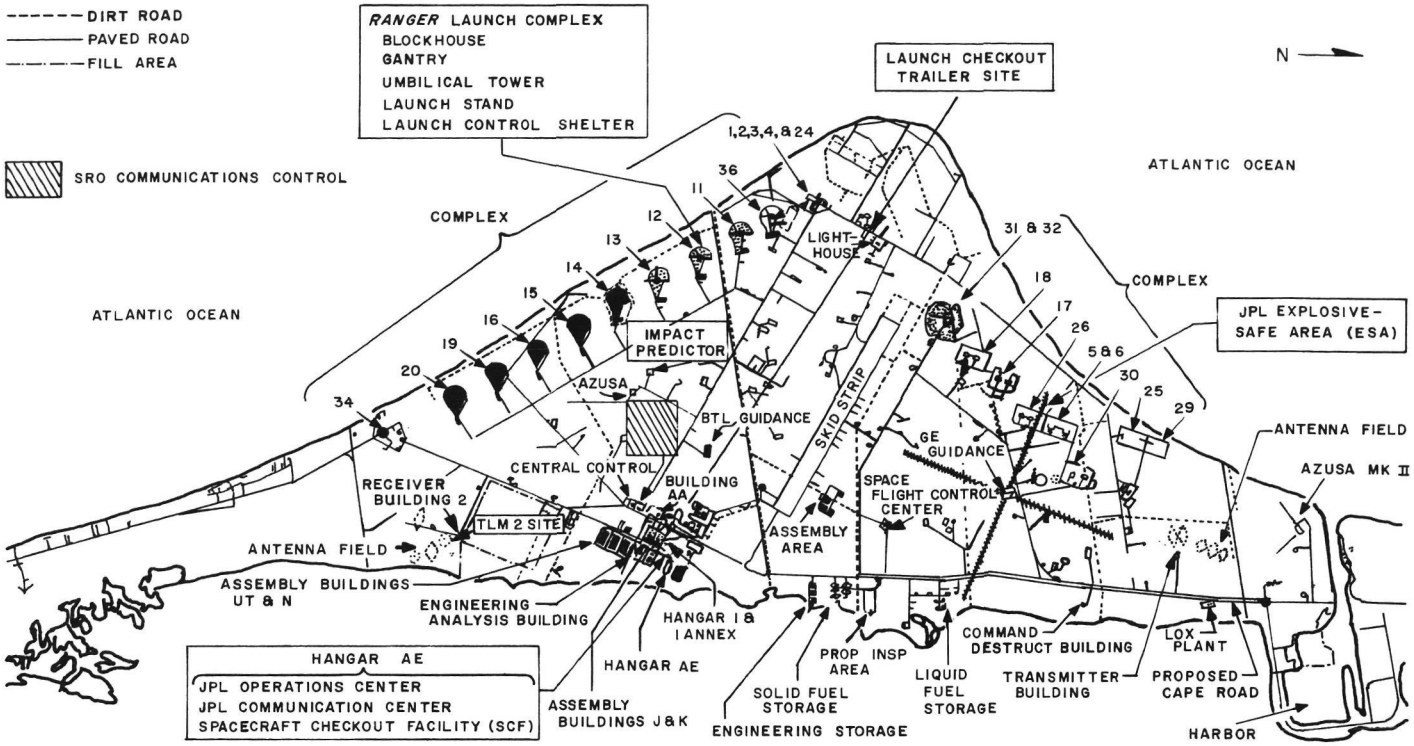

Figure 384. AMR launch complexes

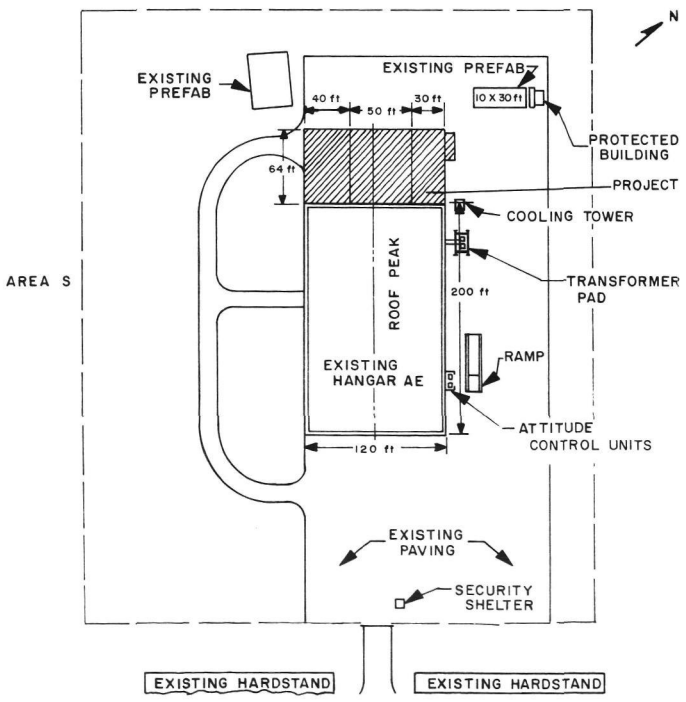

Figure 385. Hangar AE site plan

(2) *Scientific laboratory.* This facility was used for subsystem testing and repair of equipment by the scientific groups responsible for the various spacecraft scientific experiments.

(3) *Sterilization laboratory.* This installation was used for sterilization of spacecraft components and assemblies.

(4) *Solar panel laboratory.* This laboratory was used for the preparation, testing, and storage of solar panels and associated equipment.

c. JPL Operations Center. The JPL Operations Center is located in the northeast wing of the high-bay area. During those operations involving both the blockhouse and the SCF, the direction and coordination of all mission operations between JPL and other participating agencies are centered in this room. The center is also the tie-point for all JPL operational communications whenever the above-mentioned situation exists. Conference tables and consoles for the Mission Director, the Operations Center Coordinator, the Status Coordinator, and their assistants are located in the center of the room. In addition, there are three status boards along the northwest wall. One of these boards indicates the condition of the tracking and communication equipment at the various stations supporting the mission; the other two indicate the real-time events during flights (Figs 388 and 389). The Operations Center equipment is removed and stored

CONFIDENTIAL

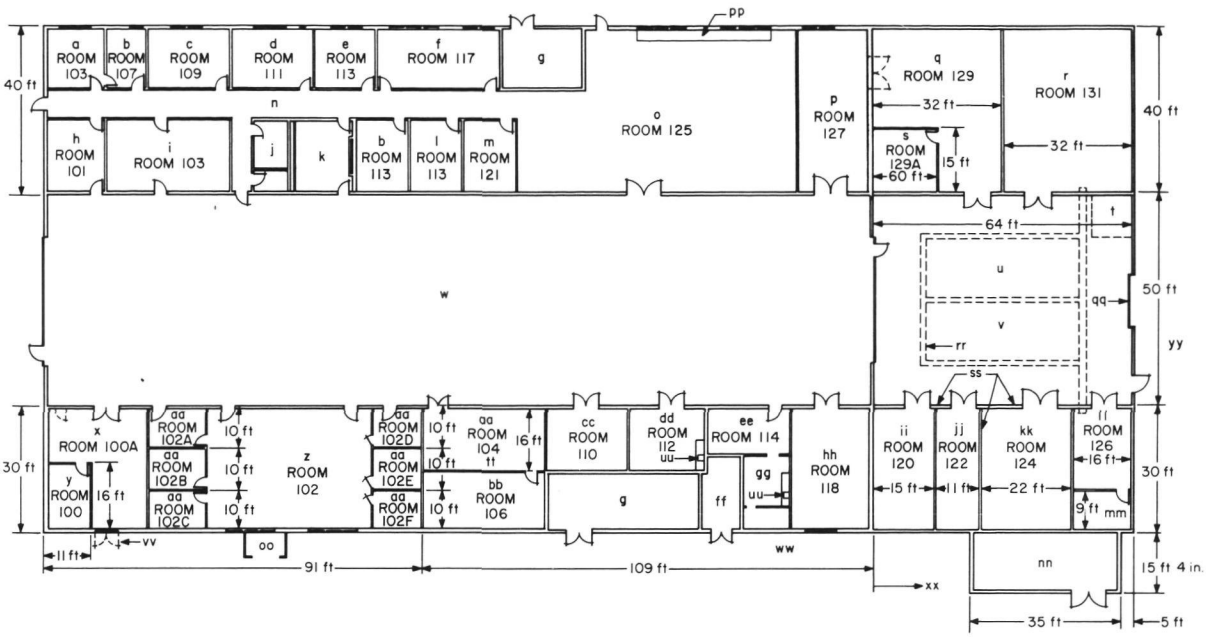

a - FIELD PROJECT HEAD
b - ADMINISTRATION
c - PAYLOAD MANAGEMENT OFFICE
d - PROJECT SUPPORT
e - DATA INSTRUMENTATION
f - CONFERENCE ROOM
g - ATTITUDE CONTROL MECHANICAL EQUIPMENT
h - ASC HEAD AND PROJECT OFFICE
i - TECHNICAL STAFF
j - WOMEN
k - MEN
l - COMPUTER AND DATA STORAGE
m - PAYLOAD ENGINEER
n - CORRIDOR
o - PAYLOAD AND DATA LABORATORY
p - PAYLOAD AND EQUIPMENT STORAGE (TO BE AIR CONDITIONED)
q - SCIENTIFIC LABORATORY
r - ELECTRONIC LABORATORY
s - OFFICE
t - RF SCREEN
u - ASSEMBLY AND SYSTEMS TEST AREA
v - 5-ton CRANE, 35-ft LIFT
w - EXISTING AE ASSEMBLY
x - SECURITY AND ADMINISTRATION OFFICE
y - FIELD STATION MANAGER
z - ENGINEERING OFFICE AND GROUP STUDY
aa - ENGINEERING OFFICE
bb - MOPS AND ADMINISTRATIVE TWX EQUIPMENT
cc - MECHANICAL LABORATORY
dd - DATA PROCESSING
ee - FACILITIES SUPPORT
ff - MOTOR GENERATOR ROOM
gg - BATTERY LABORATORY
hh - OPERATIONS ENGINEERING
ii - DATA ANALYSIS LABORATORY
jj - SOLAR PANEL LABORATORY
kk - MECHANICAL AND ELECTRICAL STOCK ROOM
ll - STERILIZATION LABORATORY
mm - STORAGE
nn - ATTITUDE CONTROL EQUIPMENT SHELTER
oo - 15-ton ATTITUDE CONTROL SHELTER
pp - FLOOR CABLE THROUGH
qq - SLIDING DOORS 12-ft WIDE × 20-ft HIGH
rr - CABLE TRENCH COVERS
ss - FILLED REINFORCED CONCRETE BLOCK WALL
tt - NEW PART
uu - SINK
vv - REMOVE DOORS AND SEAL OPENING
ww - EXISTING SAFETY SHOWER
xx - NEW CONSTRUCTION
yy - CONCRETE RAMP

Figure 386. Hangar AE spacecraft checkout facility

during local SCF operations; the room itself is used for the analysis of records and various test data in support of checkout operations while the spacecraft is within the SCF. In addition, the JPL Operations Center comprises the following equipment to be furnished and installed by AMR:

(1) Four operations consoles with equipment (Fig 389).

(2) Required MOIS amplifiers, power supplies, etc.

(3) Required amplifiers for switch and conference panels.

(4) Electric clock (24 hr).

(5) Countdown amplifier/speaker unit.

(6) Speaker w/volume control for paging system.

d. JPL Communication Center. The Communication Center, located in the northeast wing of the low bay, houses the operational TTY and MOIS equipment. It is the tie-point for JPL communication lines between Cape Canaveral and Pasadena.

The following equipment is contained in the Communication Center:

(1) MOIS terminal equipment.

(2) Cross-country leased lines terminations (two voice and two half-duplex TTY lines).

(3) AN/FGC 25 Kleinschmidt TTY.

Two of these 60 words-per-min machines are connected to the JPL-leased teletype lines to Pasadena and three are on standby. An additional teletype machine is connected to a Space Communication Net (SPACON).

The remaining area of the low bay is utilized for engineering and administrative office space, and for various supporting laboratories.

3. JPL Explosive Safe Area (ESA)

Final preparation of the completed spacecraft, installation of fueled propulsion systems and pyrotechnic devices, and sterilization of the spacecraft are accomplished in the ESA located near the east edge of the 26-56 Launch Complex.

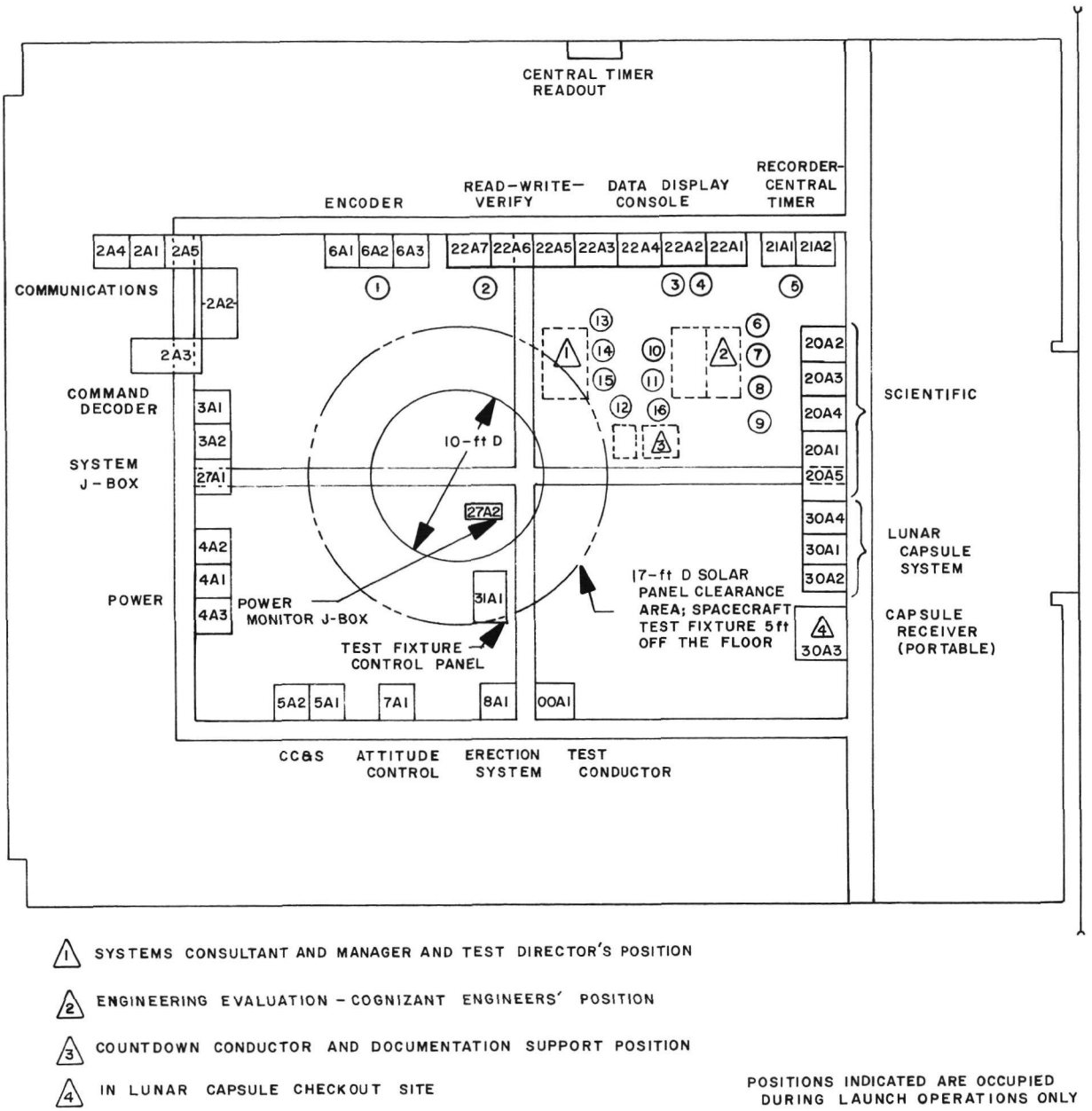

Figure 387. SCF system test area and equipment

The RA-1 and -2 spacecraft did not utilize the ESA, since neither had a midcourse propulsion unit, and the mission did not impose the requirement for spacecraft sterilization.

The site plan of this area is shown in Figure 390. Operations in the ESA take place in three separated, revetted, explosive-safe buildings interconnected by a smooth-surfaced roadway. The buildings are the Sterilization and Assembly Laboratory, the Capsule Laboratory, and the Propulsion Laboratory.

a. Sterilization and Assembly Laboratory. This laboratory is used for assembly of the lunar capsule and of the midcourse propulsion unit with the spacecraft bus; for final spacecraft weighting; for installation of the nose fairing assembly; and for gaseous sterilization of the completely assembled spacecraft within the shroud. The building is also used for monitoring and controlling the lunar capsule dynamic balancing machine in the Capsule Laboratory. The Sterilization and Assembly Laboratory is approximately 20 by 40 ft and is revetted on the north

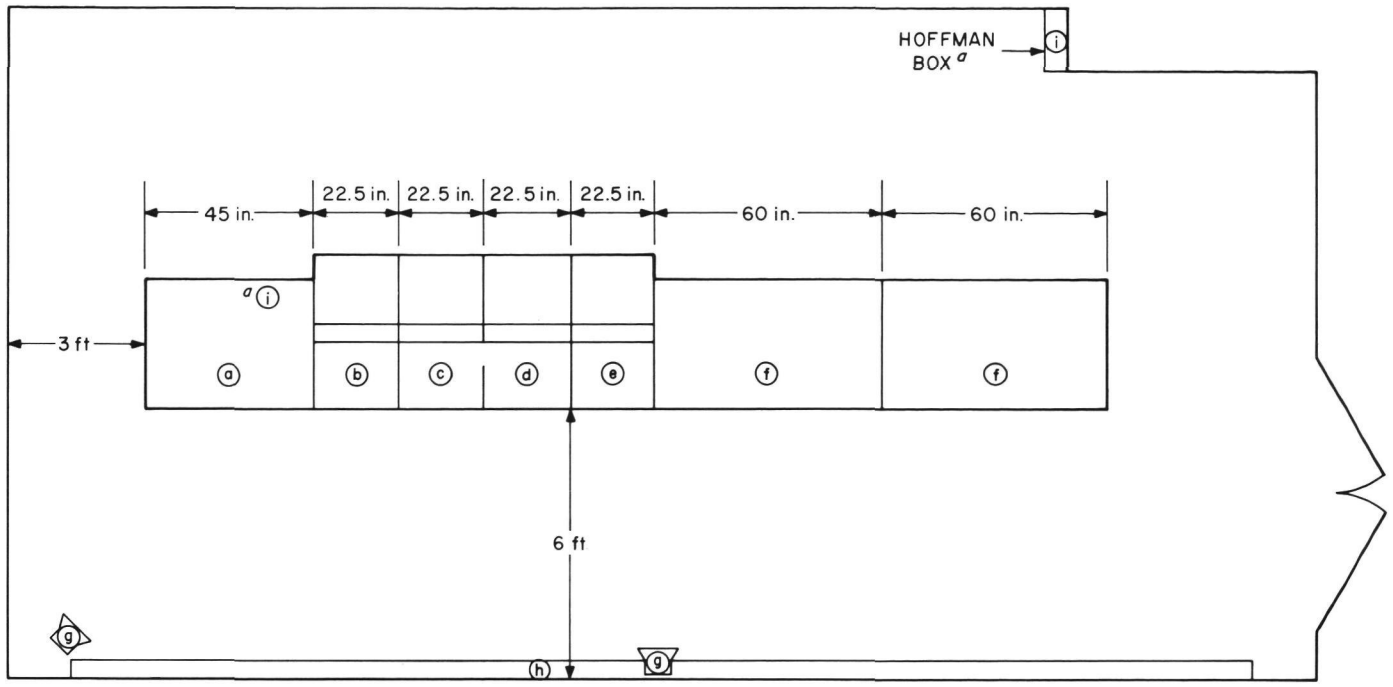

a-45-in. CONFERENCE TABLE
b-STATUS COORDINATOR'S CONSOLE
c-CONTROL CENTER COORDINATOR'S CONSOLE
d-BLANK CONSOLE
e-MISSION DIRECTOR CONSOLE
f-60-in. CONFERENCE TABLE (CFE)
g-COUNTDOWN AND PAGING SPEAKERS
h-STATUS BOARDS
i-[a]CABLES INTO ROOM TERMINATED AT HOFFMAN BOX. ADDITIONAL CABLES REQUIRED TO GO TO CONSOLES, AND WITH CONNECTORS ON BOTH ENDS

Figure 388. Hangar AE, JPL Operations Center floor plan

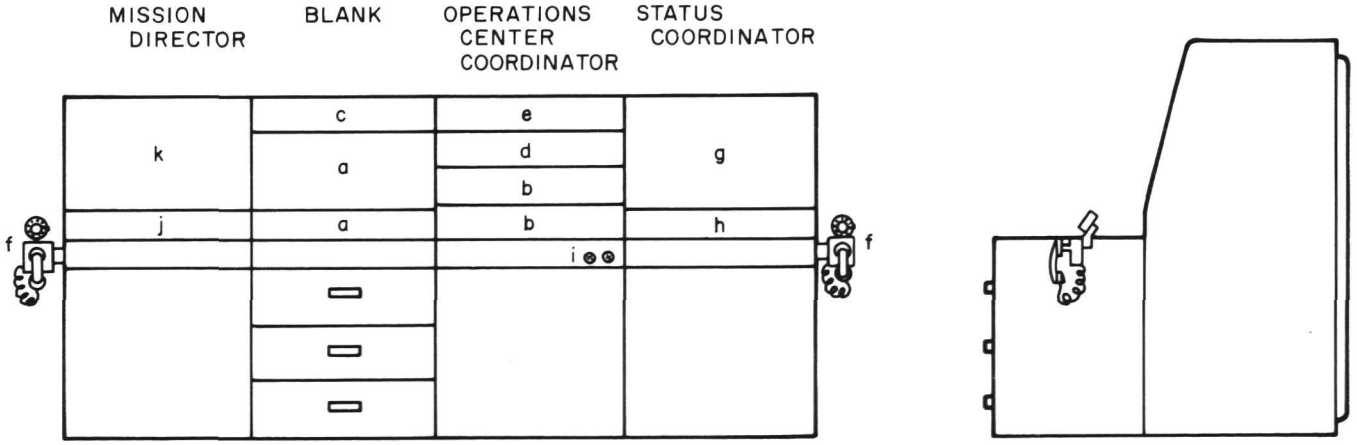

a-BLANK
b-MOPS FLASH UCSS END INSTRUMENT
c-DIGITAL COUNTDOWN CLOCK
d-CONFERENCE PANEL 1
e-CONFERENCE PANEL 2
f-TYPE 211 TELEPHONE
g-CONTROL PANEL FOR STATUS BOARD LIGHT
h-MOIS END INSTRUMENT
i-MOIS HEADSET JACK
j-MOIS END INSTRUMENT
k-COUNTDOWN MANUAL HOLDER

Figure 389. JPL Operations Center, console layout

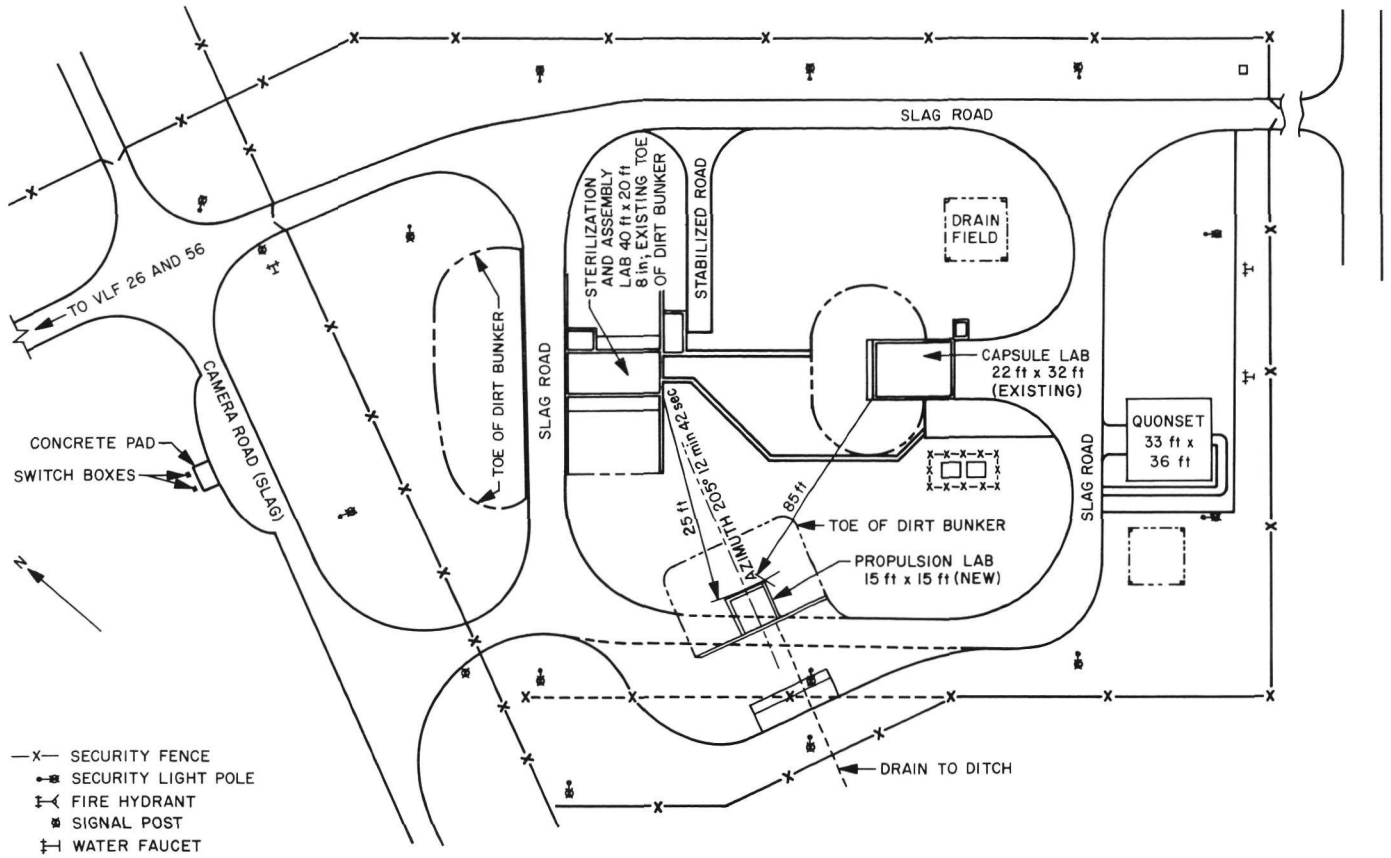

Figure 390. Explosive Safe Area

and south sides by an earth mound 27 ft high. A monorail, 2-ton capacity, traveling crane with a vertical travel of 20 ft extends the full length of the building. A stationary, 2-ton hoist, having a vertical travel of 29 ft is also provided.

b. Capsule Laboratory. This laboratory is used for assembly, checkout, and dynamic balancing of the lunar capsule and capsule subassemblies. The Capsule Laboratory is approximately 24 by 32 ft with a roof height of 20 ft. The building floor has two levels, the western portion being elevated 6 in. above the eastern portion. The lunar capsule balancing machine is approximately 13 ft high, 10 ft in length, and 4 ft in width, and contains a 3-hp, explosion-proof motor. The entire machine weighs 12,500 lb.

c. Propulsion Laboratory. This laboratory is used for checking, assembling, fueling, and pressurizing the spacecraft midcourse propulsion unit. The checkout and pressure testing of the inert, storable, liquid rocket motor is accomplished in a trailer parked adjacent to the laboratory. The remaining operations accomplished within the laboratory are monitored in the trailer. The Propulsion Laboratory is approximately 15 ft square with a ceiling height of 12 ft and a "blowout" roof. An overhead, deluge type sprinkler system, revetments on three sides of the laboratory, and other safety features required for handling liquid propellants are provided. Shed-type fuel and oxidizer shelters are located in those revetments on opposite sides of the building.

4. Launch Complex 12

a. General. The launch facilities for *Ranger* are located in Launch Complex 12. The Complex comprises the blockhouse, launch control shelter, umbilical tower, Launch Complex Equipment (LCE), spacecraft simulator, launch stand, and gantry (Figs 391 and 392). The LCE comprises equipment in the blockhouse, umbilical tower, and the launch control shelter; launch complex cabling, and the spacecraft simulator are also included. The LCE is capable of:

(1) Energizing the spacecraft to provide auxiliary power to the spacecraft and to switch the spacecraft to internal power.

Figure 391. Launch Complex 12, AMR

(2) Commanding the spacecraft, by hard-line where necessary, and verifying that the commands have been accepted.

(3) Monitoring necessary pre-launch operations from the blockhouse in order to verify proper operation. Portions of the spacecraft performance monitoring are done through the telemetry system and the data is displayed in the STA of the SCF. To facilitate monitoring of critical circuits and to allow more detailed monitoring of specific measurements as needed, the spacecraft telemetry mode selection is controlled from the blockhouse. The number of such measurements is limited, however, to simplify launch complex operations. Certain spacecraft parameters are monitored through landlines to the spacecraft.

b. Blockhouse. The blockhouse is a steel-reinforced, concrete structure located approximately 1200 ft from the launch pad. The blockhouse is the center of operations for hard-line command and monitoring of the spacecraft and for the launch vehicle during pre-launch and launch operations. The blockhouse contains GD/A-, LMSC-, and JPL-furnished consoles, with equipment for transmitting the necessary commands to the *Atlas–Agena-B–Ranger* vehicle, and for verifying proper operational modes and circuitry. JPL equipment is contained in the spacecraft monitor and control console, and the spacecraft coordinator's console. The JPL consoles are fixed-station equipment bolted to the blockhouse floor. Individual panels and chassis are easily removable and access to the rear of the racks is provided. The spacecraft monitor and control console (Fig 393) comprises five racks of equipment.

c. Launch Control Shelter. The Launch Control Shelter (Fig 394) is a 20- by 36-ft prefabricated metal building with a usable height of approximately 10 ft. It houses power equipment which must be in close proximity to the spacecraft. The building, located approximately 37 ft from the umbilical tower, houses (for JPL) one standard rack. (Fig 395) containing power supplies and other equipment which can be remotely controlled from the blockhouse. A junction box, an integral part of the rack, provides the necessary versatility to permit connection into the landlines of equipment located in the Launch Control Shelter. Access to both the front and rear of the racks is provided. An operator may be present within the shelter until $T-2$ hr.

d. Umbilical tower. The umbilical tower provides a transition point from the spacecraft catenary cable to the long-line cables and contains only that equipment which must be located in close proximity to the spacecraft. A JPL-supplied junction box is located on the tower, close to the point at which the cables enter the catenary. The junction box contains a line amplifier for the mixed modulation signal and two isolation packages for data encoder circuitry. The umbilical plug and catenary cables are for spacecraft use only and connect from the umbilical receptacle in the spacecraft adapter to the umbilical tower junction box and the trunk cables.

e. Launch Complex cabling. All spacecraft ground support cabling is discretely distributed among three junction boxes: The monitor and control console junction box, the launch control shelter junction box, and the umbilical tower junction box.

(1) *Long-line trunk cables.* Long-line trunk cables connect from the top of the umbilical tower to the blockhouse. Provision has been made to accommodate an adequate number of twisted pair, shielded, jacketed (TPSJ) lines from the blockhouse to the shelter, and from the shelter to the umbilical tower,

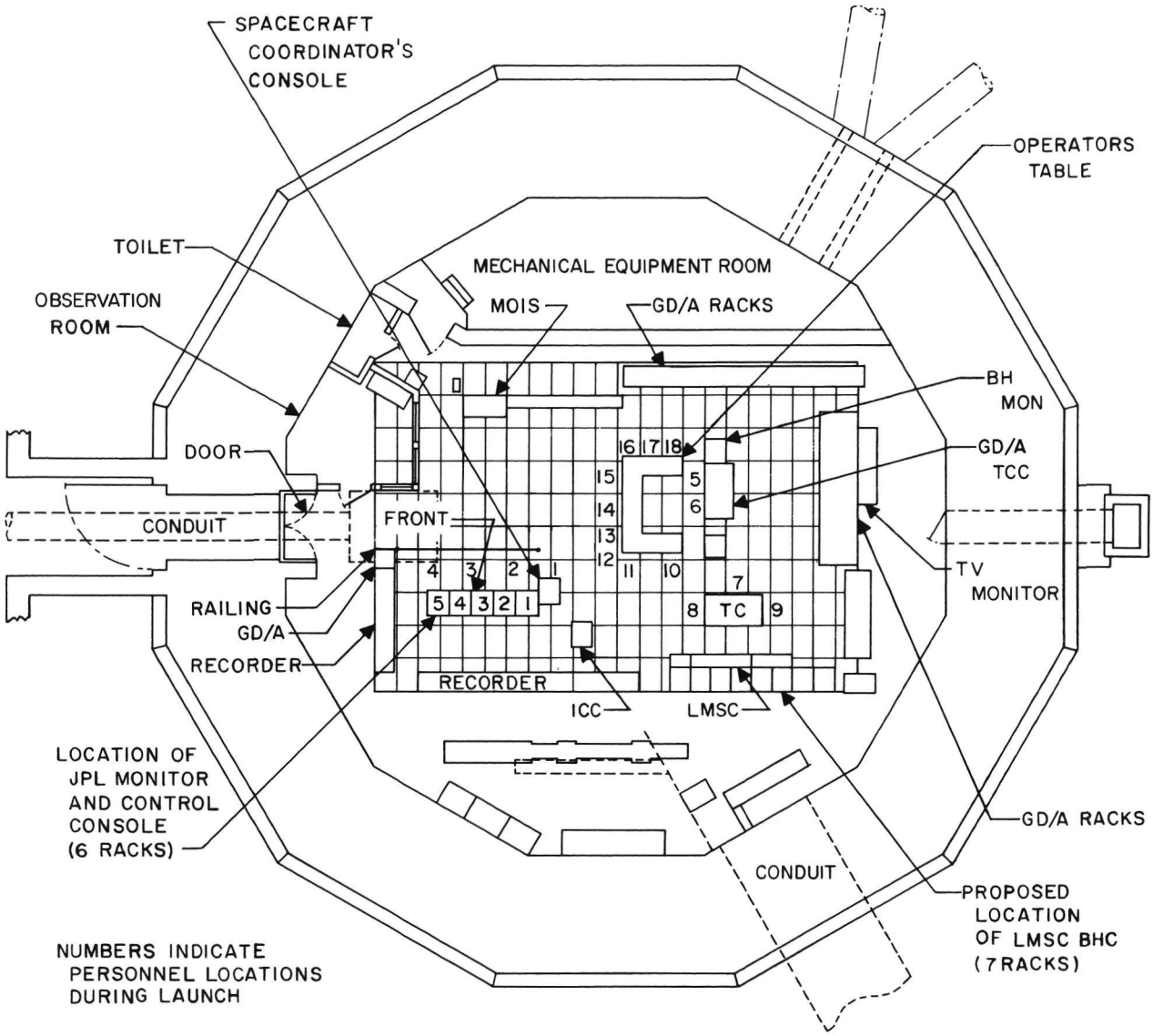

Figure 392. Blockhouse plan, Complex 12, AMR

with the addition of the required number of power cables.

(2) *Interconnecting cables.* Interconnecting cables connect equipments housed in the console racks.

As a backup when r-f reception is not available, the spacecraft mixed modulation signal, passing through the spacecraft umbilical connector, is carried from the blockhouse to the SCF by high-quality data transmission cables (video pairs).

f. Spacecraft simulator. This unit is furnished by JPL to ensure electrical compatibility of the launch complex with the spacecraft, the GSE, and the lunar capsule dynamic balancing equipment. This is accomplished by simulating, or actually duplicating the appropriate spacecraft circuitry and conducting a checkout of the unit with blockhouse GSE according to a formal procedure.

5. JPL Launch Checkout Trailer Site (LCTS)

The LCTS is located at the east corner of the evacuation site parking area, at the approximate intersection of grid coordinates $X = 635{,}900$ and $Y = 1{,}510{,}060$ (Fig 396). The following equipment is stationed at the site:

(1) JPL LCRFT (Fig 397).

(2) JPL LCTT (Fig 398).

(3) Antenna tower.

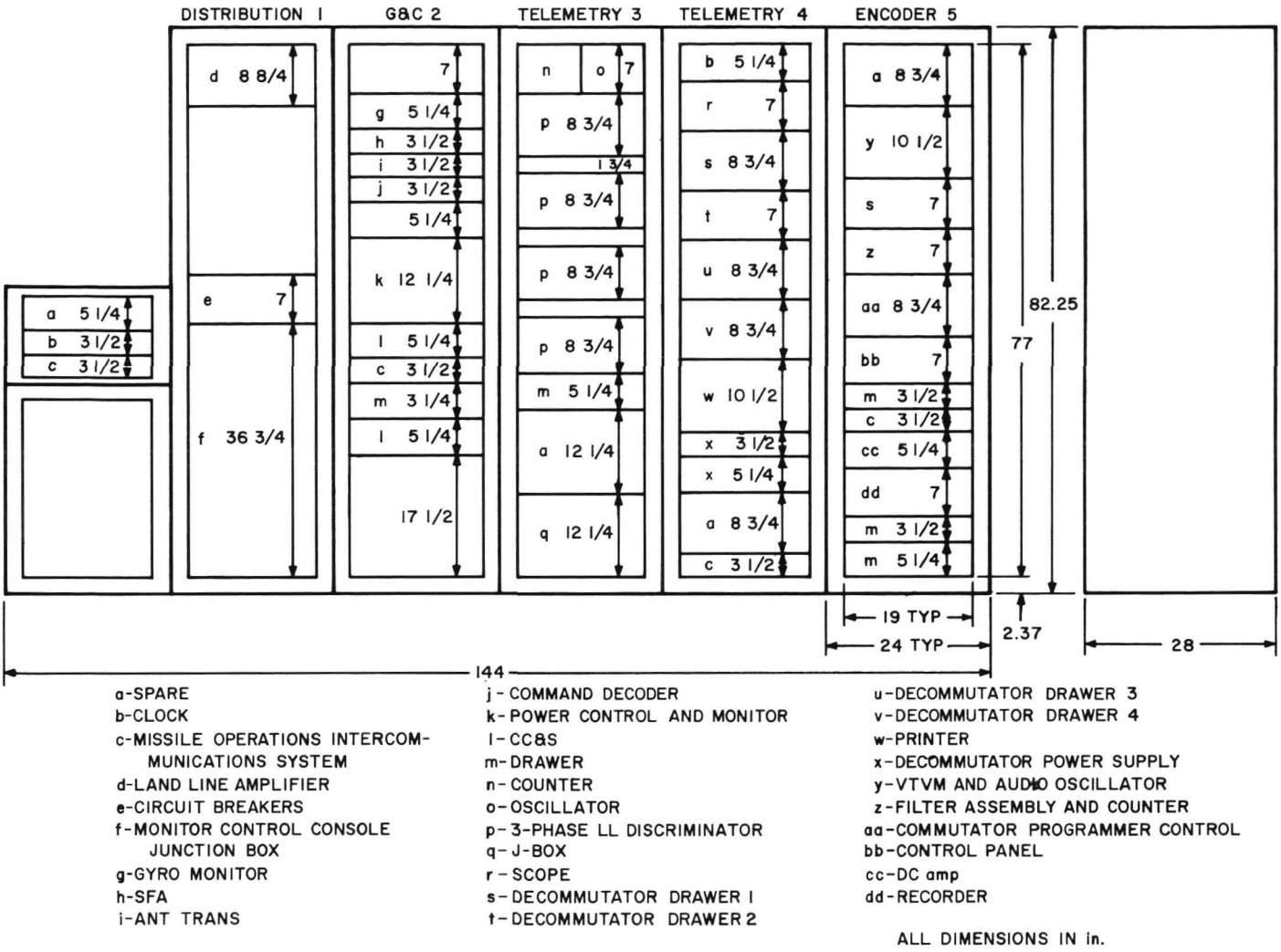

Figure 393. Typical blockhouse spacecraft monitor and control console

(4) Pole beacon collimation tower.

(5) Communication equipment building.

(6) Two mobile air-conditioning units (one unit for each of the trailers).

6. Launch Checkout RF Trailer (LCRFT)

The primary purpose of the RF trailer is to verify, by means of r-f communication, that the spacecraft is functioning properly when on the launch stand. In addition to providing this function, during the booster phase of the flight, the LCRFT (JPL-9075) contains the necessary equipment to provide an r-f link from the spacecraft to the telemetry and doppler data readout equipment. Basically, the LCRFT consists of a radio system, a command checkout system, and various types of commercial test equipment.

7. Launch Checkout Telemetry Trailer (LCTT)

The LCTT makes permanent magnetic-tape records of the results of all test operations conducted in the SCF and the blockhouse. During blockhouse operations, the LCTT is operated in conjunction with the LCRFT to record the signal received by the LCRFT and relay it to the data display equipment in the SCF. The LCTT equipment includes direct-write oscillograph recorders, magnetic-tape recorders, a time code generator, a digital printer, and the necessary discriminators.

8. Antenna Tower and Pole Beacon Collimation Tower

Both the antenna tower and the pole beacon collimation tower are approximately 18 ft high with 6- by 6-ft bases. They are of open construction and of prefabricated

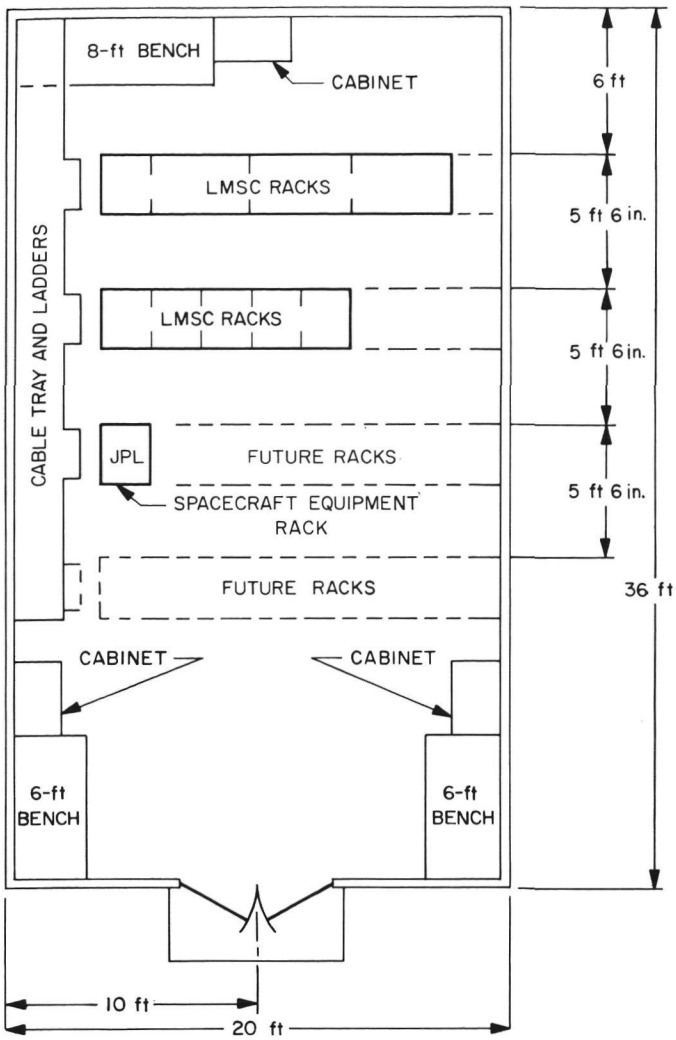

Figure 394. Launch Control Shelter

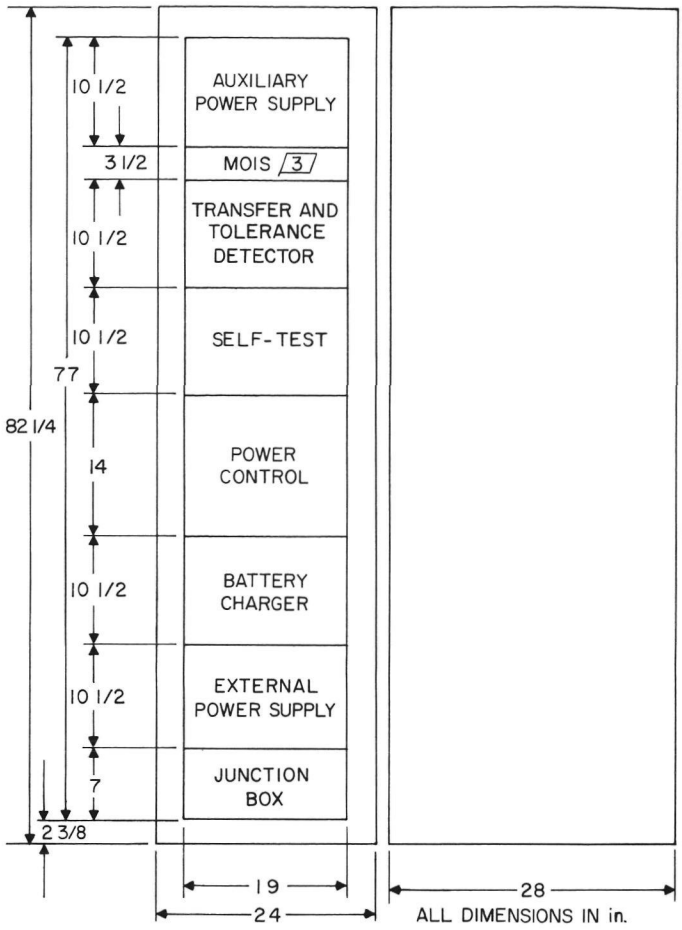

Figure 395. LCS spacecraft equipment rack

tubular metal members. The antenna tower is required for communication with the spacecraft, and the pole beacon collimation tower for checkout of the LCTS.

9. Communication Equipment Building

This small, 8- by 10-ft building contains MOIS and other power and communication terminal equipment, and provides a junction point for distribution of required cabling at the site. In addition, the building is utilized by lunar capsule personnel during on-launcher operations.

B. Pre-Flight Tests and Launch Operations

1. RA-1

a. Pre-launch test and operations. Upon arrival of the RA-1 spacecraft at AMR, a comprehensive survey was

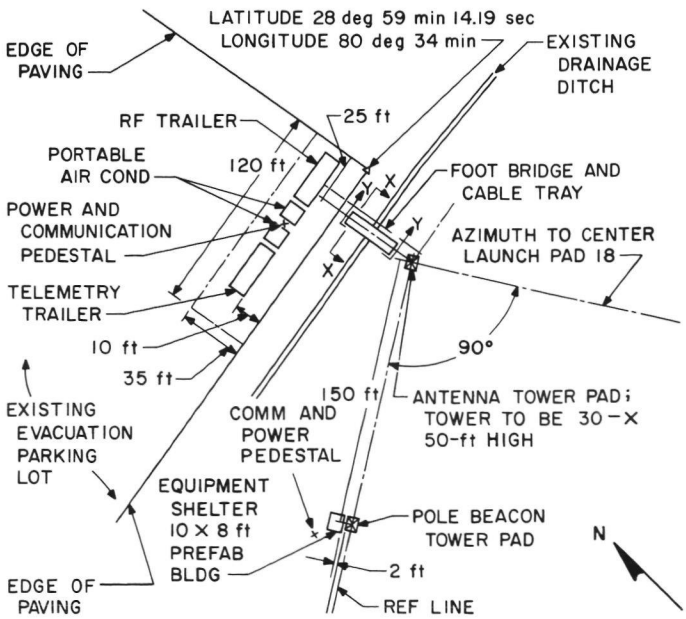

Figure 396. Launch checkout trailer site, AMR

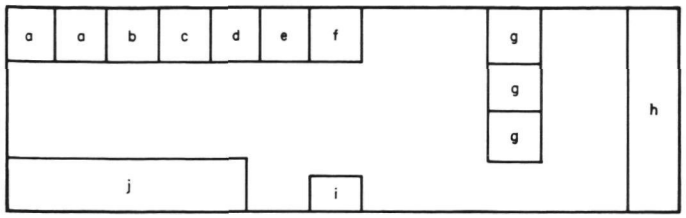

a-STORAGE
b-COMMAND EQUIPMENT
c-TRANSMITTER POWER SUPPLIES AND TERMINAL BOARDS
d-COMMUNICATION RECEIVER
e-COMMUNICATION TEST EQUIPMENT AND RECEIVER POWER SUPPLIES
f-COMMUNICATION TRANSMITTER
g-COMMUNICATION CONSOLE
h-DESK
i-POWER PANEL
j-WORK BENCH AND STORAGE

Figure 397. Launch checkout r-f trailer, floor plan

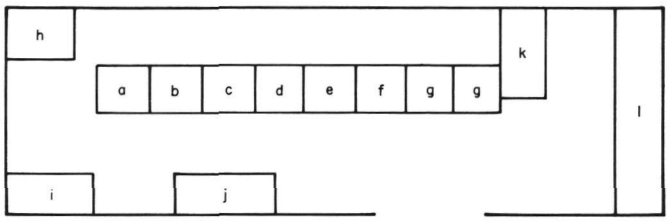

a-RACK 1, DIRECT-WRITE OSCILLOGRAPH
b-RACK 2, POWER SUPPLIES DISCRIMINATORS, VOLTAGE CONTROLLED OSCILLATORS
c-RACK 3, POWER SUPPLIES, dc VOLTMETERS
d-RACK 4, DECOMMUTATOR, PRINTER, WWV TIME
e-RACK 5, TIME CODE GENERATOR, FREQUENCY STANDARDS, BATTERIES
f-RACK 6, NEMS-CLARKE RECEIVER, INTERCOM, SPEAKERS
g-RACK 7 AND 8, AMPEX TAPE RECORDERS (2)
h-WORK BENCH DEHUMIDIFIER
i-POWER REGULATOR
j-WORK BENCH
k-DESK
l-WORK COUNTER, PARTS DRAWERS

Figure 398. Launch checkout telemetry trailer, floor plan

made of the spacecraft to determine the nature and extent of any damage which may have occurred to the spacecraft during the shipment. No damage was found. After assembly, the spacecraft was placed on the system test fixture and connected to the ground support equipment (GSE).

Figure 399 presents the JPL/AMR operations, both as actually accomplished and as planned. The six system test runs are indicated by the circled numbers, e.g., ①. Figure 399 covers the period from arrival of the spacecraft at AMR through the first launch attempt.

Grounding, wiring integrity, and power turn-on checks were then performed before undertaking the preliminary system test. The preliminary system test was performed to obtain a quick-look evaluation of how well the spacecraft was performing functionally. The results of the preliminary test allowed proper proportioning of the scheduled time for subsystem checkouts.

Subsystem checkouts were provided for rechecking of telemetry and validating calibrations of the scientific experiments. These checkouts also enabled verification of the spacecraft's permanent magnetic field, mapped at the Malibu magnetometer site.

After completing all subsystem testing, the spacecraft launch and backup battery and the ¼ w transmitter batteries were installed. The spacecraft was then readied for a complete system test prior to performing the first on-launch-pad spacecraft checkout. After this system test and corrections of the deficiencies detected, the final mechanical work (e.g., installation of the live firing squibs) was performed. The spacecraft was finally installed on the flight *Agena* adapter and the aerodynamic shroud installed. The spacecraft was then purged with dry nitrogen and then moved to Launch Complex 12 where it was mated with the *Agena* on top of the *Atlas* booster vehicle.

Approximately 1 week was then allowed for performing spacecraft functional tests. These tests were used to study the spacecraft in its new environment and to establish the actual AMR countdown procedure for RA-1. Upon completion of the spacecraft functional tests, a combined r-f interference test was performed. No r-f interference was noted. A joint flight acceptance test (J-FACT) was then performed. The purpose of this test was to demonstrate to AMR that all participating agencies (GD/A, LMSC, and NASA/JPL) would work together without interference. The J-FACT was completed and the spacecraft was returned to Hangar AE for its final functional and mechanical checkouts. Finally, in Hangar AE, after installation of flight batteries and flight solar panels, a final systems test was performed and a careful mechanical inspection (final spacecraft button-up) was performed.

The spacecraft was then certified as being in a flight-ready state, after which it once again was installed on the flight adapter, the aerodynamic shroud installed, the spacecraft purged with dry nitrogen and returned to the launch complex, 2 days prior to launch. An on-pad electrical checkout was again made.

The first launch attempt was made on July 29, 1961, but was scrubbed at 0502 EST due to electrical power outages at AMR. The second launch attempt was made on July 30, but had to be cancelled due to a leak in the spacecraft attitude control gas system. The spacecraft was again returned to Hanger AE when the defective gas pressurization was replaced with a new bottle and associated regulator. The spacecraft was returned to the Launch Complex and time was picked up on Countdown

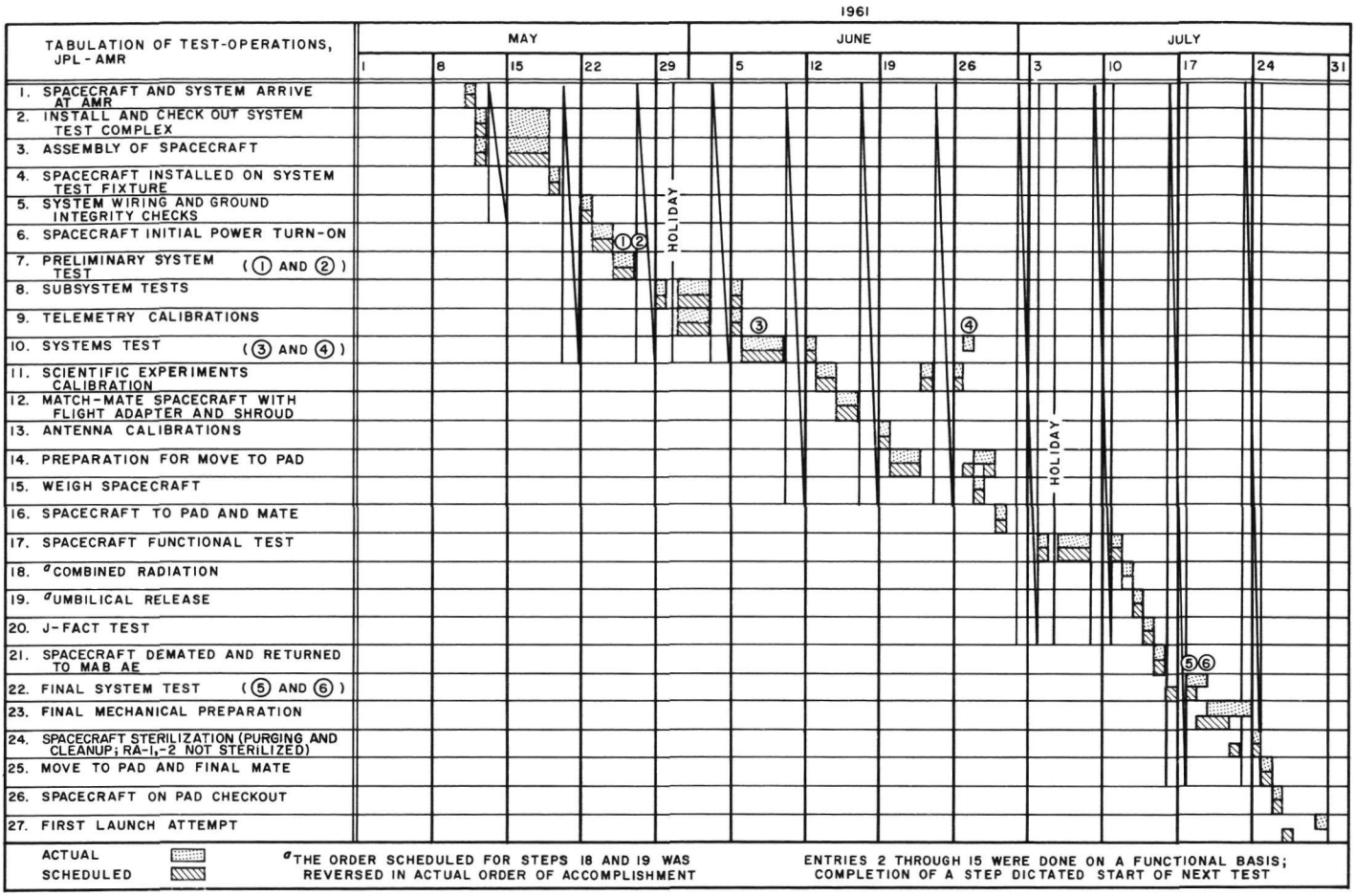

Figure 399. JPL pre-launch test operations, RA-1

3 at 1900 EST on July 31. The third launch attempt was cancelled when the *Atlas* booster vehicle experienced difficulty with a LOX tanking valve. On August 1 time was picked up on Countdown 4 which again was scrubbed because of multiple spacecraft controller commands, when Command 2 was issued. The spacecraft was returned to Hangar AE and extensive troubleshooting undertaken, which resulted in system field modifications to prevent a recurrence of this failure.

On August 22, Countdown 5 was started at 1927 EST (T −470). At 2104 EST, the Telemetry Checkout Trailer lost its air conditioning and, when the temperature started to increase, most of the electronic equipment was turned off. The tape recorder was left on and, after a portable air conditioner was installed and operating, full operation was resumed. Although both r-f silence periods were extended beyond their normal time, no holds were necessary up to T −60. In addition to the planned hold of 70 min at T −60, two unscheduled holds were called, the first at 0337 EST (T −50). Because of an *Atlas* umbilical circuit problem and an *Agena* acid leak encountered during the 70-min planned hold, the service structure could not be removed on schedule, requiring the hold. The hold continued for 28 min and countdown was resumed at 0405 EST. This unscheduled hold absorbed the second and remaining planned hold of 15 min and reduced the firing window by 13 min. The second unscheduled hold was called at 0450 EST (T-5) to permit stabilization of the high-temperature gas in the *Agena* attitude-control system. Countdown was resumed at 0459 EST with the firing window reduced by a total of 22 min. At T −3, the spacecraft controller was started on schedule; however, two momentary *Atlas* sequencer holds (at T −60 sec and T −18 sec) during the last min of the countdown resulted in the spacecraft controller being about 10 sec ahead at lift-off.

Launch was at 0504 EST, August 23, 1961, and loss of lock by the JPL/AMR Station occurred on the horizon

at 0512 EST. Loss of the communication lines between Ascension Island and Cape Canaveral delayed knowledge of the launch preinjection data until Goldstone reported their sighting. Early data from Goldstone provided the first indication of an abnormal flight.

The launch-through-parking-orbit injection portion of the trajectory was approximately nominal. Quick-look data indicated that the *Atlas* flew a 1 to 2σ trajectory, *Atlas–Agena* separation occurred successfully, and the *Agena* first burn placed the *Agena* and *Ranger* spacecraft into an approximately nominal 100-nm circular parking orbit. Later, however, near the time when final *Agena* burn should have occurred, a nonstandard behavior was observed. The *Agena* second burn imparted a small velocity impulse, which contributed only enough energy to increase slightly the parking-orbit apogee. The *Ranger I* spacecraft was therefore injected into an Earth–satellite orbit. Table 80 gives the computed orbital elements.

Table 80. Orbital elements, *Ranger I*

Orbital element	Parking orbit		Transfer orbit	
	Computed by AMR	Computed by JPL	Computed by AMR	Computed by JPL
	Data source Antigua	Data source Antigua and Ascension	Data source Ascension	Data source Ascension and DSIF
Semi-major axis of conic section (a, km)	6598.03	6580.0	6709.7	6708.9
Eccentricity of conic section (e)	0.0071	0.0052	0.0251	0.0249
Inclination (i), deg	32.72	32.85	32.93	32.93
Right ascension of ascending node (Ω) deg	279.81	279.80	279.81	279.82
Argument of perigee (ω) deg	127.41	194.6	198.07	198.36
True anomaly plus argument of perigee at epoch ($V + \omega$) deg	141.40	136.5	197.03	197.0133

2. RA-2

a. Pre-launch operations. The period of operations starts with the arrival of the spacecraft at AMR and finishes with the first scheduled launch period (Fig 400). The spacecraft arrived at Hangar AE, AMR, on the morning of August 25, 1961. The RA-2 flight spacecraft was moved to the system test fixture and updated to the final flight configuration. After system grounding checks were performed, power was applied to the spacecraft (September 31), and a satisfactory power survey was performed.

On September 6, 1961 the first system test of RA-2 at AMR was performed. The following discrepancies were noted:

(1) *Attitude-control subsystem:* when Command 4 (Sun acquisition) was activated, a negative roll valve light came on at the GSE, indicating that a valve was blowing-by gas. This function should have been initiated by Command 5. The GSE electronics were checked out in the laboratory, and the spacecraft attitude control modules were replaced.

(2) *Scientific subsystem:* the Lyman-alpha telescope would not start scanning upon coded initiation from the timer-controller. The three 1000th-sec pulses from the timer-controller were too narrow for proper initiation of the Lyman-alpha telescope scan; hence controller Set 5 was replaced with Set 9.

Telemetry and scientific subsystem calibrations were started on September 7. Telemetry calibrations of the scientific subsystem continued through September 15.

System test 2 of RA-2 at AMR was performed on September 18; during this test the following discrepancies were noted:

(1) GSE in the communications and data automation system (DAS) observed noise which caused phase errors leading to out-of-sync conditions. It was determined that the noise transients on the 60-cps primary line voltage supply had affected all hangar checkout areas at AMR.

(2) Scientific subsystems noted one procedural difficulty in the excitation of the cadmium sulfide detector, as well as a failure in the operation of the friction experiment. The failure in the friction experiment was due to a faulty output amplifier, a nonflight item, and was replaced. The SCRE–DAS calibrations were again checked after the test was completed using a spare 90-deg unit.

Telemetry calibrations of rate-gyro and nitrogen pressure transducer were completed on September 19. Mechanical preparations for match-mating the spacecraft to the *Agena* adapter continued from September 20 through September 28. The only discrepancy noted during these preparations was the damaged high-gain antenna (No. 9). It was received with a damaged ground plane, and returned to JPL for repair. Match-mate operations were completed on September 29.

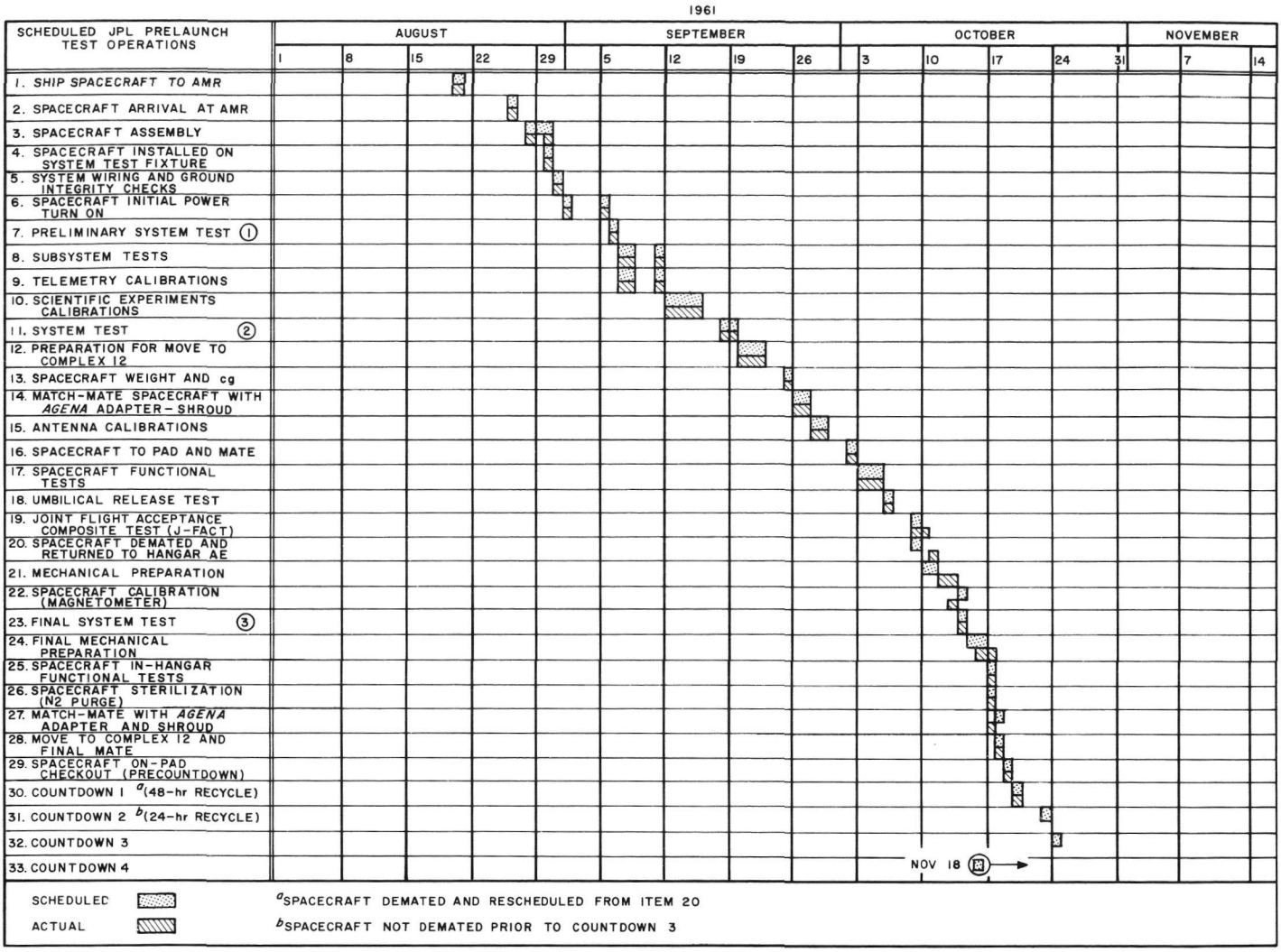

Figure 400. JPL scheduled pre-launch test operations, RA-2

In-hangar functional checkout was accomplished on September 30. The following discrepancies were noted:

(1) DAS readout of the triple coincidence telescope was out of tolerance. The faulty readings were traced to a malfunctioning transducer. It was to be repaired and replaced after the October 9 J-FACT.

(2) A magnetometer temperature translator was out of band due to miswiring. An adapter for 25A1P1 was fabricated for use during the J-FACT, but will be repaired and replaced prior to October 14.

(3) DAS readout of the boom SCRE was out of tolerance due to batteries running down. The batteries were replaced, and a recheck was normal.

Nitrogen purging of the spacecraft shroud assembly began October 1, and continued until operations were started to move the spacecraft shroud assembly to Complex 12 for mating to the *Agena* vehicle prior to the J-FACT.

Match-mating of the spacecraft with the *Agena* was completed October 2 and a dummy run was conducted from Hangar AE, the blockhouse (Complex 12), and the spacecraft umbilical tower. The following deviations were noted:

(1) R-F telemetry trailer power failed due to a 225-amp fuse blowing at $T - 225$ min. A delay of 20 min ensued, and telemetry calibrations were invalidated.

(2) Case II temperatures monitored during the test were 4 to 5°F lower than those associated with the RA-1 spacecraft.

(3) Scientific subsystems reported deterioration of the SCRE batteries.

(4) Minor procedural changes were effected to improve the operations prior to the J-FACT.

Dummy Run 2 of RA-2 spacecraft was performed on October 4. No operational problems were noted during this test.

On October 9 the joint flight-acceptance test (J-FACT) was performed. The following discrepancies were noted:

(1) Case IV temperature transducer out of tolerance.

(2) Opening of the controller-commutator during the test.

(3) Channel 4 noise spikes seen in all areas on r-f signal.

(4) Repetition of scientific subsystem problems seen in Dummy Run 2.

Final mechanical preparations were undertaken between October 9 and 14. Magnetometer mapping of the spacecraft took place after final mechanical cleanup on the morning of October 14. Final system test of the RA-2 spacecraft was conducted on October 14.

All subsystems reported normal operation during the test, except for the Lyman-alpha temperature transducer, which was out of tolerance, and a faulty frequency response was detected on the SCRE. These units were replaced on October 17.

On October 17, 1961, the spacecraft was mated with the spacecraft adapter, and the shroud was installed.

Match-mate operations between the *Ranger* spacecraft and the Agena vehicle began on October 18. These were completed and JPL began its precountdown. After about 45 min running time it was noted, at the r-f trailer and central recorder in the hangar, that no binary channels were present. Failure of these channels caused interruption of the test. The failure, while thought to be discrete, caused the spacecraft to be demated from the *Agena*, and brought back to Hangar AE for investigation of the failure.

The *Ranger* precountdown was again started on October 19. It was completed without difficulty with all subsystems and evaluation reporting in the *green*.

It was decided after the first launch attempt was scrubbed that rescheduling would be a matter of a 48-hr delay, to demate the spacecraft, return it to the hangar, and install the spare units of the scientific experiments still in doubt.

b. Launch operations. The JPL–AMR countdown began when range time was picked up at 2100 hr on October 19, 1961. The first firing period of 8 days began on October 20. After the first launch attempt a rescheduling meeting was held. Due to conflict with another scheduled firing at AMR on the second day of the *Ranger* RA-2 firing period, the shot was rescheduled to October 22, a 48-hr hold.

First launch attempt. On October 22 the operations proceeded normally until $T-226$, when Command 2 was activated.

At $T-110$ a 10-min hold was called by JPL, prior to *Agena* critical tanking operations, to enable a further evaluation of Channel 4 irregularities. At $T-102$ the hold was released with Lyman-alpha data on Channel 4 evaluation completed and a decision made to fly, even though the irregular performance data could not be adequately explained, without compromising the primary mission objective.

After the gantry had been moved back, and the built-in 70-min hold was completed, range time was again picked up at $T-60$ with the spacecraft subsystems and performance evaluation reports still *go* (green report).

At $T-40$, a series of holds began. First, a 15-min hold was called to rerun the GE guidance loop tests. Extensions of 10 min, then still another of 15 min, were called for the same reason, until at 0245 EST an extended hold of 1 hr, 15 min was called to move the gantry back around the launch vehicle to gain access to the GE guidance electronics. No 28-v power was getting through the guidance system. At 0310 EST the first launch attempt was scrubbed.

Prior to the second launch attempt, the RA-2 scientific experiments still in doubt as a result of Channel 4 evaluation (Lyman-alpha) and magnetic mapping of the friction package (Spare 5) were rechecked and the spares installed if calibration checks proved them to be better components.

Second launch attempt. The AMR Countdown 2 for RA-2 was picked up at 2100 on October 23. Operations proceeded with normal indication in all systems until $T-60$, when the 70-min built-in hold was called. At this time the test conductor reported that a leak had developed in the vernier engine hydraulic subsystem but did not expect to exceed the build-in hold time to resume the count. However, during investigation of this problem, it was found that a booster regulator in the sustainer engine had also malfunctioned.

With all other systems *go* (green report) at the end of the 70-min hold, at 0131 EST, the test conductor called an

additional 15-min hold. At 0145 EST, it was decided to replace the booster regulator and transducer in the sustainer engine, and an additional 50-min hold was called. This was accomplished with an additional 15-min hold being called for clean-up operations.

Time was picked up shortly before 0300 EST, at $T-60$ in the countdown. At $T-47$, a hydraulic leak developed again in the vernier engine system. Investigation showed that the entire engine would have to be replaced. Hence, at 0310, the launch was scrubbed.

Third launch attempt. GDA and LMSC proceeded on schedule and picked up time at 1947 EST, October 24, 1961. At 2045 EST on October 24, 1961, prior to the start of JPL and AMR portions of the countdown, it was announced that the test 4507 was scrubbed. Preparations for JPL's countdown had started when word came in from Lockheed that the *Agena* could not be cleared for launch, due to the in-flight failure of a *Discoverer* on the previous day. Telemetry data had shown abnormal drops in the *Agena* hydraulic system pressure, resulting finally in loss of engine gimbal control.

LMSC reported that the *Agena* validation could be run concurrently with the system modification of vehicle 6002, making it possible to reschedule the *Ranger* RA-2 launch for the first day of the second firing period, available November 18–26, 1961.

Fourth launch attempt. Time was picked up on RA-2 Countdown No. 4 at 2057 EST, November 17, 1961. The test proceeded without trouble until $T-60$, when, during the built-in 70-min hold, it was discovered by LMSC that they had a "cocked" quick-disconnect in the fuel pressurization system. The gantry was re-positioned around the vehicle and the quick-disconnect was properly inserted. The built-in hold was extended 30-min to achieve pressurization and move the gantry away. Time was picked up again, $T-60$ at 0200 EST.

All areas on the spacecraft, the Launch Checkout Station, blockhouse, and Hangar GSE were *go*. DSIF stations were all *green* by launch time. Downrange telemetry with the DAMP ship, Ascension, and Antigua was intermittent until 2240 EST, when both Ascension and Antigua were *green*. The DAMP ship was out until 2335 EST when a *green* report was received. The *Twin Falls Victory* ship was not on station for this operation.

A 5-min hold was called at $T-31$ min (0225 EST) to free-up a frozen liquid nitrogen valve on the loading trailer. The valve was thawed and the count resumed at 0227 EST.

The count then proceeded to $T-5$ (0249 EST), when a further hold was called to complete LOX loading. This hold was initially for 9 min, then extended another 9 min at 0300 EST. *Ranger* RA-2/*Atlas*/*Agena-B* was launched from Pad 12 at 0312:21.502 EST, November 18, 1961. The weather at launch was clear with winds SSE at 10–12 knots, temperature 71°F. (windshear 37% bending, 32% control, total 69% at 2241 EST).

The launch checkout station dropped two-way lock at 0315 EST, picked up the transponder signal again at 0317. Lock was again dropped momentarily at 0320 EST, and finally dropped the signal entirely at 0320.5 EST.

Agena cutoff was reported at 0355 EST; launch checkout station received the *Agena* signal to 0323 EST.

The *Ranger II* actual trajectory was an Earth–satellite orbit with an eccentricity near zero. The launch azimuth was 108 deg from north. Lift-off appeared to be normal. The *Atlas* discrete times were near normal (Table 81). Spacecraft showed ejection occurred one sec after nominal, followed by *Atlas/Agena* separation one-half sec after nominal. *Agena* first burn seemed to be slightly nonstandard. Ignition occurred 4 sec late, resulting in velocimeter shutoff 7 sec after nominal. Up to this point, the resulting trajectory was within the 3-σ tolerance required.

Table 81. Sequence of events, *Ranger II*

Events	Time for liftoff, sec	
	Nominal	Actual
1. Liftoff (Greenwich Mean Time)	7:37 to 9:37	8:12:21.502
2. Booster cut-off	138.0	135.898
3. Sustainer cut-off	278.4	279.728
4. Vernier cut-off	295.0	295.148
5. Spacecraft shroud ejection	296.24	297.373
6. *Atlas–Agena* separation	299.50	300.148
7. *Agena-B* first ignition	348.25	353.498
8. *Agena-B* first cut-off	499.05	507.498
9. *Agena-B* second ignition	1282.75	No indication
10. *Agena-B* second cut-off	1373.10	No indication
11. Spacecraft electrical disconnect	1524.92	?
12. *Agena-B* spacecraft separation	1531.50	?

At $T+1283$ sec, the *Agena B* was to restart and place the *Ranger II* spacecraft into a highly elliptical orbit. However, due to an unknown malfunction, *Agena* reignition apparently did not occur. As a result, the *Ranger II* spacecraft remained in the parking orbit. Table 82 presents a comparison of the nominal and actual orbital elements. The actual orbital elements were computed by the Atlantic Missile Range facilities based on Ascension Island data.

Table 82. Orbital elements, *Ranger II*

Parameter	Nominal	Actual
Epoch, t (Greenwhich Mean Time)	Injection	$8^{hr}35^{m}42^{s}$
Semi-major axis, a(km)	640,934	6576.3
Eccentricity, e	0.989760	0.004568
Inclination of the plane of the orbit to the equatorial plane(i), deg	32.6557	33.313
Longitude of the ascending node Ω, deg	325.832	336.415
Argument of perigee (Ω), deg	193.644	52.833
True anomaly plus argument of perigee, $r + \Omega$, deg	196.98310	198.318
Apogee distance, km	1,275,305	6606
Perigee distance, km	6563.4	6546
Period, min	85 to 110	88.457
Lifetime, days	120+	1 (approx)

3. RA-3

a. Schedule of operations. Scheduled operations for RA-3 took place as indicated in Figure 401. The period of operations starts with the arrival of the spacecraft at AMR and finishes with the start of the scheduled launch countdown.

b. Operations summary. The RA-3 spacecraft arrived at AMR on November 20, 1961. A complete receiving inspection did not disclose any spacecraft damage; however, several pieces of ground support equipment showed minor shipping damage. The systems test complex cabling was started November 20, 1961, and no major difficulties were encountered. The gamma-ray GSE was modified to the extent that a new rack containing a punched tape and Sanborn recorder was added.

During initial systems test preparation, the midcourse motor fuel tank was charged to 150 psi and the helium tank was charged to 500 psi. The pressurization was an attempt to gain a long-term evaluation of tank leak rates. Several subsystem problems developed during the test periods. These problems are outlined in the text to follow.

During initial power turn-on at AMR, several discrete failures were noted on the data display equipment. Some of the analog outputs to the central recorder failed during testing and were repaired. The Channel V discriminator had failed prior to AMR system test No. 1. The spare was not received at AMR in time to provide information during the systems test. A short circuit in the data display console prevented the data encoder from controlling the decommutator inhibit function.

AMR preliminary system test (spacecraft AMR system test No. 1). This was conducted on November 29, 1961.

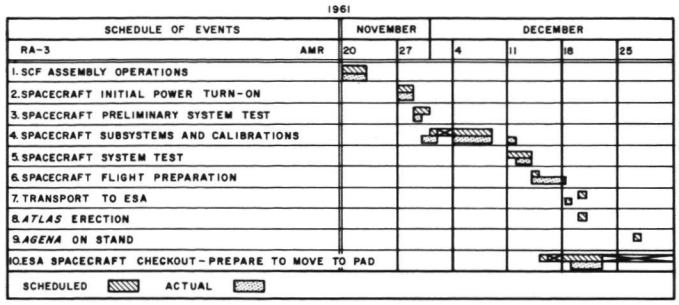

Figure 401. JPL scheduled pre-launch test operations, RA-3

No additional problems were detected as the result of shipment. The test was performed with the spacecraft in flight condition, except for the following known discrepancies:

(1) Non-flight lunar capsule and radio altimeter.

(2) Non-flight gyros and gyro electronics, secondary Sun sensors, and Earth sensor.

(3) Antenna drive module 7A3 was a flight spare.

(4) Power module 4A4 S/N 7 replaced by S/N 8.

(5) Non-flight type batteries.

(6) Antenna and cables were not used. These cables were not shipped with the other packaged cables to AMR.

(7) Module 6A5 was non-flight.

(8) Solar panels were not installed.

Spacecraft subsystem tests and calibrations.

Cabling. During initial subsystem testing, failure of the scientific 4-v monitor appeared to result from an intermittent connection at the plug on Module 4A8.

Ground integrity checks were conducted on December 6, 1961. The following problems were noted and cleared:

(1) The MOIS in the power GSE had zero ohms to the start ground (bent pin).

(2) The range time clocks were putting a d-c voltage to the start ground.

(3) The data display console was putting 40-volt ac on the start ground. (Reversing the a-c cord in the data display rack cleared the problem.)

Attitude control. The attitude-control leak rate checks were completed on December 4, 1961. The leak rate was established at 53 cc per hr, as determined over 43 hr. This rate is within the specification.

Delivery of flight gyro package (not sterilized) and Earth sensor was expected on December 8, 1961, but they did not arrive until January 9, 1962.

Data encoder. Intermittent 120-cps amplitude modulation was observed on Channel 4 subcarrier. Troubleshooting did not uncover the cause; however, various changes in the GSE complex may have removed the problem as no observations of the phenomena recurred.

All telemetry calibrations were completed except for the gyro package and radio altimeter echo strength. These had to wait until flight units arrived.

AMR system test No. 2. The system test in Hangar AE for RA-3 was postponed from December 9 to December 12, 1961, due to the late delivery of the flight radio altimeter. The test was performed with the spacecraft in flight condition except for the following known discrepancies:

(1) Flight solar panels electrically but not mechanically connected to spacecraft.

(2) Non-flight gyros and gyro electronics. Command current modification was in gyro electronics.

(3) Non-flight antenna yoke.

(4) Non-flight battery.

(5) AD/F had no simulators for both cutters.

(6) Pyro has a squib harness change due to be incorporated at a later date.

(7) Several dents were noted in the radio altimeter dish.

(8) The flight radio altimeter and electrical mock-up of the lunar capsule were used.

(9) Earth sensor temperature transducer was noted to be indicating in error. (Presumed to be a shift in resistance since original calibration.)

(10) Telemetry for gyros and gyro electronics were not valid since flight packages were not installed. Radio altimeter echo strength channel uncalibrated. No real calibration for Earth sensor and Sun sensor channels on telemetry.

(11) Antennas and cables were not used.

For AMR system test No. 2, Procedure P34300.01-1 was followed with these exceptions:

(1) Launch phase was abbreviated. CC&S commands were set manually. A/C performed exercises for Earth sensor and Sun sensor checks.

(2) Spacecraft was held quiescent for approximately 30 min to allow LCTT to make data correlation checks between LCTT, blockhouse, and hangar data display installations.

(3) Second pitch maneuver was set for 30-sec duration to allow A/C to get indication of gyro loop recovering from saturation.

(4) The terminal phase was modified to accommodate test of flight radio altimeter.

Spacecraft flight preparation. During the period from December 15 to December 22, 1961, final preflight mechanical preparation of the basic spacecraft hex was completed. This included:

(1) Change from high-gain antenna test yoke to flight yoke.

(2) High-gain antenna alignment verification.

(3) Antenna drive servo pot mechanical/electrical alignment.

(4) Complete hex tear-down and build-up.

(5) General hardware up-dating.

(6) Thermal control surface paint up-dating and extensive clean-up.

(7) Reflective surface, associated with Earth sensor reflectivity problem, modified.

(8) Spacecraft/*Agena* adapter pre-load shim verification.

The following problems appeared at this time:

(1) The Case IV critical reference surface was found to be irregular around mounting holes due to protective coating. This condition was reviewed with materials personnel.

(2) Interdependency of bay three shroud guide installation and Case III closed or open condition was noted. Field modification was performed on RA-3 shroud guide. The hex mounting is to be modified on future *Rangers.*

(3) Materials/sterilization problem was found to exist in areas of Earth sensor reflectivity. The sterilization requirements for the Earth sensor were set aside due to schedule pressures; problem to be investigated.

(4) A mechanical mating of the flight radio altimeter and retro support to the flight spacecraft disclosed a somewhat minor mechanical interference problem

between the altimeter support structure and a solar panel support leg. AD/F noted discrepancy and incorporated a change into the design.

Vehicle center of gravity was re-evaluated and the midcourse motor, both flight and spare units, was aligned and pinned.

JPL/Lockheed interface. A verification match-mate and spring constant determination was conducted between the flight *Agena* adapter and spacecraft. A minor decrease in the system (adapter and spacecraft) rigidity was noted and preload shim values were revised for flight.

Quality control inspection and spacecraft simulator checks were performed to verify proper wiring of the adapter cabling. Discrepancies were noted and reported to LMSC.

Special r-f checks. These remaining r-f tests were completed before January 3, 1962:

(1) Space loss measurements from RFT to Pad 12. Both high-and-low-gain measurements plus 890-mc path. Plans were to run this test January 2, 1962.

(2) Antenna gain check and antenna cable loss measurements were made. VSWR measurements were made on both.

(3) Complete checkout of RWV from Hangar AE to Launch Checkout Site and back. The video cables were in operation on December 14, 1961. Complete checkout followed on December 15, 1961.

Data scanner and spare modulator were installed in the r-f trailer for emergency use only. This gear was in full operation by December 20, 1961.

A special r-f test was run from the launch checkout r-f trailer to the Explosive Safe Area. Setting up an antenna on top of the ESA and checkout spacecraft from that area through r-f link to the LCRFT proved feasible. A pole beacon transponder was set up in ESA building and the LCRFT was in two-way lock with the transponder with the signal level varying ± 2 db.

Explosive Safe Area operations. After the move to the Assembly and Sterilization Laboratory of the Explosive Safe Area, (December 18, 1961), the final vehicle buildup was accomplished. The objective was to develop a valid, all-inclusive (electrical/mechanical; joint JPL/ADF) activity controlling procedure, verifying operations/facility compatibility, education of assembly personnel, and establishing valid time estimates for the various operations. The following problems were noted:

(1) Lower-than-desirable hook height caused minor handling problem. The handling equipment is to be modified.

(2) A static low voltage noted during squib firing assembly no voltage checks which may have been due to battery simulator hook-up.

(3) Undesirable lifting fixture instability was noted during composite vehicle handling. As a result, a secondary sling system is to be added to the handling fixture.

(4) An improper circuit indication was noted on capsule separation sensor which was traced to miswiring. The spare unit was corrected and the flight unit was corrected prior to final AMR system test.

During the ESA spacecraft checkout, the CCS clear function failed as the result of poor contact at the connector. This connector was not fastened as it would be in the flight configuration. After this test, the spacecraft was moved to Launch Complex 12 for mating with the *Agena B*.

c. RA-3, -4, -5 spacecraft.

Range safety. The RA-3, -4, and -5 spacecraft pyrotechnic and propulsion activation designs were reviewed with respect to assembly, pad, and launch safety. Use of the AMR-preferred shorting plug method was precluded by the terminal surface sterilization method, i.e., gassing with the nose shroud installed. Therefore, inertial integrating safety switches were inserted between power sources and pyrotechnic-propulsion devices on the bus and capsule alike. These switches were set to close at approximately 6 *g* over a period of 1 to 2 sec. Also, to gain a safer and more integrated design, all squibs involved with radio altimeter operation and lunar capsule separation were to be fired from the bus power source. Additional safety was obtained in the design of the central computer and sequencer (CC&S), the subsystem responsible for issuing activation commands. All command relays are locked open (safe) by a GSE clamp voltage that is present whenever power is applied to the spacecraft and is not removed until 2 min before launch. Command relay drivers have their inputs grounded until the first command is given, approximately 30 min after launch.

Page intentionally left blank

VII. Space Flight Operations

JPL spaceflight operations are defined as those operations necessary for the obtaining and processing of spacecraft information and commands required by JPL, retrieving and processing spacecraft information, and generating commands during that portion of flight from launch to the accomplishment of the mission. This chapter describes the space flight facilities, organization, plans, and operations for the *Ranger I and II* missions.

A. Facilities

1. Atlantic Missile Range Support

After launch, the tracking, telemetry, and computational facilities at AMR are used extensively in the *Ranger* program. Also, the South Atlantic-based DAMP ship was used to demonstrate the capability to track the *Agena B* vehicle and forward tracking and telemetry data in real time to AMR at Cape Canaveral. This ship will be replaced by the *Twin Falls Victory* for RA-4 and -5.

AMR tracking, telemetry, and the DAMP ship data are forwarded to the JPL Control Center (Hangar AE) and then to the CCF at Pasadena. Figure 402 shows the tracking facilities supporting the *Ranger* program at AMR.

2. Central Computing Facility

The Central Computing Facility (CCF) is located at JPL, Pasadena. The CCF reduces the tracking data and real-time telemetry data so that the required orbital calculations and command decisions can be made. After the magnetic tapes of telemetry data recorded by the DSIF are reduced to digital form at the Data Reduction Laboratory (DRL), the CCF facilities process the raw data into the form required by the users. All real-time data processing and non-real time digital processing are performed in the CCF.

a. Facilities. The facilities available at the CCF include:

(1) *IBM 7090 computer and associated card-handling equipment.* This large, high-speed, general-purpose digital computer has a 32,168-word core memory, and is equipped with two input-output channels, with each channel containing seven 729 IV tape units.

(2) *Telemetry-to-magnetic-tape translator.* This data translator accepts up to seven channels of digital data (asychronously), converts the data into blocked IBM format, and records them on magnetic tape for entry into the IBM 7090 computer.

(3) *Teletype-tape-to-magnetic-tape translator.* This device will take the bit configuration of a five-level teletype character and put it into channels A, 8, 4, 2, and 1 of an IBM magnetic-tape character. A total of 1026 of these characters will make up one magnetic-tape record. The normal rate in this mode is 300 characters per sec. The device is also capable of a maximum rate of 600 characters per sec. The translator can punch paper tape from IBM magnetic tape at 60 characters per sec.

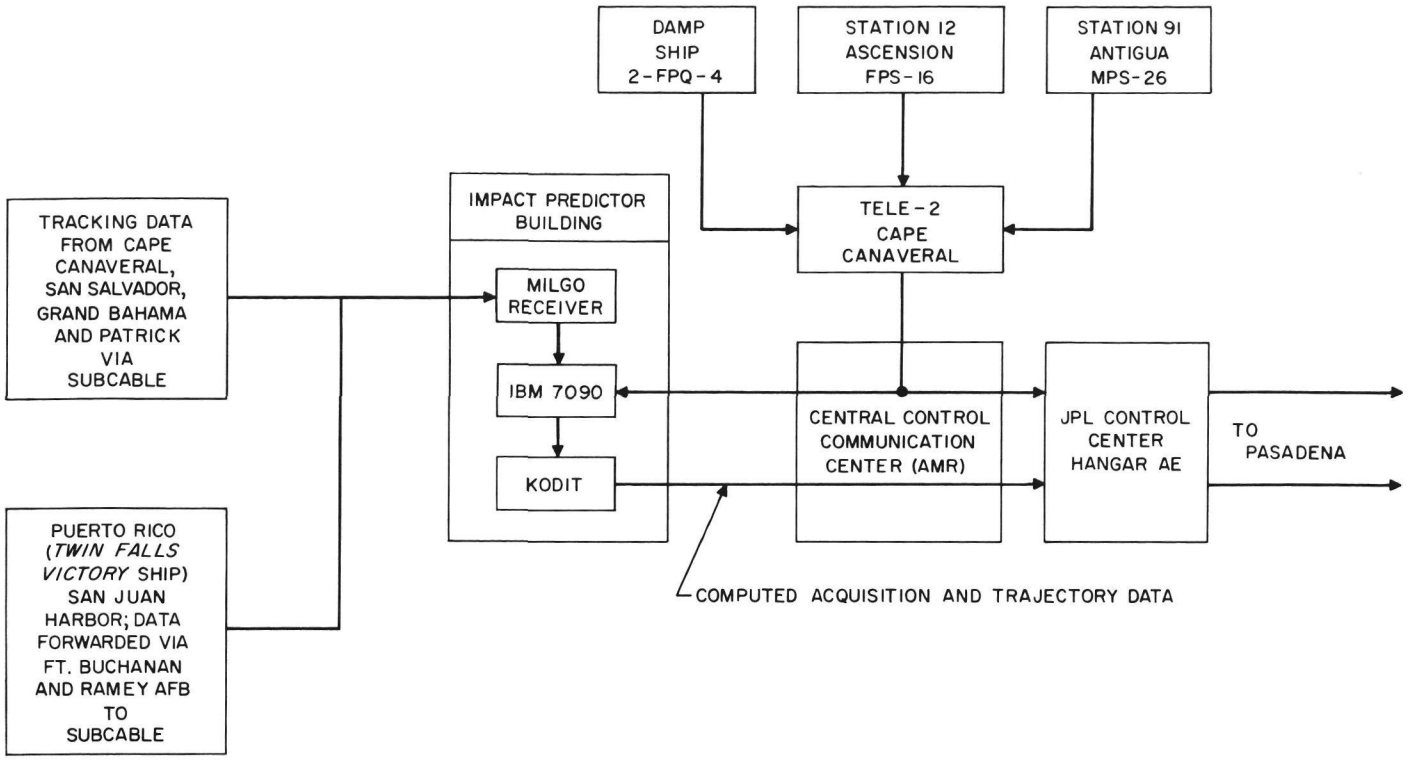

Figure 402. Tracking facilities supporting *Ranger* at AMR

(4) *IBM 1401 computer (two units).* This computer acts as a satellite to the IBM 7090. It is primarily a bookkeeping and input-output system which will relieve the 7090 of these time-consuming functions. It is equipped with a 600-line per min printer, card punch, card reader, and two magnetic-tape handlers. The 1401 will communicate with 7090 by magnetic tape, thereby eliminating card punching, card reading, and listing as on-line functions of the 7090.

(5) *Moseley 575 magnetic-tape plotter system.* This system uses IBM magnetic tape as an input, and creates an inked graph for the output. Scaling and plot control are under 7090 program control. Multiple traces may be made by selecting several traces on the input tape, and plotting one on top of the other. Strip charts may also be made with the time axis drive under 7090 program control.

(6) *Stromberg Carlson 4020 printer-plotter.* The SC 4020 is a high-speed microfilm recorder which records on microfilm real-time information supplied by the 7090 computer. Standard options extend its capabilities as a plotter and printer, and permit off-line operation from magnetic tape.

(7) *Paper-tape-to-card (IBM 047) and card-to-paper-tape (IBM 063).* These devices will be used for the tracking operations. For the initial orbit determination, the data points are entered into the computer as quickly as possible. By putting these points on cards, the transfer is more rapid than if it were put on tape, and allows human checking of transmission errors.

b. Tracking data handling. The tracking data recorded by the DSIF will be forwarded to the CCF in real time at a rate varying between 1 sample per 10 sec and 1 sample per 60 sec. The teletype tapes will be converted into IBM cards for input to the IBM 7090 computer. Paper tapes of tracking data recorded at 1 sample per 2 sec at the DSIF stations will be forwarded to the CCF in non-real time for updating the orbit, computation of future acquisition information, and final orbit determination.

c. Telemetry data handling. The CCF handling of telemetered data is influenced by two types of data: real-time data, and non-real time data. Real-time data is transmitted by teletype tape to the CCF and non-real time data is forwarded on magnetic tape to the Data Reduction Laboratory to be digitized. The CCF produces both quick-look and final report listings, and plots of

telemetered data for distribution to the cognizant scientists and engineers. Additional functions are to:

(1) Provide equipment to translate the output of the decommutators, level detectors, samplers, and time decoders used by the DRL, into IBM-compatible magnetic tape.

(2) Develop IBM 7090 programs for accomplishing the required transformations, calculations, and analyses which will be performed on the telemetered data.

(3) Operate the IBM 7090 computer, its peripheral equipment, the teletype-tape-to-magnetic-tape translator and the Moseley 575 magnetic-tape plotting system.

(4) Maintain an IBM magnetic-tape file of all telemetered data and an information retrieval system to allow recovery of information from this file.

3. Data Reduction Facility

The Data Reduction Laboratory (DRL) facility at JPL performs optimum detection of the spacecraft telemetering signal. Magnetic-tape recordings of DSIF receiver-detector output are decommutated and translated into forms suitable for analysis, computer processing, and further processing by special systems elsewhere. Capacity and scope of the DRL equipment permit reconstruction of all *Ranger* telemeter data recovered.

Oscillographic recordings of composite measurement analogs are available with 8 hr of receipt of magnetic tapes. Highly accurate digital readout of individual measurement samples are simultaneously produced for computer and scientific measurement processing equipment entries. Complete, individual-measurement, quick-look records of engineering telemetering are produced within 12 hr of the receipt of data. Ozalid duplication of quick-look records will be available for distribution within 4 hr of the completion of the various DRL reduction processes.

a. Records. DRL processing will yield these records:

(1) *Oscillographic records.*

(a) Composite analogs of all telemeter subcarrier signals.

(b) Composite analogs of all receiving station ground instrumentation recordings where required.

(c) Oscillographic records of gamma-ray measurements for manual reduction. Mode 4 will yield a combined time-shared record of vidicon data and gamma-ray data.

(d) Individual engineering measurement analog with three-place digital readout of measurement units.

(2) *Digital data stored on magnetic tape.*

(a) Measurement samples for all encoder channels, with address and time tag.

(b) Samples of gamma-ray measurement, with time tag (except Mode 4).

(c) Restored binary channel data.

(d) Spacecraft clock and reference frequencies.

(3) *Analog data stored on magnetic tape*: Vidicon measurement signal reconstruction.

(4) *Tabular printer records*: Composite digital engineering measurements.

Special end records can be produced on the DRL system in any of the forms listed above. In addition to these records, the DRL system is capable of delivering restored measurement signals to special equipment inputs in both subcarrier and binary coded decimal (BCD) form.

DRL processing is divided into several steps. All records except individual quick-look engineering measurements are produced in the *Ranger* Telemetry Data Processing System. Field station magnetic recordings are reproduced on a system compensated for tape errors, and the signal is recovered on phase-coherent discriminators. The reconstructed subcarrier signals are further processed by the telemetering decommutator for engineering measurements, and by detection and measurement reconstruction for binary data channels. Ground station instrumentation signals, including encoded timing, are demodulated. Digital data in BCD form is stored in computer format, and in a form suitable for further DRL processing. This reproduction system is operated at four times the original field recording speed. Thus, each hour of field recording can be reproduced in 15 min of DRL processing time.

The *Ranger* Telemetering Data Reduction System produces compensated records of individual spacecraft engineering measurements. Magnetic-tape stored digitized data is processed through an engineering unit conversion, and compensated for flight system drifts. A digital-to-analog converter yields an analog representation of the measurement. Digital readout of measurement samples is recorded adjacent to the analog trace.

This system operates at 128 times the real-time rate, and will produce an hour of calibrated flight measurement in less than a minute.

Facilities for data storage, display, and conference are provided in the Data Display area. Original DRL oscillograph records of current interest will be available for immediate reference. A microfilm file of all DRL record production for the *Ranger* program will be maintained, as well as microfilm readers and printers. Current *Ranger* data, stored on digital magnetic tape, will be available for processing to special requirements.

4. JPL Communications Center

The JPL Communications Center at Pasadena will be the terminus for all communications associated with the *Ranger* missions. All communications circuits providing data flow to or from any DSIF station and the Space Flight Operations Complex will be controlled from the Communications Center. The following is a description of the available circuits.

a. Teletype circuits.

(1) *Goldstone.* The Communications Center will have three half-duplex teletype circuits available for data transmission to or from either Goldstone Site. These circuits will be available for full-time usage as required. Data transmissions will be restricted on any one circuit to transmission in one direction only.

(2) *Woomera and South Africa.* One full-duplex circuit will be available to each of the overseas stations on a full-time basis. A second circuit will be available to each site on a limited basis during critical periods, or when the primary circuit fails. Due to the usage of radio teletype over a major portion of the transmission path, both circuits will be subject to failure during periods of poor high-frequency radio propagation. The primary and secondary circuits have been routed over different paths to minimize this effect as much as possible. Data transmission over these circuits can take place simultaneously in both directions.

(3) *Mobile Tracking Station.* The Mobile Tracking Station will utilize the same teletype circuits as the South Africa station.

(4) *Cape Canaveral.* Two half-duplex circuits will be available to Cape Canaveral during the launch period. These circuits will be available for about 1 month prior to each launch and will remain available until after each launch. These circuits will be used for data flow between the launch complex and the JPL Communications Center.

(5) *Central Computing Facility.* Six circuits will connect the Central Computing Facility with the Communications Center. Four of these will be full-duplex circuits with the remaining two half-duplex.

(6) *Public Information Office.* One teletype circuit will connect the Public Information Office with the Communications Center.

b. Voice circuits.

(1) *Goldstone.* Two voice circuits will be available to Goldstone. These four-wire telephone circuits will be capable of conferencing at the Communications Center with other voice circuits used as part of the DSIF operations.

(2) *South Africa.* A toll call (long distance) will be placed to South Africa prior to each launch operation. This circuit will be used as required for the first 3 operating days after launch and will not be available on a full-time basis. Approximately 10 hr per day usage is anticipated.

(3) *Woomera.* The *Mercury* voice circuit (SCAMA) will normally be used for communications to Woomera during the launch operation and the first 3 operating days thereafter. A toll call will be placed if this circuit is not available.

(4) *Cape Canaveral.* Two voice circuits will be available during the launch period for communications with the launch complex. One circuit will connect the CCF with the Cape Canaveral Computing Center, and the second will be used to coordinate the DSIF and launch activities.

(5) *Central Computing Facility.* Extensive voice communication will be provided between the Communications Center and the CCF. Two voice circuits will be established solely for operational purposes. However, due to the proximity of the two facilities, additional voice circuits will be added as required. The Communications Center has the capability of interconnecting all teletype circuits so that any station can be conferenced with any other station. During operations, all data traffic from any station will be routed directly to the CCF on a conference connection. The Communications Center also has the capability of conferencing the various voice circuits together in different configurations.

5. Space Flight Operations Center

The Space Flight Operations Center (SFOC), managed by the Space Flight Test Director, will serve as the focal point for initiation of the execution of the operating procedures. All information concerning the current performance and trajectory of the spacecraft will be routed to the SFOC for analysis, evaluation, and interpretation by the scientific data group, spacecraft data analysis team, and orbit determination group. All commands to the spacecraft will originate at the SFOC. Information to the over-all status of the operation will be kept current on status boards at the SFOC. This information will be forwarded to the Project Manager in the form of a status report.

The SFOC adjoins the CCF at JPL, Pasadena. It contains an operation room for the execution of the functions described, and a standby room providing, alternately, additional space for conference purposes and a relaxation area for SFOC and CCF personnel.

B. Organization

1. Project Manager

The Project Manager has the responsibility and authority for the execution to completion of the development and operation of the *Ranger* missions.

2. Space Flight Test Director

The Space Flight Test Director interprets the standard operating procedure and places requirements consistent with the Space Flight Operations Plan on the various operating groups. He resolves any ambiguities directly associated with the SFOP arising during its execution and also makes appropriate emergency decisions in the absence of the Project Manager.

In the fulfillment of this responsibility, the Test Director is accountable to the Project Manager and is delegated the authority of the Project Manager for placement of requirements on operating groups in accordance with the SFOP.

3. JPL Operations (Control) Center Director, AMR

The JPL Operations Center Director coordinates all activity of the Control Center at AMR during countdown and immediately after launch. He operates the communication control system to provide coordinated use of cross-country leased voice circuits.

4. Advisors

The advisors are aware of the performance of the spacecraft system, instrumentation subsystems, and DSIF during flight, and supply judgment to the Project Manager as to possible future courses of action in the event of nonstandard behavior of the spacecraft.

5. DSIF Tracking Director

The Tracking Director (called the DSIF Operations Director for RA-3) directs the operation of the Deep Space Instrumentation Facility, including the transmission of data and commands between the spacecraft and the Central Computing Facility, so as to meet the requirements placed by the Test Director in accordance with the SFOP.

6. Central Computing Facility Manager

The Central Computing Facility Manager directs the programming and operation of the computer and peripheral equipment so as to meet the requirements placed by the Test Director in accordance with the SFOP.

7. Scientific Data Group

This group controls the flow and mathematical operations on the data related to scientific experiments during the interval between its receipt from the DSIF and its transmission to the appropriate scientists. Analysis or in-flight evaluation of the scientific data is supplied by this group.

8. Tracking Data Analysis Group

This group evaluates the tracking data to obtain evaluation of the DSIF equipment.

9. Spacecraft Data Analysis Team (SDAT)

This group informs the Test Director on the status of the spacecraft performance during flight.

10. Orbit Determination Group

This group uses the tracking and pertinent telemetry data to obtain the best estimate of the actual trajectory of the spacecraft. Acquisition and prediction information are supplied to the DSIF by this group.

11. Maneuver Commands

This group determines the commands required for the midcourse and terminal maneuvers.

C. Data Handling and Flow

1. Data Handling and Flow to JPL Operations Complex

The DSIF is the primary source of data from the spacecraft and handles all communication with the spacecraft. Some data may be expected from secondary sources, such as tracking stations other than DSIF. Some data gathered from the DSIF stations after impact is that produced during the transit phase but not immediately transmitted to JPL.

The tracking data is recorded on paper teletype tape. Telemetry data is recorded on paper teletype tape and magnetic tape.

Some spacecraft data will be received from tracking stations other than DSIF, AMR, and vehicle contractors after the first 24 hr. Since the nature of the data to be received from such sources cannot be anticipated, an attempt will be made to log such data and distribute it to the appropriate personnel at JPL.

Spacecraft data received through the *Agena* telemetry system will be recorded at AMR and reduced by AMR or LMSC. The reduced data will be transmitted to the *Ranger* Project Office at JPL for internal distribution.

2. Data Handling and Flow Within the JPL Operations Complex

The handling of data within the JPL Operations Complex is determined primarily by the requirements of the users of the data. The four principal groups using spacecraft or spacecraft-related data may be categorized by the type of data that it is their primary responsibility to interpret, analyze, evaluate, and disseminate.

3. Data Handling and Flow From JPL Operations Complex

The data handling required before dissemination by the recipients is the responsibility of each group. The data that will flow from the Operations Complex is in the form of spacecraft commands, prediction and acquisition information for the DSIF, and operational documentary information about the mission.

D. Flight Operations Plans

1. RA-1 and -2

a. Standard sequence of events. The standard sequence of events specifies the expected normal operation of the spacecraft and the Space Flight Operations Complex. Normal or standard operation assumes all components of the spacecraft and Operations Complex function as designed. Only the antenna and attitude-control systems possess an in-flight capability to make corrections. Standard operation of these systems is defined as acquiring the Sun and Earth and establishing communications through the high-gain antenna. In standard operations, no commands are required and telemetered information may be received at all times after the 3-w transmitter is switched to the high-gain antenna on the transponder frequency. The procedures planned in the event standard operation is not achieved are detailed below.

b. Anticipated nonstandard sequence of events. This section considers three classes of departures from standard operation which can be anticipated and describes the procedures to be followed if they occur.

Class I: The failure of an element of the spacecraft and/or Space Flight Operations Complex to achieve standard operation which was not anticipated and for which no *a priori* corrective action was planned. The effect of such an occurrence was difficult to estimate but to the extent possible, the following failures and the procedures to be followed, were given.

Class II: The failure of an element of the spacecraft required and/or Space Flight Operations Complex to achieve standard operation which was anticipated and for which *a priori* corrective action has been planned. Such a failure constituted an anticipated nonstandard sequence of events. Since corrective action was possible, a sequence of events would be developed to execute that action. Two such sequences were required for RA-3.

Class III: An anticipated event whose occurrence cannot be predicted. Such an event would cause a nonstandard operation, since it could not be predicted. Clearly, events in this category require special attention only

when they affect the spacecraft. Since these events can be anticipated, procedures to be followed during their occurrence are given in the Space Flight Operations Plan.

E. Operations Procedures

Operating procedures are used to describe, in detail, the methods by which various critical phases of the space flight operations will be executed. Some procedures directly affect the spacecraft, others affect the conduct of the mission within the SFOC.

1. Attitude-Control and Antenna Command Procedure

The real-time commands for attitude-control and antenna command operations during RA-1 and -2 were:

(1) RTC-1 Roll override.

(2) RTC-2: Antenna hinge-angle override.

(3) RTC-3: Antenna switchover.

The attitude-control override commands are designed to aid the attitude-control subsystem in acquiring the Earth. The use of the three real-time commands, RTC-1, -2, and -3, is inter-related, especially during those parts of the mission immediately following the initial acquisition by the spacecraft of the Sun and Earth attitude reference, and immediately following the performance of the midcourse maneuver.

2. Command Decision—RTC-1, -2

No commands other than RTC-3 are necessary if DSIF 3 acquires a spacecraft signal that increases to a value commensurate with that expected from the high-gain antenna pointed at the Earth. Should no signal or a very weak signal be observed, it then is necessary to evaluate the success of the attitude-control system in pointing the antenna and to determine which other commands should be sent to the spacecraft.

The transmission of RTC-1 and/or -2, both of which affect the attitude of the spacecraft, is dependent upon several conditions. The determination of the specific command required is affected by these factors:

(1) Acquisition by the spacecraft of a body other than the Earth.

(2) Failure of the spacecraft to acquire any body as a secondary reference.

(3) The position of the Earth and Sun relative to the spacecraft.

(4) The performance of the spacecraft determined from the engineering telemetry.

3. Orbit Determination Procedure

The orbit determination procedure covers the parking orbit of the *Ranger–Agena* and the space trajectory of the spacecraft.

The parking orbit data is required by JPL to provide:

(1) Initial acquisition and prediction information for the DSIF.

(2) An estimate of the injection conditions of the spacecraft.

Knowledge of the space trajectory of the spacecraft after injection is required to provide:

(1) The path of the spacecraft in space.

(2) Successive acquisition and prediction information for the DSIF.

(3) Spatial orientation to assist in the evaluation of spacecraft performance.

(4) Spatial orientation to assist in the evaluation of the measurements obtained from the scientific experiments carried aboard the spacecraft.

a. Determination of the parking orbit. The *Ranger–Agena* vehicle is injected into a parking or Earth-satellite orbit under standard conditions at the end of the first *Agena* burning period. After a coast period, the *Agena* stage is reignited and permitted to burn until sufficient velocity is attained to place the spacecraft in the desired lunar impact trajectory.

The parking orbit will be tracked by the AMR stations. The prime responsibility for the real-time determination of the parking orbit was discharged by AMR. The orbital elements of the parking orbit and initial acquisition information will be supplied to JPL by AMR as provided in the standard sequence of events.

Prior to entry into the parking orbit, AMR fulfilled its range safety function. During, and for a short period after, entry into the parking orbit, the vehicle was tracked by the San Salvador, Puerto Rico, and Antigua radars. At the conclusion of the range safety function, at approximately $L + 325$ sec, AMR will use this tracking

data with a modified least-squares technique to determine the injection conditions of the parking orbit. The time of injection (i.e., cutoff of the first *Agena* burning period) was obtained from Antiqua in real time.

b. Determination of the spacecraft orbit. After initial acquisition by the DSIF, all post-injection tracking data will be supplied for the determination of the orbit of the spacecraft by the DSIF.

Mathematical method and computational options. The RA-1, -2 orbit was determined by finding the set of initial conditions at injection epoch, which causes the weighted sum of the squares of the differences between actual observations and the computed values of the observables to be minimized.

F. Flight Operations

1. Ranger I

a. General. *Ranger I* was launched at 10 hr 4 min and 10.26 sec GMT on August 23, 1961. The spacecraft completed 110 orbits, each of approximately 90-min duration, and re-entered the Earth's atmosphere during its 111th orbit on August 30, 1961.

b. Space Flight Operations Complex performance. The SFOC responded to the highly nonstandard *Ranger I* mission in a satisfactory manner. After initial acquisition by the DSIF and establishment of the fact that the spacecraft was in an onstandard Earth-satellite orbit, the DSIF attempted to track the spacecraft on each visible pass. The Central Computing Facility (CCF) was able to reduce all usable near-real time telemetry data obtained by the DSIF. The magnetic tapes of the telemetry recorded by the DSIF were returned to the DRL at JPL for reduction.

c. AMR tracking participation. AMR was responsible for providing JPL with (1) orbital elements of the parking and transfer orbits, (2) acquisition angles for DSIF 1 and 5, and (3) raw data for the JPL back-up role.

The parking orbit data was delayed by the necessity of having to first supply look angles to the DAMP ship and to Ascension Island. The loss of the use of the *Twin Falls Victory (Pershing)* tracking ship with its FPS-16 and high-data rate (10 points per sec) resulted in the attempt to formulate an orbit with too few Antiqua data. The lost data was subsequently retransmitted and a good orbit resulted.

The transfer orbit using Ascension data was delayed by (1) difficulty in rejecting bad data which was caused by "beacon stealing" by the DAMP ship, (2) poor radio data transmission conditions, and (3) lack of available telemetry defining the time of second *Agena* burn. When the data was edited and an assumed nominal time of second *Agena* burnout chosen, a good orbit resulted.

The raw data from AMR reached JPL with very few transmission errors. Although the Antigua data had no transmission errors, it was not used by JPL because of an input error in the 7090. The Ascension data, however, was used by JPL in real time to compute the initial orbit.

d. DSIF tracking participation. See Chapter VIII of this report for a discussion of the DSIF *Ranger I* tracking operations.

e. LOD participation. The Launch Operations Directorate (LOD) microlock tracking station at AMR supplied, in addition to launch data, one-way doppler data for all passes within their line of sight through August 30, 1961. LOD also recorded certain telemetry data on magnetic tape.

f. NORAD participation. *Ranger I* and the *Agena* were skin-tracked throughout their lifetime by the facilities of NORAD (North American Air Defense Command). The NORAD Trinidad Station tracked from launch and promptly supplied data indicating that spacecraft–*Agena* separation had occurred. After loss of communication with the spacecraft by the DSIF on August 29, 1961, skin-tracking was continued by NORAD.

NORAD has indicated that *Ranger I* re-entered the Earth's atmosphere on Orbit 111, which would have been completed at approximately 0900 GMT, August 30, 1961. The last contact made with *Ranger I* was by NORAD's Laredo, Texas, site at approximately 0830 GMT, August 30, 1961. At that time, the spacecraft's altitude was estimated at approximately 70 statute mi above the Earth.

g. LCTT participation. Although no plans had been made to use the launch checkout telemetry trailer to track beyond the launch phase, a minimum crew maintained a continuing effort from launch through the early hours of August 27, 1961. Additionally, one command was sent to the spacecraft by the LCTT, successfully effecting changeover from omni- to high-gain antenna.

h. Scientific telemetry. All the Channel B-13 data from AMR, Goldstone, and Woomera was reduced and distributed to the experimenters.

Data Automation System. This system operated correctly with the following minor exceptions:

(1) There was an occasional complete reset of all data registers between successive passes, perhaps caused by spacecraft power transients.

(2) There was an occasional program reset of undetermined origin within the DAS (i.e., it would start a new frame without finishing the preceding one).

(3) There was an occasional addition of 32 counts to the frame-count register between passes.

(4) There was an occasional malfunction of the ion chamber time register, probably because of noise.

Ion chamber, triple coincidence telescope, gold-silicon detector, and Geiger tube. All these experiments apparently operated as expected in the Earth-satellite environment.

Cadmium sulfide detectors B and C. These detectors are nearly identical in construction, location, and view angle—differing only in that Detector C has a magnetic broom for preventing low-energy electrons from being counted. Thus, Detector B should count at a rate equal to or greater than Detector C; however, Detector C consistently had the much higher counting rate. A similar, smaller discrepancy existed between Detectors A and D.

Micrometeorite detectors. Anomalously high counting rates were often recorded by the light flash detector when the spacecraft was in the sunlight. This is presumably due to direct or reflected sunlight and/or Earth light. The instrument operated correctly when in the dark.

Electrostatic analyzers. These units appear to have operated normally. However, the data was very abnormal, probably because of the presence of the ionosphere.

Lyman-alpha telescope. Part or all of four pictures and several in-flight calibrations were observed, as well as background measurements of Lyman-alpha intensity.

Magnetometer. No magnetic field data was obtained, both because the Earth's field at the *Ranger I* altitude was higher than could be measured with this experiment, and because the magnetometer temperature was usually outside the operational range.

Vela Hotel. This experiment apparently operated correctly when the Vela Hotel solar panels received enough sunlight. Most passes were too short to obtain any useful data.

i. Spacecraft performance summary. Analysis of the spacecraft performance indicated that separation from the *Agena* stage appears to have been normal. The spacecraft controller commands were all executed. The exact times are not known but there is no reason to believe the times were not nominal.

The following indications of a malfunction were noted:

(1) The attitude-control converter voltage measurement was at zero v.

(2) The Sun sensor and light detector outputs were at zero, substantiating the above indication.

(3) The rate gyro measurements had slightly more than two spikes per sec. The attitude-control converter appeared to have returned to normal by the first pass on August 25, 1961.

The attitude-control system was inoperative on August 24. While it was apparent that the attitude-control gas was exhausted by August 25, it was suspected that it had been exhausted by August 24. Because of these conditions, there were no opportunities to observe the attitude-control system in action after the first day of the mission.

The communications system functions appear to have been qualitatively normal. The radio command to transfer from the omni-antenna operation to high-gain antenna operation was sent four times and was successful each time. All commands were sent by Goldstone except the one from the JPL LCTT.

Spacecraft temperatures appear to have been normal for an orbit of this type. The solar panels and solar corpuscular radiation boom were extended successfully. These functions are deduced from the temperature and solar panel currents data since the blip channel was inconclusive.

The friction experiment was energized and operated for 17 hr. Data was received and analyzed.

j. Estimation of the orbit of Ranger I. The orbital parameters for *Ranger I* were not optimum, but they were the best obtainable using the Orbit Determination Program (ODP) with angle data only. The ODP, designed for use with deep-space probes similar to the RA-1 standard trajectory, lacked certain features which are mandatory for the determination of obits of low-altitude satellites. Consequently, Goddard Space Flight Center was requested to determine the final orbit of *Ranger I*, using the technique developed there for such a purpose.

The largest source of error in the *Ranger I* orbital parameters resulted from the exclusion of any type of drag effect which would compensate for that experienced by

the spacecraft during the decay of its orbit. This fact makes it desirable to redetermine the orbit for each excursion about the Earth, and necessary to minimize the number of excursions based upon a single set of orbital parameters. The next largest known source of error in these parameters was the exclusion of frequency data. Some of the good frequency data of each type was obtained during some view period by one of the DSIF stations.

The last known source of error resulted from the inherent difficulties experienced by the DSIF when attempting to track the spacecraft. The overwhelmingly powerful signal, coupled with the high frequency and angular rates (conditions for which the DSIF antennas were not designed), made it extremely difficult to obtain good tracking data during every view period and not to track side lobes.

2. Ranger II

a. Summary. *Ranger II* was launched from AMR on November 18, 1961. Lift-off was at 08 hr, 12 min, 21,502 sec GMT (03 hr, 21.502 sec EST). *Atlas* performance was apparently normal. The reported times of ignition and cutoff for the first *Agena* burn were normal; however, preliminary reports indicated that the *Agena* was rolling at an excessive rate during this period. Confirmation was obtained from the spacecraft gyro measurements on the AMR telemetry records.

A near-nominal parking orbit was achieved but, since no second *Agena* burn was reported, the DSIF prepared to track the spacecraft in a low-satellite orbit similar to *Ranger I*. The initial orbit had a period of 88.31 min, apogee of 147.2 statute mi, and perigee of 97.5 statute mi.

Confirmation of mechanical separation of spaccraft and *Agena* was obtained from *Agena* telemetering on the second pass over AMR. Electrical separation was verified by the fact that the programmed controller commands were executed. There was nothing in the telemetry data to indicate that the spacecraft did not perform in a manner normal for a low, Earth-satellite type of orbit. The Mobile Tracking Station (DSIF 1) provided most of the tracking and telemetry data obtained. After the fifth pass, the orbit was below the MTS horizon and no further passes were tracked. Preliminary estimates placed the time of re-entry at 0400 GMT on November 19, 1961.

b. Space Flight Operations Complex. Elements of the Space Flight Operations Complex performed most satisfactorily. The experience gained from *Ranger I* operations and that gained during the RA-2 operational tests was apparent in the manner in which the Operations Complex responded to the nonstandard situation.

c. Lift-off to injection.

AMR participation. AMR was responsible for providing JPL with (1) orbital elements of the parking and transfer orbits, (2) acquisition angles for DSIF 1 and 5, and (3) raw data for the JPL back-up role.

During the ascent phase, the vehicle was tracked and the parking orbit was established by AMR, using data from San Salvador rather than Antigua because of the poor quality of the latter. Excellent tracking data from Ascension Island was received at AMR and JPL in real time. (The preliminary indication that the second *Agena* burn had not occurred was obtained from this data.)

d. JPL launch checkout telemetry trailer (LCTT). Only one pass of *Ranger II* was tracked by the LCTT because of the low orbit. No commands were sent, nor were any interrogations made by the LCTT, which acted only as a receiver for the one pass.

e. Post-injection.

Deep Space Instrumentation Facility. Chapter VIII of report includes a discussion of the DSIF tracking operations for the *Ranger II* mission.

f. Engineering telemetry recovery.

Flight temperatures. Temperature data was obtained from all engineering system transducers except that in the Earth sensor at least once during the five passes of the spacecraft. The measurements obtained twice indicated the temperature rising with time. All other readings agreed well with this trend, with the exception of one solar panel. Temperatures in general were slightly higher than at corresponding times in the *Ranger I* flight, primarily because of the low orbit causing aerodynamic heating. In addition, the spacecraft was probably tumbling, also tending to raise the temperature above those at corresponding times in the *Ranger I* flight.

Friction experiment. The friction experiment was not running during the fourth pass over the MTS on November 18, 1961. During the fifth pass, 25 good data points were obtained from the friction experiment. Fortuitiously, one of the points was a temperature code marker and four of the points were readily comparable to data previously obtained from *Ranger I*. This combination resulted in complete tentative identification and correlation of all of the 25 data points received.

g. Scientific telemetry recovery. The data indicated that the cadium sulfide detectors, low-energy triple coincidence telescope, and the Geiger tubes operated normally. The DAS appeared to function correctly with the possible

exception of the frame-count register. Instruments which exhibited the same abnormal behavior as on *Ranger I* were the micrometeorite detector (spurious pulses, probably due to sunlight), the solar corpuscular radiation electrostatic analyzers (probably affected by the poor vacuum and the presence of the ionosphere), and the magnetometer (out of band due to high field of Earth).

h. Spacecraft performance summary. Engineering telemetry received by teletype from the DSIF during the short lifetime of *Ranger II* indicated that the spacecraft performed in a normal manner for a satellite orbit. The communications transponder and data encoder appeared to function normally. Even though no event blips were reported by the DSIF, most of the programmed controller commands were verified by other telemetry, indicating that they occurred in the proper sequence within the scheduled time brackets. This confirmed electrical separation of the spacecraft from the *Agena*, but mechanical separation could only be inferred at the time.

The attitude-control power for both Sun and Earth acquisition was turned on between the first two passes over DSIF 1. For most of this period, the spacecraft was in the Earth's shadow and no acquisition data was recovered. During the four sunlit passes tracked after that, position and rate data indicated no limit cycle operation. The spacecraft was probably tumbling much of the time in a manner similar to *Ranger I*, with Sun and Earth acquisition highly unlikely. This condition was further indicated by the very low values of solar-panel current measured.

Indicated power consumption was slightly higher than expected, which could be accounted for by the fact that the attitude-control system requirements would be higher than normal when operating in the observed manner. In all probability, the spacecraft was operating on battery power almost continously.

The few temperature measurements which were obtained indicated that the spacecraft hex temperatures were rising with each orbit, as would be expected.

The scientific instruments and friction experiment generally performed in a normal manner consistent with the orbit. Some minor abnormalities were indicated in the scientific experiments similar to those observed on *Ranger I*.

The command system was not tested on *Ranger II*. The quarter-watt transmitter signal was never tracked, but antenna drive measurements indicated that it was operating normally.

Separation of the spacecraft from the *Agena* was confirmed by analysis of *Agena* telemetry, but the separation was not normal. Magnetic tapes reduced by JPL's DRL after the flight confirmed most of the conclusions reported during the operation. Event channel blips were recovered from the first DSIF 1 pass, indicating that the command for opening panels and boom was issued at the programmed time and that the commanded extensions took place. The only programmed controller command not verified was that for reducing the modulation on the beacon transmitter.

Page intentionally left blank

VIII. Deep Space Instrumentation Facility Operations

A. *Ranger I* Pre-Launch Operations

The Deep Space Instrumentation Facility (DSIF) became fully operational as a world-wide tracking network on July 4, 1961. During the period between that date and the first scheduled launch attempt on July 26 for RA-1, the DSIF performed numerous dummy runs to test the equipment and to train personnel. The delay in actual launch to August 23, 1961, permitted the DSIF to perfect its operating procedures and achieve operational readiness for the mission.

Prior to this net preparation, each station had conducted a program of tracking system evaluation and testing. Following this program, the stations then began the series of exercises designed to acquaint them with the data handling and communications procedures required for satisfactory DSIF operation. With the postponement of the first launch, the stations were maintained in an operational readiness state until the second attempt. Two DSIF preparation exercises were conducted prior to this second launch period.

The local station evaluation tests were initiated with various star tracks which were used to evaluate station angle-pointing characteristics. R-F tracking system characteristics and performance were then evaluated. The telemetry recording and acquisition system was tested and evaluated next. Prior to the DSIF tests, local station evaluation tests were conducted, using an airborne beacon to provide practice in r-f acquisition, and with tests to enable the operators to become familiar with the data marking procedures necessary for the transmission of engineering telemetry.

The DSIF tests consisted of two types of procedure. One type, dummy run, provided practice for the data transmission personnel at each station, and allowed them to become familiar with the data transmision requirements and schedule. These tests also allowed the various required communication links to be evaluated and any required corrective action taken. The dummy runs primarily involved the data transmission personnel. However, at the discretion of the station managers, other personnel were involved by conducting aircraft acquisition tests concurrently with the dummy runs.

Other net integration tests were performed and provided a more realistic simulation of the procedures required during the first tracking period. The DSIF integration tests involved the complete station complement and were performed with full station checkouts prior to the tracking simulation and full post-mission calibrations following the simulated operation. Net preparatory operations for the initial launch were conducted on the following days: July 11 and 13, 1961: dummy runs; July 21 and 24, 1961: net integration tests. During this period, in addition to these tests, each station conducted independent exercises designed to provide the operators with additional acquisition practice.

After this preparation period, the DSIF stations participated in four launch-attempt operations prior to the rescheduling of the RA-1 mission for August 23, 1961. The four attempts occurred on July 29 and 31, and on August 1 and 2, 1961. For the launch periods when the countdown progressed to the point of imminent launch (July 29 and August 1), the DSIF was ready to participate. On August 18 and 20, the DSIF conducted two additional net integration tests prior to the successful launch attempt. When the *Ranger I* spacecraft injection was unsuccessful, the DSIF then began the difficult operational task of tracking and recording data from a near-Earth orbit.

B. *Ranger I* Tracking Operations and Evaluation

1. Tracking Operations

The scheduled standard DSIF operating procedures were not followed because the spacecraft was not injected into deep-space orbit following launch on August 23, 1961. Since at the nominal time of acquisition for the MTS and Johannesburg stations there had been no indication of nonstandard operation, the MTS searched along the nominal trajectory and heard a signal for 30 sec but was not able to acquire. Suspecting that the spacecraft was in a near-Earth orbit, the antennas of the Goldstone *Pioneer* and *Echo* stations were positioned for acquisition if the spacecraft remained in a parking orbit. Signal reception by these stations was the first conclusive indication that the spacecraft had not been injected into its nominal orbit.

Following this indication, the Johannesburg and Woomera stations were secured, since the spacecraft path was such that few good passes for tracking were visible to them. In general, the spacecraft passes at these stations were either in an area where they could not be tracked, or crossed the sky at such a rate that the antenna could not track. The primary tracking load for this nonstandard orbit was, therefore, borne, as previously planned for such an occurrence, by the Goldstone *Echo* Station and the Mobile Tracking Station. The Az-El mounted antennas at the Mobile Station and the Goldstone *Echo* Site had the rate capabilities necessary to obtain tracking data for orbit determination and telemetry data for analyzing spacecraft operation.

After successful spacecraft operation had been ascertained and after an accurate orbit had been determined, the Johannesburg and Woomera stations were put back in operation. The first official tracking by these stations occurred on August 25, 1961, at 01501Z at the Woomera station, and at 092311Z at Johannesburg. Earlier, on August 24, in an unofficial exercise, the Johannesburg station, using MTS prediction data, had tracked the spacecraft and obtained 10 good telemetry points, which were transmitted to JPL. The activation of these stations provided the DSIF with additional capability for tracking and telemetry reception. Table 83 presents a summary of the DSIF station operations for the *Ranger I* tracking mission.

The injection failure of the spacecraft made the DSIF objective more difficult. The short time (approximately 6 to 10 min) that the spacecraft was visible at each DSIF station limited the amount of tracking and telemetry data which could be obtained, and also restricted the time during which commands could be sent from Goldstone. Despite these difficulties, telemetry data was recorded, but because of the limited recording time, the recordings were never complete. Telemetry data retrieval was further hampered by the failure after Orbit 61 of the batteries used to power the transponder.

Thus, after this time, the only reliable signal was the beacon signal which carried only low-rate telemetry information. Occasionally, however, after Orbit 61, a transponder signal would be detected by a station spectrum analyzer. This was probably the result of the transponder batteries being periodically recharged by the solar panels.

During the mission, the Goldstone stations transmitted four commands to the spacecraft. The station transmitting and the commands transmitted are listed below:

Transmitting station	Command transmitted	Orbit	Time
Goldstone *Pioneer* (DSIF 2)	Hinge override	46	071504
Goldstone *Pioneer* (DSIF 2)	Hinge override	47	084715
Goldstone *Echo* (DSIF 3)	Antenna switchover	30	071258
Goldstone *Echo* (DSIF 3)	Antenna switchover	31	084800
Goldstone *Echo* (DSIF 3)	Antenna switchover	31	085056
Goldstone *Echo* (DSIF 3)	Roll override	49	115740

Table 83. Summary of DSIF participation in *Ranger I* mission

Date 1961	Station[a]	Orbit	RF one-way		RF two-way		Autotrack		Signal		Remarks
			In	Out	In	Out	In	Out	DBM	Time	
8/23	AMR										Launch time 100410.
	1	1	103611	104201							Four intermittent locks. Maximum duration was 30 sec.
	5	1	103931						−130	103931	Momentary lock. Searched until 1300. At that time DSIF-5 was instructed to secure operations.
	3	1	113133	113535					−135 *(max)*		Obtained an intermittent lock on the beacon. Autotrack *could not be attempted. Because of poor RF lock* conditions the telemetry data was erratic.
	2	1	113526	113535							Acquired transponder momentarily. Antenna servo drive was slaved to the DSIF-3 antenna after loss of lock. However, large error signals produced as DSIF-3 searched for the signal caused the servo drive system to shut down several times during the tracking attempt.
	1	2	121131	121841			121141	121841			Tracked the transponder signal until 121131 and then switched to the beacon until the end of the pass.
	2	2	130822	131426			130822	131426	−95 (avg)		Computer used to slave the DSIF-3 antenna to the DSIF-2 antenna to assist in acquisition. Tracked the transponder signal.
	3	2	130815	131036			131326	131430			Tracked the beacon signal.
			131104	131112							
			131130	131208							
			131238	131452							
	1	3	134657	135551			134657	135551	−116	134647	Went into autotrack on the transponder. At 135047 lost autotrack for 10 sec and acquired the beacon signal.
	1	4	152220	152640			152241	152631	−116	152220	Dropped out of autotrack for a total of about 120 sec.
			152841	153231			152841	153231	−111	152828	
	1	5	165951	170801					−114	165945	Tracked beacon signal using the aided track mode because the azimuth channel 455-kc IF amplifier was inoperative. This amplifier was replaced with a spare amplifier at the end of the pass.
8/24	3	13	052555	052735							Tracked the beacon signal.
	2	13									Visibility marginal. Spacecraft below horizon for the majority of the pass. No acquisition.
	2	14	065912	070202			065933	070142	−130	065912	Attempted track on beacon. Low signal strength indicated the antenna was tracking with a side lobe. The servosystem was put in aided track in an attempt to acquire with the main lobe. This was unsuccessful and tracking attempt was terminated at 0710.
	3	14	065829	070659							The antenna servosystem was slaved to the servosystem at DSIF-2 at 065932. Maintained an intermittent lock on the transponder signal.
	3	15	083226								Momentary lock on the transponder signal for 4 sec at 083226. The antenna was slaved to the DSIF-2 antenna at 083320, but no additional signal was received. Telemetry data received at DSIF-2 was transmitted over the microwave link and recorded at DSIF-3.

[a]DSIF-1: Mobile Tracking Station, -2: Goldstone *Pioneer* Site, -3: Goldstone *Echo* Site, -4: Woomera, -5: Johannesburg.
Note: All times are GMT.

Table 83. Summary of DSIF participation in *Ranger I* mission (cont'd)

Date 1961	Station[a]	Orbit	RF one-way		RF two-way		Autotrack		Signal		Remarks
			In	Out	In	Out	In	Out	DBM	Time	
8/24	2	15	083241	084111					−116 −97 (max)		Tracked the transponder signal in the aided track mode using a 6-ft "dish" mounted on the side of the 85-ft antenna. This small antenna had a beamwidth of 15 deg and a gain of 19.2 db below that of the main dish. The signal from this small antenna was used to feed the receiver reference channel.
	1	16	091441 091821	091621 092011			091511 091821	091621 092011	−116	091500	Attempted to acquire the beacon signal (960.10 mc) but acquired the transponder signal (960.05 mc) because of the doppler shift effects. Lock was lost due to rates and the beacon signal was then acquired.
	2	16	100832	101652			101502	101652	−95 (avg)		Six-ft dish used with 20-db pads in the angle error channels. The beacon was tracked in the aided track mode until told to switch to autotrack.
	3	16	100920	101810			100940	101730	−85 (avg) −70 (max)	 101439	Tracked the transponder signal. Telemetry was relayed from DSIF-2 with only fair results. After the tracking period the magnetic tape record of the telemetry received at DSIF-3 was played so that data could be recovered and sent to JPL.
	1	17	104851	105600			105204	105559	−128		Tracked the transponder signal.
	2	17	114442 114802	114702 114932							RF lock was lost at 114702 when the transponder acquired the transmitter at DSIF-3. Tracking was terminated after RF lock was finally lost because the signal from the transmitter at DSIF-3 "pulled" the transponder frequency beyond the tuning range of DSIF-2's VCO.
	3	17	114500	114821			114520	114821			Tracked the transponder signal and recorded telemetry. Two way lock was attempted but the receiver went out of lock when the transponder acquired the transmitter. Reacquisition was not accomplished. Noise pulses, which appeared in the receiver were found to originate in the blower in the transmitter. The blower was repaired.
	1	18	122525	122545			122631	123201	−117 −100	122545 122910	Tracked the transponder signal.
	2	18									Began searching for spacecraft at 131622 but the pass was marginal since the spacecraft was below the horizon. Unable to acquire.
	3	18									Too low in elevation to be successfully tracked.
	1	19	140031	140051			140101	140910	−112 (avg)		Tracked the transponder signal.
	1	20			153621	154501	153621	154501	−110	153540	
	5	20	153800								Unofficial track for acquisition practice only. Ten points of engineering telemetry passed to JPL.
	1	21	171221	171821			171321	171821	−117	171315	
8/25	4	27	015010	015220					−140	015010	Momentary locks. Attempted autotrack unsuccessful.
	4	28	032536	032825					−105 −105	032620 032753	Angle error fluctuations too large for autotrack. Telemetry discriminators were in lock occasionally. The scientific telemetry TSE was in synch and one quarter of a master frame was obtained.

[a]DSIF-1: Mobile Tracking Station, -2: Goldstone *Pioneer* Site, -3: Goldstone *Echo* Site, -4: Woomera, -5: Johannesburg.
Note: All times are GMT.

CONFIDENTIAL

CONFIDENTIAL

Table 83. Summary of DSIF participation in *Ranger I* mission (cont'd)

Date 1961	Station[a]	Orbit	RF one-way		RF two-way		Autotrack		Signal		Remarks
			In	Out	In	Out	In	Out	DBM	Time	
8/25	4	29	050627	050637					−135		
	2	29									Intended to track the beacon but corrected prediction data were late and the spacecraft was not acquired. The receiver 30/31-mc VCO was inoperative during this time but would not have affected any beacon tracking done. The 6-ft and 85-ft antennas were "in line."
	3	29	053850	054030			053900	054010	−90	053900	Tracked the transponder signal. All telemetry channels except Channel 7.7 locked up.
	4	30	063500	064340			063610	064300			
	2	30	070711	070951			070941	070951			Tracked beacon using the 6-ft dish "in line" with the 85-ft antenna. The 30/31-mc VCO was repaired before the track.
	3	30	071039	071619			071249	071609			Tracked transponder. At 071258 an antenna switch-over command was sent. The transponder static phase error was successfully zeroed out.
	1	31	074921	074931					−132	074921	Appeared to be on a sideband. Reacquisition attempts failed.
	4	31	081101	081721							Most of track on side lobe. Signal strengths varied from −115 to −140 dbm.
	2	31	084351	085021			084351	085021	−90	084600	Tracking beacon signal using 6-ft dish.
	3	31	084539	084629							DSIF-3 antenna slaved to DSIF-2 antenna to acquire the spacecraft.
			084739	085129			084749	085129	−106	085030	Antenna switchover commands were transmitted at 084800 and 085056 and a quick look at the data showed they were effective.
	1	32	092201	092841			092201	092841	−114 −94	092225 092547	Phase lock loop discriminator for Channel B-10 was later found to be bad. Tracked the transponder signal.
	5	32	092311	092621			092431	092451	−130	092540	Tracked the transponder. All telemetry channels except 7.7 were in lock for a short time.
	2	32	101741	102551			101751	102551	−89	102130	Tracking beacon signal using 6-ft dish.
	3	32	101759	101859	101859	102639	101849	102619	−86	102250	Tracked the transponder signal. All telemetry channels but 7.7 locked up. The doppler frequency multiplier was intermittently out of lock because the doppler frequency was high and out of range of the equipment.
	1	33			105733	110413	105821	110341	−123 −94	105733 110037	Phase lock loop discriminator for Channel B-10 was found to be bad after this tracking period. Subsequent investigation indicates the doppler data count was erratic because of a system maladjustment.
	2	33	115321	115951			115321	115951	−95	115600	Tracked beacon signal using 6-ft dish.
	3	33	115329	115429	115429	120039	115729	120029	−95	115958	Tracked the transponder. The transponder acquired the transmitter at 115338. All telemetry channels except 7.7 were in lock.
	1	34	123248	123258	123258	124021	123310	124001	−100 −96	123415 123800	

[a]DSIF-1: Mobile Tracking Station, -2: Goldstone *Pioneer* Site, -3: Goldstone *Echo* Site, -4: Woomera, -5: Johannesburg.
Note: All times are GMT.

CONFIDENTIAL

CONFIDENTIAL

Table 83. Summary of DSIF participation in *Ranger I* mission (cont'd)

Date 1961	Station[a]	Orbit	RF one-way		RF two-way		Autotrack		Signal		Remarks
			In	Out	In	Out	In	Out	DBM	Time	
8/25	1	35	140811	141631			140821	141621	−113	140813	
	5	35	140959	141124			140959	141124	−80	140959	Tracked transponder in autotrack until 141124 when angular rates became too great. Switched to aided track mode but were not able to reacquire the signal.
	1	36	154248	155138			154431	155138	−125 −100	154430 154947	Twice during this tracking period changes in signal level of approximately 33 db were noticed.
	5	36	154400 154457 154551	154410 154521 154721							No useful data obtained. AGC indicated receiver locked using a side lobe.
8/26	4	42	002424	002434							Poor pass for tracking. Signal varied from −112 to −145 dbm.
	4	43	015433	020033			015433	020023	−68 (max)		Telemetry in lock except channel 7.7. Two and one half frames of good TSE data.
	4	44	032921 033330	033220 033609			032959 033400	033220 033509	−70 (max)		Rate too high for antenna for short period in the middle of the track.
	4	45	050516	051116							High antenna rates.
	3	45	053619	053629			053659	054359	−94	053811	To decrease the probability of locking on a side lobe the receiver was desensitized to −100 dbm. Tracked the transponder signal. The doppler count became erratic since the doppler frequency multiplier approached its limit of operation.
	2	45	053645 054041	053731 054201			053721 054131	053731 054201	−110	054144	Tracked the beacon signal.
	4	46	063914 064454	064134 064614			064524	064616			Data marginal.
	3	46	070951	071219	Pseudo 071219	071949	071209	071909	−80	071714	DSIF-2 used their transmitter on this pass. Telemetry locked up.
	2	46	071005	071046	Pseudo 071046	071741	071041	071741	−80	071610	Hinge override command transmitted at 071504. Transponder interrogated and tracked but mode switch not thrown to pseudo-two-way. After this tracking period, examination of records indicated the command may not have been received since the transponder may not have been in lock.
	1	47	075041	075631			075041	075551	−112 −85	075041 072251	
	5	47	075141	075241			075141	075211			Autotrack was lost for an unexplained reason and reacquisition could not be accomplished.
	3	47			Pseudo 084459	085029	084619	085019	−88	084950	DSIF-2 used their transmitter on this pass. Spin modulation believed observed on telemetry recordings. After loss of RF lock at 085029 only sidebands could be acquired.
	2	47			Pseudo 084621	084931	084741	084901	−84	084906	Transponder definitely in lock two way. Sent hinge override command at 084715.
	1	48	092604	093135			092701	092911	−125 −90 (max)	092604	Three large signal level excursions were noted toward the end of the pass. Amplitude modulation (due to tumbling?) appeared worse, averaging 6 db peak to peak.

[a]DSIF-1: Mobile Tracking Station, -2: Goldstone *Pioneer* Site, -3: Goldstone *Echo* Site, -4: Woomera, -5: Johannesburg.
Note: All times are GMT.

CONFIDENTIAL

Table 83. Summary of DSIF participation in *Ranger I* mission (cont'd)

Date 1961	Station[a]	Orbit	RF one-way		RF two-way		Autotrack		Signal		Remarks
			In	Out	In	Out	In	Out	DBM	Time	
8/26	5	48									Did not attempt tracking since the spacecraft was behind the polar mask or below the local horizon.
	3	48	102019 102409	102129 102839	102129	102249	102249	102249			Receiver again desensitized to −100 dbm. Telemetry Channel 2 was in and out of lock and Channel 7.7 was not locked at all. Tracked the transponder. The signal level varied from −100 dbm to −130 dbm.
	2	48	102101	102741			102111	102741			Tracked the beacon signal.
	1	49	110020	110638			110046	110621	−116 −94 (max)	110020	Telemetry appeared good for about 6 min. Amplitude modulation of about 3 db peak to peak on the last portion.
	5	49									Did not attempt tracking since the spacecraft was behind the polar mask or below the local horizon.
	2	49	115551	115939	120001	120051	115601	115931	−90 (avg)		Tracked transponder. After this tracking period the doppler switching circuit was repaired to allow retention of RF lock when switching from the one-way to the two-way doppler mode.
	3	49	115624	115709	115709	120203	115709	120149	−94	115755	Roll override command sent at 115740.
	1	50	123511	123547	123547	124238	123624	124201	−100 −71 (max)	123511	Telemetry signal appeared good.
	5	50									Did not attempt tracking since spacecraft was behind the polar mask or below the local horizon.
	1	51	140940	141755			141014	141751	−100 (max) −92 (max)	140940	Eight min of telemetry data recorded.
	5	51	141041	141741			141041	141731	−75 (max)		Tracked the transponder signal. All telemetry channels locked up but Channel 5 was intermittent and the TSE malfunctioned.
	1	52	154514	155111			151614	154731	−117 −104 (max)	154514	The servosystem was left in the aided track mode for most of the pass because of noisy tracking conditions due to ground reflections. Telemetry system was in sync but the signal condition was poor.
	5	52									Did not attempt tracking since the spacecraft was below the horizon.
8/27	4	58	002036	002436			002346	002436	−80 (max)		Tracked the transponder signal.
	4	59	015315	015835			015325	015355	−65 (est. max)		Lost lock because of high antenna rates. Tracked the transponder signal.
	4	60	032902	033342					−90 (max)		Tracked the transponder signal manually because required rates were too fast for autotrack. Used 6-ft reflector antenna for reference channel input.
	3	60	040319								Only momentary lock, the pass was too low.
	4	61	050326	050836			050356	050646	−110 (max)		Two frames of scientific telemetry data received. The 6-ft reflector antenna was not used for this pass. The transponder signal was tracked. The automatic gain control (AGC) reading indicates the entire pass was tracked using an antena side lobe.

[a]DSIF-1: Mobile Tracking Station, -2: Goldstone *Pioneer* Site, -3: Goldstone *Echo* Site, -4: Woomera, -5: Johannesburg.
Note: All times are GMT.

Table 83. Summary of DSIF participation in *Ranger I* mission (cont'd)

Date 1961	Station[a]	Orbit	RF one-way		RF two-way		Autotrack		Signal		Remarks
			In	Out	In	Out	In	Out	DBM	Time	
8/27	2	61	053541	054011			053601	054011	−95	053807	Tracked the beacon signal.
	3	61	053711	053741	053741	054121	053741	054121	−97	054008	Tracked the transponder with the receiver desensitized to −100 dbm. Engineering telemetry locked up and Channel 7.7 was in lock about 50% of the time. The discriminator Channels 4, B-10, B-11, B-12, and B-13 had what appeared to be 1-pps modulation on the analog outputs. No scientific data were evident. At the conclusion of the pass the TSE equipment was checked and found to be functioning normally.
	4	62									Strong signal seen on the spectrum analyzer for about 3 sec at 063639. Signal appeared to be the beacon signal. Acquisition attempts were unsuccessful.
	2	62	071001	071041					−125	071000	Attempted to track the beacon signal. The prediction data were in error by approximately 4 min. No successful acquisition.
	3	62	071309 071509	071419 071559					−120 (max)	071600	Attempted to acquire the transponder and attain two-way lock. Initial signal at −144 dbm and telemetry Channels 1 and 3 were in lock. Channel 3 was in lock whenever an r-f signal was present. Could not hold a good r-f lock during this track.
	1	63	074621	074751			074621	074751	−116		Tracking data invalid due to a 90-sec error in the tuning system.
	5	63							−117 (max)		Did not acquire signal because of a 4-min error in the prediction data.
	3	63	084141	085031			084151	085001	−84	084720	The receiver was set for tracking the beacon and desensitizing to −105 dbm. The only telemetry channels which locked up were Channels 1 and 3. Channel 1 showed some very erratic change in information and no information appeared on the analog output for Channel 3. The transponder signal did not appear on the panalyzer. An audio tone detected on the telemetry signal for a short time was found to be caused by the 960.10 mc reference oscillation.
	2	63	084141	084941			084201	084941	−85	084630	Tracked the beacon signal. The time discrepancy noted in the prediction data for the last pass was corrected.
	1	64	092221	092731			092241	092731	−116	092242	No telemetry modulation was detected at acquisition, but appeared for about 3 min during the pass. The transponder signal was detected for a few seconds at 092525.
	5	64									Behind the station polar mask.
	3	64	101649	102419			101659	102359	−94	102320	Tracked the beacon with the receiver desensitized to −100 dbm. The 960.05 mc VCO was used so that the tone generated in 960.10 mc VCO would not interfere with the telemetry operation.
	2	64	101641	102311			101651	102311	−88	101930	Tracked beacon signal. At conclusion of tracking DSIF-2 ceased participation in the tracking of *Ranger I*.
	1	65	105641	110221			105711	110201	−121	105701	Telemetry tones were detected for approximately 1 min and the transponder signal was heard for 23 sec at 105934.

[a]DSIF-1: Mobile Tracking Station, -2: Goldstone *Pioneer* Site, -3: Goldstone *Echo* Site, -4: Woomera, -5: Johannesburg.
Note: All times are GMT.

CONFIDENTIAL

CONFIDENTIAL

Table 83. Summary of DSIF participation in *Ranger I* mission (cont'd)

Date 1961	Station[a]	Orbit	RF one-way		RF two-way		Autotrack		Signal		Remarks
			In	Out	In	Out	In	Out	DBM	Time	
8/27	5	65									Behind the station polar mask.
	1	66	123041	123741			123111	123721	−120		The transponder signal appeared for about 2 min beginning at 123203. Modulation appeared on the beacon signal twice.
	5	66							−130 (avg)		Pass came out of polar mask at a rate too great for the antenna. Attempted to acquire by waiting at approximately the mid-point of the pass. This attempt was unsuccessful. The receiver had several momentary locks and servo went to autotrack for a few brief periods but the signal was never acquired with the main lobe. No tracking or telemetry data obtained.
	1	67	140441	141151			140521	141111			Modulation appeared on the beacon signal three times (about 3 min total time). The transponder signal was seen twice (total appearance about 2 min).
	5	67	140531	140741			140631	140741	−93.7 (max)	140700	Tracked the beacon signal. Two momentary periods of autotrack between 140901 and 140951.
			140901	140951					−130	140758	
8/28	4	74	001025 001445	001315 001545					−130 (avg)		Attempted to track the beacon but was unsuccessful. Receiver lock was maintained long enough to show there was no modulation on the beacon signal and no transponder signal present.
	4	75	014356	015006			014416	014716	−70 (max)		Tracked beacon signal. No transponder signal evident. Some beacon modulation detected.
	4	76	031904 032234	032104 032424			032004	032054	−80 (max)		Used 6-ft dish for reference channel input. Tracked the beacon signal. The transponder signal appeared on the spectrum analyzer once during the first part of the tracking period.
	3	76	035400	035520			035400	035520	−100	035534	Tracked the beacon. Only used Channels 1 and 3 in telemetry recording to prevent damage to recorder pins because of noise on other channels. No telemetry data were obtained during this tracking period.
	4	77	045217 045627	045457 045827							Modulation appeared on the beacon signal once. No transponder signal detected. The receiver had several intermittent locks from 045457 to 045627.
	3	77	052539	053049			052539	053049	−90	052844	Tracked the beacon with the receiver desensitized to −100 dbm. Telemetry Channel 1 locked up and had a 1-sec blip on it.
	1	78	060241	060811			060301	060751	−121 −111	060240 060419	Tracked the beacon signal. Went out of lock briefly at 060650 to check receiver tuning. Twice during the tracking period two signals were seen on the spectrum analyzer.
	4	78	062728 062858 062948	062828 062950 063008					−130 (max)		Tracked beacon signal and modulation was present during all periods of receiver lock. No indication of transponder signal.
	3	78	070109 070359	070149 070429					−125 (max) −130	 070129	Attempted to track the beacon with the receiver desensitized to −100 dbm. A signal was detected at 065625 but no lock was obtained. Receiver sensitivity was increased and the antenna was moved ahead of the predictions by

[a]DSIF-1: Mobile Tracking Station, -2: Goldstone *Pioneer* Site, -3: Goldstone *Echo* Site, -4: Woomera, -5: Johannesburg.
Note: All times are GMT.

Table 83. Summary of DSIF participation in *Ranger I* mission (cont'd)

Date 1961	Station	Orbit	RF one-way		RF two-way		Autotrack		Signal		Remarks
			In	Out	In	Out	In	Out	DBM	Time	
											more than 4 min to finally obtain lock. Telemetry Channel 1 locked up at 070349.
8/28	1	79	073551	074211			073621 074051	074001 074141	−113 −100 (max)	073612 073754	Tracked the beacon signal. Modulation was detected from 073909 to 074227.
	5	79	073741	073831					−117 (max)	073700	Required antenna rates were too great after the first minutes of the pass. Tracked the beacon signal. Telemetry detected momentarily at 073900.
	3	79	083049	083839			083059	083819	−92	083400	Tracked the beacon with the receiver desensitized to −105 dbm. Telemetry Channel 1 was in lock for the complete track. Tracking predictions were off approximately 4½ min.
	1	80	091131	091551			091201	091511	−113	091134	Tracked the beacon signal. Telemetry modulation present for three periods: 091048 to 091106; 091117 to 091300; and 091405 to 091537.
	5	80									Pass was low on horizon and behind the polar mask. Did not attempt tracking.
	3	80	100459	101159			100519	101129	−95	100803	Tracked the beacon with the receiver desensitized to −105 dbm. Telemetry Channel 1 in lock. Channel 3 again locked on tone generated by faulty wideband VCO.
	1	81	104441	105021			104511	105001	−113	104441	Modulation detected from 104605 to 104735 and from 104843 to 105001.
	5	81									Pass was low on the horizon and partially behind the polar mask. Did not attempt tracking.
	1	82	121811	122451			121821	122401	−119 −95 (max)	121811	Modulation detected three times for about 1 min each time.
	5	82	122151	122331					−120 −135	122000 122312	As an aid to acquisition the 6-ft dish was used paralleled with the main antenna. The antenna rates required were rather high so the antenna was positioned at a midpoint in the pass. Approximately 1 min was available for acquisition and tracking before the probe went over the horizon.
	1	83	135211	135821			135251	135741	−121	135230	Modulation detected twice for about 1½ min each time.
	5	83	135241	135521			135341	135511	−130 −87	135220 135400	The 6-ft dish was disconnected for this pass. Telemetry Channels 1 and 3 were in lock for about 1 min.
	4	89							−120	235336	Used parallel dish configuration. Momentary receiver lock at 235336. Signal detected on spectrum analyzer appeared to be beacon signal but frequency predictions indicated the signal was that of the transponder. Doppler shift effects are believed to have caused a momentary lock on the transponder signal.
8/29	4	91									012944. Used parallel dish configuration. No signal detected.
	4	92									030254. Used 6-ft dish with servo in aided track mode and a spike antenna through the hour angle channel to a 51J4 receiver. No signal.

[a]DSIF-1: Mobile Tracking Station, -2: Goldstone *Pioneer* Site, -3: Goldstone *Echo* Site, -4: Woomera, -5: Johannesburg.
Note: All times are GMT.

CONFIDENTIAL

CONFIDENTIAL

Table 83. Summary of DSIF participation in *Ranger I* mission (cont'd)

Date 1961	Station[a]	Orbit	RF one-way		RF two-way		Autotrack		Signal		Remarks
			In	Out	In	Out	In	Out	DBM	Time	
8/29	3	92									Listened from 032730 to 034230. Receiver desensitized to −105 dbm. No signal received.
	4	93									043541. Used parallel dishes. No signal heard.
	3	93									Receiver not desensitized. Listened from 050100 to 052500 and heard nothing.
	4	94									Listened from 060912 to 061952 and heard nothing. Woomera ordered to secure operations.
	1	94									Listened from 054200 to 055100 and heard nothing.
	3	94									Receiver not desensitized. Listened from 063340 to 065200. No signal heard. *Ranger* operations terminated.
	1	95									Listened from 071500 to 072600 and heard no signal.
	1	96									Listened from 085000 to 085830 and heard no signal. *Ranger I* operations terminated.

[a]DSIF-1: Mobile Tracking Station, -2: Goldstone *Pioneer* Site, -3: Goldstone *Echo* Site, -4: Woomera, -5: Johannesburg.
Note: All times are GMT.

This command transmission was performed to demonstrate the command capability of both the primary command station, *Echo* (DSIF 3), and the back-up command station, *Pioneer* (DSIF 2). Verification of command reception and performance was received for all commands sent by DSIF 3, but no indications of success were received for commands transmitted by DSIF 2. The effects of commands sent by DSIF 3 were easier to detect since they produced a change in signal level. The command for an antenna hinge-angle change, transmitted by DSIF 2, did not produce a signal level change due to the proximity of the spacecraft to Earth.

Due to the difficulties of tracking and receiving data from the *Ranger I* spacecraft, the DSIF tried various techniques for improving acquisition and data reception attempts. The techniques used were primarily concerned with the performance of the r-f tracking system. These techniques consisted of connecting the output of the 6-ft parabolic reflector antenna mounted on the edge of the large reflector to the receiver reference channel or, at only the Goldstone Stations, desensitizing the receiver. The use of the 6-ft antenna, while decreasing the system gain by 34 db, provided a telemetry reception beamwidth of 15 deg, but left the tracking beamwidth at approximately 1 deg. Desensitizing the receiver was an attempt to keep the system from tracking on an antenna side lobe. Because of the strong spacecraft signal, both of these techniques could be used without jeopardizing the tracking capability of the stations.

In addition to the r-f changes, a modification was made to the antenna hydraulic drive system at each HA-Dec antenna installation. This modification consisted of repiping the hydraulic system to remove the anti-backlash feature. This modification increased the possible tracking rate from 1 deg/sec to 1.5 deg/sec, but decreased the tracking accuracy.

The *Ranger I* tracking mission, while obviously not a complete success, did accomplish many objectives. The successful operation of the spacecraft was indicated from the signal strength observations and telemetry information provided by the DSIF. The operations involved in tracking the spacecraft provided the DSIF Net Control Center with experience in organizing and maintaining communications with stations located at remote points around the world. At the DSIF stations, personnel received experience in operating the various systems and in performing the various operational and administrative details involved in a tracking mission. A large amount of experience was also gained in the early acquisition of a low-orbit, fast-moving space probe. During a normal operation, this important event only occurs on the first day at the station located near the spacecraft injection point.

2. Evaluation

a. Tracking by Mobile Tracking Station. Passes 2 and 3 represent somewhat better than typical examples of the MTS tracking capability. Figures 403 and 404 show the locations of the two passes with respect to the station. These, incidentally, are representative of many of the *Ranger I* orbits and serve to illustrate the visibility problems this type of satellite pass presents to a HA-dec antenna. This is the reason that the Johannesburg Station was unable to provide extended coverage of the *Ranger I* mission. Orbit 3 is probably the best tracking done on the mission by the MTS antenna. It is of particular interest for this reason and because it provides a good example of multipath effects on a wide (10 deg) beamwidth antenna.

b. Tracking by Goldstone Pioneer *and* Echo *Stations (DSIF 2 and 3).* Orbit 2 (Fig 405) was the first pass that was successfully tracked by both stations and although this pass was obviously not one that could be considered good from a visibility standpoint, it is of interest from an antenna comparison viewpoint.

c. Tracking by Woomera Station (DSIF 4). The tracking done by the Woomera Station during Orbit 30 is representative of the successful tracks performed by this station, which faced the same problems as Johannesburg. Visibility, high-angular rates, and difficulties in acquisition prevented a more extensive coverage of the *Ranger I* mission. Figure 406 presents the trajectory plot for Orbit 30.

d. Tracking by Johannesburg Station (DSIF 5). After the first orbit, DSIF 5 was formally secured because the MTS was capable of tracking all following passes over that location. DSIF 5 did attempt informal tracking of several orbits but the high angular rates and polar mount limitations prohibited the acquiring of much useful data. The most successful track occurred during Orbit 32, when 3 min, 10 sec of useful data was obtained.

C. *Ranger II* Pre-Launch Operations

The DSIF preparatory operations for *Ranger II* began during the first two weeks of October at all stations except DSIF 2 (Goldstone *Pioneer*). These preparatory

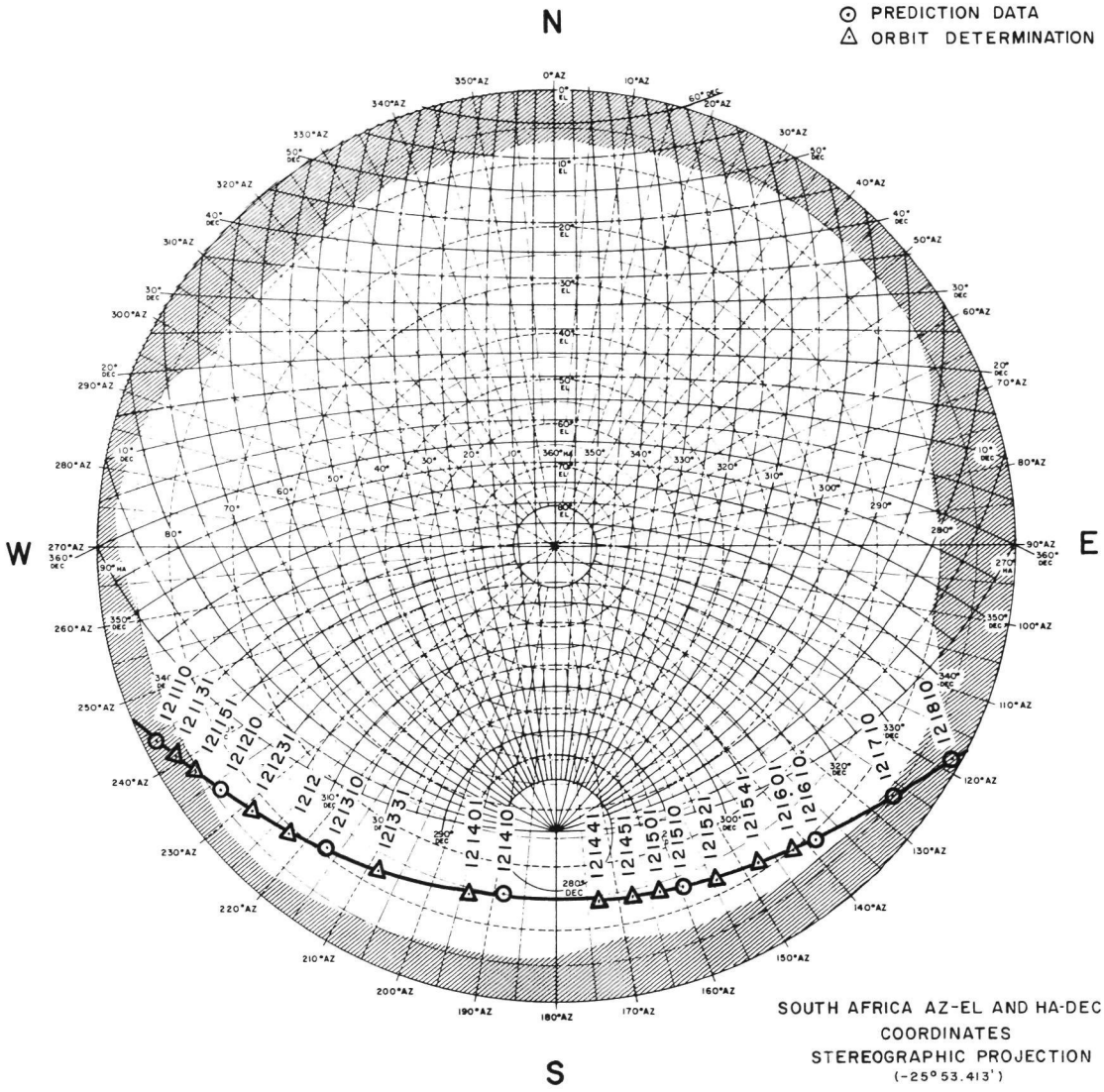

Figure 403. Comparison of predicted and computed Orbit 2 for DSIF 1 and 5

operations consisted of star tracks to evaluate antenna optical pointing accuracy and dynamic tracking tests using an airborne r-f beacon to evaluate the r-f tracking characteristics of the antennas. The Goldstone *Pioneer* Station, because of other commitments and since it was to participate as a backup for DSIF 3 (Goldstone *Echo* Station), did not begin preparation for the *Ranger II* mission until October 15. All stations participated in a net integration test on October 18. Station operations during the test were satisfactory and the DSIF was ready and operational for the launch attempt.

Three launch attempts were made: October 20, 23, and 25, 1961, and the DSIF was operational for each attempt. After these attempts, the RA-2 mission was rescheduled for November 18, 1961.

Although the DSIF was operational for all *Ranger II* events, several difficulties were encountered. One problem was that, while communications with the DSIF stations were generally good, some outages occurred on the Johannesburg circuits due to poor propagration conditions over the North Atlantic. The Goldstone *Echo* Station suffered a failure of the azimuth data encoder unit and a spare encoder unit was installed. The Woomera Station had a number of component failures in the data handling system. These problems were resolved in teletype conferences between operating personnel and the cognizant JPL engineers.

During the period before the next launch attempt, the DSIF maintained its state of operational readiness by

conducting routine maintenance and subsystem tests. The Goldstone *Pioneer* Station repeated the star tracks and dynamic tracking tests conducted prior to the first RA-2 launch attempts. The initial tests did not provide the desired data. An operational readiness test on November 16 demonstrated that the DSIF was ready for the next launch attempt.

D. *Ranger II* Tracking Operations

Ranger II was launched at 0812:21.5Z on November 18, 1961. The DSIF was ready and operational for the launch. Teletype and voice circuits between JPL Net Control and the DSIF stations were established at 0637Z. These circuits were operational until 0805Z when one South African teletype circuit failed because of propagation difficulties. This circuit was never re-established.

The launch appeared normal and prediction data were transmitted to DSIF 1 and 5 based on a nominal *Agena* second burn. The spacecraft was due over the DSIF 1 horizon at 0840 and, prior to this time, the station had begun a horizon search. At 0841, DSIF 1 began using the pointing data as a guide for antenna positioning. The spacecraft transponder signal was acquired at 084438. Tracking was done in the one-way mode until 084830, when the transponder was acquired in a two-way condi-

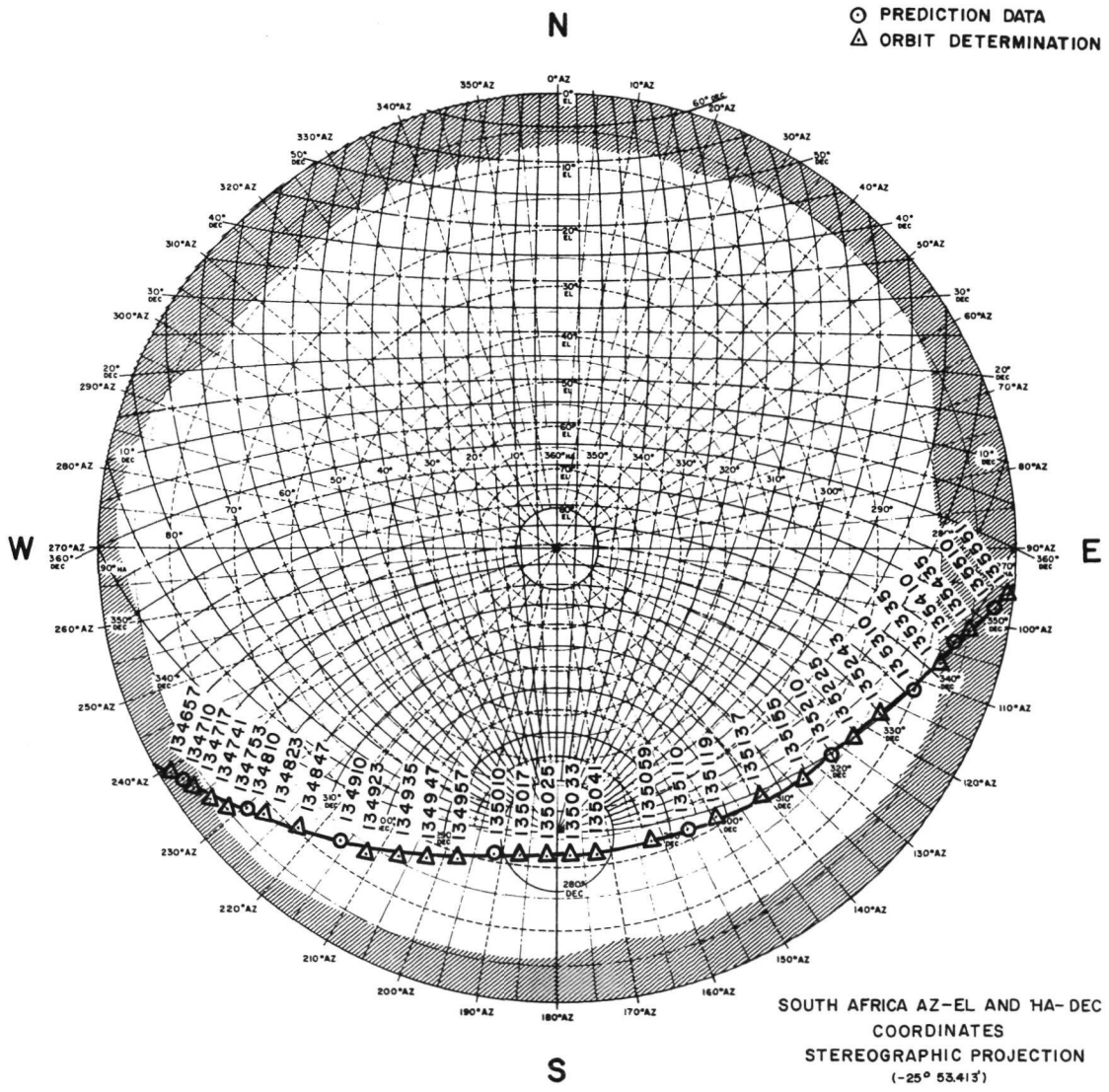

Figure 404. Comparison of predicted and computed Orbit 3 for DSIF 1 and 5

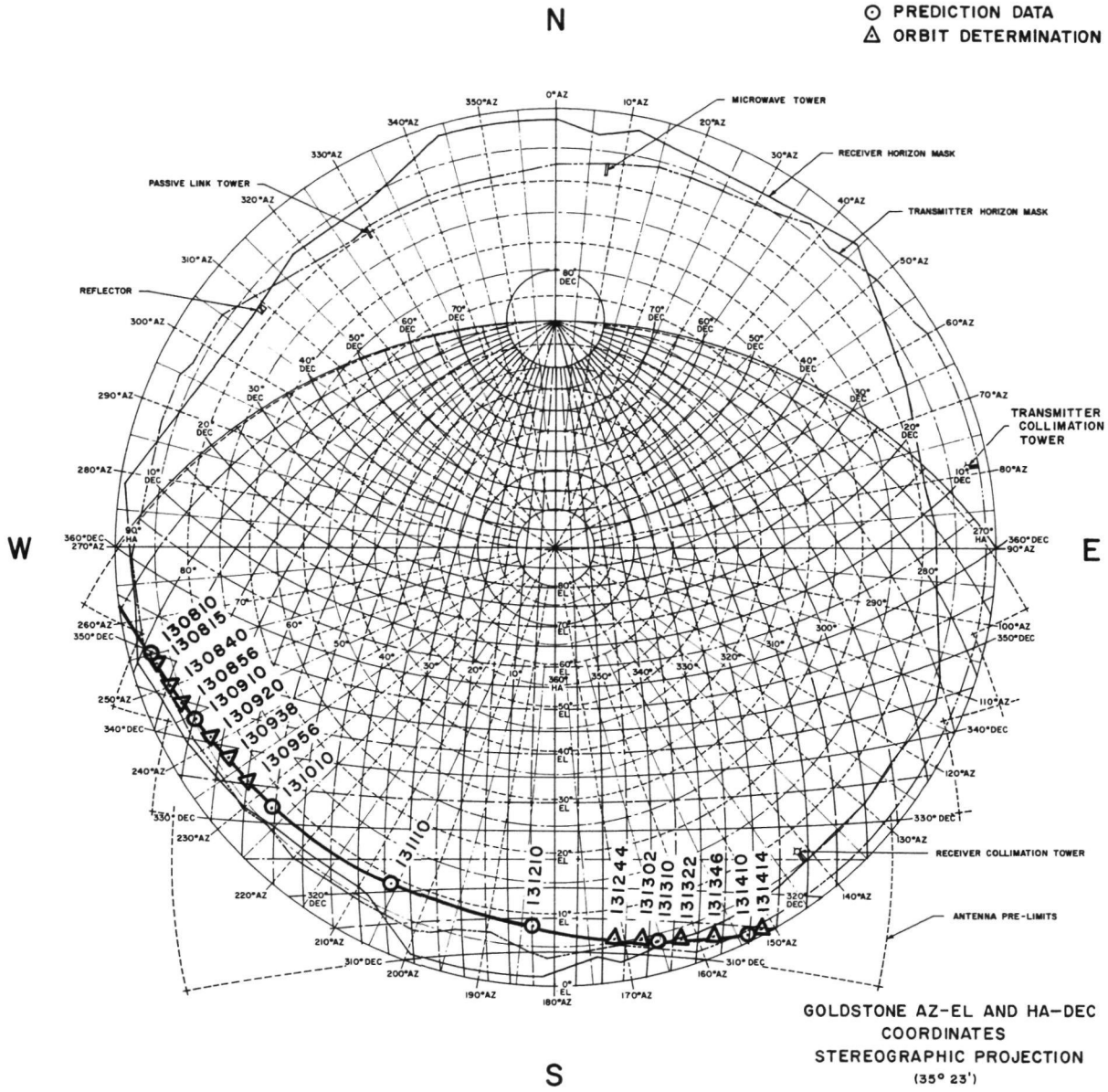

Figure 405. Comparison of predicted and computed Orbit 2 for DSIF 2 and 3

tion. By this time, because of the elevation angles and angular tracking rates required, it was apparent that the *Agena* second burn had not occurred and the spacecraft had remained in its nominal 115-mi altitude parking orbit.

The DSIF then began the task, as in the *Ranger I* mission, of tracking and communicating with a low-altitude satellite. The Woomera Station was secured since the spacecraft would not be visible there until approximately 2300Z on November 18. The other DSIF stations continued their tracking efforts until the spacecraft was no longer visible over their local horizons. Final contact with the spacecraft occurred at 1456Z, November 18, by the Mobile Tracking Station. The next scheduled acquisition by the DSIF was at approximately 2310Z at the Woomera Station, but no signal was heard. Subsequent searching by the Woomera and Goldstone Stations was unsuccessful and the *Ranger II* tracking mission was terminated. A summary of the DSIF operation is presented in Table 84.

Because of the difficulties of acquiring and tracking this satellite in the relatively brief view periods at each

station, a 6-ft diameter parabolic antenna was mounted on the large reflector. The output of this antenna was connected to the receiver reference channel. This technique was similar to that used in *Ranger I* operations and, while decreasing the system gain by 34 db, provided a telemetry reception beamwidth of 15 deg, but left the tracking beamwidth at approximately 1 deg. This acquisition aid antenna was installed at the Woomera and Goldstone Stations but was only used for acquisition at the Goldstone *Echo* Station. It was not installed at the other stations until after the probe had stopped transmitting.

E. DSIF Preparations for RA-3

Following the conclusion of *Ranger II* operations the DSIF net began preparations for RA-3. A summary of the changes incorporated into the stations by December 31, 1961, follows:

1. Goldstone Echo Site

A Read-Write-Verify (RWV) command unit was installed in place of the tone command unit employed for *Ranger II*. In addition, a 960-mc parametric pre-

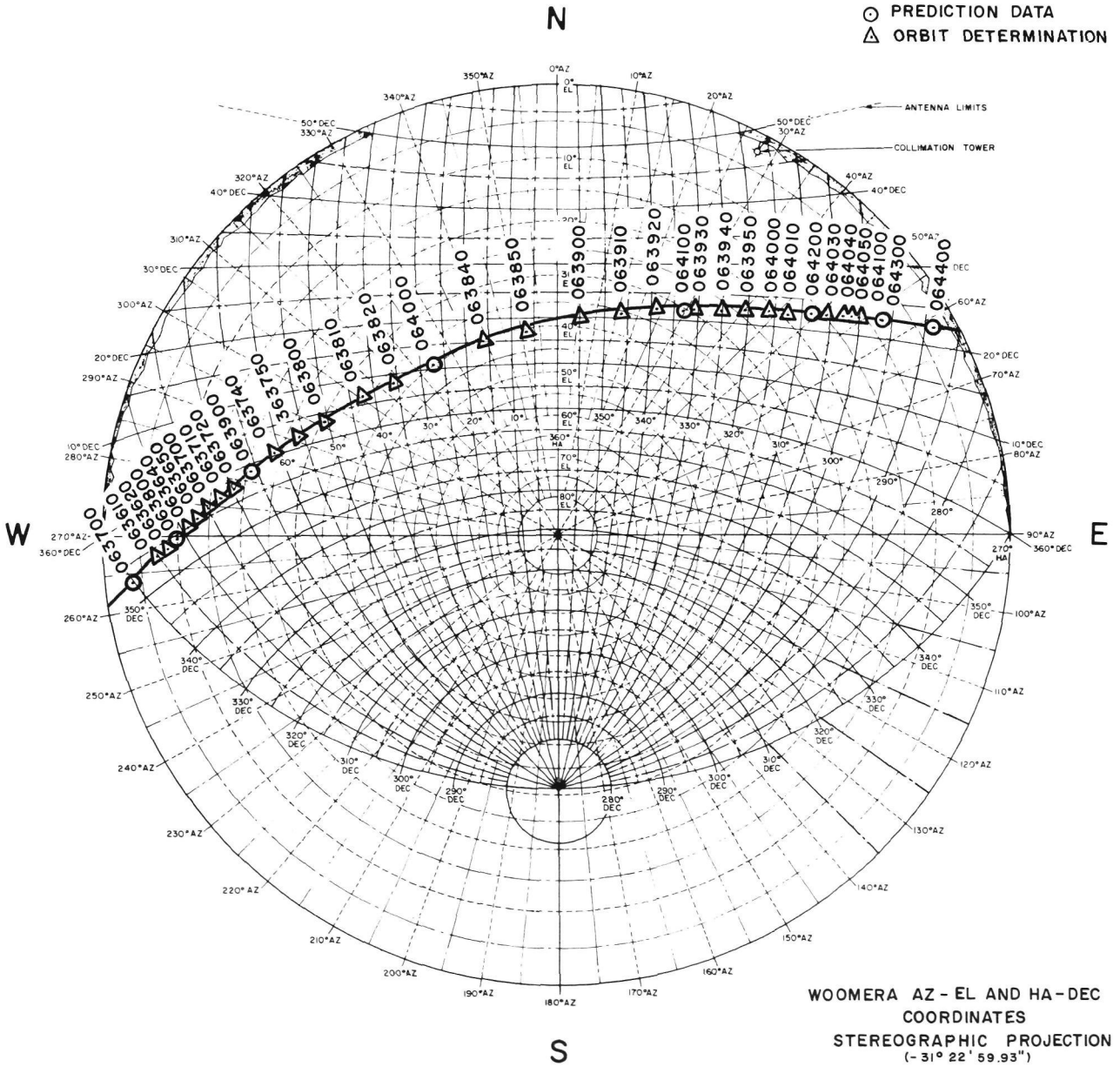

Figure 406. Comparison of predicted and computed Orbit 30 for DSIF 4

Table 84 . DSIF operations summary for *Ranger II* mission

Date 1961	Station	Orbit	RF one-way		RF two-way		Autotrack		Signal		Remarks
			In	Out	In	Out	In	Out	DBM	Time	
11/18	—	—									*Ranger II* launch at 0812:12.5.
	1	1	084438	084830	084830	085056	084445	085056	−114 to −121		Tracked the transponder. Began recording telemetry at 0848:30 and continued until loss of lock at 0850:56. Data were transmitted to JPL in near real time.
	5	1	084642	084656	—	—	—	—	—		Tracked the beacon. Obtained only momentary lock. Autotrack was not achieved and no useful data were obtained.
	2	1	094011	094021					−130 (max)		Attempted to track the transponder. The antenna was tracking using a side lobe and when an attempt was made to acquire with the main lobe the signal was lost and r-f lock could not be attained again.
	3	1	093856	094446			093923	094446	−125		Tracked the beacon signal using the six-foot dish. Intermittent RF locks were obtained during the period indicated. Because of problems in the data handling equipment the data condition code did not indicate RF lock or autotrack. No telemetry data were obtained.
	1	2	101708	101721	101721	102339	101741	102301	−114		Tracked the transponder. Obtained and transmitted telemetry data in near real time to JPL. Obtained good tracking data.
	5	2	—	—	—	—	—	—	—		Unable to track because the pass was behind the polar mask.
	3	2	111354 111438 111521 111543	111405 111442 111527 111611							Tracked the beacon with the servosystem in the aided track mode. No useful data were obtained.
	2	2									The spacecraft passed low on the horizon and according to predictions would be visible for 1 min and 30 sec. A momentary r-f lock was obtained at 111417.
	1	3	115025	115051	115051	115653	115051	115610	−115	115051	Tracked the transponder signal. Transmitted tracking and telemetry data to JPL.
	5	3									Pass not visible to the station.
11/18	1	4	132250	132316	132316	132648			−105	132350	
	5	4	132341	132632					−90 −85 −130	132341 132536 132640	*Tracked the beacon signal. Lost lock during the track* because of the high angular rates required. Tracking data and engineering and scientific telemetry data were transmitted to JPL after the pass. The station was secured after this pass since Orbit 5 would not be visible.
	1	5	145629	145647	145647	150117			−112	145833	Tracked the transponder. Transmitted tracking data in real time to JPL telemetry data were transmitted to JPL after the tracking period.
	4	11									Began searching for signal at 2310, 10 min before predicted acquisition time. Continued searching for beacon signal until 10 min after predicted loss of signal. Negative results. 6-ft dish was in parallel with the reference channel.

CONFIDENTIAL

Table 84. DSIF operations summary for *Ranger II* mission (cont'd)

Date 1961	Station	Orbit	RF one-way		RF two-way		Autotrack		Signal		Remarks
			In	Out	In	Out	In	Out	DBM	Time	
11/19	4	12									Beacon searching at 0034. The 6-ft dish was in parallel with the reference channel. Searched until 0100 with negative results.
	4	13									Used wide beam dipole and searched from 0200 to 0232. Listened at 960.1 mc but heard no signal.
	4	14									Listened at 960.1 mc using the wide beam dipole. Searched from 0330 to 0405. No signals were heard.
	2, 3	15									Conducted search for beacon and transponder frequencies. No results. All stations secured.

CONFIDENTIAL

amplifier was mounted on the antenna; an ultra-stable transmitter voltage-controlled oscillator (VCO) was installed to improve the accuracy of the two-way doppler measurement; and exhaustive tests were performed on the antenna structure and servo drive system to isolate and remedy the source of error detected by the *Ranger I* post-flight data analysis. These additions and corrections necessitated considerable re-wiring at *Echo* Site in order to be ready for scheduled January 1962 launch of RA-3.

2. *Goldstone* Pioneer *Site*

The receiver at the *Pioneer* Site was equipped with a maser (low-noise) and parametric preamplifiers in order to attempt a track of the beacon in the RA-3 capsule during the terminal retro-maneuver. After installation, the *Pioneer* Site undertook an evaluation program for the new system.

3. *Johannesburg and Woomera Stations*

The overseas DSIF stations installed parametric preamplifiers in anticipation of RA-3. The configuration for these stations is shown in Figure 254. In addition, the Johannesburg Station received and installed an additional 150-kw diesel generator during December 1961. This generator is part of a program to provide full transmitter capability at Johannesburg in time for RA-4.

4. *Mobile Tracking Station*

After the completion of the *Ranger II* mission, the MTS was secured, and the crew returned to the United States. While at JPL, the MTS crew fabricated the modification kits necessary to install an ultra-stable VCO in the mobile station for RA-3.

Page intentionally left blank

IX. Project Continuation Plan

At the close of the period covered by this report (the end of 1961), the *Ranger* Project was about one month behind schedule, as measured by launch dates. The first two flights, while they demonstrated many of the required elements of launch vehicle and spacecraft technology, had yielded little or no new scientific information. Certain vital aspects of the operation, such as the Earth-orientation of the spacecraft high-gain antenna and the controlled midcourse maneuver, were yet to be demonstrated in flight. The flight of *Ranger III*, which will be covered in the next report, remedied these deficiencies.

The project is now (March 1962) on schedule and the functions of all systems have been demonstrated, with the exception of the terminal phase and the retro-capsule landing. The changes being incorporated as a result of *Ranger III* experience are all of such a nature that they can be made without delay of the fourth launch attempt.

The plan for continuing the project now includes six flights: two more like *Ranger III*, with the vidicon, gamma-ray, radar, and rough-landed seismometer experiments, and then four with the high-resolution TV impact experiment plus radiation environment detectors. The spacecraft configurations to be used are shown in Figure 2. The *Atlas–Agena B* launch vehicles will be essentially unchanged, as will the launch-to-injection instrumentation. The U. S. Army tracking ship *American Mariner*, also known as the DAMP ship, will be replaced by the Atlantic Missile Range ship *Twin Falls Victory*.

The Data Operations and Command System will operate with the same organization and methods as in *Ranger III*, but with improved facilities and modified procedures as dictated by that experience.

The DSIF system will support the flight missions as it has in the past, and the later flights will also carry experimental equipment to assist in the planned transition from L-band to S-band for the primary tracking frequencies. The gain margins of the system will be improved through the use of more sensitive receivers as soon as these can be operationally qualified.

The objective of the project will continue to be to produce the technology, the environmental measurements, and the scientific understanding that will best support the U.S. in the drive toward human exploration of the Moon.

References

1. *Juno IV Final Report*, Report No. 20-123, Jet Propulsion Laboratory, Pasadena, November 30, 1961.
2. *The Vega Program*, Report No. 30-6, Jet Propulsion Laboratory, Pasadena, August 3, 1959.
3. *Surveyor Spacecraft System*, Technical Memorandum No. 33-54, Jet Propulsion Laboratory, Pasadena, August 30, 1961.
4. *Agena Study Report*, Jet Propulsion Laboratory, Pasadena, February 1, 1960.
5. *Scientific Experiments for Ranger-1 and -2*, Technical Report No. 32-55, Jet Propulsion Laboratory, Pasadena, March 2, 1961.
6. *Scientific Experiments for Ranger-3, -4, and -5*, Technical Report No. 32-199, Jet Propulsion Laboratory, Pasadena, January 9, 1962.
7. Dallas, S. S., *Post-Injection Standard Trajectory Ranger P-32*, Engineering Planning Document No. 36, Jet Propulsion Laboratory, Pasadena, June 26, 1961.
8. *Thirty-five Day Report, Ranger 1 System Test Evaluation and Performance Analysis Report*, LMSC-448617-01, Lockheed Missile Systems Company, Sunnyvale, Calif., September 27, 1961.
9. Johnson, M. S., *Estimation of Orbit of Ranger 1*, Interoffice Memorandum, Jet Propulsion Laboratory, Pasadena, September 13, 1961.
10. Dallas, S. S., *Post-Injection Standard Trajectory Ranger P-33 (RA-2)*, Engineering Planning Document No. 44, Jet Propulsion Laboratory, Pasadena, September 26, 1961.
11. *Launch Report for Atlas 117D/Agena-B 10205-6002 Ranger Spacecraft RA-2*, LMSC-271410, SSN-T61-102, Lockheed Missiles and Space Company Space Systems, AFMTC Test Operation, Florida, December 2, 1961.
12. Asderian, O., *Orbit Determination Group*, Jet Propulsion Laboratory, Pasadena, December 26, 1961.
13. Barnes, F. L. and Maloy, J. O., *Midcourse and Terminal Guidance Operations Program*, RFP 312-24, Jet Propulsion Laboratory, Pasadena, Calif.
14. Tross, C., *Astronomical Constants and Their Importance in Lunar Trajectory Determination*, pp. 938–941, ARS Journal, Vol. 30, No. 10, American Rocket Society, New York, October 1960.
15. *Research Summary No. 36-5*, Vol. I, pp. 13–16, Jet Propulsion Laboratory, Pasadena.
16. Coleman, P. J., Jr., Davis, L., and Sonett, C. P., *Steady Component of the Interplanetary Magnetic Field: Pioneer V*, Physical Review Letters, 5: 43–46, 1960.
17. Parker, E. N., *Dynamics of the Interplanetary Gas and Magnetic Fields*, Astrophysical Journal, 128: 664–676, 1958. See also: Parker, E. N., *The Hydrodynamic Treatment of the Expanding Solar Corona*, Astrophysical Journal, 132: 175–183, 1960.
18. Bierman, L., *Solar Corpuscular Radiation and the Interplanetary Gas*, Observatory, 107: 109–110, 1957. See also: Bierman, L., *Physical Processes in Comet Tails and Their Relation to Solar Activity*, Memoires de la société royale des sciences de Liège, 13 (Series 4): 291–301, 1953.
19. Chamberlain, J. W., *Interplanetary Gas. II. Expansion of a Model Solar Corona*, Astrophysical Journal, 131: 47–56, 1960.
20. Fan, C. Y., Meyer, P., and Simpson, J. A., *Cosmic Radiation Intensity Decreases Observed at the Earth and in the Nearby Planetary Medium*, Physical Review Letters, 4: 421–423, 1960. See also: Fan, C. Y., Meyer, P., and Simpson, J. A., *Trapped and Cosmic Radiation Measurements from Explorer VI*, pp. 951–966, Proceedings of First International Space Science Symposium (Edited by H. Kallman Bijl), North Holland Publishing Company, Amsterdam, 1960.
21. Fan, C. Y., Meyer, P., and Simpson, J. A., *Preliminary Results from the Space Probe Pioneer V*, Journal of Geophysical Research, 65: 1982–1983, 1960.
22. Neher, H. V., *An Automatic Ionization Chamber*, Review of Scientific Instruments 24, 99–102 (1953).
23. Neher, H. V. and Johnston, A. R., *Modification to the Automatic Ionization Chamber*, Review of Scientific Instruments 27, 173–174 (1956).
24. Johnson, F. S., *The Exosphere and Upper F Region*, Journal of Geophysical Research, 65: 2571–2575, 1960.
25. Kupperian, J. E., Jr., Byram, E. T., Chubb, T. A., and Friedman, H., *Far Ultraviolet Radiation in the Night Sky*, Planetary and Space Science, 1: 63–65, 1959.
26. Struve, O., *Far Ultraviolet Radiation of the Night Sky*, Sky and Telescope, 17: 445–448, 1958.
27. Shklovsky, I. S., *On Hydrogen Emission in the Night Glow*, Planetary and Space Science, 1: 63–65, 1959.
28. Johnson, F. S., and Fish, R. A., *The Telluric Hydrogen Corona*, Astrophysical Journal, 131: 502–515, 1960.
29. Purcell, J. D., and Tousey, R., *The Profile of Solar Hydrogen-Lyman-. . .*, Journal of Geophysical Research, 65: 370–372, 1960.
30. Whipple, F. L., *The Meteoritic Risk to Space Vehicles*, Vistas in Astronautics, Volume I (Edited by M. Alperin and M. Stern), Pergamon Press, New York, 1958.
31. Bjork, R. L., and Gazley, C., Jr., *Estimated Damage to Space Vehicles by Meteoroids*, Research Memorandum RM-2332, Rand Corporation, Santa Monica, Calif., February 20, 1959.
32. *Data Automation System for the Ranger Spacecraft Program*, Jet Propulsion Laboratory Manual 1, Jet Propulsion Laboratory, Pasadena, April 1, 1961.
33. Morecroft, J., *Telemetry Support Equipment (TSE) Operation and Maintenance*, Technical Memorandum No. 33-66, Jet Propulsion Laboratory, Pasadena, October 16, 1961.
34. Arnold, J. R., *Gamma Ray Spectroscopy of the Moon's Surface*, Proceedings of the Lunar and Planetary Exploration Colloquium, 1, No. 3, North American Aviation, Inc., Downey, Calif., 1958.
35. Trexler, J. H., *Lunar Radio Echoes*, Proceedings of the IRE, 46, No. 1, 286–292, 1958.
36. Pettengill, G. H., *Measurements of Lunar Reflectivity Using the Millstone Radar*, Proceedings of the IRE, 48, No. 5, 933–934, 1960.
37. Senior, T. B. A., and Siegel, K. M., *A Theory of Radar Scattering by the Moon*, Journal of Research of the National Bureau of Standards, 64D, No. 3, 217–229, 1960.
38. Brown, W. E., Jr., *A Lunar and Planetary Echo Theory*, Journal of Geophysical Research, 65, No. 10, 3087–3095, 1960.
39. Daniels, F. B., *A Theory of Radar Reflection from the Moon and Planets*, Journal of Geophysical Research, 66, No. 6, 1781–1787, 1961.
40. Straiton, A. W., and Tolbert, C. W., *Bistatic Moon-Reflection Measurements at kmcs*, University of Texas Report No. 5-28, November 30, 1959.
41. Hansen, Siegfried, *Research Program on High Vacuum Friction*, Final Report No. TR 59-97, Litton Industries, Beverly Hills, Calif., March 30, 1959.
42. *Handbook of Geophysics*, Editorial Staff, The Macmillan Company, New York, 1960.
43. *Combined Bi-Monthly Summary No. 68*, Jet Propulsion Laboratory, Pasadena, October 1, 1958 to December 1, 1958.
44. Yu, Ying-Nien, *A Summary of Design Techniques for Axisymmetric Hypersonic Wind Tunnels*, AGARDograph, 35, NATO, AGARD, November 1958.
45. Landsbaum, Ellis M., *Contour Nozzles*, Memorandum No. 20-169, Jet Propulsion Laboratory, Pasadena, September 15, 1958.

CONFIDENTIAL

This document contains information affecting the national defense of the United States, within the meaning of the Espionage Laws, Title 18, U.S.C., Sections 793 and 794, the transmission or revelation of which in any manner to an unauthorized person is prohibited by law.

CONFIDENTIAL